third
symposium on

DETONATION

JAN 1 3 1994

**JAMES FORRESTAL
RESEARCH CENTER
PRINCETON UNIVERSITY**

19950111 138

SEPTEMBER 26-28, 1960

DTIC
COPY
INSPECTED
6

Accesion For	
NTIS CRA&I	☑
DTIC TAB	☐
Unannounced	☐
Justification	

By
Distribution /

Availab...	
Dist	Avail...
A-1	

cosponsored by

**NAVAL ORDNANCE LABORATORY
WHITE OAK
and
OFFICE OF NAVAL RESEARCH**

DTIC QUALITY INSPECTED 3

Office of Naval Research • Department of the Navy

FOREWORD

The Third Symposium on Detonation is the continuation of the series of Navy-sponsored discussions of this subject, which have been scheduled at irregular intervals as new advances in the science make an assessment of the current state of the field timely. The first two symposia were sponsored by the Office of Naval Research. On this occasion, the Naval Ordnance Laboratory, White Oak, one of the laboratories under the Bureau of Naval Weapons, is joining with ONR in the continuation of these symposia.

Unlike the previous symposia, the scope of this one has been limited to condensed systems. This restriction is based on the existence of more opportunities for presentation of research on gaseous detonation at relatively frequent meetings of various scientific and engineering societies.

The object of this symposium is to bring together scientists actively engaged in research on detonation to discuss the current status of related research. To achieve this, the organizers of the symposium have invited review papers on the three topics being emphasized: Explosive Sensitivity, Detonations and Shocks, and Non-Steady Detonations. These are supplemented by contributed papers to include the results of current research.

The papers are being published in two groups, one containing the unclassified contributed papers and the second containing the review papers and classified contributed papers.

The sponsors of this symposium are of the opinion that the exchange of research information and concepts will stimulate advances in this complex field of the interaction between flow and exothermic

chemical processes. In addition, advances in the understanding of detonation phenomena are becoming more and more important to the Department of Defense and other agencies of the government. This increases the value of making certain existing knowledge is available to those having need for it.

To all those contributing to the success of the symposium, the organizers wish to express their sincerest appreciation. Special thanks go to the individuals undertaking the difficult task of preparing the review papers; to the session chairmen; to the staff of Project SQUID of the James Forrestal Research Center, Princeton University, for handling many of the arrangement details; and to Princeton University for the use of its facilities.

James E. Ablard
Chemistry and Explosives Program Chief
Naval Ordnance Laboratory
White Oak

Ralph Roberts
Head, Propulsion Chemistry Branch
Office of Naval Research

During my eight years organizing The Detonation Symposium, I have received inquiries about copies of the first three symposia (which were never published in hardback form). In response to your inquiries, the first three are now hardbound. The first two symposia are combined in a single hardbound volume. The third symposium is in a separate hardbound volume. All of the papers in these symposia are now unclassified.

Copies of these volumes, or Proceedings of any Detonation Symposium (the First through the Seventh) are available at a cost of $35.00 each. Only prepaid orders can be accepted. Make your check payable to "The Detonation Symposium." Mail your payment to:

Dr James M Short, R12
Co-Chairman, The Detonation Symposium
Naval Surface Weapons Center
White Oak, Silver Spring, MD 20903-5000

James M Short
June 1, 1987
White Oak

CONTENTS

A COLLIDING BALL HIGH EXPLOSIVE IMPACT
SENSITIVITY TESTING MACHINE

C. M. Bean, G. P. Cachia, J. Kirkham
Atomic Weapons Research Establishment,
United Kingdom Atomic Energy Authority,
Aldermaston, Berkshire, England.

INTRODUCTION

The impact sensitivity machines normally used in testing high explosives not only employ considerable impact energies but form complex elastic systems not readily variable in a defined way. An elastically much simpler system, described in this paper is therefore being developed and is based essentially on the symmetrical collision of two identical hardened steel spheres (ball bearings). The advantages of such a machine as a research tool are the ease with which the diameter of the balls can be varied and the facility of being able to calculate how much energy is deposited in the sample. This is possible merely by measuring ball velocities before and after collision and their masses, since no energy can pass across the plane of symmetry. Also by virtue of this symmetry the supporting structure plays no part in the impact and thus can be made of a simple light construction, fully portable and of low cost. The impact characteristics of colliding balls are well known and give some idea of the conditions pertaining in the sample but exactly how much the presence of the sample modifies the simple impact conditions is not yet known.

DESCRIPTION

The machine is shown diagrammatically in Fig. 1 and consists of two steel balls suspended on piano wires so that when the wires are vertical the balls just touch. The wires are provided with screw adjustments at their points of suspension so that the point of impact can be adjusted vertically. The wires each pass through a narrow hole about three inches vertically below these points so that when deflected they swing with an effective radius of thirty inches. The balls can be drawn apart by means of two electro-magnets mounted on radius arms whose angular positions can be adjusted by means of two hand-operated winches. The deflection of the piano wires from the vertical can be read on two quadrant protractors mounted behind the wires. The present machine can be fitted with balls of diameters in the range 1 to 6 inches, the wires being attached to small tufnol adaptors which are then stuck to the balls with Eastman adhesive 910.

1
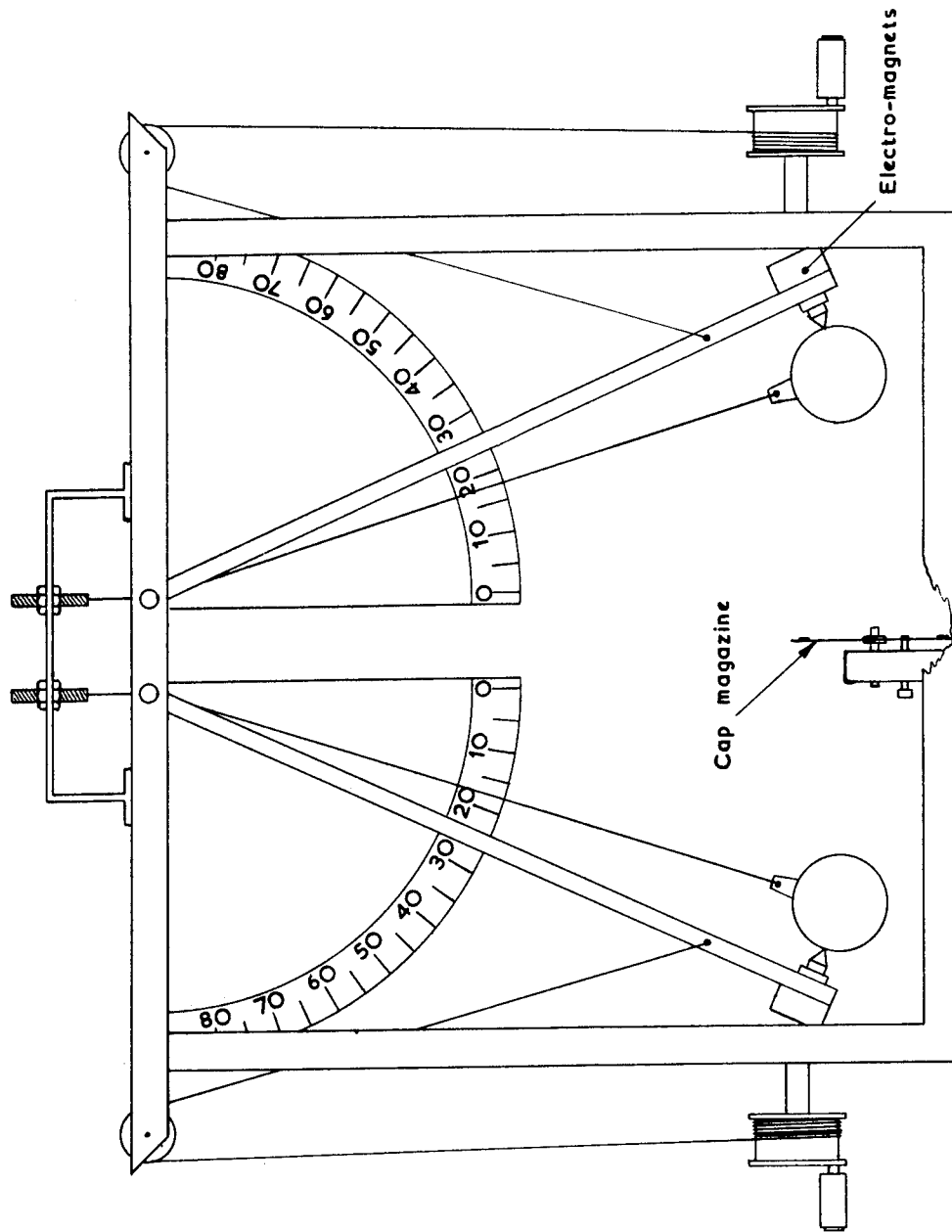
Figure 1 – Colliding ball impact sensitivity testing maching (schematic)

Measured volumes (approximately 7 mg) of the sample powder
are placed in ten depressions (diam. 0.4 cm) equally spaced around
the periphery of an 8 inch diameter disc of 1 mil aluminium glued to
a star shaped support (Fig. 2). 0.7 inch diameter discs of 1 mil
aluminium are then stuck over each sample using pressure adhesive,
care being taken to prevent contamination of the sample by the
adhesive. A magazine of ten sample caps is thus formed each (includ-
ing the aluminium) approximately 16 mils thick. The filled magazine
is mounted vertically in the plane of symmetry of the machine so that
a cap is at the point where the two balls collide when released. The
correct positioning of the cap is ensured by means of a spring loaded
dowel pin which engages in holes in the magazine disc.

In operation the two balls are drawn apart to the same angle
and then the electro-magnets are de-energised simultaneously allowing
the balls to swing towards each other and to impact the cap between
them. An event is signalled by a sharp crack often accompanied by
a flash, but with a failure little noise is produced. Attempts have
been made to provide more positive recognition of events, for example
by the installation of a peak sound intensity meter but these have
not proved to have any merit over the operator's judgement and various
operators invariably agree on the result of a test. This sharp
discrimination between fires and failures appears to be characteris-
tic of the machine and probably stems from the conditions being very
favourable to the growth of explosion; thus any event larger than a
certain critical size will grow and consume a considerable proportion
of the sample and will be easily detected. Events occurring below
this minimum magnitude will consume practically no explosive and be
recorded as failures. After each test the dowel pin is withdrawn,
the magazine disc revolved to present the next cap and the dowel pin
allowed to enter the next locating hole. The balls are then set to
the required height and the test repeated. When a violent event
occurs the surface of the ball may suffer damage in the form of sur-
face cracks and pits and for this reason the balls are changed
periodically or re-suspended from a different pole. There has how-
ever been no indication that such damage materially affects the
result of the test.

RESULTS

The tests carried out so far with this machine have been
exploratory and designed to highlight its chief characteristics.
Where 50% heights are quoted they were obtained using the Bruceton
(one up one down) procedure. Table 1 shows a series of results in
which the effect of progressive surface damage to the balls was
investigated. RDX was prepared by comminuting coarse RDX under water
in a high speed homogenizer to a surface area of approximately 3000
sq. cm/gm. and then dried. The balls were 2 inches in diameter and
each weighed 537 gm. and there appeared to be no trend in the results
throughout the series.

Adhesive

Sample cover disc

SECTIONED TEST CAP

0.001" Aluminium foil

Magazine disc

Explosive (.7 mg)

Magazine cap locating holes

FOIL HOLDING PLATE

MAGAZINE DISC

Filled caps

Moulds for caps

CAP PREPARATION
BLOCK
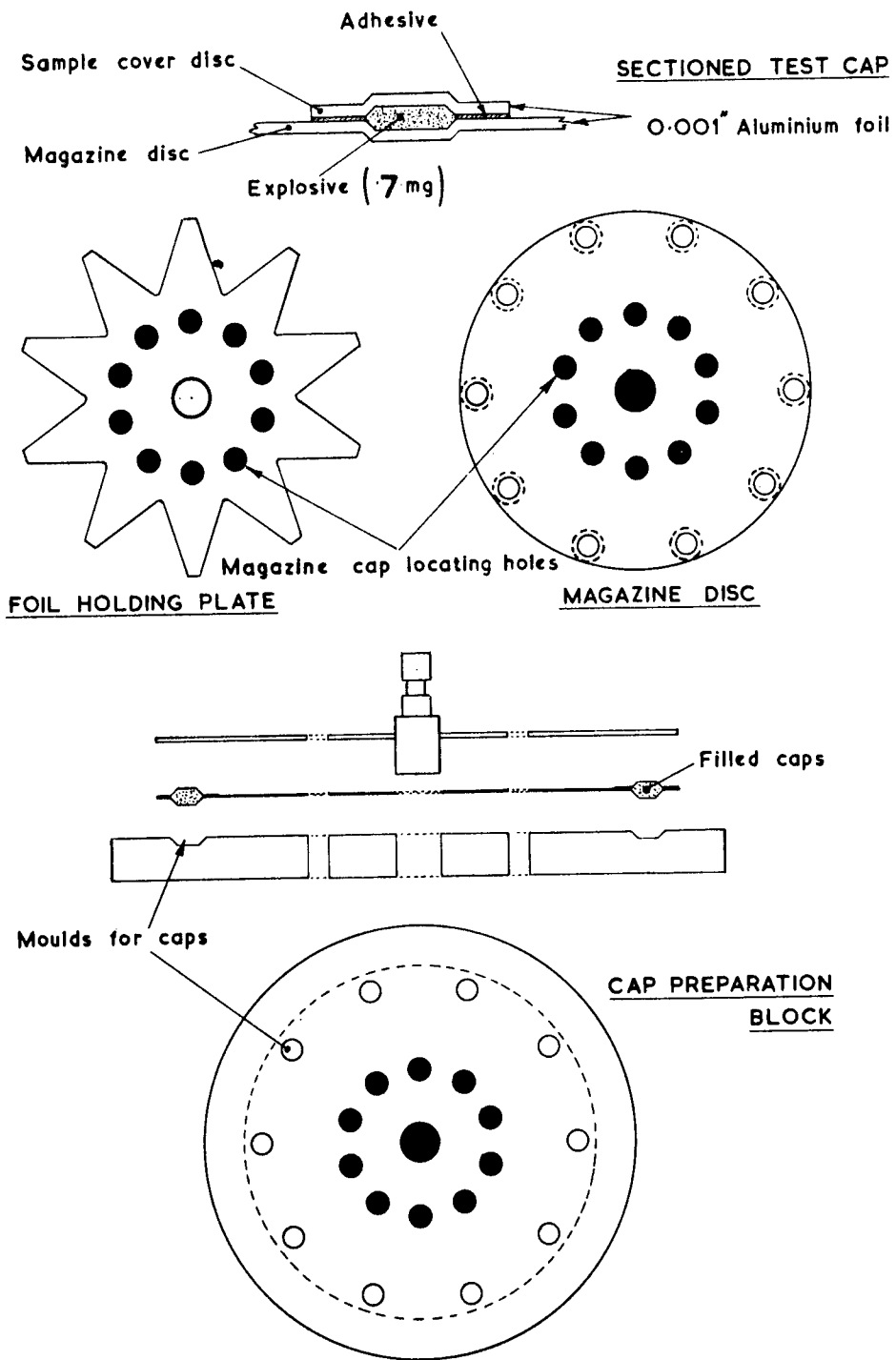
Figure 2 - Cap magazine and filling block

4

TABLE 1

Results of repeated tests on the same sample batch
without altering the balls.

Test No.	1	2	3	4	5	6	7	8	9	10	11	12
No. of caps	30	30	30	30	30	30	30	30	30	30	30	30
50% drop height (cm)	9.2	7.6	8.6	7.4	8.1	7.4	8.2	8.4	8.6	8.0	7.4	7.9
Operator	A	B	B	B	C	C	C	C	C	C	B	A

Table 2 shows the effect of varying the ball diameter over
the range 1.25 to 6 inches. Two RDX samples were used; the fine
sample as described above and a coarse sample consisting of a 60 to
100 BSS sieve fraction of the uncomminuted material. For this
series of experiments foils 0.8 mils thick were used as supplies of
the standard 1.0 mil foil were not available.

TABLE 2

The variation of 50% drop height with ball diameter

Ball diameter (ins)		1.25	1.5	2.0	2.5	3.0	3.5	5.0	5.905 (150mm)
Ball weight (gm.)		131	226	537	1048	1810	2872	8374	13796
50% drop height (cm)	Fine RDX	16.4	11.0	6.9	4.0	2.4	1.9	0.7	0.5
	Coarse RDX	18.8	14.0	8.1	4.5	2.4	1.8	0.9	0.55

Table 3 shows the comparison of RDX, HMX and PETN using
3 inch balls, each explosive again being tested both as a comminuted
sample (surface area approximately 3000 sq.cm./gm.) and as a 60 to
100 B.S.S. sieve fraction of the uncomminuted material.

TABLE 3

Comparisons of 50% drop heights of RDX, HMX and PETN.

Explosive	PETN		RDX		HMX	
	Fine	Coarse	Fine	Coarse	Fine	Coarse
50% drop height (cm).	2.3	2.5	4.4	4.8	3.5	3.9

Table 4 shows the effect of ageing on samples of 75/25
HMX/TNT and 75/25 Cyclotol which were prepared by grinding up cast-
ings in an end runner mill and testing with 3 inch balls. Also
shown are the different results obtained when samples of Composition
B were prepared by wet high speed attrition and by dry end runner
milling.

TABLE 4

The effect of ageing on TNT - containing compositions

Explosive	Method of Sample preparation	Age (days) after preparation	50% drop height (cm).
75/25 HMX/TNT	Dry end runner milling	7	3.8
-ditto-	-ditto-	23	4.2
-ditto-	-ditto-	63	no result*
75/25 Cyclotol	-ditto-	1	4.5
-ditto-	-ditto-	40	no result*
60/40 Comp. B	Wet h/speed attrition	28	13.6
-ditto-	Dry end runner milling	1	no result*

*Samples were too insensitive to give a 50% drop height
with this diameter ball.

Table 5 shows the variation of the probability of an event
with increasing drop height of 3 inch balls for a sample of Composi-
tion B3 which failed to give a 50% height when freshly prepared by
grinding a casting in an end runner mill.

TABLE 5

The variation of the probability of events with increasing
drop height for Comp B3.

Drop height (cm)	1.13	2.6	4.6	6.2	10.2	13.9	17.9	22.4
No. caps tested	20	20	20	20	20	20	20	20
No. of fires	0	0	2	1	3	4	1	0

DISCUSSION

The work carried out has confirmed the view that this
machine is a useful and versatile tool for investigating initiation
by impact and that the subject is complex and will require a good
deal of effort to isolate the important factors.

The results given in Table 2 have been used in Fig. 3 to
plot the relationships between the ball velocities and energies at
the 50% condition as a function of ball diameter not however making
any allowances for ball rebound energy. It was thought that the 50%

6
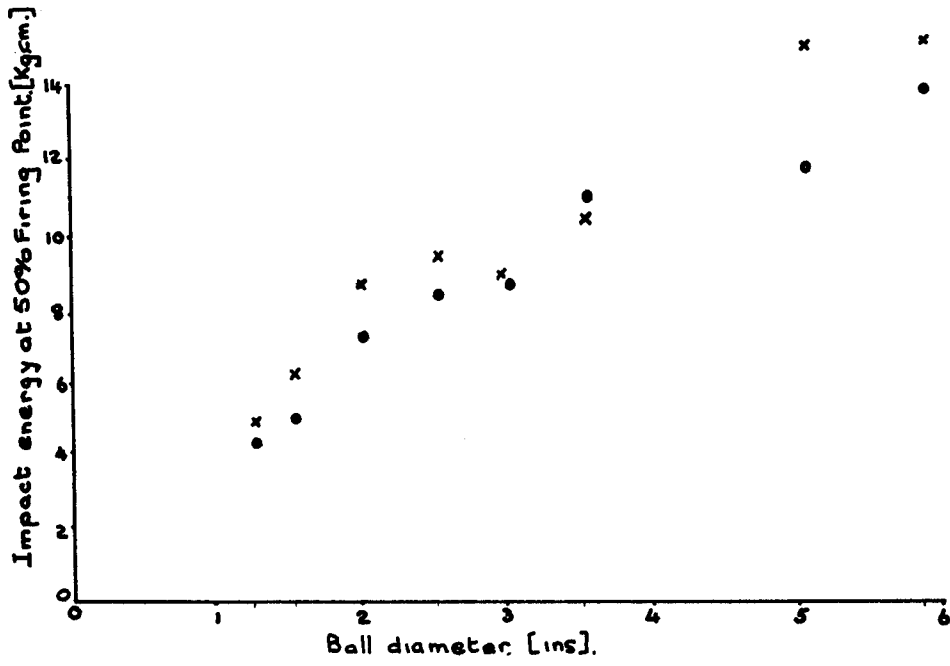
50% Firing energy vs. ball diameter.
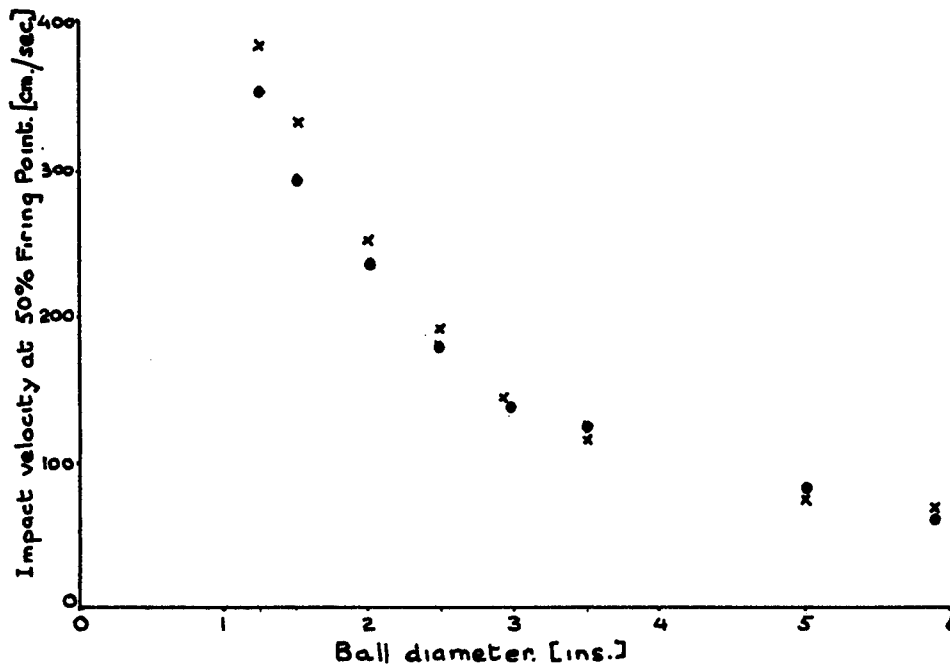
Figure 3 - 50% firing velocity vs ball diameter

velocity should approach a limiting value as the ball diameters were increased, since at some velocity the heat dissipative processes will prevent the sample reaching reaction temperatures however high the pressure. However even with the largest balls the downward trend in the 50% velocity appears to continue. The difference in results between the fine and coarse powders may be due to the extra work required to crush the coarse particles prior to the high compression phase.

Using the same two sets of results given in Table 2 a calculation has been made of the average volume of sample displaced by intrusion of the balls per unit time during impact, assuming that the sample is an infinitely extended slab of constant thickness from sample to sample and neglecting the velocity decrement of the balls and the compressibility of the sample. These results, which are given in Table 6 although moderately constant throughout the whole range of ball sizes for a given powder, show a tendency to decrease as the ball diameter increases. It is perhaps surprising that this crudely simplified treatment which gives pre-eminence to the geometry of the system and neglects the energy and momentum, gives such constant results.

TABLE 6

Ball Diameter (inches)	Mean ball volume intruded into the sample per unit time (cm^3 sec $^{-1}$)	
	Fine RDX	Coarse RDX
1.250	29.7	31.8
1.500	29.3	38.8
2.000	31.0	33.5
2.500	29.4	31.2
3.000	27.4	27.4
3.500	28.4	27.9
5.000	24.7	28.0
5.905	24.7	26.1
Mean	28.1	30.6

The results given in Tables 3 and 4 illustrate the effect variations of sample preparation procedure can produce. Whereas with pure explosive compounds such as RDX HMX and PETN, samples are not affected by ageing and only to a minor degree by the method of preparation, explosives containing TNT have been shown most sensitive to these variables. Wet high speed attrition produces much more sensitive samples than dry end-runner milling and all samples decrease in sensitivity with time. These effects are probably due to variations in the proportion of the surface of the sensitive component covered with TNT and the ageing experiments suggest that the TNT can migrate and cover crystal surfaces produced during milling processes.

The results in Table 5 show that with a given ball diameter the probability of fire does not necessarily increase continually with increasing drop height but may initially increase and then subsequently decrease without ever exceeding the 50% probability. In such a case it seems likely that if the ball diameter is increased the maximum probability will rise. This phenomenon may be related to the fact that the time of contact of two colliding balls decreases with increasing velocity of approach and that there is a dual requirement for an explosion to occur. Firstly there must be a sufficiently high pressure to raise an element of sample to a sufficiently high temperature to produce a primary event and secondly that the conditions favourable for growth and propagation of that event must be maintained for some minimum time. In Table 5 it is presumed that this second condition is not fulfilled sufficiently for the probability of fire to rise above 20%. This feature probably applies to other impact machines on similar grounds.

Some obvious parameters of the test have not yet been examined at all and these include the effect of varying the sample size and the addition of grits and desensitisers but it is hoped to proceed with this work with the ultimate object of understanding the desensitisation of explosives to impact initiation.

A PHOTOGRAPHIC STUDY OF
EXPLOSIONS INITIATED BY IMPACT

J. Wenograd*
U. S. Naval Ordnance Laboratory
White Oak, Silver Spring, Maryland

ABSTRACT: Two photographic methods have been used to observe the course of explosions as they occur in impact testing. The extent and geometry of the propagation of explosions under the conditions of impact have been studied by placing a photographic film in virtual contact with explosions on the Bruceton Research Laboratory impact machine at the Naval Ordnance Laboratory, White Oak. By means of experiments with artificial centers of initiation it has been shown that the extent of propagation of partial impact explosions is essentially independent of drop height.

A synchronization technique has been developed by means of which impact-like explosions have been initiated and photographed with a Beckman-Whitley high speed framing camera at the Explosives Research and Development Establishment, Waltham Abbey, Essex, England.

High explosives are found to react under slightly varying conditions by three distinct modes. The most frequently encountered mode is a fast burning reaction proceeding from a center of initiation. The velocity of this propagation is 460 m./sec. for PETN, about 300 m./sec. for RDX and 220 m./sec. for PETN incorporated with 10 or 20 percent of TNT. PETN has also been observed to react by an irregular slow burning reaction characterized by velocities near 100 m./sec. The third mode of reaction is a low order detonation which proceeds at rates near 1300 m./sec. in PETN samples. The primary explosives, lead azide and mercury fulminate, detonate under the conditions employed in this investigation.

INTRODUCTION

The violent and complex stresses to which explosives are subjected in impact tests are believed to result in the formation of hot spots (1), one or several of which develop a sufficiently high temperature to initiate a self-sustaining chemical reaction in the surrounding material. This initiation process is followed by the consumption of the remaining explosive by some reaction proceeding from the initially microscopic hot spot. The existence, formation, and properties of hot spots have been elucidated by considerable experimentation and speculation (1,2,3,4). The propagation phase of impact explosions is less well understood, although its nature has been the subject of several investigations (1,5).

A photographic method, wherein a film is placed in virtual contact with an impact explosion, has been used to assess the extent and geometry of these explosions. In addition, a synchronization technique has been developed by means of which impact-like explosions can be photographed with a Beckman-Whitley high speed framing camera which permits the direct observation of the nature and velocity of propagation of the explosions.

EXPERIMENTAL

A standard Explosives Research Laboratory Impact Machine (6), at the Naval Ordnance Laboratory, was used for the contact photographic experiments. It was equipped with type 12 tools and a 2.5 kg. weight. Two-inch-square pieces of Kodak, infrared sensitive, sheet film were placed on the anvil of the impact machine with the emulsion side up. The film was shielded from blast and burning effects by the use of pieces of 0.002-inch thick, transparent, sheet mica. The explosive samples, usually about 50 mg., were placed upon the mica and struck in the usual way. The explosion records shown in this report, Fig. 2-6, are positives of the films obtained in this way; thus, the dark areas represent light given off by the explosion. The presence of the film and mica serve to cushion the blow received by the explosive. This results in a change in the scale of impact sensitivities usually associated with the various explosives.

The Beckman-Whitley model 189 high speed framing camera at the Explosives Research and Development Establishment, Waltham Abbey, Essex, England, has been used to photograph impact-like explosions of several materials. The mechanical properties of such transparent anvil materials as glass and Perspex (a methyl

methacrylate polymer marketed by I.C.I.) and the synchronization requirements of the camera virtually preclude the photography of explosions initiated by a falling weight. Mechanical impact was therefore simulated by means of an explosive-driven steel plate. The experimental set-up is shown in Fig. 1. A high voltage detonator is used to detonate a half-inch-diameter half-inch-long tetryl pellet pressed to a density of 1.48 g./cc. This pellet is in contact with a 2-inch-diameter half-inch-thick steel disc which is placed on a thin layer of explosive on a 2-inch-square one-inch-thick perspex anvil. The pressure developed in the explosive is of course higher at the center under the tetryl charge. The force of the blow could be strengthened by using two tetryl pellets, or weakened by introducing thin brass discs between the tetryl pellet and the steel plate.

In most cases the luminosity spreads from the center of the impacted area in a symmetrical fashion. The patterns from successive frames were projected onto a white card and the explosion fronts traced out. The areas enclosed by the successive fronts in the sequence were measured with a planimeter and the linear propagation velocities were calculated on the assumption of a circular front.

The explosives were standard British and American production samples used without further purification. Small, compact quantities of sensitive materials were used to seed some of the contact photographic shots. Pentaerythritol tetranitrate (PETN) and diazodinitrophenol (DDNP) crystals were grown by slow evaporation of acetone solutions. Single crystals or aggregates weighing about 2 mg. were used as seeds. Lead azide seeds were obtained by pressing 5 mg. of dextrinated azide to 25,000 psi.

The nature of the pressure pulse which causes the initiation of the explosive is not too different for the two methods described in this paper. By extrapolating from known data for the equation of state of steel and Perspex and assuming that the layer of explosive reaches the same pressure as the Perspex, Jacobs (7) has estimated the pressure pulse at the center of the explosive sample to have a height of 200,000 psi. and a half width of 2-5 microseconds. For comparison, he has also estimated the pressure developed in the E.R.L. machine in use at the Naval Ordnance Laboratory to reach about 60,000 psi. with a half width of approximately 50 microseconds.

RESULTS

Figure 2 is a typical contact photograph of an explosion occurring in granular PETN. The explosion seems to have started at the center from which the striations emanate and to have continued to the boundaries of the explosive layer. The white areas in the darkened region represent places where the emulsion was blasted away. Figure 3 shows an explosion in a sample of granular RDX. The figure seems to have been traced out by a similar reaction although there is less evidence that initiation started from a single center. Figure 4 shows the explosion of a tetryl sample. The feathery nature of the outline of the luminous region is taken to indicate that the reaction spread in a slow and complex manner.

It is possible to cause reactions in an explosive by drops from heights ordinarily too low to cause initiation, by the introduction of artificial centers. Such centers consist of small compact masses of sensitive material prepared as described above. The explosion of a tetryl sample thus initiated is shown in Fig. 5. The figure bears striking similarities to Fig. 4. The indentations in the area of luminosity indicate that the explosion has failed to propagate to these regions. Indeed, upon inspection of the mica and striker, unconsumed explosive was found in these regions. Explosions of PETN and RDX initiated artifically are similar in appearance to Figures 2 and 3.

The explosion shown in Fig. 6 was most interesting. In this case a layer of about 50 mg. of tetryl was spread on the mica and a 5 mg. lead azide pellet was placed in the center. Striking the sample caused an extremely loud explosion which was far louder than the reports commonly heard in impact machine operations. The tool surfaces were badly damaged and, as can be seen, more than half of the film was blown away. The arc of blasted emulsion represents the edge of the tools. The explosion encountered here was far more violent than the previous shots and was almost certainly a detonation.

The use of artificial centers of initiation has permitted a consideration of the effect of increasing drop height on the propagation of impact explosions. Ten tetryl samples seeded with DDNP crystals were struck from heights varying from twenty to sixty cm. In eight cases this resulted in initiation of the DDNP and partial consumption of the tetryl. Tetryl alone gave no reaction at drops less than 100 cm. There was little or no noticeable difference in the extent of propagation at the higher

HIGH VOLTAGE
DETONATOR

TETRYL PELLET

MILD STEEL
CYLINDER

PERSPEX ANVIL

EXPLOSIVE

45° FRONT SURFACE
MIRROR

CAMERA
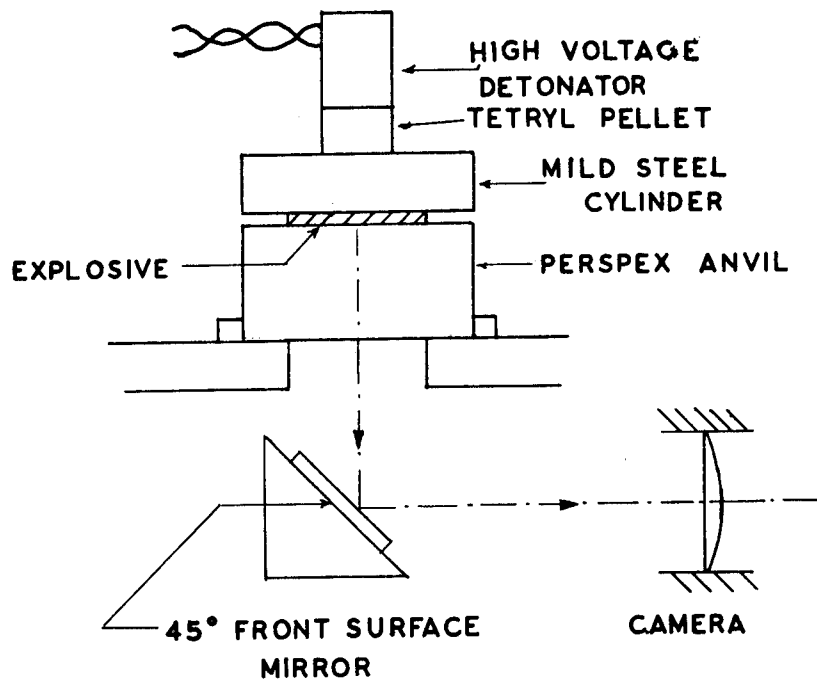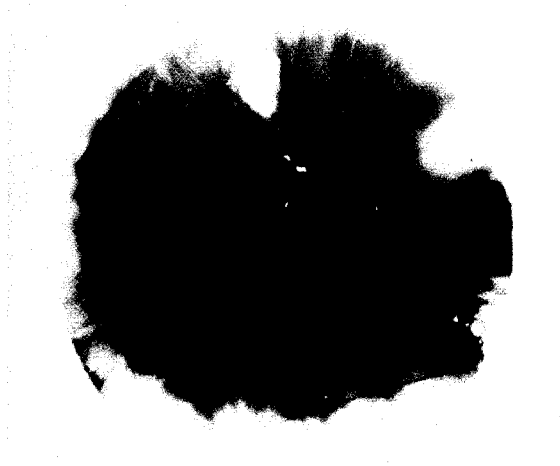
Figure 1
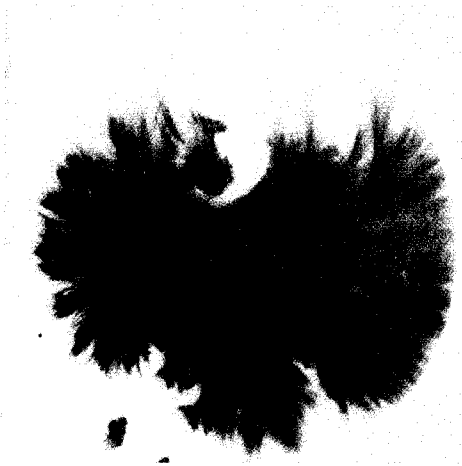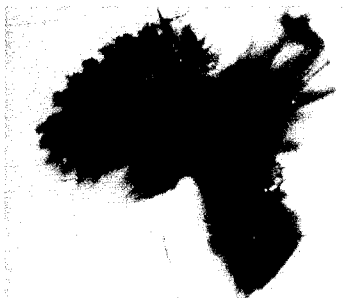
Figure 2

Figure 3

Figure 4

Figure 5

Figure 6

drop heights. Eight TNT samples seeded with DDNP and struck from heights varying between 25-150 cm. behaved similarly, although pure TNT showed no reaction at all in drops from less than 200 cm.

The explosions which occurred in pure samples were similar to those initiated by artificial centers. The nature of the propagations, as seen from the photographs, were such that they may be classified under at least three categories. Examples of the most common mode of propagation can be seen in Figures 2 and 3. This mode will be referred to as a fast burning reaction. It is characterized by a rather regular pattern with striations emanating from one or a few points which may be centers of initiation. In all cases the luminosity terminates at the boundary of the tools, indicating that the reaction is quenched by a release of pressure.

A second mode of reaction which is considered a slow burning process is illustrated in Figures 4 and 5. This type of reaction is characterized by a feathery pattern which ends at the boundary of the tools. A third mode of propagation is illustrated by Fig. 6. Because of the violence of this reaction and the amount of damage caused, it must be regarded as a detonation. Detonations are characterized by a scoring of the impact tools and a blackening of the film beyond the area of high pressure.

Three modes of propagation of impact-like explosions have also been observed in studies with the high-speed camera. The most common mode was a fast burning reaction similar to the explosion of PETN illustrated in Fig. 7. The burning appeared to begin during frame 1 over an area corresponding to that of the tetryl donor pellet. The reaction then grew from this initial area and by frame 2, four microseconds later, it had formed a sharp deflagration front. This reaction front then propagated at an approximately constant rate to the edge of the area of observation.

The explosions of a number of PETN samples were photographed and representatives of three modes of propagation observed. When the regular experimental set-up with the half-inch steel plate, unsieved or small sieved explosive, and one or two tetryl pellets were used, PETN reacted by the fast burning mode. The average frame to frame velocities for thirteen shots had a mean of 460 m./sec. and an average deviation of only 30 m./sec.

Rather slight changes in the experimental conditions caused quite drastic changes in the mode of explosion. If relatively large PETN crystals (retained on a B. S. S.
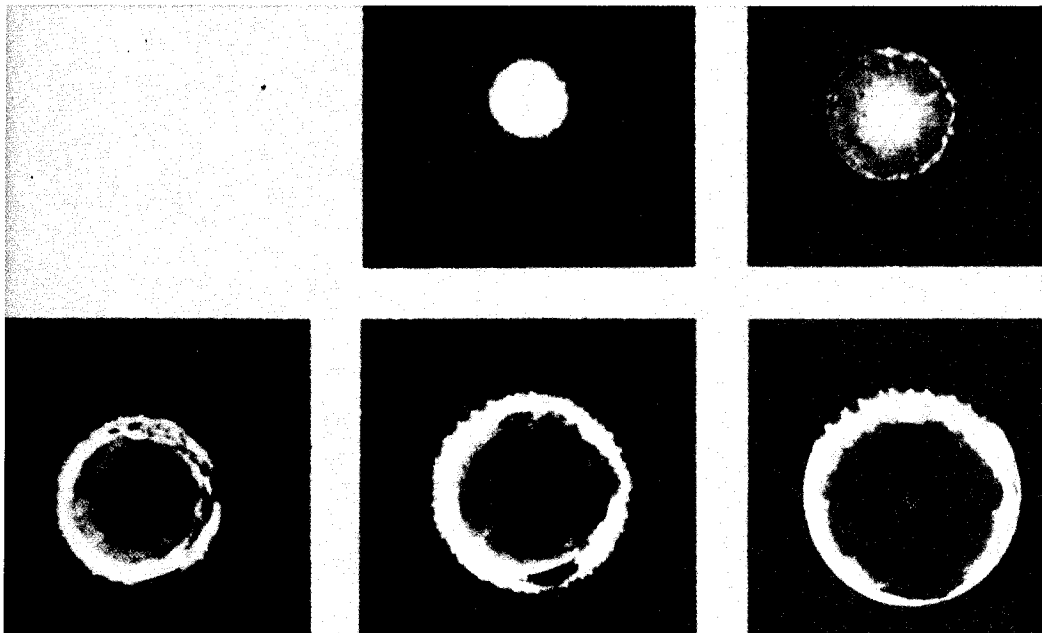
Figure 7 - PETN, fast burning. 4μseconds between frames

sieve) were used, the reaction was found to propagate at a markedly faster rate. Four separate observations showed this phenomenon. The reaction of a sample of large PETN crystals is similar to Fig. 7. These rapid reactions propagate at velocities of about 1300 m./sec. and are termed low order detonations. In only one case was a velocity of this sort observed with unsieved PETN. Figure 8 shows a reaction which, although it did not initiate centrally, seemed to begin at the normal fast burning velocity. In this one case, however, after the fast burning front had been formed and had propagated about 12 mm. into the sample, a new reaction began about 5 mm. ahead of the front and propagated at the low order detonation velocity. This example of a transition from fast burning to low order detonation was the only one observed during this series of experiments.

Yet another mode of consumption of PETN was observed if a brass gap with a thickness greater than 0.060 inches was placed between the tetryl pellet and the steel plate. This type of explosion, illustrated in Fig. 9, is thought of as a slower type burning reaction. In this case no explosion front formed, but tentacles of burning material emanated from the center of initiation which corresponded to the axis of the tetryl charge. The burning velocity along the tentacles was about 100 m./sec.

Two pentolite samples were prepared by a slurrying technique. Both samples were PETN rich containing 80 and 90 percent of this explosive. They both exploded by the fast burning mode although with a far lower velocity and luminosity than pure PETN. The richer mixture had an average propagation velocity of 200 m./sec., while the value for the other sample was 230 m./sec. It is strange that the richer pentolite should appear to have a lower velocity, but this probably is due to experimental error. The appearance of a typical pentolite shot is very similar to the RDX shot shown in Fig. 10.

The RDX samples which were observed all decomposed by the fast burning mode. The measured velocities, while they definitely fell between those of PETN and the pentolites, were very erratic. The velocities for five samples had a mean of 360 m./sec. with an average deviation of 70 m./sec. A typical explosion is shown in Fig. 10.

Two primary explosives, lead azide and mercury fulminate, were exploded and observed in these experiments. Both reacted extremely rapidly and may be considered to have detonated. Figure 11 shows the detonation of a fulminate sample. The propagation rate in the azide samples
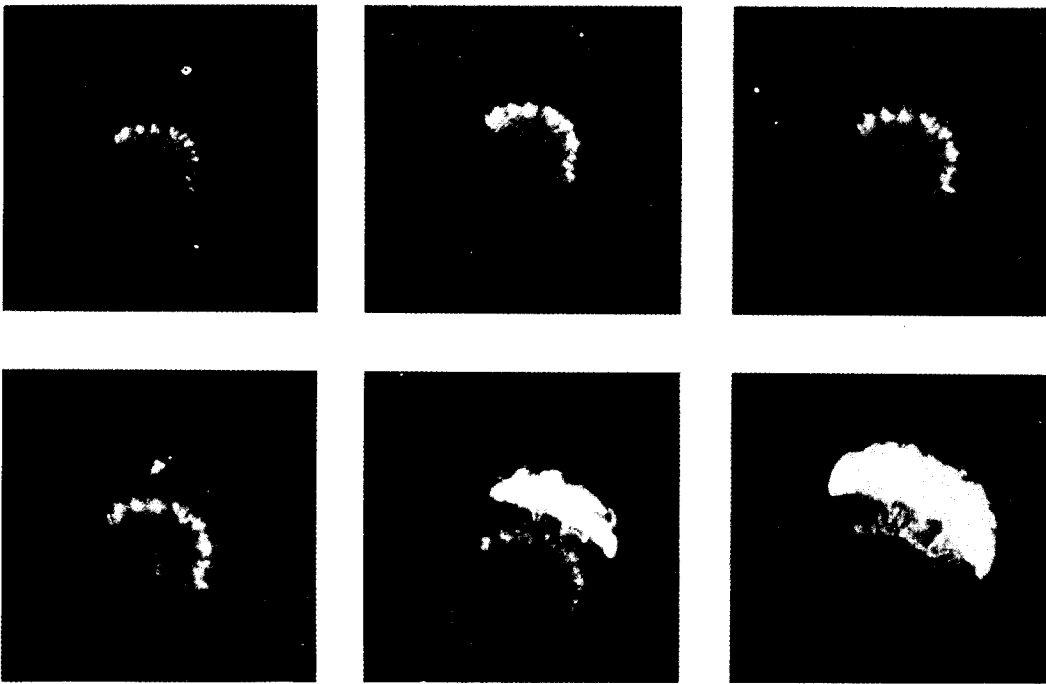
Figure 8 - PETN, fast burning-low order detonation transition
2 μseconds between frames
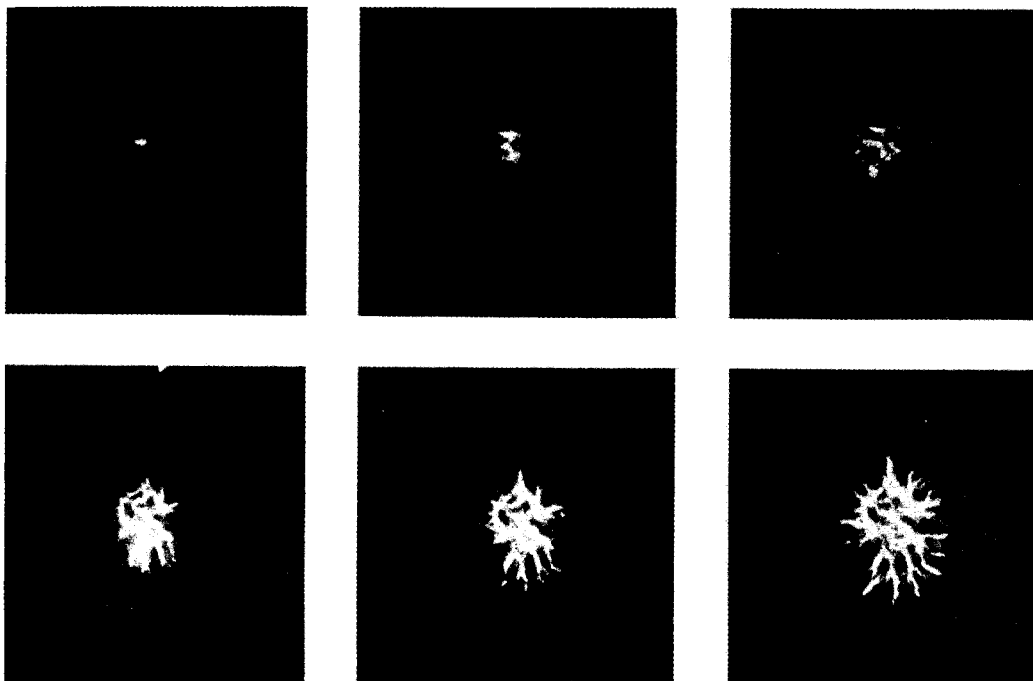
Figure 9 - PETN, slow burning. 4 μseconds between frames

Figure 10 - RDX, fast burning. 4   seconds between frames

Figure 11 - Mercury fulminate, detonation
0.8   seconds between frames

was near 3000 m./sec., while in mercury fulminate the rate varied between 3000 and 4600 m./sec.

DISCUSSION

It is evident that it is no longer possible to speak of a single mode of propagation for explosives under impact test. Clearly, since rather minor changes in experimental conditions have been shown to change the course of the reaction, the mode of explosion can change as the nature of the impact machine or even the force of the blow is varied. Apparently, however, the rate of propagation of reaction once a given mode has developed is fairly constant in various impact machines.

Using a streak camera, Bowden (1) observed explosions of several materials initiated either by falling weights or by sparks in confined layers of explosive. Most materials were observed to explode by a fast burning reaction, the propagation velocity of which varied between 100-1000 m./sec. for PETN and was somewhat slower (100-300 m./sec.) for RDX and tetryl. Low order detonations propagating at velocities around 2000 m./sec. could also be observed for these materials. In the course of a study of the time lag of impact explosions using ionization probes, Collins and Cook (5) measured burning velocities for several materials. They obtained a burning rate of 300 m./sec. for PETN, 255 m./sec. for RDX, and 320 m./sec. for mercury fulminate. The velocities obtained in this study are consistent with these values except that mercury fulminate was observed to detonate.

The contact photographs for PETN and RDX, Figures 2 and 3, show fairly uniformly blackened areas with concentric streaks radiating outward. This is just the result one would obtain by "integrating" the frames of Figures 7 or 10. The serrations in the explosion front would trace out streaks. These serrations or streaks are believed to have been caused by burning particles moving along with the explosion front. It is reasonable to conclude that in the E. R. L. impact test as employed at the Naval Ordnance Laboratory (type 12 tools) the principal mode of explosion for both PETN and RDX is a fast burning reaction propagating at rates near 500 m./sec. for the former and 350 m./sec. for the latter.

The contact photographs of explosions of tetryl are characterized by a darkened area consisting of a mass of minute lines in a feathery pattern. Figure 9 seems to represent a grosser aspect of this same phenomenon. If this is the case, it may be concluded that the mode of

reaction for tetryl in the E. R. L. impact test is a slow burning process proceeding non-directionally along tentacles emanating from a center of initiation at rates not exceeding 100 m./sec. The appearance of these pictures seems quite consistent with a slow burning mechanism consisting of ignition of successive grains of explosive by hot gases moving through pores or channels in the compressed explosive.

While materials such as lead azide certainly detonate under impact, the occurrence of detonations in impact tests of high explosives is still uncertain. Low order detonations as shown in Figure 8 and as observed by Bowden (1) can be induced by impact-like procedures. However, in the absence of any direct proof it is not possible to say where or whether they occur in practice. The nature of the damage to impact machine tools is perhaps the most valid criterion of detonation. Thus, in the E. R. L. impact test the tools are severly scored by lead azide and similar materials but are unmarked by high explosives such as PETN and RDX. On the other hand, in the Rotter test as applied in England a great variety of materials cause quite severe damage to the anvils. Thus, although it is likely that in one common test RDX and PETN undergo the fast burning reaction, it is possible that these same materials undergo a low order detonation under the conditions of the Rotter test.

Experiments with artificial centers of initiation have indicated that both the mode of propagation and the extent of the consumption of explosive are independent of the drop height for the fast and slow burning reactions. However, if the artificial center of initiation detonates, it is possible for the bulk explosive to pick up and propagate this reaction.

ACKNOWLEDGMENT

BIBLIOGRAPHY

(1) F. P. Bowden and A. D. Yoffee, "Initiation and Growth of Explosions in Liquids and Solids", Cambridge University Press, 1952.

(2) E. K. Rideal and A. J. B. Robertson, Proc. Roy. Soc., A <u>195</u> 135 (1948).

(3) J. L Copp, S. F. Napier, T. Nash, W. J. Powell, H. Shelly, H. R. Ubbelohde, and P. Woodhead, Phil. Trans. Roy. Soc., A <u>241</u> 197 (1949).

(4) J. Wenograd, NavOrd Report (NOL) 5730, "The Correlation of the Impact Sensitivity of Organic High Explosives with their Thermal Decomposition Rates", 30 September 1957.

(5) T. K. Collins and M. A. Cook, "The Measurement of the Sensitivity Time Lag of Explosion and Burning Velocity of Explosives by Drop Test Techniques", Technical Report XLVIII, University of Utah, December 1955.

(6) H. D. Mallory, NavOrd Report (NOL) 4236, "The Development of Impact Sensitivity Tests at the Explosive Research Laboratory, Bruceton, Pennsylvania During the Years 1941-46", March 1956.

(7) S. J. Jacobs, U. S. Naval Ordnance Laboratory, Private Communication.

PURE ENVIRONMENTAL SHOCK TESTING OF CONDENSED PHASES

Ted A. Erikson
Armour Research Foundation
Chicago, Illinois

INTRODUCTION

This paper reports a selected portion of a study performed on the initiation of lead azide by means of a "pure" environmental shock test (1,2). This work was supported by the Picatinny Arsenal under Contracts No. DA-11-022-501-ORD-2731 and DA-11-022-ORD-3120. Lead azide samples were exposed to the reflected shock region produced in an ordinary shock tube. Measured shock intensities in various driven gases were varied, and the time delay for the detonation response of the sample was determined.

Using a similar type of shock test technique, several investigators (3,4) developed a heat transfer analysis for the problem of initiation of composite propellants. Without in any way wishing to detract from the scope of such approaches to the problem of sensitivity, one of our objectives for this study was based on the premise that the order of response (i.e., sustaining decomposition, deflagration and detonation) for an unstable system is characterized by a unique energetic situation. Thus, contact of an energy-rich zone (e.g., the flame zone or an artificial environment) with a potentially energy-rich zone (e.g., a layer of relatively undisturbed explosive) can result in a characteristic time delay for a subsequent rate of propagation. The appropriate variation of an artificial environment might be used to evaluate such energetics.

By varying the magnitude, rate, and mode of energy release from the artificial environment to the surface, it should be possible to evaluate specific energetic susceptibilities of an unstable system. For example, in the pure environmental shock test, relative measures of the magnitude, rate, and mode of energy release from the reflected shock region to the surface of a condensed-phase system might be ascertained from the shock intensity, the pressure, and the composition of the driven gas (varying degrees of freedom), respectively.

EXPERIMENTAL

A detailed description of the total study is contained in the final reports on Contract No. DA-11-022-501-ORD-2731 (June, 1959) and Contract No. DA-11-022-ORD-3120 (June, 1960). General details of the shock tube and sample preparations are described below. (Measurements of transient electrical conductivity will not be discussed.)

Shock Tube

A schematic diagram of the shock tube is shown in Fig. 1, where an overall and a magnified view of the time-distance sequence of events are also illustrated. The shock tube was instrumented with a Kistler PZ-6 miniature pressure transducer and a PT-6 amplifier-calibrator unit for measuring transient pressures. A Tektronix 535 oscilloscope with a Beattie-Coleman camera was used for recording pressure transients. A Tektronix 545 oscilloscope with a Dumont camera was also available for supplemental records.

The sample was positioned on the back plate of the shock tube as shown in Fig. 2, which indicates the composite array of equipment, instrumentation and electrical circuitry. Triggering of the Tektronix 535 oscilloscope was effected by the reception of a shock pressure output on the Kistler gage, and both the pressure and the V_2 voltage of the conductivity circuit (see Fig. 2) were simultaneously displayed at the 100-kc chopping rate of a Tektronix 53/54 C dual pre-amplifier. Triggering of the Tektronix 545 oscilloscope was effected by less than a 0.1-volt rise in V_1 (of the conductivity circuit), and both the negative voltage output from the Kistler gage and V_1 were displayed at the 100-kc chopping rate of a CA dual pre-amplifier unit. The Kistler gage output exhibits a characteristic "ring" which is caused by explosion noise transmitted through the end plate and wall of the shock tube to the gage position. The response time, t_r, from detonation at the sample site to "ring" at the gage position was calibrated by spark initiation, and the result was 7.4 ± 0.8 microseconds. Typical photographs of oscilloscope traces are shown in Fig. 3. Photographs of similar shocks with and without azide samples are included to enable the identification of the respective traces. It can be seen that the shock pressure, a time delay (due to "ring") and conductivity voltage transients are recorded.

An examination of the magnified view of the endplate in Fig. 2 shows the sequence of events that takes place. In some tests, the oscilloscope is triggered by the pressure of the reflected rather than the incident shock. Figure 2 shows that

$$t_d = t_s - \Delta t_s - t_r \tag{1a}$$

or

$$t_d = t_{rs} + \Delta t_{rs} - t_r \tag{1b}$$
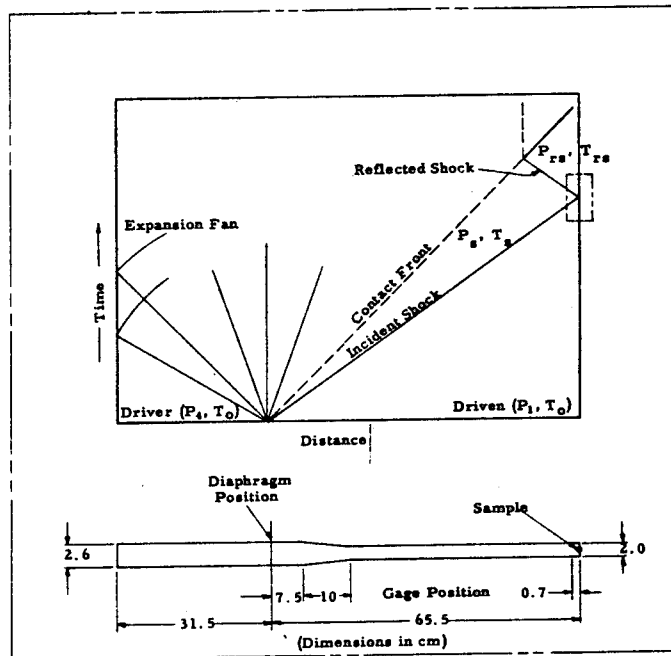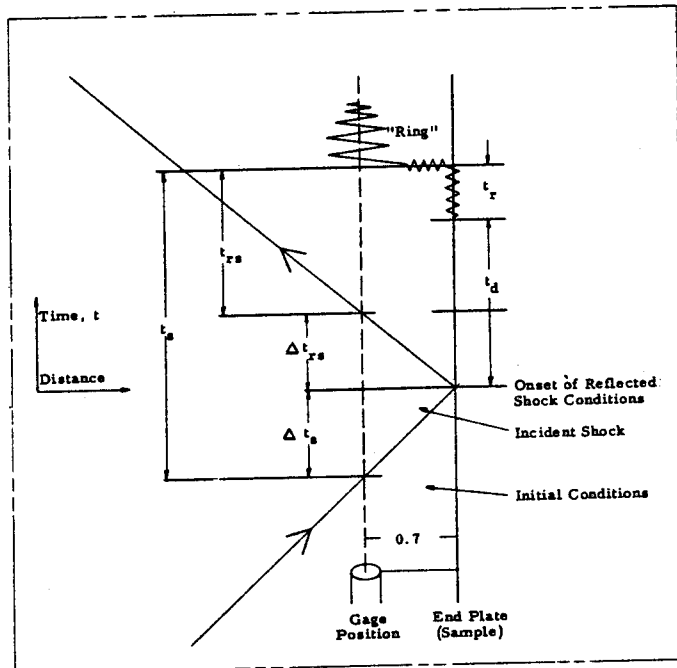
Figure 1 - Shock tube profile and diagram
of time-distance events
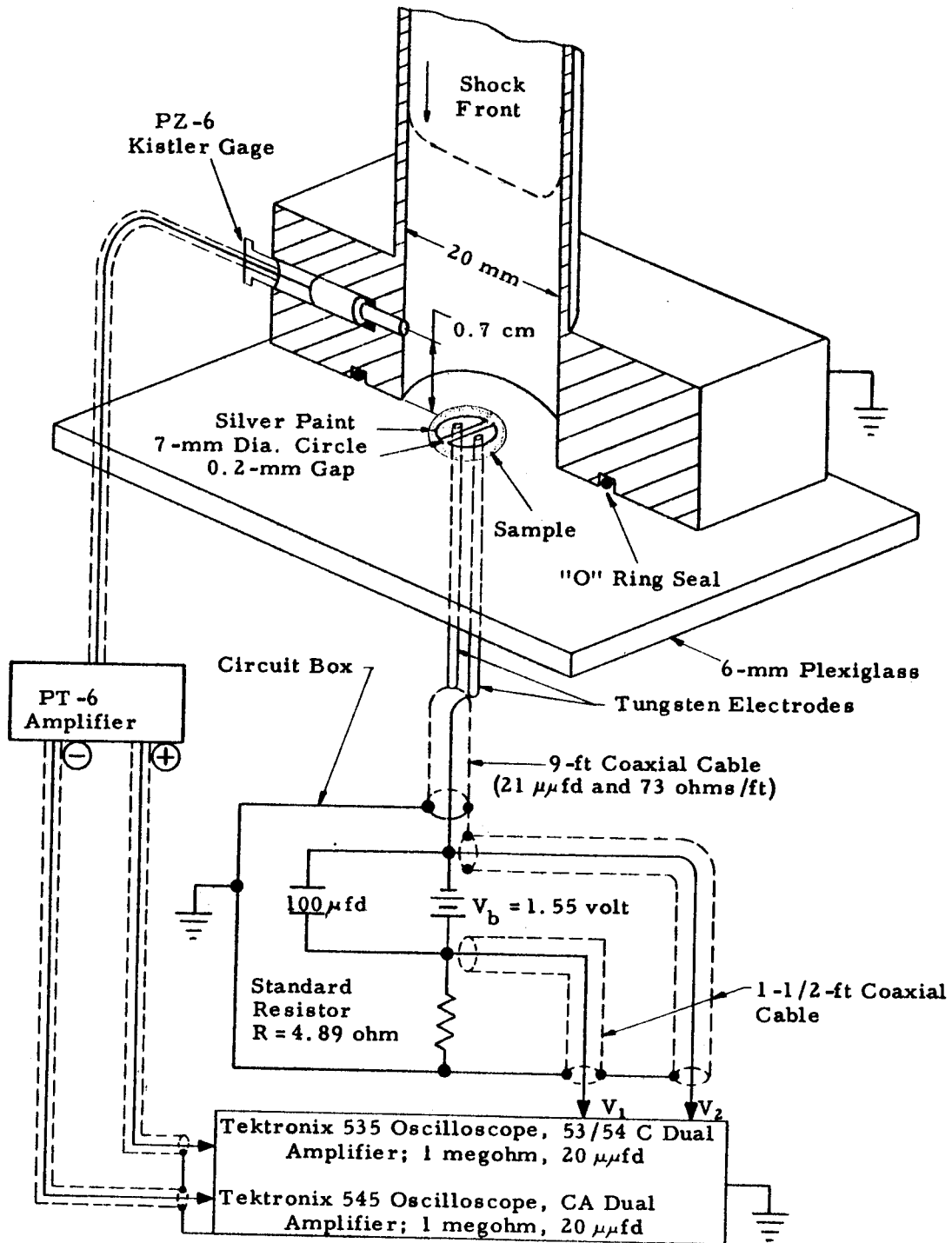
Figure 2 - Diagram of shock tube equipment and circuit

when the incident and reflected shock, respectively, trigger the Tektronix 535 oscilloscope trace. The traverse time of the incident shock (Δt_s) and the reflected shock (Δt_{rs}) have been estimated from the shock strength, and the corrections indicated by Eq (1a) and (1b) have been incorporated.

The report by Alpher and White (5) was utilized in the construction of curves which relate the initial driver-to-driven gas pressure ratio, P_4/P_1, to the Mach number of the incident shock, M_s, the ratio of the reflected shock pressure to the initial driven pressure, y', and the reflected shock temperature of the driven gas, T_{rs}. The results are shown in Fig. 4 for the ARF shock tube with helium driver gas into helium or argon, nitrogen, and carbon dioxide driven gases. An experimentally-resolved curve, as obtained from reflected shock pressure measurements with the Kistler gage, is also indicated on this figure. The bifurcation phenomenon (6) influences the choice of the correct value for the reflected shock pressure from photographs such as are shown in Fig. 3. As a consequence, the shock strength is believed to be best indicated (at least in a relative manner) by the theoretical curves shown in Fig. 4. These are confirmed, within the experimental error, by the results obtained from the Kistler gage measurements.

Since the P_4/P_1 ratio was accurately measured, this value was used to define the Mach number of the incident shock directly. From M_s, the values of T_{rs} and y' were determined on the graph. The reflected shock pressure is the product of y' and the measured initial driven gas pressure. All data have been converted to values of P_{rs} and T_{rs} by this technique.

Sample Preparation

For this study, the Picatinny Arsenal supplied 65 grams of lead azide which had been produced under carefully controlled conditions. Picatinny stated that the analysis of this lot was 100.1% lead azide; spectral analysis showed that the combined impurities were less than 0.1%, consisting of iron, magnesium, silicon, copper and aluminum. The average particle size of this lot was 6 microns, and the density was 4.52 g/cc. All samples were handled and tested in a controlled humidity room where the ambient temperature was maintained near 23°C. Only dim reflected light was used for illumination during handling operations.

Samples of the colloidal lead azide in a water solution were deposited with a medicine dropper onto the prepared end plate (see Fig. 2). Several samples deposited in this manner were placed in a black vacuum desiccator which contained phosporus pentoxide and silica gel as desiccants. The desiccator was then evacuated, and pumping was maintained for one to five hours. The history (i.e., evacuation time, storage time, and ambient room exposure) of all samples was similar, and because of their prolonged exposure to the desiccants, all samples were assumed to be completely dry.

Test No.	Tektronix 535	Sweep Speed, sec/cm	Tektronix 545	Sweep Speed, sec/cm
116 (blank)		20		2
115-56A		20		2
120 (blank)		20		2
119-58A		20		2
132 (blank)		10		1
131-65A		10		1
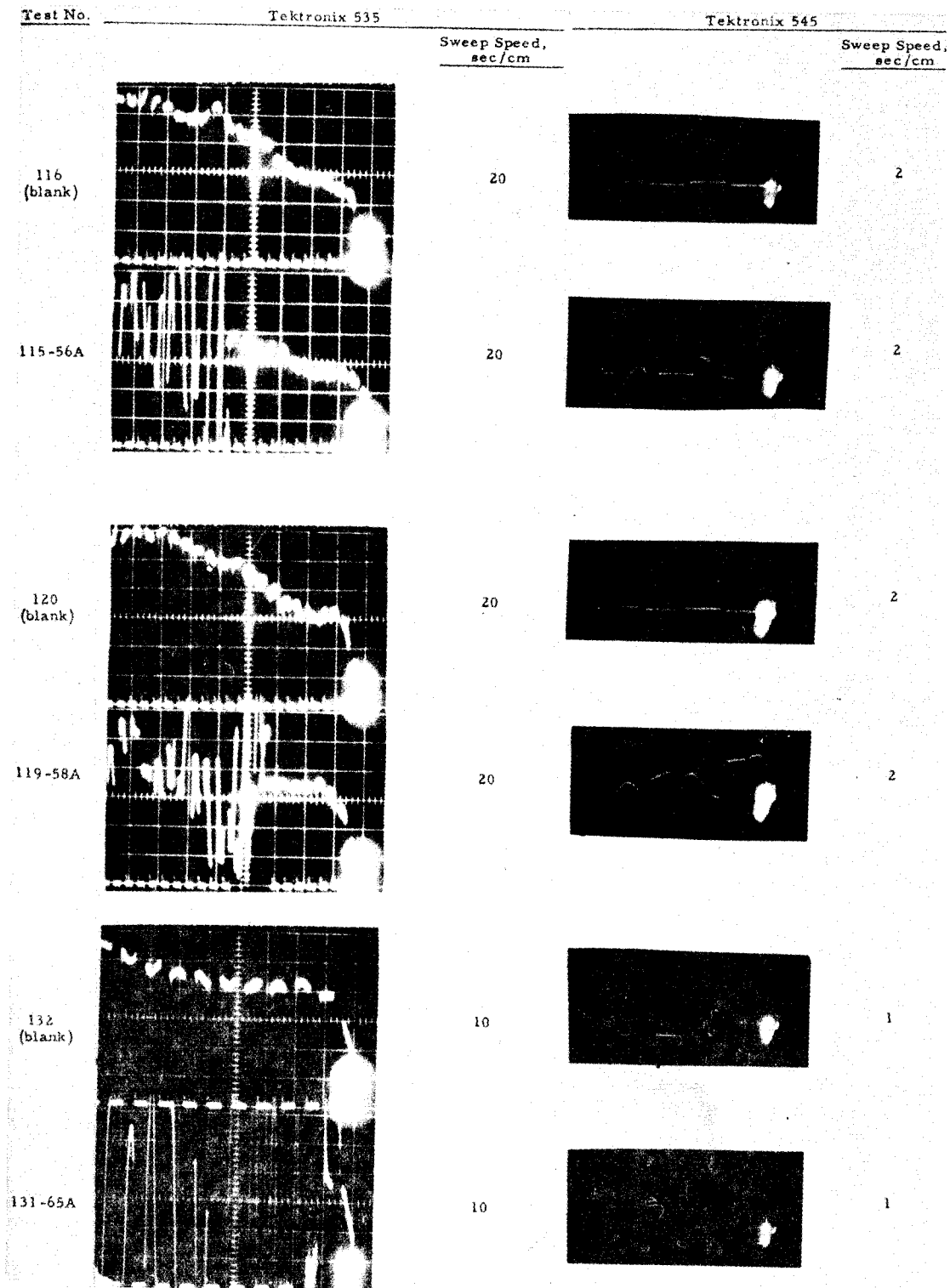
Figure 3 –Photograph of pressure-voltage transients
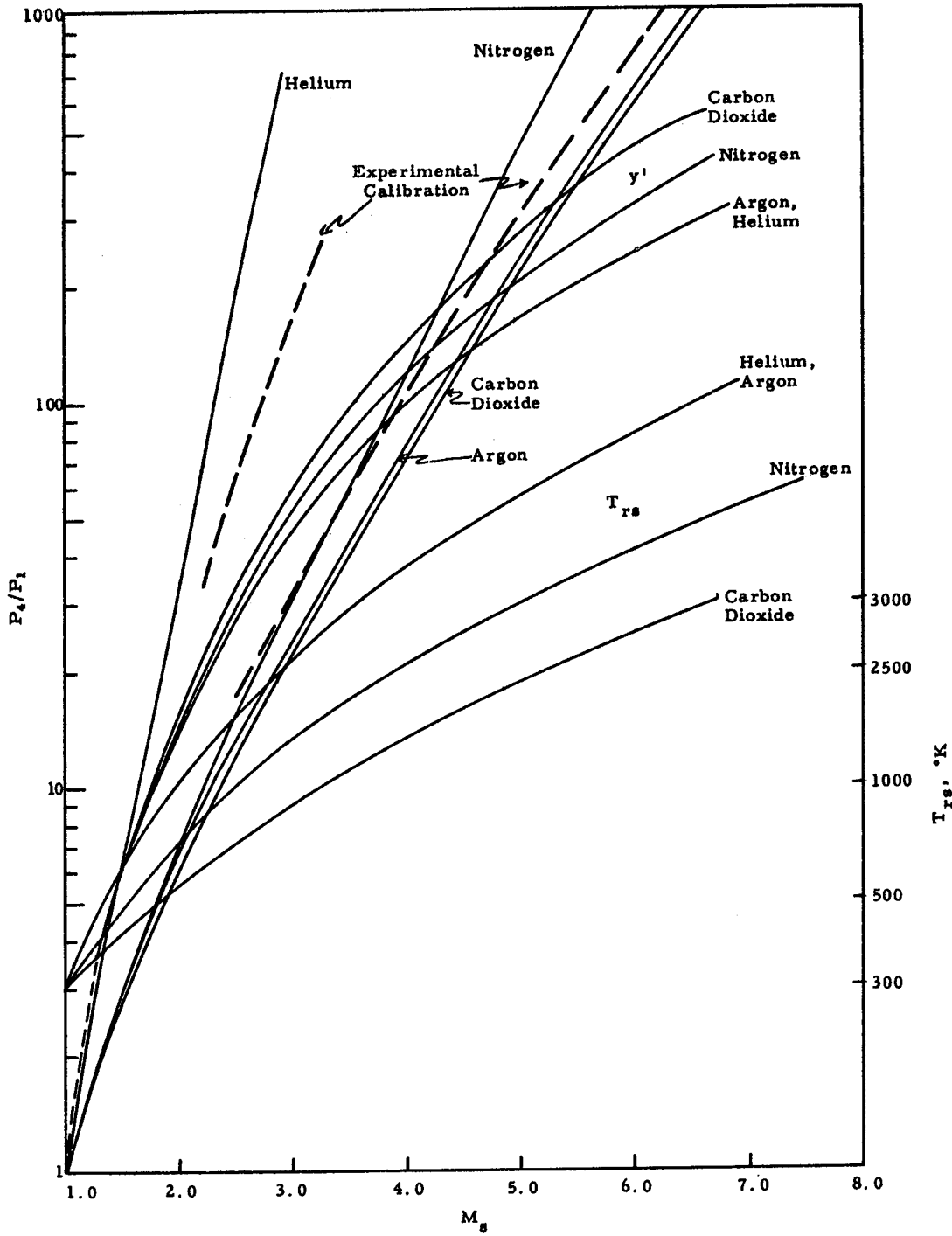
Figure 4 - Shock tube calibration curves

Those samples which were introduced into the shock tube with no further treatment are designated as unpressed samples. Other samples, which were pressed onto the plexiglass mount with a highly-polished steel plate to loading pressures usually near 40 psi, are designated as pressed samples. Normally, most samples weighed about 0.03 gram. The exposed surface area of normal samples was about 1 sq cm. The sample thickness varied from about 0.1 to 1.0 mm for pressed and unpressed samples, respectively.

RESULTS

The present collection of data includes 134 tests performed with lead azide samples exposed to shocks under varied conditions. These conditions and their approximate ranges include:

1. Shock:

   a. Incident Mach number - 2 to 7
   b. Temperature of reflected shock - 900 to 8000°K
   c. Pressure of reflected shock - 50 to 500 psia

2. Driven gas: helium, nitrogen, argon, and carbon dioxide

3. Time delay: near zero to 1000 microseconds

4. Sample density: about 0.3 (unpressed) to greater than 3 (pressed) g/cc

5. Sample weight: 0.002 to 0.08 gram (with corresponding thickness of 0.1 to 0.9 mm and frontal area of 0.1 to 1.0 sq cm).

Representative data for the three tests shown in Fig. 3 are given in Table 1. Complete data are given in the final reports on the contracts.

Table 1

DATA FROM PURE ENVIRONMENTAL SHOCK TESTS
WITH LEAD AZIDE AND NITROGEN DRIVEN GAS

Test No.	Sample Description	P_1, psia	P_4/P_1	M_s	T_{rs}, °K	P_{rs}, psia	t_d, μ sec.
115	Pressed	0.467	500	5.09	3100	97.5	103
116	Blank	0.460	517	5.11	3200	100	-
119	Pressed	0.767	301	4.69	2700	134	69
120	Blank	0.770	304	4.69	2700	135	-
131	Pressed	1.55	150	4.18	2220	206	24
132	Blank	1.545	156	4.19	2230	206	-

DISCUSSION OF RESULTS

When the surface of a condensed-phase, unstable system is exposed to the hot gas in the reflected shock region produced in an ordinary shock tube, the following experimental data are known (or measured) at time of contact:

T_{rs} - the temperature of the reflected shock gas

P_{rs} - the pressure of the reflected shock gas

T_o - the surface temperature of the condensed-phase.

A time delay to explosive decomposition (i.e., detonation, in our case) is then measured, during which interval it is practically impossible to monitor the infinitesimal variations in T_{rs}, P_{rs}, and T_t, or the extent of decomposition near the surface. Based on a heat transfer analysis, the surface temperature at time t (T_t), can be estimated. The correlation of T_t to the time delay, t_d, then serves to indicate reaction mechanisms through "runaway" temperatures, activation energies, and the like. One difficulty with this approach is the assumption that T_t can be adequately estimated by a heat transfer analysis. Because of the necessity for assuming a flat surface, little account is taken of the fact that, microscopically, the surface exhibits large irregularities. No heat transfer analysis of our data was performed, but cursory efforts indicated temperature rises at the surface were less than 40 °C (maximum) during the strongest shock exposures.

Our efforts were based on the premise that some clue with respect to the initiation process could reside in the properties (i.e., state of the surroundings) of the "hot" gas in contact with the surface of the condensed-phase system. If it is assumed that a model similar to that proposed by Tykodi and Erikson (7) for steady-rate processes can be applied, the constant properties of the "hot" driven gas represent the necessary energetics for initiation. Because data over varied shock intensities with four different driven gases were available, attempts were made to evaluate the best and most meaningful correlations. In general, such applications required the inclusive use of the kinetic theory of gases, that is, the concept that driven gas molecules colliding with the surface have the classical Boltzman distribution of energy. Accommodation coefficients for gas-solid collisions at the interface are assumed to be unity.

Initially, an overall chemical reaction of the following type was assumed:

$$x\ N_2\ (gas,\ T_{rs},\ P_{rs}) + PbN_6\ (solid,\ T_o) \longrightarrow Products \qquad (2a)$$
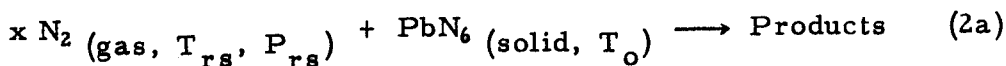
for which the rate of reaction might be expressed by an equation of the form:

$$\frac{d(PbN_6)}{dt} = A\ e^{-E^*/RT_{rs}} \left[PbN_6\right] \left[N_2\right]^x \qquad (2b)$$

where $[PbN_6]$ is the concentration of lead azide, $[N_2]$ is the concentration of the driven gas, x is a coefficient (assumed to be unity), A is a frequency factor, and E^* is an activation energy. This equation can be rearranged in the following form for a test of the data:

$$\log (P_{rs} t_d) = \frac{E^*}{2.3 R} (1/T_{rs}) - \log \frac{A(PbN_6)}{d(PbN_6)/d \ln t_d} \quad (3)$$

If it is assumed that the log term on the right side of Eq (3) is approximately constant, a plot of $\log (P_{rs} t_d)$ as a function of $1/T_{rs}$ should be a straight line with a slope of $E^*/(2.3 R)$. The data obtained on Contract No. DA-11-022-ORD-3120 are shown plotted in this form in Fig. 5. This graph suggests that different slopes (E^*) are obtained for nitrogen and helium as compared with argon and carbon dioxide driven gases. For the first two gases an E^* of about 10 kcal/mole is indicated, while for the second two an E^* near 30 kcal/mole is indicated. If E^* is to represent an overall activation energy for the initiation of lead azide, it should be independent of the inherent properties of the inert (relatively) driven gas.

It was later discovered that $\log (P_{rs}^2 t_d)$ as a function of $1/T_{rs}$ effected a considerable improvement in the correlation of the data obtained on Contract No. DA-11-022-501-ORD-2731. In retrospect, this would suggest the possibility that the coefficient, x, in Eq (2a) should actually be 2 rather than 1. These data are shown plotted in this form in Fig. 6. The E^* value was found to change from about 6 kcal/mole (as given in the final report) to about 18 kcal/mole (as shown in Fig. 6). The latter value is believed to be more in line with estimates of an activation energy for lead azide from thermal testing. However, when the data from Contract No. DA-11-022-ORD-3120 were plotted in this fashion, as shown in Fig. 7, considerable scatter was still apparent. Further, it appears that an E^* of about 14 to 18 kcal/mole represents the combined data from both contracts.

Two factors have been purposely ignored to this point, namely, the driven gas effects due to the collision frequency components (molecular weight and temperature) and the specific heat capacity at constant volume, $\overline{C}_v$ (the energy that can be accommodated upon gas-solid collision). At the present time, it appears that the most orderly integration of the data collected to date is represented by the semi-theoretical expression:

$$\dot{n}_{rs} P_{rs} t_d e^{-\frac{\left[E_{act} - \overline{C}_v (T_{rs} - T_o)\right]}{R T_{rs}}} = \beta \quad (4)$$

where E_{act} and β are constants that are characteristic of the explosive system. That is, E_{act} is defined as the activation energy of the lead azide for the rate-controlling mechanism, and β is a
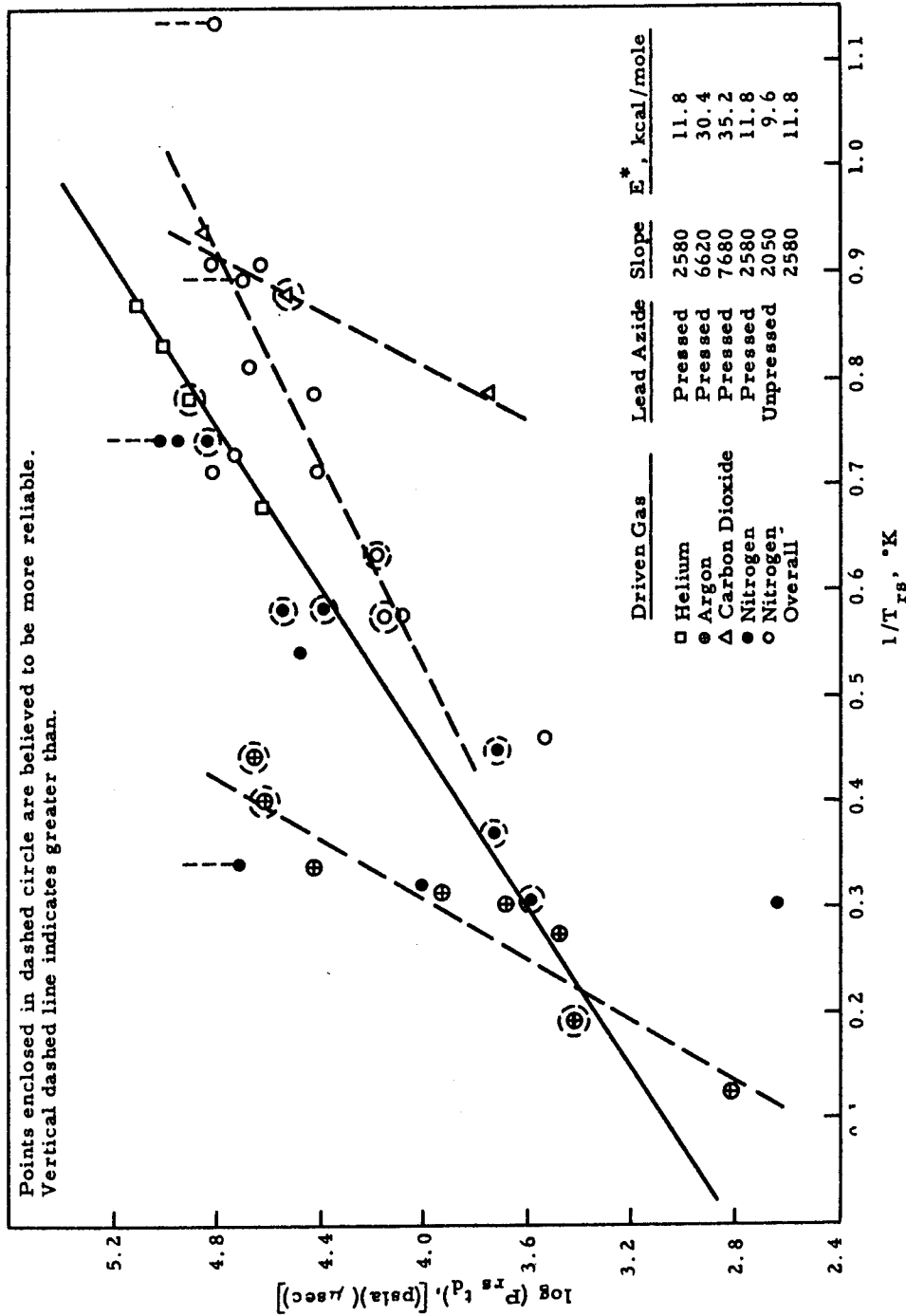
Figure 5 - Log $(P_{rs} t_d)$ as a function of $1/T_{rs}$ for shock test data
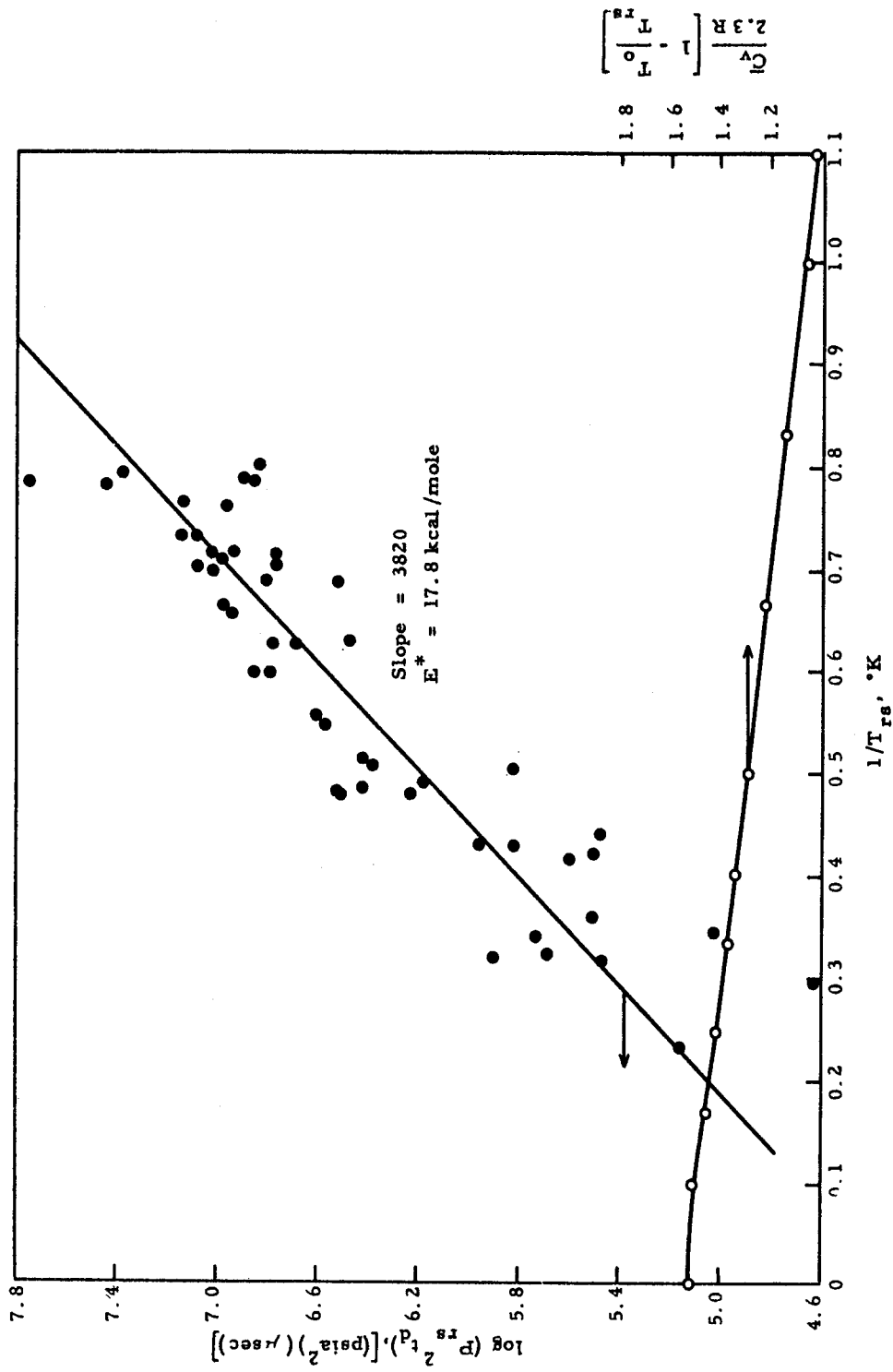
Figure 6 – Log $(P_{rs}{}^2 t_d)$ as a function of $1/T_{rs}$ for shock test data obtained with unpressed lead azide and nitrogen
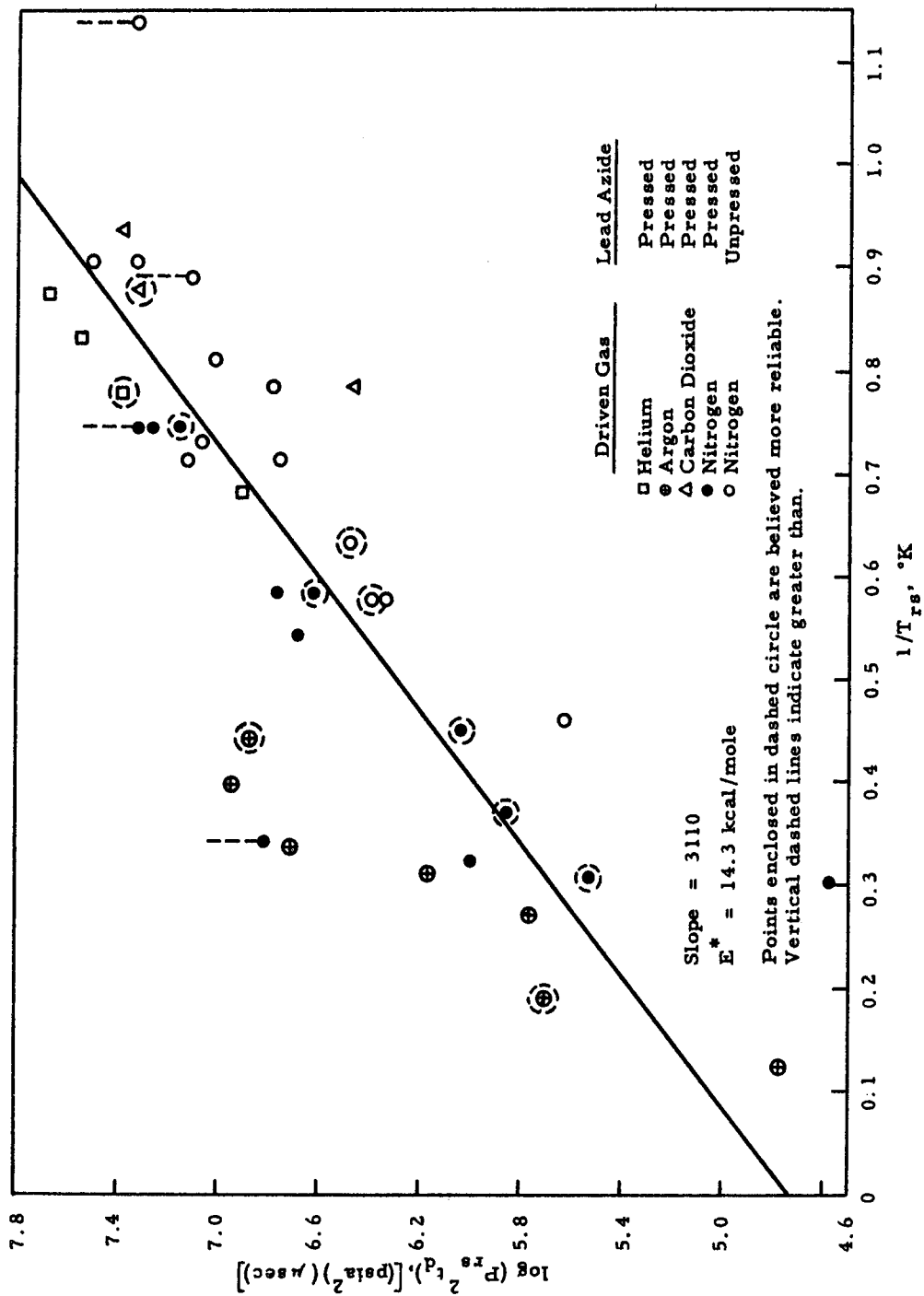
Figure 7 - Log $(P_{rs}{}^2 t_d)$ as a function of $1/T_{rs}$ for shock test data

constant believed to be characteristic of the energetics of the shock
initiation process. The time delay is for a characteristic, explosive
response. All other variables are properties of the environmental
driven gas (surroundings). Since all colliding molecules can, on
the average, deliver $\overline{C}_v(T_{rs} - T_o)$ units of energy to the surface,
the exponential factor represents the colliding fraction that has the
required E_{act} for the solid reaction mechanism.

When the usual expression for the collision frequency is
substituted, Eq (4) can be rearranged into the following form for a
graphical representation:

$$\log\left[\frac{P_{rs}\,t_d}{(M_w\,T_{rs})^{1/2}}\right] + \frac{\overline{C}_v}{2.3R}\left[1 - \frac{T_o}{T_{rs}}\right] = \frac{E_{act}}{2.3R}\left[\frac{1}{T_{rs}}\right] +$$

$$\log\left[\beta\,(2\pi R)^{1/2}\right] \tag{5}$$

Thus, a plot of the left side of the equation as a function of $1/T_{rs}$
should give a slope of $E_{act}/(2.3R)$ and an intercept of
$\log\left[\beta(2\pi R)^{1/2}\right]$.

It appears that notably less deviation results when the data
of Contract No. DA-11-022-ORD-3120 are plotted in this form.
As shown in Fig. 8, the data with the four driven gases fall near
a common line. A relatively small effect due to the bulk density
appears to exist between pressed and unpressed samples. In the
construction of this plot, classical values of $\overline{C}_v$ were used for all
gases except carbon dioxide, for which both classical and actual (8)
values of $\overline{C}_v$ were used. The slope of the line drawn to represent
the data shows an activation energy of about 16 kcal/mole. However,
an increased E_{act} of about 50 kcal/mole is indicated at temperatures
greater than about 3300°K, which is near the explosion temperature
of lead azide.

The data of Baer, et al. (3), were used to test the application
of some of the relations that were evaluated in this report. Only
three P-T-t combinations with air (one more with nitrogen was not
considered) were tabulated in the ARS reprint of Baer's paper.
Various functions, as shown in Table 2, were used to calculate
slopes and deviations for the three possible combinations available
from his data.

From Table 2, it is evident that a minimum deviation occurs
when the data are treated as shown in Fig. 6, 7, or 8. An activation
energy of 10.1 kcal/mole was calculated for their composite per-
chlorate propellant, which differs from their reported value of
28 kcal/mole (by heat transfer analysis) but which appears to be
more in agreement with the activation energy of about 7.1 kcal/mole
reported by Chaiken (9) in his discussion of the rate-controlling
mechanism (surface gasification) for similar propellants.
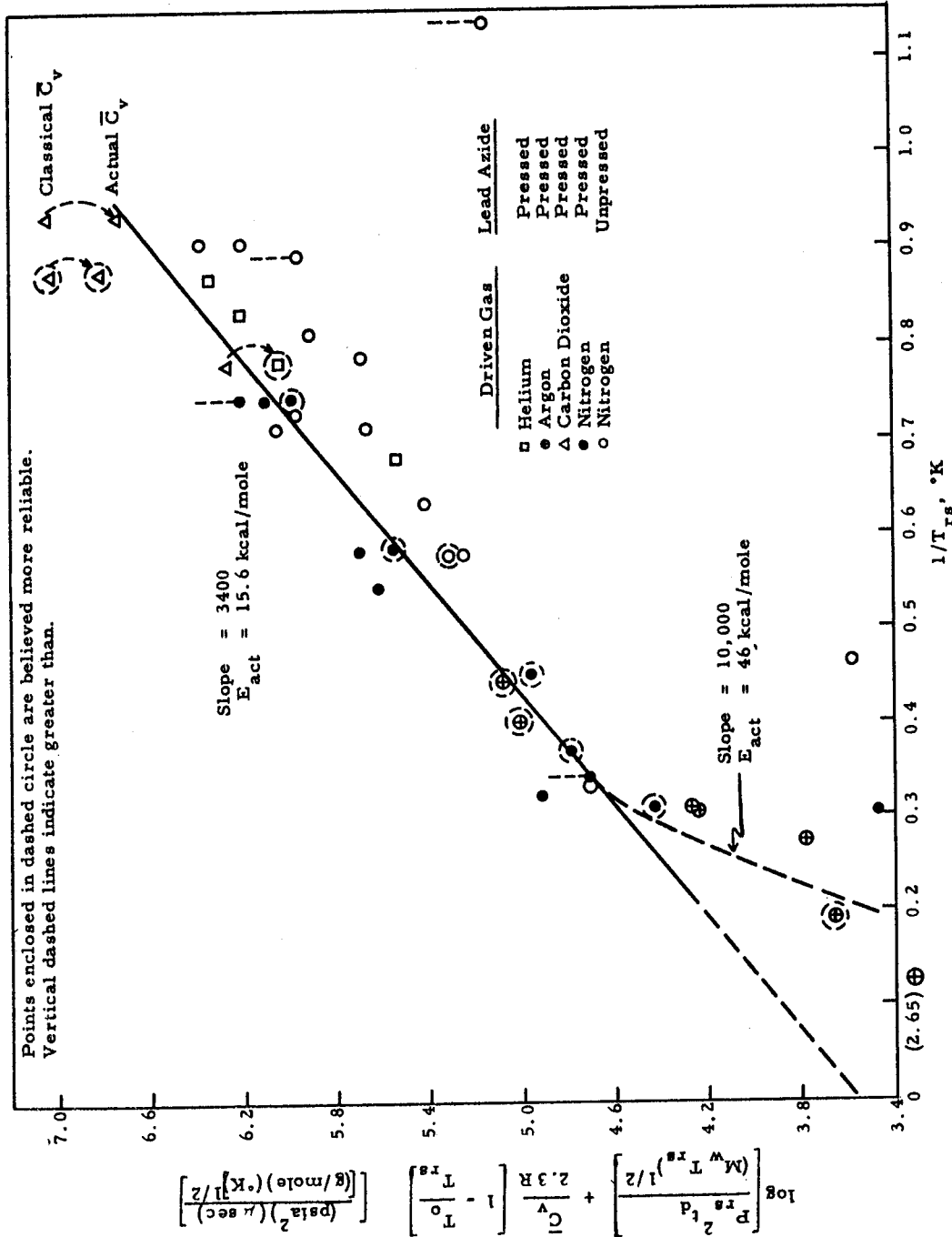
Figure 8 – Best correlation of shock tube data

Erikson

Table 2

EVALUATION OF BAER'S DATA FOR SLOPE CONSISTENCY

Baer's Data[*]

	1	2	3
Run No.:	1017-4	1016-4	1017-3
Driven Gas:	Air	Air	Air
T_g, °K:	990	1370	1505
P_g, psia:	240	245	240
t_d, millisec:	44.5	10	7.5

Treatment

Combination:[**]	Slope [relative to $(\frac{1}{T_g})$]				
Function	1-2	1-3	2-3	Average	Average Deviation
$\Delta \log t_d$	2320	2240	1920	2160	160
$\Delta \log (P_g T_g^{1/2} t_d)$	2030	1980	1750	1920	113
$\Delta \log (P_g t_d)$	2290	2240	2060	2300	90
$\Delta \log (P_g T_g^{-1/2} t_d)$	2540	2510	2380	2480	63
$\Delta \log (P_g^2 t_d)$	2190	2190	2190	2190	0
$\Delta \log \left[(P_g T_g^{-1/2} t_d) + C_v(T_g - T_o) \right]$	2210	2210	2210	2210	0

[*]Reference 3. Baer's subscript g is equivalent to the subscript rs used in the text of this paper.

[**]Numbers refer to the sets of Baer's data tabulated above.

SUMMARY AND CONCLUSIONS

This paper reports an effort to correlate the initiation condition for a condensed-phase explosive system in contact with a hot reflected shock gas environment with the properties of that environment. It has been found that the shock test data from various sources (Baer (3) and the studies conducted at Armour Research Foundation) can be uniformly represented by relations of the sort:

$$P_{rs}^2 t_d e^{-E^*/RT_{rs}} = \text{constant} \tag{6}$$

$$\dot{n}_{rs} P_{rs} t_d e^{-\frac{\left[E_{act} - \overline{C}_v(T_{rs} - T_o)\right]}{RT_{rs}}} = \beta \text{ (a constant)} \tag{4}$$

This treatment was found to give results which are not incompatible with conclusions derived from heat transfer analysis. The energy of activation for the rate-controlling mechanism in lead azide was indicated to be near 16 kcal/mole. A higher activation energy of about 50 kcal/mole is suggested at temperatures over 3000°K in the gas environment.

Should the E_{act} and constant term of Eq (4) be properties that are characteristic of an explosive system (even in a relative manner), a mathematical definition of explosive sensitivity is suggested by the equation:

$$t_d = \frac{\beta e^{+\frac{\left[E_{act} - \overline{C}_v(T_{rs} - T_o)\right]}{RT_o}}}{\dot{n} P_{rs}} \tag{7}$$

That is, for a given gas environment, the t_d of the system may be used to indicate a measure of safety by defining the time that is available before an explosive response.

The relationship suggested by Eq (6) has similar possibilities. It seems that such a definition of explosive sensitivity, which is based on semi-theoretical grounds, is a considerable improvement over the relative means of identifying instability which have been used for the last century in the explosive and, more recently, in the propellant fields. The complex nature of explosive sensitivity becomes obvious when it is realized that t_d, by this approach, must be associated with the time for various explosive responses, that is, partial decomposition, sustaining decomposition, deflagration and detonation.

REFERENCES

1. W. A. Gey and A. Bennett, "Sensitivity of Explosives to Pure Shock," J. Chem. Phys. 23, 1979 (1953).

2. T. A. Erikson, "Pure Environmental Shock Testing of Condensed-Phase, Unstable Materials," ARS Journal 30, 190 (1960).

3. A. D. Baer, N. W. Ryan, and D. L. Salt, "Propellant Ignition by High Convective Heat Fluxes," Paper presented at ARS Solid Propellant Conference, Princeton, N. J., January 28-29, 1960.

4. R. F. McAlevy, P. L. Cowan, and M. Summerfield, "Mechanism of Ignition of Composite Solid Propellants," Paper presented at ARS Solid Propellant Conference, Princeton, N. J., January 28-29, 1960.

5. R. A. Alpher and D. R. White, "Ideal Theory of Shock Tubes with Area Change near Diaphragm," GE Report No. 57-RL-1664, January 1957.

6. R. A. Strehlow and A. Cohen, "Limitations of Reflected Shock Technique," BRL Report No. 1059, December 1958.

7. R. J. Tykodi and T. A. Erikson, "Thermodynamics, Stationary States and Steady-Rate Processes,"(series of four papers) J. Chem. Phys. 31, 1506-1525 (1959).

8. NBS Circular 564, "Thermal Properties of Gases," November 1955.

9. R. F. Chaiken, "Thermal Layer Mechanism of Combustion of Solid Composite Propellants," Combustion and Flame 3, 285-300 (1959).

ON THE MEMORY EFFECT IN THE THERMAL INITIATION OF EXPLOSIVES

By

W. R. Hess and R. C. Ling
Picatinny Arsenal
Dover, New Jersey

Introduction

The "memory effect" is a quite well known phenomenon in the thermal sensitization of explosives. It manifests itself through the apparent additivity of the induction periods prior to ignition. Thus, Ubbelohde[1] found that the total induction period of lead azide which is heated at a given temperature T, is practically the same measured in one or more stages. The latter is tantamount to heating the sample at T for a shorter period followed by chilling and repeating this cycle one or more times until an explosion is finally observed. Algebraically, this can be stated by the equation

$$\tau = \tau_1 + \tau_2 + \tau_3 + \cdots \cdots \quad (1)$$

Although the phenomenon has been known for many years, an analytical treatment was not available. Jones and Jackson[2] observed that autocatalytic decomposition is a necessary precondition for the existence of the memory effect in the thermal initiation of explosives. Eyring[3] and associates treated the thermal decomposition of solid explosives as a first order reaction and arrived at a useful expression for the induction period. It is the purpose of the present report to describe the memory effect analytically in terms of the following kinetic assumptions: (1) For a first order approximation loss of heat by conduction can be neglected, and (2) thermal initiation of explosives is closely related to the autocatalysis involved in a solid decomposition reaction. A mathematical derivation of the effect is made, and the results are compared with experiments. It is also shown that true additivity of induction periods is only a special case of the memory effect in general.

Discussion of Assumptions

Consider the autocatalytic reaction

$$B \xrightarrow{A} A + C \quad (2)$$
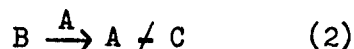
and the kinetic equation

$$\frac{dx}{dt} = K_0(a \neq x)(b-x) \qquad (3)$$

where x is the concentration of the reaction product A, a and b are the initial concentrations of A and B, respectively, and K_0 represents the specific reaction rate. Strictly speaking, Equation (3) is applicable only to gaseous systems and solutions. On the other hand, Hinshelwood[4] found that it can also be applied to the case of molten tetryl. Prout and Tompkins[5] described the decomposition of potassium permanganate by a relation derived from the expanded chain theory. This relation is very similar to the solution of equation (3) in an isothermal case, hence, there is good reason for using an autocatalytic reaction equation as an approximation for solid state decompositions. The above mentioned similarity of the relations may be better understood by considering that in the initial reaction the rate of formation of catalyst nuclei overshadows the rate of growth of the nuclei. During this initial period, one would therefore expect the reaction rate to be proportional to the catalyst concentration. As the reaction proceeds, however, the catalyst nuclei will grow and aggregate so that the catalyst becomes partly "screened" out. It is, therefore, reasonable to assume that the reaction rate is related to the interface at which the catalysis takes place. In spite of the uncertainty surrounding the exact kinetic relation, it seems very worthwhile to describe the memory effect in terms of Equation (3), particularly since we confine ourselves to the early stage of initiation. By means of the above mentioned approximate kinetic equation the memory effect can be shown to be closely related to the concentration of the catalyst formed during pre-sensitization. In our treatment of the problem, the absence of thermal conduction is assumed. As the results show later, the initial stage of pre-reaction is characterized by a very small temperature increase; consequently, omission of the later is well justified. How heat conduction may influence the temperature-time profile has, for example, been calculated by Semenov[6] for gaseous reactions (See dotted line in Fig. 1).

Mathematical Formulation

For practical reasons the kinetic equation (3) is rewritten in terms of concentrations normalized with respect to the initial value of the reactant B:

$$\frac{dx}{dt} = k \cdot e^{-E/RT}(\alpha_0 \neq x)(1 - x) \qquad (4)$$

in which x is the relative amount of the reacted material, k is a proportionality factor which includes the frequency factor, E and R represent, respectively, activation energy and the gas constant, and α_0 is the initial concentration of the catalyst which may originate from various kinds of intrinsic lattice defects. Mathematically, the non-zero value of α_0 is required for the integrability of certain integrals to be described later (i.e., $x = 0$ represents a singularity

in the treatment if $\alpha_0 = 0$). When heat loss by conduction is neglected, the heat of reaction ΔH evolved by an exothermic reaction can be used solely to raise the temperature of the explosive sample. On this basis the reacted amount x is given by

$$x = \frac{Cv(T - T_0)}{\Delta H} \qquad (5)$$

where T_0 is the bath or hot plate temperature, and C_V a mean specific heat. By introducing a hypothetical temperature T_∞ which is the maximum temperature attainable in an adiabatic reaction, equation (5) can be written

$$x = \frac{T - T_0}{T_\infty - T_0} \qquad (6)$$

From equations (4) and (6) we have

$$\frac{dt}{dt} = \frac{ke^{-E/RT}}{(T_\infty - T_0)} (T - T_1)(T_\infty - T) \qquad (7)$$

where

$$T_1 = T_0 - \alpha_0(T_\infty - T_0)$$

Integrating equation (7) we obtain t in terms of the logarithmic integral

$$t = C_1 \left\{ \left(e^{y_1} \int_{,p_0}^{\infty} \frac{e^{-p}}{p} \, dp + e^{y_\infty} \int_{-\infty}^{q_0} \frac{e^q}{q} \, dq \right) - \left(e^{y_1} \int_{,p}^{\infty} \frac{e^{-p}}{p} \, dp + e^{y_\infty} \int_{-\infty}^{q} \frac{e^q}{q} \, dq \right) \right\} \qquad (8)$$

where

$$y = E/RT , \quad y_0 = E/RT_0 , \quad y_1 = E/RT_1 , \quad y_\infty = E/RT_\infty ,$$

$$C_1 = \frac{1}{k(1+\alpha_0)} , \quad {}_,p = y_1 - y , \quad q = y - y_\infty ,$$

$${}_,p_0 = y_1 - y_0 , \quad q_0 = y_0 - y_\infty$$

Figure 1 shows the temperature-time profile schematically. (The above-mentioned influence of heat loss by conduction is indicated by the dotted line.) The steep rise of temperature represents a self-acceleratory reaction leading to ignition, and the time τ_0 required for this to occur may be defined as the induction time, characteristic of the sample under study. Such a definition implies that near t_0 t is practically independent of T, and consequently that the last two T-dependent terms in equation (8) compensate each other.
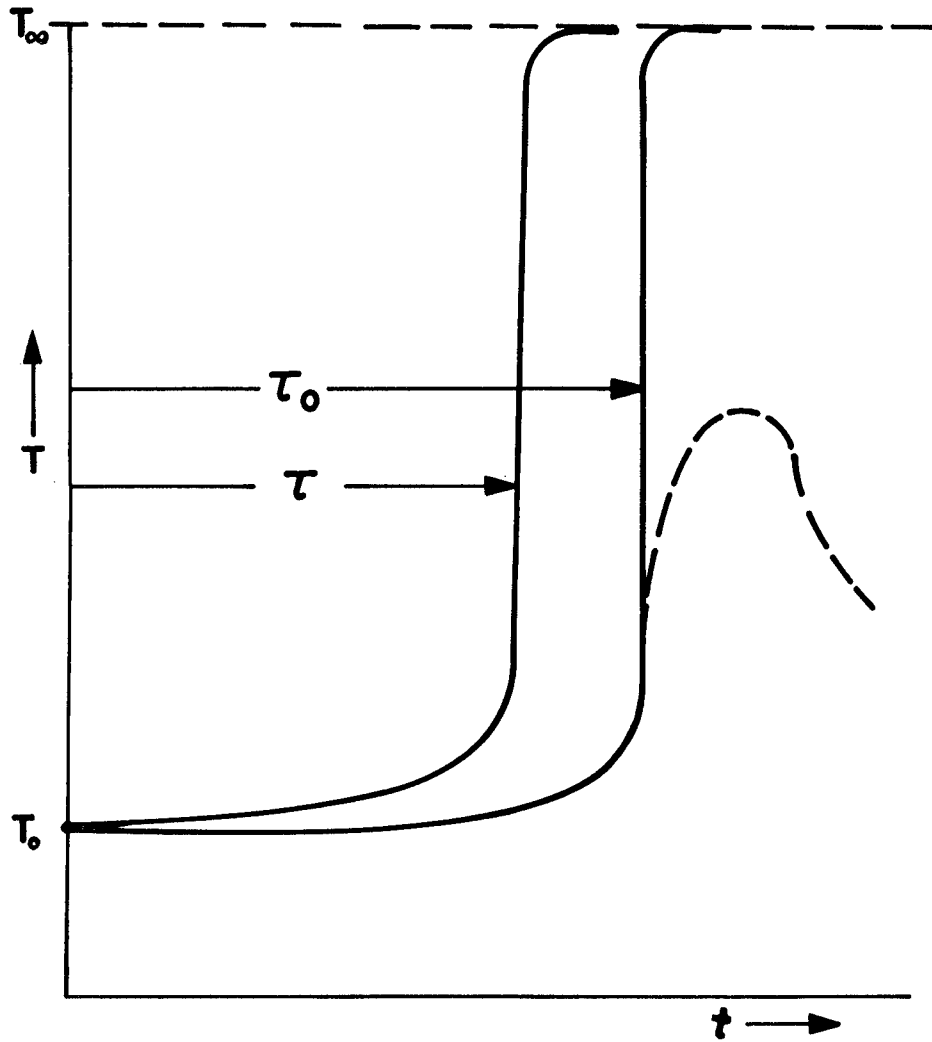
FIG. I: TEMPERATURE—TIME CHARACTERISTIC FOR DIFFERENT INITIAL CONCENTRATION α.

We then have

$$\tau_o = C_1 \left\{ e^{y_1} \int_{_1 p_o}^{\infty} \frac{e^{-p}}{p} \, dp + e^{y_\infty} \int_{-\infty}^{q_o} \frac{e^q}{q} \, dq \right\} \qquad (9)$$

which, in essence, depends only on the initial concentration of the catalyst and the bath temperature T_0. Thus the memory effect reduces to a description of the amount of auto-catalytic decomposition product formed in a given length of time. When the auto-catalytic reaction is interrupted after a heating time t by cooling the explosive sample, an amount x of the catalyst formed can be calculated by using equation (8) and the linear relationship (5) between x and T. When the reaction is resumed by heating to the previous temperature T_0, the initial concentration of the catalyst is increased by the amount x to $\alpha_1 = \alpha_o + x$, and the new, shorter induction time τ can be evaluated from a similar integral

$$\tau = C_2 \left\{ e^{y_2} \int_{_2 p_o}^{\infty} \frac{e^{-p}}{p} \, dp + e^{y_\infty} \int_{-\infty}^{q_o} \frac{e^q}{q} \, dq \right\} \qquad (10)$$

where

$$C_2 = \frac{1}{k(1+\alpha_1)} \quad , \qquad _2 p_o = y_2 - y_o \quad ,$$

and

$$y_2 = E \left\{ R(T_o - \alpha_1 (T_\infty - T_o)) \right\}^{-1}$$

The time t required to form the additional amount x of catalyst can also be calculated via equation (8).

As mentioned previously, the memory effect is described by

$$\tau_o = t + \tau$$

or

$$\frac{\tau}{\tau_o} = 1 - \frac{t}{\tau_o} \qquad (11)$$

Knowing τ_o, τ, and t from the integrals mentioned, and assuming the constancy of k, one can check the memory effect by plotting τ/τ_o against t/τ_o. For a linear memory effect as defined by equation (11) a straight line with a negative slope of unity should result. Figure 2 shows such a plot for 3 explosives with known values ΔH, E, and C_v. In all these cases the initial concentration of catalyst was taken as 10^{-6}. It is noted that the major portion of the calculated curve describes very well the linear memory effect.
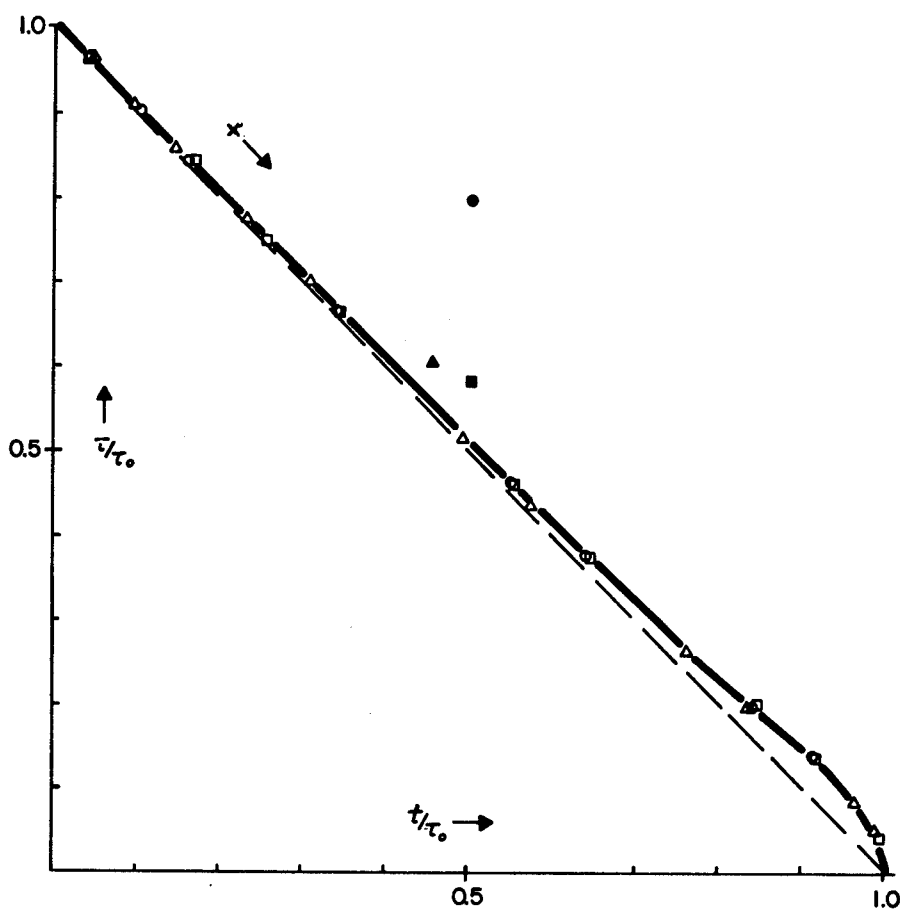
FIG. 2: CALCULATED PAIRS OF VALUES $(\tau/\tau_0, t/\tau_0)$ FOR

LEAD AZIDE $\triangle$: E=38 KCAL/MOLE, $\frac{\Delta H}{C_v}$=3336 $^{\circ}$K, T_0=603 $^{\circ}$K;

PETN   o : E=37 KCAL/MOLE, $\frac{\Delta H}{C_v}$=5130 $^{\circ}$K, T_0=521 $^{\circ}$K;

TETRYL $\square$: E=52 KCAL/MOLE, $\frac{\Delta H}{C_v}$=4804 $^{\circ}$K, T_0=525 $^{\circ}$K.

IN ALL THREE CASES α_0=10^{-6}. THE SOLID SIGNS $\blacktriangle$, $\bullet$, $\blacksquare$ REPRESENT EXPERIMENTAL VALUES.

It should be mentioned that the treatment can be extended to include a more general case, i.e., thermal sensitization involving two stages of preheating times t_1 and t_2 or, analytically,

$$\frac{\tau}{\tau_o} \approx 1 - \frac{t_1}{\tau_o} - \frac{t_2}{\tau_o} \qquad (12)$$

Figure 3 represents a plot for this more general case. (In the figure a constant initial preheating time $t_1 = const$ is chosen while the points for the variable second time t_2 are plotted together with the one stage preheating curve of Figure 2.) It is observed that the result of a second preheating also gives support to the model proposed.

It is evident from these plots that for a preheating time very close to the total induction time the calculated curve deviates appreciably from the straight line representing the linear memory effect. Such deviation might well result from a breakdown in the assumptions regarding auto-catalysis and neglect of heat loss. Furthermore, there exists some arbitrariness in the definition of τ_o owing to the very steep but not infinite rise of the $T - t$ curve near $t \approx t_0$.

Some experimental results are given in Figure 2. As found in some cases, the original induction time τ_o represents a lower limit for the sum of terms on the right side of equation 1. In Figure 2 these points will lie above the straight line. A more detailed theoretical investigation shows that the entire calculated curve of Figure 2 will be more convex when the initial concentration of catalyst is taken to be greater than 10^{-6}. Thus even the degenerated, non-linear memory effect can be explained by the model used before.

In summary, the mathematical treatment presented here provides a theoretical relation between the memory effect in an explosive and its auto-catalytic decomposition as evidenced by the validity of the additivity equation $\tau = \tau_1 + \tau_2 + \cdots$.

Bibliography

(1) A.R. Ubbelohde, Research 3,204 (1950)

(2) M.M. Jones and H.J. Jackson, Explosivstoffe 9, 177 (1959)

(3) R.B. Parlin, G. Duffy, R.E. Powell, and E. Eyring, OSRD No. 2026 "The Theory of Explosive Initiation"

(4) C.N. Hinshelwood, J.Chem.Soc. 119, 721 (1921)

(5) Prout and Tompkins, Trans. Faraday Soc. 40, 488 (1944)

(6) N.N. Semenov, Uspekhi Fiz. Nauk 23 (3), 251-292 (1940)
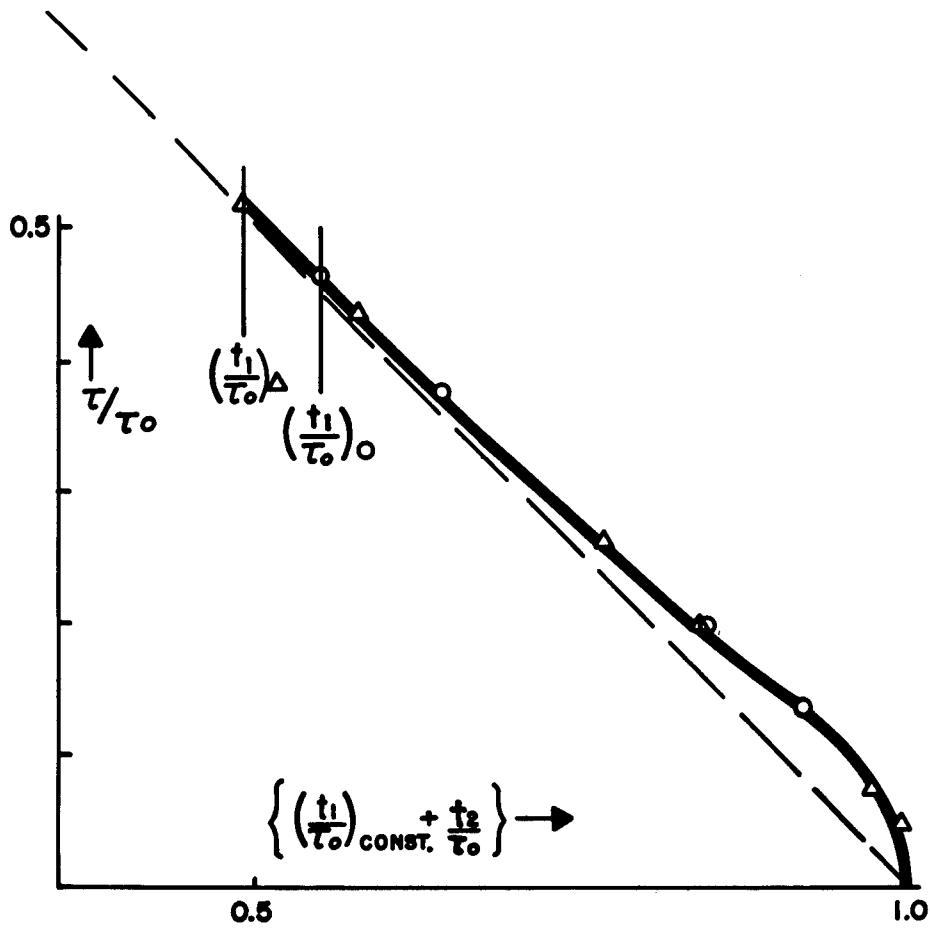
FIG. 3 : CALCULATED PAIRS OF VALUES CONCERNING TO PRE—
HEATING TIMES (t_1/τ_o =CONST.) FOR LEAD AZIDE $\triangle$
AND PETN $\circ$.

THE THERMAL DECOMPOSITION OF $[Co(NH_3)_6](N_3)_3$

Taylor B. Joyner and Frank H. Verhoek
U. S. Naval Ordnance Test Station
China Lake, California

INTRODUCTION

The thermal decompositions of a series of complex cobalt ammine azides, $[Co(NH_3)_6](N_3)_3$, $[Co(NH_3)_5N_3](N_3)_2$, cis- and trans- $[Co(NH_3)_4(N_3)_2]N_3$, and $Co(NH_3)_3(N_3)_3$ have been studied with the goal of understanding the mechanisms of the slow reactions prior to explosion. This would bear on the processes by which initiation begins in an exothermic crystal and grows through a slow stage to release the energy which will convert the reaction to rapid burning and detonation.

The compounds studied relate directly to the simple metal azides (NaN_3, $Pb(N_3)_2$, AgN_3) in that the principal reaction is the reduction of a metal cation by an azide ion. (Recent extensive reviews summarize the considerable information now available on the simple azides.[1,2,3,4,5] The complexes differ in that they have a more difficult chemistry, a 3-electron reduction complicated by the ligand molecules, but they also have the major advantage of metal-azide relationships clearly defined by the ligand sphere. This definition permits the recognition of two distinct types of azides. In $[Co(NH_3)_6](N_3)_3$ the azides are ionic. They are isolated from the cobalt by the coordinated ammonias, occupy anionic sites in a salt-like lattice, and are presumably symmetrical with the structure

$$N \underset{1.16}{\text{———}} N \underset{1.16}{\text{———}} N$$

as in simple metal azides.[6] In $Co(NH_3)_3(N_3)_3$ they are bonded directly to a specific cobalt and are presumably assymetric as in the case of such covalent compounds as methyl azide

$$H_3C \overset{1.47}{\diagup} N \underset{1.24}{\text{———}} N \underset{1.12}{\text{———}} N. \quad [7,8]$$

$120°$

The remaining three compounds have both types of azides. The behavior of $[Co(NH_3)_6](N_3)_3$ is quite typical of the four ionic members of the series and will be specifically discussed in the remainder of the paper.

EXPERIMENTAL

Preparation.--The hexammine was prepared as previously described.[9] Visibly crystalline samples (crystals 0.05 to 0.5 mm. long) were obtained by a simple recrystallization from water. Powder samples were prepared by dissolving the complex in water and rapidly precipitating with a large excess of alcohol. In reality the powder consists of micro-crystals. X-ray powder patterns revealed sharp lines and established a minimum crystal diameter of about 0.1 μ.[10] Microscopic examination fixed an upper limit of about 5 μ. Both powder and crystals were stored in a vacuum desiccator over sulfuric acid and kept in the dark.

Apparatus.--The apparatus consists of a simple vacuum line with a comparatively small volume (50 to 100 ml.). The glass reaction vessel is protected from explosions by placing the sample (ca. 10 mg.) in a stainless steel cup (6 mm. in diameter and depth) cushioned with glass wool plugs. The reaction vessel is arranged to permit rotation about a standard-taper joint into a hot oil bath maintained to $\pm$ 0.1° at temperatures of 120 to 150°C. The pressure of the evolved gases is measured manometrically. Empirical corrections obtained with known samples of nitrogen account for the small volume of the system at high temperature.

RESULTS

Three distinct overall reactions have been recognized: A slow reaction to a cobalt(II) complex

$$[Co(NH_3)_6](N_3)_3 \longrightarrow Co(NH_3)_2(N_3)_2 + 4NH_3 + 1.5N_2 \quad (1);$$
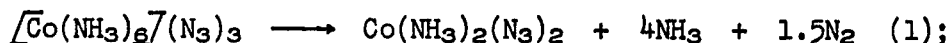
a slow reaction followed by an explosion to a final stoichiometry

$$[Co(NH_3)_6](N_3)_3 \longrightarrow Co + \sim 4NH_3 + \sim 5.5N_2 + \sim 3H_2 \quad (2);$$
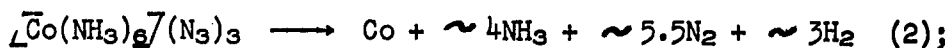
and a reaction with a lengthy induction period followed by rapid but non-explosive production of a nitride

$$[Co(NH_3)_6](N_3)_3 \longrightarrow CoN + 6NH_3 + 4N_2 \quad (3);$$
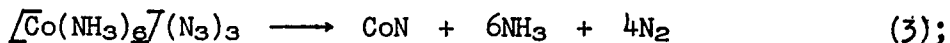
Temperature, particle size, and ammonia pressure affect the kinetics and lead to these various reactions.

The influence of temperature and the impressive effect of particle size are illustrated in Fig. 1. Crystalline samples show a long induction period with little gas evolution followed by a fast but non-explosive reaction to the nitride (Eq. 3). The more labile powder samples show an immediate slow reaction evolving considerable gas (Eq. 1). At lower temperatures the reaction ceases with the formation of the cobalt(II) compound, but above 130° an explosion to cobalt ultimately occurs (Eq. 2).

Ammonia pressure above the solid shows two marked effects (Fig. 2). In the case of the powder it accelerates the 1-electron reduction and inhibits the explosion of the resulting $Co(NH_3)_2(N_3)_2$. While the latter is reasonable in view of the well known lability of cobalt(II) compounds to ammonia loss and absorption[11] (a decomposition mechanism involving a loss of ammonia as a rate controlling step would be inhibited by excess ammonia), the more surprising acceleration of the 1-electron reaction is not yet understood. In the case of crystalline samples ammonia produces a very marked departure from normal behavior. An initial reaction (probably the 1-electron reduction) is accelerated. This is followed by a long quiescent period and a final explosion.

A liquid nitrogen trap on the line some distance from the hot bath also produces interesting effects (Fig. 3). In the case of both powder and crystals the time to explosion or rapid reaction is shortened. This is understandable for the powder at the higher temperatures. Since ammonia has been found to inhibit the explosion of $Co(NH_3)_2(N_3)_2$, its removal by the cold trap would lead to earlier explosions. More surprising is the marked shortening of the induction period of crystalline samples and the powder in the 120° run. This is so pronounced in some cases (curves E and F) that reaction occurs at a time when very little nitrogen has been noted in the trapped run and no gas evolution at all had been detected in a corresponding untrapped run. While this acceleration may most reasonably be attributed to the removal of ammonia, it is quite remarkable that trapping small amounts -- virtually undetectable manometrically -- could have such a marked effect. It is also noteworthy that at 120° the behavior of the powder is altered from the explosive reaction to a smooth production of CoN.

DISCUSSION

The complicated effects of ammonia have so far prevented a very successful quantitative analysis of our kinetic data. Nevertheless, the complex (and at first glance contradictory) behavior of the system in actuality permits considerable insight into some features of the reaction. These must be recognized before a detailed inquiry into the mechanism can hope to succeed. What is desired now is a self-consistent, qualitative explanation of the marked differences in behavior of crystalline and powder samples taking into account the following points: (1) powder samples are more labile than crystals;

THERMAL DECOMPOSITION OF $[Co(NH_3)_6](N_3)_3$

A. Powder, 120°
B. Powder, 130°   E. Crystals, 130°
C. Powder, 140°   F. Crystals, 140°
D. Powder, 150°
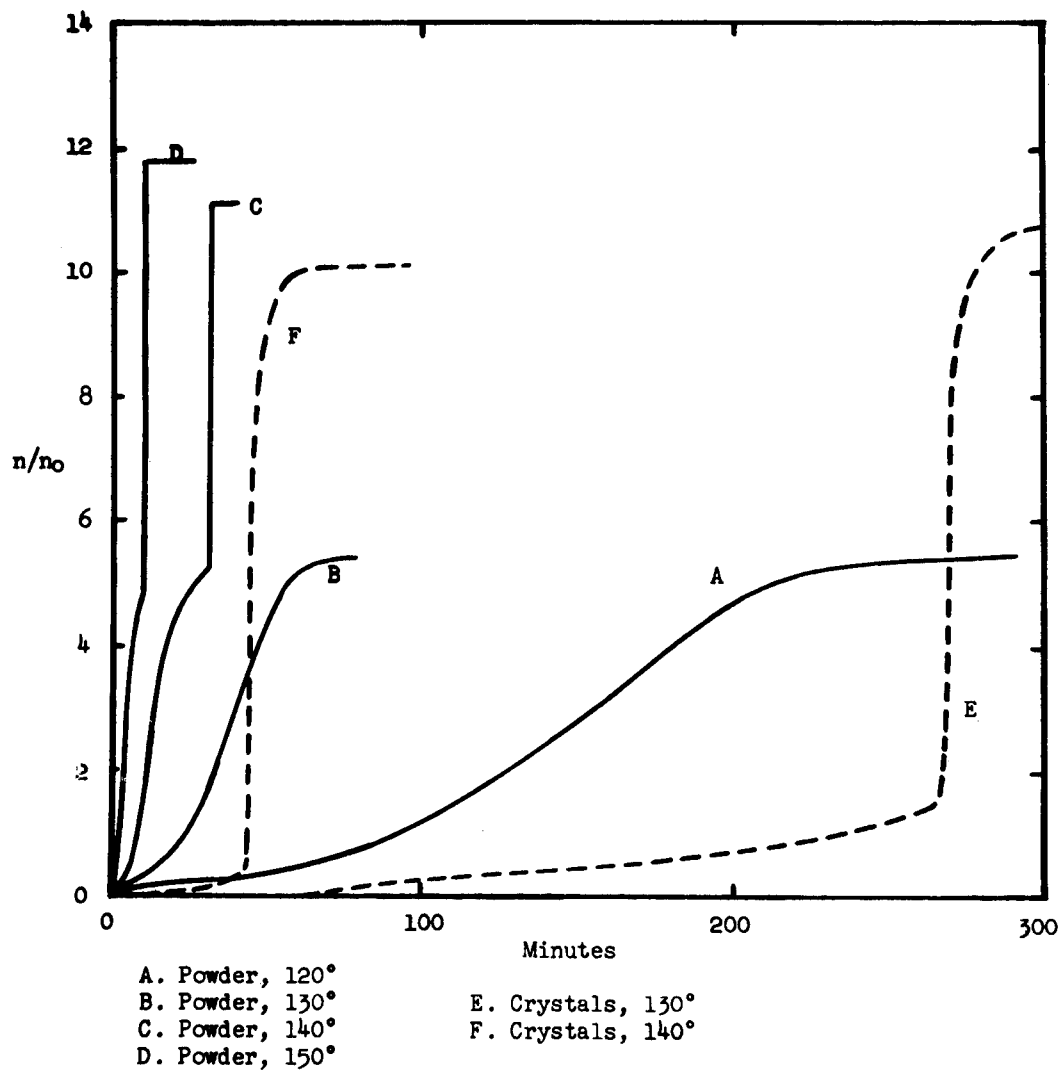
FIGURE 1.   THE EFFECTS OF TEMPERATURE AND CRYSTAL SIZE.
The moles of evolved gas per mole of complex
(n/n_0) versus time.

DECOMPOSITION OF $[Co(NH_3)_6](N_3)_3$

140°

A--Powder, initially evacuated
B--Powder, initial pressure of 103 mm. NH_3
C--Crystals, initially evacuated
D--Crystals, initial pressure of 101 mm. NH_3
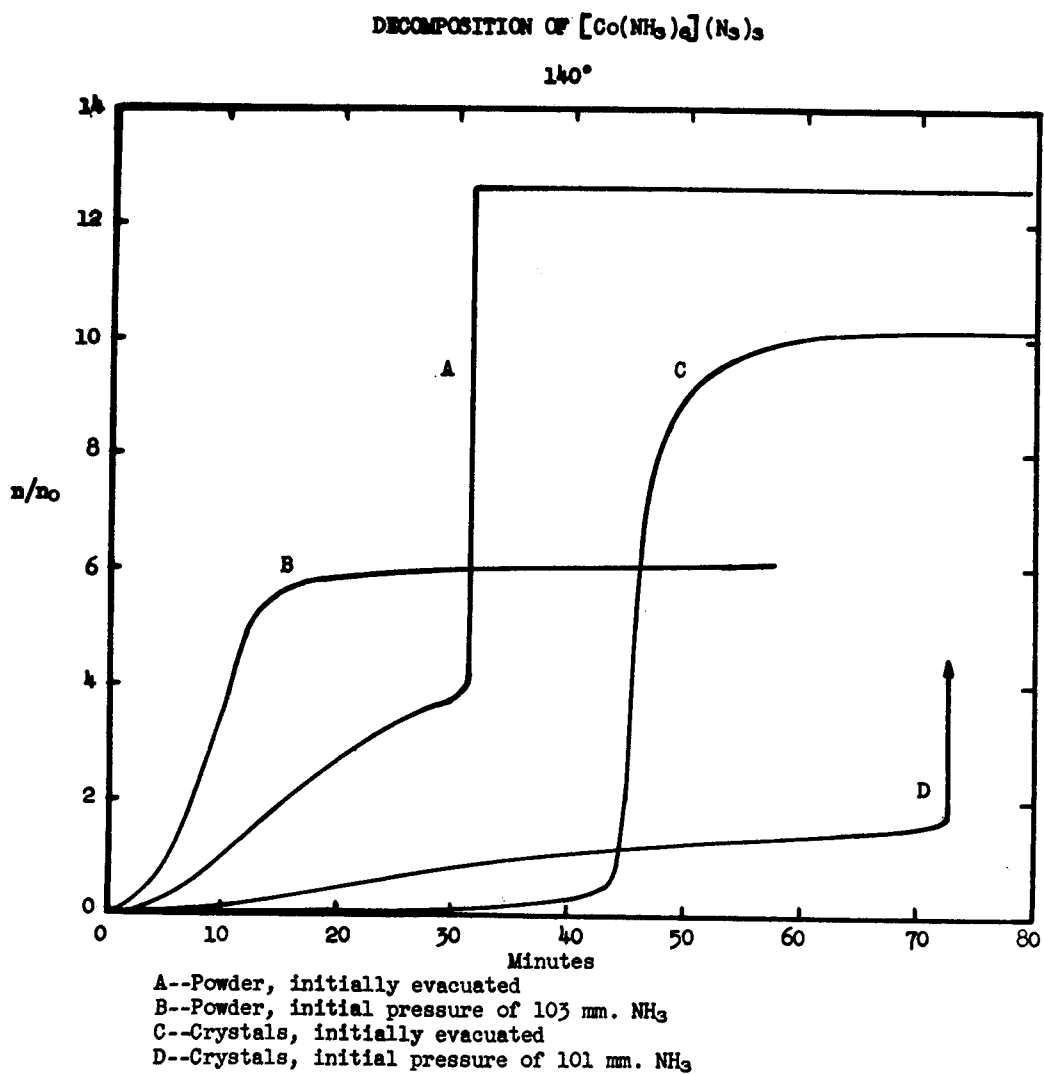
FIGURE 2.   THE EFFECT OF AMMONIA.   The moles of evolved gas
            (n/n_O) versus time.

THERMAL DECOMPOSITION OF $[Co(NH_3)_6](N_3)_3$

A. Powder, 120°
B. Powder, 120°, trapped
C. Powder, 140°
D. Powder, 140°, trapped
E. Crystals, 140°
F. Crystals, 140°, trapped
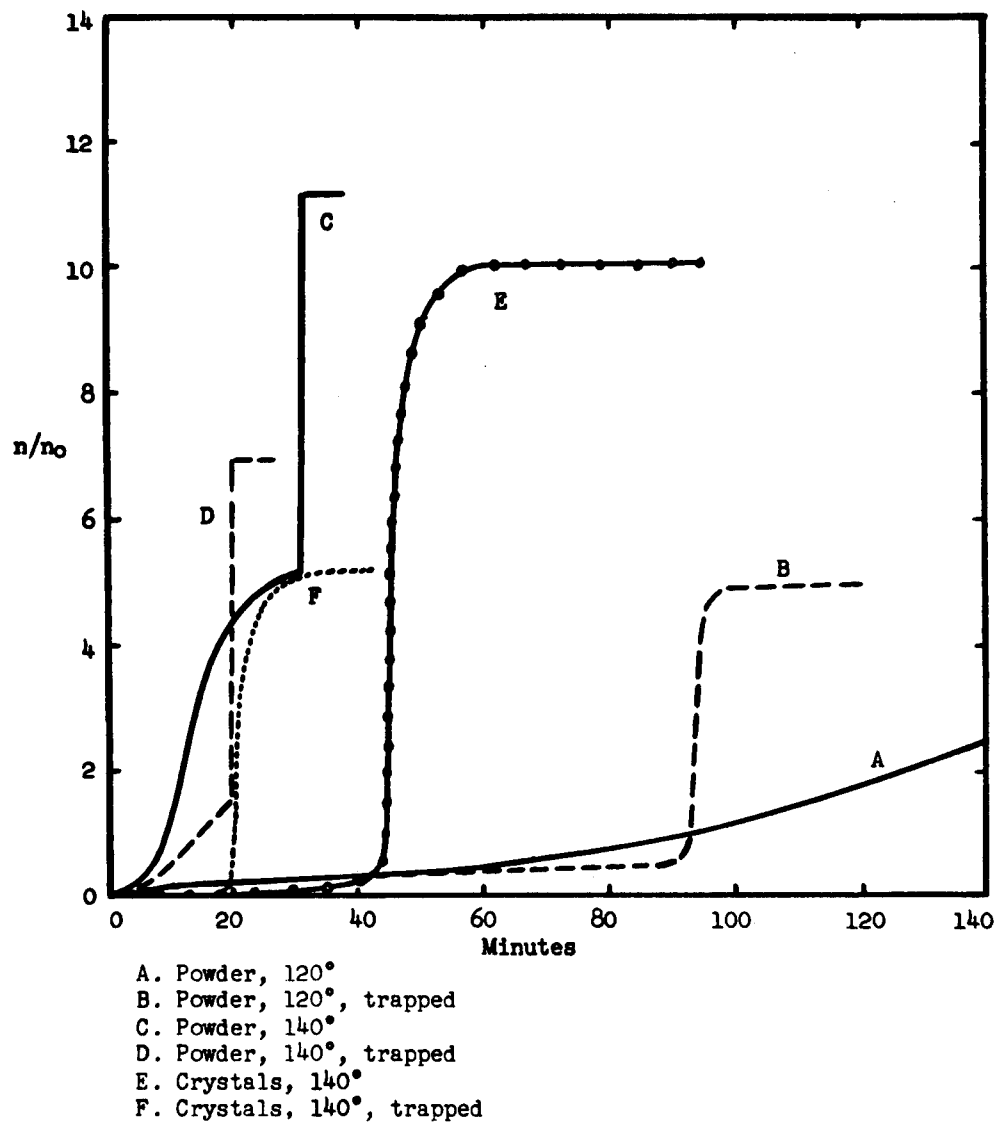
FIGURE 3. THE EFFECT OF A LIQUID NITROGEN TRAP. The moles of evolved gas (n/n_0) versus time.

(2) crystals proceed smoothly to CoN (except in the presence of added ammonia which promotes an initial reaction, inhibits the rapid CoN reaction, and finally results in an explosion to cobalt); (3) crystals exposed to a cold trap proceed smoothly to CoN with shortened induction periods; (4) powder proceeds explosively to cobalt (except below 130° or in the presence of added ammonia when a smooth reaction to $Co(NH_3)_2(N_3)_2$ may occur); (5) powder exposed to a cold trap goes explosively to cobalt with shortened induction periods (except at 120° when a smooth reaction to CoN occurs); (6) the action of ammonia may be summed up as accelerating the 1-electron reduction, inhibiting the explosion of $Co(NH_3)_2(N_3)_2$, and inhibiting the rapid reaction to CoN when present in tiny amounts.

A reasonable picture may be formed in terms of a strong surface adsorption of ammonia and an overall decomposition involving two major steps. The first step is the only moderately energetic (possibly endothermic) 1-electron reduction to $Co(NH_3)_2(N_3)_2$, (Eq. 1). The second is a very exothermic decomposition to the final products, cobalt or CoN. The initiation of this second step is particularly important to a general understanding of the system. The actual initiating reaction may very probably be the decomposition of a small amount of the diammine according to an overall stoichiometry of

$$Co(NH_3)_2(N_3)_2 \longrightarrow Co + 2NH_3 + 3N_2 \qquad (4)$$

however, this cannot at present be established with certainty and, hence, the following discussion is kept in general terms. Regardless of the mechanism of initiation of the exothermic reaction, once it occurs the energy liberated is sufficient to insure very rapid propagation through the solid by means of either the fast (but smooth) reaction to CoN or an explosion to cobalt. Which of these paths will be followed will depend very strongly on the time of initiation of the energetic reaction relative to the progress of the 1-electron reduction.

At this point it may be useful to think of the overall decomposition in terms of a competition between the 1-electron reduction and the initiating mechanism of the exothermic reaction. Both are influenced by ammonia. The reduction is accelerated while the initiating mechanism is inhibited. Once the energetic reaction does begin, whether it explodes or goes smoothly to the nitride will depend on the quantity of $Co(NH_3)_2(N_3)_2$ present; in other words, on the extent the 1-electron reduction has already proceeded. If initiation occurs relatively early and a large amount of $/Co(NH_3)_6/(N_3)_3$ still remains the energetic decomposition proceeds smoothly to CoN. Conversely, if it is late the composition of the solid will have been altered by the accumulation of a considerable amount of the diammine. This material, upon initiation, explodes to cobalt.

The important effects of minute quantities of ammonia on these reactions may be understood in terms of surface adsorption. It is

reasonable to assume that reaction begins and proceeds most readily on the surface of the crystals since the powder, with a high surface to volume ratio, is more labile than the visibly crystalline samples. If it is further assumed that the ammonia produced in the very early stages of the reaction can be adsorbed on the surface an explanation of the inhibiting effect of small quantities of ammonia is possible. While the reaction is still young, having produced a microscopic amount of solid product and a manometrically undetectable quantity of gases, sufficient decomposition will have occurred to immerse the site in a sea of adsorbed ammonia. This ammonia, by acting directly on the young reaction site, can then exert a very large influence on the course of the reaction.

Considering fairly large crystals in some detail, after initiation on the surface the 1-electron reaction in the presence of its own adsorbed ammonia can proceed into the crystal. Once away from the surface the reaction slows and the total gas evolved remains small. Eventually, the energetic reaction will be initiated, possibly by the decomposition of a little of the recently formed $Co(NH_3)_2(N_3)_2$ in a locally overheated region, and propagates through the crystal which still consists primarily of undisturbed $[Co(NH_3)_6](N_3)_3$. In the process the reaction will overcome the ammonia's inhibition and destroy the small amount of diammine already produced.

In the presence of a cold trap the ammonia adsorbed on the surface of the crystal will be removed (or at least reduced). This will slow the 1-electron reduction but permit an earlier initiation of the energetic reaction thus shortening the induction period. Conversely, in the presence of excess ammonia the inhibition is more effective. Consequently, a larger quantity of diammine may be produced prior to initiation, partially because of the acceleration of the 1-electron reduction and partially because of the delay of the rapid reaction. When the energetic reaction finally does occur, this accumulated diammine will explode rather than reacting smoothly.

In the case of the powder the situation is altered by the large surface area of the micro-crystals, an area 100 to 1000 times greater than in visibly crystalline samples. The original surface reaction is thus able to generate considerable amounts of ammonia which will again accelerate the 1-electron reduction and inhibit the energetic reaction. Moreover, the increase in the surface to volume ratio means that a reaction proceeding inward to a given depth prior to initiation will consume a much greater percentage of the crystal. For example, with crystal sizes in the 0.1 to 1 μ region a uniform penetration of 100 molecular layers will consume on the order of 10 percent of the crystal. Consequently, when initiation finally occurs the sample will contain large amounts of $Co(NH_3)_2(N_3)_2$ and the reaction will rapidly go over into an explosion consuming any remaining $[Co(NH_3)_6](N_3)_3$ and yielding cobalt as a final product.

The explosion can be avoided by completely inhibiting its initiation by the presence of excess ammonia (at the lower temperatures the ammonia generated by the reaction itself is sufficient). Removal of this ammonia results in explosions. Alternately, the decomposition can be altered from the powder's usual explosive behavior to the smooth CoN path by markedly slowing the 1-electron reduction relative to the initiation reaction. This is accomplished at 120° in the presence of a cold trap. Here the low temperature slows the reduction while the trap provides the most favorable situation for the initiation reaction. Consequently, the energetic reaction commences at a time when relatively little of the hexammine has been converted to $Co(NH_3)_2(N_3)_2$ and the rapid reaction takes the form of a smooth decomposition to CoN.

In conclusion, this discussion has presented a consistent (but not necessarily exclusive) explanation of the principal features of the thermal decomposition of crystalline and powder samples of $[Co(NH_3)_6](N_3)_3$. However, it has said virtually nothing as to the detailed reaction mechanisms and, therefore, should be considered only as a necessary foundation for efforts to arrive at a more complete understanding of the system. While several quite plausible reaction mechanisms can be formulated, at present our kinetic data provides no convincing distinction between them. Nevertheless, it may be of some interest to mention that the 1-electron reaction (in particular) is suspected of being quite analogous to the simple metal azides in that the formation of the azide radical is believed to play an important and possibly rate-determining role in the decomposition. The mechanism by which ammonia accelerates this reaction and the intriguing problem of the means by which electrons are transferred through the ligand sphere to the cobalt atom are now under investigation.

REFERENCES

(1) W. E. Garner, "Chemistry of the Solid State", Butterworths Scientific Publications, London, 1955, Chap. 9.

(2) F. P. Bowden and A. D. Yoffe, "Fast Reactions in Solids", Academic Press, Inc., New York, N. Y., 1958.

(3) B. L. Evans, A. D. Yoffe, and P. Gray, Chem. Rev. 59, 515 (1959).

(4) H. Rosenwasser, "Hydrazoic Acid and the Metal Azides (A Literature Survey)", Report 1551-TR, U. S. Army Engineer Research and Development Laboratories, Fort Belvoir, Virginia, 1958.

(5) H. Rosenwasser, "Hydrazoic Acid and the Metal Azides (A Literature Survey), Supplement 1", ibid. 1959.

(6) Reference 2, page 46.

(7) L. Pauling and L. O. Brockway, J. Am. Chem. Soc. 59, 13 (1937).

(8) R. L. Livingston and R. Rao, "Abstracts", 135th Meeting, American Chemical Society, 1958, p. 64R.

(9) T. B. Joyner, D. S. Stewart, and L. A. Burkardt, Anal. Chem. 30, 194, (1958).

(10) C. W. Bunn, "Chemical Crystallography", Clarendon Press, Oxford, 1946, page 367.

(11) "Gmelins Handbuch der anorganischen Chemie, Kobalt, Teil B: Die Ammine des Kobalts", System-Nummer 58, Verlag Chemie, Berlin, 1930, pages 9-45.

THE BEHAVIOR OF EXPLOSIVES AT VERY HIGH TEMPERATURES

Joseph Wenograd
U. S. Naval Ordnance Laboratory
White Oak, Silver Spring, Maryland

ABSTRACT: Recent work at the Naval Ordnance Laboratory has indicated that the impact sensitivities of organic high explosives are related in a simple manner to the velocities of their thermal decomposition reactions at very high temperatures, 300°-1000°C.

It has been possible, by means of a new experimental technique, to measure the time delay to explosion for a series of explosives in this hitherto unexplored range of temperature and reaction rate.

This has been accomplished by loading the explosive into fine hypodermic needle tubing which can then be heated, essentially instantaneously, by a capacitor discharge. The temperature and explosive event are recorded by monitoring the resistance of the tube.

The measured delay times are related to the impact sensitivities of high explosives as sensitive materials are found to explode more rapidly at a given high temperature than less sensitive ones.

INTRODUCTION

A wide variety of the physical, chemical and mechanical properties of an explosive determine the absolute value of its impact sensitivity (1,2,3). The author has proposed (4) that of these properties only one, the thermal decomposition velocity at initiation temperature, varies sufficiently among the organic high explosives to account for the differences in relative sensitivity which are observed. The explosives which are most sensitive also prove to be the ones which are least stable at very high temperatures.

High temperature thermal decomposition rates were estimated by extrapolations based on the most reliable values for the Arrhenius parameters of a series of explosives in the available literature. These parameters were obtained in isothermal studies of molten explosives carried out at relatively low temperatures. The direct observation of the behavior of explosives at very high temperatures would avoid reliance on a long extrapolation of low temperature measurements.

In the temperature and time range of interest in impact sensitivity studies, chemical decomposition is so rapid compared to the process of heat transfer as virtually to preclude any isothermal measurements on condensed explosives. Moreover, these temperatures are sufficient to cause the very rapid vaporization of most organic materials and the formation of an insulating layer similar to that supporting a drop of water on a hot skillet. Any experiment designed to ascertain the behavior of explosives in the temperature range 300°-1000°C must apply heat to the material very rapidly, yet hold the material under heavy confinement to prevent vaporization and to contain the material in the hot region.

Another method, apart from decomposition kinetics, which has been used to assess the stability of explosives has been the study of explosion induction times and their temperature dependence (5). Delays do not appear to have been measured for any explosives for times shorter than 0.1 seconds. There have been several attempts to relate these delay times to decomposition kinetics, none of which met with clear success.

This paper describes a new technique which permits the measurement of very brief delay times at high temperatures and considers the application of the measurements to the understanding of the sensitivity of explosives.

EXPERIMENTAL

The major difficulties hindering the observation of explosives subjected to very high temperatures have been overcome by enclosing them in lengths of fine stainless steel hypodermic needle tubing. The low heat capacity and rather high resistivity of the tubes permit them to be electrically heated to high temperatures very quickly. The explosive, being a non-conductor, is unaffected by the ohmic heating but is soon heated by conduction. The small, but significant, temperature coefficient of resistance of the material permits its temperature to be determined through a resistance measurement. The explosion of the contents of a tube can be observed by the change in resistance which it causes. Although the tubes are fine, their geometry and construction are such that they have considerable strength and are able to provide heavy confinement for the explosive. Moreover, the tubing proves to be sufficiently massive that its heat loss to the surrounding air is quite slow in the time scale of these experiments. The situation appears to correspond to the ideal case of an infinite cylinder of explosive at T_0, the surfact of which is heated to T_1 at zero time and maintained at this temperature. Thermal explosion equations have been solved with just these boundary conditions, but, as will be seen, the results do not seem to describe these experiments.

The explosives are loaded into #28 hypodermic needle tubing fabricated from type 304 stainless steel by the Superior Tube Company, Collegeville, Pennsylvania. This size has an outside diameter of 0.014 inches and an inside diameter of 0.007 inches. The individual experimental tubes are made by soft soldering the tubing to brass binding posts which can be mounted in the circuit with set screws. Before loading, the tubes are annealed to give a constant resistance. This is done by heating them to a cherry red heat by passing about 2 amps through them. The resistance of the tubes at room temperature (R_0) is determined by measuring the voltage drop across the tubing on passage of a very low current. The tubes are nominally two and one-half inches long between the binding posts and have a resistance of approximately 0.600 ohms.

The resistivity-temperature curve for these tubes was determined by measuring the resistance of tubes heated to known temperatures. This curve is shown in Figure 1. The square points represent temperature measurements made with thermocouples and resistances measured with a Wheatstone bridge. For the round points, the temperatures were measured with an optical pyrometer assuming an

FIGURE 1

$$\frac{R_1}{R_0}$$

○ Optical Pyrometer-Volts-Amps

□ Thermocouple Wheatstone Bridge

TEMPERATURE °C
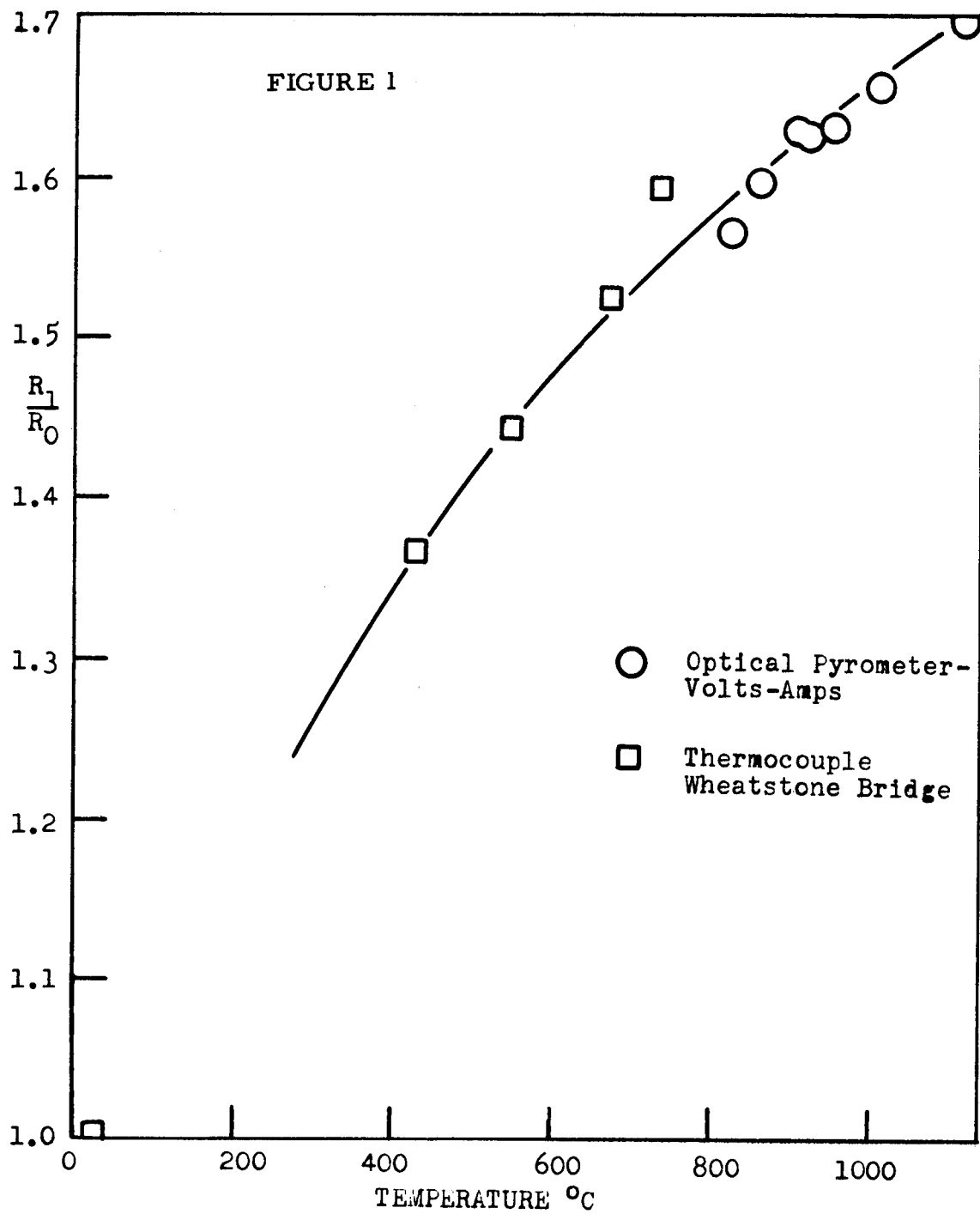
emissivity of 0.85 and the resistance values were obtained using a voltmeter and ammeter in a D. C. heating circuit.

In order to fill the tubes, they are prepared with one end open and one end closed*. The open end of the tubing is rested against the bottom of a small beaker containing a small amount of the explosive to be tested. Liquids are placed in a vacuum dessicator and solids in a vacuum oven regulated a few degrees above the melting point. The system including the tubes is then evacuated. Explosive is then forced into the tube by the readmission of air.

Of the explosives tested, only PETN and tetryl are markedly unstable at their melting points. It is felt, however, that the extent of decomposition in the roughly ten minutes they remain at elevated temperature is insufficient to affect these results.

The tubes are studied in the circuit shown schematically in Figure 2. The high voltage pulser consists of a high voltage power supply, which charges a 2 microfarad capacitor to voltages ranging to about 7 kilovolts, and a 5C22 thyratron for switching this charge. The capacitor discharges its energy through all three branches of the circuit, but because of the lower resistance of $R_1 + R_2$, the bulk of the current flows through this path. When the capacitor has finished discharging, the high voltage pulse represents an open circuit and only the simple Wheatstone bridge powered by E_b through R_A remains.

The unbalance voltage of the bridge which is related to the temperature of the tube under test is recorded on a type 535 Tektronix oscilloscope with a type D plug in unit and a DuMont type 2614 oscillographic record camera. Usable sweep rates for these experiments vary from 20 microseconds/cm to 10 milliseconds/cm. By means of a simple zero calibrating circuit, the scope scale has been expanded so voltages can be read to within 1 millivolt in the range 0-0.6 volts.

---

* Tubing can be cut without collapsing the walls if a sharp, scissors type of wire cutter is used. Diagonal or side cutters do a good job of sealing off the end of the tubing.
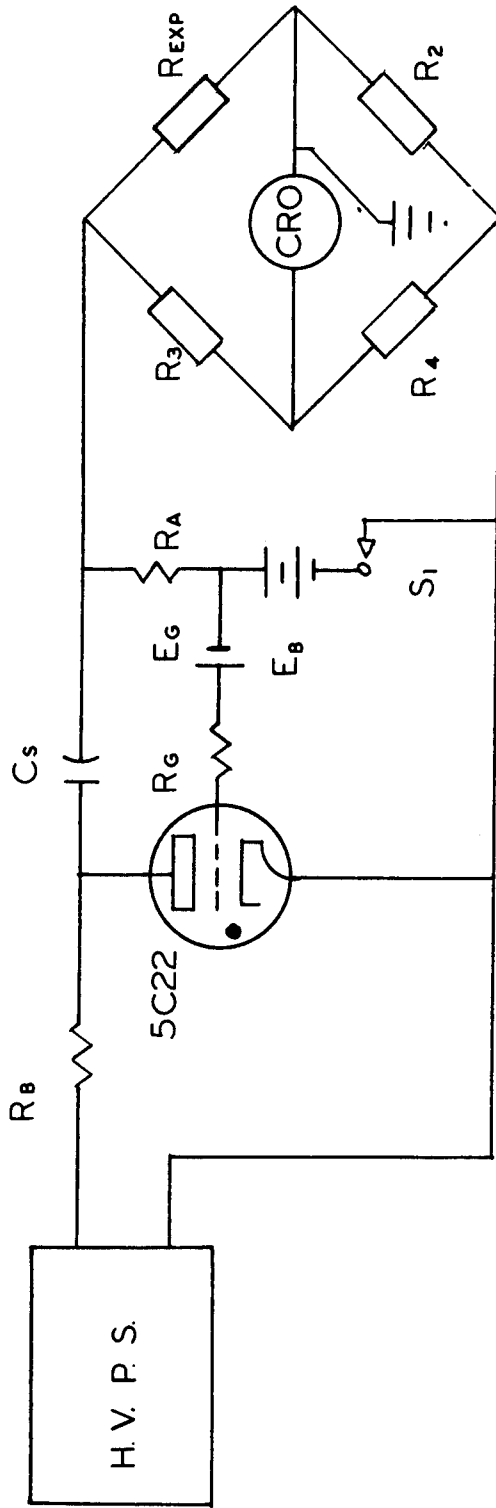
FIGURE 2

H. V. P. S.- High Voltage Power Supply and Associated
Circuitry

R₃= R₄   25 ohm non-inductive resistor

R_A 10 ohm non-inductive resistor

R_2 constantan resistor

R_{exp} tube under test ($R=R_0$ at room temperature,
$R=R_1$ at elevated temperature)

R_G 1000 ohm resistor

R_B 1 megohm resistor

E_G 7.5 volt battery

E_B 24 volt storage battery

S_1 mercury relay

C_s 2 microfarad capacitor

65

The resistance of the tube under test can be computed from the bridge output voltage E and the known parameters of the circuit using the expression

$$R_1 = \frac{25E_BR_2 + ER_AR_2 + 50ER_2 + 50ER_A}{25E_B - ER_A - 50E} \qquad (1)$$

The scope is triggered internally by the capacitor discharge. The discharge heats the tube close to its final temperature in about 20 microseconds. After the circuit has settled down, the value of E can be used to compute the temperature of the wire. When the material in the tube explodes, the tube is ruptured and its resistance changes in an abrupt manner which is clearly visible on the scope trace. The temperature just before this abrupt change is taken as the explosion temperature. The explosion time is the time at which the sharp break in the trace occurs minus the 20 microsecond heating time.

RESULTS AND DISCUSSION

For a given explosive, a plot of the logarithm of the time delay against the reciprocal of the absolute temperature is generally linear over a considerable range of temperatures. That is, the materials conform to the expression:

$$\tau = A\exp(B/RT) \qquad (2)$$

where τ is the time delay, T is the absolute temperature of the tube at the time of explosion and A and B are constants.

The explosives studied have been subjected to temperatures in the range 260°C to 1100°C and time delays varying between 50 milliseconds and 50 microseconds have been measured. The lower measurable time limit is determined by the duration of the capacitor discharge pulse. The measurement of times longer than 50 milliseconds is complicated by the cooling of the tubing and by the evaporation of the explosive out of the end of the tubes.

The results for two typical high explosives, 2,4,6-trinitrotoluene (TNT) and pentaerythritol tetranitrate (PETN), are shown in Figure 3. Despite the scatter, the results are fairly linear over the wide ranges of temperature studied. Figure 4 shows the results for 1,3,5-trinitrobenzene (TNB), di-β-nitroxyethyl nitramine (DINA) and nitroglycerine (NG). Again, the results appear linear over the range of study. The coefficients A and B obtained for all the explosives studied are included in Table I.

FIGURE 3

FIGURE 4
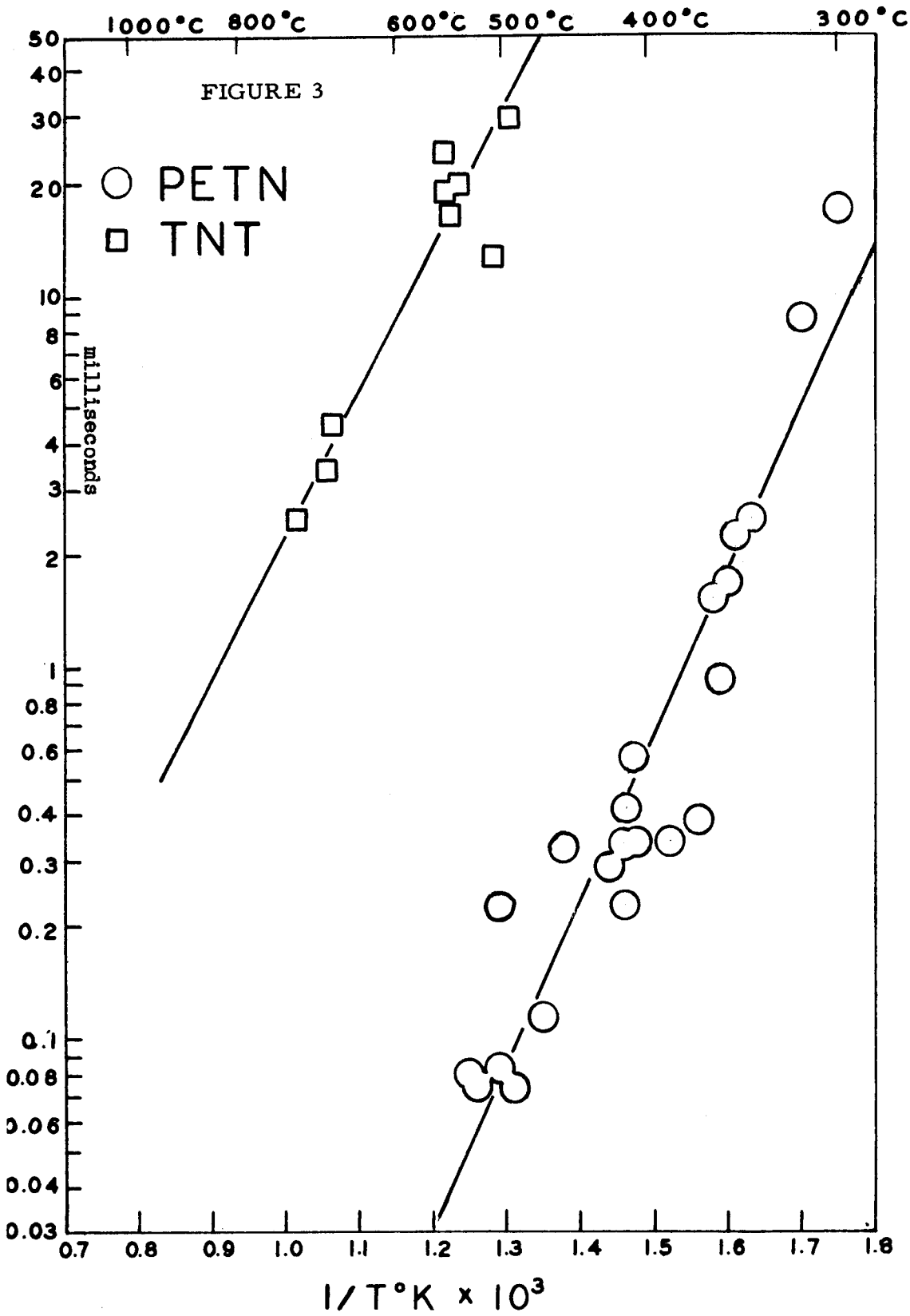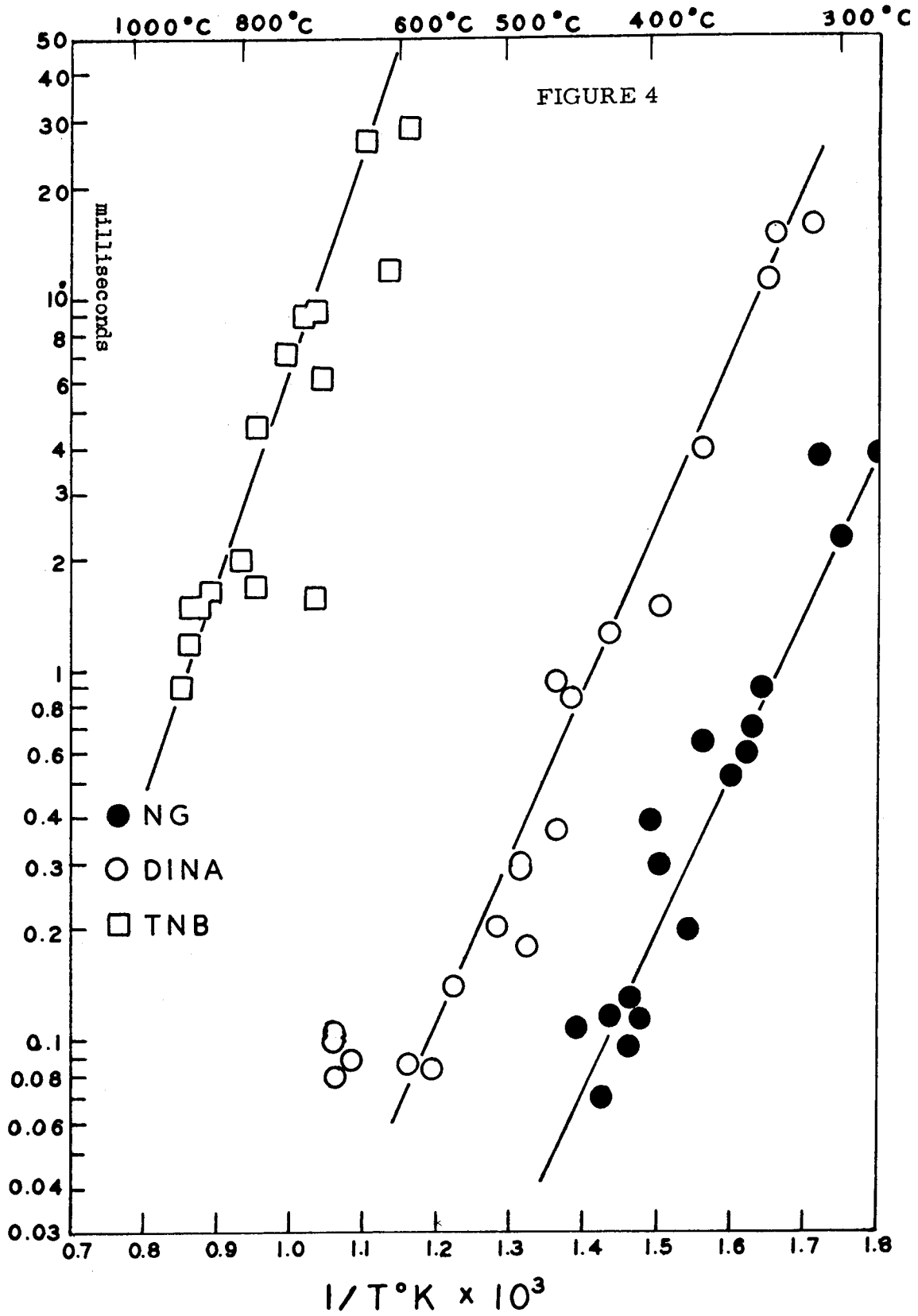
TABLE I

Explosive	Impact Sensitivity 50% ht. cm. 2.5 Kg. weight	A	Bx10^{-3}	Literature Values for E* kcal/mole	Critical Temperature for Explosion in 250 Microsec. °C
Nitroglycerine	4-8	-10.8	21.8	48.0 (10)	390
PETN	13	- 9.9	20.4	47.0 (10)	430
BTNEN	11	- 9.8*	20.2*	42.5 (11)	440*
TNETB	18	- 9.5*	21.0*	43.4 (12)	500*
DINA	30	- 9.3	20.5	49.8 (11)	510
DNPTB	32	-11.9*	28.4*	-	830**
Tetryl	36	- 5.7	11.1	38.4 (13)	880
Trinitrobenzene	100	- 7.9	26.3	-	1060
TNT	160	- 6.6	18.0	43.3 (14)	1040

* Values refer to low temperature portion of curve.

** Values refer to high temperature portion of curve.

The slopes of the delay time-reciprocal temperature curves reported in Table I (B values) may be regarded as adiabatic activation energies for the compounds studied. These results are comparable to those obtained by others doing measurements at lower temperatures (5). Cook (7) and Zinn and Mader (8), who have integrated the equation which Frank-Kamenetskii (9) proposed to describe the development of thermal explosions, predict that this adiabatic activation energy should correspond to the activation energy of the heat producing thermal decomposition reaction. Isothermal gas evolution or weight loss measurements generally yield values for the activation energy of the thermal decomposition of explosives in the range 30-60 kcal/mole. There is a suggestion in Table I of a rough relationship between the adiabatic and the isothermal activation energies. The two sets of data do not correspond. The reasons for this discrepancy are at present obscure.

An unexpected phenomenon has come to light in the course of experiments with three explosives containing the terminal trinitromethyl group. This is illustrated in Figure 5 which shows experimental points for 2,2-dinitropropyl 4,4,4-trinitrobutyrate (DNPTB) in #28 hypodermic needle tubing. There is a definite inflection with comparatively little scatter in the middle of the range of accurate measurements. Similar but more pronounced inflections have been observed for 2,2,2-trinitroethyl 4,4,4-trinitrobutyrate (TNETB) and bis-(2,2,2-trinitroethyl) nitramine (BTNEN). In fact, in these cases, there is evidence of an upward turn in the explosion delay times above the inflection temperature.

It appears that the behavior of these explosives at temperatures below the inflection point govern their sensitivity. Thus the A and B values in Table I refer to the lower temperature portions of the curves for these materials. It is extremely unlikely that these inflections reflect any basic change in the chemical kinetics of the decomposition process. Any such change would require that a process of higher activation energy become rate determining above the inflection temperature. This should lead to greater slopes for the time-reciprocal temperature curves rather than the lower slopes which are observed.

Experiments in which the diameter of the steel tubing is varied show drastic changes in the higher temperature portions of the plots. When smaller sizes of tubing are employed, suggestions of humps in the curves vanish. The lower temperature portion of the curves and the points of

FIGURE 5
DNPTB
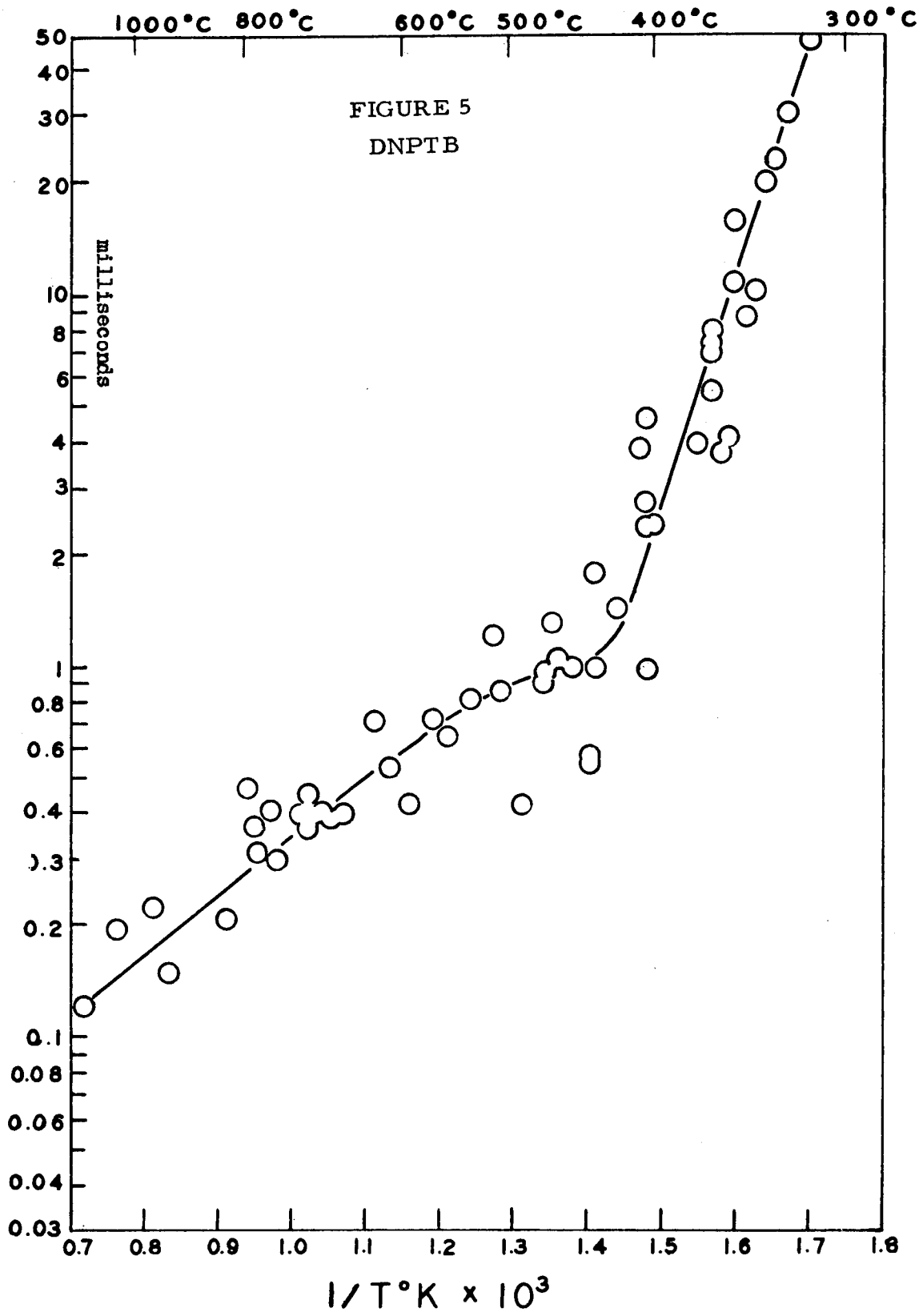
inflection do not seem to vary with tube size. It is possible that inflections of this nature occur with other explosives outside the time ranges measured.

The proposal that the high temperature decomposition velocity is the most important factor determining the relative impact sensitivity of an explosive can now be tested. The hot tube experiments employ a purely thermal initiation process and none of the mechanical properties of the explosive can influence the result. If a scale of sensitivities based on the hot tube experiments can be established which corresponds with the scale observed in impact testing, it would imply that the effect of differences in mechanical properties on relative impact heights might be regarded as being of lesser importance.

One would expect more sensitive explosives to explode more rapidly at a given high temperature than less sensitive ones. Thus, in a graph such as Figure 6 it would be expected that the sensitive explosives would tend towards the lower right-hand corner. In going towards the upper left, lines representing successively less sensitive materials would be intersected. The impact sensitivities of the explosives represented in Figure 6 are reported in Table I. It can be seen that the more sensitive materials do indeed explode more rapidly and at lower temperatures than insensitive ones.

In an impact experiment there is a rather short period of time during which the explosive is heavily confined. In order for an impact explosion to occur, the initiation of the reaction must occur before the pressure is released by the rebound of the tools. Warner and Smith (6) have measured the duration of impact by studying the variation with time of the pressure in the anvil of an impact machine similar to that employed at the Naval Ordnance Laboratory. The found that the anvil was under pressure for about 250 microseconds although the presence of a sample complicated the picture somewhat. The ease of initiating impact explosions can thus be related to the ease of forming centers capable of build-up in 250 microseconds or less. For each explosive there is a temperature above which initiation in hot tubes occurs within this interval. These critical temperatures are recorded in Table I.

A plot of these critical temperatures against impact sensitivities is shown in Figure 7. With the exception of the values for tetryl and DNPTB,the data are seen to fit a smooth curve fairly well. Both of the explosives which deviate have low slopes which render their critical
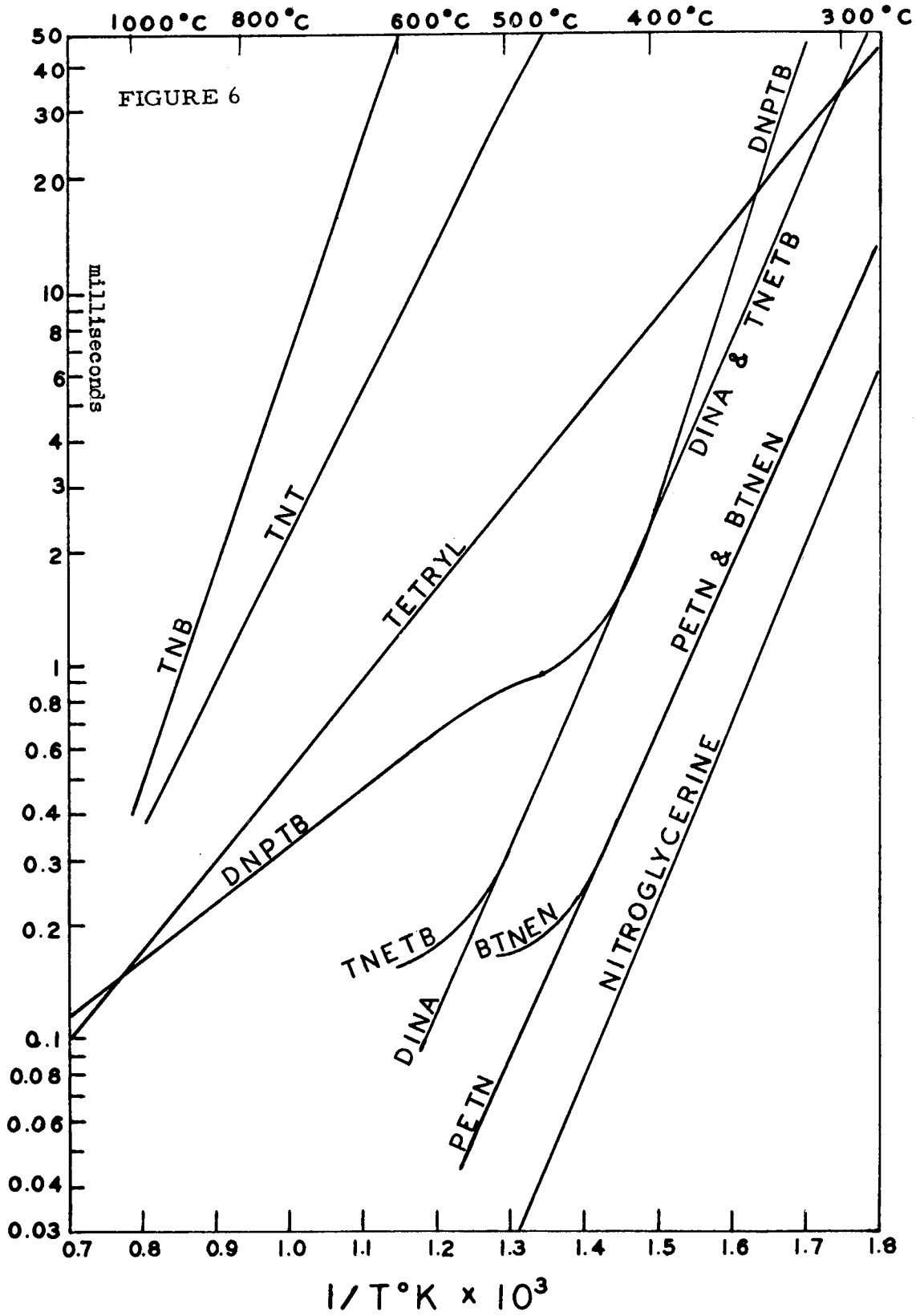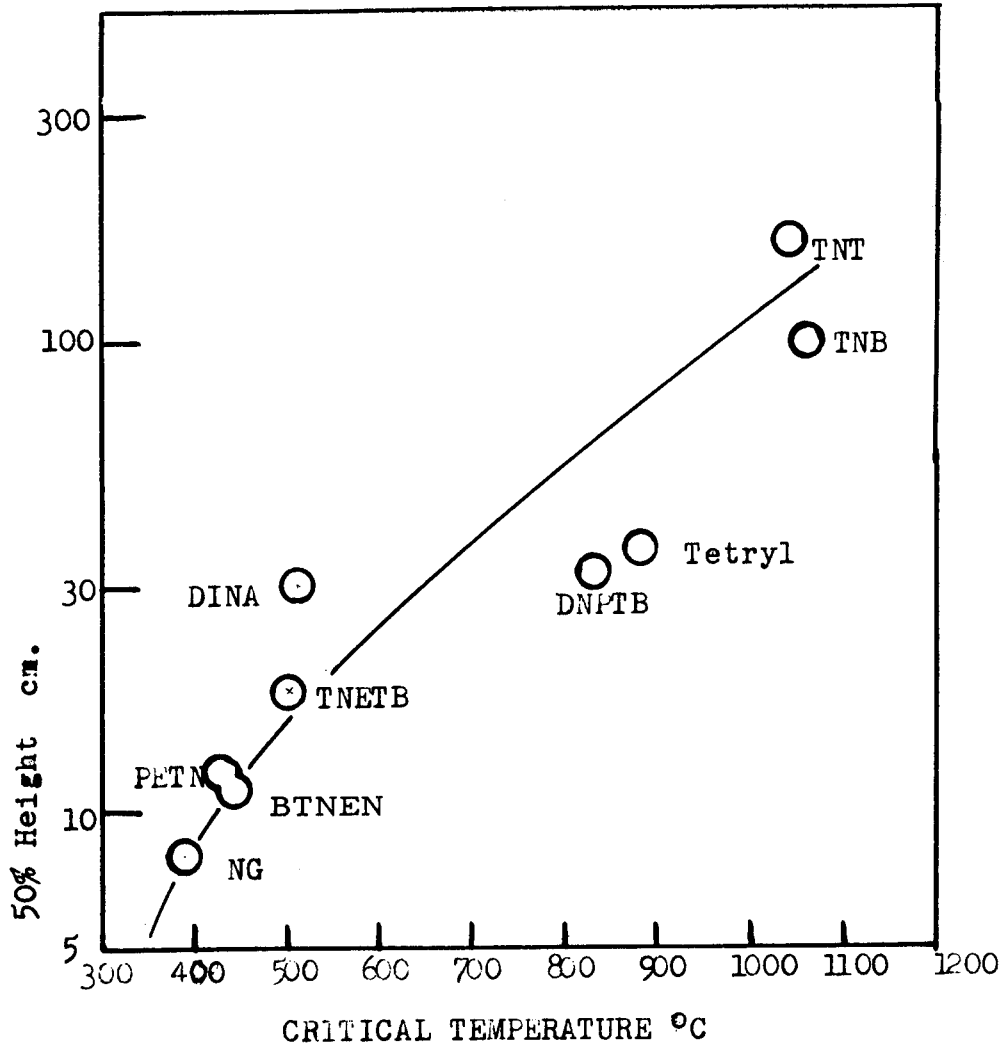
FIGURE 6

FIGURE 7

temperatures particularly sensitive to the selection of
the confinement interval. The agreement which exists
serves to corroborate the view that the relative sensi-
tivities of organic high explosives are determined
largely by their thermal decomposition rates at high
temperatures.

ACKNOWLEDGMENT

BIBLIOGRAPHY

(1) F. P. Bowden and A. D. Yoffe, "Initiation and Growth of Explosions in Liquids and Solids", University Press, Cambridge, 1952.

(2) E. K. Rideal and A. J. B. Robertson, Proc. Roy. Soc., A $\underline{195}$ 135 (1948).

(3) J. L. Copp, S. E. Napier, T. Nash, W. J. Powell, H. Shelley, A. R. Ubbelohde and P. Woodword, Phil. Trans. Roy. Soc. A $\underline{241}$, 197 (1948).

(4) J. Wenograd, NavOrd Report (NOL) 5730, "The Correlation of the Impact Sensitivity of Organic High Explosives with their Thermal Decomposition Rates", 30 September 1957.

(5) H. Henkin and R. McGill, Ind. Eng. Chem. $\underline{44}$ 1391, (1952).

(6) L. C. Smith and R. F. Warner, Private Communication.

(7) G. B. Cook, Proc. Roy. Soc. A $\underline{246}$, 154 (1958).

(8) J. Zinn and C. L. Mader, J. App. Phys. $\underline{31}$, 323 (1960).

(9) D. A. Frank-Kamenetskii, Acta. Physiochim, U.R.S.S. $\underline{10}$, 365 (1939).

(10) A. J. B. Robertson, J. Soc. Chem. Ind. $\underline{67}$, 221 (1948).

(11) J. Wenograd, unpublished results.

(12) A. D. Little Inc. Private Communication, April 1954.

(13) A. J. B. Robertson, Trans. Faraday Soc. $\underline{44}$, 677 (1948).

(14) M. A. Cook and M. T. Abegg, Ind. Eng. Chem., $\underline{48}$, 1090 (1956).

THE RAPID BURNING OF SECONDARY EXPLOSIVES BY A CONVECTIVE MECHANISM

John Watson Taylor
Atomic Weapons Research Establishment
United Kingdom Atomic Energy Authority
Aldermaston Berkshire
England

Summary

Rates of burning of PETN, RDX and HMX powders have been measured in a strand burner at elevated pressures. Some of the rates were remarkably high compared with the remainder which were low values typical of burning rates of high density explosives. The high rates correspond to flames which propagate by a convective mechanism in which the hot product gases are driven by the pressure gradients which they produce, into the porous solid. The slow flames remain on the surface of the mass of powder which becomes melted to form a continuous molten layer just ahead of the burning zone so that there is no possibility of gas penetration into the solid beyond. For any given powder there is a certain transition pressure below which it burns in the slow manner and above which it burns by the convective mechanism. Increasing the pressure up to the transition value is presumed to have the effect of thinning the molten layer until it is too thin to maintain a continuous coverage over the pores; convective burning then sets in. To reach this stage requires higher pressures if the pore size is small or if the explosive is one which, in general, burns with a thick molten layer. The relevance of these results to the development of detonation in solids is discussed.

Introduction

In any description of the processes by which the burning of an explosive medium may lead to the development of a detonation wave in the medium, it is necessary to explain how the pressure can rise rapidly enough to enable the extremely high detonation pressure to be reached in the face of the ever present pressure dissipating tendencies. This means that it is necessary to show how the rate of burning can be very great especially in the early stages of the pressure rise whilst the pressure is still relatively low and when a very large rate of burning cannot be expected from pressure considerations alone. Rates of burning are increased by increase of temperature or by the presence of certain catalysts but the effects are comparatively small and virtually the only way by which a given explosive medium can burn at a very large rate at moderate pressures is by the

burning occuring over a large specific surface area. This can arise in gases and liquids by the burning zone becoming turbulent. The present paper is concerned with showing how a large (internal) burning surface can arise in solids.

Assuming that an explosive mass becomes ignited at one end, then if this mass is completely impermeable and remains so, it must be presumed impossible for the burning at the end to produce burning over a large internal surface of the mass by any means other than such compression as the end-burning can generate. If the end-burning occurs under highly confined conditions the pressure produced may be sufficient to produce internal ignition by compression in explosive having suitably susceptible centres at which reaction can develop, and there appears to be some evidence that this can happen (1). Often, however, as for example in considering the safety of explosives, interest is focussed on the possibility of detonation developing in the absence of heavy confinement and in this case the pressure which could be developed by end-burning alone must be very much less and may be assumed to be inadequate to lead to internal ignition by compression of the explosive. In such cases therefore, an impermeable explosive which remains impermeable cannot be expected to burn over any but a small area of its outer surface and so has no means of developing really high pressures and cannot therefore be expected to develop a detonation wave from a simple ignition.

A different state of affairs exists when the explosive mass is permeable, as with powders or low density pressed explosive, or can become permeable as when a charge is damaged by crushing. In these cases it is possible to imagine that burning which starts at one end of the permeable mass might under some conditions be able to spread into the pores and propagate rapidly along them leading to burning over a very large internal surface. This type of burning seems first to have been considered by Andreev (2) who supposed that, in his experiments on burning to detonation in tubes, burning over an enlarged surface area must have arisen by a process of gas flow into the pores of the solid, i.e. by a convective mechanism. See also ref. (3). The present work establishes the reality of this type of burning and also elucidates some of the conditions which must be satisfied before it can occur.

Measurements of Burning Rates

Burning rates of compacted explosive powders were measured at elevated pressure in a strand burner either by a fuse wire technique using electric stop clocks, or by high speed cine photography. The explosive powder, PETN, RDX or HMX, was lightly pressed in increments into six millimetre bore tubes of paper or perspex having respective wall thicknesses of 0.002 inch and 0.198 inch. The paper tubes were formed from a single sheet of paper with a cemented seam down one side and a plastic plug of the same diameter was cemented into them to form a base. During burning, the paper burned down just above the flame front but because of the construction, the remainder of the tube cannot be thought of as having been gas tight. The types of perspex tube assemblies which were used are illustrated in figure 3. The incremental pressing of powder into these tubes was

actually carried out with the tube inverted and using a detachable base; this was in order to ensure identical pressing with both open and closed ended tubes. The strand burner, shown in figure 1, is a development of that which was described by Crawford (4) and is essentially a pressure vessel, with internal dimensions 3 inches diameter by 24 inches, and into the bottom of which a tube of the explosive was mounted. Slot windows on either side of the burner allowed the burning explosive to be photographed, and electrical leads through the end-cap at the bottom of the burner allowed current to be passed when the fuse wire technique was used. The burner was connected through a wide bore tube to a gas cylinder, which was large enough to ensure that the pressure remained constant during burning. This combined system was pressurized with nitrogen before an experiment and then isolated. Ignition of the explosive was accomplished by means of a hot wire via a small piece of cordite.

Results and Discussion

The most striking result of the study of the burning rates of low density PETN, RDX and HMX was that it was observed that in each case, some of the flames propagated remarkably rapidly compared with the remainder which corresponded to mass burning rates typical of high density explosives in the same pressure region i.e. of the order of 1 g.cm.$^{-2}$.sec^{-1}. This can be seen in table I which presents the few results which have been obtained for PETN and RDX, and in figure 2, which gives the results of a much more extensive investigation with HMX. The slow burning results for the latter lie on the gently sloping line near the bottom of figure 2 and it can be seen that for any given particle size of powder, slow burning always occurs at low enough pressures but that as the pressure is raised the powder will begin to burn much more rapidly above a certain transition pressure.

Table I   Burning Rates of PETN and RDX

(Standard deviations in brackets)

Explosive	Method	Density g.cm^{-3}	Pressure p.s.i.g.	Apparent Mass Burning Rate g.cm^{-2}.sec^{-1}.
PETN, 500–853 micron	As in fig.II(c)	0.928	375	0.544 (.011)
" "	"	0.918	375	0.531 (.006)
" "	"	0.936	450	8.86 (.17)
" "	"	0.912	525	13.9 (.53)
" "	"	0.939	750	47.7 (.56)
" "	"	0.917	750	59.0 (.70)
RDX, approx. 5 micron	Paper tube	1.07	750	1.66 (.08)
RDX, approx. 200 "	"	1.16	750	33.3 (3.9)

The essential features of the rapid flames and of the slow flames, and the significance of the transition pressures at which the one type of burning changes to the other, are discussed in the following

STRAND

A

O-RING

FIG. 1 Strand Burner

SIDE ELEVATION OF WINDOW

LOOKING IN DIRECTION OF ARROW A.
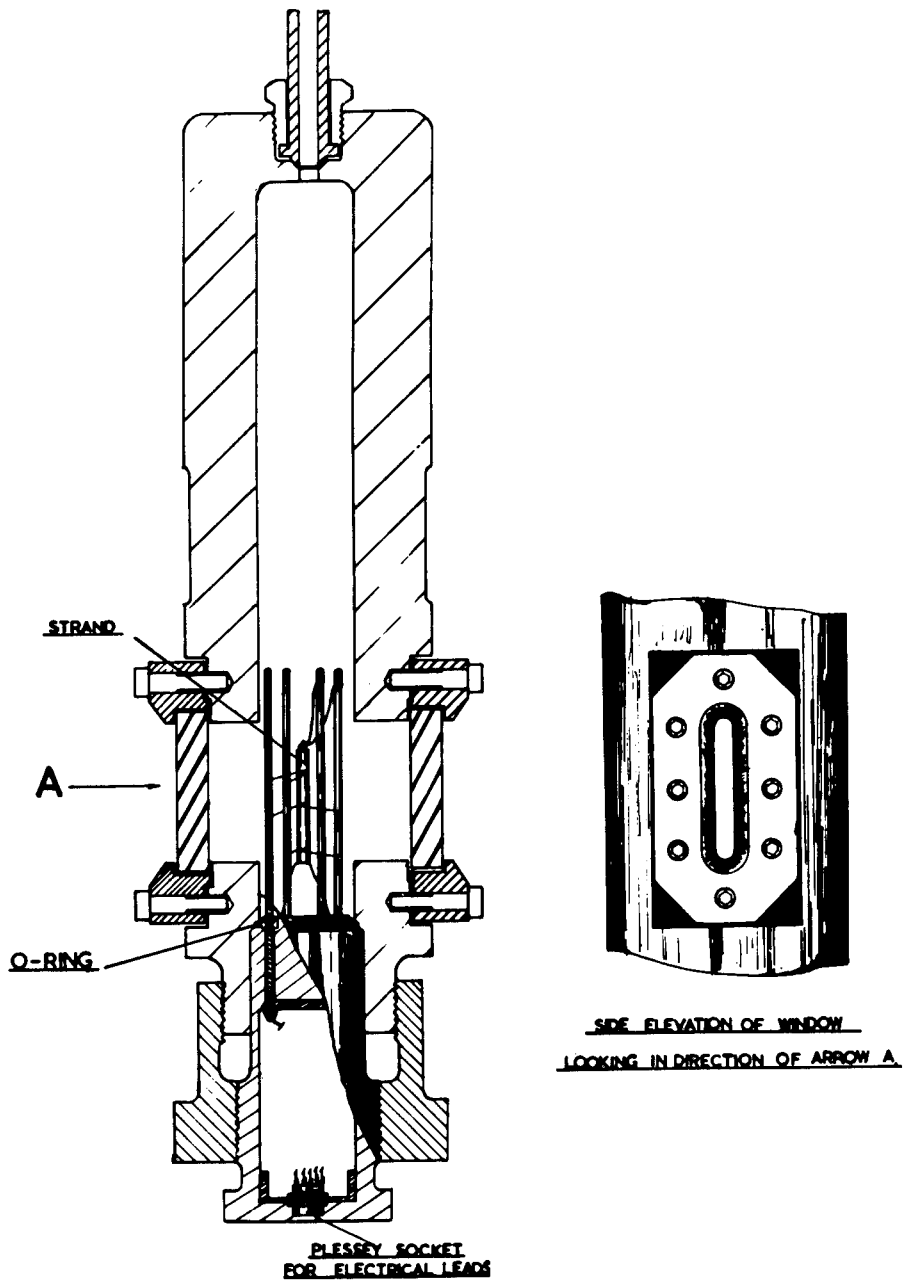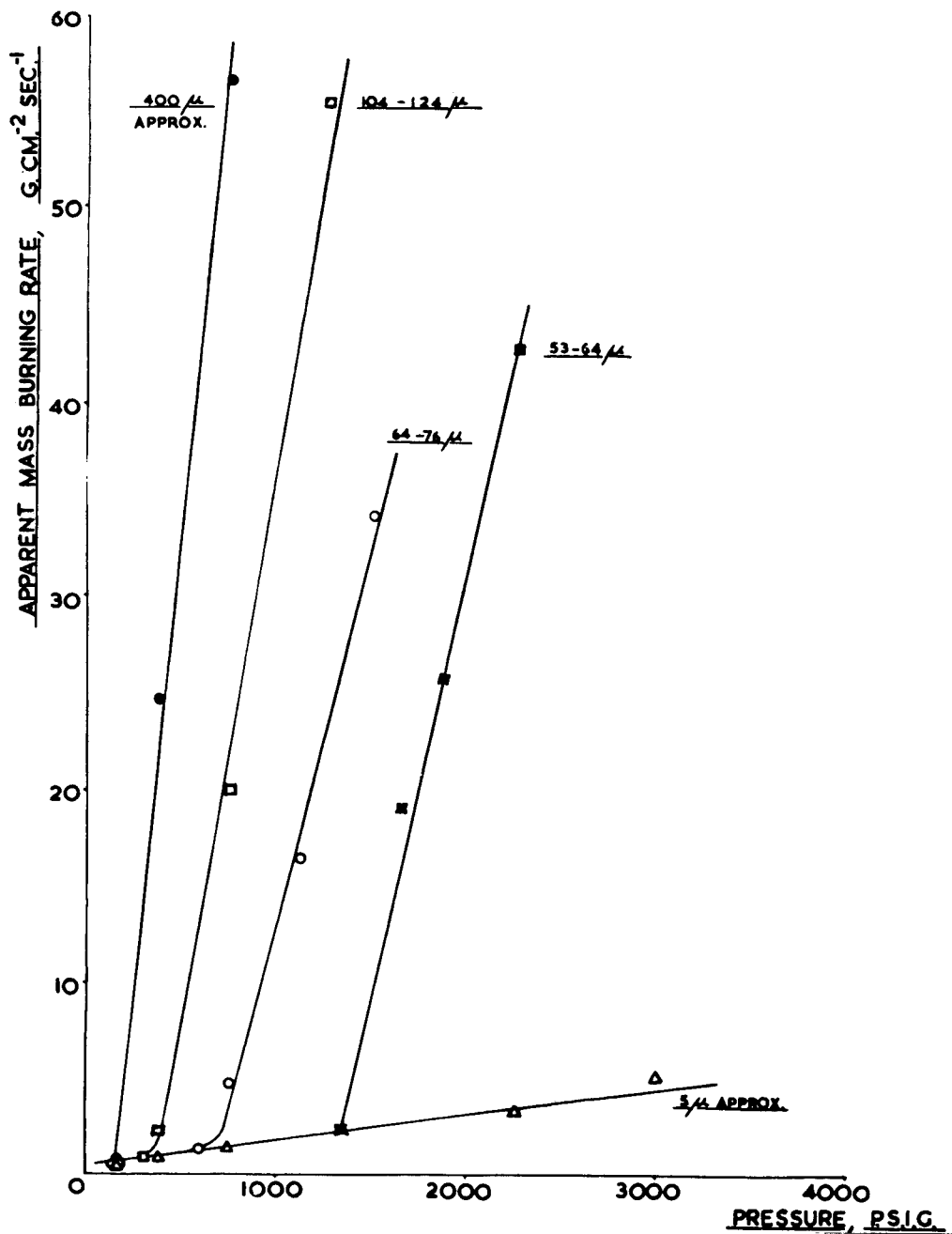
FIG. 2 Burning rates of pressed HMX powder at various pressures
(paper tube method).
Mean loading densities 1.20, 1.05, 1.07, 1.08 and 1.02.
respectively for 400μ, 104-124μ, 64-76μ, 53-64μ
and 5μ powders.

sections. High speed cine photographs of the burning strands of PETN, RDX and HMX could not be distinguished from one another in their qualitative features either as regards the rapid flames on the one hand or the slow ones on the other, and although most of the subsequent discussion is confined to HMX, there is no reason to believe that it would not apply equally well in its qualitative aspects to PETN or RDX or indeed to any secondary explosive compound.

(a) Rapid burning

On cine films of the rapid flames the particles of explosive could be seen to be loosened up to form a fluidised mass just ahead of the flame front and in the flame front the particles could be seen to begin to rise along with the product gases, burning as they accelerated upwards. This is considered to be direct evidence that the rapid flames involve the explosive burning over the large area within the pores of the powder. In the case of the coarser powders, the particles were finally ejected from the gas stream and could be partially recovered at the bottom of the burner after an experiment.

The way in which the rapid flames propagate along the explosive column was investigated by experiments in which the flow of the product gases out of the perspex containing-tube was slightly restricted by a small reduction of the area of the tube outlet to form a convergent nozzle. A diagram of the tube assembly is given in figures 3 (a) and (b) and typical results are illustrated by curves (a) and (b) in figure 4. It can be seen that a greater flame speed is obtained over most of the length of the tube when the product gas stream passes through a convergent nozzle than when a blank nozzle is used and moreover in both cases the flame speed is greater the nearer the flame gets to the lower end of the tube.

These results are interpreted as being effects of changing pressure gradients. Thus, the lower ends of the tubes must remain at ambient pressure whilst, as in all simple flames, the pressure in the region of the flame front will be greater than the ambient pressure by a certain amount (which may be called the dynamic pressure). There must therefore be a pressure gradient between the flame front and the lower end of the tube and this pressure gradient will be greater the greater the dynamic pressure (which is increased by the convergent nozzle), or the nearer the flame front is to the lower end of the tube. The effect of these pressure gradients will be to cause the nitrogen gas initially present in the pores of the powder to be flowing towards the lower end of the tube at a rate which increases with the pressure gradient. Any hot product gas ahead of the position of peak pressure would likewise flow along with the nitrogen and would be expected to ignite the pore surfaces as it advanced thus leading to the flame advancing more rapidly when the pressure gradient was greater, due to the presence of a convergent nozzle, or due to the flame being nearer to the lower end of the tube. This is clearly a satisfactory explanation of the principal features of curves (a) and (b) in figure 4 and shows that the mechanism of flame propagation is essentially a convective one, the flame being a process of rapid flow of hot product gas into the permeable solid, igniting it as it goes and displacing the gas initially present in the pores and setting it flowing ahead. This general conclusion is supported by
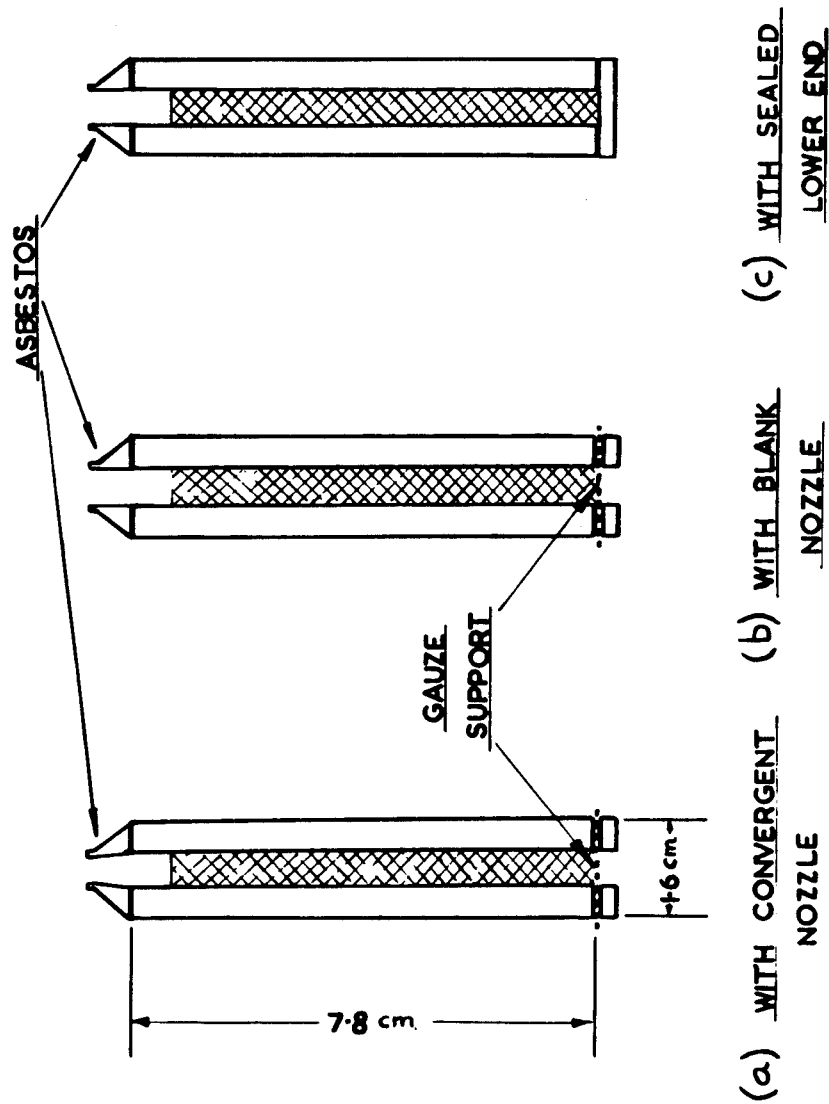
FIG. 3   Perspex tube assemblies containing explosive
powder for burning velocity measurements.

(a) WITH CONVERGENT NOZZLE   (b) WITH BLANK NOZZLE   (c) WITH SEALED LOWER END

ASBESTOS

GAUZE SUPPORT

7·8 cm.

·6 cm
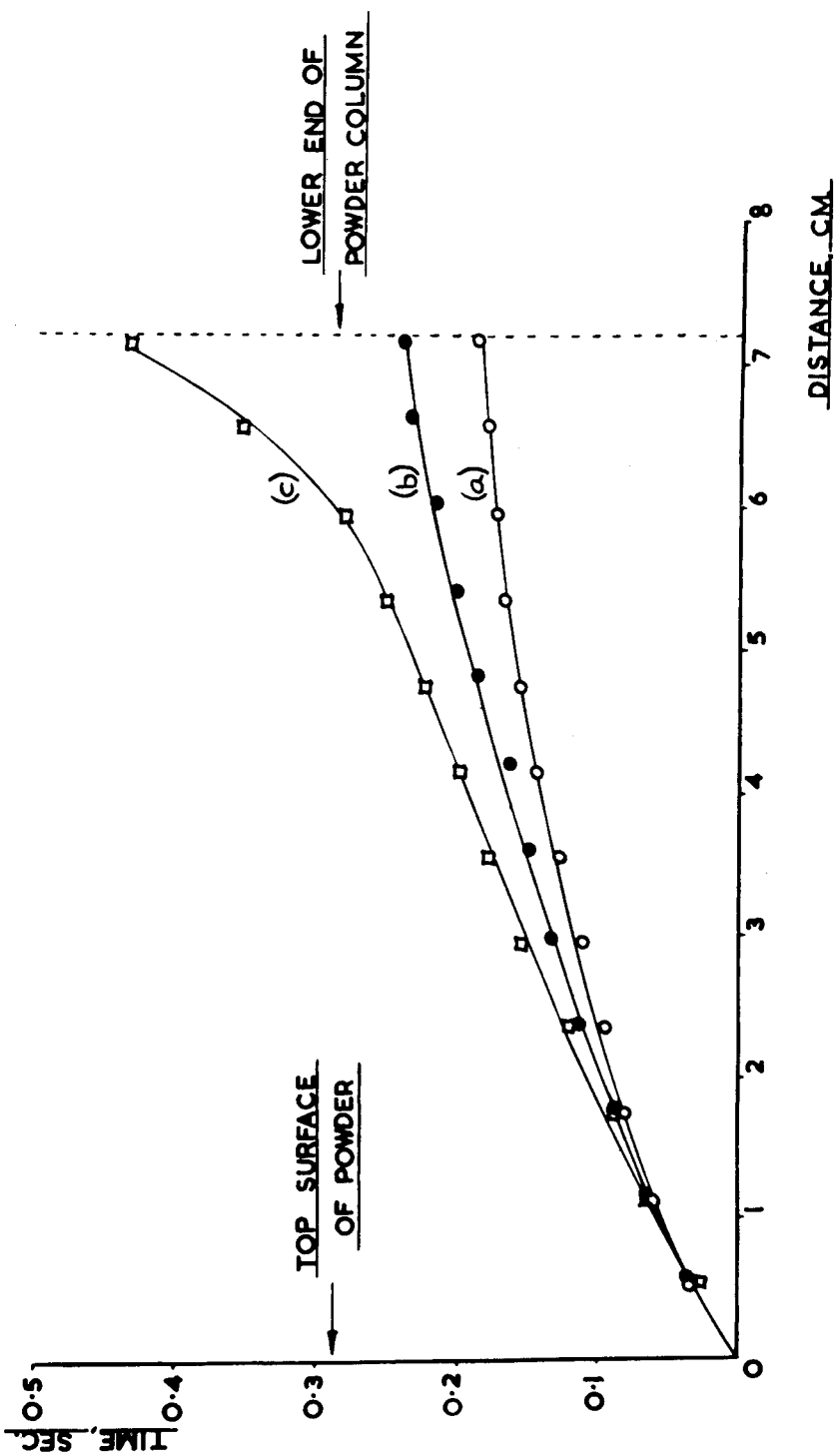
FIG. 4   Distance-time plots of the flame front for HMX loaded
into the corresponding tubes shown in figure 3.   Nitrogen
pressure 375 p.s.i.g., approximate particle size 400 microns,
loading density 1.08 g.cm^{-3}.

results of similar experiments which were carried out using perspex
tubes which were closed and gas-tight at the lower end, as shown in
figure 3 (c). A typical result is given in curve (c) of figure 4.
In contrast to curve (b) in the same figure, it can be seen that there
is now no continuous increase in flame speed as the flame advances,
corresponding to the fact that there is no reason why the pressure
should remain at ambient at the lower end of the tube and in fact the
pressure at the end of the tube must slowly rise due to the accumula-
tion of nitrogen which has been displaced by the flame from the upper
parts of the tube. The absence of a constant pressure condition at
the lower end of the tube makes a more detailed interpretation of
curve (c) rather difficult, but it is very likely that the advance of
the visible flame in this case depends in part upon other effects such
as diffusion, especially as the flame approaches the lower end of the
tube.

It is important to note that the convergent nozzle would
produce only a very small increase in the total pressure in the
perspex tube. This can be seen from the fact that the dynamic
pressure corresponding to curve (b) would be roughly a quarter of an
atmosphere and also that the throat area in the convergent nozzle used
was 0.51 of the tube cross sectional area and corresponds to an
increase in dynamic pressure by a factor of only four, as estimated
on the basis of frozen-equilibrium flow. The convergent nozzle would
therefore only increase the total pressure by about three quarters of
an atmosphere, at an ambient pressure of about 25 atmospheres. This
calculated effect of the convergent nozzle is assumed to give the
correct order of magnitude for the pressures which must have been
present during actual experiments, and using these values, the
increase in flame speed which could be accounted for simply by an
increase in the total pressure in the tube would be less by a power
of ten than that actually observed. This emphasises the importance
of pressure <u>differences</u> in this type of flame.

(b) <u>Slow burning and the significance of transition pressures</u>

It is clear from Table I and figure 2 that a low density
powder does not always burn rapidly by the convective mechanism
described above but that it may burn at low rates typical of high
density explosives. Cine films of powders burning at these low rates
show that the flame front is essentially flat with no sign of the
fluidised appearance referred to in connection with the rapid flames,
and related work by the author has shown that when burning occurs at
these low rates a molten layer of explosive is present in the burning
zone. The latter fact has the result that the mass rate of burning
equals that for high density explosive burning under the same condi-
tions. It also suggests that the main difference between the condi-
tions which lead to the convective type of burning and those leading
to the slow type of burning rests upon whether the conditions are
such as to allow an incipient molten layer to be continuous and so
lead to slow burning by preventing the flame gases having access to
the pores of the solid, or whether such a continuous molten layer
would be unstable, in which case convective burning should set in.

---

* To be published

On this basis a transition from slow burning to convective burning
would be expected when the conditions had been changed sufficiently
to make it just impossible for the molten layer to remain continuous.
This is presumed to be the case under the conditions at each of the
bends of the curves shown in figure 2. It will be noted from this
figure that the transition pressure corresponding to each of the bends
is greater the finer the particles and since the loading density is
approximately constant, this means that the transition pressure
increases with decrease in pore size. A plausible explanation of
this variation can be based on a consideration of molten layer thick-
ness. Thus, because of the steady increase in (slow) burning rate
with pressure, the preheating zone and therefore the molten zone will
get thinner as the pressure is raised, and a stage will be reached
when the molten zone is just too thin to form a continuous layer over
the pores of the powder so that the pores are exposed to the flame
gases and convective burning is possible. If the pore size of the
explosive is less, then a greater pressure must be applied to the
explosive before the molten layer is thin enough to be inadequate to
cover the pores, i.e. for smaller pores the transition pressure should
be greater; this agrees with the facts.

   An important consequence of this explanation is that if two
different explosives burn with different molten layer thicknesses at
the same pressure, then under the same conditions of particle size
and loading density a greater transition pressure would be expected
for the explosive which burns with the thicker molten layer. Now the
molten layer in burning PETN is almost certainly thicker than that of
HMX because of the big difference between the melting points (140°C
and 278°C respectively) and so a greater transition pressure would be
expected for PETN than for HMX under the same conditions. This is
confirmed by the results in table I and figure 2 which show that the
transition pressure of 500-853 micron PETN is about 400 p.s.i.g.
whereas that of the same particle size of HMX would be below the
value of 150 p.s.i.g. obtained for the transition pressure of HMX
of approximately 400 micron particle size, the latter statement being
based on the previously described evidence that the transition
pressure of HMX decreases with increase in particle size. It there-
fore seems very likely that the explanation of transition pressures,
based on the variation of molten layer thickness in relation to pore
size, is correct.

Conclusion
   The importance of burning over the internal surface of a
solid explosive in facilitating the development of detonation was
discussed in the introduction. It has been shown that such internal
burning can arise by the convective spreading of flame from the surface
of an explosive mass into its interior at a rate which increases with
the pressure gradient just ahead of the flame front, and therefore,
in most practical cases, with the pressure in the flame. It has also
been shown that melting of the explosive may prevent this spreading
if the pressure at the burning surface is below a certain transition
pressure, the value of which depends upon the porosity of the explo-
sive. Experiments have not yet been carried out to see to what
extent melting can prevent the onset of convective burning when there

is a large pressure difference across the liquid film as would tend to
be the case in more practical situations such as the ignition of a
locally confined region of an explosive mass. However assuming that
the general behaviour would be the same in these cases, the effect of
melting should be to prevent, or greatly reduce the chance of, the
development of detonation provided the pressure remained below an
appropriate transition pressure. If the effective confinement were
such that the pressure could exceed the transition pressure, detona-
tion would be much more likely to develop.

Acknowledgments

The author would like to thank his colleagues, especially
Mr. G. P. Cachia, for the benefit of stimulating discussion. Experi-
mental assistance was provided by Mr. A. R. Evans and Mr. E. G. Baker.

References

1. A. Maček, J.Chem. Phys. 31, 162, (1959)

2. K. K. Andreev, Compte rend.acad.sci. URSS, 29, 469 (1940)

3. N. Griffiths and J. M. Groocock, A.R.D.E. Report (MX) 5/59,
   (Unclassified)

4. B. L. Crawford, C. Huggett, F. Daniels and R. E. Wilfong,
   Analytical Chem. 19, 630, (1947).

ELECTRICAL INITIATION OF RDX

G. M. Muller, D. B. Moore, and D. Bernstein
Poulter Laboratories, Stanford Research Institute
Menlo Park, California

The object of this paper is to present the principal results obtained in the course of two different studies of the electrical initiation of RDX*. The first of these studies[1] was concerned with the initiation of loosely-packed, powdered RDX by a bridgewire; in the second,[2] initiation of pressed pellets of RDX was achieved by incorporating in each pellet a central core consisting of an RDX-graphite mixture through which current could be passed. The results from the two sets of experiments illustrate the overwhelming importance which the state of aggregation of the explosive plays in determining, not merely the minimum energy required for initiation, but also the nature of the explosion which follows successful initiation.

I BRIDGEWIRE INITIATION OF POWDERED RDX

A. APPARATUS AND PROCEDURE

The various types of charges and bridgewire arrangements used are shown in Figure 1. The charge was assembled by placing a lucite plate of the appropriate type on one of the metal cover plates, filling the resulting cavity with powdered RDX, and completing the assembly as shown in Figure 1(a). A charge of type B3, already loaded with RDX but prior to final assembly, is shown in Figure 2. (Note the dab of silver ink used to hold the bridgewire in place.) All lucite plates were 1/4 inch thick; the remaining dimensions (w and ℓ in Figure 2) of each charge used will be indicated whenever appropriate. The cover plates were of 3/16-inch steel or aluminum; in addition to confining the charge on top and bottom, they provide electrical contact to each end of the bridgewire whose effective length, with the charge fully assembled, is thus equal to the thickness of the lucite plate.

In most of the shots reported, the grain size of the RDX used was about 80 to 100 μ; inadvertently, some of the charges probably consisted of 100 to 300 μ material. Except for an occasional

*Throughout this paper, the term "RDX" refers to the pure (unwaxed) material.

(a)

(b)

TYPE A

TYPE C

(1)   (2)   (3)   (4)
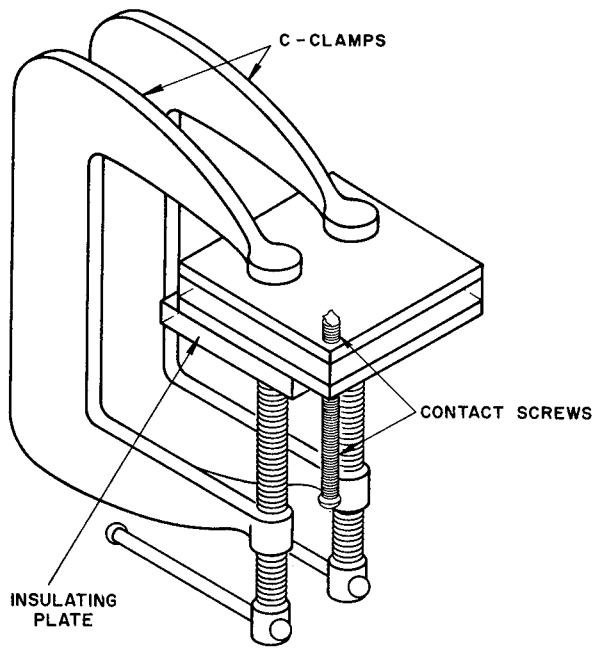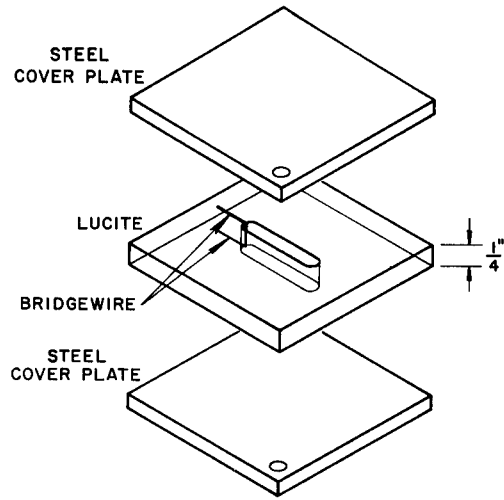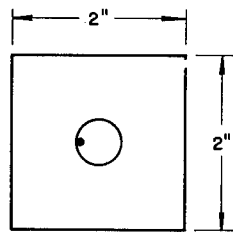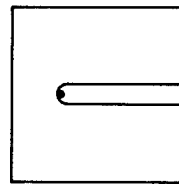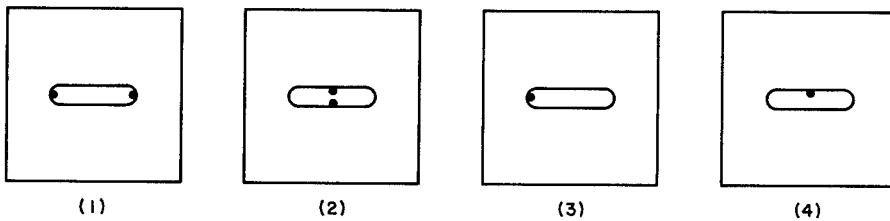
TYPE B

(c)

FIG. 1

EXPLOSIVE DEVICES

FIG. 2

TYPE B3 CHARGE

(a) $\frac{1}{4}$ x 1 INCH CHARGE
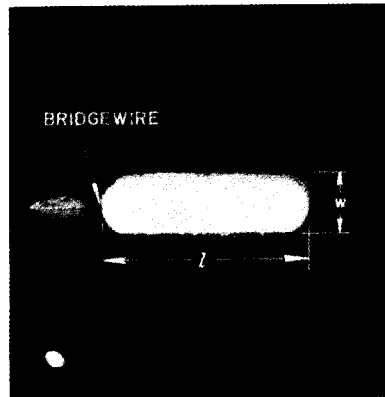
(b) $\frac{1}{8}$ x 1 INCH CHARGE
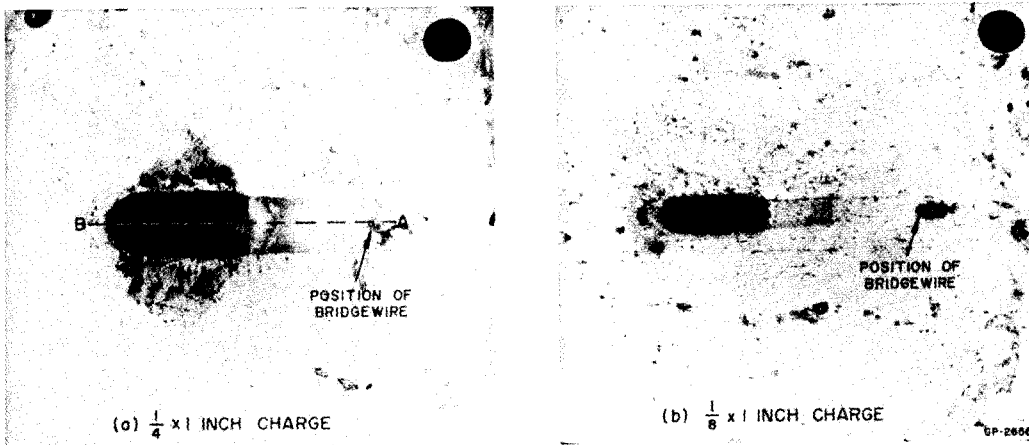
FIG. 3

INSIDE FACE OF TWO COVER PLATES FROM B3 CHARGES
SHOWING HIGH ORDER DETONATION MARKINGS

90

deliberate variation, no particular attempt was made to control the loading density; some auxiliary measurements indicate that the usual value (referred to as "normal" in the remainder of this section) was 1.15 g cm^{-3} ($\pm$ 10%).

The electrical energy for firing the charges was supplied by a 4-μf power supply, triggered by a three-electrode spark gap. The circuit had a switching time of about 0.1 μsec and a short-circuit period of about 11 μsec. The power supply terminated in two copper electrode clamps mounted inside a large wooden box; the assembled charge was connected to the clamps by the two contact screws shown in Figure 1(a). Current and the voltage across the load were measured, respectively, by a current viewing resistor and a voltage dividing network, and displayed on a Tektronix 551 dual beam oscilloscope.

B. RESULTS: SINGLE-BRIDGEWIRE CHARGES

1. <u>General</u>. To fix ideas, consider a specific B3 charge, 1/4- x 1-inch, normal packing density, No. 38 (4-mil diameter) copper bridge-wire.* With a condenser voltage of 1.5 kv or above, this charge always exploded. (It will become clear in the sequel why the more general term "exploded" is used rather than "detonated.") Putting aside for the moment the question of a threshold voltage for explosion, let us consider the explosion itself. Terminal observation of the steel cover plates proved to be very enlightening because in each case the reaction wave progressing through the RDX from the bridgewire left a distinctive footprint. Figure 3(a) is a photograph of a typical steel cover plate of a 1/4- x 1-inch charge after firing at 2 kv. For the first 11 or 12 mm from the position of the bridgewire (A) there is very little marking on the plate; over the region corresponding to the remainder of the RDX charge, the plate is blackened and feels dis-tinctly rough to the touch. The transition from the unmarked to the blackened zone was, in most cases, fairly abrupt and reasonably uni-form transverse to the line AB. Several cover plates were sectioned along lines parallel to AB, and the sections examined metallograph-ically. Figure 4 displays a series of three micrographs taken at dif-ferent points along the surface of a sectioned plate. Figure 4(a) is centered at about 10.5 mm from the bridgewire and shows no significant surface deformation or damage to the crystal structure. Figure 4(b) at 11.5 mm shows distinct surface rippling and a few isolated crystal-lographic twins; visual observation of the specimen in a metallograph also shows deposition of amorphous black material (probably carbon), not visible on the photograph. At 12.5 mm [Figure 4(c)] the twinning

---

* The nominal diameter and resistivity of the various wire types referred to in this paper are as follows:

MATERIAL	B & S GAGE NO.	DIAMETER (mils)	RESISTIVITY AT 20°C (ohms/foot)
Copper	32	7.95	0.164
Copper	38	3.695	0.660
Copper	44	1.978	2.66
Nichrome	40	3.145	61.0
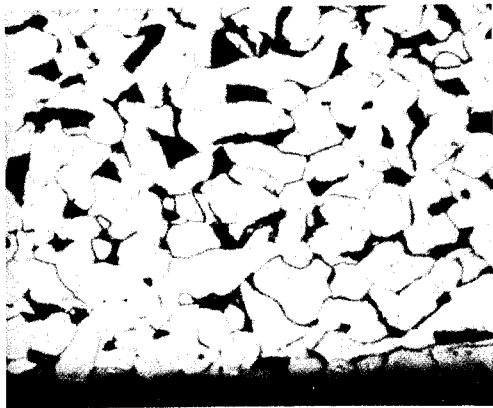
(a) 10.5 mm FROM BRIDGEWIRE
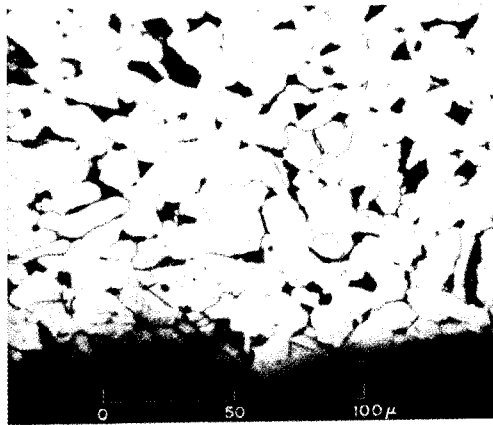
(b) 11.5 mm FROM BRIDGEWIRE
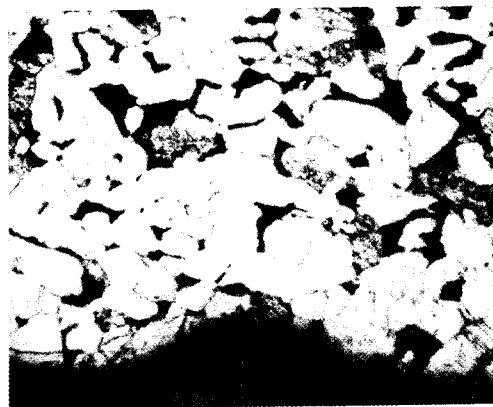
(c) 12.5 mm FROM BRIDGEWIRE

FIG. 4

CROSS SECTIONS OF COVER PLATE FROM B3 CHARGE AFTER FIRING

has become extremely severe. These terminal observations strongly indicate that the reaction initiated by the bridgewire travels a distance of about 11.5 mm (under the conditions of the particular experiments just discussed) and then undergoes an abrupt change; in particular, past experience at this Laboratory[3] indicates that the heavy twinning mentioned above is evidence of pressures in excess of 130 kilobars. It is, therefore, reasonable to infer that this abrupt change corresponds to a transition from deflagration or low order detonation to high order detonation.

A few of the shots were fired with several pin-pairs inserted through one of the cover plates; while these were not intended to be high-precision experiments, they showed quite clearly the existence of two velocity regimes, an initial one of 2-3 mm/μsec in the unmarked zone followed by one of 6-8 mm/μsec in the blackened zone.

That the reaction initiated in a train of powdered RDX by a bursting bridgewire eventually turns into a high order detonation was also shown in an experiment not requiring metallographic examination. In this experiment a Type C charge was used; two shots were fired with a 3/16-inch steel plate butted up against the free end of the charge (Figure 5). In each case, an end spall was driven off the far side of the plate (Figure 6), indicating high order detonation in the RDX.

Finally, two Type C charges were fired under photographic observation, using a Beckman and Whitley framing camera. The photographs show the front of a reaction wave which starts at the bridgewire, travels through that portion of the RDX corresponding to the unmarked region of the cover plate at an average (and possibly slightly increasing) velocity of about 2.7 mm/μsec, and then at the boundary of the blackened zone very rapidly speeds up to 6.8 mm/μsec, at the same time sharply increasing in luminosity. One of the shots was fired with lucite rather than steel cover plates; this decrease in confinement did not appear to have a substantial effect on the distance at which the high order detonation began.

2. <u>Induction Distance</u>. With the evidence presented above, it becomes clear that with each explosion of powdered RDX initiated by a bursting bridgewire there is associated an induction distance for high order detonation. For the purpose of reporting the experimental results, "induction distance" will be used simply to denote the distance measured on a steel cover plate from the position of the bridgewire to the nearest point at which the characteristic blackening can be observed by superficial examination.* The uncertainty in these measurements was of the order $\pm$0.5 mm; moreover, in those shots where two steel plates were used, any difference between the two separate measurements of induction distance fell within this same range.

---

*i.e., without the use of metallographic techniques.
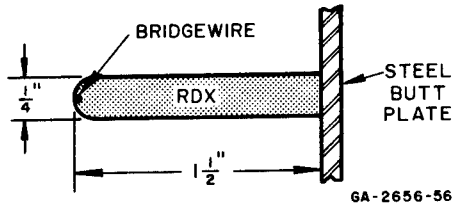
FIG. 5

TYPE C CHARGE ARRANGED
TO SPALL A STEEL PLATE

FIG. 6

STEEL PLATE SPALLED BY
HIGH ORDER DETONATION
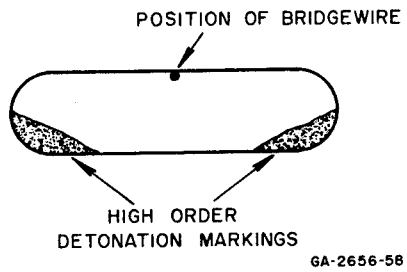
FIG. 7

APPEARANCE OF COVER PLATE
FROM TYPE B4 CHARGE
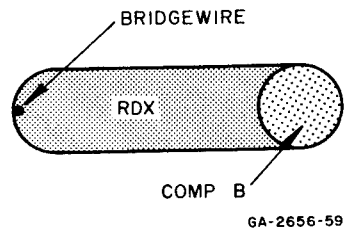
FIG. 8

B3 CHARGE MODIFIED TO
INVESTIGATE SECONDARY
DETONATION OF COMP B

To show the dependence of induction distance on various parameters, Table I presents a list of firings of Type B3 charges with steel cover plates, indicating charge dimension (w x ℓ, in the notation of Figure 2), shot number (for reference purposes), condenser voltage, and induction distance. Unless otherwise indicated, the bridgewire was No. 38 copper wire, and the loading density normal. (No measurement of induction distance could be made with charges having two aluminum cover plates because of the severe damage to the plates.)

It is apparent that, at most, only a slight decrease in induction distance results from increasing the condenser voltage from 2 kv to 8 kv; the difference between 12 mm and 10.5 mm is, in view of the experimental uncertainty just on the threshold of being significant. To what extent an increase in stored electrical energy corresponds to increased effective energy dissipation in the RDX is a matter of some speculation; in this connection, note also that going from a 4-mil (No. 38) to an 8-mil (No. 32) bridgewire (Shots No. 267 and 266) at constant voltage led to no significant change in induction distance.

The consistency of the data referred to in the last paragraph can be taken as an indication that the moderate variations in packing density which may be expected to have occurred from shot to shot did not have a large effect on the induction distance. On the other hand, a very marked increase in induction distance (from 12 mm to 17.5 mm) resulted from lowering the packing density by 50%. No measurement was made at the time, but it is estimated that the packing density in Shot No. 270 was about one-half of normal. (As was pointed out in connection with the framing camera shots, the substitution of lucite for steel as the cover plate material seems to have no significant effect on induction distance; there is no reason to believe, therefore, that the validity of the conclusion just stated is affected by the fact that one of the cover plates in this shot was made of aluminum.)

Decreasing the channel cross section (i.e., the cross section transverse to AB) from 1/4 x 1/4 inch to 1/8 x 1/4 inch (Shot No. 265) produced a moderate (from 12 mm to 14 mm) increase in induction distance. Figure 3(b) shows one of the cover plates from this shot.

TABLE I

SINGLE BRIDGEWIRE CHARGES

TYPE B3

SIZE (in.)	SHOT NO.	CONDENSER VOLTAGE (kv)	INDUCTION DISTANCE (mm)
1/4 x 1	254	2.0	12
1/4 x 1	255	2.0	12
1/4 x 1	264	2.0	12
1/4 x 1	267	8.0	11
1/4 x 1	266	8.0	10.5^1
1/4 x 1	270	2.0	17.5^2
1/4 x 1/2	262	5.0	10.5
1/8 x 1	265	2.0	14

[1] No. 32 copper bridgewire

[2] RDX lightly packed-density perhaps 1/2 normal; 1 steel, 1 Al plate

95

Two 1/4- x 1-inch charges of Type B4 were fired at 2.5 kv and 5.5 kv, respectively. These charges differ from B3 only in the position of the bridgewire. The markings on the cover plates are shown schematically in Figure 7. The induction distances (measured from the wire to either blackened zone) were all about 11 mm.

3. <u>Secondary Initiation of Insensitive Explosives by RDX</u>. To determine the effect of single-bridgewire initiated RDX on an insensitive explosive, two shots were fired using B3 devices in which part of the RDX charge was replaced by a 1/4-inch equilateral cylinder of Composition B. Schematically, the arrangement is shown in Figure 8.

Both devices had No. 38 copper bridgewires. Shot No. 259 employed a 1/4- x 1-inch charge (over-all dimension, including the Composition B cylinder), fired at 3.5 kv. From the markings on the cover plates, it was quite evident that high order detonation had occurred in the Composition B. Shot No. 273 employed a 1/4- x 1/2-inch charge, fired at 5 kv; in this shot the Composition B was merely shattered. These results are readily explainable in terms of induction distance. The RDX charge in Shot No. 259 was large enough to allow the reaction wave in the RDX to go as a high order detonation for approximately 6 mm before striking the insensitive explosive, thus causing the latter to detonate also. In Shot No. 273, the longest distance between the bridgewire and any part of the RDX charge was only about 9 mm; no high order detonation could develop in the RDX, and the pressure and temperature developed in the pre-high order wave were insufficient to detonate the Composition B.

For some further results relating to the initiation of detonation in Composition B, see also Shot No. 261 described under C, below.

4. <u>The Threshold for Initiation</u>. The principal reason for presenting the material on induction distance prior to discussing the process of initiation itself is to show that, within the range of the present experiments, the growth to high order detonation is reasonably independent of the details of initiation. (This certainly would not be true when reaction in the RDX is initiated by another explosive.) In almost all of these experiments, there was either failure to explode with no substantial reaction induced in the RDX (as evidenced by the presence of unburned RDX even though in some cases the explosive device came apart); or else the device exploded, with the RDX completely consumed. It is clear that explosion implies the presence of a high order detonation only where the charge is larger than the induction distance.

For determining threshold voltages, it is only that part of the charge (and possibly its environment) in the neighborhood of the bridgewire which is significant. Thus, for present purposes, the experiments involving charges of Type B3 may be considered concomitantly with a previous series of shots involving 1/2-inch diameter charges of Type A, with aluminum cover plates.

In Table II, explosion or failure to explode is indicated for a number of shots, some of them already listed in Table I.

TABLE II

SINGLE BRIDGEWIRE CHARGES

BRIDGEWIRE		CHARGE		SHOT NO.	CONDENSER VOLTAGE (kv)	RESULT: CHARGE EXPLODED INDUCTION DISTANCE (mm) (where measured) UNLESS OTHERWISE INDICATED
Material	Diameter (gage)	Type	Size (in.)			
Cu	38	A	1/2	231	2.8	
Cu	38	A	1/2	232	2.3	
Cu	38	A	1/2	242	2.0	
Cu	38	A	1/2	233	1.8	
Cu	38	A	1/2	243	1.5	
Cu	38	A	1/2	244	1.2	Failed
Cu	38	B3	1/4 x 1	267	8.0	11
Cu	38	B3	1/4 x 1/2	262	5.0	10.5
Cu	38	B3	1/4 x 1	256	2.5	
Cu	38	B3	1/4 x 1	254	2.0	12
Cu	38	B3	1/4 x 1	255	2.0	12
Cu	38	B3	1/4 x 1	264	2.0	12
Cu	38	B3	1/4 x 1	270[1]	2.0	17.5[2]
Cu	38	B3	1/8 x 1	265	2.0	14
Cu	38	B3	1/4 x 1	245	1.9	
Cu	38	B3	1/4 x 1	246	1.5	
Cu	38	B3	1/4 x 1	271[1]	1.2	Failed
Cu	32	B3	1/4 x 1	266	8.0	10.5
Cu	32	B3	1/4 x 1	253	2.0	Failed
Cu	44	B3	1/4 x 1	248	1.75	Failed
Nichrome	40	B3	1/4 x 1	247	1.75	Failed
Nichrome	40(4)[3]	A	1/2	227	3.8	
Nichrome	40(4)	A	1/2	228	3.3	
Nichrome	40(4)	A	1/2	229	2.8	
Nichrome	40(4)	A	1/2	230	2.3	Failed

[1] Packing density of RDX about 1/2 normal

[2] 1 steel, 1 aluminum cover plate

[3] 4 strands of No. 40 wire twisted together

With a No. 38 copper bridgewire, explosion occurred consistently at 1.5 kv and above, failure at 1.2 kv; the threshold voltage under present experimental conditions thus lies between these values. One shot (No. 271) was fired at 1.2 kv and with a very low packing density to see whether loose packing might have a significant effect in lowering the threshold voltage; this charge, too, failed to explode. No systematic series of shots was run on No. 32 and No. 44 copper wire but it is clear that the threshold voltage for these gages is higher; in fact, the No. 32 wire barely broke at 2.0 kv. A systematic series was run on a bridgewire consisting of four strands of No. 40 nichrome wire twisted together; the threshold voltage is between 2.3 and 2.8 kv.

A single strand of No. 40 nichrome wire failed to initiate RDX at
1.75 kv.

Generally, if firing of a charge did not lead to initiation,
the RDX was left more or less in place. Usually, the RDX adjacent to
the exploded wire(s) showed spotty discoloration, at first believed to
be burn marks. On closer examination, it was determined that this dis-
coloration was at least partly due to very fine copper particles dis-
persed for as much as 2 mm from the original position of the bridgewire.

5. Bridgewire Oscillograms; Energy Considerations. Figure 9(a)
is the 10-μsec record for Shot No. 264. The probable sequence of
events is as follows. On a 1-μsec time scale, the switching is es-
sentially instantaneous at t = 0.1 μsec. The current begins to rise,
governed by the time constant of the external circuit. The bridgewire
is heated with a gradual rise in resistance, accounting for the slight
rise in measured voltage between 2.0 μsec and 2.7 μsec. At this point,
the wire bursts, leading to a very sharp increase in resistance which
is reflected in the almost discontinuous increase in voltage and the
simultaneous discontinuity in dI/dt. Some slight conduction continues
to take place, the resistance at 4 μsec being of the order of several
ohms. At 7 μsec the current has fallen to a negligible value, with
the voltage remaining constant at about 800 volts which corresponds to
the residual voltage.

Figure 9(b) covers the first 20 μsec of Shot No. 246. Except
for the lower voltage, the record is very similar to the previous one;
the residual condenser voltage is 400 volts.

Figure 9(c) covers 20 μsec of Shot No. 271. In this case,
the wire did not break until about 4 μsec with the current already
rapidly declining. The peak in measured voltage associated with the
breaking is much less pronounced. This shot, at 1.2 kv, did not lead
to initiation of the RDX.

In the foregoing, fired at a relatively low voltage, very
little conduction took place following the bursting of the wire. In
Shot No. 227 [Figure 9(d)] with nichrome No. 40(4)* wire fired at
somewhat under 4 kv, the wire broke in about 2 μsec; moreover, the
dwell time (the time of non-conductance following the bursting of the
wire) is no more than about 0.1 μsec. At an even higher voltage, the
breaking of the wire is farther advanced; the resulting arc behaves
effectively like a short [Figure 9(e), Shot No. 260].

The bursting of the wire can also be advanced by going to a
smaller wire diameter. Figure 9(f) (Shot No. 248) is the record for
a No. 44 copper bridgewire fired at 1.75 kv. Here the wire burst in
less than 2 μsec; the process required little enough energy so that,
in spite of the low initial condenser voltage, considerable current
flow took place for approximately the next 8 μsec. It is interesting
to note that in this shot the RDX was not initiated.

The lowest voltage (1.5 kv) at which initiation took place
corresponds to a stored energy of 4.5 joules. A rough integration of
the power dissipated in the wire for Shots No. 246 [Figure 15(b)] and

*See Table II, Note (3) for notation.

98

SHOT NO.

(a)

1 μsec/cm

0- 5000 amp/cm 264

0- 2000 v/cm

(b)

2 μsec/cm

5000 amp/cm 246

1000 v/cm

(c)

2 μsec/cm

5000 amp/cm 271

1000 v/cm

(d)

2 μsec/cm

5000 amp/cm 227

(NOT CALIBRATED)

(e)

1 μsec/cm

5000 amp/cm 260

4000 v/cm

(f)

2 μsec/cm

5000 amp/cm 248

1000 v/cm

UPPER TRACE IS CURRENT
LOWER TRACE IS VOLTAGE
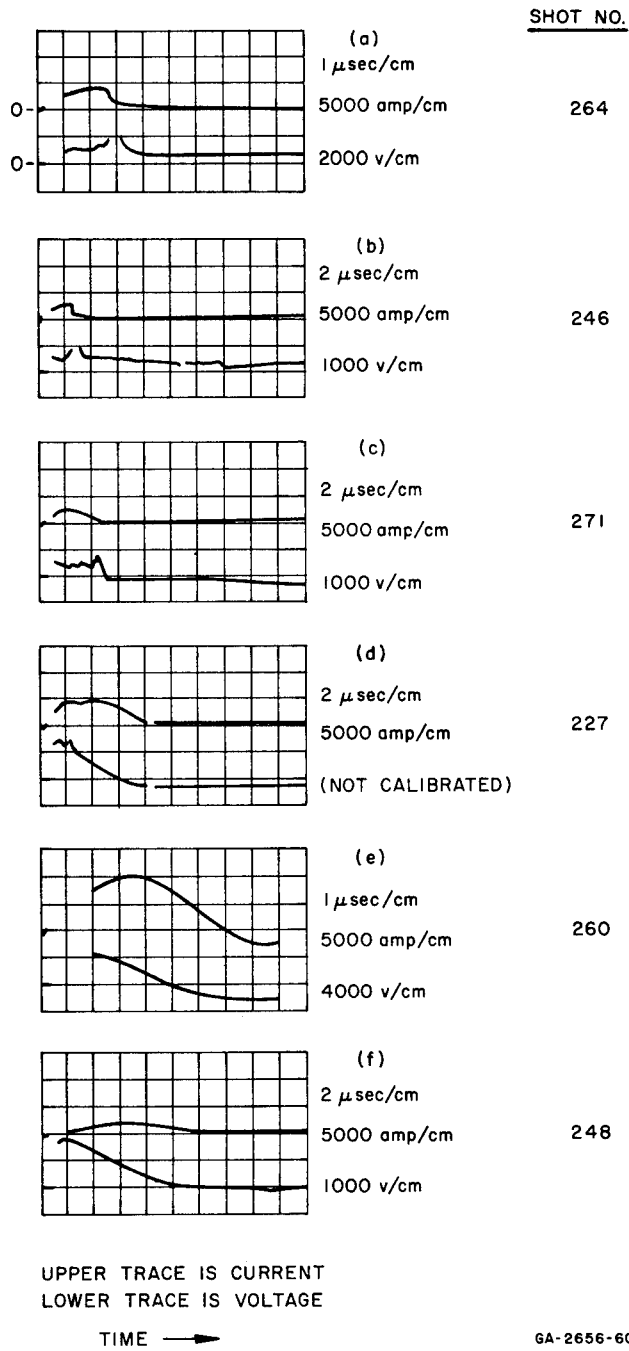
TIME ⟶   GA-2656-60

FIG. 9

TYPICAL BRIDGEWIRE OSCILLOGRAMS

243 (both with No. 38 copper bridgewire) shows that approximately 3-4 joules, i.e., a substantial part of the stored energy, was delivered to the wire prior to bursting in each case. On the other hand, it is clear that in those cases where the stored energy is greatly in excess of that required to burst the wire, at least a large part of this additional energy is dissipated in whatever conductive path (arc, etc.) replaces the wire--See Figures 9(d), (e), (f). Thus, if it is the energy delivered to the wire before it breaks which is significant in determining whether or not the RDX is initiated, it would appear that to minimize the stored energy (for a given power supply and a fixed wire length), it is most efficient to choose the wire diameter such that the threshold energy required for bursting the wire is equal to or slightly less than the energy which must be delivered to the RDX for initiation.

It should be noted that in the shot involving the No. 44 wire fired at 1.75 kv (Shot No. 248), with a stored energy of 6 joules, the energy delivered after the wire broke was less effective in promoting reaction than energy delivered prior to the breaking of the No. 38 bridgewires in Shots No. 246 and 243, since in both of the latter, with a stored energy of only 4.5 joules, initiation took place whereas Shot No. 248 failed. It may, however, be that a circuit with a sufficiently short resonant period can deliver most of its stored energy before even a very thin wire, subject to the effects of inertia and magnetic pressure, has significantly expanded. Now, a given amount of energy stored in a thin wire, being available at a higher temperature, is probably more effective in the initiation of chemical reaction than an equal amount stored in a thicker wire. Therefore, while No. 44 copper wire is uneconomic compared with No. 38 wire under the present experimental conditions, the use of a power supply with a much higher resonant frequency may well reverse this situation and lower the minimum initiation energy.

It may also be noted in this connection that the time during which most of the energy is delivered to a No. 38 wire with the power supply used is rather shorter than one might suspect from the 11-μsec resonant period of the detonator unit. The calculation of the power dissipation for Shots No. 246 and 243 mentioned above indicates that relatively little power is dissipated until just before the current flow reaches its first maximum; after that, the power dissipation increases very rapidly because of the heating and consequent increase in resistance, and the wire bursts within a microsecond.

Unfortunately, it was impossible to include in this study any experiments on the effect which the length of the bridgewire has on minimum initiation energy. Since initiation in a given volume of RDX probably depends principally on achieving a certain initial energy density, the minimum initiation energy may be expected to be roughly proportional to the wire length. End effects may, however, be significant. Recent experiments[4] on exploding wires indicate that in most of the bridgewire devices, energy may be released preferentially in the vicinity of the two points of contact between bridgewire and cover plate; in this case, a large part of the dissipated electrical

energy may be lost to the initiation process by thermal conduction to the cover plates.

C. RESULTS: INTERACTION OF TWO REACTION WAVES

Several B1 charges were fired to investigate whether the collision of two pre-high order reaction waves could lead to high order detonation. These charges are identical with the B3 charge, except that they have No. 38 copper bridgewires at both ends of the charge. (The wires are electrically in parallel.) Three 1/4- x 1/2-inch charges were fired at 3, 5, and 7.5 kv, respectively (Shots No. 274, 263, 268). A photograph of one of the cover plates is shown in Figure 10. The sharp indentation midway between the bridgewire positions shows, on metallographic examination, none of the surface rippling, deposition of black amorphous material, and twinning indicative of high order detonation. Thus the indentation must be essentially due to the intensification of pressure which is produced when any two high-amplitude compression waves collide.* The general evidence from the experiments discussed, as well as from earlier ones not covered in this paper, is that the terminal damage and noise produced by a given amount of initiated RDX is independent of the fraction of the charge, if any, which underwent high order detonation. (This observation may not be true under radically different experimental conditions such as complete lack of confinement.) It seems quite likely, therefore, that the reaction which occurs behind the pre-high order wave front leads to the same total energy release as that occurring behind the high order wave front but at a much slower rate. If this surmise is correct, then the failure to produce high order detonation in the above two shots may be ascribed to the fact that when the two wave fronts collided there was no longer a sufficient amount of unreacted material available in which a high order detonation could have been initiated by the sudden increase in temperature and pressure resulting from the collision.

A shot (No. 272) which may confirm the statement just made (although the evidence is not conclusive) involved a 1/4- x 1-inch B1 device in which the central part of the RDX charge had been replaced by a 1/4-inch equilateral Composition B cylinder (Figure 11).

This shot, fired at 5 kv, led to complete high order detonation of the Composition B. On the basis of even as short an induction distance as 10.5 mm, the amount of RDX which could have undergone high order detonation (shown black in the figure) is very small. It seems likely, therefore, that the Composition B was actually detonated by the collision of the two shock waves which resulted when it was struck by the two reaction waves in the RDX.

One shot (No. 258) was fired at 3 kv with a 1/4- x 1-inch RDX charge. The cover plates showed a deep indentation surrounded by 1 to 2 mm of typical high order markings, midway between the bridge-wires. Since each reaction wave had an available run of about 12 mm,

---

*It is, in a way, ironic that high order detonation can be produced in a charge of the same dimensions by initiating it with a single bridge-wire. Compare Shot No. 263 (Table I).
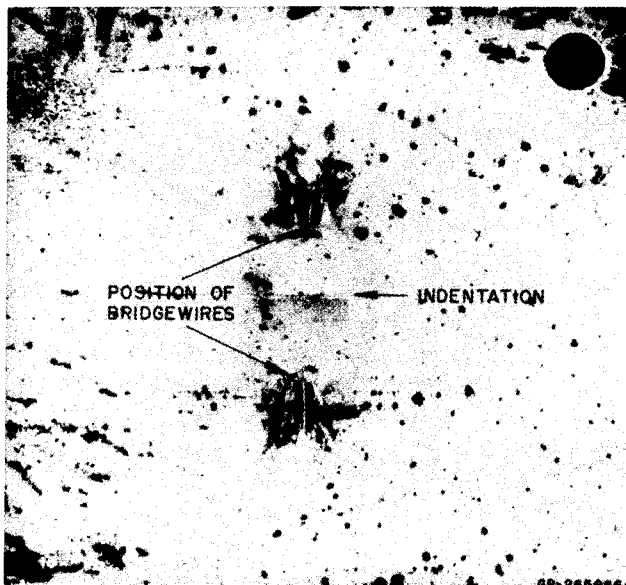
FIG. 10

COVER PLATE FROM A B1 CHARGE SHOWING THE PRESSURE
MARK RESULTING FROM THE COLLISION OF TWO PRE-HIGH
ORDER REACTION WAVES
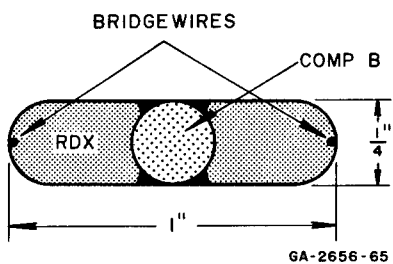
FIG. 11

CHARGE FOR SHOT NO. 272
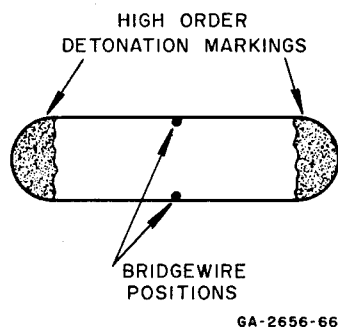
FIG. 12

APPEARANCE OF COVER PLATE
FROM A TYPE B2 CHARGE

this result is entirely what one would expect.

One shot (No. 261) was fired at 4.8 kv using a 1/4- x 1-inch type B2 charge. The bridgewire arrangement and cover plate markings are shown schematically in Figure 12.

The measured induction distance was 9.5 mm, the lowest found in any experiment. Apparently the two reaction waves starting out from the bridgewires reinforced each other under conditions where this reinforcement could be effective in shortening the induction distance (contrast with the three shots discussed at the beginning of this section).

II   INITIATION OF PRESSED RDX BY INTERNAL HEATING

A.   BACKGROUND

Like most solid explosives, RDX in the form of pressed pellets is much less sensitive to initiation than is the granular material. At BRL, pressed RDX pellets have been initiated by a bridgewire; the required energy was of the order of 50 joules.* Having the explosive powdered rather than pressed probably facilitates bridgewire initiation in two ways:

(a) Liquid metal droplets from the exploding wire can penetrate more readily into the interior of the mass of explosive where they ignite individual grains.

(b) Either the pressure generated by the explosion of individual grains is large enough to compress nearby air pockets to a sufficiently high temperature where ignition of adjacent grains of explosive takes place, or else hot gas jets from one burning grain penetrate among adjacent grains, with the same result.

Bowden and Gurton[5] suggested that the first of the two mechanisms under (b) is responsible for the propagation of the steady low-order detonation found in thin films of various explosives which contain air or gas inclusions. (In contrast to a high order detonation, the pressure developed in a low order detonation is too small to induce substantial reaction at the wave front by shock compression of the explosive itself.) Some such mechanism can account for the almost immediate appearance of the pre-high order reaction wave following the bursting of the bridgewire in a charge of powdered RDX; moreover, if the individual grains of RDX are ignited at the surface, the energy release behind the advancing reaction front is, of course, slower than in a high order detonation.

In the experiments to be described, the transfer of energy to the explosive takes place in a way which eliminates that particular

---

*Private communication from George Hauver. In the BRL experiment high order detonation apparently occurred within a very short distance from the site of the bridgewire; it may be, therefore, that if enough energy is delivered to a bridgewire to initiate a pressed or cast explosive at all, the resulting pressure-temperature conditions will generally be extreme enough for a high order detonation to start immediately.

difference in the initiation of pressed and powdered RDX which arises
from consideration (a), above. Pressed cylindrical RDX charges were
used containing a 1/32-inch diameter cylindrical central core of RDX
mixed with a conducting powder. Current from a condenser was passed
through this central core, substantially all the stored energy being
delivered in from two to seven microseconds. Some preliminary calcu-
lations[2] based on assumptions commonly used in the theory of the
thermal initiation of explosives or propellants[6,7,8] had indicated
that if the initial temperature through the core following the electrical
discharge exceeds 600°K, the temperature reached as the result of the
reaction of the explosive will have been only slightly affected by heat
conduction by the time that the chemical reaction in the core is sub-
stantially complete. For initial core temperatures exceeding 750°K,
this latter point should be reached within about one microsecond following
the discharge; to reach this initial core temperature requires an energy
of about 4 joules, assuming that all the electrical energy is converted
into heat, and that the heating of the core is uniform. With a suf-
ficiently high energy input, it is conceivable that the core pressure
might rise rapidly enough to induce detonation in the surrounding ex-
plosive; the only other mechanism available for causing the surrounding
explosive to undergo reaction is a progressive thermal explosion which
propagates by heat conduction. (If the explosive charge is large enough,
such a thermal explosion wave will probably ultimately turn into a
detonation.) Because heat conduction is a comparatively slow process,
this mechanism will fail to operate if the core temperature falls because
of the leakage of the explosion products, or if the charge breaks apart
because of mechanical effects resulting from the high pressure at the
center. (It may be mentioned in this connection that explosion and
eventual detonation of pressed RDX had been obtained by Stresau and
Weber at Armour Research Foundation* by delivering 200,000 ergs of
electrical energy to a volume of the order 10^{-5} cm^3.)

B. APPARATUS AND PROCEDURE

All charges were cylindrical, 1/4-inch high and of 1/4-inch
diameter. Each charge consisted of an inner cylindrical core 1/32-inch
in diameter and of a surrounding cylindrical shell. The shell was
first pressed out of pure, unwaxed RDX to a density of 1.7 gm^{-3} and the
core was then pressed into the shell, core materials being mixtures of
RDX (grain size 80 to 100 μ) and graphite (grain size 15 to 40 μ) or
RDX and silver flake. The pressing operations were performed in a
specially constructed die. While the density of the outer shell could
be quite well controlled, it is likely that in some of the charges the
core density may have been somewhat below 1.7 g cm^{-3}.

The electrical energy was supplied by a 1/2-μf coaxial con-
denser, fired by a spark gap. This power supply was mounted in a co-
axial system with very low inductance; the resonant period on short-
circuit was 1.6 μsec. The power supply terminated in a steel pedestal

---

* Private communication from J. Savitt to G. E. Duvall.

Muller, Moore & Bernstein

which provided the ground connection; a hole in the pedestal allowed
access to a coaxial fitting for the high voltage connection. The
pedestal was mounted inside the wooden box used for the experiments
described in Part I.

Except for a few preliminary experiments, the charges were
fired in the assembly shown in place on the power supply pedestal in
Figure 13. The charge was placed in a cavity inside a 2-inch by
2-inch lucite cylinder; brass pistons provided confinement on the top
and bottom of the charge (with a view to simulating a very long cyl-
inder) and also supplied the electrical connections to the core of the
charge. The weight on the top piston prevented the latter from tearing
through the wooden box; as it was, we found it necessary to tape a
piece of styrofoam to the weight to prevent it from damaging the box.

The power supply circuit included a current viewing resistor
and access for a high voltage probe; the output from these devices was
monitored on a Tektronix 551 dual beam oscilloscope.

The steel sleeve surrounding the lucite cylinder had a
1/8-inch diameter hole drilled perpendicular to the axis of the assem-
bly at the height of the explosive pellet; light coming through this
hole was viewed by a photomultiplier whose output was monitored on a
Tektronix 535 oscilloscope.

From some preliminary measurements, it was clear that the
specific conductivity of finely powdered conductors depends strongly
on the density and hence on the pressure applied in loading. Thus,
pure silver flake (silver in the form of approximately 50-micron
diameter platelets) is essentially nonconducting when piled in a small
heap; if this same material is placed inside a 1/32-inch hole in a
piece of lucite, and then manually compressed between two pieces of
piano wire of about the same diameter as the hole, the resistance very
suddenly falls to a negligible value as the force applied to one of
the wires reaches a few pounds (by casual estimate). This same kind
of dependence of resistance on loading density was found to hold for
mixtures of conducting and nonconducting powders. Moreover, we found
that dextrin containing as much as 20 percent graphite was noncon-
ducting even when pressed into 1-inch-diameter pellets at 5,000 psi;
presumably, the dextrin, because of its smaller grain-size, completely
coated the individual graphite particles.

In view of these preliminary findings, it is not surprising
that attempts to measure the DC resistance of some of the pellets pro-
duced somewhat random results. The lowest resistance measured between
the two pistons (see Figure 13) with a 10%-graphite core pellet in
place was about 50,000 ohms. Contact resistance played an important
part. For example, the condenser failed to discharge in one attempted
shot involving a 15%-graphite core pellet. On removing the assembled
charge holder from the pedestal, a measurement of the resistance be-
tween the pistons showed effectively infinite ($>10^8$ ohms) resistance.
The charge holder was then disassembled and the pellet and piston
faces cleaned off to remove any ungraphited RDX which might be inter-
fering with the contact between the pistons and the graphited pellet
core. The charge was reassembled, and a second resistance measurement
gave a value of about 2 megohms. The pellet was then successfully

exploded; the oscilloscope record indicated a delay of no more than 1/2 μsec between the appearance of the voltage across the pistons and the beginning of appreciable current flow.

C. RESULTS

Table III lists the twelve shots which were fired using the charge assembly shown in Figure 13. The identifying shot numbers refer to our laboratory records. The entry under "Core" shows the kind and amount of conducting powder mixed with RDX to form the core material, "C" and "Ag" indicating graphite and silver flake, respectively. For each shot, the voltage and stored energy are given.

TABLE III

SHOT	CORE	VOLTAGE (kv)	STORED ENERGY (joules)	TERMINAL OBSERVATION
7	20% Ag	5.0	6.25	Entire charge exploded
8	20% C	3.85	3.7	Entire charge exploded
9	20% C	3.25	2.65	Entire charge exploded
10	20% C	2.9	2.1	Entire charge exploded
11	20% C	2.9	2.1	Entire charge exploded
12	20% C	2.7	1.8	Entire charge exploded
13	20% C	5.6	7.8	Entire charge exploded
14	15% C	5.6	7.8	Entire charge exploded
15	15% C	5.6	7.8	Entire charge exploded
16	15% C	6.15	9.4	Core only exploded*
17	10% C	5.6	7.8	Entire charge exploded
18	10% C	6.15	9.4	Entire charge exploded

* The outer RDX shell remains substantially intact; the lucite holder was cracked into four pieces.

The electrical energy dissipated in the charge was determined by numerical integration from the voltage and current records for several shots; in each case the value thus obtained agreed with the stored energy to within 10%. The voltage-current record reproduced in Figure 14 is typical of the shots fired at 5 kv or above; the capacitor is generally substantially discharged within 1.5 to 2.5 μsec from the time the circuit is closed. The load resistance at time of maximum current is usually about 1 ohm. (Unfortunately, no voltage-current or photomultiplier records were obtained from the single shot, No. 7, which involved a silver-RDX core.) At the lower voltages used, the time required for complete discharge increases to about 5 to 7 μsec, and the resistance at maximum current is about 3 ohms. An exception is Shot No. 9 where discharge was completed in 2 μsec and the resistance at maximum current was about 1 ohm, both values being typical of the higher voltage discharges.
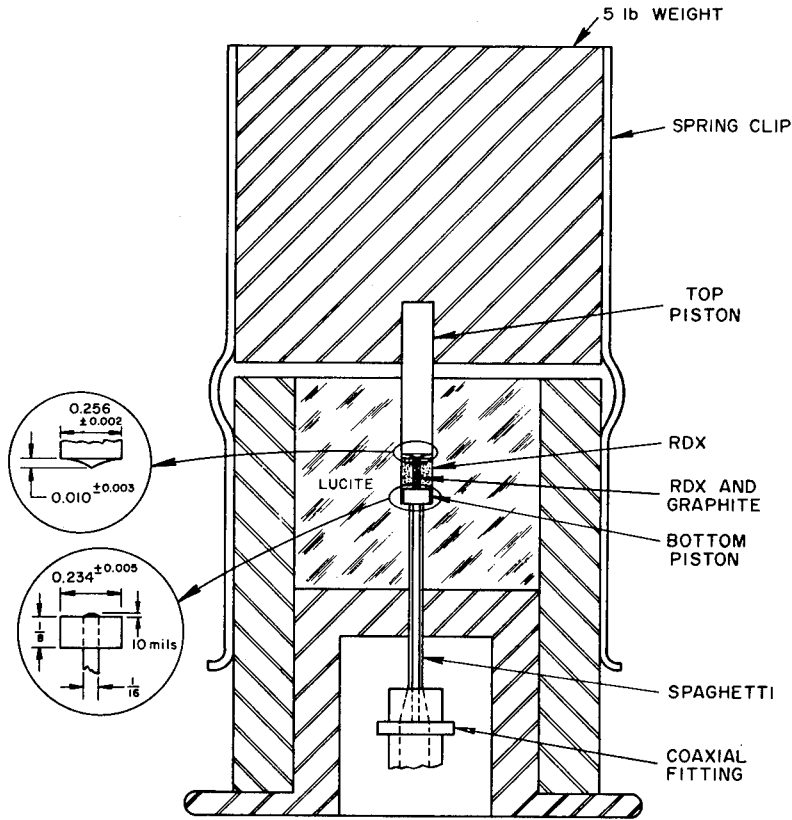
FIG. 13

CHARGE AND CHARGE HOLDER
(Pressed RDX)
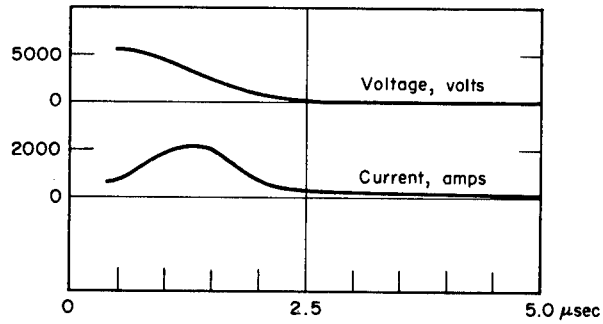
FIG. 14

TYPICAL VOLTAGE-CURRENT RECORD
(Pressed RDX, Shot No. 15)

Figure 15 shows the photomultiplier records from Shots No. 12 and 17 on rather long time-scales. Each oscillogram records two major luminous events, the interval between these being about 200 μsec for the high energy shot and about 1200 μsec for the low energy shot. The first event is definitely associated with explosion of the conducting core and possibly with the electrical discharge itself; the second one, by elimination, with explosion of the main charge. To verify the first statement, consider the photomultiplier records from Shots No. 15 and 16 fired at comparable voltages (Fig. 16). In Shot No. 16 the core only exploded; this misfire was perhaps due to the leakage of the explosion gases during the apparently quite extended induction period required for substantial reaction to buildup in the remainder of the charge. For present purposes, the significance of the shot lies in the great qualitative similarity which the first 50 μsec of the resulting photomultiplier output bear to the corresponding period of Shot No. 15 in which the main charge did explode. Moreover, a careful examination of the original photomultiplier oscillogram from Shot No. 12 (Fig. 7) shows that the first luminous event has a two-peak structure substantially like those shown in Figure 8; the first peak in this shot did not appear, however, until about 40 μsec after the electrical circuit was closed, hence long after completion of the electrical discharge. We must conclude that the first luminous event, although it may contain contributions (see below) due to the discharge as such, is principally related to the explosion of the RDX-graphite core.

The first peak of the two peak structure is probably due to the light emitted when the pressure wave from the reacting core (possibly reinforced by pressure generated by the electrical discharge itself) suddenly heats, by compression, the air trapped at the pellet-lucite interface; the second peak likely arises in a similar manner at the lucite-steel interface. There is the possibility that stray light emitted from the region of contact between the pistons and the core may come within the view of the photomultiplier by internal reflections from the lucite-steel interface and thus contribute to the photomultiplier output; such light emission could be the immediate result of the electrical discharge, or arise from the subsequent chemical reaction. It may be noted, incidentally, that in Shot No. 16 the intensity of the photomultiplier output begins to rise toward the second peak at about the time (12 μsec) at which the front of a compressional wave generated in the core within two microseconds of the closing of the circuit would be expected to arrive at the lucite-steel interface. In other high-energy shots where usable photomultiplier records were obtained, the time delay to the beginning of the second peak is somewhat longer; one cannot discount the possibility that a further contribution to the light intensity arises when the air at the pellet-lucite interface is reheated by the inward-moving compressional wave reflected from the lucite-steel interface.

While these questions of detailed interpretation of the photomultiplier records could hardly be settled without further experiments, it is clear at this point that the explosion of the charge takes place in two quite distinct stages. The core explodes first;

SHOT NO. 12
STORED ENERGY: 1.8 joules

0   1   2 msec

SHOT NO. 17
STORED ENERGY: 7.8 joules

0   1   2 msec
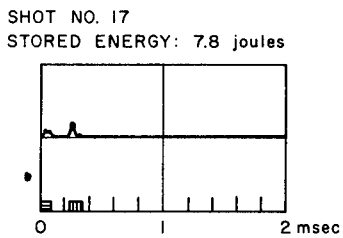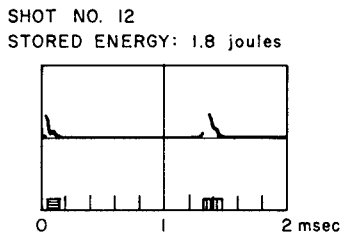
FIG. 15

PHOTOMULTIPLIER RECORDS
Showing the energy dependence
of the timing of the first (▦)
and second (▦▦) major
luminous events

SHOT NO. 15
STORED ENERGY: 7.8 joules

FIRST   SECOND
PEAK   PEAK

0   50   100 μsec

SHOT NO. 16
STORED ENERGY: 9.3 joules

FIRST   SECOND
PEAK   PEAK

0   25   50 μsec
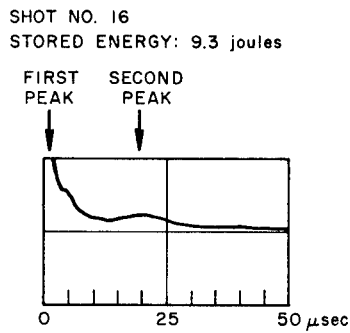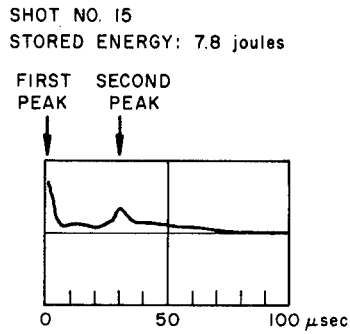
FIG. 16

PHOTOMULTIPLIER RECORDS
Showing the two-peak structure
of the first major luminous event

109

substantial reaction occurs within at most a few microseconds from the closing of the circuit at an applied voltage of 5 kv or above, or with a delay ("first induction period") of as much as 40 μsec at an applied voltage of 2.7 kv. Then follows a second induction period, ranging from 200 μsec at 5.5 kv to 1.2 msec at 2.7 kv, at the end of which the main charge explodes. If there is insufficient confinement of the charge during this second induction period, escape of the hot explosion gases from the core and the consequent loss of the heat available for inducing reaction in the remaining explosive may cause failure of the main charge to explode. In the case of very slight confinement, the main charge may simply break apart and be scattered. This is substantiated by two shots fired prior to those listed in Table III but employing the same kind of explosive pellets (with a 10% graphite core). The charge holder consisted merely of a thin-walled lucite shell within which the pellet was held by two small brass pistons under negligible pressure. The shots were fired at 5.6 and 6.1 kv, respectively. The voltage-current records are substantially identical with those from the later shots fired at comparable voltages but in each case there was merely a loud pop, and terminal examination of the debris disclosed fairly large pieces of lucite and unreacted grains of RDX.

D. DISCUSSION

For Shot No. 12, with a stored energy of 1.8 joules, the initial core temperature calculated on the basis of uniform heating and with conservatively low values of heat capacity and density is only 550°K (assuming the pellet to be at 290°K prior to the discharge). According to the calculations mentioned in Section A, above, at this temperature explosion of the core would require an induction time of some 30 msec even if heat conduction is neglected, whereas the observed induction time was 40 μsec. This discrepancy is too great to be explained by errors in the values of the various constants used in the computation. A first induction period of 40 μsec corresponds to an initial core temperature of about 660°K, hence to a temperature rise due to the discharge of about 370°K rather than 260°K. This difference can be readily accounted for if we take into consideration the nonuniformity of the electrical discharge. From the drop in resistance of the core during the discharge it is clear that (at least with the RDX-graphite cores) the electrical process is not simply an ohmic heating of the solid core but probably involves typical electric breakdown phenomena such as a multiplicity of minute (on the scale of the core diameter) gaseous conduction channels. Thus, if in the shot under consideration, these channels were distributed over roughly 70 percent of the core volume, the average temperature rise in the affected mass of RDX-graphite mixture would indeed be about 370°K.

In Section A an estimate of 4 joules was given as the energy required for immediate explosion of the core; in view of the nonuniformity of the discharge, a somewhat lower energy will generally be sufficient.

Since the time-scales of the explosions observed in the pressed RDX strongly suggest a mechanism dominated by thermal conductivity, it is worthwhile to develop a theory which may explain the second induction period on the basis of a model based on heat conduction with a temperature dependent heat source provided by the chemical reaction. The model must take into account the depletion of unreacted explosive in order to avoid a meaningless indefinite rise in the core temperature. Calculations based on such a model are currently in progress at this Laboratory, and will be reported at a later time; the equations describing the model are given in Reference 2.

The experiments show that, with increasing energy input, the second induction period becomes progressively shorter; very likely, a point is eventually reached where detonation occurs almost immediately. Below this point, whether or not substantial explosion or detonation of the main charge occurs will depend strongly on the degree of confinement.

REFERENCES

1. Moore, D. B. and G. M. Muller, Electrical Initiation of Insensitive Explosives, Poulter Laboratories Technical Report 016-59, Stanford Research Institute, 1959.

2. Muller, G. M. and D. Bernstein, Initiation of Explosives by Internal Heating, Poulter Laboratories Technical Report 007-59, Stanford Research Institute, 1960.

3. Curran, D. R., S. Katz, J. J. Kelly and M. E. Nicholson, Trans. Metallurgical Soc. AIME, 215, 151 (1959).

4. Chace, W. G. (ed.), Exploding Wires, New York, 1959.

5. Bowden, F. P. and O. A. Gurton, Proc. Roy. Soc. A, 198, 337,350 (1949).

6. Hicks, B. L., J. Chem. Phys. 22, 414 (1954).

7. Cook, G. B., Proc. Roy. Soc. A 246, 154 (1958).

8. Zinn, John and C. L. Mader, J. Appl. Phys. 31, 323 (1960).

DETONATION STUDIES IN ELECTRIC AND MAGNETIC FIELDS[*]

Floyd E. Allison
Carnegie Institute of Technology
Pittsburgh, Pennsylvania

Introduction

While investigating the behavior of sensing probes used to obtain detonation velocities by electronic methods, Birk, Erez, Manheimer, and Nahmani[1] studied the electrical conductivity between two electrodes placed in contact with a detonating charge. From their work, they concluded that the voltage to current ratio in the detonation zone was practically independent of voltage and could be regarded as an "ionization resistance," the value of which decreased when the area of the electrodes is increased or the distance between them decreased. Using 0.6 mm diameter copper wire electrodes placed along the sides of a 20 mm diameter rod of 50/50 Pentolite, they obtained a voltage to current ratio of 5.5 ohms. Because the current did not continue to rise after 1 μ sec, they concluded that conduction was limited to a zone about 7 mm wide either because their probes disintegrated or because the explosive products contained a 7 mm wide zone of much higher conductivity. Values of the electrical conductivity have also been determined for a number of condensed explosives by workers at the University of Utah[2,3]. Typical values of the resistivity reported by this group range from 1 to 3 ohm cm while conduction zone widths (measured at the axis) range from 2 to 3 cm. Recently experiments have been undertaken at the Ballistic Research Laboratories, Aberdeen Proving Ground[4] and at the Carnegie Institute of Technology (CIT) in an effort to obtain additional information concerning the conduction zone.

Electrical Resistance of the Ionized Zone

At CIT, the electrical resistance of the ionized zone in Composition B (D = 7.7 mm/μ sec) and 50/50 Pentolite (D = 7.4mm/μ sec)

has been determined using the experimental arrangement shown in Fig.
I. The polyethylene insulators were a necessary part of an experiment
to be described later and were used in this experiment in an effort to
maintain identical boundary conditions. Within the range of currents
used in this experiment, the applied voltage is seen to be a linear
function of the current, the resistance of the conduction zone being
4.3 ohms for Composition B and 3.7 ohms for 50/50 Pentolite.
Additional experiments were performed without polyethylene insulators
using similar charges placed between 1/16 in. thick copper electrodes.
For these "unconfined" charges, the resistance was found to be 6.1
ohms in Composition B and 5.8 ohms in 50/50 Pentolite.

By firing the charges in a transverse magnetic field as
shown in Fig. II, the ionized explosive products, by virtue of their
flow velocity, will produce a current in the external load resistance.
In this experiment the polyethylene sheets serve to insulate the deto-
nation products from the metal pole faces of the magnet. If the con-
duction zone is regarded as a MHD generator, one can determine an in-
ternal resistance for the generator by observing the terminal voltage
as a function of load resistance. According to the relation

$$\frac{1}{V_T} = \frac{1}{EMF} \left(1 + \frac{R_i}{R_L} \right) , \qquad (1)$$

the reciprocal of the terminal voltage is a linear function of the
reciprocal of the load resistance, whose intercept is the reciprocal
of the generator EMF and whose slope is the internal resistance
divided by the EMF. Experimental results obtained from firing Compo-
sition B and Pentolite charges in a magnetic field of 0.28 w/m^2 are
shown in Fig. II, and a summary of the resistance values are presented
below.

	"Confined Charges"		"Unconfined Charges"
Explosives	E Field (ohms)	B Field (ohms)	E Field (ohms)
Composition B	4.3	4.2	6.1
50/50 Pentolite	3.7	3.5	5.8

Width of the Conduction Zone

The width of the conduction zone has been estimated from
results obtained with the experimental arrangement shown in Fig. III.
While one cannot bound the conduction zone by a geometrical plane
behind which the conductivity suddenly drops to zero, the major
portion of the current is limited to a region 1/2 to 3/4 inch wide
for Composition B and to a slightly wider region for 50/50 Pentolite.
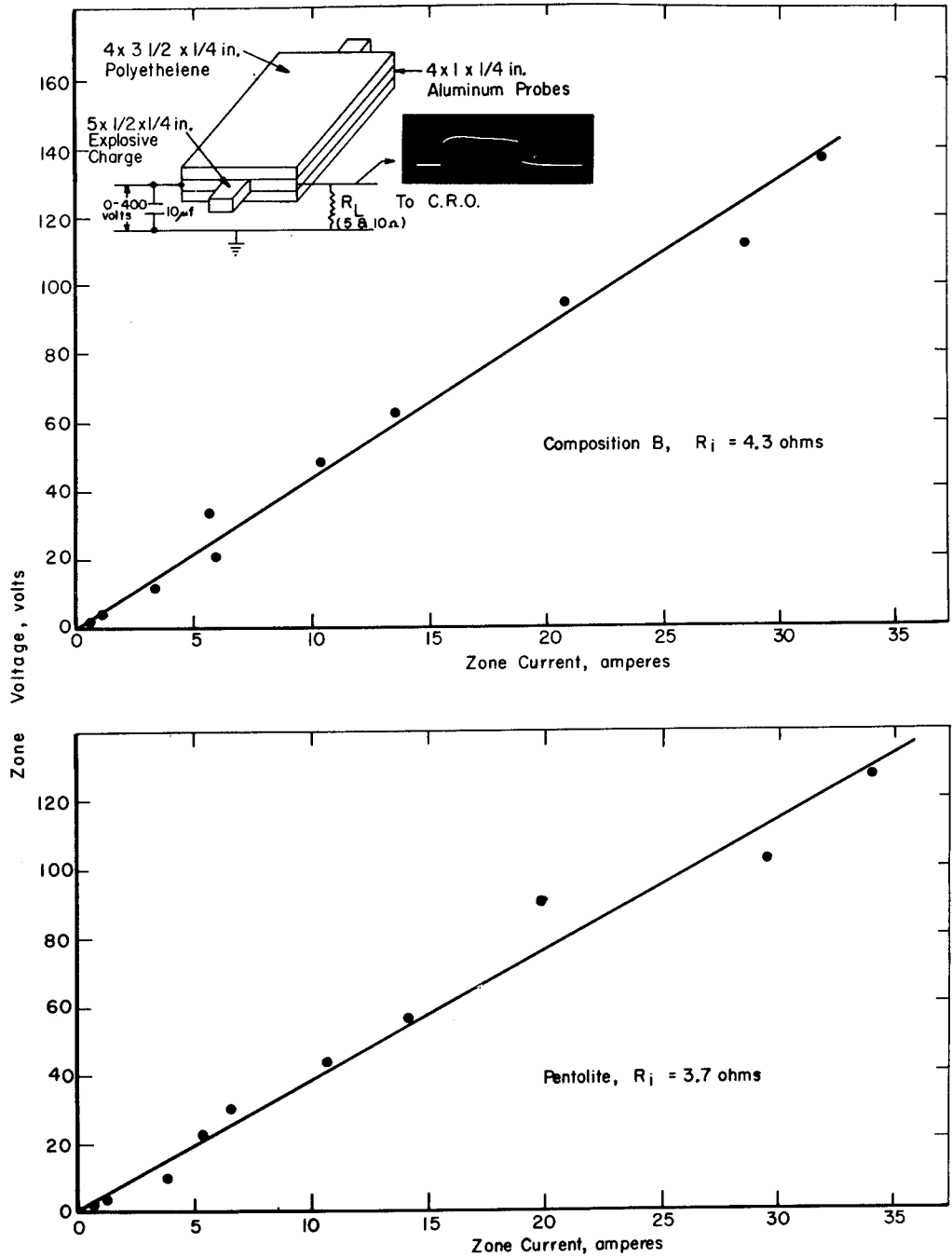
Figure I Experimental arrangement and results of tests performed to determine the internal resistance of the conduction zone of explosive charges detonated in an external electrical field. For the particular charge geometry investigated values of 4.3 ohms and 3.7 ohms were obtained for Composition B (60 RDX / 40 TNT) and Pentolite, respectively.
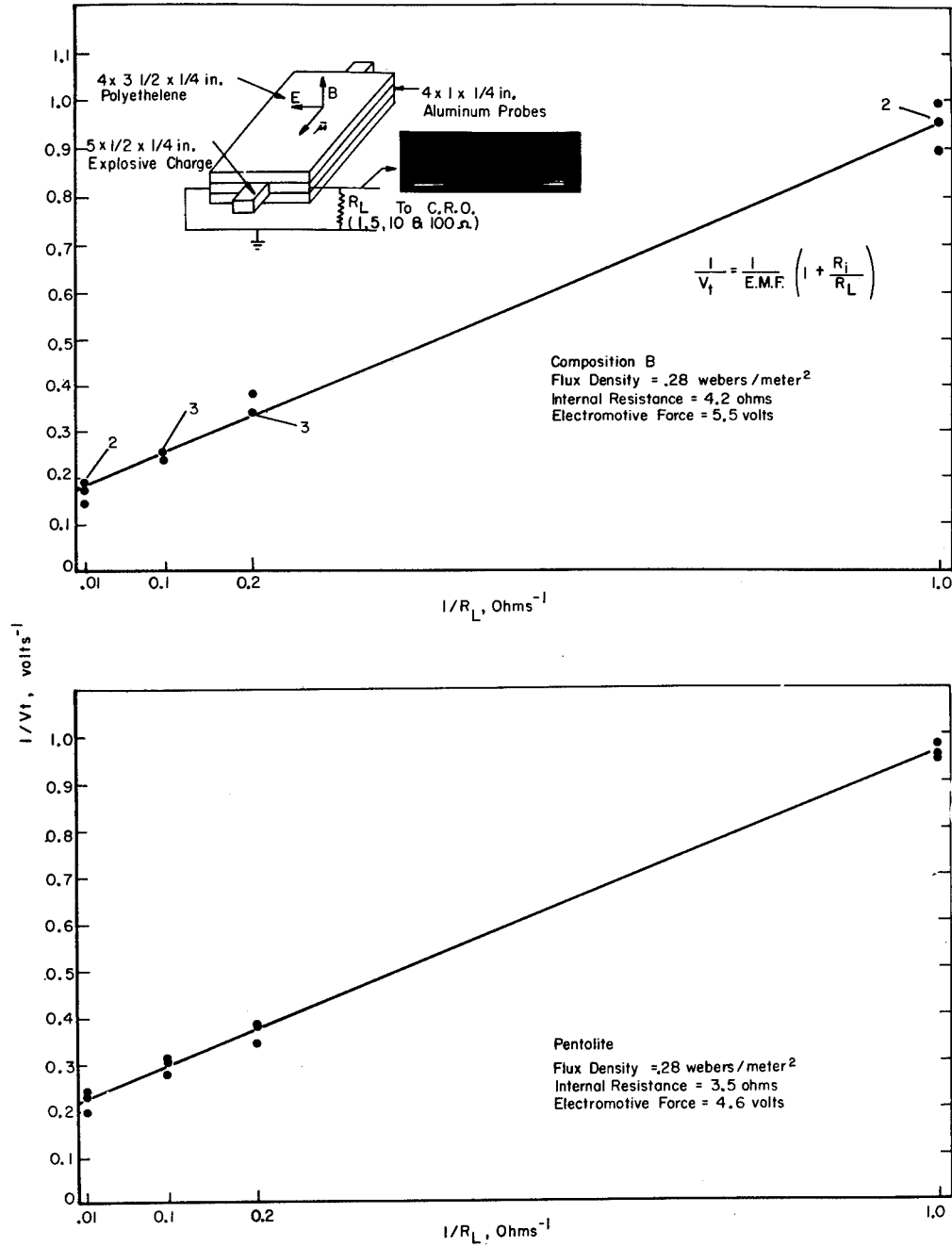
Figure II Experimental arrangement and results of tests performed to determine the internal resistance and electromotive force of the conduction zone of explosive charges detonated in an external magnetic field. For Composition B (60 RDX/40 TNT) values of 4.2 ohms and 5.5 volts were obtained for the internal resistance and electromotive force, respectively. Pentolite charges of identical geometry yielded values of 3.5 ohms and 4.6 volts.
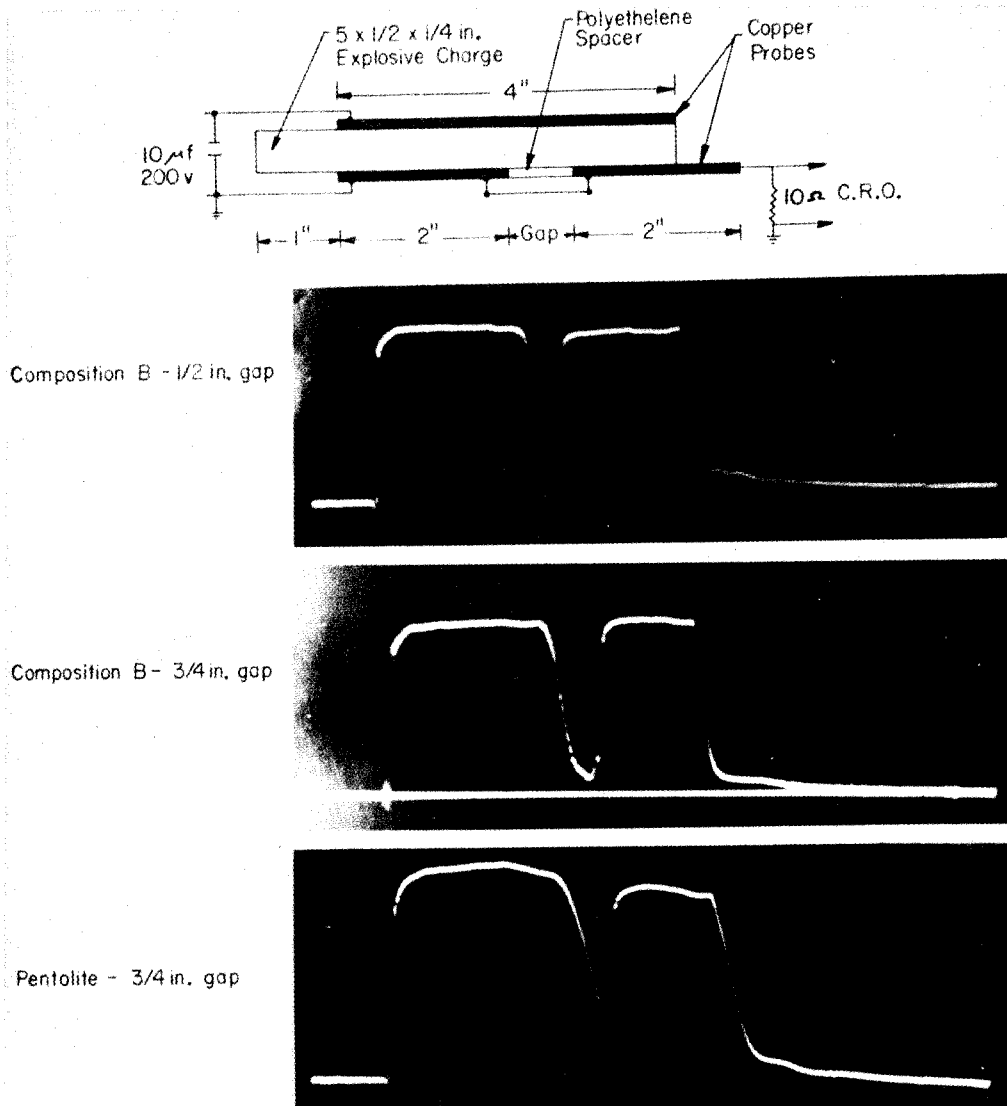
Figure III   Experimental arrangement and results of tests performed in an attempt to define the effective width of the conduction zone in detonating Composition B and Pentolite. Since the values of applied voltage and load resistance used here give rise to a steady state zone current of approximately 13 amperes, the oscillograms indicate that the high conduction region extends approximately 1/2 to 3/4 inches behind the detonation front.

Although the width of conduction zone for 50/50 Pentolite is somewhat wider than that reported by the Israeli group, the difference in zone width is probably due to differences in the degree of confinement. For purposes of estimating the order of magnitude of the resistivity one might assume a zone width of 3/4 in. for Composition B and use the relation $R = \bar{\rho} \ell /A$, which leads to a value of 4.0 ohm cm for $\bar{\rho}$. Thus, the order of magnitude for the zone width and the resistivity are in reasonable agreement with values reported by the Utah group.

The EMF Generated by the Conduction Zone

An estimate of the flow velocity associated with the conduction zone can be obtained from the observed values of the EMF produced by charges detonated in an external magnetic field. Assuming one-dimensional flow the EMF will be related to a mean flow velocity by the relation

$$EMF = B \ell \bar{u} \tag{2}$$

where ℓ is the distance between the probes and

$$\bar{u} = \frac{\int \sigma \, u dx}{\int \sigma \, dx} \tag{3}$$

is an average flow velocity weighted in favor of regions having higher electrical conductivity. In actual practice, one observes the voltage V_T developed across a load resistance, which according to equations (1) and (2) is a linear function of B whose slope is $\ell \bar{u}/(1 + R_i/R_L)$. Experimental results obtained with Composition B and 50/50 Pentolite are shown in Fig. IV. These experimental results indicate values of 1.8 mm/μ sec and 1.2 mm/μ sec for $\bar{u}$ in Composition B and Pentolite, respectively. The use of a 1/2 in. thick charge and heavier confinement, in an effort to reduce effects of lateral expansion, did not significantly increase the measured mean particle velocity. Since these values are significantly lower than the anticipated C-J flow velocity, the conduction zone evidently extends well into the expansion region behind the C-J plane.

Conclusions

For a given configuration of charge and lateral confinement there is a zone of ionization in the detonation products that offers a well defined resistance to the passage of an electric current. Values of the width and resistivity of the conduction zone determined at CIT are in reasonable agreement with those reported by other workers. Observed values of the weighted mean particle velocity, assuming one-dimensional flow, are smaller than the anticipated flow velocity at the C-J plane indicating that the conduction zone extends into the expansion region behind the C-J plane.

Composition B — R_L = 100 ohms

V_t = 21.5 volts, E.M.F = 22.6 volts at $\frac{1\ weber}{meter^2}$

Pentolite — R_L = 100 ohms

V_t = 14.0 volts, E.M.F. = 14.7 volts at $\frac{1\ weber}{meter^2}$
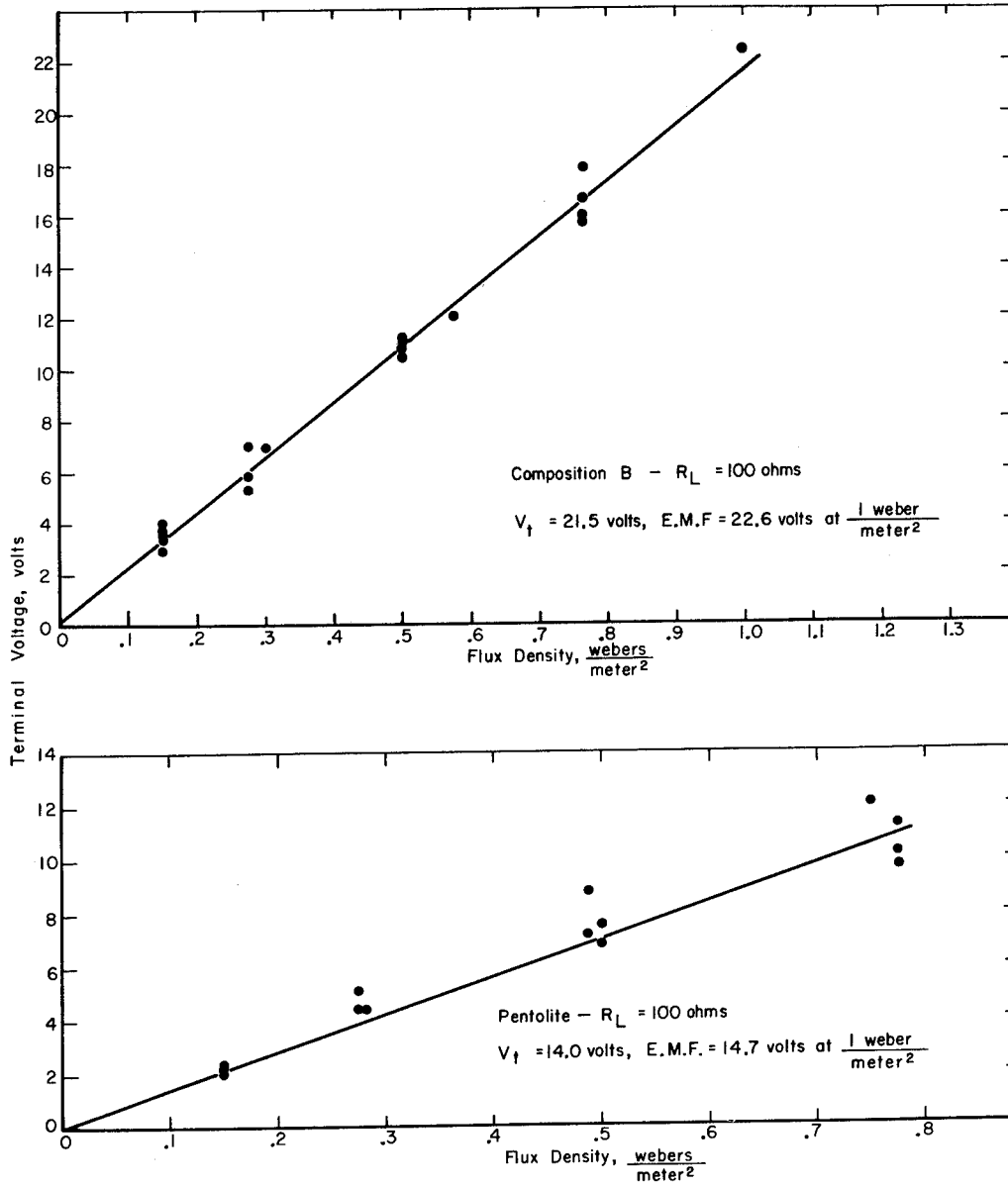
Figure IV   Plots of terminal voltage as a function of field strength for explosive charges detonated in an external magnetic field. On correcting the above results for the potential drop across the zone resistance values of 22.6 volts and 14.7 volts are obtained for the electromotive force at 1 weber/meter² for Composition B and Pentolite, respectively.

118

Acknowledgements

The author wishes to acknowledge the valuable assistance of Mr. R. W. Watson who developed the experimental techniques used at CIT for making the measurements discussed in this paper.

Bibliography

1. M. Birk, A. Erez, Y. Manheimer, and G. Nahmani, Bulletin of the Research Council of Israel, Vol. III, No. 4, 398 (1954).

2. M. A. Cook, R. T. Keyes, and L. D. Lee "Measurements of Ionization and Electron Densities in the Detonation Wave of Solid Explosives," Technical Report No. 1, Contract AF-18(603)-100, ERG, University of Utah, September, 1956.

3. Melvin A. Cook, The Science of High Explosives, Reinhold Publishing Company, New York, 1958.

4. R. L. Jameson, "Electrical Measurements in Detonating Pentolite and Composition B," (Presented at this Conference).

ELECTRICAL MEASUREMENTS IN DETONATING PENTOLITE AND COMPOSITION B

R. L. Jameson
Ballistic Research Laboratories
Aberdeen Proving Ground, Maryland

Introduction

The ability of a detonating high explosive to conduct electrical current has been known for many years. Early uses of this phenomena are found in the work of Peters[1] and Nisewanger and Brown[2] who applied this characteristic of the detonation to the development of explosive switches.

More recently Birk, Erez, Manheimer, and Nahmani[3] investigated the electrical characteristics of a detonation more closely. Their work was once again aimed at developing switches but did include measurements of electrical resistance as well as an estimate of the charge concentration within the conducting media.

Cook, Keyes, Lee, and Pound[4] applied a capacitor discharge method similar to Birk et al to their work in various condensed explosives. The Cook investigation relates various electrical phenomena to the "Detonation head" theory. This investigation, which is the most extensive published to date, lists resistivities for seven explosives and includes a discussion of various possible methods of ionization within the detonation.

Other work is under way in solid explosives at Carnegie Institute of Technology[5] under the direction of Dr. Allison and at Steven's Institute of Technology under the direction of Dr. Lukasik[6] Soviet interest in this work is reflected in an article by Brisk, Turasov and Tsukermann[7] in JETP. These authors used electrode and electrodeless techniques to measure resistance, and included an analysis of the relation of conductivity to pressure in their discussion. Investigations into the electrical nature of intense shocks in gases and of gaseous detonation have been and are being carried out. The techniques of Lin, Resler and Kantrowitz[8] with shock waves in argon has become standard with experimenters dealing in the gaseous state; it has been applied successfully to gaseous detonation by Basu[9] of M. I. T and Gibson and Bowser[10] of Bureau of Mines.

The work described in this paper is intended to be used as ground work for further investigation into the electrical effects of detonation. Emphasis has been placed on the determination of the

resistivity of the explosive products by measuring the resistance and geometry of the conducting zone. Using these measurements and drawing from the experience of other investigators, a value of electron concentration within the conducting zone has been calculated.

Theory

In a simple resistance sample of rectangular cross section, width w and height h, with length l, the resistance R is related to the volume resistivity, ρ, by the equation

$$R = \rho \frac{l}{h\,w} \, . \tag{1}$$

The coefficient of ρ, l/hw, is only defineable for simple regular bodies. In the case of a sample with varying cross section the equation would be better stated as

$$R = K\rho, \tag{2}$$

where K is the coefficient of resistivity, and is considered to be a purely geometrical quantity. If K can be found experimentally, a measurement of R can be made to compute the volume resistivity. The reciprocal of volume resistivity is called the conductivity:

$$\sigma = \frac{1}{\rho} \, . \tag{3}$$

The total conductivity within a material is the sum of the contributions from all charged particles.

$$\sigma_T = \Sigma \sigma_j \tag{4}$$

$$\sigma = nqU \tag{5}$$

n is the number of ions per unit volume, q the charge of the ions, U the mobility of the ions. If the particles within the conductivity zone are limited to electrons and positive ions, then the assumption that

$$\sigma = \sigma_e + \sigma_{pi} \approx \sigma_{eg} \tag{6}$$

because $U_e \gg U_{pi}$, is valid

$$\sigma = n_e U_e \tag{7}$$

where e is the charge on the electron.

In order to compute the electron concentration n_e, a value for the mobility of an electron must be established. Birk et al used relations found in the work of Compton and Langmuir, while Cook et al applied Drude's "Elementary Theory of Electronic Mobility". The work of Compton and Langmuir, an application of kinetic theory; Drude's theory, as published in 1900, was originally intended to apply to electrons in metals, but the form used by Cook contains kinetic theory assumptions and the mobility computed from it is approximately

equal to that computed from the Compton equation. The use of kinetic theory at 0.2 megabars pressure and doubtful conditions of equilibrium can only be considered as an approximation. It must be remembered that values of molecular diameter used to estimate the mean free path are measured for pressures less than one atmosphere and, therefore, the actual mean free path is probably shorter than calculated. With the statement of these limitations the ion concentration was calculated from this equation.

$$n_e = \frac{\sigma}{e\,U_e} = \frac{\sigma}{e} \left(\frac{3\pi \sqrt{m\bar{M}}\;E}{8\,e\,L_e} \right)^{1/2} \tag{8}$$

where m is the mass of the electron, $\bar{M}$ the average mass of the positive ion, E the field intensity, and L_e the mean free path of the electron. L_e is estimated from

$$L_e = 4\sqrt{2L} \tag{9}$$

where L is the mean free path for the gas. The determination of the conductivity was made by the following experiments.

Experimental Details and Results

1. Resistance

Measurements of conductivity in shocks and detonating explosives had previously been made by two general techniques: the Lin method, using field and search coils; and a simple capacitor discharge electrode method. Although the Lin method eliminates the interference of electrodes, it was prohibitively expensive in the present case due to the destructive nature of the experiment. Therefore, an electrode technique was decided upon for the experiment.

In order to eliminate as much of the influence of the electrodes as possible a method of determining resistivities from several shots was devised. The resistance across a charge was determined by measurements made with the circuit shown as Figure 1. All resistance measurements were made with electrodes placed along the length of the charge as shown in Figure 2. In order to confine the conduction to the charge as much as possible, each shot was fired in an atmosphere of propane (Figure 3). Propane has been shown by Hauver[14] to be many orders of magnitude less conducting than air at very high shock pressures. Many measurements of resistance were made with this set-up, using various charge sizes and electrode widths. The resistances are tabulated in Table I

2. Geometry of Conducting Zone

To determine the resistivity from equation 2 of the theory section, a value of the coefficient of resistivity had to be determined. A first approximation could be made by considering the limits of $K = \frac{1}{A}$. The lower limit of K is obtained when l is equal to the distance between the electrodes and A is the product of
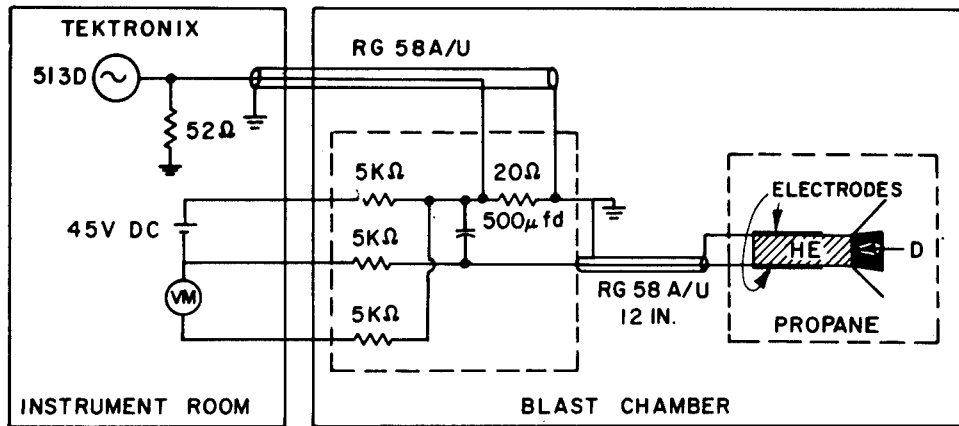
Fig. 1 Schematic diagram of resistance
measurement equipment
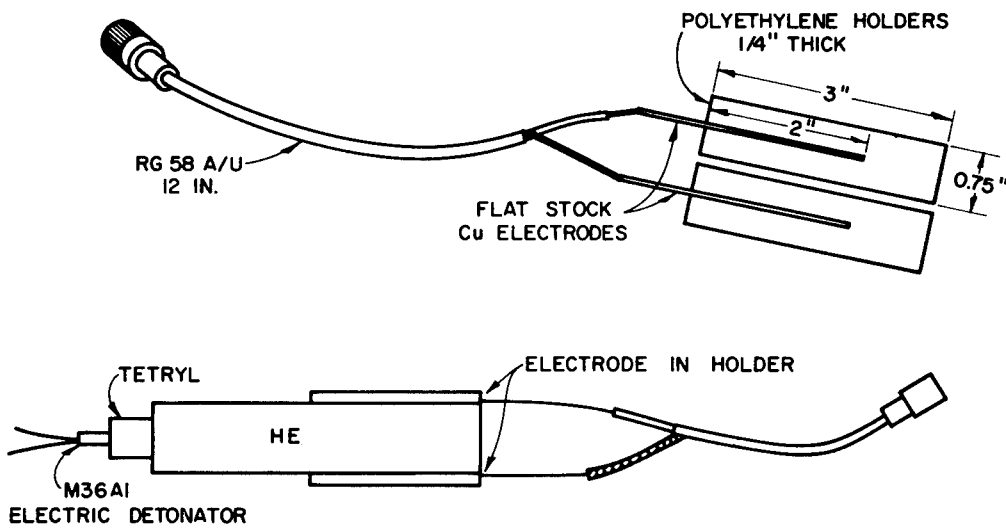
Fig. 2 - Electrodes with attached cable and
electrode arrangement on charge
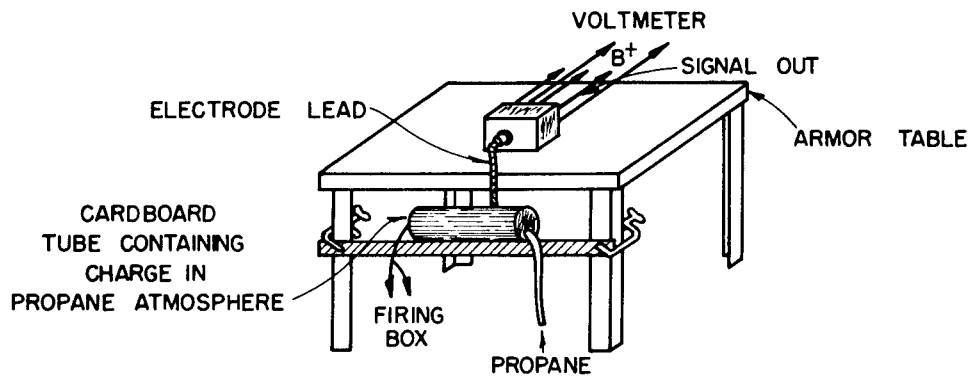
Fig. 3 - Blast chamber set-up of
test box and charge

Table I

Resistance Measurements in Detonating Exllosives

A. Pentolite

Thickness cm	Electrode Width cm	Confinement Thickness cm	Coefficient of Resistivity cm^{-1}	R ohms	Volts	I amps
1.27	0.159	0.635	7.53	2.4	6.1	2.6
1.27	0.318	0.635	5.91	2.0	5.4	2.6
1.27	0.635	0.635	4.33	1.3	3.7	2.8
1.91	0.159	0.635	8.08	3.1	7.8	2.5
1.91	0.318	0.635	6.90	2.9	7.2	2.5
1.91	0.625	0.635	5.27	2.1	5.3	2.5
2.54	0.159	0.635	9.48	3.8	9.1	2.4
2.54	0.318	0.635	7.53	3.0	7.5	2.5
2.54	0.635	0.635	5.98	2.3	5.9	2.6
2.54	0.635	0.635	5.98	3.2	7.8	2.5
2.54	0.318	0.635	7.53	3.4	8.4	2.5

B. Composition B

Thickness cm	Electrode Width cm	Confinement Thickness cm	Coefficient of Resistivity cm^{-1}	R ohms	Volts	I amps
1.27	0.159	0.635	7.53	2.3	6.1	2.6
1.27	0.318	0.635	5.91	2.2	5.8	2.6
1.27	0.159	0.635	7.53	3.8	9.0	2.4
1.27	0.318	0.635	5.91	1.9	5.0	2.6
1.27	0.318	NC	NM	2.9	7.1	2.5
1.27	0.159	0.635	7.53	2.8	8.3	3.0
1.91	0.159	0.635	8.08	3.9	9.2	2.4
1.91	0.318	0.635	6.90	2.2	5.9	2.6

Table I

Resistance Measurements in Detonating Explosives

B. Composition B

Thickness cm	Electrode Width cm	Confinement Thickness cm	Coefficient of Resistivity cm^{-1}	R ohms	V Volts	I amps
1.91	0.318	0.635	6.90	2.1	5.5	2.6
1.91	0.318	NC	NM*	3.7	8.8	2.4
2.54	0.159	0.635	9.48	3.3	8.1	2.5
2.54	0.318	0.635	7.53	2.6	6.8	2.6
2.54	0.159	0.635	9.48	3.2	7.8	2.4
2.54	0.318	0.635	7.53*	2.5	6.3	2.6
2.54	0.318	NC	NM*	3.8	9.0	2.4
2.54	0.159	0.635	9.48	3.2	9.5	3.0

*Not Measured

the conduction zone width at the surface of the charge and the charge width; that is to say, the conduction zone is considered a slab. This conduction would be true as $\rho \rightarrow \infty$. The upper limit of $\frac{1}{A}$ is obtained when 1 is equal to the distance between electrodes and A is the product of conduction zone width at the surface and the width of the electrode. This condition would be true for $\rho \rightarrow 0$. The actual value for K should be between these limits if the zone geometry is a slab. In the determination of A, the zone width at the surface was measured for both unconfined and semiconfined cases. Electrodes were placed on the surface perpendicular to the long axis of the charge and were directly opposing. Oscilloscope records of these firings are shown as Figure 4. Using the length of the electrodes in the direction of detonation and the detonation velocity, values of zone width can be calculated. The length of the conducting zone on the surface for a semiconfined Pentolite or Composition B charge was determined to be 1.7mm; unconfined, the zone is 0.2mm long. The limits of K for semiconfined charges are: $1 = 2.54$cm, $K = 7.9 - 94.1$cm^{-1} (upper limit computed width narrowest electrode); $1 = 1.90$cm, $K = 5.9 - 70.4$cm^{-1}; $1 = 1.27$cm, $K = 4.0 - 47.0$cm^{-1}. The limits of K unconfined are: $1 = 2.54$cm, $K = 66.8 - 798.7$cm^{-1}; $1 = 1.90$cm, $K = 50.0 - 597.5$cm^{-1}; and $1 = 1.27$cm; $K = 33.4 - 399.4$cm^{-1}.

To further define K, an experiment was performed in which 3.2mm diameter brass electrodes were embedded into square cross section charges as shown in Figure 5. A typical oscilloscope record of these firings is shown as Figure 6. The duration of the signal from each electrode set was used to calculate the width of the conduction zone at that distance from the axis of the charge. Plots of these points are shown as conduction region profiles in Figure 7. Conduction for this geometry is highest in a pyramidal region. Profile measurements were also made in 2.54cm diameter confined charges with the electrode arrangement shown as Figure 8. The profiles drawn from the data are shown as Figures 9 and 10. Conduction for this geometry is highest in a conical region.

3. Resistivity

A method of calibrating the electrodes was derived from the shape of the zone of highest conductivity determined by the probes. Graphite sheets with a resistivity of 0.235 ohm-cm were used to make models of the conductivity zone. The electrodes were placed across the sample in the same manner as in the explosive experiment and resistance measurements were made using a Wheatstone Bridge. Knowing the resistance and the resistivity, the value of K was calculated. The values of K are tabulated in Table II.

With these values of K, it was now possible to plot the resistance vs K to determine the value of the resistivity from the slope of the lines. These plots are shown in Figure 11 for 50/50 Pentolite (density, 1.6 gm/cc; detonation velocity, 7.5 mm/μsec) and in Figure 12 for 60/40 Composition B (density, 1.6 gm/cc and
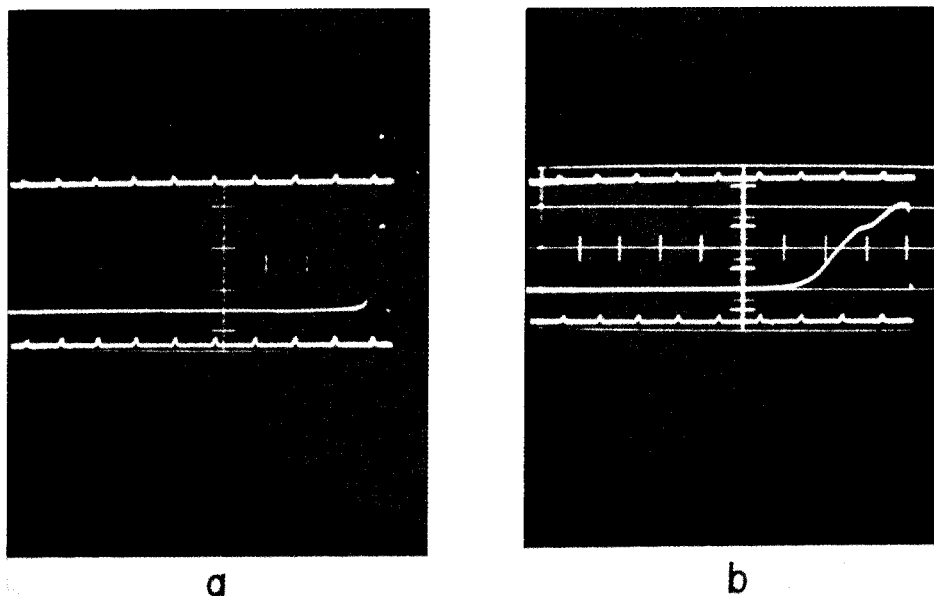
Fig. 4 - Surface electrode conduction traces for unconfined pentolite (a) and semiconfined penolite (b) (one microsecond time marks)

ELECTRODE SETS A, B & C
CONNECTED IN PARALLEL
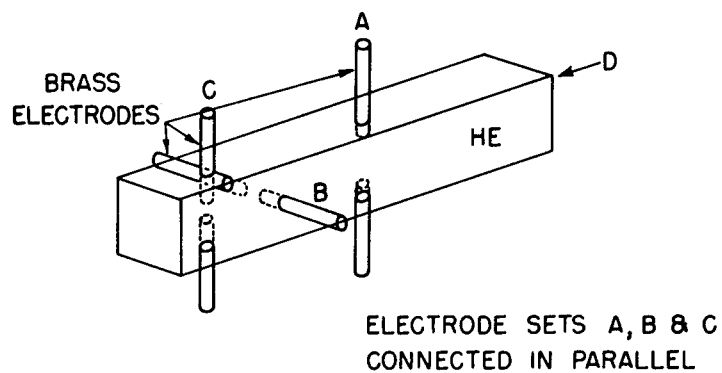
Fig. 5 - Electrode arrangement in square cross section charge
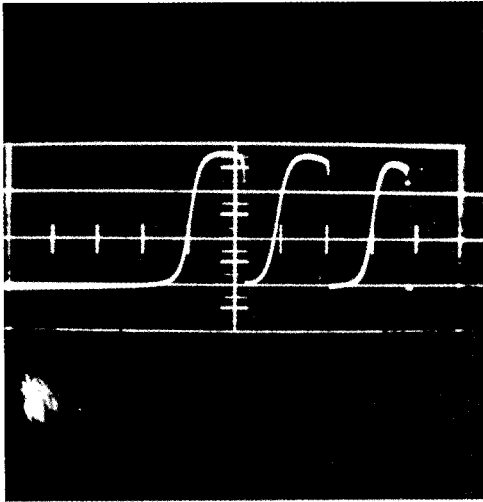
TIME I μ SEC/CM

Fig. 6 - Conduction trace from three sets of electrodes placed within a pentolite charge at decreasing distances from the axis (from right to left)

10 MM

19 MM

□ = I MM
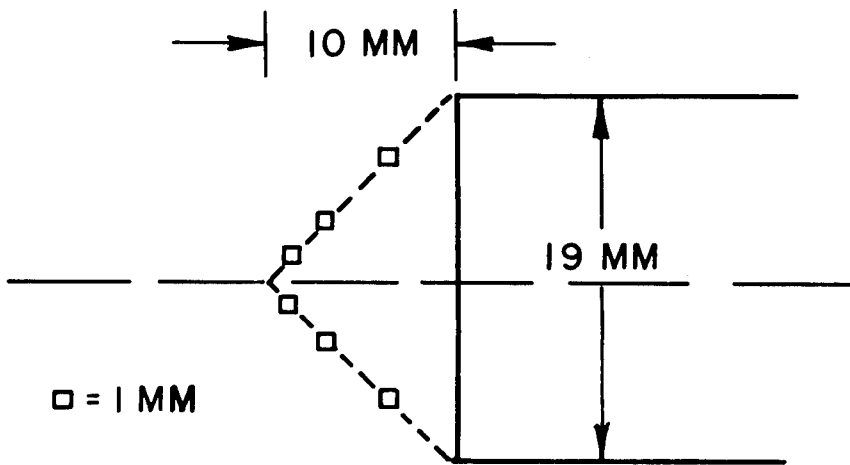
Fig. 7 - Constant conductivity profile 19 mm sq. x 152 mm long 50/50 pentolite stick unconfined

129

POLYETHYLENE
1/8" WALL

1/8" DIA. BRASS ELECTRODES

A ROTATED 60° FROM, B ROTATED 60° FROM C
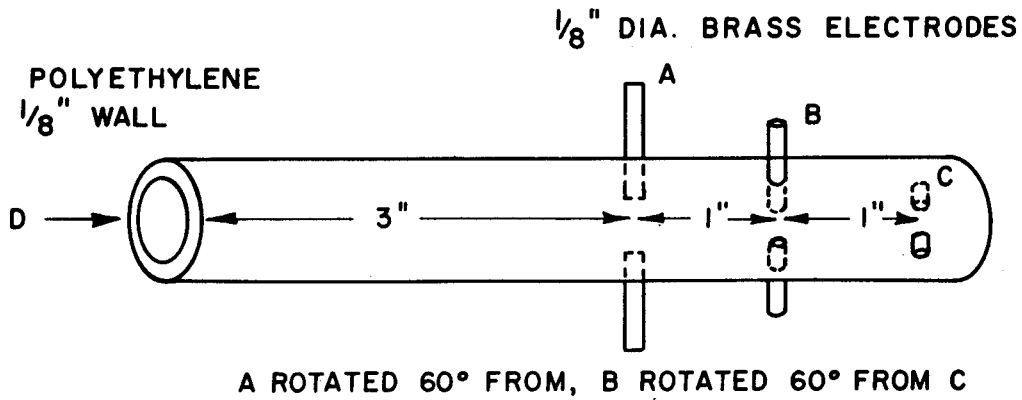
Fig. 8 - Electrode arrangement in confined cylindrical charges
for profile measurements

11.3MM

□ = 1 MM
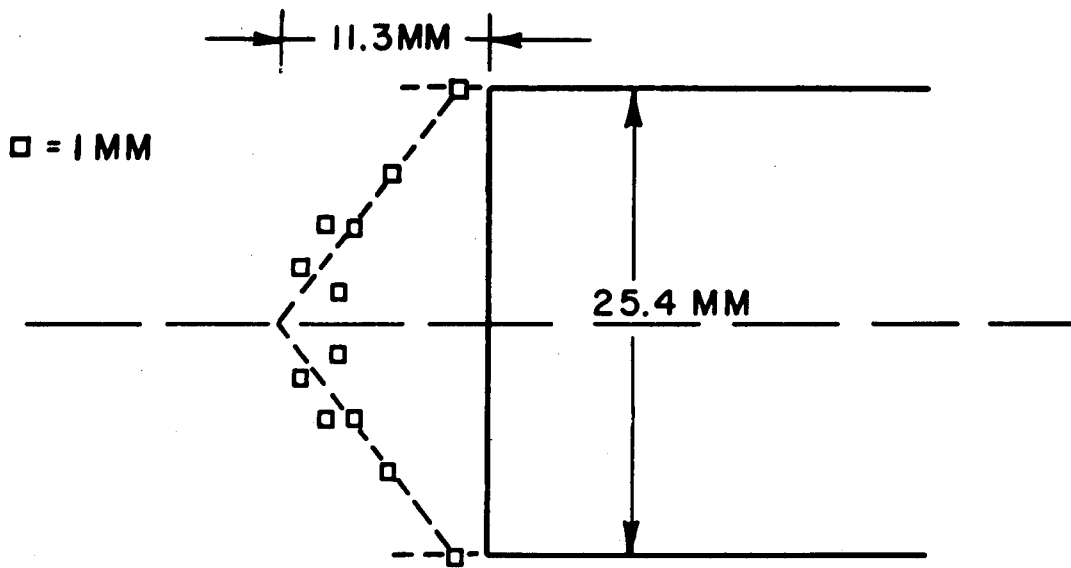
25.4 MM

Fig. 9 - Constant conductivity profile 25.4 mm dia., 50/50
pentolite confined by 3 mm polyethylene
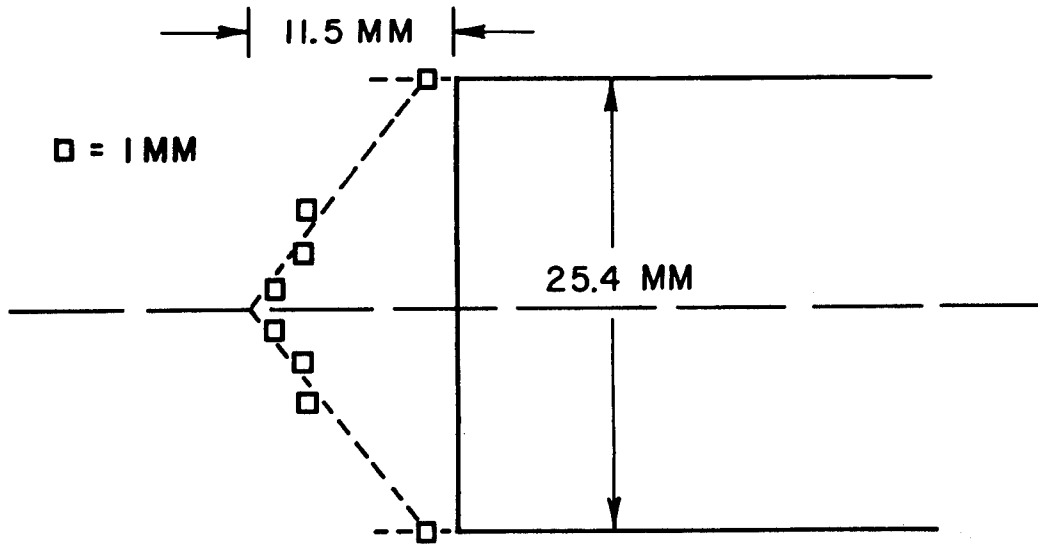
Fig. 10 - Constant conductivity profile 25.4 mm dia., comp. B
confined by 3 mm polyethylene
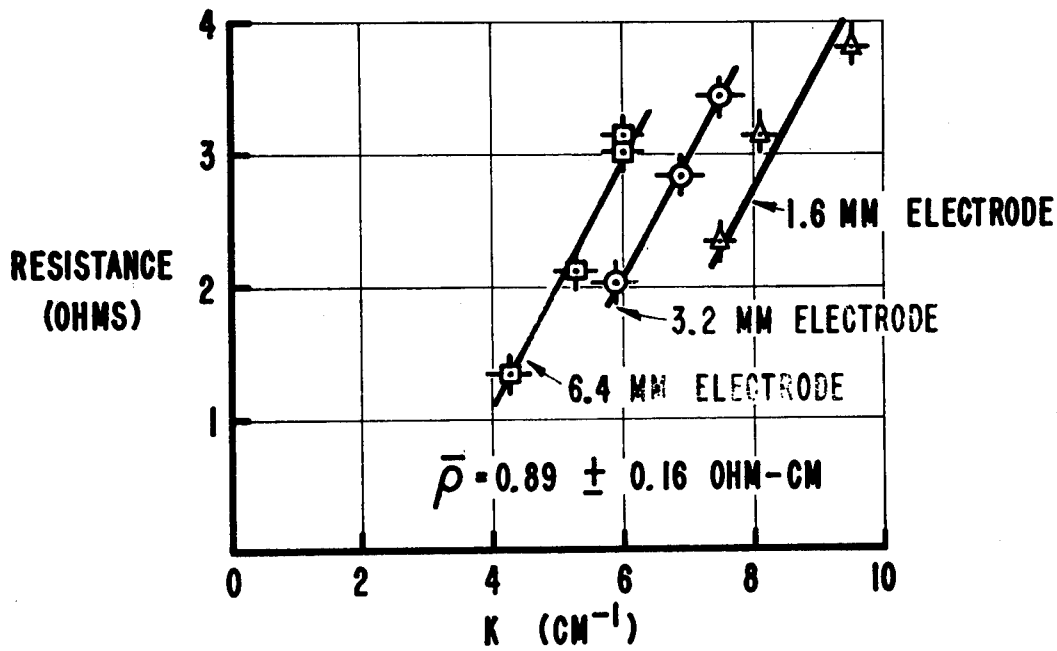
Fig. 11 - Resistance vs geometrical coefficient of
restivity for 50/50 pentolite
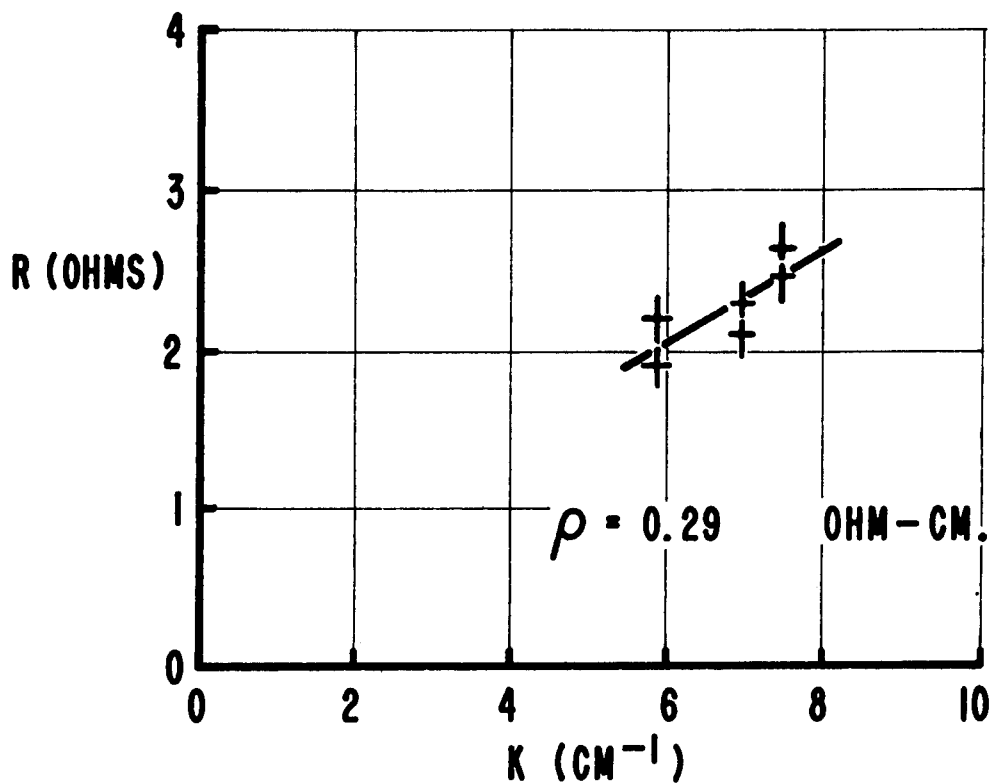
Fig. 12 - Resistance vs geometrical coefficient of
resistivity for 60/40 composition B

Table II

Electrode Width cm.	Distance between electrodes cm.		
	1.27	1.90	2.54
0.159	7.53	8.08	2.54*
0.318	5.91	6.90*	7.53*
0.635	4.33	5.27*	5.98*

* Fall outside theoretical limits due to the experimentally determined zone geometry deviating from idealized slab.

detonation velocity, 7.8 mm/μsec). Only the 0.318 cm electrode results are plotted for Composition B. Due to the dispersion in the results using the 0.159 cm electrodes, it was impossible to calculate a significant slope from the data. The dispersion is attributed to non-uniformity of explosives due to a change of explosive lots. An average value of the resistivity was calculated for 50/50 Pentolite to be 0.89 ohm-cm. The Composition B resistivity was calculated to be 0.29 ohm-cm.

The values of the resistivity were calculated from data taken with the semiconfined charges. However, it is believed to be valid for the unconfined charges as well. Figure 13 shows the difference in voltage drop across semiconfined and unconfined charges. The resistance of an unconfined charge is about 50% higher than that of a semiconfined charge. This can be explained by the difference in the contact area at the charge surface; thus the conduction cross section is different in each case. The ion concentration should be the same for both conditions.

4. Ion Concentration

From the values of resistivity that have been computed, it is possible to form an estimate of ion concentration, using equation 8. The values of n_e thus computed are: $n_e = 1.2 \times 10^{19}$ electron/cc for Pentolite; and $n_e = 3.6 \times 10^{19}$ electron/cc for Composition B These calculations are based on an assumption that there is only single ionization and that electrons contribute to conduction very much more than the positive ions. The values used in these calculations were: $e = 1.6 \times 10^{-19}$ coulombs; $L_e \approx 5 \times 10^{-7}$ cm; $m = 9.1 \times 10^{-28}$ grams; $\bar{M} = 4 \times 10^{-23}$ grams; and $E = 1$ volt/cm.

The location of the conduction zone with reference to the reaction zone was determined by a combination of electronic and optical techniques. A Pentolite charge was cast in a manner that allowed 3 mm diameter electrodes to be inserted 3mm into the charge directly opposing each other. These electrodes were connected by RG 58 A/U coaxial cable to the conductivity test circuit and its signal displayed on one
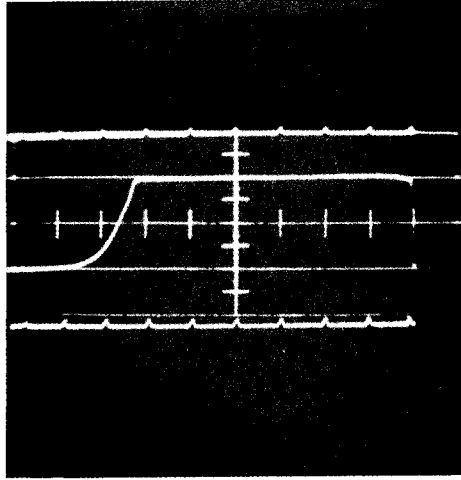
a
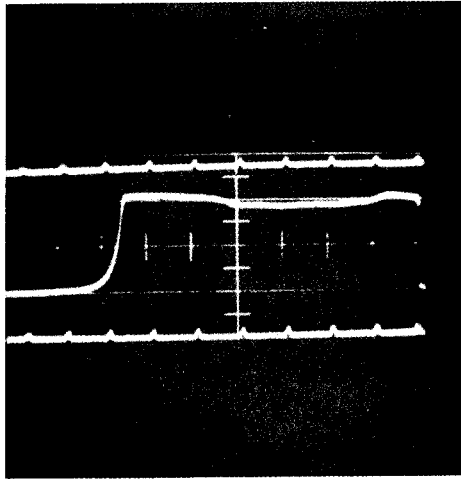
b

Fig. 13 - Conduction traces for pentolite semiconfined (a) and composition B with unconfined center section (b)

channel of a Tektronix 551 dual beam Oscilloscope. The shutter signal
of a Kerr Cell camera used to observe the event was displayed on the
second channel of the oscilloscope. A box with a saran window was
prepared and the explosive charge placed in it. The box was filled
with propane, as in other conductivity experiments. Front lighting
for the event was furnished by an Argon flash bomb. An ionization
switch, capacitor trigger circuit was used to syncronize the camera
and trigger the oscilloscope. The Kerr Cell photograph and oscilloscope
record are shown as Figure 14. After the correction for the time
difference of conduction and picture is made and correction for curvature
of the front, the front of the conduction zone is located at the rear
of the reaction zone.

Discussion of Results

Resistance measurements made by this author are generally in
agreement with those made by other groups working in similar phases of
the explosive conduction problem. There have been different methods
used to calibrate the equipment that have led to some differences
in the calculated resistivities. Values of resistivity for Composition
B have been measured by three groups; Cook reported 2.56 ohm-cm; the
Soviet group, 0.2 ohm-cm; and this author, 0.29 ohm-cm.

Ion concentrations have been reported by Cook to be about
10^{18} electron/cc; Birk et al, about 10^{20} electron/cc; and this author,
about 10^{19} electron/cc. The difference arise from differences in
computing the mobility. However, the values are only approximations
and can therefore be considered in good agreement.

There is some disagreement about the location of the conduction
zone. Cook locates the conduction zone ahead of the Chapman-Jouquet
plane; the Soviet group, at the detonation zone; and this author, at
the end of the reaction zone, which could be considered at the Chap-
man-Jouguet plane in an ideal explosive.

The shape of the zone of high conduction seems to depend on
the geometry of the explosive itself. For a square cross section charge,
the shape is pyramidal with a square base, and for a circular cross
section charge the zone shape is a cone with a circular base. Some
authors report the decay of conduction traces to be due to recombination;
however, there is evidence to support the argument that the high con-
duction zone is the zone of highest density within the detonating
charge and that the decrease in conduction is due mainly to the expan-
sion in the gases accompanying the release wave moving into the dense
gases from the charge boundaries. The Soviets have found the conduction
to be directly proportional to some power of the pressure and density.
This would seem logical, since conductivity is proportional to con-
centration of charge carriers, which would be a function of pressure.
The conduction profiles computed from probe measurements have approx-
imately the same dimensions as the high density zone seen in the radio-
graph shown as Figure 15. Larger charges must be fired to determine
the range of conditions under which the release wave is more important
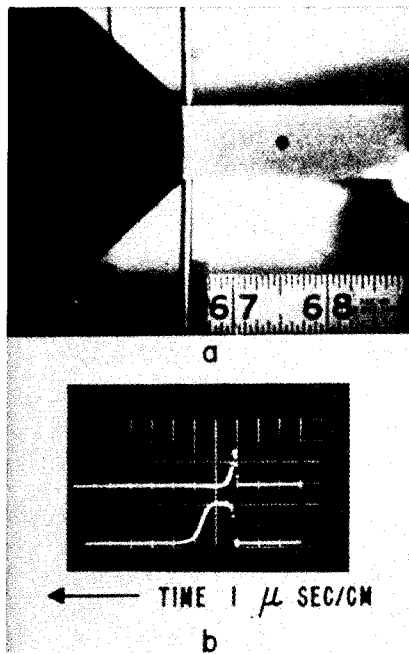
Fig. 14 - Kerr cell camera photograph of pentolite charge in propane at time of conduction (a) and oscillograph record of Kerr cell pulse and conduction pulse (b)
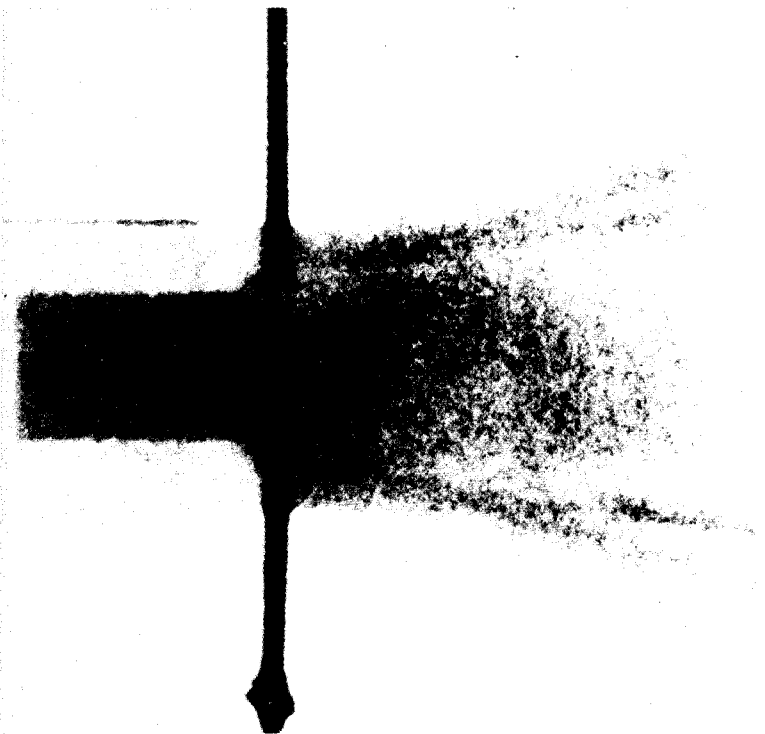
Fig. 15 - Flash radiograph of semiconfined pentolite charge showing electrode position and high density gas zone

than recombination.

Conclusion

Resistivities that have been calculated from the resistance and geometry of the conducting region agree quite closely with those determined by other authors using less direct approaches. The conducting zone in detonating explosives is bounded by the reaction zone in the front and the release wave on the sides. In large charges recombination is more important in determining the length of the conducting zone than in the smaller charges used in this experiment.

Bibliography

1. Peters, M., Z ges. Schiess Spreng. 39, 75, (1944).

2. Nisewanger, G. R. and Brown, F W., Bureau of Mines, R. I. 3879, (1946)

3. Birk, M., Erez, A , Manheimer, Y. and Nahmani, G., Bulletin of the Res. Coun. of Isreal, 3, 4 (1954).

4. Cook, M. A., Keyes, R. T., Lee, L. D., and Pound, E. F., Technical Report I, University of Utah, (1956)

5. Allison, F., Carnegie Institute of Technology (present at this meeting).

6. Lukasik, S., Stevens Institute of Technology, Quarterly Progress Report, December 1959, Contract DA-28-017-501-ORD-3450.

7. Birsk, A. A., Tarasov, M. S., and Tsukerman, U. A., JETP, 1095, V. 37, No. 6.

9. Lin, S. C. Resler, E. L., and Kantrowitz, A., Journal of Applied Physics, 26, 95, 1955.

9. Basu, S., M. I. T., Thesis for degree Doctor of Science.

10. Gibson, F. and Bowser, M., Bureau of Mines, Quarterly Report Project 1102, 1959.

11. Compton, K. T. and Langmuir, I. Rev. Mod. Phys., 2, 204, 1930.

12. & 13. Kennard E., Kinetic Theory of Gases, McGraw-Hill 1938, 470-475

14. Hauver, G., Private communication.

ON THE ELECTRICAL CONDUCTIVITY OF DETONATING HIGH EXPLOSIVES*

Bernard Hayes
University of California, Los Alamos Scientific Laboratory
Los Alamos, New Mexico

Ordinary condensed organic explosives are nearly perfect insulators under normal conditions of temperature and pressure. This situation changes drastically when their molecular structures are altered either by a strong shock or by detonation; and, consequently, they become highly conductive. The nature of the conduction process is not known. Undoubtedly, electrons bear most of the charge transferred, but the motion of the massive ions should not be completely discounted. If electronic conduction predominates, there is some justification in applying Ohm's law and obtaining a conductivity coefficient relating the current density to the electric field strength. However, one should resist the temptation then to assume collision cross sections and temperatures in order to calculate electron concentrations.

Practical use may be made of the fact that the high conductivity causes essentially 100% reflection of a microwave electromagnetic field; and it also allows one to obtain excellent time-of-arrival signals. As an example of the latter function consider Fig. 1. For this pin-signal record the explosive consisted of ten discs of Composition B stacked one on top of the other. Each disc was 1 in. in diameter and only 0.060 in. thick. The pin machine time marks on the raster record are $\frac{1}{2}$ μsec apart. The next to last foil was broken causing the void between the last two signals on the signal line. It is interesting to note that before the first signal was recorded, the second and third signals were also progressing down the signal line. Before discussing the details of the circuit used to produce this record we shall first determine the conductivity to be expected from detonating Composition B and the equivalent circuit of pin circuits in general.

One technique for determining the conductivity of the reaction products of a detonating high explosive is illustrated in Fig. 2. In this figure are shown the experimental arrangement of the explosive and a coaxial test cell. In addition to containing a portion of the

-- -- -- -- -- -- --
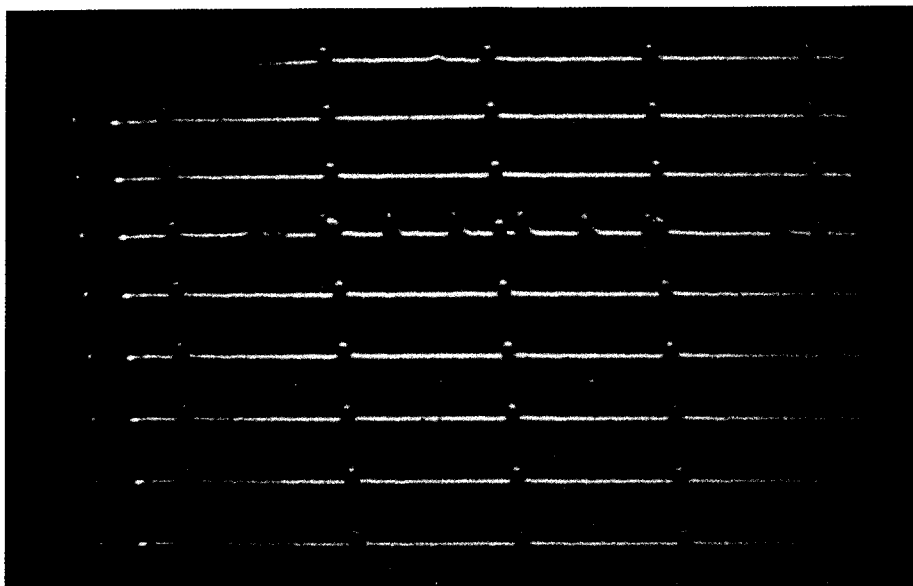
Fig. 1. Fast Pin-Signal Record.
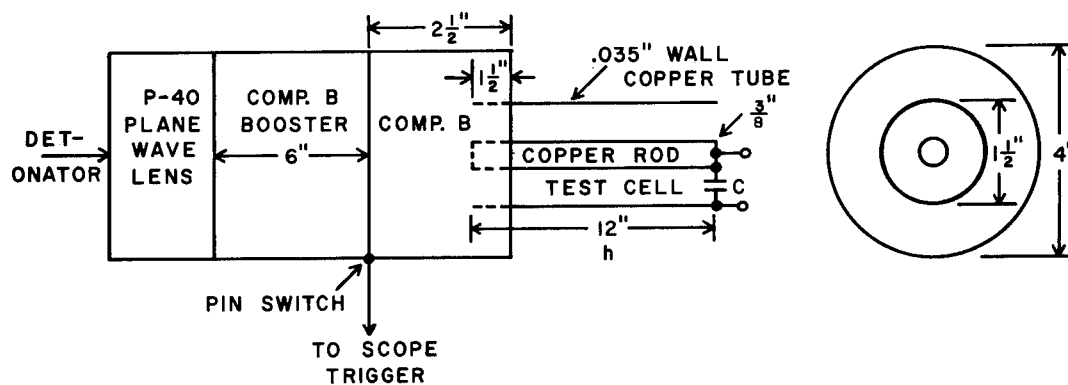
Fig. 2. Experimental Conductivity Setup.

explosive, the test cell proper acts as a high-quality inductance.[1] Also, for this type of test cell the conductivity of the explosion products between the inner and outer coaxial copper cylinders is directly proportional to the conductance. Across the open end of the inductance is a high-quality capacitor to complete the series resistance, inductance, capacitance, ringing circuit. The chief advantages of such a system is that the device does not require calibra-

tion, it maintains a high degree of symmetry, and causes a minimum of disturbance to the detonation products.

The interpretation of the experimental results is based on the premise that the decay in the amplitude of oscillations of this ringing circuit is due to the energy absorbed in the resistive component, which in this case is the explosion products. The resistive component, however, is not constant, but decreases with time as the detonation progresses through the test cell. Consequently, the decay of the envelope of the oscillations does not fall exponentially, but rather is a function of the total resistance between the inner and outer conductors of the test cell.

The equivalent series circuit and recording method for the test cell are shown in Fig. 3, along with the defining circuit equations. There is an initial DC voltage present across the capacitor prior to the detonation front entering the test cell. R_L is the resistance of the copper electrodes while r_s is the resistance of the explosion products in the test cell.

$$L\frac{di}{dt} + (R_L + r_s)i + \frac{1}{C}\int i\,dt = 0$$

$$q = \int i\,dt = CV$$

$$LC\frac{d^2V}{dt^2} + C(R_L + r_s)\frac{dV}{dt} + V = 0$$

$$V_c = V_o \exp\left\{-\frac{1}{2L}\int(R_L + r_s)dt\right\}\cos g(t)$$

$$\sigma = \left\{2\mu hut\frac{d}{dt}(\ln V)\right\}^{-1}$$
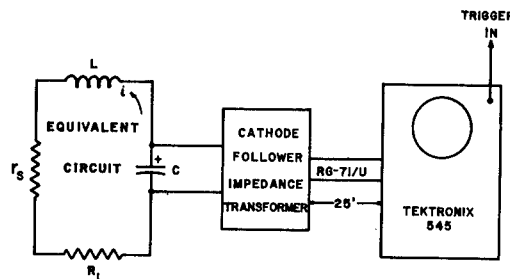
Fig. 3. Circuit Schematic and Defining Equations.

A solution of the homogeneous differential voltage equation for the voltage across the capacitor as a function of time is of the form

$$V_c = V_o \exp\left\{-\frac{1}{2L}\int(R_L + r_s)dt\right\}\cos g(t)$$

where V_o is the initial voltage across the condenser. The exact expression for $g(t)$ can be written out, but it is not necessary in this case to know the function since the recorded waveform is measured at the peaks of the periodic waveform where the function $\cos g(t)$ equals approximately one.

By neglecting the resistance of the copper electrodes in comparison to the resistance of the explosion products it can be shown that the conductivity becomes

$$\sigma = \left\{2\mu hut\frac{d}{dt}(\ln V)\right\}^{-1}$$

where μ is the permeability of the copper, h is the height of the coaxial cylinders, u is the detonation velocity of the wave entering the test cell and V is the ratio of the initial voltage on the condenser to the voltage at the peaks at the time t. Thus the conductivity is seen to be inversely proportional to the slope of the logarithmic decrement and the time. Information on these latter two variables is obtained from the experimental record.

The cathode follower, in addition to maintaining an initial charge on the condenser prior to detonation, also acts as an impedance transformer between the high-impedance oscillatory circuit and the terminated signal cable. Furthermore, the cathode follower must be especially designed to operate as a linear device since it must not introduce any amplitude distortion. The gain of the device is not important since voltage ratios are ultimately desired.

A typical voltage waveform is shown in Fig. 4. The waveform at
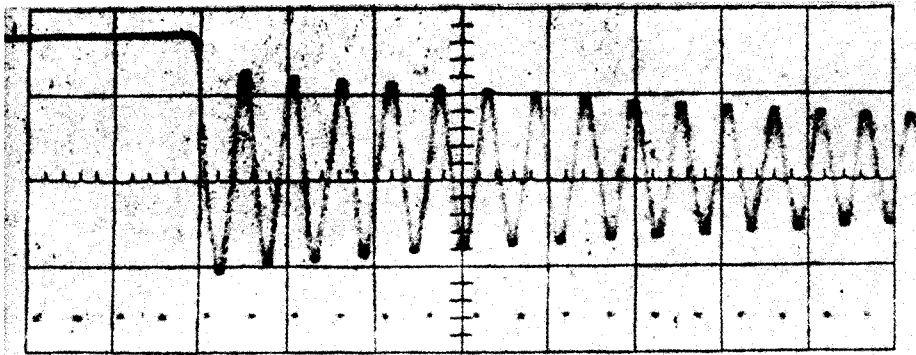
Fig. 4. Recorded Experimental Waveform.

the nodes has been intensified somewhat for reproduction purposes. However, measurements are made only at the peaks of the waveform and

these points are quite distinct. The timing marks for this record are made from a 20-megacycle pulsed oscillator. The total sweep length is one microsecond, and is close to the maximum attainable for single-shot photography utilizing our present equipment. Higher operating frequencies are desirable for greater resolution as we shall shortly see.

The conductivity profile for Composition B as determined from the preceding analysis is shown in Fig. 5 for two different operating frequencies.[2] Although the frequency of operation of the test cell is
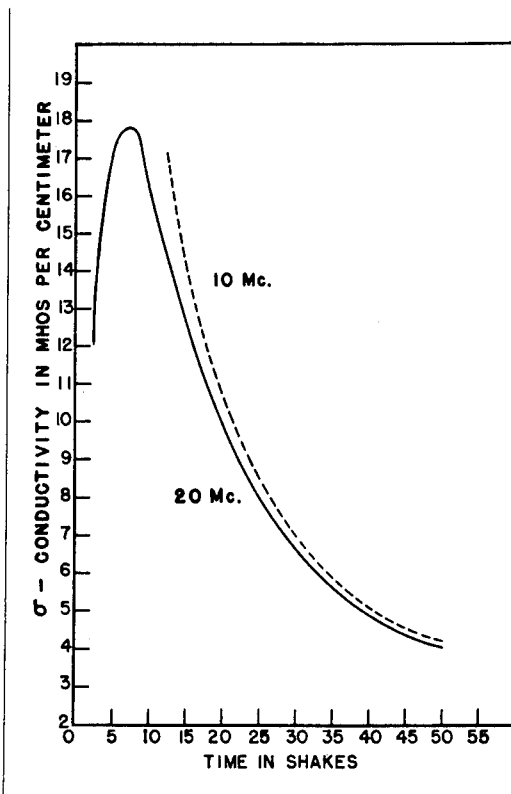
Fig. 5. Composition B Conductivity Profile.

not explicit in the expression for the conductivity, the frequency of operation is primarily determined by the choice of the inductance and capacitance. Resolution is determined by the time to reach the first nodal point. If the frequency is low the details near the detonation front are obscured. For the top curve in Fig. 5, the operating frequency was approximately 10 megacycles. The height of the test cell was only 2 in. and the capacitance was 30,000 pico farad. The time between the peaks of the periodic waveform was about 5 shakes, and this time is not sufficient to resolve the shape of the curve near the detonation front. The resolution for the bottom curve was about $2\frac{1}{2}$ shakes and consequently is sufficient to determine that a peak in the conductivity occurs between 5 and 10 shakes. No claim is made as

to the absolute accuracy of these curves; but they do show the order of magnitude and the approximate shape of the conductivity profile.

In particular, no account has been taken of the motion of the electrodes. It is true that the electrodes do not have the same motion as a flat plate would, and therefore, a full correction does not apply. Calculation suggests that about a 6% reduction in detonation velocity would account for electrode motion. Also, the effect of rarefactions and the cooling of the explosion products by the copper electrodes has not been assessed. These latter two effects may account for the rapid decrease in conductivity behind the reaction zone. These disadvantages are inherent to one degree or another in any measurement system, but it appears that the advantages of this test-cell arrangement outweigh the disadvantages. Conductivity measurements on explosives other than Composition B have not been carried out because it is our feeling that the qualitative behavior of other explosives will be very similar to that for Composition B. Instead, this present knowledge of the conductivity profile has been used in designing pin circuits for fast breaks and good response.

For example, a pin circuit[3] may be represented schematically by the diagram in Fig. 6. Here the impedance Z is the input impedance of

Circuit Response

$$V = \frac{2V_0 e^{-\frac{Zt}{2L}}}{\sqrt{1-4L/Z^2C}} \sinh\left(\frac{t}{\sqrt{LC}}\sqrt{Z^2C/4L-1}\right)$$

Damped Response when

$$\frac{Z^2C}{4L} > 1 \qquad \hat{t} = \frac{2L}{Z}$$
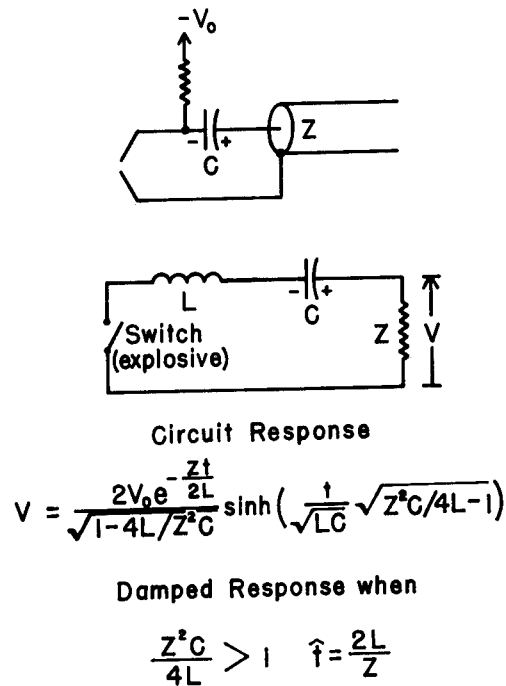
Fig. 6. Pin Circuit and Design Equations.

a properly terminated signal cable, and the inductance L is the self inductance of the wires leading to the pins, while C is the charge storage capacitor. The inductance of a tenth of a microhenry or so

of a foot of wire is sufficient to cause ringing if the circuit is not properly damped. The resistance of the reaction products can be considered small compared to the cable impedance when close-spaced pin pairs are employed. The geometry of the pin foils is quite important in order to achieve a small resistance from a small conductivity. It may be readily shown that the voltage across the input to the cable may be written

$$V_z = V_o \frac{2e^{-Zt/2L}}{\sqrt{1 - 4L/Z^2C}} \sinh\left\{\frac{t}{\sqrt{LC}} \sqrt{Z^2C/4L - 1}\right\}$$

This expression results in three possible modes of operation, namely, oscillatory, critically damped, and overdamped. For proper pin circuit response it is desirable to operate in the overdamped mode. This means that the term $Z^2C/4L$ must be greater than one.

The rate of rise of the initial signal may be obtained by setting the derivative of the voltage with respect to time equal to zero and solving for the time to the peak of the response waveform. When this is done it may be shown that a first approximation leads to

$$\hat{t} = 2L/Z$$

This means that the rise time is directly proportional to the amount of inductance in the circuit leads. Incidentally, a rule of thumb for the peak voltage amplitude under these conditions is that the maximum voltage will be about 75% of the initial voltage across the condenser.

As an illustration of the effect of lead inductance on the circuit response, Fig. 7 is a photograph of two rate-stick shots where
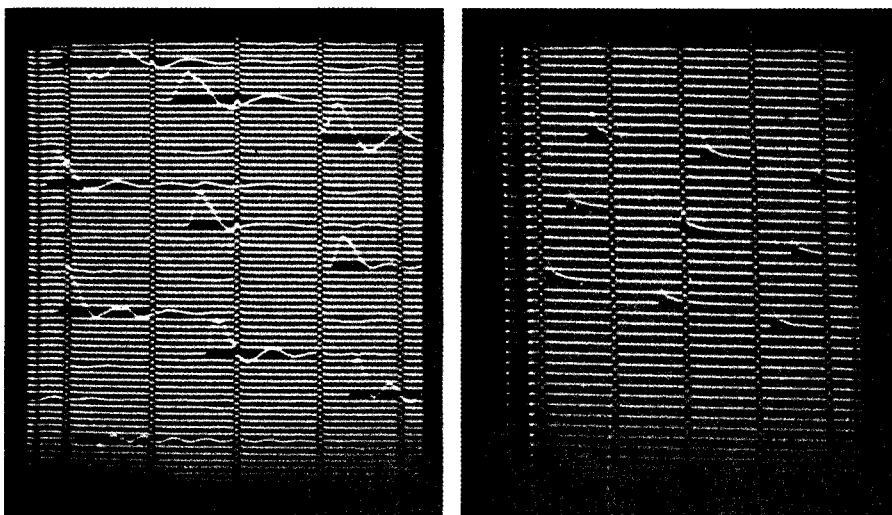
Fig. 7. Underdamped and Overdamped Pin-Signal Waveforms.

145

the only difference is the length of wire leading to the pins. In the left photograph the waveform is seen to be oscillatory and does not exhibit sharp breaks. For the photograph on the right the circuit is damped by using shorter leads and a distinct improvement in the leading edge may be seen. The pin and mixer arrangement used to obtain these waveforms is shown in Fig. 8. As many circuits as are necessary may be added since the diodes isolate the inactive circuits from the cable.
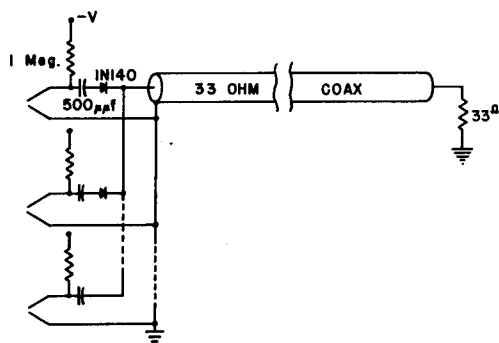
Fig. 8. Pin Circuit and Signal Mixer.

Turning now to the problem encountered at microwave frequencies, a somewhat different technique than the one previously employed must be used since the period of oscillation of the electric field is exceedingly short. In this region of the electromagnetic spectrum the interference waveform[4] between the incident and reflected waves may be analyzed to determine the electrical properties of the reaction products only when the reaction products may be considered homogeneous and when the density of these products is sufficiently low that the dielectric constant of the reaction products can be considered to have a value of one. A cursory examination of Maxwell's second field equation will show that one cannot distinguish between a change in the complex dielectric constant and a change in the electron concentration, since a change in either one affects the reflection coefficient or transmission coefficient in exactly the same manner. Furthermore, at the presently usable microwave frequencies, nearly 100% reflection of an incident electromagnetic wave can be expected.

This does not imply that microwaves cannot be useful as a diagnostic tool in explosives research. On the contrary, much use can be made of this fact. The next two figures will illustrate the point.

Figure 9 shows a microwave interferometer waveform obtained from detonating 24-mesh spherical-grain TNT in a 2-in. ID brass tube, 30 in. long. The timing marks are separated by 1 μsec and the nodes at the voltage minima (horizontal line) represent the location along the circular waveguide where impedance minima exist. The fact that the voltage at a minimum is essentially zero means that the conductivity of the detonation front is quite high. The time differences between
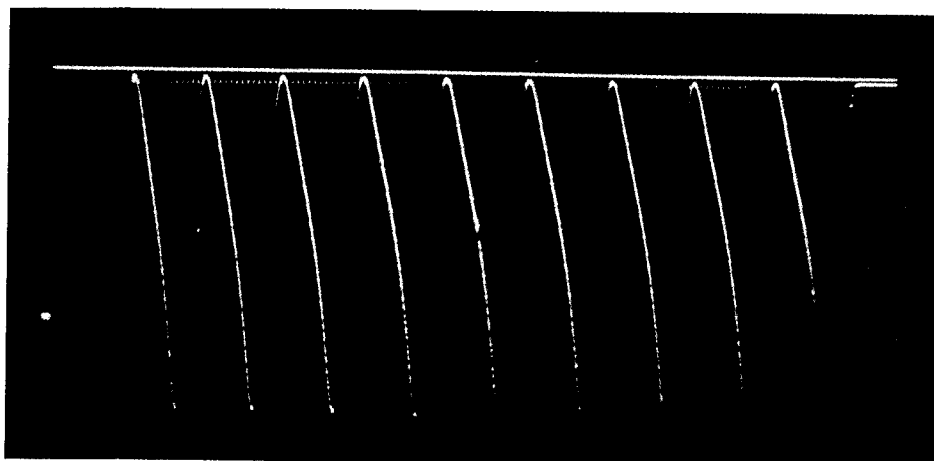
Fig. 9. Microwave Interferometer Waveform.

nodes are inversely proportional to the velocity of the front since the space separation of the nodes is fixed by the waveguide wavelength. The resolution which can be achieved is limited only by the operating frequency and technical limitations which are too complicated to go into here.

Another interesting shot which depends on the high conductivity of the explosion products to reflect back the incident microwave energy is shown in Fig. 10. In this figure are shown the experimental arrangement of the explosive and the test equipment used to obtain the interferometer waveform. The purpose of this experiment was to observe standoff initiation and to follow the detonation front as it traveled through the explosive and the shock front as it traveled across an air gap into the next piece of explosive. Furthermore, it was desired to note the effects of increased charge separation on the initiation of the explosive.

The explosive used was a plastic-bonded one in a 6-ft. long, 3-in. diameter brass tube. The explosive cylinders were 5 in. high and separated from one another by one, three, and five charge diameters, respectively. The particular operating frequency was so chosen that the unreacted explosive was reflectionless in addition to being transparent. Consequently, only the moving detonation or shock front influences the waveform.

The first charge was initiated high order from a plane wave lens; and the detonation front proceeded through this charge and emerged out into the air space between the first and second charge. The shock wave progressed across the air space and into the second charge. There appears to be very little if any delay before the second charge detonates at high order. However, this is not the case for the third charge. The change in slope of the interference waveform is indicative of a slow shock wave entering the explosive. But, the charge eventually goes high order. However, when the shock emerges from the front of the charge it is no longer plane as indicated by the generation of a lower-order microwave mode generated by a non-planar shock

front. This condition is greatly exaggerated in the fourth charge as evidenced by the increase in interference generated by the asymmetric detonation.
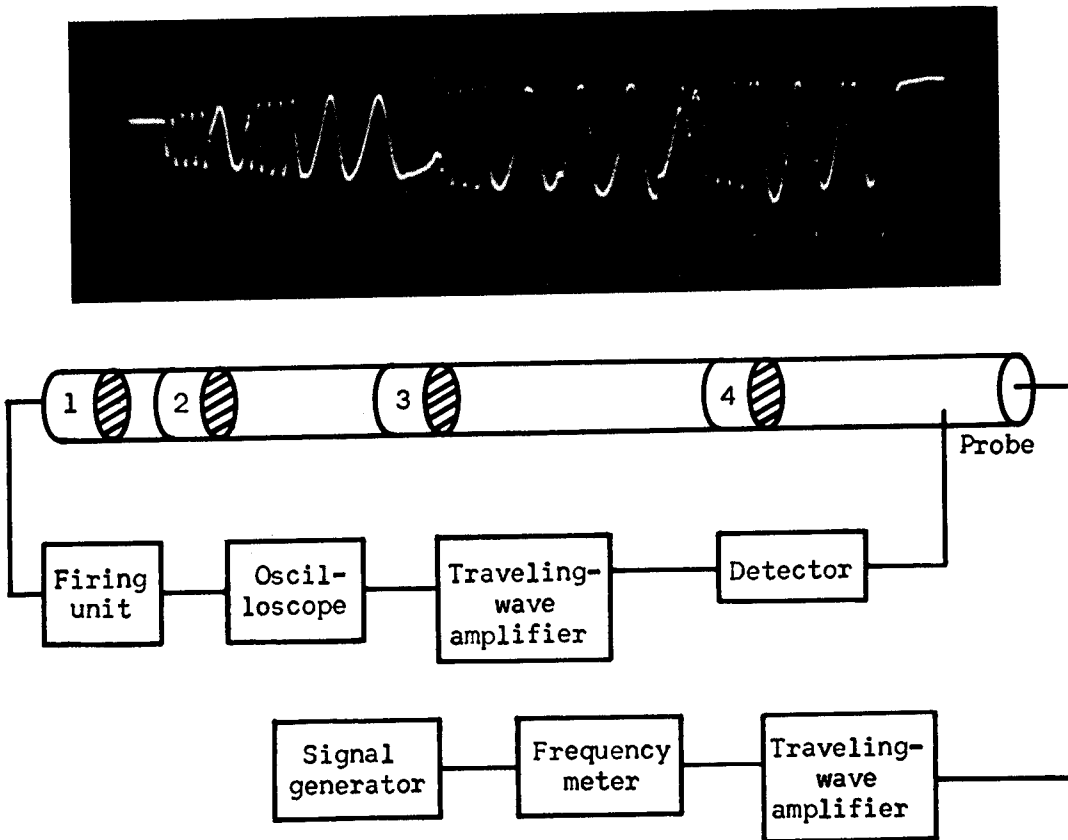
Fig. 10. Standoff Initiation of a Plastic-Bonded Explosive.

These last two records were included as further evidence of the high conductivity of a detonation and to point out that although microwave conductivity experiments are not feasible, microwaves can be a useful diagnostic tool.

REFERENCES

1. R. I. Sarbacher and W. A. Edson, "Hyper and Ultrahigh Frequency Engineering", John Wiley & Sons, Inc., New York, 1943, Chapter 7, Coaxial Lines.
2. A. A. Brish, M. S. Tarasov, and V. A. Tsukerman, "Electrical Conductivity of the Explosion Products of Condensed Explosives", Soviet Physics - J.E.T.P., Dec. 1959.

3. A. W. Campbell, M. E. Malin, T. J. Boyd, Jr., and J. A. Hull, "Precision Measurement of Detonation Velocities in Liquid and Solid Explosives", Rev. Sci. Inst., 27, 567-574 (1956).
4. A. von Hippel, "Dielectrics and Waves", John Wiley & Sons, Inc., New York, 1954, Chapter 17, Standing Waves.

IONIZATION IN THE SHOCK INITIATION OF DETONATION*

R. B. Clay, M. A. Cook, R. T. Keyes, O. K. Shupe and L. L. Udy
Institute of Metals and Explosives Research, University of Utah
Salt Lake City, Utah

ABSTRACT

Conductance-distance (or time) curves measured by both the
"parallel" and "perpendicular" probe methods in receptors of the
modified card-gap or "SPHF plate" method are presented and com-
pared with corresponding pressure-distance curves obtained by the
new aquarium method. Results show that the initiation of deto-
nation by shock correlates directly with an <u>ionization pulse</u>
observed to propagate in the predetonation regime.

By the use of high shock impedance end plates on short
receptor charges and double-donor systems on longer receptors,
causing powerful shock reflections and interactions during the
initiation of detonation, it is shown that ionization is the
major factor in the initiation of detonation, although the shock
wave is also a factor of importance. The great importance of
ionization is seen by the fact that the initiation time lag and
position X of the initiation process in the receptor are determined
by the coincidence of the ionization pulse and the shock wave.
Detonation does not occur until this coincidence is established.
As a result the time lag τ is, in general, independent of shock
intensity, reflections and/or interactions. Ionization is thus
seen to be a fundamental criterion of detonation in condensed
explosives.

Introduction

Although the details governing the initiation of high explosives
by shock are not yet completely understood the most widely held
mechanism is that of Kistiakowsky[1] which has been described also
by Jacobs,[2] and by Groocock and Griffiths.[3] The latter described
this mechanism as follows: "Entry of an intense shock wave into a
receptor charge raises the temperature and pressure of the explosive.
This causes the explosive to decompose exothermally and, if the rate
of reaction is sufficiently high, more energy is fed into the shock
wave than is lost by dissipative processes. The shock wave, which
already has a very high velocity, is accelerated and its amplitude
is increased causing a further acceleration of the reaction rate.
There is thus a smooth conversion of a shock wave into a detonation
wave, i.e., into a self-sustaining, shock-propagated reaction
governed by hydrodynamic laws." The explanation of the process
maintained by this laboratory, however, is that, while the influence
of the factors of initial heating and shock reinforcement are not
denied, a more essential factor is that detonation is a process
associated with high ionization and heat-conduction,[4,5] and that
these factors play a determining role. Indeed, it is here maintained
that detonations in condensed explosives are characterized by the
fact that their reaction zones are highly ionized even to the extent
that they may be described as "dilute plasmas." It has been sug-
gested, in fact, that initiation can occur only when the total
enthalpy at the front of the reaction zone becomes approximately
equal to the heat of reaction Q plus the Hugionot energy ϕ, that is,
where the enthalpy $H = Q + \phi$. This is made possible by transport
of enthalpy from regions behind to the front of the wave. This
enthalpy transport, in fact, requires abnormally high heat conduc-
tivity which is made possible by the large concentration of
electrons existing in the ionized reaction zone, or the internal
detonation-generated plasma first recognized as such by Cook, Keyes
and Lee.[6]

Cook, Pack and Gey found considerable evidence for this
"plasma" mechanism of detonation in their studies of the transition
from deflagration to detonation by means of high speed color
photography.[7,8] The discovery by Cook, Pack and Gey of the
detonation-generated external plasmas, namely the brilliant,
detonation-generated, dilute plasmas emitted from free surfaces of
high explosives, constituted, we believe, a major development in
the theory of detonation. The key to the formation of these
plasmas was given by Cook and McEwan in their quasi-metallic
lattice model of high density plasmas.[9] In this model one may
readily see how explosives (and other dielectrics for that matter)
may be converted to plasmas (under the influence of pressures and
temperatures in the range of those encountered in the detonation
of high explosives)with low activation energy from the normal
localized states of dielectrics to the collective electronic states
of dilute (one or two electrons per molecule) plasmas. The.

quasi-metallic model of the reaction zone of detonation has been subjected to considerable experimental investigation. The model, in fact, seems to explain very well the observed properties of the internal and external plasmas existing in the detonation of high explosives. The external detonation-generated plasmas have been discussed in detail by Cook, Keyes and Udy,[10] who employed electrical conduction measurements to elucidate their electronic character. It is a fact that the external plasmas are generated only at the free surfaces of condensed high explosives.

Other contributions to this mechanism are the studies of the shock initiation process using the modified card gap or SPHF method by Cook, Pack, Cosner and Gey,[11] and the recent development in this laboratory of an accurate method for the measurement of pressures in detonation and shock waves by means of a new "aquarium" method. This method is described in a recent paper by Cook, Pack and McEwan.[12] The aquarium method was employed by Cook and Udy to provide an absolute calibration in direct pressure units of the card-gap test for monopropellants.[13] This work contributed a great deal to an understanding of the shock generator systems of the card gap and the modified card gap systems.

More recently the Bureau of Mines has undertaken to investigate the detonation-generated plasmas by means of the high speed framing camera and so far have verified that the plasma is not simply a shock wave propagated into the surrounding gaseous medium, although these investigators have questioned the plasma character of these highly luminous clouds emitted from the free surfaces of high explosives.

It is the purpose of this paper to present still further evidence to aid in the differentiation of the shock and heat conduction mechanisms. For this purpose, direct comparisons of the pressure in the shock wave prior to and at the moment of initiation of detonation, as measured in the new aquarium method, with electrical conduction during the same stages of the shock initiation of detonation in the receptor of the modified card-gap or SPHF plate methods, are developed. Also observations of the $\tau(S_2)$ relations under conditions of shock interactions and reflections at the ends of short receptors are used to show the relative importance of shock pressures and shock interactions.

Experimental

The experimental observations of ionization and pressure were made by means of the rotating mirror streak camera in conjunction with pin techniques similar to those used in the measurements of conduction in the external detonation-generated plasmas.[10] Both parallel and perpendicular probe techniques were used. However, instead of being supported by a constraining tube as described in Ref. 10, the probes were assembled and the Composition B explosive

cast into the assembly, thus insuring good contact between the probe surface and the explosive. Since the cast explosive gives the probe support, small piano wires were substituted for the larger, stiffer, copper-coated steel probes used in the studies of Ref. 10. The circuit diagram shown in Fig. 1 was used in these tests with the only modification being the value of the resistance r_1. The conduction trace was observed with either a Tektronix Type 545 or a Tektronix Type 533 oscilloscope. The oscilloscope traces were recorded with either a Beattie-Coleman oscilloscope camera with a roll-film adapter or with an Edgerton-Germeshausen and Grier oscilloscope camera on a 4" x 5" plate film.

The modified card-gap type assembly was used with glass or lucite as the medium between the donor and the receptor charges. By virtue of the transparency of glass and lucite the shock could be observed as it moved through the SPHF plate by backlighting with a high explosive flashbomb in a manner analogous to that used in the card-gap calibration test of Ref. 13. The donor charges used throughout were 5 cm (d) x 20 cm (L) cast Composition B. The receptor charges were also made of cast Composition B of 5 cm (d); however, the charge lengths were varied depending on the particular parameter being considered. The aquarium setup used in the pressure determinations is illustrated in Fig. 2a and b. The setup of Fig. 2b is a modification of the aquarium technique in which the aquarium was replaced by 5 cm (d) piece of transparent lucite rod approximately 2.5 cm long. To transform the resulting shock velocities into pressure measurements the lucite rod was calibrated by the aquarium technique to obtain the necessary $p(V)$ calibration data. (The techniques involved and the actual calibration curves are presented in the paper by Cook, Keyes and Ursenbach - this symposium.)

In order to correlate the pressure measurements with the conduction data, perpendicular probe measurements were made simultaneously with the pressure measurements on the same charge as indicated in Figs. 2a and b. The probes were placed 0.5 cm from the end of the receptor charge immersed in the aquarium with care being taken that the probes were not wet by the water in the case of the assembly of Fig. 2a. The donor charge was then fired and the resulting shock waves through the SPHF plate and the aquarium or lucite rod were recorded by the streak camera and the conduction across the perpendicular probes was recorded by the oscillograph camera. The oscillograph was triggered in all cases by the detonation wave of the donor charge completing a circuit between two fine copper wires placed in a small V-notch filed in the end of the donor charge against the SPHF barrier.
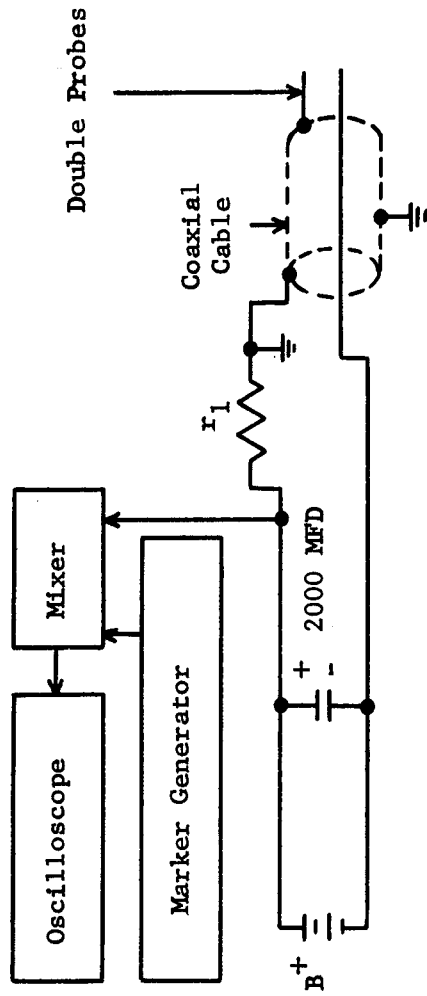
Fig. 1: Diagram of equipment for electrical probe measurements.
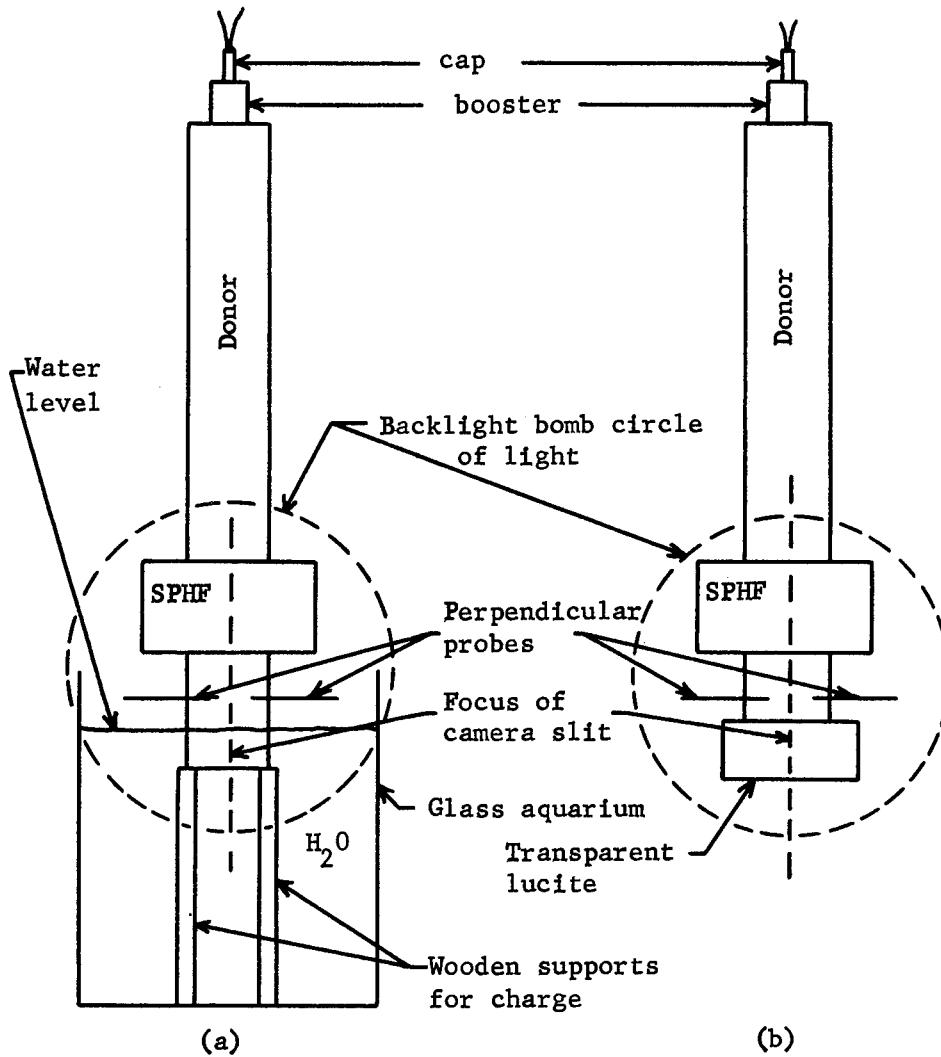
Fig. 2: Experimental setup used to determine pressure-
distance and conduction-distance curves simultaneously.
(a) Aquarium method, (b) lucite method.

Results and Discussion

Parallel probe measurements of conduction

Fig. 3 shows five traces from typical parallel probe shots near the sensitiveness limit, i.e., using SPHF barriers of glass with relative thickness S_1/S_1^* between 0.9 and 1.05. The parallel probe method integrates all conduction along the length of the receptor charge. The perpendicular probe system gives directly "point" conductance. Significant information is obtained by careful correlation of results of the parallel and perpendicular probe measurements. In the results of Fig. 3 the probes were separated 0.5 cm and ran the entire length of the receptor charge. The sweep was 5 μsec/cm, and the gain adjusted to 5 volts/cm with a battery voltage of + 20.2 volts and a resistance r_1 = 12.0 ohms.

First, it may be noted that the relative magnitude of the conductance in the receptor (conduction being proportional to the height of the voltage rise) was found to decrease sharply with small increases of length S_1 of the SPHF plate near the sensitiveness limit. Since all initiating waves were generated by identical donors the initial shock pressures in the SPHF plates were equal. However, the thickness S_1 varied enough in the different examples shown in Fig. 3 to allow slightly different degrees of shock attenuation before entering the receptor. It is interesting to observe such large variations in the integrated conduction with such small variations in S_1 near the sensitiveness limit, i.e., as S_1 approaches S_1^*. At small values of S_1 the total (integrated) conduction increased with the time in the interval τ between entrance of the shock into the receptor and initiation of detonation as in Fig. 3a. However, we usually observed a slight inflection in the rise portion as in Fig. 3a. Near the sensitiveness limit S_1^*, however, the trace separated into two separate regions, the first having a maximum, followed by decay, and the second having a sharp increase in ionization when detonation was initiated (see Fig. 3b-d). Above S_1^* the second rise portion corresponding to detonation was, of course, absent (see Fig. 3e).

Since the maximum or the inflection point in the conduction curve generally increases with an increasing shock intensity, it is evident from the traces of Fig. 3 that the shock intensity must actually be decaying as the shock wave moves down the receptor charge in those cases which exhibit a maximum, namely those where S_1 approaches the sensitiveness limit.

The relative times between the peak of the conduction pulse and the initiation of detonation as recorded in traces b, c and d of Fig. 3 were found to be 1.9 μsec, 4.4 μsec, and 8.9 μsec, respectively. These rapidly growing time differences as S_1 approached S_1^* are associated with a complicated balance between total induction time τ, rate of chemical reaction in the deflagration
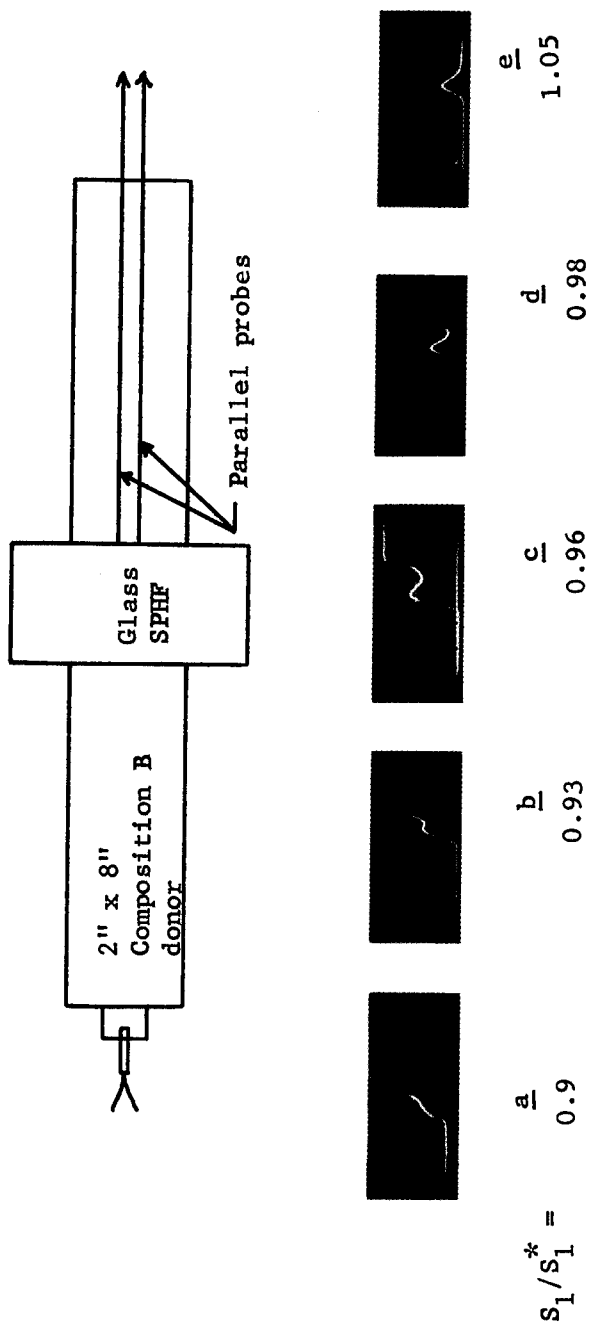
Fig. 3: Parallel probe traces of conduction in initiation of detonation in receptor for $0.9\ S_1^* < S_1 < 1.05\ S_1^*$ and $L_r \gg S_2$.

stage prior to the DDT, the tendency for decay of the shock during the interval before the final sudden transition from deflagration to detonation, or the DDT, especially near the sensitiveness limit, and the influence of (slight) differences in initial shock intensity on most of these factors, particularly the rate of chemical reaction, at the sensitiveness limit. Since these significant differences, as well as the separation of the inflection into a maximum point, and a decay correspond so closely to the sensitiveness limit it is obvious that they provide an accurate criterion of the approach to the sensitiveness limit, and that therefore ionization is a fundamental factor in the initiation of detonation.

Perpendicular probe measurements of conductance at X = 1.0 and $L_r > S_2$.

Fig. 4 shows five representative traces obtained by the perpendicular probe method with probes placed in the receptor 1.0 cm from the SPHF plate-receptor interface. Table I summarizes results obtained in this arrangement including those obtained from streak camera traces of the DDT recorded simultaneously with the probe measurements by focusing the slit and observing the charge in air along the longitudinal axis as in Ref. 11, no pressure measurements being made in this series. The ionization traces showed either two or three peaks when detonations occurred and only one when failure occurred. The first peak occurred 7.0 to 8.2 µsec after the shock entered the receptor. The beginning of the rise, however, appeared 3.4 ± 0.2 µsec after the shock entered the receptor. Since the initiation wave travels 2.9 cm/sec[11] the rise time to the first peak ranged from 3.3 to 4.8 µsec. It is believed that this situation reflects both the shape of the pressure profile in the wave emerging from the glass SPHF plate associated with the propagation of a plastic wave at a lower velocity than an elastic wave in glass at the intensities in question[14] and to the influence of chemical reaction. At small values of S_1 the chemical reaction effect is more pronounced than at large S_1 but is probably never absent except at $S_1 > S_1^*$.

Since detonation started at a distance S_2-1 cm from the probe, the return of the detonation to the probes or the peak of the second ionization pulse occurred at the time t_2, given by $\tau + (S_2-1)/D' +$ rise time, as measured from entrance of the initiating wave into the receptor, D' being the velocity of the rearward detonation. This rearward velocity has been observed on the streak camera to be about 7 km/sec. The calculated τ's given in Table I were based on these relations. One expects τ' to agree with τ only when S_1 is sufficiently lower than S_1^* that detonation initiates uniformly across the entire surface of the DDT. As S_1 approaches S_1^* initiation may occur only in the most favorable position, namely near the axis of the charge. Under this condition $\tau'-\tau$ would be about 3.2 µsec. The maximum observed difference was only 2.0 µsec and the minimum close to zero.
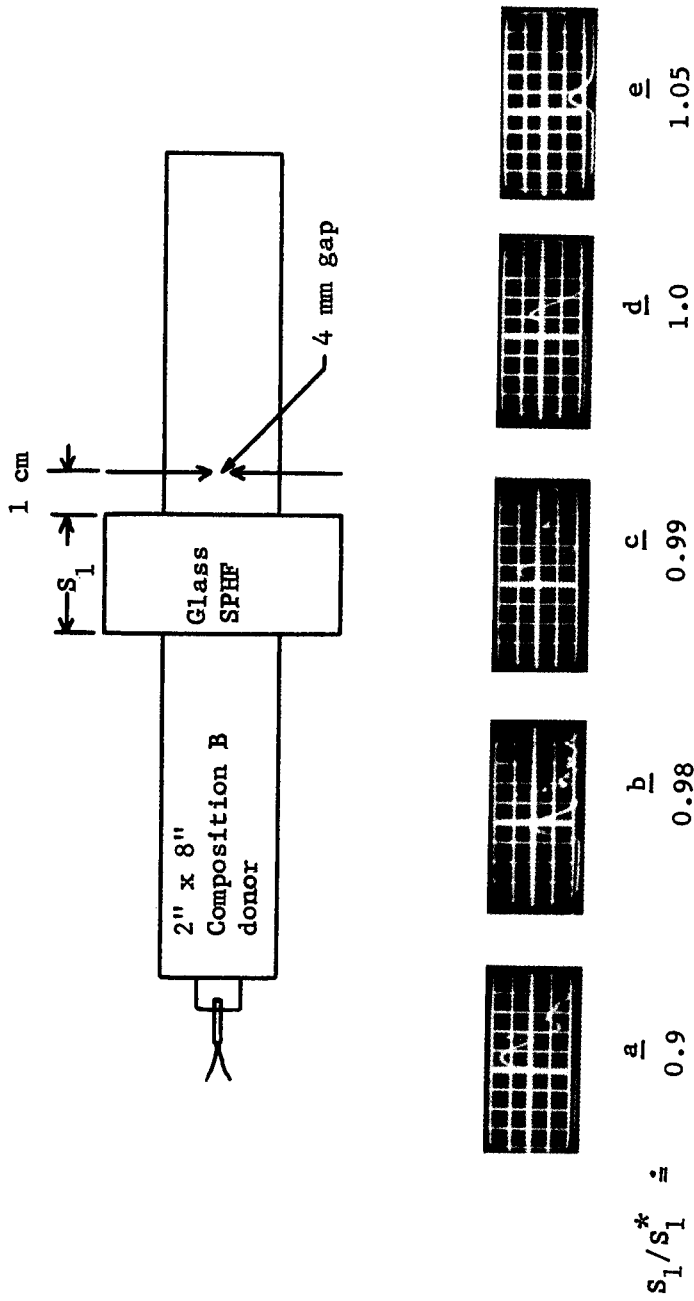
Fig. 4: Perpendicular probe traces of conduction 1 cm inside the receptor for $0.9\ S_1^* < S_1 < 1.05\ S_1^*$.

Table I: Perpendicular probes (at $X = 1.0 \pm 0.1$ cm) and streak camera results (recorded simultaneously on same charge) for glass SPHF plate ($L_r > S_2$).

Series	No.	S_1 (cm)	S_2 (cm)	τ' (μsec)	t_1 (μsec)	t_2 (μsec)	$(S_2-1)/D'$ (μsec)	τ (calc)	$(S_2-1)/(\tau-t_1)$ (km/sec)	Λ_1 (mhos)
A	1	7.2	2.9	10.2	8.0	13.6	2.7	10.0	9.5	0.55
A	2	7.3	3.3	11.8	8.2	16.1	3.3	11.9	6.2	0.28
A	3	7.3	3.6	12.2	7.7	15.8	3.7	10.8	8.1	0.26
A	4	8.4	4.6	15.7	7.8	20.2	5.2	14.5	5.4	0.17
B	1	4.8	2.5	10.5	7.4	12.1	2.1	8.7	11.5	0.34
B	2	6.0	3.6	13.1	7.0	14.8	3.7	9.9	9.0	0.10
B	3	7.2	F	--	7.0	--	--	--	--	0.003
C	1	5.4	3.1	11.8	6.8	12.9	3.0	9.6	7.5	0.25
C	2	6.1	4.2	16.0	7.0	18.3	4.6	13.0	5.3	0.15
C	3	6.6	4.3	15.0	7.2	17.8	4.7	12.1	6.7	0.25
C	4	7.2	F	--	7.0	--	--	--	--	0.003
C	5	7.8	F	--	7.0	--	--	--	--	0.002

t_1 = time to first conductance peak (measured from arrival of shock at SPHF plate-receptor interface).

t_2 = time to second conductance peak (same reference)

Λ_1 = conductance at first peak (Λ following detonation was about 0.5 to 1.0 mhos)

τ' = the apparent time lag; a correction downward is needed to account for the interval required for the wave to propagate from its place of origin on, or symmetrically about, the axis to the surface of the charge. The maximum correction is 3.2 μsec. This maximum correction applies, if at all, only at the sensitiveness limit.

τ = t_2 - $(S_2-1)/D'$ = rise time; $D' \approx 0.7$ km/sec.

It is interesting to note that the rise time from the point on the first ionization pulse, where the ionization began to increase, to the second peak amounted to 1.1 ± 0.25 μsec. This presumably reflects the actual rise time of the ionization in the rearward detonation wave.

The third pulse is evidently associated with reflection from the disintegrating, but still intact, SPHF plate.

The perpendicular probe method with probes at $X = 1.0$ cm was originally designed to record the "flash-across" observed in the liquid explosives nitromethane and dithekite[5,7,8] and in liquid TNT (by Gey and Kinaga at NOTS). Since the velocity V^* of the flash-across in these liquids ranged from 35 to 100 km/sec it was looked for at about the time $\tau - (S_2-1)/V^*$ or about 0.5 to 1.0 μsec before the DDT and should be seen at that time if an ionization surge were associated with it. It is interesting, however, to consider the velocity $(S_2-1)/(\tau-t_1)$ which should be the effective velocity of the peak of the ionization pulse between the time of observing it and the DDT on the assumption that it is really this ionization pulse that causes the initiation detonation. This result is given also in Table I. Note that this velocity ranged from 11.5 km/sec at $S_1/S_1^* \doteq 0.7$ (B-1) to an average of 7.0 km/sec at $S_1/S_1^* \doteq 1.0$ (A-4, B-2, C-2 and 3). (Incidently, the flash-across velocities mentioned above were measured at $S_1/S_1^* \leq 0.5$). This evidence thus seems to show that the first ionization pulse of Fig. 4a-e may be identically the flash-across phenomenon.

Perpendicular probe measurements at variable X and $L_r = X + 0.5$ cm

Fig. 5 shows six oscilloscope traces of electrical conduction in the shock initiation of detonation in the receptor of the modified card-gap test obtained by perpendicular probes in the arrangement of Fig. 2(b) in which the charges were only 0.5 cm longer than the distance X of the probe from (lucite) SPHF plate, this distance being varied from 0.5 to 4 cm and S_1 being close to S_1^*. The lucite SPHF barrier length was held constant at 4.75 cm in all the shots of Fig. 5. The sweep rate of the scope was 5 μsec/cm, the gain was set at 5 volts/cm, the battery voltage was + 21.6 volts and r_1 was 22.0 ohms. Traces a, b, c and d show the conduction results obtained as the shock wave passed over the probes placed about 0.5, 1.1, 1.5 and 2.1 cm, respectively, from a lucite SPHF plate-receptor interface. Pressures were measured by the lucite system as well as by the aquarium method on these same charges. In these four receptor charges the charge lengths were all too short for the initiation of detonation or the DDT to occur. However, in trace (e) the DDT occurred after the shock had passed by the perpendicular probes placed 2.60 cm from the interface and the effect of the detonation wave moving back across the probes can be seen. In trace (f) the DDT occurred before the shock wave passed the probes placed

(a)

(b)

(c)

(d)

(e)

(f)
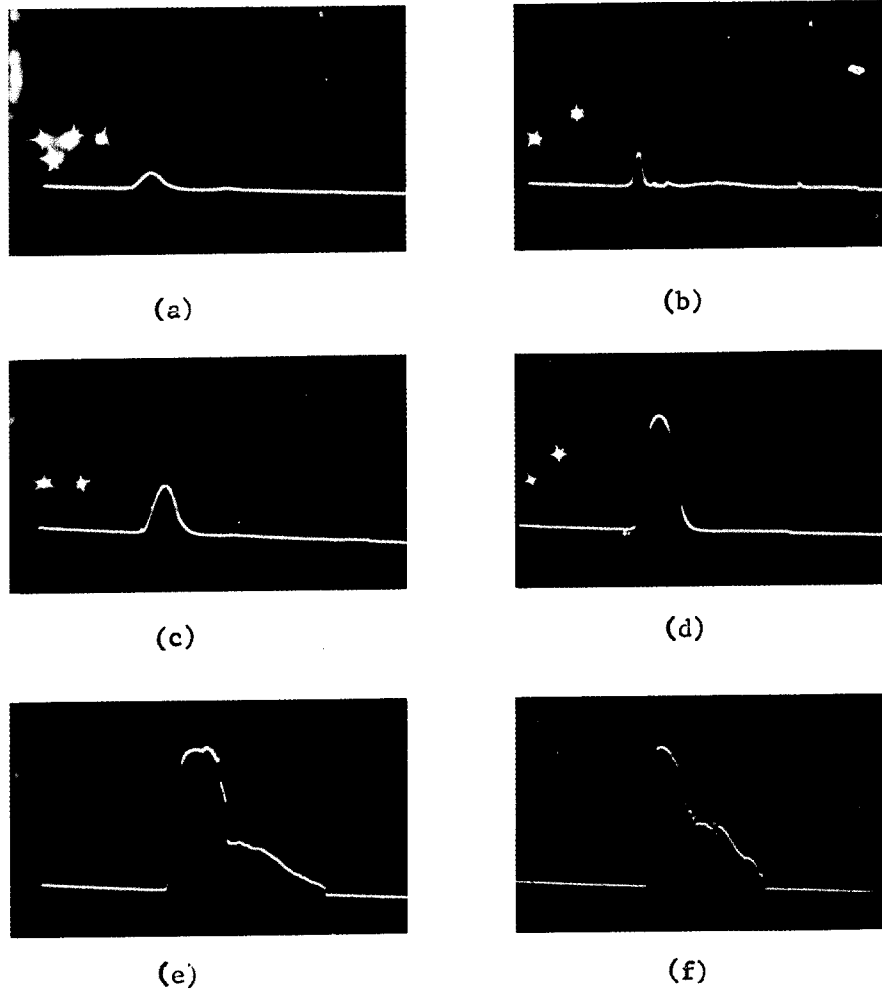
Fig. 5: Traces of conduction using perpendicular probe method; probe separation = 0.5 cm; bias = +21.6 volts; gain = 5 v/cm; sweep rate = 5 μsec/cm; r_1 = 22.0 ohms; lucite SPHF with S_1 = 4.75 cm; distance x of probes from SPHF-receptor interface, (a) x = 0.48 cm, (b) x = 1.08 cm, (c) x = 1.48 cm, (d) x = 2.06 cm, (e) x = 2.60 cm, and (f) x = 4.05 cm.

4.05 cm from the interface and only the conduction of the internal plasma was recorded as the detonation wave propagated across the probes. The increase of conduction with distance X from the SPHF plate-receptor interface is striking in the traces of Fig. 5. However, as shown below, this situation is characteristic only of these short charges and does not represent the true state of affairs in a receptor long enough to detonate. The conduction-distance curve (2) of Fig. 6 represents the values obtained from the series of shots in Fig. 5. Curve (1) of Fig. 6 was obtained from a similar series using glass SPHF barriers, and curve (3) from a series with lucite SPHF barriers of slightly shorter length (S_1 = 4.70 cm) than those of curve (2), S_1^* in this case being greater than 5.0 cm for lucite. As the curves of Fig. 6 demonstrate, the conduction across the perpendicular probes increased rapidly with distance from the SPHF barrier-receptor interface. This is evidently associated with release wave effects as shown below. It appears, in fact, that the conduction (ionization) increased at an accelerating rate until a level of ionization comparable to that within the internal plasma or the detonation wave itself was reached whereupon the DDT took place.

An astounding fact, which no doubt has an important bearing on the mechanism of the shock initiation of detonation in condensed explosives, is seen by comparing the conductances measured by the perpendicular probe method at 1 cm from the SPHF barrier for charges of L_r = 1.6 cm (Fig. 5b) with those for $L_r \gg S_2$ at effectively the same initial shock strength. The peak conductance corresponding to the first maxima in Fig. 4a-d where $L_r \gg S_2$ were from 0.5 to 0.1 mhos. On the other hand, the conductance in the case shown in Fig. 5b in which L_r = 1.6 cm was only 0.01 mho which is only 0.1 to 0.02, the conductance observed for $L_r > S_2$.

It has already been noted that when $L_r < S_2$ no detonation is initiated (unless as shown below a shock reflection plate is placed on the end of the charge, lucite or water not having high enough impedances to reflect a shock but only a release wave when placed on the end of Composition B). It is evident, therefore, that the conductance at X $\doteq$ 1 cm depends on L_r; unless L_r is somewhat larger than S_2 ionization sufficient to trigger the DDT does not develop. This suggests that a (probably elastic) wave propagates far enough ahead of the (plastic) wave responsible for initiation to be reflected as a release wave into the region measured by the probes before the intense plastic wave (or peak of the composite wave) reaches the probe, thus destroying the effect of the initiating shock before it has a chance to initiate a detonation. This apparently explains receptor failures when $L_r < S_2$ even with donor-SPHF plate systems generating very high shock intensities, i.e., for $S_1 \ll S_1^*$. Evidently, therefore, the curves of Fig. 6 are associated largely with the influence of release waves reflected from the end of the charge before the plastic wave, or rather the

Clay, Cook, Keyes,
Shupe and Udy
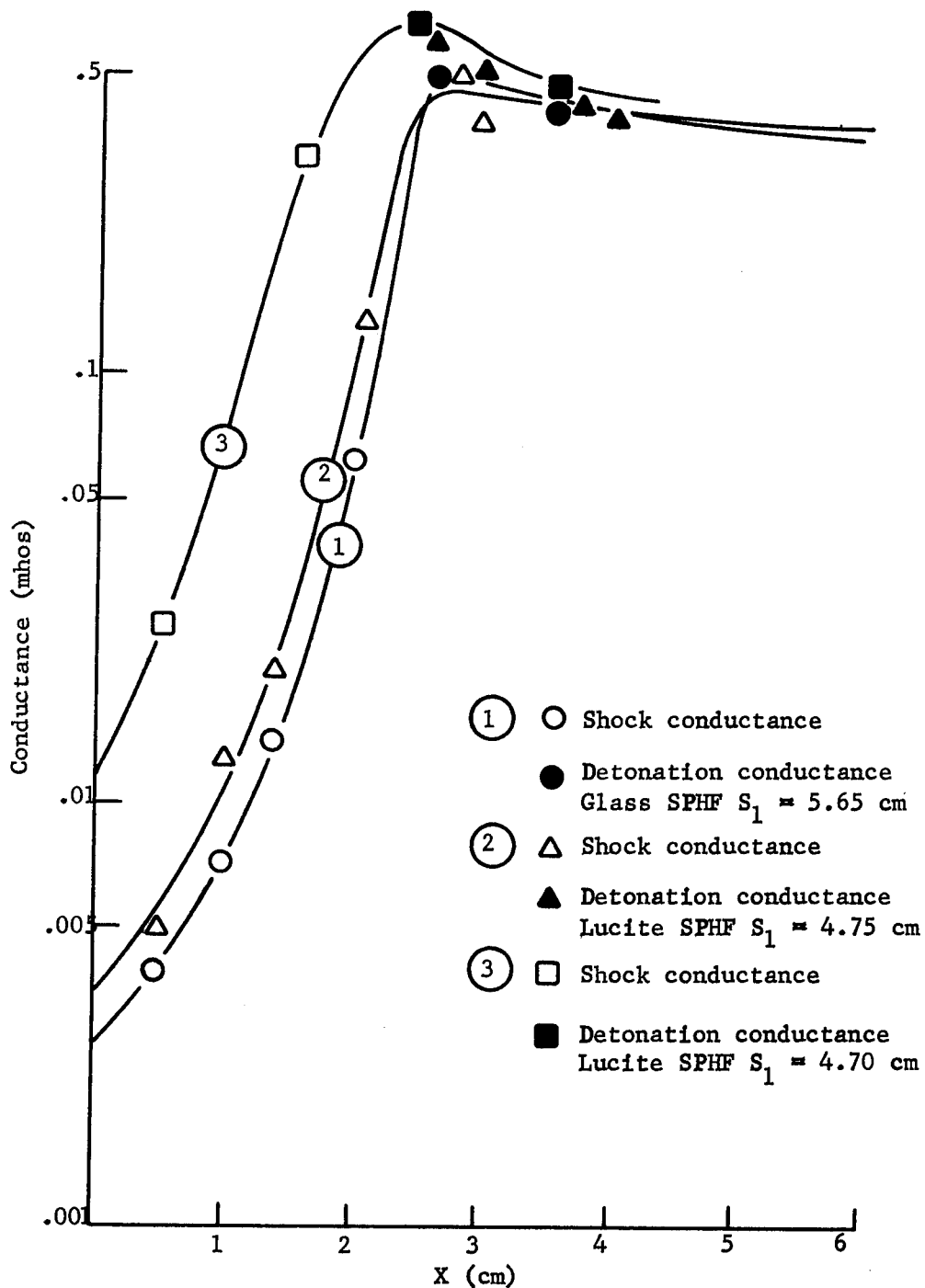
Fig. 6: Conduction-distance curves measured from plate-
receptor interface in SPHF method.

peak of the ionization (and pressure) pulse responsible for initiating detonation actually reaching the probes. In the absence of these release waves the ionization pulse is one or two orders of magnitude larger. As a matter of fact, in the absence of reflected release waves the intensity of the initial ionization pulse shown in Fig. 4 approaches, or even exceeds in some instances. i.e., at $S_1 \ll S_1^*$, that in the detonation wave.

This release wave attenuation concept is given substantial support by the observed streak camera traces of shocks from these systems propagated into water. A striking demonstration of the separation of shocks in a Composition B donor-thin glass SPHF barrier system is illustrated by the streak camera trace of Fig. 7. Note that the initial wave transmitted into the aquarium is suddenly overtaken by a wave of greater intensity, about 1.5 cm from the SPHF plate-water interface, showing that a second (plastic) wave from the donor-glass SPHF plate system traveled at lower velocity than an initial (elastic) wave and was enough more intense than the initial wave to overtake it upon entering the medium of zero shear strength. This was also seen by Clay[14] in studies of velocities of shock waves of various intensities in media of appropriate shear strength to develop instability of shock and follows from the von Neumann criterion of shock stability (Ref. 5, Cht. 9).

While the results with perpendicular probes presented in Fig. 5 and Fig. 6 are, therefore, of great interest, they do not reflect the true nature of the ionization pulse but only the release wave-attenuated ionization pulse. Still, the great influence of pressure on ionization is brought out strikingly by these studies. On the other hand, there is no reason to suspect that the pressures measured on these short charges do not reflect the actual shock pressures at the interface.

Pressure-distance relations

In measurements of the pressure variations in the receptor charges as a function of distance X from the SPHF plate-receptor interface, several series of shots were made using the setups of Fig. 2a and b. Fig. 8 shows several curves of p(X) using glass and lucite SPHF barriers of different S_1/S_1^*. The initial velocities of the shock waves were measured by reading the slopes of the distance-time curves recorded by the streak camera at the receptor-water or receptor-lucite interfaces as the case may be. These velocities were then transformed into pressures by use of the p(V) calibration curves for water and lucite presented in this symposium by Cook, Keyes and Ursenbach. The results shown in Fig. 8 indicate a pressure increase with distance whenever S_1 is appreciably less than S_1^*. However, at $S_1 \doteq S_1^*$ this may not be the case, the results showing a tendency for the pressure to drop initially with distance from the SPHF barrier near the sensitiveness limit, realizing that $S_1^* \approx 6.6$ to 8.0 cm for the glass SPHF plates in the situation
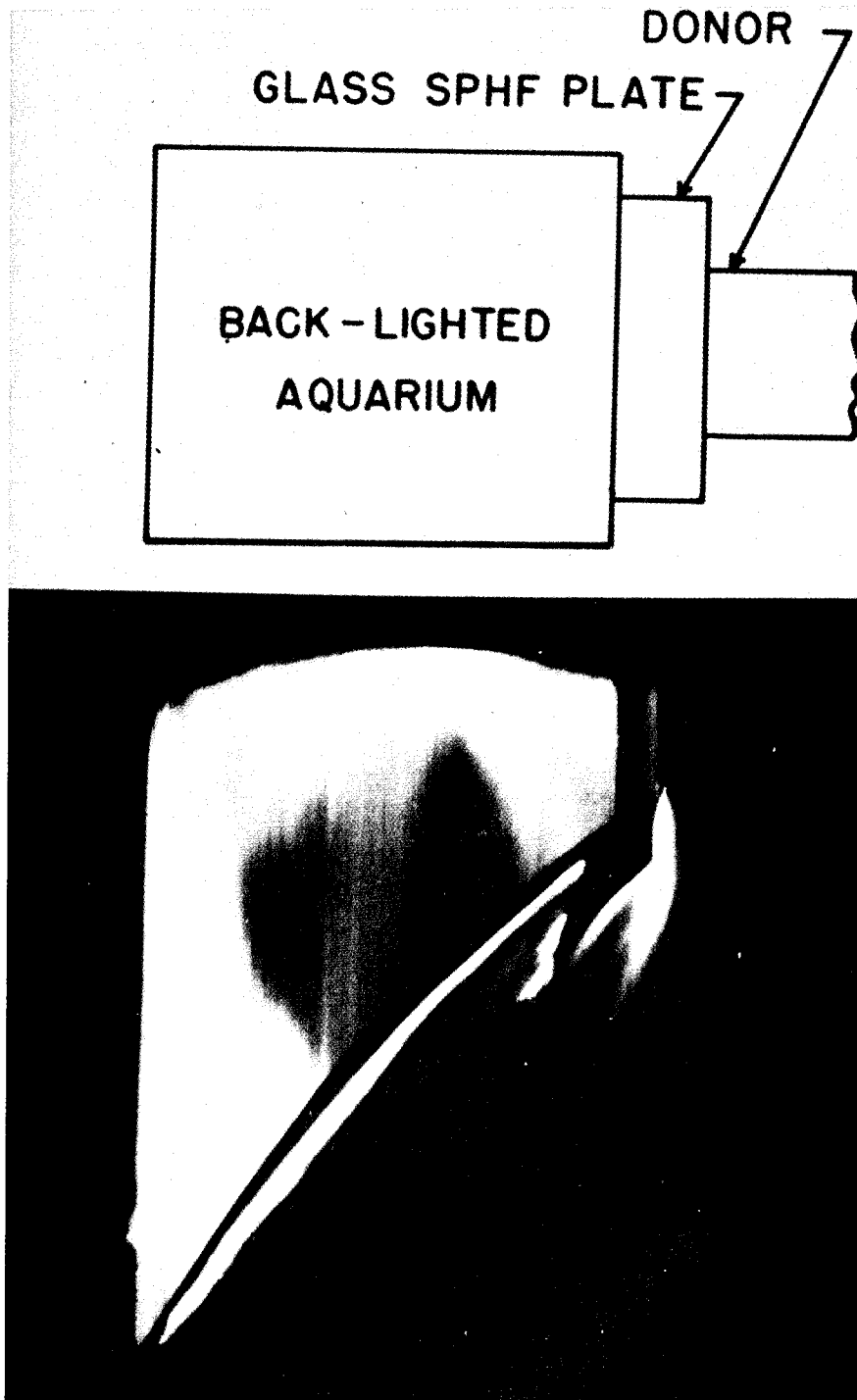
Fig. 7: Shock waves in aquarium showing intense wave overtaking initial wave about 1 cm from interface.
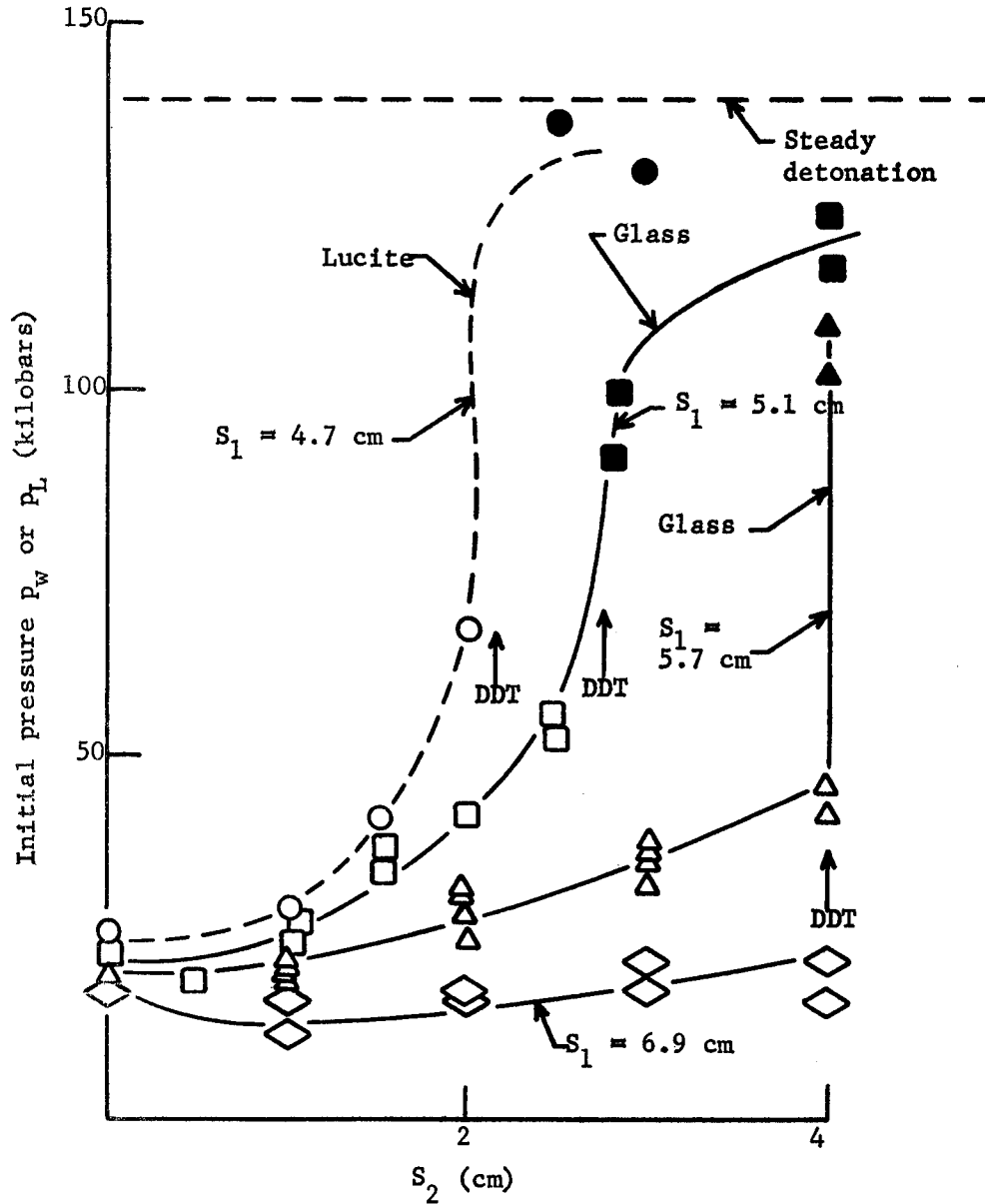
Fig. 8: Pressure (p_W)-distance curves measured from
plate-receptor interface in SPHF method.

shown in Fig. 8.

It was observed, as illustrated in Fig. 7, that the velocity of the shock wave transmitted into the aquarium or lucite from the end of the receptor in general underwent a slight increase before it attenuated in most cases owing to the fact that the peak of the pressure pulse entering the aquarium or lucite from the receptor lagged behind the front. This velocity variation made it difficult to measure with high accuracy the slope of these distance-time curves.

Trapped detonation-initiation waves

The experimental arrangements used in this phase of study were of three types as shown in Fig. 9, the Composition B donors being 5 cm (d) x 20 cm (L) (detonated with 20g of cast 50/50 pentolite) and the Composition B receptors being 5 cm (d) and of variable length. With the arrangement of Fig. 9a a glass thickness S_1 was selected at 5.6 cm for which S_2 was 3.0 cm for a long receptor charge. Here, however, the length L_r of the receptor was chosen to be less than S_2. (Note that for $L_r < S_2$ no detonation occurs with a bare Composition B receptor.[8]). By using an end plate of high impedance (ρV) as in Fig. 9a initiation of detonation occurred at a position X (measured from the SPHF barrier) and at a time τ obeying the following relations:

$$\begin{cases} X = 2L_r - S_2; \quad S_2/2 < L_r < S_2 & (1) \\ \tau = S_2/C & (2) \end{cases}$$

where C is the plastic wave velocity in Composition B, namely 2.9 km/sec. This situation is illustrated by the framing camera sequences in Fig. 10a and b for $L_r = 5S_2/6$ and $L_r = 0.5 S_2$, respectively. Table II summarizes the data obtained in the method shown in Fig. 9a with various plates. The results bear out the conditions (1) and (2) and, moreover, that the initiation of detonation is caused only in shock reflections; as noted above, initiation of detonation in a receptor of $L_r < S_2$ does not occur when the impedance (ρV) of the plate is less than that ($\rho_1 D$) of the explosive or for a free surface, i.e., when the reflected wave is a release wave. Moreover, when $L_r < 0.5S_2$ no initiation of detonation occurred, the shock evidently propagating back through the disintegrating SPHF plate before the necessary conditions developed to cause the initiation of detonation.

When a high impedance plate was placed not only on the end of the receptor, but also between the SPHF plate and the receptor as illustrated in Fig. 9b, the initiation of detonation then obeyed (in addition to condition 1) the conditions
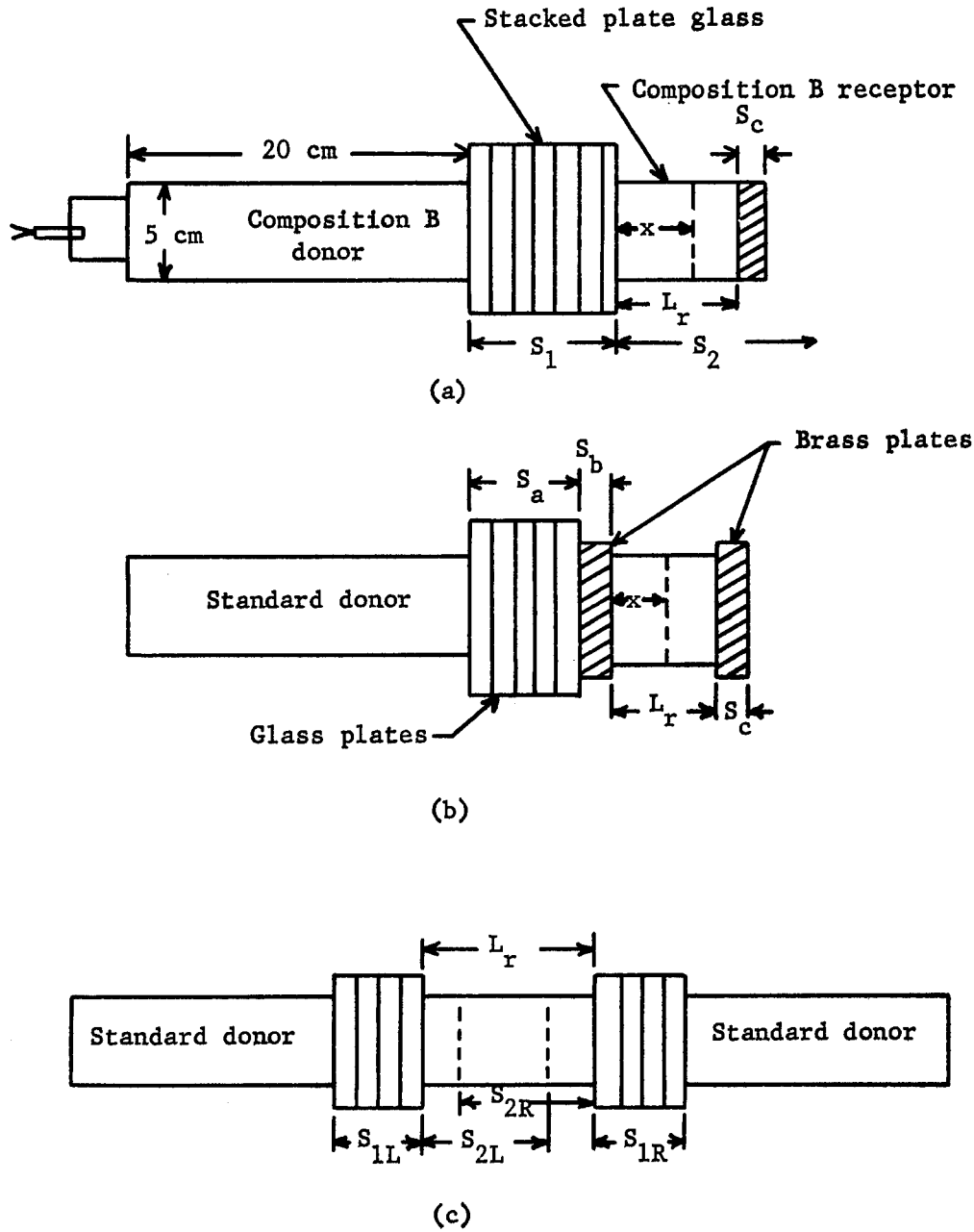
Fig. 9: Experimental arrangements for study of trapped
detonation-initiation waves in Composition B.

(a)   (b)
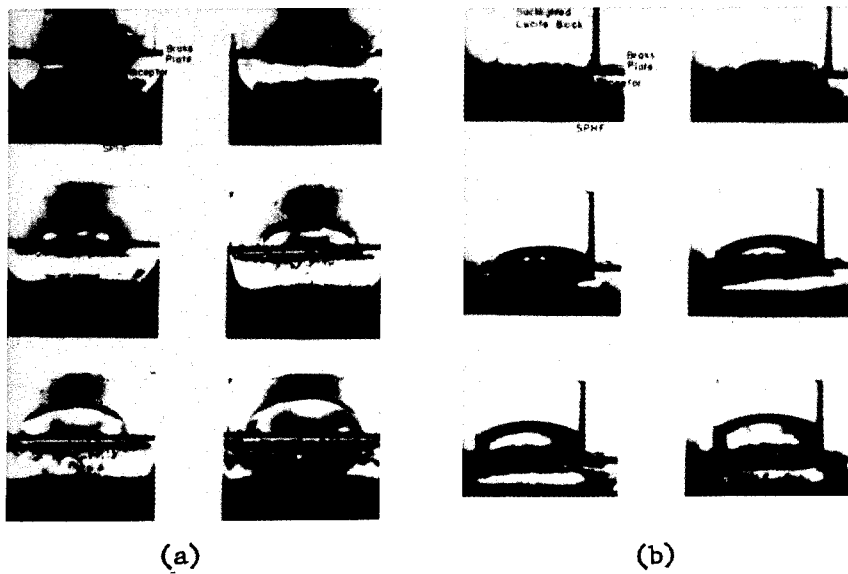
Fig. 10:   Photographs from high speed framing camera sequences.
           (a) S_1 = 5.6 cm, L_r = 2.5 cm, S_c = 0.34 cm brass
           (b) S_1 = 5.6 cm, L_r = 1.5 cm, S_c = 0.32 cm brass

           NOTE: A "backlighted" lucite block was placed adjacent
                  to the brass plate in order to show the emergent
                  shock pattern from the receptor.

Clay, Cook, Keyes,
Shupe and Udy

Table II: Results obtained in Fig. 9a arrangement using 5.6 cm (S_1) glass plate.*

End Plate	S_c (cm)	L_r (cm)	X (cm)	τ' (μsec)	S_2/τ (mm/μsec)	Method
None	Standard	Long	3.0±0.3	11±0.2	2.9±0.2	a**
Brass	0.32	2.5	2±0.3	10.5±0.2	2.9±0.2	"
Brass	0.32	2.0	1±0.3	10.5±0.2	2.9±0.2	"
Brass	0.32	1.5	0±0.3	10.5±0.2	2.9±0.2	"
Brass	0.32	1.0	No initiation			"
Copper	0.16	2.0	1.46	10.0	2.8	b
Copper	0.08	2.0	1.64	9.6	2.8	"
Copper	0.025	2.0	No initiation			"
Iron	0.058	2.0	0.6	10.8	2.7	'.
Iron	0.030	2.0	0.9	11.5	2.8	"
Iron	0.025	?.0	No initiation			"
Lead	0.37	2.0	1.0	11.6	2.8	"
Lead	0.18	2.0	0.8	12.8	2.7	"
Aluminum	0.24	2.0	No initiation			"
Aluminum	0.43	2.0	No initiation			"
Aluminum	0.75	2.0	No initiation			"
Aluminum	3.0	2.0	No initiation			"
Glass	2.5	2.0	No initiation			"
Alumina	0.6	2.0	1.55	9.6	2.0	"
Magnesia	2.25	2.0	No initiation			"
$BaTiO_3$	2.5	2.0	0.8	11.2	2.8	"

* X = distance from interruptor plate where initiation of detonation occurred.

τ' = apparent time between shock entrance into receptor and the initiation of detonation (actual time lag about 1 μsec less).

S_2/τ = average velocity of trapped initiation wave before initiation of detonation.

**a = framing camera, b = streak camera.

171

$$\begin{cases} X = S_2 - 2L_r; \quad S_2/3 < L_r < S_2/2 & \text{(3)} \\ \tau = S_2/C & \text{(2)} \end{cases}$$

Results bearing out this situation are shown in Table III. It should be noted, however, that when $L_r < S_2/2$, i.e., after three reflections of the (trapped) initiation wave, no initiation was observed in several attempts.

Results obtained by the Fig. 9c assembly are summarized in Table IV along with those obtained for a long receptor (for calibration). Note the excellent correlation; even though the shock from the right had to propagate through that from the left, and vice versa, at $2S_2 < L_r < S_2$ the $S_1(S_2)$ relations and S_2/τ were unaffected. This clearly demonstrates that the initiation of detonation does not depend on the initiation wave pressure. That is, S_2 and τ were not influenced by interaction of the two separate initiating waves. An interesting and important aspect of the measurements summarized in Table IV is the fact that each initiation of detonation occurring in the assembly shown in Fig. 9c knew its own donor and was not influenced by the opposite donor even though the initiation of detonation occurred inside the region over which the shock from the opposite donor had passed. This is strikingly illustrated by the streak camera record of Fig. 11. In this case the donor charge on the left was delayed slightly from that on the right. Note that $S_{2L} = S_{2R}$ and $\tau'_L = \tau'_R$, and moreover, the time-distance data agreed with those obtained with the same donor-barrier system but with a long ($L_r \gg S_2$) receptor charge.

Fig. 12 shows a microsecond, framing camera sequence of a backlighted shot made according to Fig. 9c using $L_r = 4.0$ cm and $S_{1R} = S_{1L} = 5.55$ cm. It is indeed interesting to observe two initiation waves run into and pass through each other without initiating a detonation, but at the same time to observe each separate wave produce initiation independently at the same S_2 that it would have produced detonation if a long receptor had been used instead of the Fig. 9c arrangement.

The strong interaction of the two waves of approximately equal magnitude without producing detonation upon collision but each producing detonation later at the same characteristic distance S_2 as though the other shock were not present, shows clearly that shock alone is not responsible for initiation of detonation. In spite of the fact that the pressure resulting from the collision of two waves is greater than the sum of the pressures of the two interacting waves before collision,[15] the combined waves were no more effective in initiating detonation than either one alone. The same reasoning can be applied to the reflection of a wave at a high impedance interface. If shock alone were to induce detonation, it would be expected to take place at the receptor-end plate interface for the case $L_r < S_2$, or at least where S_2 exceeded L_r only a small amount

172

Table III: Results by Fig. 9b arrangement for S_a = 3.55, S_b = 0.32 brass, S_c = 0.32 brass.

L_r (cm)	X (cm)	τ' (cm)	S_2/τ' (mm/μsec)
Long	3.7	13.0	2.9
1.5	3.7	10.8	3.4
1.35	3.4	11.4	3.2
1.3	0.9	11.2	3.2
1.1	No initiation		

Table IV: Comparison of results in standard charge with long receptor and in Fig. 9c arrangement with $S_{1L} = S_{1R}$.

Method	S_{1R} (cm)	S_{1L} (cm)	L_r (cm)	S_{2L} (cm)	τ'_L (μsec)	S_{2R} (cm)	τ'_R (μsec)
Fig. 1, Ref. 11	6.15	Standard	Long	5.2	19.0		
" "	6.15	"	"	5.1	19.2		
" "	6.00	"	"	4.1	15.4		
" "	5.90	"	"	3.8	13.9		
" "	5.85	"	"	5.1	15.7		
Average	5.9*			4.3	15.0		
Fig. 9c	5.85	5.85	5.5	4.3	15.0	5.0	17.6
"	5.90	5.90	5.5	3.8	13.9	3.9	13.3
"	5.95	5.95	5.5	4.9	17.8	5.2	18.9
"	6.00	6.00	5.5	4.2	14.4	4.2	14.6
"	5.85	5.85	5.5	4.0	13.8	5.2	16.5
Average	5.9	5.9	5.5	4.2	15.8	4.7	16.2

*The standard value for S_1^* at $L_r \gg S_2$ was only 6.6 cm in this lot of Composition B.
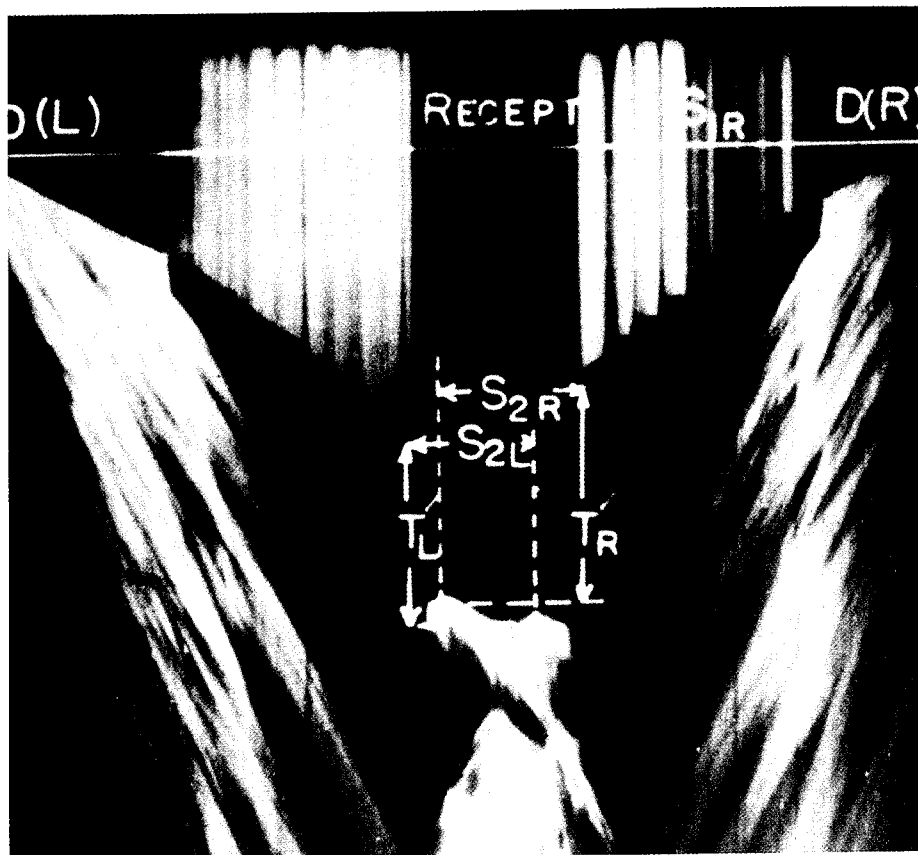
Fig. 11: Streak camera trace of initiation of detonation by method of Fig. 9c, $S_{1L} = S_{1R}$ with left-hand charge slightly delayed.

Clay, Cook, Keyes,
Shupe and Udy
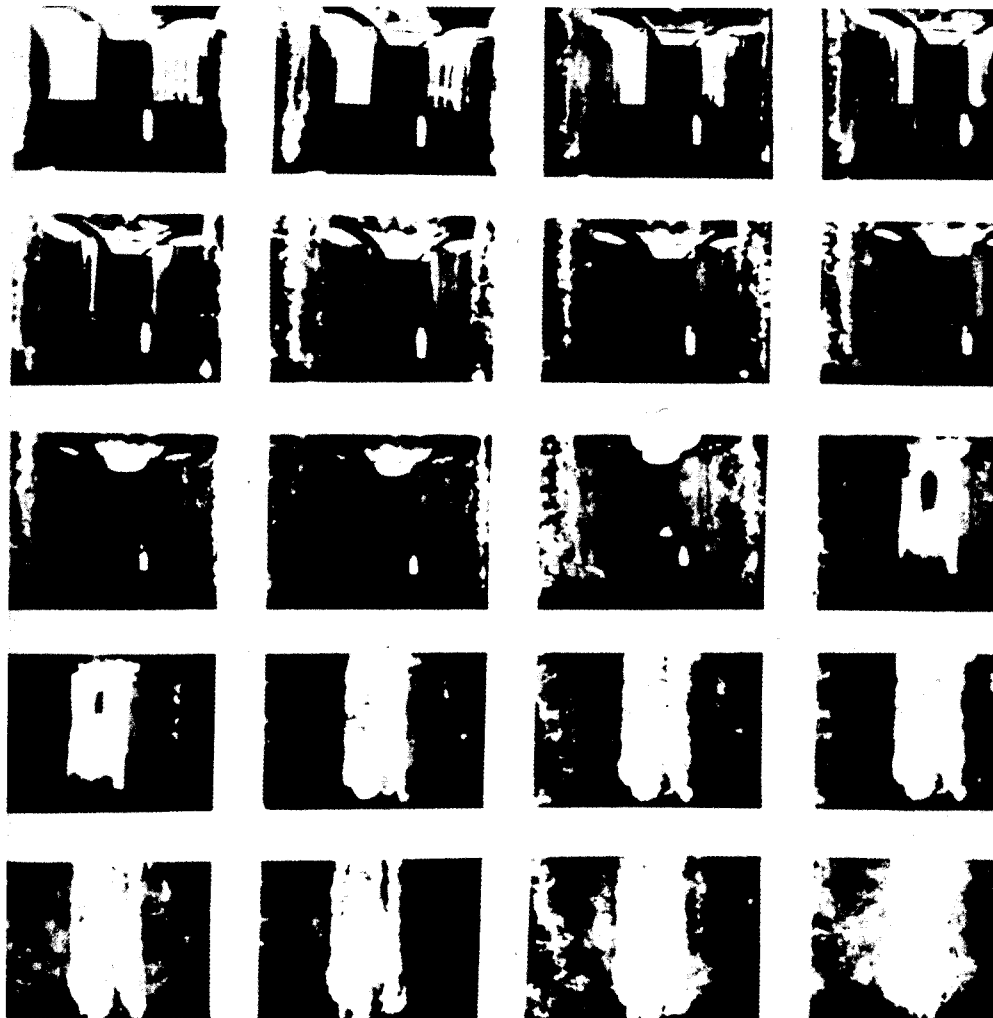
Fig. 12: Framing camera sequence of symmetrically induced
initiations by method of Fig. 9c.

(e.g., by 20%) because at this position the shock intensity is greatly intensified. Therefore, since detonation occurred at the front of the initial sonic disturbance, evidently this discontinuity is a necessary, but not a sufficient, condition to initiate detonation in the receptor.

Table V compares the sensitiveness limit or limiting barrier thickness, S_1^*, of preshocked receptors and standard receptors. Data from three different type experiments are presented. The first utilized donor and receptor charges arranged as in the standard card-gap test. The second utilized the double-donor arrangement of Fig. 9c with $S_{1L} = S_{1R}$ and $S_2 < L_r < 2S_2$. The donor charges were initiated simultaneously such that the initiation waves would collide at the center of the receptor. The third type experiment used the Fig. 9c arrangement with S_{1R} selected to be greater than the sensitiveness limit. The receptor length, L_r, and plate thickness, S_{1L}, were then varied. Initiations of the two donors were timed so that the wave through the thicker barrier traversed most of the receptor before the wave from the thinner barrier entered the receptor. The time delay between events as measured from the streak camera traces as well as the calculated distance through the receptor traversed by the initial wave before entrance of the second wave are given in Table V. Since the sensitiveness limit, S_1^*, of Composition B may vary from batch to batch, the batch number also was noted.

For batch #1 Composition B the sensitiveness limit was 6.55 cm. On the other hand, with the symmetrical double-donor arrangement of Fig. 9c no detonations resulted in five trials when the barrier thickness was 6.55 cm. This result indicated that Composition B was less sensitive to initiation under conditions wherein the initial waves collided and passed through each other than when initiation occurred in undisturbed receptors.

Further comparisons of sensitivity in standard and preshocked receptors were carried out using the Fig. 9c arrangement with $S_{1L} < S_1^*$ and $S_{1R} < S_1^*$ as described previously. Using the standard arrangement initiations were observed in batch #2 Composition B for barrier thickness up to 8.8 cm. However, with $L_r = 5.5$ cm, $S_{1R} = 9.7$ cm, and $S_{1L} = 6.85$ cm no initiations resulted in two trials when the receptors were preshocked before the wave from the left-hand barrier entered the receptor. Similarly, with $L_r = 8.0$ cm no initiations occurred through the left hand or thinner barrier after the receptor was shocked from the right. In one case, however, an initiation occurred through the right-hand barrier due to an initiating wave propagating in the undisturbed receptor. With 12.0 cm receptors one initiation was produced by the wave through the thicker barrier before entrance of the wave through the thinner barrier, and one initiation was caused by the wave through the thinner barrier propagating in the preshocked region of the receptor. The results again indicate that preshocked receptors are less sensitive to initiation than normal receptors, even when the

176

Table V: Sensitiveness limits for standard and pre-shocked receptors using glass barriers.

S_{1L} (cm)	S_{1R} (cm)	L_r (cm)	S_{2L} (cm)	S_{2R} (cm)	τ'_L (μsec)	τ'_R (μsec)	τ_L (μsec)	τ_R (μsec)	Δt* (μsec)	ΔS** (cm)	Comp.B Batch No.	Remarks
7.1	--	--	--	--	--	--	--	--	--	--	1	Failed
6.60	--	--	--	--	--	--	--	--	--	--	1	Failed
6.55	--	--	4.4	--	15.1	--	14.1	--	--	--	1	
6.60	--	--	--	--	--	--	--	--	--	--	1	Failed
6.60	--	--	8.3	--	82.6	--	81.8	--	--	--	1	***
6.60	--	--	--	--	--	--	--	--	--	--	1	Failed
6.55	--	--	9.2	--	92.2	--	90.0	--	--	--	1	***
6.55	6.55	5.5	--	--	--	--	--	--	0	0	1	Failed
6.55	6.55	5.5	--	--	--	--	--	--	0	0	1	Failed
6.55	6.55	5.5	--	--	--	--	--	--	0	0	1	Failed
6.55	6.55	5.5	--	--	--	--	--	--	0	0	1	Failed
6.55	6.55	5.5	--	--	--	--	--	--	0	0	1	Failed
7.4	--	--	6.4	--	69.1	--	67.2	--	--	--	1	***
8.1	--	--	--	--	--	Not measured	--	--	--	--	2	Detonation
8.8	--	--	2.6	--	11.8	--	9.9	--	--	--	2	
6.85	9.75	5.5	--	--	--	--	--	--	17.3	50	2	Failed
6.85	9.75	5.5	--	--	--	--	--	--	15.7	4.6	2	Failed
6.85	9.75	8.0	--	2.3	--	7.9	--	6.7	24.5	--	2	****
6.85	9.75	8.0	--	2.0	--	8.2	--	6.6	24.5	7.1	2	Failed
6.85	9.78	12.0	--	--	--	--	--	--	42.4	--	2	***
6.87	9.75	12.0	6.0	--	26	--	--	--	42.4	12	2	*****

* Δt indicates time delay between entrance of the initial wave into the receptor from the thicker barrier and entrance from the thinner barrier.

** ΔS indicates distance initial wave from the thicker barrier would propagate through the receptor before wave from the thinner barrier entered the receptor.

*** Illustrates initiation with barrier thickness near the sensitiveness limit where $S_2/\tau = 1000$ m/sec rather than the usual case of $S_2/\tau = 2950$ m/sec.

**** Wave through right hand barrier produced detonation.

***** Initiated from left after receptor was shocked.

177

initiating waves collided within the receptor. The results with batch #2 Composition B also indicated that the sensitiveness limit of preshocked receptors increased as the wafer length increased. This might be explained on the basis that the wave from the right-hand barrier attenuated with distance diminishing the desensitization effect of initiation through the thinner barrier. These results would appear to show that initiation of detonation, rather than being promoted by shock, is actually inhibited by shock.

Finally, some results obtained (a) by having axial holes of various diameters in the brass and plate, and (b) the use of end cylinders or plates of diameters less than the receptor diameter are shown in Table VI. In the case of axial holes in the 0.3 cm and plates of diameter 1.4 cm or less the re-initiation of detonation occurred normally in accord with condition (1). However, at a hole diameter greater than 1.4 cm no initiation occurred. The ratio of the hole area to the charge (cross-sectional) area was about 0.1 at the failure point. Correlating these results, end cylinders of 1.9 cm diameter or larger produced reflected initiation waves with a corresponding area ratio at the failure point of about 0.14. These results show that the receptors tended to initiate at the charge axis which is in agreement with photographs of the process.

The results of these studies show that, while they play an essential part in the process, shock waves are not solely responsible for the initiation of detonation in the receptor of the card-gap and the SPHF plate tests. While one might therefore conclude that the additional factor needed to effect the initiation of the receptor is the plasma generated at the instant of the flash-across, one important consequence of the trapped detonation-initiation wave studies is that the plasma, if it is the other essential part, must run into the shock from behind in order to effect a detonation; it clearly does not effect a detonation by running head-on into the shock. This result follows from the fact that each initiation of detonation in the method of Fig. 9c knew its own donor.

Summary and Conclusions

1. Parallel probe ionization measurements were found to correlate on an S_1/S_1^* basis with the initiation of detonation in the receptors in the SPHF plate "sensitiveness" test. In Composition B receptors at $0 < S_1/S_1^* < 0.9$ the total ionization-time curve exhibited a uniform rise from the instant the shock from the donor entered the receptor until the initiation of detonation occurred, a slight inflection being evident in the rise curve becoming more prominent toward the upper limit of this range. At $0.9 < S_1/S_1^* < 0.95$ the inflection point changed over to a maximum-minimum ionization region at an ionization level about 2/3 to 3/4 that in the initial detonation wave. In the range $0.95 < S_1/S_1^* < 1.0$ the

Table VI: Effect of geometry of (brass) end plate in method of Fig. 9a (a) 0.32 brass end plates with center holes, and (b) brass cylinders.

S_1 (cm)	L_r (cm)	End Plate	S_c (cm)	Hole Diameter (cm)	Cylinder Diameter (cm)	X (cm)	τ' (μsec)	S_2/τ (mm/μsec)
5.55	2.0	(a) Brass-center hole	0.32	.1.27		0.9	11.2	3.0
5.55	2.0	"	0.32	1.42		1.4	10.4	2.8
5.65	2.0	"	0.32	1.42		No initiation		
5.55	2.0	"	0.32	1.90		No initiation		
5.55	2.0	"	0.32	2.54		No initiation		
5.65	2.0	(b) Brass cylinder	1.27		1.90	No initiation		
5.55	2.0	"	1.27		1.90	0.46	14.6	2.6
5.65	2.0	"	1.27		2.24	1.65	9.0	2.6
5.55	2.0	"	1.27		3.40	0.5	14.0	2.7

maximum and minimum in the ionization-time curve separated progressively in magnitude and time as S_1/S_1^* increased. Precisely at $S_1/S_1^* = 1.0$ the minimum in the curve became zero, the maximum occurring then at an ionization level about 1/3 of the level existing in detonation. At $S_1/S_1^* > 1.0$ the ionization pulse consisted of the initial pulse only and became progressively smaller with increasing S_1/S_1^* disappearing only at S_1 values appreciably above S_1^*. This excellent correlation with the sensitiveness limit seems to demonstrate the dependence of detonation on ionization, the latter being considered effective in creating detonation by rendering the reaction zone strongly thermally conducting.

2. Perpendicular probes at 1.0 cm inside the (long) receptor from the inert (here glass or lucite) barrier showed two important ionization pulses (and a third unimportant circumstantial one). The first pulse, for measurements in the range $0.7 < S_1/S_1^* < 1.0$, exhibited a maximum about 4.0 μsec after the initial rise and evidently propagated into the shock front (where it initiated detonation) at a rate which increased from about 7 km/sec at $S_1/S_1^* \doteq 1.0$ to 11.5 km/sec at $S_1/S_1^* \doteq 0.7$. While further study is required using, for example, two or more sets of perpendicular probes, making measurements at different distances from the barrier and using different S_1/S_1^* ratios, it appears that this ionization pulse is to be identified with the flash-across phenomenon observed in transparent liquid explosives.

3. In the range $0 < S_1/S_1^* \lesssim 0.7$ the pressure in the initiating shock in the receptor was observed to build up progressively and uniformly with distance from the barrier going smoothly into detonation as predicted by Kistiakowsky. However, in the range $0.7 \lesssim S_1/S_1^* < 1.0$ the shock pressure changed very little, if at all, in the interval τ, increasing discontinuously from the critically low level that it had upon entering the receptor to the detonation level right at S_2.

(4) Perpendicular probe measurements at variable distance X (from 0.5 cm to S_2) with receptors of X + 0.5 cm length yielded rapidly rising conduction-time curves. These were shown to be associated with the effects of a release wave reflected from the end of the receptor. These studies provided unique information on the influence of pressure on the conduction level in the ionization (effective initiation) pulse; the initial low levels of ionization at X = 0.5 was caused by release wave-attenuation of the pressure pulse from the donor system caused by a finite rise time to a peak pressure a μsec or so behind the shock front owing to the lower velocity of the plastic compared with elastic wave in the explosive and donor system. This effect disappeared gradually as X was increased thus causing the conductance to increase rapidly with X.

(5) By using high impedance end-plates on the receptor it was found possible to explode it at $0.5 < L_r < S_2$ which is impossible

with bare receptors or for receptor charges in contact with any low impedance medium. A striking observation was the fact that the total time τ and total shock travel distance $2L_r - X$ (=S_2) were both constant in these tests. This is a striking confirmation that the effective initiation pulse is the ionization pulse and not the shock wave.

The conditions in (4) and (5) not only provide a simple explanation of receptor length effects but also the reason for the ionization minimum in the parallel probe studies. If initiation does not occur at some time during the interval of entrance of the compressional portion of the wave into the receptor, the ionization pulse is required upon complete development to pass through a rare-faction zone before it moves into the shock front. Since ionization in the predetonation region depends strongly on pressure, it sub-sides while in the rarefaction region of the shock wave but builds up again (explosively) upon moving into the compression portion of the wave. Detonation occurs only when the pressure and ionization pulses combine; in the absence of the ionization pulse strong shocks many times greater in magnitude than the critical value to initiate the ionization pulse, which then builds to its critical level via chemical reaction, can even collide without triggering a detonation as shown by double-donor studies.

(6) Double-donor systems with $S_1 < S_1^*$ for both donors and with $S_2 < L_r < 2S_2$ exhibited double DDT's each knowing its own donor. This and other similar shock interaction experiments in which $S_1 < S_1^*$ for one and $S_1 > S_1^*$ for the other donor demonstrated clearly the importance of the ionization pulse in the initiation of detonation in the modified card-gap or SPHF plate test and showed that shock pressure is important only in its effect on promoting ionization but not as a direct means of initiating detonation.

BIBLIOGRAPHY

1. Kistiakowsky, G.B., "Third Symposium on Combustion, Flame and Explosion Phenomena," Williams and Wilkins, Baltimore (1959).

2. Jacobs, S.J., "Conference on Wave Shaping", Pasadena, California, June 1956.

3. Groocock, J.M., and Griffiths, N., "The Burning to Detonation in Solid Explosives," ARDE Report (MX) 5/59, March 1959.

4. Cook, M.A., Keyes, R.T., and Filler, A.S., Trans. Fara. Soc. 52, 369 (1956).

5. Cook, M.A., "The Science of High Explosives," Reinhold Publishing Corp., New York (1958).

6. Cook, M.A., Keyes, R.T., and Lee, L.L., "Measurements of Ionization and Electron Densities in the Detonation Wave of Solid Explosives," Technical Report No. 1, Contract AF-18(603)-100, Explosives Research Group, University of Utah, September 15, 1956. (See Chapter 7, Ref. 5)

7. Cook, M.A., Pack, D.H., and Gey, W.A., Proc. Roy. Soc. (London) A246, 281 (1958).

8. Cook, M.A., Pack, D.H., and Gey, W.A., "The Deflagration to Detonation Transition," Seventh Symposium (International) on Combustion, Oxford, August 29-September 3, 1958. Butterworth's Scientific Publications (London) 1959, p. 820-836.

9. Cook, M.A., and McEwan, W.S., J. Appl. Phys. 29, 1612 (1958).

10. Cook, M.A., Keyes, R.T., and Udy, L.L., J. Appl. Phys. 30, 1881, (1959).

11. Cook, M.A., Pack, D.H., Cosner, L.N., and Gey, W.A., J. Appl. Phys. 30, 1579 (1959).

12. Cook, M.A., Pack, D.H., and McEwan, W.S., Trans. Fara. Soc. No. 451, Vol. 56, Part 7, July 1960.

13. (Cook, M.A., and Udy, L.L., "Calibration of the Card-Gap Test," (to be published).

14. Clay, R.B., "Shock Waves in Solids," Doctorate Thesis, University of Utah, June 1960.

15. Courant, R., and Friedrichs, K.O., "Supersonic Flow and Shock Waves," Interscience Publishers Inc., New York (1948).

16. Jacobs, S.J., "Properties of Detonation Waves," Discussion, p. 879, Seventh Symposium (International) on Combustion. Butterworth's Scientific Publications, (London), 1959.

CHEMICAL FACTORS IN EXTERNAL DETONATION-GENERATED PLASMAS*

M. A. Cook, A. G. Funk, and R. T. Keyes
Institute of Metals and Explosives Research, University of Utah
Salt Lake City, Utah

ABSTRACT

Results obtained in studies of detonation-generated plasmas pertaining to thickness, velocity, and luminosity as a function of the composition of the explosive and various bulk and surface additives are presented. The term detonation-generated plasma refers to the highly luminous and ionized zone generated at charge surfaces by detonation waves. These plasmas are to be classified as dilute plasmas (i.e., plasmas with one or less free electron per atom or molecule) in contrast to concentrated plasmas in which complete ionization of the planetary electrons occurs. Shock waves are shown to produce relatively little luminosity in comparison to that emitted by detonation-generated plasmas. Differentiation is thus made between the luminosity resulting from a shock wave traveling through air and that of a detonation-generated plasma. The plasma resulting from collision of like plasmas is compared with that obtained in collision of chemically different plasmas, and the effects of oxygen balance are discussed in terms of the mechanism of the generation of plasmas.

Introduction

An external detonation-generated plasma is the region of intense luminosity formed at the surface of a condensed explosive when the detonation front emerges. Plasmas propagating from the ends of charges have been observed to last for more than 250 μsec and to exhibit remarkable cohesive properties. Six selected pictures from a framing camera sequence showing the propagation of a plasma from Dithekite-13 were reproduced on the cover of the Journal of Applied Physics for November 1958. Previous to the recognition of the plasma character of the emission phenomenon the luminosity was generally considered to result from decay of ionization that was thermally induced by the shock wave propagating through the gaseous medium surrounding the detonation. On the basis of electron density measurements in the detonation reaction zone,[1] which showed average electron densities to be at least $10^{17}/cm^3$ in the detonation reaction zone and perhaps at the detonation front to exceed $10^{19}/cm^3$, it was proposed that external detonation-generated plasmas consisted of ions and electrons propelled from the detonation reaction zone at the charge surface.[2] The terms internal and external plasmas were used to signify the ionization within the charge and exterior to the charge, respectively.

Based upon the cohesive properties exhibited by external plasmas the quasi-lattice model for their structure was proposed.[3] Assuming that the same type structure existed in the much higher density internal plasmas, which would seem plausible because such a structure would be even more likely to exist under such conditions, it was possible to account for the extremely high degrees of ionization existing in reaction zones where temperatures were only of the order of 5000°K or less and densities were about 2.2 g/cm^3.

In the internal plasmas the expected life of an electron was estimated to be only of the order of 10^{-8} sec[1] and thus the internal plasmas decayed very rapidly, existing only as long as free electrons were being generated by chemical reactions in the reaction zone. However, at the charge surface, free ions and electrons are propelled into the low density region outside the charge as long as the detonation reaction persists, the decay rate of the external plasma then being much slower because of the much lower density in the surrounding medium. The length of the external plasma would then be expected to be proportional to the reaction zone length. Cook, Pack and Gey[2] found this to be the case, which was later substantiated by Cook, Keyes and Udy.[4]

Decay of ionization in external detonation generated plasmas was also studied as a function of the gaseous medium through which the plasmas were propagated. The decay rate was found to be strongly dependent upon the electron affinity but not upon the ionization potential or the heat capacity[4] of the gas comprising the medium of propagation. Also interesting plasma pulsations

were observed when plasmas were propagated into a constraining tube the diameter of which was larger than the diameter of the charge. A striking confirmation of the quasi-lattice structure of the external detonation-generated plasma was that the plasma exploded in some cases into gas clouds possessing volumes many times the original volume of the plasma.

A later study[5] proved that external plasmas could be extruded and readily conveyed by thin-walled glass tubing. That external plasmas possessed structure was further demonstrated by the fact that they could be made to explode relatively early when subjected to violent agitation such as that produced by a rapid compression in a constraining tube and then an expansion into the atmosphere or upon impact with a solid surface. This study also showed that an intense shock was generated at the rear surface of the external plasma. This shock was interpreted to be a recombination shock generated by decay of the plasma which occurs greatest at the rear where the density begins to fall off rapidly. On this basis it became evident that plasmas were self-propelled by their own recombination shocks and that this was the cause of their very high velocities relative to the detonation wave and external shock waves.

Since external plasmas apparently are formed by chemionization during chemical reaction of explosive at the surface of the charge, their characteristics should be influenced by the chemical composition of the explosive and by material on the charge surface. This paper presents, therefore, results of an investigation of the chemical nature of the external detonation-generated plasmas.

Experimental

The observations carried out in this study of the chemical characteristics of external plasmas were primarily (1) propagation velocity, (2) intensity of light emission, and (3) color. Velocities were measured with a rotating mirror streak camera while intensity of light emission and color were observed qualitatively from rotating mirror framing camera sequences taken in color with Super-Anscochrome film using a ruled, white background for contrast and semi-quantitative measurements of luminosity. When comparisons were to be made between two or more plasmas the photographic records of both were taken when possible on the same photographic sequence. If this were not possible, care was taken that the speed of development and the conditions under which the exposures were taken were uniform.

The chemical compositions of the external plasmas were varied by using a variety of explosives including PETN, RDX, tetryl, 50/50 pentolite, Composition B, TNT, and the blasting agent 94/6 AN/fuel oil (AN/FO). Since only a few selected oxygen balances were available with these explosives, however, the Sprengel explosive Dithekite, a mixture of nitric acid, nitrobenzene and

186

water, was used most extensively. With this explosive the oxygen balance (O.B.) could be varied at will over the whole range of detonability from the oxygen excess side to the oxygen deficient side simply by varying the proportions of the nitric acid solution and the nitrobenzene. In all cases the nitric acid solution used was 82.8% HNO$_3$ which was combined with purified nitrobenzene to make Dithekite.

One series of studies was devoted to the influence on the external plasma from surface layers comprising various materials that were applied to the end of Composition B charges. Single layered applications were made of aluminum, magnesium, lead, zinc, (all in powdered form), NH$_4$ClO$_4$, LiClO$_4$, NaCl (all in granular form), aluminum foil, grease, and polyethylene. Since grease proved to be a very effective material for quenching the plasma, in order to determine if quenched plasmas could be regenerated, some bi-layered tests were carried out in which a layer of grease was first applied, followed by a layer of powdered aluminum, NH$_4$ClO$_4$, LiClO$_4$, or NaCl each in granular form.

A series of experiments was also carried out to determine if a secondary explosion resulted when a strongly oxygen rich plasma collided with a strongly oxygen deficient one, more specifically a plasma from an explosive of high positive O.B. and a plasma from one of strongly negative O.B. The results were then compared in control tests with colliding plasmas from an explosive of zero O.B. If the plasmas consisted of partially ionized material from the explosive, then the combination of an oxygen rich with a fuel rich plasma should result in a minor explosion.

In order to elucidate further whether the external plasma resulted from chemionization of the explosive or thermal ionization in the shock propagating through the gaseous medium surrounding a charge, the external plasma generated by AN/FO was compared with the shock wave (not plasma) from Composition B passing through a thin glass plate or grease, each of which served to eliminate the plasma. The Composition B charge was backlighted in order to render the shocks visible. Then by means of streak camera traces the velocity and luminosity of the plasma from 94/6 AN/FO were compared to the velocity and luminosity of the shock from the Composition B assembly. In order to make comparisons of luminosity, non-backlighted streak camera traces for the Composition B and the 94/6 AN/FO charges were used.

Measurements of plasma velocity and detonation velocity for Dithekite of varying oxygan balance were carried out over the entire range of detonability, the Dithekite being contained in 200 ml long-form pyrex beakers (height approximately 10 cm and diameter 5.3 cm) and initiated by 4.8 cm (diameter) x 15 cm (length) cast TNT charges through 1/4" thick glass plates which served both to support the beaker and to retain the detonation products of TNT. The height

of Dithekite in the beakers was maintained at 6 cm in all of these experiments. Thus, the remaining 4 cm of the beaker served as a constraining tube. Since the plasma velocity varies (through plasma oscillations) in the early stages of formation the _average_ velocity over the first 4 cm of travel was recorded. Measurement of the detonation velocity required backlighting in order to record the motion of the detonation front.

The effect of compression of plasma on velocity was also investigated. These studies were carried out by detonating Dithekite in 250 ml Erlenmeyer flasks, the height of the Dithekite being 3.7 cm, the top of the flask being stoppered with a cork into which was inserted a 16" length of 1/2" I.D. glass tubing. In order that the plasma be allowed to flow unimpeded into the glass tube the hole in the bottom of the cork was tapered smoothly from the neck diameter of the Erlenmeyer flask to the diameter of the glass tube.

Results and Discussion

The influence of surface films on external plasmas from Composition B is illustrated in Fig. 1 which reproduces selected pictures from several framing camera sequences. Fig. 1a shows the plasma from a bare Composition B charge, included for comparison purposes. For the plasma shown in Fig. 1b the end of the charge was covered with 0.02 mm thick Al foil. Aluminum foil caused a marked increase in luminosity and in the density of the blue color associated with the plasma, and a several-fold increase in thickness of the plasma. This increase in luminosity cannot be explained on the basis of a stronger shock wave in the atmosphere because the plasma from the bare Composition B charge was measured to possess a velocity about 300 m/sec higher than the plasma from the charge covered with aluminum foil, the velocities being 6700 m/sec and 6400 m/sec, respectively. The phenomenal effect of aluminum can be explained, however, on the basis of chemical reaction of the aluminum with the detonation products and accompanying chemionization. This conclusion was verified by results with surface layers of powdered magnesium and powdered lead. The magnesium was found to influence the plasma luminosity and thickness in a manner similar to but less pronounced than that of aluminum. The lead, on the other hand, markedly decreased the plasma luminosity as would be anticipated because of the low heats of formation of the lead compounds. Surface layers 1 mm thick of NH_4ClO_4 and $LiClO_4$ on Composition B also produced increased luminosity as shown in Fig. 1c. This would be expected on the basis that these oxygen-rich compounds should react with the oxygen-negative detonation products from Composition B.

A 1 mm layer of grease and the 0.0875" glass layer completely quenched the external plasma from Composition B. In the case of glass it is because the plasma is held back and the shock wave alone

(a) (b) (c) (d)
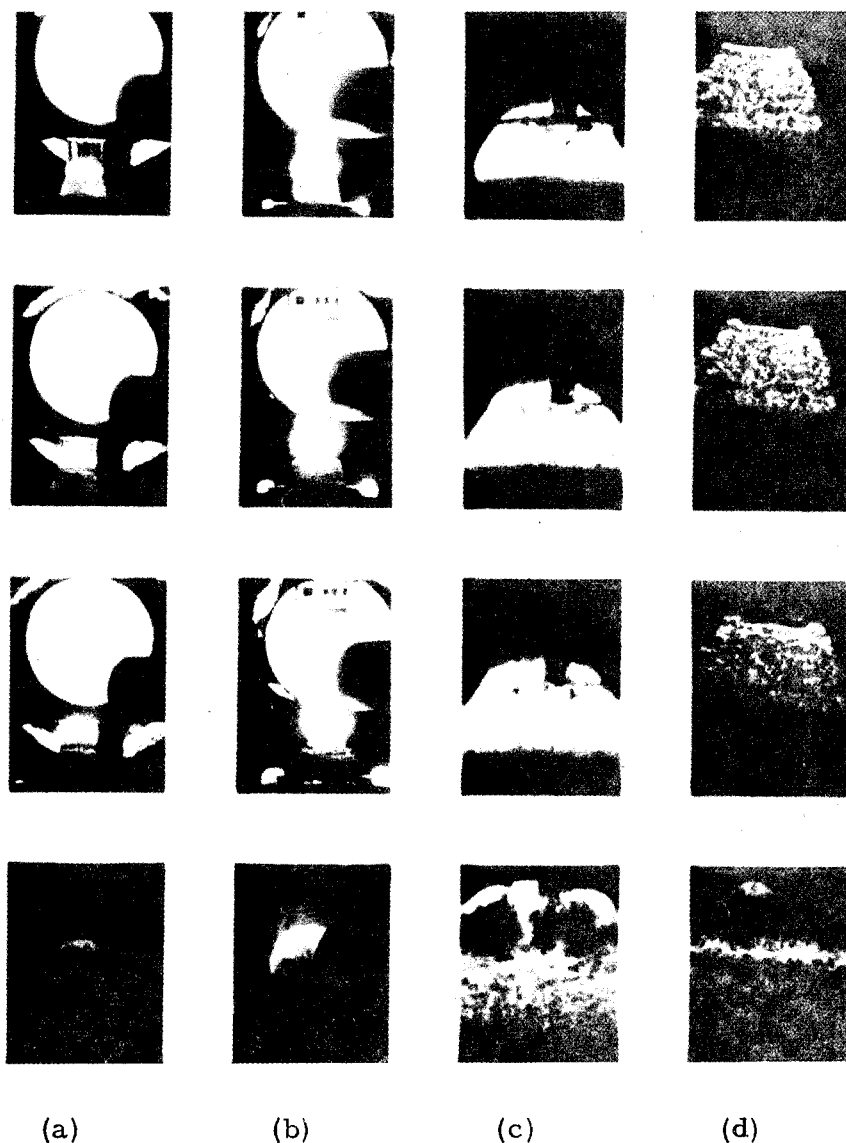
Fig. 1: Influence of surface films on plasmas from
Composition B. (a) Bare Comp B; (b) 0.02 mm
Al film; (c) left to right, 1 mm NH_4ClO_4, 1 mm
$LiClO_4$, 1 mm grease, 0.32 mm polyethylene;
(d) 0.0875 in. glass. (2 μsec/frame. Frames 1,
2,3, and 11 shown.)

(e)   (f)   (g)   (h)   (i)
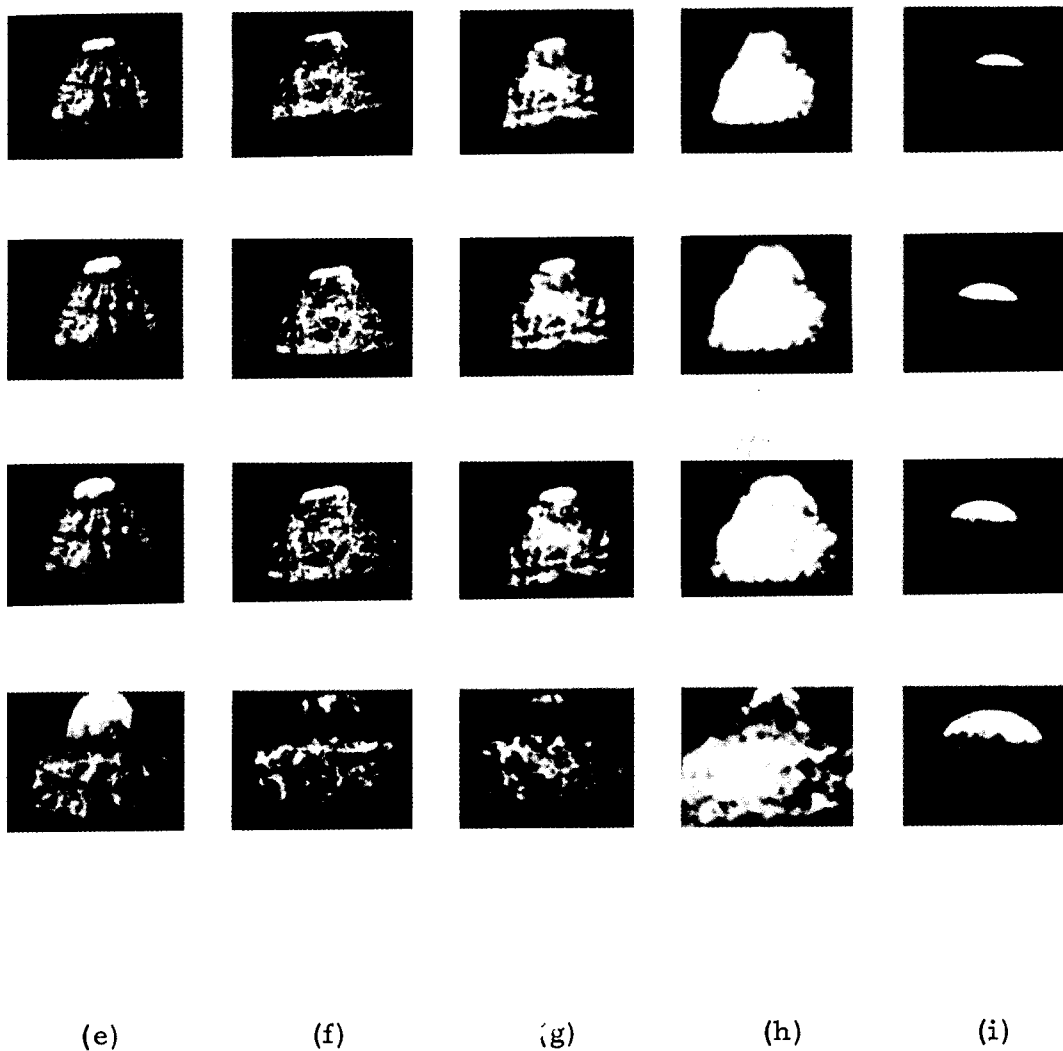
Fig. 1(Continued): Influence of surface films on plasmas from Composition B. (e) 1.5 mm grease plus 1.0 cm powdered Al; (f) 1.5 mm grease plus 1.0 cm $LiClO_4$; (g) 1.5 mm grease plus 1.0 cm NaCl; (h) 1.0 cm NaCl, (i) Bare 94/6 AN/fuel oil.

is able to penetrate the glass. This is adequate proof that the brilliant luminosity is not caused by a shock wave propagating in air. In the case of grease, however, the quenching of luminosity is a chemical one brought about by free radical formation and the large electron affinities of free radicals as explained by Cook, Keyes and Udy.[4]

Fig. 1c also shows the effect of several layers of polyethylene having a total thickness of 0.32 mm. The polyethylene film proved to exert little or no effect on the external plasma.

Fig. 1 (continued) shows some effects of bi-layered applications, the first layer being grease to quench the plasma and the second layer being usually a material expected to cause the plasma to reappear. In the case of aluminum powder and $LiClO_4$ powder on grease the plasma reappeared as shown in Fig. 1(e) and (f) as expected owing to chemical reaction. On the other hand, as shown by Fig. 1(g) considerable luminosity also reappeared with NaCl on grease even though NaCl does not react chemically under these conditions. The results shown in Fig. 1h where a similar layer of NaCl on Composition B alone was found to decrease luminosity, indicate that the mechanism for NaCl is different. Probably the light produced by NaCl when traversed by a shock is electrokinetic in origin, as suggested previously.[6]

Fig. 1(i) presents selected frames showing the external plasma from 94/6 AN/FO generated at the end of a 6" diameter x 36" long (bare end) charge. Even though the detonation velocity in this case was only 2700 m/sec a bright external plasma was generated. Further verification of the fact that external plasmas are not the result of shock-induced ionization in the gaseous medium is evident from comparisons of the characteristics of the plasma from 94/6 AN/FO with the shocks from Composition B charges terminated by a 0.0875" glass plate or a 1 mm layer of grease (the layer of grease on Composition B as shown in Fig. 1c was only about 0.1 mm thick). Firstly, as previously mentioned, the glass plate or the grease completely eliminated the plasma from Composition B. This result was verified from streak camera photographs as well as framing camera photographs. However, when the glass-terminated Composition B charges were backlighted and photographed with a streak camera to show the shock moving from the glass plate, the shock was found to have a velocity in excess of 4400 m/sec. On the other hand, the plasma from 94/6 AN/FO propagated at a velocity below 3700 m/sec and remained highly luminous over a relatively long time. The backlighted, streak camera record of the wave propagated from the end of the grease-covered Composition B charge gave a velocity of 6000 m/sec. As shown by Cook, Keyes and Udy[4] and in Fig. 6.14a, Ref. 6, however, this wave is not a shock wave but simply the luminosity-quenched plasma. Indeed, since glass is a good impedance match for Composition B there is no reason to expect that the true shock for the grease covered charge should not

also possess a velocity about equal to 4400 m/sec.

Fig. 2 contains plots of plasma velocity (averaged over the first 4 cm of propagation) and detonation velocity of various Dithekite mixtures as a function of oxygen balance. The oxygen balance was varied from -75 to +25 weight percent oxygen which covered almost the entire range of detonability of the Dithekite mixtures. Given abscissa on the graph are the oxygen balance as well as percent water in the mixtures. Both the detonation velocity and the plasma velocity vs O.B. curves exhibited maxima corresponding to a slightly negative oxygen balance with the velocities dropping more sharply on the oxygen rich side than on the oxygen deficient side. The densities of the Dithekite mixtures, on the other hand, increased continually from 1.29 g/cm^3 for D-7 to 1.43 g/cm^3 for D-15. Particular attention is directed to the fact, which was well verified experimentally, that the average plasma velocity was less than the detonation velocity near the two extremes of oxygen balance, the trend being more pronounced on the oxygen rich side, while for near zero oxygen balance the average plasma velocity exceeded appreciably the detonation velocity.

The shape of the detonation velocity vs O.B. curve is precisely what one would predict from thermohydrodynamic theory, the enthalpy of the detonation reaction being a maximum for a slight oxygen deficiency. The fact that the average plasma velocity generally exceeded the detonation velocity, but at the extremes of oxygen balance and especially on the oxygen rich side was less than the detonation velocity, is believed to be significant in regard to the mode of propulsion of plasmas.

Fig. 3 presents selected pictures from framing camera sequences showing examples of the collision of plasmas. Fig. 3a shows the collision of two plasmas from D-13 (O.B. = 0) while, for contrast, the Fig. 3b shows the collision of the plasma from D-14 (O.B. = 12.5) with that from D-12 (O.B. = -12.5). As mentioned above if external plasmas result from chemionization in detonation reactions at the surface of the charge rather than from shock-induced, thermal ionization in the gaseous medium surrounding the charge, one would expect that the interaction of two unlike plasmas, specifically a plasma from an explosive with a positive oxygen balance and the plasma from an explosive with a negative oxygen balance, would produce a greater enhancement of luminosity than would occur during the interaction of two plasmas having the same composition. Two factors are, in fact, expected to contribute to increased luminosity resulting from the impact of two plasmas: first the relative compression of the plasmas[5] and second, rapid chemical reaction between the species comprising the two plasmas. The latter effect, of course, can only occur if the plasmas contain species that originate primarily from the explosive, and the species contained in the two plasmas were sufficiently different that they could react chemically during mixing.
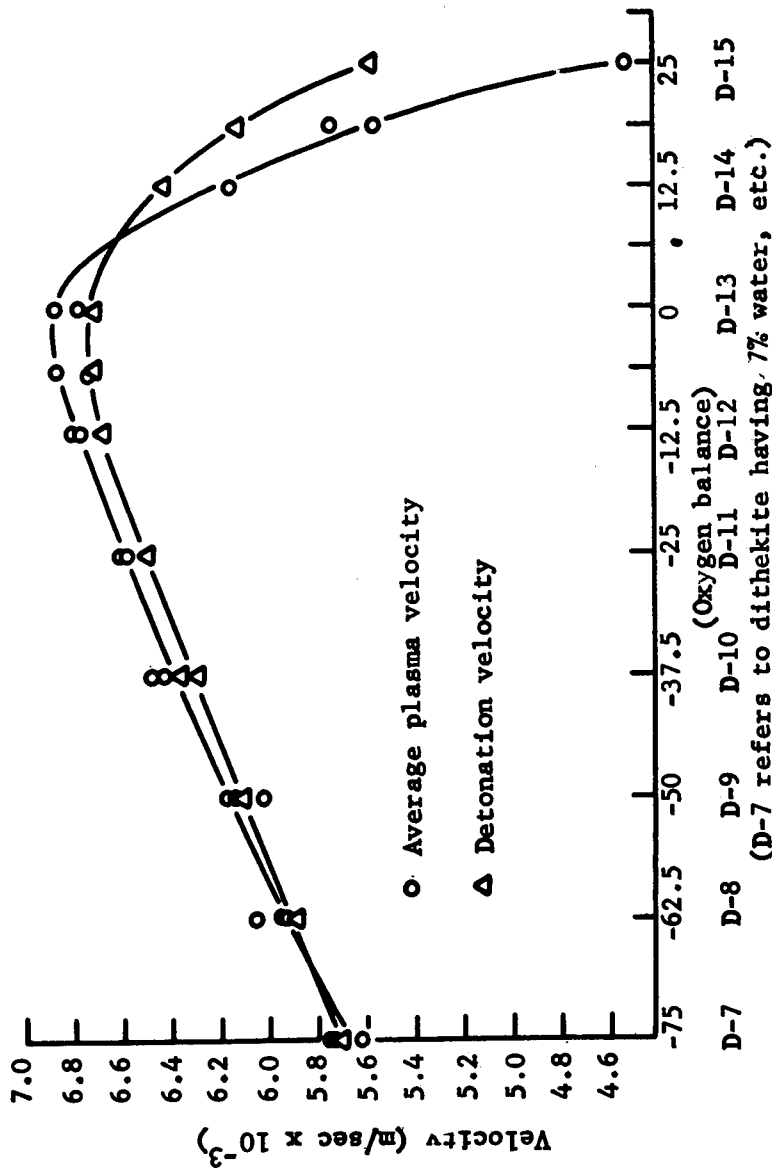
Fig. 2: Detonation velocity and average plasma velocity (over the first four cm propagation) as a function of oxygen balance.

(a)   (b)   (c)
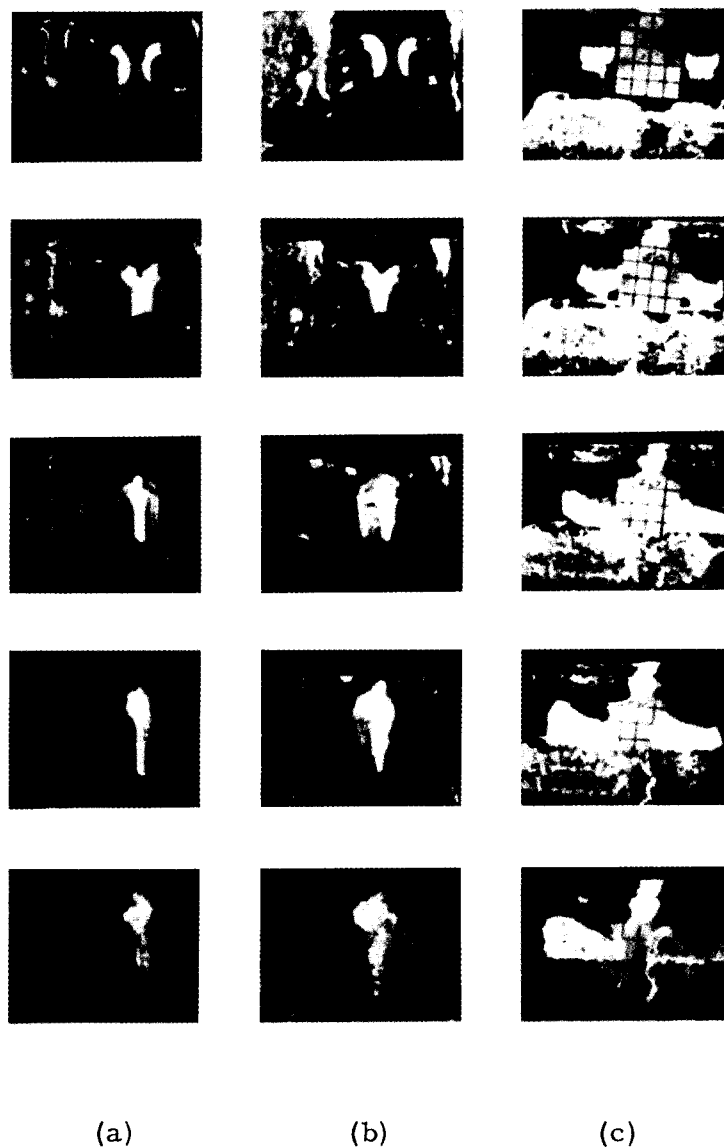
Fig. 3: Collisions of chemically similar and chemically disimilar plasmas. (a) Both D-13 plasmas (O.B. = 0); (b) D-14, left (O.B. = 12.5) with D-12, right (O.B. = 12.5; (c) Plasma from cast TNT (O.B. = -74.5) colliding with plasma from D-15 (O.B. = +25) and plasma from pressed PETN (O.B. = -10) colliding with plasma from D-15. (2 μsec/frame, frames 1,4,7, and 10 shown.)

In examining the photographs of Fig. 3a and Fig. 3b one will note, especially in comparing the last three frames in each series, that a more marked increase in luminosity resulted from the collision of the plasma from the D-14 with the plasma from D-12 (Fig. 3b) than occurred upon the collision of two D-13 plasmas (Fig. 3a). .(This effect is considerably more noticeable on the original films than on the reproductions where detail has been lost.) In addition, the luminosity persisted longer in the collision of the plasma from D-14 and D-12 than in the collision of two D-13 plasmas. This is further substantiated by the fact that the two D-13 plasmas collided at a relative velocity approximately 600 m/sec greater than in the collision of the D-14 with the D-12 plasmas. Thus the plasma compression and resulting increase in luminosity by this mechanism should have been much greater for the collision of like plasmas than for the collision of the unlike ones. This result, therefore, demonstrates the importance of chemionization as the main source of luminosity of these plasmas.

One will note from examination of frame 2 in each of the two series of Fig. 3 that the depth of the enhanced luminous region was greater for the like (D-13) plasmas than for the unlike ones (D-12 into D-14). This result is to be expected because the relative velocity of the two plasmas from D-13 was greater than the relative velocity of the plasmas from D-14 and D-12.

Fig. 3c shows selected frames from a framing camera sequence of the collision of a plasma from cast TNT (O.B. = -74.5) and a plasma from PETN (O.B. = -10) on the left and the collision of a plasma from cast TNT with a plasma from D-15 (O.B. = 25) on the right. The results again demonstrate the importance of chemionization as the source of the luminosity in the external detonation-generated plasmas. A comparatively greater increase in luminosity, which lasted for a longer period of time, occurred in the collision of the plasmas from TNT and D-15 where extensive exothermic chemical reaction would be expected following collision. This situation is particularly noticeable in the last two frames of the series. Again the effect of chemionization was made more striking by the fact that the plasma from PETN had a velocity about 1200 m/sec greater than that from TNT and thus the compressional effect should have been correspondingly greater.

External plasmas may be readily compressed by directing them into constraining tubes of a smaller diameter. Charges of Dithekite were detonated in 250 ml Erlenmeyer flaska producing plasmas which were compressed smoothly into 1/2" I.D. thin-walled glass constraining tubes. The ratio of the surface area of the Dithekite charge or the area of the original plasma to the cross-sectional area of the 1/2" I.D. tube was 38. Fig. 4 reproduces selected frames of sequences showing plasmas from Dithekite mixtures possessing oxygen balances from -75 to +25 which were compressed in the above manner. For the particular case shown in Fig. 4 D-7 and D-8,

(a)   (b)   (c)
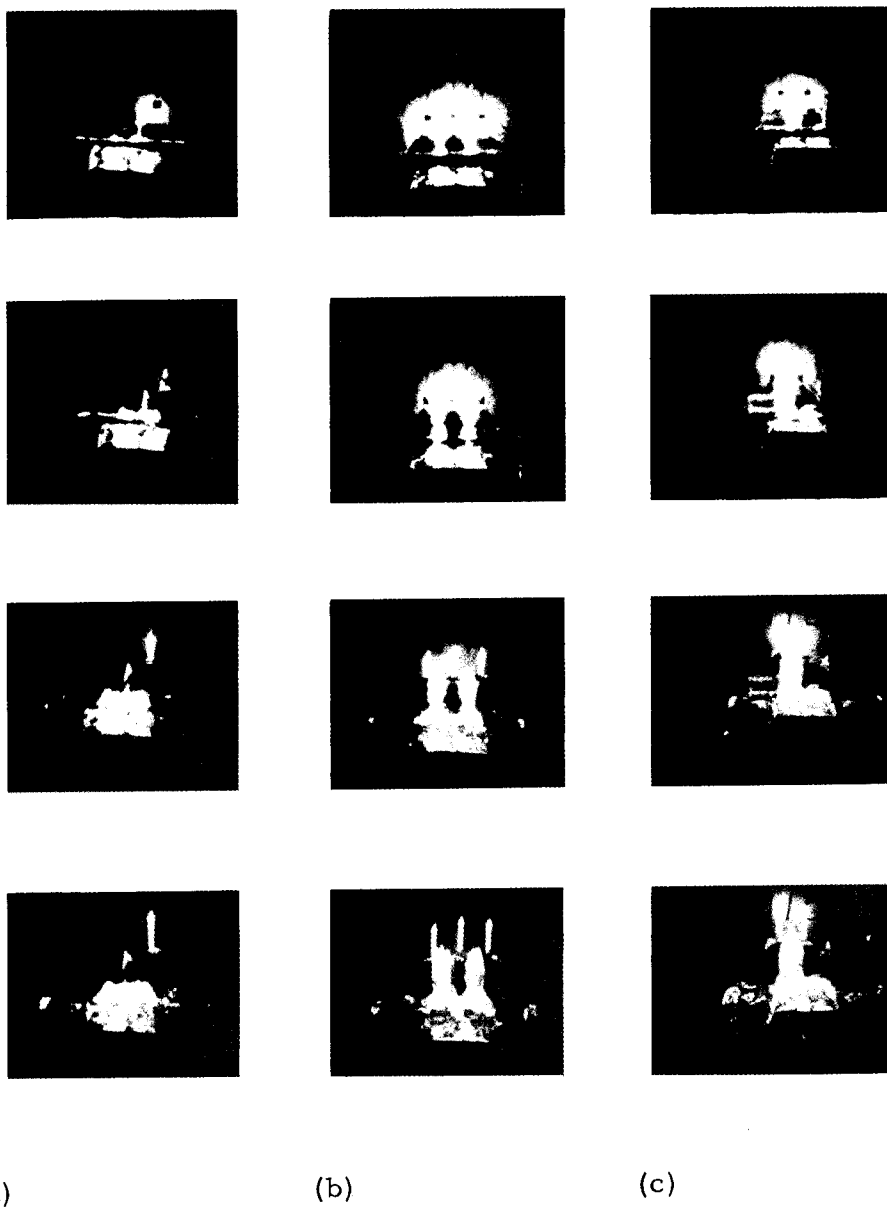
Fig. 4: Selected frames showing Dithekite plasmas com-
pressed into 1/2-in. tubes. (a) D-7, 8, and 9 (left
to right); (b) D-10, 11, and 12; (c) D-13, 14, and
15. (2 μsec/frame, frames 1,4,7, and 10 shown.)

the two charges on the left, and D-15, the charge on the extreme
right, did not detonate. The latter mixture lies near the failure
point because instances have occurred both where this mixture
detonated, and it failed. However, the D-7 and D-8 failure must
have occurred because of some mechanical difficulty because these
mixtures detonated consistently in previous tests.

With the mixtures that detonated, namely D-9 to D-14, large
increases in luminosity occurred as the plasmas were compressed
into the 1/2" tubes. In addition to the increase in luminosity
the plasmas were extended in length to roughly 12 cm. There did
not, however, appear to be any marked, consistent variation in
length of these compressed plasmas as a function of oxygen balance.
When the plasmas were compressed into the 1/2" diameter tubes there
was also an increase in velocity which reached values as high as
13,000 m/sec in the case of D-13. Actually higher velocities and
greater extensions of plasma length have been observed. The velocity
and the length of plasma after being compressed in a tube are
determined to a great extent by the ratio of the cross-sectional
area of the original plasma and the cross-section of the tube, the
greater the compression, the greater the velocity of the compressed
plasma, and the longer its length inside the compression tube. The
velocities of the various compressed plasmas shown in Fig. 4 could
not be resolved sufficiently accurately from the framing camera
sequences to determine the dependence on oxygen balance, and the
appropriate streak camera traces required for such measurements as
yet have not been obtained.

The framing camera sequences shown in Fig. 4 illustrate another
salient factor, namely that the glass did not fracture at the
plasma front even during the compression process. Instead, the
fracturing took place at the rear of the plasmas where the strong
recombination shock was located. Since similar results have been
obtained for very thin-walled tubing this fact demonstrates
further the cohesive nature of external plasmas.

In addition to the plasma compressions shown in Fig. 4 a
plasma from RDX was compressed from an Erlenmeyer flask into a
hole through a lucite block and forced to make a 90° turn. The
plasma flowed around the corner with no change in luminosity
resulting. The lucite assembly was backlighted to observe shocks
in the lucite produced when the plasma reached the 90° turn, but
any such shocks generated were too weak to be observed.

The results of these plasma compression experiments, especially
the extension of plasma length, the delayed fracture of glass, and
the unimpeded flow of the plasma around a 90° corner do not appear
to be explainable on the basis of a shock mechanism for formation
of the ionization.

Plasmas from the Dithekite series D-7 through D-15 detonated in 200 ml long-form beakers, which was the arrangement used for the streak camera measurements of detonation velocity and plasma velocity given in Fig. 2, are illustrated in Fig. 5 by selected frames from framing camera sequences. Sharp decreases in luminosity, velocity, and length of the plasma are particularly noticeable as the oxygen balance was increased from zero through 12.5 to 25, although decreases may also be observed as the O.B. was made more negative. The explosive D-15 (O.B. = 25) exhibited a plasma that was hardly visible, which (because D-15 lies at the limit of detonability) is just the result one would expect on the basis that the detonation state is a plasma state, and the external plasma stems from chemionization at the charge surface. It is interesting to note further that the plasma from the 6" diameter 94/6 AN/FO charge, which was relatively bright, possessed a velocity roughly 1000 m/sec slower than the "dim" plasma from D-15.

Attention is also drawn to the fact that the plasma decay products from D-13 were almost perfectly transparent while the decay products from plasmas whose O.B. deviated from zero tended to be opaque with the tendency increasing the greater the deviation from zero oxygen balance. Similar results were also observed in comparing the decay products of plasmas from TNT, 50/50 pentolite, RDX, and PETN.

Some streak camera traces obtained using the same long form beaker arrangement are reproduced in Fig. 6, many of the streak camera pictures, in fact, being taken simultaneously with the framing camera sequences. Such traces were used to obtain the data of Fig. 2. These traces also illustrate strikingly the decrease in velocity, intensity and thickness of external plasmas that are encountered with Dithekite mixtures as the oxygen balance is varied.
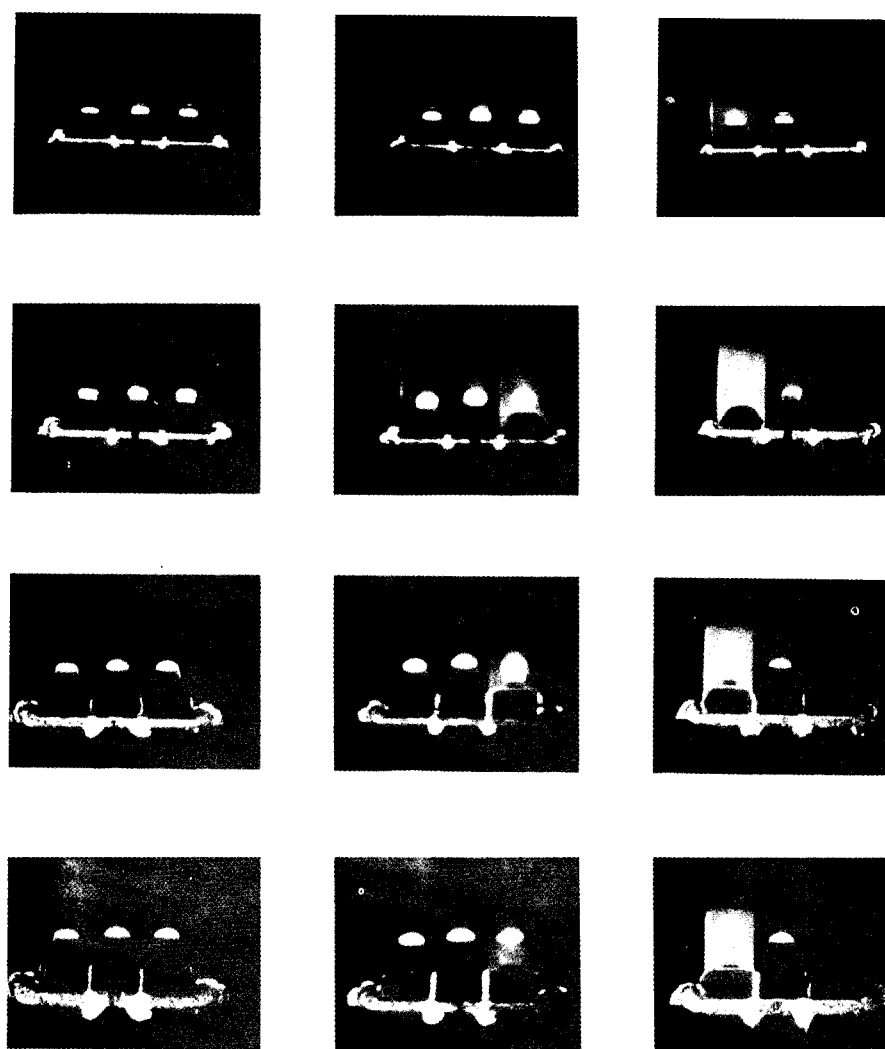
(a)   (b)   (c)

Fig. 5: Selected frames showing Dithekite plasmas.
(a) D-7, 8, and 9 (left to right); (b) D-10, 11,
and 12; (c) D-13, 14, and 15. (2 sec/frame,
frames 1,4,7, and 10 shown.)
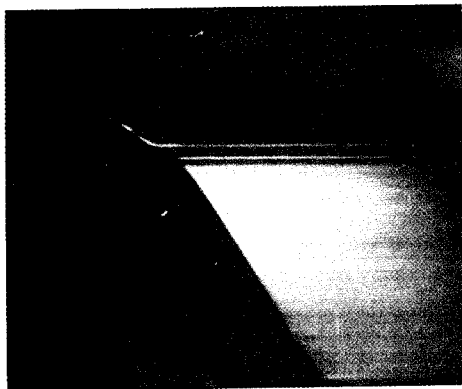
(a)

(b)

(c)
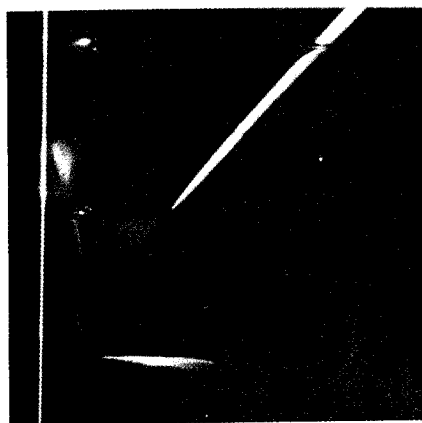
(d)
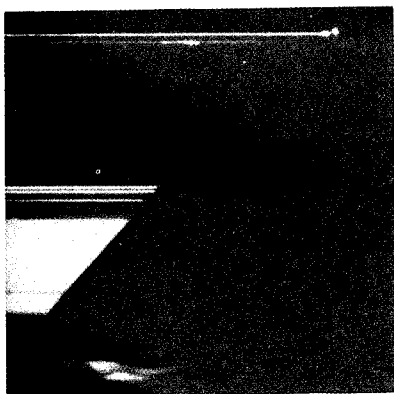
(e)

Fig. 6: Streak camera traces of Dithekite plasmas. (a) D-6; (b) D-7; (c) D-12; (d) D-14; (e) D-15.

BIBLIOGRAPHY

1. M. A. Cook, R. T. Keyes, and L. D. Lee, "Measurements of Ionization and Electron Densities in the Detonation Waves of Solid Explosives," Technical Report No. 1, Contract No. AF-18(603)-100, Explosives Research Group, University of Utah, September 15, 1956.

2. M. A. Cook, D. H. Pack, W. A. Gey, Proc. Roy. Soc. (London) A246, 281 (1958), Butterworth Scientific Publications.

3. M. A. Cook, W. S. McEwan, J. Appl. Phys. 29, 1612 (1958).

4. M. A. Cook, R. T. Keyes, and L. L. Udy, J. Appl. Phys. 30, 1881-1892, (1959).

5. A. Bauer, M. A. Cook, and R. T. Keyes, "Detonation-Generated Plasmas," (submitted for publication).

6. M. A. Cook, "The Science of High Explosives," Reinhold Publishing Corporation, New York (1958).

DETONATION PLASMA

E.L. Kendrew and E.G. Whitbread

Explosives Research and Development Establishment
Waltham Abbey, England.

INTRODUCTION

The detonation of high explosives is always accompanied by a luminous phenomenon which is so characteristic that it is sometimes confused with the detonation itself. It became important to the study of initiation when coupled by M.A. Cook to his "heat pulse" theory. Briefly, an initiating shock in the body of the explosive charge is overtaken by a "heat pulse". At this point the reactions then produce a high degree of ionisation which, when the detonation is established, is restricted to the detonation zone itself. To quote Cook (1) on the generation of the light produced when the detonation zone reaches the surface of the charge: "Apparently the surface layers of explosive begin to spray ions and "electrons into the low-density region of the gas phase when they "start to react, and cease as soon as the reaction is over. "The plasma thus formed has a long half life owing to the low density, "that formed under the high-density conditions inside the explosive "disappears rapidly".

The experiments described here are a study of the connection between the luminous phenomena and the charge's immediate environment.

EXPERIMENTAL

1. Cook's experiment was repeated, with a beaker part full of 60/40 RDX/TNT. The luminous cloud appeared attached to the top of the expanding explosion products.

2. A glass cell, 5 x 4 x 1 cm. half filled with dithekite was detonated from the bottom and photographed in a schlieren field. When the luminous cloud is about 2 to 3 cm. above the cell lateral shock waves in air can be seen as dark lines joining the top of the cell to the edges of the cloud itself. The end shock

(i.e. out of the top of the cell) is not distinguishable from the cloud itself.

3. Experiment 2 was repeated but without schlieren lighting. A box with perspex (lucite) sides, cardboard top and a cellulose film bottom was fixed so that the base was 12 mm above the top of the cell. The box was filled with propane. When the luminous cloud passed into the box a dense black cloud immediately surrounded or replaced it.

4. Experiment 3 was repeated with carbon dioxide in the box. A result similar to that obtained with propane was observed, except that in this case the cloud was not quite so dense.

5. Experiment 3 again repeated but with the box full of neon. The luminous cloud remained luminous but on entering the box the lilac colour observed in air was replaced by pink in the neon.

6. Small explosive charges were detonated in propane, carbon dioxide and neon. These gave results similar to those observed in the perspex box experiments.

7. A gap test type of experiment using RDX/TNT was fired in a vacuum of 5×10^{-5} mm. Hg. The main luminous effects were entirely quenched by the vacuum and the detonated explosive is seen expanding as a very dark mass. There is a flash of light when the detonation reaches the witness block. A small charge of RDX/TNT was similarly fired in vacuo but no luminous cloud was ejected from the end.

DISCUSSION

There is no reason to doubt that the light is due to the recombination of ions and electrons in ionised gas. This is supported by the change in colour when the atmosphere is changed from air to neon. The experiments in propane and carbon dioxide support Cook's theory that the absence of "plasma" when propane is used to surround the charge is due to its decomposition.

It is also certain that the phenomenon is closely attached to the products of the explosion. The appearance of separation of the "plasma" in the dithekite experiments is due to the fact that this explosive is oxygen balanced and the products nearly invisible.

The experiments in vacuo make clear that the light is in fact emitted by the compression of the gas surrounding the charge. The only other explanation is that the light is caused by a strong shock reflected into the products. Light can indeed be generated by this mechanism and the flash seen from the witness

block used in the evacuated gap test arises this way. In the more usual circumstances however the shock impedance of the products will be greater than that of the atmosphere and the reflected wave will be a rarefaction.

ILLUSTRATION

The effective illustration of the foregoing calls for a large number of photographs in colour and a short cine film has been prepared.

BIBLIOGRAPHY

1.   "The Science of High Explosives", Melvin A. Cook,
      Reinhold Publishing Corp. Page 157.

ENERGY TRANSFER TO A RIGID PISTON UNDER DETONATION LOADING

A. K. Aziz, H. Hurwitz and H. M. Sternberg
U. S. Naval Ordnance Laboratory
White Oak, Maryland

ABSTRACT: The flow following the impact of a plane
detonation front, in a condensed explosive, on a rigid
piston is obtained by a finite difference procedure.
Computations are described wherein the equation of state
$E = Pv/\gamma - 1$ is used for the gaseous explosion products,
and the constant γ is taken equal to 2.5, 3.0 and 3.5.
Explicit formulas for the piston motion are obtained
analytically for the special case where γ is equal to
three. The effects of the detonation parameters and the
explosive mass to piston mass ratio on the terminal
velocity of the piston, and the energy transmitted to the
piston, are described. In the range where $\gamma = 2.5 - 3.5$
the terminal velocity of the piston is found to depend
almost entirely on the chemical energy released in the
explosion and the explosive mass to piston mass ratio,
i.e., for a fixed chemical energy, the total energy
transmitted to the piston is insensitive to the form of
the detonation wave.

I.   Introduction

The flow behind a plane detonation front in a con-
densed explosive has been described by G. I. Taylor (1).
A natural offshoot of this problem consists of determin-
ing the flow following the impact of a plane detonation
front on a rigid piston. Of particular interest in
explosives work is the amount of energy transmitted to
the piston and the effect on the energy transmission
process of such factors as the explosive mass to piston
mass ratio and the explosive density, heat of formation
and detonation velocity. The initial configuration is
shown in Figure 1.1.

Free back
expansion into
vacuum

High
Explosive

Plane detonation starts
at this surface.

Rigid Piston
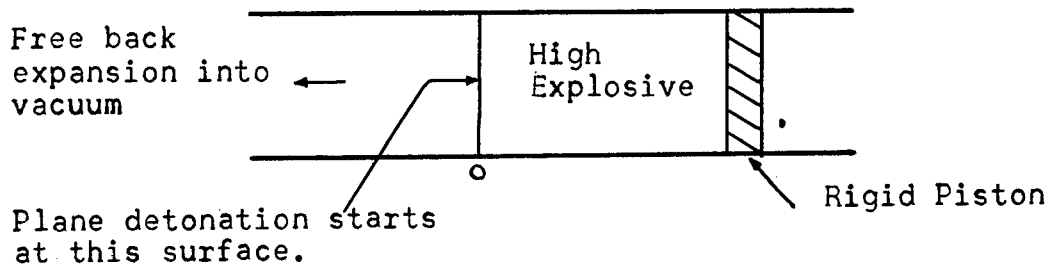
Figure 1.1

The essential features of the gas dynamic problem
are the following: The flow after initiation at the
surface 0 in Figure 1.1, and before the detonation front
reaches the piston is given by a simple wave centered at
0. When the detonation front reaches the piston a shock
is reflected. The rigid piston assumption implies an
initial velocity of zero for the piston followed by a
smooth acceleration. Figure 1.2 is a space-time diagram
indicating the flow regions.

t

reflected shock

III

piston path

gas
boundary

II

A

I

O

X
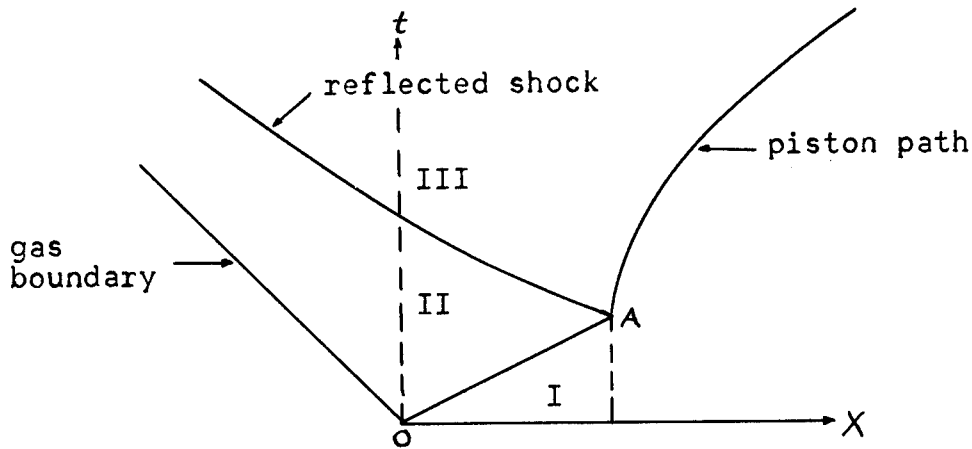
Figure 1.2

Region I in Figure 1.2 consists of solid, unreacted,
explosive. Region II is the simple wave (Taylor wave)
region. Region III is a region of interaction between
the wave crossing the reflected shock and the wave
reflected from the piston.

The equation of state of the form

$$E = Pv/(\gamma - 1)$$

(1.1)

has been used throughout for the gaseous explosion products. Here E is the specific internal energy, P is the pressure, v is the specific volume and γ is constant for each explosive composition. This equation, with γ in the range of 2.5 - 3.5, has been used for the gaseous products of condensed explosives with considerable success, (see Jacobs (2), Price (3), Jackson and Clark (4) and Deal (5)).

A number of relations between the detonation parameters, and the Taylor solution, are listed in Section II. The special case where the adiabatic exponent, γ, is equal to three is considered in Section III. The reflected shock in Figure 1.2, being a weak shock is approximated, in this section, by a compression wave. The validity of this approximation is discussed by Courant and Friedrichs (6). Simple explicit formulas for the motion of the piston are obtained for this special case.

In Section IV a finite difference scheme programmed for the IBM 704 computer is described. This scheme is capable of treating the problem considered here when a more general equation of state than 1.1 is used. The program uses the staggered difference method due to Lax (7) in the shock region and a straightforward differencing of the hydrodynamic equations in the adjoining rarefaction regions.

The results of the computations, in which the equation of state 1.1 was used with γ equal to 2.5, 3 and 3.5 are given in Section V. The quantities u_f/D, $E_f/m_e E_o$, and $u_f/\sqrt{E_o}$ are plotted, for constant γ, against the explosive mass to piston mass ratio, m_e/m_p. Here u_f is the terminal velocity of the piston, D is the detonation velocity, E_f is the total energy transmitted to the piston and E_o is the specific chemical energy released in the explosion. Since γ can be expressed in various ways in terms of the detonation parameters (Section II), the effect of any detonation parameter on the terminal velocity of the piston and on the energy transmitted to the piston can be found from these plots.

II. The Detonation Parameters and the Taylor Wave

In this section a number of relations between the detonation parameters are listed and explicit formulas for the flow variables are given at the time the detonation first reaches the piston in Figure 1.2. This information provides the initial data for the problem dealing with the piston motion.

The following dimensionless variables will be used:

$$\bar{X} = \frac{X}{L} \quad , \quad \bar{t} = \frac{D}{L}t, \quad \bar{u} = \frac{u}{D} \quad , \bar{V} = \frac{V}{V_o}, \quad \bar{c} = \frac{c}{D}$$

$$\bar{P} = \frac{P}{\rho_o D^2} \quad , \quad \bar{E} = \frac{E}{D^2} \quad , \quad \bar{\rho} = \frac{\rho}{\rho_o} \quad , \quad \bar{M} = \frac{M}{\rho_o L} = \frac{M}{m_e} \tag{2.1}$$

Here X is the distance, D is the detonation velocity, t is the time, u is the particle velocity, M is the mass, c is the sound speed, L is the explosive charge length, ρ is the density, and ρ_o is the density of the solid unreacted explosive.

Simple relations between the detonation parameters can be obtained by using the equation of state 1.1 together with the Chapman-Jouguet hypothesis and the conservation equations (see, for example, Jacobs (2), or Price (3)). Denoting by J the conditions immediately behind the detonation front, i.e., the conditions on the line OA in Figure 1.2, a number of these relations can be written

$$\bar{u}_J = \frac{1}{\gamma+1} \quad , \quad \bar{c}_J = \frac{\gamma}{\gamma+1} \quad , \quad \bar{V}_J = \frac{\gamma}{\gamma+1}$$

$$\bar{P}_J = \frac{1}{\gamma+1} \quad \bar{E}_J = \frac{\gamma}{(\gamma^2-1)(\gamma+1)} \quad \bar{E}_o = \frac{1}{2(\gamma^2-1)} \tag{2.2}$$

The flow in regions II and III of Figure 1.2 must satisfy the continuity and momentum equations

$$\frac{\partial \rho}{\partial t} + \frac{\partial(\rho u)}{\partial X} = 0 \quad , \tag{2.3}$$

and

$$\frac{\partial u}{\partial t} + u\frac{\partial u}{\partial X} = -\frac{1}{\rho}\frac{\partial P}{\partial X} \tag{2.4}$$

When the equation of state 1.1 is used, Taylor's solution
for the flow in region II of Figure 1.2 is the centered
simple wave with the properties

$$\bar{u} + \bar{c} = \frac{\bar{X}}{\bar{t}} \tag{2.5}$$

$$\bar{u} - \frac{2}{\gamma-1} \bar{c} = -\frac{1}{\gamma-1} . \tag{2.6}$$

In region II, since the flow in this region is isentropic

$$\bar{\rho} = \bar{\rho}_J \left(\frac{\bar{c}}{\bar{c}_J} \right)^{\frac{2}{\gamma-1}} , \tag{2.7}$$

and

$$\bar{P} = \bar{P}_J \left(\frac{\bar{c}}{\bar{c}_J} \right)^{\frac{2\gamma}{\gamma-1}} . \tag{2.8}$$

From 2.5 - 2.8 and 1.1,

$$\bar{u} = \frac{2\bar{c}-1}{\gamma-1} \tag{2.9}$$

$$\bar{X} = \left[\frac{(\gamma+1)\bar{c}-1}{\gamma-1} \right] \bar{t} \tag{2.10}$$

$$\bar{P} = \frac{1}{\gamma+1} \left(\frac{\gamma+1}{\gamma} \right)^{\frac{2\gamma}{\gamma-1}} \bar{c}^{\frac{2\gamma}{\gamma-1}} \tag{2.11}$$

$$\bar{\rho} = \left(\frac{\gamma+1}{\gamma} \right)^{\frac{\gamma+1}{\gamma-1}} \bar{c}^{\frac{2}{\gamma-1}} \tag{2.12}$$

$$\bar{E} = \frac{\bar{c}^2}{\gamma(\gamma-1)} \tag{2.13}$$

Consider the explosive charge to be divided into zones
of equal mass, m, and let the zone interfaces be labeled
by the subscript j and numbered from one through j max.
Conservation of mass requires that

$$\frac{j-1}{jmax-1} = \int_0^{\bar{c}(j,\bar{t})} \bar{\rho} \, \frac{\partial \bar{X}(\bar{c},\bar{t})}{\partial \bar{c}} \, d\bar{c} . \tag{2.14}$$

Inserting 2.10 and 2.12 into 2.14 and integrating gives

$$\dot{j} = (j_{max} - 1)\, \bar{t} \left(\frac{\gamma+1}{\gamma} \bar{c} \right)^{\frac{\gamma+1}{\gamma-1}}$$

(2.15)

or

$$\bar{c} = \frac{\gamma}{\gamma+1} \left[\frac{\dot{j}-1}{j_{max}-1} \; \frac{1}{\bar{t}} \right]^{\frac{\gamma-1}{\gamma+1}}$$

(2.16)

III. The Special Case Where γ is Equal to Three.

Simple formulas for the piston motion and the energy transmitted to the piston are obtained when the constant, γ , in 1.1 is taken equal to three and the weak reflected shock is approximated by a compression wave. The wave approximation for the reflected shock implies that the characteristics in the rarefaction fan in region II, of Figure 1.2, do not change slope after crossing the shock. When γ is equal to three all of the characteristics are straight lines. The positive characteristics intersecting the piston path in Figure 1.2 are then straight lines emanating from the point 0. The above stipulations and equation 2.5 imply that 2.5 is satisfied on the piston path. Let m_p be the mass of the piston and let

$$n = \frac{m_e}{m_p} = \frac{\rho_0 L}{m_p} \; .$$

(3.1)

The set of equations which must be solved to obtain the piston motion, for the special case considered here, can now be written

$$\bar{u} + \bar{c} = \frac{\bar{X}}{\bar{t}}$$

(3.2)

$$\frac{d\bar{u}}{d\bar{t}} = n\, \bar{P}$$

(3.3)

$$\bar{P} = \frac{16}{27} \bar{c}^3$$

(3.4)

$$\frac{d\bar{X}}{d\bar{t}} = \bar{u} \; .$$

(3.5)

Here, 3.4 is obtained from 2.11 by setting γ equal to three. The required starting values for the piston motion, assuming a rigid piston, are

$$\bar{u}_A = 0, \quad \bar{c}_A = 1, \quad \bar{p}_A = \frac{16}{27}, \quad \bar{X}_A = 1, \quad \bar{t}_A = 1. \tag{3.6}$$

The starting value for $\bar{c}_A$ results from the fact that

$\bar{u} + \bar{c}$ is equal to one on the line OA in Figure 1.2 (see 2.2), and from the wave approximation which implies that $u + c$ does not change slope on crossing the reflected shock.

On the piston path let

$$\alpha = \bar{c}\,\bar{t}. \tag{3.7}$$

From 3.7 and 3.2,

$$\bar{X} = \alpha + \bar{t}\,\bar{u}, \tag{3.8}$$

and differentiation of (3.8) gives

$$\frac{d\alpha}{d\bar{t}} = -\bar{t}\,\frac{d\bar{u}}{d\bar{t}}. \tag{3.9}$$

From 3.9, 3.3, 3.4 and 3.7,

$$\frac{d\alpha}{d\bar{t}} = -\frac{16}{27}\,n\,\frac{\alpha^3}{\bar{t}^2}. \tag{3.10}$$

Integration of 3.10 along the piston path, starting at A in Figure 1.2, results in

$$\bar{t} = \left[1 + \frac{27}{32}n\left(1 - \frac{1}{\alpha^2}\right)\right]^{-1}. \tag{3.11}$$

Insertion of 3.11 into 3.9 gives

$$\frac{d\alpha}{d\bar{u}} = -\left[1 + \frac{27}{32n}\left(1 - \frac{1}{\alpha^2}\right)\right]^{-1}, \tag{3.12}$$

which, on integration gives the piston velocity as

$$\bar{u} = 1 - \frac{27}{32\,n}\left[1 + \frac{32\,n}{27}\alpha - 2 + \frac{1}{\alpha}\right]. \tag{3.13}$$

211

Formulas 3.11, 3.13 and 3.8 give $\bar{t}$, $\bar{u}$ and $\bar{X}$, on the piston path, in parametric form. The terminal velocity of the piston can be obtained as follows: From 3.11, $t \to \infty$ implies

$$\alpha_f = \lim_{t \to \infty} \alpha = \left[1 + \frac{32 \pi}{27} \right]^{-\frac{1}{2}}$$

(3.14)

Inserting 3.14 into 3.13 gives the terminal piston velocity as

$$\bar{u}_f = 1 - \frac{27}{16 \pi} \left[\left(1 + \frac{32 \pi}{27} \right)^{\frac{1}{2}} - 1 \right] .$$

(3.15)

The formula 3.15 can be written

$$\bar{u}_f = \frac{Z - 1}{Z + 1}$$

(3.16)

where

$$Z = \left(1 + \frac{32 \pi}{27} \right)^{\frac{1}{2}} .$$

(3.17)

The fraction of the chemical energy transmitted to the piston is given by

$$\frac{E_f}{m_e E_o} = \frac{\bar{E}_f}{m_e \bar{E}_o} = \frac{8 \bar{u}_f^2}{\pi} .$$

(3.18)

The value of $\bar{E}_0$ given by 2.2 has been used in 3.18. Using 3.16 and 3.17 in 3.18 leads to

$$\frac{E_f}{m_e E_o} = \frac{256}{27} \frac{(Z - 1)}{(Z + 1)^3} .$$

(3.19)

Maximizing 3.19 yields the result that the fraction of the chemical energy transmitted to the piston is greatest when Z is equal to two. From 3.17, this corresponds to a ratio of explosive mass to piston mass of 81/32. Formula 3.19 shows that the fraction of the chemical energy transmitted, for this value of π, is 256/729.

IV. The Finite Difference Method

The flow behind the accelerating piston and the piston motion for the cases where γ is different from three were determined by a finite difference procedure, programmed for the IBM 704 computer. The method used is an explicit Lagrangian scheme in which the shock is replaced by an abrupt but continuous transition in the

Aziz, Hurwitz, Sternberg

flow variables. The von-Neumann and Richtmyer "q" method (8, 9), usually employed to effect this transition, is not used here. Instead the Lax stagger method (7) is used in the shock region, i.e. for those mesh points with the property $U_{j+1}^{n-1} < U_{j-1}^{n-1}$, and a conventional differencing of the hydrodynamic equations is used in the rarefaction regions.

To write the hydrodynamic equations for plane unsteady flow in Lagrangian form let

$$M = \int_{1}^{j} \rho_j^{\circ} \frac{dX_j^{\circ}}{dj} \, dj \quad,$$

(4.1)

where ρ_j° and X_j° are the density and position of the jth particle at zero time. Then

$$\frac{\partial U}{\partial t} = - \frac{\partial P}{\partial M}$$

(4.2)

$$\frac{\partial v}{\partial t} = \frac{\partial U}{\partial M}$$

(4.3)

$$\frac{\partial X}{\partial t} = U$$

(4.4)

$$dE = - P \, dv \, .$$

(4.5)

The energy equation in conservation form is used in the Lax stagger scheme. Here 4.5 is replaced by

$$\frac{\partial}{\partial t} \left(E + \frac{U^2}{2} \right) = \frac{\partial (P U)}{\partial M} \, .$$

(4.6)

The above equations were differenced in the following way: The mass, m_j, of the two zones which meet at the interface labelel j is obtained, for $j = 2$ through j max-1, from

$$m_j = \frac{X_{j+1}^{\circ} - X_{j-1}^{\circ}}{V_j^{\circ}} \, .$$

(4.7)

The two difference schemes are then:

213

Normal Scheme (used for rarefaction points, $U_{j+1}^{n-1} > U_{j-1}^{n-1}$)

$$U_j^n = U_j^{n-1} - \frac{P_{j+1}^{n-1} - P_{j-1}^{n-1}}{m_j} \Delta t \qquad (4.8)$$

$$X_j^n = X_j^{n-1} + U_j^n \Delta t \qquad (4.9)$$

$$V_j^n = V_j^{n-1} + \frac{U_{j+1}^n - U_{j-1}^n}{m_j} \Delta t \qquad (4.10)$$

$$E_j^n = E_j^{n-1} - P_j^{n-1}(V_j^n - V_j^{n-1}) \qquad (4.11)$$

$$P_j^n = \frac{(\gamma-1)E_j^n}{V_j^n} . \qquad (4.12)$$

Stagger Scheme (used for shock and constant state points $U_{j+1}^{n-1} \leq U_{j-1}^{n-1}$)

$$U_j^n = \frac{U_{j+1}^{n-1} + U_{j-1}^{n-1}}{2} - \frac{P_{j+1}^{n-1} - P_{j-1}^{n-1}}{m_j} \Delta t \qquad (4.13)$$

$$X_j^n = \frac{X_{j+1}^{n-1} + X_{j-1}^{n-1}}{2} + U_j^n \Delta t \qquad (4.14)$$

$$V_j^n = \frac{V_{j+1}^{n-1} + V_{j-1}^{n-1}}{2} + \frac{U_{j+1}^{n-1} - U_{j-1}^{n-1}}{m_j} \Delta t \qquad (4.15)$$

$$E_j^n = \frac{E_{j+1}^{n-1} + E_{j-1}^{n-1}}{2} - \frac{(U_j^n)^2}{2} + \frac{(U_{j+1}^{n-1})^2 + (U_{j-1}^{n-1})^2}{4}$$
$$- \frac{P_{j+1}^{n-1} U_{j+1}^{n-1} - P_{j-1}^{n-1} U_{j-1}^{n-1}}{m_j} \Delta t \qquad (4.16)$$

$$P_j^n = \frac{(\gamma-1)E_j^n}{V_j^n} \qquad (4.17)$$

For the present problem the explosion products were divided into zones of equal mass so that, for $j = 2$ through j max-1,

$$m_j = \frac{2\rho_o L}{jmax-1} \qquad (4.18)$$

214

A single stability criterion was used for all points, the time step for each cycle being chosen by

$$\Delta t = \text{minimum over all } j \text{ of } \frac{V_j^{n-1} m_j}{2 c_j^{n-1}} . \qquad (4.19)$$

The machine computation was started at the time t_A in Figure 1.2, i.e., when the detonation front has just reached the piston. Initial values for the flow variables, for the points $j = 1$ through j max-1, were computed from the Taylor solution (formulas 2.9 - 2.17). The initial value of the particle velocity at the point j max, being the initial piston velocity, was taken equal to zero. The initial pressure, volume and energy at j max were then obtained by applying the Rankine-Hugoniot equations across the reflected shock. This gives

$$P_{jmax}^o = P_J + \frac{\frac{\gamma+1}{4} U_J^2 + U_J \left(\frac{(\gamma+1)^2}{16} U_J^2 + \gamma P_J V_J \right)^{1/2}}{V_J} \qquad (4.20)$$

$$V_{jmax}^o = V_J - \frac{U_J^2}{P_{jmax}^o - P_J} \qquad (4.21)$$

$$E_{jmax}^o = \frac{P_{jmax}^o V_{jmax}^o}{\gamma - 1} \qquad (4.22)$$

Here, as before, the subscript J refers to the Chapman-Jouguet conditions.

During each time cycle the boundary points, $j = 1$ and $j = j$ max, were treated as follows: At $j = 1$, the zero pressure boundary condition leads to the difference equation, for the velocity,

$$U_1^n = U_1^{n-1} - \frac{2 P_2^{n-1}}{m_2} \qquad (4.23)$$

The position of the first point, X_1^n, was computed from 4.9, using U_1^n from 4.23. The normal scheme (4.8 - 4.12) was always used for $j = 2$, so that P_1^n and V_1^n were never used, directly, in the computation. At $j = j$ max the acceleration of the piston is given by

$$m_p \frac{du}{dt} = P \qquad (4.24)$$

or

$$\frac{du}{dt} = \frac{r}{m(jmax-1)} P , \qquad (4.25)$$

where π is defined by 3.1 and m is the mass of one zone. The corresponding difference equation, centered in time, is

$$U_{jmax}^{n} = U_{jmax}^{n-1} + \frac{\pi}{m(jmax-1)} \; \frac{P_{jmax}^{n-1} + P_{jmax}^{n}}{2} \; \Delta t$$

$$(4.26)$$

The pressure and specific volume at $j = j$ max were obtained by extrapolation. Consider the pressure gradients at the points 1, 2 and j max in Figure 4.1.
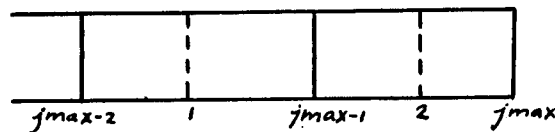
Figure 4.1

Linear extrapolation of the gradients gives

$$2\left(\frac{\partial P}{\partial M}\right)_{jmax}^{n} = 3\left(\frac{\partial P}{\partial m}\right)_{2}^{n} - \left(\frac{\partial P}{\partial M}\right)_{1}^{n}$$

$$(4.27)$$

Here,

$$\left(\frac{\partial P}{\partial M}\right)_{2}^{n} = \frac{P_{jmax}^{n} - P_{jmax-1}^{n}}{m} \; ,$$

$$(4.28)$$

and

$$\left(\frac{\partial P}{\partial M}\right)_{1}^{n} = \frac{P_{jmax-1}^{n} - P_{jmax-2}^{n}}{m} \; .$$

$$(4.29)$$

From 4.2 and 4.25

$$\left(\frac{\partial P}{\partial M}\right)_{jmax}^{n} = -\left(\frac{dU}{dt}\right)_{jmax}^{n} = -\frac{\pi \, P_{jmax}^{n}}{m(jmax-1)}$$

$$(4.30)$$

Inserting 4.28 - 4.30 into 4.27 gives

$$P_{jmax}^{n} = \left(4P_{jmax-1}^{n} - P_{jmax-2}^{n}\right) \bigg/ \left(3 + \frac{2\pi}{jmax-1}\right)$$

$$(4.31)$$

A similar procedure was used to obtain V_{jmax}^{n}. Using the equation of state 1.1 to replace E in 4.5 gives

$$dV = -\frac{V}{\gamma P} \, dP \; ,$$

$$(4.32)$$

so that for j = j max, using 4. 32 and 4.30,

$$\left(\frac{\partial v}{\partial M}\right)^n_{jmax} = \frac{n\, v^n_{jmax}}{Y_m(jmax-1)}$$

(4.33)

The same process used to extrapolate the pressure now gives

$$v^n_{jmax} = \left(4 v^n_{jmax-1} - v^n_{jmax-2}\right)\Big/\left(3 - \frac{2n}{Y(jmax-1)}\right)$$

(4.34)

An additional restriction was inserted, namely, if P^n_{jmax} computed from 4.31 is greater than P^{n-1}_{jmax} , then

$$P^n_{jmax} = P^{n-1}_{jmax} \quad , \quad V^n_{jmax} = V^{n-1}_{jmax}$$

are used in place of 4.31 and 4.34. This restriction is needed during the first few cycles where it prevents the pressure at the piston from exceeding the initial pressure, P^o_{jmax} calculated from 4.20.

The computer program consists of the following steps:

1. Read data: $n, \; Y, \; \rho_o, \; L, \; D$

2. Initialize. Divide gas into zones and use the Taylor solution (2.9 - 2.17) to obtain $P^o_j, \; U^o_j, \; X^o_j, \; V^o_j, \; E^o_j$ for j = 1 through j max-1. Compute $P^o_{jmax}, V^o_{jmax}, E^o_{jmax}$ from 4.20 - 4.22.

3. Print initial conditions.

4. Advance time cycle number.

5. Compute time step, using 4.19.

6. Compute $(\Delta u)_j = U^{n-1}_{j+1} - U^{n-1}_{j-1}$ for j = 2 through j max-1.

7. Compute U^n_j , X^n_j for j = 2 through j max-1, using the normal scheme for $(\Delta u)_j > 0$ and the stagger scheme for $(\Delta u)_j \leqslant 0$.

8. Compute $U^n_1, X^n_1, U^n_{jmax}, X^n_{jmax}$.

9. Compute V^n_j for j = 3 through j max-1, using the normal scheme for $(\Delta u)_j > 0$ and the stagger scheme for $(\Delta u)_j \leqslant 0$. Use the normal scheme to compute V^n_2 .

10. Compute E^n_j , P^n_j , $(c^2)^n_j$, for j = 3 through j max-1, using the normal scheme for $(\Delta u)_j > 0$ and the stagger scheme for $(\Delta u)_j \leqslant 0$. Use the normal scheme for E^n_2, P^n_2 and $(c^2)^n_2$.

11. Compute P_{jmax}^n, V_{jmax}^n using 4.31 and 4.34.

12. Iterate for U_{jmax}^n, V_{jmax-1}^n, P_{jmax-1}^n, E_{jmax-1}^n, V_{jmax}^n, P_{jmax}^n, E_{jmax}^n.

13. Print the time, time step and values of the flow variables for specified time cycle numbers.

14. Test for piston acceleration equal to zero;

    If no - return to 4.

    If yes - print time, time step, values of flow variables for each j, and stop.

V. Computation Results and Conclusions

Machine computations were made for twelve cases, covering the explosive charge to piston mass ratios 1, 3, 6 and 10, and values of 2.5, 3.0 and 3.5 for the constant γ in the equation of state 1.1. The finite difference procedure described in Section IV was started at the time the detonation front first reaches the piston (Figure 1.2), the initial values of the flow variables being obtained from the Taylor solution (2.9 - 2.16) and the formulas 4.20 -- 4.22.

The pressure distribution at various times after the start of the piston motion is shown, for a typical machine run, in Figure 5.1. The Taylor wave, the reflected shock, and the rarefaction wave emanating from the piston may be seen here.

Figure 5.2 consists of plots, for $\gamma = 3$, of U/U_f versus time, where U is the piston velocity and U_f is the terminal piston velocity. For a typical experimental arrangement, where the charge length is 10 centimeters, the detonation velocity is 0.8 centimeters/microsecond, and the explosive mass to piston mass ratio is 3, it is seen from the figure that ninety percent of the terminal piston velocity is acquired within the first 12.5 microseconds after the detonation front first reaches the piston.

As a consequence of the scaling properties (see 2.1) which apply when the equation of state 1.1 is used, the twelve machine runs suffice to determine the effect of the detonation parameters on the energy transmission process, for most practical problems encountered with military explosives. The values of U_f/D obtained in the machine computations are listed in Table 5.1, for the different values of γ and the mass ratio μ.

218
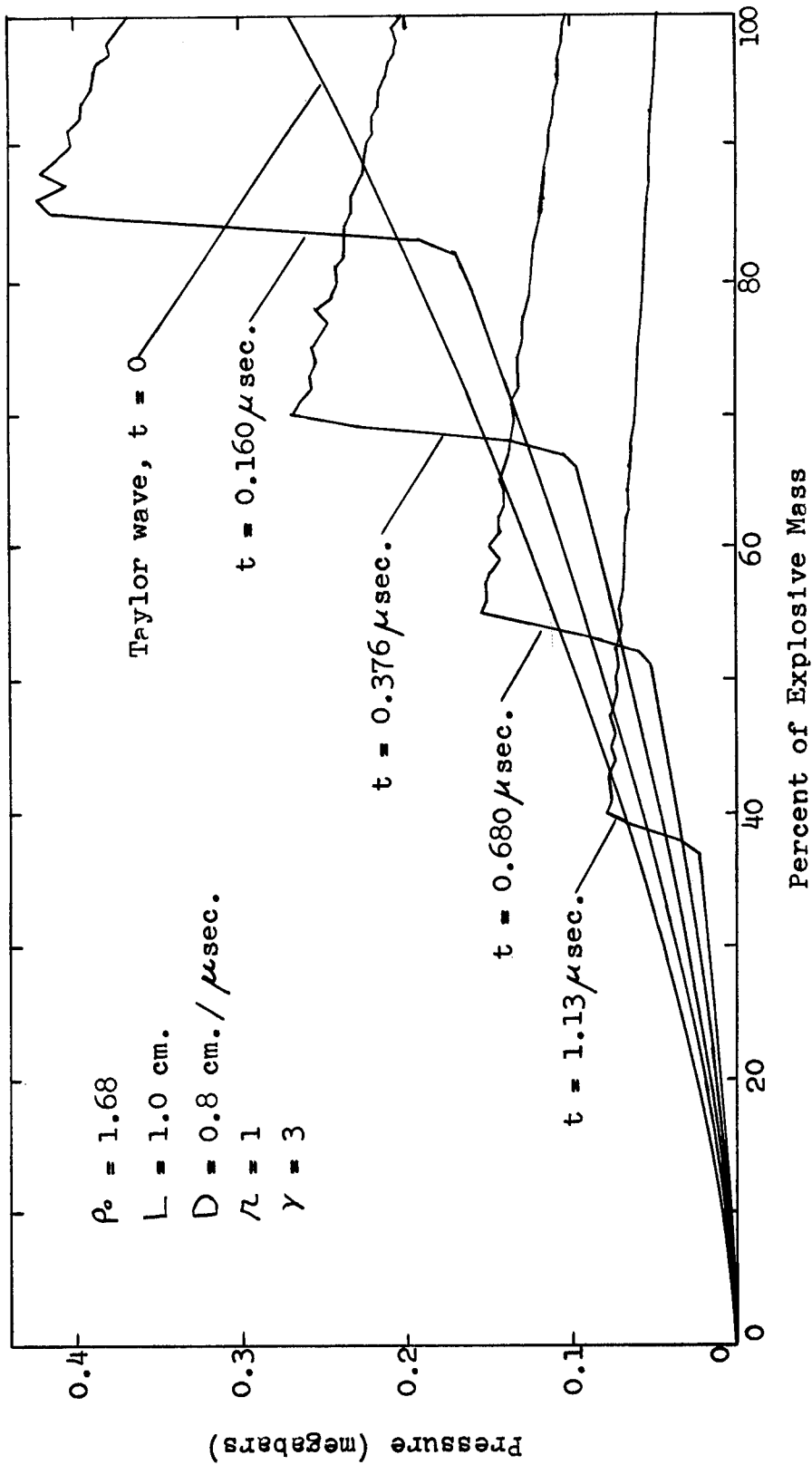
Figure 5.1 Pressure plots showing the Taylor wave and the reflected shock for a typical piston motion problem.
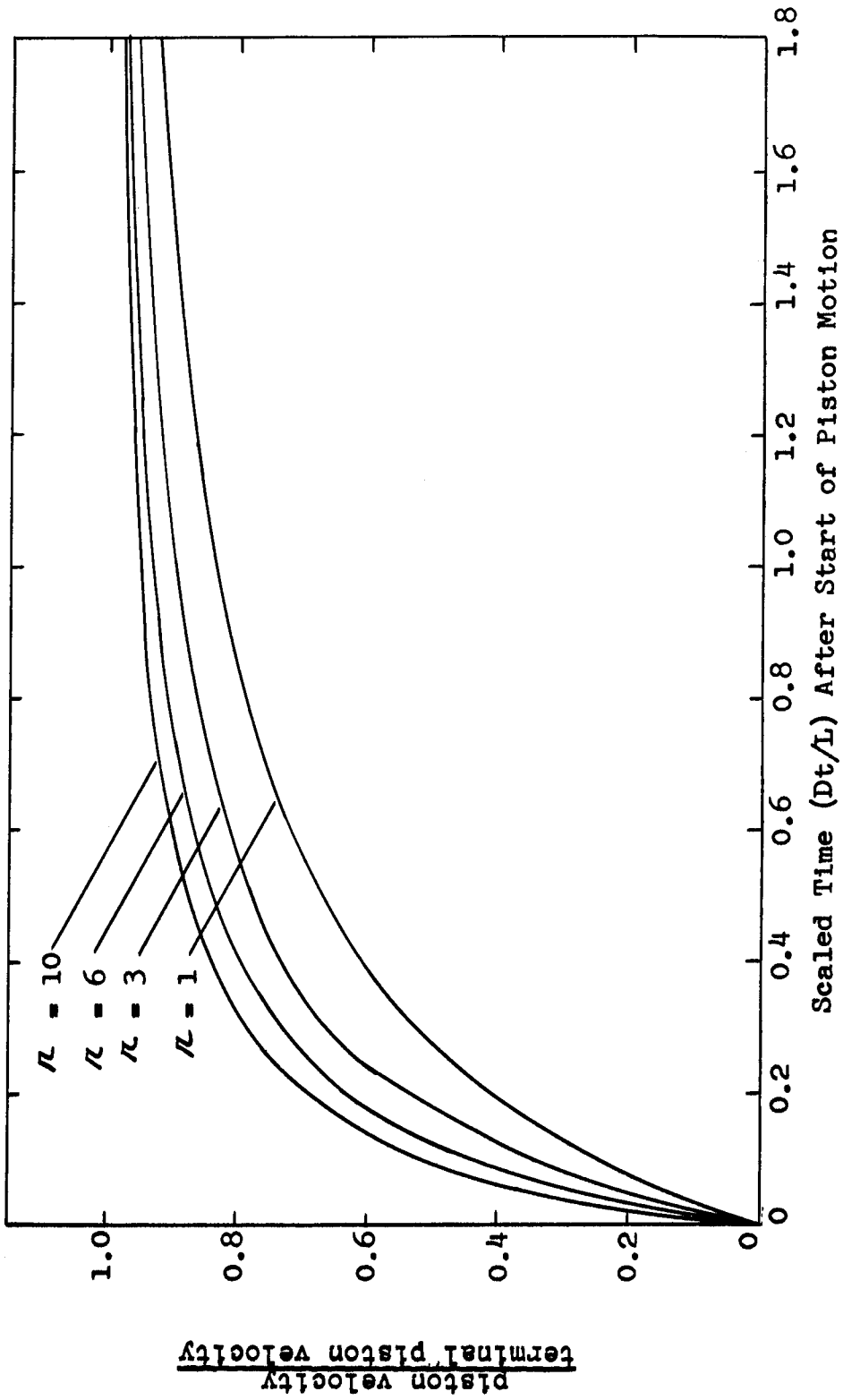
Figure 5.2 Fraction of terminal piston velocity versus time ($\gamma = 3$).

Table 5.1

Scaled Terminal Piston Velocity versus $\hbar$ and γ

$$u_f/D$$

	Machine Computations			Analytic Solution
$\hbar$	$\gamma = 2.5$	$\gamma = 3.0$	$\gamma = 3.5$	$\gamma = 3.0$
1	0.2363	0.1932	0.1635	.1930
3	0.4420	0.3623	0.3083	.3619
6	0.5857	0.4809	0.4097	.4803
10	0.6860	0.5634	0.4809	.5637

The explicit solutions for the special cases where γ is equal to three (formula 3.15) are also given in Table 5.1. for comparison with the machine computations. These results are plotted in Figure 5.3. Figure 5.4 consists of plots of the fraction, $E_f/m_e E_o$, of the chemical energy transmitted to the piston versus $\hbar$, for the three values of γ . These were obtained from Table 5.1 via the formula

$$\frac{\overline{E}_f}{m_e \overline{E}_o} = \frac{\overline{u}_f^2 (\gamma^2 - 1)}{\hbar},$$

(5.1)

where 2.2 has been used for $\overline{E}_o$. Since, from 2.2,

$$\frac{u_f}{\sqrt{E_o}} = \sqrt{2(\gamma^2 - 1)} \ \overline{u}_f \ ,$$

(5.2)

the results in Table 5.1 can be plotted in the form $u_f/\sqrt{E_o}$ versus $\hbar$ for the different values of γ . This is done in Figure 5.5, where the three curves are found to coincide within about 2.5 percent in the values of the ordinate. Since the quantity $u_f/\sqrt{E_o}$ is insensitive to the value of γ , the explicit formula obtained for $\gamma = 3$ gives a good approximation for any γ in the range of 2.5 - 3.5. From 3.15 and 5.2,

$$u_f \sim 4\sqrt{E_o} \left\{ 1 - \frac{27}{16\hbar} \left[\left(1 + \frac{32\hbar}{27} \right)^{1/2} - 1 \right] \right\}$$

$$(2.5 \leq \gamma \leq 3.5). \ (5.3)$$

The result that the terminal piston velocity depends almost entirely on E_o and $\hbar$, and is insensitive to the form of the detonation wave, appears significant for practical work with condensed explosives. For a fixed
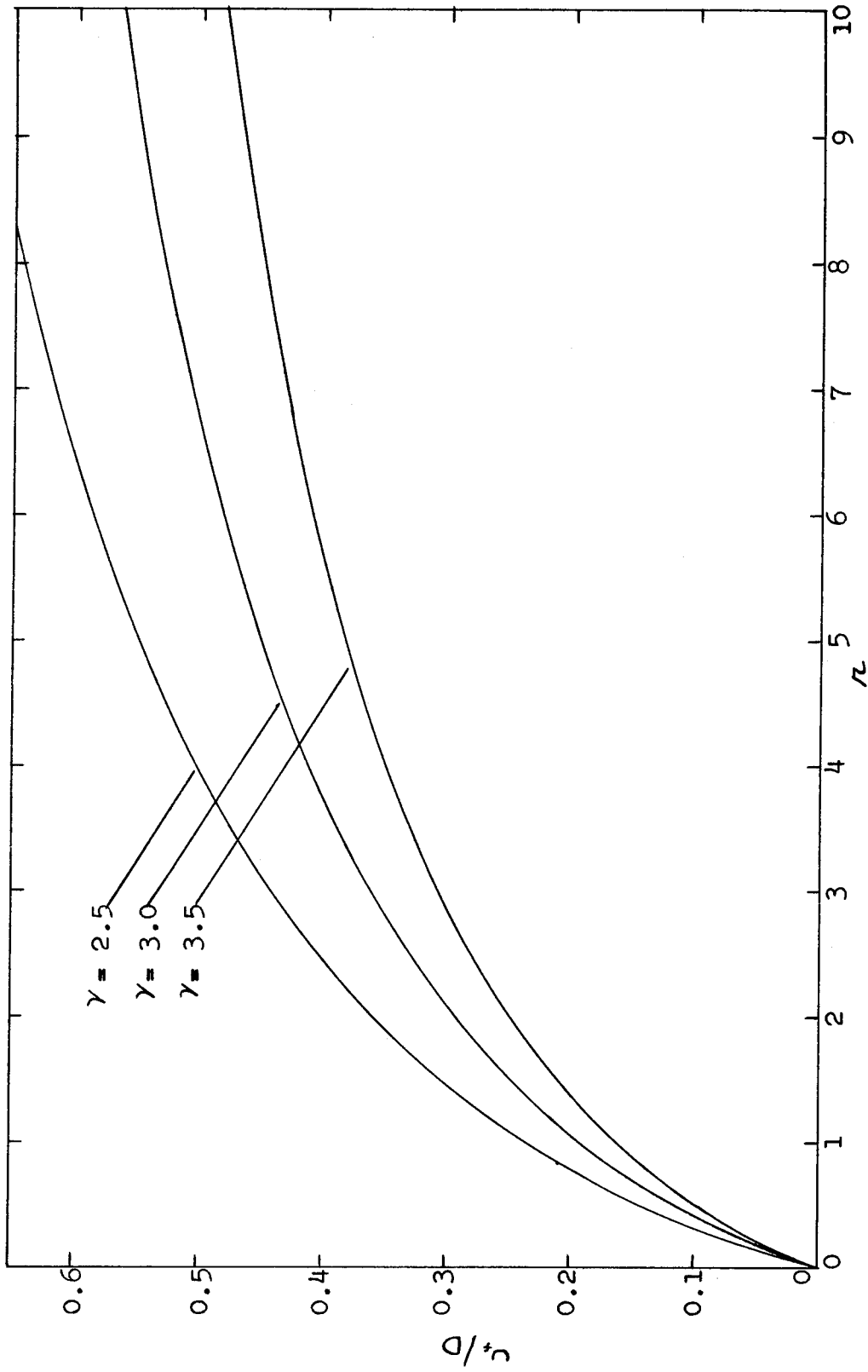
Figure 5.3 Scaled terminal piston velocity (u_f/D) versus explosive mass to piston mass ratio.
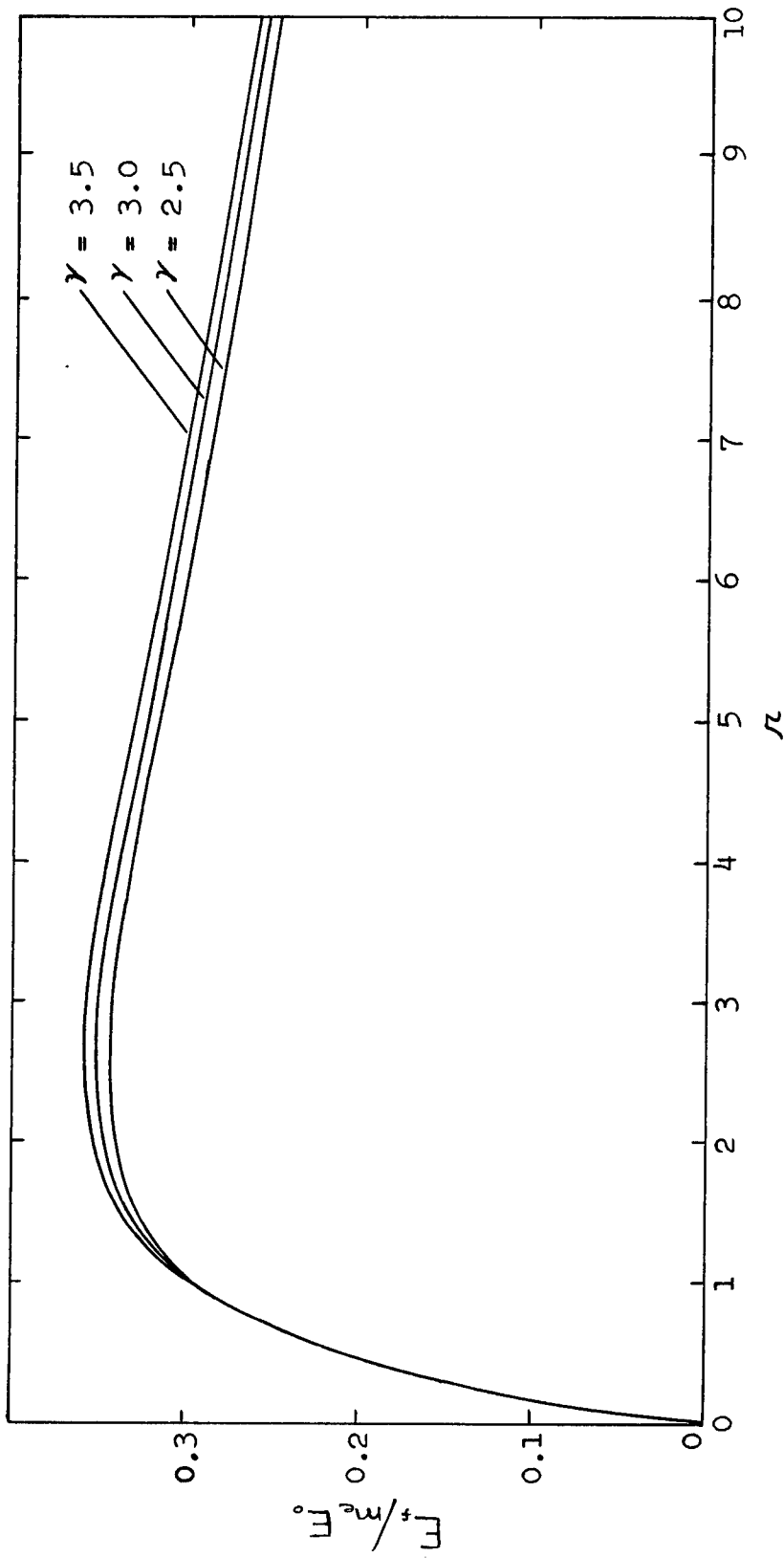
Figure 5.4 The fraction of the chemical explosive energy transmitted to the piston versus the explosive mass to piston mass ratio.
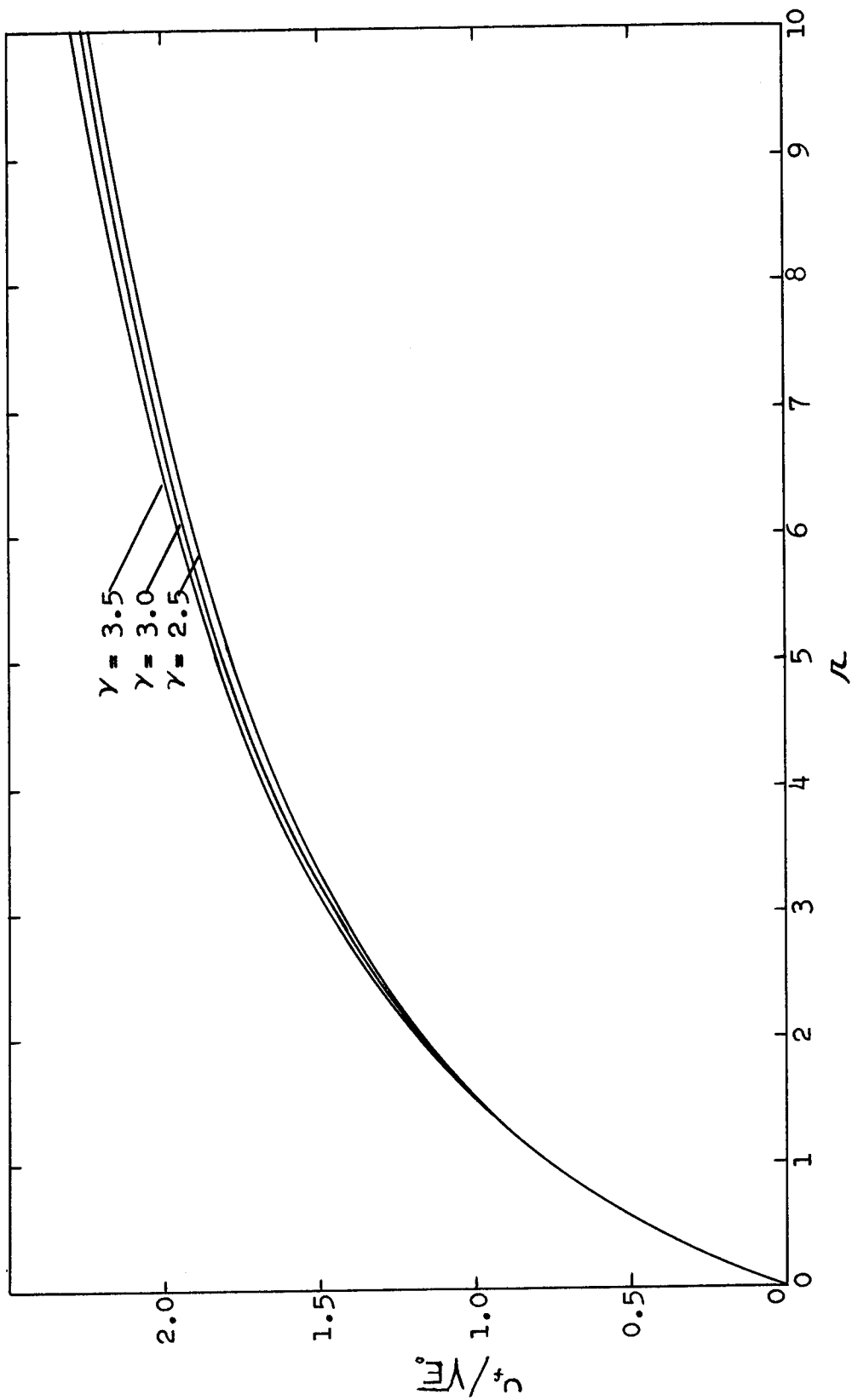
Figure 5.5 $U_f/\sqrt{E_o}$ versus the explosive mass to piston mass ratio.

chemical energy E_o , a change in γ from 2.5 to 3.5 will, from 2.2, redistribute the energy in the Taylor wave so that the Chapman-Jouguet pressure is increased by 67 percent and the detonation velocity is increased by 50 percent; yet the increase in the total energy transmitted to the piston is, from Figure 5.4, only 0.6 percent for n = 1, 1.5 percent for n = 3 and 1.2 percent for n = 10. This seems to explain the success, in the past, of formulas in which U_f is given as a function of E_o and n .

References

(1) G. I. Taylor, "The dynamics of the combustion products behind plane and spherical detonation fronts in explosives", Proc. Roy. Soc. (London) A-200, 235 (1950).

(2) S. J. Jacobs, "The energy of detonation", NavOrd Report 4366 (17 September 1956).

(3) D. Price, "Dependence of damage effects upon detonation parameters of organic high explosives", Chem. Revs. 59, 801 (1959).

(4) R. Jackson, D. B. Clark, "Lagrange's problem for confined high explosives", B.R.L. Report No. 943 (July 1955).

(5) W. E. Deal, "Measurement of the reflected shock hugoniot and isentrope for explosive reaction products", Phys. Fluids 1, 523 (1958).

(6) R. Courant and K. O. Friedrichs, "Supersonic Flow and Shock Waves" (Interscience Publishers, Inc., N. Y., 1948).

(7) P. D. Lax, "Weak solutions of non-linear hyperbolic equations and their numerical computations", Pure Appl. Math. 7, 199 (1954).

(8) J. von Neumann and R. D. Richtmyer, "A method for the numerical calculation of hydrodynamic shocks, J. Appl. Plys. 21, 232 (1950).

(9) R. D. Richtmyer, "Difference Methods for Initial Value Problems" (Interscience Publishers, Inc., N. Y., 1957).

A COMPUTER PROGRAM FOR THE ANALYSIS
OF TRANSIENT AXIALLY SYMMETRIC EXPLOSION
AND SHOCK DYNAMICS PROBLEMS

T. Orlow, D. Piacesi and H. M. Sternberg
U. S. Naval Ordnance Laboratory
White Oak, Maryland

ABSTRACT: The main features of a high speed computer
program for the analysis of transient axially symmetric
explosion and shock dynamics problems are described. The
hydrodynamic equations determining the material flow are
solved numerically by the von Neumann-Richtmyer method.
The program contains routines to accommodate slippage
along interfaces between dissimilar materials; e.g., it
can be used to determine the flow of gaseous explosion
products venting from a metal tube. Results are given
showing the computed two-dimensional flow of metals and
gases following the detonation of cased solid explosive
charges.

I. Introduction

The computation of the flow of gases and metals
following initiation of a detonating explosive system can
be characterized mathematically as a problem in transient,
compressible, flow. Many configurations of practical
interest are axially symmetric and contain several flowing
materials, each with its own equation of state. Further
complications arise due to the presence of shocks and
violent rarefactions. The solution of detonation problems
of this type, out of the question ten years ago, is now
quite practicable by means of present day electronic compu-
ters. A major factor in this development has been the
advance in experimental physics (1, 2) that has resulted
in the equations of state of metals and gaseous products
at the extreme pressures encountered in the detonation
of condensed explosives.

The AEC laboratories appear to have made the greatest
effort to exploit the possibilities for the high speed
machine computation of transient flow problems in two space

226

dimensions. A number of unclassified AEC reports (see, for example, (3) and (4)) deal with Lagrangian and combined Eulerian-Lagrangian machine programs wherein the shocks are treated by the von Neumann-Richtmyer "q" method (5, 6), as abrupt but continuous transitions in the flow variables. The NOL work has been influenced and substantially benefited by contacts with Lawrence Radiation Laboratory personnel working in this field.

The Naval Ordnance Laboratory has, for some time, been engaged in the construction of a computing machine program, or "code", for the solution of axially symmetric, time dependent, explosion hydrodynamic problems. This initial effort has been centered about an explicit, Lagrangian, finite difference scheme, based on the "q" method. Sufficient generality has been maintained so that many different materials, each with its own equation of state, can be incorporated into a single problem. Provision for slippage of one moving boundary past another has been included, mainly for use in venting gases from expanding metal tubes.

Our intention in this paper is to describe the main features of the NOL code, called "Cyclone", and to give some results obtained in a test problem. The test problem is concerned with the flow following the initiation at the center of a steel tube filled with a condensed explosive. The hydrodynamic theory and the difference equations are discussed in Section II. The slippage routine and the test problem are considered in Sections III. and IV.

The Cyclone code was originally prepared at NOL by A. Gleyzal. The first version was described in September 1959 in a classified paper by A. Gleyzal, H. M. Sternberg and A. D. Solem. The code has been substantially rewritten by the present authors, who added the boundary, axis, and slippage routines now in use. The stability criteria are due to J. Enig (7).

II. The Hydrodynamic Theory and the Difference Equations

To write the hydrodynamic equations for axially symmetric flow in Lagrangian form denote the Lagrangian coordinates by k, ℓ, the Eulerian coordinates by R, Z, the velocity components by u, v, the density by ρ, the specific volume by V, the internal energy by E, and the pressure by p. The continuity equation is then

$$\frac{\rho_0}{\rho} = \frac{R A}{R^0 A^0} ,$$
(2.1)

where

$$A = \frac{\partial(R,Z)}{\partial(k,\ell)} ,$$
(2.2)

and the superscript o refers to initial values of the variables. Following the von Neumann-Richtmyer idea, an artificial viscosity q is introduced and the pressure in the equation of motion, and in the energy equation, is replaced by

$$P = p + q \qquad (2.3)$$

In the present work, the variable q is taken as

$$q = \frac{b A}{V^3} \left(\frac{\partial V}{\partial t}\right)^2 , \qquad (2.4)$$

where b is a constant that is adjusted to give the desired sharpness to the shock. The equations of motion are now

$$\frac{d^2 R}{dt^2} = \frac{-R}{\rho^\circ R^\circ A^\circ} \left[\frac{\partial P}{\partial k} \frac{\partial Z}{\partial \ell} - \frac{\partial P}{\partial \ell} \frac{\partial Z}{\partial k} \right] , \qquad (2.5)$$

$$\frac{d^2 Z}{dt^2} = \frac{-R}{\rho^\circ R^\circ A^\circ} \left[\frac{\partial P}{\partial \ell} \frac{\partial R}{\partial k} - \frac{\partial P}{\partial k} \frac{\partial R}{\partial \ell} \right] , \qquad (2.6)$$

$$\frac{dR}{dt} = \int \frac{d^2 R}{dt^2} dt \quad , \quad \frac{dZ}{dt} = \int \frac{d^2 Z}{dt^2} dt , \qquad (2.7)$$

$$R = \int \frac{dR}{dt} dt \quad , \quad Z = \int \frac{dZ}{dt} dt , \qquad (2.8)$$

and the energy equation is

$$\frac{\partial E}{\partial t} = - P \frac{\partial V}{\partial t} . \qquad (2.9)$$

The equation of state of each material present in the problem is assumed given in the form

$$p = p(E, V) . \qquad (2.10)$$

A simple mechanical model is useful in connection with the finite difference approach. In this model, we consider the material to be divided, by mesh lines, into zones, as in Figure 2.1, with integer values of k and ℓ used to label the mesh points.
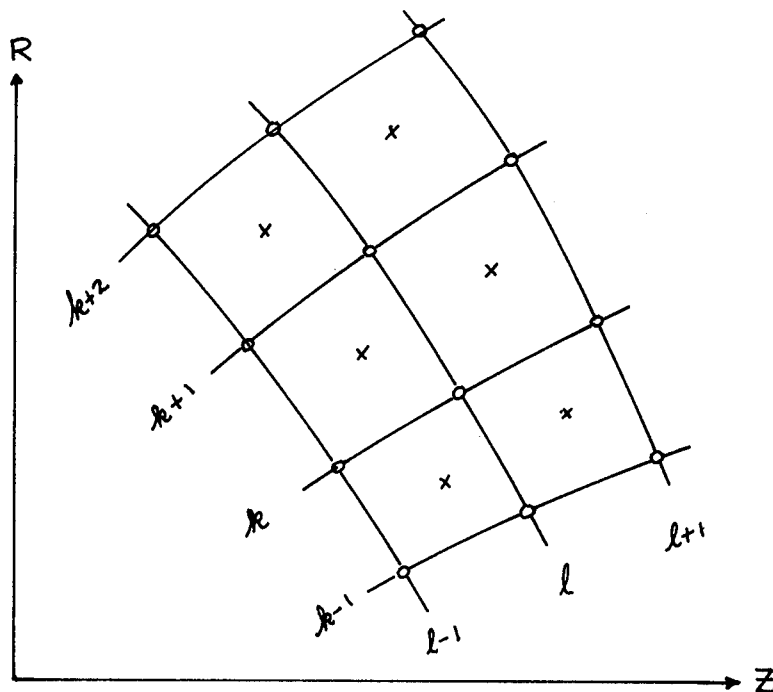
Figure 2.1

The variable A, in equation 2.1, can now be interpreted as the area of the zone as it moves. Mass is conserved by requiring that the mass of each zone remains constant as its density and configuration change. To each mesh point a mass is assigned consisting of one-fourth the mass of the four surrounding zones. We think of the problem as one of determining the motion of these mass points. Suppose that the values of all the flow variables are known at time t^n. Having chosen a time step, Δt, the acceleration of each mass point is determined from the pressures in the four surrounding zones. The new velocity components and positions of the points are then found. This is followed by computations which give the new specific volumes, pressures and energies associated with each zone. A new time step is then chosen and the entire process is repeated.

The difference equations used to represent 2.1-2.10 in the Cyclone code are given below. Positions and velocities are centered at the mesh points and subscripted (k, ℓ). Specific volumes, areas, pressures, artificial viscosities, and internal energies are located at the

centers of the zones and carry the subscripts $(k-\frac{1}{2}, l-\frac{1}{2})$. Superscripts are used to denote the time cycle numbers.

At the beginning of each time cycle, the time t^n is computed from

$$t^n = t^{n-1} + \Delta t^{n-\frac{1}{2}}, \tag{2.11}$$

where t^{n-1} is the time at the previous cycle and $\Delta t^{n-\frac{1}{2}}$ is the time step, usually determined from stability considerations. At time t^n, the quantities

$$R_{k,l}^{n-1}, \quad Z_{k,l}^{n-1}, \quad U_{k,l}^{n-\frac{1}{2}}, \quad V_{k,l}^{n-\frac{1}{2}}, \quad E_{k-\frac{1}{2}, l-\frac{1}{2}}^{n-1},$$

$$V_{k-\frac{1}{2}, l-\frac{1}{2}}^{n-1}, \quad P_{k-\frac{1}{2}, l-\frac{1}{2}}^{n-1}$$

are known; for n = 1, from the given initial data and for $n > 1$, from the computation for the previous cycle. We first calculate the new positions of the mesh points from

$$R_{k,l}^n = R_{k,l}^{n-1} + \Delta t^{n-\frac{1}{2}} U_{k,l}^{n-\frac{1}{2}} \tag{2.12}$$

$$Z_{k,l}^n = Z_{k,l}^{n-1} + \Delta t^{n-\frac{1}{2}} V_{k,l}^{n-\frac{1}{2}}. \tag{2.13}$$

The new positions are used to obtain the approximate areas of the zones by a straightforward differencing of 2.2. This gives

$$A_{k-\frac{1}{2}, l-\frac{1}{2}}^n = \left(\frac{\partial R}{\partial k}\right)_{k-\frac{1}{2}, l-\frac{1}{2}}^n \left(\frac{\partial Z}{\partial l}\right)_{k-\frac{1}{2}, l-\frac{1}{2}}^n - \left(\frac{\partial R}{\partial l}\right)_{k-\frac{1}{2}, l-\frac{1}{2}}^n \left(\frac{\partial Z}{\partial k}\right)_{k-\frac{1}{2}, l-\frac{1}{2}}^n, \tag{2.14}$$

where

$$\left(\frac{\partial R}{\partial k}\right)_{k-\frac{1}{2}, l-\frac{1}{2}}^n = \frac{1}{2}\left(R_{k,l}^n - R_{k-1,l}^n + R_{k,l-1}^n - R_{k-1,l-1}^n\right), \tag{2.15}$$

and

$$\left(\frac{\partial R}{\partial l}\right)_{k-\frac{1}{2}, l-\frac{1}{2}}^n, \quad \left(\frac{\partial Z}{\partial k}\right)_{k-\frac{1}{2}, l-\frac{1}{2}}^n, \quad \left(\frac{\partial Z}{\partial l}\right)_{k-\frac{1}{2}, l-\frac{1}{2}}^n$$

are computed in a similar manner. Insertion of these gradients into 2.14 gives the result

$$A_{k-\frac{1}{2}, l-\frac{1}{2}}^n = \frac{1}{2}\left[\left(R_{k,l_1} - R_{k-1,l}\right)\left(Z_{k,l} - Z_{k-1,l-1}\right) + \left(R_{k,l} - R_{k-1,l-1}\right)\left(Z_{k-1,l} - Z_{k,l-1}\right)\right]. \tag{2.16}$$

The value of R at the center of each zone is computed from

$$R^n_{k-1/2,\,l-1/2} = \frac{1}{4}\left[R^n_{k,l} + R^n_{k-1,l} + R^n_{k,l-1} + R^n_{k-1,l-1}\right]. \qquad (2.17)$$

The new specific volumes are now obtained by using 2.1 in the form

$$V^n_{k-1/2,\,l-1/2} = \frac{A^n_{k-1/2,\,l-1/2}\, R^n_{k-1/2,\,l-1/2}}{W_{k-1/2,\,l-1/2}}, \qquad (2.18)$$

where

$$W_{k-1/2,\,l-1/2} = \frac{A^o_{k-1/2,\,l-1/2}\, R^o_{k-1/2,\,l-1/2}}{V^\bullet_{k-1/2,\,l-1/2}}. \qquad (2.19)$$

The quantities $W_{k-1/2,\,l-1/2}$ are computed once, at the start of the problem after applying 2.14 and 2.16 when $n = 0$. Following $V^n_{k-1/2,\,l-1/2}$ we compute

$$\dot{V}^{n-1/2}_{k-1/2,\,l-1/2} = \frac{V^n_{k-1/2,\,l-1/2} - V^{n-1}_{k-1/2,\,l-1/2}}{\Delta t^{n-1/2}}, \qquad (2.20)$$

$$V^{n-1/2} = \frac{V^n + V^{n-1}}{2}$$

$$q^{n-1/2}_{k-1/2,\,l-1/2} = \begin{cases} b\, \dfrac{A^{n-1/2}_{k-1/2,\,l-1/2}\left(\dot{V}^{n-1/2}_{k-1/2,\,l-1/2}\right)^2}{\left(V^{n-1/2}_{k-1/2,\,l-1/2}\right)^3}, & \dot{V} < 0 \\[4mm] = 0, & \dot{V} \geq 0 \end{cases} \qquad (2.21)$$

We now obtain $P^n_{k-1/2,\,l-1/2}$ and $E^n_{k-1/2,\,l-1/2}$ from the following difference equations for 2.3, 2.9 and 2.10:

$$\left[\; P^n_{k-1/2,\,l-1/2} = p\left(E^n_{k-1/2,\,l-1/2}, V^n_{k-1/2,\,l-1/2}\right) \qquad (2.22)\right.$$

$$\left\{\; P^n_{k-1/2,\,l-1/2} = p^n_{k-1/2,\,l-1/2} + q^{n-1/2}_{k-1/2,\,l-1/2} \qquad (2.23)\right.$$

$$\left[\; E^n_{k-1/2,\,l-1/2} = E^{n-1}_{k-1/2,\,l-1/2} - \frac{P^n_{k-1/2,\,l-1/2} + P^{n-1}_{k-1/2,\,l-1/2}}{2}\left(V^n_{k-1/2,\,l-1/2} - V^{n-1}_{k-1/2,\,l-1/2}\right)\right.$$

$$(2.24)$$

The bracket equations are solved for $P^n_{k-1/2,\,l-1/2}$ and $E^n_{k-1/2,\,l-1/2}$ with one iteration.

In calculating the internal energy $E^{n}_{k-1/2, \ell-1/2}$ for an explosive, we assume a detonation wave, with a known detonation velocity, starts from some point, or surface, where the explosive is initiated. If the detonation front has arrived at a point (k, ℓ), we add to $E^{n}_{k-1/2, \ell-1/2}$ the chemical energy of the explosive contained in the zone with the center $(k-1/2, \ell-1/2)$. The equation of state for the gaseous explosion products is used for this zone from this time onward. If the detonation front has not passed through the zone, we use the equation of state for the solid undetonated explosive.

At this stage in the cycle, a time increment is computed by means of the stability criteria (7). Let c be the sound speed and define

$$B^{n}_{k-1/2, \ell-1/2} = \left[\left(\frac{\partial R}{\partial k}\right)^{n}_{k-1/2, \ell-1/2}\right]^{2} + \left[\left(\frac{\partial Z}{\partial k}\right)^{n}_{k-1/2, \ell-1/2}\right]^{2}$$
$$+ \left[\left(\frac{\partial R}{\partial \ell}\right)^{n}_{k-1/2, \ell-1/2}\right]^{2} + \left[\left(\frac{\partial Z}{\partial \ell}\right)^{n}_{k-1/2, \ell-1/2}\right]^{2} \qquad (2.25)$$

Then, for all zones, we compute

$$\left(\Delta t_{k-1/2, \ell-1/2}\right)^{2}_{N} = \frac{0.8 \left(A^{n}_{k-1/2, \ell-1/2}\right)^{2}}{(c^{2})^{n}_{k-1/2, \ell-1/2} \, B^{n}_{k-1/2, \ell-1/2}} \qquad (2.26)$$

and, for the zones where $\dot{V}^{n-1/2}_{k-1/2, \ell-1/2} < 0$, we compute

$$\left(\Delta t_{k-1/2, \ell-1/2}\right)^{2}_{S} = \left[0.9 \, \frac{A^{n}_{k-1/2, \ell-1/2} \, V^{n}_{k-1/2, \ell-1/2}}{4b \, \dot{V}^{n-1/2}_{k-1/2, \ell-1/2} \, B^{n}_{k-1/2, \ell-1/2}}\right]^{2}. \qquad (2.27)$$

We then take

$$\left(\Delta t_{k-1/2, \ell-1/2}\right)^{2} = \min\left[\left(\Delta t_{k-1/2, \ell-1/2}\right)^{2}_{N}, \left(\Delta t_{k-1/2, \ell-1/2}\right)^{2}_{S}\right] \qquad (2.28)$$

$$\left(\Delta t_{min}\right)^{2} = \min \left(\Delta t_{k-1/2, \ell-1/2}\right)^{2} \quad \text{over all } k, \ell \qquad (2.29)$$

$$\Delta t^{n+1/2} = \min\left[\sqrt{(\Delta t_{min})^{2}}, 1.4 \, \Delta t^{n-1/2}\right] \qquad (2.30)$$

$$\Delta t^{n} = \frac{\Delta t^{n+1/2} + \Delta t^{n-1/2}}{2}. \qquad (2.31)$$

The total energy, kinetic plus internal, is summed at this point in the cycle and compared with the total energy known to be in the system.

The pressure gradients and acceleration components are now computed by means of

$$\left(\frac{\partial P}{\partial k}\right)^n_{k,\ell} = \frac{1}{2}\left(P^n_{k+\frac{1}{2},\ell+\frac{1}{2}} - P^n_{k-\frac{1}{2},\ell+\frac{1}{2}} + P^n_{k+\frac{1}{2},\ell-\frac{1}{2}} - P^n_{k-\frac{1}{2},\ell-\frac{1}{2}}\right) \qquad (2.32)$$

$$\left(\frac{\partial P}{\partial \ell}\right)^n_{k,\ell} = \frac{1}{2}\left(P^n_{k+\frac{1}{2},\ell+\frac{1}{2}} - P^n_{k-\frac{1}{2},\ell-\frac{1}{2}} + P^n_{k-\frac{1}{2},\ell+\frac{1}{2}} - P^n_{k+\frac{1}{2},\ell-\frac{1}{2}}\right) \qquad (2.33)$$

$$\dot{u}^n_{k,\ell} = \frac{-R^n_{k,\ell}}{M_{k,\ell}}\left[\left(\frac{\partial P}{\partial k}\right)^n_{k,\ell}\left(\frac{\partial Z}{\partial \ell}\right)^n_{k,\ell} - \left(\frac{\partial P}{\partial \ell}\right)^n_{k,\ell}\left(\frac{\partial Z}{\partial k}\right)^n_{k,\ell}\right] \qquad (2.34)$$

$$\dot{v}^n_{k,\ell} = \frac{-R^n_{k,\ell}}{M_{k,\ell}}\left[\left(\frac{\partial P}{\partial \ell}\right)^n_{k,\ell}\left(\frac{\partial R}{\partial k}\right)^n_{k,\ell} - \left(\frac{\partial P}{\partial k}\right)^n_{k,\ell}\left(\frac{\partial R}{\partial \ell}\right)^n_{k,\ell}\right], \qquad (2.35)$$

where

$$M_{k,\ell} = \frac{1}{4}\left[W_{k+\frac{1}{2},\ell+\frac{1}{2}} + W_{k-\frac{1}{2},\ell-\frac{1}{2}} + W_{k+\frac{1}{2},\ell-\frac{1}{2}} + W_{k-\frac{1}{2},\ell+\frac{1}{2}}\right]. \qquad (2.36)$$

The new velocity components are then obtained from

$$u^{n+\frac{1}{2}}_{k,\ell} = u^{n-\frac{1}{2}}_{k,\ell} + \Delta t^n\, \dot{u}^n_{k,\ell}, \qquad (2.37)$$

$$v^{n+\frac{1}{2}}_{k,\ell} = v^{n-\frac{1}{2}}_{k,\ell} + \Delta t^n\, \dot{v}^n_{k,\ell}. \qquad (2.38)$$

We now have R, Z, E, P, q, V, u, v and c for the entire mesh. The time is now advanced, via 2.11, and the cycle is repeated.

The Cyclone code is designed to accommodate an arbitrary number of rectangular regions in the fixed Lagrangian (k, ℓ) grid, each with its own equation of state. Input consists of first assigning numbers and boundaries to the regions, e.g.,

$$\left.\begin{array}{l} 3 \le k \le 7 \\ 9 \le \ell \le 15 \end{array}\right\} \text{region 5.}$$

Values of the Eulerian coordinates of the mesh points and the flow variables, at time t = o, can be inserted by means of tables. It is more convenient, however, to insert

the functions $R(k, \ell)$, $Z(k, \ell)$, $\cup(k, \ell)$, $\vee(k, \ell)$, $V(k-1/2, \ell-1/2)$ and $E(k-1/2, \ell-1/2)$ for each region at $t = 0$. An initialization routine then computes and stores the initial values of the Eulerian coordinates and the flow variables. Following the initialization, a first time step is assigned and the process outlined above is started.

Machine output consists of a listing of R, Z, $\cup$, and v for all the grid points; P, E and V for all the zones; and other variables of interest, at specified cycle numbers. In addition, during each time cycle, the position of every mass point appears as a dot on a cathode ray oscilloscope screen. These arrays of dots are photographed, thereby providing a film record of the motion of the mass points.

III   The Slippage Routine

The finite difference scheme based on the Lagrangian formulation of the flow problem suffers from the disadvantage that large distortions in the zones occur when neighboring points, in the Lagrangian grid, develop different velocities. These distortions introduce serious errors through their effect of the accuracy of the pressure gradient computations. The slippage scheme,to be described here,is designed to overcome this difficulty in the case where a gas is venting from an expanding metal tube. The scheme makes use of the fact that the pressure must be continuous across the gas-metal boundary. During each time step, the pressure at the boundary is determined by interpolation involving pressures in both the gas and the metal. The motion of the gas and metal during the time step are then determined independently.

The grid system, where the slippage routine is to be used, is shown in Figure 3.1.
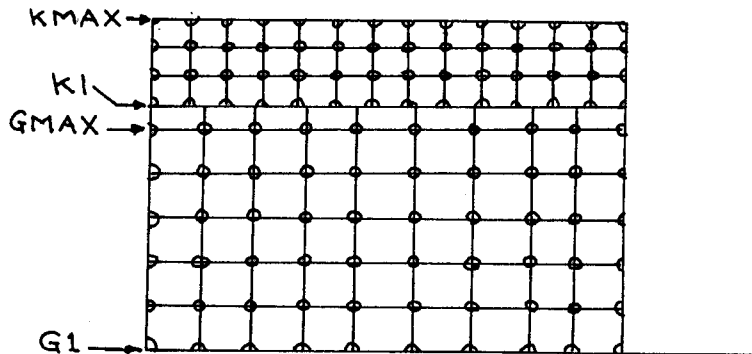
Figure 3.1

The region between the k lines Kl and KMAX, in Figure 3.1, consists of metal. The gas is contained in Gl through Kl. It should be noticed that the gas region is zoned so that all mass points are interior points, i.e., the space between the lines GMAX and Kl is occupied by a half zone of gas, for which the mass is contained in the mass points on the line GMAX. The Lagrangian ℓ lines in the gas are not connected to the ℓ lines in the metal. Figure 3.2 is an enlarged view of a section of the gas-metal boundary after both the gas and the metal have been set into motion.
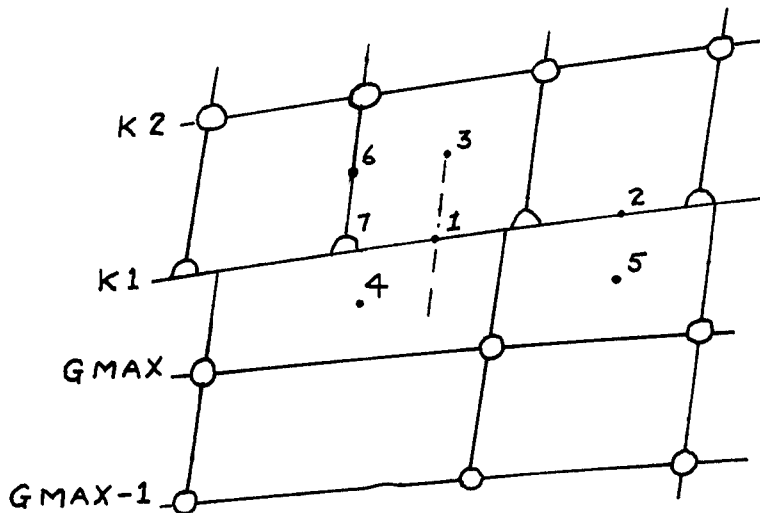
Figure 3.2

The computations, which include the slippage along the gas-metal boundary, proceed as follows: At the beginning of each time cycle, the velocities of all the mass points are known. The new positions, for all the points, are computed in the usual way, via 2.12 and 2.13. The new zone areas are also computed in the usual way for Gl through GMAX and Kl through KMAX. To find the areas of the half zones between the lines GMAX and Kl, the ℓ lines through GMAX-1 and GMAX are extended to meet the metal boundary Kl and the points of intersection are computed. The areas of the half zones, formed by this process, are then computed in the usual way, using 2.16. The specific volumes, pressures and internal energies are then found, via 2.18-2.24, for all the zones, including the half zones. We next determine the pressures along the gas-metal boundary in the following way: Consider the point labeled 1 in Figure 3.2. A line through the points 3 and 1 is extended into the gas region and the closest half zone centers, 4

and 5 on both sides of the line are found. Since the pressures at 3, 4 and 5 are known, the pressure at 1 can be obtained by interpolation. To do this, we use the areas of the triangles shown in Figure 3.3.
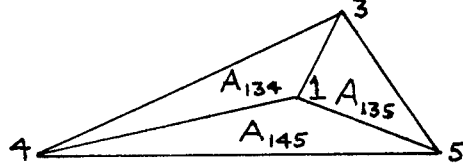
Figure 3.3

Denote these areas by A_{134}, A_{153} and A_{145}, as shown in the figure. The interpolation formula used is then

$$P_1 = \frac{A_{135} P_4 + A_{145} P_3 + A_{134} P_5}{A_{134} + A_{135} + A_{145}}$$

Since the gas-metal boundary pressures are now available, the motion of the metal half masses located on the interface can be determined by the same method used for the points on the outer metal boundary KMAX (Figure 3.1). One scheme, which appears to work quite well, consists of computing the acceleration at the points between K1 and K2 and assigning these accelerations to points on K1, e.g. the acceleration centered at the point 6 in Figure 3.2 is assigned to the point 7.

IV A Test Problem

The application of the Cyclone code to the solution of a detonation problem is illustrated in this section. The problem consists of determining the axially symmetric flow following initiation at the center of a steel tube filled with high explosive. The configuration is shown in Figure 4.1.

Figure 4.1

236
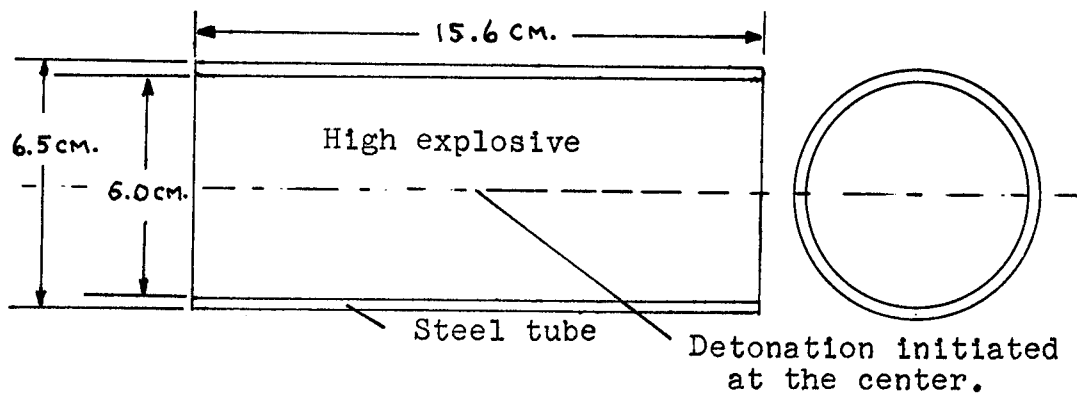
The flow is symmetric about both the R and Z axes; hence, only one-fourth of the cross section shown in Figure 4.1 need be considered in the computation. The zoning of the problem for the Cyclone code was done as in Figure 3.1, with 38 grid lines in the Z direction and 19 grid lines in the R direction. The outer five zones consisted of metal and the gas-metal boundary was considered as a sliding interface. The equation of state of the steel was taken, from a fit to data given in (1), as

$$p = 0.293\mu + 7.28\mu^2$$

where

$$\mu = \frac{\rho}{\rho_0} - 1.$$

The equation of state of the solid unreacted high explosive was taken as

$$p = 0.128\mu + 1.19\mu^3$$

with the initial density $\rho_0 = 1.68$. The equation of state

$$E = pv/\gamma - 1 \quad ,$$

with $\gamma = 2.82$ and the detonation velocity 0.781 cm per microsecond, was used for the gaseous explosion products. Expansion into a vacuum was assumed.

The detonation was started at the center of the tube in Figure 4.1, i.e., at the origin in Figure 3.1. The spherical detonation front emanating from the center first reaches the steel tube, and sends a shock into it, at the plane $Z = 0$. The initial layout and subsequent positions of the metal and gas points are shown in Figures 4.2, 4.3 and 4.4. Figure 4.2 is the initial configuration. In Figure 4.3, the detonation front has just reached the outer surface of the explosive, at the axis. Figure 4.4 shows the configuration at a later time after part of the gas has vented and the tube has expanded to about 1.6 times its initial diameter.
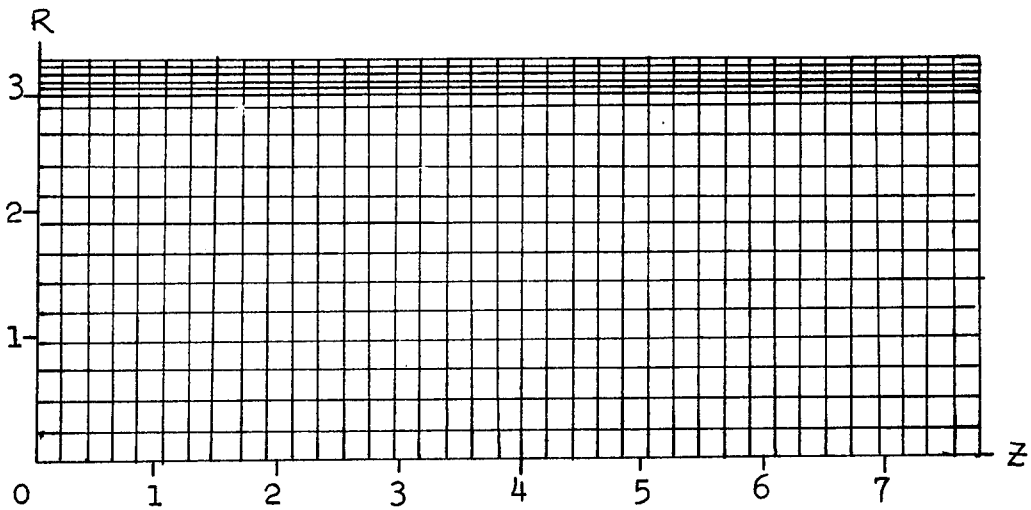
Figure 4.2   The computation grid for the case expansion
problem (t = o).   The outer five zones consist of steel.
The remaining zones contain a solid high explosive.
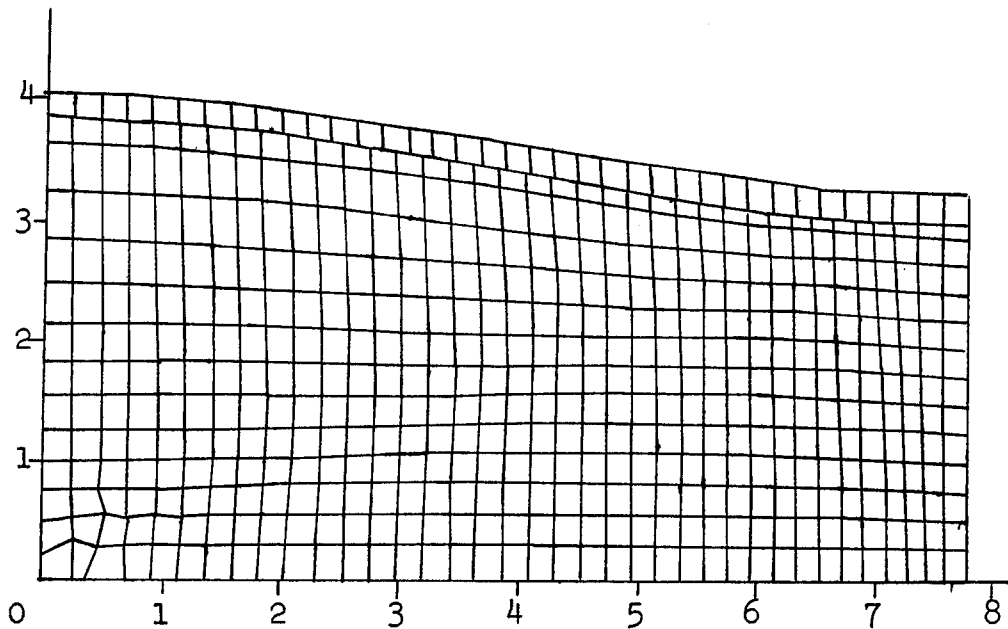
Figure 4.3   The grid points, for the case expansion
problem, at 9.7 microseconds after initiation at the
center.   The detonation front has just reached the
explosive surface at the axis.   The k lines in the
metal are not shown.
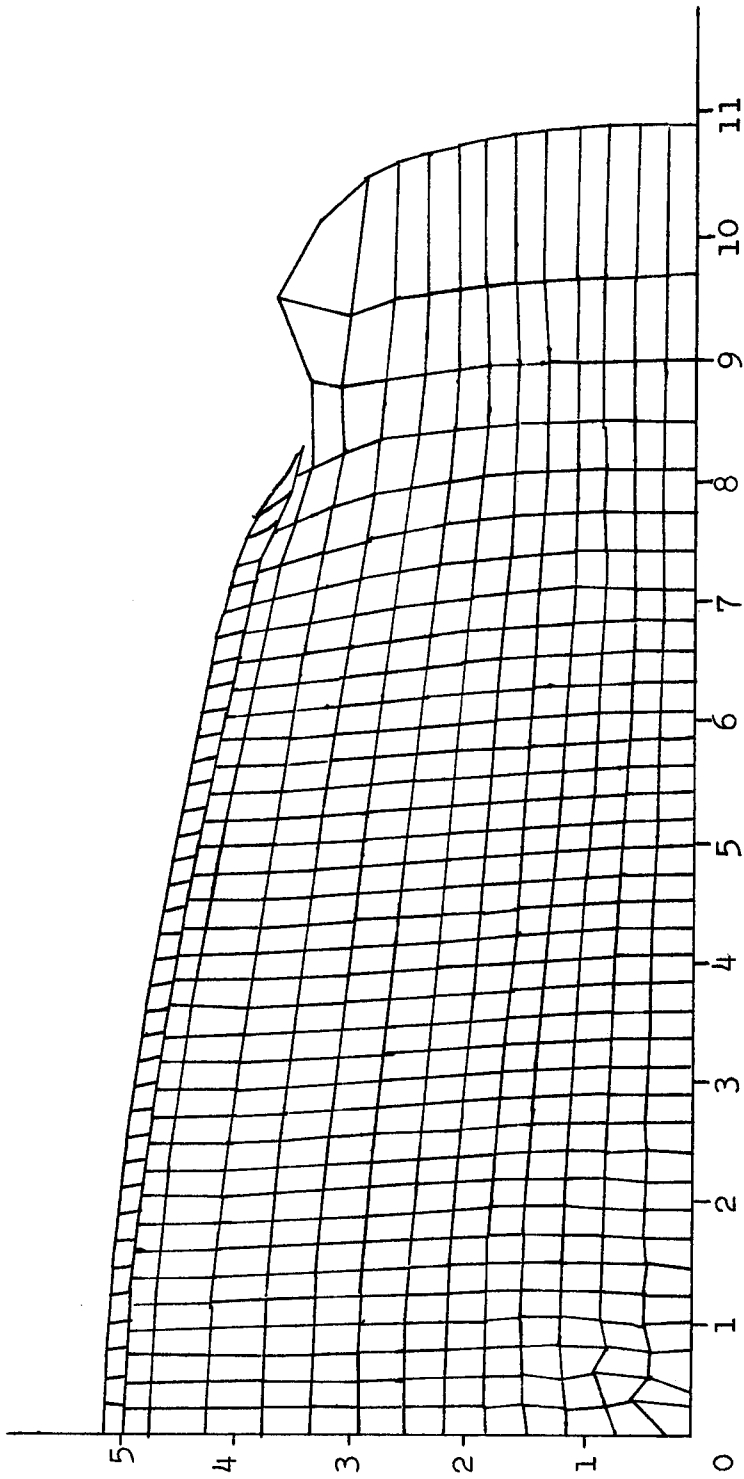
Figure 4.4 The grid points, for the case expansion problem, at 15.0 microseconds after initiation at the center. The k lines in the metal are not shown.

REFERENCES

1. M. H. Rice, R. G. McQueen and J. M. Walsh, "Solid State Physics", Vol. 6, pp. 1-63, Academic Press, Inc., New York, 1958.

2. W. E. Deal, Physics of Fluids $\underline{1}$, 6, 523 (1958).

3. Harwood G. Kolsky, Los Alamos Scientific Laboratory Report LA-1867, Sep. 1954.

4. Martha W. Evans and Francis H. Harlow, Los Alamos Scientific Laboratory Report LA-2139, June 1957.

5. J. von Neumann and R. D. Richtmyer, J. Appl. Phys., $\underline{21}$, 232 (1950).

6. R. D. Richtmyer, "Difference Methods for Initial Value Problems", Interscience Publishers, Inc., New York, 1957.

7. Julius W. Enig, NAVORD Report 6726 (May 1960).

PRESSURE PROFILES IN DETONATING SOLID EXPLOSIVE

G. E. Hauver
Ballistic Research Laboratories
Aberdeen Proving Ground, Maryland

Abstract

The dependence of the electrical conductivity of sulphur upon pressure is used to measure a pressure-time profile for detonating Baratol. The measurements indicate an initial pressure spike and lend further confirmation to the hydrodynamic theory of detonation proposed by von Neumann. Preparation of a sulphur pressure transducer is described, along with the method of calibration and preliminary performance tests.

Introduction

Alder and Christian[1], in 1956, reported a large increase in the electrical conductivity of some ionic and molecular crystals when these materials are subjected to transient pressure in the order of 250 kilobars. They proposed that the materials undergo a transition to the metallic state. Joigneau and Thouvenin[2], in 1958, reported a large increase in the electrical conductivity of crystalline sulphur when it is subjected to high transient pressure, but detected no sudden or discontinuous transition to metallic conduction. The experimental arrangement for their investigation is shown in Figure 1. From their results, it was inferred that a modified system should permit the use of sulphur as the active element of a pressure transducer for measurements well into the kilobar range.

Preparation of a Sulphur Pressure Transducer

Figure 2 shows the modified system that has been used for the investigation to be described. A thin disc of sulphur, 0.0050 inch thick and 9/32 inch in diameter, is insulated in Teflon. Teflon was selected for two reasons. First, it is nearly a perfect impedance match for crystalline sulphur. Second, it is a non-polar plastic and does not generate spurious current signals when subjected to high
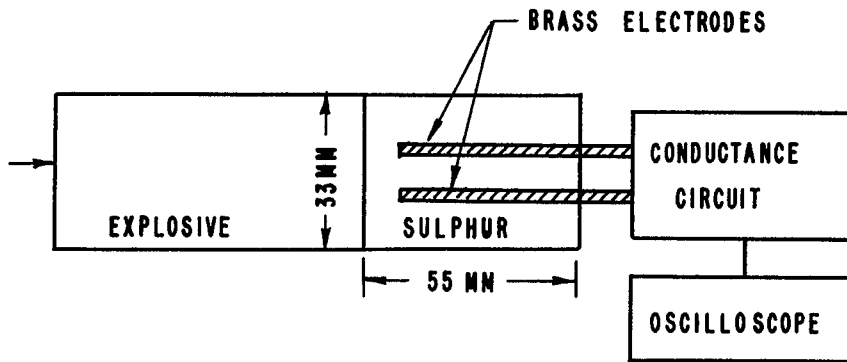
FIGURE I

Conductivity Setup
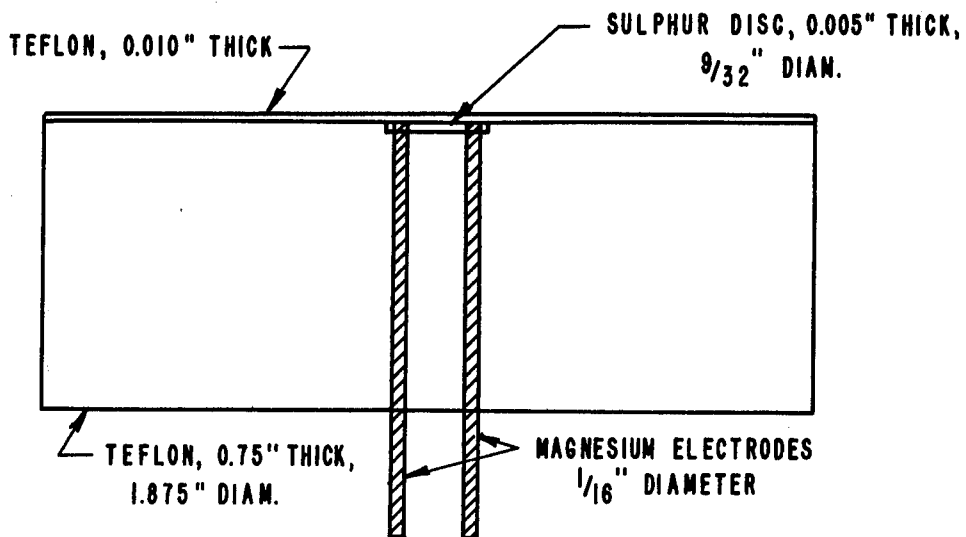
FIGURE 2

Modified Sulphur System

transient pressure[3,4]. Magnesium electrodes are used in a further effort to match impedances. The system is prepared by machining a shallow cavity in the Teflon base. The Teflon is drilled and the electrodes are pressed into place, with care taken not to deform the Teflon. Vacuum melted sulphur is cast into the cavity, and after solidifying, the excess is ground away leaving a thin disc of sulphur to bridge the electrodes. Teflon front insulation, usually 0.010 inch thick is bonded to the surface with an epoxy. The epoxy is now the greatest source of impedance mismatch, but work is in progress to prepare an epoxy with the correct impedance. Care must be taken not to subject the sulphur disc to thermal or mechanical shock, as fine cracks are readily formed. If a crack extends between electrodes, air apparently is introduced, and a long duration signal results. Transverse cracks in the interelectrode area apparently are filled with epoxy when the Teflon front is bonded on, and this tends to reduce or eliminate conduction through the interelectrode sulphur.

With care, the 0.0050-inch sulphur dimension can be held to within 0.0001 inch, and this thickness permits adequate time resolution for most measurements. A 0.010-inch Teflon front permits the sulphur to be close to the point where the measurement is desired, and minimizes attenuation. The Teflon front can be reduced in thickness, but the magnesium electrodes punch through sooner. For measurements to be reported, a punch-through time of about 5 microseconds is found for the 0.010-inch thickness.

Calibration

Figure 3 shows the experimental arrangement used for calibration. A plane detonation wave impacts an aluminum plate that is

maintained at ground potential to remove any charge effects that might be associated with the detonating explosive. The plate thickness controls the pressure to which the sulphur is subjected. A representative conductance-time signal for the sulphur is shown at the left. The minimum sulphur resistance (maximum conductance) is related to the shock front pressure. Figure 4 shows sulphur-resistance vs. pressure. Resistivity values appear along the right ordinate. The upper curve relates the resistance to the pressure in the aluminum determined from the known equation of state by measured values of free surface velocity. The lower curve relates resistance to the estimated pressure to which the sulphur was actually subjected.
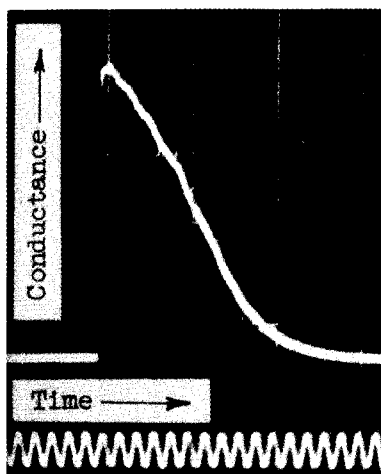
For resistance greater than 5000 ohms, the accuracy of the calibration is doubtful. Two sources apparently contribute to the conductance signal. The sulphur conducts, but there is also a small contribution believed to come from ionized gaseous impurities in the
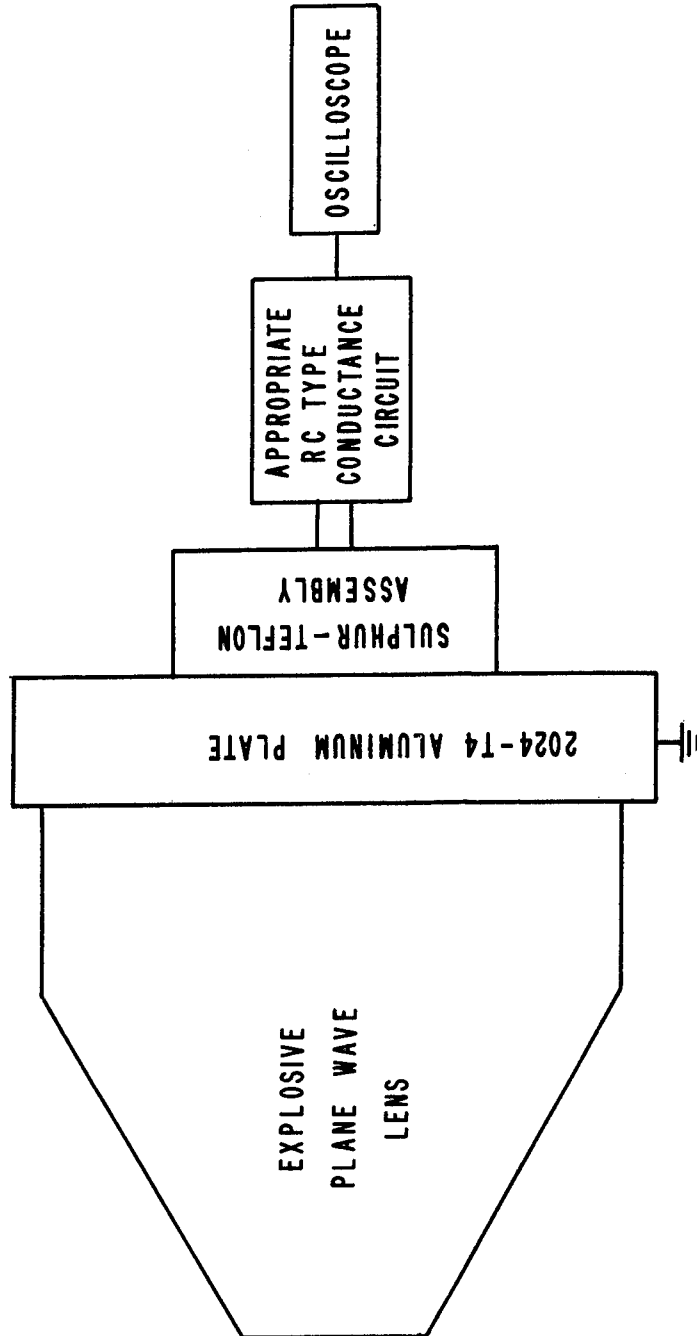
FIGURE 3

Calibration System
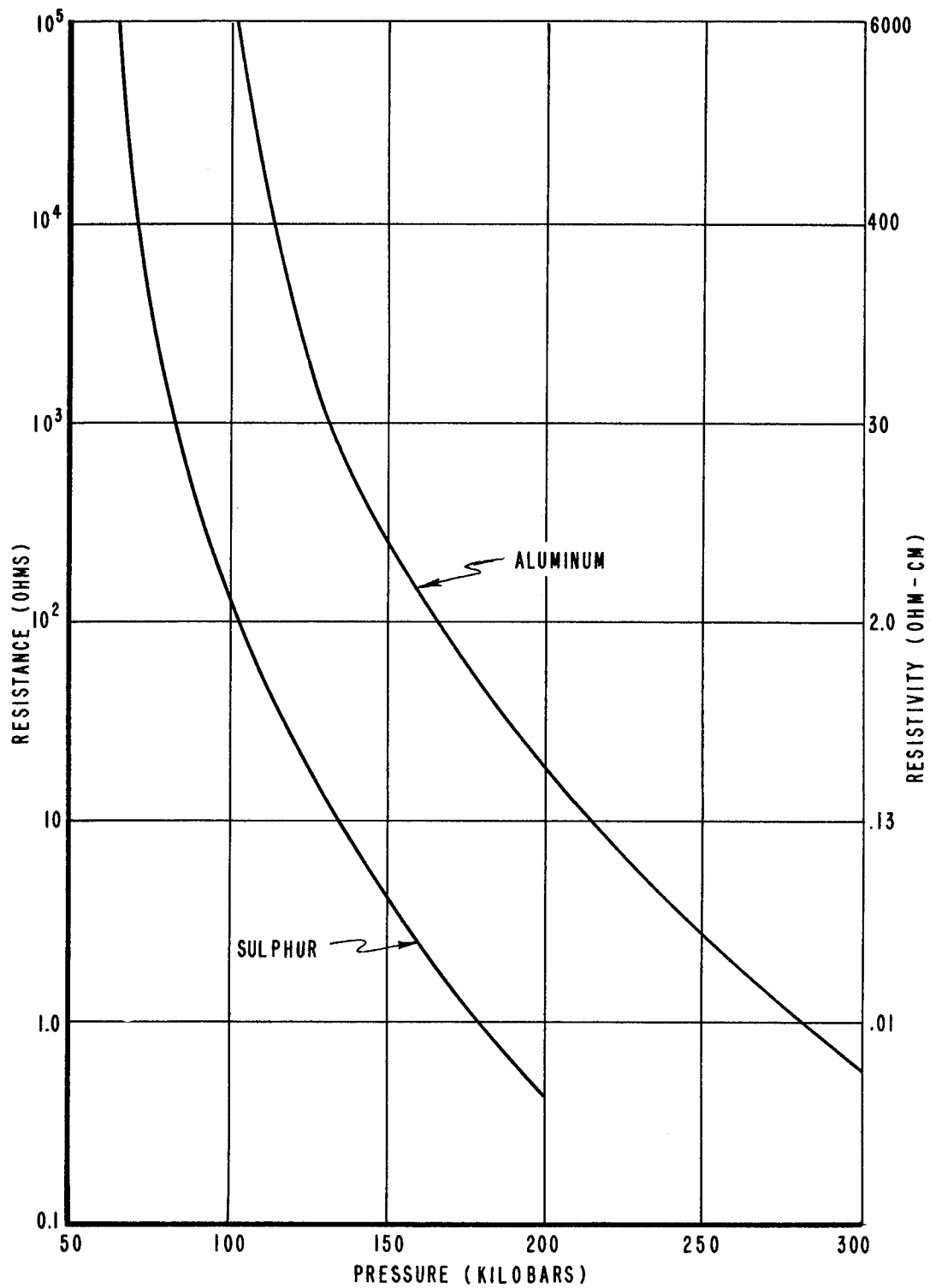
FIGURE 4 – CALIBRATION CURVE

system. When the pressure is above 75 kilobars, conduction by the sulphur dominates, and the contribution by impurities is not significant. Below this pressure, the contribution by ionization becomes more significant and measurements are progressively less significant.

Appropriate RC circuits are used for the measurements. They consist of a known resistor in series with the sulphur element. A constant voltage is maintained across the combination, and potential drop across the resistor is recorded with an oscilloscope. From this measurement, the resistance of the sulphur is determined and related to pressure by the calibration curve.

Plate Impact Tests

To show, in a more or less semi-quantitative way, that the sulphur is indicating true pressure-time profiles, several tests were performed with impacting plates. Figure 5 shows a sketch of the system that was used because data and component parts were immediately available. Teflon-front thickness of 1/16, 1/8 and 3/16 inch was used to allow different degrees of attenuation before measurement of the pressure-time profile by the sulphur. Figure 6 shows the measured pressure-time profiles. Unfortunately, the impacting plate produced pressures near the confidence-borderline region of the calibration curve (about 75 kilobars). Nevertheless, some significant features are evident. As the Teflon thickness increases, it is evident that the rarefaction is reducing the pressure-time profile to a spike. In going from 1/16" to 3/16" of Teflon, the width of the pulse top is reduced from 0.35 to 0.12 microsecond. The width of the pulse top is in the order to be expected, but little can be said about the pulse width at lower pressure. Of the four curves, 1 and 2 show the most evidence of conduction by ionized impurities. It is not known why the pressure in the test with a 1/8-inch thick front was about 7 kilobars higher than in other tests. More informative tests, with impacting plates producing maximum pressures of 150 to 200 kilobars in the sulphur, are planned.

Profile Measurements with Detonating Explosive

A number of tests were performed in which a sulphur trans-ducer was placed against the end of a Baratol cylinder. 67-33 Baratol was selected because the present sulphur configuration does not lend itself to accurate measurement of pressures as high as those encountered with more energetic explosives. The Baratol cylinder was 2 inches in diameter and 3 inches long, with a 2 x 3 inch Pentolite booster. Figure 7 shows the pressure-time curves obtained. The lower curve indicates the pressure-time profile at the interface as recorded by the sulphur. Actually, three tests were used to cover the pressure range. Figure 9 shows the transducer signal for the first portion of the curve. To join the curves from the three tests, it was necessary to make slight displacements in the time direction. However, the maximum displacement necessary was 0.06 microsecond, but this is not considered excessive since zero time is not established with much
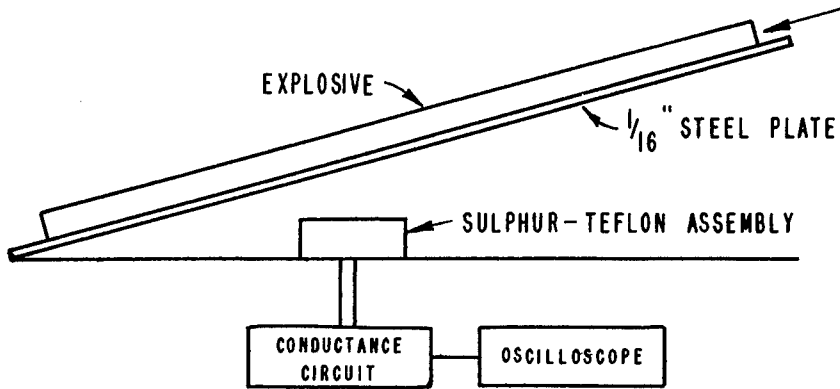
Figure 5.   Plate Impact Test
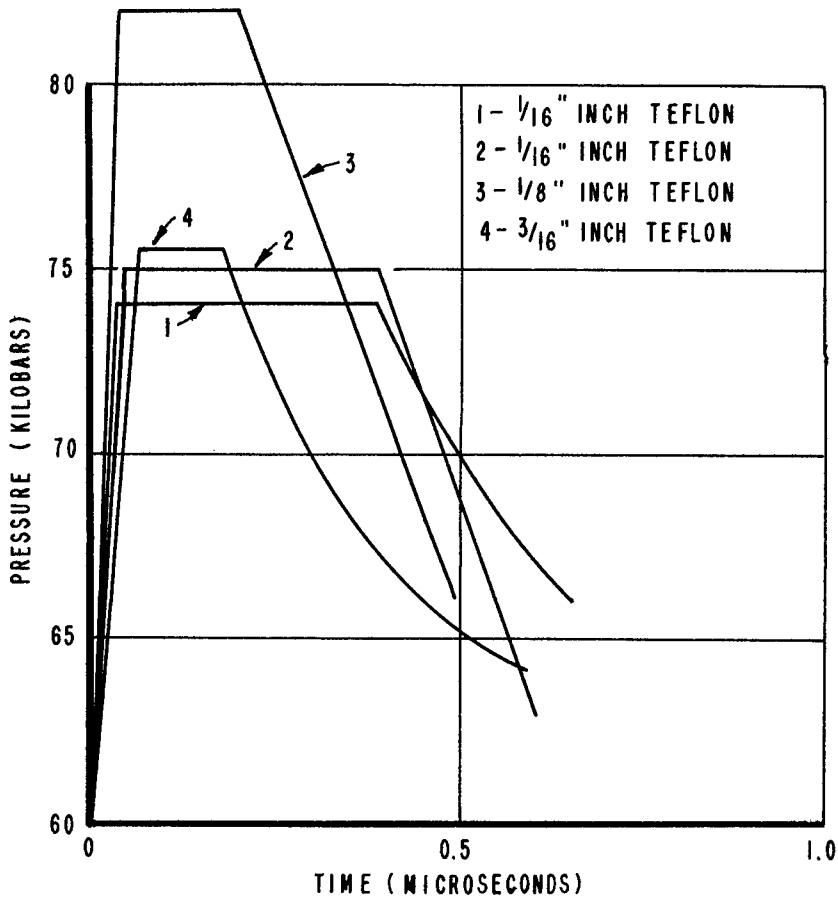
Figure 6.   Plate Impact Pressure Profiles
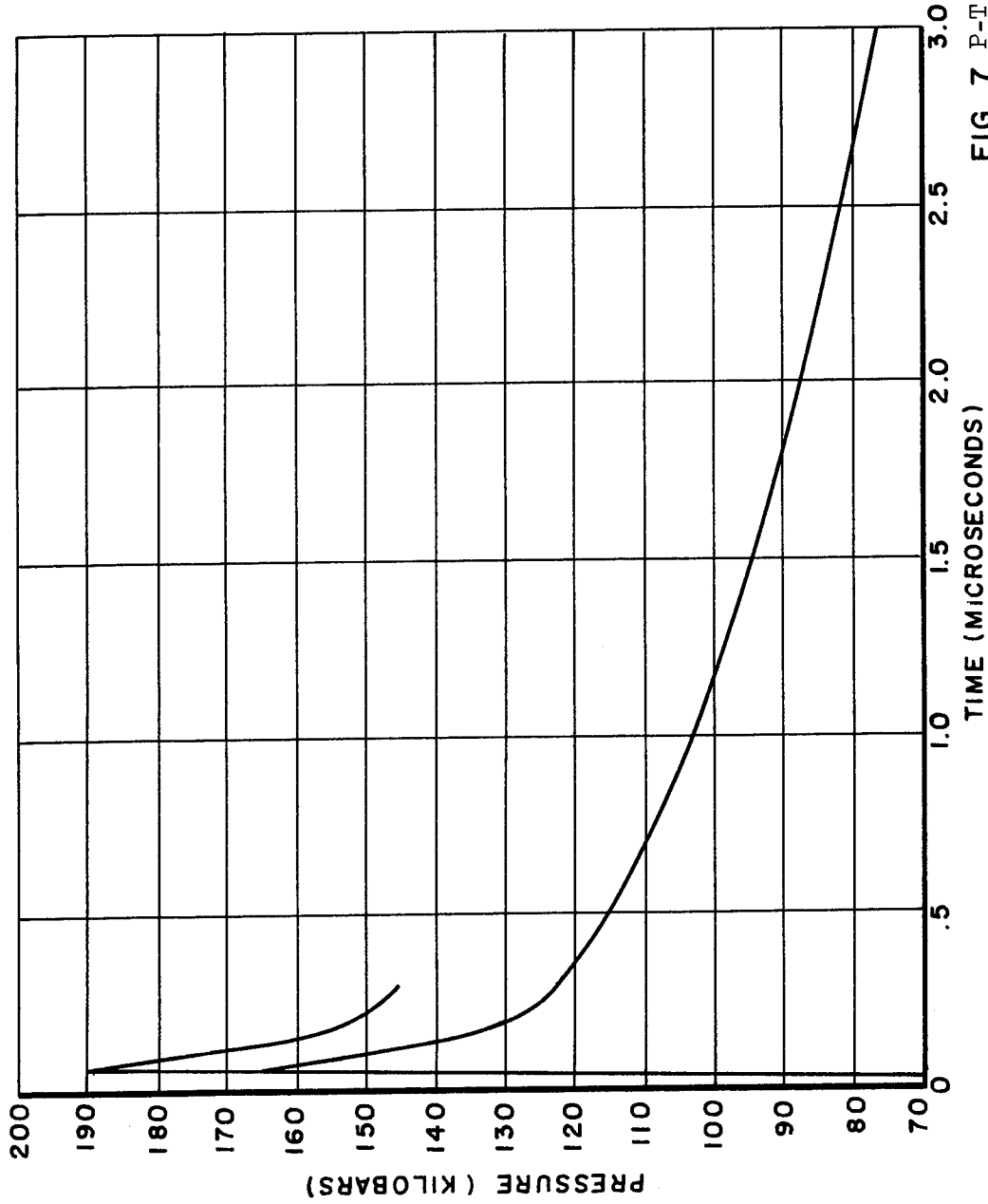
FIG. 7 P-T Profiles

better accuracy.

A pressure profile for detonating Baratol was calculated from the first portion of the interface pressure-time curve, which is the portion interpreted to represent the reaction zone. The interface equation[5]

$$P_x = \frac{P_s\,(\rho_x\,D_x + \rho_s\,D_s)}{2\,\rho_s\,D_s}$$

was used. In this equation, P, ρ and D are pressure, density and shock (detonation) velocity. Subscripts x and s refer to the explosive and sulphur.

The pressure-time curve indicates the von Neumann spike followed by the Taylor wave. The initial pressure of 190 kilobars is not the maximum. The initial pressure is limited by the rise time of the conductance circuit, and attenuation during passage through the thickness of Teflon between the explosive and the sulphur. For measuring the initial portion of the pressure-time curve, 0.005-inch thick Teflon insulation was used. A 5-mil Teflon front has consistently indicated a pressure from 5 to 10 kilobars higher than that measured with a 10-mil front. The curve indicates a C-J pressure of approximately 150 kilobars, although this point is not sharply defined. The accuracy of these pressure values depends upon the accuracy with which the interface pressure was estimated when the sulphur was calibrated. The aluminum pressure as determined by free surface measurements and the equation of state is not in doubt, but at present there is some doubt as to the exact position of the Hugoniots for the materials in the sulphur-Teflon system.

The spike width is judged to be 0.2 microsecond, indicating a reaction zone width of one millimeter. An expanded view of the spike is shown in Figure 8. (Figure 10 shows the actual transducer signal). The lower curve in Figure 8 is the pressure-time profile at the interface as recorded by the sulphur. The upper curve is the profile estimated for detonating Baratol. The profile is believed to suggest a reaction rate determined by grain burning[5]. No sharp change of slope is observed between the spike and the Taylor wave, and it is not presently known if this is a characteristic of the reaction, the explosive dimensions or circuit limitations. For this measurement, 0.010-inch thick Teflon front insulation was used, limiting the measured pressure to about 180 kilobars. Rise time limitations are evident, and for this particular test the rise time is judged to be 0.07 or 0.08 microsecond.

Conclusions

The use of sulphur as a pressure transducer is not in a state of perfection, but the elimination of spurious contributions to the conductance signal, better impedance match throughout the system and modified configurations for use at higher pressures should achieve greater accuracy and usefulness.
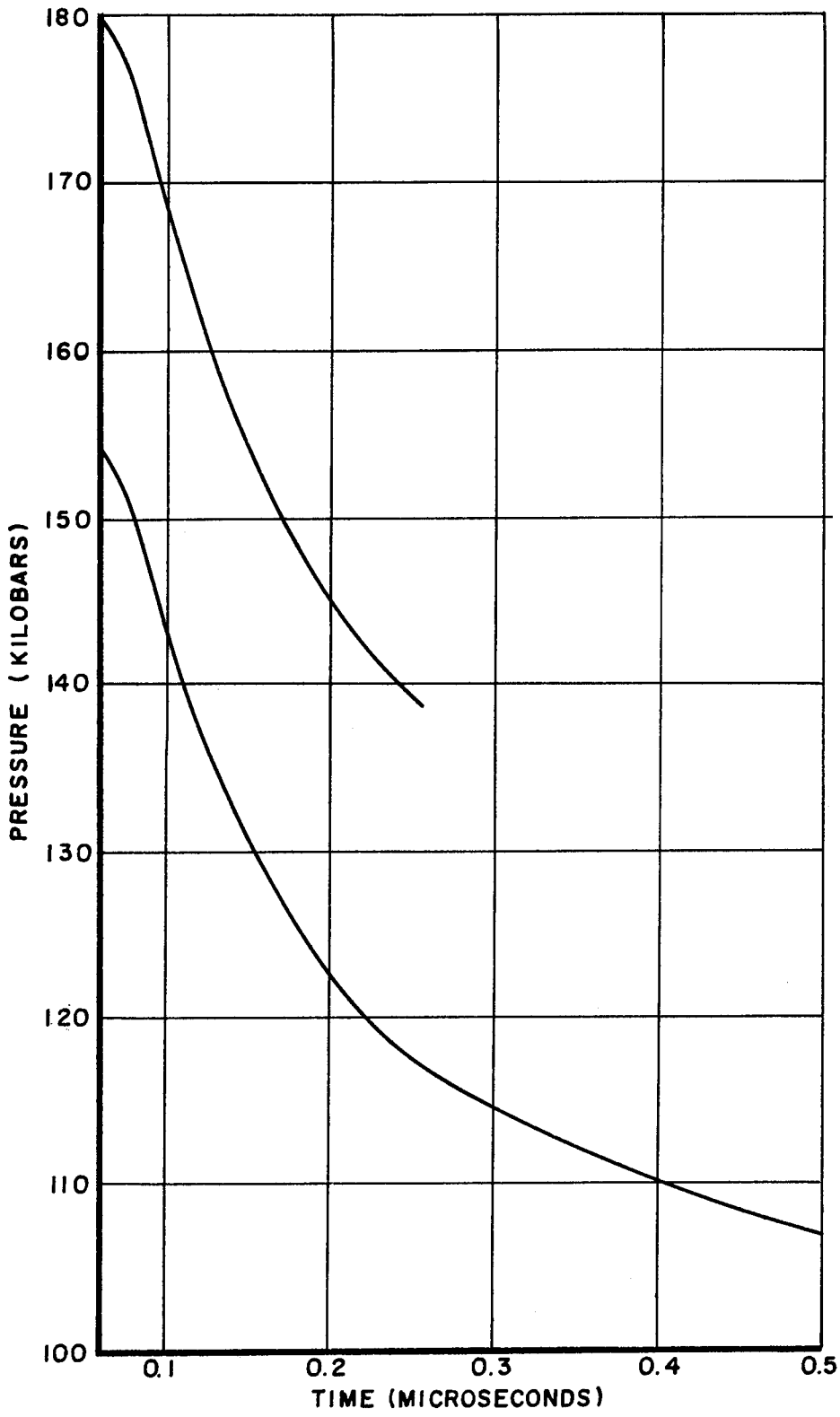
Figure 8.   P-T Profiles
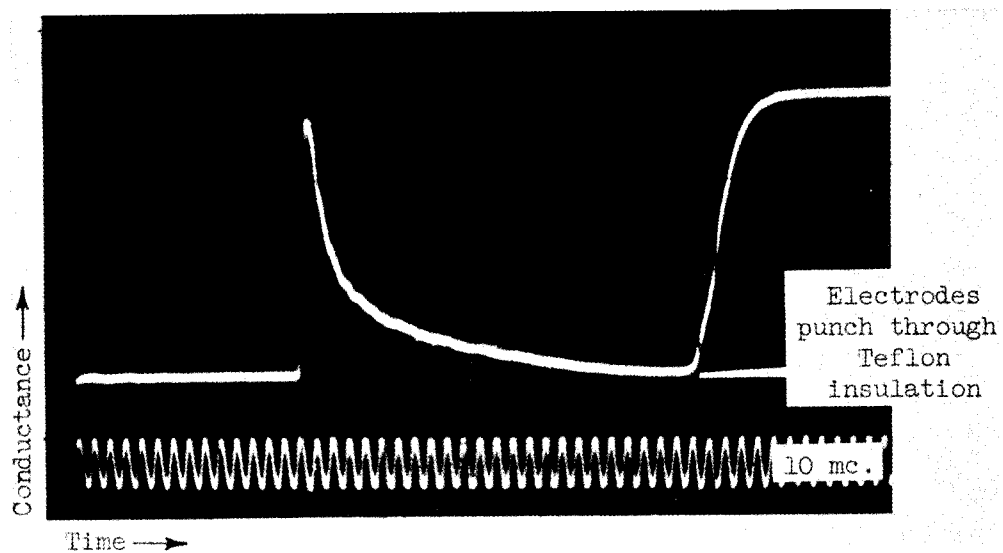
Figure 9
Transducer Signal
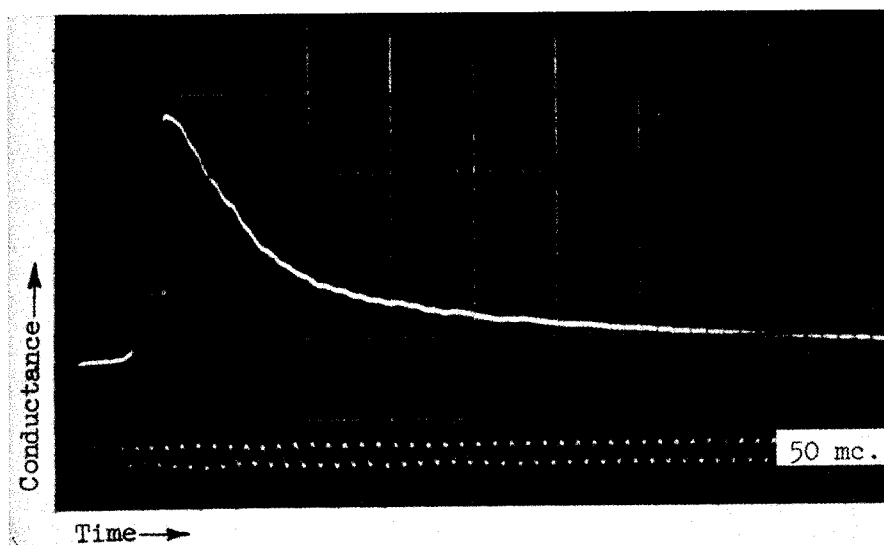
Figure 10
Transducer Signal

Pressure-time measurement with the present sulphur transducer in contact with detonating Baratol, gives clear evidence of an initial pressure spike, and lends additional confirmation to the hydrodynamic theory of detonation proposed by von Neumann and others. The sulphur transducer appears capable of good resolution over that portion of the pressure-time curve corresponding to the reaction zone, and may offer a method for investigation of the reaction process.

Bibliography

1. J Alder and R H. Christian, "Metallic Transition in Ionic and Molecular Crystals", Phys. Rev. 104, 550-1, 15 October 1956.

2. S. Joigneau and J Thouvenin, "Electrical Conductivity of Sulphur Under the Action of a Shock Wave", C. R. Acad. Sc. (Paris) 246, 3422-5, 23 June 1958.

3. R. J. Eichelberger, "Effect of Very Intense Stress Waves in Solids", International Symposium on Stress Wave Propagation in Materials, Interscience Publishers Inc., New York, 1960.

4. G. E. Hauver, BRL Technical Note, Aberdeen Proving Ground, Md. (to be published)

5. R. E. Duff and E Houston, "Measurement of the Chapman-Jouguet Pressure and Reaction Zone Length in a Detonating Explosive", J. Chem. Phys. 23, 1268-73, July 1955.

DECAY OF EXPLOSIVELY-INDUCED SHOCK WAVES
IN SOLIDS AND SPALLINGS OF ALUMINUM

John O. Erkman
Poulter Laboratories, Stanford Research Institute
Menlo Park, California

ABSTRACT

Experiments are reported in which aluminum plates were
caused to spall by explosively-induced oblique shock waves. The
work is principally directed toward developing techniques for per-
forming reproducible experiments with aluminum, and for testing
the scaling laws for spalling. Results indicate that simple
scaling laws apply to the phenomenon of spalling of aluminum plates
if the explosive load exceeds 1/4 inch in thickness and the plate
thickness exceeds 1/2 inch.

Flow in the plates is essentially steady state and two-
dimensional. Such flows, when supersonic, may be calculated by the
method of characteristics for hydrodynamics. These calculations
give the value of the flow variables, including the pressure, every-
where in the plate. Comparison with experimental data indicates
that aluminum spalls at a pressure of about -33 kilobars.

I INTRODUCTION

After a high amplitude shock wave is reflected from a
free surface of a specimen, one or more thin layers of material
may be separated from it. This phenomenon is known as spalling
or scabbing. The shock wave may be induced by the detonation of
a high explosive (HE) charge, usually in contact with the specimen.
Inasmuch as the shape of the pressure pulse, along with the
properties of the material, determines the thickness and number
of spalls, all charges of HE will not cause spalling. Work reported
herein was undertaken to investigate the dynamic tensile strength
of aluminum by observing the spalling of explosively loaded aluminum
plates. The ultimate goal of the present study is to determine dynamic
tensile strength of aluminum as observed in spalling; an important
part of the work has been to develop methods for producing stable
flow and to establish validity limits for geometric scaling, which
is important for theoretical interpretation.

For ease of interpretation the induced shock wave must be
plane, propagating in the direction of a normal to its wave front,

or two dimensional and steady with the medium in a state of plane strain. Spalling resulting from explosively induced one-dimensional shock waves has been studied by Rinehart [1] and Broberg. [2,3] Rinehart analyzed his experiments with the aid of elastic theory and arrived at values for the normal fracture stress for five metals, which are 2 to 5 times greater than static tensile strengths. Broberg considered both elastic and plastic waves and predicted the number of spalls by assuming a value for the rupture stress. His experimental results indicate that the spall thickness for steel did not scale when all linear dimensions of the experiments were simultaneously increased by a given factor.

Further theoretical work based on elasticity and plasticity assumptions has been given by Kumar. [4] At these Laboratories, Dally [5] reported on the spalling of mild steel under explosive attack in one- and two-dimensional geometry. Analysis of Dally's experiments, as well as of Broberg's scaling experiments, are complicated by the multiple waves generated in steel. [6] Analysis of all one-dimensional experiments is difficult as far as scaling is concerned, because the explosive thickness is not well defined. For example, Dally used a plane-wave generator to produce a plane detonation front in the high explosive pad. This added an unknown confinement to the detonation product gases, so that the effect of changing the thickness of the explosive is not clearly discernible. In this report, only the two-dimensional case is considered. Results of several experiments are reported, as well as the calculated pressure-time curves along stream-lines in aluminum.

II EXPERIMENTAL PROGRAM

A. EXPERIMENTAL SETUP

In order to investigate scaling for aluminum spalls, several experiments were performed, in each of which the ratio of the thickness of the aluminum plate to the thickness of the explosive was the same. A ratio of 2:1 was used for most of the work reported herein; the basic experimental arrangement is shown in Figure 1. One surface of the aluminum was lapped so that the explosive made good contact with the metal surface. As an aid in determining the spall thickness, a grid with a 1/2-inch spacing was engraved on the free surface of the metal so that a piece with a known area could be cut from the recovered spall and weighed. Point initiation was used in all shots, the point of initiation being separated from the end of the metal by a distance approximately equal to the width of the specimen, as shown in Figure 1.

Breakup of aluminum spalls was minimized in some experiments by the use of aluminum side and an end bar for momentum traps, as shown in Figure 2. The assembly was loaded with explosive as shown in Figures 3 and 4: Composition B-3 was used over the specimen, and Composition C-3, a plastic explosive, served as the leader and the loading over the end bar and the side bars. The loaded shot was then placed in a bag of thin plastic, floated on water, and fired. The
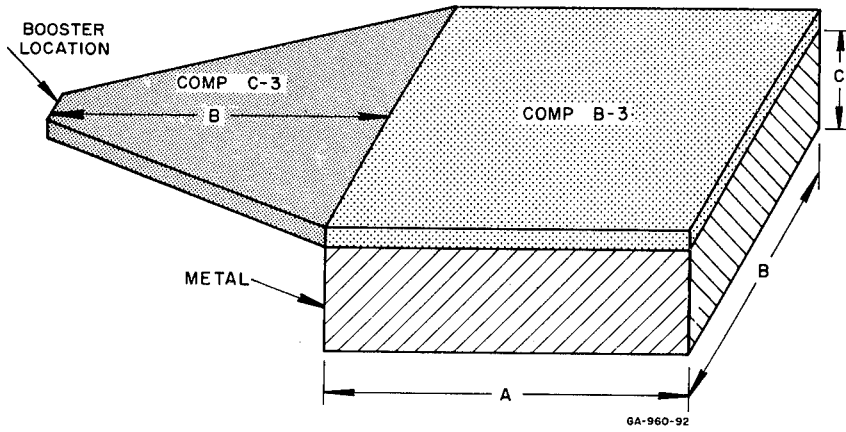
FIG. 1

EXPERIMENTAL ARRANGEMENT
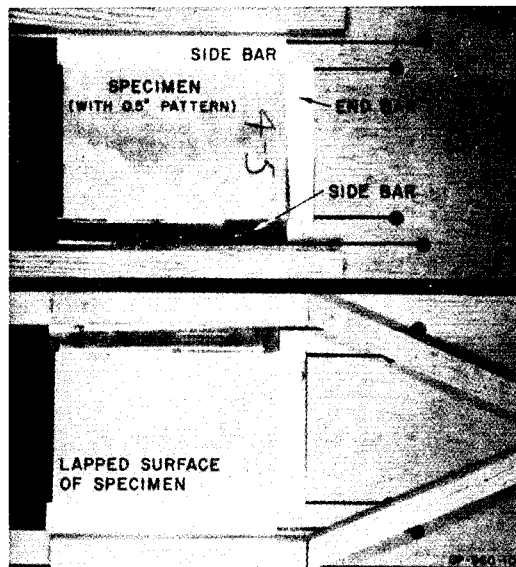
FIG. 2

ALUMINUM SPECIMEN READY FOR LOADING

255
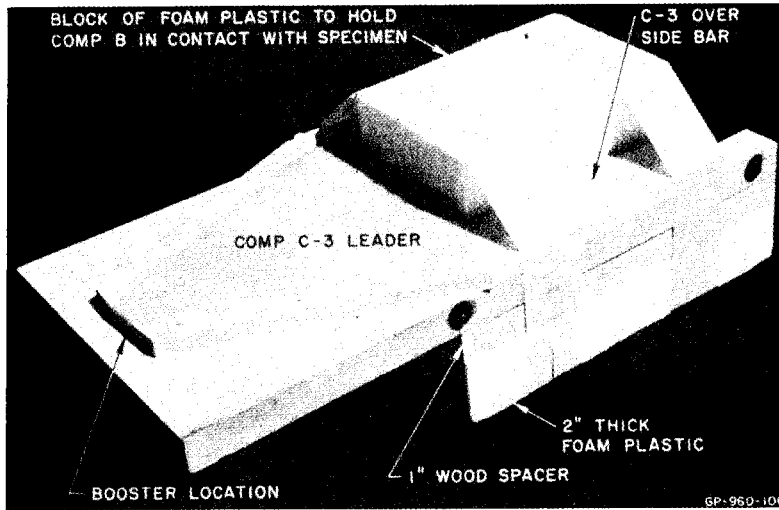
FIG. 3

LOADED SHOT READY FOR BOOSTER AND ELECTRIC DETONATOR
The Composition B-3 slab is held in contact with the aluminum
by the block of foam plastic and tape. The wood spacer separates
the aluminum free surface from the bottom block of foam plastic
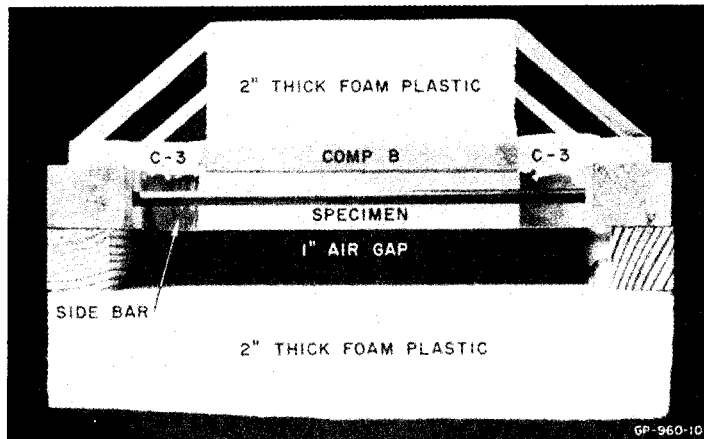
FIG. 4

END VIEW OF LOADED SHOT SHOWING COMPOSITION B-3
OVER SPECIMEN AND C-3 OVER SIDE BARS

spall traversed a 1-inch air gap and 2 inches of low density foam plastic before encountering the water barrier. Excellent recovery was made as shown in Figures 5 and 6.

B. RESULTS AND REPRODUCIBILITY OF EXPERIMENTS USING ALUMINUM

Results of twelve experiments for which the ratio of plate to explosive thickness is 2:1 and 4:1 are listed in Table I.

TABLE I

EXPERIMENTAL RESULTS FOR ALUMINUM SPALLS

(Columns Labeled A, B, and C Refer to Fig. 1)

SHOT NO.	A (In.)	B (In.)	C (In.)	EXPLOSIVE (In. thick)	SPALL (In. thick)	SPALL TO EXPLOSIVE THICKNESS RATIO	PLATE TO EXPLOSIVE THICKNESS RATIO
4547[a]	3	4	0.253	0.125	0.087	0.696	2.02
4548[a]	3	4	0.502	0.250	0.155	0.620	2.01
4549[a]	4	6	1.003	0.500	0.268	0.536	2.01
4550[a]	4	6	1.502	0.750	0.480	0.640	2.00
6383[a]	7	12	1.980	0.990	0.531	0.536	2.00
4442[b]	4	6	0.326	0.082	0.081	0.99	3.98
4443[b]	4	6	0.489	0.125	0.116	0.93	3.91
4543[a]	4	6	1.003	0.250	0.180	0.720	4.01
4054[c]	4	6	0.997	0.250	0.173	0.693	3.99
4544[a]	4	6	1.503	0.375	0.267	0.712	4.01
4444[b]	4	6	1.994	0.500	0.382	0.765	3.99
4546[b]	6	8	3.003	0.750	0.463	0.617	4.00

[a] 2024 T4 aluminum

[b] 2017 T4 aluminum

[c] 1100F aluminum

As side and end bars were not used in most of these experiments, some of the spalls were badly broken, so that thickness was not reliably determined for the thicker spalls. In most cases, the spall thickness was determined by cutting out a portion of the spall, using the engraved grid lines as a guide, and weighing the sample. Reliable measurements require a piece of the spall with no taper and with an area of at least 2 square inches.

Eight additional experiments are reported in Table II. These were designed to minimize side effects by using the side bars shown in Figures 2,3, and 4. Two sets of experiments were performed to test the reproducibility of spall production by 0.5-inch and 0.75-inch explosive. In each set of four experiments, the aluminum was
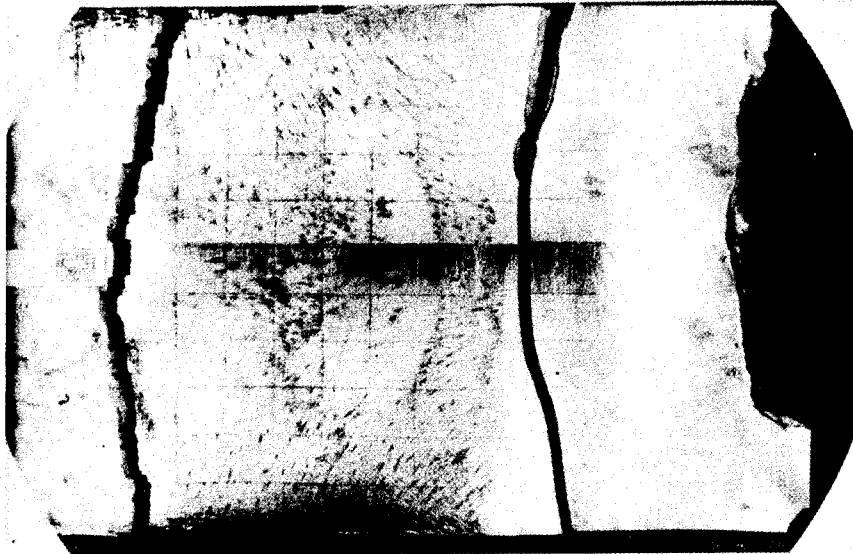
FIG. 5

RECOVERED SPALL SHOWING ORIGINAL FREE SURFACE SIDE
Detonation traveled from right to left

FIG. 6

FRACTURE SURFACE OF ALUMINUM SPALL

TABLE II

REPRODUCIBILITY OF ALUMINUM SPALLS FROM 5.5 x 8 INCH PLATES
WITH SIDE AND END BARS

SHOT NO.	PLATE THICKNESS (inches)	EXPLOSIVE THICKNESS (inches)	SPALL THICKNESS (inches)	SPALL TO EXPLOSIVE THICKNESS RATIO
4640	1.0055	0.5015	0.270	0.54
4641	1.0074	0.5015	0.277	0.55
4642	1.0065	0.5015	0.283	0.56
4643	1.0062	0.5015	0.278	0.55
4729	1.5042	0.752	0.423	0.56
4730	1.5060	0.752	0.424	0.56
4731	1.5038	0.752	0.422	0.56
4732	1.5064	0.752	0.430	0.57

twice as thick as the explosive. Spalls from the 1.5-inch aluminum show an end effect, as indicated by the taper in the cross section of the thick spall in Figure 7. This effect required that the spall thickness be measured near the end of the spall, farthest removed from the detonator, in order to approximate the steady state spall thickness. With this precaution, reproducibility was good for both sets of experiments.

Results for aluminum are presented graphically in Figure 8. For a ratio of 2:1, the spall thickness is observed to be relatively independent of the dimensions of the experiment, particularly for explosive thickness greater than 1/4 inch. This indicates that absolute lengths, such as the reaction zone length in the explosive, or absolute times, such as the delay time for fracturing, are relatively unimportant. If these observations can be substantiated by further experimental work, the theoretical treatment of the spalling problem will be simplified.

Those experiments for which the aluminum plate was four times as thick as the explosive did not yield good results because they were performed before techniques were perfected for recovering aluminum spalls. Those data must be confirmed with further experimental work.

III HYDRODYNAMICS AND SPALLING

A. INCIDENT SHOCK WAVE

Intensity and location of an explosively-induced oblique shock and the flow behind the shock may be calculated by applying hydrodynamic theory. Both the explosive product gas and the specimen material are regarded as nonviscous, non-heat-conducting fluids, with known equations of state. Calculations are further restricted to those cases for which the flow is supersonic in both the specimen and in the gas, so that the method of characteristics applies.
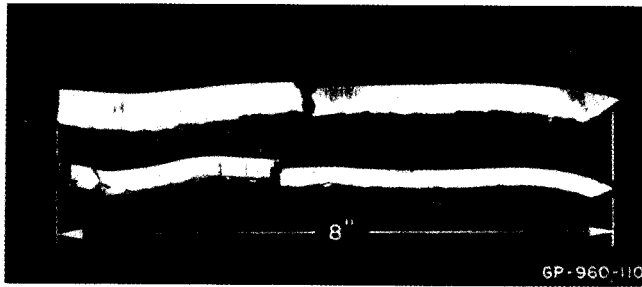
FIG. 7

END TO END CROSS SECTION OF ALUMINUM SPALLS
Thin spall from 1.0 inch-plate, thick spall from
1.5 inch-plate.   Detonation propagated from left
to right leaving noticeable taper in the thick spall
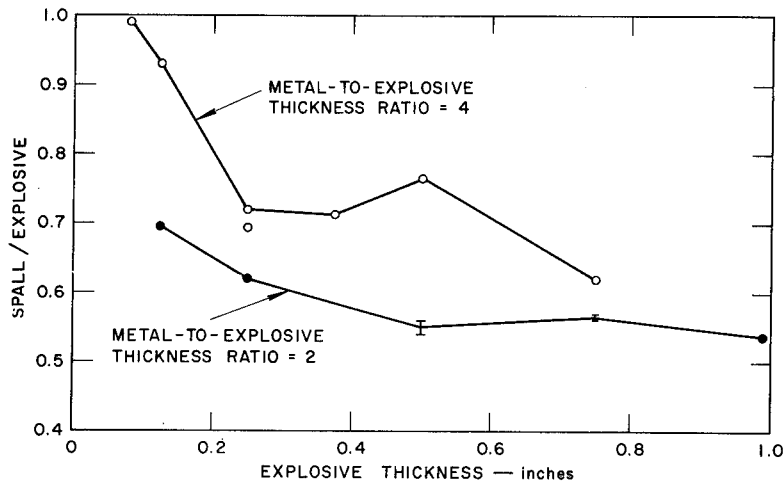
FIG. 8

RESULTS OF SCALING INVESTIGATIONS FOR ALUMINUM SPALLS

Circulation in both media has been neglected. A Chapman-Jouguet detonation is assumed, and the front is assumed to lie in a plane.

Figure 9 shows in cross section a slab of explosive of unit thickness in contact with a semi-infinite slab of metal. Flow in the detonation product gas has been described previously, as well as the flow in a semi-infinite specimen. ([7],[8],[9]) In the specimen, the shock ABCD . . . is overtaken by elements of a simple wave originating at the free surface of the explosive and which are refracted into the metal at points MNO . . . . These elements are characteristics of Family II,* and a point such as C is located by the intersection of a segment of an oblique shock BC with the characteristic NC. Pressure and all fluid properties are assumed to be constant in a polygon or field such as MBCN in Figure 9.
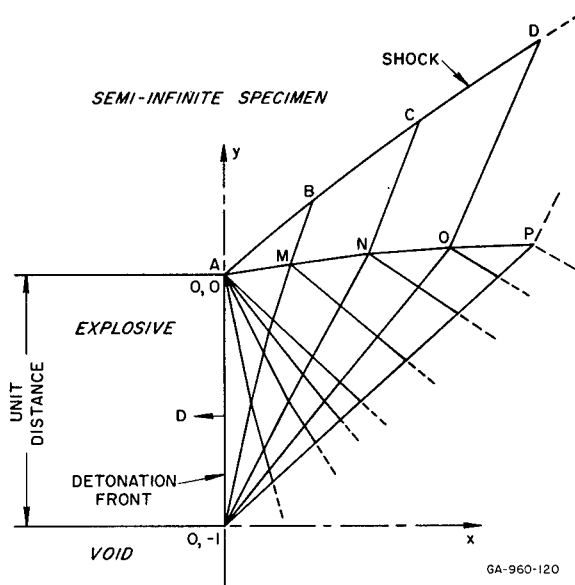
FIG. 9

PHYSICAL PLANE FOR A SLAB OF EXPLOSIVE OF
UNIT THICKNESS AGAINST A SEMI-INFINITE
SPECIMEN

For aluminum, pressure P in megabars and density ρ in g/c.c. are related by

$$P = 0.189 \left[\left(\frac{\rho}{\rho_0} \right)^{4.27} - 1 \right] \tag{1}$$

---

*

The notation of References 7, 8, and 9 is used in this section.

where ρ_0 is the normal density, 2.785 g/c.c. Constants in Equation (1) where obtained by fitting the data of Walsh et al. [10] For the gas, the polytropic equation is used,

$$P = 0.0275\rho^{2.77} . \qquad (2)$$

Constants in this equation were obtained by fitting the Chapman – Jouguet point for Composition B-3. This explosive contains 60% RDX, 40% TNT, and has a detonation velocity and density of 0.80 cm/μsec and 1.73 g/c.c. respectively. Such an equation of state is useful over a wide range of pressure, [11] and gives good results when employed in calculating the pressure-time profile of an explosively-induced oblique shock in water.[12]

B. REFLECTION OF THE SHOCK AT THE FREE SURFACE

Introduction of the free surface at y = t complicates the problem as shown in Figure 10, which shows the flow pattern near the point at which the shock contacts the free surface of the specimen. The shock is reflected at the point T as a simple, centered wave, elements of which are characteristics of Family I. Characteristics of Family II, refracted through the interface at point 0 and beyond, interact with the centered simple wave, and are finally reflected at the free surface as characteristics of Family I. Flow near the specimen-gas interface is unaffected by the presence of the free surface until the characteristic TUVW . . . comes into contact with the interface. Since the spall is thin, the region of interest lies close to the point T and the interaction of

GB-960-121
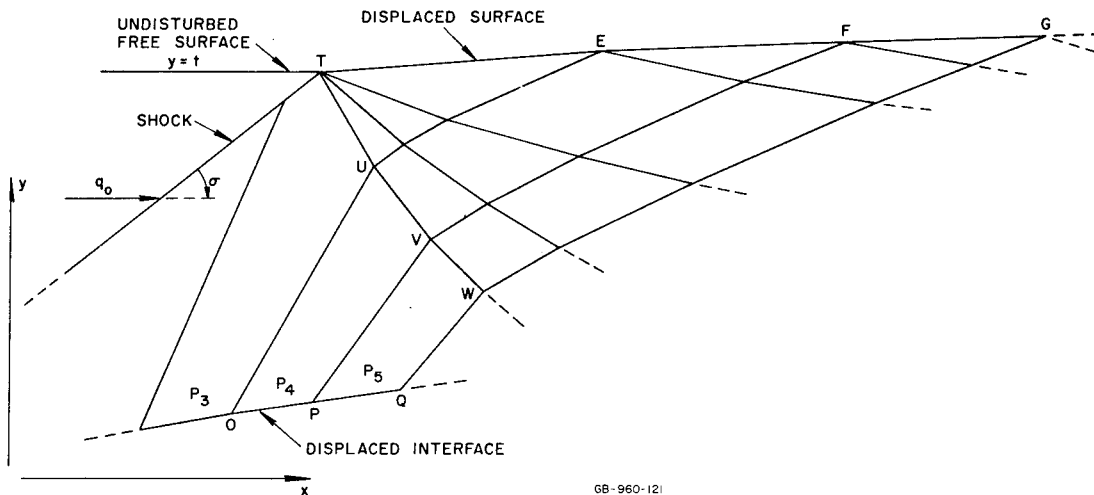
FIG. 10

CHARACTERISTIC NET NEAR FREE SURFACE OF SPECIMEN
Origin of Coordinates same as in Figure 8

characteristic TUVW . . . with the interface need not be considered. Hence, the previous results may be used and all that remains is to determine the interactions of the waves to the right of the point T in Figure 10.

The shock is approximated as a series of straight line segments, so point T may be located by intersecting two straight lines. This point, and the known points OPQ . . . are the boundaries imposed on the step-wise solution of the problem in the physical plane. Pressure is zero (or negligible) along the free surface TEF . . ., so that fields having the free surface as a boundary are represented in the hodograph plane by states on the zero pressure circle; for the equation of state used here, Equation (1), the zero pressure circle lies inside the zero density circle. Metals are capable of supporting relatively large "negative pressures" for which the density ρ is less than the normal density ρ_0; in order to work wi `ı states in the hodograph plane between the zero pressure circle and the zero density circle, it is necessary to assume that Equation (1) is valid for negative pressures. With this assumption, the flow in the metal specimen is obtained by the method used in References 7, 8, and 9. Sound speed for any point in the specimen is obtained from the Hugoniot equation of state just as in the case of a fluid. This is probably the most drastic assumption made in the solution of the problem.

C. RESULTS

Results of the calculations are partially represented by Figure 11, where many of the fields in the flow pattern are labeled with a number giving the pressure in kilobars for that field. The calculations are done with a great deal more detail than are shown in the figure. Three streamlines are drawn in Figure 11, for which the y-coordinates are 2.35, 2.45, and 2.55 ahead of the shock. Pressure as a function of x is given for these streamlines in Figure 12, as well as for the streamline for which y is 1.0 ahead of the shock, i.e., the interface. The abscissa, x in Figures 11 and 12 may be converted to time τ by the relation

$$\tau = xd/D$$

where d is the explosive thickness in cm, and D is the detonation velocity in cm/μsec. The time scale used in Figure 12 is for d = 1 cm and D = 0.8 cm/μsec. For the three streamlines, the time from maximum pressure to a pressure of less than −20 kilobars is about 1.5 μsec. Pressure decreases slightly thereafter to the point where the solution was terminated. Along the streamlines, the pressure eventually increases because of the finite pulse duration and its eventual reflection from the interface as a compression wave. The brief duration of the positive pressure phase on the interior stream-lines compared to that along the interface (y= 1.0) is characteristic of the interaction between incident shock and reflected rarefaction.

The dynamic tensile strength of the spalled specimen is estimated by comparing the measured spall thickness with the pressure profile along a streamline corresponding to that thickness. The mean
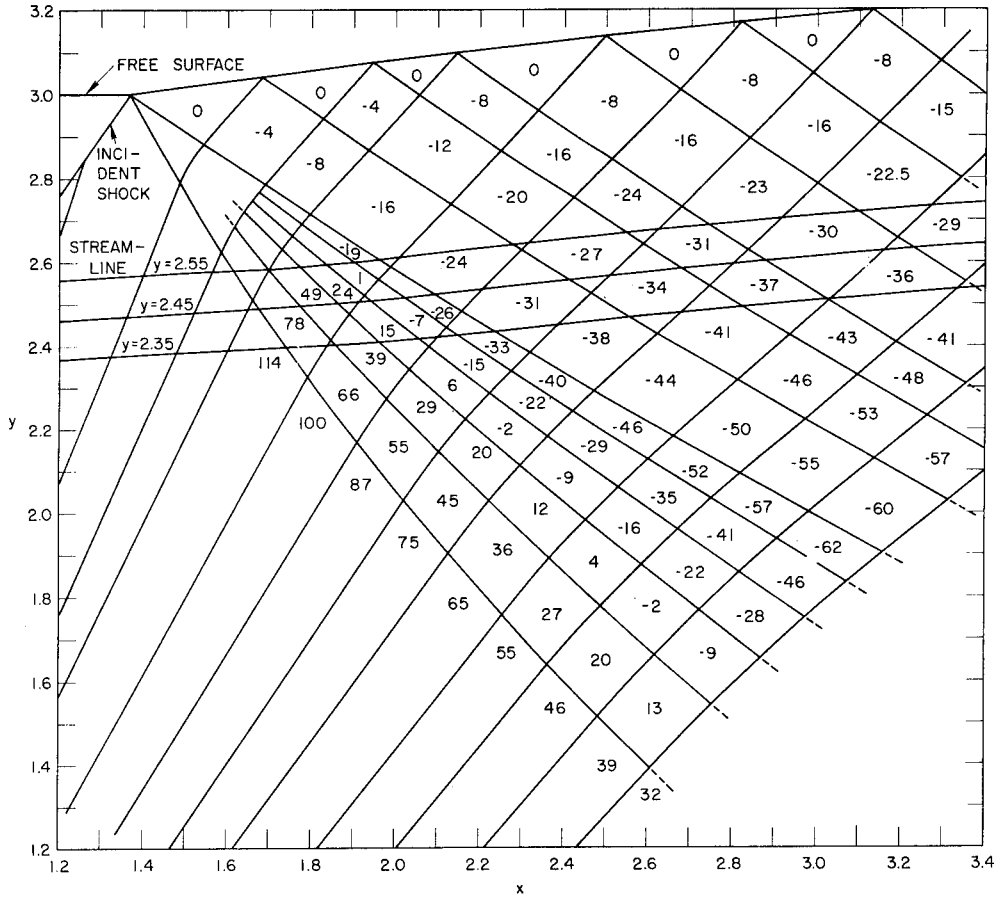
FIG. 11

HYDRODYNAMIC SOLUTION FOR A SHOCK IN ALUMINUM REFLECTED AT A FREE SURFACE
The number in each polygon gives the local pressure in kilobars.
Coordinates are the same as in Figure 8.
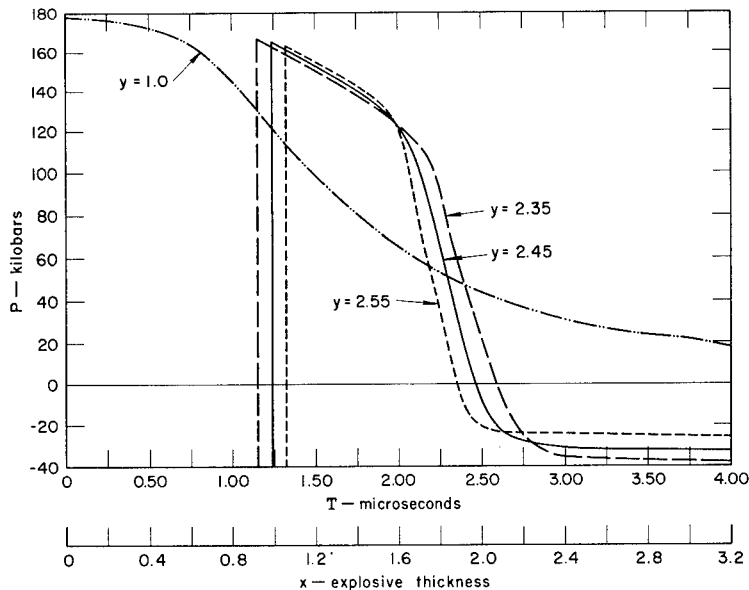
FIG. 12

PULSE SHAPES FOR EXPLOSIVELY INDUCED SHOCKS IN ALUMINUM

spall thickness from Figure 8 is 0.55 times the explosive thickness
for explosive thickness of 1/2 inch or greater and for a metal
to explosive thickness ratio of two. This corresponds to the stream-
line labelled y = 2.45 in Figure 12, along which pressure reaches
the minimum value of -33 kilobars.The stress required for spalling
is then not less than -33 kilobars. Values greater than this are
reached earlier on streamlines corresponding to thinner spalls, as
indicated by the profile labelled 2.55 in Figure 12. On the basis
of the assumptions made in calculating the pressure field of Figure 11,
it must be concluded that the fracture stress for aluminum in
triaxial tension is 33 kilobars at strain rates less than approximately
4×10^4 sec $^{-1}$ This strain rate is estimated from the slope of the
2.45 curve in Figure 12 where it intersects the 2.35 curve and from
Equation (1). Failure of scaling for smaller explosive thickness
may reflect the effects of a time delay to fracture or finite
length of the explosive reaction zone, or both.

IV CONCLUSIONS

Experimental results reported here indicate that spalling
of aluminum plates in two-dimensional steady flow scales geometrically
for explosive thickness equal to or greater than 1/2 inch and for a
metal to explosive thickness ratio of two. Comparison of spall
thickness with hydrodynamic calculations yields a unique value of
33 kilobars for fracture stress in triaxial tension. This value
appears to be independent of small variations in aluminum com-
position; it is three times the value reported by Rinehart ([1]).

265

Results with a metal to explosive ratio of four are not definitive.

REFERENCES

1. Rinehart, J. S. "Some Quantitative Data Bearing on the Scabbing of Metals under Explosive Attack," Journ. Appl. Phys., 22, 5, 555-560 (1950)

2. Broberg, K. B., "Studies on Scabbing of Solids under Explosive Attack," J. Appl. Mech., Paper No. 54-A95 (1954)

3. Broberg, K. B., Shock Waves in Elastic and Elastic-Plastic Media, Kungl. Fortifikations-forvaltningen Befastningsbyran Forskings-Och Forsokssektionen, Rapport nr 109:12, Stockholm, 1956

4. Kumar, S., "Scabbing and Pulse Propagation in Materials," Penn. State Univ. ITR-14, Aug. 1, 1958

5. Dally, E. B., "Spalling Experiments in Mild Steel," Poulter Labs Int. Rpt. 037-56 (1956)

6. D. Bancroft, E. L. Peterson, S. Minshall, "Polymorphism of Iron at High Pressures," J. Appl. Phys. 27, 291 (1956)

7. Erkman, J. O., Explosively Induced Oblique Shocks, Phys. of Fluids, 1, No. 6, Nov.-Dec. 1958

8. Erkman, J. O., Explosively Induced Oblique Shocks, Technical Report No. 14, Contract DA-104-200-509-ORD-294, Ballistics Research Laboratories.

9. Erkman, J. O., Explosively Induced Oblique Shocks, Technical Report No. 17, Contract DA-04-200-509-ORD-294, BRL.

10. Walsh, John M., Melvin H. Rice, Robert G. McQueen, and Frederick L. Yarger, Shock Wave Compressions of Twenty-Seven Metals. Equations of State of Metals. Physical Review, Vol. 108, No. 2, Oct. 15, 1957

11. Deal, W. E., Measurement of the Reflected Shock Hugoniot and Isentrope for Explosive Reaction Products, the Physics of Fluids, Vol. 1, No. 6, Nov.-Dec., 1958

12. Erkman, J. O., Pressure Profile for an Explosively Induced Oblique Shock in Water. Poulter Laboratories Internal Report 007-60, 1960.

EFFECTS OF BOUNDARY RAREFACTIONS ON IMPULSE
DELIVERED BY EXPLOSIVE CHARGE

Boyd C. Taylor
Ballistic Research Laboratories
Aberdeen Proving Ground, Maryland

Introduction

In order to calculate the velocity imparted to elemental areas of metal liners in contact with explosive charges of arbitrary shape, it is necessary to make drastic simplifications in the theoretical description of the process. If this is not done, then long runs on large size computing machines are required to handle problems that can be represented in two-dimensional form if no shear occurs between the explosive products and the liner. Problems more complicated than this require enlargement of existing computers. Thus there is a need for a model of the detonation process that is simple enough to permit accurate calculations to be made on three-dimensional charges by medium size computing machines. Construction of such a model requires mathematical investigation of the possible simplifying assumptions that can be made in the theory and accurate experimental data by which these simplications or models can be tested.

This is a report of the initial results of a program for acquiring experimental data of the velocity imparted to metal elements in several simple configurations. These data are then compared with predictions calculated by rigorous and approximate methods. Experimental data are presented for the velocity imparted to steel elements by three charge configurations: (a) from the ends of radially confined cylindrical Composition B charges of 1.625 inch diameter (D), from 1/2D to 2 1/2D long, with steel elements or liner from 1/64 inch to 1/2 inch thick; (b) from the ends of unconfined cylindrical Composition B charges as in (a), but with steel elements from 1/64 inch to 1/8 inch thick; (c) from the ends of unconfined rectangular Composition B charges with cross-section dimension ratios of 1, 2, and 3.

The experimental results are compared with predictions from the one-dimensional theory developed by Rostoker, and with predictions from the "release wave" approximation developed by Eichelberger for

three-dimensional charges. In the case of confined cylindrical charges, Rostoker's one-dimensional theory is in good agreement with the experimental results for those elements close to the axis for those charges where the gas flow presumably is nearly one-dimensional. This occurs for charges of 2D or shorter length having steel liners of 1/16 inch or less thickness. The simplifications made in developing original details of release wave approximation appear to be too drastic since velocity calculations made by this method show very limited agreement with the experimental data. However, the release wave concept still appears to be a valid base on which to construct a simple model.

Experimental

In using the results of experiment to determine the valid simplifications and approximations that can be made to render the time dependent three-dimensional equations that describe the interaction of the metal-explosive system susceptable to calculation by computing machines like the EDVAC or ORDVAC, the instantaneous pressure variable would be the preferable one to measure. However, no such pressure transducer was available when this program was started. Although some recent developments appear promising[1], the experimental measurements, out of necessity, were restricted to measuring the asymptotic velocity attained by identifiable elements of the metal liner. Although it is precisely this velocity which we desire to compute theoretically, experimental knowledge of the velocity does not provide much insight as to how the theoretical equations can be simplified so that calculation is economically feasible.

Flash radiographs of the spacial positions of the liner elements in flight and electronic measurement of the time of flight give the experimental average velocity of each element. This velocity is then corrected for air drag to yield the initial asymptotic velocity for each element. Although acceleration time is neglected in this computation a correction for it can also be included when the acceleration curve is known.

Since the object in most of the experiments is to determine the effects of charge boundaries on the impulse delivered to elements of the metal liner, it is necessary to pre-cut the metal liner into the desired size elements to prevent the strength of the material from causing interaction among the elements. It is important to cut the elements small enough so that the impulse gradient does not break them up further, since it is difficult to determine the total impulse of such an element if it breaks into several pieces of unknown mass, each traveling at a different velocity. However, in those cases where an element breaks up into several fragments, all traveling at the same velocity, the impulse can be measured. This is sometimes the case with elements shaped in the form of a ring such as would be used on the end of a cylindrical charge.

Confined Cylindrical Charges: For this series of tests 1.625 inch diameter charges of Composition B as shown in Figure 1

were used. Lengths varied from 1/2D to 2 1/2D, and the steel liner
thickness varied from 1/64 inch to 1/2 inch. The confinement was
mild steel of 1/4 inch wall thickness. Since the charges have circular
symmetry, the liner was cut into a series of nested rings of diameter
5/32 inch, 15/32 inch, 25/32 inch, 35/32 inch, 45/32 inch, and 1.625
inch. The rings were further cut into segments for some of the
charges. The velocity of each ring has been plotted at the radial
distance of the center of area of each ring. This is not quite correct
when the impulse gradient is changing rapidly with radial position, in
which case the radial position at which the ring should be plotted must
be computed taking into account the impulse gradient. Figure 1 is
a sketch of the charge configuration used. All charges were point
initiated at the rear end, using a booster small enough to have no
effect on the liner velocity. As shown by Figure 2, 1/4 inch steel
was equivalent to an infinite thickness of steel confinement for a
2D long charge with 1/16 inch steel liner. Figure 3 is for 1/64 inch,
1/32 inch, 1/16 inch, and 1/8 inch thick steel liners with various
charge lengths, and Figure 4 shows the velocity curves for 1/16 inch,
1/32 inch, 1/16 inch, 1/8 inch, 1/4 inch, and 1/2 inch thick steel
liners with 2D long charges. Figure 3 indicates, based on a one shot
sample, that a 2D long charge is equivalent to an infinitely long
charge for a 1/16 inch thick steel liner in 1/4 inch wall steel
confinement.

The velocity of the outermost ring for the 1/2 inch thick
steel on Figure 4 is low due to interference from the inner corner of
the confining steel cylinder which has spalled off and is observed
on the radiograph traveling ahead of the segments of the outermost ring.

Unconfined Cylindrical Charges: For this series, 1.625 inch
diameter charges of Composition B were used also. Lengths varied
from 1/2D to 2 1/2D, and the steel liner thickness varied from 1/64 inch
to 1/8 inch. The liners were pre-cut into a series of nested rings
and mounted in a 1.625 inch ID by 2 inch OD steel surround of the same
thickness. The purpose of this surround was to provide radial support
for the outermost ring during the shock acceleration process to
minimize breakup of this ring. However, the procedure was not entirely
successful, and the accuracy of velocity of the outermost ring reported
for these unconfined shots is questionable on account of the extreme
break-up suffered by this outermost ring. Figure 5 is for 1/64 inch,
1/32 inch, 1/16 inch steel liners with various charge lengths, and
Figure 6 is for 1/64 inch, 1/32 inch, 1/16 inch, and 1/8 inch steel
liners with 2D long charges.

Unconfined Rectangular Charges: For this series, the thick-
ness of the unconfined rectangular Composition B charges was held
fixed at 1.125 inch, while the width was made 1, 2, and 3 times the thick-
ness. The length of the charge was 6.75 inch in all cases, which is
effectively an infinite length. The velocities of the elements along
the short centerline (1.125 inch) of the charge are plotted in
Figure 7.
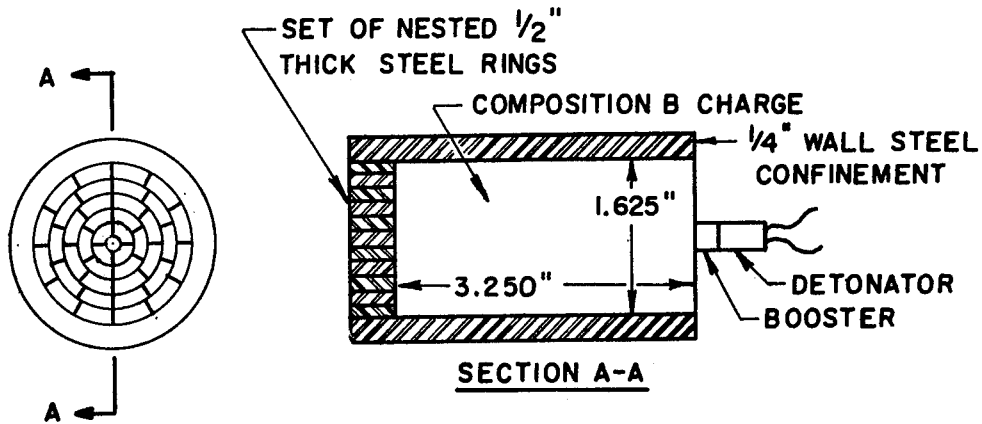
FIGURE I-DETAILS OF CONFINED CHARGE 2 D LONG
WITH 1/2" THICK STEEL LINER.
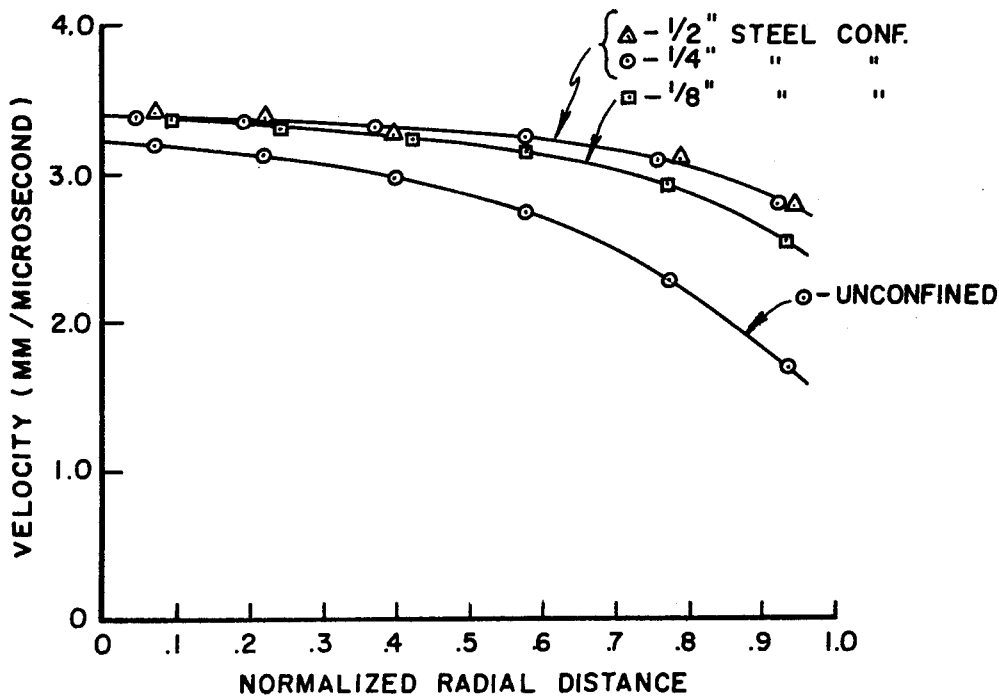
FIG. 2- COMPARISON OF VELOCITIES IMPARTED TO 1/16" THICK
STEEL FRAGMENTS BY CONFINED AND UNCONFINED 15/8" DIA.
BY 31/4" LONG COMP. B CYLINDRICAL CHARGES.
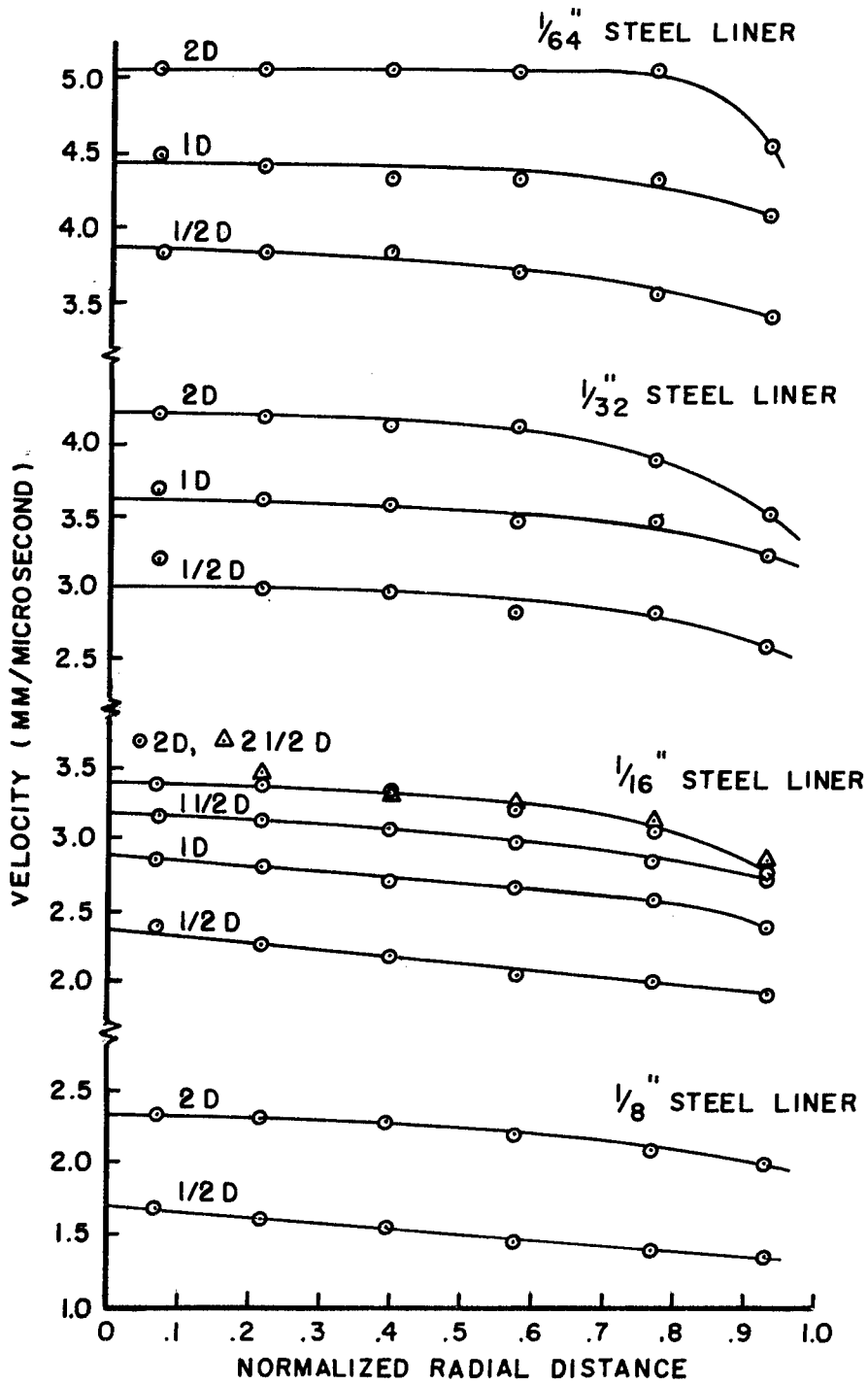
FIGURE 3 - COMPARISON OF VELOCITIES IMPARTED TO STEEL FRAGMENTS OF VARIOUS THICKNESSES BY 1 5/8" DIAMETER CYLINDRICAL COMP. B CHARGES OF VARIOUS LENGTHS IN 1/4" WALL STEEL CONFINEMENT.
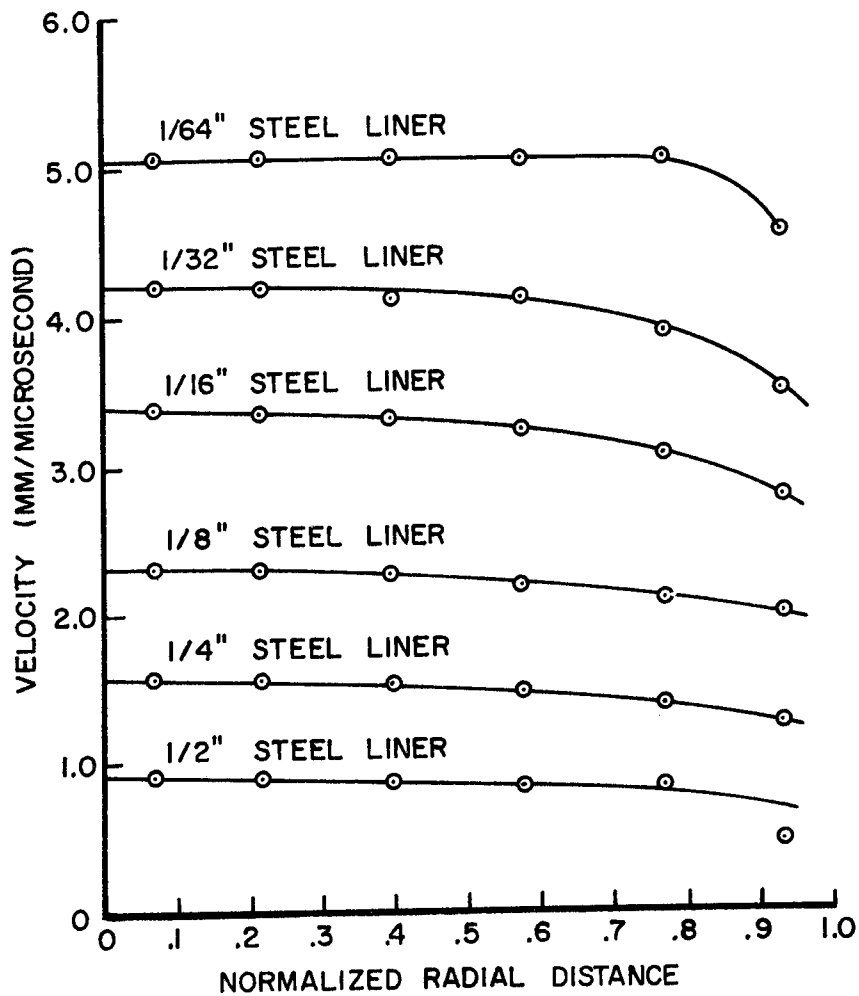
FIGURE 4. COMPARISON OF VELOCITIES IMPARTED TO STEEL FRAGMENTS OF VARIOUS THICKNESSES BY $1\frac{5}{8}$" DIAMETER BY $3\frac{1}{4}$" LONG (2D) CYLINDRICAL COMP. B CHARGES IN 1/4" WALL STEEL CONFINEMENT.
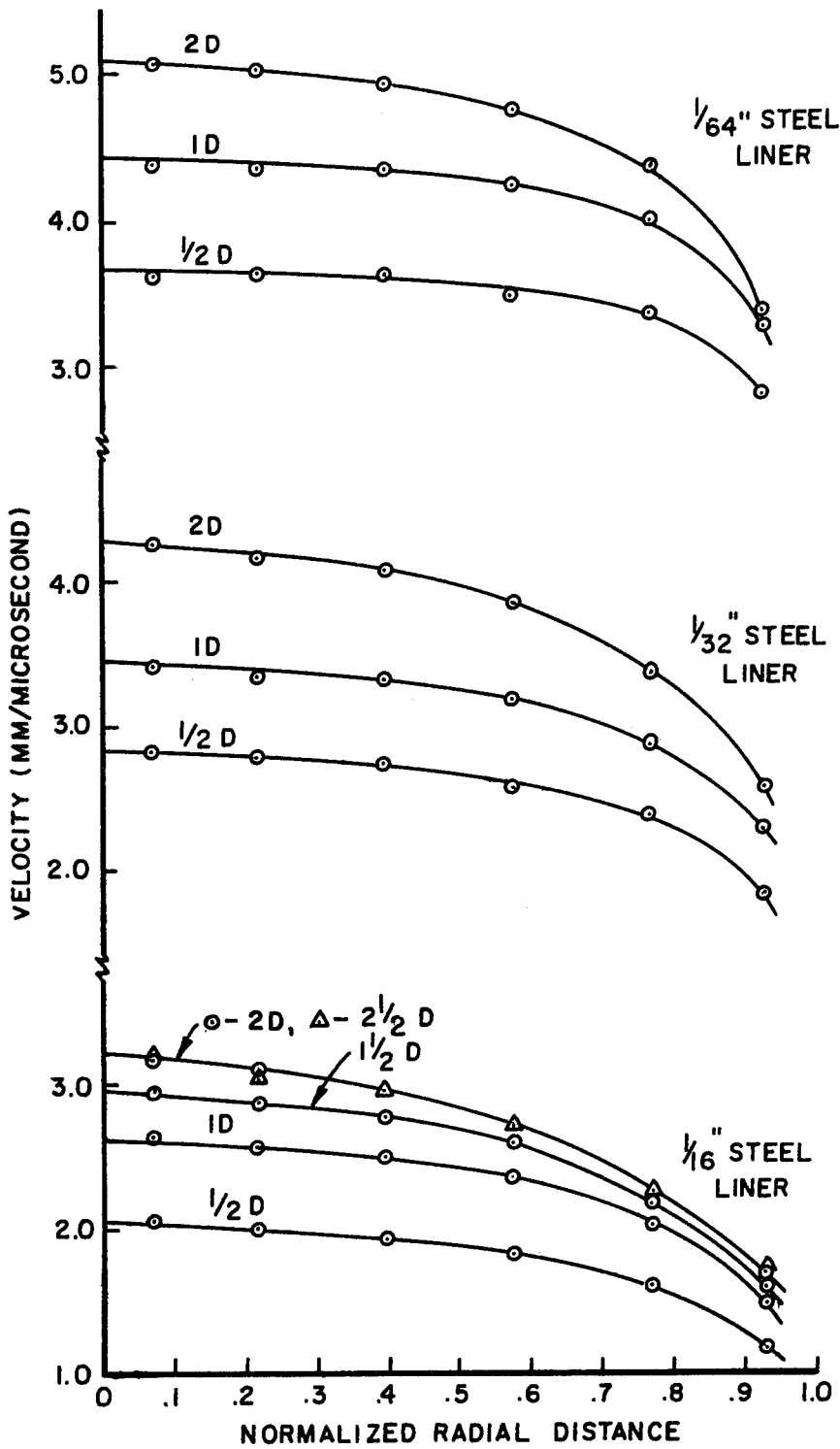
FIG. 5 – COMPARISON OF VELOCITIES IMPARTED TO STEEL FRAGMENTS OF VARIOUS THICKNESSES BY 1⅝" DIAMETER CYLINDRICAL COMP. B CHARGES OF VARIOUS LENGTHS. (UNCONFINED)
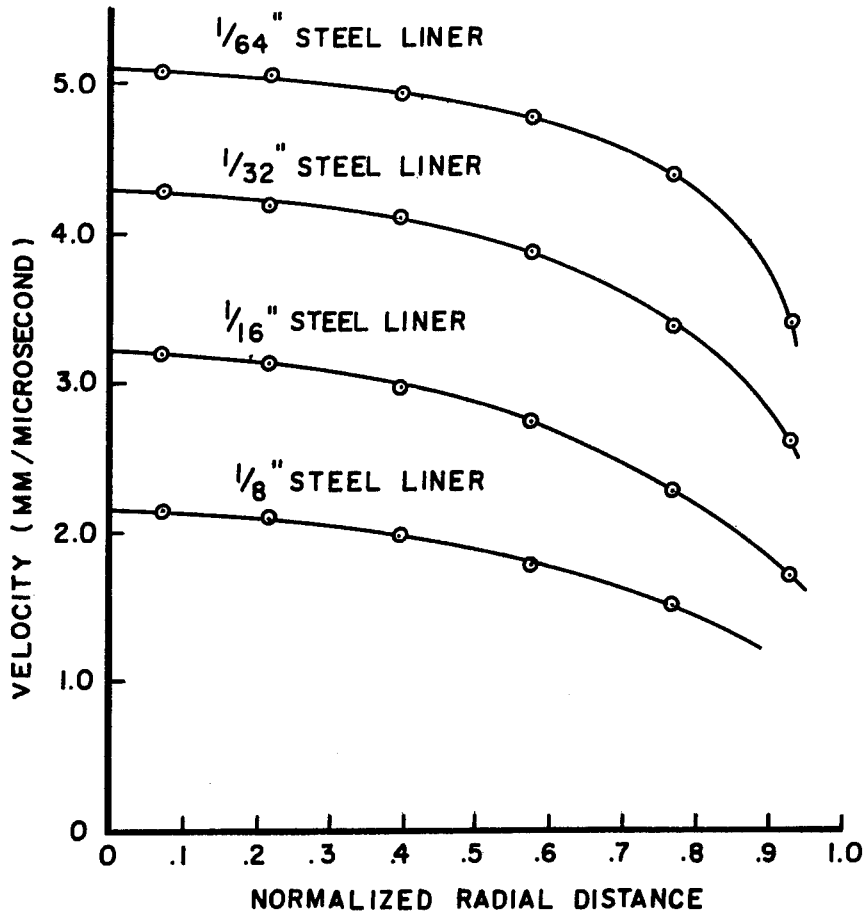
FIG. 6 - COMPARISON OF VELOCITIES IMPARTED TO
STEEL FRAGMENTS OF VARIOUS THICK-
NESSES BY 1⅝" DIAMETER BY 3¼" LONG
(2D) CYLINDRICAL COMP. B CHARGES.
(UNCONFINED)

Theory and Approximations

Rostoker[2] has given a theoretical treatment of the one-dimensional problem of the shock motion of a liner of finite thickness driven by a semi-infinite explosive charge, making simplifying assumptions as to the equation of state of the liner and of the detonation products (polytropic gas law with gamma of 3). He has also developed the equation of motion of a finite liner driven by an explosive charge of finite length (with rear end expanding into a vacuum) under the assumptions of a rigid liner (one whose shock velocity is infinite) and a polytpopic equation of state:

$$1) \quad u_L(T_L) = U_D \left\{ 1 - \frac{27}{16\Omega} \left[\sqrt{1 + \frac{32}{27} \Omega \left(\frac{1}{1 + \ell/U_D T_L} \right)} - 1 \right] - \frac{1}{I + \frac{U_D T_L}{\ell} \sqrt{1 + \frac{32}{27} \Omega \left(\frac{1}{1 + \ell/U_D T_L} \right)}} \right\}$$

in which $u_L(T_L)$ = liner velocity at time T_L

T_L = elapsed time after detonation wave reaches liner

Ω = ratio of mass of charge to mass of liner, per unit area

ℓ = length of charge

U_D = detonation wave velocity

As the time $T_L \to \infty$, then $u_L(\infty)$ is given by:

$$2) \quad u_L(\infty) = U_D \left\{ 1 + \frac{27}{16\Omega} \left[1 - \sqrt{1 + \frac{32}{27} \Omega} \right] \right\}$$

Eichelberger[3] in his "release wave" approximation starts with the above equation and makes the assumption that a rarefaction from the charge boundary propagates into the detonation products at a constant velocity U_R and acts so as to drop the pressure instantaneously to zero as it passes over any point. The time which elapses between the detonation wave reaching a point, and the first of the rarefaction waves from any of the charge boundaries reaching the same point is used to calculate the effective length of the explosive charge which acts on that point. This effective charge length is used in equation 2 above to calculate the resultant liner velocity. In this approximation, the value of $K = U_R/U_D$ is equal to 0.6 on the basis of hydrodynamic considerations, although in the past sometimes it has been used as a disposeable constant. This release wave approximation is in use at C. I. T. and B. R L for computing the performance of shaped charges of various configurations.

Discussion of Results

It is of interest to determine the degree of agreement between

Rostoker's one-dimensional theory and the experimental firings which are most likely to behave in a one-dimensional manner. These are the axial elements of the liners of the confined cylindrical charges. The experimental velocities of the axial elements, the asymptotic velocities calculated by Rostoker's equation 2, and the ratios of these velocities are presented in Table 1 for various steel liner thicknesses and Composition B charge lengths.

Table 1

Experimental and Theoretical Velocities
For 1 5/8 inch Diameter
Composition B Charges in 1/4 inch Wall
Steel Confinement

Charge Length		Steel Liner Thickness					
		1/64"	1/32"	1/16"	1/8"	1/4"	1/2"
1/2D	Experimental Velocity (MM/μSec)	3.89	3.04	2.34	1.65	-----	----
	Theoretical Velocity (MM/μSec)	4.54	3.66	2.74	1.86	-----	----
	Ratio of Velocities	0.86	0.83	0.85	0.88	-----	----
2D	Experimental Velocity (MM/μSec)	5.07	4.20	3.35	2.33	1.57	0.91
	Theoretical Velocity (MM/μSec)	5.93	5.31	4.54	3.66	2.74	1.87
	Ratio of Velocities	0.86	0.79	0.74	0.64	0.57	0.46

Two items are of immediate interest: (a) the fact that the velocity ratio reaches an upper limit at about 0.83 to 0.88; and (b) the fact that the velocity ratio decreases as the liner thickness increases for 2D long charges.

Referring to Figure 1, it can be seen that when the liner moves forward a distance equal to its own thickness, it has moved out of the confinement and the detonation products can escape radially. It was thought that this process could account for at least part of the velocity defect shown by the upper limit of 0.83 to 0.88 for the ratio. To examine this further, two shots were fired, one with the confinement extended 1/4 inch beyond the liner surface, and the other with it extended 1 inch. The results are plotted in Figure 8, for a 1/16 inch thick steel liner and a 2D charge length. The velocity was increased about 6.5%. Thus a further complication will be introduced into any scheme for computing velocities of confined liners. Gas leakage thru the joints of the pre-cut liner is another
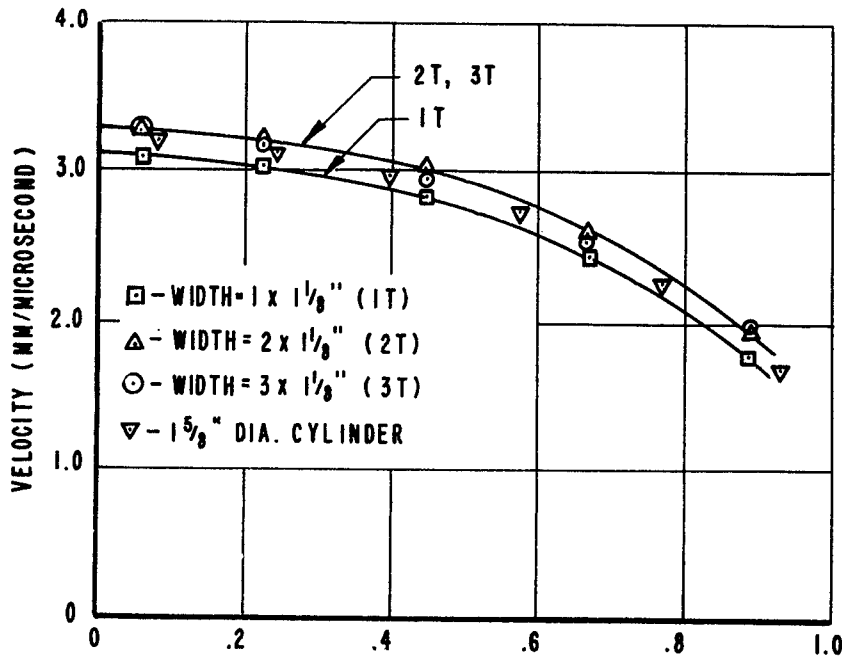
FIG.7-COMPARISON OF VELOCITIES IMPARTED TO 1/16" THICK STEEL FRAGMENTS BY UNCONFINED RECTANGULAR COMP. B CHARGES 1⅛" THICK AND OF VARIOUS WIDTHS AND BY A 1⅝" CONFINED CYLINDRICAL COMP. B CHARGE. ALL CHARGE LENGTHS EFFECTIVELY INFINITE.
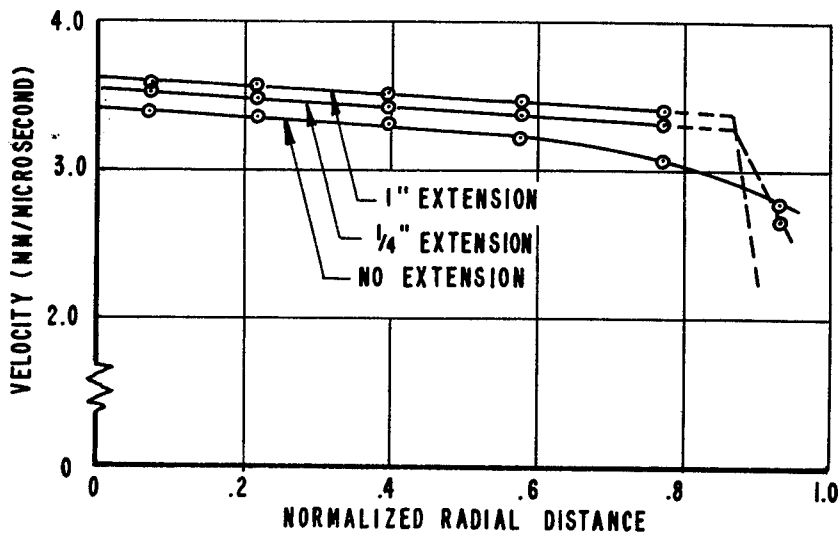
FIG.8-EFFECT OF EXTENDING CONFINEMENT BEYOND LINER ON VELOCITIES IMPARTED TO 1/16" THICK STEEL LINERS BY 1⅝" DIAMETER BY 3¼" LONG (2D) COMP. B CYLINDRICAL CHARGES IN 1/4" WALL STEEL CONFINEMENT.

277

process that might cause losses sufficient to limit the maximum velocity, but this has not been investigated. There is also the possibility that the asymptotic velocity predicted by Rostoker's equation 2 is in error since it depends ultimately on assumptions made concerning the equation of state of the detonation products.

Rostoker[2] in comparing the equation of motion of a liner driven by a semi-infinite charge with the equation of motion of the same liner driven by a charge of finite length, remarks that the curves are almost identical over some initial interval of time. That is, it takes some time before the rarefaction from the rear surface appreciably alters conditions at the liner. If the curves for liner motion according to equation 1 are examined, Figures 9, 10, and 11, it can be seen that for a 2D charge length that the experimental velocities correspond to a time of 2.05, 2.10, 2.35, 2.20, and 2.5 respectively. In other words, over the steel liner thickness range from 1/64 inch to 1/2 inch, Rostoker's one-dimensional equation yields the correct experimental velocity if one assumes the acceleration process is terminated after about 2.0 to 2.5 microseconds. This holds whether the liner has acquired 0.86 of the theoretical asymptotic velocity as in the case of 1/64 inch steel or whether it has only acquired 0.46 as in the case of 1/2 inch steel. Since this departure from one-dimensional behavior must be caused by the expansion of the steel confinement, the question arises of how a confined charge of equal length but of a larger diameter would behave. For such a charge, one would expect that it would take longer for the rarefaction caused by the confinement expansion to affect the center of the charge, and consequently the experimental velocity should increase somewhat because of the longer acceleration time available.

In Figure 10 the velocity curves for both confined and unconfined charges with 1/16 inch steel liners have been plotted along with $u_L(T_L)$ calculated by Rostoker's equation 1. One can use these curves to graphically obtain the time, as a function of radial position, at which the one-dimensional acceleration process described by Rostoker's equation would have to be terminated to produce the particular experimental velocity obtained at that radial position. This time vs radial position is plotted in the lower graph for both confined and unconfined charges and in Figure 11 for 1/32 inch and 1/8 inch liners. Examination of these curves, particularly for the unconfined charges, shows that a possible "explanation" of the experimental velocities could be made by postulating the existence of a delayed release wave which drops the pressure instantaneously to zero and travels at constant velocity from the boundary toward the axis for about 2/3 of the distance and then speeds up slightly for the remaining 1/3 of the distance. In the case of the unconfined charges with 1/32 inch, 1/16 inch, and 1/8 inch thick steel liners, the delay in the start of the release wave would be about 0.5 microsecond and the release wave velocity would vary from 6.3 mm/microsecond for the 1/32 inch and 1/16 inch to 6.75 mm/microsecond for the 1/8 inch steel liner. In the case of the confined charges, the delay would be about 1.0 microsecond and the velocity would be higher than for the
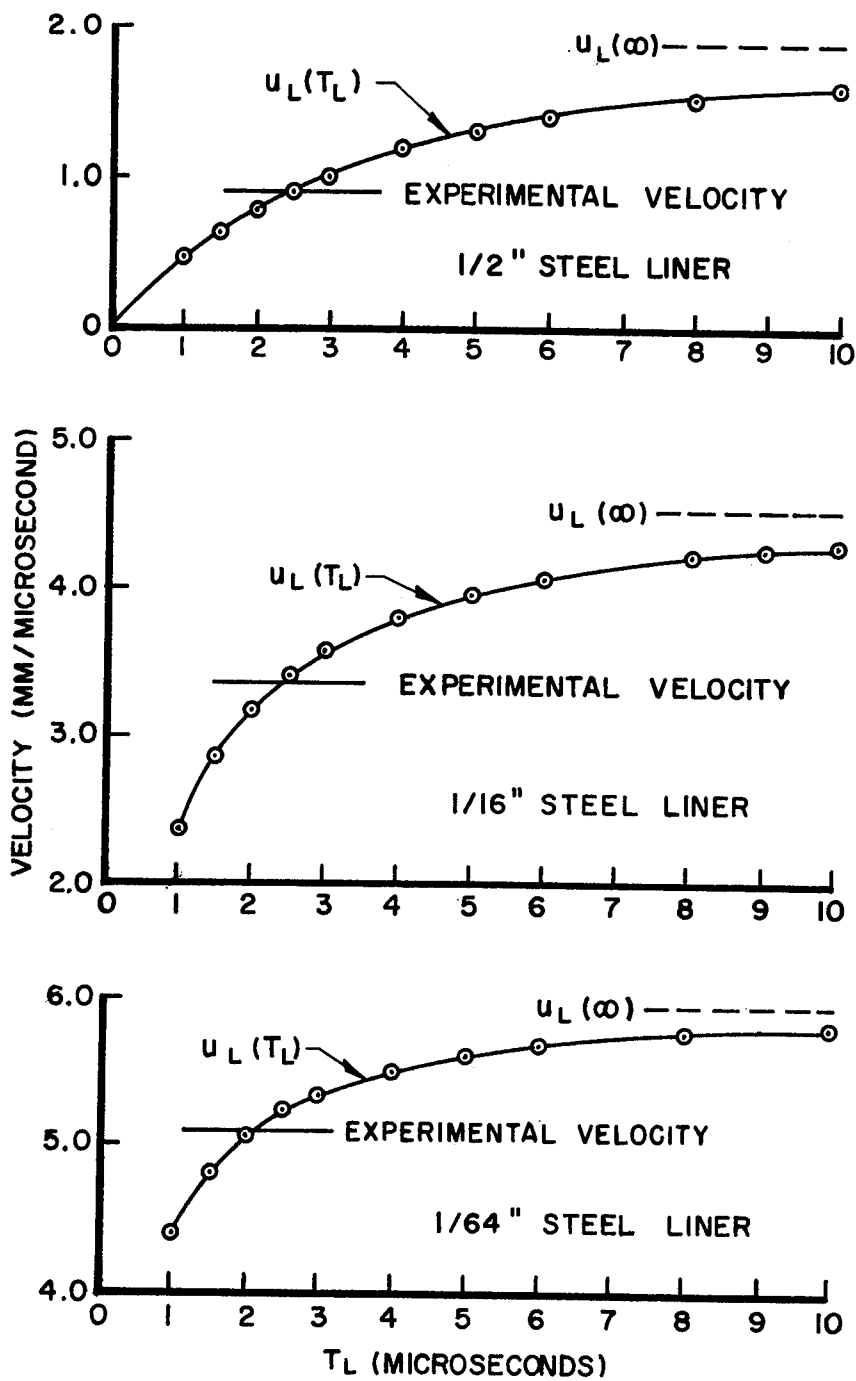
FIGURE 9. LINER MOTION CURVES CALCULATED BY ONE-DIMENSIONAL THEORY FOR 3¼" LONG COMP. B CHARGES AND STEEL LINER THICKNESSES SHOWN.
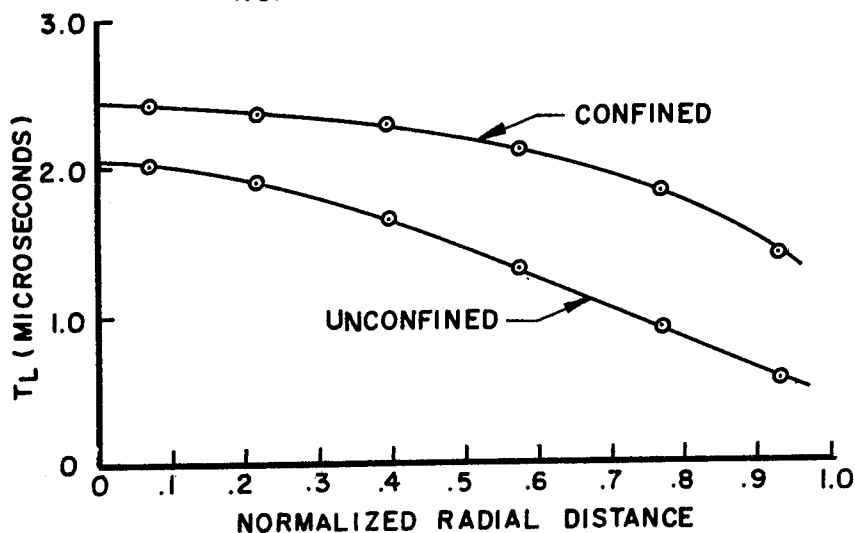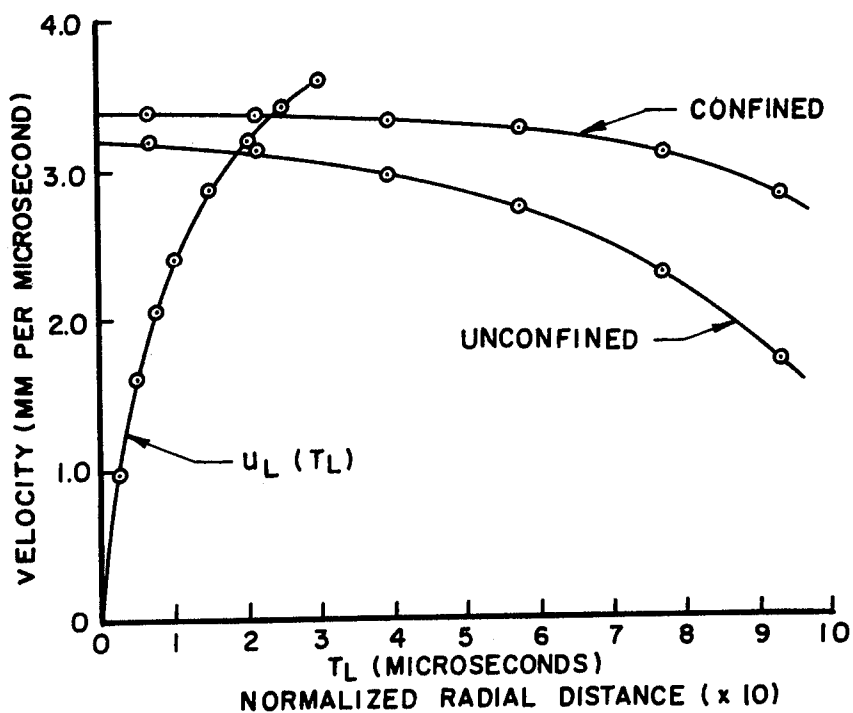
FIGURE 10- PLOT OF ACCELERATION TIME (T$_L$), BOTTOM, AS
DETERMINED FROM EXPERIMENTAL VELOCITIES AND
THE ONE-DIMENSIONAL LINER MOTION CURVE, TOP,
FOR 1/16" THICK STEEL FRAGMENTS DRIVEN BY
1 5/8" DIA. BY 3 1/4" LONG (2D) CYLINDRICAL COMP.
B CHARGES IN 1/4" WALL STEEL CONFINEMENT
AND UNCONFINED.
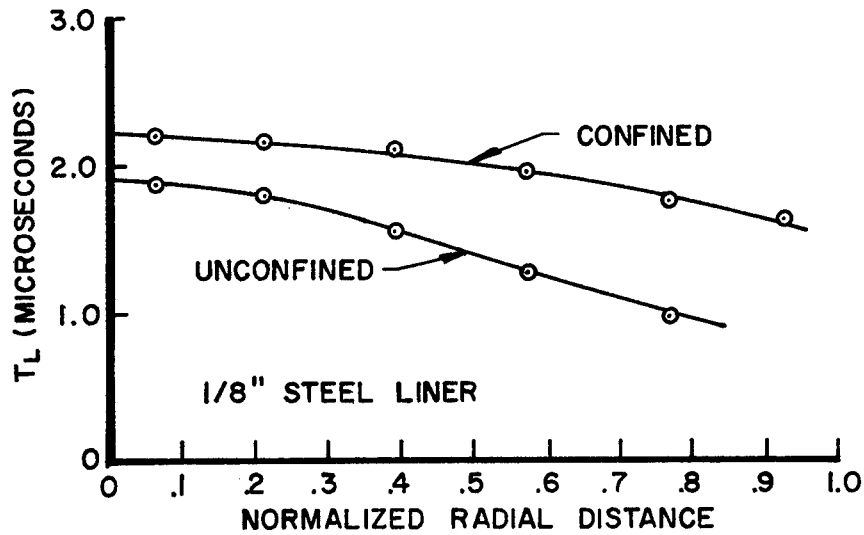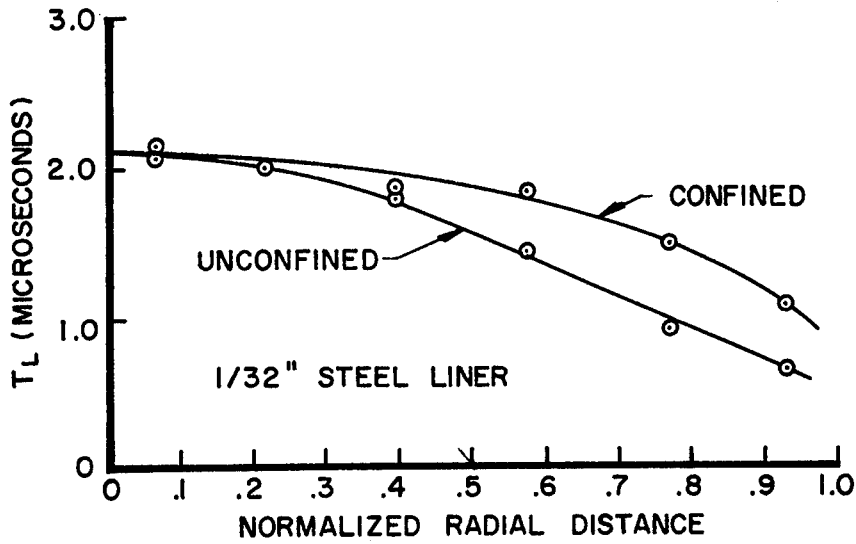
FIGURE 11. PLOT OF ACCELERATION TIME(T_L) FOR 1/32" AND 1/8" THICK STEEL FRAGMENTS DRIVEN BY $1^5/_8$" DIAMETER BY $3\frac{1}{4}$" LONG (2D) CYLINDRICAL COMP. B CHARGES IN 1/4" WALL STEEL CONFINEMENT AND UN-CONFINED.

unconfined charge and increase continuously toward the center. In examining these curves, two points should be kept in mind: First, the velocity given directly by the slope of these time-position curves is the phase velocity, not the propagation velocity; second, the time used in these plots is the acceleration time during which a particular element of the liner is being accelerated. The acceleration times for each element cannot be referred to a common real time origin unless the detonation wave is a plane wave perpendicular to the charge axis. In the case of a curved detonation wave, a correction for the time of arrival of the detonation front must be made to refer the acceleration times to a common real time origin.

The above "explanation" can be accepted only as a possible computational aid, since it tortures the one-dimensional theory on which it rests. The fact that such an explanation can be made is almost obvious, since it is known that the liner velocity decreases from the axis to the boundary of the charge, and if one employs an equation such as 1 in which the length is maintained constant and the velocity is an increasing function of time, then to yield the desired velocity distribution, the time of action must increase from the boundary to the axis. This then can be interpreted as a signal propagating inward from the boundary. That such can be done should not be taken as proof of the physical existence of a delayed discontinuous release wave.

Figure 12 is a comparison of experimental velocities for a 1/16 inch thick steel liner with an unconfined charge 2D long with calculations made using the form of the release wave approximation developed by Eichelberger and discussed in "Theory and Approximations". Here "K" is the velocity ratio of the release wave to detonation wave. If can be seen that while the correct value for the velocity of a limited radial range of the liner can be obtained by empirical adjustment of the parameter "K" that the shapes of the calculated and experimental velocity curves differ considerably.

Results for several unconfined rectangular Composition B charges were previously presented in Figure 7. The velocities are for elements positioned along the short center liner of 1.125 inch ($=T$) thick charges of Composition B in which the width was 1T, 2T, and 3T and the length was kept at 6T to provide an essentially infinitely long charge. The liner thickness was 1/16 inch steel. This limited series suggests that a width of 2T is essentially infinite for this liner thickness. A further item of considerable interest is that this 1.125 inch thick charge (and essentially infinite width and length) imparts the same velocity to a 1/16 inch steel liner as does a 1.625 inch diameter unconfined cylindrical charge and furthermore the shape of velocity vs normalized position curve is the same for the slab and cylindrical charges.

Conclusions

Results obtained from the release wave approximation and from the empirical interpretation of Rostoker's one-dimensional equation to
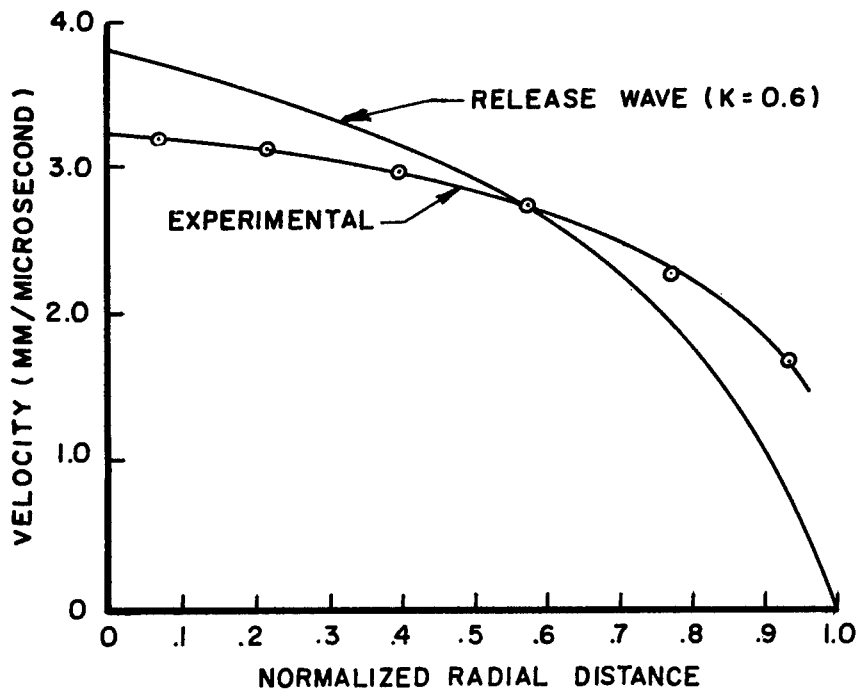
FIGURE 12 - COMPARISON OF EXPERIMENTAL VELOCITIES WITH CALCULATED VELOCITIES USING THE RELEASE WAVE APPROXIMATION FOR A 1/16" THICK STEEL LINER DRIVEN BY A $1\frac{5}{8}$" DIAMETER BY $3\frac{1}{4}$" LONG (2D) UNCONFINED CYLINDRICAL COMP. B CHARGE

obtain the time of cut-off of acceleration illustrate difficulties that can occur when one attempts to construct a simple model of a complicated process. In the case of the release wave approximation where one attempts to simplify by making the initial assumption of a constant velocity release wave (or rarefaction shock) which is physically unrealistic, then the calculated results do not agree closely with experiment. If one starts with the experimental data and uses it to interpret a theory beyond the conditions for which it is applicable, then one may end up with conclusions that are physically unrealistic. This was the case where the time of cut-off of Rostoker's equation leads to a release wave originating at an unconfined charge surface with a delay of 0.5 microsecond after passage of the detonation front. If such models are used as computational aids with the realization that some features are physically unrealistic, then no harm is done. Because of this physically unrealistic content one hesitates to use them for predictions beyond the range for which they have been verified experimentally. Thus when an unusual charge design is attempted, a firing program must be run to extend the model, which practice is not too far removed from trial and error design. On the other hand, if the content of the model is physically realistic, it should be valid for predictions beyond the immediate range of experimental knowledge.

Thus further efforts at constructing a model will be concentrated on removing the physical inconsistencies from the present release wave approximation, since the approach taken by this particular approximation appears to be the most promising.

Bibliography

1. Hauver, G. E., "Pressure Profiles in Detonating Solid Explosives" (Presented at this Symposium).

2. Rostoker, N. and Murray, T. P., "The Motion of a Liner Propelled by a One-Dimensional Charge", Second Bimonthly Report, Fundamentals of Shaped Charges, Carnegie Institute of Technology, Contract No. DA-36-061-ORD-122, February 29, 1952.

3. Eichelberger, R. J., "Predictions of Shaped Charge Performance from the Release Wave Theory", First Quarterly Status Report, Fundamentals of Shaped Charges, Carnegie Institute of Technology, Contract No. DA-36-061-ORD-394, January 31, 1954.

EXPERIMENTAL DETERMINATION OF STRESSES GENERATED BY AN ELECTRIC DETONATOR*

John S. Rinehart
Colorado School of Mines
Golden, Colorado

The magnitude, duration and spatial distribution within a solid body (plexiglas) of the transient stress disturbance generated by an electric detonator detonated in intimate contact with the body has been experimentally determined. The technique is to affix to one surface of the body a small pellet of the same material, which flies off when the disturbance reaches the surface, the velocity of the pellet being determined. The complete stress-time curves are built up by using pellets of several thicknesses. Three types of detonators have been used with these being placed flat ended against the surface of a plexiglas block. A few were confined. The stress in the plexiglas was found to be distributed more or less uniformly about the axis of the detonator. Along the axis both peak pressure and total momentum decreased with distance from the detonator: peak pressure exerted by an Olin Mathieson No. 6 Plasti-cap ranged from 9500 lb/in^2 at 1.25 in from the detonator to 7000 lb/in^2 at 2.0 in; and the momentum ranged from 16 x 10^{-3} lb-sec/in^2 at 1.25 in to 9.0 x 10^{-3} lb-sec/in^2 at 2.0 in. The disturbance lasted about two microseconds. Similar results were obtained with the other detonators.

INTRODUCTION

Small detonators or blasting caps are commonly
used to initiate the explosion of a ponderable mass of
explosive. And there exists a wide variety of such de-
tonators, each designed for one or more specialized uses,
some being electrically activated and others mechanically.
The electrically activated cap usually contains a match
in a small cylindrical case made of plastic or metal
which, when heated by the passage of an electric current,
ignites, thereby setting off a few grains of highly sensi-
tive explosive also contained in the case. The force of
the small explosion is usually sufficient to initiate de-
tonation of a much larger mass of less sensitive explo-
sive placed in intimate contact with the cap. Construc-
tional details of caps manufactured by different companies
are not the same, there being variation in type of ex-
plosive, explosive content, match composition, and case
design, with much of the detailed information being
proprietary in nature. The external and case features of
three common No. 6 electric caps are illustrated in
Fig. 1, the one on the left being a plastic cased, flat
ended cap manufactured by the Olin Mathieson Co; the one
in the center, a copper cased, rounded end cap manufac-
tured by the Atlas Powder Company; and the one on the
right, a copper cased cap manufactured by E. I. duPont
de Nemours Company, which differs from the Atlas cap by
having the front of the cap indented, thereby creating a
situation conducive to the formation of a shaped charge
jet (1). Although these caps are widely used and several
engineering tests have been devised for testing their
efficacy, there is essentially no quantitative data on
the magnitude and duration of the stress generated within
a body when the cap is exploded while in close contact
with the body (which normally would be an explosive). In
this study detailed quantitative data on these stresses
have been obtained for the first time from experiments
made using three types of No. 6 instantaneous electric
blasting caps.

METHOD

The experimental arrangement used in many of the
tests is shown schematically in Fig. 2, the cap being
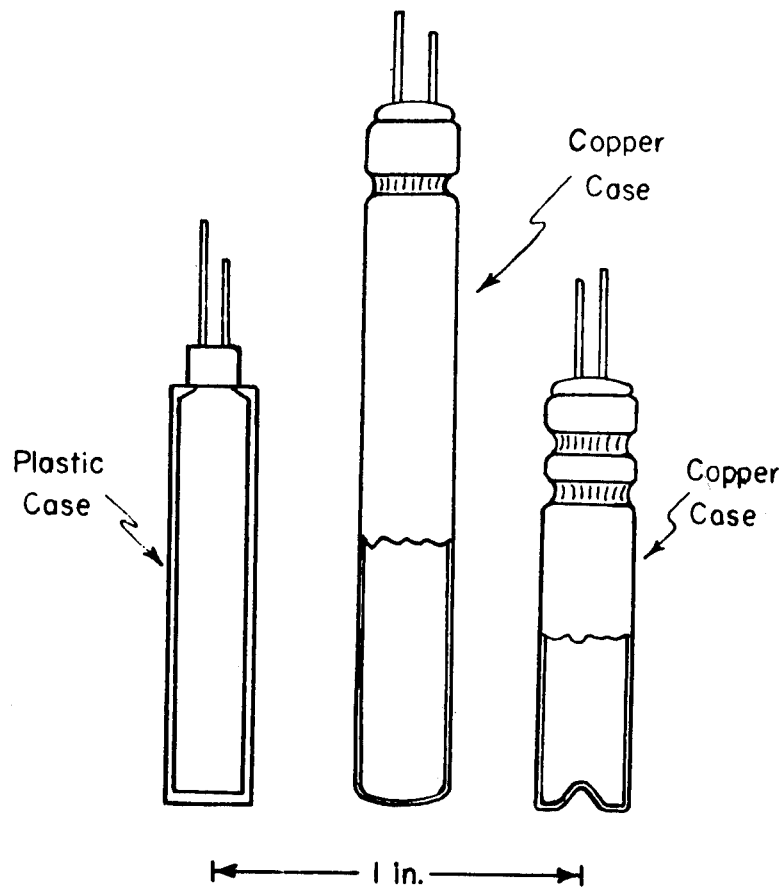
Fig. 1. External features of three caps studies.
Left: plastic cased, flat ended cap manu-
factured by Olin Mathieson; middle: copper
cased, rounded end cap manufactured by
Atlas Powder; right: copper cased, reen-
trant ended cap manufactured by duPont.
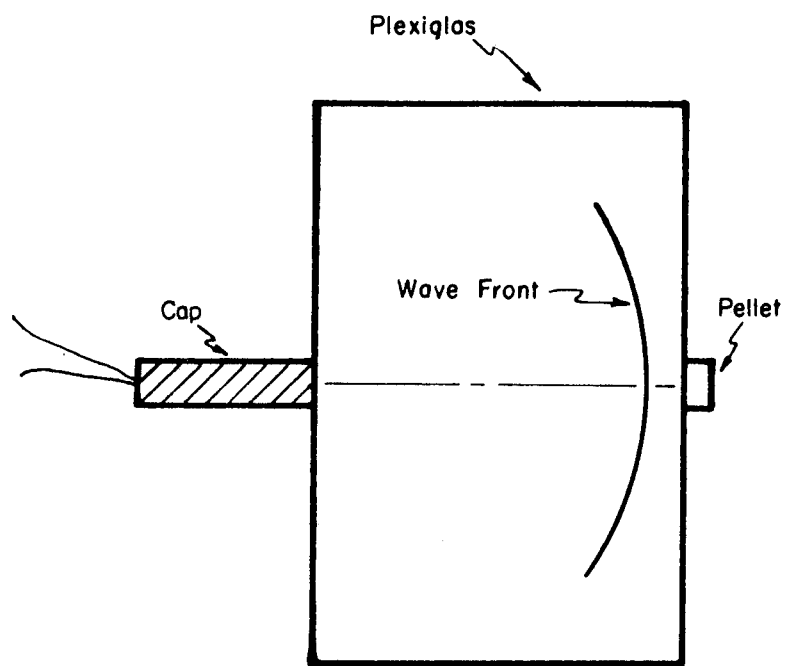
Fig. 2. Experimental arrangement for along-the-axis tests.

unconfined and butted end on against a small block of plexiglas, usually an inch thick and of a few inches in other dimensions. A sharp-fronted transient compressional stress disturbance of the form illustrated in Fig. 3 is developed when the cap is exploded; on striking the far (right) surface, it causes a pellet of the same material, affixed lightly thereto with oil, to fly off with some of the momentum of the disturbance trapped in it. By using successively thicker pellets and repeating the experiment, complete and detailed stress-time profiles of the pulse can be drawn: this technique has been successfully employed by several investigators (2, 3, 4). In the present tests plexiglas cylindrical pellets 1/4 in in diameter were used, with pellet thicknesses ranging from 1/32 in to 1/4 in, roughly in 1/32 in steps. The velocity of each pellet, which usually lay in the range from 30 ft/sec to 180 ft/sec, was measured by photographing its flight over a several inch long path, using either a high intensity, short duration stroboscopic light or a slotted rotating disk light source in conjunction with an open shutter Polaroid camera, containing ultra-fast film, 3000 ASA.

A typical momentum trapped (reduced to momentum per unit area) versus thickness of pellet curve is drawn in Fig. 4, the distance from cap to pellet being 2 in and the cap an Olin Mathieson No. 6 Plasti-cap. The curve has become substantially flat for a pellet thickness of 1/8 in, implying that most of the impulse or momentum of the disturbance lies in a region just twice this thickness, or 1/4 in. The longitudinal wave velocity of the plexiglas used in these experiments was measured using a standard pulse technique and found to be 9070 ft/sec; the duration of the 1/4 in pulse would therefore be about 2.3 microsec.

Both stress-distance and stress-time curves for the disturbance can be derived from the momentum per unit area versus pellet thickness curve, provided certain assumptions are made: The first of these is that the particle velocity in the disturbance is linearly related to stress through the equation

$$\sigma = \rho cv$$

289
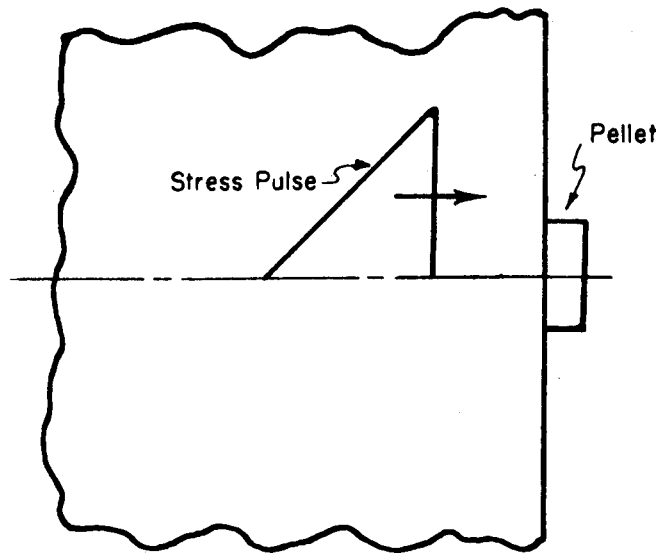
Fig. 3.   Dynamics of momentum entrappment.
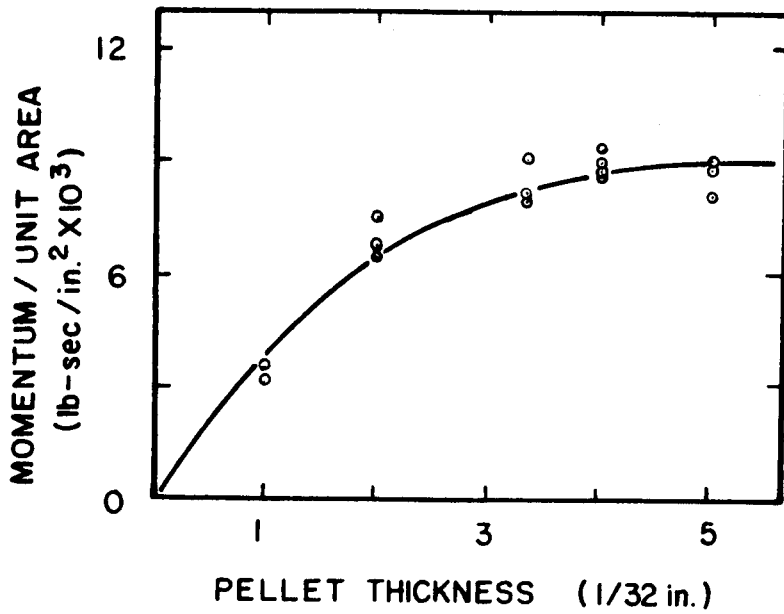
Fig. 4.   Momentum per unit area versus thickness of pellet.
Free surface perpendicular to axis of cap.   Olin
Plasti-cap.   Cap to pellet distance, 2 in.

where σ is the instantaneous value of the stress; ρ is the density of the material (73.6 lb/ft^3 for plexiglas); c is the longitudinal wave velocity (taken in all calculations as 9070 ft/sec); and v is the instantaneous value of particle velocity in the disturbance. The second assumption, needed only in drawing the stress-distance curve, is that the pulse does not change shape over the distance under consideration as it progresses through the body. This is not a particularly good assumption, as will be seen later, since measurable attenuation, dispersion, and divergence do occur. Stress versus distance and stress versus time curves, deduced from the curve of Fig. 4, are plotted in Figs. 5 and 6, respectively. The stress, initially about 10,000 lb/in^2, decays essentially to zero in 2 to 3 microsec with the length of the pulse being about 1/4 in.

CHANGE OF PULSE SHAPE WITH DISTANCE

It is to be expected that a pulse of this type will change its shape due to divergence, attenuation, and dispersion as it moves through the plexiglas. Tests were run for cap to pellet distances of 1.25 in, 1.50 in, 1.75 in, and 2.0 in, with the results plotted in Figs. 7 and 8, Fig. 7 being a log-log plot of total momentum per unit area in the pulse versus cap to pellet distance, and Fig. 8 being plots of the four respective stress versus time curves. The straight line in the log-log plot, (Fig. 7), drawn with a slope of minus one, is a good fit to the data, indicating that the total impulse delivered by the disturbance varies inversely with the first power of distance, a more or less reasonable result since in a spherically expanding wave stress decays inversely with the first power of the distance (5). The principal change in pulse shape with distance, (Fig. 8), is a decay in stress at all points along the pulse; there is also a tendency for the wave to sharpen up, losing some of its bell shape and becoming more nearly exponential as the distance from the cap increases. This change may be due to a frequency dependent absorption, strongly felt in this frequency range (6); but more probably it arises from the fact, as illustrated in Fig. 9, that the front of the disturbance is not precisely spherical, this lack
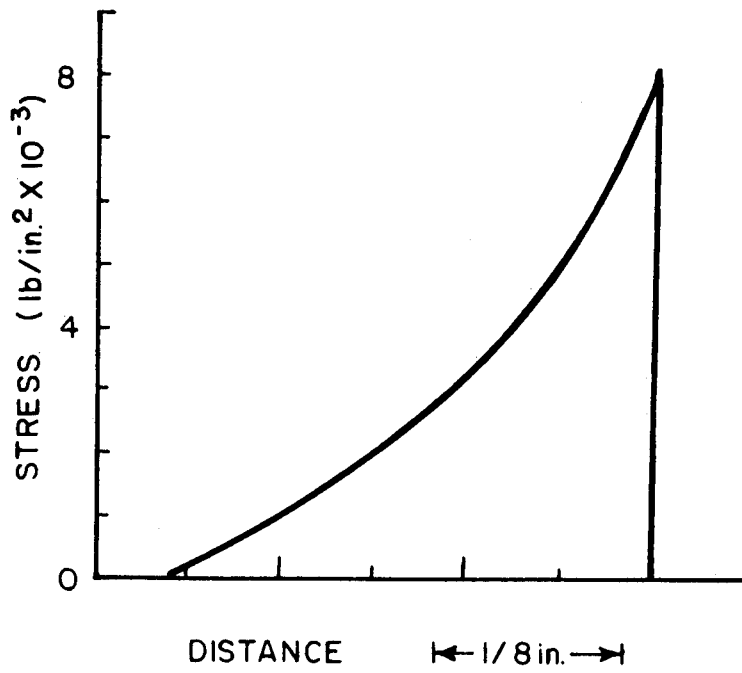
Fig. 5.   Stress versus distance.   Derived from Fig. 4.
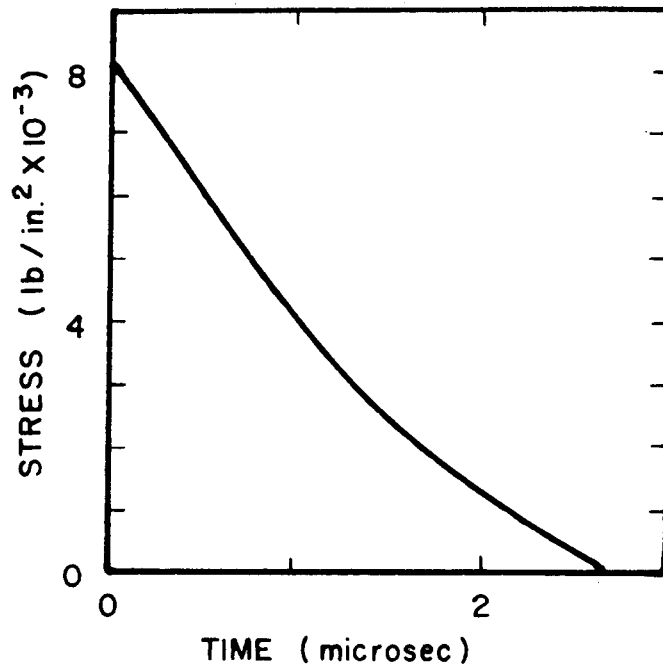
Fig. 6.   Stress versus time.   Derived from Fig. 4.
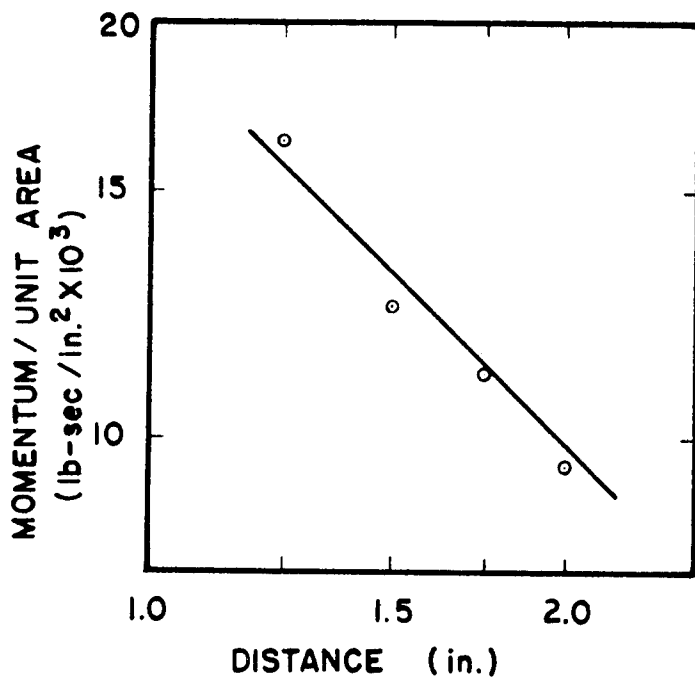
Fig. 7. Log. of total momentum per unit area versus
        log. of distance from cap. Experimental
        arrangement shown in Fig. 2. Olin Plasti-
        cap. Line has slope of minus one.
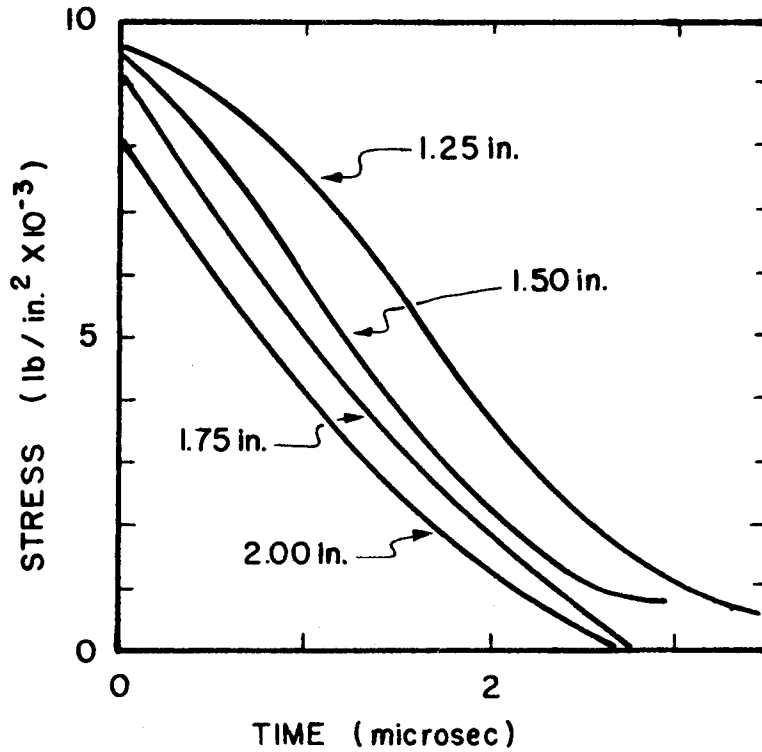
Fig. 8. Stress versus time for four cap to pellet distances. Data taken on axis. Olin Plasti-cap.
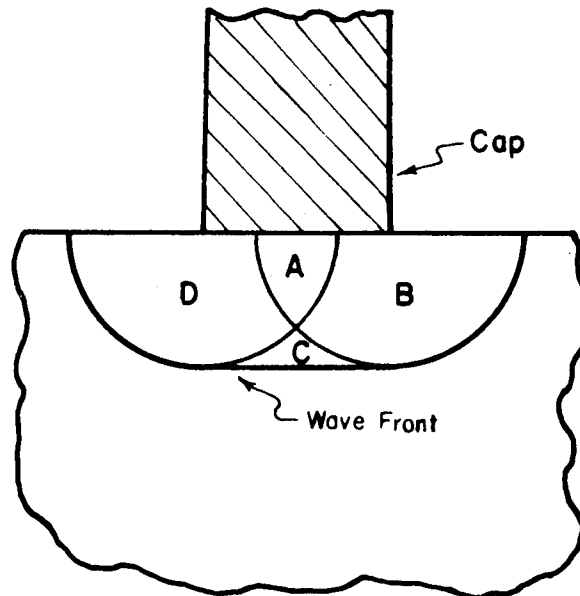
Fig. 9. Schematic of longitudinal wave pattern generated by unconfined cap.

of sphericity having its origin in the finite lateral dimensions of the detonator. This particular stress situation has been treated (7) for the elastic case, the salient relevant features being sketched in Fig. 9. Rarefaction waves moving inward create several distinct regions, labeled A, B, C, and D. Region C, originally quite thick, becomes thinner and thinner as the wave expands, with the wave approaching sphericity more and more closely. The stress near the center of the wave will be sustained a shorter and shorter time with increasing distance from cap, supporting the present observation.

EFFECT OF CAP CONFINEMENT

If the cap is confined by placing it in a hole in the block, as illustrated in Fig. 10, the stress situation ought to be quite different, both because there is no opportunity for rarefaction waves originating at a free surface to move into the solid hard on the heels of the front of the disturbance, and because the explosion products can not disperse as readily, causing the pressure to be sustained longer. A few tests were run with confined caps, the cap being inserted into a one inch deep hole bored in the plexiglas block. Only Plasticaps were used. The results are compared with similar results for unconfined caps in Figs. 11 and 12, the figures containing plots of momentum per unit area as a function of time, and stress as a function of time, respectively. Cap to pellet distance was 2 in in each case. Under these conditions the total impulse per unit area, about 16×10^{-3} lb-sec/in^2 in the disturbance created by the confined cap, is nearly twice that of 9.0×10^{-3} lb-sec/in^2 in the disturbance produced by the unconfined cap. The maximum stress, 10,000 lb/in^2 for the confined cap is only somewhat, 20 percent, higher than the 8,000 lb/in^2 stress of the unconfined cap. But the stress is maintained at this high level for a longer time.

DIFFERENT CAPS

Results for the three types of caps are compared in Fig. 13; momentum per unit area is plotted against
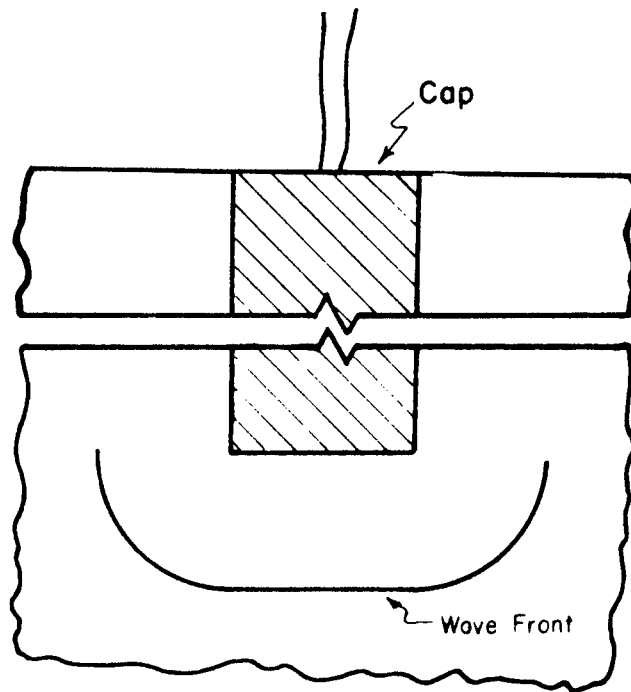
Fig. 10. Schematic of longitudinal wave
pattern generated by confined
cap.
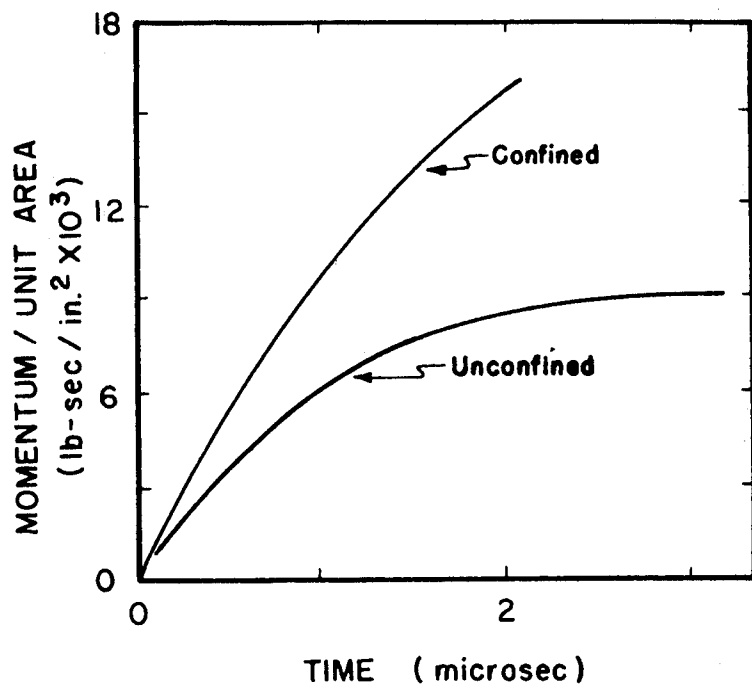
Fig. 11. Comparison of momentum per unit area as a function of time for confined and unconfined caps. Along axis. Cap to pellet distance, 2 in. Olin Plasti-cap.
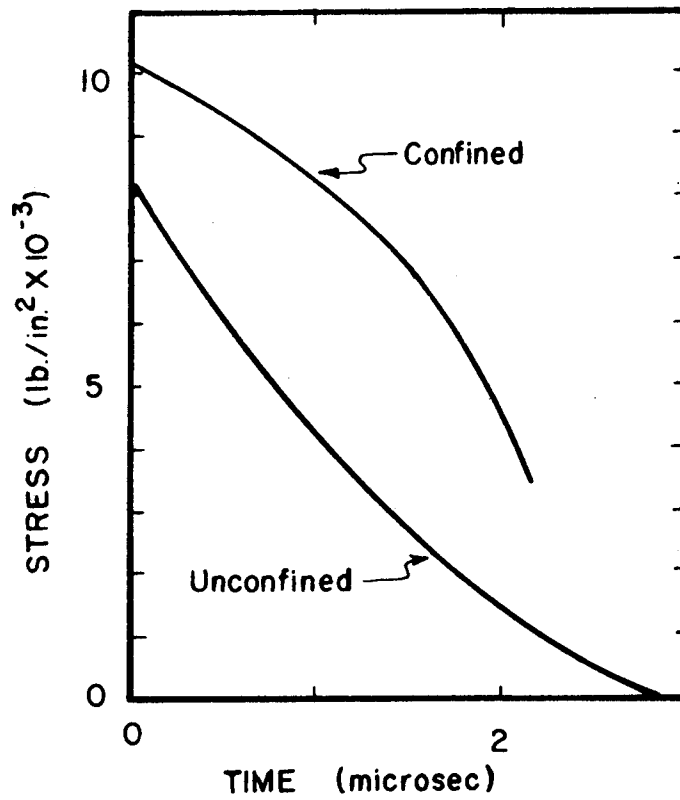
Fig. 12. Comparison of stress versus time curves for confined caps. Derived from Fig. 11.
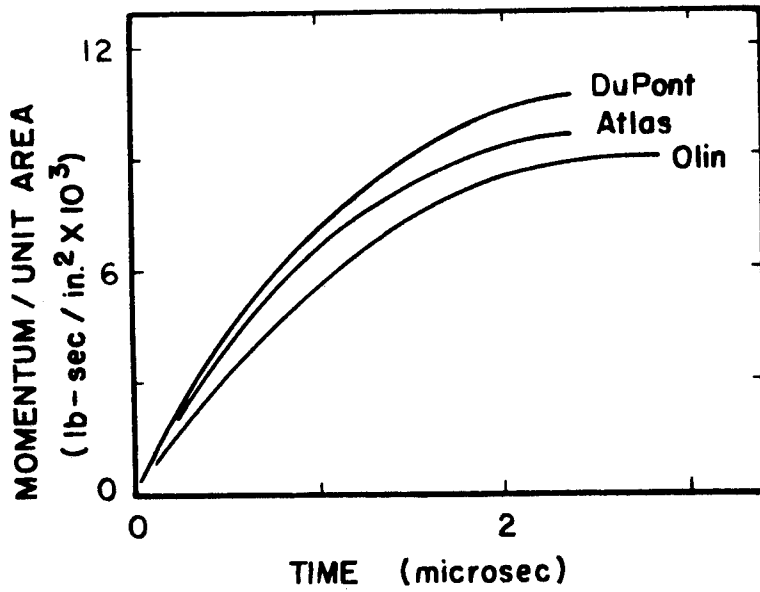
Fig. 13. Momentum per unit area versus time for three types of No. 6 caps. Along axis. Cap to pellet distance, 2 in.

time for each cap for a cap to pellet distance of 2 in. In general, the impulse delivered by each of the caps is about the same, differences in construction shown in Fig. 1 appearing to be not especially significant. This result is to be anticipated since in practice the three caps are similarly and competitively used.

ANGULAR DISTRIBUTION OF IMPULSE

In the tests discussed thus far the pellet was placed along an extension of the axis of the cylindrical cap. Of equal interest is the magnitude and duration of the off-axis stress and impulse. The experimental arrangement shown in Fig. 14 was used to make such determinations. Here the front of the disturbance, assumed spherical, is made to strike normally a surface so cut that the normal to it forms an angle θ with an extension of the axis of the cap. Results of these off-axis measurements are summarized in Fig. 15, a plot of momentum per unit area against the angle θ. Only the Plasti-cap was tested over a complete hemisphere, tests on the other caps being limited to off-axis angles of 60 degrees. The curve for the Plasti-cap indicates remarkable uniformity of impulse over the whole wave front, with the 90 degree value, 7.2×10^{-3} lb-sec/in^2, being only 18 percent lower than the zero degree value of 8.8×10^{-3} lb-sec/in^2. The Atlas rounded nose cap follows essentially the same pattern. Although the data are not definitive, the duPont cap, with its indented shaped charge like front face, appears to concentrate the impulse somewhat more in the forward direction. At θ equal to 60 degrees the impulse seems to be dropping rapidly.

The upper curve of Fig. 15, with its steep slope, indicates that confinement greatly enhances the magnitude of the impulse delivered off-axis.
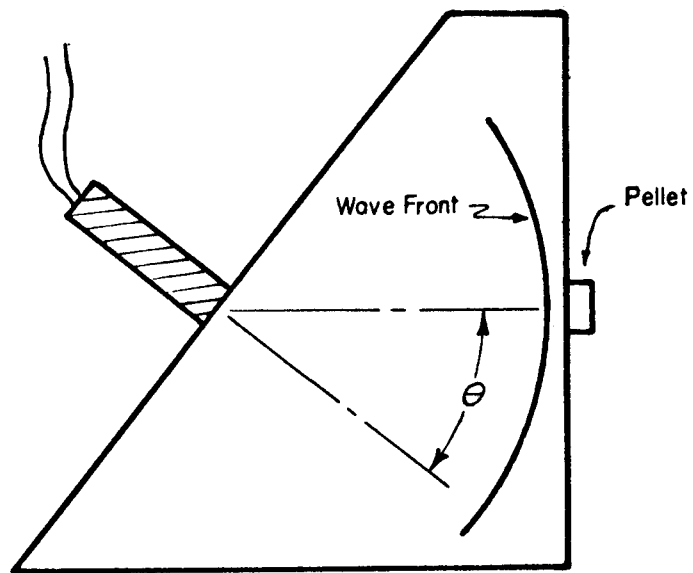
Fig. 14.   Experimental arrangement for deter-
mining distribution of impulse
off-axis.
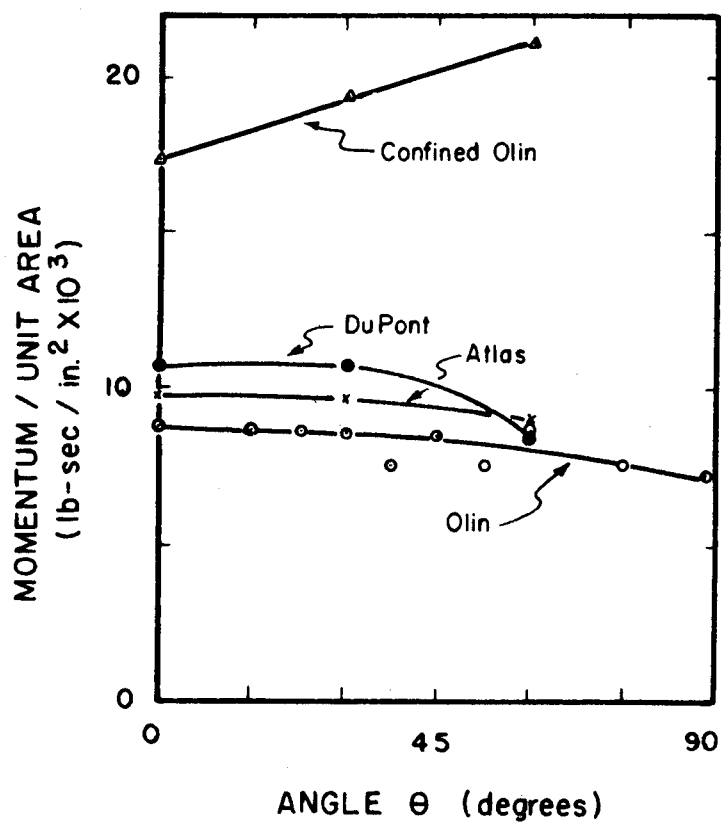
Fig. 15. Momentum per unit area as function of
angle off-axis for confined and uncon-
fined caps of three types. Experimental
arrangement shown in Fig. 14. Distance
from cap to pellet, 2 in.

REFERENCES

1. R. W. Wood "Optical and physical effects of high explosives" Proc. Roy. Soc. (London) 157A, 249 (1936)

2. B. Hopkinson "A method of measuring the pressure produced in the detonation of high explosives or by the impact of bullets" Trans. Roy. Soc. (London) 213A, (1914)

3. J. S. Rinehart and J. Pearson Behavior of Metals under Impulsive Loads (Amer. Soc. Metals, Cleveland, 1954) p. 78

4. J. S. Buchanan and H. J. James "Measurement of high intensity stress pulses" British Journal of Applied Physics 10, 290 (1959)

5. H. J. Selberg "Transient compression waves from spherical and cylindrical cavities" Arkiv för Fysik 5, 97 (1952)

6. Unpublished results

7. J. H. Huth and J. D. Cole "Impulsive loading on an elastic half space" J. App. Mech. 21, 294 (1954)

COMMENTS ON HYPERVELOCITY WAVE PHENOMENA IN CONDENSED EXPLOSIVES*

R. F. Chaiken
Chemical Division, Aerojet-General Corporation
Azusa, California

The direct observation of hypervelocity wave phenomena during detonation initiation by strong shocks in single crystals of PETN and liquid nitromethane have been reported by Holland, Campbell and Malin (1) and by Cook, Pack and Gey (2) respectively.

Holland et. al. noted, by means of streak camera photography of shock impacted large crystals of PETN, that the growth of detonation towards steady-state apparently proceeded in several stages. First, a relatively low velocity wave front (5.56 mm/μsec) appeared which abruptly changed to a very high velocity compression wave (~ 10.45 mm/μsec). Within ~0.5μsec, the high velocity front changed to an apparent steady-state detonation (8.28 mm/μsec) which consumed the crystal. No explanation was offered as to the nature of these events.

From similar space-time high speed camera studies of the shock initiation to detonation in nitromethane, Cook and his coworkers observed a "flash across" phenomena in which an apparent wave of luminescence originated in the explosive behind the initial compression front, and propagated at a reported velocity of ~35 mm/μsec to overtake the initial compression front. This "flash across" phenomena was interpreted as a heat transfer wave caused by a sudden increase in the thermal conductivity of the shock compressed nitromethane. The phenomenon was taken as a direct observation of the "heat pulse" which Cook, Keyes and Filler (3) had predicted.

Several years prior to the CPG (i.e. Cook, Pack and Gey) studies, the author carried out a streak camera study of the shock initiation to detonation in nitromethane.(4) At that time, evidence was found to indicate the existence of a hypervelocity wave moving behind the initiating shock front. It was suggested that the detonation reaction wave originated behind the initial compression front, and traveled at a "super-velocity" in the compressed explosive to overtake the initiating shock front.

The author believes that this detonation initiation process could be an alternate explanation for the "flash across" phenomena observed by CPG, and at the same time offers an explanation for the velocity steps in PETN which were observed by Holland et. al.

Figure 1 depicts a space-time plot of the wave phenomena occuring during detonation initiation in nitromethane based upon the author's studies.(4) Referring for the time being, only to time zones I and II, D_i is the initiating shock velocity (i.e., the velocity of the shock wave entering the explosive from an external source); D' is the hypervelocity wave velocity; u is the velocity imparted to the explosive by the initiating shock wave; τ is the time lag after compression, for any element of fluid at an initial distance S from the point where the initiating shock front enters the explosive, to reach the observed luminous stage; τ_0 refers to the observed time lag for the fluid element at S = 0.

In the time zones I and II, CPG's observations apparently coincide with the author's except for the magnitude and interpretation of τ_0 and D'.

Assuming the D_i and D' are independent of S (i.e. negligible attenuation of the wave fronts in the explosive), it is possible to express τ as a linear function of S.

From figure 1 the following relations hold:

$$S = u \left(\tau_0 - \tau \right) + S' \qquad [1]$$

and

$$S' = D' \Delta t = \Delta S_1 + u \Delta t \qquad [2]$$

From the Rankine-Hugoniot (R-H) relationships for one-dimensional steady-state shock propagation,

$$\Delta S_1 = \left(V/V_0 \right) S \qquad [3]$$

where V/V_0 = the ratio of specific volumes across the shock front (subscript o referring to the initial state).

Equations 1 - 3 can be rearranged to yield

$$\tau = \tau_0 - (S/u) \left[D' \left(1 - V/V_0 \right) - u \right] \bigg/ \left[D' - u \right] \qquad [4]$$

From the R-H equations, $u/D_i = 1 - V/V_0$; therefore, equation 4 becomes

$$\tau = \tau_0 - \left[\left(D'/D_i - 1 \right) \bigg/ \left(D' - u \right) \right] S \qquad [5]$$

Equation 5 is the same as CPG's experimental equation, i.e.,

$$\tau = \tau_0 - a' S \qquad [6]$$

where a' is a positive constant having the measured value of ~1.7μsec/cm. For this value of a', and taking D' = 35mm/μsec and u = 0.45 D_i, the initiating shock velocity in CPG's experiments turns out to be ~5.3 mm/μsec. This value of D_i falls within the range of values studied by the author.

In figure 2, a plot of a' vs. D' is given for the conditions D_i = 5.3 mm/μsec and u = 2.4 mm/μsec. Superimposed upon this curve are

$$\text{PLOT OF } a' \text{ vs. } D'$$

$$a' = (D'/D_i - 1)/(D' - u)$$

$$D_i = 5.3 \text{ mm}/\mu \text{ sec}$$

$$u = 2.4 \text{ mm}/\mu \text{ sec}$$

Figure 2

TIME ZONES

SPACE-TIME PLOT OF WAVE
PROPAGATION UPON SHOCK
INITIATION OF DETONATION

D_i = INITIATING SHOCK VELOCITY
u = VELOCITY IMPARTED TO THE MASS
    BY D_i
D' = "HYPERVELOCITY" WAVE VELOCITY
D_3 = STEADY-STATE DETONATION
    VELOCITY

Figure 1

the results of the two studies. It is seen that CPG's values for a' and D' differ by the respective factors of ~0.25 and ~3 from the author's values. However, it is easily seen that in the range of a' = 1.7μsec/cm, it would be very difficult to calculate an accurate value for D' on the basis of an experimentally measured a'. This might be a reason for the discrepancy in the two sets of results.

It is interesting to note that if one assumes that the chemical reaction wave resulting in D' has a velocity comparable to a steady-state detonation velocity (D_s) at the shock density $(\rho = 1/V)$, it might be possible to obtain an estimate of D' from extrapolated $D_s(\rho)$ data. From the work of Campbell, Malin and Holland (5) on the detonation velocity of nitromethane as a function of initial temperature the following expression for $D_s(\rho)$ can be obtained:

$$D_s = 2.78 \times 10^3 \rho + 3110 \text{ meters/sec} \qquad [7]$$

Estimating that $\rho \simeq 2.1 \text{ gm/cm}^3$ for $D_i \simeq 5.3 \text{ mm/μsec}$, yields a steady-state detonation velocity of 8.86 mm/μsec. Since this reaction wave would be traveling in a moving medium,

$$D' = D_s + u \simeq 11.5 \text{ mm/μsec} \qquad [8]$$

which is consistent with the author's value.

The formation of a propagated "super-velocity" reaction wave is also consistent with an adiabatic reaction model in which the chemical reaction rate exhibits an apparent induction time (τ_o). After τ_o seconds pass, the molecules of explosive which were first compressed by the initiating shock front suddenly decompose. The rapid release of energy propagates a high pressure reaction wave moving with velocity $D' > D_i$ behind the initiating shock front. This "super-velocity" reaction wave overtakes the initiating shock front and passes into the unshocked region. The detonation reaction in the nitromethane which has not yet been compressed is then greatly over-initiated (i.e. it occurs with a higher than steady-state velocity), and the detonation front rapidly decays to its normal steady-state value. Thus referring to time zones III and IV in figure 1, a small portion of the explosive will be consumed by a detonation front moving at a hypervelocity before steady-state is achieved. This general picture now explains the detonation steps in PETN. (1) Additional support for this general description of the detonation initiation process comes from the recent work by Hubbard and Johnson (6). Calculations of the shock initiation detonation conditions utilizing time dependent one-dimension hydrodynamic equations with an Arrhenius form of chemical energy release indicate the formation of a hypervelocity reaction wave behind the initiating shock front.

Literature References

1. T. E. Holland, A. W. Campbell, and M. E. Malin, J.Appl.Phys. 28, 1212 (1957)

2. M. A. Cook, D. H. Pack and W. A. Gey, Seventh Symposium (International) on Combustion, Butterworths, London (1959) 820.

3. M. A. Cook, R. Keyes and A. S. Filler, Trans.Faraday Soc. 52, 363 (1955)

4. R. F. Chaiken "The Kinetic Theory of Detonation of High Explosives," M.S. Thesis, Polytechnic Institute of Brooklyn, Brooklyn, New York, (1958); also submitted to the Eighth Symposium (International) on Combustion, Pasadena, California (1960).

5. A. W. Campbell, M. E. Malin and T. E. Holland, J.Appl.Phys., 27, 963 (1956)

6. H. W. Hubbard and M. H. Johnson, J.Appl.Phys., 30 765 (1959)

NONIDEAL DETONATION
OF AMMONIUM NITRATE-FUEL MIXTURES

L. D. Sadwin, R. H. Stresau,[*] S. J. Porter,[**] J. Savitt
Armour Research Foundation
of Illinois Institute of Technology
Chicago, Illinois

INTRODUCTION

Because of their relatively long reaction zones, mixtures of ammonium nitrate and fuels are well suited media for the investigation and study of nonideal detonation. Nonideal detonation is defined for the purposes of this paper, as detonation in which movements of material and energy along coordinates other than that normal to the detonation front are sufficient to significantly affect the propagation and other conditions of the detonation. As Eyring and his associates[1] as well as many others have pointed out, these effects become appreciable as the charge dimensions approach the length of the reaction zone.

In the course of their efforts to gain a better understanding of the explosive behavior of ammonium nitrate-fuel mixtures, the Spencer Chemical Company and its various contractors have developed an appreciable mass of data which is of general interest, in that it seems to contain several keys to a better understanding of nonideal detonation processes. It should be pointed out that this paper is concerned specifically with a 94/6 mixture of Spencer's N-IV, prilled, ammonium nitrate with No. 2 Diesel fuel.

ANALYTICAL OBSERVATIONS

All explosive reactions, whether thermal decomposition, deflagration, or detonation, are affected by the geometry of the charge, the particle size of the explosive, the confinement afforded by the surroundings, and the density and composition of the explosive. Experiments with pure organic explosive compounds in granular form indicate that the reaction zone length is directly related to the particle

---

[*] Consultant: 7 Summit Rd., Lake Zurich, Illinois

[**] Consultant to Spencer Chemical Co., Kansas City, Missouri

size of the explosive. Jacobs[2] found that ammonium picrate charges composed of large particles detonated at lower velocities than those composed of smaller particles, but that those composed of mixtures of large and small particles detonated at still lower velocities. These effects were most pronounced in small diameter charges and tended to disappear if sufficiently large diameters were used. For some combinations of charge diameter and density, detonation failed to propagate in the mixed-particle-size material, although it was stable in charges composed of all-large or all-small particles. These findings tend to support the view that the reaction behind the detonation front is a surface burning or deflagration type of reaction rather than an adiabatic thermal decomposition.

The curved front theory of Eyring and his associates[1] gives the relationship:

$$\frac{D}{D_i} = 1 - \frac{ka}{R} \tag{1}$$

between the detonation velocity, D, of a column of explosive of radius, R, whose ideal velocity is equal to D_i and reaction zone length equal to a. The constant k is determined by confinement conditions.

By the assumption of an Arrhenius type relationship between temperature and reaction rate, taking into account the thermodynamic relationship between pressure and temperature and the hydrodynamic relationship between detonation velocity and temperature, Eyring and his associates derived a relationship between detonation velocity and reaction rate which was combined with Eq. (1) in an iterative process. This relationship was used to plot the familiar re-entrant curve (Fig. 1) relating detonation velocity to charge radius.

Although they proposed the grain burning model of the reaction in the detonation zone of a high explosive and pointed out that the reaction time for this model is proportional to the grain radius, R_g, Eyring and his associates did not carry these ideas to their logical conclusion regarding the relationship between the ratio of the grain radius to the charge radius and that of the detonation velocity of a column to the ideal plane wave detonation velocity of the explosive used.

If it is assumed that the surface burning rate of the grain, W, is proportional to the pressure and that the pressure is proportional to ρD^2 as has been observed by Jacobs[3] for several military explosives at somewhat more moderate pressures than those of detonation, the reaction zone length is equal to:

$$a = \frac{D R_g}{W} = \frac{D R_g}{k_1 P} = \frac{k_2 R_g}{\rho D} \tag{2}$$
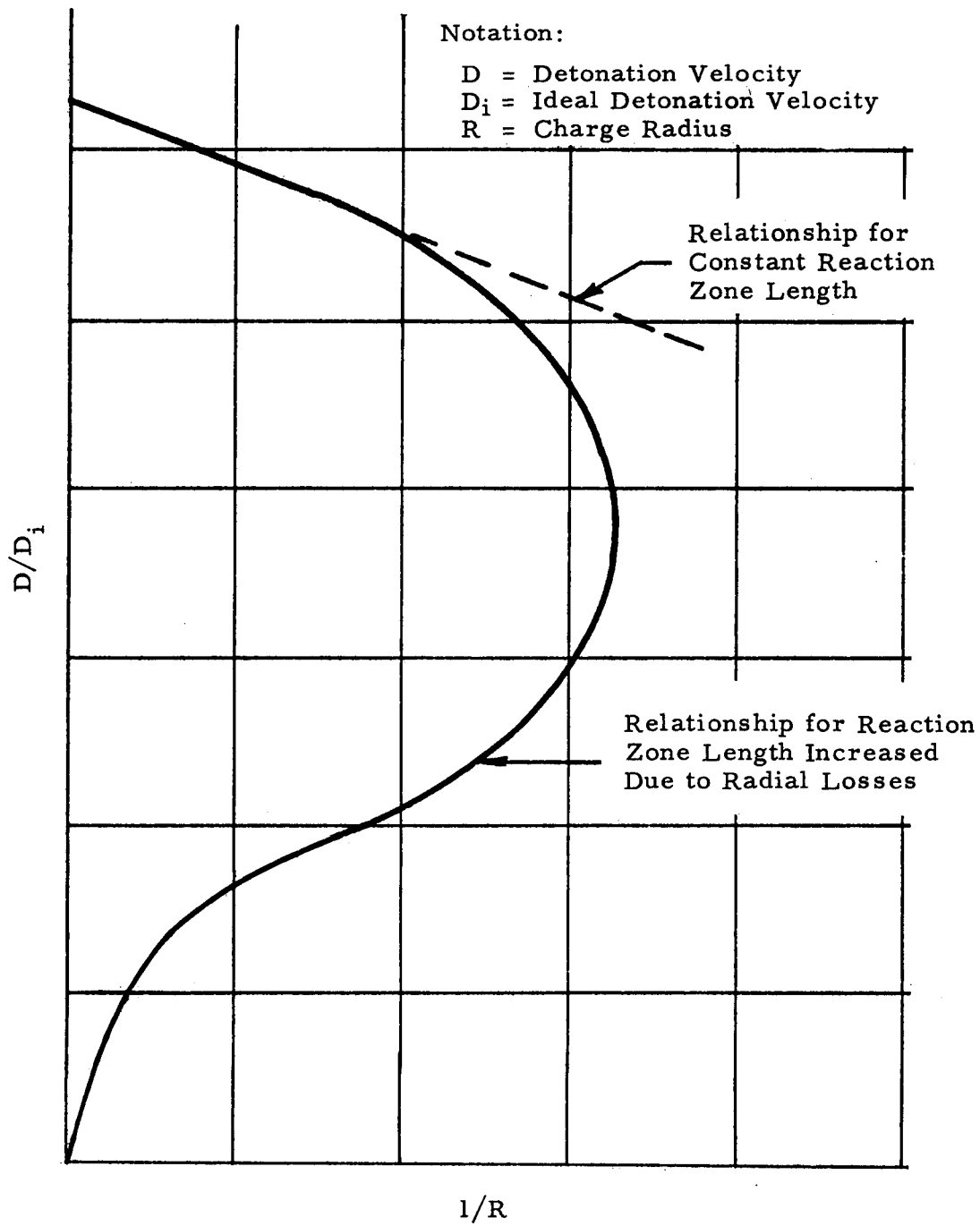
Figure 1 - General relationship between detonation velocity
and charge dimension

By substitution, Eq. (1) becomes:

$$D = \frac{D_i}{2} \left[1 \pm \sqrt{1 - \frac{4 k_3 R_g}{R \rho D_i}} \right] \qquad (3)$$

EXPERIMENTAL OBSERVATIONS

The reaction zones of the detonation of ammonium nitrate-fuel mixtures are quite long. In this respect, the velocity measurements made with ammonium nitrate-fuel mixtures presented in Fig. 2, which were essentially identical except for particle size are particularly significant. The 4200 m/sec detonation velocity observed for the finest grain material is an indication that the 2000 m/sec for the same mixtures in the coarser granulation is appreciably lower than the ideal velocity.

In Fig. 2, particle size effects data for 94/6 ammonium nitrate-fuel oil are plotted on coordinates of particle size to charge dimension ratio and detonation velocity. Note that these data fit the pattern predicted by Eq. (3) quite well. Lower velocities observed for the run-of-mill ammonium nitrate prill, which had a broad distribution of particle sizes, are consistent with the results of the investigation of particle size effects in ammonium picrate by Jacobs.[2]

Ideal detonation velocities of solid explosives increase linearly with density. The effect of density upon the reaction zone length is somewhat complex. Experimental data seem to indicate that the reaction zone length goes through a minimum at a density which is characteristic of both the composition and the particle size of the explosive. This might be explained on the following basis. At low densities the mass of granular explosive is quite nonhomogeneous in its distribution. This nonhomogeneity of mass distribution is reflected in a similar nonhomogeneity in heat distribution when the material is compressed by the shock. Because of the exponential nature of the Arrhenius equation, this nonhomogeneity of heat distribution results in a larger initial average reaction rate. However, the lower density explosive has a lower detonation pressure so that the subsequent deflagration within the reaction zone is slower. As the density is increased, the mass distribution and, hence, the temperature become more uniform, reducing the initial reaction rate while the increased pressure raises the burning rate.

Detonation velocities of ammonium nitrate-fuel explosives reach maxima in the mid range of the densities used in most experiments (Fig. 3). The drooping of the curve at high densities may be attributable to increasing nonideality with increasing density. If so, it should straighten with increasing diameter, confinement, and vigor of initiation.
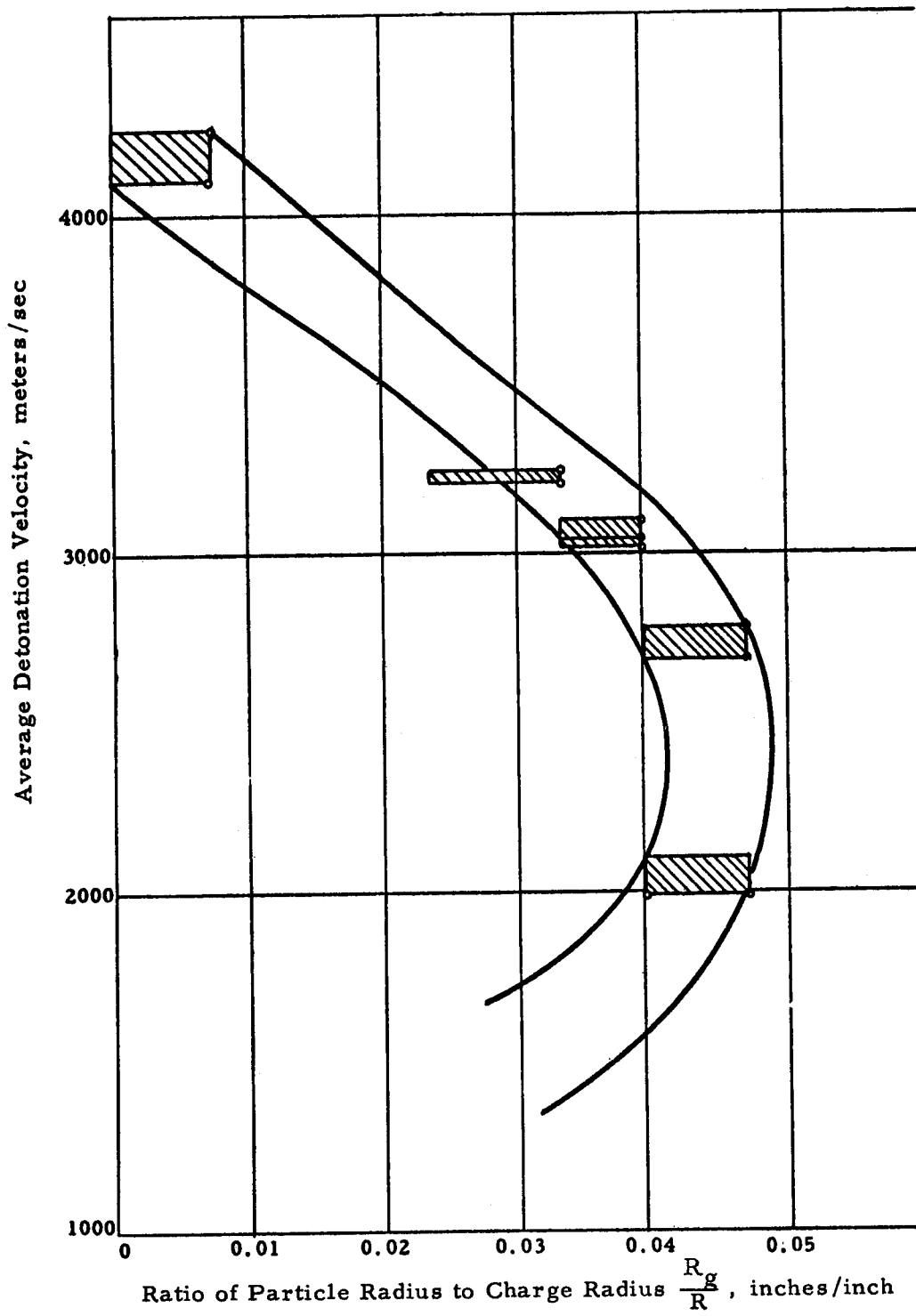
Figure 2 - Detonation velocity as related to particle size
for ammonium nitrate-fuel explosive charges
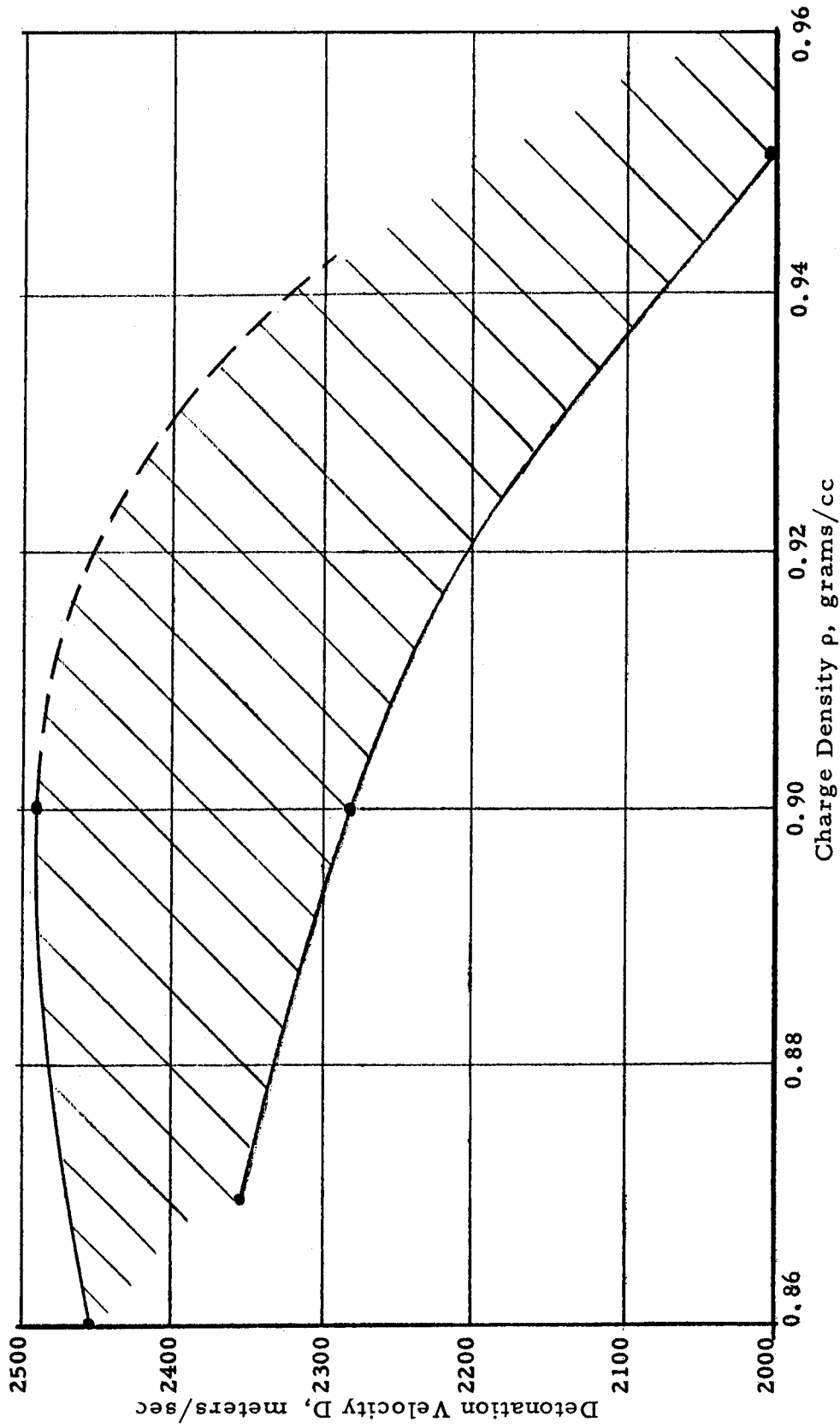
Figure 3 - Detonation velocity as a function of charge density. Explosive: 94/6
Spencer N-IV ammonium nitrate-fuel oil

With other explosives, it has been found that the range of nonideal detonation velocities which can persist for a reasonable fraction of the detonation time of a charge in the size range used in ordnance increases with decreasing densities. For lower densities, the range between the failure velocity and the stable velocity is increased, while the buildup from intermediate velocities to the stable rate is stretched out in time and distance. These observations are consistent with the fact pointed out by Eyring, that the Hugoniot temperatures of the nonreactive shocks (based on the assumption that the explosive is a homogeneous solid) is insufficient to result in a self propagating reaction, so the fact that such low velocity reactions are observed must be explained on the basis of nonuniform heating due to the inhomogeneity of the low density material. It may be surmised that much of the variability of the detonation velocity of ammonium nitrate-fuel mixtures is attributable to the very low bulk density at which these materials are generally used.

In addition to the factors mentioned above, nonideal detonation is affected by the confinement of surrounding materials (Table I). As has been pointed out in earlier work with other materials, the effectiveness of a confining medium is closely related to the ratio of its shock impedance (the product of the shock velocity and density) to the detonation impedance of the explosive. Because of its low detonation impedance, the mixture of ammonium nitrate with an organic fuel is well confined by materials which are negligible in their confining effects upon military high explosives. We have observed, for example, that an eighth-inch thick tube of lucite is appreciably more effective as a confining medium than a similar tube of cardboard. Results of underwater explosion measurements indicate that water is also a very effective confining medium for these mixtures.

Most of the energy of an underwater explosion is divided between that which produces a compression wave of the water, the shock energy, and that which causes gross movement of the water as a result of the relatively slow expansion of the reaction products, the bubble energy. The ratio of this partition is determined, for ideal detonations, by the equation of state of the reaction products. In nonideal detonations, substantial fractions of the reactions may be too slow to contribute to the propagation of detonation or, in turn, to the shock wave. In such situations, the output is strongly biased toward bubble energy. In materials such as HBX, the aluminum may be said to introduce an element of nonideality in addition to enhancing the total energy available.

Both the equation of state and the course of the reaction also affect the pressure-time profile of the wave. Where the destructive effects of a charge are of primary interest, the details of the pressure-time profile are of secondary interest. However, their effectiveness against various structures is not necessarily directly related to the energy of the pulse. In this respect, the peak pressure, the momentum (the time integral of pressure) and the energy (the time integral of pressure squared) are listed as properties of explosives. The

TABLE I. Results of Effects of Confinement and End Initiation
on the Axial Detonation Velocity

(Explosive: 94/6 Ammonium Nitrate Fuel Oil)

Charge Weight, lb	Density, grams/cc	Initiation System	Geometry of Confinement	Average Detonation Velocity, meters/sec
0.55	0.9	19.9 grams sheet explosive	acrylic tube 1.8" inside diameter X 7" long	1510
0.174	0.81	18.6 grams sheet explosive	acrylic tube 1.25" inside diameter X 1/8" wall X 5" long	1420
0.168	0.80	28.1 grams sheet explosive	acrylic tube 1.25" inside diameter X 1/8" wall X 5" long	1530
0.168	0.80	38.3 grams sheet explosive	acrylic tube 1.25" inside diameter X 1/8" wall X 5" long	3400
1.01	0.85	32 grams sheet explosive	acrylic tube 2.25" inside diameter X 1/8" wall X 8" long	2080
0.946	0.80	60.5 grams sheet explosive	acrylic tube 2.25" inside diameter X 1/8" wall X 8" long	2000
4.01	0.86	150 grams sheet explosive	cast acrylic tube 3.5" inside diameter X 1/8" wall X 13" long	2980
4.0	0.87	113 grams loose tetryl	cast acrylic tube 3.5" inside diameter X 1/8" wall X 13" long	1900
5.46	0.85	184 grams loose tetryl	cardboard tube 3.4" inside diameter X 1/8" wall X 22" long	1700

relationship of these quantities is, of course, determined by the gross characteristics of the pressure-time profile.

For most military organic explosives, the detonation is essentially ideal and for the aluminized explosives in charge sizes of military interest, the nonideality is a reproducible property of the explosive. In these cases, the shock pressure, energy and momentum, and the bubble energy are, for all practical purposes, properties of the explosive, which may be compared with a standard such as TNT. The nonideality of the detonation of ammonium nitrate-fuel explosives is a controllable variable, as illustrated in Figs. 4, 5 and 6, and may be expected to result in substantial predeterminable variability in the relationships of these quantities. Where an explosive charge is to be used as an acoustic source, the effects of this nonideality on some of the details of the profile which are not characterized by these quantities may be even more important. The underwater explosion measurements of 94/6 ammonium nitrate-fuel oil indicate that the nonideality observed in the detonation velocity experiments discussed above has significant and reproducible effects upon the nature of the output of the explosive to surrounding water. These effects are quite apparent in the tabulation of the underwater measurements (Table II). It is of interest to note that the systematic variation in detonation velocity as related to initiation is reflected in a parallel variation in pressure-time profile.

A frequent practice in commercial blasting is that of initiating ammonium nitrate-fuel explosives with Primacord. A common technique is that of stretching the Primacord down the blast hole, approximately centered and filling the hole with the explosive mixture. The longitudinal velocity of propagation of the detonation in such charges is, of course, that of the Primacord and yields little information regarding the behavior of the ammonium nitrate-fuel mixture. In an attempt to characterize this behavior as affected by the vigor of initiation, a series of centrally initiated charges of the configuration shown in Fig. 7, were observed end on by means of the Beckman-Whitley high-speed framing camera. The results, in Fig. 8 and Table III, show a progressive change in radial propagation velocity, D_R, ranging from 900 meters per second for charges axially initiated by means of 100 grains per foot Primacord to 3900 meters per second for charges initiated by means of 1.5 inch diameter tetryl pellets.

CONCLUSIONS

In light of the preceding explanation of the behavior of ammonium nitrate-fuel mixtures, and the experimental data herein presented, the following inferences and observations may be made:

(1) The detonation of most of the ammonium nitrate-fuel mixtures was quite significantly nonideal.

(2) The hammermilled material detonated at very nearly the ideal velocity for the 94/6 ammonium nitrate-fuel oil mixture.

317

Initiation: 3 inches of 100 gpf Primacord. Pressure attenuation: 1

Initiation: 3 inches of 400 gpf Primacord. Pressure attenuation: 1

Initiation: 125 grams of 40% gelatin extra. Total charge weight: 1 pound.
Pressure attenuation: 1

Figure 4 - Pressure-time profiles of one pound, 94/6, ammonium nitrate-fuel oil charges with varied initiation. Recorded 25 feet from charges 25 feet deep.

Sadwin, Stresau, Porter, Savitt
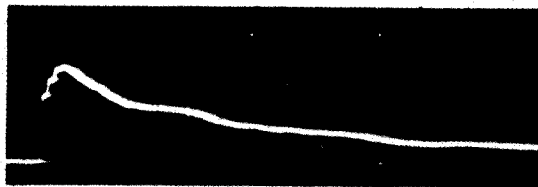
Initiation: 6 inches of 100 gpf Primacord. Pressure attenuation: 1
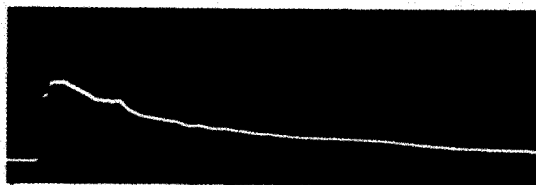
Initiation: 6 inches of 400 gpf Primacord. Pressure attenuation: 1
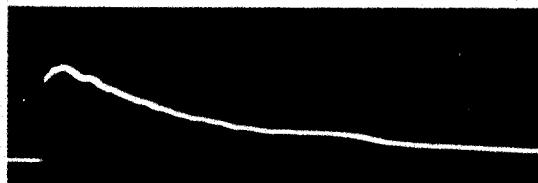
Initiation: 245 grams 40% gelatin extra. Total charge weight: 3 pounds.
Pressure attenuation: 1

Figure 5 - Pressure-time profiles of three pound, 94/6, ammonium nitrate-fuel oil charges with varied initiation. Recorded 25 feet from charges 25 feet deep.

Charge: 10 feet of 400 gpf Prima-
cord. Pressure attenua-
tion: 1

Charge: 196 grams (TNT +
initiation system)

Initiation: 29 grams of sheet
explosive. Pressure
attentuation: 1

Charge: 587 grams of 60% high
pressure gelatin.
Pressure attenuation: 1

Charge: 1 pound of 94/6 ammonium
nitrate-fuel oil.

Initiation: 3 inches of 100 gpf
Primacord.
Pressure attenuation: 1

Charge: 1 pound of 94/6 ammonium
nitrate-fuel oil.
Initiation: No. 8 ebc.
Pressure attenuation: 1

Charge: 8 pounds (ammonium
nitrate + molasses +
initiation system)
Initiation: 295 grams of 60% high
pressure gelatin.
Pressure attenuation: 2

Charge: 8 pounds (94/6 ammonium
nitrate-fuel oil +
initiation system)
Initiation: 295 grams of 60% high
pressure gelatin.
Pressure attenuation: 2

Figure 6 - Comparison of pressure-time profiles produced by
various explosive charges. Recorded 25 feet from charges
25 feet deep.
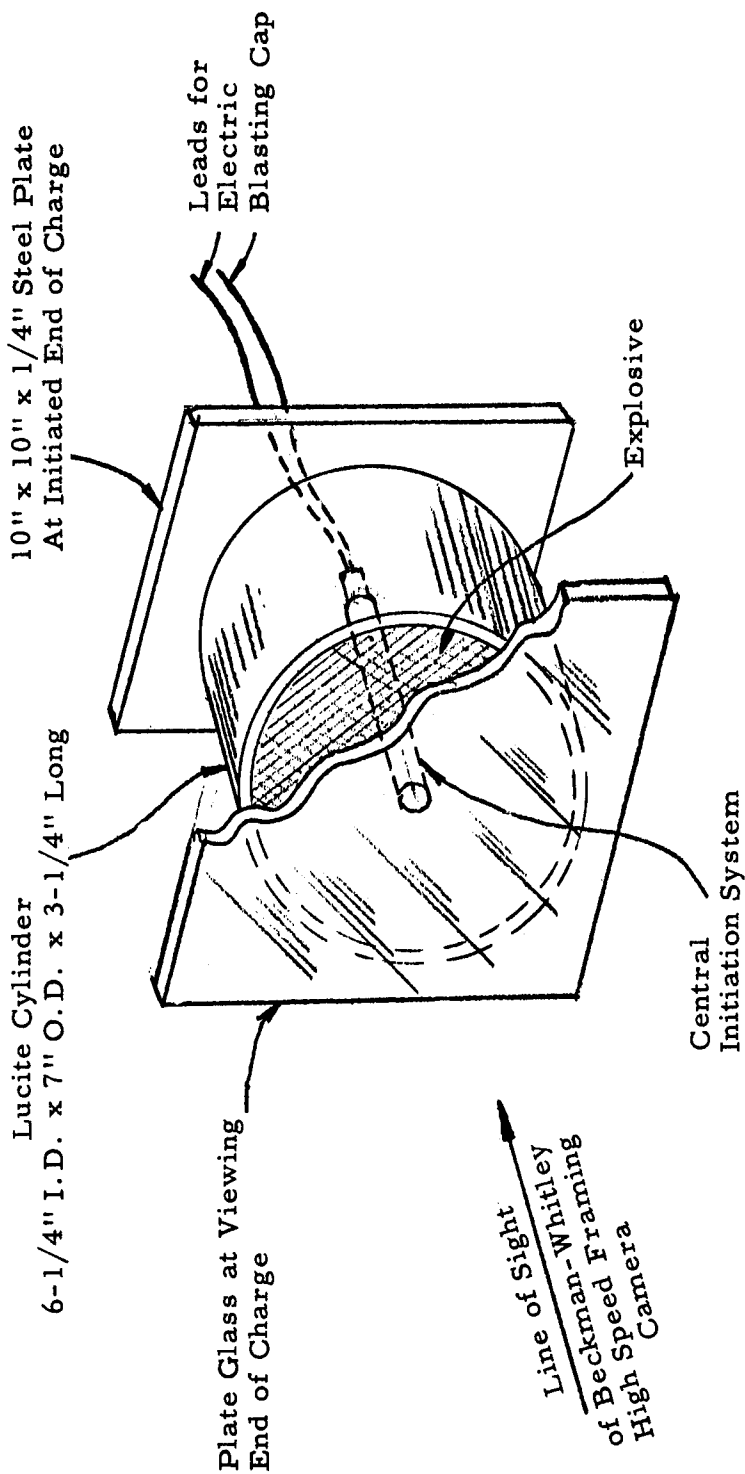
Figure 7 – Centrally initiated charge configuration used in studies of effects of vigor of initiation

Explosive: Spencer Chemical Co. N-IV Ammonium Nitrate plus 6% No. 2 Fuel Oil

Initiation: 100 gpf Primacord
D_R = 900 meters/sec

Initiation: 400 gpf
Primacord
D_R = 1100 meters/sec

Initiation: 9/16 inch
diameter tetryl pellets
D_R = 1900 meters/sec

Initiation: 2 inch diameter,
60% high pressure gelatin
D_R = 2300 meters/sec
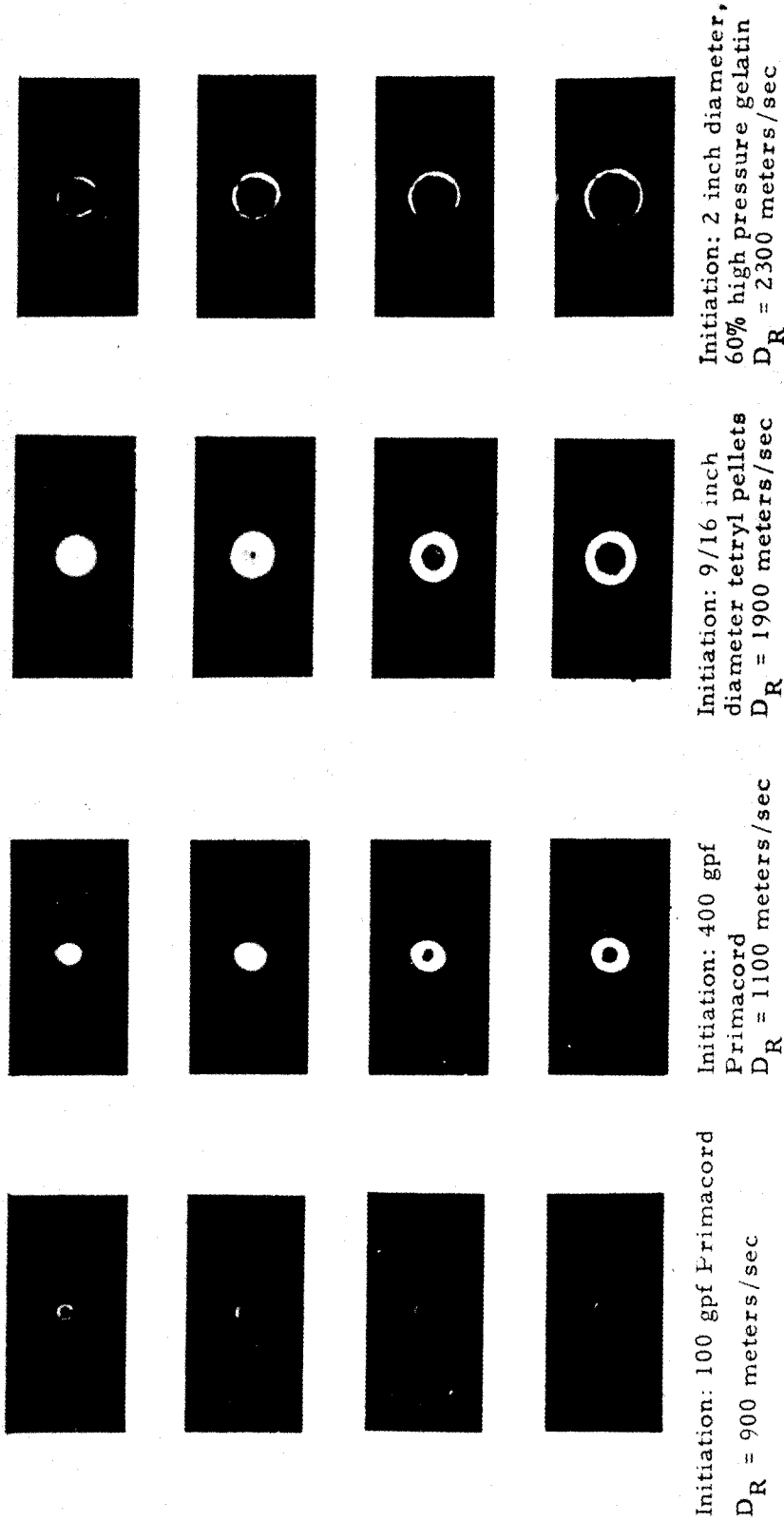
Figure 8 - Effects of vigor of initiation on detonation front expansion. Viewed by Beckman-Whitley high speed framing camera. Time between successive frames— 2 microseconds. Charge configuration of Figure 7.

TABLE II

Underwater Explosion Measurements, Explosive:
94/6 N-IV Ammonium Nitrate Prill -- No. 2 Diesel Fuel

Initiation System	Charge Weight lb.	Bubble Energy cal/gram	Shock Energy cal/gram
3 inches of 100 gpf Pc*	1.0	276	43
3 inches of 100 gpf Pc	1.0	300	--
12 inches of 100 gpf Pc	1.0	388	--
6 inches of 100 gpf Pc	3.0	357	56
4 inches of 100 gpf Pc	8.0	543	71
3 inches of 200 gpf Pc	1.0	373	--
3 inches of 400 gpf Pc	1.0	471	27
6 inches of 400 gpf Pc	3.0	550	49
125 grams of 40% gelatin extra	1.0 Total	400	104
127 grams of 40% gelatin extra	1.0 Total	347	--
245 grams of 40% gelatin extra	3.0 Total	521	47
107 grams of 60% high-pressure gelatin	1.0 Total	540	--
295 grams of 60% high-pressure gelatin	8.0 Total	605	86
No. 8 ebc**	1.0	20	--

* gpf Pc = grains per foot Primacord

** ebc = electric blasting cap

NOTE: Measured 25 feet from charges 25 feet deep

TABLE III

Results of Effects of Central Initiation
on the Radial Propagation Velocity

(Explosive: 94/6 Ammonium Nitrate-Fuel Oil)

Central Initiation System	Average Radial Propagation Velocity, meters/sec
0.56 " diameter tetryl pellet	1900
0.75" diameter tetryl pellet	2750
1.5" diameter tetryl pellet	3900
100 gpf Primacord	900
200 gpf Primacord	1050
400 gpf Primacord	1100
2" diameter 60% high-pressure gelatin	2300

(3) The bimodal velocity distribution, which is predicted by the relationship derived by Eyring and associates,[1] and which has been observed in other explosives, is quite apparent in much of the data.

(4) A large fraction of the measured velocities correspond with the knee of the rate-diameter relationship, (Fig. 1). In this region, small variations, not only in initiation, but in intimacy of mixture, confinement, particle size distribution, and charge size, can cause substantial variations in velocity.

(5) The larger charges now used in most commercial applications of ammonium nitrate-fuel explosives probably fall farther from the knee of the curve, so they may be expected to have a more definitely bi-modal distribution. If so, their detonation velocities, if they are adequately initiated, will be higher than those observed in most of the experiments. The lower velocity mode of detonation propagation becomes more and more metastable as the charge diameter is increased. Slight variations in vigor of initiation, confinement, or other conditions can cause the detonation to either decay to failure or build up to the stable rate. Of course, even if curves of the type shown in Fig. 2 are generally applicable to these explosives, the abscissa of the coordinate system must contain a confinement factor. The relationship between this factor for a particular application and that for the experiments conducted remains to be investigated.

ACKNOWLEDGEMENT

REFERENCES

(1) H. Eyring, R. E. Powell, G. H. Duffy, and R. B. Parlin, "The Stability of Detonation," Chemical Reviews, Vol. 45, 1949, pp 69-181.

(2) S. J Jacobs, et al, OSRD Report No. 1755.

(3) S. J. Jacobs, "Closed Bomb Burning of High Explosives and Propellants," OSRD Report No. 6329, Jan. 22, 1946.

THE DETONATION VELOCITY OF PRESSED TNT*

M. J. Urizar, E. James, Jr., and L. C. Smith
Los Alamos Scientific Laboratory
University of California
Los Alamos, New Mexico

ABSTRACT

The detonation velocity of pressed TNT has been determined as a function of charge diameter at each of a series of loading densities. Current theories of the diameter effect are discussed and used to compute infinite diameter detonation velocities (D_∞) and detonation reaction zone lengths from the experimental data. The results for the velocity-density dependence may be summarized as follows:

$$D_\infty = 1872.7 + 3187.2\,\rho \qquad (0.9 \leq \rho \leq 1.5342 \text{ gm/cc})$$

$$D_\infty = 6762.5 + 3187.2\,(\rho - 1.5342) - 25{,}102\,(\rho - 1.5342)^2$$

$$+ 115{,}056\,(\rho - 1.5342)^3 \qquad (1.5342 \leq \rho \leq 1.636 \text{ gm/cc})$$

The reaction zone lengths computed from the data are a decreasing function of the charge density and are in good agreement with predictions based on the grain-burning model of the reaction zone.

I. INTRODUCTION

The velocity of detonation is a fundamental and readily measured characteristic property of a high explosive, and it has received considerable study, both experimental and theoretical. Phenomenologically, the detonation velocity of a given explosive depends most importantly on the loading density, the size, and the amount and type of lateral confinement of the charge. Theoretical studies of the detonation process have shown that the density dependence has a thermodynamic origin -- specifically, in the nonideality of the equation of state of the detonation products at the temperatures

---

327

and pressures involved. The remaining two factors have similarly been shown to be related to the kinetics of the reaction which converts the unburned explosive to its detonation products.

The detonation process is most simply studied theoretically on the basis of an idealized, one-dimensional hydrodynamic model. The detonation properties deduced from such a model are independent of both the size and confinement of the system (of its kinetics, in fact), and the detonation velocity, in particular, is customarily referred to as the infinite diameter, plane-wave velocity. It is of importance in such studies to have available accurate experimental data on the infinite diameter velocities of various explosives, and in this paper we present the results of an experimental program whose principal objective was to obtain such data on pressed TNT over the accessible range of loading densities.

It is obvious that to achieve this objective requires some sort of an extrapolation from finite charge data. Our work is based on the assumption that the detonation velocity of a finite charge is related to the infinite diameter velocity by the equation [1]

$$D = D_\infty \left(1 - \frac{a}{2R}\right).$$ (1)

Here D is the detonation velocity of a cylindrical charge of radius R, a is assumed independent of R (but a function of the explosive, loading density, and confinement), and D_∞, as the notation suggests, is the infinite diameter velocity. This equation accurately represents our results over the range of charge diameters included in this study. Other work done at this Laboratory, both by others and by us[2], indicates that the equation does not necessarily hold in the region of very small charge diameters, and this has recently been verified in the case of TNT, in particular, in a contemporary study of this explosive by Stesik and Akimova.[3]

The procedure, then, was to determine the detonation velocity as a function of charge diameter at each of a series of loading densities. The corresponding values of D_∞ are then estimated from least square fits of equation (1) to the experimental data. It is obvious that this procedure simultaneously provides estimates of the quantity a under various conditions, and in the discussion the significance of this quantity is discussed in terms of current theories of the diameter effect.

II. EXPERIMENTAL

A. Explosive

All the data reported here were obtained with a single lot of commercial TNT (2,4,6-trinitrotoluene) manufactured in August 1944 by the Atlas Powder Company. Its melting point, as determined from a cooling curve, was 80.55°C, and its purity was estimated as 99.6 mole percent. The principal impurities are presumed to be the other

TNT isomers and the dinitrotoluenes, as these are usually found in the typical commercial product. The results of a sieve analysis of the granular material, before pressing, are given in Table I.

TABLE I

TNT PARTICLE SIZE ANALYSIS

U.S. Std Sieve No.	Sieve Opening (microns)	Cumulative (% Retained on)	Differential (%)
40	420	0.4	1.2
50	300	1.6	9.6
70	210	11.2	48.8
100	149	60.0	13.8
120	125	73.8	14.8
140	105	88.6	7.8
200	74	96.4	0.8
230	62	97.2	1.2
325	44	98.4	

B. Charge Preparation

All the low-density charges (below 1.4 gm/cc) were prepared and fired in 0.2" wall brass tubes, primarily to contain, and prevent damage to, the more fragile low-density pressings, but these tubes also provided confinement in the detonation velocity measurements, reducing the magnitude of the diameter effect and thereby permitting a more accurate estimate of D_∞. Unpublished measurements made at this Laboratory indicate that the limiting effectiveness of brass in reducing the diameter effect in Composition B is reached at a wall thickness of less than 0.1",[4] while, for 60/40 Amatol, Copp and Ubbelohde[5] found that limiting effectiveness of steel was reached with a wall thickness of less than 0.2". Confinement by 0.2" of brass is thought to be more than adequate for pressed TNT, and the use of thicker tubes in any event would have created difficulties in obtaining accurate weights on the loaded tubes with the balances which were available.

It is important to note in this connection that the shock velocity in the confining medium must not exceed the detonation velocity of the explosive, as the explosive will otherwise be compressed at the wall by the shock in the tube, and the velocity obtained will not be that corresponding to the initial charge density. Roughly speaking, brass is a satisfactory confining medium for velocity measurements down to about 4000 m/sec.

Most of the data reported here on high-density TNT were obtained with unconfined charges, although in a few cases confined high-density charges were fired to verify that the value of D_∞ obtained was independent of the technique used.

The brass tubes were prepared and measured by professional machinists, starting with extruded tubing of convenient size. The nominal inside diameters and lengths of the finished tubes were as follows:

ID (in.)	Length (in.)
0.7683	3.000
1.0250	3.000
1.5385	3.000
3.077	6.000

A 0.5" wide by 0.005" deep notch was milled in one end of each tube to provide space for the pin foils in the shot assembly.

Each tube was carefully weighed on an analytical balance of the appropriate capacity before and after loading to obtain the total weight of explosive in the finished charge. The tubes were loaded to the desired density, one inch at a time, by pressing the explosive directly into them. For the last increment or two, an auxiliary loading sleeve which meshed with the notch on the upper end of the tube was used to contain the loose explosive and to serve as a guide for the punch. The loading was done in increments to minimize density variations along the length of the charge. Radial density variations were controlled by carefully distributing the loose powder in the tube before pressing the increment. The desired finished height of each loading increment was obtained by using punches of different lengths, together with spacers of the appropriate heights inserted between the upper flange of the punch and the end of the tube or loading sleeve.

During the pressing, the bottom end of the tube rested on a flat Lucite plate, and at this end the face of the charge after pressing was flat and flush with the end of the tube to within 0.001" or better. At the top the situation was somewhat different. In the first place, to provide space for the pin foils without introducing gaps between successive tubes in the shot assembly, the finished height of the explosive was held at $^{+0.000}_{-0.003}$" relative to the end of the tube. In addition, in the case of the larger diameter, medium-density charges, there was a tendency for this end of the charge to bow out as a result of reexpansion. This could be corrected by placing a 1/2" thick Lucite plate on the end of the charge and pressing on its center with an undersized punch. With some experience this could be done in such a way that after reexpansion had occurred, the charge was flat and of the desired length.

The high-density unconfined charges were made by pressing 6" diameter by 4" high stock pieces in a locally available die, and machining from these cylindrical charges of the desired sizes. The same diameters and lengths were used as before in most cases, except that the 6" long pieces were made up of two 3" long cylinders. Only those parts of the stock pieces were used which were reasonably

uniform in density. The finished cylinders were quite rigid and could be measured and handled without difficulty.

The high-density confined charges were prepared in the same way, except that after machining, the cylinders of explosive were cooled slightly and slipped into the confining tubes. Upon rewarming to room temperature, the explosive expanded, giving a snug fit in the tube.

C. Velocity Measurements

The detonation velocity measurements were made by a group working under the supervision of A. W. Campbell, using a technique which has already been described in detail elsewhere.[6] Only a few special features of the shot assembly, as it evolved after considerable experimentation, will be described here.

Each shot was made up of approximately nine increments, with transit-time pin foils inserted at the end of each increment (see Fig. 6 of ref. 6). Thus the 3" diameter charges were (generally) 54" long, the others 27" long. The charges were initiated by means of a detonator, a small tetryl pellet, and a 1" thick pad of Composition B. With this type of initiation the detonation velocity of the charge had become stable after it had traveled through two, or at most three, of the nine increments, so that six or seven data points were normally obtained from each shot. The whole assembly was held together by clamps to insure good contact between successive components of the train. In the case of small-diameter unconfined charges this must be done carefully, for if excessive clamping pressure is used, the charge will be shortened significantly and the velocity obtained will be too high. It is necessary to check the total length of the charge, after clamping, against the sum of the lengths of the individual increments to insure that the proper amount of pressure is being applied.

After each shot had been assembled, it was placed in an insulated box and its temperature was adjusted to 75 ± 5°F before it was fired.

D. Sources of Error

The velocity measuring technique described above and in ref. 6 has been developed to such an extent that charge quality has become the determining factor in the over-all precision of the data. Accordingly, our discussion here will be largely devoted to the problem of measuring charge density, and to the control and effects of density variations within the charge.

From the data presented later it can be seen that an error of 0.001 gm/cc in determining the density of a charge corresponds to an error of about 3 m/sec in the detonation velocity. It is therefore essential that the charge density be determined with considerable accuracy. In our experiments this problem was most serious in the

case of the smallest diameter charges. Therefore only these will be discussed, and it will be left as understood that the errors are proportionately smaller for the larger charges.

The densities of all confined charges prepared by pressing the explosive directly into the confining tubes were derived from measurements of the inside diameters and lengths of the tubes, and from their weights before and after loading. Our best estimates for the uncertainties in these quantities are as follows:

Measurement	Uncertainty
Weight of explosive (corrected for buoyancy)	< 1/10,000
Length	2/10,000
Diameter	7/10,000

It follows that the maximum uncertainty in the density is somewhat less than 0.003 gm/cc. We believe that the errors in these measurements are primarily random, and hence their effect would be expected to appear as a loss of precision rather than accuracy.

It will be recalled that in pressing the final increment into the tube, the finished surface of the explosive was allowed to be as much as 0.003" below the end of the tube. The reason the length of the tube, rather than the actual height of the explosive, is the dimension used in the volume calculations is that compensating effects are present. If the actual height of explosive in a particular increment were 2.997" instead of 3.000", the actual density of that increment would be higher than our recorded density by one part in a thousand. As a result, the transit time through the column of explosive would be 0.02 - 0.03 μsec less than it would be if the actual height of explosive were 3.000". However, we estimate that this is just about the time required for the product gases to move across the 0.003" gap and initiate the next increment, so that the two effects should cancel very closely. Since the size of the gap between various increments of the charge varied from zero to three mils, the over-all error in the measurements from this source is probably negligible. The variation in the length of the gap, and in the position of the pin foils within the gaps, will contribute slightly to the standard deviation of the data.

The densities of the high-density charges were determined directly from measurements of the weights and dimensions of the pieces and were corrected for buoyancy. The reported densities are estimated to be accurate to +0.002 gm/cc for the 3/4" diameter charges. The water displacement method was used to check the results in some cases, and the densities determined by the two methods of measurement agreed to within the assigned experimental error.

Density variations within the charge also are a problem in precise detonation velocity measurements on pressed explosives, and two types are recognizable in charges such as we are describing here. The first, which we refer to as axial, is a periodic variation in density along the length of the charge which is an unavoidable consequence of the incremental loading procedure. As each loading increment is pressed, the material next to the punch is compressed to a higher density than the material at the bottom of the increment. The result is a sawtooth variation in density along the charge whose wavelength and amplitude are direct functions of the length of the loading increment (one inch in our work). The shorter the increment, the lower the amplitude, and, of course, the shorter the wavelength. The second type, referred to as radial, is a nonuniformity in density in any plane perpendicular to the axis of the charge. Careful distribution of the powder in the tube or die before pressing will decrease the radial density variations, but it will not eliminate them entirely unless the bulk explosive is very uniform. Radial density variations become worse when very short increments are pressed, since a slight unevenness in the distribution or packing of the loose powder will produce a proportionately larger variation in density.

We attempted to evaluate the effect of axial density variations by deliberately introducing large variations in an experimental charge. First, a 3"ID x 4" OD x 6" long polystyrene tube was loaded in one-inch increments. The increments were weighed out to give alternating densities of 1.35 and 1.25 gm/cc. After the tube was loaded, the densities of the successive increments were determined by X-ray absorption technique.[7] The results were as follows:

Increment	Intended Density (gm/cc)	Measured Density (gm/cc)
Top	1.25	1.25
5	1.35	1.29
4	1.25	1.30
3	1.35	1.31
2	1.25	1.31
Bottom	1.35	1.36

The precision of the X-ray method used is about 1% in density, and it is obvious that only the top and bottom increments are significantly different from the average. Nevertheless, this loading procedure would be expected to exaggerate whatever axial density spreads are present in our rate sticks, so a 3" diameter rate stick was prepared in brass tubes by this method, and a second was prepared at the same time using our usual loading procedure. The velocities of the two charges were measured with the following results:

Loading Method	Ave Over-all Density(gm/cc)	No. Velocity Increments	Average Velocity	$\pm$ L_{95}
Nonuniform	1.300	7	5987.9	6.1
Uniform	1.300	7	5985.3	6.4

Our conclusion is that axial density fluctuations of this wavelength are not a limiting factor in the over-all precision of our results.

This is not entirely unexpected, since the detonation wave does not respond instantaneously to changes in local conditions,[1] and hence there is a significant damping out of the effects of density variations providing these are commensurable in size with the build-up (or build-down) distance of the detonation wave. This is true both for axial and radial inhomogeneities in density.

We have also attempted to use the X-ray absorption method to estimate the magnitude of the radial density variations in a single increment. These appear to amount to about $\pm$ 0.010 gm/cc in typical charges. It is important to avoid systematic radial density variations. For example, if the loose explosive is simply poured into the tube in such a manner as to assume a cone shape, and the increment is then pressed without redistributing the explosive, the central core of the whole charge will be above average density, and this high-density core will control the rate of propagation of the wave. In other words, the observed velocity will correspond to the density of the core, rather than to the average density of the charge. We have verified this statement experimentally with other explosives, but the results are not sufficiently novel to merit detailed reporting here.

Density variations as large as 0.010 gm/cc are known to be present in the lower density pieces cut from the 6" x 4" stock charges. An attempt was made to minimize systematic errors from this source by cutting the rate sticks from selected regions of the stock charge.

At densities near crystal density, such problems as internal density spreads, errors in the measurement of over-all density, and gaps in the shot assembly, are eliminated or greatly reduced in magnitude, and generally somewhat better statistics were obtained in the velocity measurements on the highest density charges.

III. DATA AND ANALYSIS

The rate stick data were analyzed by the difference method, which has been shown to be the correct procedure for cumulative straight-line data such as we obtain.[8] After discarding the first two or three observations (representing the booster section), we compute the detonation velocities over the remaining individual increments, and then obtain the average velocity, and its variance and 95% confidence limit ($\pm$ L_{95}), in the usual way.

In some cases this procedure had to be modified to correct for nontrivial variations in the densities of the individual increments within the charge. The correction is made by adjusting the incremental velocities by an amount

$$(\bar{\rho} - \rho) \left(\frac{\partial D}{\partial \rho} \right)_{\bar{\rho}}$$

where $\bar{\rho}$ is the average density of the rate section, ρ is the density of the increment in question, and $\left(\frac{\partial D}{\partial \rho} \right)_{\bar{\rho}}$ is the slope of the velocity -density curve at $\bar{\rho}$. For reasons already mentioned, this probably represents an over-correction, but it is usually small, and in any event its only effect is on the variance and confidence limit.

One additional adjustment is usually necessary before proceeding to the next step in the analysis. In fitting equation (1) we require that the velocities corresponding to the various diameters be obtained at a common density. In practice this could not always be achieved, and hence in each diameter series it was usually necessary to adjust one or more of the velocities, using the same correction factor as before. The corrections in this case can be made with considerable confidence.

The data analysis of a typical shot is displayed in Table II. A summary of the charge data and final velocities is given in Table III. We attach little significance to the individual $\pm L_{95}$'s appearing in this table since the sampling errors in estimating such a statistic in a single experiment are large. They do provide an indication of the dispersion of the incremental velocities observed in the various shots. However, in making the least squares fits to equation (1) we have elected to treat each shot as a single independent observation of weight unity, and no further use is made of these particular $\pm L_{95}$'s in the subsequent discussion.

The remainder of the analysis is carried out in two steps, the first of which involves obtaining the least squares fits of equation (1) to the experimental data. This is straightforward, and the results are summarized in Table IV. From each fit we obtain an independent estimate of the variance of the underlying population, S_i^2. These were tested and found to be homogeneous by Bartlett's test, [9] implying that the true variance, σ^2, is independent of ρ (the test also was made on the confined and unconfined shots separately, with the same result). The variances were therefore pooled and a value of 19.1, with 42 degrees of freedom, was obtained.

The second step is somewhat more complicated and involves obtaining a least squares fit of a suitable equation to the velocity-density data $(D_\infty \text{ vs } \rho)$. Preliminary computation indicated that, with considerable accuracy, D_∞ is a linear function of ρ up to a density of about 1.53 gm/cc, but that at higher densities a polynomial fit would be required. The fitting procedure finally adopted was as

335

TABLE II - TYPICAL SHOT DATA ANALYSIS

Nominal Density 1.5127 gm/cc - Diameter 2.603 cm - Unconfined

Increment No.	Uncorrected Density (gm/cc)	Increment Length (cm)	Average Incremental Transit Time (μsec)	Uncorrected Det Vel (m/sec)	$\bar{\rho} - \rho$ (gm/cc)	$\left(\dfrac{\partial D}{\partial \rho}\right)(\bar{\rho}-\rho)$ (m/sec)	Corrected Det Vel (m/sec)
1	1.516	7.6225	(Booster)				
2	1.498	7.6200	(Booster)				
3	1.515	7.6200	11.4579	6650.4	-0.009	-28.5	6621.9
4	1.502	7.6200	11.5204	6614.3	0.004	12.7	6627.0
5	1.504	7.6197	11.5129	6618.4	0.002	6.3	6624.7
6	1.506	7.6208	11.5031	6625.0	0.000	0.0	6625.0
7	1.505	7.6200	11.5054	6623.0	0.001	3.2	6626.2
8	1.505	7.5692	11.4305	6621.9	0.001	3.2	6625.1
9	1.505	7.6200	11.4997	6626.2	0.001	3.2	6629.4
Averages (Incr. 3 - 9)	1.5069[a]			6625.6			6625.6
Variance				135.9			5.3
Std Dev				11.6			2.3
95% Conf. Interval				± 10.7			± 2.1
Adjustment of D to Nominal Density	1.5127				0.0058	18.4	6644.0

[a] After buoyancy correction.

TABLE III - SUMMARY OF SHOT DATA

Confined Charges

| Density (gm/cc) | Dia (cm) | Length of Increment (cm) | No. of Increments | | D(m/sec) | $\pm$ L$_{95}$ |
			Booster Section	Rate Section		
0.9009	1.951	7.620	3	6	4587.2	3.2
0.9009	2.603	7.620	2	7	4632.3	6.8
0.9009	3.906	7.620	2	7	4663.6	5.7
0.9009	7.816	15.240	2	7	4713.4	5.1
1.0511	1.951	7.620	2	7	5052.4	13.1
1.0511	2.603	7.620	2	7	5103.0	4.6
1.0511	3.906	7.620	2	7	5133.7	9.7
1.0511	7.816	15.240	2	7	5180.8	6.8
1.2008	1.954	7.620	2	7	5568.8	8.0
1.2008	2.605	7.620	2	7	5598.3	4.7
1.2008	3.908	7.620	2	7	5623.6	3.1
1.2008	7.815	15.240	2	7	5662.1	5.6
1.3005	1.905	7.620	2	7	5900.0	7.7
1.3005	2.605	7.620	3	6	5926.9	10.7
1.3005	2.605	7.620	2	7	5925.7	5.6
1.3005	3.908	7.620	2	7	5951.9	6.6
1.3005	3.908	7.620	2	7	5955.4	8.6
1.3005	7.815	15.240	2	7	5990.0	4.8
1.3005	7.816	15.240	2	7	5982.2	6.0
1.4470	1.951	7.620	3	6	6401.2	10.4
1.4470	1.951	7.620	2	7	6398.9	11.6
1.4470	2.603	7.620	2	7	6417.7	2.7
1.4470	2.603	7.620	2	7	6425.9	11.9
1.4470	3.908	7.620	2	7	6442.1	11.1
1.4470	3.906	7.620	2	6	6443.9	7.0
1.4470	7.816	15.240	2	6	6466.9	2.1
1.4470	7.823	15.240	2	7	6469.8	5.4
1.5342	1.951	7.620	2	7	6732.9	6.3
1.5342	2.603	7.620	2	7	6722.0	11.7
1.5342	3.906	7.620	3	6	6742.2	10.4
1.5342	7.813	15.240	2	7	6743.6	5.9
1.5695	1.951	7.620	2	7	6816.5	4.0
1.5695	2.603	7.620	2	7	6824.9	2.4
1.5695	3.906	7.620	2	7	6833.8	0.8
1.5695	7.816	15.240	2	7	6831.6	1.8

TABLE III - Continued

SUMMARY OF SHOT DATA

Confined Charges

Density (gm/cc)	Dia (cm)	Length of Increment (cm)	No. of Increments Booster Section	Rate Section	D(m/sec)	$\pm L_{95}$
1.6359	1.951	7.620	2	7	6933.0	2.1
1.6359	2.603	7.620	2	7	6934.6	1.6
1.6359	3.909	7.620	2	7	6938.5	4.0
1.6359	7.823	15.240	2	7	6941.4	3.1

Unconfined Charges

Density (gm/cc)	Dia (cm)	Length of Increment (cm)	No. of Increments Booster Section	Rate Section	D(m/sec)	$\pm L_{95}$
1.4407	1.951	7.620	2	6	6372.1	8.6
1.4407	3.906	7.620	2	7	6423.3	5.2
1.4407	7.823	12.700	3	6	6447.5	5.4
1.5127	1.951	7.620	1	8	6624.9	1.7
1.5127	2.603	7.620	2	7	6644.0	2.1
1.5127	3.906	7.620	3	6	6661.7	7.6
1.5127	7.818	7.620	4	5	6684.5	9.4
1.5127	7.818	7.620	4	5	6681.1	23.9
1.5627	1.951	7.620	1	8	6802.7	3.4
1.5627	2.603	7.620	2	7	6812.9	2.3
1.5627	3.906	7.620	3	6	6831.9	30.3
1.5627	7.818	7.620	4	5	6823.2	8.6
1.5627	7.818	7.620	4	5	6832.1	14.7
1.6094	1.951	7.620	1	8	6901.8	3.5
1.6094	2.603	7.620	2	7	6907.4	21.3
1.6094	3.906	7.620	2	7	6902.9	16.9
1.6094	7.816	7.620	4	5	6909.7	3.0
1.6094	7.816	7.620	4	5	6907.4	5.2
1.6238	1.951	7.620	2	6	6933.3	3.2
1.6238	2.603	7.620	2	7	6929.1	5.4
1.6238	3.909	7.620	2	5	6926.8	6.3
1.6238	7.823	15.240	5	4	6930.3	1.9
1.6251	0.693	5.080	2	7	6906.4	10.8
1.6251	0.846	5.080	1	3	6905.3	5.7
1.6251	1.090	5.080	2	7	6922.1	2.3
1.6251	1.524	5.080	2	7	6923.6	1.3
1.6251	2.540	5.080	2	7	6926.4	5.2
1.6251	7.620	5.080	2	7	6928.3	4.1

TABLE III - Continued

SUMMARY OF SHOT DATA

Unconfined Charges

Density (gm/cc)	Dia (cm)	Length of Increment (cm)	No. of Increments		D(m/sec)	$\pm L_{95}$
			Booster Section	Rate Section		
1.6324	1.951	7.620	1	8	6936.6	2.3
1.6324	2.606	7.620	1	7	6941.1	7.9
1.6324	3.909	7.620	2	7	6943.6	9.0
1.6324	7.818	7.620	4	5	6941.2	3.7
1.6324	7.818	7.620	4	5	6941.9	5.2

TABLE IV - ANALYSIS OF DATA

Density Index i	Density (gm/cc)	No of Shots at i^{th} Dens N_i	First Stage of Analysis				Second Stage of Analysis	
			D_∞ (m/sec)	S_1^2	a (mm)	$\pm L_{95}$ [a]	D_∞ (m/sec) [b]	$\pm L_{95}$
	Confined Charges							
1	0.9009	4	4751.5	28.8	0.673	0.102	4,744.3	15.1
2	1.0511	4	5221.3	34.3	0.621	0.093	5,222.9	11.0
3	1.2008	4	5689.5	17.7	0.419	0.085	5,700.0	7.7
4	1.3005	7	6012.2	14.1	0.366	0.053	6,017.8	6.3
5	1.4470	8	6489.8	8.5	0.272	0.049	6,484.7	6.9
6	1.5342	4	6748.2	31.2	0.060	0.071	6,762.6	8.5
7	1.5695	4	6840.2	17.4	0.062	0.071	6,848.9	8.5
8	1.6359	4	6944.1	0.5	0.033	0.070	6,948.2	13.4
	Unconfined Charges							
9	1.4407	3	6473.0	00.7	0.304	0.077	6,464.6	6.8
10	1.5127	5	6701.6	2.7	0.224	0.061	6,694.1	8.0
11	1.5627	5	6839.2	53.0	0.097	0.061	6,835.7	7.6
12	1.6094	5	6909.7	7.9	0.020	0.061	6,909.3	12.1
13	1.6238	4	6927.0	7.8	-0.013	0.033	6,929.4	8.0
14	1.6251	6	6933.6	20.8	0.027	0.018	6,931.3	7.9
15	1.6324	5	6944.0	4.4	0.016	0.059	6,942.5	10.2

a Computed from S_1^2

b Detonation velocity predicted by equation (3).

follows:[10] We define a step function

$$F(\rho, \rho^*) = 0 \qquad \rho \leq \rho^*$$

$$= 1 \qquad \rho > \rho^*$$

and write

$$D_\infty = a_0 + a_1 \rho + F(\rho, \rho^*) \left[a_2(\rho - \rho^*)^2 + a_3(\rho - \rho^*)^3 \right] \qquad (2)$$

The least squares normal equations are readily obtained for this function in the usual way. However, since the experimental design was not symmetrical (i.e., the diameters and numbers of shots fired are not the same for all densities), the correct procedure is a weighted least squares analysis with weight factors

$$w_i = \frac{N_i \displaystyle\sum_{j=1}^{N_i} (\delta_{ij} - \bar{\delta}_i)^2}{\displaystyle\sum_{j=1}^{N_i} \delta_{ij}^2}$$

where $\delta = 1/2R$, and i and N_i are as in Table IV. By a trial and error method it was determined that an appropriate value for ρ^* was 1.5342 gm/cc; that is, values of D_∞ for densities greater than this exhibit significant departure from the linear part of equation (2). The final result of the analysis is as follows:

$$D_\infty = 1872.7 \pm 37.2 + (3187.2 \pm 27.1)\, \rho + F(\rho,\, 1.5342) \left[(-25,102 \right.$$

$$\left. \pm 10,212)\, (\rho - 1.5342)^2 + (115,056 \pm 103,667)\, (\rho - 1.5342)^3 \right] \qquad (3)$$

The $\pm$ values in this equation are the 95% confidence limits of the coefficients.

This part of the analysis also provides an independent estimate, S_2^2, of the variance of the underlying population. We find $S_2^2 = 47.3$ with 11 degrees of freedom. The ratio S_2^2/S_1^2 is 2.48, from which it is concluded by the v^2 test[11] that the two variances are from different populations. The observed ratio only slightly exceeds the critical ratio, 2.32 (5% level), and it is quite possible that this conclusion is the result of a small fitting error introduced into the analysis by our assumption as to the form of equation (2). However, the use of a more complicated expression hardly seems justifiable.

The last two columns of Table IV contain the values of D_∞ computed from equation (3) and their 95% confidence intervals. The confidence intervals are obtained from the equation.

$$\pm L_{95} \text{ of } D_\infty = \text{"t"}(0.95,11) \, S_2 \left[\frac{1}{15} + \sum_{k=1}^{3} (X_k - \bar{X}_k)^2 \, C_{kk} + \sum_{\ell} \sum_{k \neq \ell} (X_k - \bar{X}_k)(X_\ell - \bar{X}_\ell) \, C_{k\ell} \right]^{1/2}$$

where $X_1 = \rho$, $X_2 = (\rho - \rho*)^2$, and $X_3 = (\rho - \rho*)^3$. The $C_{k\ell}$ are the elements of the covariance matrix. Their values are

$$C_{11} = 3.2232 \qquad\qquad C_{12} = -4.846 \times 10^2$$

$$C_{22} = 4.564 \times 10^5 \qquad\qquad C_{13} = 4.036 \times 10^3$$

$$C_{33} = 4.674 \times 10^7 \qquad\qquad C_{23} = -4.582 \times 10^6.$$

Figures 1 and 2 are deviation plots for the reciprocal diameter fits. They indicate quite clearly that our diameter effect data do not depart from the form of equation (1) in any systematic way. In Fig. 3, the upper curve is a deviation plot for the whole of equation (3), while the lower curve illustrates the manner in which the high-density data depart from the extrapolated linear portion of that equation.

IV. DISCUSSION

We have seen that equation (1) accurately represents our data over the range of diameters studied by us, but its use for extrapolation purposes needs to be justified. To this end we will want to make use of the observation that in our experiments we have

$$\frac{D}{D_\infty} \geq 0.985 \text{ (unconfined charges)} \qquad \frac{D}{D_\infty} \geq 0.965 \text{ (confined charges)}$$

where these relations hold for all diameters and densities.

Two theories of the diameter effect have been proposed, the curved-front theory of Eyring and coworkers[1] and the nozzle theory of H. Jones.[12] In both cases the theory was developed for three types of confinement -- no confinement, light confinement, and heavy confinement. We are here concerned only with the first and last of these.

In both theories the existence of a detonation reaction zone of finite length x is assumed, and we need only replace $\underline{a}$ by x in equation (1) to obtain the result given by the curved-front theory
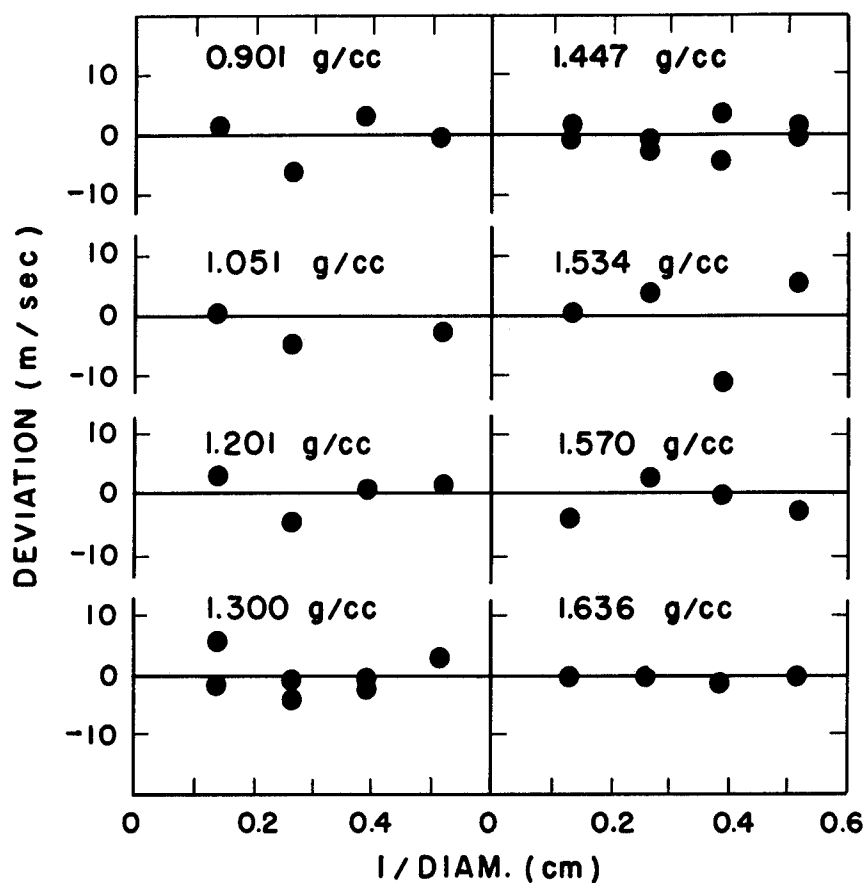
Figure 1

Deviation plots (experimental-calculated)
for reciprocal diameter fits -- confined
charges.
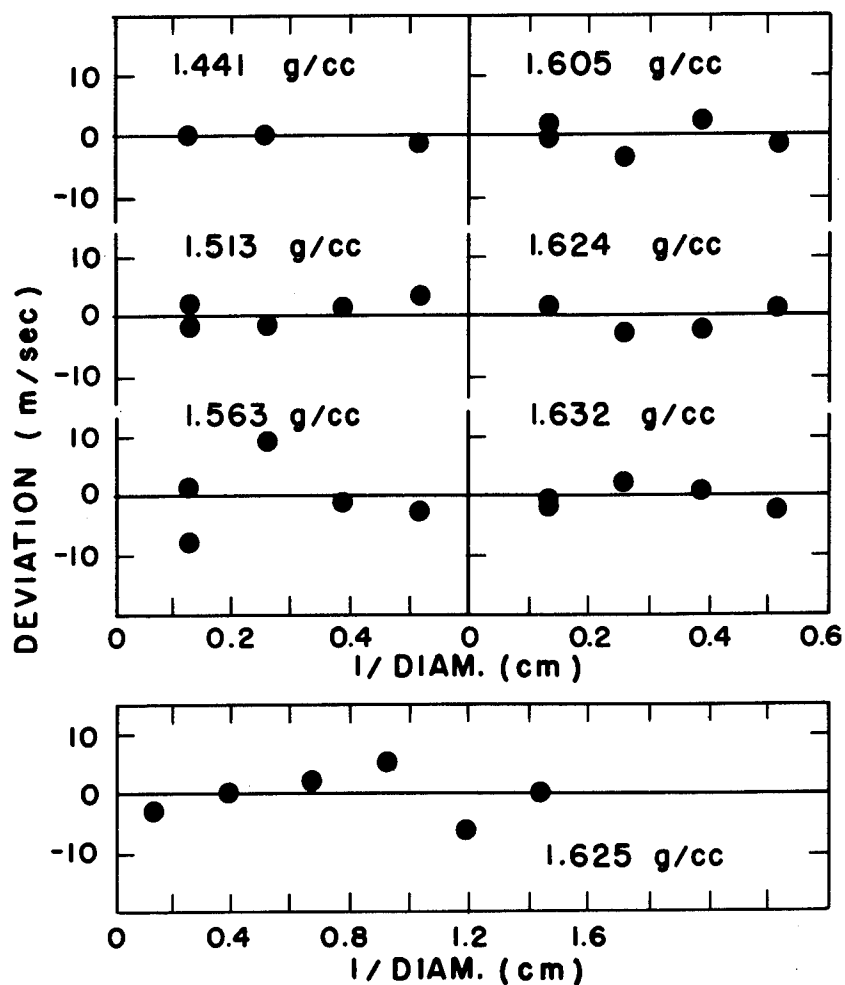
Figure 2

Deviation plots (experimental-calculated) for reciprocal diameter fits -- unconfined charges.
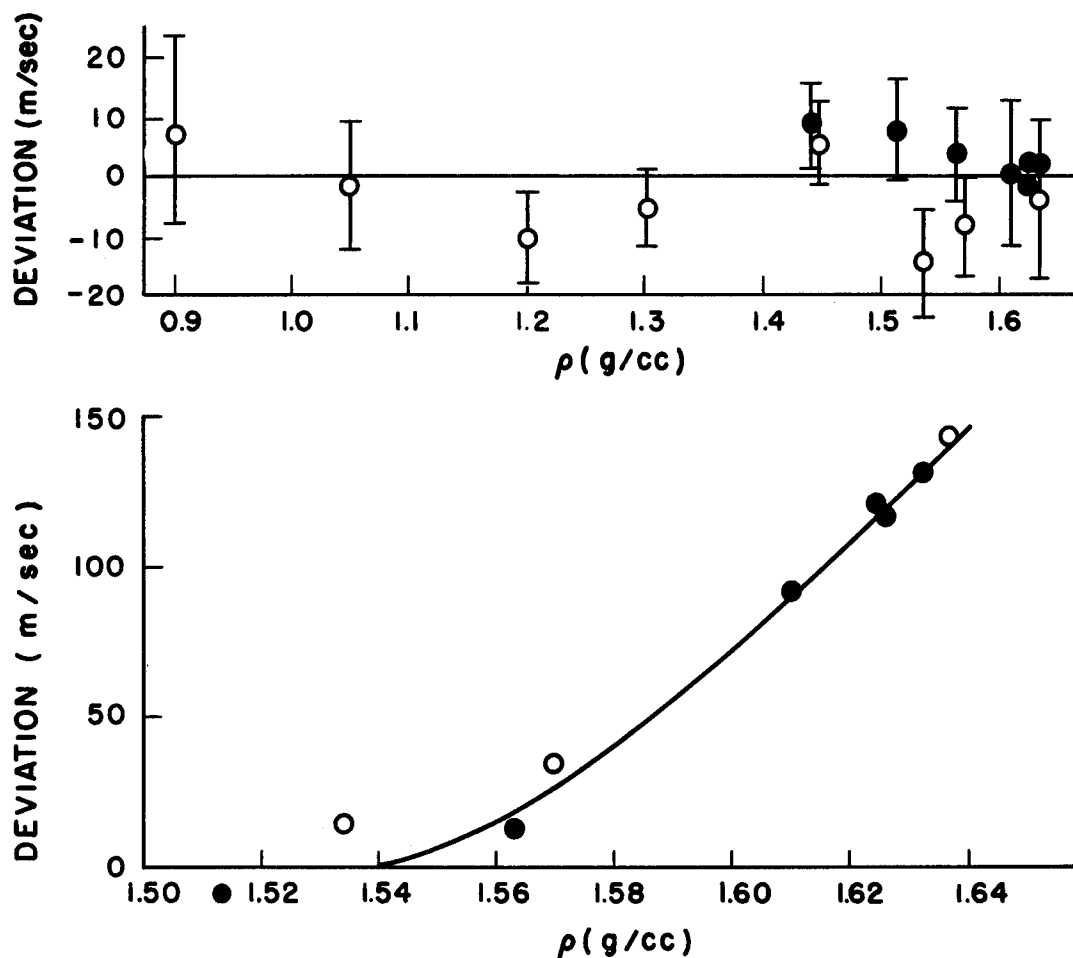
Figure 3

Deviation plots (experimental-predicted) for the D_∞ vs ρ data. Open circles: Confined charges. Full circles: Unconfined charges. The upper graph is for the whole density range and shows the deviation of the experimental points from the velocities predicted by equation (3). The error flags (where shown) are the 95% confidence intervals calculated from S_2^2 (see text). In the lower graph, the high-density region has been expanded to emphasize the departure from linearity (first two terms of equation (3)) in this region. The curved line represents the contribution of the higher order terms of equation (3).

for unconfined charges (we assume that x is not sensibly dependent on R). The corresponding result for heavily cased charges is

$$\frac{D}{D_\infty} = 1 - 0.88 \; \frac{x}{R} \; \sin \phi$$

with ϕ given by

$$\tan \phi = \frac{\rho}{\rho_c} \sqrt{\frac{D^2}{D_c^2} - 1} \; .$$

Here ρ_c and D_c are the initial density and shock velocity in the confining material, respectively, and the other symbols have already been defined. Upon inserting reasonable values for D_c in the last equation, we find that in our experiments $\tan \phi < 0.25$, and hence to a sufficiently good approximation $\sin \phi \cong \tan \phi$. Furthermore, at a given density ρ, the expression under the radical sign varies by about twenty percent or less, while R varies by a factor of four. Hence well within the precision of our data we may set

$$1.76 \sin \phi \cong 1.76 \frac{\rho}{\rho_c} \sqrt{\frac{D^2}{D_c^2}} \cong C (\rho) \qquad (4)$$

and we then have

$$\frac{D}{D_\infty} = 1 - \frac{C}{2} \; \frac{x}{R}$$

which is of the desired form. Our estimates of the values of C at the densities of interest, obtained from equation (4), are as follows:

ρ	C
0.9	0.12
1.05	0.18
1.2	0.24
1.3	0.28
1.45	0.34
1.53	0.38
1.57	0.40
1.64	0.43

An approximate form of Jones' equation for heavily cased charges is

$$\frac{1}{D^2} = \frac{1}{D_\infty^2} \left(1 + \frac{9 \; x \; \tan \phi}{R} \right) \; .$$

Here ϕ is the expansion angle of the case, and the other symbols have the meanings already assigned. It is assumed that $\frac{x}{R} \tan \phi$ is small, and indeed we have $\frac{x}{R} \tan \phi < 0.01$ for $D/D_\infty > 0.96$. Under these conditions we can equally well write

$$D = D_\infty \left(1 - \frac{4.5 \, x \, \tan \phi}{R}\right)$$

which is of the desired form providing the expansion angle is constant at a given loading density. This would appear to be an entirely reasonable assumption. We note in passing that, to within about a factor of two, $x = 4a$ for heavily cased charges by both theories.

The Jones theory for unconfined charges is a quite different matter. For $D/D_\infty \cong 1$ these equations can be written

$$D = D_\infty \left[1 - 4.5 \, (r - 1)\right]$$

where r is defined parametrically by

$$r = 1.85 \left(1 - \frac{x}{R} \cot \theta \right)$$

$$\frac{x}{R} = 0.919 \, \frac{\sin \theta}{1 + \cos \sqrt{2} \, \theta}$$

If in this case we assume that x is independent of R, we find that a plot of D/D_∞ vs x/R curves rather sharply as $D/D_\infty \to 1$, so that it is not possible to obtain a reasonable representation of our results by means of these equations unless x is allowed to vary with R. The functional form which such a dependence might assume is not contained in either theory, and hence a unique solution for D_∞ cannot be obtained.

To summarize, then, for x independent of R, and for $D/D_\infty \cong 1$, equation (1) is of the form predicted by both theories for heavily confined charges, and by the curved-front theory for unconfined charges. It is, under these same conditions, inconsistent with the results of the nozzle theory for unconfined charges. Nevertheless, we feel that its use in estimating infinite diameter velocities from our finite charge data has been adequately justified on both experimental and theoretical grounds.

Corresponding to the reaction zone length x which appeared in the foregoing discussion, there is a reaction time τ. These are quantities of considerable physico-chemical interest which are difficult to measure by any direct method. From elementary conservation of mass considerations, they are related by the equation

$$\tau = \frac{x}{D} \frac{\bar{\rho}}{\rho}$$

where ρ is the initial density of the explosive and $\bar{\rho}$ is the average density (unburned explosive plus products) in the reaction zone. The value of the ratio $\bar{\rho}/\rho$ is not known, but from the presumed structure of the reaction zone [1] we can assert that ρ_{CJ}/ρ is a lower bound where ρ_{CJ} is the density at the Chapman-Jouguet plane. For many explosives $\rho_{CJ}/\rho \cong \frac{4}{3}$. With this in mind, but otherwise quite arbitrarily, we set $\tau = \frac{1.5 \, x}{D}$, and, in Table V, we have summarized the values of x and τ computed from our data, using the results of the curved-front theory. In Fig. 4, x is plotted as a function of ρ. From this figure we see that x is a smoothly decreasing function of ρ over the whole density range, becoming quite small as crystal density (1.654 gm/cc) is approached. Similar results were obtained by Stesik and Akimova, although these investigators used a quite different, empirically calibrated relationship between D/D_∞ and x/R. The dashed line in Fig. 4 represents the dependence of x on ρ according to the data of their paper. The differences in the two curves are readily explainable, qualitatively at least, if the TNT used by Stesik and Akimova was of a smaller average particle size (around 40 microns) than that used by us. It is not unlikely that this was the case, as they state that their TNT had been ball milled.

These results must be interpreted with some reserve, since the theories of the diameter effect are imprecise, and also because little is known about the actual kinetic structure of the reaction zone. Regarding the latter, one reaction mechanism which appears consistent with much of the available experimental data is surface ignition, followed by inward burning, of the individual grains.[13] This mechanism is generally referred to as the grain-burning theory. A decrease in x with ρ would be expected on the basis of this theory, and may be viewed as the result of two effects -- a decrease in grain size due to crushing of the grains in the pressing operation, and an increase in burning rate with increasing pressure in the reaction zone. It is of some interest to compare the data of Table V with corresponding estimates made on the basis of the grain-burning theory. The comparison is most readily made using the reaction times τ. If the explosive grains are assumed to be uniform spheres of radius r, and if $\dot{r}$ is their linear (radial) burning rate, than we have $\tau = r/\dot{r}$. In practice the explosive grains are neither spherical nor uniform in size; furthermore, many of them are agglomerates of smaller crystals, and even the individual crystals may have internal fissures and voids. Finally, some attrition of the grains must occur during their passage through the shock front (by spalling, for example). The data of Table I cannot, therefore, be used in any straightforward way to estimate an average effective grain radius for the reaction time calculations. For this reason, to make the comparison we have turned the calculation around, and from the values of τ given in Table V and estimated values of $\dot{r}$ we have calculated r. The values of r so obtained are then to be compared with the data of Table I, keeping

TABLE V

Reaction Zone Length x and Reaction Time τ - Curved-Front Theory

	Confined			Unconfined	
ρ	x (mm)	τ^a(μsec)		x (mm)	τ^a(μsec)
0.901	5.61 $\pm$ 0.85	1.78			
1.051	3.45 $\pm$ 0.52	0.99			
1.201	1.75 $\pm$ 0.35	0.46			
1.300	1.31 $\pm$ 0.19	0.33			
1.441				0.30 $\pm$ 0.08	0.07
1.447	0.80 $\pm$ 0.14	0.19			
1.513				0.22 $\pm$ 0.06	0.05
1.534	0.16 $\pm$ 0.19	0.04			
1.563				0.10 $\pm$ 0.06	0.02
1.570	0.15 $\pm$ 0.18	0.04			
1.609				0.02 $\pm$ 0.06	<0.01
1.624				- 0.01 $\pm$ 0.03	<0.01
1.625				0.03 $\pm$ 0.02	<0.01
1.632				0.02 $\pm$ 0.06	<0.01
1.636	0.08 $\pm$ 0.16	0.02			

[a] Computed from $\tau = 1.5 \dfrac{x}{D}$. See text.
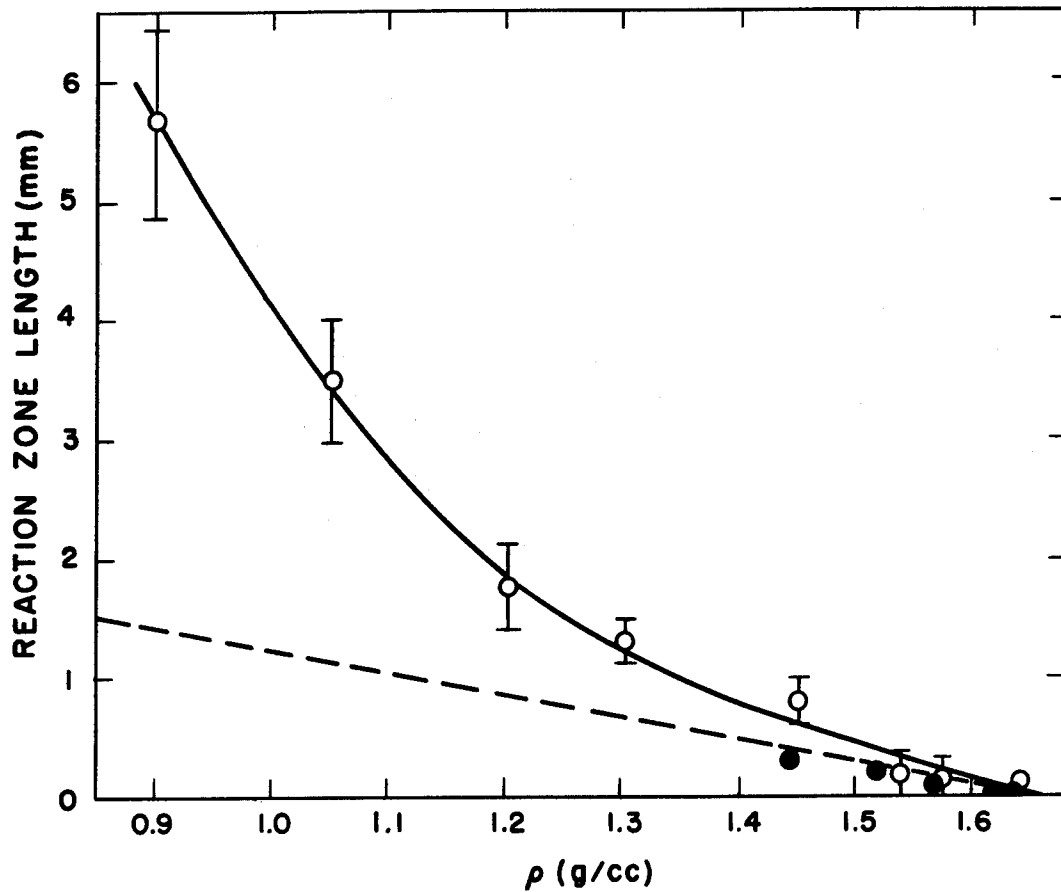
Figure 4

Detonation reaction zone length as a function of loading density.
Open circles: Confined charges.
Full circles: Unconfined charges.
Error flags shown are 95% confidence intervals.
The dashed line represents data by Stesik and Akimova, ref 3 (see
text).

in mind the above comments regarding the expected relative magnitudes of the two sets of data.

The linear burning rate of TNT crystals has been measured by Jacobs as a function of pressure up to about 3000 atm. The details of this investigation have never been published in the open literature,[14] but the burning rate of TNT was found to follow an equation of the form

$$\dot{r} = k \, P^n .$$

The coefficient k is temperature dependent, increasing at the rate of about 2% for each 10°C rise in temperature. At room temperature, $k = 0.53 \times 10^{-6}$ for $\dot{r}$ in mm/μsec and P in atmospheres. If we assume that the temperature of the shocked (but unreacted) explosive is 900°C (vide infra), then k has the value 3.0×10^{-6}. The exponent n was found by Jacobs to be equal to 0.81. Therefore, for the burning rate we use the equation

$$\dot{r} = 3.0 \times 10^{-6} \, P^{0.81}$$

and hopefully extrapolate this into the range of detonation pressures. The latter also must be estimated in the density range of interest. For this purpose we have used the equation

$$P_{CJ} = 2.75 \times 10^{-3} \, \rho \, D^2 \tag{5}$$

where P is given in atmospheres for D in m/sec. This choice is based in part on the results of hydrodynamic calculations[15] and in part on an experimental value at $\rho = 1.455$ gm/cc.[16] The pressure varies considerably throughout the reaction zone, perhaps by as much as a factor of two,[1] being higher at the front of the zone. For this reason we have computed the burning rates using a pressure (assumed constant throughout the reaction zone) 20% higher than that given by equation (5). The results of these calculations may be summarized as follows:

TABLE VI

ρ (gm/cc)	$P \times 10^{-3}$ (atm)	$\dot{r} \times 10^3$ (mm/μsec)	$r \times 10^3$ (mm)	Grain Dia (microns)
0.90	67	24.4	43.5	87
1.05	94	32.4	32.1	64
1.20	128	41.3	19.0	38
1.30	155	47.6	15.7	31
1.45	201	59.2	11.3	23

The agreement between the numbers appearing in the last column of this table and the numbers which might have been predicted from the sieve analysis data is surprisingly good, particularly in view of the impressive extrapolation of Jacobs' burning rate equation which was involved in the calculations.

An alternative model for the detonation reaction is the homogeneous adiabatic decomposition of the shock-heated explosive, assuming an Arrhenius rate law. Under these conditions the reaction time is given by the equation[17]

$$\tau = \frac{cRT_o^2}{ZQE} \, e^{E/RT_Q}$$

where c is the heat capacity, Q is the heat of reaction, T_o is the temperature of the shocked explosive, R is the gas constant, and Z and E are the preexponential factor and activation energy, respectively, in the Arrhenius law. In this equation everything but R is uncertain in the regime of interest here. We begin by setting c = 0.5 cal/gm/°C and Q = 1000 cal/gm. Temperatures on the Hugoniot of unreacted TNT have been computed [15] for two assumed equations of state, one of the Mie-Gruneisen form, and the other of the form cited by Cowan and Fickett for graphite.[18] In both cases the parameters in the equation of state were adjusted to fit experimental Hugoniot data for unreacted TNT.[19] Similar temperatures were obtained with both equations of state, and, for the pressures and densities listed in Table VI, we have $T_o \cong 1200°K$. It is of interest to note that, in this range, a 100° change in T_o changes τ by about a factor of three.

The greatest uncertainty arises in the values to be assigned to E and Z. From studies of the thermal decomposition of liquid TNT, Robertson[20] obtained $Z = 10^{11.4}$ sec^{-1} and E = 34.4 kcal/mole, while Cook and Abegg[21] obtained $Z = 10^{12.2}$ sec^{-1} and E = 43.4 kcal/mole. Inserted in the above equation, with the previously assigned values of c, Q, and T_o, these rate laws lead to the following estimates of the reaction time:

0.3 μsec (Robertson)
1.5 μsec (Cook and Abegg)

Thus these estimates also are in good agreement with the "experimental" values. On the other hand, we view them as even less reliable, and by a considerable margin, than the burning rate calculations summarized in Table VI.

We conclude this discussion of reaction zone lengths with a few general comments. First of all, while the interpretation of our data in terms of the combined curved-front/grain-burning theories has led to surprisingly good agreement in the computed reaction zone lengths, this agreement cannot be cited as proof of any part of the theory. The agreement could be accidental, and the only justifiable

conclusion to be drawn from these results is that this interpretation of the data has not led to any gross inconsistencies.

Secondly, and in spite of this agreement, we feel that some modification of the grain-burning theory might be profitable. The argument is as follows: When a soft granular material is shocked to a density well above its crystal density, it would seem reasonable to expect that the individual grains would completely lose their identity, so that the model of inward burning grains becomes somewhat implausible. On the other hand, the discontinuities in the material (voids and intergranular contact points) are likely places for burning to start -- by spalling, intercrystalline friction, or adiabatic compression as the material passes through the shock front. These considerations suggest that the reaction may proceed through the outward burning of numerous small hot spots (holes) more or less randomly distributed throughout the compressed material. Both the number and size distribution of such hot spots presumably would depend on the strength of the shock in such a manner that a decrease in reaction zone length with increasing charge density would result from this effect as well as from the increase in burning rate. Reaction zone lengths deduced from this "hole burning" model would not be expected to be grossly different from those computed from the grain burning model. Its principal advantage, aside from plausibility considerations, is that it can explain a wider range of reaction times. Unfortunately, this same flexibility, which is an inherent feature of the model, makes simple calculations of reaction zone lengths somewhat more difficult to justify in terms of the conditions assumed to hold initially behind the shock front. Some of the consequences of the model are currently being explored at this Laboratory.

The literature abounds in detonation velocity data on TNT, but most of it was obtained before the development of accurate instrumental methods and also before the importance of charge geometry and confinement was fully appreciated. We will here consider only the more recent studies.

Cybulski, Payman, and Woodhead,[22] using a rotating mirror camera, made a number of measurements, mostly on cast TNT, in which they studied the effect of purity, crystal size, charge diameter, and confinement. From their data they deduce a limiting velocity of 6950 m/sec for cast TNT at a density of 1.624 gm/cc. This is some 25 m/sec above our curve. As a check on the reproducibility of the method they also determined the detonation velocity of pressed TNT at a density of 1.00 gm/cc in 1.25" diameter unconfined charges, using a TNT having a particle size two to three times larger than that of the TNT we used. Their velocity of 4650 m/sec is over 300 m/sec below what we would predict from our results for confined charges of this diameter and density. This emphasizes the importance of the effects of confinement and particle size on detonation velocities determined at low loading densities.

Copp and Ubbelohde[23] used a careful application of the Dautriche method to obtain detonation velocity data on confined charges of cast TNT at a density of 1.60 gm/cc with various charge diameters. From their results they deduce a limiting velocity of 6970 m/sec. This is some 70 m/sec above our curve and indeed lies very close to the extrapolation of our least squares line. We believe the discrepancy lies in the method used by Copp and Ubbelohde to extrapolate their experimental points to obtain an infinite diameter velocity. The velocity actually reported by them for 3" diameter charges is 6850 m/sec, and the correlation between velocity and diameter is not statistically significant in the case of their data.

The wartime work of the Explosives Research Laboratory at Bruceton has never been published in the open literature but has been summarized in an OSRD report.[24] Over a hundred velocity measurements were made on TNT at a variety of densities, charge diameters, particle sizes, and degrees of confinement. The data are difficult to analyze in a systematic way, but a limiting velocity curve deduced by the investigators is given as

$$D = 1785 + 3225 \, \rho$$

which is in good agreement with our results.

Stesik and Akimova's work most nearly parallels ours in plan and objective, although it differs considerably from ours in experimental details and in the treatment of the data. Their infinite diameter velocities are a linear function of ρ up to 1.55 gm/cc and are described by the equation

$$D_\infty = 1669 + 3342 \, \rho \, .$$

This is only in fair agreement with our equation (3). Their infinite diameter velocities are some 70 m/sec below ours in the low-density region and are higher than ours by a similar amount at high density. We can only speculate as to the reasons for this. The difference at low density may be a consequence of their extrapolation procedure and, more directly, of the method they used to calibrate it. The situation at high density is more obscure, as many of their experimental velocities are higher than our infinite diameter velocities.

It is interesting to note that their highest density point, at 1.62 gm/cc, lies some 83 m/sec below the straight line determined by their other four experimental points. Thus their data also contain evidence of the downward curvature of the D_∞-ρ line observed by us in the high-density region.

ACKNOWLEDGMENTS

We especially wish to acknowledge the valuable contributions of
W. W. Wood and A. W. Campbell of this Laboratory, and of R. J. Hader
of the Institute of Statistics at the University of North Carolina.
We also are indebted to W. H. Rogers, now deceased, who determined
the cooling curve of the TNT used in this investigation, and to
R. G. Shreffler for helpful discussions and criticisms.

REFERENCES

(1) Eyring, Powell, Duffey, and Parlin, Chem. Rev. 45, 69 (1949).

(2) Malin, Campbell, and Mautz, J. Appl. Phys. 28, 63 (1957).

(3) Stesik and Akimova, Zhur. Fiz. Khim. 33, 1762 (1959).

(4) Private communication from A. W. Campbell of this Laboratory.

(5) Copp and Ubbelohde, Trans. Faraday Soc. 44, 646 (1948).

(6) Campbell, Malin, Boyd, and Hull, Rev. Sci. Instru. 27, 567 (1956).

(7) We are indebted to Grover Taylor for these measurements.

(8) Mandel, J. Amer. Stat. Assoc. 52, 552 (1957).

(9) A. Hald, Statistical Theory with Engineering Applications, (John Wiley and Sons, Inc., New York, 1952), p 291.

(10) We are greatly indebted to R. J. Hader and W. W. Wood, who suggested this method of analysis.

(11) Ref 9, p 379.

(12) Jones, Proc. Roy. Soc. A189, 415 (1947). See also ref 1.

(13) Kistiakowsky, Third Symposium on Combustion, Flame, and Explosion Phenomena, p 560. Williams and Wilkins Co., Baltimore.

(14) The work is briefly described in Science in World War II, Chemistry volume. Little, Brown and Co., 1948. See also ref 13.

(15) By C. L. Mader of this Laboratory.

(16) W. Garn, J. Chem. Phys. 32, 653 (1960).

(17) This is, for example, readily obtained from equation (6), p 174 of ref 1, after correcting an error in sign in the two exponentials.

(18)   Cowan and Fickett, J. Chem. Phys. $\underline{24}$, 932 (1956).

(19)   Unpublished data by W. Garn of this Laboratory.

(20)   Robertson, Trans. Faraday Soc. $\underline{44}$, 977 (1948).

(21)   Cook and Abegg, Ind. Eng. Chem. $\underline{48}$, 1090 (1956).

(22)   Cybulski, Payman, and Woodhead, Proc. Roy. Soc. $\underline{A197}$, 51 (1949).

(23)   Copp and Ubbelohde, Trans. Faraday Soc. $\underline{44}$, 658 (1948).

(24)   MacDougall, Messerly, Hurwitz, et al, OSRD-5611, "The Rate of Detonation of Various Explosive Compounds and Mixtures".

MEASUREMENTS OF DETONATION, SHOCK, AND IMPACT PRESSURES*

M. A. Cook, R. T. Keyes, W. O. Ursenbach
Institute of Metals and Explosives Research, University of Utah
Salt Lake City, Utah

ABSTRACT

An "aquarium technique" for the measurement of detonation, shock, and impact pressures is described which is capable of measuring accurately pressures over a range extending from roughly one to several hundred kilobars. An experimental determination of the equation of state for water, upon which use of the aquarium technique relies, is presented and compared with results obtained by other investigators. Similar data are presented for lucite. Measurements of pressures for a variety of explosives including both ideal and non-ideal ones are presented for various charge diameters and lengths using explosives of widely different reaction zone lengths. These pressures were found to correspond to the Chapman-Jouguet value of the detonation pressure calculated from thermohydrodynamic theory.

Introduction

When a shock wave propagates through an undisturbed medium of density ρ_1, all the remaining shock wave parameters may be expressed uniquely in terms of any one chosen parameter. For example, pressure, temperature, and particle velocity may each be expressed uniquely in terms of the velocity of the shock wave. The fact that disturbances, even of relatively low pressure, propagate in water as shocks, coupled with the fact that water is transparent, thereby permitting convenient and continuous observation of shock velocity by a streak or framing camera, suggest that water can be used as a pressure gauge for measuring transient pressures. For instance, it may be used to measure the peak pressures in detonation waves of condensed explosives, in impact-generated shocks produced by the collision of a moving plate with a fixed plate, or, for that matter, it may be used to measure the peak pressures of shocks in various other media irrespective of the mode of shock generation.

Before water can be used as a pressure measuring medium its shock parameters must be known. The Rankine Hugoniot curves for water have been derived by a number of investigators including Kirkwood and Montrall,[1] Kirkwood and Richardson,[2] Richardson, Arons and Halverson,[3] Arons and Halverson,[4] and Doering and Burkhardt.[5] In these treatments systematic extrapolations of Bridgman's[6,7] PVT data for water were made. Probably the most comprehensive extrapolation of Bridgman's PVT data, however, was carried out by Snay and Rosenbaum[8] who used more recent data of Bridgman[9,10] which for water extended to 36,500 kg/cm^2 and for ice VII to 50,000 kg/cm^2.

A different approach was used in a later study by Walsh and Rice.[11] In their method an intense plane shock wave was generated in an aluminum plate by the detonation of a slab of Composition B in contact with one side of the plate. The shock through a portion of the plate was then transmitted into water. Higher pressures in the aluminum plate were reported by "slapping" the aluminum plate with a thin, high velocity, explosively driven plate rather than detonating the charge directly in contact with the test aluminum. By application of a special streak camera technique pioneered by Walsh and co-workers and through use of a previously derived equation of state for aluminum the shock velocity in water as a function of the corresponding shock pressure in the aluminum at the interface was determined. Continuity conditions of pressure and particle velocity across the interface between the aluminum and water were then applied to determine the Hugoniot curves for water.

In determining shock parameters for water a factor which should be considered is the possibility of a phase change of the medium within the shock wave. This possibility was investigated by Snay and Rosenbaum[8] and by Walsh and Rice.[11] According to Snay and Rosenbaum the Rankine Hugoniot curve for supercooled water and the Rankine Hugoniot curve for partially frozen water are never far

apart, and thus the shock velocity would not be materially affected
if freezing did occur. Since partial freezing of a liquid should
lead to reduced transparency, because of differences in indices of
refraction of water and ice, Walsh and Rice carried out some trans-
parency experiments of water being traversed by a shock wave in the
pressure range of 30 to 100 kilobars. No sign of opacity due to
freezing was observed. They concluded therefore that even though
P,T conditions might be proper for freezing under static conditions,
the time the liquid was under the correct conditions within the
shock wave apparently was too short for freezing to occur.

In using water as a pressure gauge (by observing the trans-
mission of the shock into it) one must calculate from the measured
shock pressure in water the pressure in the adjacent medium of
interest from which the water shock was transmitted. In a previous
application of the "aquarium technique" for the measurement of
pressure, two procedures were used to perform such a calculation.[12]
The first method, which was considered the more exact one, was
patterned after a treatment given by Riemann for a shock propagating
across a boundary into a medium of lower impedance. The second
method utilized the shock "impedance mismatch" equation

$$ p_i = \frac{p_t(\rho_t V_t + \rho_i V_i)}{2\rho_t V_t} \qquad (1) $$

where p is pressure, ρ is initial density of the medium before being
traversed by a shock, V is the velocity of the shock, and subscripts
i and t designate the incident medium and the transmitting medium,
respectively. Although the shock impedance mismatch equation
theoretically should only be accurate when the wave reflected at
the interface is a weak shock, in the investigations covered by
Ref. 12 where the reflected wave was a rarefaction, equation (1)
was found to yield results in very good agreement with the first
method. Consequently, in the present study equation (1) was used
to calculate p_i from measured values irrespective of whether the
reflected wave was a release wave or a shock wave.

This paper presents results obtained by application of the
aquarium method for the measurement of detonation pressures of a
number of explosives.

Furthermore, since the results of Snay and Rosenbaum were
derived from an extrapolation of low pressure PVT data, and since
the curve of Walsh and Rice is dependent upon the equation of state
of aluminum and application of continuity conditions across the
aluminum-water interface, results of a shock parameter study for
water by a third, independent method are described. Less compre-
hensive results are also presented for lucite which, like water,
possesses desirable characteristics for use as the transmitting
medium of a pressure gauge.

Experimental

(a) Shock parameter determinations

The shock parameters which are of interest in this study are related by the familiar hydrodynamic equations

$$p - p_o = \rho_1 VW \qquad (2a)$$

$$W/V = [1-(\rho_1/\rho)] \qquad (2b)$$

and the approximate relation

$$W \doteq V_{fs}/2 \qquad (3)$$

where p is the pressure, ρ is the density, V is the shock velocity, V_{fs} the free surface velocity, and W is the particle velocity, the subscript 1 indicating initial conditions before passage of the shock wave. Equation (3) expresses the fact that the particle velocity in the shock at a free surface is approximately twice the particle velocity in the shock in the medium in question.

The method used for determining the shock-parameter data for water and some of the data for lucite consisted of simultaneous measurements of the shock velocity immediately inside the free surface and the free surface velocity as the shock emerged from the water or lucite. Observations of the shock and free surface velocities were made with a rotating mirror streak camera using diffuse backlighting from an explosive flash bomb to show the propagation of the shock wave and the free surface. Fig. 1 illustrates the aquarium setup. Note that point-initiated charges were used. For this reason it was necessary that the slit view of the streak camera lie along the charge axis in order to obtain the correct values of shock velocity and the corresponding free surface velocity. Care was also taken in the alignment for the free surface in the cases of both the water and the lucite to lie on the optic axis of the system so that the view of the camera was flush with the free surface.

Two sizes of aquaria were used, the smaller being 6" x 6" x 6" and the larger 12" x 12" x 8", the size of the aquarium being dictated by the height, h, of water above the receptor charge. As h was increased above a certain limit the dimensions of the aquarium had to be increased due to the fact that the shattering of the glass propagated with a velocity which exceeded the shock velocity in the liquid. Increasing the size of the aquarium, of course, resulted in an increased path length for fracture which permitted the events of interest at the water-air interface to be photographed before they were obscured.

The pressure or velocity of the shock wave when it reached the air surface was varied primarily by one of two methods: (1) By

varying the height, h, of the liquid above the surface of the genera-
tor charge, and (2) by varying the size of the shock-generator charge,
since use of smaller diameter generator charges resulted in a greater
attenuation of the shock in water. With 3" diameter x 3" length
shock-generator charges and 2" diameter x 2" length donor charges
of Composition B the pressure of the shock wave, when it reached the
water-air interface, could be varied conveniently between an upper
limit of about 130 kb when the height of the liquid was 0.5 cm and
a lower limit of about 30 kb using a liquid height of about 7 cm.
For lower pressure, rather than employing further increases of
water height, it was more convenient to reduce the size of the charge.
Consequently, for pressures below roughly 30 kb and down to as low
as 1 kb, 1" diameter x 1" length Composition B shock-generator
charges and 1" diameter x 3" length donor charges were used. The
calibration curve was extended to 155 kb by using a charge based on
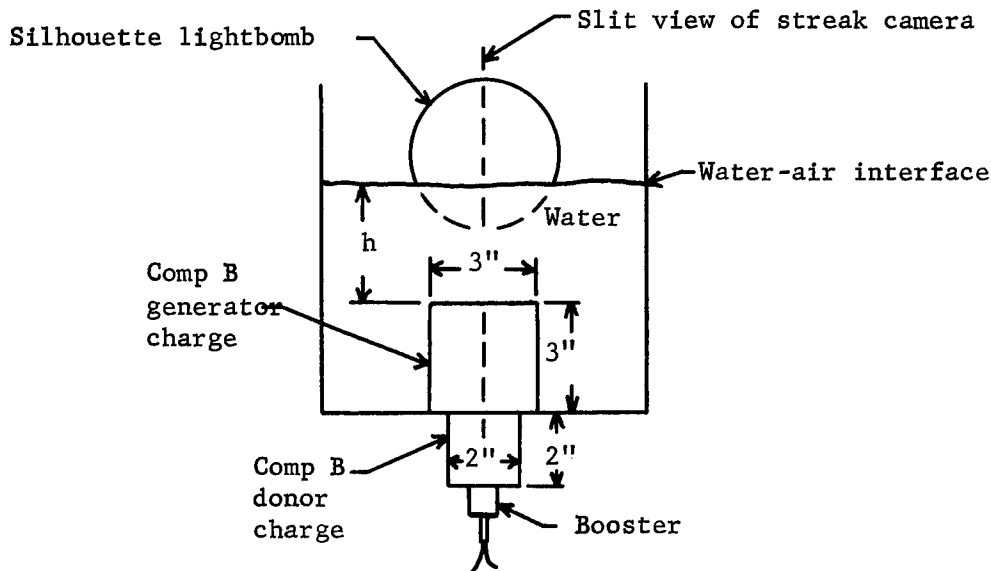
Fig. 1: Aquarium setup for measuring velocity of water shock
along the charge axis and free surface velocity.

HMX as the shock-generator charge. This value was sufficiently
high for measurements of detonation pressures of the explosives of
interest. Walsh and Rice reported, however, extending shock para-
meter data to above 300 kb by hurling an explosively driven, thin,
flat plate across a short air gap.

The silhouette-type lightbomb comprised a 4" diameter x 3"
length 50/50 TNT/Composition B charge inserted in a 4" x 30" paste-
board tube of about 1/16" wall thickness. A sheet of translucent
polyethylene plastic was taped to the front of the tube which
served as a diffusing screen. The height of the lightbomb was

adjusted so that the surface of the water in the aquarium was approximately in line with the center of the front of the lightbomb as viewed by the camera. The aquarium assembly and the streak camera were arranged such that the slit view of the streak camera was as shown in Fig. 1, i.e., perpendicular to the water-air interface and lying along the axis of the generator charge. Consequently, with proper synchronization of the lightbomb, a streak camera trace was obtained of the shock propagating through the liquid to the water-air interface. When the shock front reached the surface of the water the trace showed a rarefaction wave propagating back into the water and the spalling of the water surface. This spall apparently is in the form of a very fine spray because it is relatively opaque and permits photographing the motion of its front and thus the direct recording of the free surface velocity.

Fig. 2 reproduces a typical streak camera trace showing the attenuating shock wave, the release wave, and spall. Note that the spall velocity is very constant. The results of interest obtained from the films are the shock velocity just as the shock reached the interface and the free surface or spall velocity. Both these measurements were obtained from the slopes of the traces at the interface through application of the proper magnification factors and camera writing speed. The writing speed of the camera in general was chosen such that the slopes of the shock wave trace and the free surface trace about equally bracketed the slope corresponding to a 45° angle.

The water used in this investigation was ordinary tap water rather than distilled water because the amounts required were rather large (some aquaria holding seven gallons) and the difference between the compressibility of distilled water and tap water is small. The temperature of the water was $20°C \pm 5C°$.

A few shock-parameter determinations for lucite were made in the same manner as those for water, i.e., by simultaneous measurements of shock velocity at the free surface and the free surface velocity. However, a greater number of determinations were made by transmitting the shock from lucite into water, measuring the final velocity of the shock in lucite and the initial velocity of the shock in water by means of a streak camera (utilizing a silhouette backlight bomb to render the shocks visible), and then by means of the previously obtained equation of state for water and equation (1) calculating the shock pressure in lucite immediately inside the lucite-water interface. The shocks in lucite were generated by the detonation of 4.8 cm diameter x 18 cm length point initiated, cylindrical Composition B charges. As in the aquarium method the assemblies were carefully aligned in order that the slit view of the streak camera fell along the charge axis which made the use of expensive plane wave initiators unnecessary. The strength of the shock in lucite at the lucite-water interface was regulated by varying the thickness of lucite between the charge and the water.

362
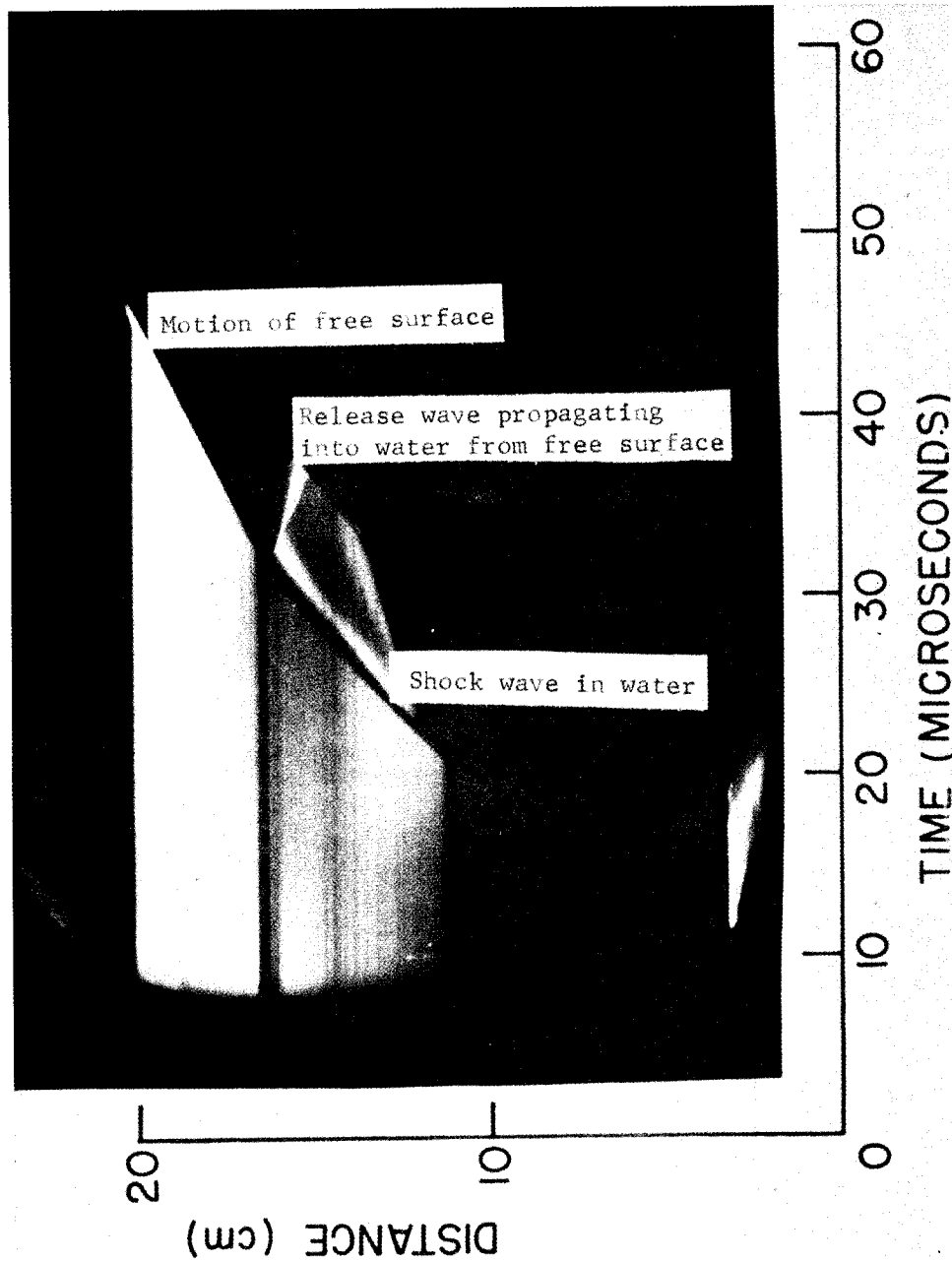
Fig. 2: Typical streak camera trace obtained using the arrangement of Fig. 1 (shock parameter determination for water).

The diameter of the lucite was in all cases sufficiently large to shield the detonation products from the region where the motion of the shock wave was observed.

(b) Detonation pressure determinations

Fig. 3 illustrates the aquarium assembly used for measuring the initial velocity of the shock (and pressure) in water transmitted directly from a detonation wave. As in the previous cases the assembly was aligned such that the streak camera observations were made along the charge axis, the height and tilt of the assembly being such that the bottom face of the charge in this case was coincident with (and parallel) to the optical axis of the camera. The streak camera at this installation viewed upward through a periscope in which the line of sight was reflected to a horizontal direction by a front surface mirror. The camera was mounted on a turntable and three supporting casters, permitting rotation of the camera about its optic axis. Thus the slit view of the camera could conveniently be adjusted to either the horizontal or vertical direction or to any position between them simply by rotation of the turntable. This method of mounting the camera therefore permitted the proper alignment to be made with ease.

The cast charges were detonated with the bare end immersed in the aquarium. However, in cases where there existed the possibility of absorption of water or solution of some of the charge components the charges were sprayed with Krylon for waterproofing. Charges made up from granular or loose material were vibrator-packed in thin-walled (approximately 1/16" thick) cardboard tubes. The ends of the charges which were immersed in water in these cases were "closed off" with a layer of polyethylene 3 mils thick which was too thin to affect appreciably the shock transmitted into the water.

The average densities of all charges were determined just prior to firing. In addition to the determination of the initial velocity of the shock transmitted into water the detonation rate of the charge was measured, and thus all variables were evaluated whose magnitudes were required in the impedance mismatch equation for calculation of pressure in the incident medium in terms of that in the transmission medium. Detonation velocities as well as the initial shock velocities were calculated from the slopes of the traces. This procedure when carefully applied was found to yield satisfactory results even for the initial shock velocity determinations because case was taken to obtain traces of approximately 45° slope but more importantly because in many cases (with the primary exception of short charges) the attenuation of the water shock during the initial stages proved not to be rapid.

Numerous measurements of the peak pressure in the detonation wave to detect pressures higher than the C-J pressure have been carried out previously.[13,14] However, these experiments utilized

364
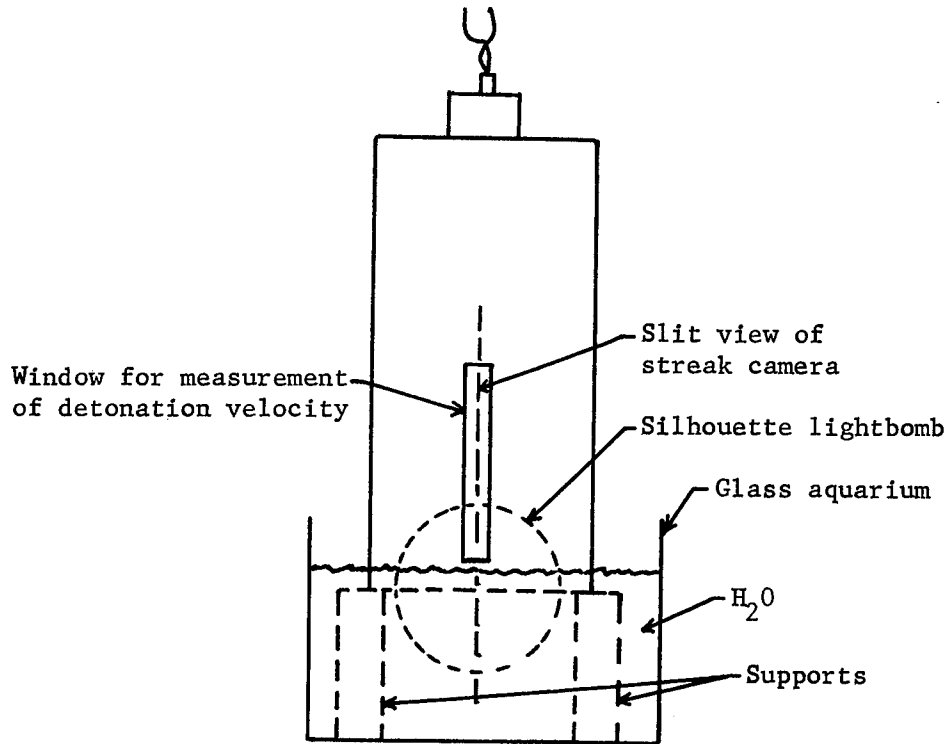
Fig. 3: Aquarium assembly for measurement of velocity along
the axis (and pressure) of the transmitted shock
in water from a detonation wave.

measurements of free surface velocity from aluminum acting as the
transmission medium for shocks generated by detonation of the
explosive in contact with the test sample. Since the observations
were carried out on the free surface or exit side of the aluminum
rather than at the explosive-metal interface, questionable measure-
ments with very thin plates were required,[15,16] requiring also
extrapolations to zero thickness to determine the pressure or
particle velocity at the detonation front.

The difficulties in using excessively thin plates in the method
of Ref. 13 and 14 were amplified by the fact that experiments were
devoted mainly to explosives of short reaction zone length, such as
Composition B, cast TNT, and fine, granular TNT for which the
detonation "spike" would be "erased" quickly as it propagated into
the aluminum. In the aquarium method, however, where a continuous
observation of the shock wave velocity from the explosive-water
interface outward into the liquid is possible, one does not need to
use thin layers of the transmitting medium. Admittedly a streak
camera may not be able to resolve very rapid changes in velocity

365

(or pressure) in a short distance near the explosive-water interface. Consequently, in this study emphasis was placed upon the use of explosives known to possess long reaction zone lengths and especially those whose characteristic impedances very nearly equalled the shock impedance of water, thus assuring that the impedance mismatch equation represented a good approximation for the pressure in the explosive.

The explosives included in this study were pelleted TNT of standard Tyler mesh sizes, -4+6, -6+8, -8+10; -48+65 granular TNT; and cast 50/50 amatol. Also included here are measurements made by Bauer[17] for the "blasting agents", 94/6 AN/fuel oil and the coarse TNT and Composition B "slurries"[18], because the reaction zone lengths of blasting agents are quite likely among the greatest of all detonating explosives. Also additional measurements are included for explosives of much shorter reaction zone length, namely granular RDX, granular RDX-salt, cast TNT, cast 65/35 baratol, 50/50 pentolite, Composition B, HBX-1, and a special explosive X. Measurements of this sort have been presented previously for pento- lite, Composition B, TNT and tetryl by Cook, Pack and McEwan.[16]

Except for a study with Composition B and one with a special explosive X where charge length was varied to observe transient effects of pressure vs charge length the charge lengths used in this investigation were all at least four charge diameters in order to insure that the detonation velocity was constant before the deto- nation front reached the end of the charge. In the case of the pelleted TNT and the blasting agents, all of which possessed long reaction zone lengths, the charge diameters were varied between values extending in some cases from the critical diameter to a diameter sufficiently large for the detonation velocity to be nearly ideal.

Results

(a) Shock parameter determinations

Table I presents the experimental shock velocity, free surface velocity, particle velocity ($W \doteq V_{fs}/2$) and pressure results for water. In Fig. 4 are plotted the experimental points with pressure as the ordinate and shock velocity as the abscissa. Fig. 5 presents a similar plot in which the low pressure part of the curve of Fig. 4 has been expanded to a larger scale. On both figures the smooth curve through the points represents an approximate best fit as "drawn by eye" to the data. Velocity-pressure values from this curve of best fit are given in Table II and represent the most reliable values.

Results of Snay and Rosenbaum,[8] and Walsh and Rice[11] also are plotted in Fig. 4. Note that Snay and Rosenbaum's results agree with the results of the present study at pressures up to about

Table I: Experimental shock parameter data for water
(20°C ± 5C°)

Shot No.*	Shock Velocity (m/sec)	Free Surface Velocity (m/sec)	Particle Velocity (m/sec)	Shock Pressure (kilobars)
170	1630	143	72	1.16
182	1710	229	115	1.96
167	1810	355	178	3.21
168	1890	377	189	3.57
178	1780	360	180	3.20
179	1820	368	184	3.35
169	2050	556	278	5.70
177	2070	550	275	5.69
176	2110	605	303	6.38
29	2410	940	470	11.3
40	2260	900	450	10.2
41	2300	920	460	10.6
174	2800	1010	505	14.1
175	2760	1020	510	14.1
171	3540	1600	800	28.3
199	3510	1780	890	31.2
21	3680	1740	870	32.0
187	4000	2150	1080	43.0
6	4330	2760	1380	59.8
19	4240	2830	1420	60.0
193	4250	3160	1580	67.2
195	4490	3080	1540	69.1
194	4750	3130	1570	74.3
196	4720	3040	1520	71.7
5	4650	3160	1580	73.5
13	4810	3310	1660	79.6
32	4610	3080	1540	70.9
201	4930	3230	1620	79.6
202	4750	3230	1620	77.8
203	4750	3280	1640	77.9
17	4680	3420	1710	80.0
30	4900	3290	1650	80.6
204	5070	3540	1770	89.7
205	4900	3560	1780	87.2
206	4900	3570	1790	87.5
207	4870	3540	1770	86.2
200	4810	3380	1690	81.2
18	4960	3800	1900	94.2
	5070	3840	1920	97.3

* Note: Shot number has been included for convenience of the writers.

Table I: Continued

Shot No.*	Shock Velocity (m/sec)	Free Surface Velocity (m/sec)	Particle Velocity (m/sec)	Shock Pressure (kilobars)
4	5080	3850	1930	98.0
190	5070	4200	2100	106
11	5470	4100	2050	112
189	5380	4210	2110	113
192	5530	4120	2060	114
213	5570	4110	2060	114
1	5480	4690	2350	128
2	5580	4440	2220	124
3	5320	4500	2250	120
10	5610	4400	2200	123
36	5420	4440	2220	120
37	5330	4490	2250	120
38	5410	4530	2270	122
34	5660	4730	2370	134
9	6050	4720	2360	143
183	6010	5040	2520	151
181	6130	4980	2490	153
184	6270	5090	2550	160
185	6200	5150	2580	160
186	6290	4980	2490	157
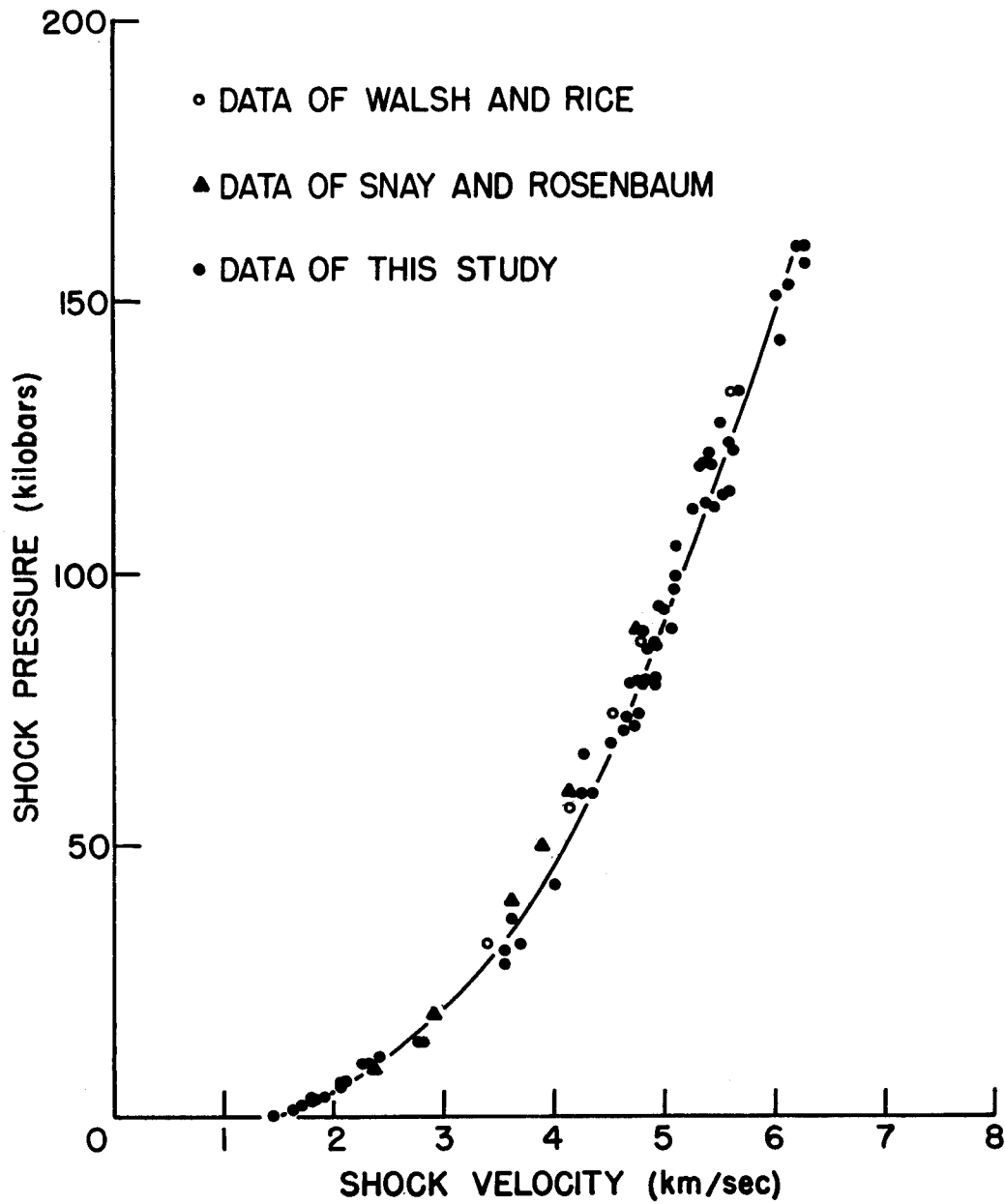
Fig. 4: Experimental shock velocity vs pressure data for water.
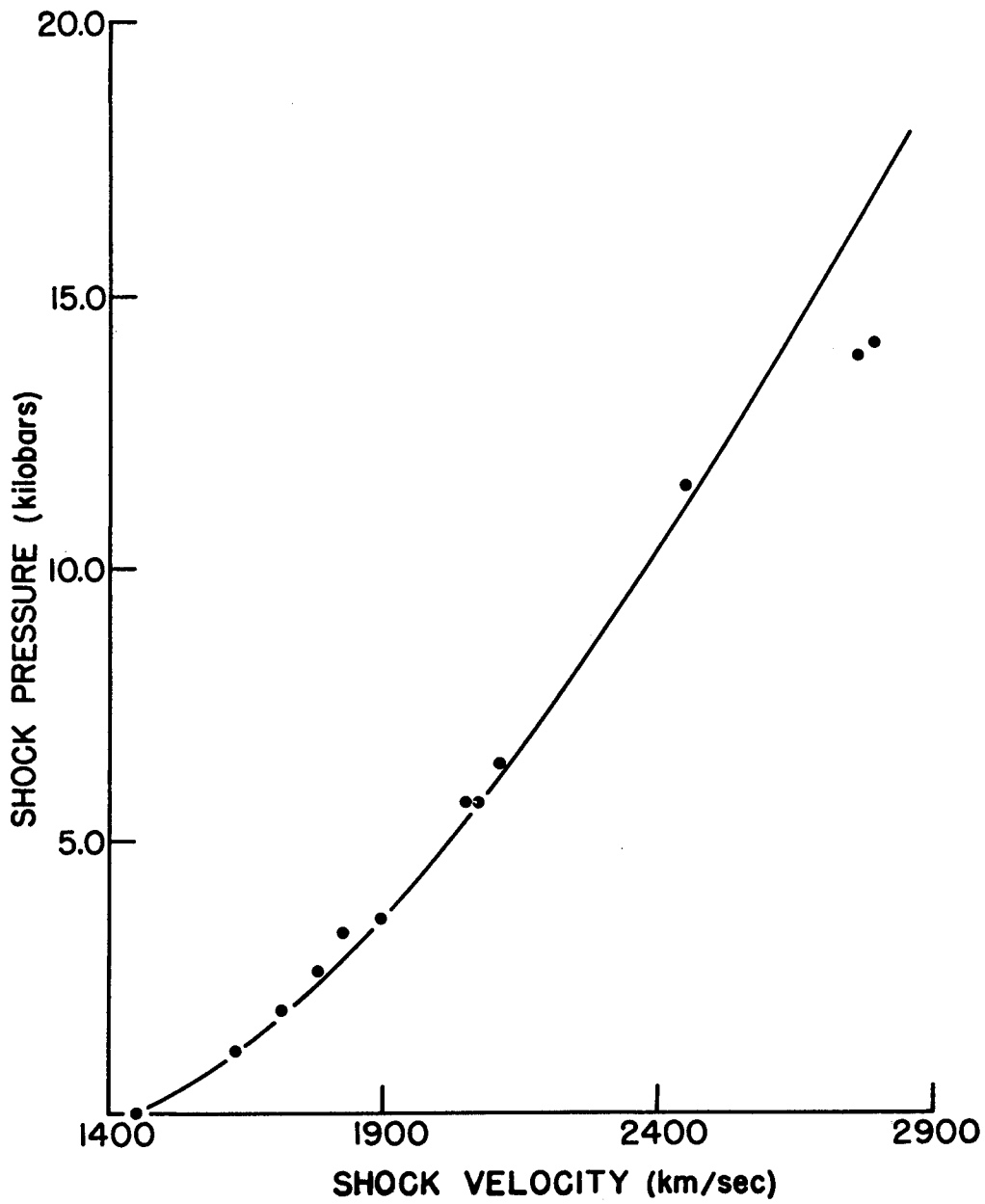
Fig. 5: Experimental shock velocity vs pressure data for water (low pressures).

Table II: Smoothed shock parameter results for water
(20°C ± 5C°)

Shock Velocity (m/sec)	Shock Pressure (kilobars)	Shock Velocity (m/sec)	Shock Pressure (kilobars)
1450	Sonic	3450	30.0
1620	1.0	3820	40.0
1740	2.0	4120	50.0
1840	3.0	4350	60.0
1940	4.0	4570	70.0
2020	5.0	4780	80.0
2100	6.0	4980	90.0
2170	7.0	5170	100.0
2240	8.0	5350	110.0
2310	9.0	5530	120.0
2380	10.0	5700	130.0
2680	15.0	5870	140.0
2980	20.0	6040	150.0
		6200	160.0

10 kb, and from thence there is a tendency for their data to bear to the left showing that their results indicate a greater compressibility. The results of Walsh and Rice fall about midway between those of Snay and Rosenbaum and this study. The differences in compression between the results of Walsh and Rice, which should be more comprehensive than Snay and Rosenbaum's data, and the data of this study were 3.2% for a shock velocity in water of 3500 m/sec and 2.8% for a shock velocity of 5500 m/sec, corresponding to pressures of 31 kb and 125 kb, respectively. The disagreement in pressures at these two velocities amounts to 9.7% for the lower velocity and 4.2% for the higher one.

The agreement between the shock parameter data for water obtained by Walsh and Rice and the data of this investigation is reasonably good. One may conclude, therefore, that the Rankine Hugoniot curves for water are now known with sufficient accuracy that water may reliably be used as the transmission medium for the measurement of pressures in shock and detonation waves.

In Table III are listed shock-parameter results for lucite in the form of shock velocity vs shock pressure, the data being portrayed graphically in Fig. 6. No differentiation was made in either case as to which of the two methods was used to obtain a given $p(V)$ point because the results of the two methods were indistinguishable within the limits of the experimental error involved. The smoothed results representing the most reliable values are given in Table IV. Note that in Fig. 6 the curve was not extended to the sonic velocity because it was found that considerable variation existed in values of sonic velocity available for lucite, and thus the true value was uncertain.

(b) Detonation pressure measurements

Results obtained for the military-type explosives in which the charge length was maintained at approximately 4 diameters to assure that the detonation wave was steady are listed in Table V. All the charges in this case may be considered to be unconfined, the cast charges being bare and the loose charges being contained in 1/16" thick pasteboard tubing. In Table V are listed the type explosive, the charge density, the charge diameter, the measured detonation velocity (D), the initial velocity of the shock transmitted into water (V_t), the initial pressure of the shock front in water (p_t), the ideal or hydrodynamic velocity D^* corresponding to the given density, the pressure of the detonation wave or incident wave (p_i) calculated through application of equation (1) (the impedance mismatch equation), the ideal detonation pressure calculated by means of thermohydrodynamic theory as outlined in Ref. 19, the ratio of pressure of the incident wave or detonation wave to ideal detonation pressure, and the $(D/D^*)^2$ ratio.

Table III: Experimental shock parameter data for lucite.

Shock Velocity (m/sec)	Shock Pressure (kilobars)	Shock Velocity (m/sec)	Shock Pressure (kilobars)
3300	19	4000	33
3400	23	4000	35
3520	23	4400	48
3700	27	4620	59
3740	29	5370	105
3800	30	6040	134
3800	31	6200	166
3950	32	6360	169
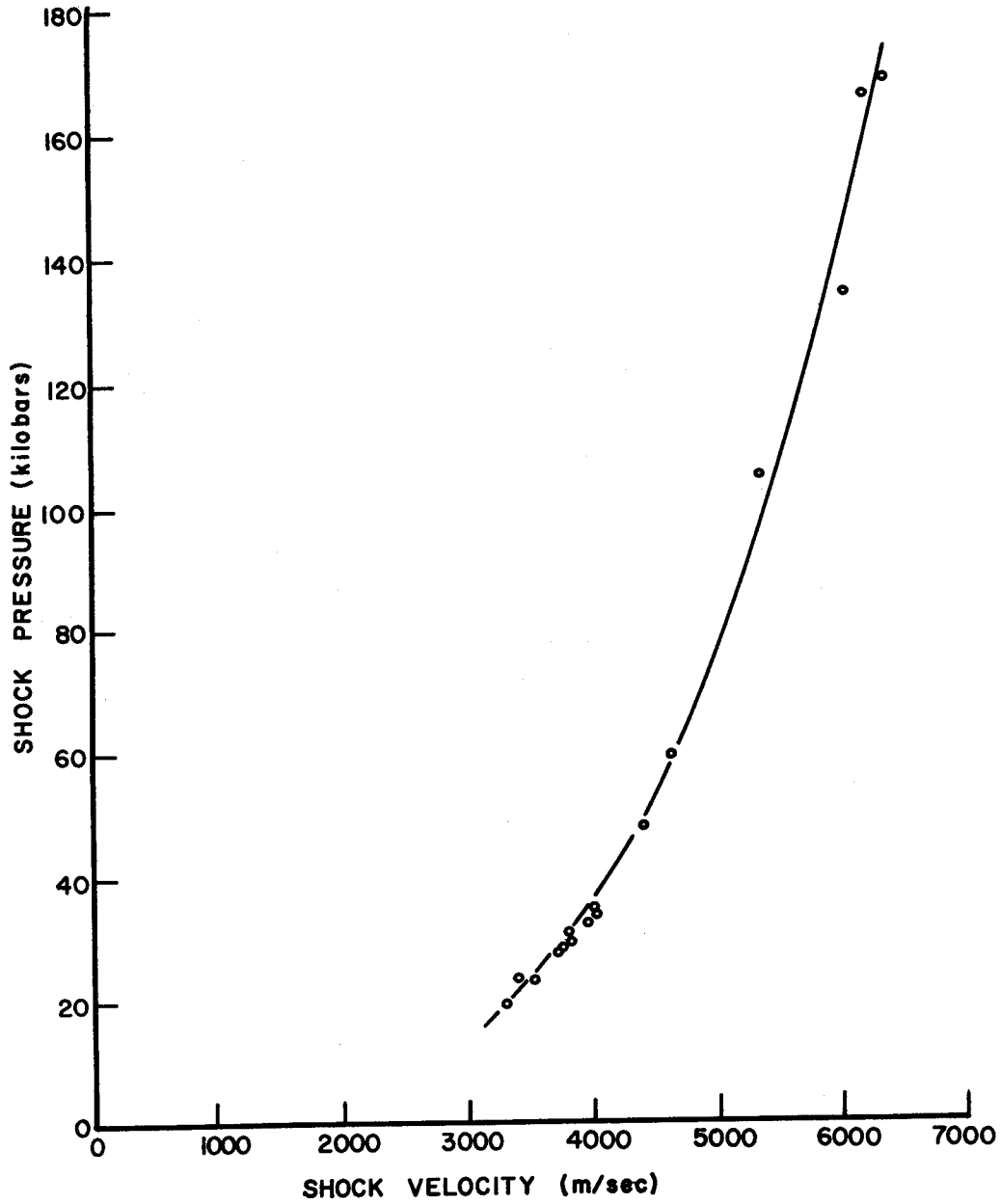
Fig. 6: Experimental shock velocity vs pressure data for lucite.

Table IV: Smoothed shock parameter data for lucite.

Shock Velocity (m/sec)	Shock Pressure (kilobars)	Shock Velocity (m/sec)	Shock Pressure (kilobars)
3350	20	5410	100
3820	30	5560	110
4160	40	5700	120
4430	50	5840	130
4670	60	5960	140
4880	70	6100	150
5070	80	6210	160
5250	90	6330	170

Table V: Experimental pressure measurement results for military type explosives

Explosive	ρ_1 (gm/cm³)	d_{exp} (cm)	D (m/sec)	V_t (m/sec)	P_t (kb)	D* (m/sec)	P_i (kb)	P_2^* (kb)	P_i/P_2^*	$(D/D*)^2$
RDX	1.10	1.25	5830	4640	75	6400	89	115	.78	.91
RDX	1.23	2.53	6410	5250	108	6850	135	145	.93	.90
RDX	1.17	2.53	6360	4760	80	6660	103	130	.79	.90
RDX	1.22	2.53	6535	5520	120	6830	147	142	1.02	.98
RDX	1.21	2.53	6610	5470	115	6800	141	139	1.01	.94
RDX	1.18	3.77	6750	4920	89	6730	118	130	.91	1.00
RDX	1.21	4.40	6665	5010	94	6800	123	139	.90	.96
RDX	1.21	5.05	6825	5325	113	6800	143	139	1.04	1.01
RDX	1.17	5.05	6750	5270	105	6670	131	130	1.01	1.00
RDX	1.17	5.05	6730	5400	112	6670	138	130	1.07	1.02
RDX	1.10	6.30	6400	5085	94	6370	112	115	.98	1.00
RDX	1.13	7.62	6620	5115	97	6550	119	122	.98	1.02
65/35 Ba(NO₃)₂ TNT	2.35	5.00	5150	4420	62	5600	116	156*	.74	.85
HBX-1	1.75	5.00	7160	5485	116	7400	190	190*	1.00	.94
50/50 NH₄NO₃ TNT (AN #1)**	1.58	4.80	5720	4860	84	6600	120	144	.84	.76
50/50 NH₄NO₃ TNT (AN #2)**	1.53	4.80	5550	4610	72	6450	102	136	.75	.74
50/50 NH₄NO₃ TNT (AN #1)**	1.58	7.62	6230	5160	100	6600	145	144	1.00	.89
50/50 NH₄NO₃ TNT (AN #2)**	1.53	7.62	6040	4850	85	6450	121	136	.89	.94
80/20 RDX Salt	1.32	2.53	5790	4850	85	6310	110	125	.88	.85
80/20 RDX Salt	1.30	4.40	6198	4925	87	6240	115	121	.95	.98
80/20 RDX Salt	1.28	5.00	6198	5000	92	6180	119	118	1.01	1.01
TNT -8+10 mesh	.95	5.05	3670	3810	40	4850	38	62	.61	.58
TNT -8+10 mesh	.95	5.05	3790	3906	43	4850	41.5	62	.67	.61
TNT -8+10 mesh	.97	7.62	4630	4080	49	4920	52	64	.81	.69

Table V: Continued

Explosive	ρ_1 (gm/cm^3)	d_{exp} (cm)	D (m/sec)	V_t (m/sec)	P_t (kb)	D^* (m/sec)	P_i (kb)	P_2^* (kb)	P_i/P_2^*	$(D/D^*)^2$
TNT -8+10 mesh	1.01	7.62	4660	4395	62	5050	64	70	.91	.85
TNT -8+10 mesh	1.00	7.62	4711	4220	56	5010	59	68	.87	.88
TNT -8+10 mesh	.99	10.00	4765	4410	63	4960	65	66	.98	.92
TNT -8+10 mesh	1.01	10.00	4835	4272	58	5060	62.5	70	.88	.92
TNT -8+10 mesh	1.00	7.62	4505	4410	63	5010	64	68	.94	.81
TNT -6+8 mesh	.99	7.62	4507	4000	47	4980	50	67	.75	.82
TNT -6+8 mesh	1.01	10.00	4675	4420	63	5060	65	70	.93	.85
TNT -6+8 mesh	1.02	10.00	4966	4362	61	5100	66	72	.92	.96
TNT -6+8 mesh	.97	16.10	4880	4350	60	4880	63	63	1.00	1.00
TNT -4+6 mesh	1.00	7.62	4414	3865	43	5010	45.5	68	.67	.77
TNT -4+6 mesh	1.02	10.00	4669	4206	55	5090	59	72	.82	.85
TNT -4+6 mesh	1.01	10.00	4645	4365	60	5030	62	68	.91	.85
TNT -4+6 mesh	1.06	12.35	4995	4410	63	5200	69	77	.90	.92
TNT -4+6 mesh	1.00	15.9	4800	4480	65	5010	66	68	.96	.92
TNT -4+6 mesh	.99	25.3	4600	4425	64	4980	65	67	.97	.97
TNT -48+65 mesh	.80	2.53	3840	4075	49	4350	43	46	.93	.77
TNT -48+65 mesh	.87	2.53	3870	4080	49	4600	45	52	.86	.72
TNT -48+65 mesh	.86	3.77	4550	4045	47.5	4550	47	51	.92	.93
TNT -48+65 mesh	.87	3.80	4445	4225	54	4650	52	52	1.00	.93
TNT -48+65 mesh	.86	4.40	4385	4080	49.0	4550	47	51	.92	.93
TNT -48+65 mesh	.87	5.05	4550	4385	62	4550	59	52	1.00	1.10
TNT -48+65 mesh	.87	5.05	4580	4262	56	4600	54	52	1.00	1.04
TNT -48+65 mesh	.91	5.05	4430	3910	45	4750	46	57	.81	.86
TNT -48+65 mesh	.91	5.05	4680	3910	45	4750	47	57	.82	.96
TNT -48+65 mesh	.81	7.62	4400	3915	43	4350	41	46	.89	1.00
TNT -48+65 mesh	.86	7.60	4525	4400	62	4540	57	51	1.11	.99
Composition B***	1.71		5800		140		230	230	1.00	
50/50 pentolite**	1.65		5680		134		214	215	.995	

Table V: Concluded

Explosive	ρ_1 (gm/cm³)	d_{exp} (cm)	D (m/sec)	V_t (m/sec)	ρ P_t (kb)	D* (m/sec)	P_i (kb)	P_2^* (kb)	P_i/P_2^*	$(D/D^*)^2$
Tetryl***	1.50			5400	115		172	175	.982	
TNT***	1.58			5100	96		159	160	.994	
TNT***	.87			3600	34		37	42	.881	

* Computed from $P_2^* = (\rho D^2)/4$

** AN #2 $\doteq$ 35 mesh
AN #1 was somewhat finer

*** Data from Ref. 16. (Detonation velocities were not measured. However, Composition B, 50/50 pentolite, pressed tetryl, and cast TNT should have propagated at ideal velocity.)

ρ = average density of the explosive
D = measured detonation velocity
D* = ideal or hydrodynamic value of detonation velocity
V_t = initial velocity of shock wave in the transmitted medium (water)
P_t = initial pressure of the shock wave in the transmitted medium (water)
P_i = pressure of the wave in the incident medium (the explosive) calculated from the impedance mismatch equation in terms of P_t
P_2^* = Chapman-Jouguet value of the detonation pressure at ideal detonation velocity calculated from thermohydrodynamics.

Fig. 7 presents results for special explosive X in 5 cm diameter and Composition B in 4.8 cm diameter for which the charge length was varied from 1 cm to 6 cm to determine if a pressure-buildup effect existed in explosives of very short reaction zone lengths where one would expect no detonation velocity transient. These charges were all boostered with identical 1/2" x 1" pressed RDX boosters. With such short charges, however, difficulty was encountered in measuring the initial velocity of the shock wave in water because of a rapid attenuation in velocity of the shock in the aquarium. The plot of the results indicates, despite of the observed scatter, a small pickup in detonation pressure as the charge length was increased. Whether or not the detonation velocity increased slightly over this region in order to produce the pressure pickup could not be determined.

Data for the commercial blasting agents are given in Table VI through the courtesy of the Intermountain Research and Engineering Company, Salt Lake City, Utah. These results are given both for unconfined charges and charges confined in 3/8" thick or 1/4" thick steel tubing. One will note that the detonation velocity and pressure of the low density AN/fuel oil mix was very sensitive to confinement. In 5" diameter unconfined charges the detonation velocity was only 2770 m/sec which corresponded to a D/D^* ratio of only 0.66 while with 3/8" steel confinement in the same diameter the detonation velocity was 3930 m/sec corresponding to a D/D^* ratio of 0.94. The DBA series of coarse TNT or Composition B "slurries" were much less sensitive to confinement probably because their detonation pressure is much higher.

In comparing the measured values for pressure in the explosive, that is, pressures of the incident waves (p_i) obtained by the aquarium technique, one will note that in every case where the detonation wave propagated at ideal velocity, p_i was found to agree within experimental error with the Chapman-Jouguet pressure p_2^*, i.e., to the detonation pressure calculat ed from thermohydrodynamic theory. A similar result was found in the study of Ref. 12. It should also be stressed that in most of the loose packed explosives the impedance match between the explosive and water was very good . Therefore, calculations of pressure in the incident medium in terms of pressure of the transmitted medium, through applications of the shock impedance mismatch equation, should be very reliable.

Since the pressure through a detonation wave is given by the relation $p = \rho_1 DW$ one would expect that in non-ideal detonations the Chapman-Jouguet pressure, which is defined as the pressure at the surface in the wave ahead of which chemical reaction supports propagation and behind which chemical reaction lends no support, should be given by

$$p \doteq (D/D^*)^2 p_2^*\qquad(4)$$
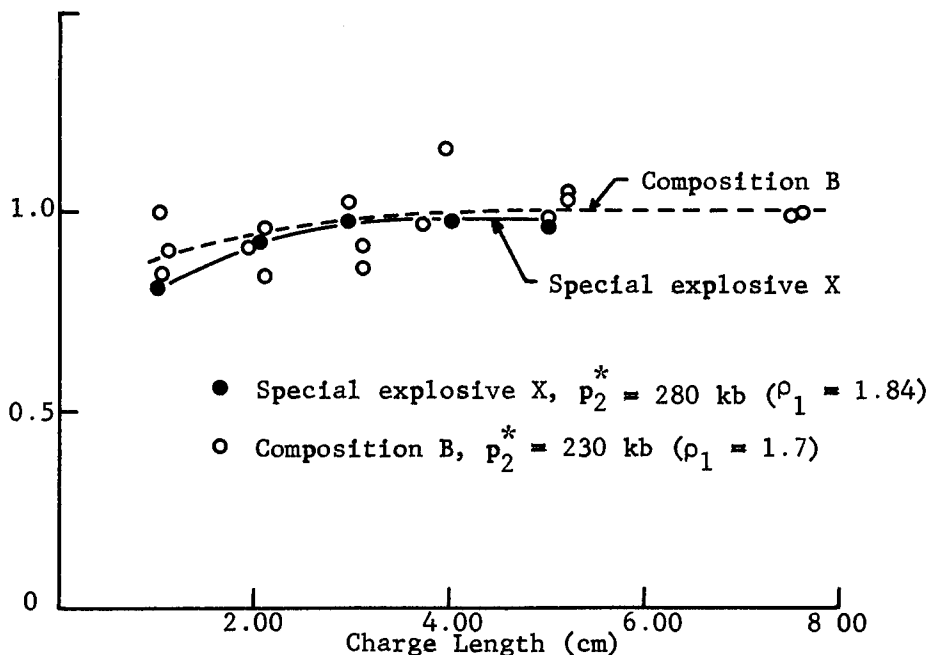
Fig. 7: Pressure of the detonation wave (measured by the aquarium technique) as a function of charge length for 5 cm diameter special explosive X and 4.8 cm diameter Composition B boostered with 1/2" x 1" pressed RDX.

where asterisks signify ideal values, p_2^* being the ideal detonation pressure. Equation (4) assumes that W/D depends only on ρ_1 and not on D/D^*, an assumption well justified by the generality of the covolume-specific volume $(\alpha[v]$ curve for high explosives)[19] Comparisons of $(D/D^*)^2$ with p/p_2^* given in Tables V and VI indeed show a striking agreement in most cases.

Some very important information regarding the pressure or particle velocity profiles of detonation waves are also apparent from this study. According to the Zeldovich-von Neumann concept, which is based upon transport phenomena being negligible in a detonation wave, the pressure at the detonation front should be approximately twice the Chapman-Jouguet pressure. Then as chemical reaction proceeds the pressure decays along the Rayleigh line to the Chapman Jouguet value at the end of the reaction zone. For explosives of reaction zone length of the order of a few mm or less, e.g., Composition B, the presence of the von Neumann spike would be very difficult to detect. As mentioned earlier previous experiments to determine the pressure profiles through reaction zones by means of the aluminum free surface velocity technique were devoted primarily to explosives of very short reaction zone length, i.e., Composition B.

380

Table VI: Experimental pressure measurement results for commercial blasting agents

Blasting Agent	ρ (g/cm³)	d (in)	Confinement	No. Measurements	D (m/sec)	V_t (m/sec)	P_t (kb)	D* (m/sec)	P_i (kb)	P_2^* (kb)	P_i/P_2^*	$(D/D*)^2$
94/6 AN/FO	0.82	5	None	3	2770±50	2550±70	12±.5	4200	13.5±1.0	40	0.34	0.43
94/6 AN/FO	0.82	5	Steel*	2	3930±20	3900±170	42.5±3	4200	37.5±1.5	40	0.93	0.88
DBA-1	1.52	5	None	5	4900±100	4000±100	46±3	6400	85±3	150	0.57	0.59
DBA-1	1.52	5	Steel*	1	5120	4720	77	6400	103	150	0.69	0.64
DBA-2	1.68	5	None	2	5500±100	4480±120	64±4	6800	97±5	180	0.54	0.66
DBA-2	1.60	5	Steel*	2	5270±70	4800±100	80±5	6500	111±10	155	0.71	0.66
DBA-3	1.58	5	None	4	5800±80	4600±200	71±10	6800	126±8	180	0.70	0.72
DBA-3	1.58	5	Steel*	2	6180±80	5530±190	125±10	6800	172±11	180	0.95	0.83
DBA-3	1.58	2	None	3	5300±100	4700±100	74±5	6800	101±5	180	0.56	0.63
DBA-3	1.58	2	Steel*	2	5885±15	5050±150	94±7	6800	134±6	180	0.75	0.75

* Steel confinement was 3/8" tubing for 5" diameter and 1/4" tubing for 2" diameter

ρ = average density of the explosive

D = measured detonation velocity

D* = ideal or hydrodynamic value of detonation velocity

V_t = initial velocity of shock wave in the transmitted medium (water)

P_t = initial pressure of the shock wave in the transmitted medium (water)

P_i = pressure of the wave in the incident medium (the explosive) calculated from the impedance mismatch equation in terms of P_t

P_2^* = Chapman-Jouguet value of the detonation pressure at ideal detonation velocity calculated from thermohydrodynamics.

Note: The plus and minus variations cover the spread in the experimental data.

381

This choice of explosive necessitated the use of very thin plates for which the free surface velocity measurements were in question.
Since there is no reason to believe that an overpressure, if present, would exist in a rapidly reacting explosive and not in a slowly reacting one, it would seem prudent to look for evidence of a spike in slowly reacting explosives. The blasting agents listed in Table VI represent a class of explosives known to possess the longest reaction zones of the detonating type explosives and, according to any published theory, possess reaction zone lengths sufficiently great that a spike could easily be detected by the aquarium technique, but no evidence of a spike was observed. The coarse TNT series, especially -4+6 mesh TNT, also have reaction zone lengths which are ample for easy detection of a spike by the aquarium technique. And yet with -4+6 mesh TNT in 25.3 cm diameter, where the detonation velocity was in close agreement with the ideal value, and the impedance match was very good, the pressure of the incident wave corresponding to the initial velocity of the transmitted wave was found to equal the Chapman-Jouguet value.

Fig. 8 shows a streak camera trace illustrating the aquarium technique for measuring detonation pressures by transmitted shock waves in water. In this case the charge consisted of a slurry explosive detonated in a 5" I.D. steel tube. Note the slow attenuation of the velocity of the shock wave in water. This is typical of large charges which permits an accurate measurement of the initial velocity of the shock.

In conclusion, therefore, since even with explosives possessing the longest known reaction zone lengths, the aquarium technique measured the Chapman-Jouguet value of the detonation pressure, it appears that the highest pressure in the detonation wave is the Chapman-Jouguet pressure. This conclusion is strengthened by the fact that such results have been obtained in those cases where the characteristic impedance of the explosive very nearly equalled the shock impedance of the water under which condition computations from the impedance mismatch equation would be expected to be very reliable.

Acknowledgment
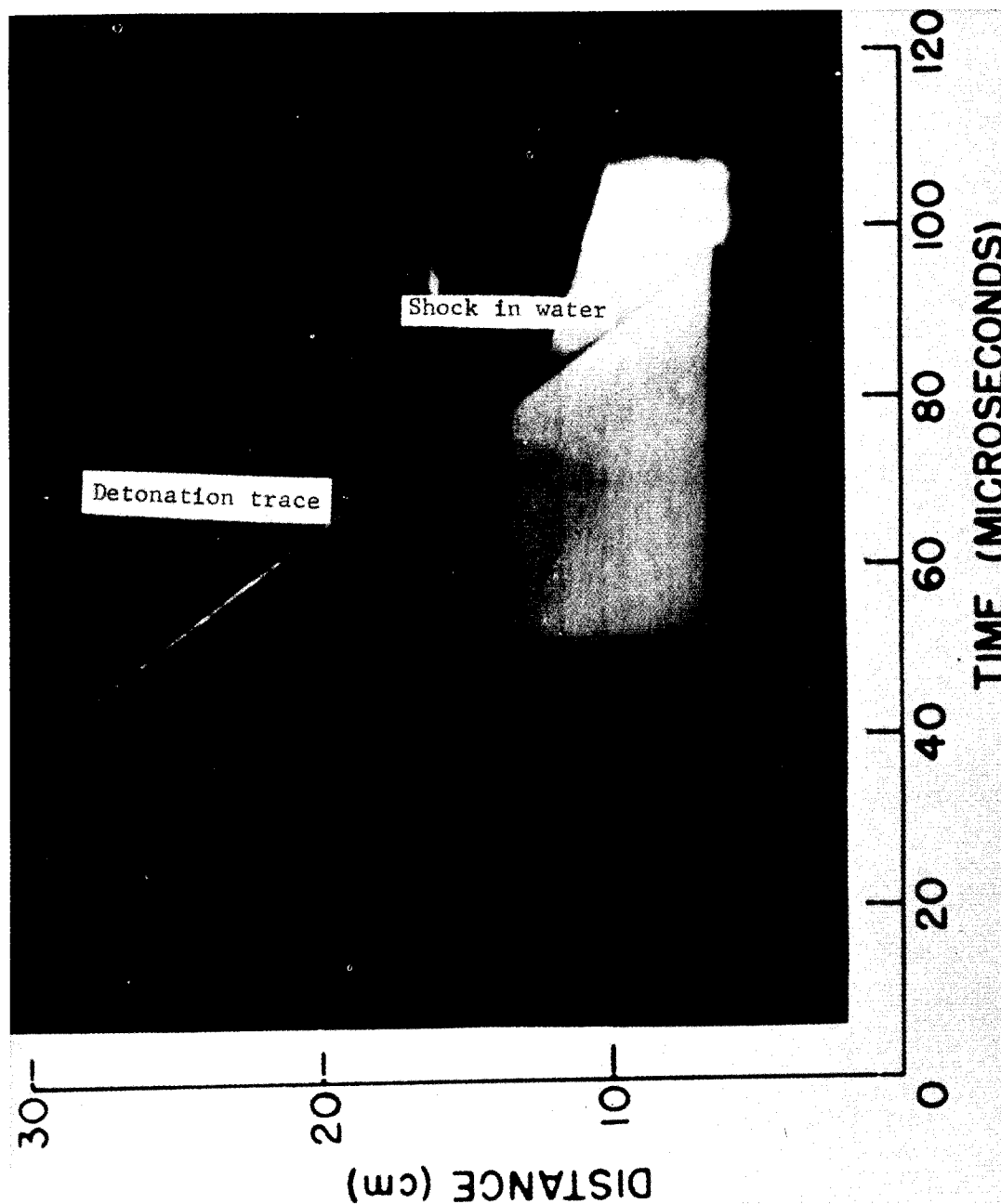
Fig. 8: Streak camera trace illustrating the aquarium
technique for measurement of detonation pressure
(explosive, slurry in 5" I.D. steel tube).

BIBLIOGRAPHY

1. J. G. Kirkwood and E. W. Montrall, "The Pressure Wave Produced by an Underwater Explosion II," OSRD No. 670, June 1942.

2. J. G. Kirkwood and J. M. Richardson, "The Pressure Wave Produced by an Underwater Explosion III," OSRD No. 813, August 1942.

3. J. M. Richardson, J. M. Arons, and R. R. Halverson, "Hydrodynamic Properties of Sea Water at the Front of a Shock Wave," J. Chem. Phys. 15, 785-794 (1947).

4. A. B. Arons and R. R. Halverson, "Calculations for Sea Water at the Shock Front," OSRD No. 6577, March 1946.

5. W. Doering and G. Burkhardt, "Contribution to the Theory of Detonation," HEC Accession List No. 60, Page 4, Bias Group.

6. P. W. Bridgman, "Water in the Liquid and Five Solid Forms under Pressure," Proc. American Academy of Arts and Sciences, 47, 441-558 (1912).

7. P. W. Bridgman, "The Phase Diagram of Water to 45,000 kg/cm^2", J. Chem. Phys. 5, 964-966 (1937).

8. H. G. Snay and J. H. Rosenbaum, "Shockwave Parameters in Fresh Water for Pressures up to 95 Kilobars", NAVORD Report 2383, U.S. Naval Ordnance Laboratory, White Oak, Maryland, April 1952.

9. P. W. Bridgman, "Freezing and Compressions to 50,000 kg/cm^2", J. Chem. Phys. 9, 794-797 (1941).

10. P. W. Bridgman, "Freezing Parameters and Compression of Twenty-One Substances to 50,000 kg/cm^2," Proc. American Academy of Arts and Sciences, 74, 399-424 (1942).

11. J. M. Walsh and M. H. Rice, "Dynamic Compression of Liquids from Measurements in Strong Shockwaves", J. Chem. Phys. 26 (1957).

12. W. C. Holton, "The Detonation Pressures in Explosives as Measured by Transmitted Shocks in Water," NAVORD 3968, U.S. Naval Ordnance Laboratory, White Oak, Maryland, 1 Dec 1954.

13. R. E. Duff and E. Houston, "Measurement of the Chapman-Jouguet Pressure and Reaction Zone Length in a Detonating High Explosive," Second ONR Symposium on Detonation, Washington, D.C., February 9-11 (1955), page 225.

14. H. D. Mallory and S. J. Jacobs, "The Detonation Zone in Condensed Explosives," Second ONR Symposium on Detonation, Washington, D.C. February 9-11 (1955) page 240.

15. R. B. Clay, M. A. Cook, and R. T. Keyes, "Plate Velocities in the Impulse Loading by Detonation Waves," Preprint 9, Symposium on Shock Waves in Process Equipment, Annual Meeting, Chicago, Illinois, American Institute of Chemical Engineers, Dec 8-11, 1957.

16. M. A.Cook, D. H. Pack and W. S. McEwan, "Promotion of Shock Initiation of Detonation by Metallic Surfaces", Trans. Fara. Soc. No. 451, Vol. 56, Part 7, July 1960.

17. A. Bauer and M. A. Cook, "Observed Detonation Pressures of Blasting Agents", Submitted for publication in the Canadian Mining Journal.

18. M. A. Cook and H. E. Farnam, U.S. Patent No. 2,930,685, March 29, 1960.

19. M. A. Cook, "The Science of High Explosives," Reinhold Publishing Corporation, New York (1958).

LOW PRESSURE POINTS ON THE ISENTROPES
OF SEVERAL HIGH EXPLOSIVES

W. E. Deal
University of California
Los Alamos Scientific Laboratory
Los Alamos, New Mexico

Basic Principles

When a plane detonation wave travelling perpendicular to a plane explosive-air interface arrives at that interface, a shock is driven forward into the air by the expanding explosive reaction products and a rarefaction is reflected back through these reaction products. Assuming the detonation wave to be a shock followed by a reaction zone of rapidly decreasing pressure (von Neumann spike) terminating at the Chapman-Jouguet (C-J) plane which in turn is followed by the rarefaction wave from the rear of the explosive (Taylor wave), one might expect the air shock velocity to exhibit an initial value which decays rapidly[*] followed by a region of more gradual decay. The state behind the air shock after decay of the von Neumann spike effect and before appreciable Taylor wave decay would correspond to expansion of the explosive reaction products from the C-J state[**]. The interaction at the interface between the air and reaction products after decay of spike effects is shown in the pressure-particle velocity plane in Fig. 1. The coordinates of the intersection between the air shock Hugoniot and the reaction products isentrope in this plane are the pressure and particle velocity behind both the forward moving air shock and the backward

---

[*] If, however, the rarefaction reflected into the explosive quenches the reaction, there will be a thin layer of unreacted explosive carried ahead of the reaction products. The interaction of this thin layer of unreacted or partially reacted explosive with the reaction products from the C-J state is analogous to the problem of a thin foil on the free surface of a moving thick plate of lower shock impedance. The thin layer equilibrates rapidly to the velocity of the thick pushing medium.

[**] The C-J state may not be clearly defined for charges of finite length and diameter in which case the state at the terminus of the reaction zone is intended.

moving rarefaction wave into the reaction products (i.e., these two quantities are continuous across the interface). Determination of the pressure and particle velocity for the air shock thus gives a point on the reaction products isentrope from the C-J state.
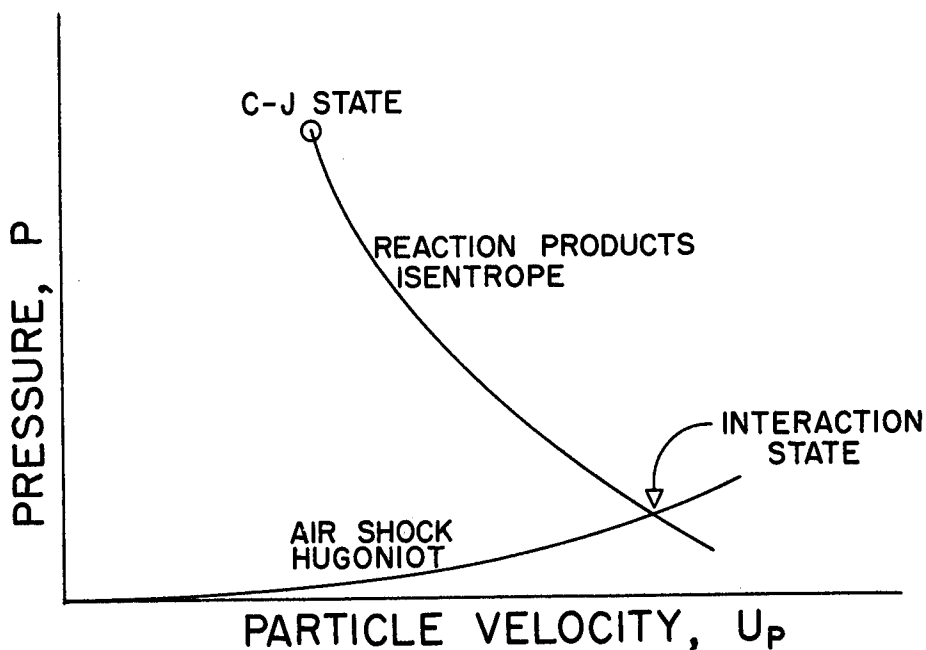
Fig. 1 - Interaction at Air-Reaction Products Interface

C-J pressures are of the order of 300 kilobars and the air shock pressures are of the order of one kilobar, consequently such determinations allow checking of an equation of state at two widely separated pressures. For a gamma-law equation of state (i.e., P/ρ^γ = const.), the P-U_p isentrope from the C-J state is given by (1):

$$U_p = \left[P_{cj}/(\alpha \rho_o D)\right]\left[1 + \alpha - (P/P_{cj})^\alpha\right], \qquad 1$$

$$\text{where } \alpha = (\gamma - 1)/2\gamma, \qquad 2$$

$$\text{and } \gamma = (\rho_o D^2/P_{cj}) - 1. \qquad 3$$

Insertion of known values for explosive initial density ρ_o and detonation velocity D as well as pressure P and particle velocity U_p from air shock determinations yields gamma and C-J pressure P_{cj} by successive iteration. These quantities may then be compared to values obtained from measurements in metals (2). Error analysis of these equations shows that a 1% error in U_p corresponds to very nearly 1% change in the calculated γ and 3/4% change in the calculated P_{cj}.

Experimental Technique

The explosive system for these experiments consisted of an explosive plane wave lens of 8-in. aperture which detonated a cylinder of the explosive to be studied on one end. The expansion of the reaction products from the opposite end of the cylinder after complete detonation then acted as the piston which drove the air shock. A schematic of the shot arrangement is shown in Fig. 2.

DETONATOR

CHARGE
TO BE STUDIED

AIR SHOCK POSITION
DURING MEASUREMENT

EXPLOSIVE
PLANE LENS

SLIT PLATE

MARKER
TAPES

CAMERA VIEW
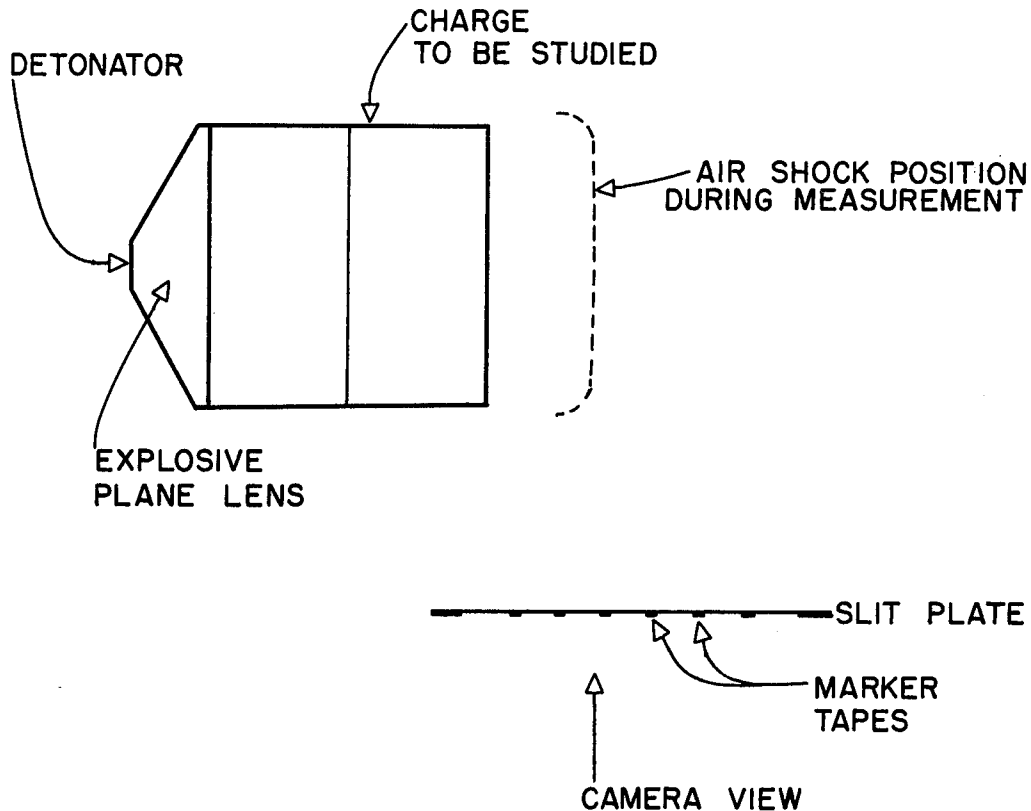
Fig. 2 - Schematic of Shot Arrangement

The velocity of this air shock was determined using a sweeping image camera to view the luminous* shock through a slit

---

* The use of the self-luminosity of the shock introduces uncertainties in measurements of rapidly varying shock velocity because of possible emission relaxation times long compared to the period of shock velocity change; however, results quoted here are for essentially steady state shocks as can be seen from the typical record shown in Fig. 3.

parallel to the direction of shock travel. An image of the slit with
its scaling markers was swept on the film perpendicular to its
length. The writing speed of the camera was adjusted to yield a
trace angle of about 45°. A typical good quality record is shown in
Fig. 3. The slope of the leading edge of luminosity along with
camera demagnification and writing speed yield a value for the air
shock velocity.

It is possible to deduce particle velocity from the shot
record by use of the slope of the line of extinction of luminosity;
however, because of effects at the explosive periphery, this edge is
so much more diffuse than the leading edge that attempts to measure
it were abandoned in favor of calculating it using an IBM 704
program (3) developed by Dr. R. E. Duff of this laboratory. The
program was used to calculate shock parameters for an air mixture
of 78.11, 20.96 and 0.93 mole percent of N_2, O_2, and A respectively.
Species N_2, O_2, A, NO, N, O, N_2^+, O_2^+, A^+, NO^+, N^+, O^+, O^-, and
electrons were included in the calculation. Thermodynamic functions
given by F. R. Gilmore (4) were used. An individual calculation was
performed for each shot; thus initial air temperature and pressure
needed only to be measured for each experiment, not controlled.

Charges of 8-in. diameter and 8-in. thickness made up of
two 4-in. layers were used in all experiments reported here. Three
shots each were fired for charges of pressed TNT, Composition B,
77/23 Cyclotol, and Octol. Charge densities were obtained for the
pieces fired; composition analysis, composition spread and density
spread within a charge were obtained by sectioning charges prepared
in an identical manner. These quantities are listed in Table I
along with the other data.

Camera demagnification was obtained for each shot from a
photograph of the slit plate by the shot camera with the image
stationary. A correction was then applied to this demagnification
value because the point of origin of the light in the shock front
was behind the slit a small distance. Careful alignment of the axis
of the charge relative to the optical axis of the camera was neces-
sary such that these axes were perpendicular at the point in front
of the charge where the precise measurement was desired. With an
object distance of about 400 inches, variation of the point of light
emission across the face of a 4-in. radius charge could cause as much
as $\pm 1\%$ variation in the demagnification factor. In fact, the air
shock is not perfectly plane as is seen in the framing camera
pictures of Fig. 4 and except for the very first motion this error
could not be greater than $\pm 0.5\%$.

Data and Results

The coordinates of the leading edge of luminosity of the
camera record were read with a two-axis comparator after first
aligning the time direction with one axis. The slope of this edge
was then determined by a linear least squares fit to the coordinates
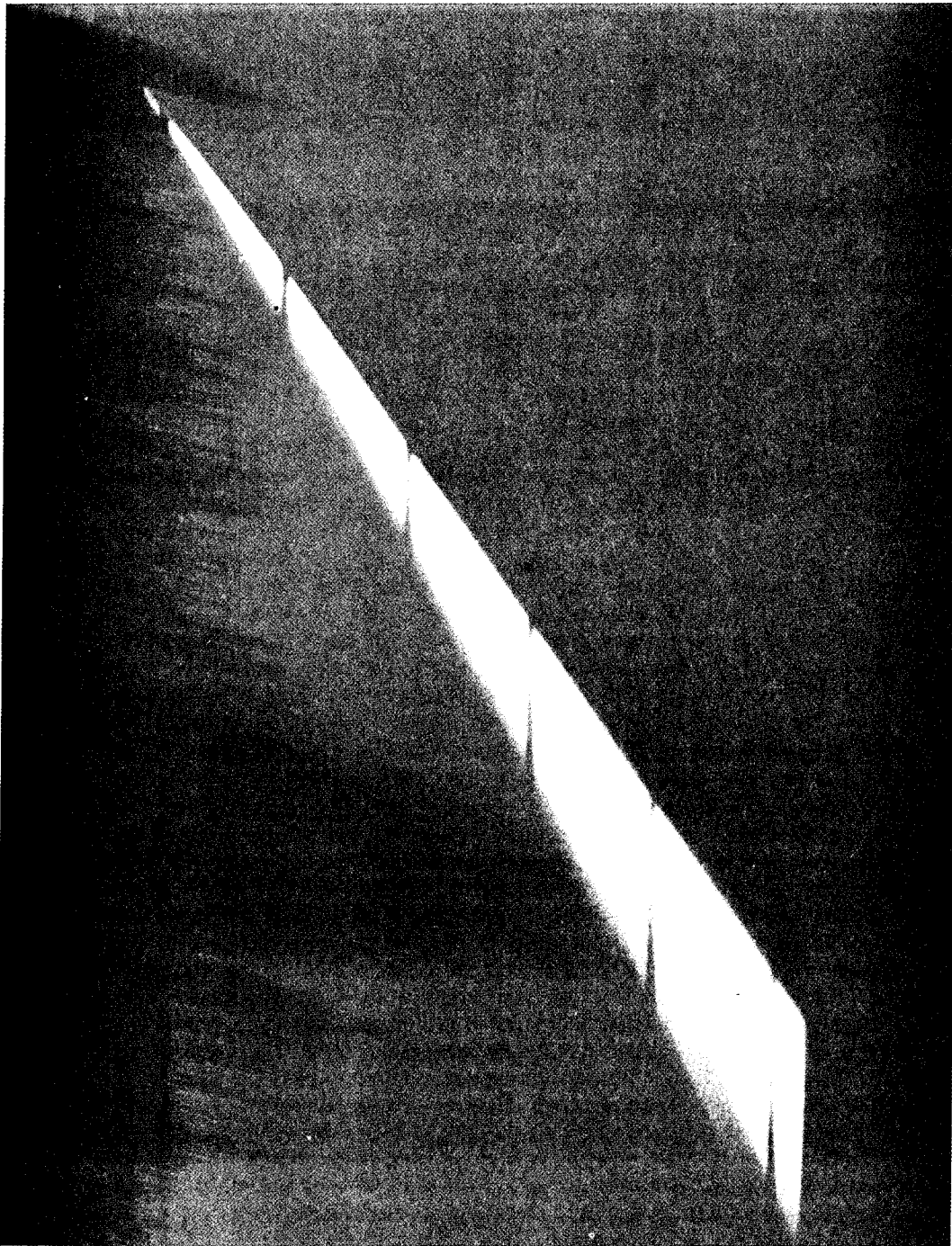
Fig. 3 - Typical good quality smear-camera record. Time increases downward; the air shock is moving from left to right. The gaps in the trace are from the fiducial tapes on the slit.

Table I - Results of Twelve Experiments

A - Pressed TNT
Pure TNT
$\rho_o = 1.636 \pm .002$ gm/cc
$D = .6932$ cm/μsec.

Shot No.	T_o °K	P_o bars	U_s cm/μsec	U_p cm/μsec	P bars
2172	285.7	.7959	.7340	.6708	478.4
2173	293.7	.8091	.7567	.6924	503.3
2174	297.2	.8091	.7417	.6781	477.6

B - Grade A Composition B
$62.8 \pm 0.8\%$ RDX
$\rho_o = 1.717 \pm .002$ gm/cc
$D = .7985$ cm/μsec

2167	293.2	.7972	.8673	.7966	654.9
2168	292.7	.7972	.8699	.7990	660.0
2182	301.2	.8100	.8679	.7972	648.7

C - 77/23 Cyclotol
$77.0 \pm 0.7\%$ RDX
$\rho_o = 1.752 \pm .002$ gm/cc
$D = .8274$ cm/μsec

2186	298.7	.8021	.8640	.7935	641.9
2190	293.7	.8014	.8763	.8050	671.0
2191	294.2	.8013	.8867	.8147	685.9

D - Octol
$77.6 \pm 1.5\%$ HMX
$\rho_o = 1.821 \pm .002$ gm/cc
$D = .8494$ cm/μsec

2181	299.2	.8101	.8862	.8142	681.1
2184	295.2	.8099	.8777	.8063	676.9
2185	301.2	.8020	.9074	.8339	702.4
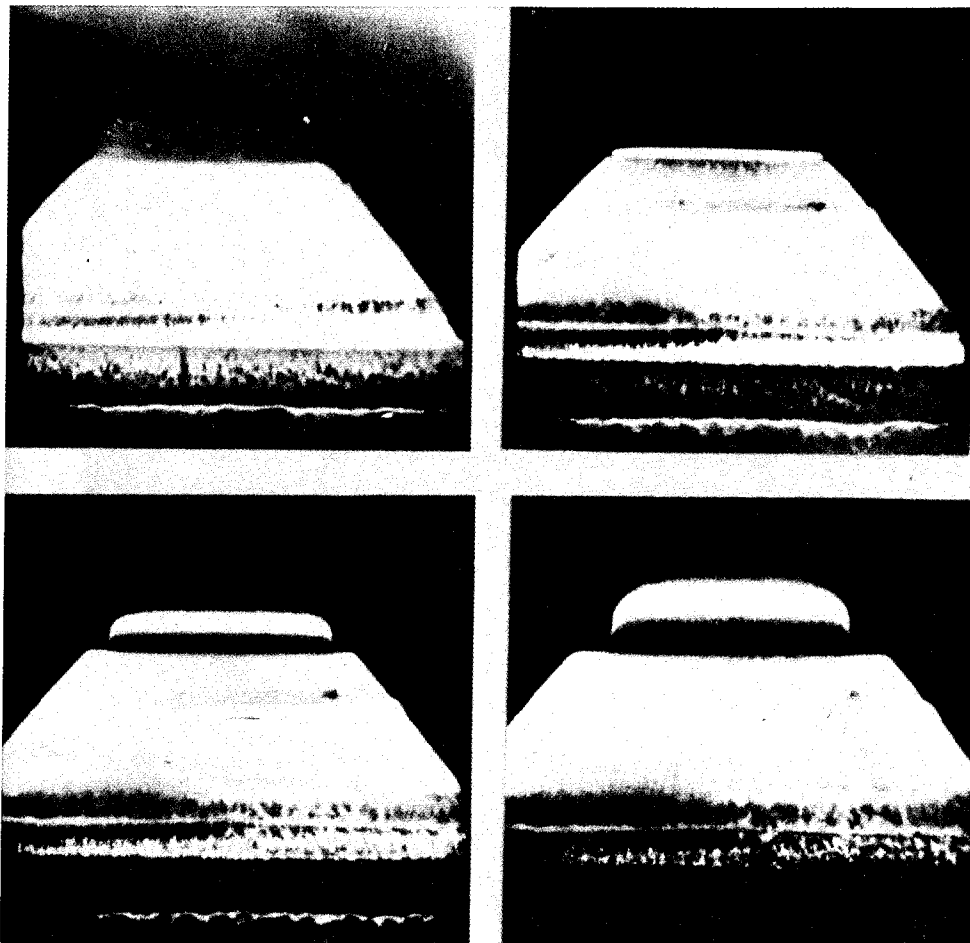
Fig. 4 - Four pictures selected from a framing-camera sequence of twenty-five. The time interval between the pictures shown is five microseconds. The detonation and shock waves are moving upward. The first picture shows the explosive before emergence of the detonation wave, the second shows the air shock within one microsecond after formation, and the third and fourth pictures show the air shock after 1.7 in. and 3.4 in. of further travel respectively.

after first deleting data for about the first 1/4-in. of motion where some evidence of curvature was seen and for distances greater than the charge radius where edge effects might affect the velocity. The resulting shock velocities (U_s) are listed in Table I for the twelve shots (three shots for each of four explosives) along with initial conditions (T_o, P_o) and calculated particle velocities (U_p) and shock pressures (P). The detonation velocities given were calculated from experimental D-ρ_o relations obtained by previously described methods (5). The difference between the air shock velocities off Composition B given in Table I and that quoted in Reference 1 is due to the failure to apply a 5% parallax correction to the Reference 1 gas data. Insertion of values of P, U_p, ρ_o, and D from Table I into Equations 1, 2, and 3 yield γ and P_{cj} by successive iteration. The values so obtained are given in Table II and compared with values, corrected to the same density, obtained from measurements of the shock attenuation in dural (2).

The rather distinct difference in the TNT γ and P_{cj} obtained by the two methods indicates that assumption of constant gamma equation of state to approximately 500 bars is not justified for TNT. The γ and P_{cj} from the two methods for the other three explosives agree rather well, however. It is indeed remarkable that the assumption of constant gamma holds so well at these widely separated pressures, at least so far as hydrodynamic variables are concerned. While this agreement does not assure constancy of gamma in the intervening region, the data of Reference 1 at eleven pressure points for Composition B prejudices one to expect constancy of gamma in the intervening region for Cyclotol and Octol also.

Table II - Calculated γ and P_{cj} Compared with Dural Data

A - Pressed TNT

| | Shot No. | | | | | % Differ- |
	2172	2173	2174	Average	Ref. 2	ence
γ	2.794	2.704	2.765	2.754 ± 1.4%	3.172	-13.2
P_{cj} (kb)	207.2	212.2	208.8	209.4 ± 1.0%	188.4	+11.1

B - Composition B

| | Shot No. | | | | | % Differ- |
	2167	2168	2182	Average	Ref. 2	ence
γ	2.714	2.707	2.714	2.712 ± 0.1%	2.769	-2.1
P_{cj} (kb)	294.7	295.3	294.7	294.9 ± 0.1%	290.4	+1.5

C - Cyclotol

| | Shot No. | | | | | % Differ- |
	2186	2190	2191	Average	Ref. 2	ence
γ	2.831	2.789	2.753	2.791 ± 1.1%	2.798	-0.3
P_{cj} (kb)	313.1	316.6	319.6	316.4 ± 0.9%	315.8	+0.2

D - Octol

| | Shot No. | | | | | % Differ- |
	2181	2184	2185	Average	Ref. 2*	ence
γ	2.836	2.864	2.769	2.823 ± 1.4%	2.844	-0.7
P_{cj} (kb)	342.5	340.0	348.6	343.7 ± 1.0%	341.8	+0.6

* This explosive was not reported in Reference 2
but data were obtained in the identical manner
described there.

References

1. W. E. Deal, Phys. Fluids $\underline{1}$, 523 (1958).

2. W. E. Deal, J. Chem. Phys. $\underline{27}$, 796 (1957).

3. IBM 704 Code HUG.

4. F. R. Gilmore, Rand Corp. Report No. RM 1543 (1955).

5. Campbell, Malin, Boyd, and Hull, Rev. Sci. Instr. $\underline{27}$, 567 (1956).

STRONG SHOCKS IN POROUS MEDIA[*]

James L. Austing
H. S. Napadensky
R. H. Stresau[**]
J. Savitt
Armour Research Foundation
Chicago 16, Illinois

INTRODUCTION

Various theories have been advanced to explain qualitatively the complex phenomena encountered in the detonation process. The most widely quoted of these theories is that proposed by von Neumann (1). This theory makes the argument that the initial shock at the detonation front is a non-reactive one in which the explosive is compressed to a high pressure-density point on the Hugoniot curve for the unreacted explosive. Then there follows a period of chemical reaction in which each of the intermediate unreacted explosive-reaction product mixtures follows the Rankine-Hugoniot assumptions. Such a theory gives rise to a pressure spike in the detonation head, and this pressure in the non-reactive shock is higher than the Chapman-Jouguet pressure at the end of the reaction zone. While this theory is broadly accepted, some investigators have failed to observe the predicted spike. Cook (2), for example, has proposed an alternate mechanism, particularly for gaseous explosives. This mechanism suggests that the initial shock compresses the explosive to a pressure equal to that of the Chapman-Jouguet point. Then the pressure across the reaction zone is equal to the Chapman-Jouguet pressure, due to a high thermal conductivity in the reaction zone itself. Similar reasoning is then extended to solid explosives, and data are presented which seem to support the contention that there is no spike in the detonation head.

Some of the investigators who have detected the von Neumann spike have found variations in its shape. For example, Mallory and Jacobs (3) detected a plateau in the spike for TNT which they interpreted as an indication that the reaction proceeded at an appreciable rate only after an inception period. This was evidence that the reaction in TNT proceeds according to a thermal mechanism. On the other hand, Duff and Houston (4) observed a sharply peaked pressure profile for Composition B with no evidence of a plateau. This was

an indication that the reaction is essentially a surface burning re-
action. Other investigators may find different profiles in the
reaction zone, depending on the types of explosives studied and
the experimental techniques used.

It is readily seen that there are differing views as to which
model correctly predicts the behavior of the detonation process. All
of these models are based on purely speculative reasoning which in
some cases appears to be supported by adequate experimental evidence.
But in the past the conclusions which were made on the basis of evi
dence from these various experiments have been contradictory, and this
in turn leads to the different detonation models. At this point we
should ask ourselves why has it not been possible to predict an adequate
model which is based on fundamental considerations and which ties
together all facets of experimental data. One reason for this is the
complete lack of quantitative equations of state for unreacted explo
sives, particularly solid explosives. But in attempting to arrive
at a reasonable equation of state, the porosity of the medium must
not be ignored. Therefore, an experimental technique which enables
us to obtain data for the derivation of an equation of state for a
porous material, we believe, should be extended to the application
of determining equations of state of unreacted solid explosives.

For the past several years, Armour Research Foundation has
been engaged in a fundamental research program in the field of nuclear
reactor safety. This program has resulted in the development of an
experimental technique to observe the dynamic response of porous media
used in the design of blast shields for nuclear reactors. Various
porous materials such as Flintkote Insulboard, pine, maple, and redwood
have been studied at high rates of loading by means of this technique.
However, this paper is concerned entirely with data on the Flintkote.
A Hugoniot curve has been constructed based on the data obtained from
the propagation of the shock wave in the medium. This curve, together
with basic thermodynamic identities, has led directly to the calculation
of the temperature rise across the shock front. The combination of the
Hugoniot curve and the temperature data provides the necessary infor
mation from which an equation of state of the Insulboard material
may be derived. We recognize that these data in themselves have no
direct bearing on the behavior of explosives. However, the results we
have obtained are of interest at a meeting of this type because in
some ways Flintkote is similar to a solid explosive, especially with
respect to its porosity.

EXPERIMENTAL TECHNIQUE

Shocks in porous media such as Flintkote and wood have been observed by means of an experimental technique which also allows us to obtain the dynamic stress-strain data of these materials at very high rates of loading. A schematic diagram of the experimental arrangement is shown in Fig. 1. Essentially, the experimental set-up consists of a cylindrical porous specimen on which a reference grid is painted. The specimen rests between a very heavy steel anvil and a cylindrical aluminum or steel plate, weighing anywhere from one to twelve pounds, as shown in Portion A of Fig. 1. We have referred to this plate as the "driving plate". The top of the driving plate contains a cup into which a low density charge of loose tetryl is loaded. The initiation system is supported six to eight inches above the tetryl charge, and consists of an electric blasting cap and a tetryl pellet which rests on an aluminum sheet. The aluminum sheet serves as a source of fragments to insure a more or less uniform plane wave initiation of the tetryl charge.

We will return to Fig. 1 shortly, but it is of interest to observe photographs of the set-up first. Figure 2 shows a typical specimen and its reference grid. The specimen in this instance is 1/2 inch thick pine. Figures 3 and 4 are photographs which depict the set-up in its various stages of assembly. Figure 3 shows a 1-inch thick specimen mounted between the anvil and the driving plate, with the tetryl charge on top of the driving plate. Figure 4 shows the specimen and driving plate assembly mounted in a shield which prevents fragments and smoke from obscuring the reference grid on the specimen.

We will now return to Fig. 1. Here we see a schematic representation of the method which we have used to observe the dynamic response of these porous media. This consists of a smear camera, which contains a narrow slit which is cut in the direction of displacement and which is immediately in front of the film. The image of the reference grid is focused on this slit, and the film travels in a direction perpendicular to the direction of displacement of the driving plate. A suitable time interval reference mark is photographed onto the moving film, with the result that we are able to obtain a displacement-time record of the dynamic event. Figure 5 is a photograph of the entire experimental set-up. The smear camera and the associated gear for the timing mark and firing pulse are shown in this photograph. The driving plate is also clearly visible.

In each experiment then, the sequence of events is as follows: A 100-foot roll of film begins its travel through the camera, and after it has reached proper speed the blasting cap receives the firing pulse automatically from the gear used with the camera. The detonation of the tetryl pellet hurls a spray of fragments from the aluminum sheet toward the loose tetryl charge, as shown in Portion B of Fig. 1. The detonation of the loose charge

BLASTING CAP

BOOSTER
$\frac{1}{2} \times \frac{1}{2}$ TETRYL

ALUMINUM TRANSFER
FRAGMENT SHEET

LOW DENSITY
EXPLOSIVE

DRIVING PLATE

FRAGMENT
SPRAY

REFERENCE
GRID

SPECIMEN

3-3/4 DIAMETER
ANVIL (Steel)

BASE
(Steel)

LENS

FILM
TRAVEL

SLIT PLATE

SLIT

35mm ROLL
FILM

A

B

C

Fig. 1 – Test arrangement

399
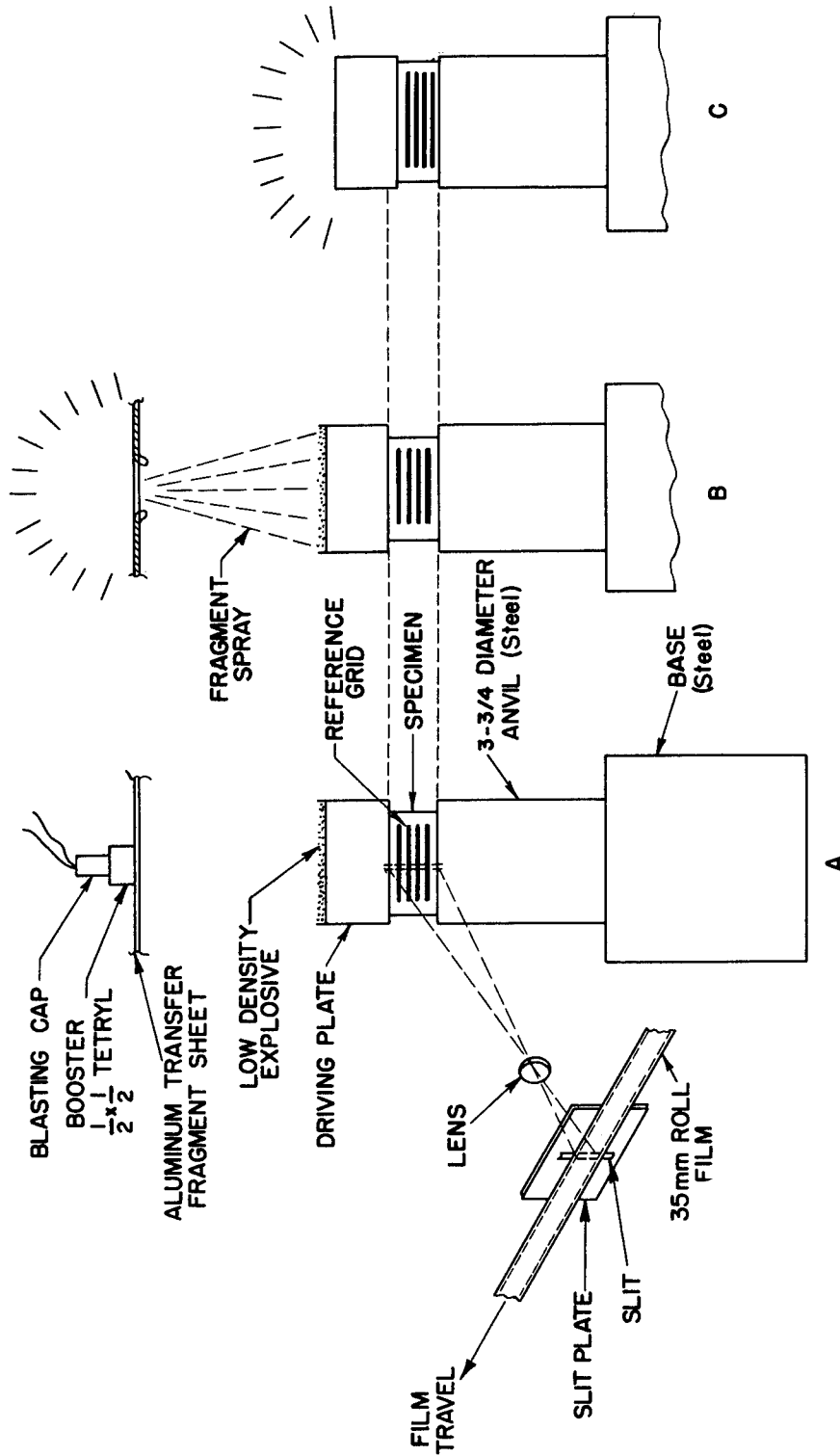
Fig. 2 - One-half inch thick pine specimen
showing reference grid
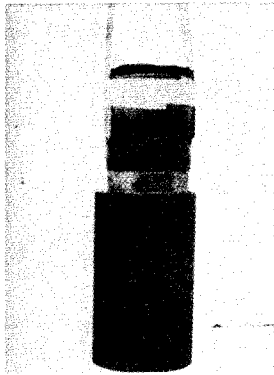
Fig. 3 - Specimen
mounted between
anvil and driving
plate

Fig. 4 - Assembly
of Fig. 3 mounted
in fragment and
smoke shield
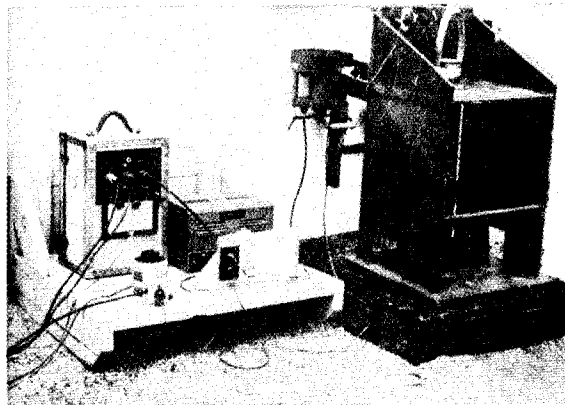
Fig. 5 - The complete experimental
set-up showing associated electronic
gear

causes a nearly instantaneous acceleration of the driving plate, and the driving plate moves downward so as to compress the specimen, as shown in Portion C of Fig. 1. The specimen in turn resists this compression, so that eventually the driving plate comes to rest, at which time the specimen imparts an upward velocity to the driving plate. Figure 6 shows a 1/2-inch pine specimen, before and after compression.

TYPICAL RECORDS OBTAINABLE

At this point it is of interest to view some of the typical records which are obtained on the film of the smear camera. Such a record, for Flintkote-Insulboard, is shown in Fig. 7. In this figure, the bounds of the specimen, the lower bound of the driving plate, and the upper bound of the anvil have been clearly identified. The reference grid on the specimen enables us to observe the propagation of the shock wave, as well as multiple reflections of the shock wave. The driving plate reference lines are also apparent, and these are used to obtain a dynamic stress-strain curve for the material.

Figure 8 shows a typical smear record obtained for a pine specimen in which the grain was oriented for application of force radial to growth rings. Here, the shock wave travels at a much higher velocity than that through the Flintkote, and the multiple reflections are not apparent.

HUGONIOT CURVE AND EQUATION OF STATE

The data which can be obtained from these smear camera records which we have just considered enables us to construct a Hugoniot curve for the material, and from this it is possible to calculate the temperature rise across the shock front. This has been done for Flintkote-Insulboard, and the procedure which we have used will now be discussed.

The construction of the Hugoniot curve, first of all, is accomplished through the use of the well-known equations for conservation of mass and momentum across a shock front. These equations are, respectively:

$$\rho_o D = \rho(D-u) \tag{1}$$

$$P = \rho_o Du + P_o \tag{2}$$

where: ρ_o is the density of the medium ahead of the shock front

     ρ is the density of the medium behind the shock front

     D   is the velocity of the shock

     u   is the particle velocity behind the shock front

     P_o is the pressure ahead of the shock front

     P   is the pressure behind the shock front
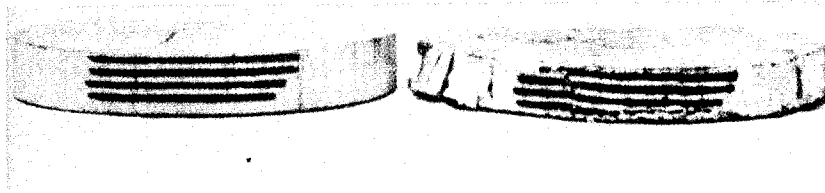
Fig. 6 - One-half inch thick pine specimen
before and after compression
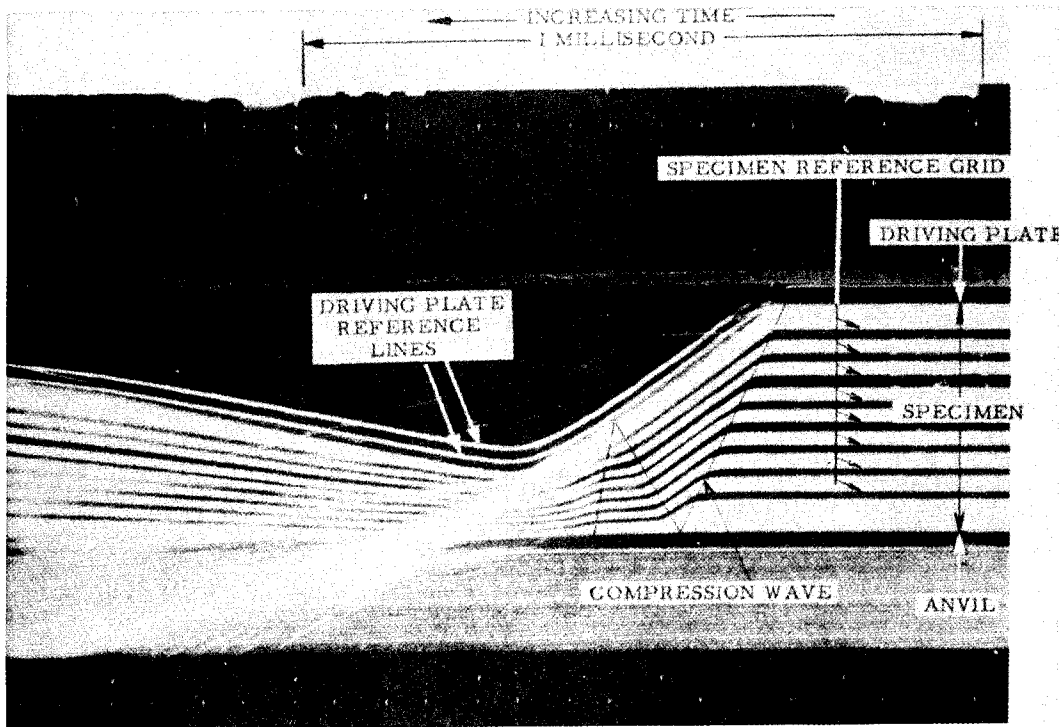
Fig. 7 - Smear camera record of the dynamic
response of Flintkote insulboard
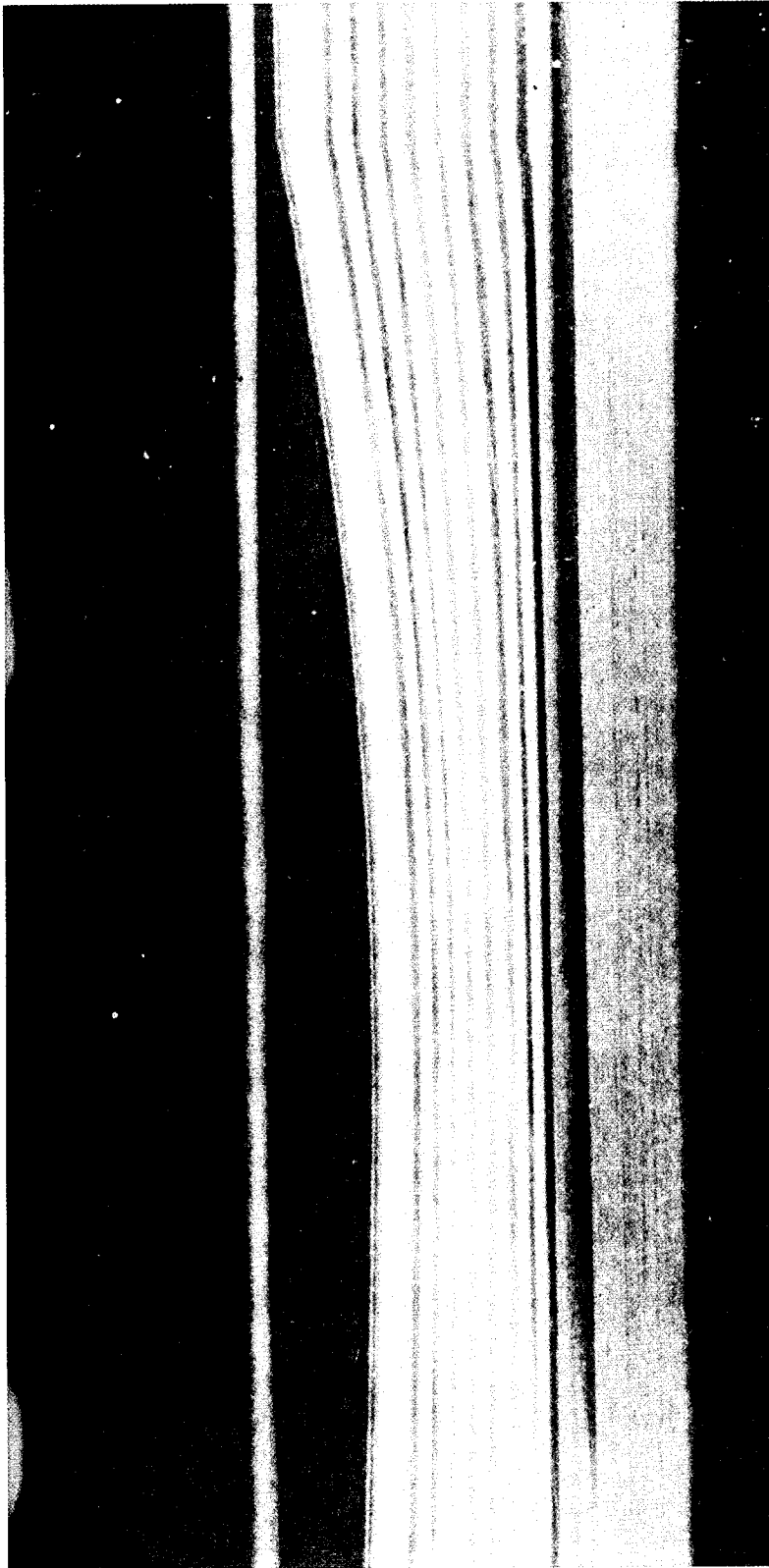
Fig. 8 - Smear camera record of dynamic response of pine, grain oriented for application of force radial to growth rings

These equations are in a form which assumes that the particle velocity ahead of the shock front is zero. In terms of specific volumes, Equation (1) becomes

$$\frac{V}{V_o} = \frac{D-u}{D} \tag{3}$$

where:

$V_o \ (= \frac{1}{\rho_o})$ is the specific volume of the media ahead of the shock front

V is the specific volume of the media behind the shock front

From each record, the shock velocity of the compression wave and the particle velocity behind the shock front can be calculated directly from the time-displacement slopes of the reference grid. These velocities then lead directly to the calculation of the relative volume V/V_o from Equation (3). If it is assumed that the initial pressure is atmospheric, the pressure P can be calculated from Equation (2) with the knowledge that ρ_o, the density of the medium ahead of the shock front, is also the density of the sample before being subjected to compression. This procedure has been employed for a whole series of records of experiments on Flintkote-Insulboard, and the resulting data points which determine the Hugoniot curves for the first shock are summarized in Tables I and II. On most records, the velocity of the shock wave appeared to be constant, but there seemed to be a rather random variation in the particle velocities as the shock wave propagated through the medium. We were unable to explain this. Consequently, the particle velocities as calculated are reported in the tables. This causes a corresponding variation in the pressure and relative volume.

The pressure-relative volume points in Tables I and II form the basis for the Hugoniot curve which is shown in Fig. 9. Each dotted line corresponds to one set of experimental points from one of these tables. As stated above, the unexplained variation in the particle velocity, together with the assumption of constant shock velocity, causes a corresponding variation in the calculated pressure and relative volume across the shock front, and this is reflected in the figure. For purposes of comparison, the curve for static compression of the medium is shown in Fig. 9 along with the Hugoniots. The static curve was calculated from load-deformation data which were obtained on a standard compression test machine.

TABLE I

Hugoniot Data for First Shock in Flintkote Insulboard,

1" Thick Specimens

Shot Number	Original Density, lb/in^3	Shock Velocity, ft/sec	Particle Velocity, ft/sec	Pressure, psi	Relative Volume, $\frac{V}{V_o}$
52	0.0103	590	253	586	0.571
			249	577	0.578
			240	556	0.593
			240	556	0.593
			241	559	0.592
			241	559	0.592
			240	556	0.593
			240	556	0.593
			241	559	0.592
			232	539	0.606
			230	534	0.610
			228	529	0.613
			228	529	0.613
			234	543	0.602
			234	543	0.602
			226	525	0.617
			230	534	0.610
53	0.0105	565	184	421	0.674
			182	416	0.678
			184	421	0.674
			187	427	0.669
			186	425	0.671
			183	419	0.676
			180	412	0.681
			164	377	0.710
			167	383	0.704
			164	383	0.710
			167	377	0.704
			167	377	0.704
			168	385	0.703
			162	372	0.713
			170	390	0.699
			161	370	0.715
			174	399	0.692

TABLE I (Cont'd)

Shot Number	Original Density, lb/in^3	Shock Velocity, ft/sec	Particle Velocity, ft/sec	Pressure, psi	Relative Volume, $\frac{V}{V_o}$
57	0.0102	467	53	107	0.885
			48	99	0.897
			45	94	0.903
			44	92	0.905
			45	94	0.903
			43	91	0.907
			46	96	0.900
			46	96	0.900
			47	97	0.898
			44	92	0.905
			44	92	0.905
			42	88	0.909
			43	90	0.907
			49	101	0.894
			44	92	0.905
132	0.0115	534	181	428	0.662
			169	401	0.684
			166	394	0.690
			162	384	0.698
			170	402	0.684
			172	406	0.679
			168	398	0.686
135	0.0113	542	126	301	0.786
			121	291	0.777
			116	278	0.787
			115	277	0.788
			117	282	0.784
			117	282	0.784
			117	282	0.784
			114	274	0.791
			137	328	0.747

TABLE I (Cont'd)

Shot Number	Original Density, lb/in^3	Shock Velocity, ft/sec	Particle Velocity, ft/sec	Pressure, psi	Relative Volume $\frac{V}{V_o}$
136	0.0113	506	156	347	0.692
			157	349	0.690
			160	355	0.684
			162	360	0.679
			160	355	0.684
			158	351	0.688
			157	349	0.690
			156	346	0.692
			156	346	0.692
			160	355	0.684
			159	353	0.686
			157	349	0.690
			157	349	0.690
			157	349	0.690
			157	349	0.690
			157	349	0.690
			157	349	0.690
137	0.0113	519	75	177	0.856
			68	162	0.869
			68	162	0.869
			69	164	0.867
			69	164	0.867
			70	165	0.866
			67	161	0.870
			64	152	0.878
			52	126	0.901
139	0.0116	528	137	326	0.738
			136	325	0.738
			135	323	0.744
			133	317	0.749
			132	315	0.750
			131	314	0.754
			132	315	0.750
			132	315	0.750
			133	317	0.749

TABLE I (Cont'd)

Shot Number	Original Density, lb/in^3	Shock Velocity, ft/sec	Particle Velocity, ft/sec	Pressure, psi	Relative Volume, $\frac{V}{V_o}$
140	0.0113	541	136	323	0.750
			130	310	0.760
			127	303	0.766
			124	297	0.771
			124	297	0.771
			124	297	0.771
			124	297	0.771
			124	297	0.771
			124	297	0.771
143	0.0114	443	65	136	0.855
			62	130	0.858
			65	136	0.855
			66	138	0.849
			65	136	0.855
			66	138	0.849
			65	136	0.855
			61	127	0.861
			65	136	0.855
			55	117	0.875
			57	122	0.868
			53	113	0.879
			55	117	0.875
			67	140	0.847
			67	140	0.847
			65	136	0.855
			65	136	0.855

TABLE II

Hugoniot Data for First Shock in Flintkote Insulboard

1/2" Thick Specimens

Shot Number	Original Density, lb/in^3	Shock Velocity, ft/sec	Particle Velocity, ft/sec	Pressure, psi	Relative Volume, $\frac{V}{V_o}$
54	0.0100	540	167	351	0.690
			175	367	0.676
			169	355	0.685
			177	372	0.671
			161	339	0.704
			162	341	0.699
			155	327	0.714
			160	337	0.704
			160	337	0.704
58	0.0103	692	220	600	0.681
			214	584	0.690
			199	544	0.712
			187	512	0.729
			181	496	0.738
59	0.0106	620	53	143	0.915
			52	142	0.916
			49	135	0.920
			48	133	0.921
			60	162	0.902
62	0.0104	845	25	94	0.970
			24	91	0.983
			27	102	0.968
			27	102	0.968
133	0.0112	564	162	395	0.713
			154	376	0.726
			152	372	0.730
			153	373	0.728
			148	360	0.737

TABLE II (Cont'd)

Shot Number	Original Density, lb/in^3	Shock Velocity, ft/sec	Particle Velocity, ft/sec	Pressure, psi	Relative Volume, $\frac{V}{V_o}$
142	0.0112	528	122	284	0.769
			118	275	0.775
			118	275	0.775
			122	284	0.769
			135	312	0.746
			132	305	0.751
			135	312	0.746
			132	305	0.751
			131	303	0.752
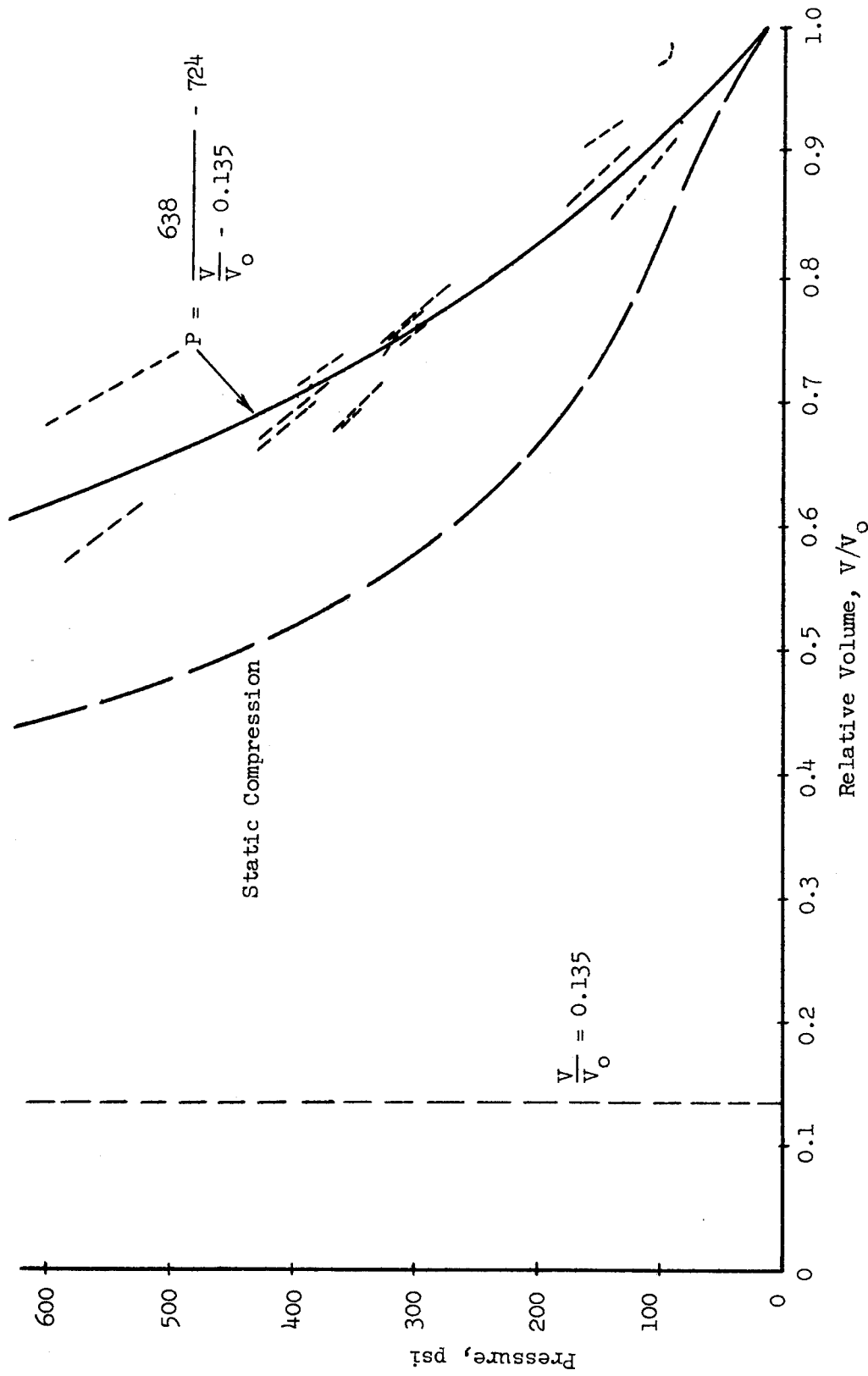
Fig. 9 - Curves of Hugoniot compression and static compression in Flintkote insulboard

$$P = \frac{638}{\frac{V}{V_o} - 0.135} - 724$$

Static Compression

$\frac{V}{V_o} = 0.135$

Pressure, psi

Relative Volume, V/V_o

Several considerations were involved in attempting to fit an equation through the experimental Hugoniot points: (1) Since a Hugoniot curve is a locus of end points on a shock compression, the curve must pass through the initial point ($V/V_0 = 1$, $P = 14$ psi) and a point which represents a reasonable average of the Hugoniot points; (2) the equation should have an asymptote at some finite relative volume between zero and one, since a porous material will approach a limiting density as the compressive stress increases to very high values; and (3) the equation should be as simple as possible. The static stress-strain data for Flintkote-Insulboard (the same data which are represented in Fig. 9) at very high stresses were used to calculate the relative volume asymptote, with the result that

$$\lim_{P \to \infty} \frac{V}{V_0} = 0.135$$

This is shown as a vertical dotted line in Fig. 9. To determine what mathematical function would best describe the experimental points, we attempted to rectify the data. In so doing we discovered that two types of plots yielded essentially straight lines. These included the plots of pressure P versus $1/(V/V_0 - 0.135)$ and log P versus $\log(V/V_0 - 0.135)$. Since the former of these plots was simpler and would yield a function with a relative volume asymptote, the equation of the Hugoniot was assumed to fit a hyperbola of the form

$$(P + a) \left(\frac{V}{V_0} - 0.135\right) = k$$

Determination of the constants $\underline{a}$ and $\underline{k}$ showed that this equation is as follows:

$$P = \frac{638}{\dfrac{V}{V_0} - 0.135} - 724 \tag{4}$$

Equation (4) has been plotted in Fig. 9.

The method for the calculation of the temperature rise across the shock front was suggested to us in a published article by Walsh and Christian (5). We have used this method, but have derived the working equations in a slightly different manner.[*] Our derivation begins by assuming that energy is a function of temperature and volume, that is

$$E = E(T, V)$$

---

[*]The thermodynamic identities used in this derivation can be verified in any good thermodynamics text. For example, reference (6) is suggested.

from which

$$dE = \left(\frac{\partial E}{\partial T}\right)_V dT + \left(\frac{\partial E}{\partial V}\right)_T dV$$

$$dE = C_V dT + \left(\frac{\partial E}{\partial V}\right)_T dV \tag{5}$$

where C_V is the heat capacity at constant volume. From the first law of thermodynamics,

$$dE = TdS - PdV \tag{6}$$

Differentiating equation (6) with respect to volume at constant temperature, we have

$$\left(\frac{\partial E}{\partial V}\right)_T = T\left(\frac{\partial S}{\partial V}\right)_T - P \tag{7}$$

However, the thermodynamic identity

$$\left(\frac{\partial S}{\partial V}\right)_T = \left(\frac{\partial P}{\partial T}\right)_V$$

may be substituted into equation (7) with the result that

$$\left(\frac{\partial E}{\partial V}\right)_T = T\left(\frac{\partial P}{\partial T}\right)_V - P \tag{8}$$

Substitution of equation (8) into equation (5) results in

$$dE = C_V dT + \left[T\left(\frac{\partial P}{\partial T}\right)_V - P\right] dV$$

from which

$$\frac{dE}{dV} = C_V \left(\frac{dT}{dV}\right) + T\left(\frac{\partial P}{\partial T}\right)_V - P \tag{9}$$

The Hugoniot equation for conservation of energy across a shock front is

$$E - E_o = \frac{1}{2}(P + P_o)(V_o - V)$$

Differentiating this equation, we obtain

$$\frac{dE}{dV} = -\frac{1}{2}(P + P_o) + \frac{1}{2}(V_o - V)\left(\frac{dP}{dV}\right)_{\text{Hugoniot}} \quad (10)$$

Substitution of equation (10) into equation (9) results in the **following** differential equation:

$$\frac{dT}{dV} + \frac{\left(\frac{\partial P}{\partial T}\right)_V}{C_V} T = \left[\left(\frac{V_o - V}{2}\right)\left(\frac{dP}{dV}\right)_{\text{Hugoniot}} + \frac{P - P_o}{2}\right]\frac{1}{C_V} \quad (11)$$

Equation (4), the empirical Hugoniot equation, may be differentiated with respect to volume as follows:

$$\left(\frac{dP}{dV}\right)_{\text{Hugoniot}} = -\frac{638}{V_o\left(\frac{V}{V_o} - 0.135\right)^2} \quad (12)$$

Equations (4) and (12) may be substituted into equation (11). If P_o is assumed to be equal to 14 psi, equation (11) reduces to the following:

$$\frac{dT}{dV} + \frac{\left(\frac{\partial P}{\partial T}\right)_V}{C_V} T = \left[319\frac{\left(\frac{V}{V_o} - 1\right)}{\left(\frac{V}{V_o} - 0.135\right)^2}\right.$$

$$\left. + \frac{319}{\left(\frac{V}{V_o} - 0.135\right)} - 369\right]\frac{1}{C_V} \quad (13)$$

Equation (13) is a linear differential equation in which C_V is assumed to be constant, and in which $(\partial P/\partial T)_V$ and

$$319\frac{\left(\frac{V}{V_o} - 1\right)}{\left(\frac{V}{V_o} - 0.135\right)^2} + \frac{319}{\left(\frac{V}{V_o} - 0.135\right)} - 369$$

are functions of volume alone. For purposes of simplification, let

$$
b = \frac{\left(\frac{\partial P}{\partial T}\right)_V}{C_V} \tag{14}
$$

$$
f\left(\frac{V}{V_o}\right) = 319\frac{\left(\frac{V}{V_o} - 1\right)}{\left(\frac{V}{V_o} - 0.135\right)^2} + \frac{319}{\left(\frac{V}{V_o} - 0.135\right)^2} - 369 \tag{15}
$$

so that equation (13) simplifies to

$$
\frac{dT}{d\left(\frac{V}{V_o}\right)} + V_o b\, T = \frac{V_o}{C_V}\, f\left(\frac{V}{V_o}\right) \tag{16}
$$

where the differential $d(V/V_o)$ has been introduced to put equation (16) into a from which is consistent with equation (15). To solve equation (16), it is necessary to introduce the integrating factor

$$
e^{\int V_o b\, d\left(\frac{V}{V_o}\right)} = e^{V_o b\left(\frac{V}{V_o}\right)}
$$

such that

$$
\left[e^{V_o b\left(\frac{V}{V_o}\right)}\right]\frac{dT}{d\left(\frac{V}{V_o}\right)} + V_o b T\left[e^{V_o b\left(\frac{V}{V_o}\right)}\right]
$$
$$
= \frac{V_o}{C_V}\, f\left(\frac{V}{V_o}\right)\left[e^{V_o b\left(\frac{V}{V_o}\right)}\right] \tag{17}
$$

Integration of equation (17) results in

$$
T\, e^{V_o b\left(\frac{V}{V_o}\right)} = c + \frac{V_o}{C_V}\int f\left(\frac{V}{V_o}\right) e^{V_o b\left(\frac{V}{V_o}\right)} d\left(\frac{V}{V_o}\right) \tag{18}
$$

The integration constant $\underline{c}$ can be evaluated from the following boundary conditions,

$$T = T_o \, , \quad \frac{V}{V_o} = 1$$

Equation (18) then reduces to the following expression for temperature as a function of relative volume:

$$T = T_o \, e^{V_o b(1- \frac{V}{V_o})} + \frac{V_o}{C_V} \int_1^{V/V_o} f(\frac{V}{V_o}) \, e^{V_o b(\frac{V}{V_o})} \, d(\frac{V}{V_o}) \quad (19)$$

Equation (19) is the working equation which enables the calculation of the temperature rise across the shock front.

The integration of the function

$$f(\frac{V}{V_o}) \quad e^{V_o b(\frac{V}{V_o})} \quad d(\frac{V}{V_o})$$

in equation (19) was performed graphically. The value of the specific volume V_o was obtained from the average of the experimentally determined values from each experiment. The value of the heat capacity C_V was estimated to be 0.25 cal/gm °C. The exponent b contains the partial derivative $(\partial P/\partial T)_V$ which can be evaluated from the thermodynamic identity

$$(\frac{\partial P}{\partial T})_V = -\left(\frac{\partial (\frac{V}{V_o})}{\partial T}\right)_P \left(\frac{\partial P}{\partial (\frac{V}{V_o})}\right)_T$$

Here, $\left(\partial (V/V_o)/\partial T\right)_P$ is the thermal coefficient of volume expansion (estimated to be 0.00001/°C), and $\left(\partial P/\partial (V/V_o)\right)_T$ can be obtained from the static curve in Fig. 9. The exponents in equation (19) were of such small magnitude that

416

$$e^{V_o b(1-\frac{V}{V_o})} \approx 1$$

$$e^{V_o b(\frac{V}{V_o})} \approx 1$$

so that to a very good approximation

$$\Delta T = \frac{V_o}{C_V} \int_1^{\frac{V}{V_o}} f(\frac{V}{V_o}) \; d(\frac{V}{V_o}) \tag{20}$$

Thus, the graphical evaluation of equation (20) leads directly to the determination of the temperature increase. The results of this calculation as a function of relative volume are as follows, assuming that the specific heat of the medium remains constant:

Relative Volume , V/V_o	Temperature Rise, °C
1.0	0
0.9	0.01
0.8	0.05
0.7	0.19
0.6	0.58
0.5	1.58

These data are plotted in Fig. 10, and show an almost insignificant temperature rise even in the region of our strongest shock at about $V/V_o = 0.65$.

DISCUSSION

The experimental technique which was described earlier in this paper has made it possible to calculate data which may be used to derive an equation of state for a porous material. The Hugoniot can be calculated directly from one record. This has been done for Flintkote-Insulboard, with the result that the strongest Hugoniot compressions have been to pressures of about 550 psi and relative volumes of about 0.65. The temperature rise associated with a shock wave of this strength is in the neighborhood of 0.3°C. This data appears to be consistent in general with that reported by Walsh and Christian (5), who report a rise of 15°C, for example, at a shock pressure of 15 kilobars in aluminum.
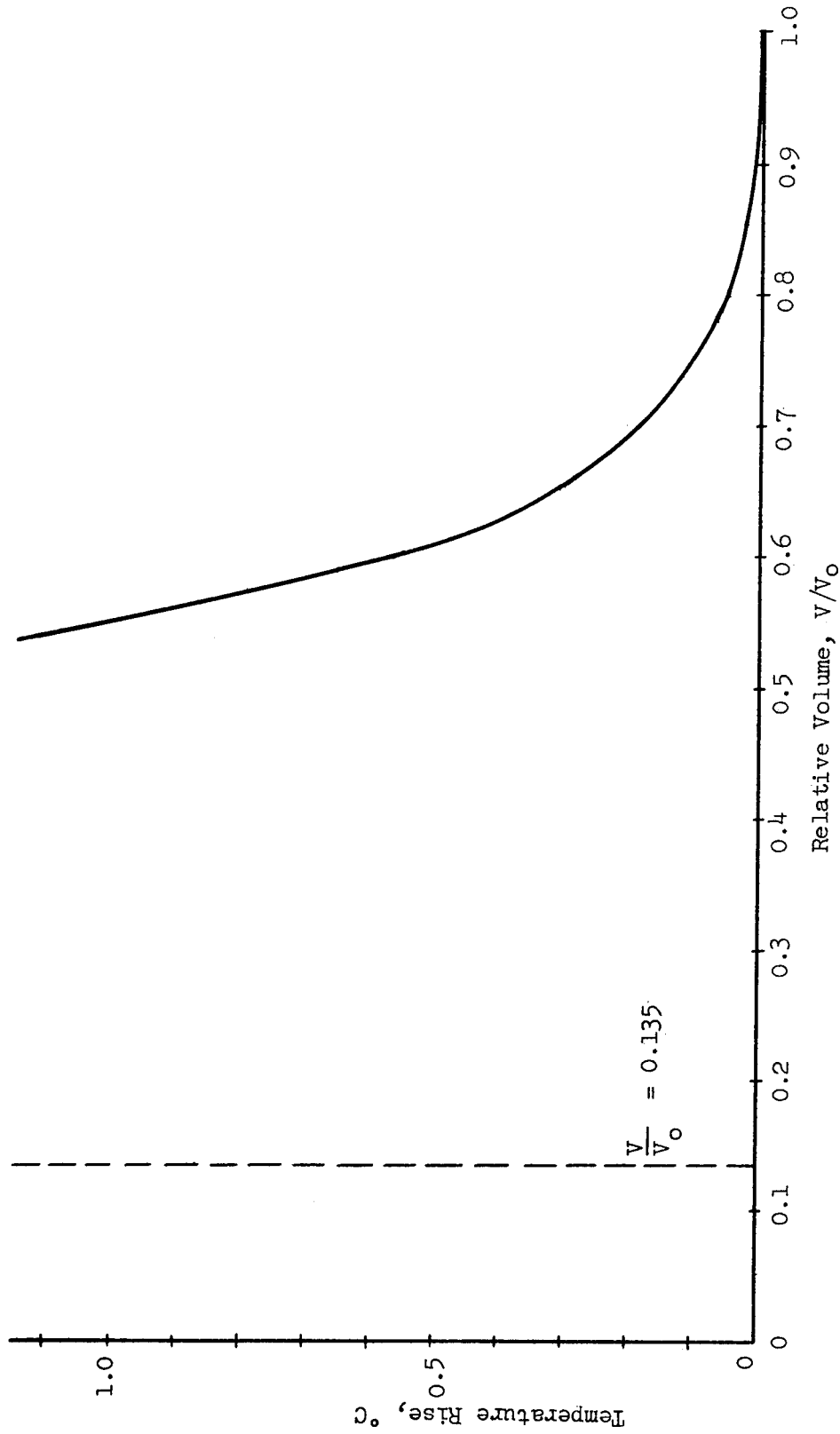
Fig. 10 - Graph of the temperature rise due to Hugoniot compression in Flintkote insulboard

We feel that this experimental technique can be used to obtain similar data for the construction of an equation of state for non-reacting explosives. Napadensky, Stresau, and Savitt (7) have obtained smear camera records of the propagation of non-reactive shocks in explosives. These records are similar to those shown in Fig. 7 and 8, but the velocity of the shock wave is too great for accurate analysis. This problem will be solved by the use of smear cameras which write at higher speeds.

ACKNOWLEDGEMENTS

The authors wish to express their appreciation to all persons who assisted in the various phases of the work reported in this paper. These persons include W. Mandleco who constructed the various pieces of equipment used in the experimental portions of the program; W. Hartman and J. Wagner who assisted in the firing of the experiments; and R. Blomquist and C. Love who performed a significant portion of the numerical calculations.

REFERENCES

1. von Neumann, J., "Theory of Detonation Waves",
        OSRD Report No. 549 (1942)

2. Cook, M. A., Filler, A. S., Keyes, R. T., "Mechanism of Detonation",
        Technical Report No. XLI,
        University of Utah, November 15, 1954

3. Mallory, H. D. and Jacobs, S. J., "The Detonation Zone in Condensed
        Explosives", Paper No. 17, 2nd ONR Symposium
        on Detonation, Washington, D. C.,
        February 9-11, 1955.

4. Duff, Russell E. and Houston, Edwin, " Measurement of the
        Chapman-Jouguet Pressure and Reaction Zone
        Length in Detonating High Explosive",
        Paper No. 16, 2nd ONR Symposium on Detonation,
        Washington, D. C., February 9-11, 1955.

5. Walsh, John M. and Christian, Russel H., "Equation of State of
        Metals from Shock Wave Measurements",
        Phys. Rev., 97, 6 (March 15, 1955)

6. Zemansky, Mark W., "Heat and Thermodynamics",
        McGraw-Hill Book Company, New York (1957)

7. Napadensky, H. S., Stresau, R. H., and Savitt, J.,
        "The Behavior of Explosives at Impulsively
        Induced High Rates of Strain", presented
        at this meeting.

THE BEHAVIOR OF EXPLOSIVES AT IMPULSIVELY INDUCED HIGH RATES OF STRAIN[*]

H. S. Napadensky, R. H. Stresau[**], and J. Savitt
Armour Research Foundation
Chicago 16, Illinois

Experimental Technique

A sensitivity test has been devised wherein cylindrical specimens of explosives of the order of a pound in weight are squeezed between an explosive driven plate and a massive anvil. The experimental technique is illustrated in Fig. 1. Essentially, the metal plate is accelerated by means of the plane wave initiation of a low density charge of high explosive in such a manner as to compress the explosive test specimen. The motions of the plate and the lines of a reference grid which is stencilled on the specimen are observed either by means of a Fastax Streak Camera which records time-displacement histories, or by means of the Beckman and Whitley Model 189 Framing Carmera which records the behavior of the whole surface of the sample under impact.

A typical streak camera record is shown in Fig. 2. The acceleration of the plate is so nearly instantaneous that the acceleration time is barely resolved by the streak camera. The subsequent negative acceleration by the action of the specimen. which shows as a quite measurable curvature of the streak camera record, is a measure of the pressure exerted upon the driving plate by the specimen and, hence, of the stress within the specimen. For each point on the curve it is then possible to measure the displacement which is proportional to the strain of the specimen; the first time derivative (or slope) which is proportional to the rate of strain; and the second time derivative (or curvature) which is proportional to the stress in the material. Dynamic stress-strain data are thus obtainable. The propagation of compression waves through the sample is visible as the progressive displacement of the reference lines stencilled on the specimen. Thus, both the non-reactive shock wave propagation velocity and the particle velocities can be measured almost point-to-point

over the area of a record such as Fig. 2. Continuity and momentum conservation conditions may be applied to reduce these data to shock pressure-density relationships for the explosive.

An example of a Beckman & Whitley Framing Camera record of the dynamic compression of an unconfined cast Comp B specimen is seen in Fig. 3. (The event is front lighted by means of an Argon Flash Bomb). The deformation of the specimen is clearly seen. The over-all geometrical change in the specimen is noticeable as a gradual "mushrooming" of the cylinder with time. Stripes were drawn on the explosive every 1/4 of an inch. The changes in distance between stripes, as one proceeds from frame to frame, can be used as a measure of local changes in density with time. One can observe the non-reactive shock wave as it travels through the specimen. This is noticeable on the prints as a progressive brightening of the surface of the sample. From Fig. 3, the non-reactive shock velocity and pressure within the specimen are readily calculated.

Typical Records and Interpretation

With an experimental technique as the one described above, it is possible to observe the behavior of the explosive over a wide range of impulsive loading conditions, by varying the mass of the driving plate, the quantity of driving charge used, and the size of the explosive test specimen. At one extreme the shock transmitted through the driving plate is of sufficient intensity to initiate detonation before or at the instant it reaches the face of the anvil. Examples of this are seen in Figs. 4, 5, and 6. Figure 4 shows selected frames, taken 4 microseconds apart, of the compression and initiation of an unconfined cylinder of Comp B, 3 inches in diameter by 3 inches high, weighing 570 grams. The force was applied by means of a steel plate weighing 1418 grams which impacted the explosive specimen at approximately 600 ft/sec. The time between impact and initiation was about 26 microseconds. A high-order detonation of the explosive appears to have started at the bottom of the specimen as evidenced by the bright spot at the bottom of frame 6, indicating the inception of the reaction at the explosive-anvil interface. The shape of the detonation profile as seen in frames 7 and 8 also shows that the detonation starts at the bottom of the explosive and moves upward into the previously shocked specimen. Figure 5, showing selected frames 1.05 microseconds apart, is another example of detonation occurring at the instant the shock wave reaches the anvil. In this case the center of reaction appears to begin in the lower left-hand corner of frame 4, 12.5 microseconds after impact, and progresses back upward into the specimen. The explosive sample was 9404 PBX, 2.5 inches in diameter by 2.34 inches high. Figure 6 shows the impact and the initiation of a cylinder of 9404 PBX, 2.5 inches in diameter by 2.34 inches high. The time between the frames is 1.05 microseconds. In this case the shock intensity was of sufficient strength to initiate detonation before it reached the face of the anvil. The detonation is first observed in frame 7 and appears to have started at about

421
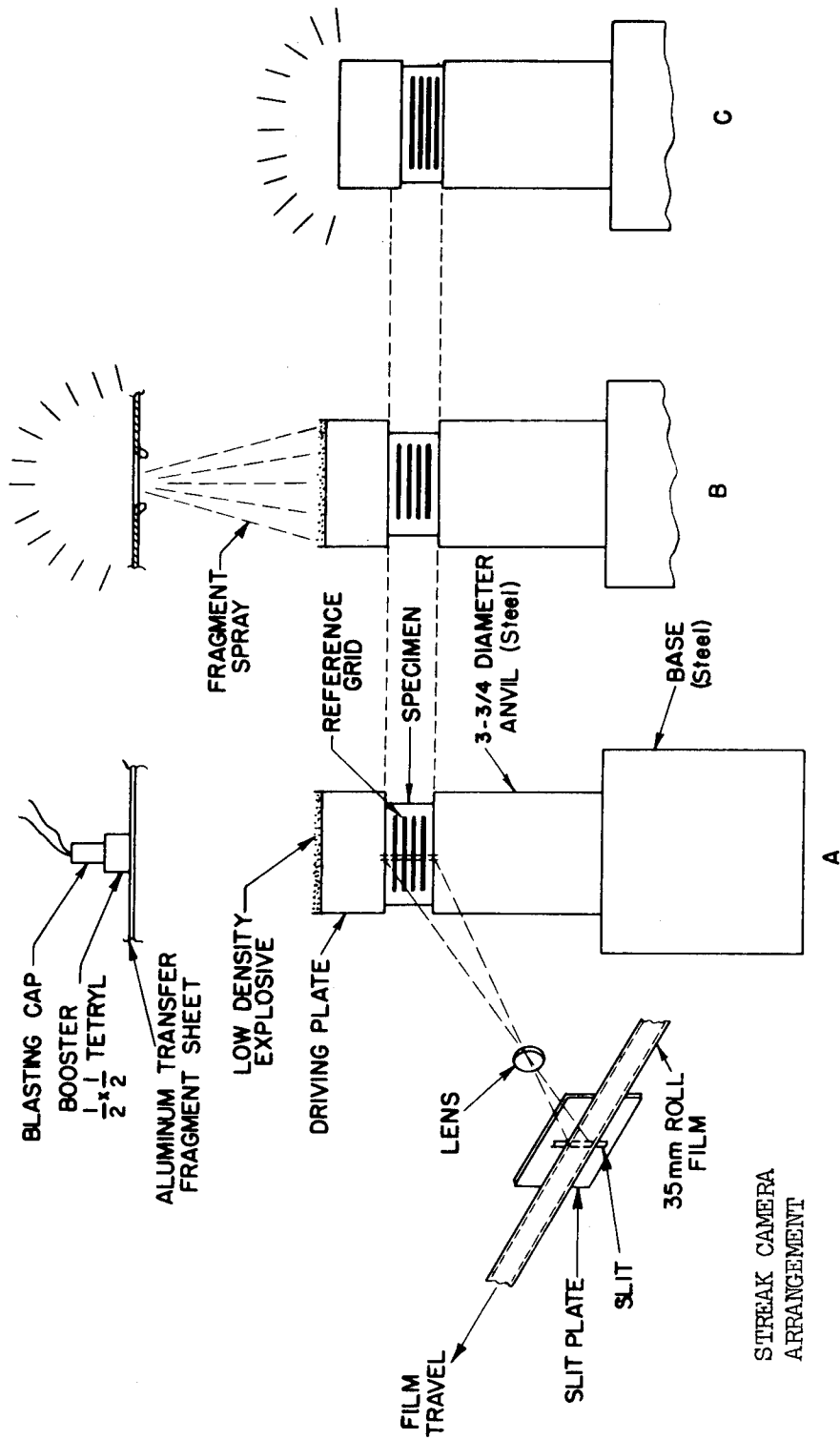
Fig. 1 - Test arrangement
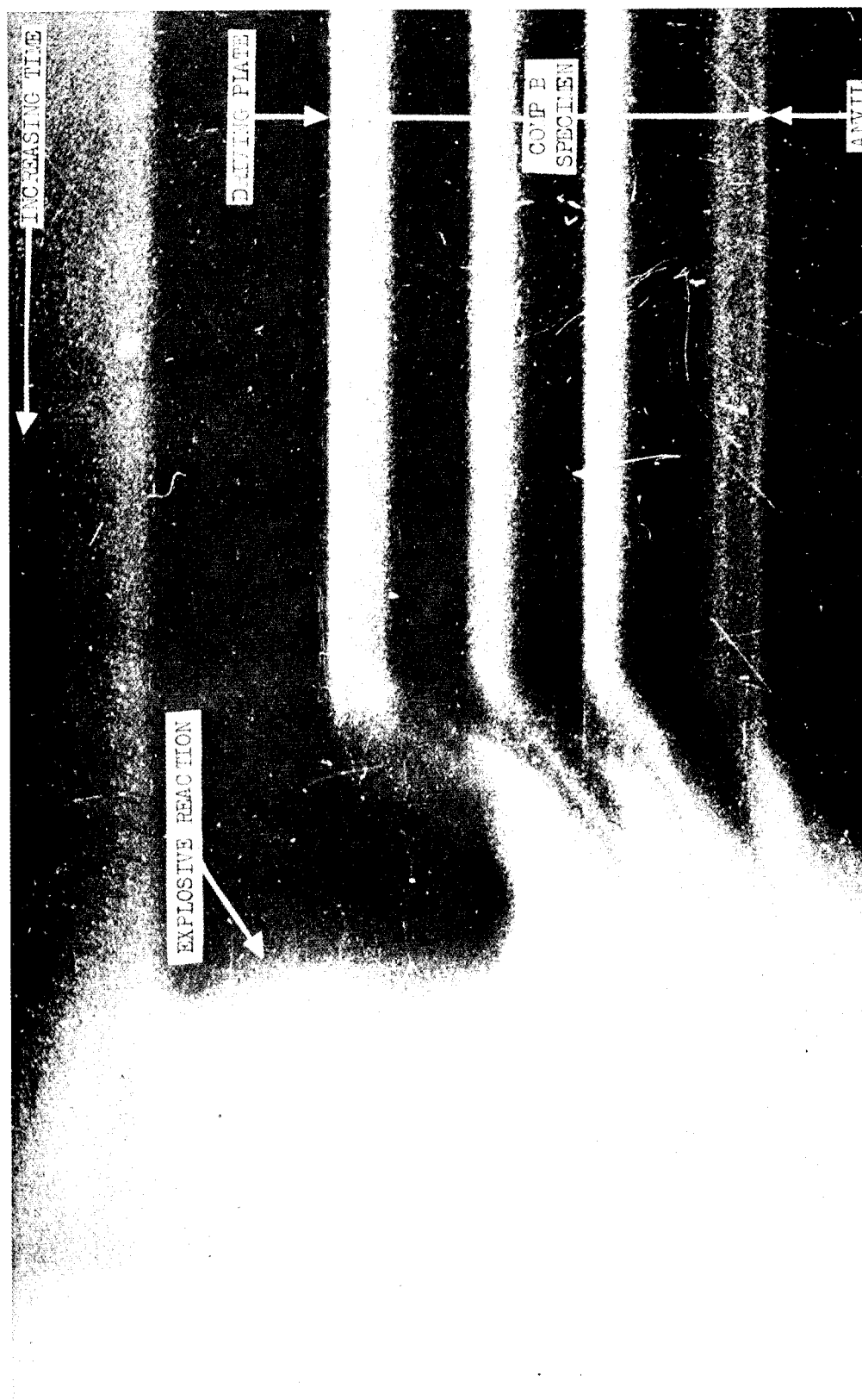
Fig. 2 - Streak camera record of dynamic response to impact of Comp B,
time from impact to initiation - 200 microseconds
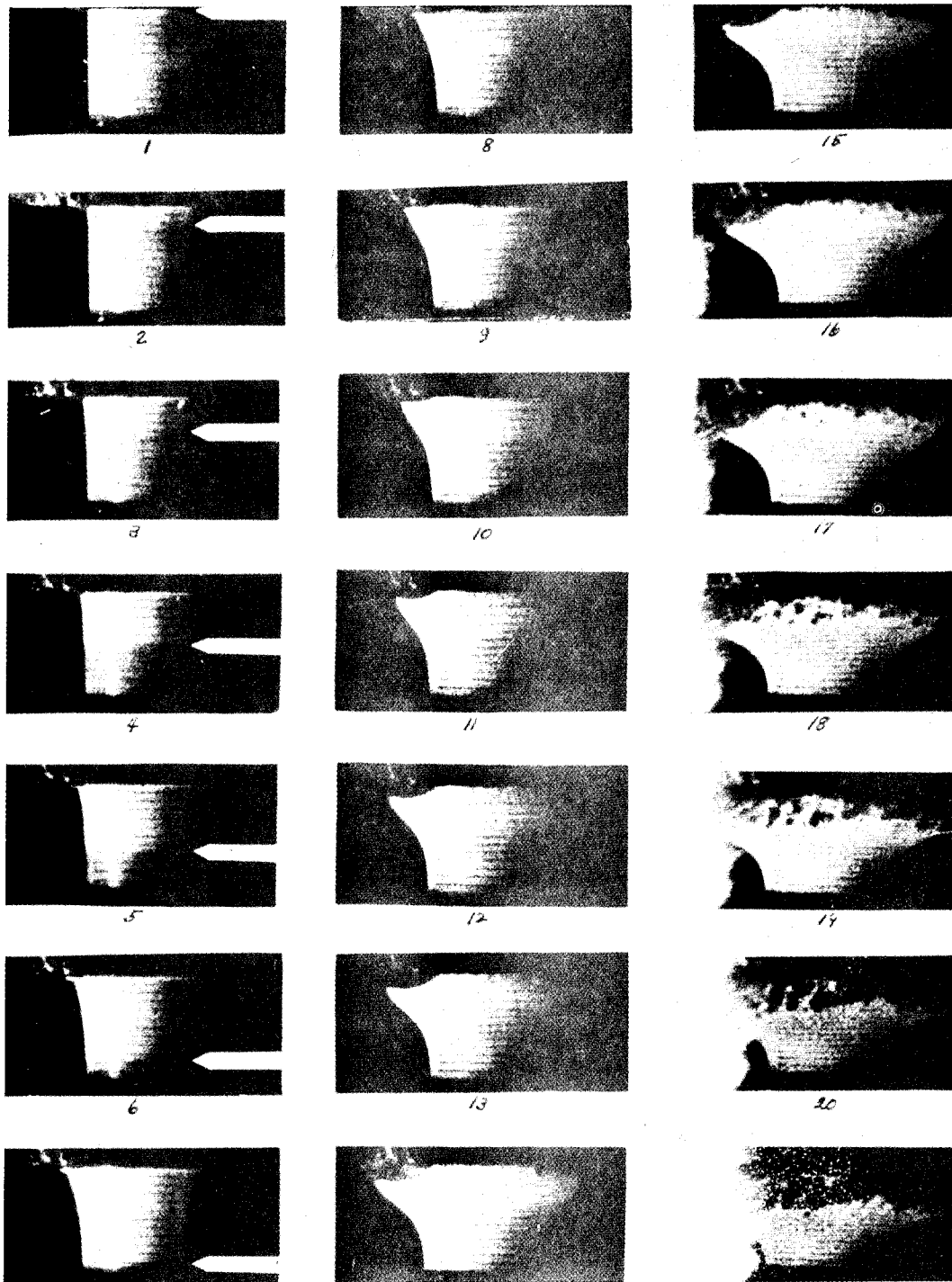
Fig. 3 - Framing camera sequence showing deformation under impact of a cast Comp B cylinder, arrows indicate shock front, 4 microseconds between frames. (Bright light to the left of frames 16-21 is that of explosive light source appearing in the field of view.)
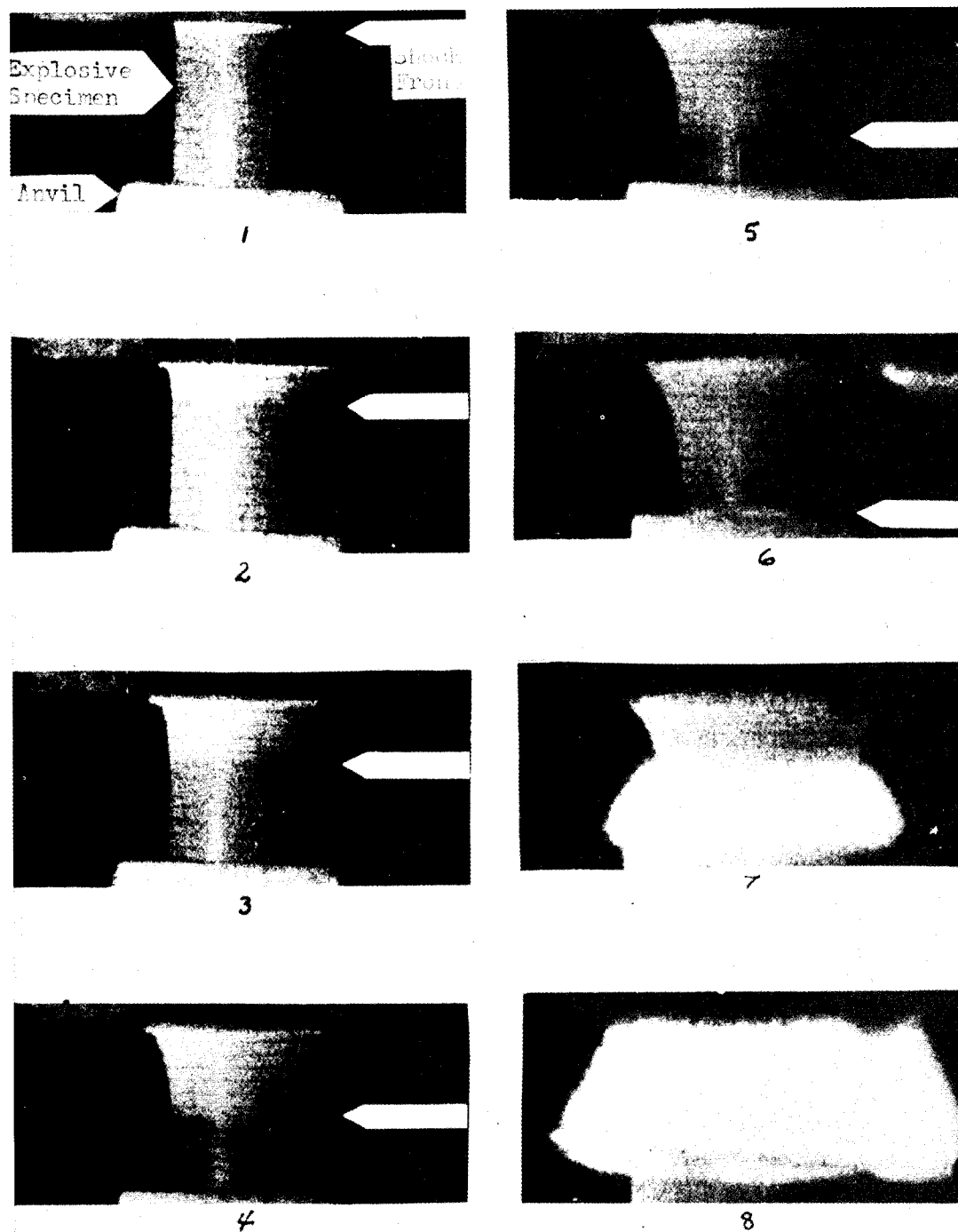
Fig. 4 - Framing camera sequence showing impact initiation of an unconfined Comp B cylinder 3 inches diameter by 3 inches high. 4 microseconds between frames.
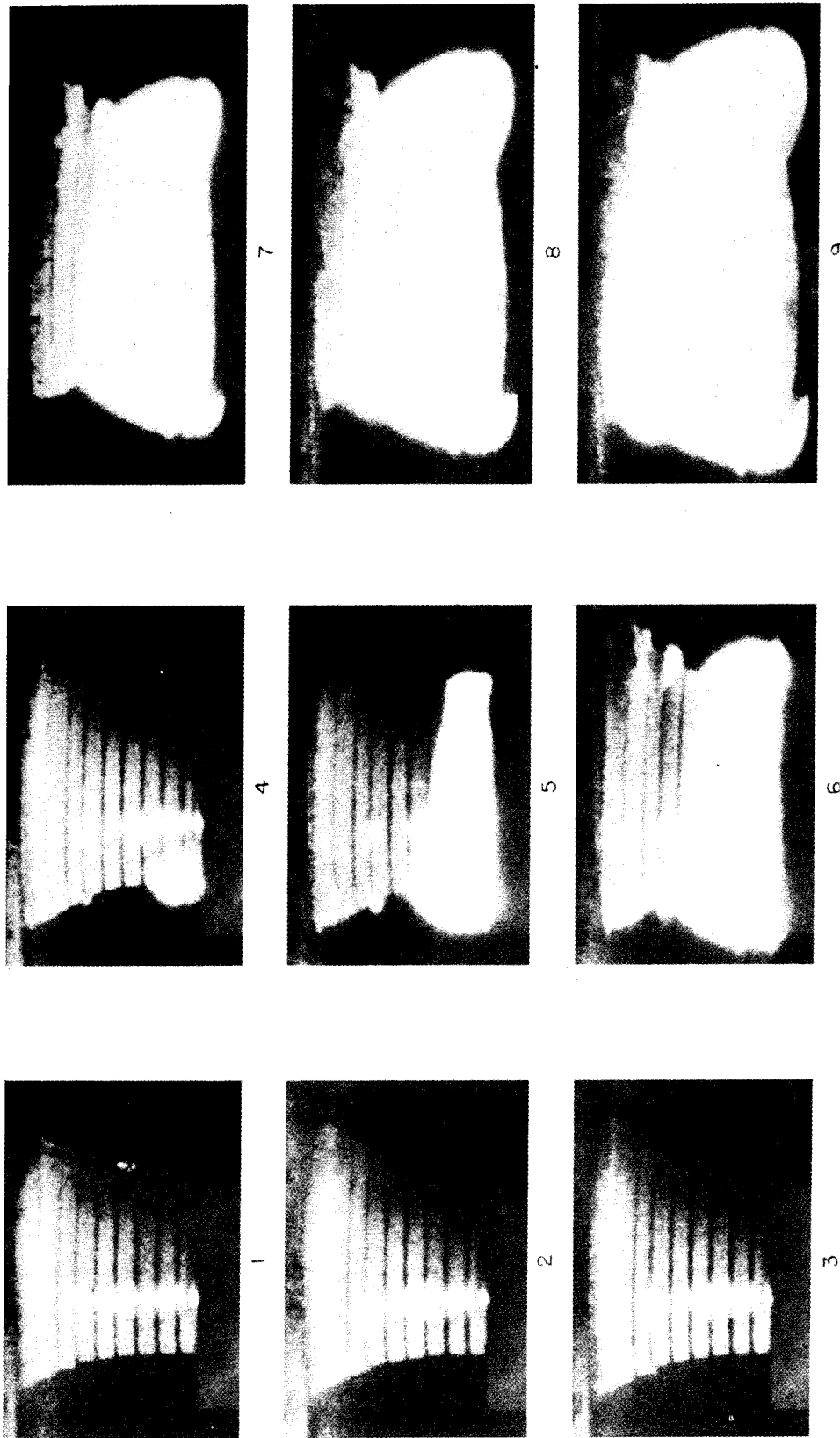
Fig. 5 - Framing camera sequence showing the inception and growth of a detonation in 9404 PBX, 1 microsecond between frames
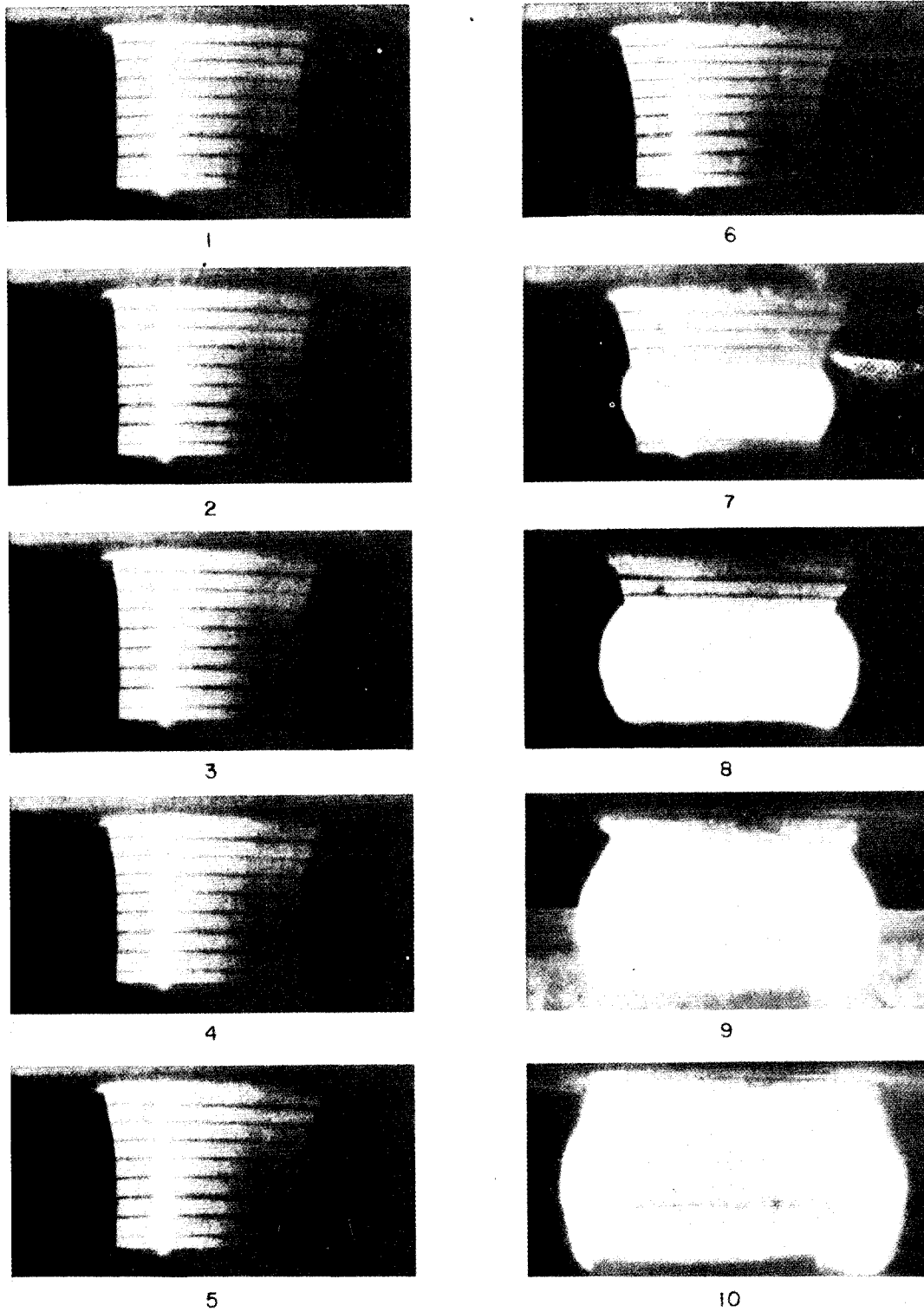
Fig. 6 - Framing camera sequence showing forward and reverse propagation of a detonation in 9404 PBX, 1 microsecond between frames.

1.6 inches from the top of the sample. The reaction occurs 10.5 micro-
seconds after impact, and propagates both in the forward and reverse
direction. In these cases the initiation mechanism is probably
similar to that of earlier experiments of Cachia and Whitbread (1),
Eichelberger and Sultanoff (2); Cook, Pack and Gey (3); Marlow and
Skidmore (4); and Savitt (5). They have observed that the depth in
the explosive at which initiation occurs depends upon the pressure
of the incident shock, the lower the pressure the deeper the point of
initiation. This has been explained by Cosner and Sewell (6) by the
fact that if the shock wave entering the charge is above a minimum
intensity it will be supplemented by a chemical reaction; the pressure
build-up from the reaction is dependent on the shock intensity. There-
fore, when the initial shock intensity is high, the pressure build-up
from chemical reaction is fast, and so initiation takes place near the
explosive-metal interface. When the initial shock intensity is lower,
the pressure build-up from the chemical reaction is slower, and
initiation takes place farther from the explosive-metal interface.
An alternate explanation may be based on the generality that reaction
rates in explosives are so highly dependent upon temperature, that
for a rate of any given order of magnitude, it is described with fair
accuracy in terms of a threshold or ignition temperature, combined
with applications of the general principles of the behavior of non-
reactive compressive waves. A shock traversing a barrier or gap, is
generally modified, particularly in its pressure-time profile, by
impedance discontinuities and the reverberations of the gap or medium.
The important contrast of the emergent wave to the incident wave is
the lack of the nearly discontinuous increase in peak pressure which
is characteristic of a stable shock. As the emergent wave propagates
through the acceptor explosive, the higher pressure components of the
wave tend to overtake the front so that the discontinuous pressure
rise at the front increases in magnitude. Since the temperature
increase associated with a single Hugoniot compression to a given
pressure is appreciably greater than that associated with either
adiabatic compression or a series of Hugoniot compressions to the
same maximum pressure, the threshold temperature for a reaction rate
of the order of magnitude of that associated with detonation is
attained when the discontinuous rise at the front acquires sufficient
magnitude. It is probable that, in some cases, this mechanism is
combined with that suggested by Jacobs (7) in which the overtaking
wavelets are evolved as a result of incipient reaction of the explo-
sive, due to the passage of the essentially nonreactive shock.

At the threshold of initiation, however, the time between
initial movement of the plate and the evidence of explosion is long
enough for many reverberations of the shock between the driving plate
and the anvil. The streak camera record shown in Fig. 2 is an example
of an observation of this type. It shows the impact and subsequent
initiation of a Comp B specimen, 3 inches in diameter by 1/2 inches
in height, weighing 90 grams. It was impacted by a steel plate
weighing 1475 grams, at a velocity of 206 ft/sec. The time from
initial impact to initiation was about 200 microseconds. Here the

mechanism of initiation is probably similar to that proposed by Wenograd (8), whose comparison of impact experiments with reaction kinetic data suggests that an impact explosion of high explosives is a phenomenon intermediate between a low temperature thermal decomposition and a detonation. It might be noted that the time to reaction observed here is of the order of that assumed by Wenograd for the duration of impact.

A third mechanism is implied by observations, in some instances, where the explosion originates in explosive dust external to the original charge dimensions. The streak camera record of Fig. 7 is one of many observations of this behavior. It illustrates the response to impact of a Comp B specimen, 3 inches in diameter by 1 inch high, weighing 181 grams. It was impacted by an aluminum plate weighing 504 grams, at a velocity of about 600 ft/sec. In this example wide stripes were painted on the specimen. The broad bright vertical bands seen on the left of Fig. 7 is light from the reacting explosive. In this case the time from impact to reaction is about 280 microseconds.

Where no explosion results, data are obtained regarding the shock pressure-density relationships for the unreacted explosive as well as the inter-relationship of stress, strain, and strain-rate in the impulsively loaded explosive specimen. Some of the data obtained thus far are plotted in Fig. 8, stress vs strain, and Fig. 9, strain vs strain-rate for Comp B.

Conclusion

The importance of nonuniformity of energy distribution in initiation is clearly illustrated in these experiments. The change in internal energy density as calculated from shock hydrodynamics or from changes in kinetic energy of the driving plate is never sufficient to raise the average temperature to a point where rapid reaction should be expected. An example of this can be shown by referring to the experiment whose framing camera record is illustrated in Fig. 4. One can observe the non-reactive shock wave as it travels through the specimen. This is noticeable as the progressive brightening of the surface of the explosive. From this observation, a shock velocity of about 10,000 ft/sec is calculated. A particle velocity of 600 ft/sec is obtained from streak camera observations. From the conservation equations for a shock wave one readily calculates; a pressure of 9 kilobars, and a density of 1.7 grams/cm^3, which results in an energy increase of 4.07 cal/gram for the shocked explosive. The maximum possible temperature rise due to the internal energy increase calculated (assuming a specific heat of 0.24 cal/gm for Comp B) is only 17°C. However, if one calculates the temperature rise due to the adiabatic compression of a trapped gas bubble, by
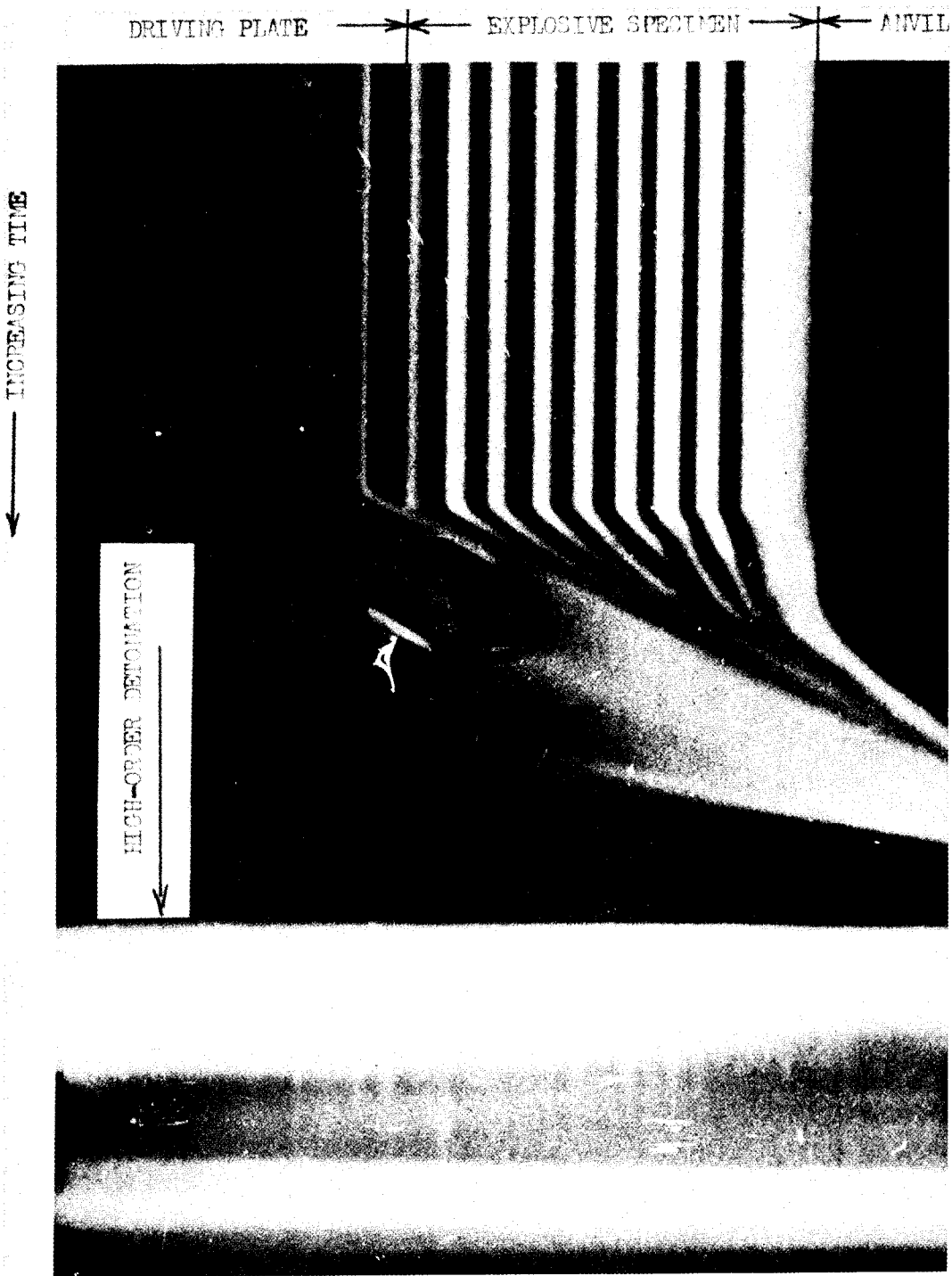
Fig. 7 – Streak camera record of dynamic response to impact of Comp B, time from impact to initiation – 280 microseconds.
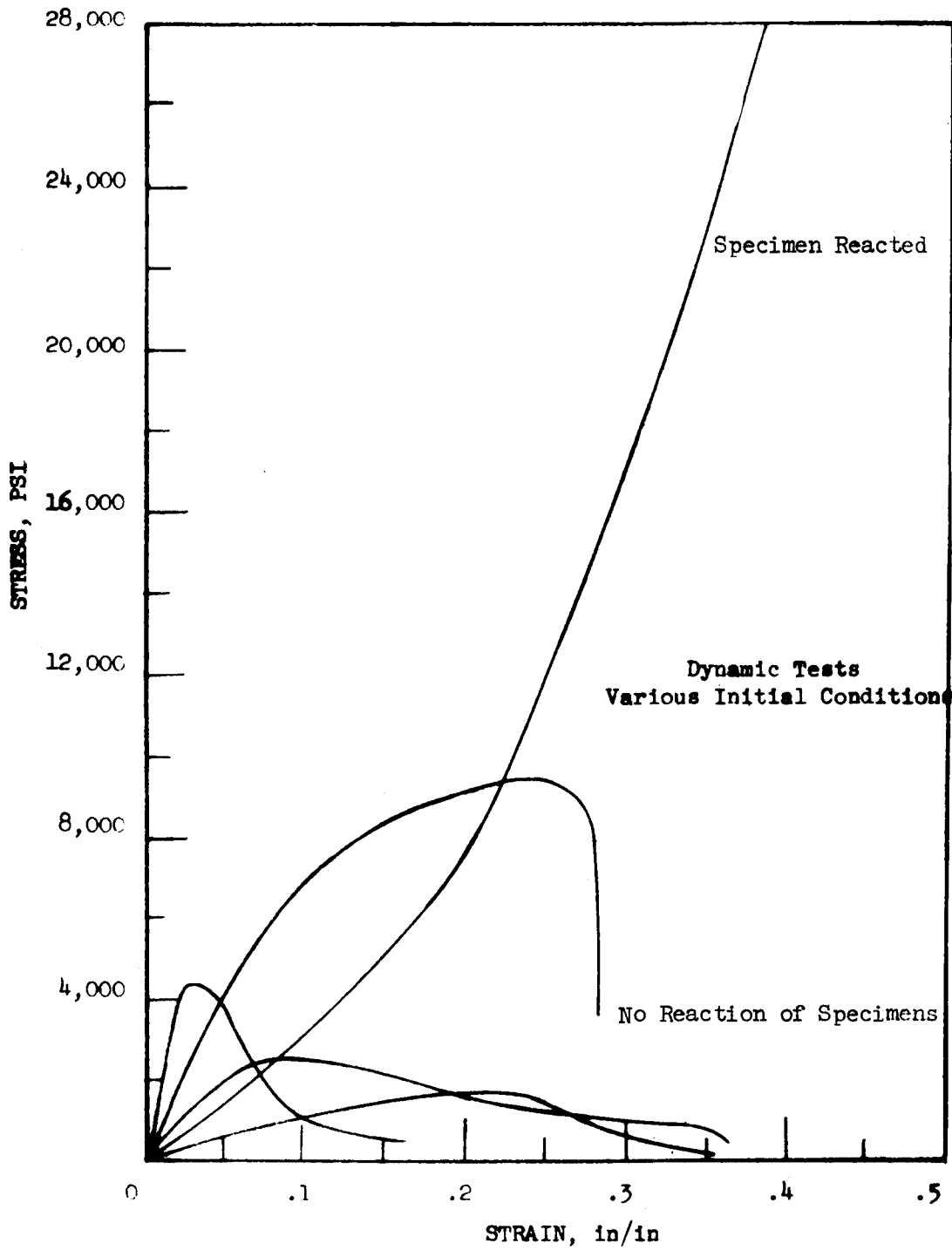
Fig. 8 - Stress vs strain curves for Comp B
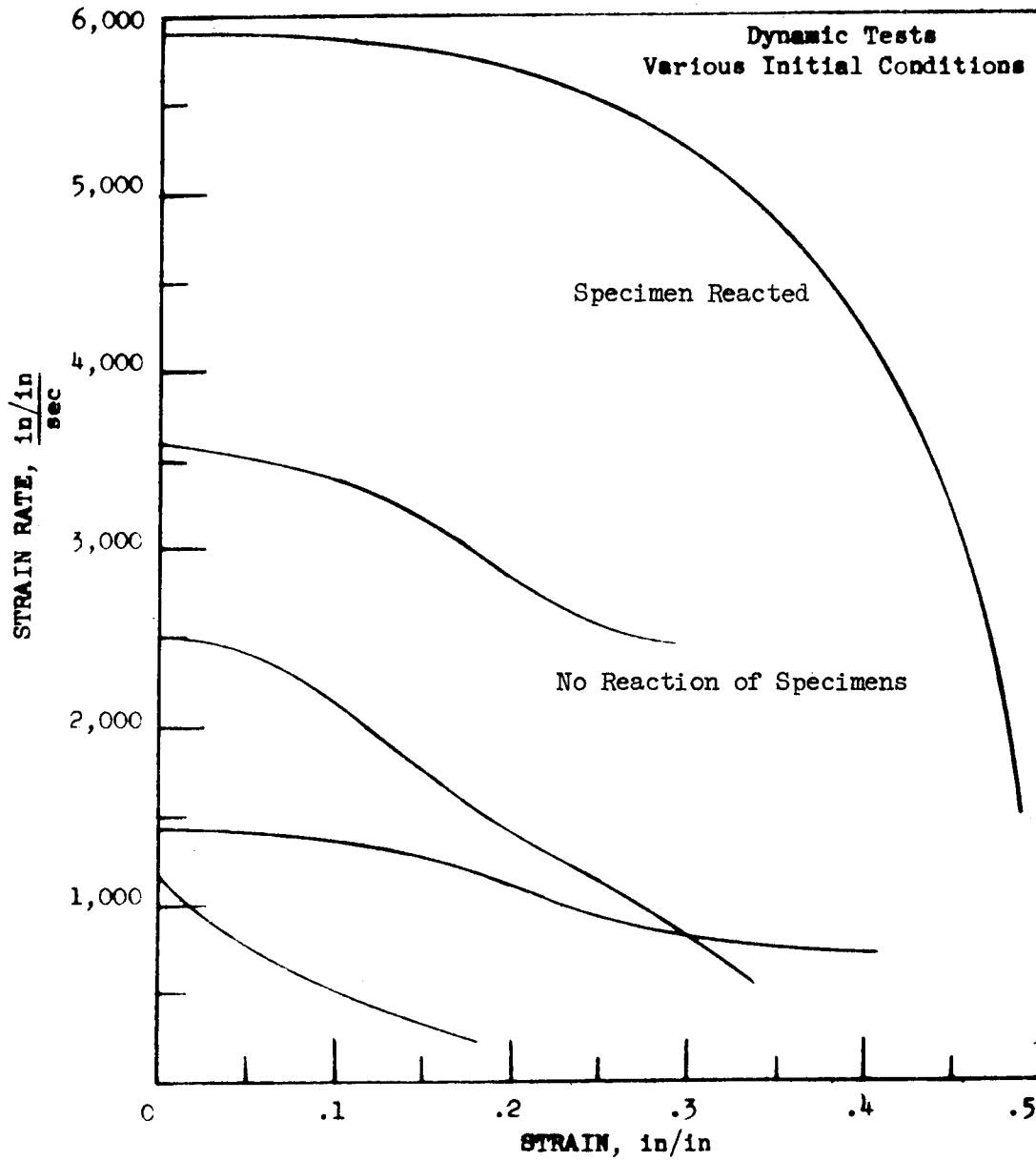
Fig. 9 - Strain rate vs strain curves for Comp B

the relationship $T/T = (P/P_0)^{\frac{\gamma-1}{\gamma}}$, a temperature rise of about 3500°C is obtained. But even this temperature rise, which is about 10 times the critical hot spot temperature needed for initiation, does not insure a reaction growing to completion. The heat and gaseous products generated as a result of the compression must evolve in the explosive charge more rapidly than they are dissipated in order for the reaction to accelerate.

One can easily realize that the value of the data obtained in impact sensitivity experiments may be increased considerably by theoretical considerations of the impact initiation process. The initiation process is clearly quite complex. However the analysis of simplified models which are still representative of the condition within the explosive, after impact, might be tractable. One such model has been suggested by the authors in an earlier paper (9). This model assumes that in a porous explosive material:

(1) A sudden impact load has resulted in the compression of interstitial gases.
(2) This compression is not uniformly distributed.
(3) At some point in the explosive the pressure is appreciably higher than elsewhere.
(4) The compression has heated the gas to above the "ignition temperature" for the explosive.
(5) The principal mechanism of reaction propagation is that of "deflagration".
(6) The principal mechanisms of heat dissipations is the flow of the product gases through the interstices.

In this model of a porous explosive medium, we assume that the interstitial spaces, a volume which is small compared to the explosive charge and large compared with an individual particle or pore, are filled with hot compressed gas. The gas flows through the porous medium at a rate that is related to the pressure gradient by the partial differential equation

$$\frac{k}{\mu(1+m)f} \, \nabla^2 \, P^{1+m} \;=\; \frac{\partial P^m}{\partial t} \; ,$$

where m = ratio of specific heat at constant volume to that at constant pressure, μ = viscosity of the gas, f = porosity of the explosive, k = permeability of the explosive, t = time and P = pressure of the gas.

At the same time the explosive deflagrates at the grain surface at a rate related to the pressure by an empirical formula of the form $U = a+bP^\nu$. Since $PV = nRT$, and $dn/dt = (V/RT)(dP/dt)$, and $UA = (a+bP^\nu) \; A = dn/dt$ the substitution $dP/dt = 1/m \; P^{1-m} \; dP^m/dt$ results in the equation $(a+bP^\nu) \; ARTm/VP^{1-m} = dP^m/dt$, where A is the surface area of particles per unit volume.

The complete relation between the evolution and the dissipation of gas in our system is now given by

$$\frac{k}{\mu(1+m)f} \nabla^2 P^{1+m} + (a+bP)P^{m-1} \quad \frac{ART\ m}{V} = \frac{dP^m}{dt}$$

In the three-dimensional case, because of spherical symmetry we can write the above equation as

$$\frac{k}{\mu(1+m)f}\left(\frac{\partial^2 P^{1+m}}{\partial r^2} + \frac{2}{r}\frac{\partial P^{1+m}}{\partial r}\right) + (a+bP^{\nu})\ P^{m-1}\frac{ARTm}{V} = \frac{dP^m}{dt},$$

with the boundary conditions, $P(r,o) = p_1 + p_2 e^{-r^2 p_3^2}$ $(o < r < r_1)$,

$$P(r_1,t) = P_1 \qquad (t > o)$$

$$\frac{dP(o,t)}{dr} = o$$

The solution of the above equation will enable us to determine under what conditions an expanding reaction will occur which will carry on to detonation, and when the reaction is dying. This dying reaction can occur when the rate at which the gas is flowing out of the system is greater than the rate at which it is being evolved, due to burning of the explosive material. Data of the type reported herein will aid in the interpretation of solutions to the equation.

Acknowledgement

The authors are especially indebted to J. Gershon and W. Hartman for their assistance in the photographic work and in performing the experiments.

:mc

Bibliography

(1)   G. P. Cachia and E. G. Whitbread, "The Initiation of Explosives by Shock", Proceedings of the Royal Society, Series A, Vol. 246, No. 1245, 29 July 1958, p. 268

(2)   R. J. Eichelberger and M. Sultanoff, "Sympathetic Detonation and Initiation by Impact", Ibid, p. 274

(3)   M. A. Cook, D. H. Pack and W. A. Gey "Deflagration to Detonation Transition in Solid and Liquid Explosives", Ibid, p.281

(4)   W. R. Marlow and I. C. Skidmore "The Initiation of Condensed Explosive by Shock Waves from Metals", Ibid, p. 284.

(5)   J. Savitt, "Some Observations on the Growth of Detonations" Navord Report No. 3753, 25 August 1954

(6)   L. N. Cosner and R. G. S. Sewell, "Initiation of Explosives
        Through Metal Barriers", <u>Proceedings of Detonation Wave
        Shaping Conference</u>, 5-7 June 1956 p. 235

(7)   S. J. Jacobs, "A Theory Concerning the Initiation of Detona-
        tions by Shocks", <u>Ibid</u>, p. 248

(8)   J. Wenograd, "The Correlation of the Impact Sensitivity of
        Organic High Explosives With Their Thermal Decomposition Rates"
        <u>Proceedings of the Gilbert B. L. Smith Memorial Conference
        on Explosive Sensitivity</u>, 2 June 1958, p. 130

(9)   R. H. Stresau and H. S. Napadensky "Thermal Unbalance and
        Initiation", <u>Ibid</u>, p. 191.

INITIATION AND GROWTH OF DETONATION IN LIQUID EXPLOSIVES

F. C. Gibson, C. R. Summers,
C. M. Mason, and R. W. Van Dolah
Bureau of Mines
Pittsburgh, Pennsylvania

Introduction

The mechanism whereby detonation is initiated in condensed phase explosive systems, though the subject of many experimental and theoretical investigations, continues to elude definition. Of continuing interest in the high-explosives field, sensitivity to initiation of detonation has assumed increased importance in the liquid monopropellant and high-energy solid propellant fields. This sensitivity is typically evaluated, among other methods, by a gap-sensitivity test where the sample, suitably contained, is subjected to shock from a standard explosive donor after attenuation by passage through an inert barrier. The development of this test is described by Jacobs (1). One form has been recommended as a "standard test" for evaluating the sensitivity of liquid monopropellants (2).

Although the gap test is capable of yielding quite reproducible results when applied to many systems, many anomalous results occur. As an example, neat nitromethane will yield nearly identical "gap values" whether the containing cup is of aluminum or steel. Other systems, such as 50-50 nitroglycerine-ethylene glycol dinitrate, (NG/EGDN), show a much lower apparent sensitivity (smaller gap value) in steel cups than in aluminum cups, with glass cups giving even smaller gap values. Clearly, the test does not measure a sensitivity that is characteristic only of the liquid explosive alone; rather, the sensitivity measured depends, in part, upon the nature of the containers. Further, Cook and associates (3) have pointed out that the mechanism whereby initiation occurs under card-gap test conditions may be extremely pertinent to the problem of deflagration-to-detonation transition in solid propellants. With these problems in mind, the Bureau of Mines began studying the card-gap test.

Many theories of initiation have been proposed (3-7). Bowden's hot-spot theory, originally developed for the drop-weight case -- which relies on the adiabatic compressional heating of

bubbles -- has been criticized by Bolkhovitinov (8) and by Johannson and Selberg (9), who point out that the relaxation times for the min-ute bubbles postulated to be present are too short for the compres-sion to be adiabatic. Bolkhovitinov hypothesizes an alternative mechanism where the crystallization of the liquid under pressure is the causative heat source. Johannson (10) proposes that vapor or droplet burning in the bubbles must be responsible for the initiation at low-impact energies. Indeed, Bowden and Jafee recognized the im-portance of the vapor-phase decomposition in the initiation of liq-uid explosives. Andreev (7) suggests that the burning of a droplet suspension is important in the transformation of deflagration to detonation. Interestingly enough, this same idea of a burning sus-pension of particles of explosive is postulated by Cachia and Whit-bread (11) as being important in their experiments on the shock ini-tiation of single crystals of Cyclonite (RDX). In considering the initiation of air-free nitroglycerin, Selberg (12) attempts to cal-culate the particle velocity of the shock wave required. In con-trast, Cook and comtemporaries (3) suggest that initiation occurs only with the development of both a pressure-generated "metallic state" and a "plasma" which can provide the postulated requirement of high heat conductivity. A further consequence of this theory is the projection of a "plasma" from the end of the charge under some conditions (13). Jacobs (1), however, has suggested that the exper-iments described by Cook may be explained by alternate hypotheses.

We believe the results reported herein suggest a mechanism for initiation under card-gap test conditions and provide, as well, a possible explanation for the off-the-charge-end "plasma" phenome-non.

Experimental Details

Liquid systems were chosen by the Bureau of Mines because they are more amenable to photographic study. Shock and detonation phenomena were examined by direct- and schlieren-photographic meth-ods and by a resistance element technique recently developed to measure continuously detonation velocities (14). The photographs were made both with an instantaneous (0.5 μ sec. exposure) Rapa-tronic camera[1] and the Cordin high-speed framing camera[2] of the U. S. Naval Propellant Plant at Indian Head, Maryland.

---

[1] A product of Edgerton, Germeshausen and Grier, Inc., 160 Brook-line Ave., Boston, Mass.

[2] A product of the Cordin Company, 1637 Pioneer Rd., Salt Lake City 4, Utah.

Several charge configurations were used in these experiments. Initiation was accomplished by an attenuated shock wave, from an explosive donor, into the transparent vessel containing the liquid explosive. A drawing of a typical charge configuration is shown in Figure 1.

Preliminary work indicated that a rubber barrier would be a satisfactory shock attenuator to yield delayed ignitions and considerable predetonation activity of interest. Typically, it was found that a rubber barrier 2.6 cm. thick would provide initiation delay times of 5 to 15 μ sec. for granular explosives and about 50 μ sec. for the 50-50 nitroglycerin-ethylene glycol-dinitrate (NG/EGDN) mixtures used for most of this investigation. In some experiments, the usual stack of cellulose acetate cards (2) was employed with comparable results.

To permit a study of the effects of geometry and wall materials, the confining vessels used were either round Plexiglas tubes or tubes having square cross sections where the front and rear (viewing sides) were Plexiglas; the side walls were steel, aluminum, or Plexiglas. In most cases a mirror was positioned at 45° above the tube to provide a simultaneous end-on view of the event. In other cases, a steel witness plate, 1/4 inch thick, was positioned on top the charge.

Because the early stage of the shock excitation is nonluminous, it was necessary to provide background light to silhouette the event. This was provided by an exploding wire fabricated of a 10-cm. length of 5 mil. aluminum wire. A simple white paper corner reflector was positioned behind the wire. A capacitive discharge energy of 216 joules was applied to the wire through a synchronizing hydrogen thyratron with suitable delay provided to allow optimum buildup of luminosity. The exploding wire was placed 7-1/2 cm. behind a translucent paper screen which was, in most cases, ruled with lines one centimeter apart to provide convenient reference.

The donors were 14 gram tetryl pellets initiated either by a No. 8 electric blasting cap or a short length of Primacord which was, in turn, initiated by a No. 8 blasting cap. All tests were conducted with the liquid at a temperature of 25°C.

Experimental Results

A complete framing-camera sequence of one explosive test, Figure 2, illustrates the complexity of the initiation process. This charge configuration was identical to that shown in Figure 1, except that the charge contained a resistance element. The vessel was a 23 mm. i.d. Plexiglas tube, 11 cm. long, filled with NG/EGDN and shocked by a 14-gram tetryl donor through a 2.6 cm.-thick rubber

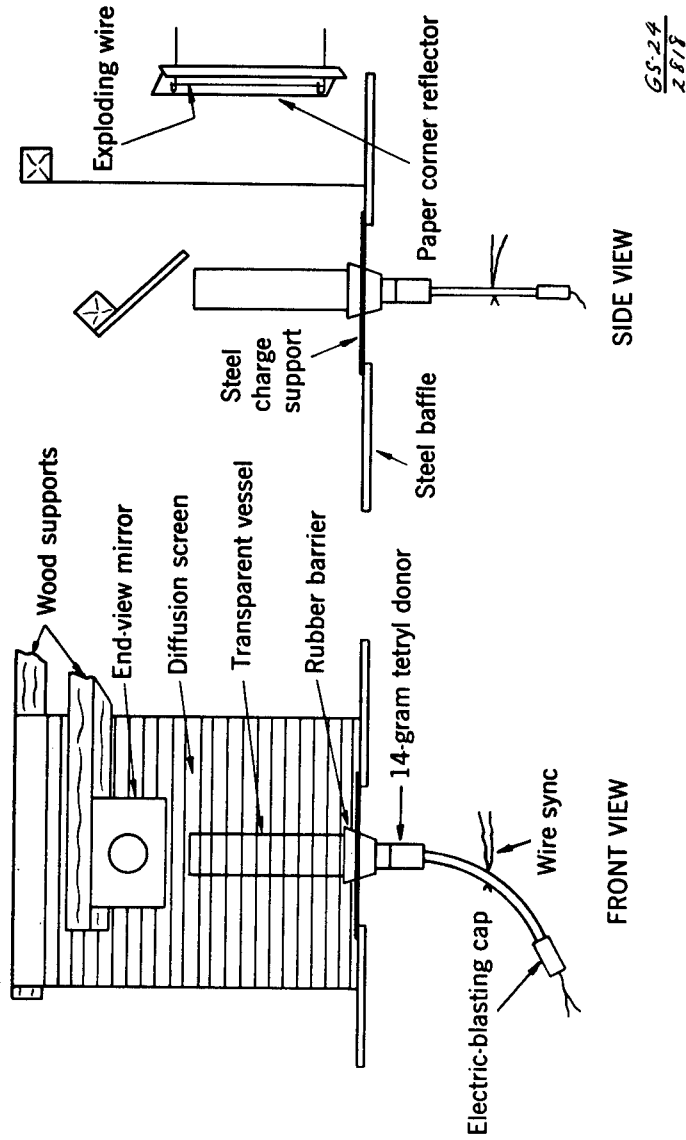Fig. 1 - Drawing of a typical test vessel configuration used for initiation and growth studies in liquid explosives
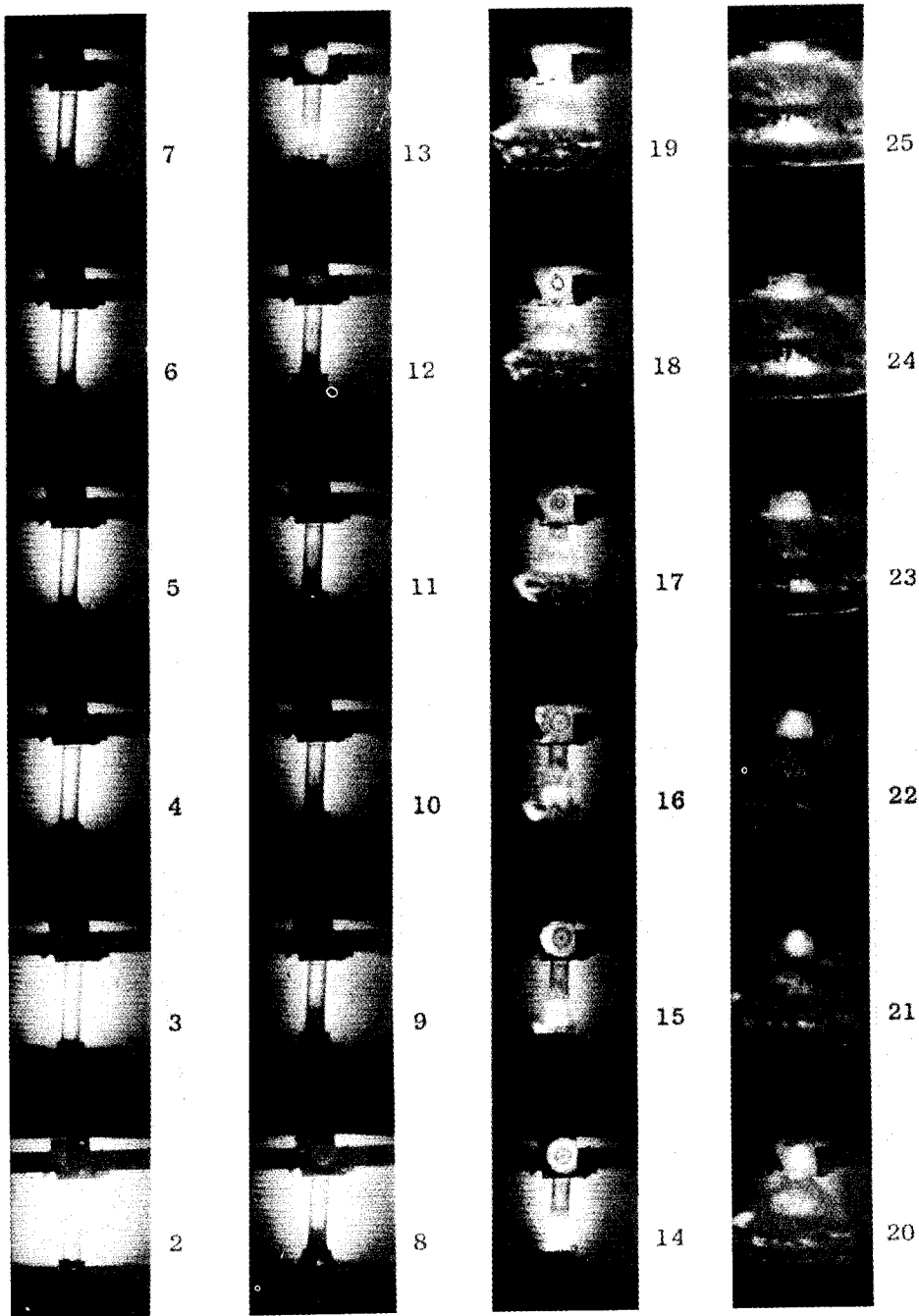
439

Fig. 2 - A framing camera sequence of the initiation and growth of detonation in a NG/EGDN mixture, contained in a 23 mm. i.d. tube. Both axial and peripheral initiation is shown. The interframe time is 4.2 sec. and the frame exposure time is 1.4 μsec. A resistance element was prepositioned in the charge.

barrier. Interframe time was 4.2 μ sec. and the exposure time per frame was 1.4 μ sec. The end-on view of the event appears in the mirror inclined at about 45° to the charge axis and positioned off the charge end.

In frame 3, the shock wave is seen emerging from the barrier. A nonluminous disturbance moves up the tube at a rate of about 1.6 mm/μ sec.; this is slightly higher than sonic velocity for the liquid. In frame 9, about 25 μ sec. later, an axial disturbance, nonluminous in its early stages, begins to appear. Later, this disturbance develops into a spearhead, showing a lateral, luminous growth at its base and moving downstream through the column at 2.5 mm/μ sec. This is approximately sonic velocity for the cylindrical plastic container. This axial disturbance would thus appear to result from the interaction of the transverse waves generated in the liquid by the compression waves in the vessel wall.

In frame No. 12, the reaction occurs not only on the axis, but early peripheral initiation also is seen in the mirror view. In frame 13, the luminous reactive region is seen to develop at the interface between the liquid and the vessel wall, but little lateral pressure is created. By frames 15 and 16, two initiation regions are indicated and the vessel has begun to yield. The axial disturbance has reached the charge end and has spread along the meniscus in frame 15 and a suspension of droplets is driven off the end in a fountain-like ejection. These particles decompose during passage through the atmosphere above the charge, as indicated in the end-on view of frame 18 and later frames.

The peripheral initiation of the NG/EGDN mixture is more clearly shown in the selected frames (18, 20, 22, and 24) taken from another shot, Figure 3. This sequence was photographed with an interframe time of 1.4 μ sec. and an exposure time of 0.90 μ sec. The diameter of the confining vessel was 35 mm. i.d., about 50 percent larger than that used in the tests described in Figure 2; the length was the same. Because of the greater diameter, the axial disturbance was less severe and initial luminous reaction occurred only at the liquid explosive-vessel wall interface, as shown clearly in the end-on view (Figure 3). The hairy structure of the products cloud is perhaps caused by the ejection and subsequent reaction of explosive after passage through the longitudinal tension cracks in the plastic vessel wall. The broad luminous zone is propagating at a rate of about 7 mm/μ sec. This is approximately the normal hydrodynamic velocity for detonating NG/EGDN.

The intense spearheaded axial disturbance, evidenced in Figure 2, is further illustrated in Figure 4. In Figure 4, the vessel was not instrumented with a resistance element. This single frame 0.5 μ sec. Rapatronic camera photograph shows the opacity caused by the wall-liquid interaction at the vessel top and the cracks at the base from which liquid explosive is later ejected.

18 20 22 24

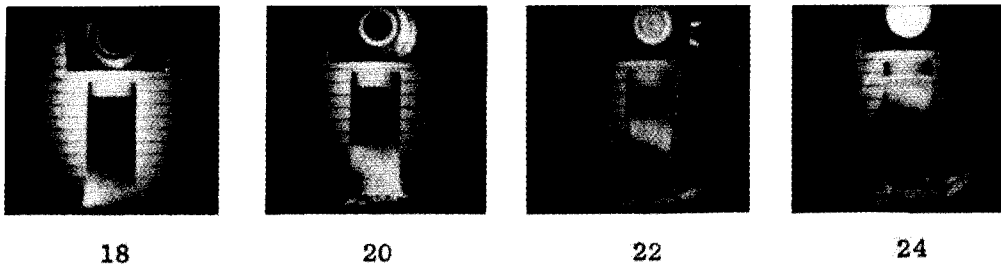Fig. 3 - Selected frames of a sequence in a 35 mm. i.d. vessel showing only peripheral initiation in a NG/EGDN mixture. The interframe time between adjacent frames was 1.4 μsec. and the frame exposure time was 0.90 μsec.
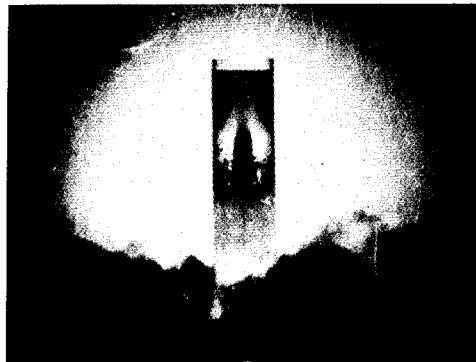

Fig. 4 - A Rapatronic camera photograph, single frame exposure, showing the predetonation activity in a column of NG/ EGDN. No resistance element was employed. Exposure time was approximately 0.5 sec.

The early suspicion that the formation of an axial spearhead depended upon the presence of the resistance wire element was thus eliminated. In other similar pictures, taken without back lighting, the luminosity of the base of the spearhead is clearly evident.

By employing a square plastic tube, the complex wave interaction can be further examined. Figure 5 illustrates the beautifully symmetrical pattern of luminous and nonluminous phenomena occurring at an intermediate point in the initiation process. This frame, selected from a full sequence, had an exposure time of 1.4 μ sec. The tube was 22 mm. x 22 mm. x 75 mm. and had been shocked through a rubber barrier in the usual manner. The top of the grey zone, seen in the front view, represents the position of the compression wave in the plastic container and also seen where the luminous zones merge in the center, is the point where the transverse sonic waves intersect in the liquid.

In Figure 6, four selected frames are shown from a framing camera sequence where a standard card-gap (2) configuration was used. The time between adjacent frames is 4.2 μ sec.; the exposure time is 1.4 μ sec. Again, a square plastic tube was used with a 2.6-inch card-gap (plastic) and two 1-5/8-inch-diameter by 1/2-inch-long tetryl boosters. This result was a high-order detonation, as evidenced by the photographic sequence and also by the clean-cut hole that resulted in the witness plate. The failure of the plate is evident in the fourth frame shown. Again, the wall is the locus for initiation, but the reaction is seen to spread quickly and uniformly across the vessel. The bright spot under the witness plate in frame 9 is an air bubble, but it did not serve as a nucleus for initiation.

A rather similar card-gap test configuration is shown in Figure 7. Here, two sides of the tube were steel and the plastic barrier was only 3.75 cm. thick. The same type donor was used in this test as for that shown in Figure 6, the framing rate was also the same. In this sequence the reaction is predominately along the side walls of the vessel and although reaction developed throughout the entire container by frame 16, the detonation reaction was incomplete and the witness plate was recovered essentially undamaged. These two shots indicate an anomaly which may result from using a witness plate as a criterion for detonation.

In another experiment (Figure 8), a square cross-section tube with two sides of aluminum was employed, together with a rubber barrier. The early stage of the initiation is not unlike that obtained with a plastic card barrier as shown in Figure 6. Instead of a witness plate, an end viewing mirror was used. The incipient ignition, seen in frame 7, has, 4.2 μ sec. later, developed into a reaction which has engulfed the base of the charge. In frame 10, a luminous cloud, giving the appearance of the plasma reported by Cook (3), is seen at the end of the charge resting on the liquid explosive meniscus.
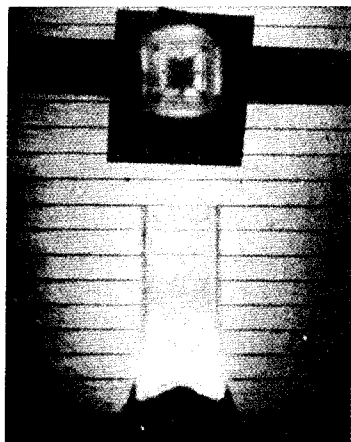
Fig. 5 - A single frame, from a sequence, of detonating NG/EGDN in a plastic vessel having a square cross section. The end-on mirror shows the symmetry of shock interaction and peripheral initiation. The exposure time was 1.4 μsec.

7   9   11   15
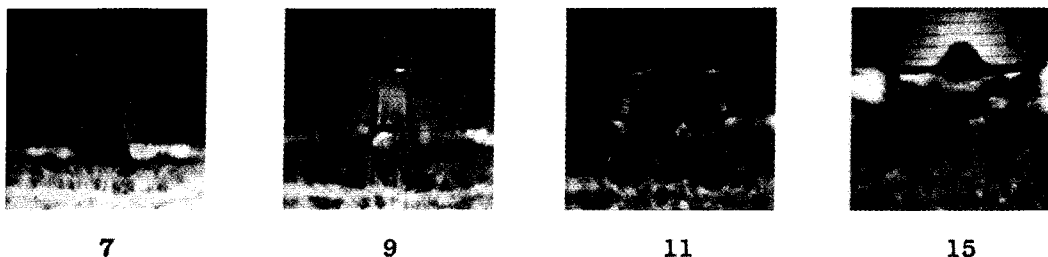
Fig. 6 - Selected frames from a sequence of a detonation in NG/EGDN for a typical card-gap configuration. A plastic tube having a square cross section, a plastic barrier thickness of 2.6 inches, and a 4 inch x 4 inch x 1/4 inch witness plate were used. A high order detonation resulted which punched a clean hole in the witness plate. The adjacent interframe time was 4.2 μsec. and the frame exposure time was 1.4 μsec.
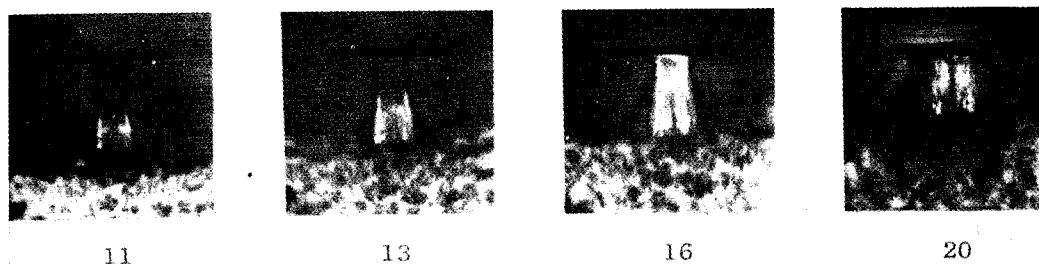
Fig. 7 - Photograph of a card-gap configuration in which the side walls were steel; gap thickness was 1.5 inches (vs. 2.6 inches for Fig. 6). Initiation is at the metal wall surfaces. Reaction was predominately low-order, little witness plate damage resulted. The interframe is 4.2 μsec. and frame exposure time is 1.4 μsec.
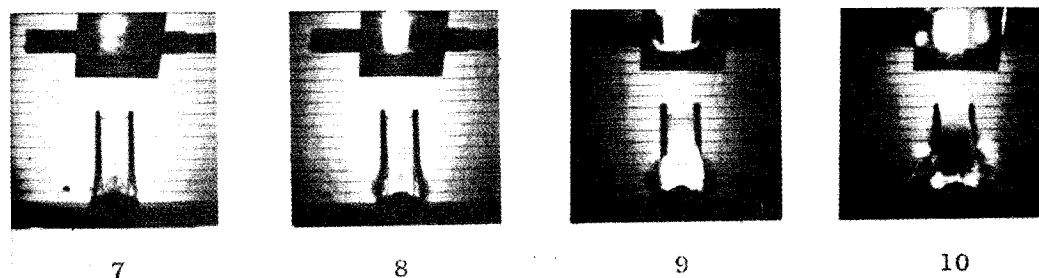
Fig. 8 - Frames selected from a sequence of detonating NG/EGDN in a vessel of square cross section and with two aluminum side walls. A rubber shock attenuation-barrier was used. Early initiation stages are similar to the card-gap tests, except that the locus for initiation appears to be in a central region. In frame 10 a luminous cloud is seen at the end of the charge resting on the meniscus although the reaction has not as yet reached the end of the charge.

The nature of the off-end luminous zone, seen in the preceding photograph, may be explained by the results in Figure 9. The vessel is a 35 mm. i.d. cylinder. Frame 6 shows the shock wave entering the column; in frame 8, two zones are discernible, the uppermost caused by the shock wave in the wall and the opaque region at the base of the charge due to shock activity in the unreacted liquid. Merging in frames 10 and 12, these zones have enveloped the entire charge by frame 14. A reaction at the wall, occurring at the base of the column in frame 16, has, by frame 18, reached the end of the charge; however, at this instant an opaque fountain (dark cloud) of unreacted droplets or mist of explosive is ejected from the surface of the liquid. In frame 19 this cloud has grown and is reacting as a droplet suspension in the off-end atmosphere. Also visible in frame 19 is an annular droplet formation caused by ejection of material near the wall subsequent to the central fountain shown in frame 18. The appearance of this off-end phenomenon could readily be misconstrued as a "plasma", since it would probably have electrical characteristics of a "plasma" when evaluated by probe techniques and certainly appears to have the photographic attributes of the "plasma" described in the literature by Cook, et al. (3, 13).

The results obtained using a hybrid confining vessel are shown in Figure 10. In this experiment, one side wall is aluminum and the other is steel; a rubber barrier is employed. Selected frames from the sequence indicate effects caused by the nature of wall material. The interframe time is 2.1 μ sec. and the exposure is 1.4 μ sec/frame. The event is symmetrical in the early stages; by frame 5 the effect of the difference in wall composition becomes noticeable in that the side view shows the precursor wave along the steel to be advancing ahead of the wave along the aluminum. In contrast to this, the end view indicates that the locus of an early reaction, which appears to die out, is at the aluminum wall. In frame 6 a symmetrical axial disturbance forms which, by frame 9, appears to bend toward the aluminum wall. In frame 12 the ejection of a droplet formation is evident with the greater jet action in the vicinity of the steel. By frames 14 and 15, pockets of reaction appear along the steel interface and in frame 16 the off-end droplet cloud has reacted in passage into the air at the charge end.

The schlieren photograph in Figure 11 clearly shows the multiplicity of lateral waves induced in the explosive by shock waves in the steel side walls. This is a single-frame Rapatronic camera photograph taken 25 μ sec. after entry of the shock wave into the NG-EGDN filled vessel. The charge contained a resistance element. The opaque region at the base of the charge represents the disturbance in the liquid explosive.

The effect of the presence of metal surfaces in repressing detonation failures in nitromethane was reported by Campbell and associates (15). The experiments involved streak camera studies of detonation in tubes of glass, dural, and glass tubes lined with
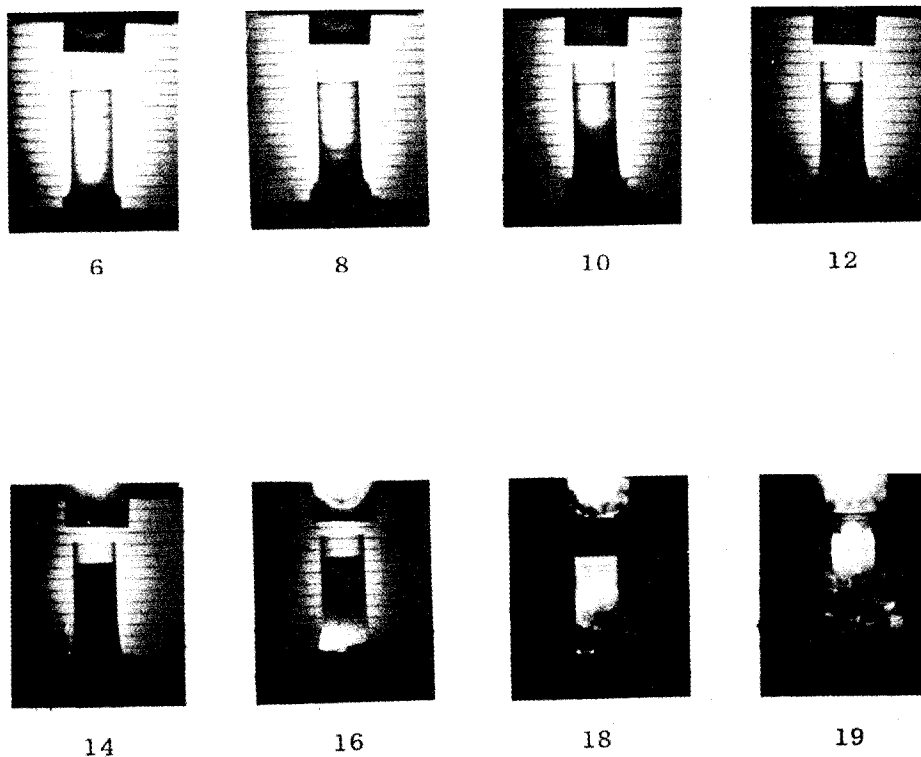
Fig. 9 -- The development of the off-end luminous cloud is shown in the selected frames from a sequence of detonating NG/EGDN in a 35 mm. i.d. Plexiglas tube. Predetonation activity is shown in the early stages of the event and in frame 18 an opaque axial droplet ejection is clearly evident, in frame 19 (4.2 μsec. later) this material has reacted on its passage into the atmosphere. In addition, an annular formation has developed during the interframe time of 4.2 μsec. and exposure time of 1.4 μsec. This may be an example of the phenomena referred to in the literature as a "plasma."

2   5   6   9

12   14   15   16
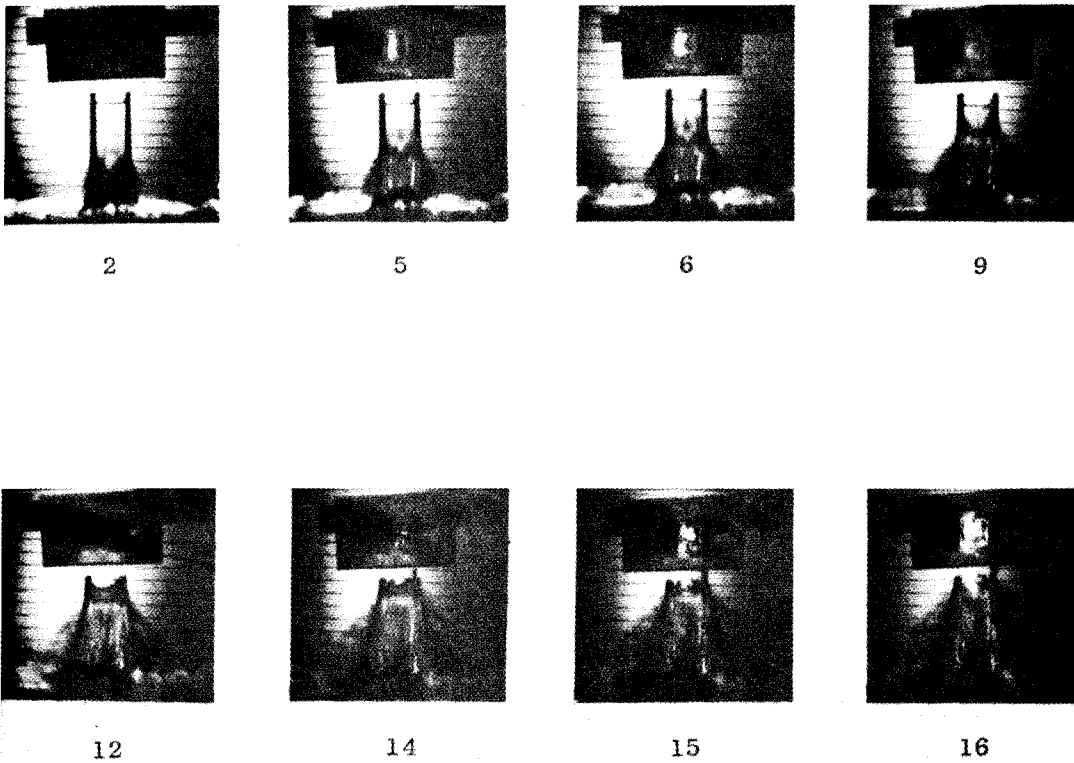
Fig. 10 - Selected frames from a sequence of detonating NG/EGDN showing the effect of wall material. The left side wall is aluminum and the right wall steel. Luminosity is first discernible in the region of the aluminum but is later followed by reaction at the steel wall. Adjacent frames were 2.1 μsec. apart and frame exposure was 0.14 μsec. The jet of unreacted explosive is visible and the locus of reaction is shown in the end-on mirror view.
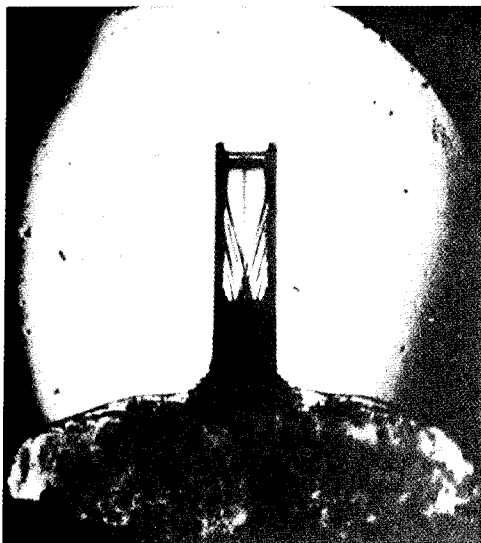
Fig. 11 - A Rapatronic camera schlieren photograph of the lateral waves in the body of a detonating NG/EGDN mixture.

448

various metal foils. Campbell and his fellows concluded that the action of metal foils in repressing failures was due to the confinement provided by the foil where the density, compressibility, and thickness of the material are the important parameters. No discernible effect was observed due to the specific nature of the surface. In our experiments, using relatively thick (3.1 mm.) side walls, the wall material seemed to play an important role in establishing the locus of initiation.

Resistance-element records for two types of initiation of detonation in NG/EGDN are shown in Figure 12. In one case (Figure 12(a)) in which the barrier was a 2.6 cm. long rubber cylinder snugly fitting into the plastic acceptor tube, the shock waves were sufficiently intense to cause the detonation to occur after a delay of 25 μ sec. and at a point about 1.6 cm. into the charge. In the other case (Figure 12(b)), where shock attenuation was provided by the conventional-type rubber barrier (shown in Figure 1), a delay of about 45 μ sec. resulted and initiation to detonation originated at a distance of 5.2 cm. from the barrier. During the delay, the wire-element record shows a period of erratic behavior where no orderly propagation is indicated; however, ultimately, at least on the axis, the hydrodynamic velocity was attained. Our conclusion is that had these tests been instrumented only by witness plates, the first result would have been "positive," the second a "failure". Under these conditions, the detonation velocities measured over discrete intervals would have been recorded as high and low, respectively.

Discussion and Conclusions

These photographic studies indicate that the stimulus given to a sample in the card-gap test is anything but simple. Evidently, the usual concept of a sample being subjected to a "pure shock" is rather naive and quite inadequate. Rather, the sample is subjected to a wide range of interacting forces. Consideration of these interactions leads us to suggest a new mechanism for the initiation of detonation in liquid explosives. The mechanism is essentially one of cavitation established by shock excitation (16), possibly with additional heating of the liquid provided by shear forces resulting from differential particle velocities in the liquid and between the liquid and the container walls. A minor contribution to heating may result from compression of the liquid.

If a liquid body is exposed to intense acoustic vibrations -- and the intensity of the stimulus in the tests described is unquestionably high -- gas bubbles will be formed from the dissolved gases. Such gas pockets may first exist as small invisible bubbles of microscopic dimensions. These bubbles, finely dispersed throughout the liquid, constitute weak points in a liquid whose tensile strength is determined by the largest bubble present. In addition,

(a)   (b)
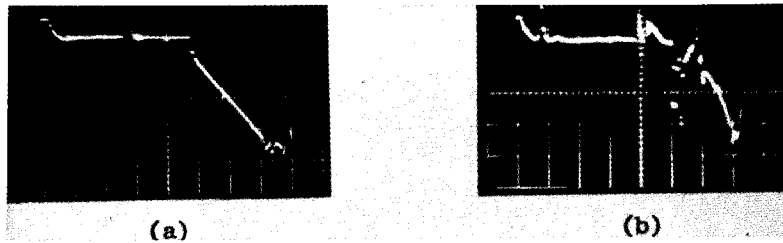
Fig. 12 - Oscillographic record of a wire element
employed for the continuous determination of
detonation velocities. (a) Waveform resulting
from a high order propagation in NG/EGDN in
which the steady state velocity is 8.6 mm/μsec.
A piston type rubber barrier was used giving an
abnormally high apparent velocity which may have
been due to precompression during the 25 μsec.
delay before reaction began. (b) Waveform result-
ing from a test using the conventional charge con-
figuration (Fig. 1). A period of erratic behavior
is indicated prior to establishment of a 7.5 mm/μ
sec. propagation. Time base if 5 μsec/div on the
abscissa and distance is 3.6 cm/div on the
ordinate.

impurities, such as dust particles, provide nuclei for the formation of additional cavities. Other weak points would be found in the gas nuclei contained in small imperfections in the container wall. In a reactive system, such as NG/EGDN, the vapors in the voids would be capable of exothermic decomposition. Bowden and associates (4), have postulated that the adiabatic heating of such cavities would be a sourcs of local reaction; however, Bolkhovitinov (8) and Selberg (12) disagree with this theory, based on consideration of thermal relaxation times for the very small bubbles (10^{-3} to 10^{-5} mm.).

During cavitation, the small bubbles may coalesce into larger bubbles of a size sufficient for compression to result in adiabatic heating. Importantly, any decomposition of the vapor or droplets in the bubbles which results in the production of gas, also results in an increase in bubble size. The time required for the foci to grow through coalescence and reaction may well account for the long delays observed in the initiation process.

An analogy of the cavitation process has been observed in solid plastic rods. Figure 13 shows a section of 1-1/4 inch Plexiglas rod after it has been subjected to the shock waves from a 1-1/4 inch diameter explosive donor. That part of the rod immediately adjacent to the explosive was completely destroyed but a portion of the rod recovered shows a well defined spearhead of multiple tensional fractures. This is to be compared with Figures 2 and 4 showing the spearhead observed in 50-50 NG/EGDN. Each fracture gives the appearance of a small cone pointed toward the explosive donor. This solid analog lends support to the suggestion that initiation processes comparable to those observed here in liquids may play an important role in the sensitivity of solid propellants.

The nature of "low-order detonations" continues to elude definition. These phenomena are characterized by low apparent velocities of a luminous, pressurized, or ionized front. Because the luminosity, pressure, and ionization are all less than that associated with a normal detonation, less than complete reaction is the usual assumption. Tacitly, the process is otherwise assumed to resemble a detonation (17). The broad luminous zone, the complex pressure interactions between wall and contents, and the erratic ionization observed with the resistance element raises questions as to the validity of this assumption. Further investigation of "low-order detonations" are planned by the Bureau of Mines because of their potential importance in the safe handling of explosives and propellants.

<u>Acknowledgment</u>
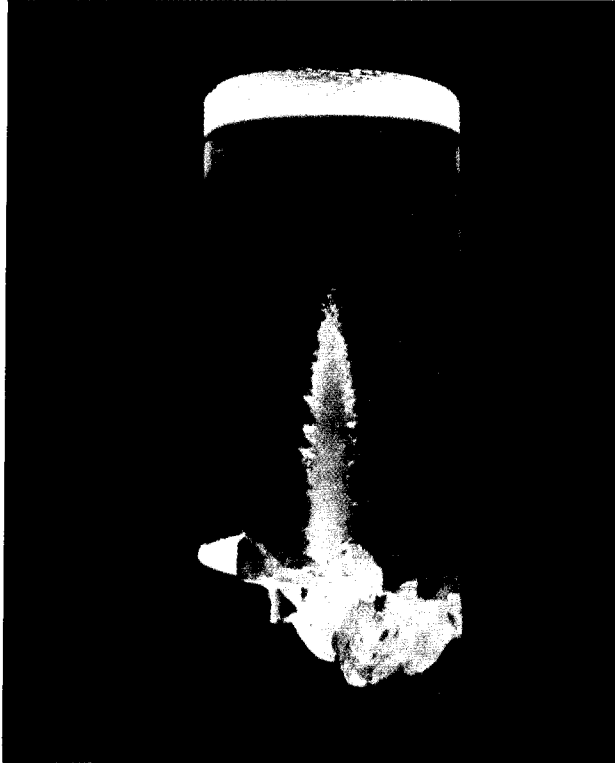
Fig. 13 - Photograph showing the effect
of shock wave interaction in a solid
Plexiglas rod which had been used as a
barrier in a card-gap test. The effect
of tension and the attenuation of the
shock wave with distance into the rod
is clearly shown. Similar effects in
liquids would produce cavitation.

List of References

1. S. J. Jacobs, Recent Advances in Condensed Media Detonations, J. Am. Roc. Soc. 30, 151-8 (1960).

2. Liquid Propellant Test Methods, Test No. 1, Card-Gap Test for Shock Sensitivity of Liquid Monopropellants, The Liquid Propellant Information Agency, Applied Physics Laboratory, The Johns Hopkins University, March 1960.

3. M. A. Cook, D. H. Pack, L. N. Cosner, and W. A. Gey, Instrumented Card-Gap or SPHF-Plate Test, J. Appl. Phys. 30, 1579-84, (1959).

4. F. P. Bowden and A. D. Yoffe, Initiation and Growth of Explosion in Liquids and Solids, Cambridge University Press, Cambridge, England, (1952).

5. G. B. Kistiakowsky, Initiation of Detonation of Explosives, Third Symposium on Combustion and Flame and Explosion Phenomena, The Williams and Wilkins Company, Baltimore, Maryland, (1949), 560-5.

6. A. J. B. Robertson, The Thermal Initiation of Explosion in Liquid-Explosives, ibid. 545-51.

7. K. K. Andreev, Some Considerations on the Mechanism of Initiation of Detonation in Explosives, Proc. Roy. Soc., 246, 257-67, (1958).

8. (a.) L. G. Bolkhovitinov, On the Theory of the Initiation of an Explosion by the Falling Weight Tests, Dokl. Akad. Nauk, USSR, 125 (3), 570-2 (1959). (b.) L. G. Bolkhovitinov, A Possible Mechanism for the Initiation of Liquid Explosives, ibid. 126 (2), 322-4 (1959). Translated and issued by Technical Information and Library Services, Ministry of Aviation, December 1959.

9. C. H. Johannson and H. L. Selberg, The Ignition Mechanism of High Explosives, App. Sci. Res. A 5, 439-49 (1955).

10. C. H. Johannson and others, The Initiation of Liquid Explosives by Shock and the Importance of Liquid Break Up, Proc. Roy. Soc., 246, 160-7 (1958).

11. G. P. Cachia and E. G. Whitbread, The Initiation of Explosives by Shock, Proc. Roy. Soc., 246, 268-73 (1958).

12. H. L. Selberg, Initiation of Nitroglycerin by Shock Waves, Appl. Sci. Res. A 5, 450-2 (1955).

13. M. A. Cook, R. T. Keyes, and L. L. Udy, Propagation Characteristics of Detonation-Generated Plasmas, J. Appl. Phys., 30, 1881-92 (1959).

14. F. C. Gibson, M. L. Bowser and C. M. Mason, Method for the Study of Deflagration to Detonation Transition, Rev. Sci. Inst., 30, 916-9 (1959).

15. A. W. Campbell, M. E. Malin, and T. E. Holland, Detonation in Homogeneous Explosives, Proceedings of Second ONR Symposium on Detonation, Office of Naval Research, Department of the Navy, Washington, D. C. (1955), 336-59.

16. I. R. Jones and D. H. Edwards, An Experimental Study of the Forces Generated by the Collapse of Transient Cavities in Water, J. Fluid Mechanics, 7, 596-609 (1960).

17. Rudi Schall, The Stability of Slow Detonation, Z. fur angew. Phys., 6, 470-5 (1954).

INITIATION CHARACTERISTICS OF MILDLY
CONFINED, BUBBLE-FREE NITROGLYCERIN

C. H. Winning
E.I. du Pont de Nemours and Company
Gibbstown, New Jersey

Background Information

The many initiation studies that have been conducted indicate that initiation, especially by near-minimum influences, is controlled by many physical conditions. Nitroglycerin was first prepared in 1846 and much information has been obtained about the initiation process and associated conditions since the initial work on nitroglycerin by Sobrero and Nobel.

Prior to 1892, Berthelot concluded that the impact energy in the drop-weight initiation test was sufficient to heat only a small portion of a nitroglycerin sample to the detonation temperature (Ref. 1). Direct evidence concerning energy requirements and the details of the localized process was obtained many years later by Bowden and co-workers (Ref. 2). These investigators found that the applied energy required for impact-initiation was only $5-25 \times 10^{-4}$ cal. in the presence of an air bubble. The heat developed within a small bubble by adiabatic compression accounts for 10^{-10} to 10^{-7} cal. In the absence of bubbles the applied energy required for impact initiation was higher by many orders of magnitude, namely, 2.5-25 cal.

The importance of air bubbles in dense, gelatinized nitroglycerin explosives is well known in the explosives industry. For instance, blasting gelatin (approximately 91% nitroglycerin, 8% nitrocotton, 1% chalk) may become so insensitive from loss of occluded air during storage that initiation by a commercial blasting cap is well-nigh impossible.

Bowden often found the build-up time from deflagration to detonation of nitroglycerin to be 20-150 μs starting from a hot spot in a confined film. In some unpublished work by the writer the build-up times for the underwater shock-wave initiation of nitroglycerin in polyethylene bags often were much longer, namely 1-15 ms, if the near limiting conditions for initiation existed. This work involved sympathetic detonation tests between primer and receptor charges spaced to obtain various shock wave energies, or pressures. At a distance for consistent propagation from a 73 g. cast pentolite primer, namely 8 ft., the shock-wave energy was only about 0.025 cal./cm^2,

and the pressure 75 atmospheres (Ref. 3). Undoubtedly air bubbles were present in the nitroglycerin. Bowden found that the building-up process of initiation of nitroglycerin from an adiabatically compressed air bubble in a film could be accomplished if the bubble volume was compressed by a ratio of 20/1, which corresponds to a pressure increase from 1 atmosphere to about 50, or to an initial adiabatic bubble temperature of about 500°C. In both Bowden's work and ours the build-up to detonation was slowest if a minimum intensity initiating influence was exerted.

Earlier work at this Laboratory gave reason to consider that more than microscopic or very localized effects might be involved in the initiation of bubble-free, unconfined nitroglycerin. Whereas nitroglycerin may readily be caused to detonate from a small hot spot in a thin, confined film, it fails to propagate far from even a large primer if confined only in a paper tube (soda straw) having a diameter of about 4 mm. This diameter is approximately the critical size for propagation of slightly confined nitroglycerin.

Method of Investigation

A framing camera was used to take a sequence of 25 pictures of the initiation process in 20 to 60 μs. The subjects were back-lighted with an argon flash lamp in order to reveal shocks, rarefaction clouds, and gas clouds.

A commercial blend of 70/30-nitroglycerin/ethylene glycol dinitrate (EGD) which had the characteristic yellow tint of the clear liquid was used. The material was passed through double dry filter papers prior to use. For brevity, and in accord with common industrial usage, the blend of nitrate esters will be referred to as NG throughout this paper.

The cells containing NG were either rectangular or cylindrical. The rectangular cells had windows of either glass of 1 mil "Mylar"* (10^{-3} in. thick). The latter material was used for most of the investigation. The cylindrical cells were made of "Mylar" that was cemented to a disk-shaped base of "Lucite"**. The smallest dimension of the cell in different experiments ranged between 3/4 in. and 3 in.

In order to minimize shock reflections and rarefaction clouds in the undetonated NG near a slow-acting initiating influence, some of the cells were immersed in tanks containing either water or a denser aqueous salt solution.

Initiating influences were applied by several methods. Arc discharges and exploding bridge wires were set off within NG-filled cells, using a source of 5000 v. from a 3 μfd condenser that was triggered through a 5C22 hydrogen thyratron tube. No. 8 and other blasting caps of the arc-firing type also were used as initiators. The No. 8 caps started to expand about 2-1/2 μs after the spark discharge.

Other experimental details will be mentioned where they apply.

*Registered trademark for polyester film of E.I. du Pont de Nemours & Co., Inc.

**Registered trademark for acrylic resin of E.I. du Pont de Nemours & Co., Inc.

Initiation Studies

Arc Discharge in NG

The photographs revealed that the initial highly luminous reaction about a spark discharge (0.01 cm. gap) in NG soon diminished in luminosity. The photographic record is indicative of an initial temperature greatly exceeding 3000°K. The initial radial expansion rate of the hot gas globe in the NG was 150-200 m./sec., but this rate diminished to about 50 or 60 m./sec. 25 μs after the discharge. The rate decreased to about 35 m./sec. in another 25 μs.

The approximate energy of the spark discharge in NG was 4.5 cal. if we assume that half of the condenser energy was transmitted to the discharge points.

An attempt was made to produce an accelerated reaction in the vicinity of sparks by firing two successive ones 0.2 cm. apart, in a time interval of 10 μs. The objectives were as follows: (1) to project compressed liquid, preferably as spray, into the first hot gas globe, (2) to create additional pressure between arcing regions, and (3) to start a larger hot reaction zone. Johansson, Selberg (Ref. 4) and co-workers (Ref. 5) considered some of these effects when invest-igating the shock initiation of NG and of another liquid, nitric acid-dinitrotoluene. Fig. 1 shows the events 13-47 us after firing the first of two sparks in NG. The second spark, fired 10 us after the first, produced no significant acceleration of the reaction in the NG. The radial rate of gas expansion around the initial discharge dimin-ished to about 70 m./sec. between 20 and 40 μs after the first dis-charge. The two cylindrical objects (0.6 cm. x 1.3 cm.) evident on either side of the arcs were solid rubber supports for the terminal wires that were set to provide a gap distance of 0.01 cm.

Exploding Bridge Wire in NG

A high voltage pulse was applied to a resistance bridge wire that was immersed in NG. The wire was about 0.25 cm. long and 0.005 cm. in diameter. The very luminous, high-temperature reaction around this exploding bridge wire also proceeded with diminishing luminosity and rate of radial expansion. The radial expansion rate was about 60 m./sec. after 35 μs, and about 22 m./sec. after 200 μs.

No. 8 Blasting Cap in NG

An initiator having the strength of a No. 8 blasting cap is considered an adequate, dependable initiator for practically all explosives that are capable of propagating a stable detonation at diameters up to about one inch. The heat of reaction of the explos-ive charge in the cap is about 600 cal. However, in the absence of adhering bubbles on a cap immersed in NG, usually only a very slow or a partial reaction of the NG occurred.

Fig. 2 shows two NG cells (2 in. x 2 in. x 3 in., inside dimensions; glass windows), each of which contained a No. 8 cap hav-ing a transparent plastic shell instead of the usual metal shell. Thus the luminosity of the cap reaction was evident from its beginning. The left cell contained water, the right one NG. A delayed-action, destroying pellet for the NG is evident outside the cell at the right. The third picture in the sequence shows similar luminosity and gas expansion, and similar shock waves in the two liquids. Thus

13 µs

30 µs
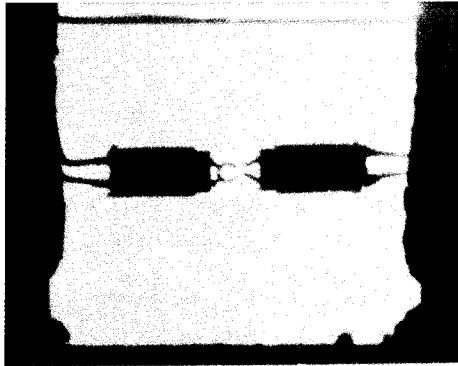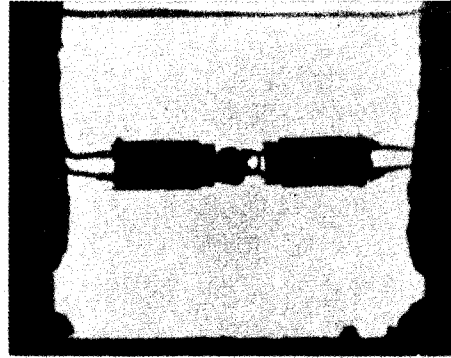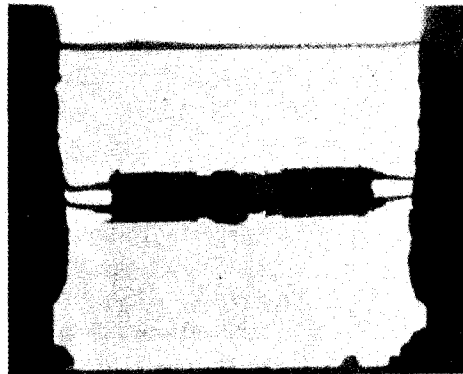
47 µs

Fig. 1 - Consecutive sparks in NG. Stated times are
relative to the firing of the first spark

1.0 µs

1.8 µs

11.1 µs

19.5 µs
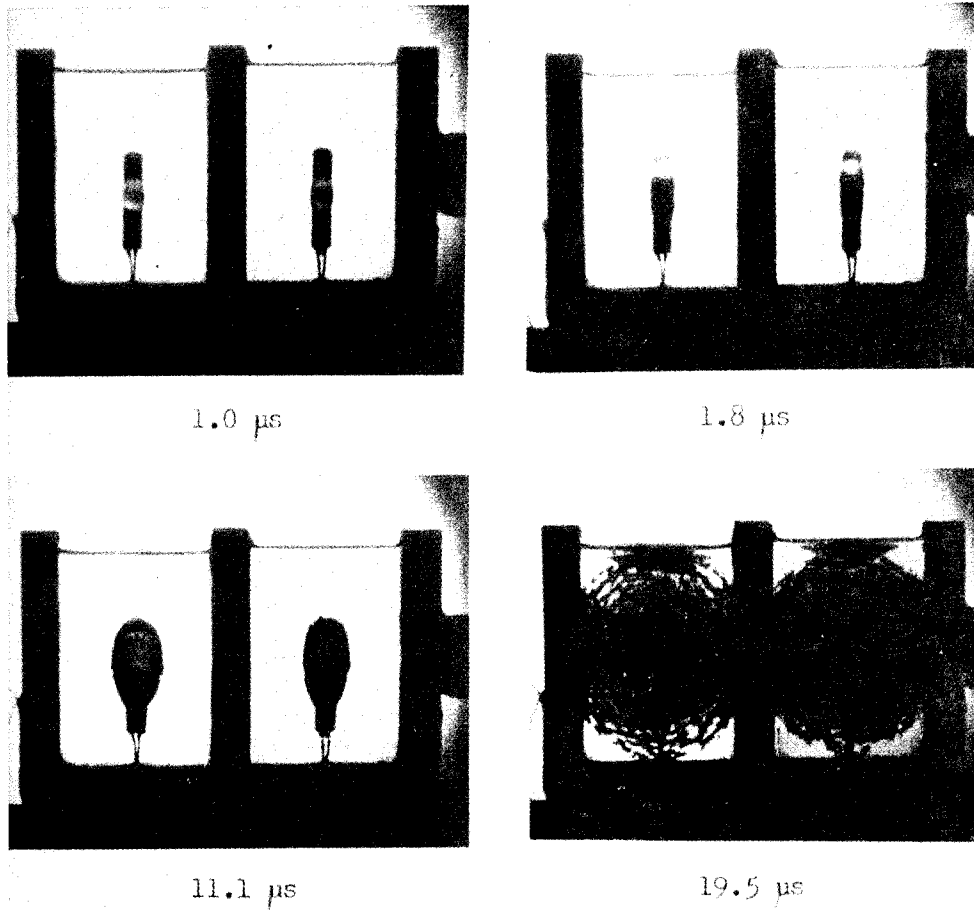
Fig. 2 - No. 8 plastic shell caps fired in water (left) and in NG (right). Stated times are relative to the start of cap expansion.

neither a high velocity detonation nor appreciable deflagration started in the NG. The fourth photograph shows comparable glass breakage and also the start of a dark rarefaction cloud below the surface of both liquids. The over-all result is typical of that obtained with caps having the standard cap shell of metal.

The effect of occluded air on initiation is shown in Fig. 3. Fine, aerated powders, (cork dust and "Microballoons"*) were secured in narrow lines on opposite sides of a No. 8 cap by use of a thin film of rubber cement. Luminous detonation at about 7500 m./sec. started very suddenly from each aerated region.

Although not illustrated in Figs. 2 and 3 a high velocity detonation occasionally started suddenly at the shock front about 0.3 cm. from the end of a cap having a conical indented end, which is standard construction. This end-initiation by converging shock influence did not depend on the presence of an air bubble in the indentation. The tests were conducted with the indented end of the cap up, and, as usual, the adhering bubbles were dislodged with a wire probe.

The indented end of a No. 8 cap (shell of commercial bronze) is the source of a high-velocity metal jet if a cap is detonated in air, but not if it is detonated in NG without a bubble in the cavity. A cap jet in air having a characteristic velocity of 2800-3500 m./sec. may be shot into NG from a distance of 2.5 cm. above the NG surface without starting a high-velocity detonation during a penetration exceeding 4 cm. During this penetration, the jet hole in the NG typically attained a diameter of 0.7 cm., and a surface layer of NG burned to a depth of 0.8 cm. In the absence of a delayed-action destroying pellet, it is possible that in some tests the NG would burn partially or completely without detonating. On the other hand, a cap jet caused a pulverulent, aerated dynamite containing 50% NG to detonate at nearly its characteristic velocity (for cartridges of 1-1/4 in. diameter) within 5 us after jet impact.

The third picture in Fig. 4 shows the delayed, luminous initiation of NG at high velocity by a No. 8 cap that was centrally situated within the cell. In this experiment the cell width was only 7/8 in. (front to back). In the third picture the faintly visible shock from the cap (in the clear NG) has a velocity of 1700 m./sec. The initial shock velocity at the cap boundary was about 3500 m./sec. The shock front in this NG cell was followed within about 0.6 cm. by a dark appearing rarefaction cloud, in which the luminous detonation started 5.4 us after the initial cap expansion. The gas cloud from the cap is obscured by the rarefaction cloud around it. The start of delayed, high-velocity, luminous detonation within a rarefaction cloud prompted further investigation of this phenomenon. Additional interest arose because the hot gas cloud was sufficiently transparent for a brief interval to reveal the presence of the non-luminous gas cloud from the cap. Photographs 3 and 4 in Fig. 4 also show the surface effect of hot gas projected from above by a blasting cap having no metal end.

Fig. 5 shows a single picture from a sequence which was
*Registered trademark for hollow, unicellular, urea-formaldehyde plastic spheres of Standard Oil Co. of Ohio

0 µs   2.5 µs
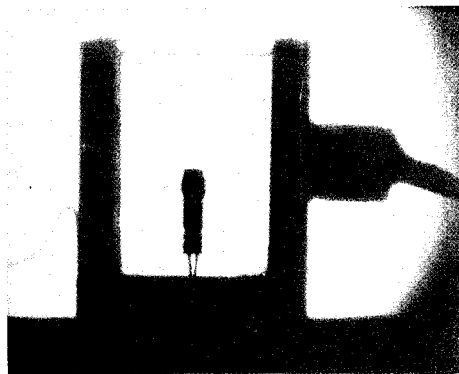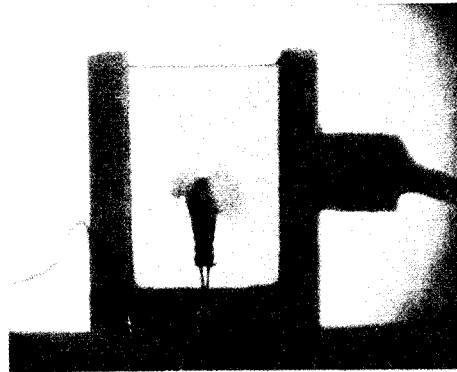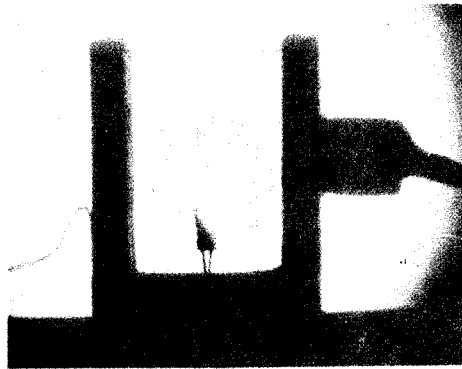
4.2 µs

Fig. 3 - No. 8 cap fired in NG - "Microballoons" and cork
dust, respectively, on opposite sides of cap.
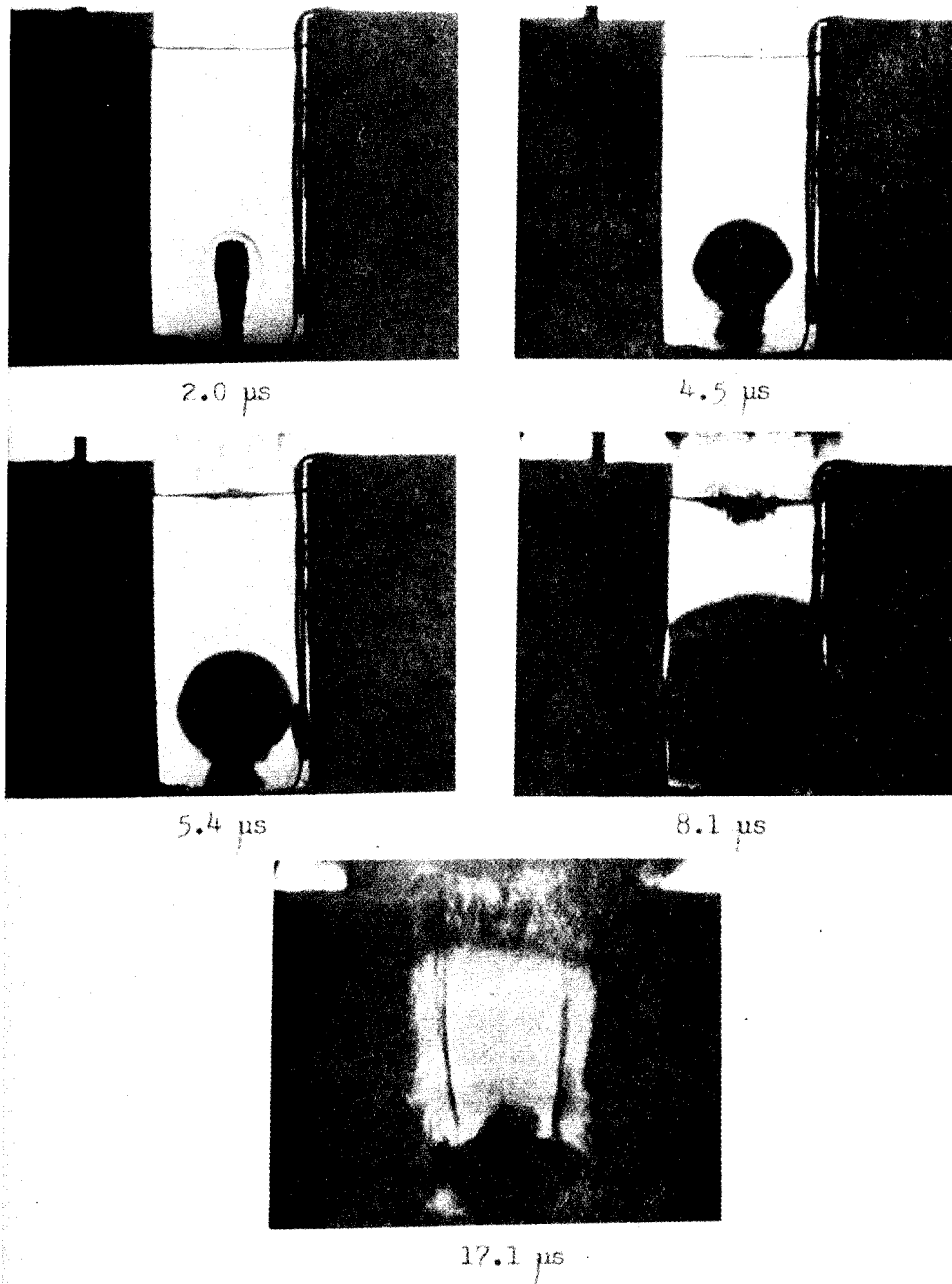
Fig. 4 - No. 8 cap fired in NG cell 7/8 in. thick. Open-end cap
fired 1-1/2 in. above the NG surface.

similar to that in Fig. 4. The width of the cell in Fig. 5 was 1/4 inch more than that in Fig. 4, namely 1-1/8 in. The dark rarefaction cloud and the delayed initiation therein again occurred. The highly transparent gas cloud from the detonation of NG is of additional interest, for in it the dark gas cloud from the cap and also the cap wires are clearly evident. An equally transparent gas cloud was not consistently reproducible. Its formation appeared to depend on the high-velocity detonation (at about 8000 m./sec.) of preshocked NG in a rectangular cell, containing a rarefaction cloud.

Initiation of NG by caps under other physical conditions was then investigated, as shown in Fig. 6. Cylindrical cells of NG were immersed in water to modify the shock reflections. At the right a single cap was located in a cylinder of NG having a diameter of 3/4 in. To the left of a plywood barrier was a larger cell containing two caps 3/8 in. apart. This large cell had a diameter of 3 in. The third picture shows the absence of luminous, high-velocity detonation 58 us after simultaneous firing of the three caps. However, it is of interest to note in the second picture that a faintly luminous region existed temporarily in the small cylinder; that is, in the rarefaction region above the oval gas cloud from the cap. The intersecting shocks between the adjacent caps in the large cell did not initiate any noticeable reaction. A flat rarefaction cloud is evident above the two caps in the third picture. This cloud appeared and disappeared intermittently during the picture sequence.

Shock reflections in NG were essentially eliminated by immersing an NG cell in a dense salt solution. (The solution density was 1.34 at 25°C. The composition was as follows: NH_4NO_3 - 33.0%, $NaNO_3$ - 23.0%, H_2O - 44.0%). The solution was contained in a cubic tank, 10 in. in each dimension. Thus the effect with regard to shock reflections was essentially that of shooting a cap at the center of a 10 in. cube of NG, except that the "Lucite" base of the cylinder produced a near-by rarefaction cloud. The diameter of the cylinder containing the NG was 3 in. The two pictures of Fig. 7 reveal a slow, nonluminous expansion around the cap. Cracks in the glass window of the tank started to obscure the view after about 148 µs. The radial expansion rate was accelerating slowly toward the end of the observation period, and had attained 440 m./sec. after 148 µs.

Because NG reacted so slowly to the influence of a blasting cap, it was of interest to know the effect of a cap in a nonexplosive liquid having comparable density. Fig. 8 shows the effect of No. 8 caps in a chlorinated hydrocarbon, "Aroclor"* No. 1254 (a liquid having a density 1.54 at 25°C.). The two cylinders of "Aroclor", 1-1/4 in. and 3 in. diameter, were immersed in water. A transient rarefaction cloud was formed in the upper portion of the small cylinder, but not in the large one. In the large cell the reflected rarefaction from the more distant wall was weak and thus no rarefaction cloud was formed. The gas globe around the cap in the small cylinder was only slightly smaller after 25 µs than the globe around the cap in NG shown in Fig. 5 (after 29 µs). The radial rate of gas expansion in the large cylinder of "Aroclor" was 300 m./sec. 25 µs after the
*Registered trademark for chlorinated hydrocarbons of Monsanto Chemical Co.
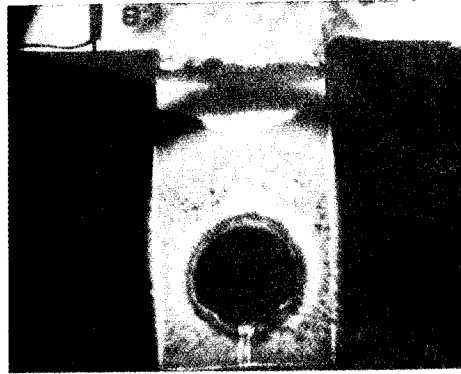
24 µs

Fig. 5 - No. 8 cap fired in NG
cell 1-1/8 in. thick. Open-end
cap fired 1-1/2 in. above the
NG surface.

0 µs

29 µs
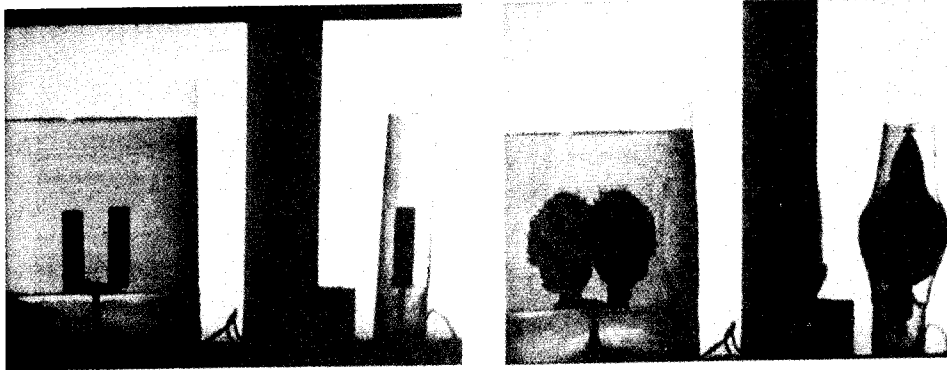
58 µs

Fig. 6 - No. 8 caps fired simultaneously in cylindrical
NG cells that were immersed in water.

464

90 µs   148 µs

Fig. 7 - No. 8 cap fired in cylindrical NG cell that was
immersed in dense aqueous solution.

8.4 µs   22.4 µs
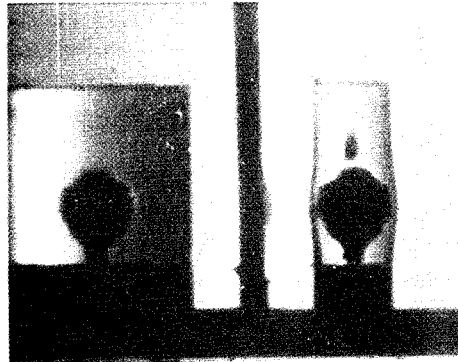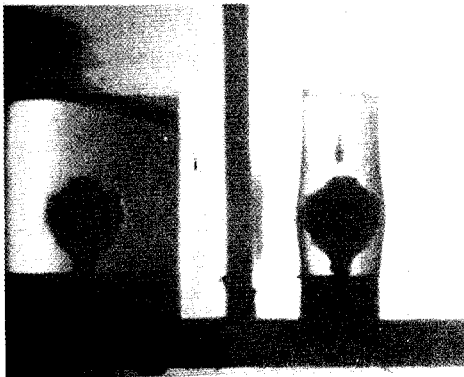
25.2 µs   30.2 µs

Fig. 8 - No. 8 caps fired in cylindrical cells containing
"Aroclor". The cells were immersed in water.

465

start of cap expansion, but the rate was diminishing.

Pictures not shown here indicate that the radial rate of
gas expansion in water-immersed "Aroclor" diminished to almost zero
after 100 μs, when the gas globe radius was 2.6 cm. After the same
time interval a cap in water-immersed NG caused radial gas globe
expansion at 350 m./sec., when the gas globe radius was 4.3 cm. The
hot gas volume in NG was about twice that in "Aroclor" after 50 μs,
but after 10 μs the volume in NG was five times that in "Aroclor",
indicating that a small amount of reacting NG added its effect to that
of the cap.

Intersecting Shocks from Special Large Caps

Intersecting shock conditions tending to promote delayed
initiation of NG are shown in Fig. 9. A mirror above the cell permit-
ted photographing a downward view in addition to the direct view.
The inside length, width, and depth of the cell were 4 in., 3 in.,
and 2-1/2 in., respectively. The two special caps contained 14 gr.
of PETN in the base charge, and were 1/2 in. in diameter to provide
an approximately symmetrical charge. The second cap was electrically
fired 18 μs after the first, at which time a rarefaction shock from
the first cap was reflected from the upper surface, and after re-
flected rarefaction shocks had collided in the bisecting plane of the
lower left corner. Delayed initiation of the NG, 29 μs after firing
the first cap, was evident in the lower left corner of the cell,
rather than at the cap location, indicating that this rarefaction zone
was more favorable for the development of the deflagration to deto-
nation process. The mirror view of a luminous crescent between the
caps indicates the possible existence of a second initiation center
between the two caps, where the shock from the second cap acted on
the rarefaction cloud proceeding downward from the surface above the
first cap.

Discussion

The application of different types of intense initiating
influences to the interior of essentially unconfined, bubble-free NG
gives evidence of low sensitivity and reluctant build-up of defla-
gration to detonation in a liquid explosive that has been used suc-
cessfully as a sensitizer for many dynamites, but generally in dis-
persed, aerated form.

The reaction started in NG by a No. 8 blasting cap proceeds
slowly and may not lead to detonation of the sample, as indicated on
occasion by recovery of residual material. The relatively small
amount of reaction of NG caused by a cap in 50-100 μs is indicated
approximately by the difference in gas volume in comparison with the
gas volume produced by a similar cap in "Aroclor".

A rough estimate may be made of the pressure and temper-
ature in the NG adjacent to the strong shock sources, such as the
No. 8 blasting cap. Extrapolation of time-distance curves for shock
travel give initial velocities of 3000-3500 m./sec. The correspond-

Note: The possibility of initiation at dust spots on the surface of
the NG was eliminated by providing a thin layer of Nujol on the sur-
face. Undesirable absorption of NG by the wood of the cell was
prevented by coating the inner surface with shellac.)
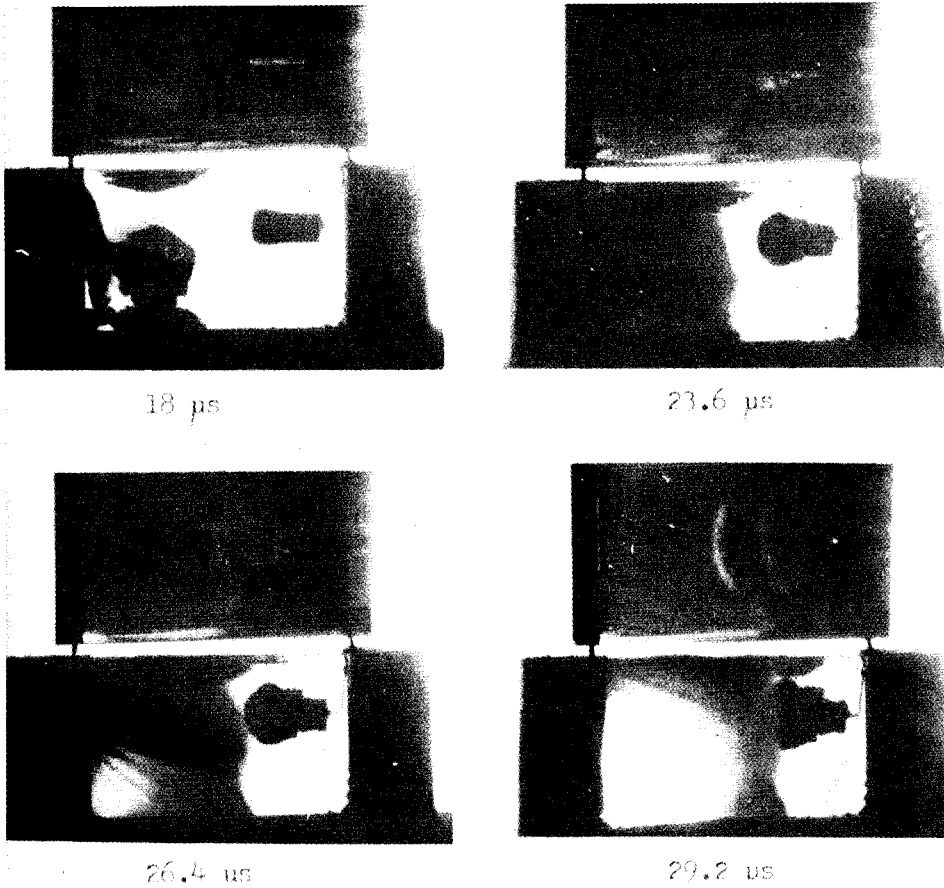
Fig. 9 - Delayed initiation of NG. Special caps contained 14 gr. PETN. Stated times are relative to the firing of the first cap.

ing initial movement of the expanded copper cap shells is not always clearly evident, and the measurements of boundary positions are not accurate because these boundaries were viewed through shock fronts that initially were highly curved. A material velocity of 600-800 m./sec. corresponds approximately to the aforementioned shock velocities. Applying the relationship, $P = \rho U\mu$, gives an initial shock pressure of about 40,000 atmospheres. (P = pressure, = density, U = shock velocity, μ = particle velocity). The associated transient temperature elevation at the shock front may be estimated by the simplified assumption that also was applied by Selberg (Ref. 6). Accordingly, $\Delta T = \dfrac{\mu^2}{2C}$, where C, the heat capacity, is 1.7×10^7 ergs/g. If $\mu = 8 \times 10^4$ cm./s., then $\Delta T = 192°C$. Since the ambient temperature was about 25°C. the peak transient temperature was 217°C.

The failure of NG to develop a rapidly accelerating detonation when exposed to a highly luminous arc discharge or to a high-velocity cap jet (from outside the NG) is evidence of rapid energy dispersion within the nitroglycerin. The energy is dispersed mainly by shock waves of insufficient duration and/or temperature to produce initiation. The cap jet velocity of 3500 m./sec. is much higher than the bullet velocity of 1100 m./sec. which Zippermayr found inadequate for the initiation of NG contained in a synthetic rubber bag. He employed a steel bullet having a diameter of 4.4 mm. (Ref. 7).

The occurrence of delayed initiation in an opaque rarefaction zone raises questions about the mechanism of the event. The creation of the opaque obscuring region can be delayed in increasing the cell dimension in the direction of the field of observation and work along this line is in progress.

References

1. Berthelot, M., _Explosives and Their Power_. English translation by C. Napier and William Macnab, John Murray, London, 1892.
2. Bowden, F.P. and Yoffe, A.D., _Initiation and Growth of Explosions in Liquids and Solids_. Cambridge at the University Press, 1952.
3. Cole, R.H., _Underwater Explosions_. Princeton University Press, 1948.
4. Johansson, C.H. and Selberg, H.L., Appl. Sci. Res., V, A, 439 (1955).
5. Johansson, C.H. and others, Proc. Roy. Soc. (London) Discussion, A246, 160 (1957).
6. Selberg, H.L., Appl. Sci. Res., V, A, 450 (1955).
7. Zippermayr, M., Explosivstoffe, 3, 25 (1955).

SHOCK INITIATION OF DETONATION IN LIQUID EXPLOSIVES*

A. W. Campbell, W. C. Davis, and J. R. Travis
University of California, Los Alamos Scientific Laboratory
Los Alamos, New Mexico

INTRODUCTION

The processes involved in the initiation of explosives have been the subject of much experimentation and theoretical speculation, and many investigators have contributed to an understanding of the problem. An excellent review of recent work has been made by S. J. Jacobs.[1] Of particular relevance to the work to be described here is the paper of Hubbard and Johnson,[2] who, in calculational experiments, have studied shock induced thermal explosion. Their calculations agree very well with the conclusions from the work described here.

In this paper experiments are described which show that nitromethane and other explosives in the homogeneous state are initiated as a result of shock heating. The initiation process is essentially a thermal explosion. Before describing the experiments, some of which are indirect, the general sequence of events which take place in the explosive will be described to aid in understanding the purpose of each experiment.

The general plan was to study the behavior of explosive when subjected to a smooth, plane shock wave of constant amplitude. Plane wave lenses[3] were combined with additional high explosive and inert shock-attenuator plates to produce a shock wave of the desired amplitude in the test explosive (see Fig. 1). The behavior of the test explosive was then observed before the intrusion of edge effects or of reverberations in the attenuator. When a shock wave, strong enough to produce detonation within a few microseconds, is generated in nitromethane, the explosive behind the shock front is compressed to about 5/8 of its original volume and simultaneously is heated to a high temperature estimated to be 1140°K. It has been possible to calculate the compression by impedance-matching calculations, and also measure the compression directly with fair accuracy. On the other hand, it has not been possible to measure the shock temperature; instead,

the temperature has been calculated by approximate methods.

The shock-heated explosive reacts very slowly at first, but the reaction rate accelerates due to self-heating, and detonation results. This acceleration of the reaction rate first becomes important at the attenuator-explosive interface, where the high temperature has prevailed longest. In the laboratory frame of reference the resulting detonation wave sweeps forward at a velocity which is the sum of the particle velocity behind the initial shock front and the detonation velocity of compressed, unreacted explosive. This detonation wave overtakes the initial shock wave and temporarily overdrives detonation in the unshocked explosive ahead of it.

The conclusions drawn in this paper are based on more than 300 separate experiments. Because not all of them can be presented in detail, they have been grouped into types of experiments. Many of each type have been done, and a few selected ones are described in enough detail for the reader to see what data can be obtained and how it has been used. We have tried to furnish enough of the experimental results to provide evidence to support every conclusion. In no case does a conclusion rest upon a single experiment, although in several cases only one experiment is described.

Recording Equipment

The equipment used in the experimental work described in this paper included a smear camera, a framing camera, and raster chronographs. The smear camera had a maximum writing speed of 9.2 mm/μsec at F/6 and had correction for the elastic distortion of the rotating mirror.[4] In the space direction the maximum resolution amounted to 400 line pairs. The time resolution was 5×10^{-9} sec.

The framing camera was capable of 15-frame sequence with a minimum exposure time of 2×10^{-7} sec and a time interval between frames of 2.5×10^{-7} sec. Resolution was 300 line pairs vertically and 200 line pairs horizontally. Maximum aperture was F/20.

The electronic chronographs and techniques for using them are described elsewhere.[5] Maximum time coverage per chronograph was about 150 μsec with a standard error per transit-time reading of about 3×10^{-9} sec.

Type I Experiment: External Velocity Profile

In the experiments designated as Type I a smear camera was used to record the progress of the initial shock wave in the explosive under study and to observe the transition to high-order detonation. The charge arrangement is diagrammed in Fig. 1.

A shock wave of appropriate amplitude was sent into a nitromethane charge from the booster-attenuator system. The nitromethane was illuminated from behind by an argon flash for a shadowgraph picture. The smear camera recorded the vertical progress of this shock wave and of the ensuing detonation wave over a distance as shown by the scale in Fig. 2. After the detonation wave left the field of view of the camera it passed into a 5.08-cm diam tube in which the steady-state

"stick" velocity was measured by the pin technique[5] with the electronic chronographs.
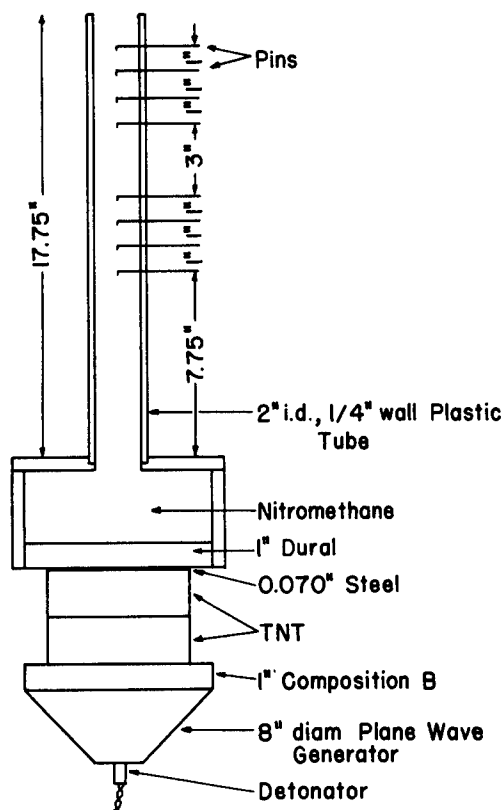
Fig. 1. Charge setup for nitromethane velocity profile experiment. Shot D-5772. The camera optic axis was parallel to and about 2 cm about the dural attenuator plate. The nitromethane was backlit by an argon flash charge.

In Fig. 2 are displayed both the field of view of the smear camera and a space-time record of the initiation process. It should be pointed out that the optic axis of the camera obviously could not be arranged to be tangent to the shock wave throughout its travel. The optic axis was aligned parallel to the bottom of the nitromethane box and at a distance above it coinciding with the anticipated shock transition point. This geometrical compromise contributed a maximum error of 2% to the observed velocities.

The results of two shots are listed in Table I. These shots were chosen because only in these two were steady-state stick velocities obtained in addition to the plane-wave velocities of the initial shock and of the detonation wave immediately after the transition. Unfortunately, the shock waves from these booster-attenuator systems were

not sufficiently uniform for accurate measurements and the plane-wave velocities in Table I are low. Best estimates of these velocities from additional experiments are entered at the bottom of the table.
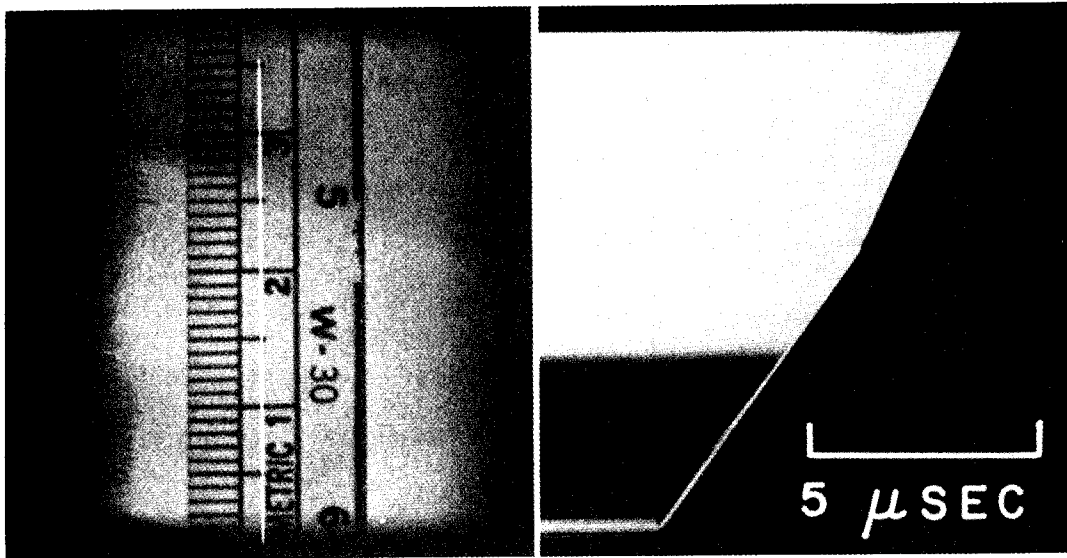
Fig. 2.   Left half of picture shows camera view of scale
mounted in nitromethane box shown in Fig. 1 with
slit image superimposed as a white line. Right
half of picture is the smear camera record from
the charge of Fig. 1. Time increases to the right.
The lighting is such that the lower record is a
shadowgraph, and shows the shock front as a bright
line. The shock moves up at constant or slightly
decreasing velocity from the bottom. At about
21 mm from the bottom, the detonation wave over-
takes the shock, as evidenced by the sudden
change in velocity. The detonation in the com-
pressed nitromethane can not be seen in this
picture. This picture can be compared directly
with Fig. 3, Lines III and VI.

A booster-attenuator system of the type used for these experi-
ments was fired to determine the velocity of the free surface of the
attenuator plate. A knowledge of the equation of state of the plate
and the shock velocity in the nitromethane allows a determination of
the pressure and the particle velocity in the nitromethane, using
standard impedance matching methods.[17] The pressure was determined
to be 81 kbar, and the particle velocity 1.6 mm/μsec, with an accura-
cy of about 5%. As will be shown later, the induction time is a very
sensitive function of the shock pressure, and since the range of in-
duction times over which it is possible to work is limited, the pres-
sure in all experiments is about the same.

TABLE I

External Velocity Data For Nitromethane

Shot Number	Initial Shock Velocity (mm/μsec)	Detonation Velocity (mm/μsec)	Stick Velocities	
			Pin Numbers	(mm/μsec)
D-5772	4.33	6.57	1-5	6.24
			2-6	6.36
			3-7	6.24
			4-8	6.22
D-5773	4.24	6.85	1-5	6.24
			2-6	6.25
			3-7	6.26
			4-8	--
			AVE.	6.26
	(4.50)*	(6.90)*		

* Best estimates from camera records of other shots.

The camera records of the initiation process show three interesting features. The initial shock wave proceeds at a constant or slightly decaying velocity, indicating that it is essentially a nonreactive wave; the transition is very abrupt, which we have found to be characteristic of homogeneous explosives; and the detonation velocity immediately after the transition shows an overshoot of about 10%, decreasing in a few microseconds to the normal detonation velocity.

The presence of overshoot can be demonstrated with the use of the average stick velocity as follows. From the work of Campbell, Malin, and Holland[6] we find the stick velocity of nitromethane to be given by the following equations,

$$\text{at } 91.3^\circ\text{F} \qquad D = 6.2125 - 0.00517 \ (1/d) \qquad (1)$$
$$\text{at } 22.5^\circ\text{F} \qquad D = 6.3745 - 0.01705 \ (1/d) \qquad (2)$$

where D is the detonation velocity in mm/usec and d is the explosive diameter in centimeters (confined in glass tubes). A linear interpolation is made to obtain an expression for the velocity at 70°F, the temperature of the nitromethane in the experiments discussed here.

$$\text{at } 70^\circ\text{F} \qquad D = 6.2627 - 0.00885 \ (1/d) \qquad (3)$$

From (3) the velocity for a stick of 5.08-cm diam is found to be 6.25 mm/μsec. This value is compared with the average stick velocity in Table I, and the difference is added to the constant term of (3) to obtain a corrected estimate of the plane-wave detonation velocity for the lot of nitromethane used in the experiments discussed here. Comparison of this estimate (6.27 mm/μsec) with the best estimate for the overdriven velocity entered in Table I (6.90 mm/μsec) reveals the overshoot to be 0.63 mm/μsec, or approximately 10%.

474

Type II Experiment: Internal Velocity Measurements

Given the results of the Type I experiments, the next problem was to locate the origin of the high-order detonation wave. This was done in Type II experiments.

It was assumed that the chemical reaction accompanying detonation could best be identified by observing the change in electrical resistivity accompanying it. To this end nitromethane could be prepared with a resistivity up to 5 megohm-cm. In contrast, the reaction zone of the high-order detonation in this explosive was known to be quite conducting.

After several preliminary experiments had been carried out using a pin technique, it became apparent that high-order detonation originated at the attenuator-explosive interface. The general sequence of events is as shown in Fig. 3. Curve I represents the shock wave in the attenuator moving toward the attenuator-explosive interface. Along II, the interface moves to the right with local particle velocity while a rather non-reactive shock wave precedes it along III. High-order detonation originates at the interface and follows Curve IV to the transition point, V, where it overtakes the initial shock wave and passes into the unshocked explosive, proceeding along VI.
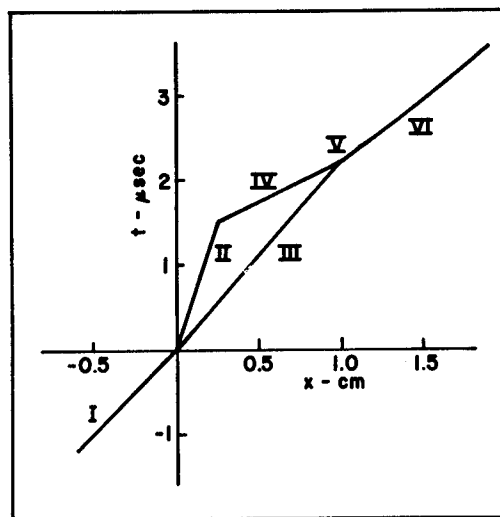
Fig. 3. Sequence of events in the initiation of a homogeneous explosive.

Because it was very difficult to obtain sufficiently uniform initiation over a sufficiently large area, a detailed pin record of the events in a single shot, as diagrammed in Fig. 3, was not attempted. (A camera record of these events is given in the section on Type IV Experiments below.) Instead, the pin technique was employed to measure the particle velocity U_p and the detonation velocity D^* in the

compressed nitromethane behind the initial shock wave .
In Fig. 4 is shown the experimental arrangement. The plastic at
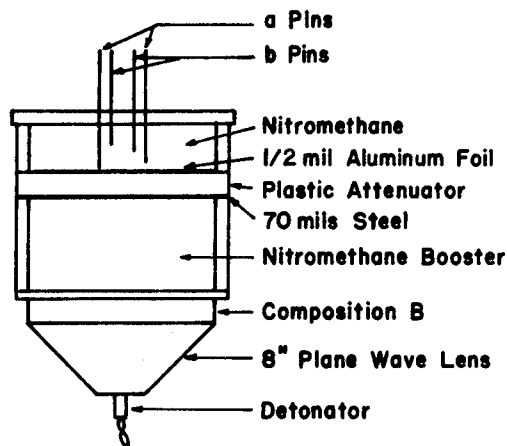
Fig. 4. Charge arrangement for Type II experiments. Six-
teen a pins were arranged in a 1-in. diam circle
at distances alternately 10 mils and 160 mils from
the aluminum foil. Sixteen b pins were arranged
in a 5/8-in. diam circle, half of them at 315 mils
and the other half at 750 mils standoff.

the plastic-explosive interface was coated with a $\frac{1}{2}$-mil (5×10^{-4} in.)
aluminum foil as a ground electrode. Eight pairs of pins were ar-
ranged above the interface in a 1-in. circle to yield eight measures
of the interface velocity, Curve II of Fig. 3. Eight additional pairs
of pins were arranged in a 5/8-in. diam circle to yield eight measures
of the detonation velocity, Curve IV of Fig. 3.

The pins were designed so as to minimize pin drift in the sur-
rounding mass flow. The first 16 pins were made of 3-mil diam tung-
sten wire, and the second 16 were made of 15-mil wire with the ends
tapered 1 in 4. The tapered section was terminated with a flat sur-
face 5 mils in diameter to facilitate measurement of the pin location
relative to the plastic-explosive interface.

The apparent values obtained in an experiment of this type are
listed in Table II. These values are in error by an unknown amount
because of drift of the pins in the mass flow of the surrounding ex-
plosive. This drift causes the observed values of the particle ve-
locity to be lower than the true one and causes the detonation veloc-
ity values to be too high.

A first-order correction to the apparent values of U_p and D^* can
be made as follows. Referring to the schematic drawing, Fig. 5, Pins
1, 2 sense the motion of the plastic-explosive interface; high-order
detonation occurs in Interval c; Pins 17, 18 sense the motion of the
detonation wave; and the detonation wave overtakes the initial shock

TABLE II

Internal Velocity Data for Nitromethane

Shot Number E-0374

Pin Numbers	Apparent Particle Velocity U_p (mm/μsec)	Pin Numbers	Apparent Detonation Velocity D^* (mm/μsec)
1-2	1.356	17-18	12.644
3-4	1.438	19-20	12.835
5-6	1.256	21-22	10.894
7-8	1.177	23-24	10.257
9-10	1.286	25-26	10.455
11-12	1.286	27-28	10.330
13-14	---	29-30	---
15-16	1.351	31-32	9.779
	AVE. 1.307		AVE. 11.027
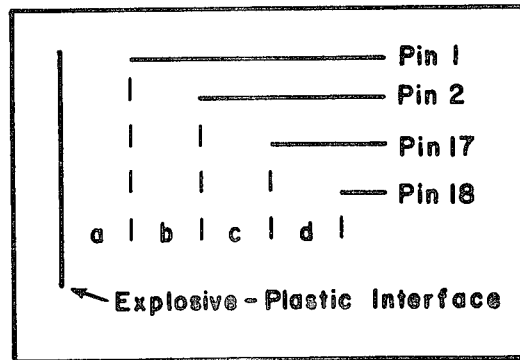
Fig. 5. Diagram for use in velocity calculations in Type II experiments.

477

wave beyond Interval $\underline{d}$. The following symbols are defined:

W   Pin drift velocity.

U_p Interface velocity.

D^* Detonation velocity in compressed nitromethane.

$\underline{b}$ Distance between Pins 1, 2, measured normal to interface.

$\underline{d}$ Distance between Pins 17, 18, normal to interface.

t_1 Time between signals from Pins 1, 2.

t_2 Time between signals from Pins 17, 18.

The assumption is made that the pins drift at constant velocity, W, after contact by the initial shock wave. The further assumption is made that the velocity of the initial shock wave is 4.5 mm/μsec (see Table I). The following relation then holds,

$$U_p t_1 = b - \frac{b}{4.5} W + W t_1 \qquad (4)$$

where $\frac{b}{4.5}$ W is the distance Pin 1 drifts during the time required for the initial shock wave to traverse the Interval $\underline{b}$. $W t_1$ is the distance Pin 2 drifts during the time required for the interface to move from the tip of Pin 1 to the tip of Pin 2. A similar relation holds for the motion of the high-order detonation wave.

$$D^* t_2 = d - \frac{d}{4.5} W + W t_2 \qquad (5)$$

It is assumed that the detonation velocity, D^*, is equal to the detonation velocity of uncompressed nitromethane (rounded to 6.30 mm/μsec) plus an increment due to the density increase behind the initial shock wave plus the local particle velocity:

$$D^* = 6.30 + 3.20 \left(\rho - \rho_0 \right) + U_0 \qquad (6)$$

where the velocity dependence on density is taken to be 3.20 mm/μsec g/cc, [6] and ρ_0 and ρ are the initial (1.125 g/cc) and final densities, respectively, of the nitromethane. Since

$$\rho - \rho_0 = \frac{U_p}{U_s - U_p} \rho_0 \qquad (7)$$

$$D^* = 6.30 + 3.20 \frac{U_p}{4.5 - U_p} \rho_0 + U_p \qquad (8)$$

In solving Equations 4, 5, 8 simultaneously, the value of b/t_1 is taken to be 1.30 (Table II) and d/t_2 is taken to be 11.0 mm/μsec. The following results are then obtained:

W = 0.56 mm/μsec
U_p = 1.70 mm/μsec
D^* = 10.19 mm/μsec

478

From the expression,

$$P = \rho_0 U_p U_s, \qquad (9)$$

the pressure behind the initial shock wave can be calculated. Taking the value of 1.70 mm/μsec for U_p and 4.5 mm/μsec for U_s the pressure is found to be 86 kb.

The approximation made in Equation (6) is not justified by any simple theory. There must be additional velocity changes from the change in pressure and the change in initial internal energy. These will be of opposite sign and may cancel, but they cannot be shown to be small by any method yet found. The calculation is included because it seems to agree so well with the results of the pressure measurements described for the Type I experiments. It would also be possible to estimate the pin drift velocity and arrive at about the same result, because the corrections to the pin data are small. The fact that the detonation velocity in the compressed explosive can be found by making only the density correction and using the coefficient found from experiments performed by varying the initial temperature at ambient pressure is interesting, but has not yet been related to the theory. The detonation velocity in compressed liquid TNT can also be closely approximated by making a similar density correction.

Type III Experiment: Observation of Detonation Light

For nitromethane and other transparent explosives, clarification
of initiation behavior can be obtained by viewing a test charge normal
to the shock wave and photographing the light generated by the charge
itself. The charge setup is shown in Fig. 6.
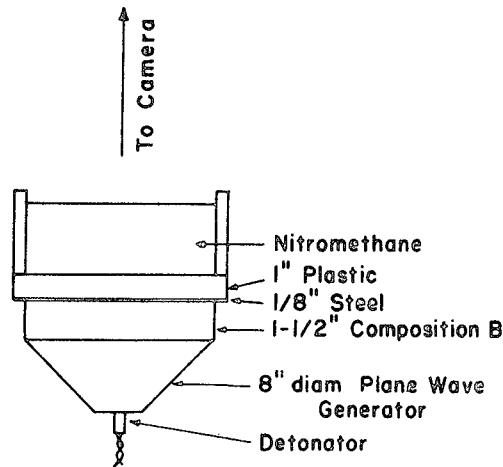
Fig. 6. Charge setup for Type III Experiments. Shot E-0609

The smear camera record obtained for nitromethane initiated by
the attenuator-booster system of Fig. 6, is shown in Fig. 7. At time
$\underline{F}$, the initial shock wave entered the nitromethane as indicated by the
flash of light from a bubble mounted on the attenuator surface. A de-
tonation spread from this bubble (see Experiment VIII for discussion
of effects of bubbles). At time $\underline{A}$, detonation appeared across 4 in. of
the attenuator surface, simultaneous within 0.08 usec. This weak
light comes from detonation in the nitromethane which has been com-
pressed by the initial shock. This detonation overtakes the shock,
giving a sharp increase in intensity on the film at time $\underline{B}$ which soon
decays to the intensity of steady-state detonation.

Better measurement of U_p and D^* can be made from records of this
type than from Type II experiments in which it is necessary to assume
constant pin drift velocity.

The distance $\underline{d}$ at which the detonation D^* overtakes the shock can
be computed along two paths as can be seen in Fig. 8. Equating the
expressions so obtained gives a relation between the velocities, U_p,
U_s, and D^*. Thus

$$d = U_s \, t_1 = U_p \, (t_1 - t_2) + D^* \, t_2$$

his equation can be solved for D^* by substituting into it the meas-
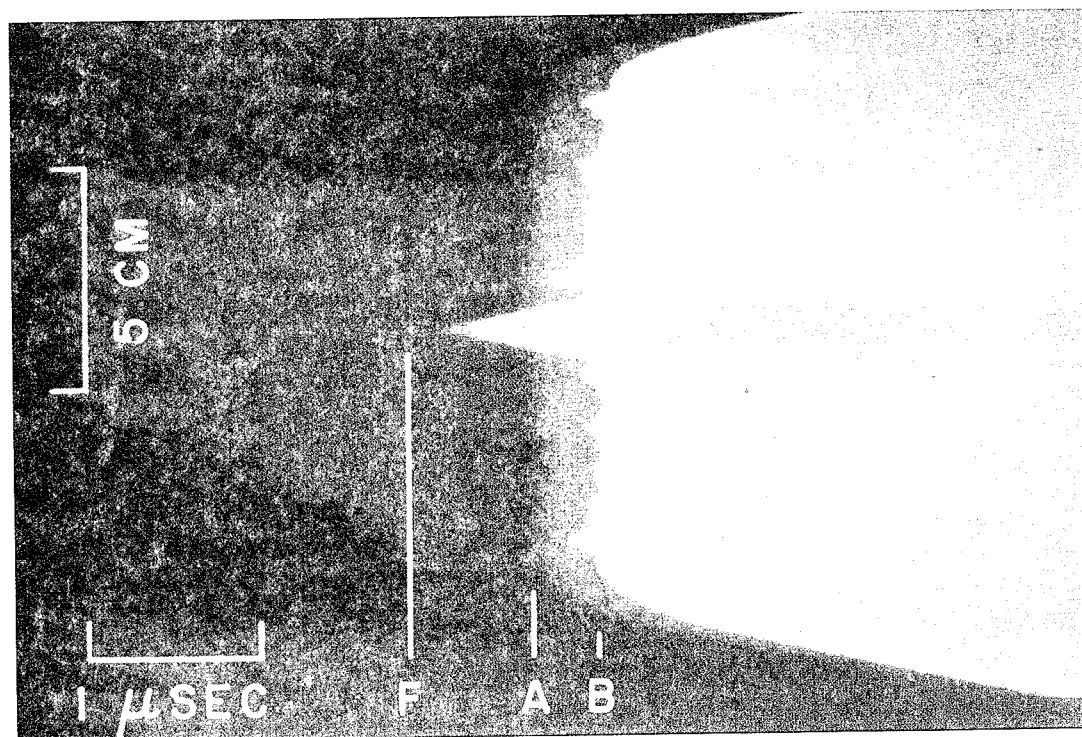
Fig. 7. Smear camera record of detonation light from nitro-
methane charge of Fig. 6. Shot E-0609. Time in-
creases to the right.
F: The flash of a bubble marks the time of entry
of the shock wave into the nitromethane.
A: Detonation initiates at the attenuator-nitro-
methane interface.
B: Time at which the detonation in the compressed
nitromethane overtakes the shock wave.
The times used in the text are defined as follows:

$$t_1 = B - F$$

$$t_2 = B - A$$

$$t^* = A - F = \text{induction time}$$

ured values of U_s, U_p, t_1 and t_2. The free-surface velocity of one
booster-attenuator system was measured, and the impedance match tech-
nique gave $U_s = 4.5$ mm/μsec and $U_p = 1.6$ mm/μsec as described in the
section on Type I Experiments. These values correspond to a pressure
of 81 kbar. These values will be assumed to be identical in all the
experiments, because the pressure changes from one experiment to an-
other are only about 5%. The values of t_1 and t_2 from several ex-
periments, and the calculated values of D* are given in Table III,
Column 4. The four shots for which data are given in the table are
those which illustrate this paper, and averages are presented for

481

another series of shots.
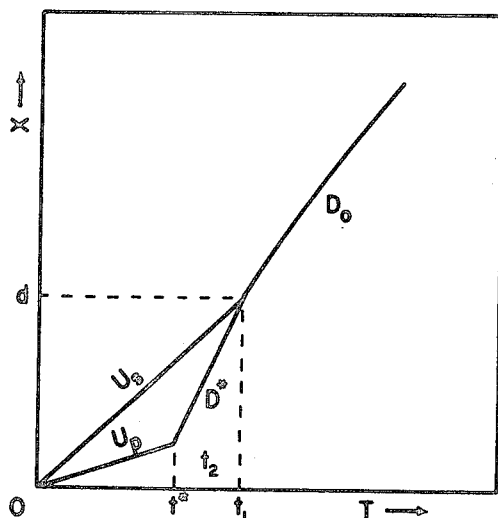
Fig. 8. Space-time representation of initiation behavior of nitromethane. The initial shock enters the nitromethane at time 0.

U_s = Shock velocity

U_p = Particle velocity

D_0 = Detonation velocity, steady-state

D^* = Detonation velocity in compressed nitro-methane

t^* = Induction time

It is instructive to compare the results obtained for D^* with the solutions to Equation (9) obtained by substituting from Equation (8) to eliminate D^*. Equation (9) may then be solved for U_p, giving

$$U_p = U_s - \tfrac{1}{2}(D_0 - \alpha/\rho_0)t - \left(\left[U_s - \tfrac{1}{2}(D_0 - \alpha/\rho_0)t\right]^2 + U_s D_0 t - U_s^2\right)^{\frac{1}{2}} \tag{10}$$

where $t = t_2/t_1$, D_0 is the normal detonation velocity, and α is the velocity dependence on density used in Equation (6). For the same values used in Experiment II,

$$U_p = 4.5 - 1.35t - (16.2t + 1.82t^2)^{\frac{1}{2}} \tag{11}$$

The assumptions made in this analysis are that initiation occurs at the nitromethane-attenuator interface, that D^* is adequately repre-sented by Equation (8), and that both D^* and U_s are constant. The re-sults are given in Columns 6, 7, and 8 of Table III.

The light from the detonation in the compressed nitromethane is

weaker than that from the normal steady-state detonation. The difference in brightness corresponds to a temperature difference of about 180°K between two black bodies of brightnesses equal to those of the two detonations. We interpret this brightness difference to mean that the detonation in compressed nitromethane has a lower temperature than detonation in normal explosive. Little of the light from the former explosive is absorbed by the nitromethane behind the shock front, since its intensity remains constant as the detonation approaches the shock wave.

It is important in these shots that the initial shock wave be plane and smooth. Although the time of arrival of the shock which entered the nitromethane of Fig. 7 was the same at every point within 0.01 μsec, some fuzziness in the initiation is apparent. This is due to small pressure variations across the wave front. Several points detonated 0.1 μsec before the rest and a strong interaction is visible where the shock was overtaken by the by the detonation. Further discussion of this point is included in Type VII experiments.

TABLE III

Results of Detonation Light Observations

Shot Number	t_1 (μsec)	t_2 (μsec)	D* (a) (mm/μsec)	t	U_p (mm/μsec)	D* (b) (mm/μsec)	P (kb)
E-0609	1.07	0.37	9.99	0.346	1.62	9.95	82
D-6207	1.22	0.41	10.25	0.336	1.67	10.10	85
	2.94	1.00	10.14	0.340	1.65	10.03	84
E-0577	4.53	1.39	11.08	0.306	1.82	10.57	92
E-0634	1.07	0.36	10.16	0.339	1.65	10.05	84
	1.61	0.53	10.50	0.326	1.72	10.25	87
Averages of 13 shots:			10.44	0.328	1.71	10.22	86.6
Mean Deviations:			± 0.50	±0.020	±0.10	± 0.30	± 5.0

(a) Calculated assuming U_s = 4.5 mm/μsec, U_p = 1.6 mm/μsec, and P = 81 kbar.
(b) Calculated assuming Equation (8).

Type IV Experiments:
Smear Camera Record of Complete Initiation Process

Each of the three preceding types of experiments was aimed at ob-
taining information about some part of the initiation process. The
combined experimental results gave a picture of events as diagrammed
in Fig. 8. When this stage of the investigation had been reached it
was felt to be desirable to obtain a single record showing all of the
events in their proper relationship. For this purpose the charge
arrangement shown in Fig. 9 was designed.
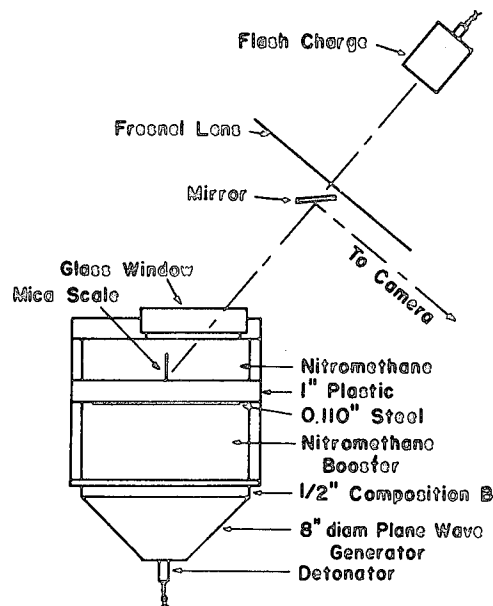
Fig. 9. Charge arrangement for Type IV Experiments.

A scale was inserted in the nitromethane to be studied to aid in
recording the progress of the various waves. This scale was designed
to have as little mass as possible so as to minimize its effect on
the initiation process. It was made of two sheets of mica, each less
than 1-mil thick. One face of one sheet was finely ground so as to
make it a good scatterer of light. Then a scale was formed on the
surface by depositing evaporated aluminum through a grid, leaving
narrow uncoated lines as graduations. Finally, the coated surface was
cemented to the second sheet of mica with Canada balsam. This filled
the scratches, leaving the graduations transparent. The distance from
the bottom of the scale to the first line was 1/8 in.; the distance
between lines was 1/4 in.
The scale was illuminated with light from an argon shock light-

source using a plastic Fresnel lens to image the source on the subject. After the light left the Fresnel lens, it passed by successive reflection from the front surface of the plastic attenuator, to the scale, to a small mirror before the Fresnel lens and, finally, to the objective lens of the smear camera.
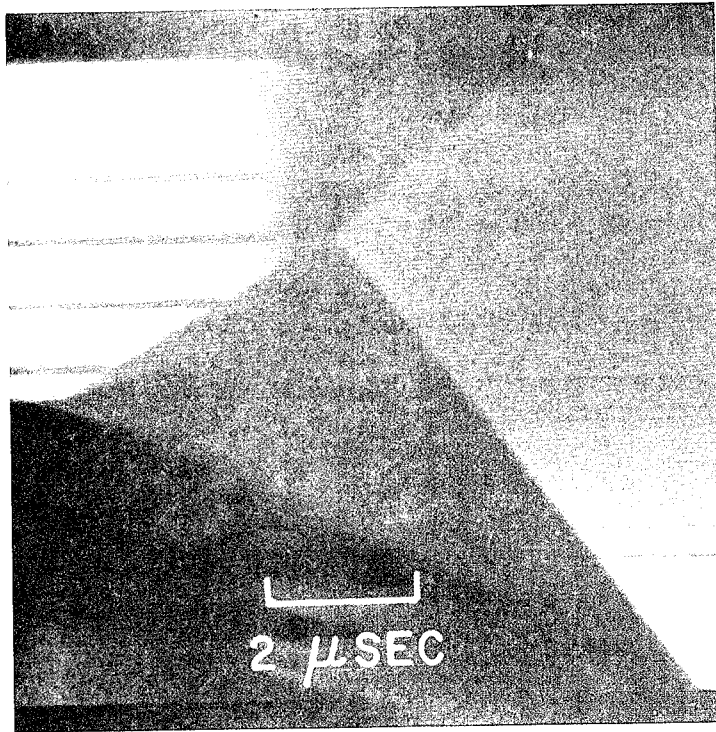
Fig. 10. Smear camera record of Type IV Experiment.

Figure 10 shows the smear camera record from such a shot, and Fig. 11 is a diagrammatic interpretation of the record. The explanation is as follows. At Time $\underline{1}$ the argon light source began to illuminate the scale, the graduations producing the Lines $\underline{a}$, $\underline{b}$, $\underline{c}$, $\underline{d}$. At Time $\underline{2}$, the attenuated shock wave entered the nitromethane and proceeded up the scale as shown by Line $\underline{A}$. Line $\underline{B}$ shows the motion of the attenuator-explosive interface, and just above it is a line formed by the motion of Graduation $\underline{a}$ and a second line due to a flaw in the scale.

At Time $\underline{3}$, initiation occurred at the plastic-nitromethane interface, and argon shock light was no longer reflected from the plastic to the scale. Consequently, the scale appeared less bright and detonation light was recorded through the transparent Graduation $\underline{d}$. High-order detonation in the compressed nitromethane followed the Line $\underline{C}$. The intersection of Lines $\underline{C}$ and $\underline{B}$ shows that initiation occurred at the plastic-nitromethane interface.

The intersection of Lines $\underline{C}$ and $\underline{D}$ is the point on the scale at
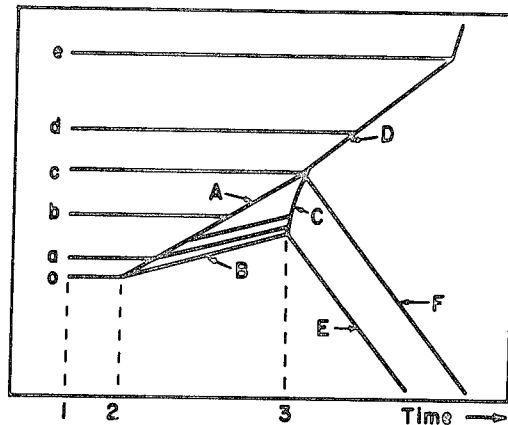
Fig. 11. Explanatory diagram of Fig. 10. Time 2-3 is in-
duction time.

which the detonation wave in the shocked nitromethane overtook the
initial shock wave. Detonation in unshocked nitromethane then pro-
ceeded along Line D. Along Line E the initiation of detonation at the
attenuator-explosive interface spread to points progressively farther
from the charge axis, and along Line F the detonation wave overtook
the initial shock wave, the departure from verticality (simultaneity)
showing that the latter wave was not flat.

Type V Experiment. Dependence of Induction Time on Initial Temperature

The time between the entrance of the initial shock and initiation, the induction time, should be strongly dependent on the initial temperature of the nitromethane. A series of Type III experiments was performed in which the initial temperature of the nitromethane was varied from 1.5°C to 45°C. The same booster-attenuator system, shown in Fig. 6, was used for all shots. Since the pressure of the initial shock wave was dependent on the density, a small correction should be made for the change of density with temperature. The booster-attenuator system was kept at 25°C for all shots. The nitromethane in a plastic box was controlled at the desired shot temperature to within 1°C, then mounted on the attenuator a few minutes before firing. The temperature at several points in the nitromethane was monitored with thermocouples throughout the experiment. Results of several shots with different lots of nitromethane are given below.

TABLE IV

Results of Induction Time vs Initial Temperature Experiments

	Shot Number	Temperature (°C)	Induction Time (μsec)
Lot 1	E-0590	1.7	5.0
	E-0588	26.8	1.8
Lot 2	E-0602	6.3	1.5
	E-0603	36.7	0.57
	E-0598	45.5	0.45

These results illustrate the strong dependence on the ambient temperature. About 10% decrease (30°K) in the ambient temperature produces an increase of 300% in the induction time. The two lots of nitromethane came from different bottles from the same supplier. The effects of sensitizing and desensitizing agents are large. For any quantitative measurement of induction time it is necessary that all the nitromethane come from the same bottle and be used within a few days.

Type VI Experiment. Dependence of the Induction
Time on the Initial Shock Pressure

In performing the experiments already described, it soon was discovered that the induction time depended strongly on the initial shock pressure, and close control of the booster-attenuator system was nec-

essary to get reproducible results.

To measure this dependence a shot was made following the pattern of Type III experiments. A step was machined into the upper surface of the attenuator so that one half was $\frac{1}{4}$ in. thicker than the other. This resulted in pressures into the nitromethane on either side of the step which differed by 3.3%. This pressure difference was determined on a replicate booster-attenuator system by optical measurements of the shock and free-surface velocities of the plastic and by subsequent impedance-matching calculations. As can be seen from the data in Table V, the inductions times differed by 26%. This result was supported by additional experiments. These data may be interpolated to show that a 10-mil change in the thickness of the plastic attenuator produces a 1% change in the induction time.

TABLE V

Results of Induction Time vs Shock Pressure Experiments

Shot Numbers B-4485, B-4488

Attenuator Thickness (inches of plastic)	P (kb)	t* (μsec)
1.20	86	2.26
0.95	89	1.74

Type VII Experiment. Effect of Rough Initiating Shock Wave

The variations in induction time observed across the attenuator plate of every shot fired indicated that very small pressure variations caused large effects. The plastics used in most shots were of optical quality, because the standard quality showed more pronounced variations. These facts suggested that variations in the attenuator caused tiny shock wave interactions in the liquid nitromethane, with consequent formation of small local hot spots. The experiments to be described were designed to discover how much the induction time would be shortened by interactions of controlled size purposely introduced.

These shots were identical with those of Type III experiments, except that grooves were ruled in one half of each Plexiglas attenuator plate. In the shot illustrated in Fig. 12, the grooves, of triangular cross section, were 20 mils deep and spaced 25 mils apart so that the tops were sharp. The Plexiglas was coated with a thin layer of paint to prevent attack by the nitromethane. The two induction times, 1.9 and 0.8 μsec, are strikingly different. The smallest grooves tried, 6 mils deep and 8 mils apart, still caused a decrease in the induction time, but only by 15%. The shock impedance of the Plexiglas and the nitromethane are so close together that the amplitude of the ripples in the emergent shock is only 5% as large as the grooves themselves. It is easy to see that if the wave emerging from
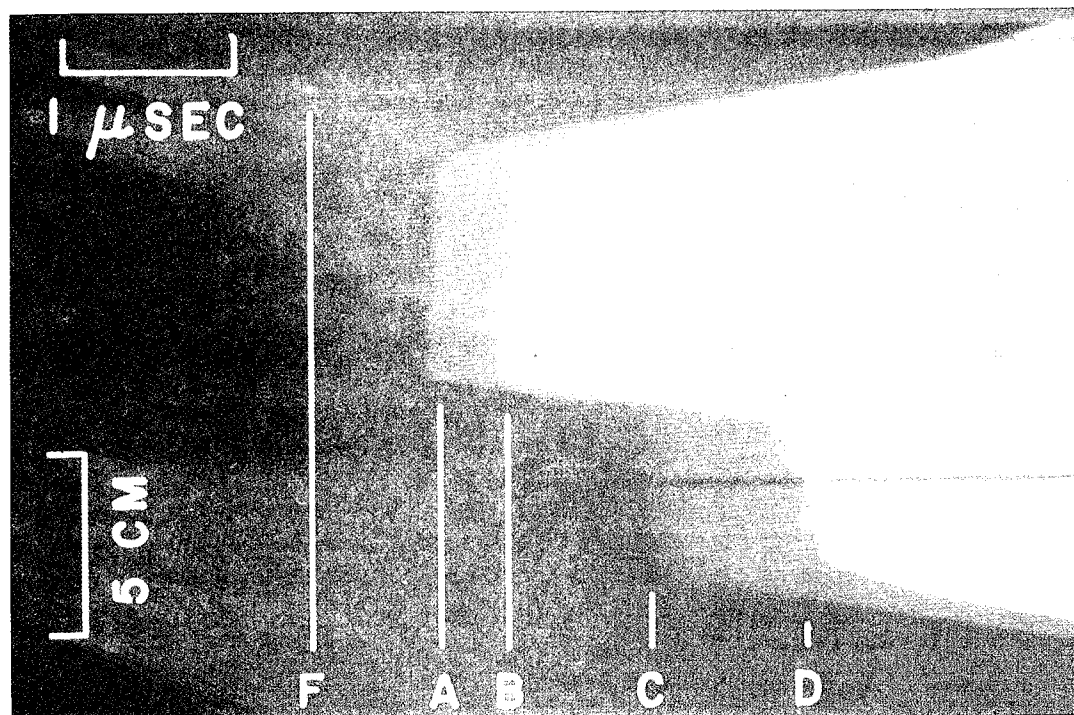
Fig. 12. Smear camera record of effect of rough shock wave
on induction time.
F: Shock enters nitromethane.
A: Detonation is initiated in compressed nitro-
methane at interface between nitromethane and
grooved attenuator plate.
B: D* overtakes shock.
C: Detonation is initiated at interface of nitro-
methane and smooth attenuator plate.
D: D* overtakes shock.
Induction time, t*: Over grooved plate A - F.
                    Over grooved plate C - A.
Shot D-6207.

the attenuator is not almost perfect, the induction time will be arti-
ficially shortened. It is apparently impossible to be sure that any
of these experiments gives the induction time corresponding to a per-
fectly plane shock wave.

Type VIII Experiment. Effect of Bubbles

In the description of Type III experiments it has been pointed
out that a gas bubble can cause initiation as soon as the shock hits
it. The experiments to be described here were performed to investi-
gate initiation by bubbles of various gases. In the course of the

investigation, knowledge of the effects of shock wave interactions suggested that the major effect of the bubble was to produce a shock interaction. Therefore, "bubbles" of solids were also introduced.

The experiments were done exactly as those of Type III, with the gas bubbles on the surface of the attenuator plate. It was found that a very small amount of silicone vacuum grease on the plastic plate would hold the bubbles in place under the surface of the nitromethane.

Bubbles, formed by forcing gas through a capillary into nitromethane, were caught under clean glass. Because the contact angle between the nitromethane and glass was zero, the trapped bubbles were spherical. The diameter of each bubble was measured and each bubble was transferred under nitromethane to the shot box. In position on the attenuator plate, the shape of the bubble was no longer spherical. Hereafter, the diameter measure is used to mean a bubble having the volume of a sphere of that diameter.

Several kinds of initiation behavior, for a shock of given strength, result from the presence of a bubble in nitromethane. If the bubble is sufficiently large, in the order of 0.7 mm in diameter, detonation will spread almost immediately from it after it is shocked. Smaller bubbles, in the order of 0.4 mm, cause some reaction to take place in the nitromethane, but detonation occurs at or near the shock front after it has run a distance dependent on bubble size and the initiating conditions. From still smaller bubbles, initiation will not occur on our time scale, although the bubble may glow for several microseconds. Figure 13 shows these three cases for argon bubbles mounted in nitromethane.

To determine whether shock heating of the gas, or heating of the explosive in a local region due to the pressure interaction at the bubble is the more important cause of this initiation behavior, bubbles of gases with different γ's were introduced. Argon ($\gamma = 1.67$) and butane ($\gamma = 1.1$) should be heated to quite different temperatures when shocked. The argon bubbles caused initiation in a slightly smaller time than butane bubbles of the same diameter, but the effect was much less than would be expected from the anticipated large temperature difference. To show conclusively that the pressure interaction is the effective cause, small pieces of plastic and tungsten, as well as bubbles, were introduced into nitromethane. Both of these, although raised to a relatively low temperature by the shock wave, caused initiation with close to the same induction time as the bubbles, as can be seen in Fig. 14. Most of the apparent delay occurs because the plastic and tungsten extended farther into the nitromethane than the bubbles.
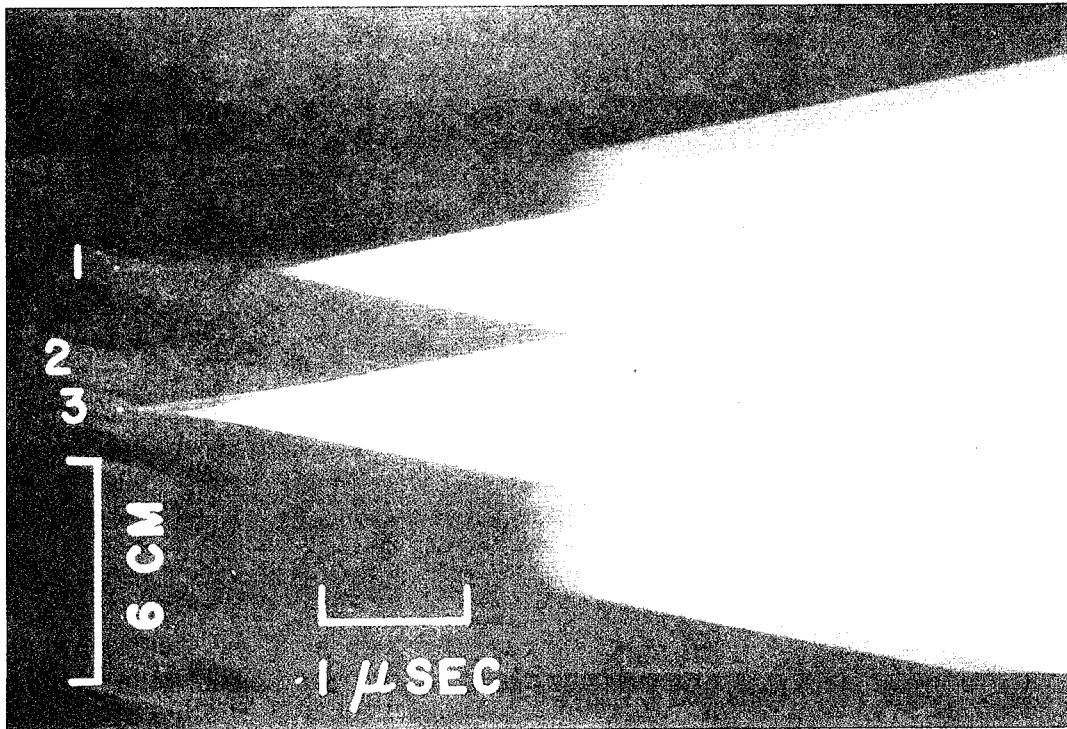
Fig. 13. Smear camera record of bubbles in nitromethane.
Time increases to right.
Argon bubbles: 1. 3/4 mm diam.
2. 1/2 mm diam.
3. 1 mm diam.
Shot E-0577.
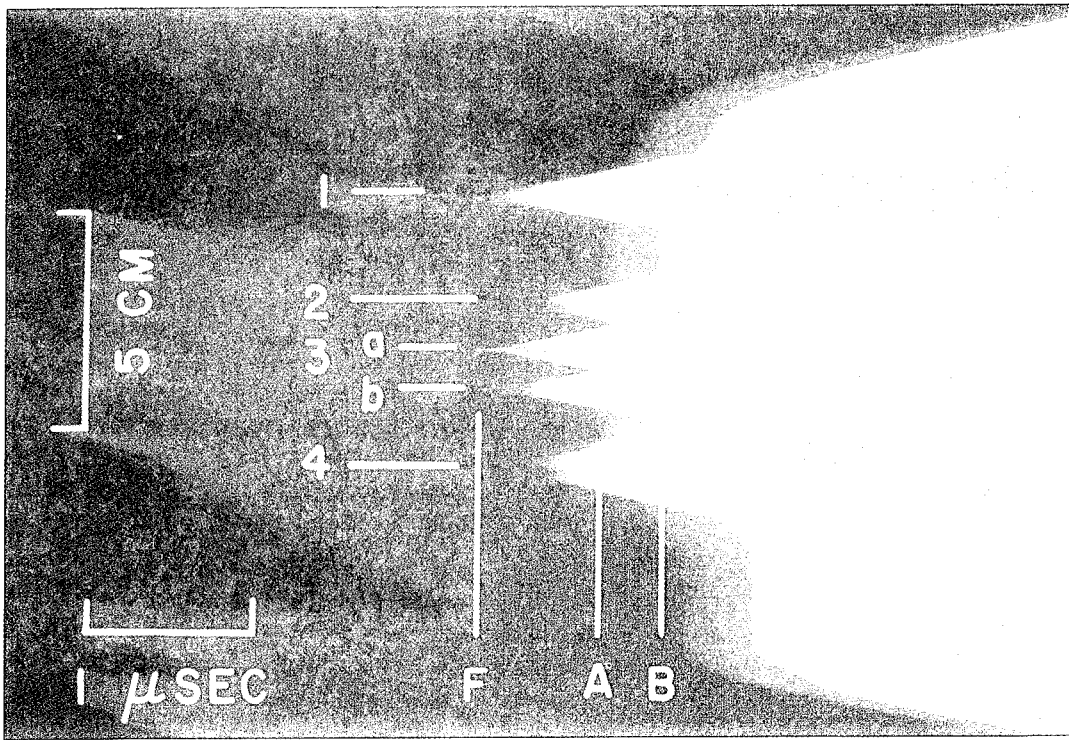
Fig. 14. Smear camera record of initiation of nitromethane
by pressure interactions. Time increases to the
right.
F: Shock enters nitromethane.
A: Detonation is initiated at attenuator-nitro-
methane interface.
B: Detonation overtakes shock.
1: Air-filled hole in attenuator, 1-mm diam,
1/2-mm deep covered with 1/2-mil Mylar.
2. Tungsten rod, 1-mm diam, 2-1/2-mm long (1-3/4-mm
extension into nitromethane).
3a. Air bubble.
3b. Argon bubble, 0.8-mm diam.
4. Plastic, approximately 1-mm diam.
The lower part of the picture shows delayed ini-
tiation, probably due to a defect in the plastic
attenuator.
Shot E-0634.

Type IX Experiment. Other Explosives

The results described thus far were obtained with nitromethane. To be sure they were not unique to nitromethane, twenty-five experiments, chiefly of Types I and III, were done with other liquids, namely, molten DINA, molten TNT, and Dithekite 13 (63/24/13 HNO_3, nitrobenzene, H_2O). One striking difference appeared. The weak light from the detonation in the shocked liquid was not observed for any of these. All three are yellow but transparent enough to transmit enough light from a source as bright as the detonation in compressed nitromethane to be photographed. Otherwise, the behavior was the same as for nitromethane. The overshoot brightness which quickly decreased to steady-state intensity was observed. Bubbles produced the same effects as in nitromethane. We believe that the same mechanisms are active in these explosives as in nitromethane but the detonation behind the initial shock has an even lower temperature than was found for nitromethane.

Finally, the initiation of single crystals of PETN has been found to occur exactly as does initiation of nitromethane. The experiments are described in Reference 7. The smear camera record reproduced there, similar to Fig. 2, can be interpreted in the same way as are Type I experiments here.

Preliminary information about three of these explosives is listed in Table VI. The values are approximate.

TABLE VI

Initiation Data for Other Explosives

Explosive	P (kb)	T (°C)	t* (μsec)	D* (mm/μsec)
TNT	125	85	0.7	11.0
Dithekite 13	85	25	1.8	12.2
PETN	112	25	0.3	10.9

DISCUSSION OF RESULTS

Many authors have considered thermal explosion theory to be important in explaining the process of initiation.[1] Among these the recent treatment by Hubbard and Johnson[2] is perhaps the most pertinent here. They developed a theory for a semi-infinite homogeneous explosive, and from calculations observed the general behavior which we have observed independently in experiments. They found that when an element of explosive had been subjected to a shock wave of the proper strength, a time interval, referred to as a "time delay" or an "induction time", ensued in which almost no chemical reaction took place. Then complete reaction occurred in a relatively very short

time, and this reaction then moved forward as a detonation wave.

Unfortunately, Hubbard and Johnson attempted to apply their theory to the experimental results of Majowicz and Jacobs[8] for physically inhomogeneous explosives, where the initiation mechanism was quite different.[9] The theory is more suitably applied to the process of initiation in nitromethane. In what follows, the attempt will be made to follow the notation and treatment of Hubbard and Johnson.

The assumption is made that the reaction in nitromethane follows an Arrhenius rate law containing the term $\exp E_A/RT$, where E_A is the activation energy, R is the gas constant, and T is the local temperature. The substitution is made for T,

$$T = (E_0/C_V) + (Qf/C_V) \tag{1}$$

where E_0 is the specific internal energy behind the initial shock wave, Q is the heat of explosion per gram, f is the fraction of unit mass reacted, and C_V is the average specific heat at constant volume. The following expression is ultimately obtained for the reaction time:

$$t = \nu^{-1} \int_0^f (1 - f')^{-N} \exp\left[\epsilon/E_0 + Qf'\right] df' \tag{2}$$

where t is the induction time, ν is the "collision frequency", N is the order of the reaction, and $\epsilon = C_V E_A/R$. Since most of the reaction time is due to values $f \simeq 0$, the integral becomes

$$t = \nu^{-1}(E_0/C_V)^2(Q/C_V)^{-1}(E_A/R)^{-1} \exp\left[(E_A/R)(E_0/C_V)^{-1}\right] \tag{3}$$

The values in parentheses correspond to temperatures.

$$E_0/C_V = T_0 \tag{4a}$$

$$Q/C_V = T_f \tag{4b}$$

$$E_A/R = T_A \tag{4c}$$

Here, T_0 is the temperature behind the initiating shock, T_f is the temperature of the reaction products, and T_A is the activation temperature. In Equation (4b) C_V is the average specific heat of the reaction products, and the value is taken to be the same as that for the unreacted explosive. Equation (3) may then be rewritten in the form

$$t = \nu^{-1} T_0^2 (T_f T_A)^{-1} \exp T_A/T_0 \tag{5}$$

We now wish to calculate a value of t using the following experimental data for nitromethane.

$$\nu \quad : \quad 10^{14.6}/sec \qquad \text{Ref. 10}$$

$$E_A \quad : \quad 53,600 \text{ cal/g} \qquad \text{Ref. 10}$$

$$U_s \quad : \quad 4.5 \text{ mm/}\mu sec$$

$$U_p \quad : \quad 1.70 \text{ mm/}\mu sec$$

$$P \quad : \quad 86 \text{ kbar}$$

$$\rho_0 \quad : \quad 1.125 \text{ g/cc} \qquad \text{Ref. 11}$$

$$Q \quad : \quad 1.28 \text{ kcal/g} \qquad \text{Ref. 12}$$

$$C_v \quad : \quad 0.41 \text{ cal/g/°C} \qquad \text{Ref. 13}$$

The value of T_0 is computed from the following two relations,

$$\Delta E = \tfrac{1}{2} p \Delta v \qquad (6)$$

and

$$T_0 = 300 + \Delta E/C_v \qquad (7)$$

where ΔE is the increase in internal energy across the initiating shock. ΔE was found to be 345 cal/g giving the result

$$T_0 = 1140°K \qquad (8)$$

T_f corresponds to the temperature of the reaction products in the detonation wave in the compressed nitromethane. Estimated from Q/C_v the value of T_f is found to be 4260°K. (This value may be compared with the value of 3200°K obtained by W. C. Davis[14] from photographic brightness measurements.) Inserting appropriate values in Equation (4c)

$$T_A = 27,000°K \qquad (9)$$

Substitution of these temperature values in Equation (5) gives

$$t = 0.6 \text{ }\mu sec \qquad (10)$$

This value of t is in good agreement with our experimental observations when due regard is given to the uncertainties in the numerical values used in the calculation. These very crude calculations can be used only as order-of-magnitude confirmation. The agreement is no doubt in large part fortuitous, because the thermochemical numbers may change as the pressure is increased.

A similar calculation for the PETN data, using the measured thermochemical data of Robertson[15] or of Cook and Abegg[16] shows rea-

sonable agreement. The two sets of data give values which bracket our experimental values.

An estimate of the sensitivity of the induction time to variation of the temperature behind the initial shock wave is obtained from Equation (5) by taking logarithms and differentiating

$$\frac{dt}{t} = 2 \frac{dT_0}{T_0} - \frac{T_A}{T_0} \frac{dT_0}{T_0} \tag{11}$$

Substituting the values calculated above for T_A and T_0 and collecting terms gives

$$\frac{dt}{t} = - 21.7 \frac{dT_0}{T_0} \tag{12}$$

Equation (12) shows that for a change in the initial shock temperature of 1%, or 11.4°K, in the calculation leading to Equation (10), the re-action time is changed by 21.7% or 0.13 μsec. This agrees with the experimentally observed sensitivity of the induction time to initial shock strength found in Type VI experiments, although the sensitivity is expressed in terms of temperature rather than pressure.

The extreme sensitivity of the induction time to changes in the initial shock temperature is characteristic of homogeneous explosives and is responsible for the extreme difficulty found in obtaining ex-perimentally reproducible induction times. Intrusion of strong rare-factions, as Hubbard and Johnson's calculations showed, lowered the local temperature and stopped chemical reaction. It was this effect of rarefaction from the charge boundaries and in the Taylor wave from the booster system which forced the use of the large-diameter charges described in this paper, and which prevented even then the study of initiation involving induction times of more than a few microseconds.

Local increases in the shock temperature can also be effected by reflecting the mass flow from inclusions of higher shock impedance than nitromethane, or by causing local convergences in the mass flow, which result in increased compressional heating of the explosive. If these local increases in temperature are great enough, reaction will take place. The results of this reaction may be to hasten the onset of detonation throughout the shocked explosive, as in the Type VII ex-periments, or if a single defect is large enough, the result may be the onset of detonation over a very small area, as shown by the Type VIII experiments. It follows that the stronger the initial shock wave the more easily can chemical reaction be effected at hot spots.

These experiments have presented severe problems of technique, not all of which have been solved satisfactorily. The quantitative measurements for use in an accurate comparison with thermochemical calculations can not yet be made. The explosive varies enough from batch to batch, even with the most careful purification, that one can-not specify the explosive properly. Even though one may determine an activation energy and "frequency" factor, one does not know to what explosive they belong. The shock waves used were not flat-topped pressure pulses, having been generated from detonation waves with

drooping Taylor waves even when very large charges were used. The sensitivity of the initiation to small shock wave interactions has been demonstrated, but it has not yet been possible to demonstrate that the attenuator plates do not have small inhomogeneities which are present in all experiments. These, if they are present, do not affect the qualitative conclusions, but they might invalidate quantitative results. All of these difficulties must be overcome before quantitative measurements can be presented as dependable.

The qualitative results are, however, completely unambiguous. The experiments show clearly a thermal explosion resulting from shock heating. Excellent agreement with the simple theory is demonstrated. The details of the process have all been examined. The experiments also show that small shock-wave interactions have large effects on the initiation process. These interaction experiments give a very useful insight into the differences between the initiation of homogeneous explosives and the more complicated problem of the initiation of inhomogeneous explosives, because they provide some view of the common ground between the two.

ACKNOWLEDGEMENTS

REFERENCES

1. S. J. Jacobs, Am. Roc. Soc. J. 30, 151 (1960).
2. H. W. Hubbard and M. H. Johnson, J. Appl. Phys., 30, 765 (1959).
3. J. H. Cook, Research, 1, 474 (1948).
4. T. E. Holland and W. C. Davis, J. Opt. Soc. Am., 48, 365 (1958).
5. A. W. Campbell, M. E. Malin, T. J. Boyd, Jr., J. A. Hull, Rev. Sci. Instr., 27, 567 (1956).
6. A. W. Campbell, M. E. Malin, and T. E. Holland, Second ONR Symposium on Detonation, Washington, D. C. (1955).
7. T. E. Holland, A. W. Campbell, M. E. Malin, J. Appl. Phys., 28, 1217 (1957).
8. J. M. Majowicz and S. J. Jacobs, "Initiation to Detonation of High Explosives by Shocks", presented at Lehigh Meeting of Fluid Dynamics Division, American Physical Society, Nov. 1957.
9. A. W. Campbell, W. C. Davis, J. B. Ramsay, J. R. Travis, "Shock Initiation of Solid Explosives". This Symposium.
10. T. L. Cottrell, T. E. Graham, T. Y. Reid, Trans-Faraday Soc., 47, 584 (1951).
11. A. Makovky and L. Lenji, Chem. Revs., 58, 627 (1958).

12. Personal communication from C. L. Mader, Los Alamos Scientific Laboratory.

13. W. M. Jones and W. F. Giauque, J. Am. Chem. Soc., 69, 938 (1947).

14. Unpublished data, W. C. Davis, Los Alamos Scientific Laboratory.

15. A. J. B. Robertson, Trans-Faraday Soc., 44, 977 (1948).

16. M. A. Cook and M. T. Abegg, Ind. Eng. Chem., 48, 1090 (1956).

17. M. H. Rice, R. G. McQueen, and J. M. Walsh, "Compression of Solids by Strong Shock Waves", Solid State Physics, Advances in Research and Applications, Volume VI, Eds. F. Seitz and D. Turnbull (Academic Press, Inc., New York, 1958).

SHOCK INITIATION OF SOLID EXPLOSIVES*

A. W. Campbell, W. C. Davis, J. B. Ramsay, and J. R. Travis
University of California, Los Alamos Scientific Laboratory
Los Alamos, New Mexico

INTRODUCTION

In this paper we shall describe an experimental investigation of
the initiation of inhomogeneous solid explosives by strong, plane
shock waves, with high-order detonation taking place in less than 10
μsec. The initiation process is observed to be very complicated, and
still is not understood in detail. A previous paper[1] has discussed
the initiation of liquid and other homogeneous explosives, which show
a behavior much different from that of solid inhomogeneous explosives.

There has been much experimentation on the initiation of solid
explosives, and recent papers are well reviewed elsewhere.[2-5] No
attempt will be made in this paper to review the published work on the
subject. The work of Majowicz and Jacobs[6] is especially pertinent,
because their experiments are similar to ours, and their observations
agree with ours in many respects.

The conclusions of this paper are based on more than 200 separate
experiments, and not all of them can be described or even discussed
here. A selected few of the experiments are described to provide evi-
dence in support of the conclusions drawn. No conclusion is based on
an isolated result, although in some cases only one result is present-
ed here.

Experiments[1] with liquids and other homogeneous explosives have
shown that initiation results from shock heating of the liquid, and
that the simple ideas of thermal explosion explain all of the phenom-
ena adequately if the shock wave is plane and smooth. If the shock
wave is uneven, regions of convergent flow exist, and the local in-
crease in compression results in "hot spots" which, because of the
strong dependence of the reaction rate on the temperature, strongly
influence initiation.

In polycrystalline explosives, the shock wave is rough with lo-
cal convergences caused by the inhomogeneous nature of the explosive.

----

* Work done under the auspices of the U. S. Atomic Energy Commission.

Smear camera photographs show that the detonation wave front in pressed or cast explosive is rough, indicating that the flow is irregular in its fine detail. Reaction takes place in these very small regions of convergence distributed throughout the explosive, and makes a major contribution to initiation. Initiation thus depends strongly on the type, number, and distribution of the inhomogeneities which cause the shock interactions.

The techniques employed, which have evolved in the course of the work, are sometimes elaborate and difficult. The descriptions of the experiments have been grouped as types of experiments, and often the grouping is according to technique rather than scientific purpose. To help the reader to understand why some of the experiments were done, a brief description of the initiation behavior of solid explosives, as shown by these experiments, is presented here without any evidence or detail.

When the shock wave enters the explosive, it proceeds at a slowly-increasing velocity for a distance which is a function of the shock pressure. Then the velocity increases in a short but measurable time to the value associated with high-order detonation. The velocity transition is not abrupt as it is in the case of liquids, nor is there any strong overshoot in the detonation velocity after the transition, again in contrast to the behavior of liquids. Retonation (detonation backwards through the partially-reacted explosive) has not been observed, although retonation in small diameter sticks has been reported by Cook[7] and others.

The initial pressure of the shock wave in the explosive under study has been determined by the use of a method which is not completely satisfactory, but which is the only method available at present. In the experiments described in this paper, the shock wave enters the explosive from a booster-attenuator system, which has an inert (usually metal) plate in contact with the explosive. The assumption is made that the pressure and particle velocity are the same on both sides of the attenuator-explosive interface, the usual boundary conditions when dealing with shock waves in inert materials. Because we are studying initiation, which cannot be a steady state, these boundary conditions cannot be exactly correct. The free-surface velocity of the attenuator is measured and the approximation is made that the particle velocity, U_{PA}, is equal to one-half the free-surface velocity. Other experimental data include the initial density, ρ_{OE}, and the initial shock velocity, U_{SE}, in the explosive. Assuming that the shock Hugoniot of the attenuator material is known, the free-surface velocity measurement permits the evaluation of the shock pressure, P_A, and the particle velocity, U_{PA}, in the attenuator. The pressure, P_E, and the particle velocity, U_{PE}, in the explosive are then found by determining the intersection of the attenuator rarefaction locus, approximated by reflecting the attenuator Hugoniot about the line U_{PA} = constant, and the locus for the state of the explosive, given by the conservation of momentum relation

$$P_E / U_{SE} = \rho_{OE} \, U_{PE} .$$

This process is illustrated in Fig. 1. For a more detailed discussion of the method of calculation, see, for example, Reference 8.

When the shocked material is an explosive, the equation $P_E = \rho_{OE} U_{SE} U_{PE}$ holds for a steady state detonation, but the process of initiation cannot be regarded as a steady state. In the experiments to be described, the explosive reacts to some small extent immediately behind the shock front, and the extent of reaction increases as the shock wave proceeds. In the region near the explosive-metal interface where only a small part of the explosive reacts, the above expression for the pressure will hold with sufficient accuracy to be useful. Throughout this paper values of the pressure in the explosive will be understood to include some error from this source.
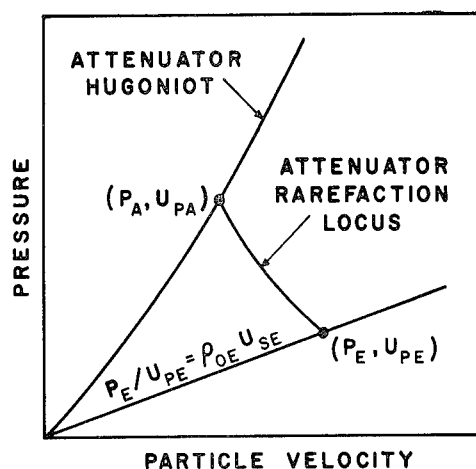
Fig. 1. Graphic method of obtaining shock pressure and particle velocity in under-initiated explosive.

EXPERIMENTAL

Type I Experiment: Wedge Technique with Smear-Camera Records

The solid explosives studied here are not transparent and must therefore be studied by observing a free surface, if camera techniques are to be used. An explosive booster-attenuator system used to send a shock wave into the explosive to be studied is shown in Fig. 2. The latter explosive is in the form of a wedge, so that progress of the shock or detonation wave can be seen as motion along the slant face. This motion can be observed best if the slant face has been covered with a thin (0.00025 in.) film of aluminized Mylar plastic[6] and illuminated with an intense light source. The alignment is such as to reflect the light from the plastic film to the camera.
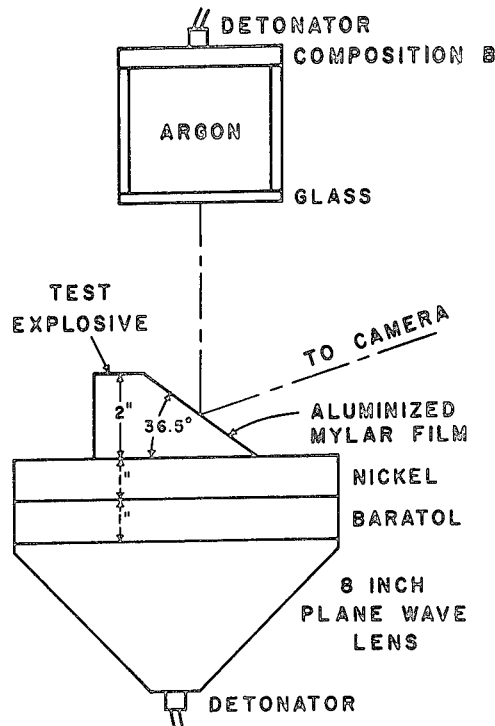
Fig. 2. Charge arrangement for Type I experiments.

As the shock wave proceeds along the slant face, the mass motion of the explosive causes a tilt of the reflecting surface so that the light is no longer reflected to the camera. This arrangement gives a sharp cut-off of light and a well-defined record. The smear camera is aligned along a line of steepest descent of the wedge and is focussed on the slant face.

Figure 3 shows a smear camera record, which is just a space-time plot, obtained with this technique, and Fig. 4 shows the interpreta- tion. The velocity of the shock wave is obtained from the slope of the space-time plot. The free-surface velocity of the attenuator plate is measured with electrical contactors spaced above the plate, or with camera techniques applied to a duplicate booster-attenuator system. Using the method described in the Introduction the pressure and particle velocity behind the initial shock in the explosive can be estimated.

The results of the analysis of the record reproduced in Fig. 3 are given here as an example of the information obtainable from ex- periments of this type. The explosive wedge was made of cyclotol (65/35 RDX/TNT) with an initial density, ρ_{OE}, of 1.71 g/cc and a base angle of the wedge of 36° 25'.
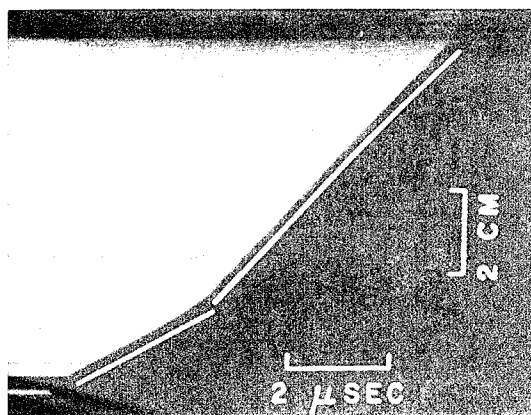
Fig. 3. Smear camera record of the cyclotol (65/35 RDX/TNT)
wedge shown in Fig. 2. Light reflected from the
slant face of the wedge is cut off as the shock wave
moves up the wedge. Two straight lines have been
added for ease in visualizing the curvature of the
space-time plot. Time increases to the right; the
toe of the wedge is at the bottom. Space scale
applies to the slant face. Shot D-6082.
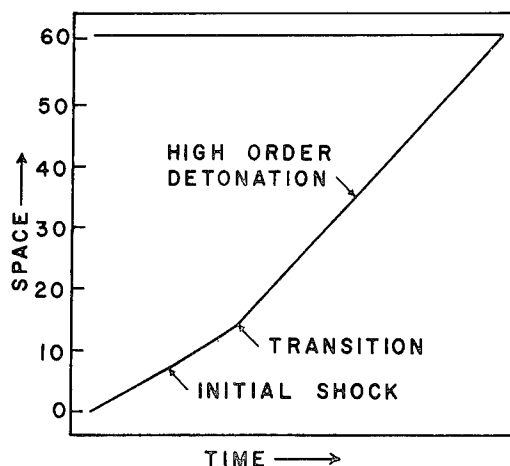
Fig. 4. Interpretation of smear camera record of Fig. 3.
This figure is a tracing of the camera record.

A space-time plot was made of the smear-camera record by dividing
the space dimension into 61 equal parts, as shown in Fig. 4, and read-
ing the corresponding time values. After converting the space values
to distance of shock travel in the wedge, polynomials of first, second
and third degree were fitted to the first 14 points and to the last
45 points, thus omitting the region of the greatest curvature. It was

found for the initial shock that the second-degree polynomial gave a better fit than either the first- or third-degree polynomials. For the portion of the curve above the transition to high-order detonation a second-degree equation also gave the best fit. In the latter fit, although the quadratic coefficient was statistically significant, its magnitude indicated that it could have resulted from imperfections in the booster wave. The equations obtained for the smear camera record shown in Fig. 3 were the following:

Initial Shock
$$X = 0.1198 + 3.5334t + 0.2452t^2$$
$$(0.0263) \ (0.0406) \ \ (0.0134)$$

High-order Detonation
$$X = -9.152 + 7.521t + 0.0457t^2$$
$$(0.169) \ (0.0665) \ (0.0062)$$

where the standard deviation of each parameter is shown in parentheses. The units of X, the space coordinate taken perpendicular to the wave front, are mm, and the units of t, the time coordinate, are μsec. The constant terms have no significance, but both equations have the same origin. For the initial shock equation, the coefficient of the linear term is the initial velocity, and the coefficient of the quadratic term is the acceleration. The high-order detonation begins at about 2.8 μsec, and the velocity at that time is, from the equation, 7780 m/sec. The high-order, steady-state, plane detonation wave velocity for this explosive is 8000 ± 20 m/sec. The difference is not significant, as it may be due to small imperfections in the wave.

The significant value of the quadratic term in the polynomials for the initial shock indicates a steady acceleration of the shock wave. No significant indication of overshoot was obtained by fitting higher-order polynomials to the high-order detonation region. Analytical fits to the data in the region of maximum curvature do not reveal any departures from a smooth acceleration of the shock prior to the onset of high-order detonation. It should be noted that all results obtained with this technique assume that the shock wave comes through the attenuator simultaneously over the region covered by the wedge to be studied, and that the pressure profile is identical at each point over the same area. Tests of the booster systems used justify these assumptions.

A very large number of experiments of this type have been done using the cyclotol mentioned, both pressed and cast, pressed TNT of various grain sizes and densities, plastic-bonded HMX, and plastic-bonded RDX. All of these experiments have shown the same qualitative behavior, and with good explosive the quantitative results are reproducible.

Type II Experiment: Wedge Technique with Framing Camera Records

Framing camera photographs often give qualitative information in a more rapidly assimilated form than do smear camera photographs.

The accuracy of measurements from framing camera pictures is usually not very good, but the photograph can be easily understood. Figure 5 shows a series of frames of a wedge of the same type as described in Experiment I. The wedge is immersed in a saturated aqueous solution of zinc chloride (ρ= 1.9 g/cc), which is a fairly good impedance match to the explosive (65/35 RDX/TNT) of the wedge. The shock pressure in the solution supports the wedge at the sides and along the slant face so that the wedge holds together throughout the entire interval covered by the framing sequence.

In the first 5 frames the shock can be seen moving up the slant face of the wedge and reducing the reflectivity of the explosive surface, which is brilliantly illuminated by an argon-flash light source. Then in Frame 6 the detonation wave begins as revealed by a change in reflectivity of the wedge surface. The detonation wave runs to the top of the wedge and the strong shock in the zinc-chloride solution emerges into the atmosphere producing a bright air shock which moves downward, obscuring the subject. The demarcation between the region traversed by the initial, weak shock wave and the region of complete detonation remains stationary and sharply defined to the end of the framing sequence; no retonation is observed.

- - - - - - -

Fig. 5.   (On following page.) Framing camera sequence showing the transition between the initial shock wave and the high-order detonation wave in a cyclotol wedge immersed in a saturated aqueous solution of zinc chloride. Time between frames: 0.5 μsec. Time increases from left to right and from top to bottom. In the setup photograph, A is the light source, B is the subject wedge, C is the opening through which the camera views the subject reflected in the mirror D. Shot C-1437.

- - - - - - -

Type III Experiment: Resistivity Technique

The purpose of this type of experiment was to study the resistivity of shocked, inhomogeneous solid explosive during the initiation process. It seemed reasonable to assume that chemical reaction in the explosive would be accompanied by a decrease in the resistivity. For electrical field strengths up to a few thousand volts per centimeter cyclotol exhibits a resistivity like that of a good plastic, i. e., of the order of 10^{15} ohm-cm. On the other hand the resistivity of a detonation wave is quite low, of the order of 10^{-1} ohm-cm. (See, for example, Refs. 9, 10.)

Figure 6 shows an experimental arrangement used to study the changes in resistivity of shocked solid explosive. The electrodes used were made of silver foil 0.0005 in. thick and 1/16 in. wide. These electrodes were inserted between 4-in. cubes of explosive which had been lapped flat; the blocks were then clamped together under a
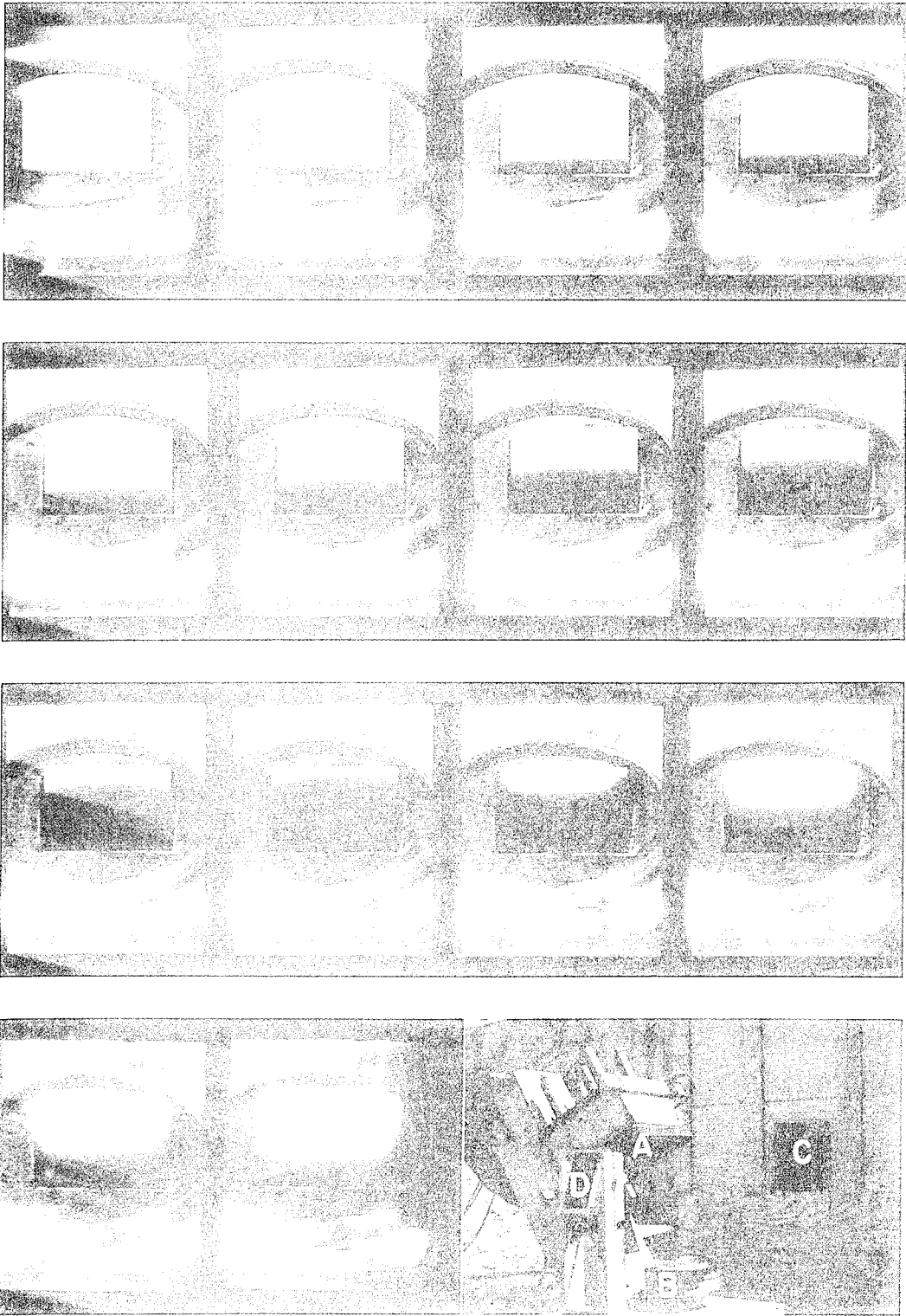
Figure 5

pressure of approximately 60 psi in an effort to eliminate any air gap from the joint. The experiment was arranged with the long axis of the foils perpendicular to the shock wave.
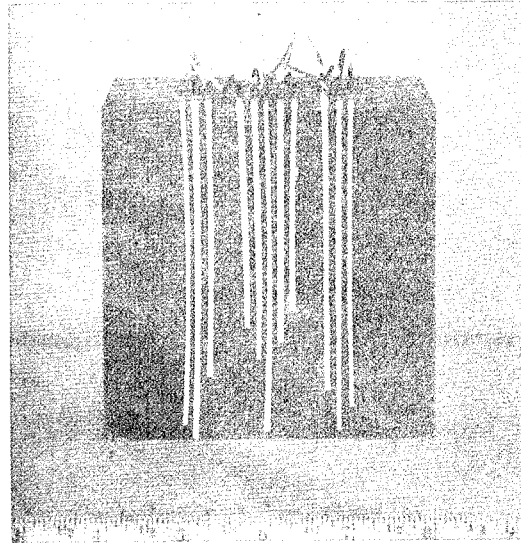
Fig. 6. Electrode placement for resistivity experiments. The center electrode in each of the three groups is connected to ground. The two fiducial signal electrodes are not shown. Shot B-4696.

Usually ten signals were taken from a single shot. The first signal was produced by the first motion of the brass driving plate and denoted the entry of the shock into the explosive under study. This signal was sent to all recording channels as an initial fiducial. The next four signals were taken from the region traversed by the initial shock wave, and a second four were taken in the region traversed by the detonation wave. One signal from each of these groups was sent to each of the four recording channels. The tenth signal, taken from the top of one of the blocks of explosive, which were 4 in. thick, was again distributed to all four channels as a final fiducial.

The signal circuits used with the electrodes are shown in Fig. 7. Selected batteries were used as low-impedance sources of current in the circuits intended to sense the resistivity behind the initial shock wave. Figure 8c shows the signal in a battery circuit when the electrodes were connected by a shock-driven brass plate. Comparison of this signal with the other two of Fig. 8 shows that the rise times of these two signals are not limited by circuit parameters but were controlled by conditions behind the shock wave.

The records from these resistivity experiments (see Ref. 11 for a description of the recording equipment) showed first of all that the explosive immediately behind the initial shock wave was quite conducting, but not so conducting as that behind a detonation wave. They also showed that the onset of conductivity occurred immediately behind

507
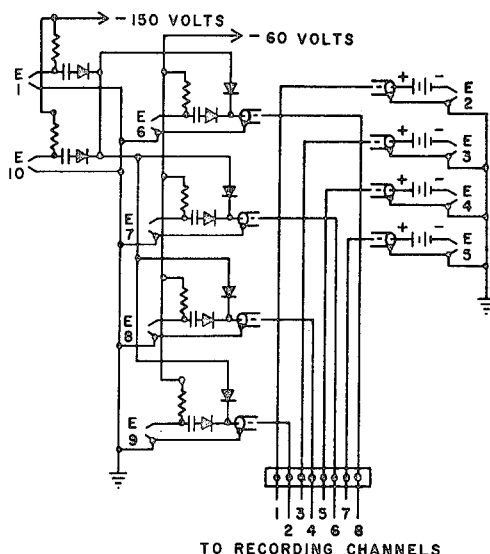
Fig. 7. Circuit used in resistivity experiments. Circuit components: resistors, 1 megohm; capacitors, 500 μμF; diodes, IN140; batteries 45 V, Eveready Type W365F; coaxial cables, 33 ohm. Electrodes are numbered as listed in Table I.
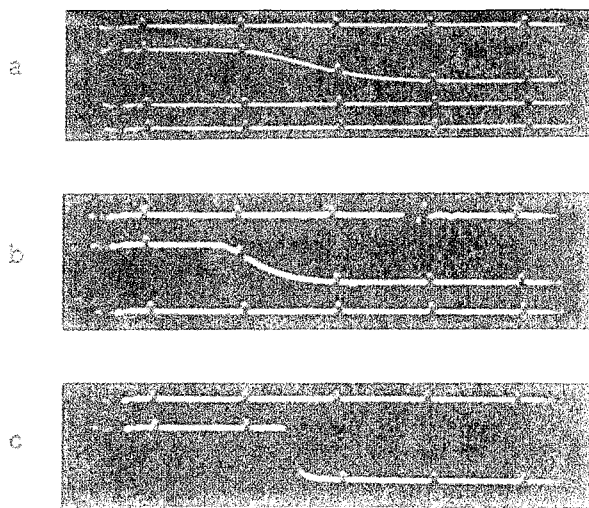
Fig. 8. Chronograph records from resistivity experiments. Time between marks, 0.50 μsec. Time proceeds from left to right and from top to bottom. (a) Signal E2 of Table I. (b) Signal E5 of Table I. (c) Signal from battery circuit of Fig. 7 when signal electrode is grounded by shock-driven brass plate. Shots D-4695, B-4703.

508

the shock front. The space-time data of a single shot are displayed in Table I. A straight line was fitted to the first five points by the method of least squares, and a second straight line was fitted to the second five points. By referring to the results of Type I experiments it can be seen that the velocities obtained as the slopes of the least-squares curves, listed in Table I, are not inconsistent with velocities for the initial shock wave and for the detonation wave from previous work. The agreement is as good as can be expected, since with the few points available the quadratic terms cannot be resolved.

TABLE I

Shot No. B-4695. Explosive: 65/35 RDX/TNT, ρ_0 = 1.71 g/cc.

Electrode Number	$x^{(a)}$ (mm)	$t^{(a)}$ (μsec)	$\Delta t^{(b)}$ (μsec)	Velocity$^{(c)}$ (mm/μsec)	Distance to Transition$^{(c)}$ (mm)
E1	0	0	− .038		
E2	1.95	(0.73−)	(+ .253)$^{(d)}$		
E3	2.95	0.781	+ .077		
E4	5.56	1.266	− .027		
E5	6.57	1.510	− .011	4.43	7.96
E6	12.76	2.437	− .006		
E7	24.91	3.998	+ .018		
E8	32.88	4.999	+ .010		
E9	50.37	7.173	− .029		
E10	101.60	13.693	+ .008	7.90	

(a) $\underline{x}$ is the distance from the attenuator-explosive interface to the end of the electrode. $\underline{t}$ is the time interval from entry of the wave into the explosive to contact of the wave with the electrode.

(b) $\Delta t = t_{obs} - t_{calc}$. t_{calc} is obtained from the least-squares fits to the data.

(c) Calculated from least-squares fits to data. Transition point is taken as the intersection of the two curves.

(d) This error seems to be due to the very slow rise of the signal and the resultant difficulty in locating the beginning of the signal. See Fig. 8a.

In Fig. 8a is shown the signal from electrode E2 of Table I, while Fig. 8b is the record from electrode E5. Although it would be difficult, if not impossible, to measure from such records the resistivity of any volume element behind the initial shock wave, the records do show that the resistivity behind the wave decreases as the point of transition to high-order detonation is approached. It is instructive to plot the rise-time of the signals against the distances of the corresponding electrodes from the transition point, the rise-time being defined as the time to 50% of maximum deflection. A curve drawn through these points tends to zero rise-time in the neighborhood of the velocity transition. At 50% deflection point the battery voltage was equally divided between the impedance of the coaxial cable (33 ohms) and the sum of the impedances of the battery and the gap between the electrodes. The battery impedance was about 4.5 ohms, and the impedance of the gap between the electrodes was therefore 28.5 ohms. If the region of low resistivity extends for a considerable distance behind the shock, the resistance between a pair of electrodes will decrease as the shock moves along them. The plot shows that the resistance decreases more rapidly as the shock progresses, which means that the resistivity of the explosive immediately behind the shock front becomes smaller as the shock approaches transition to detonation. Six experiments of this type using the same lot of explosive show excellent agreement of velocities, transition distance, and even conductivity at each level.

Type IV Experiment: Doubly-Shocked Explosive

The results reported thus far raised the question as to whether the explosive traversed by the initial shock wave ever reacted completely. For example, the framing-camera sequence presented in the discussion of the Type II experiments showed the boundary, corresponding to the transition to high-order detonation, to remain sharply defined throughout the period of observation; this implies that the explosive traversed by the initial shock wave had not detonated and that the initial shock wave was converted into a detonation wave without the contribution of a large fraction of the chemical energy available in the initial layer.

The state of this initially-shocked layer, the imminence of complete reaction, and the susceptibility of this layer to initiation by a second shock was investigated by the experimental arrangement shown in Fig. 9. A layer of Styrofoam of density 10.5 lbs/cu ft was used as the shock attenuator immediately adjacent to the explosive under study (HMX/plastic-94/6). The first reverberation in the foam supplied a second shock to the explosive. The wedge was immersed in an impedance matching solution of $ZnCl_2$, so that no rarefaction was reflected into the wedge.

Figure 10 shows the smear-camera record of such a shot. The values of the initial shock velocity, U_s, and the high-order detonation velocity, D, were found to be 3.93 mm/μsec and 9.20 mm/μsec, respectively. From Type I experiments on the plastic-bonded HMX the particle velocity, U_p, was interpolated to be 0.55 mm/μsec. Using

these data, the base angle, θ, of the explosive wedge after passage of the initial shock wave was calculated from the relationship

$$\tan\theta = \tan 20^\circ\ (U_S-U_p)/U_S$$

where the initial wedge angle was 20°. Using this value of θ and the camera record of the second shock, the velocity of the latter was calculated to be 5.62 mm/μsec.
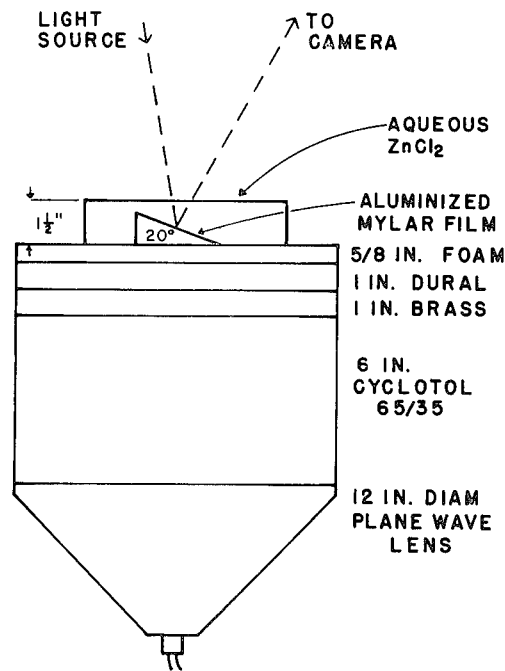
Fig. 9. Charge arrangement for doubly-shocking plastic bonded HMX. Shot D-6851.
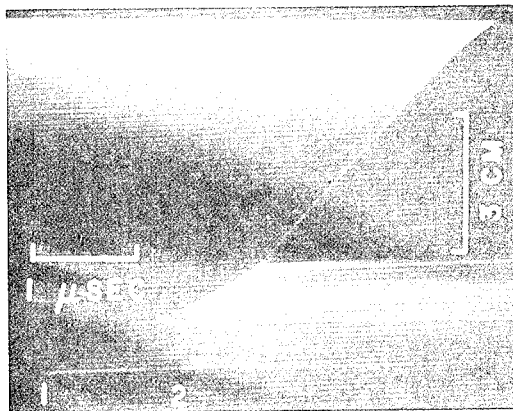
Fig. 10. Smear camera record of doubly-shocked wedge of

plastic-bonded HMX. First and second shocks are
labeled 1, 2, respectively. The first shock
starts at the bottom and moves up and to the
right at almost constant slope, until detonation
begins and the slope becomes greater. The curva-
ture at the upper right in the detonation line
is an edge effect. The second shock starts at
the bottom about 1.4 μsec later and moves at
higher velocity. The space scale applies to the
slant face. Shot D-5861.

The second shock wave corresponds to an important increase in
pressure over the 39 kbar of the first shock, although sufficient data
are lacking for an accurate calculation of this increase. The Ray-
leigh line intersects the initial Hugoniot at 100 kbar, however, so
the pressure is near 100 kbar. That it is not a detonation wave is
evident from the wave's low velocity relative to that of the deto-
nation wave observed in the upper part of the wedge. This result
suggests both that complete reaction was not imminent in the initial-
ly-shocked layer of explosive and that the initial shock has in fact
desensitized this layer.

Type V Experiment: Nitromethane-Carborundum Mixtures

Following the hypothesis that the difference in the initiation
behavior of physically homogeneous and inhomogeneous explosives is in
fact due to the inhomogeneities, an experiment was designed to convert
nitromethane, which had been extensively studied in the homogeneous
state[1], into an inhomogeneous explosive by the addition of Carborun-
dum grit. The charge was arranged as shown in Fig. 2, except that the
booster-attenuator system was 12 in. in diameter. It consisted of a
plane-wave lens, 2 in. of baratol, 3/4 in. of brass, 3/4 in. of
Lucite, and 3/4 in. of brass.

The charge of nitromethane and Carborundum is shown in Fig. 11.
A wedge-shaped container made of Homolite plastic was used to hold the
explosive mixture in contact with the brass attenuator plate. The
Carborundum was #150 grit settled to a density of 1.90 g/cc with a re-
producibility better than 0.003 g/cc. Nitromethane was introduced at
the bottom of the wedge by means of a hypodermic needle as shown in
Fig. 11. The addition of the nitromethane was carried out slowly to
displace the air in the interstices and brought the final charge den-
sity to 2.32 g/cc. Finally, a narrow strip of aluminized Mylar was
stretched along the slant face of the wedge to act as a mirror as re-
quired in the Type I experiments.

The firing record obtained from the Carborundum-nitromethane mix-
ture is shown in Fig. 12. It can be seen that the velocity tran-
sition is characteristic of inhomogeneous explosives, i. e., it is a
smooth, gradual process. The velocity of the initial shock wave was
2.47 mm/μsec and the pressure was 23 kbar. These values are to be
compared with 4.5 mm/μsec and 85 kbar for the initiating shock in
pure nitromethane. The detonation velocity in the mixture was 4.44

mm/μsec as compared to 6.30 mm/μsec for pure nitromethane. Thus, addition of Carborundum to nitromethane sensitizes it and the resulting mixture initiates in the same way as do inhomogeneous solids. Five experiments of this type have shown excellent agreement.
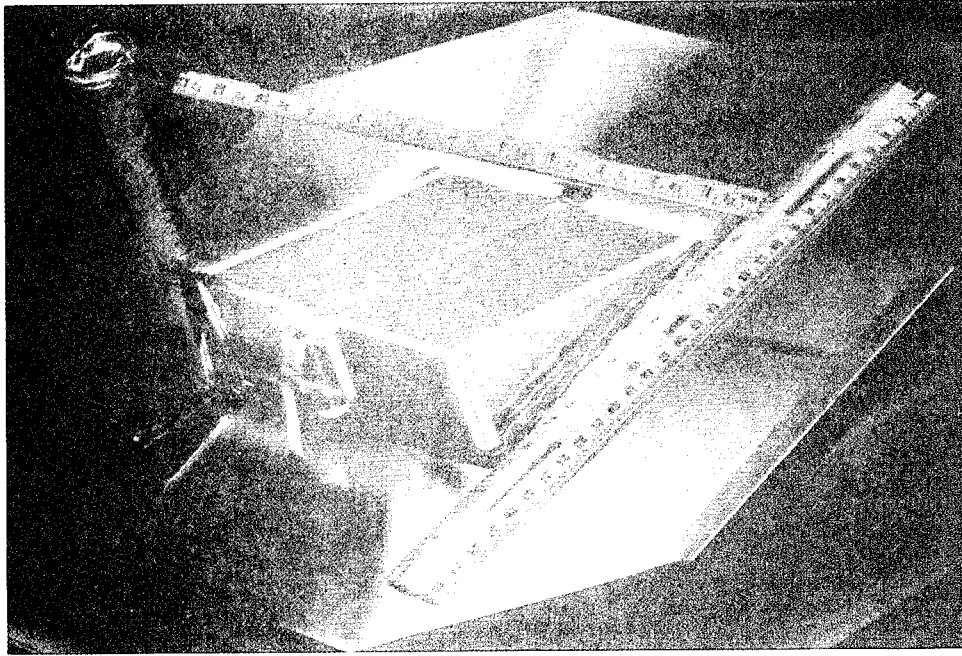
Fig. 11. Nitromethane-Carborundum charge mounted on brass shock-attenuator. Base angle of wedge: 20° Shot D-6853.
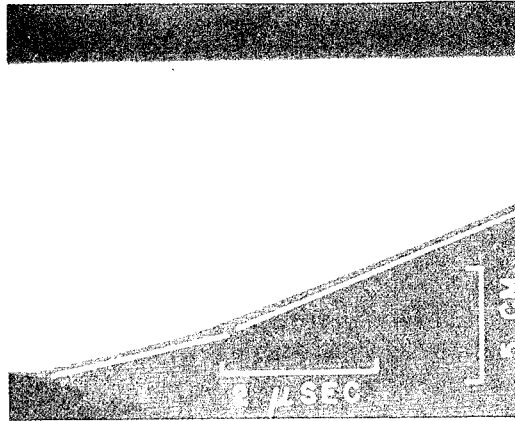
Fig. 12. Smear camera record from nitromethane-Carborundum charge in Fig. 11. The space scale applies to the slant face. Shot D-6853

513

Additional Experimental Results

In the course of the work on initiation, many data have been collected in addition to those already mentioned. In order to design an experiment to study initiation, it is necessary first to know what pressure is needed to initiate the explosive in a time convenient for the equipment available. Also, it is possible to get meaningful data only if the results can be reproduced. Reproducibility requires reproducible behavior of both the experimental piece and the booster system. Since the initiation behavior of a charge depends upon the nature and extent of the inhomogeneities present in it, it is these which must be evaluated in order to characterize and obtain the quality necessary in a charge to allow one to obtain valid results in initiation experiments. Type I experiments were used to explore these problems. Some of the results illustrate general behavior, and will be presented for that reason.

Wedges of the cyclotol described in the section Type I experiments were initiated with different boosters to determine where high-order detonation begins for different initial shock pressures. The pressures were obtained from the free-surface velocity of the attenuator plate used in the usual impedance match calculation with the initial shock velocity in the explosive. The data are plotted in Fig. 13.
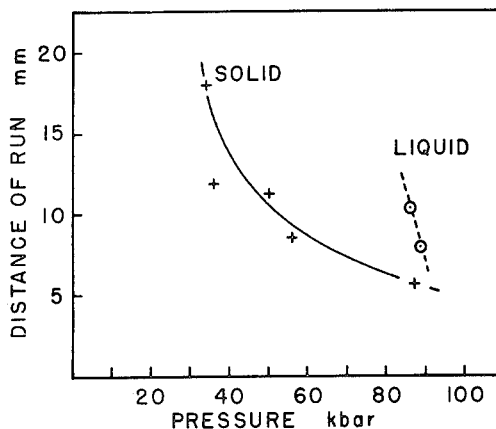
Fig. 13. Plot of distance of run of the shock wave before
high-order detonation begins versus initial shock
pressure. The solid explosive is cyclotol, and
the liquid is nitromethane.

The errors result in large part from uncertainty about which point on the accelerating curve one should pick. The contrast between the behavior of liquid[1] and solid explosives is illustrated in Fig. 13 by including the similar curve for nitromethane. The distance in this case is the position of the shock wave when detonation begins at the

back surface. The great difference in the slope of the two curves is evidence that while in liquids the shock must heat all the explosive to a high uniform temperature, resulting in a very strong dependence of the induction time on the temperature or shock pressure, in solid inhomogeneous explosive the important heating is at the defects in the structure where the temperature depends more strongly upon the nature of the defect than upon the shock pressure. It is easy to show that the average temperature in the shocked solid is too low at any of the pressures used to make the reaction proceed at a sufficient rate for detonation to occur in a few microseconds.

In Fig. 14 are plotted the results of some initiation experiments on TNT charges pressed from coarse- and fine-grained material. The coarse-grainted TNT had a median particle size in the range 200-250 μ, while the fine-grained material, which was prepared by grinding the coarse, fell largely in the range 20-50 μ. One booster design was used for all of the shots, and the measured values of the pressure were 60 kbar ± 5%.
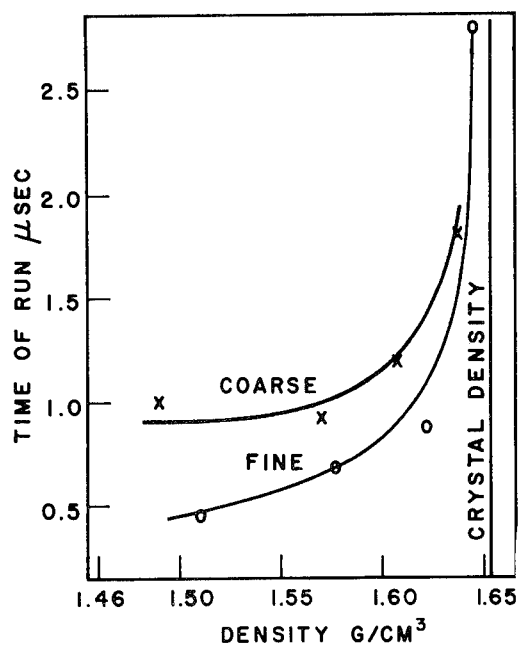
Fig. 14. Effects of initial density and particle size on the sensitivity of pressed TNT charges. Ordinates are times of run of initial shock waves as shown in Fig. 4.

From the plots of the data it can be seen that the charges made from fine-grained TNT were more sensitive than those made from coarse material. This agrees with general experience. Another important feature is the rapid decrease in sensitivity of both types of charges

as the density approaches crystal density (1.654 g/cc).

Figure 15 shows the results of initiation experiments on charges pressed from two lots of plastic-bonded HMX. The lots differed slightly in particle-size distribution. Again it can be seen that, as the limiting density is approached, the sensitivity decreases rapidly.

From these two sets of experiments it appears that at intermediate densities the particle size is more important than is the density in affecting the sensitivity, whereas at densities approaching the limiting value, the density becomes the more important factor. Furthermore, it seems reasonable to suppose that the initiation behavior gradually changes from that of an inhomogeneous explosive to that of a homogeneous one.
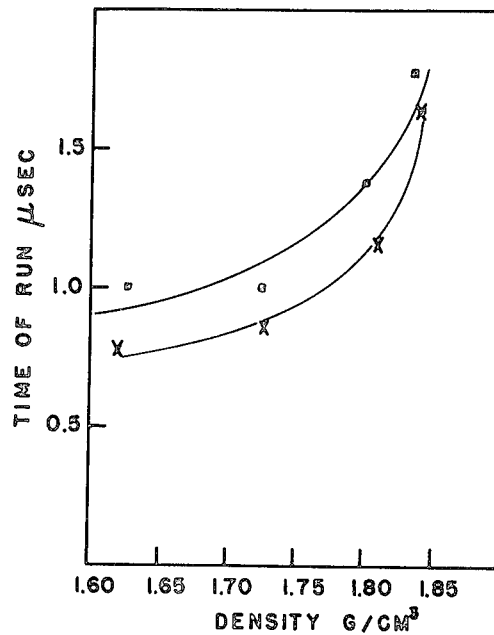
Fig. 15. Effect of density on the sensitivities of two lots of plastic-bonded HMX. Ordinates are times of run of initial shock waves as shown in Fig. 4.

516

DISCUSSION OF RESULTS

In most of the experiments described in this paper our goal has been to put a smooth, plane shock wave with a sharply rising front and constant amplitude into the explosive charge to be studied and to observe the initiation behavior before the intrusion of edge effects or of reverberations in the shock attenuator. While edge effects were eliminated, the pressure profile was not flat-topped. To achieve the latter condition to good approximation would have required either very large charges, or that a good technique for throwing big metal plates be developed. Nevertheless, the shock waves were of sufficient quality to permit the drawing of a number of conclusions from the experimental results.

It is of interest first to contrast the initiation behavior of homogeneous and inhomogeneous explosives using Reference 1 as the source of information for the former. The contrasts are as follows:

(a) The initial shock wave in a homogeneous explosive shows a constant or slightly decaying velocity as a function of time; the corresponding wave in inhomogeneous explosive accelerates throughout its travel.

(b) The transition to high-order detonation is very abrupt in homogeneous explosive; the transition in inhomogeneous explosive is less so.

(c) The onset of high-order detonation in homogeneous explosive is accompanied by an overshoot in the velocity, amounting to about 10% in the case of nitromethane; no demonstrable overshoot has been recorded for inhomogeneous explosive in our experiments.

(d) Detonation is observed to originate at the shock attenuator-explosive interface in homogeneous explosive; at present it is believed probable that detonation occurs at or near the shock front in inhomogeneous explosives. It may be possible to clarify this point in the future by conductivity measurements.

(e) The experiments with nitromethane-Carborundum mixtures have shown that the mixtures are much more sensitive than the homogeneous liquid nitromethane. The inhomogeneities in the mixture cause shock interactions with resultant local heating. For initiation, the detailed structure of the shock properties of the explosive is more important than are the values of the thermochemical constants.

(f) The material behind the initial shock wave in homogeneous explosive is relatively non-conducting for electricity until the onset of detonation; in inhomogeneous explosive the material behind the initial shock front is quite conducting and becomes even more so as the transition to high-order detonation is approached.

(g) The initiation process in homogeneous explosive is much more sensitive to variation of the initial temperature or to variation of the shock pressure than it is in inhomogeneous explosive.

It is logical to attribute the differences between the initiation behavior of inhomogeneous and homogeneous explosives to the voids and other defects in the former. Work with nitromethane in Reference 1 and the results with nitromethane-Carborundum mixtures reported here show that convergences in the mass flow and impedance mismatches can

cause local reaction which influences importantly the initiation process. It is easy to show with a smear camera record that the detonation front in a pressed or cast explosive is quite rough, from which one can deduce that the mass flow is quite irregular in fine detail.

On the other hand gas bubbles and voids are perhaps the most commonly occurring defects in cast and pressed explosives. If we may assume that the number of voids between grains of explosive is proportional to the number of grains, then the coarse-grained TNT discussed above should have fewer, but larger, voids than the fine-grained TNT at the same density. Experimental results show that the latter explosive is more sensitive, and therefore, it may be concluded that a volume of fine voids is more efficient in producing chemical reaction than the same volume of coarse voids. This suggests the importance of a surface reaction.

The effect of increasing the number of voids and other sources of hot spots is to render a given explosive more sensitive. It is well known that an explosive becomes easier to initiate as the density is decreased. This effect of hot spots is supported here by the results obtained for nitromethane-Carborundum mixtures and by the data plotted in Figs. 14 and 15. When an explosive exists in an inhomogeneous state, the shock strength necessary to cause initiation need not be great enough to raise the entire mass to a sufficient temperature for a rapid reaction (thermal explosion) to occur, but need only activate a sufficient number of hot spots. This effect of hot spots also accounts for the small dependence of the sensitivity of inhomogeneous explosives on the initial temperature.

The amount of energy obtainable from a single hot spot must depend, among other things, upon the shock strength. Following the model of Rideal and Robertson[12] the higher the temperature around a hot spot, the longer the hot spot will continue to react and the more energy it will produce before being deactivated by loss of heat to the surroundings. An increase in shock strength will increase the temperature of the homogeneous explosive about a hot spot as well as, perhaps, increasing the dimensions and temperature of the hot spot itself.

The behavior of the undetonated layer of explosive in the Type IV experiments becomes understandable on the basis of hot-spot action. The primary sources of hot spots in the plastic-bonded HMX pressings are the impedance mismatch between the HMX and the plastic, and the small bubbles present. Passage of the first shock wave creates hot spots and causes some chemical reaction to take place. After the hot spots have been deactivated by loss of heat to their surroundings, the explosive is left in a more homogeneous state than before. The bubbles will have been collapsed and the impedance mismatches reduced by the greater compression of the less dense component. The explosive will then be much less sensitive to a second shock.

In view of the above considerations, the following picture of the initiation process has evolved. A shock entirely too weak to initiate a homogeneous explosive can activate hot spots and cause detonation when the explosive is sufficiently inhomogeneous. In an explosive pressed to near crystal density the hot spots due to bubbles are quite small and are deactivated quickly after passage of the shock.

The energy contribution to the shock wave by a particular hot spot is completed soon after the passage of the wave front. Detonation occurs at or near the front of the wave; explosive located before the transition does not detonate and is relatively insensitive to subsequent shocks. Because the detonation takes place near or at the front of the wave, there is little or no overshoot in the detonation velocity.

ACKNOWLEDGEMENTS

REFERENCES

1. A. W. Campbell, W. C. Davis, J. R. Travis, "Shock Initiation of Detonation in Liquid Explosives". This Symposium.
2. Henry Eyring, R. E. Powell, G. H. Duffey, R. B. Parlin, Chem. Revs. 45, 69 (1949).
3. F. P. Bowden, et al., "A Discussion on the Initiation and Growth of Explosion in Solids", Proc. Roy. Soc. (London) 246, 146(1958).
4. F. P. Bowden and A. D. Yoffee, Initiation and Growth of Explosion in Liquids and Solids (Cambridge University Press, 1952).
5. S. J. Jacobs, "Recent Advances in Condensed Media Detonations", 30, 151 (1960), Am. Roc. Soc.
6. J. M. Majowicz and S. J. Jacobs, "Initiation to Detonation of High Explosives by Shocks", presented at Lehigh Meeting of Fluid Dynamics Division, American Physical Society, Nov. 1957.
7. M. A. Cook, The Science of Explosives (Reinhold Publishing Corporation, New York, 1958), p. 187.
8. M. H. Rice, R. G. McQueen, and J. M. Walsh, "Compression of Solids by Strong Shock Waves", Solid State Physics, Advances in Research and Applications, Volume VI, Eds: F. Seitz and D. Turnbull (Academic Press, Inc., New York, 1958).
9. B. Hayes, "On the Electrical Conductivity of Detonating High Explosives". This Symposium.
10. A. A. Brish, M. S. Tarasov, V. A. Tsukerman, Zhur. Eksp. i Teoret. Fiz. 37, 1543 (1960).
11. A. W. Campbell, M. E. Malin, T. J. Boyd, Jr., J. A. Hull, Rev. Sci. Instr. 27, 567 (1956).
12. E. K. Rideal and A. J. B. Robertson, Proc. Roy. Soc. A (London) 195, 135 (1948a).

SHOCK INDUCED SYMPATHETIC DETONATION IN SOLID EXPLOSIVE CHARGES

Morton Sultanoff
Vincent M. Boyle
John Paszek
Ballistic Research Laboratories
Aberdeen Proving Ground, Maryland

Abstract

A study of the basic physical parameters for sympathetic initiation of high explosive receptor charges by the pressure pulse from a donor charge transmitted through barriers of air, steel, aluminum, lead, and copper has been conducted. A surface phenomenon, which has been shown to be a front of mechanical discontinuity supported by a chemically reacting core, has been observed to propagate at a constant, supersonic velocity. The core reaction is initiated provided the intensity of the incident pressure pulse is less than the detonation pressure of the explosive but above a threshold value which depends on the chemical composition and physical condition. The initial core reaction is a "low-order" chemical decomposition which produces a pressure considerably less than that associated with high-order detonation, and propagates at a supersonic rate, but much slower than a higher-order detonation. This reaction is confined to the central core of the explosive and its rate of propagation is determined by the intensity of the incident wave. The distances and times required for the reaction to change abruptly to high order detonation are uniquely determined, for a given explosive, by the intensity of the incident pressure wave. High order detonation is first observed at the surface of the charge coincident to the front of the mechanical discontinuity. However, the shape of that front, on emergence, indicates that initiation originated in the reacting core.

Invariably, for a considerable time after the beginning of the high-order reaction in the receptor charge, it propagates at a rate slightly greater than normal detonation rate.

While details of behavior vary with composition and geometry of the explosive, the qualitative features appear to be generally valid.

Introduction

Studies have been made of the fundamental physical processes involved in the detonation reaction of solid explosives. These studies have led to an analysis of the parameters that control the sympathetic detonation of a receptor charge subjected to strong shocks transmitted through barriers of various materials. It is felt that these studies might lead to a fuller understanding of the detonation process and could also indicate a criterion of sensitivity based on physical quantities directly related to the explosive charges. Continuation of the research project reported formally first in a Ballistic Research Laboratories Report[1] in 1953 and subsequently in later reports[2,3] indicate the direction of this continued research with finer time and space resolution, employing new techniques for the investigation of the regime of transition from initiation to high-order detonation. Much of the earlier data were inferred from the observation of the surface conditions of receptor charges. The work covered by this report deals with the direct observations of the core reaction in the receptor. These new observations eliminate the errors and uncertainties introduced by the earlier inferences.

Experimental Proceedure

Except for some preliminary experiments with internally cast resistance wires[4] all of the data were obtained from photographic records[5]. Self-luminosity and auxiliary front lighting were used with streak-cameras, Kerr-cell single exposure shutters and multiframe, high repetition rate, framing cameras.

The charges were arranged as shown in Figure 1 and, except where noted, were cast 50/50 pentolite sticks of 3/4 inch square cross-section, 3 inches long. Barriers of air, steel, dural, copper, lead and plastic have been tested. However, most of the data presented in this report represent a variety of barrier thicknesses of air, lead and dural.

Data for initiation by pellet impact were obtained with steel discs, driven intact, at velocities ranging from 500 to 1500 meters per second by metal-padded explosive sticks.

Discussion-Specific Results

As a result of the methods for the determination of initial conditions in the receptor charges, the quantitative data obtained in these tests fall into three general catagories, i.e. air-gap, metal barrier and pellet impact. However, the conditions leading to high order detonation can be described by a single physical model.

1. Initiation by Shock Through Air Gaps

The earliest investigations of shock initiation were conerned primarily with air barriers, and the time "t" and distance "d"
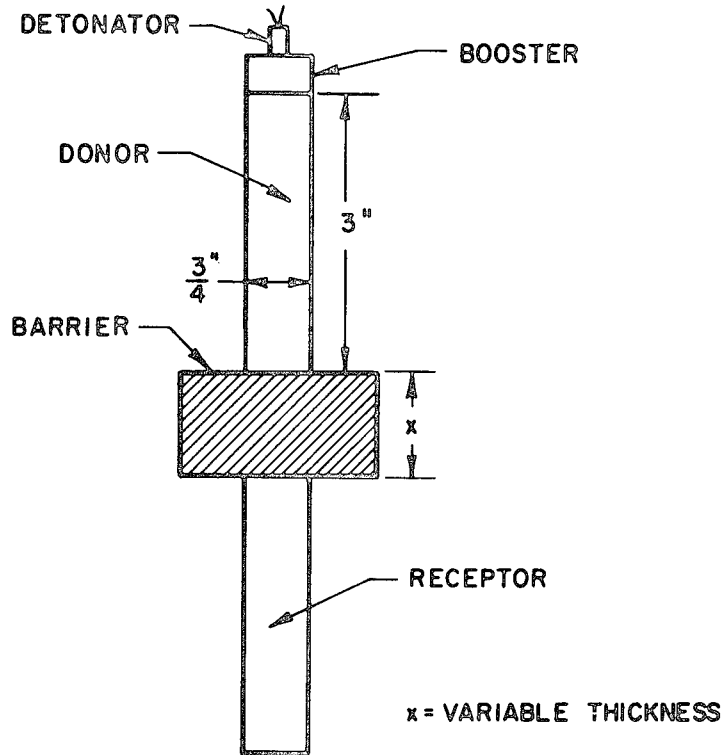
Fig.1 - Basic experimental arrangement

shown in Figure 2A, which is a typical streak-camera record, were the first observations made of the delay to detonation. More recent, front lighted records (Figure 2B) have shown that this time "t" consisted of at least two individual delays, i.e., the delay to ignition and the delay to high order detonation after ignition established a core reaction in the receptor stick. The direct measurements of the supersonic surface velocity[3] as a function of the width of the air gap in comparison with the velocities computed from the "t-d" data are shown in Figure 3.

For detonation induced by the air shock it is necessary to separate the contributions of peak pressure, impulse and possibly heat, to the reaction in the receptor. The pressure in the air shock at the face of the receptor is directly obtained from the Hugoniot relations for air, which are well known for the velocities involved. The pressure so obtained, cannot be used directly to obtain the pressure in the receptor, however. Theory and experiment both show that the peak pressure occurs when the high density detonation products, which are following closely behind and driving the air shock, impact the face of the receptor charge. A single rough measurement made at these Laboratories, (by Mr. Boyd Taylor) of the pressure developed in a Plexiglas receptor separated by a 1 inch air gap from a standard pentolite donor yielded an estimate of 300,000 PSI. At this gap distance, the pressure in the incident air shock is about 8,500 PSI and, allowing for a maximum theoretical eight-fold magnification in the reflected shock from a perfectly rigid wall, the pressure at the receptor face could be expected not to exceed 68,000 PSI as a result of the shock impact. The quantitative data presented relate the surface velocity and the delay to detonation in the receptor to the pressure in the incident wave. Recomputing to include the results of the single test with the Plexiglas receptor will increase the magnitude of this pressure, and will throw the air gap data into agreement with the metal barrier data.

2. Initiation by Shock Through Metal Barriers

The delay time and distance to detonation in receptor charges have been studied as functions of both the barrier thickness and barrier material with lead, dural, copper, and steel. However, sufficient data for quantitative as well as qualitative analysis have only been obtained with the lead and dural barriers.

Direct measurements of the pressure induced in the receptor charges could not be made with existing instrumentation and techniques. However, once the pressure in the barrier at the barrier-receptor interface is known, this information can be used with the extended high pressure Hugoniot curve published by Los Alamos[6]. By use of the pin technique, Dr. Floyd Allison at Carnegie Institute of Technology supplied the free surface velocities of barrier materials driven by contact donor charges. Using the relationship:

$$P = \rho_o U_s U_p$$
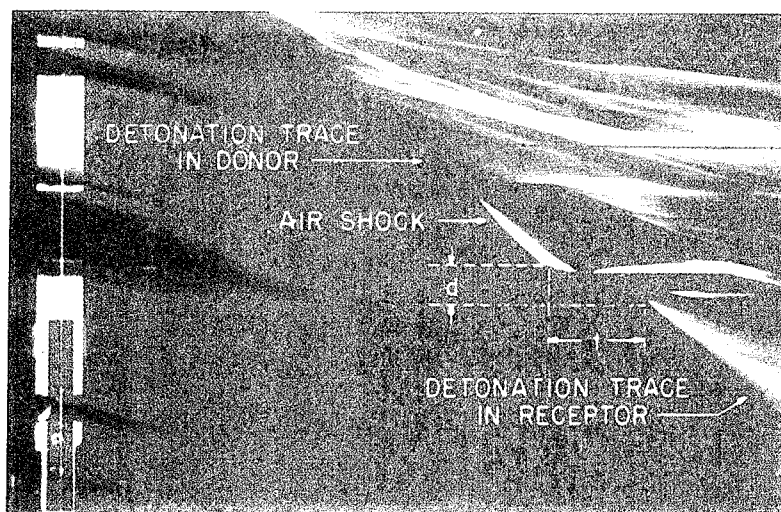
(a)

(b)
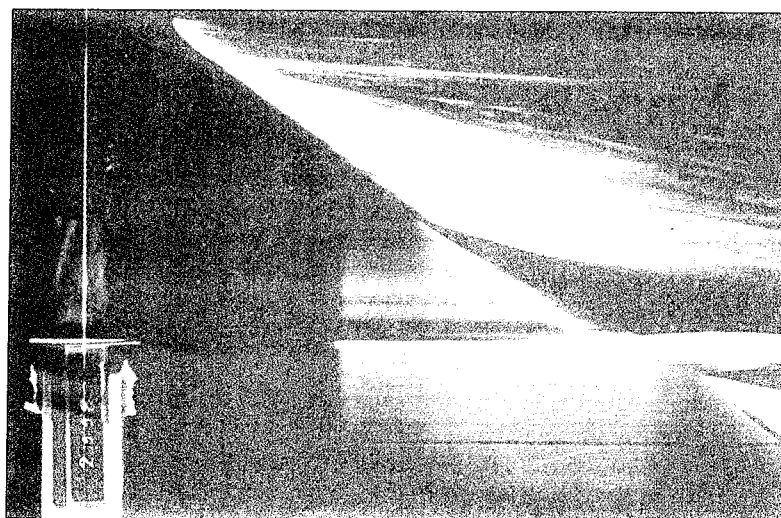
Fig. 2 - (a) Streak camera record of sympathetic detonation by air shock showing the distance and delay time to detonation; (b) front lighted record of sympathetic detonation by air shock showing the surface shock propagating along the receptor.
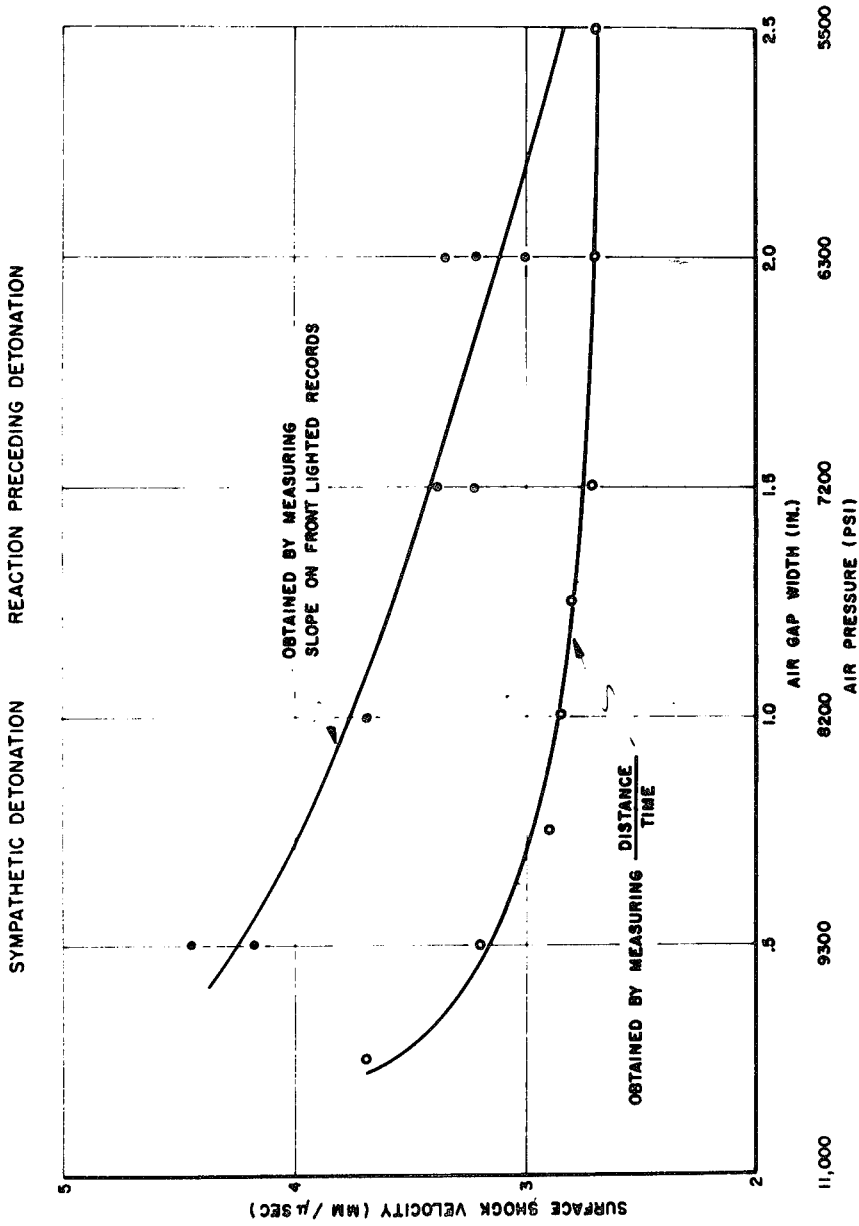
Fig. 3 – A comparison of front-lighted and distance/time measurements

where: P is pressure $(dynes/cm^2)$
ρ_o is barrier density (gms/cm^3)
U_s is shock velocity in the barrier (cm/sec)
U_p^s is the barrier particle velocity (cm/sec),
and is approximately 1/2 the free surface velocity,

the pressure transmitted to the receptor charge is computed. The relationship of the delay to detonation for lead and dural is shown as a function of these computed pressures in Figure 4.

To date, the pressure profile and consequently the impulse delivered to the receptor charge have not been measured. With new pressure transducer techniques, a program to determine values for this parameter is being initiated. However, the contribution of total impulse appears negligible in the comparison, shown in Figure 4, of data for two materials of widely different density and physical characteristics.

3. Initiation by Pellet Impact

Aluminum pads of various thickness were used on the ends of large explosive cylinders separating the charge and disc to be propelled. Tests were conducted with steel discs 1.5 inches in diameter and 0.125 inches thick weighing 28.32 grams with velocity of impact at the receptor ranging from 0.58 to 1.52 mm/μsec. Earlier evidence that peak pressure, not total energy delivered to the receptor, controlled the delays and velocities in the receptor led to the treatment of the plate as a free surface. Computations identical to those for metal barriers were made and the plot shown in Figure 5 indicates the close agreement of these data to those for metal barriers.

It appears most likely that the excessive scatter in the impact data resulted from oblique collision of the plate with the end of the receptor. Additional testing of the effects of oblique impact is being conducted to amplify this possibility.

Discussion-General Results

An examination of the photographic exposures made in tests conducted with the air and metal barriers and impacting pellets made it immediately obvious that the initiation, the pre-detonation, and the "break-out" of high order detonation have the same physical characteristics for all these methods of transfer of energy to the receptor charge. Four conditions have been found to exist in the impacted receptors:

1. Detonation occurs with no measurable delay at the impacted face of the receptor.
2. A measurable supersonic surface shock of mechanical discontinuity proceeds at constant velocity in the receptor, and eventually high order detonation breaks out in this front.
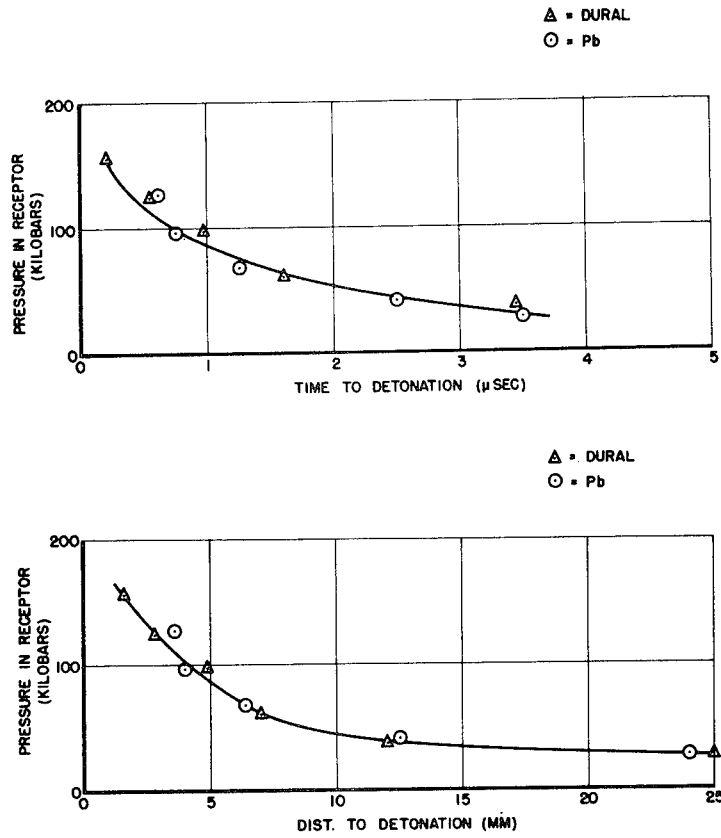
Fig. 4 - Pressure in receptor vs time to detonation, pressure in receptor vs distance to detonation

3. A measurable supersonic surface shock of mechanical discontinuity proceeds at constant velocity for the entire length of the stick and high order detonation is not observed.

4. A measurable supersonic surface shock of mechanical discontinuity is observed to gradually decay and be no longer observable as it approaches sonic velocity. High-order detonation does not occur.

The first of these conditions was not covered in this study, and the results which follow are only related to 2, 3 and 4 above.

The observation of a supersonic shock along the surface of the charge, proceeding at constant velocity, requires that energy be fed into that shock. This indicates that a chemical reaction has been initiated in the receptor. The lack of observation of this reaction at the surface does not preclude its existence. With receptors cut to lengths equal to, shorter than and longer than that distance at which high order detonation would be expected to occur for a given barrier condition, the results shown in Figure 6, which is a composite of a series of streak-camera records, were obtained for the core reaction. The profile of this reacting core can be observed to be changing shape in these records. Figure 7 is a plot of the velocity of the reaction (measured in the direction of the axis of the charge) at the center of the charge and at various radial distances from the center, as indicated. The shape of the reacting core at any given time is directly related to the difference in velocity, which is highest at the axis of the charge and decreases with radial distance. The non-reactive surface shock is joined by a continuous extension of the shock profile of the reactive core, and has the lowest velocity observed during the pre-high-order detonation regime.

The velocity of the surface shock has been found to be constant in each record. However, the magnitude of this velocity is a function of the barrier conditions. The core velocity along the axis has been measured and also shown to be constant from the photographic record of charges of different lengths, and measured as constant in a given charge by the resistance wire method mentioned earlier[4]. The magnitude of the axial velocity is also dependent on the barrier conditions.

The surface observation obtained for dural and lead barriers is plotted vs the transmitted pressure in the receptor charge (Figure 4), and it is indicated in this diagram that delay time and distance are directly dependent on pressure alone, and independent of impulse. A similar graph, Figure 3, is shown for air barriers but, as described under "Discussion" the pressure shown is that of the incident air shock. Figure 5 shows the similarity of data for pellet impact to those for metal barriers.
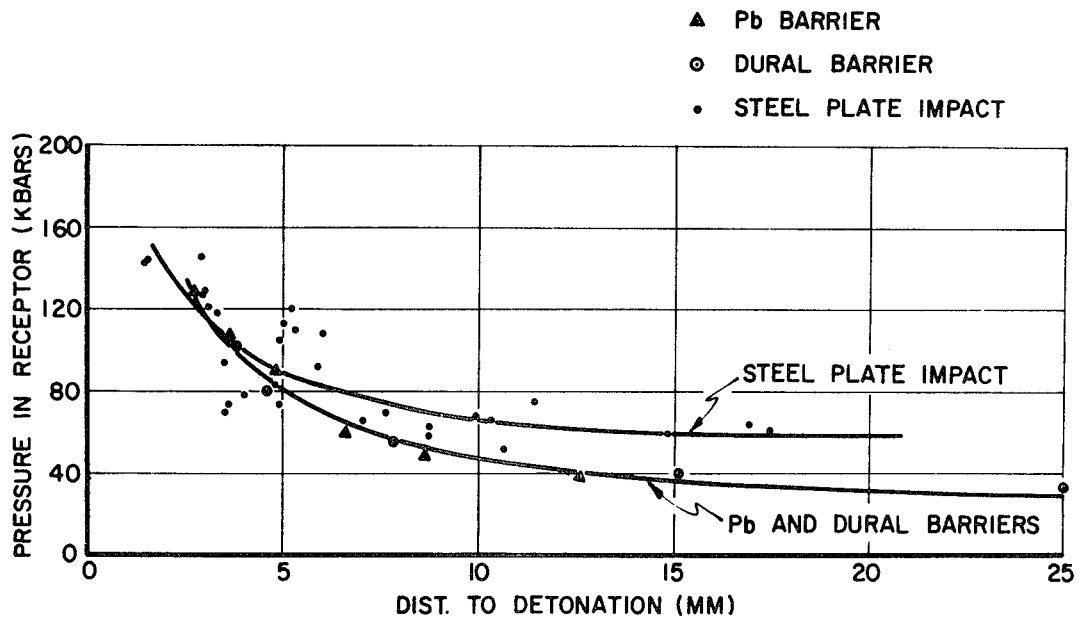
Fig. 5 - Impact initiation. Pressure in the receptor vs the distance to detonation
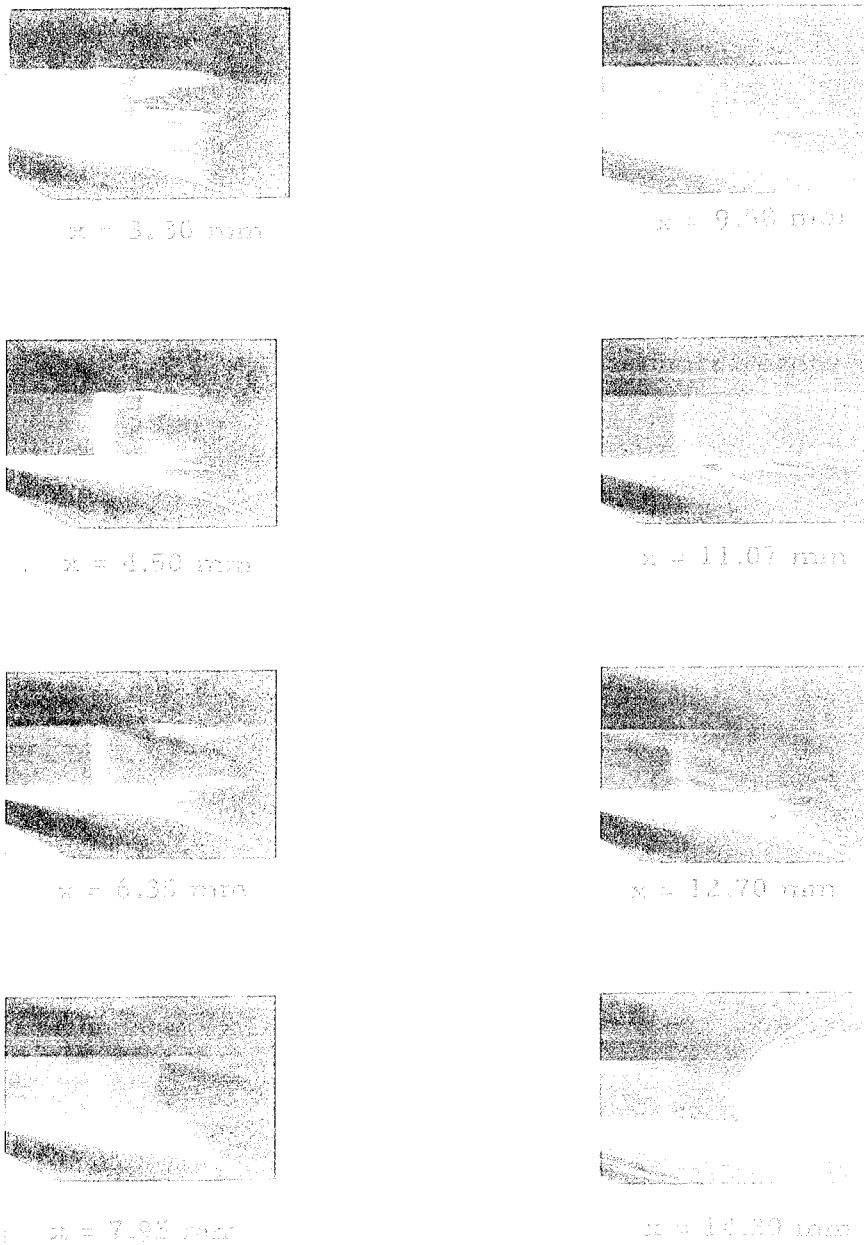
Fig. 6 - Series of streak camera records showing the core reaction emerging from the ends of short receptors (x = length of receptor)
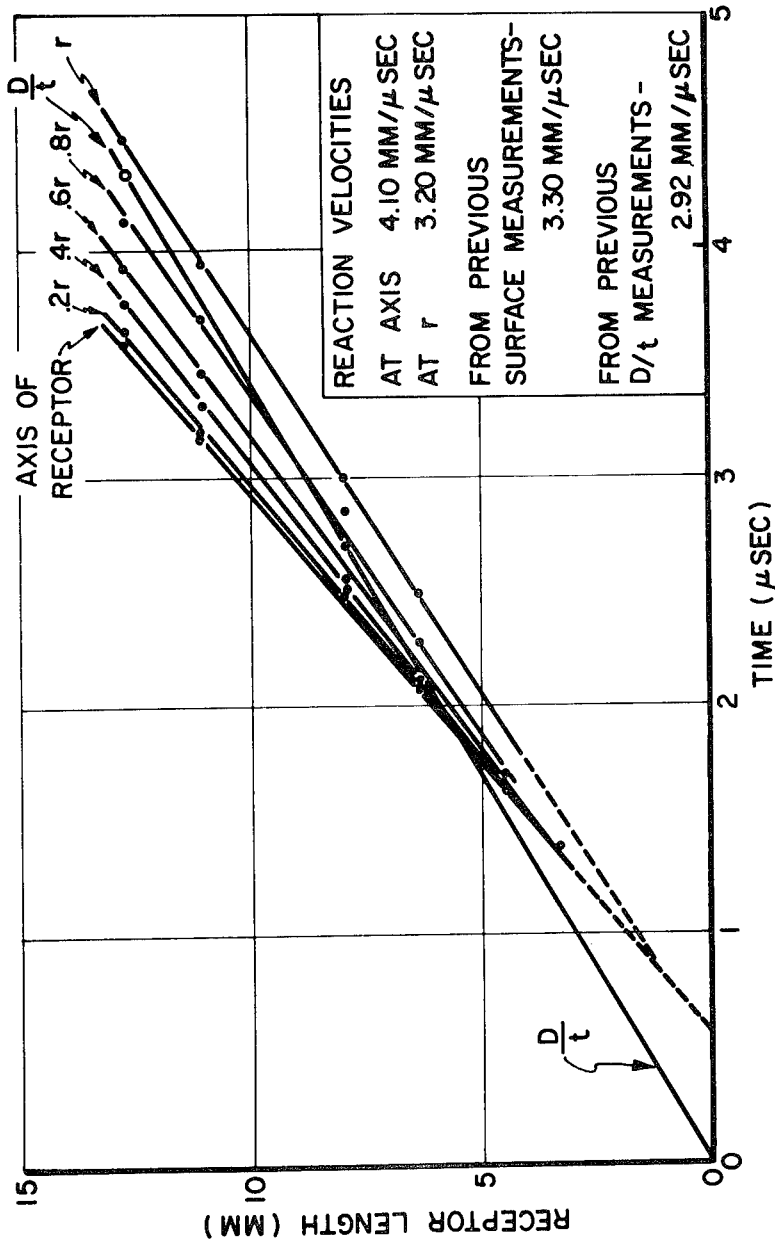
Fig. 7 - Sympathetic initiation - 1.5 in. air gap. Shock transit time in receptor vs receptor length plotted for different radii at rear surface of receptor.

In over three hundred tests conducted, the velocity of the high-order detonation that is induced in the receptor has been invariably about 1 1/2% higher than the velocity of detonation in the donor sticks. In two of these receptor sticks the detonation velocity has dropped abruptly to its normal value. A valid physical explanation for this observation cannot be made on the basis of information obtained in these firings.

Conclusions

It follows from the results obtained with the air gaps, metal barriers and pellet impact studies of sympathetic initiation that a single physical model can be established for all of these conditions.

Although the nature of the initiation of the reaction is not known, there is no evidence to contradict the hot spot theory of Yoffe And Bowden[7]. Allowing that the reaction does start by adiabatic compression of trapped gases, mechanical heating, or a combination of both, the volume of this reaction and, as a consequence, its pressure and propagation velocity, are functions of the pressure of the initial shock transmitted to the receptor. As this reaction propagates internally, as seen in the results presented here, the rarefaction wave from the boundary is sufficiently strong to prevent surface detonation. However, the pressure of this internal shock is sufficiently great to manifest mechanical surface changes in the solid explosives, observable by front lighting techniques. If the rarefaction loss rate is less than the energy release rate, the internal pressure builds up to a point at which a discontinuous jump to a high order detonation occurs in a manner similar to that proposed by Von Neumann[8]. However, in this case the reaction moves from an n=k Hugoniot, in which $1 > k > 0$, to the n=1 Hugoniot when the pressure reaches a value equal to that at the intersection of the n=k Hugoniot and the Chapman-Joguet plane. If the rate of energy release is such that the pressure does not build up at a rate higher than the rate of dissipation in the rarefaction, then the reaction either continues at a constant rate or at a decreasing rate until it is no longer detectable.

It is also concluded that the contribution to this reaction by the shock from a donor charge passing through a barrier to the receptor charge is a function of the initial pressure in the receptor. Although the significance of the total energy in the pressure pulse is not evident in these experiments it is being investigated further to determine its role in the total reaction.

Bibliography

1. Sultanoff, M. and Bailey, R. A. "Induction Time to Sympathetic High Order Detonation in an Explosive Receptor Induced by Explosive Air Shock", Ballistic Research Laboratories Report No. 865, May 1953.

2. Sultanoff, M. "Explosive Wave Shaping by Delayed Detonation", Proceedings of First Symposium on Detonation Wave Shaping (sponsored by Picatinny Arsenal at the Jet Propulsion Laboratory, Pasadena, Calif.), 5-7 June 1956.

3. Eichelberger, R. J. and Sultanoff, M. "Sympathetic Detonation and Initiation by Impact", Proc. Roy. Soc. A, Vol. 246, pages 274-281.

4. Gibson, F. C., Bowser, M. L. and Mason, C. M. "Method for the Study of Deflagration to Detonation Transition", Review of Scientific Instruments, Vol. 30, No. 10, pages 916-919, October 1959.

5. Sultanoff, M. "Instrumentation for the Study of Explosive Reactions", Proceedings of the Third International Congress on High Speed Photography, Paris, France, October 1956.

6. Walsh, John M, Rice, Melvin H., McQueen, Robert G. and Yarger, Frederick L., "Shock Wave Compressions of Twenty-seven Metals. Equations of State of Metals", Physical Review, Vol. 108, No. 2 October 1957. Pressure in receptor gotten from Los Alamos curves for C-J pressure vs. particle velocity in Comp B.

7. Bowden, F P. and Yoffe, A. D., "Initiation and Growth of Explosion in Liquids and Solids", University of Cambridge Press, London, 1952.

8. Von Neumann, John, "Theory of Detonation Waves" National Research Committee, OSRD Report, Institute for Advanced Study, Princeton, N. J. April 1, 1942.

GROWTH OF DETONATION FROM AN INITIATING SHOCK

Julius W. Enig
U. S. Naval Ordnance Laboratory
Silver Spring, Maryland

ABSTRACT: Numerical computations have been carried
out which depict the formation and structure of unsteady
detonation waves in solid explosives. Two different
methods were employed in the calculations. One takes into
account the dissipative mechanisms of heat conduction and
viscosity and the other is an application of Lax's method
to a chemically reacting fluid. A simple chemical re-
action is introduced which converts solid explosive to
gaseous products through intermediate states, each of
which has an appropriate equation of state.

A piston pushes with constant velocity against one
surface of a chemically inert slab whose other surface is
in intimate contact with a semi-infinite solid explosive
and the growth of the resultant shock is followed. For
sufficiently strong shocks, the chemical decomposition is
initiated and the shock grows into a detonation wave.
Other sample problems involving shock, detonation, or rare-
faction waves are given.

I. INTRODUCTION

In this paper we depict the formation and structure
of unsteady one-dimensional detonation waves in solid ex-
plosives. In particular our attention is directed to the
growth and structure of the reaction zone, the coupling of
the latter with the shock region, and the critical time
necessary for growth from initiation to detonation.
Hirschfelder and Curtiss [1] have given the first dis-
cussion of steady-state detonations based on a complete
set of hydrodynamic relations, including coefficients of
diffusion, thermal conductivity, and viscosity, as well as
chemical kinetics. They computed the composition, temper-

ature, and pressure as functions of distance in a steady state, plane gaseous detonation in which the irreversible unimolecular reaction [A] → [B] takes place with the release of energy. Hubbard and Johnson [2] have utilized the von Neumann and Richtmyer "q" method [3], which was originally introduced in unsteady shock problems, for calculating unsteady detonation waves in solid explosives. This method involves the introduction of a psuedo-viscosity term into the hydrodynamic equations and has the effect of giving the correct entropy change across the shock front and arbitrarily limiting the width of the shock front to several mesh size thicknesses. In the cases that they treated it was found that the hydrodynamic motion and the release of chemical energy are practically independent as a consequence of the extreme temperature sensitivity of the reaction rate. The calculations showed that for a given pressure pulse applied to the boundary of an explosive, there exists a well defined delay time before a detonation is formed. Should the pressure pulse be of such finite duration that a rarefaction wave reaches the explosive particle before it has been maintained at high temperature for the appropriate delay time, then there will be no detonation. In their application to detonation problems all of the previously mentioned authors [1], [2] used the same equation of state for both the reactants and the detonation products. Ludford, Polachek, and Seeger [4] have obtained numerical solutions for unsteady flow containing shocks, in a perfect gas, in the absence of any chemical reaction or heat conduction.

In this paper we consider unsteady one-dimensional detonation waves in solid explosives where for the first time the dissipative mechanisms of heat conduction and viscosity are taken into account. While there is considerable doubt that the notions of viscosity and heat conduction can be used to describe the internal mechanism of the shock process because of the extremely small shock width ($\approx 10^{-5}$ cm), they certainly do provide a process for changing the entropy across the shock. If, for example, a piston is driven with constant velocity into a fluid, a shock is set up which rapidly takes on steady state characteristics. The viscosity and thermal conductivity will determine the exact shape of the shock front, but the characteristics of the shock a sufficient distance behind the front are independent of the transport properties and do indeed satisfy the Rankine-Hugoniot relations. It has been known for a long time that in steady state solutions, the smaller the viscosity and thermal conductivity, the steeper the shock front. Indeed it is just these solutions which cast doubt on the applicability of these dissipative mechanisms to adequately describe the shock zone for at

535

least strong shocks。 If however deflagration waves are considered then the transport properties must play an important role in determining the flow [5]。 While we will in the future discuss deflagration and transition from initiation to deflagration to detonation we restrict ourselves now to detonation。 In any case the use of transport phenomena should be at least as applicable as the "q" method to detonation problems。

Suppose a piston is driven with constant velocity against one surface of a slab of chemically inert material whose other surface is in intimate contact with a semi-infinite solid explosive。 A shock will form and rapidly approach steady state values as it moves into the inert。 This situation is depicted in Fig。 1。
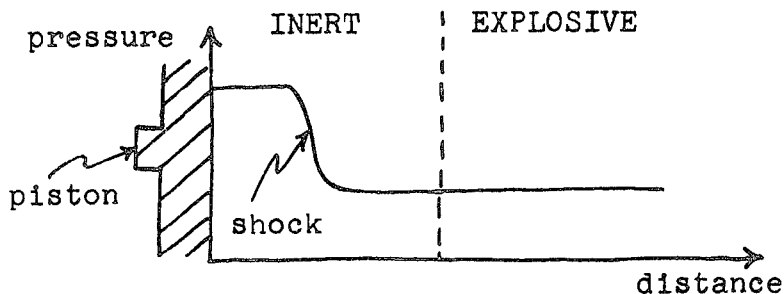
Fig。 1

What will happen when the shock reaches the inert-explosive interface? For simplicity assume that the equation of state and the physical properties of both materials are identical (only the chemical properties are different)。 As the shock passes over the inert and into the explosive it heats both to a temperature which can be easily calculated from the Rankine-Hugoniot relations and the caloric and thermal equations of state。 Now the chemical decomposition of the explosive is governed by an Arrhenius term which is extremely sensitive to temperature; and if the latter is sufficiently low such that there exist only negligible reaction rates, then the steady shock merely propagates into the explosive。 If on the other hand somewhere in the shock front the temperature is sufficiently high so that there do exist appreciable reaction rates, then the explosive material at the interface, which has been heated the longest, will eventually undergo a very rapid exothermic reaction。 The pressure in that region will rapidly increase and drive a shock back into the inert and a high pressure zone of chemical reaction will move into the explosive。 This is the process of initiation to detonation which will be discussed quantitatively in Section V。

To what extent do the transport properties, viscosity and thermal conductivity, affect the structure of the detonation wave? Von Neumann [6], Döring [7], and Zeldovitch [8], independently concluded that a detonation is a shock wave followed by a zone of chemical reaction provided transport properties are neglected. They assumed that the time for reaction to take place is long compared to the time for passage of the shock. If this assumption is true it should not make very much difference exactly how the shock is calculated, i.e. whether transport phenomena are included or the "q" method is used. In the examples that were considered Hirschfelder and Curtiss [1] found that there exists a strong coupling between the reaction zone and the shock zone when transport properties are included and therefore the solutions never come close to the von Neumann "spike". If the coupling is strong in the steady state detonation, must it have been strong during the initial stages of growth?

We now briefly describe another method that can be used for unsteady detonation calculations. This consists of applying the Lax [9] scheme to problems involving unsteady one-dimensional flow <u>with</u> chemical reaction. P. Lax has described a finite difference scheme for calculation of time dependent one-dimensional compressible fluid flows containing strong shocks. The novel feature of this method is the use of the conservation form of the hydrodynamic equations and, to a lesser extent, the particular way of differencing the equations. Putting the Lagrangean hydrodynamic equations in conservation form for the plane case is equivalent to writing each equation in the form

$$\frac{\partial A}{\partial t} + \frac{\partial F}{\partial x} = 0 ,$$

where A and F are dependent variables. The finite difference representation is taken as

$$A(x, t+\Delta t) - \tfrac{1}{2}\left[A(x+\Delta x, t) + A(x-\Delta x, t)\right] = \frac{\Delta t}{2\Delta x}\left[F(x+\Delta x, t) - F(x-\Delta x, t)\right] .$$

With this scheme there are no explicit dissipative mechanisms such as heat conduction or viscosity, or a "q" term, yet the entropy change across the shock is correctly given. We have introduced chemical reaction and find that the scheme also enables us to solve unsteady detonation problems. One advantage this method has over the Richtmyer and von Neumann and the viscosity, heat conduction methods is that the computational time is appreciably less than either. This will be explained in further detail in Section IV. Just as the "q" method, the Lax

scheme arbitrarily limits the width of the shock front to several mesh thicknesses.

II. HYDRODYNAMIC EQUATIONS

A. Viscosity and Heat-Conduction Scheme

If we consider the irreversible first order chemical reaction

$$(2.1) \qquad [S] \longrightarrow [G] \,,$$

then the equations of one-dimensional unsteady flow of a viscous heat-conducting compressible fluid consisting of species [S] and [G] may be written in the Eulerian form

$$(2.2) \qquad \frac{1}{V}\frac{DV}{Dt} = \frac{\partial u}{\partial X}$$

$$(2.3) \qquad \frac{1}{V}\frac{Du}{Dt} = -\frac{\partial}{\partial X}\left(p - \frac{4}{3}\mu\frac{\partial u}{\partial X}\right)$$

$$(2.4) \qquad \frac{1}{V}\left(\frac{De}{Dt} + p\frac{DV}{Dt}\right) = \frac{\partial}{\partial X}\left(\lambda\frac{\partial T}{\partial X}\right) + \frac{4}{3}\mu\left(\frac{\partial u}{\partial X}\right)^2$$

$$(2.5) \qquad e = e\left(T, \omega\right)$$

$$(2.6) \qquad p = p\left(V, T, \omega\right)$$

$$(2.7) \qquad \frac{1}{\omega}\frac{D\omega}{Dt} = -Z\, e^{-\frac{E^{\ddagger}}{RT}}$$

$$\frac{D}{Dt} = \frac{\partial}{\partial t} + u\frac{\partial}{\partial X}$$

where $t, X, V, u, p, e, T, \omega, \mu, \lambda, E^{\ddagger}, Z$ and R are respectively the time, Eulerian position, specific volume, particle velocity, pressure, specific energy, temperature, mass fraction of species [S] , coefficient of viscosity, thermal conductivity, activation energy, frequency factor, and specific gas constant. Equations (2.2),(2.3),(2.4), (2.5),(2.6) and (2.7) are respectively the equations for the conservation of mass, momentum, and energy, and the caloric and thermal equations of state, and the chemical kinetic equation which governs the conversion of unreacted solid explosive [S] to product gas [G] . It will be assumed that $\mu, \lambda, E^{\ddagger}$, and Z are constants.

For one-dimensional problems it is more convenient to use the Lagrangean form of the hydrodynamic equations since they reveal where each particle of fluid came from initially and hence supplies more information than the Eulerian form. In addition shocks and moving contact discontinuities can be more easily followed, and mass is automatically conserved.

To transform to Lagrangean coordinates we let x denote the X-coordinate of a small fluid element at time $t = 0$ and $X = X(x,t)$ denote that same fluid element at $t > 0$, so that x and t are regarded as independent variables. In this new coordinate system Eqs. (2.2)-(2.7) are respectively

$$(2.8) \qquad \frac{\partial V}{\partial t} = V_0 \frac{\partial u}{\partial x}$$

$$(2.9) \qquad \frac{\partial u}{\partial t} = V_0 \frac{\partial}{\partial x}\left(\frac{4}{3}\mu \frac{V_0}{V} \frac{\partial u}{\partial x} - p\right)$$

$$(2.10) \qquad \frac{\partial e}{\partial t} = V_0 \left[\frac{\partial}{\partial x}\left(\lambda \frac{V_0}{V} \frac{\partial T}{\partial x}\right) + \left(\frac{4}{3}\mu \frac{V_0}{V} \frac{\partial u}{\partial x} - p\right)\frac{\partial u}{\partial x}\right]$$

$$(2.11) \qquad e = e(T, w)$$

$$(2.12) \qquad p = p(V, T, w)$$

$$(2.13) \qquad \frac{\partial w}{\partial t} = -Z\, w\, e^{-\frac{E^{\ddagger}}{RT}}$$

where x is the Lagrangean space coordinate and the subscript 0 will always refer to initial values which in this paper will be assumed to be constant. The value of the Eulerian position $X(x,t)$ is found from the relation

$$(2.14) \qquad \frac{\partial X}{\partial t} = u$$

The equations may be made non-dimensional by the transformations

$$(2.15) \qquad \begin{aligned} &u = U(p_0 V_0)^{\frac{1}{2}}, \quad V = GV_0, \quad p = P p_0, \quad e = E\, p_0 V_0, \quad T = \theta T_0, \\ &X = SL, \quad x = \xi L, \quad t = \frac{\tau L}{(p_0 V_0)^{\frac{1}{2}}}, \quad a = \frac{4\mu}{3L}\left(\frac{V_0}{p_0}\right)^{\frac{1}{2}}, \quad b = \frac{\lambda T_0}{p_0 L (p_0 V_0)^{\frac{1}{2}}} \\ &\nu = \frac{LZ}{(p_0 V_0)^{\frac{1}{2}}}, \quad \omega = \frac{E^{\ddagger}}{RT_0}, \end{aligned}$$

where L is a characteristic length. In non-dimensional form the new equations are

(2.16) $\quad \dfrac{\partial C}{\partial \tau} = \dfrac{\partial U}{\partial \xi}$

(2.17) $\quad \dfrac{\partial U}{\partial \tau} = \dfrac{\partial G}{\partial \xi} - \dfrac{\partial P}{\partial \xi}$

(2.18) $\quad \dfrac{\partial E}{\partial \tau} = \dfrac{\partial F}{\partial \xi} + (G-P)\dfrac{\partial U}{\partial \xi}$

(2.19) $\quad G = \dfrac{a}{C}\dfrac{\partial C}{\partial \tau}$

(2.20) $\quad F = \dfrac{b}{C}\dfrac{\partial \theta}{\partial \xi}$

(2.21) $\quad E = E(\theta, \omega)$

(2.22) $\quad P = P(C, \theta, \omega)$

(2.23) $\quad \dfrac{\partial \omega}{\partial \tau} = -\nu\omega\, e^{-\frac{\epsilon}{\theta}}$

(2.24) $\quad \dfrac{\partial S}{\partial \tau} = U.$

B.   Lax Scheme

If we utilize the Lax scheme then the non-dimensional Lagrangean equations for one-dimensional unsteady flow of a chemically reacting fluid are

(2.25) $\quad \dfrac{\partial C}{\partial \tau} = \dfrac{\partial U}{\partial \xi}$

(2.26) $\quad \dfrac{\partial U}{\partial \tau} = -\dfrac{\partial P}{\partial \xi}$

(2.27) $\quad \dfrac{\partial}{\partial \tau}\left(E + \dfrac{U^2}{2}\right) = -\dfrac{\partial}{\partial \xi}(PU)$

(2.28) $\quad E = E(\theta, \omega)$

(2.29) $\quad P = P(C, \theta, \omega)$

(2.30) $\quad \dfrac{\partial \omega}{\partial \tau} = -\nu \, \omega \, e^{-\frac{\omega}{\theta}}$

(2.31) $\quad \dfrac{\partial S}{\partial \tau} = U$

where Eq. (2.27) can be obtained from Eqs. (2.17) and (2.18) after setting $F \equiv 0$ and $G \equiv 0$.

C. Initial and Boundary Conditions

The initial conditions valid for $0 \le \xi \le 1$ are

(2.32)
$$C(\xi,0)=1 \,, \; P(\xi,0)=1 \,, \; \theta(\xi,0)=1 \,, \; \omega(\xi,0)=1 \,,$$
$$U(\xi,0)=0 \,, \; G(\xi,0)=0 \,, \; F(\xi,0)=0 \,, \; S(\xi,0)=\xi \,, \; E(\xi,0)=E_0$$

where E_0 is a constant which depends on the caloric equation of state, and the initial particle velocity is assumed to be zero.

The boundary conditions valid for $\tau > 0$ are

(2.33) $\quad U(0,\tau) = U^{(0)} \,, \quad U(1,\tau) = U^{(1)}$

(2.34) $\quad F(0,\tau) = 0 \,, \; F(1,\tau) = 0$

(2.35)
$$\begin{cases} \dfrac{\partial P}{\partial \xi} = 0 \,, \; \dfrac{\partial \theta}{\partial \xi} = 0 \,, \; \dfrac{\partial C}{\partial \xi} = 0 \,, \; \dfrac{\partial G}{\partial \xi} = 0 \\[2mm] \dfrac{\partial \omega}{\partial \tau} = -\nu \, \omega \, e^{-\frac{\omega}{\theta}} \\[2mm] E = E(\theta, \omega) \\[2mm] \dfrac{\partial S}{\partial \tau} = U \end{cases} \qquad \text{for } \xi = 0, 1$$

where $U^{(0)}$ and $U^{(1)}$ are taken to be constants. The boundary conditions, Eqs. (2.33) and (2.34), are prescribed while Eq. (2.35) are implied by Eqs. (2.33) and (2.34) and the differential equations (2.16)-(2.24). The boundary condition $U(1,\tau) = U^{(1)}$ corresponds to a piston, initially at a distance L from the left hand piston, moving with constant velocity $U^{(1)}$.

III. EQUATIONS OF STATE

When a detonation wave propagates in a solid explosive it converts the solid unreacted material [S] to gaseous detonation products [G]. It is therefore very necessary to describe these two states, and in fact all the intermediate states (which exist since the detonation is assumed not to take place instantaneously), by appropriate equations of state. This can be done in the following very simple manner if we assume that the specific energy and volume at any point vary linearly with the mass fractions of solid explosive and gaseous product, i.e.,

$$(3.1) \qquad V = \omega \tilde{V}_S + (1-\omega)\tilde{V}_G$$

$$(3.2) \qquad e = \omega \tilde{e}_S + (1-\omega)\tilde{e}_G$$

where $\tilde{V}_S$, $\tilde{e}_S$, $\tilde{V}_G$, and $\tilde{e}_G$ are the specific volume and energy for the pure solid and gas respectively. We now choose for the caloric and thermal equations of state of the unreacted explosive [S] and gaseous detonation products [G] the following:

$$(3.3) \qquad \tilde{e}_S = c_S T + \tilde{e}_S^*$$

$$(3.4) \qquad \tilde{e}_S = \tilde{e}_{S_0} + \frac{1}{\gamma_S-1}\left[(p+B)\tilde{V}_S - (p_0+B)\tilde{V}_{S_0}\right]$$

$$(3.5) \qquad \tilde{e}_G = c_G T + \tilde{e}_G^*$$

$$(3.6) \qquad \tilde{e}_G = \frac{p\tilde{V}_G}{\gamma_G-1} + \tilde{e}_G^*$$

where c_S and c_G are the specific heat capacities of the solid and gas respectively, $\tilde{e}_S^*$ and $\tilde{e}_G^*$ are the heats of formation, and γ_S, γ_G, and B are constants. The subscript o as usual refers to initial values. Eliminating $\tilde{e}_S$, $\tilde{e}_G$, $\tilde{V}_S$, and $\tilde{V}_G$ between the six equations Eqs. (3.1)-(3.6), and defining

$$(3.7) \qquad E^* = \frac{\tilde{e}_S^* - \tilde{e}_G^*}{p_0 V_0}, \beta = \frac{B}{p_0}, K = (\gamma_S-1)\frac{c_S T_0}{p_0 V_0}, L = (\gamma_G-1)\frac{c_G T_0}{p_0 V_0}$$
$$m = \frac{c_S - c_G}{p_0 V_0}T_0, n = \frac{c_G T_0}{p_0 V_0},$$

leads to the non-dimensional caloric and thermal equations of state

$$(3.8) \qquad E = (m\theta + E^*)\omega + n\theta$$

$$(3.9) \qquad C = \omega \,\frac{K(\theta-1)+1+\beta}{P+\beta} + (1-\omega)\,\frac{L\theta}{P} \,,$$

where $V_o \equiv \tilde{V}_{s_o}$ (since initially only explosive exists) and $\tilde{e}_s^{*o} - \tilde{e}_G^{*o}$ is the specific heat of reaction. It is of importance to recognize that Eqs. (3.8) and (3.9) give <u>different</u> relationships between energy and temperature, and pressure, volume, and temperature for <u>different</u> mixtures of the two chemical species [S] and [G] (i.e. for different values of ω).

The temperature θ can be eliminated between Eqs. (3.8) and (3.9) giving

$$(3.10) \qquad \frac{E-\omega E^*}{m\omega+n} = \frac{P(P+\beta)C - \omega(1+\beta-K)P}{(P+\beta)(1-\omega)L + \omega KP}$$

The local sound speed c can be defined by the thermodynamic identity

$$(3.11) \qquad \frac{c^2}{V^2} = P\,\frac{\partial P}{\partial e} - \frac{\partial P}{\partial V} = \frac{V_o}{P_o}\left(P\,\frac{\partial P}{\partial E} - \frac{\partial P}{\partial C}\right).$$

We then find

$$(3.12) \qquad P\,\frac{\partial P}{\partial E} - \frac{\partial P}{\partial C} = \begin{cases} \dfrac{PK}{C(m+n)} + \dfrac{1}{C}\left(1+\dfrac{\beta}{P}\right) & \text{if } \omega=1 \\[2ex] \dfrac{P}{C}\left(\dfrac{L}{n}+1\right) & \text{if } \omega=0 \end{cases}$$

$$(3.13) \qquad \frac{d\theta}{dE} = \begin{cases} \dfrac{1}{m+n} & \text{if } \omega=1 \\[2ex] \dfrac{1}{n} & \text{if } \omega=0 \,, \end{cases}$$

which are quantitites that will be needed in Section IV when we discuss the stability of the finite difference equations.

IV. FINITE DIFFERENCE EQUATIONS

A. Viscosity and Heat Conduction Scheme

In order to carry out the numerical solution of Eqs. (2.16)-(2.24), they must be replaced by an equivalent system of finite difference equations. The exact form of these equations is of course governed by stability considerations and a stability analysis as proposed by von Neumann must be carried out in order to verify that small errors will not grow during the computations. The following set of difference equations was used for the numerical calculations:

$$(4.1) \qquad C_j^{n+1} - C_j^n = \frac{\Delta \tau}{2\Delta\xi}\left(U_{j+1}^{n+1} - U_{j-1}^{n+1}\right) =$$

$$(4.2) \qquad U_j^{n+1} - U_j^n = \frac{\Delta \tau}{2\Delta\xi}\left[G_{j+1}^n - G_{j-1}^n - (P_{j+1}^n - P_{j-1}^n)\right]$$

$$(4.3) \qquad E_j^{n+1} - E_j^n = \frac{\Delta \tau}{2\Delta\xi}\left[F_{j+1}^n - F_{j-1}^n + (G_j^{n+1} - P_j^n)(U_{j+1}^{n+1} - U_{j-1}^{n+1})\right]$$

$$(4.4) \qquad G_j^{n+1} = \frac{a}{2\Delta\xi}\frac{1}{C_j^{n+1}}\left(U_{j+1}^{n+1} - U_{j-1}^{n+1}\right)$$

$$(4.5) \qquad F_j^{n+1} = \frac{b}{2\Delta\xi}\frac{1}{C_j^{n+1}}\left(\theta_{j+1}^{n+1} - \theta_{j-1}^{n+1}\right)$$

$$(4.6) \qquad \theta_j^{n+1} = \theta\left(E_j^{n+1}, \omega_j^{n+1}\right)$$

$$(4.7) \qquad P_j^{n+1} = P\left(C_j^{n+1}, \theta_j^{n+1}, \omega_j^{n+1}\right)$$

$$(4.8) \qquad \omega_j^{n+1} - \omega_j^n = -\frac{\nu\Delta\tau}{2}\left(\omega_j^{n+1} + \omega_j^n\right)e^{-\frac{\omega}{\theta_j^n}}$$

$$(4.9) \qquad S_j^{n+1} - S_j^n = \frac{\Delta\tau}{2}\left(U_j^{n+1} + U_j^n\right)$$

where we use the notation,

$$\xi = j\Delta\xi \quad, \quad j = 0, 1, 2, \cdots, J$$

$$\tau = n\Delta\tau \quad, \quad n = 0, 1, 2, \cdots,$$

$$U_{j-1}^{n+1} \equiv U\left(\xi - \Delta\xi, \tau + \Delta\tau\right) \quad, \text{ etc.}$$

For our particular problem, θ_j^{n+1}, and P_j^{n+1}, in Eqs. (2.21) and (2.22) are evaluated from Eqs. (3.8) and (3.9). The system, Eqs. (4.1)-(4.9), is as a whole correct to

$$O(\Delta\tau) + O(\Delta\xi^2)$$

, and the system is explicit provided the quantities are solved for in the proper order. If all the variables are known at $\tau = n\Delta\tau$ and there are boundary conditions at $j=0$ and $j=J$, then the values at the new time $\tau = (n+1)\Delta\tau$ can be computed in the following order:

$$U_j^{n+1}, S_j^{n+1}, C_j^{n+1}, G_j^{n+1}, E_j^{n+1}, \omega_j^{n+1}, \theta_j^{n+1}, F_j^{n+1}, P_j^{n+1}, \quad j = 2, 3, \cdots, J-1.$$

An analysis of the stability of Eqs. (4.1)-(4.9) has been carried out and the results indicate that in the normal region, i.e. the region where the viscosity, heat conduction, and chemical reaction are negligible, the solution is stable provided the following criterion is satisfied :

$$(4.10) \qquad \left[P_j^n \left(\frac{\partial P}{\partial E}\right)_j^n - \left(\frac{\partial P}{\partial C}\right)_j^n \right]^{\frac{1}{2}} \frac{\Delta\tau}{\Delta\xi} \le 2.$$

Here $\Delta\tau$ is the time step from τ^n to τ^{n+1}. The term in brackets has already been evaluated in Eq. (3.12). In the shock region, i.e. the region where the viscosity and/or heat conduction dominate and the chemical reaction is negligible, the stability criterion is

$$(4.11) \qquad \frac{\Delta\tau}{C_j^{n+1}(\Delta\xi)^2} \left[\frac{a}{2}\left(1 + \frac{C_j^n}{C_j^{n+1}}\right) + b\left(\frac{d\theta}{dE}\right)_j^{n+1} \right] \le 2.$$

In the detonation region, i.e. the region where the chemical reaction is so rapid such that a relative change in mass fraction of, say, 0.1 occurs in a time step which is negligible compared to the hydrodynamic time step as determined by Eqs. (4.10) or (4.11), the stability criterion is determined by the condition

$$(4.12) \qquad \omega_j^n - \omega_j^{n+1} \le \epsilon_n \omega_j^n \quad, \quad 0 < \epsilon_n < 1,$$

where ϵ_n is a small number which may depend on the time step if desired. This leads to the condition

$$(4.13) \qquad \Delta\tau \le \frac{2\epsilon_n}{(2-\epsilon_n)\nu} e^{\frac{\omega}{\theta_j^n}}.$$

A condition which appears to be sufficient to insure stability is

$$(4.14) \quad \Delta\tau \leq \min_{0 \leq j \leq J} \left\{ 2\Delta\xi \left(P_j^n \left(\frac{\partial P}{\partial E}\right)_j^n - \left(\frac{\partial P}{\partial C}\right)_j^n + \frac{1}{C_j^{n+1}(\Delta\xi)^2}\left[\frac{a}{2}\left(1 + \frac{C_j^n}{C_j^{n+1}}\right) + b\left(\frac{d\theta}{dE}\right)_j^{n+1}\right]^2 \right)^{-\frac{1}{2}}, \right.$$
$$\left. , \frac{2\epsilon_n}{(2-\epsilon_n)\nu} e^{\frac{\omega}{\theta_j^n}} \right\}$$

where the criteria for the normal and shock regions have been combined.

B.   Lax Scheme

The appropriate set of difference equations is

$$(4.15) \quad C_j^{n+1} - \tfrac{1}{2}\left(C_{j+1}^n + C_{j-1}^n\right) = \frac{\Delta\tau}{2\Delta\xi}\left(U_{j+1}^n - U_{j-1}^n\right)$$

$$(4.16) \quad U_j^{n+1} - \tfrac{1}{2}\left(U_{j+1}^n + U_{j-1}^n\right) = -\frac{\Delta\tau}{2\Delta\xi}\left(P_{j+1}^n - P_{j-1}^n\right)$$

$$(4.17) \quad E_j^{n+1} - \tfrac{1}{2}\left(E_{j+1}^n + E_{j-1}^n\right) + \tfrac{1}{2}\left[U_j^{n+1^2} - \tfrac{1}{2}\left(U_{j+1}^{n^2} + U_{j-1}^{n^2}\right)\right] = -\frac{\Delta\tau}{2\Delta\xi}\left(P_{j+1}^n U_{j+1}^n - P_{j-1}^n U_{j-1}^n\right)$$

$$(4.18) \quad \theta_j^{n+1} = \theta\left(E_j^{n+1}, \omega_j^{n+1}\right)$$

$$(4.19) \quad P_j^{n+1} = P\left(C_j^{n+1}, \theta_j^{n+1}, \omega_j^{n+1}\right)$$

$$(4.20) \quad \omega_j^{n+1} - \tfrac{1}{2}\left(\omega_{j+1}^n + \omega_{j-1}^n\right) = -\nu\Delta\tau \; \omega_j^n \; e^{-\frac{\omega}{\theta_j^n}}$$

$$(4.21) \quad S_j^{n+1} - \tfrac{1}{2}\left(S_{j+1}^n + S_{j-1}^n\right) = \Delta\tau \; U_j^n.$$

The stability criterion valid everywhere is

$$(4.22) \quad \left[P_j^n \left(\frac{\partial P}{\partial E}\right)_j^n - \left(\frac{\partial P}{\partial C}\right)_j^n\right]^{\frac{1}{2}} \frac{\Delta\tau}{\Delta\xi} \leq 1.$$

If $\Delta\tau$ as chosen by Eq. (4.22) makes $\omega_j^{n+1} < 0$, set $\omega_j^{n+1} = 0$.

Comparing Eqs. (4.14) and (4.22), it is seen that the Lax scheme allows for the use of much larger time steps, since Eq. (4.11) is a much more restrictive criterion than Eq. (4.10) when shocks are present.

C. Initial and Boundary Conditions

The initial conditions valid for $j = 0, 1, 2, \cdots, J$ are

$$(4.23) \quad C_j^0 = P_j^0 = \theta_j^0 = \omega_j^0 = 1, \quad U_j^0 = G_j^0 = F_j^0 = 0, \quad S_j^0 = j\Delta\xi, \quad E_j^0 = m + n + E^*$$

The boundary conditions valid for $n > 0$ are

$$U_0^n = U^{(0)}, \quad U_J^n = U^{(1)}$$

$$F_0^n = F_J^n = 0$$

$$P_0^n = \frac{1}{11}\left(18 P_1^n - 9 P_2^n + 2 P_3^n\right), \quad P_J^n = \frac{1}{11}\left(18 P_{J-1}^n - 9 P_{J-2}^n + 2 P_{J-3}^n\right)$$

$$\theta_0^n = \frac{1}{11}\left(18 \theta_1^n - 9 \theta_2^n + 2 \theta_3^n\right), \quad \theta_J^n = \frac{1}{11}\left(18 \theta_{J-1}^n - 9 \theta_{J-2}^n + 2 \theta_{J-3}^n\right)$$

$$(4.24) \quad C_0^n = \frac{1}{11}\left(18 C_1^n - 9 C_2^n + 2 C_3^n\right), \quad C_J^n = \frac{1}{11}\left(18 C_{J-1}^n - 9 C_{J-2}^n + 2 C_{J-3}^n\right)$$

$$G_0^n = \frac{1}{11}\left(18 G_1^n - 9 G_2^n + 2 G_3^n\right), \quad G_J^n = \frac{1}{11}\left(18 G_{J-1}^n - 9 G_{J-2}^n + 2 G_{J-3}^n\right)$$

$$\omega_0^n = \omega_0^{n-1} - \frac{1}{2}\nu\Delta\tau\left(\omega_0^n + \omega_0^{n-1}\right)e^{-\frac{\omega}{\theta_0^{n-1}}}, \quad \omega_J^n = \omega_J^{n-1} - \frac{1}{2}\nu\Delta\tau\left(\omega_J^n + \omega_0^{n-1}\right)e^{-\frac{\omega}{\theta_0^{n-1}}}$$

$$E_0^n = \left(m\theta_0^n + E^*\right)\omega_0^n + n\theta_0^n, \quad E_J^n = \left(m\theta_J^n + E^*\right)\omega_J^n + n\theta_J^n$$

$$S_0^n = S_0^{n-1} + \frac{1}{2}\Delta\tau\left(U_0^n + U_0^{n-1}\right), \quad S_J^n = S_J^{n-1} + \frac{1}{2}\Delta\tau\left(U_J^n + U_J^{n-1}\right).$$

P_0^n is obtained by expanding P_1^n, P_2^n, and P_3^n in a Taylor series about the point P_0^n and keeping terms up to $O(\Delta\xi^3)$. We then solve for $\left(\frac{\partial P}{\partial\xi}\right)_0^n$ in terms of P_0^n, P_1^n, P_2^n, P_3^n and then set $\left(\frac{\partial P}{\partial\xi}\right)_0^n = 0$ to give the desired result. In similar manner we obtain P_J^n, θ_0^n, θ_J^n, C_0^n, C_J^n, G_0^n, and G_J^n.

V. SAMPLE CALCULATIONS

In order to demonstrate the feasibility of carrying out the solution of one-dimensional flow problems involving detonation waves by the proposed techniques, sample calculations were performed. In all the calculations the following data were used:

$$J = 100 \; ; \; U_J^n = 0 \; , \; n = 0, 1, \cdots$$

Inert and unreacted explosive: $\beta = 10^5$, $K = 2.4584 \times 10^4$,

$$L = 2.00688 \times 10^4, \; m = -3.01032 \times 10^3,$$

$$\eta = 1.00344 \times 10^4$$

Explosive: $\omega = 50$, $E^{\ast} = 3.92997 \times 10^4$

The initial conditions are given by Eqs. (4.23). The boundary condition $U_J^n = 0$ corresponds to a rigid wall at a distance L from the initial position of the left hand piston.

Case 1

Type of problem: Shock in a chemically inert material.

Boundary conditions: $U_0^n = 198.241$, $n > 0$

Constants: $a = 10$, $b = 0$, $\nu = 0$

A chemically inert material is contained by a moving piston and a rigid wall.

Case 2

Type of problem: Shock initiation to detonation at inert-explosive interface.

Boundary conditions: $U_0^n = 119.101$, $n > 0$

Constants: $a = 10$, $b = 0$, $\nu = \begin{cases} 0 & \text{if} \quad 0 \le j \le 29 \\ 10^{14} & \text{if} \quad 30 \le j \le 100 \end{cases}$

The situation depicted here corresponds to a composite material of identical equation of state and physical properties, where the chemically inert material lies in the region $0 \le \xi < 0.3$, and the explosive is contained in $0.3 \le \xi \le 1$. A piston moves with constant velocity into the inert, and a rigid wall contains the explosive.

548

Enig

Case 3

Type of problem: Shock initiation to detonation near
inert-explosive interface.

Boundary conditions: $U_0^n = 119.101$, $n > 0$

Constants: $a = 4$, $b = 5 \times 10^4$, $\nu = \begin{cases} 0 & \text{if} \quad 0 \leq j \leq 29 \\ 5 \times 10^{12} & \text{if} \quad 30 \leq j \leq 100 \end{cases}$

Case 4

Type of problem: Shock initiation to detonation near
inert-explosive interface.

Boundary conditions: $U_0^n = 119.101$, $n > 0$

Constants: $a = 4$, $b = 5 \times 10^4$, $\nu = \begin{cases} 0 & \text{if} \quad 0 \leq j \leq 29 \\ 10^{14} & \text{if} \quad 30 \leq j \leq 100 \end{cases}$

Case 5

Type of problem: Shock initiation to detonation at inert-
explosive interface.

Boundary conditions: $U_0^n = \begin{cases} 119.101 & \text{if} \quad \tau \leq 0.000896 \\ 0 & \text{if} \quad \tau > 0.000896 \end{cases}$

Constants: $a = 10$, $b = 0$, $\nu = \begin{cases} 0 & \text{if} \quad 0 \leq j \leq 38 \\ 5 \times 10^{12} & \text{if} \quad 39 \leq j \leq 100 \end{cases}$

A piston moves with constant velocity into the inert
and after a finite time is suddenly stopped.

Case 6 (Lax Scheme)

Type of problem: Shock initiation to detonation in an
explosive.

Boundary conditions: $U_0^n = 198.241$

A piston moves with constant velocity into a solid
explosive which is confined by the piston and a rigid
wall.

In computations involving the use of viscosity or
heat conduction, the use of realistic values for the
transport phenomena demand that the characteristic mesh
size used in the numerical solution be of the order of
the shock thickness in gases [4] or a few angstroms in
solids. Since this is impossible for practical problems,
then μ and λ must be made larger by at least several

549

orders of magnitude if the mesh width is to take on reasonable size. It has been found experimentally (numerical experimentation, that is!) that for the equations of state used here, the values of a and b that lead to stable shocks are approximately of $O(10)$ and $O(10^5)$ respectively.

For the piston velocity given in Case 1 we compute the steady state values behind the shock, shown in Fig. 2, to be $P \simeq 1.35 \times 10^5, C \simeq 0.712$, $\theta \simeq 3.68$. These compare with the values $P_H = 1.36864 \times 10^5, C_H = 0.712727, \theta_H = 3.79754$ which are obtained from the solution of the Rankine-Hugoniot equations. Actually the values very close to the piston are not those quoted above but we find that C and θ are about 10% and 19% too large respectively. This type of behavior is also common to the "q" method and can be readily understood when it is noted that a linear or quadratic viscosity term gives rise to an abnormally high energy production in the region of a velocity discontinuity. Notice that in Case 1, $\lambda = 0$.

In Case 2, where the thermal conductivity is equal to zero, the first explosive particle that is heated by the steady shock crossing the interface must go to complete reaction first. This is clearly shown in Fig. 3. The value of ν is sufficiently large so that reaction starts and goes to completion in the shock region. The detonation progresses to the right while a shock travels back into the inert.

In Case 3 the value of ν is chosen so that appreciable chemical reaction starts only after the entire shock zone has heated the explosive particle. While the interface is first to react, heat conduction to the inert soon controls the temperature rise and complete reaction first occurs at some interior explosive particle. The pressure here goes up to about 1.3×10^5 at $\tau = 0.00130296$ as shown in Fig. 4. A rarefaction wave lowers the pressure at that point as shocks move toward the right and left. The latter shocks compress and bring about complete reaction of the neighboring partially reacted explosive particles which go to higher pressures. Hence the pressure curves contain a valley, a situation which did not occur in Case 2 where $\lambda = 0$.

Having $\lambda \neq 0$ in Case 3 has an effect on the steady state values of the inert particles near the piston in a pure shock. The Rankine-Hugoniot equations lead to the values $P_H = 6.19202 \times 10^4$, $1/C_H = 1.29716$, $\theta_H = 2.00978$, for the dimensionless piston velocity $U_H = 119.101$. Comparing

550

Case 1

On each curve the dots when read from left to right are the mass particles labeled j = 0,2,4,....
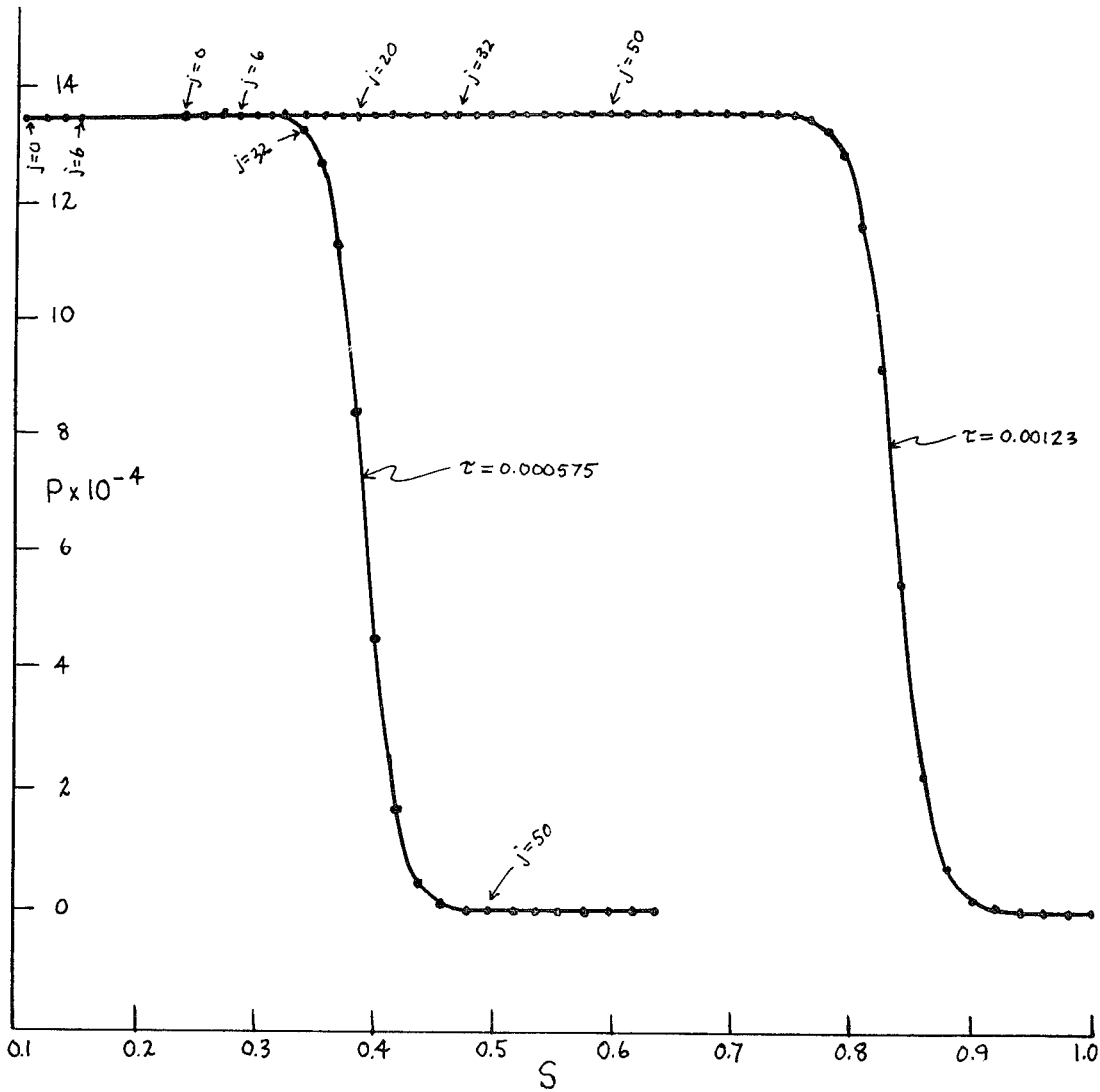
Figure 2.   Pressure P vs. Eulerian position S for various values of the time τ .

Case 2

On each curve the dots when read from left to right are the mass particles labeled $j = 0,2,4,\ldots$.
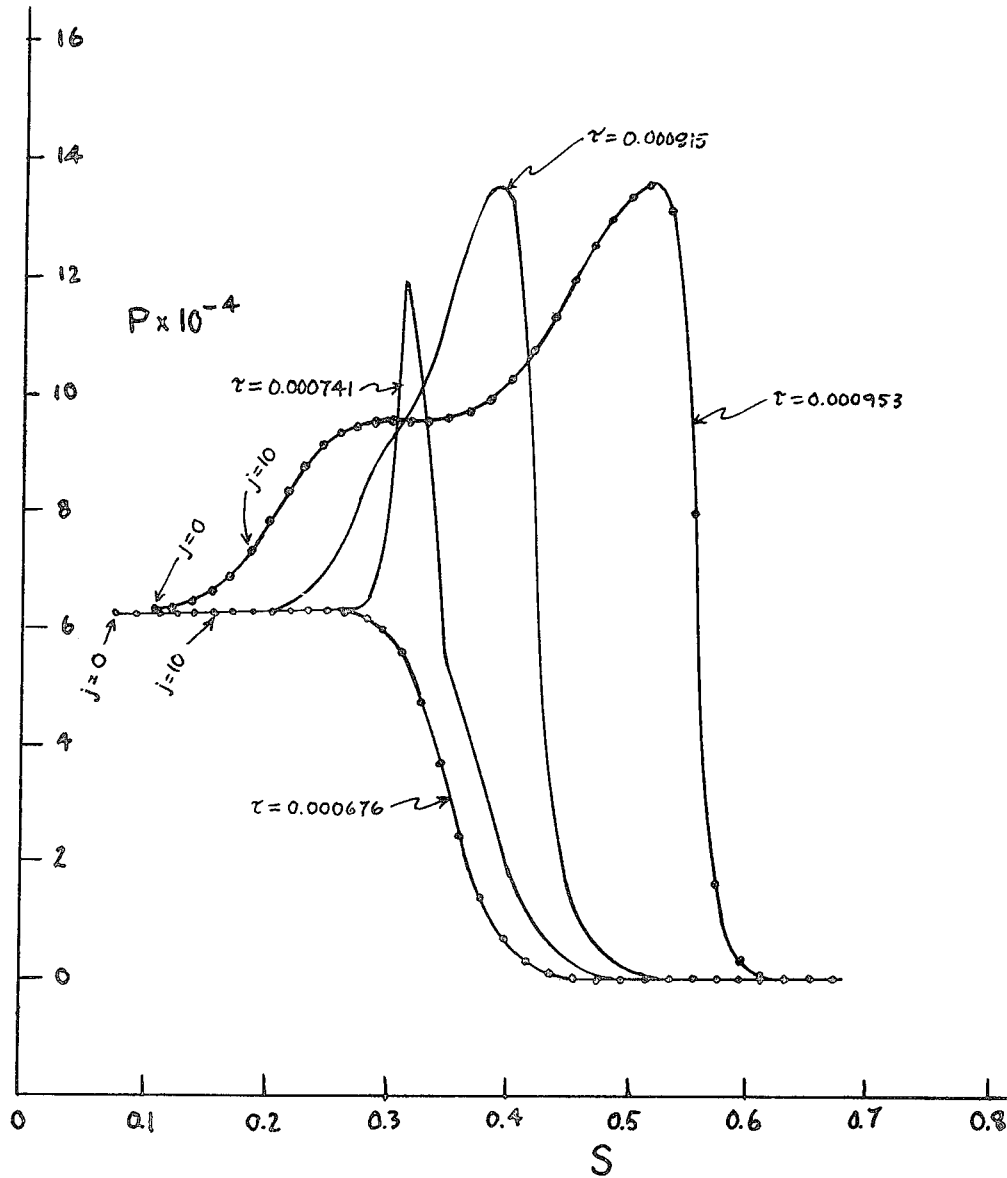
Figure 3. Pressure P vs. Eulerian position S for various values of the time τ .

Case 3

On each curve the dots when read from left to
right are the mass particles labeled J = 0,2,4,....
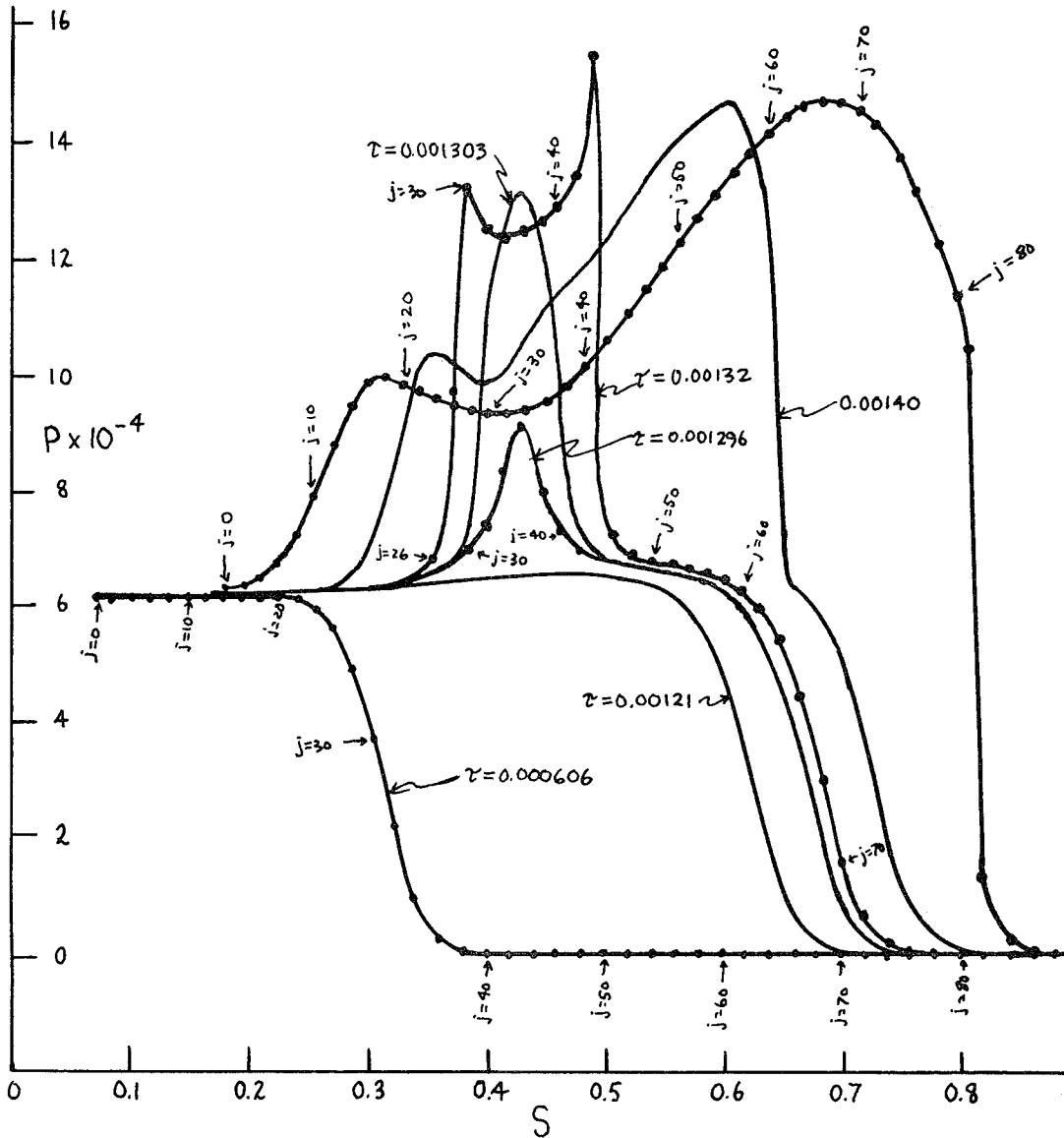
Figure 4.   Pressure P vs. Eulerian position S for various
values of the time τ .

these values with computed values for the shock profile shown in Table I, we see that even in the region of piston, there is very good agreement in contrast with what is found when $\lambda = 0$. This can be explained as follows. We have already noted that the viscosity terms lead to abnormally high energies in the neighborhood of a velocity discontinuity. These high energy gradients can be considered, by use of the caloric equation of state, as abnormally high thermal gradients which in turn tend to remove the excess energy by heat conduction to the colder regions. Therefore while the temperature gradients are also falsified, they tend to compensate for the viscosity effect. By proper adjustment of the values of a and b, the correct values for the state variables can be found near the piston. Finding the correct value of the temperature near the piston is very important for problems where the piston strikes a highly temperature-sensitive explosive surface directly. For if the temperature is falsified in the direction of too high a value, as is done when we let $\lambda = 0$, or even more so when the "q" method is used, then detonation may occur when in reality the shock temperature is not sufficient to cause it.

Comparison of Figs. 4 and 5 representing Cases 3 and 4 respectively shows the effect of increasing the value of ν so that complete reaction takes place in the shock zone. In Case 4 the reaction zone (i.e., the zone where

$0.001 \leq \omega \leq 0.999$) is never spread out over more than five or six particles. For Case 3, by the time the computation has reached $\tau = 0.00144109$ (see Fig. 4), the reaction zone

has been compressed to encompass two particles. Initially it was very much larger as can be seen from Table II where the mass fraction of unreacted explosive ω at different particle numbers j is given for different values of τ. Those points j such that $0 < \omega_j^n < 1$ and that lie to the right of the zone of complete reaction, are in the shock zone.

In Case 5 the head of the centered rarefaction wave reached the interface at the time the latter had already undergone about 5% reaction ($\omega(0.4, 0.0012) = 0.952$). The reaction was already extremely rapid so that it could not be quenched by the rarefaction wave. The interaction of the rarefaction wave and the detonation wave during the initial stages of growth of the latter is shown in Fig. 6.

In Case 6 we have extended the Lax scheme to detonation problems. The value of $\nu = 10^8$ is sufficiently small so that as the shock travels through the explosive, the

TABLE I

Case 3 at $\gamma = 0.000606$, time cycle $n=60$

j	S_j^{60}	$1/C_j^{60}$	$10^2 U_j^{60}$	θ_j^{60}	$10^4 P_j^{60}$
0	.0714	1.304	1.191	1.992	6.1634
2	.0869	1.298	1.192	1.995	6.1632
4	.1023	1.296	1.193	2.003	6.1632
6	.1178	1.294	1.194	2.011	6.1631
8	.1332	1.292	1.194	2.019	6.1635
10	.1487	1.291	1.193	2.023	6.1639
12	.1642	1.291	1.193	2.024	6.1648
14	.1796	1.291	1.193	2.023	6.1655
16	.1951	1.292	1.192	2.019	6.1643
18	.2106	1.293	1.192	2.014	6.1571
20	.2260	1.293	1.189	2.007	6.1335
22	.2415	1.291	1.181	1.995	6.0694
24	.2570	1.284	1.160	1.971	5.9124
26	.2727	1.268	1.111	1.921	5.5607
28	.2886	1.236	1.008	1.818	4.8552
30	.3051	1.182	.818	1.633	3.6656
32	.3225	1.113	.538	1.376	2.1632
34	.3409	1.054	.267	1.155	.9433
36	.3603	1.020	.102	1.047	.3217
38	.3800	1.006	.032	1.011	.0939
40	.4000	1.001	.009	1.002	.0249
42	.4200	1.000	.002	1.000	.0062
44	.4400	1.000	.000	1.000	.0015
46	.4600	1.000	.000	1.000	.0004
48	.4800	1.000	.000	1.000	.0001
50	.5000	1.000	.000	1.000	.0001
100	1.0000	1.000	.000	1.000	.0001

Case 4

On each curve the dots when read from left to
right are the mass particles labeled $j = 0, 2, 4, \ldots$.
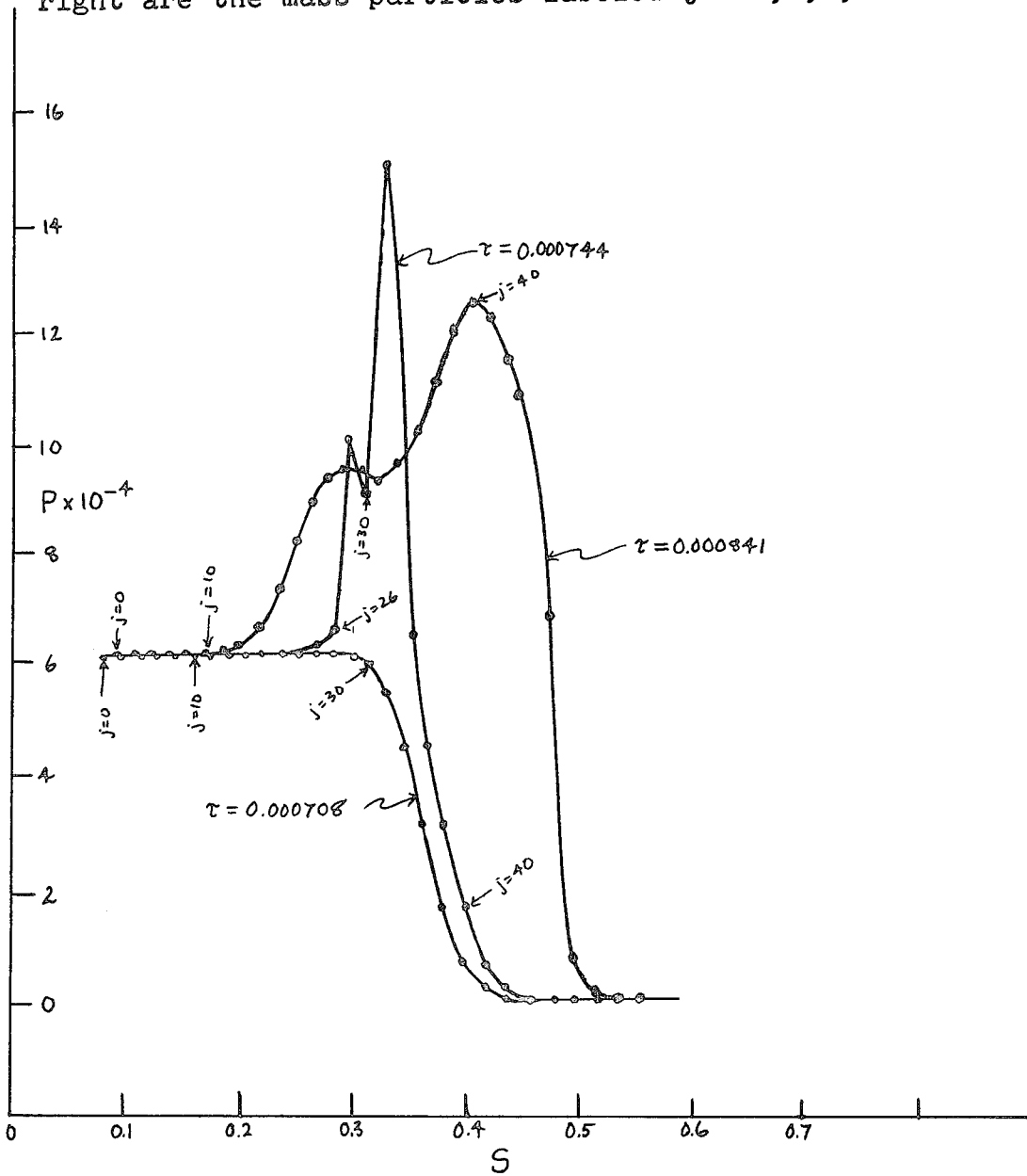
Figure 5. Pressure P vs. Eulerian position S for various
values of the time τ.

TABLE II

Size of the Reaction Zone for Different Values of τ for Case 3

j	ω_j^{90}	ω_j^{110}	ω_j^{120}	ω_j^{130}	ω_j^{140}	ω_j^{160}	ω_j^{230}	ω_j^{330}	ω_j^{360}	ω_j^{410}
28	1.000	1.000	1.000	1.000	1.000	1.000	1.000	1.000	1.000	1.000
30	.985	.961	.941	.898	.897	.886	0	0	0	0
32	.988	.962	.936	.842	.837	.664	0	0	0	0
34	.991	.966	.937	.728	.547	0	0	0	0	0
36	.994	.971	.943	.649	0	0	0	0	0	0
38	.996	.976	.951	.789	.743	0	0	0	0	0
40	.998	.981	.960	.874	.869	.734	0	0	0	0
42	.999	.985	.967	.915	.914	.897	0	0	0	0
44	.999	.989	.974	.939	.939	.932	.933	0	0	0
46	1.000	.993	.980	.955	.955	.951	.954	0	0	0
48	.	.996	.985	.966	.966	.964	.967	0	0	0
50	.	.998	.990	.975	.975	.973	.976	0	0	0
52	.	.999	.994	.982	.982	.981	.983	0	0	0
54	.	.999	.996	.988	.988	.987	.989	0	0	0
56	.	1.000	.998	.992	.992	.991	.993	.490	0	0
58	.	.	.999	.996	.996	.995	.996	.984	0	0
60	.	.	.999	.998	.998	.998	.998	.990	0	0
62	.	.	1.000	.999	.999	.999	.999	.994	0	0
64	.	.	.	.999	.999	.999	.999	.997	.735	0
66	.	.	.	1.000	1.000	1.000	1.000	.999	.995	0
68	.	.	.	.	.	.	.	.999	.998	0
70	.	.	.	.	.	.	.	1.000	.999	0
72	.	.	.	.	.	.	.	.	.999	.817
74	.	.	.	.	.	.	.	.	1.000	.999
..	.	.	.	.	.	.	.	.	.	1.000

where

$\tau^{90} = 0.000909$
$\tau^{110} = 0.001111$
$\tau^{120} = 0.001120$
$\tau^{130} = 0.001212$
$\tau^{140} = 0.0012965$
$\tau^{140} = 0.0012970$
$\tau^{160} = 0.001303$
$\tau^{230} = 0.001320$
$\tau^{330} = 0.001376$
$\tau^{360} = 0.001404$
$\tau^{420} = 0.001441$

Case 5

On each curve the dots when read from left to
right are the mass particles labeled j = 0,2,4,....
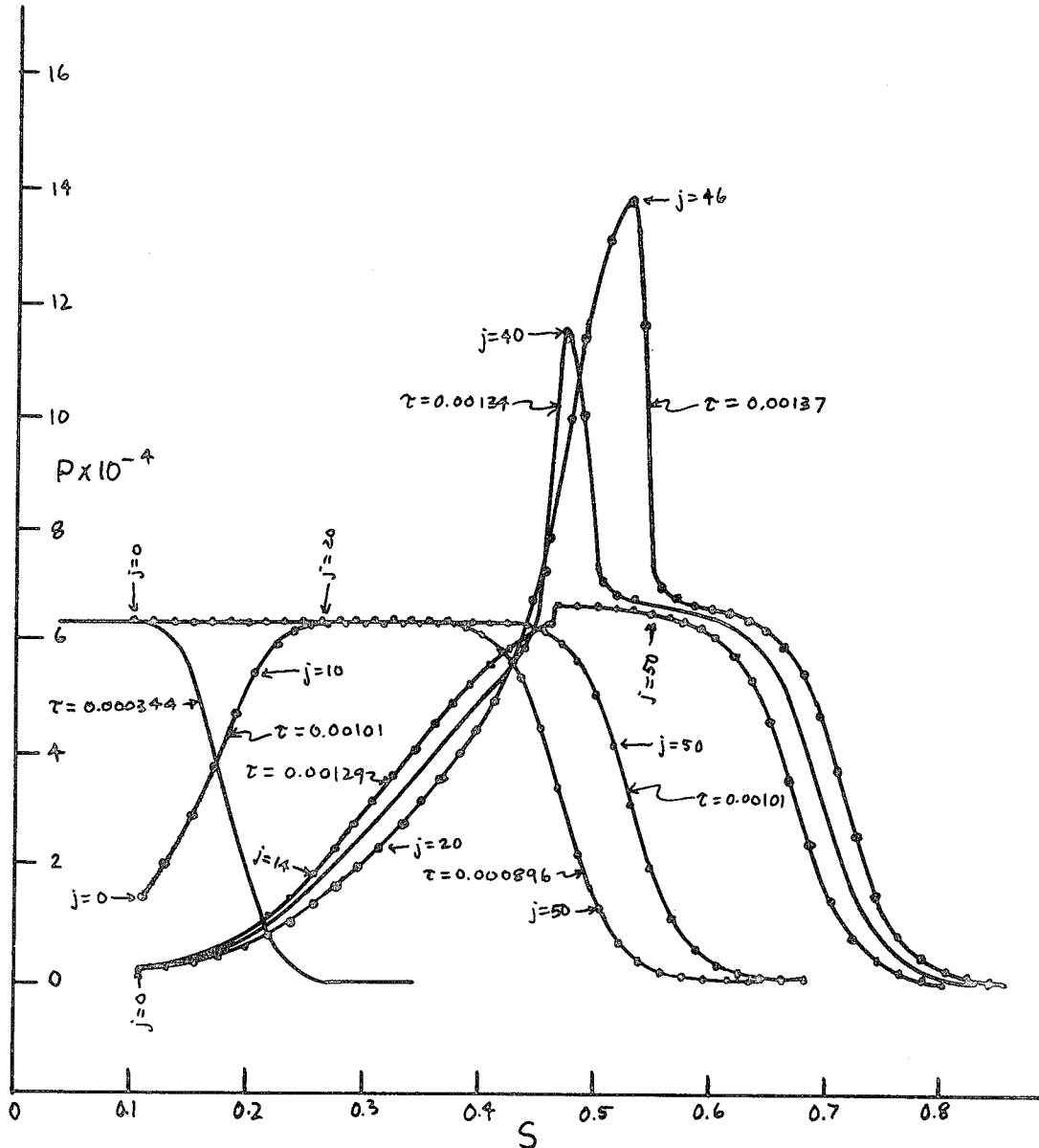
Figure 6.   Pressure P vs. Eulerian position S for various
values of the time τ .

chemical reaction behind the shock zone is quite slow.
Eventually a high pressure region of reaction forms ahead
of the piston and well behind the shock front as is shown
in Fig. 7. This high pressure region rapidly catches up
to the shock front during the transition to steady state.
The detonation wave is reflected off the rigid wall as a
shock since all of the explosive has already been converted
to detonation products. The steady state values for the
dimensionless density, temperature, and pressure are 1.34,
6.15, and 1.66×10^5 respectively. These compare with the
Chapman-Jouguet values of 1.333, 5.87 and 1.569×10^5. It
is felt that the correspondence between the two sets of
values can be further improved by a more judicious choice
of the finite difference representation of the boundary
conditions for the Lax scheme.

Concerning the question of critical time necessary
for growth from initiation to detonation, all our numerical
calculations indicate that for one-dimensional problems if
as little as one or two percent of the explosive has re-
acted, then a detonation wave will be established and will
not be quenched by any reasonably strong rarefaction waves
which may appear on the scene. Just as has been found by
Hubbard and Johnson [2], we find that for very temperature
sensitive reactions the time necessary to react the major
portion of the explosive is small compared to the hydro-
dynamic time step necessary to influence motion.

ACKNOWLEDGMENT

Case 6
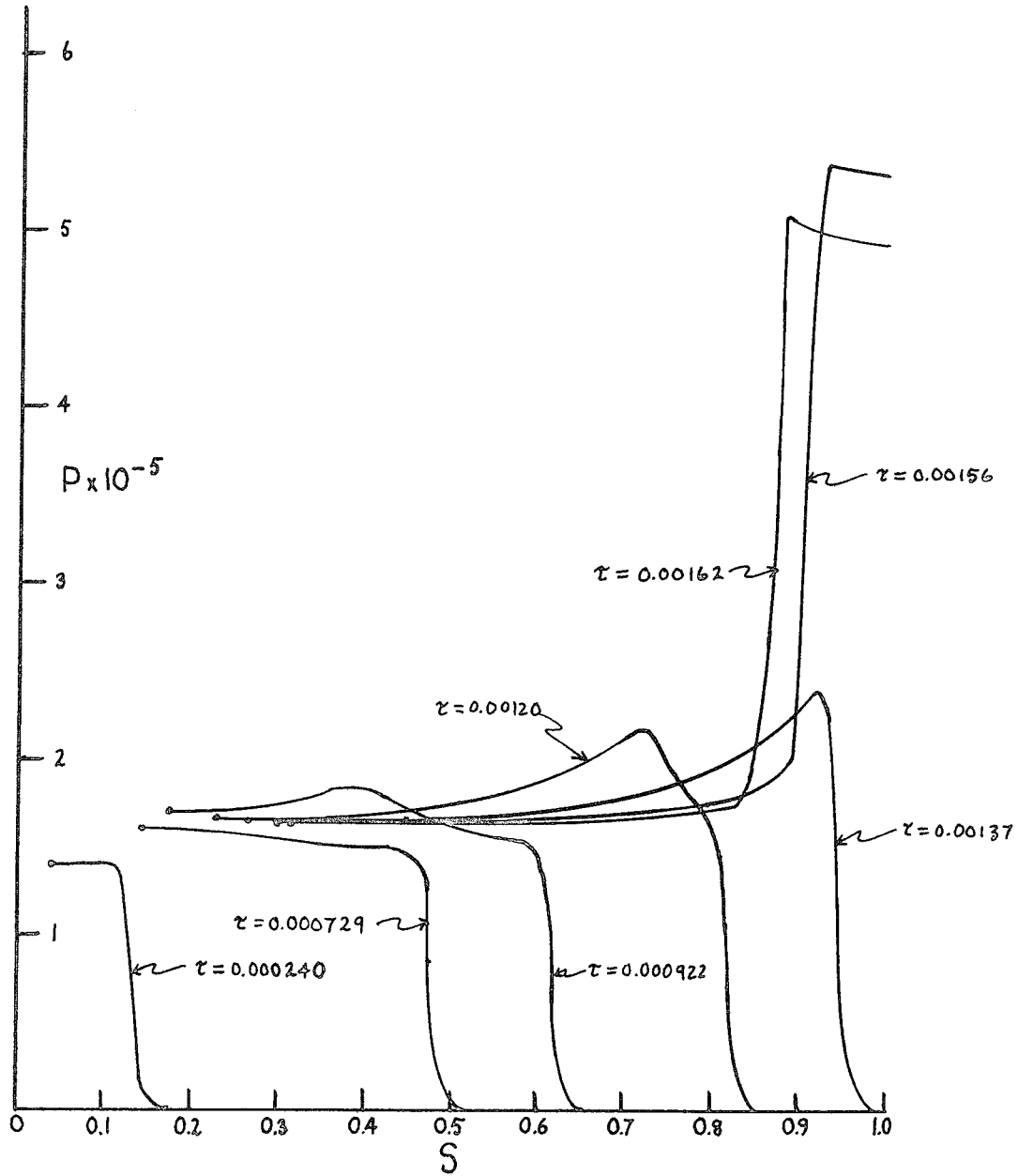
Figure 7.   Pressure P vs. Eulerian position S for various
values of the time τ .

REFERENCES

1. J. O. Hirschfelder and C. F. Curtiss, J. Chem. Phys., <u>28</u>, 1130 (1958).

2. H. W. Hubbard and M. H. Johnson, J. Appl. Phys., <u>30</u>, 765 (1959).

3. J. von Neumann and R. D. Richtmyer, J. Appl. Phys., <u>21</u>, 232 (1950).

4. G. Ludford, H. Polachek and R. J. Seeger, J. Appl. Phys., <u>24</u>, 490 (1953).

5. R. Courant and K. O. Friedrichs, "Supersonic Flow and Shock Waves", (Interscience Publishers, New York, 1948).

6. J. von Neumann, O.S.R.D., Rept. No. 549 (1942).

7. W. Döring, Ann. Physik, <u>43</u>, 421 (1943).

8. Y. B. Zeldovitch, J. Expt. Theoretical Phys. (USSR), <u>10</u>, 542 (1940).

9. P. Lax, Comm. Pure and Appl. Math, <u>7</u>, 159 (1954).

INITIATION OF A LOW-DENSITY PETN PRESSING BY A PLANE SHOCK WAVE*

G. E. Seay and L. B. Seely, Jr.
Los Alamos Scientific Laboratory
Los Alamos, New Mexico

The initiation of explosives by shocks has been studied most extensively by means of various gap sensitivity tests (1-3) where in general the geometry is somewhat complicated. Usually such tests employ non-planar shocks with large pressure gradients behind the front, and give results only in terms of the maximum thickness of the gap material which can cause detonation of the explosive. In principle, however, it should be possible to define the conditions of the initiating shock in the explosive itself (4,5). Tests in plane geometry, which can be designed for easier characterization of the shock, have been made on homogeneous explosives (6,7) and on high density solid explosives (8,9). For explosives pressed or cast to high densities, the importance of the discontinuities in the material is not in every case clear, there being some evidence that the type of initiation and even the mode of propagation change as the density approaches that of the crystal. Our interest lies in the sensitivity of granular explosives pressed to low densities, where the spaces between the particles constitute a large fraction of the total volume of the pressing. Here the interstitial gases or the discontinuities might be expected to play an important part in the initiation process. We have conducted tests on granular PETN pressed to a density of 1.0 gm/cm^3, corresponding to about 44% voids in the pressing. It is the purpose of this paper to present our first results and to discuss some of the difficulties involved in characterizing shocks in pressings of this density.

EXPERIMENTAL

The experiments were carried out on wedge-shaped (6,9) PETN charges using a streak camera to record the initiation phenomena. A shock was produced by a special plane-detonation-wave generator and reduced to the proper pressure by means of impedance mismatching in an attenuator system. The surface of the attenuator, on which the wedge was placed, was illuminated by an explosive argon flash (10-12) so that the time of entry of the shock into the wedge could be determined from the start of motion of the attenuator surface. The appearance of first light from the PETN was taken to indicate the onset of detonation. Thus, we could determine the average velocity of the initiating disturbance and the distance it traveled into the charge before the detonation became apparent.

The Shock System

It is possible to initiate explosives by means of a shock wave whose front has almost any shape in space and for which the pressure in the region behind the front drops in almost any way with time, but in general these characteristics of the wave are expected to affect the peak pressure necessary for initiation. For simplicity we desired a plane shock front followed by a constant-pressure region for the duration of the experiment, and in fact close approximations to both of these ideals were achieved. The shock system is sketched in Fig. 1.
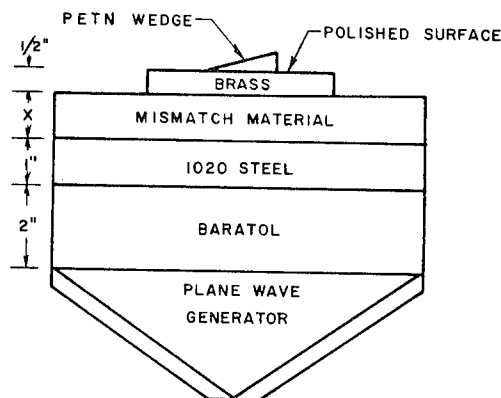
Fig. 1   Charge Arrangement for
PETN Wedge Experiments.

An 8" diameter plane wave generator of the type described by J. H. Cook (13) was used to form a detonation wave which was plane to about ±0.12 mm. Since a comparatively low pressure is sufficient to initiate PETN, 76/24 $Ba(NO_3)_2$/TNT (Baratol), which has a detonation pressure of about 140 kb, was used for the main charge. A one-inch thickness of SAE 1020 steel was placed on the Baratol. On this was placed a mismatch material, usually Lucite, in which the wave produced a pressure of about 30 kb. The next component in the attenuator was

563

brass (60.6% Cu, 39.3% Zn), in which a pressure of about 60 kb was produced. The PETN wedge sat on the surface of this brass, but, because of the mismatch at the brass-PETN interface, the pressure in the wedge was only a few kilobars.

Various attenuators, designed on this general plan, were evaluated in detail by use of an optical method for the measurement of free surface motion developed by Craig and Davis (14). As shown in Fig. 2, a wire (or other object with a well-defined edge) is placed above the surface to be measured and viewed at an angle with a streak camera. The surface is illuminated by an argon flash so that the wire and its image on the polished surface can be photographed. When the surface begins to move in the direction of the shock, the virtual image behind the surface will appear to move across the camera slit toward the wire. If we know the magnification M, the camera angle θ, and the angle α which the moving image makes with the wire on the film, then the free surface velocity is

$$U_{fs} = \frac{U_c \tan \alpha}{2M \sin \theta}$$

where U_c is the camera writing speed. Imperfections on the polished surface move at one-half the speed of the image of the wire, and can sometimes be used for measurements. Traces of such imperfections will show sudden bends at the onset of free surface motion, and, when there are many of them across the surface, they can be used to examine the planarity of the shocks.

By use of the quite accurate approximation (15) that the particle velocity U_p in the brass is one-half the measured free surface velocity U_{fs}, the shock pressure P in the brass plate was deduced from the published data on the Hugoniot for brass (16). It can be assumed that in most practical shock systems the pressure will drop to some extent behind the shock front. Such a falling pressure contour should produce a gradual lowering of the peak pressure as the wave progresses through a material. However, measurements of the free surface velocity for thicknesses of brass between 1/4" and 3/4" showed no detectable change. This indicated that the falloff in pressure produced a free surface velocity effect that lay within our experimental reproducibility, and from this we have estimated that the pressure decreased less than 4% as it travelled through this 1/2" thickness of brass.

The peak pressure was varied by changing the mismatch material or, when using Lucite, by changing its thickness. The thickness method of adjusting the pressure probably depends on the existence of the pressure drop postulated above.
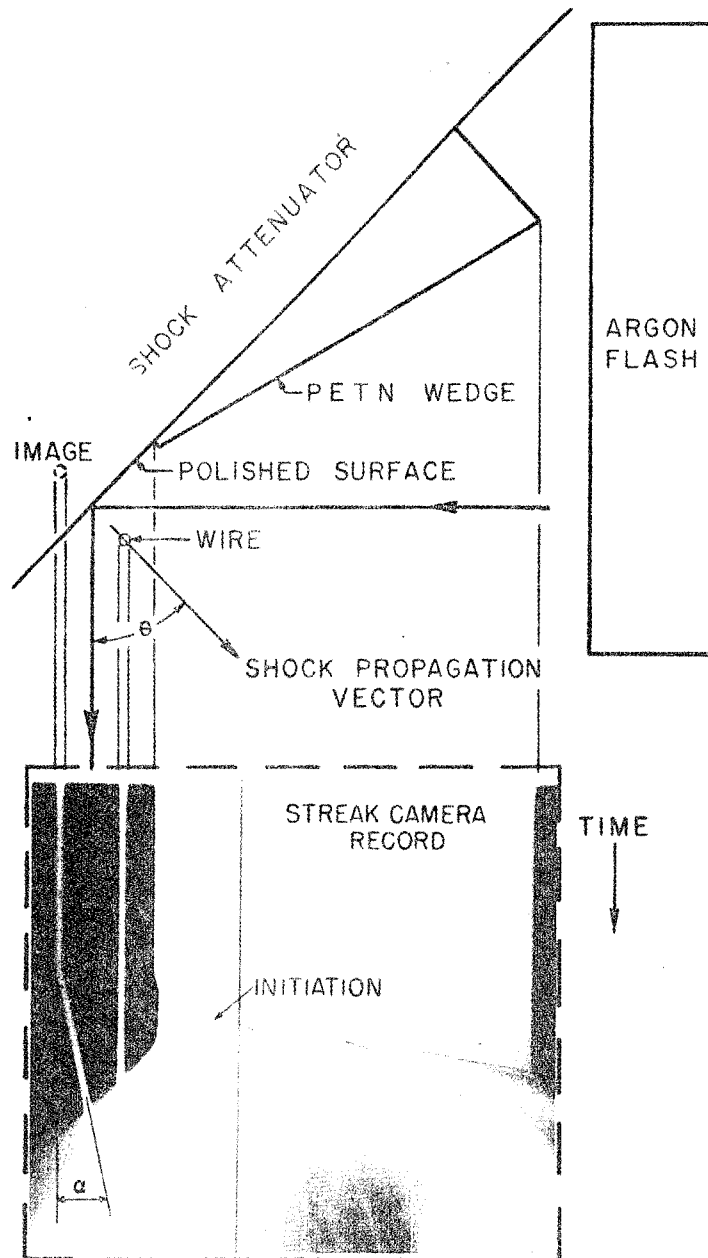
Fig. 2 Diagram of the Experimental Arrangement. A streak camera
record, printed as a negative, has been positioned so as
to show corresponding features. A wire and its image in
the polished brass surface are used to determine the free
surface velocity. The irregular line on the part of the
film corresponding to wedge-face is the detonation.
Irregularities are ascribed to uneven initiation across
the surface of the shock within the PETN pressing.

Explosives

In order to perform experiments at low density by the wedge technique it was necessary to obtain an explosive in a crystal form that would press easily to a reasonably uniform density and produce a pressing strong enough to permit shaping and handling. We also wished to pick a material that could be or had been studied (6) in the form of homogeneous large crystals. We believed there would be some advantage in using low shock strengths so that the contrast with the single crystal work would be striking. The sensitivity of low density PETN pressings recommended them on this score. There is a considerable amount of information on the crystallization of PETN (17). By fairly rapid crystallization long thin and irregular crystals can be produced which have a low bulk density and might be expected to press well. For all these reasons, PETN was chosen for study. Precipitation was accomplished by adding water to an acetone solution. This gave elongated prismatic crystals, somewhat twinned, a good fraction having re-entrant cavities along the main axis of the crystal. The specific surface, as measured with an air permeability apparatus, was about 3000 cm^2/gm. Wedges were fabricated by pressing such PETN to a density of 1.0 gm/cm^3 in cylindrical pellets in a special die. This die could be partially disassembled so that the PETN contained in the remaining section could be shaved into a wedge at an angle of 19.5 degrees. The wedge was then removed from the second die section.

The first experiments were attempted with the PETN wedge surrounded peripherally by a part of the steel pressing die, but after a method had been developed for removing the wedge from the die it became clear that the die had perturbed the shock sufficiently to give erroneous results. In some early experiments a mirror was used on the angled wedge surface in the hope that it would permit observation of the initiating disturbance. This also was shown to give results that were misleading. Low density pressings of PETN are probably especially sensitive to these effects, since the velocity of the initiating shock is so low. The abandonment of mirrors and similar materials over the surface of the wedge meant that most of the experiments were performed in such a way that the initiating shock could not be observed in the PETN, since it was so weak as to be non-luminous. Therefore, we have measured the time and distance from the entry of the shock, as shown by the start of surface motion of the brass, to the start of detonation, as indicated by the first appearance of light intense enough to be recorded by our camera.

RESULTS

A diagram of the experimental setup is shown in Fig. 2 together with a print of a typical camera record. Data from the experiments are presented in Table I. The values of Brass Free Surface Velocity could be determined to within about ±5%. The greater variation among the three free surface velocities for 1 1/2" thick Lucite is believed due to wave tilt introduced by the use of two 3/4" pieces that had not been selected for flatness. Data in the Depth of Initiation and Time of Initiation columns were obtained by measuring the position and time where light was first recorded from the PETN. This was a difficult point to measure, and it could not be done with much accuracy. Nevertheless, the accuracy is sufficient to permit determination of the conditions under which the depth of initiation becomes very large.

The luminous trace from the wedge was identified as a detonation by comparison with strongly initiated wedges. In the first three shots listed in Table I the initiating shocks were strong, the delays were so short as to be almost obscured by the toe of the wedge, and the light from the waves travelled across the wedge with nearly constant velocity (corresponding to 5.8, 5.7, and 5.7 mm/sec through the pressing for shots 1, 2, and 3 respectively). We therefore assumed that the self-luminous disturbance was in fact a detonation wave even when determination of the velocity was impossible. The irregularity of some traces, an example of which is given in Fig. 2, is taken to mean that the initiation did not take place simultaneously over the surface of the shock wave in the low density PETN pressing. This is a cause for lack of precision in measuring the depth of initiation.

Figure 3 is a graph of Depth of Initiation vs Brass Free Surface Velocity and gives some indication of the reproducibility. The corresponding shock pressures in brass are also given along the abscissa. These pressures were determined from an extrapolation of the shock Hugoniot data published by Walsh, et al (16). Their Hugoniot curve for brass is shown in the pressure/particle-velocity plane in Fig. 4 with a typical state point S indicated.

Fig. 3   Depth of Initiation vs Brass Free Surface Velocity. The depth of initiation is the distance from the original position of the brass surface to the level in the charge indicated by the position of first light on the film. Depths of initiation less than 1 mm or greater than 8 mm could not be accurately measured, and are indicated by the open-sided symbols.

567
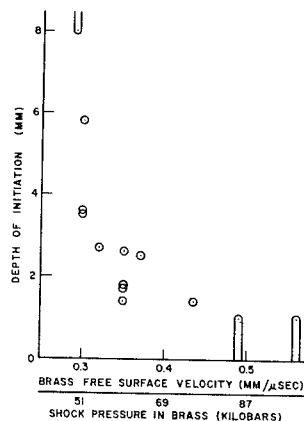
TABLE I

Data from PETN Wedge Initiation Experiments

PETN density = 1.0 gm/cm^3

Wedge angle = 19.5 degrees

PETN specific surface = 3000 cm^2/gm

Shot No.	"X" in Shock Attenuator Material	Thickness (in.)	Brass Free Surface Velocity (mm/μsec)	Depth of Initiation in PETN (mm)	Time of Initiation in PETN (μsec)
1	[a]Devcon-C	1	0.56	1	--
2	[b]Pentite	1	0.49	1	--
3	Lucite	1	0.43	1.4	1.25
4	Lucite	1 1/4	0.37	1.8	1.75
5	Lucite	1 1/4	0.38	1.4	1.39
6	Lucite	1 1/4	0.37	1.7	1.75
7	Lucite	1 1/2	0.37	2.5	2.53
8	Lucite	1 1/2	0.36	2.6	2.83
9	Lucite	1 1/2	0.33	2.7	3.03
10	Lucite	1 3/4	0.34	5.9	6.78
11	Lucite	1 3/4	0.33	3.6	3.91
12	Lucite	1 3/4	0.33	3.5	4.17
13	Lucite	2	0.29	8	--

[a]Devcon-C is an aluminum-filled epoxy resin manufactured by Devcon Corp., Danvers, Mass.

[b]Pentite is a plastic-bonded pentaerythritol, pressed close to theoretical density.

DISCUSSION

The shocked state of the brass can be determined simply from the experimental results. However, defining the state of the shocked PETN is less straightforward. The PETN has been treated as a homogeneous material and the initiating shock has been assumed to move with a velocity, in the neighborhood of 1 mm/μsec, equal in each case to the quotient of the numbers in the last two columns in Table I. We have used what Walsh, et al have called the Graphical Solution of the interface equations. A more complete description of this procedure can be found in their article (16). Starting from a typical shocked state such as S in Fig. 4, subsequent state points of the expanding brass must lie along the adiabat through point S. We have used the approximation that the adiabat can be replaced by the mirror image of the Hugoniot about the line corresponding to the value of U_p at the point S. Such a curve is shown dotted in Fig. 4. From the values of shock velocity we have then constructed lines having slopes equal to $\rho_o U_s$ for the PETN, one of which is shown as a dashed line in Fig. 4. In order for the pressure and particle velocity to be continuous across the PETN-brass interface, the state point of the PETN for a given experiment must be at the intersection I of the two curves. Repeating this process for each experiment we arrived at a series of PETN state points which, with certain reservations, can be regarded as defining a PETN Hugoniot, shown in Fig. 5.

These reservations regarding the reality of the PETN pressure and particle-velocity arise because of the assumptions made concerning the initiating shock and because the heterogeneous PETN pressing has been treated as homogeneous for hydrodynamic purposes. These questions deserve considerable discussion and have been the subject of the special experiments described below.

Fig. 4 Pressure vs Particle Velocity Plots for Brass and PETN. The brass Hugoniot is from Reference 16. See text.

The Initiating Shock

By increasing the illumination of the surface of the wedge and eliminating the simultaneous free surface velocity measurement it has been possible to obtain records of the initiating disturbance in its travel through the PETN. Such experiments have shown that this disturbance accelerates continuously. Although the early part of the smear camera record looks almost straight in some cases, the curvature increases progressively as the point of initiation is approached. Since this is

the case, the method used in the work reported above to estimate shock velocities has yielded values too high by perhaps 10%. Thus the derived PETN pressures should be reduced approximately 10%. On the other hand, this inaccuracy is about the same magnitude as some of the other uncertainties in calculation of the pressure. The important point is not that the pressure be known with great absolute accuracy but that the fact be established that PETN can be initiated by shock pressures as low as a few kilobars.

When acceleration of the initial disturbance is taking place, chemical reaction is clearly present. It seems reasonable that the shock is essentially unsupported in the early stages when it is moving into the PETN with almost constant velocity. However, it must be admitted that this has not been proven, and that the existence of a meta-stable supported shock is still a possibility as far as the present experiments are concerned. If this is in fact the situation, the curve in Fig. 5 would be considered as a Hugoniot for partially reacted PETN, but only if the constant velocity region is considered to represent a steady state. However, different initial velocities seem to indicate that each point would represent, under these assumptions, a different degree of reaction and that Fig. 5 would then not represent a Hugoniot at all. The variation of the initial velocities do not have this implication for a shock with extremely small amount of chemical reaction, and in this case Fig. 5 could be a fairly close approximation to the Hugoniot for unreacting PETN.

Fig. 5 PETN "Shock Hugoniot". The pressures and particle velocities were derived from measured properties in the last element of the attenuator, employing a number of assumptions whose validity is discussed in the text.

PETN Shock Hugoniot

There is a question as to whether it is legitimate to speak of a Hugoniot for a PETN pressing, which consists of individual PETN grains at crystal density and air spaces at very low density. The quantities ρ_0 and U_s, used to arrive at the pressure and particle velocity values for the Hugoniot, are both averages. When the shock first crosses the interface between the attenuator and the explosive, it seems questionable that any small region in the PETN pressing actually exists at the pressure and particle velocity given by the point I in Fig. 4. In other words, the appropriateness of considering the pressing to be homogeneous depends on how much small scale detail is required for the purpose at hand; and consideration of initiation would seem to require details for individual grains.

570

For purely hydrodynamic purposes, the "average Hugoniot" of the pressing may be a very useful curve. To check this, points on the PETN Hugoniot were also determined when the PETN was shocked from a material which was hydrodynamically quite different from the brass that was used in the original experiments. The 1/2-inch-thick final attenuator element of brass was replaced by a dual element consisting of 1/2-inch of uranium and 1/2-inch of Lucite. The shock entered the PETN from the Lucite and the pressure and particle velocity in the PETN were determined from the intersection of the approximation to the Lucite (18) adiabat and the $\rho_o U_s$ line, U_s having been determined as before. In Fig. 5, two points from such experiments are seen to lie on the PETN Hugoniot determined from the data collected when brass was the last attenuator element. This means that the PETN Hugoniot is satisfactory for predicting shock velocities in the pressing if the hydrodynamic properties have been determined for the material from which the shock enters the PETN. A distinction has been made here between the prediction of the shock velocity (which can be checked in absolute terms by measurement) and the derivation of the corresponding pressure (which we have not measured directly).

The PETN "shock Hugoniot" in Fig. 5 is probably more accurate than the individual points. Therefore the intersections of this curve with the appropriate brass adiabats have been used to evaluate the PETN "shock pressures", which are plotted against the depths of initiation in Fig. 6. On this basis, the minimum initiating pressure of 50 kb in the brass is seen to correspond to a derived pressure of about 2.5 kb in the PETN.

There is another aspect of these experiments which could in principle be quite distinct from the hydrodynamic properties of the pressing; namely, the question of the sensitivity of the PETN when shocked from the two materials, brass and Lucite. In the microscopic sense it is clear that the impedance match is different for these two materials as the shock enters the individual PETN grains or the air spaces between them. Strictly, it could not be taken for granted that the sensitivity of the PETN would be the same for shocks from the two materials even though they eventually produced the same macroscopic average shock velocity in the pressing. However, the depths of initiation have turned out to be consistent with the hydrodynamic behavior. This is shown by the triangular points in Fig. 6.
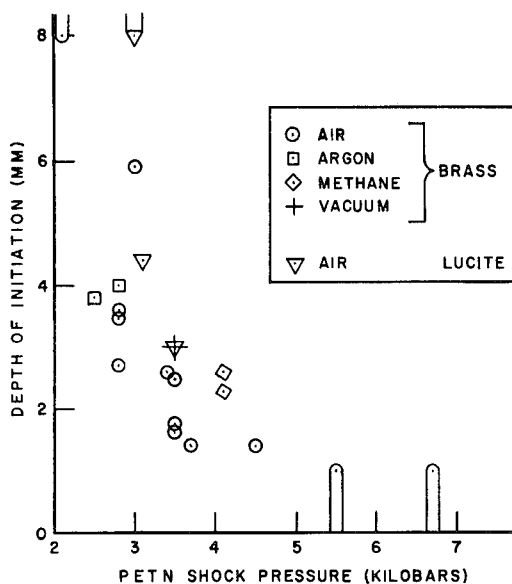
Fig. 6 Depth of Initiation vs PETN "Shock Pressure". The meaning of the pressure values is subject to the qualifications applying to the PETN Hugoniot.

In spite of the difficulties, the shock velocity in the PETN pressing can be calculated, and the initiation of the PETN will take place according to this velocity. The relative pressures, naturally, will also serve as such an index.

Effect of Interstitial Gases

One proposal for the mechanism of initiation of detonation involves grain-burning started by means of the compressional temperature of interstitial gases in the pressing. Compression may be considered to take place by a single shock along the Hugoniot, by a series of compressions along a curve approximating an adiabat, or even by means of a clear-cut shock reflection. Regardless of these details the temperature can be altered at least 500°C by choosing gases with widely different hydrodynamic and thermodynamic properties. In order to achieve extremes in this sort of behavior, we have evacuated wedges and replaced the air, either with argon to produce high gas temperatures, or with methane to produce low gas temperatures. The results of these tests are shown in Fig. 6, and the fact that these depths of initiation agree within experimental error with the values for air is taken as strong indication that the temperature of the interstitial gas has nothing to do with the mechanism of initiation. Temperature differences of several hundred degrees would have a profound effect on the rate of grain burning or on the rate of chemical reaction if such temperature changes could be brought to bear on these processes.

An experiment was also performed in which the pressure of the interstitial air was reduced to the range between 50 to 100 microns. The temperature of the compressed residual air in this case was not much different from that achieved at normal density but the total amount of energy available for transfer from gas to PETN was lowered by a factor of about 10^4. This low-pressure shot is also shown in Fig. 6, and again demonstrates that the interstitial gases did not affect the initiation process.

CONCLUSIONS

By use of a special low-bulk-density PETN it has been possible to extend wedge-type initiation measurements to low-density pressings. For such pressings it is to be expected that the nature of the crystals and the properties of the interstitial gases would affect the initiation characteristics, if they are ever to be important. The experiments reported on the lack of effect of interstitial gases seem to eliminate this component from the mechanism. Further experiments need to be done to assess the importance of the properties of the solid grains.

The particular type of PETN we have used has been shown, at 1.0 gm cm^{-3} density, to be sensitive to shocks that are quite weak compared to those required for the initiation of high density explosives. The hydrodynamics of the interface between the material

used to carry the shock and the particulate explosives can apparently
be treated satisfactorily by using methods developed for homogeneous
materials. On this basis we arrive at a pressure of about 2 1/2 kb in
the PETN pressing as the lowest pressure with which we have been able
to produce initiation. In future experiments this pressure will be
compared to the pressure necessary to initiate pressings in other den-
sities. It is hoped that the changed interface conditions can be
properly taken into account in this manner.

ACKNOWLEDGMENT

The authors wish to thank Donald Wilson for assistance in making
the experiments and for preparing the illustrations. The PETN wedges
were supplied by A. E. Marchand.

REFERENCES

1. H. Muraour, Mem. d' Artill. Fr. 12, 559 (1933).
2. H. Eyring, R. E. Powell, G. H. Duffey, and R. B. Parlin, Chem.
   Rev. 45, pp. 138-142 (1949).
3. M. A. Cook, D. H. Pack, L. N. Cosner, and W. A. Gey, J. Appl.
   Phys. 30, 1579 (1959).
4. G. P. Cachia and E. G. Whitbread, Proc. Roy. Soc. (London) A 246,
   268 (1958).
5. W. R. Marlow and I. C. Skidmore, Proc. Roy, Soc. (London) A 246,
   284 (1958).
6. T. E. Holland, A. W. Campbell, and M. E. Malin, J. Appl. Phys.
   28, 1217 (1957).
7. A. W. Campbell, W. C. Davis, and J. R. Travis, Shock Initiation
   of Detonation in Liquid Explosives, this symposium.
8. A. W. Campbell, W. C. Davis, J. B. Ramsay, and J: R. Travis,
   Shock Initiation of Solid Explosives, this symposium.
9. J. M. Majowicz and S. J. Jacobs, Initiation to Detonation of High
   Explosives by Shocks, Lehigh Meeting, Fluid Dynamics Div. APS
   November 1957.
10. A. Michel-Levy, H. Muraour, Compt. Rend, 204, 576 (1937).
11. C. H. Winning and H. E. Edgerton, J. Soc. Mot. Pict. Engr. 59,
    178 (1952).
12. R. G. Shreffler and W. E. Deal, J. Appl. Phys. 24, 44 (1953).
13. J. H. Cook, Research 1, 474 (1948).
14. B. G. Craig and W. C. Davis, to be published.
15. J. M. Walsh, M. H. Rice, Solid State Physics (Academic Press,
    New York and London, 1958) Vol. 6, p. 29.
16. J. M. Walsh, M. H. Rice, R. G. McQueen, E. L. Yarger, Phys. Rev.
    108, 196 (1957).
17. E. Berlow, R. H. Barth and J. E. Snow, The Pentaerythritols,
    (Reinhold, New York, 1958), p. 57.
18. W. E. Deal and R. G. McQueen, Private Communication (1957).

THE TRANSITION FROM SHOCK WAVE TO DETONATION
IN 60/40 RDX/TNT

E.L. Kendrew and E.G. Whitbread
Explosives Research and Development Establishment
Ministry of Aviation
Waltham Abbey, England.

INTRODUCTION

In recent years an increasing amount of attention has been paid
to the initiation of detonation by shock; this is important for
both the design of weapons and the general understanding of sensiti-
vity.

Hertzberg (1) was the first to observe that if a charge is
detonated by a shock wave the detonation occurs at a point inside
the charge and not where the shock wave entered. As the shock
has a lower velocity than the detonation the concept of a 'delay'
is thereby introduced, i.e. the charge takes longer to detonate than
the time calculated by dividing length by detonation velocity.
The concept depends on the reasonable but incorrect assumption that
the detonation ought to start at the entry face. The weakness of
this assumption is well illustrated by the behaviour of large, near
perfect, RDX crystals which usually detonate backwards from the
face by which the shock wave leaves the crystal (2).

There are at present two theories on the shock initiation of
explosives. It is common to both that the shock wave initiates
some reaction in that part of the charge through which it first
passes; one theory (3) holds that the energy from this reaction
reinforces the shock in a continuous manner, while the other theory
(4) postulates that the rising temperature of the reacting material
ultimately results in the production of a condition of thermal
super-conductivity and a "heat-pulse" flashes through the charge,
setting up a detonation when it overtakes the shock front.

It is a consequence of the first theory that the ensuing
detonation will propagate only in the direction of the initial shock
wave, since with a continuous build-up process the region immediately

behind the detonation zone must be greatly depleted of chemical
energy, and such a region, if thick enough, would act as a barrier
to a detonation propagating back into the shocked material.   In
the second theory however there is nothing to prevent a detonation
developing in both directions at once.

In general the first theory is founded on experiments with
charges of small cross section and the second with charges of larger
section.

The programme, of which a part is described here, has two
objects: first, to resolve this difference, and second, either
(i) to study the formation and transmission of the "heat pulse" or
(ii) to demonstrate the dependance of the acceleration process
(and hence the so called delay time) on the initial shock pressure.

EXPERIMENTAL

A novel feature of the explosive charges used in this work is
that in most of the experiments the shock wave passes successively
through a number of thin layers of explosive each separated from its
neighbours by metal foil.   The purpose of this is twofold:
The metal foil will prevent the flow of a "heat pulse" from layer
to layer (5) and the entire assembly is an approximate but
practical representation of a one-dimensional system in Lagrangian
co-ordinates of mass and time (6).   It is appreciated that for the
latter purpose the system has obvious limitations but it is most
valuable as a first step.

In future work it is intended to utilise measurements made of
the movement of the interface between layers, since the particle
velocity changes with pressure more than 5 times as rapidly as does
wave front velocity.   As discussed later this has not yet been
carried out.

The basic test assembly is shown in figure 1.   The "donor
charge" was an explosive lens designed to give a slightly concave
wave form.   The "gap" always contained a large sheet of 16 g. mild
steel which also acted as a shield to prevent the products of the
donor charge obscuring the camera's view of the "receptor".   The
"gap" was made up to the necessary thickness with laminated brass
(for the smallest assemblies) or with sheets of card (for the
larger charges).

Three sizes of receptor charge were used:
15 x 15 x 38 mm, 50 x 50 x 150 mm and 75 x 75 x 200 mm with "donor"
charges to suit.   The "receptors" were usually made up as stacks
of laminae each separated from its neighbours by sheets of brass
foil 0.04 mm. thick and with alternate layers coloured black.   The
laminae were 2.5 mm thick for the smallest charges and 7.5 mm thick
for the others.   On occasion solid charges were used, as some
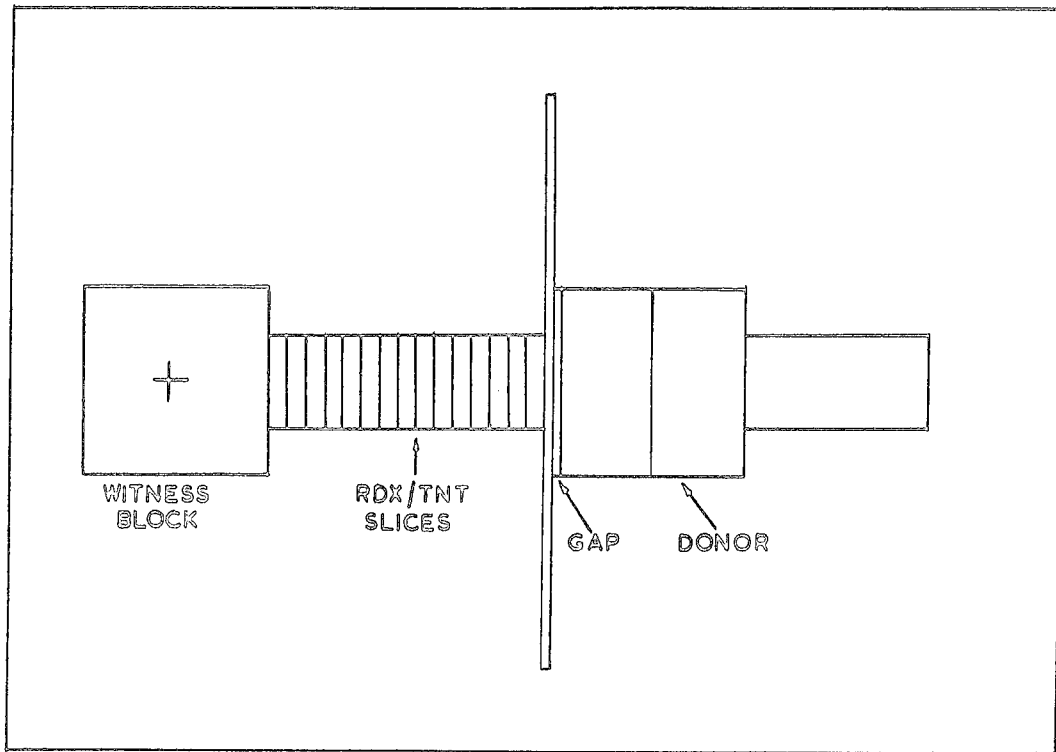
FIGURE I

qualitative information is more easily obtained with this type.

All explosive components (with the exception of the smallest donor charges) were made from RDX/TNT Grade A, cast under a pressure of 100 p.s.i. and with controlled cooling of the moulds by hot water jackets. Selected sections were cut from the casts and machined to size by standard methods. To obtain a better surface each section of the laminated charges was hand scraped and tested on a surface plate. The charges were assembled with the least possible amount of rubber cement and under some pressure.

The smallest donor charges were machined from pressed tetryl pellets.

The experiments were photographed using a Beckman and Whitley 189 framing camera at 1.2×10^6 and 5×10^5 f.p.s. Kodak tri-X, developed normally, was used for the major part of the work but a few shots were taken in colour on Anscochrome for illustrative purposes. Conventional synchronisation, argon flash bomb and blast shutter techniques were used throughout.

The charges were photographed from the side, with the optical axis at right angles to the motion of the shock front. All measurements were made on the centre line of the side face.

To the present time the quantitative study has been concentrated on the smallest (15 mm square section) size of charge. Of these 56 have been fired, in 37 a detonation developed at distances from the "gap" varying from 10 mm to the full length of the charge (38 mm) and in 19 no detonation resulted.

The shock front measurements for each film were first recorded as a space-time curve and the velocities at each point taken as the tangent to the curve. The distance between the "gap" and the onset of detonation varied from shot to shot, the velocities were not therefore plotted against the distance from the "gap" but against the distance measured backwards from the point of transition from shock wave to detonation (i.e. from where the air shock becomes luminous and toward the "gap"). The results may be grouped as a single relation (figure 2); as the velocities themselves are taken from smoothed curves the individual points are not marked but the braces indicate the spread of the data.

DISCUSSION

In previous work it had been found that a minimum shock pressure of 90 Kb was necessary to initiate RDX/TNT charges of 12.5 mm square cross section. The wave front velocity was of the order of 4000 mps. Much lower initial velocities have now been observed in the 15 mm square section charges which ultimately detonated. The difference is not yet fully explicable but must be mainly due to the fact that the measurements now put forward were made on the

surface of the charge, the previously recorded data referring to the interior. As the charge expands behind the shock front rarefaction waves move into the compressed material reducing the pressure and velocity and this reduction is immediately effective at the surface.

This has so far prevented effective use of the surface particle velocity measurements but could be overcome if the way in which the expansion takes place were properly understood.

A superficial examination of the photographs obtained so far shows a similarity to the expansion of material flowing through an orifice and subjected to the influence of the so called "simple" waves (Prandtl-Meyer expansion, ref. 6 but p 267 et seq). However an exact analysis has not yet been attempted.

On the first theory of transition, in which the shock is not reinforced until overtaken by the "heat pulse", a laminated charge of the type used in these experiments must either: (i) Detonate in the first layer, the detonation being quenched and reformed in each subsequent layer in the manner described by Cook (5) or (ii) fail, since if the heat pulse generated in the first layer does not overtake the shock wave in that layer it will be stopped by the metal foil; the shock wave will be weaker in the second layer so the heat pulse in this layer will arise later than in the first and must suffer a similar fate. Thus a laminated explosive/metal charge must detonate in the first layer or fail.

With laminated charges of all cross sections described earlier it has always been possible to obtain a transition from shock to detonation when the shock wave had traversed most of the charge. This in itself is a strong argument against the "heat pulse".

Three kinds of behaviour of the wave were found, according to the cross section of the charge used.

1. With charges of 15 mm square cross section there is a continuous acceleration from near sonic speed to detonation. The velocities in the individual shots vary considerably but all show an increase of the same form. The minimum velocity possible cannot be below sonic, and assuming this to be about 3000 m.p.s. it can be seen from figure 2 that no less than 54% of the acceleration occurs in the last 2.5 mm before detonation, 20% in the 2.5 mm before that and 10% in the previous 2.5 mm. This implies that nearly 85% of the acceleration occurs in the last 7.5 mm before detonation and only about 15% in the 12.5 mm before that.

It was not found possible to measure acceleration more than 20 mm before detonation. In those shots where the shock traversed more than 20 mm before detonation (7 out of the 56) the acceleration, if present, was too slight. A further complication was that the concave wave shape generated by the donor charge rapidly inverted,

producing spurious effects which rendered measurements in the first few millimetres useless.

In the region of gentle acceleration there is a slight change in the colour of the charge in that the yellow of the explosive becomes tinted with blue, in the region of rapid acceleration (the last three layers or so) there is a very marked colour change to deep brown. It is probable that in both cases these changes are due to chemical reaction although in the first instance (light blue) it could be due to the air shock surrounding the expanding charge.

In no case was "reverse detonation" observed. This is presumably because the layer of explosive immediately behind the detonation is too devoid of chemical energy, having supported half the acceleration within 2.5 mm.

2. With charges of 75 mm cross section the initial shock is of 3000 m.p.s. velocity, which is probably very near sonic speed, there is no measurable acceleration and the detonation develops in both directions. The velocity of the forward propagating detonation is initially above the accepted value of 7900 m.p.s. by as much as 500 m.p.s. but rapidly (within 20 mm) falls to the normal rate. The reverse wave velocity is initially about 1000 m.p.s. low and falls to a yet lower rate as the wave moves farther into the shocked region.

3. The most interesting phenomenon occurred with the intermediate size charges, i.e. of 50 mm square section. The shock wave is initially of about sonic velocity and does not accelerate until 10 mm before the transition point. When acceleration occurs it is limited to the centre of the wave (as seen on the side of the charge) which develops a thin, dark pre-detonation region followed by a detonation propagating, forward in the centre, sideways to the corners and then backwards in the corners only (fig. 3). This is exactly as if there were a short cylindrical region, in the charge centre and normal to the axis, in which the reverse detonation is inhibited. This cylinder is of such a diameter (60 mm in this instance) that it cuts into the faces of the square section charge, leaving the corners free.

An alternative possibility is that there is a critical diameter below which the reverse detonation is prohibited. But if the effective diameter is reduced asymetrically by removing two adjacent corners at the point where transition occurs, the reverse detonation is not inhibited altogether but restricted to the two remaining corners. (fig. 4).

The most probable explanation is that the lateral rarefaction waves restrict the rapid acceleration to the central region. This will result in the wave distorting into an extremely convex
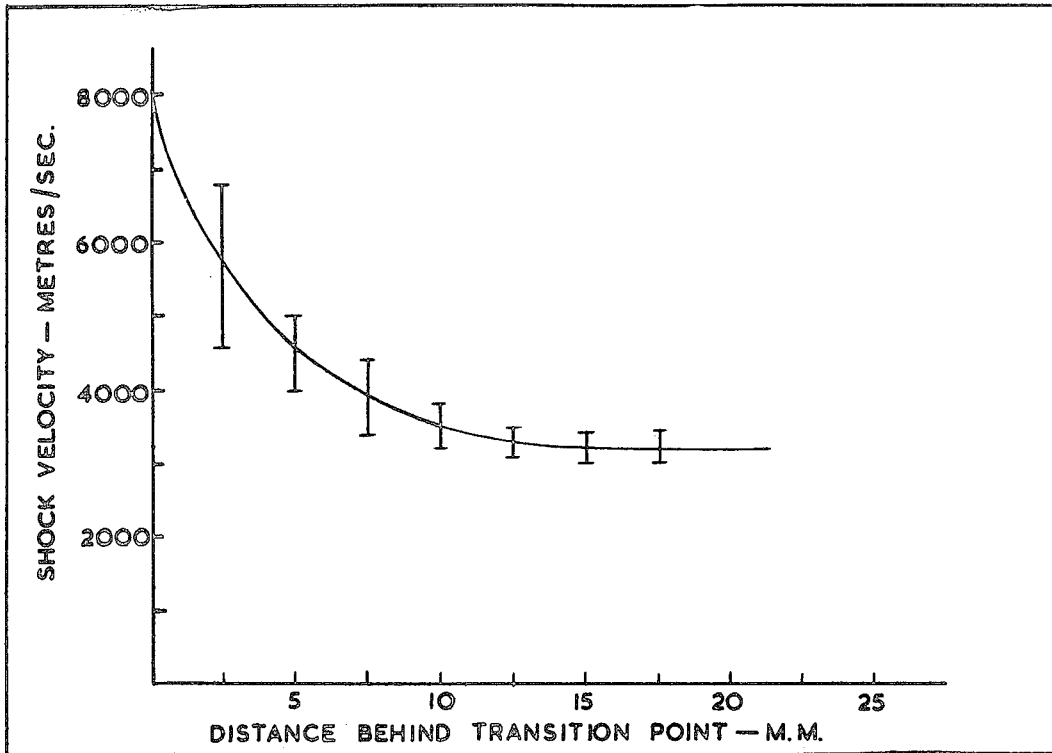
FIGURE 2
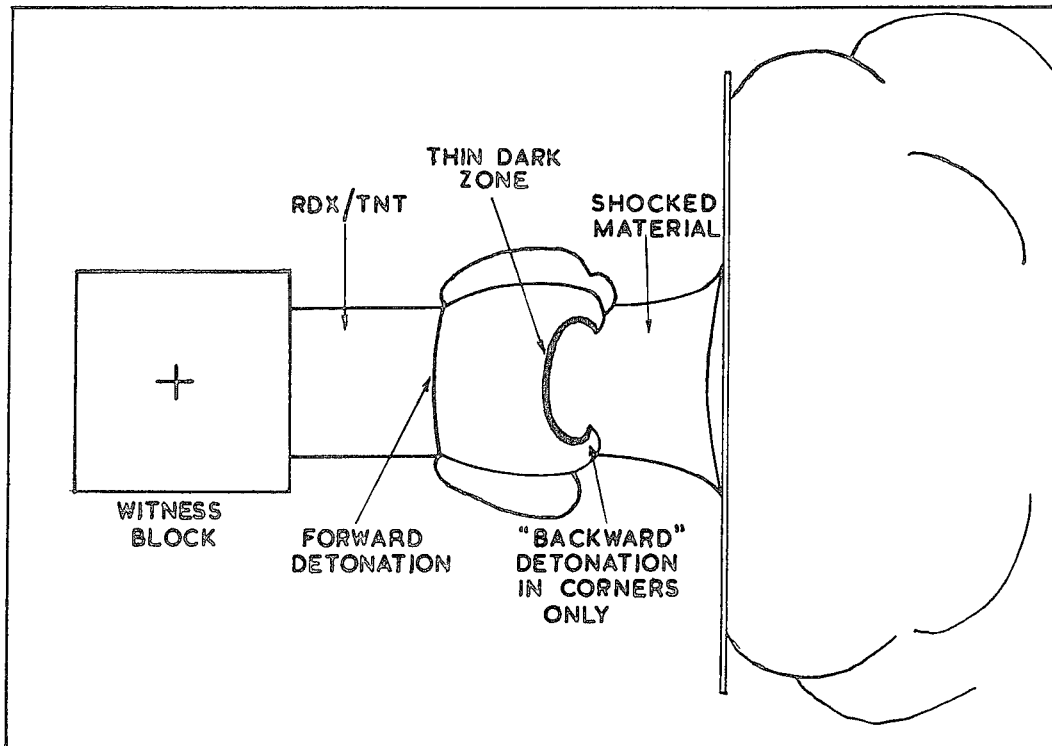
FIGURE 3

shape as transition occurs, with the result that the detonation can spread laterally into unreacted material. If the charge has a much bigger section than the central accelerating "core" the latter will not be seen at the sides until it has spread into unreacted material and a detonation is propagating in both directions. The velocities initially observed on the surface are easily explained by the geometry of such a system.

Some confirmation has been provided by an experiment in which the detonation occurs just before the end of a 50 mm square cross section charge. The detonation is seen to emerge from the centre of the end face when the shock wave in the side face is still 10 mm from the end of the charge (fig. 5). A similar result has also been obtained by Sultanoff (7).

The diameter of this accelerating "core" is, in an ideal case with rectangular pulses, the diameter at which the converging lateral rarefaction waves meet the tail of the initial pulse and will therefore be a function of charge diameter, rarefaction velocity and initial pulse length. Further work is needed to amplify this point.

BIBLIOGRAPHY

1. "Initiation of High Explosives" G.Hartzberg R.Walker Nature 161 1948 pp 647-8

2. "The Explosive Initiation of a Single Crystal of Cyclotrimethylene Trinitramine (RDX)" G.K. Adams J. Holden. E.G. Whitbread. Compte Rendu du XXXIe Congrès International de Chemie Industrielle - Liege Sept. 1958.

3. "The Initiation of Explosives by Shock" G.P. Cachia and E.G. Whitbread. Proc Roy Soc A 246 p.268 et seq.

4. "Instrumented Card-Gap or S.P.H.F. - Plate test", M.A. Cook D.H. Pack L.N. Cosner W.A. Gey. J. App. Phys 30 No. 10 p.1579 et seq.

5. "The Science of High Explosives" M.A. Cook, Reinhold Publishing Corp. p.83-4

6. "Supersonic Flow and Shock Waves" R. Courant, K.O. Friedrichs. Interscience Publishers Inc. p.30.

7. "New Observations of Explosive Phenomena by Submicrosecond Color Photography" M. Sultanoff 85th Semi Annual Convention S.M.P.T.E.
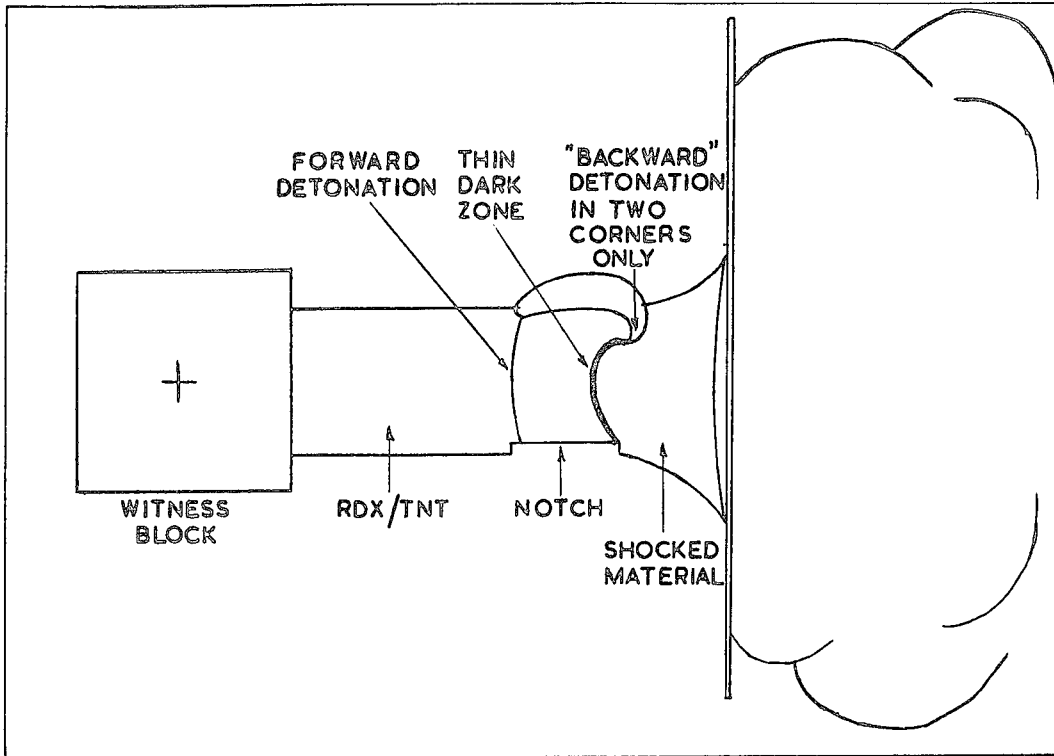
FORWARD
DETONATION
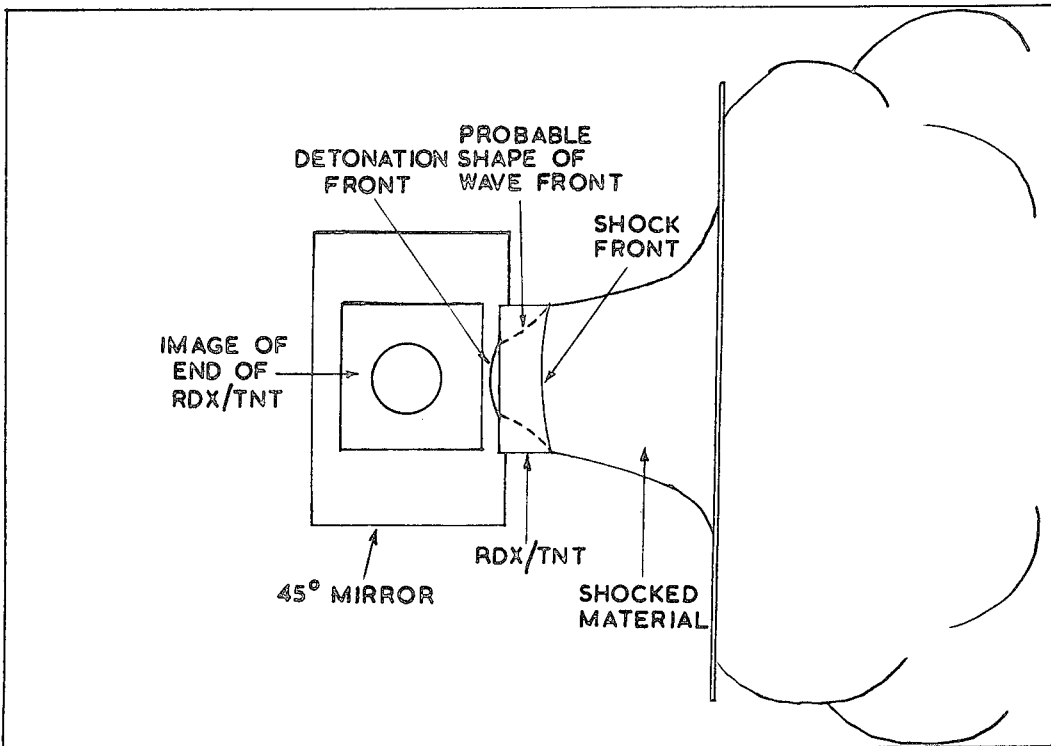
THIN
DARK
ZONE

"BACKWARD"
DETONATION
IN TWO
CORNERS
ONLY

WITNESS
BLOCK

RDX/TNT

NOTCH

SHOCKED
MATERIAL

FIGURE 4

PROBABLE
DETONATION SHAPE OF
FRONT WAVE FRONT

SHOCK
FRONT

IMAGE OF
END OF
RDX/TNT

45° MIRROR

RDX/TNT

SHOCKED
MATERIAL

FIGURE 5

582

ACKNOWLEDGEMENT

ILLUSTRATION

A 16 mm film has been printed from the original high speed camera records of the experiments described.

DETERMINATION OF THE SHOCK PRESSURE
REQUIRED TO INITIATE DETONATION OF AN ACCEPTOR
IN THE SHOCK SENSITIVITY TEST

I. Jaffe, R. Beauregard, A. Amster
U. S. Naval Ordnance Laboratory
Silver Spring, Maryland

ABSTRACT: The attenuation of the velocity of a shock
wave was measured in Lucite under conditions similar to
those of the shock sensitivity test. Two systems, one
based upon the reaction of pressure probes to the pressure
pulse of the shock wave and the other a smear camera, were
used to record the events. The reliability of the pressure
probe in recording the events was comparable to the smear
camera record of the shock for the first three inches of
Lucite after which the response of the pressure probes
lagged behind the camera record. With the aid of the smear
camera, additional data were calculated for Lucite in the
low pressure region (4-5 kbar) by measuring the shock
velocity in Lucite and water. These data were used to
extend the equation of state for Lucite to the region
applicable to this investigation.

The shock pressure in Lucite was calculated as a
function of the Lucite length from the velocity obtained
experimentally and the equation of state for Lucite. This
was compared to the length of the gap in the shock sensi-
tivity tests to obtain an approximate value of the pressure
required for the initiation to detonation of various ex-
plosives.

I.   Introduction

Shock sensitivity tests for explosives, in which the
sensitivity of an explosive is measured by interposing a
gap of some inert material between a high explosive donor
and the explosive under test, have been in use for a
number of years. The sensitivity of the explosives were
rated on an arbitrary gap scale peculiar to the conditions
of the test and the inert material used for the gap. This

investigation was made to interpret the shock sensitivity test results in terms of shock pressure required to initiate the explosive. In effect, the gap distance was calibrated.

The present work was carried out on Lucite rods, since it was determined cellulose acetate (used in forming the gap) and Lucite were similar shock attenuators. The investigation consisted of extending the equation of state data of Lucite to the lower pressures in the gap and of using the data obtained to relate pressure and gap thickness for the conditions under which the gap tests are made.

The equation of state data were obtained by initiating a shock with two cylindrical tetryl pellets (each 2 inches dia. x 1 inch thick) and measuring the shock velocity as a function of distance in Lucite rods and in water (the equation of state of which is known) as it progresses from the Lucite to the water. Using the customary approximation at the Lucite-water interface, the pressure and particle velocity in Lucite before the interface may be obtained.

II. Experimental Methods

The attenuation of the shock velocity in Lucite was determined by two different experimental techniques. One was based upon recording the passage of a pressure pulse by an electronic system, and the other used high speed photography to follow the shock front. This latter technique was used to obtain additional data to determine a more accurate curve for the equation of state of Lucite.

A. Electronic Method Used to Measure Shock Velocity

Figure I is a schematic drawing of the experimental assembly used to measure the attenuation of a shock wave in a Lucite rod. A donor, consisting of two tetryl pellets, was initiated by a Seismo* detonator. The detonation wave developed in the tetryl becomes a shock wave in the Lucite rod. The progress of the shock wave was followed by a series of pressure probes carefully placed in the assembly. The pressure pulse impinged on a copper tube 0.033 inches away from a copper wire. When the copper tube made contact with the copper wire, a circuit was closed and an impulse was transmitted to an oscilloscope (Tektronic No. 535). A Polaroid camera was used to make permanent records of the oscillograph tracings.

---

* Detonators were obtained from Olin Mathieson
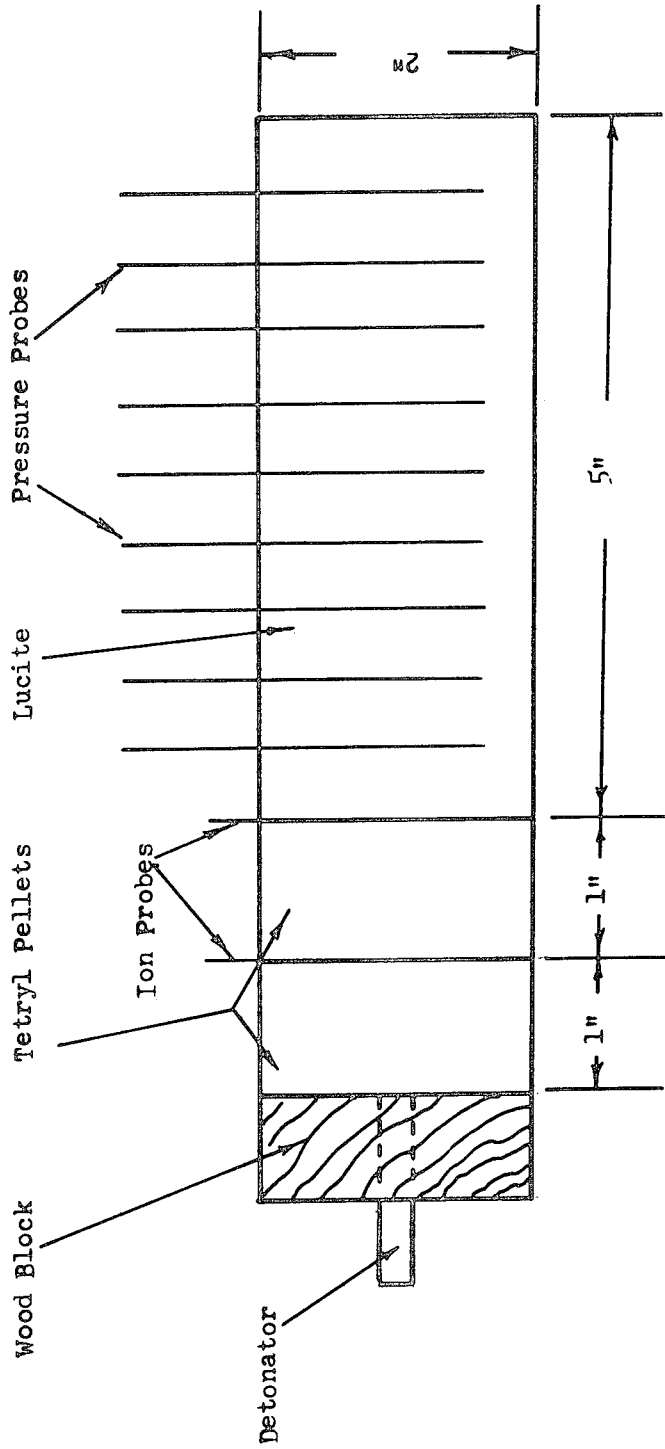
FIGURE I- Assembly for the Measurement of Shock Attenuation in Lucite

A series of holes 0.053 inches in diameter were carefully made at specified intervals in a Lucite rod. The pressure probes were inserted and the necessary leads were soldered to the probes. The tetryl pellets were securely taped to the Lucite rod. An ionization probe was inserted between the two tetryl pellets, and at the tetryl-Lucite interface. The entire ensemble was placed in the bombproof chamber where the leads were connected to the oscilloscope leads and the detonator put in place. Meanwhile a series of calibrated time marks was obtained on the oscilloscope by using a Tektronic No. 181 Time-Mark Generator. The time scale was recorded on the film just prior to the experiment.

The oscilloscope was triggered by the ionization probe placed between the two tetryl pellets. By beginning the oscilloscope sweep prior to the arrival of the detonation at the tetryl-Lucite interface, a much more definitive and precise measurement was obtained of the time of arrival of the shock in the Lucite. The arrival of the reactive shock at the tetryl-Lucite interface was recorded by the second ionization probe. The further progress of the shock wave down the Lucite rod was followed by the pressure probes. A more comprehensive discussion of the pressure probe and the electronic system used is given elsewhere (1,4).

The system contained a donor made up of two tetryl pellets, identical to those used in the shock sensitivity test at the laboratory. Cellulose acetate cards, 0.01 inches thick by 2 inches in diameter were used to build gaps less than one-half inch thick. For larger gaps, Lucite discs, one-half inch and 1 inch thick were used with the cellulose acetate cards to build the required gap. A number of charges were prepared in the exact manner used for the shock sensitivity tests and ionization probes were placed at designated positions in the Lucite-cellulose acetate gap. The gap was prepared by stacking the cards and discs in units one to two inches high. Each unit was compressed to form a compact pile and a hole was drilled in it for a pressure probe. The attenuation of the shock velocity was measured at 0.5, 1.0 and 1.5 inches and compares with the shock velocity measured in the Lucite rod.

B. High Speed Photography

The objects of this experiment were three-fold:

1) to measure the attenuation of the shock wave in Lucite by an alternate method;

2) to determine the reliability of the measurements made by the pressure probes; and

3) to obtain data which will define more precisely the equation of state of Lucite for the lower shock pressures.

Figure II is a schematic drawing which shows the arrangement of the various components. The Lucite rod was machined from a bar 2 inches x 2 1/4 inches in cross section to a rod approximately 2 1/16 inches in diameter with two parallel flat surfaces 2 inches apart and 5/8 inches wide. These parallel flats eliminated distortion of the light by the curved surfaces as the light passed through the Lucite rod. Pressure probes were inserted at designated points in the usual manner. The rod was supported vertically with its end submerged approximately 1/4 inch below the surface of the water contained in a small trough. A Lucite blast shield of known thickness was placed on top of the Lucite rod to prevent the products, resulting from the detonation of the tetryl pellets, from obscuring the view of the camera. Above this shield were placed the two tetryl pellets and the detonator. The ionization probe used to trigger the camera and the oscilloscopes was placed at the tetryl-Lucite interface.

To record the reaction two oscilloscopes, a Tektronic No. 535 and a raster oscilloscope were used in conjunction with the smear camera. A spark was arranged to go off at the end of the reaction to provide a common point, on both the oscilloscope and the camera records, from which the time intervals could be measured and compared. The illumination for the camera was obtained from an exploding wire set behind the Lucite rod. Four experiments were performed, two using four-inch long Lucite rods and two using three-inch long Lucite rods.

III. Results

Figure III is a typical record of the attenuation of a shock wave measured by the pressure probes in a Lucite rod using the sweep oscilloscope. The time scale is 1 μsec per division, and can be read to ± 0.5 μsec. The alternate positive and negative response of the pressure probes, as they were activated, made it possible to determine the position of any malfunctioning probe. Table I contains the results of the experiments performed using two tetryl pellets with the Lucite rods and the gap card units.

Of the four experiments (Expt. #5,6,7 and 8) made using the electronic system and the smear camera, only two
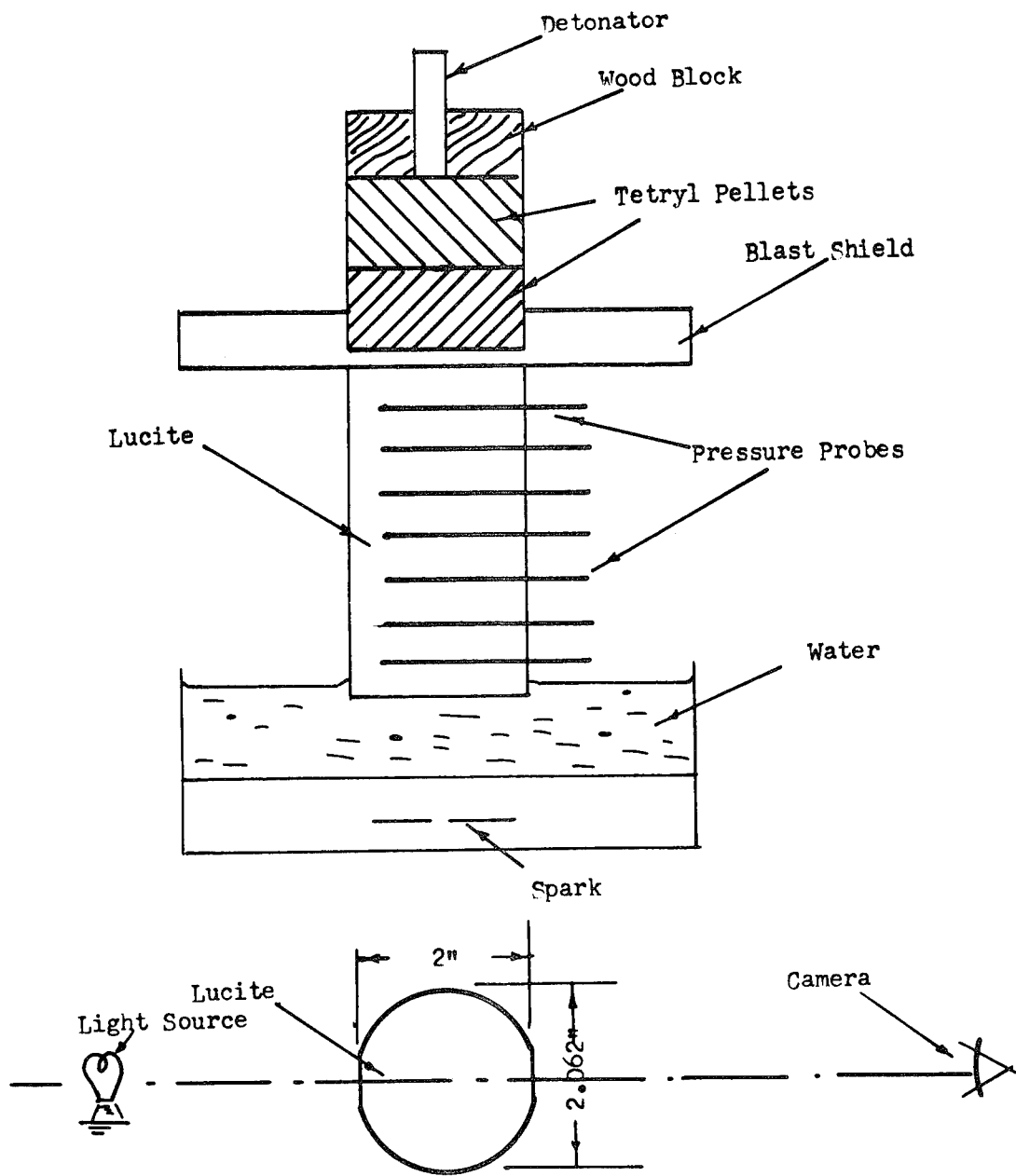
FIGURE 2- Shock Attenuation in Lucite and Water
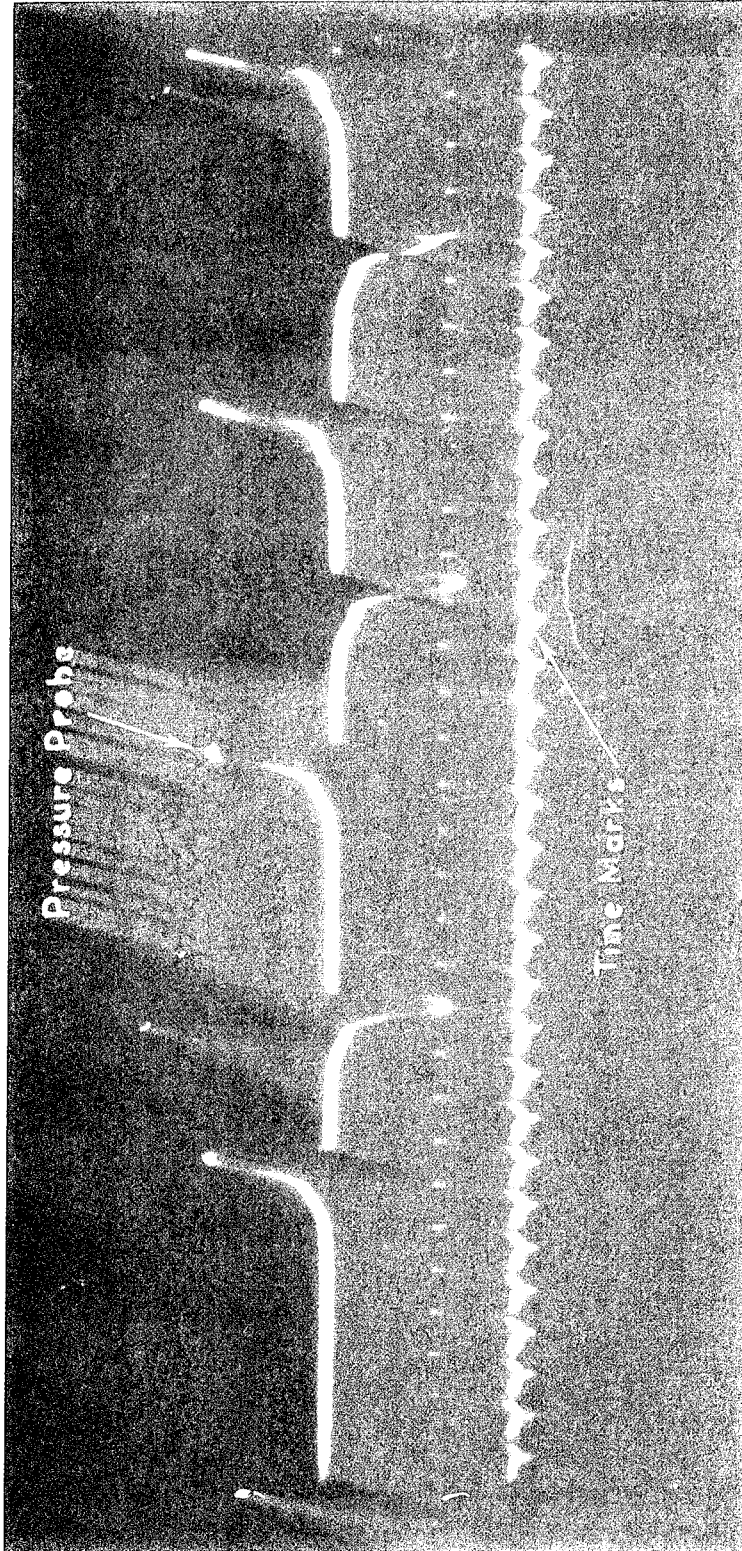
Figure 3 – Pressure probe record

TABLE I

ATTENUATION OF SHOCK IN A LUCITE ROD (Pressure Probe)

(Two Tetryl Pellets)

Distance of Probe		Time (Microseconds)				Mean
in.	mm.	Expt.#1	Expt.#2	Expt.#3	Expt.#4	microsec
0.5	12.7	-	-	2.5	3.0	2.8
1.0	25.4	5.2	6.0	5.5	6.2	5.7
1.5	38.1	8.6	9.6	9.2	9.5	9.2
2.0	50.8	12.0	13.5	12.8	-	12.8
2.5	63.5	16.1	17.8	17.0	17.4	17.1
3.0	76.2	20.5	-	21.1	21.4	21.0
3.5	88.9	25.1	26.5	25.2	26.0	25.7
4.0	101.6	29.7	31.0	29.6	31.1	30.4
4.5	114.3	33.7	37.0	33.7	35.5	35.0
5.0	127.0	-	-	-	-	-

ATTENUATION OF SHOCK IN GAP UNITS

0.53	13.4	2.7	-	75 - 0.01 in. acetate cards
1.00	25.4	6.1	6.0	1/2 in. Lucite disc and 75 - 0.01 in. cards
1.50	38.2	9.5	9.5	1 in. Lucite disc and 75 - 0.01 in. cards

could be used for comparison between the two systems. In experiment #7 the fiducial point was not obtained while in experiment #8 the electronic system did not respond satisfactorily. Figure IV shows the records obtained from the smear camera.

The time scale on the raster oscilloscope was 0.1 microseconds per division and could be read to ± 0.02 microseconds. The time scale for the photographic records was 1.26 mm per microsecond and could be read with a microcomparator to better than ± 0.02 microsecond. The magnification factor for the camera was determined for each experiment by measuring the distance between the probes on the film and relating this to the actual distance between probes. The same magnification factor was used to interpret distance for the shock wave in the water.

Table II contains the results obtained by the smear camera, measured from the fiducial point (spark).

IV. Discussion

In the hydrodynamic theory of shock waves, the conservation of momentum requires that

$$P = \rho_0 uU \tag{1}$$

where the initial pressure (P_0) and particle velocity (u_0) are assumed to be zero and where

P = shock pressure

ρ_0 = initial density of the material

u = particle velocity

U = shock velocity.

In order to obtain the pressure at any point in a shocked homogeneous medium, it is necessary to measure the shock velocity and the particle velocity. However, if a set of data corresponding to equation (1) is known, i.e. the equation of state of the medium is known, a measurement of U vs the attenuation path length (X) for the test geometry can be combined with the known data to give a P - X curve. Since it was desired to use the pressure probes to obtain the U - X data, their adequacy for such measurements was investigated.
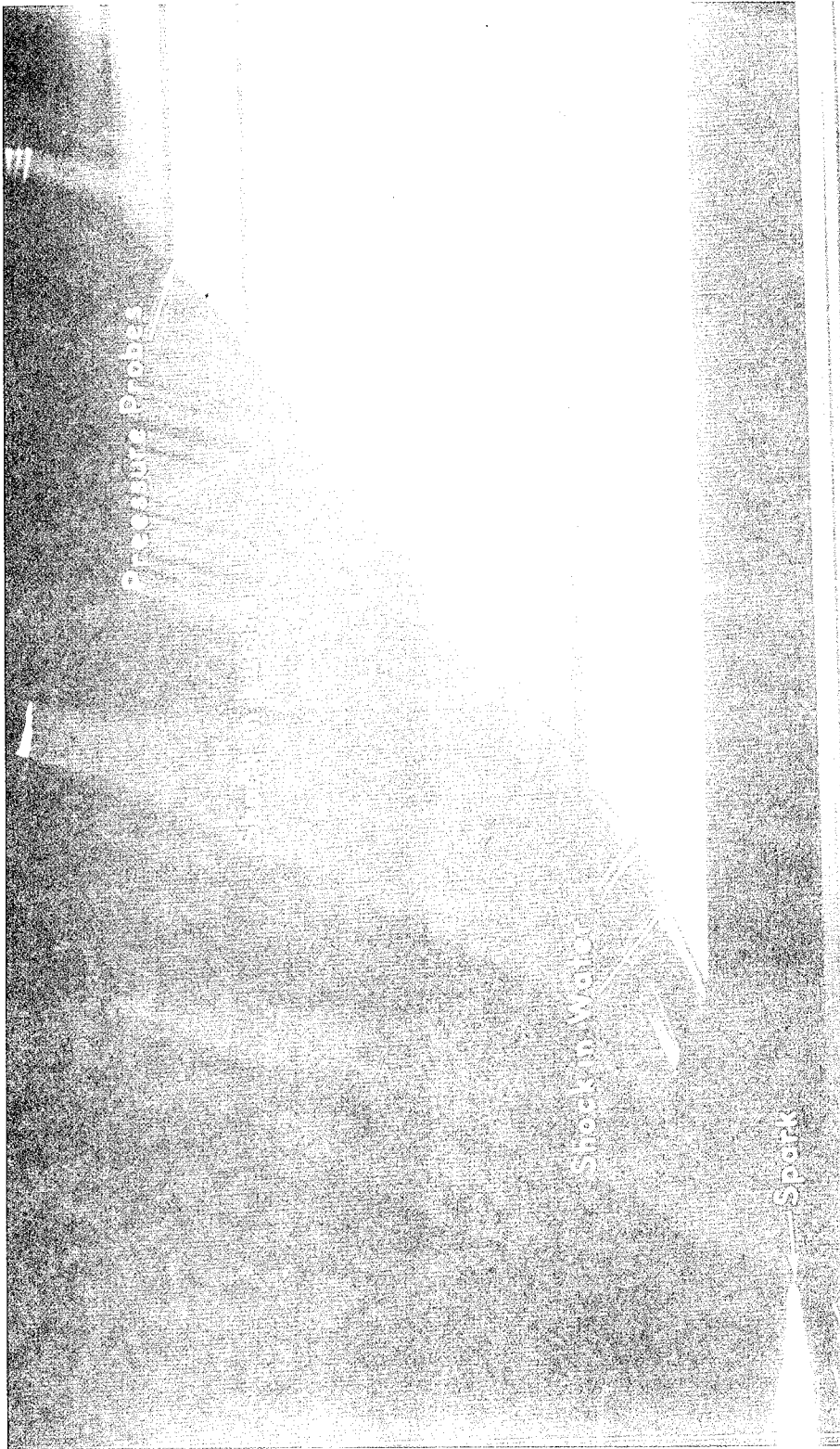
Figure 4 – Shock velocity in Lucite and water

TABLE II

RESULTS OF EXPERIMENTS #5 AND #6 USING THE CAMERA, RASTER AND SWEEP OSCILLOSCOPE

Expt. #5						
Probe No.	Distance from Donor (mm)	Distance from Spark			C - S (µsec)	C - R (µsec)
		Sweep Scope S(µsec)	Raster Scope R(µsec)	Camera C(µsec)		
1	4.2	47.43	47.72	48.0	+ 0.6	+ 0.3
2	12.0	45.73	46.08	46.31	0.6	0.2
3	22.1	43.37	43.65	43.90	0.5	0.3
4	34.6	40.27	40.36	40.48	0.2	0.1
5	47.4	36.59	36.59	36.89	0.3	0.3
6	60.1	31.97	32.14	32.66	0.7	0.5
7	72.7	28.27	28.24	28.80	0.5	0.6
8	85.3	23.29	23.38	24.42	1.1	1.0
Spark		0	0	0		
Expt. #6						
1	4.2	46.52	47.01	-	-	-
2	12.0	45.12	45.56	44.97	- 0.1	- 0.6
3	22.1	42.32	42.77	42.77	+ 0.4	+ 0.0
4	34.6	39.25	39.61	39.61	0.4	0.0
5	47.4	35.34	35.68	35.75	0.4	0.1
6	60.1	-	-	31.74	-	-
7	72.7	26.70	27.01	27.71	0.9	0.6
8	85.3	22.50	22.74	23.56	1.1	0.8
Spark		0	0	0		

A. Pressure Probe Reliability

The construction of the pressure probe causes a time lag between the arrival of the shock and its recording. The distance between the bare copper wire and the outer copper tube is approximately 0.033 inches. To record the shock, the copper must travel this distance to make contact with the inner core. Moreover, the time lag should increase as the shock pressure and velocity decrease and the response of the pressure probes should fall further behind as the shock is attenuated. In Table II a comparison is made between data from the smear camera and the sweep oscilloscope (Col. 6) and between the smear camera and the raster oscilloscope (Col. 7). In all but one instance the camera did record the process before the electronic systems did. However, with the exception of probes #7 and #8, placed at a distance of 72.7 and 85.3 mm from the donor, the time lag was, on the whole, less than 0.5 microseconds. The sweep oscilloscope data were slightly higher, 0.6 microseconds.

Thus, the pressure probe may be used to interpret the shock velocity for the initial three inches of Lucite with fair accuracy and reliability. Beyond this, as the shock wave becomes more attenuated, the time lag increases. At its worst (four inches of Lucite) the divergence of the probe results from the optical results does not exceed 6%. The sensitivity of most propellants and explosives tested lie below the three inch limit. Consequently, the pressure probe measurements can be considered fairly adequate for this work.

B. Velocity vs Distance for Lucite

The results of the experiments are plotted in Figures V and VI. The data obtained with the pressure probes are plotted in Figure V. The precision of these measurements varied from a standard deviation of $\pm$ 2.3% to 4%. This precision includes any variation due to the probe, the position of the probe, or any variation of the Lucite or the tetryl booster. Included in this plot is the data obtained by the pressure probes placed in the gap material (see above. It is quite apparent that for the distances measured the cellulose acetate and Lucite systems are comparable.

In Figure VI, a comparison is made between the data obtained with the camera and the pressure probes. The lag of the pressure data behind the data recorded by the smear camera is quite evident after the shock was attenuated by traveling through three inches of Lucite.
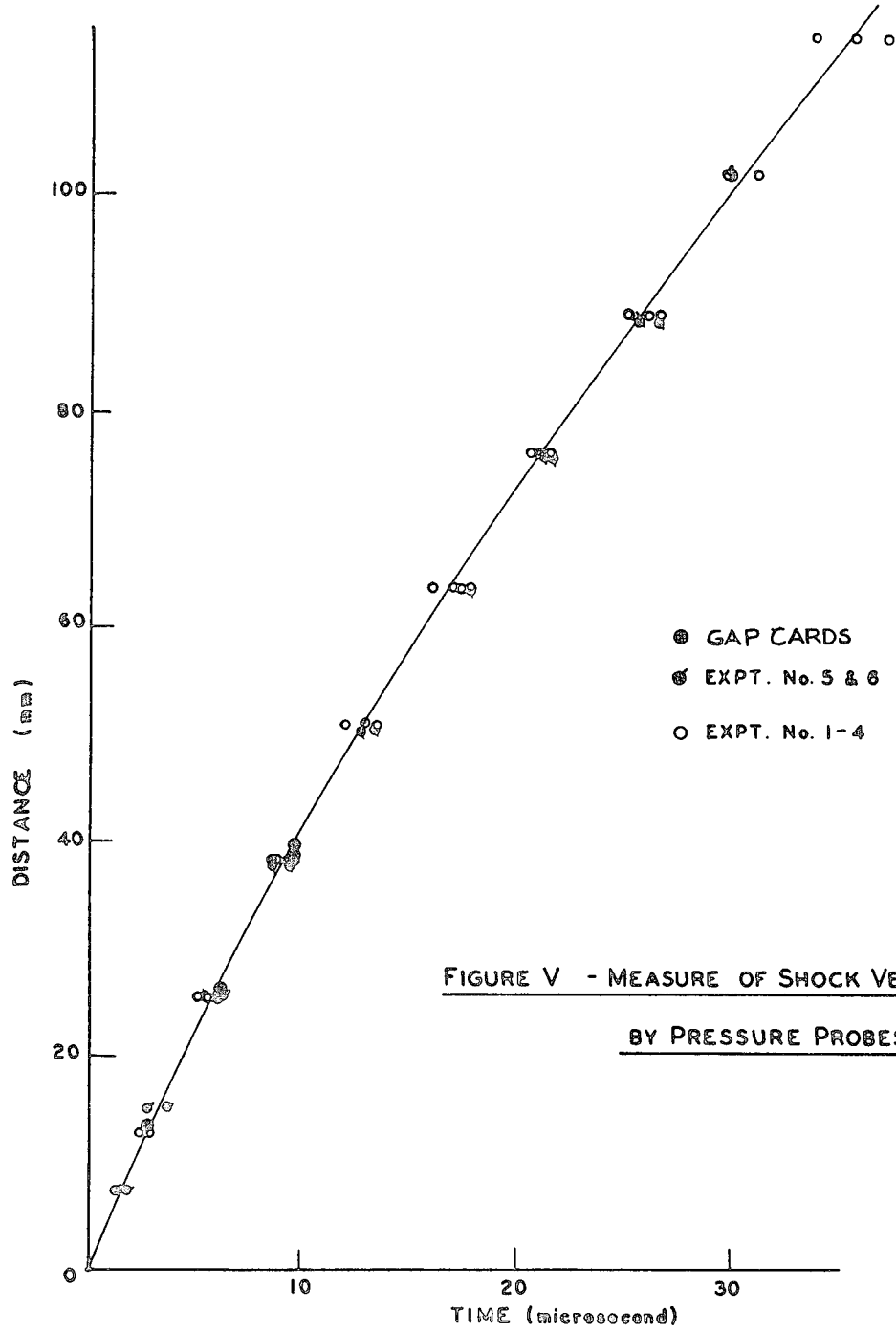
FIGURE V - MEASURE OF SHOCK VELOCITY

BY PRESSURE PROBES
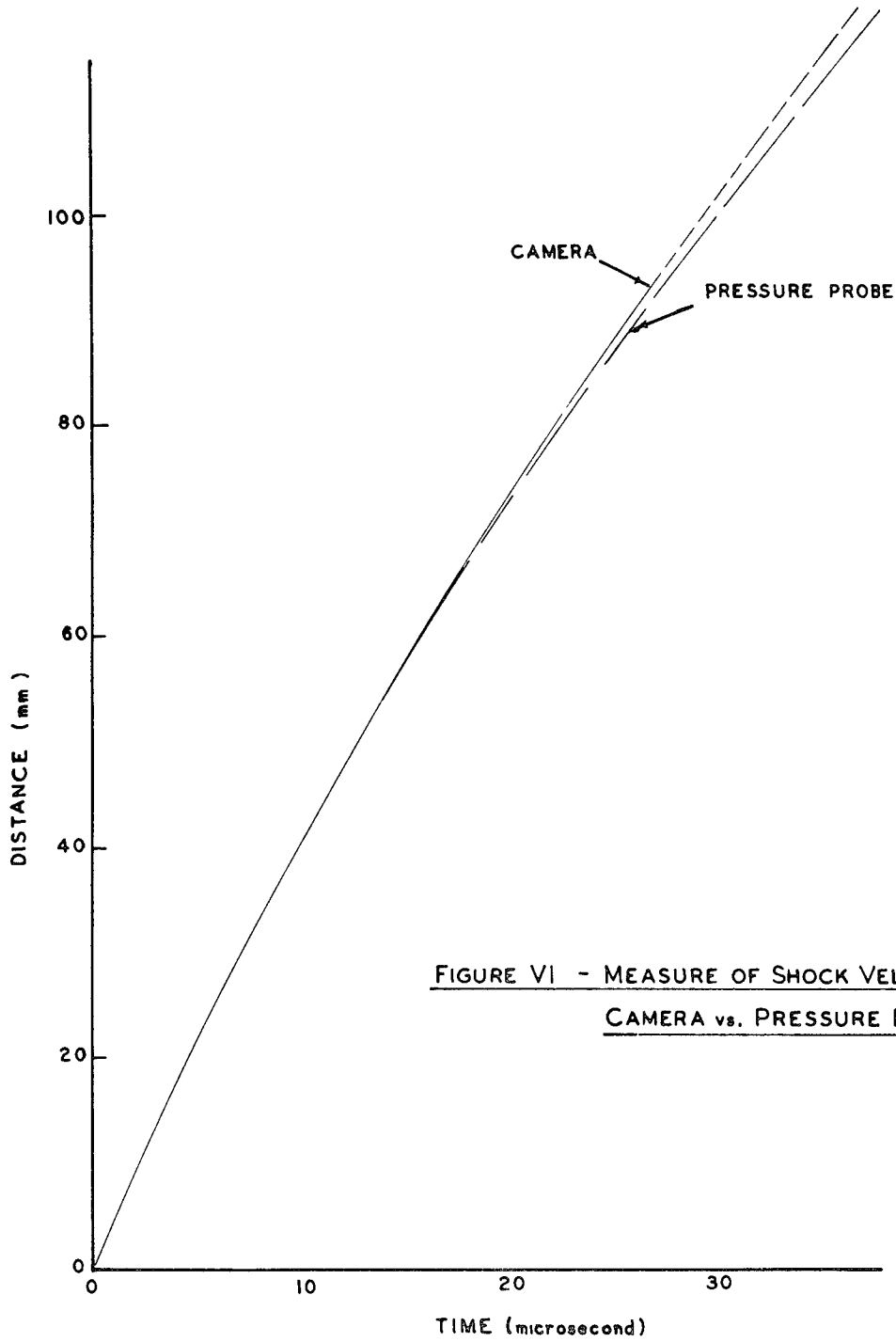
FIGURE VI – MEASURE OF SHOCK VELOCITY
CAMERA vs. PRESSURE PROBE

C. Pressure vs Distance for Lucite

In Figure VII the particle velocity was plotted as a function of the shock velocity from the experimental data obtained on Lucite (5), Plexiglass (6) and Perspex (7). These substances are quite similar in characteristics and it is assumed that their properties in the shock region do not differ from each other. However, the lowest shock strength obtained experimentally is at the upper end of the region critical to this investigation. Most shock sensitivity results on explosives are within the gap range of 30 to 65 mm and the maximum transmitted shock velocity obtained by the two tetryl pellets is about 4.6 mm per microsecond. The extrapolation to u = 0 is difficult since the shock pressure is obtained as a product of the particle and shock velocities.

The approximate shock pressures were obtained from the usual boundary approximations (8,9),

$$\mu_L = \mu_{H_2O} \frac{(\rho_0 U)_{H_2O} + (\rho_0 U)_L}{2(\rho_0 U)_L} \tag{2}$$

where

μ_L = particle velocity in Lucite

μ_{H_2O} = particle velocity in H_2O

ρ_0 = density of Lucite or water

U = shock velocity in Lucite or water

in conjunction with the experimental data obtained for the shock velocity in Lucite and water, and the particle velocity for water obtained from the literature (10). The calculated particle velocity for Lucite in Eqn. (1) yields the corresponding shock pressure.

Figure VIII is a typical plot of the results (Table II) obtained by the smear camera. The shock velocities for both Lucite and water are determined at the intersection of the respective curves which corresponds to the Lucite-water interface. Table III contains the measured shock velocities and the corresponding particle velocities calculated by Eqn. (2). Using these points for the lower pressure region and the other data already available in the higher pressure region a straight line was drawn through all the data. This curve (Fig. VII) was extrapolated to U = 2.59 mm per microsecond at μ = 0; the

FIGURE Ⅶ -U vs u FOR LUCITE
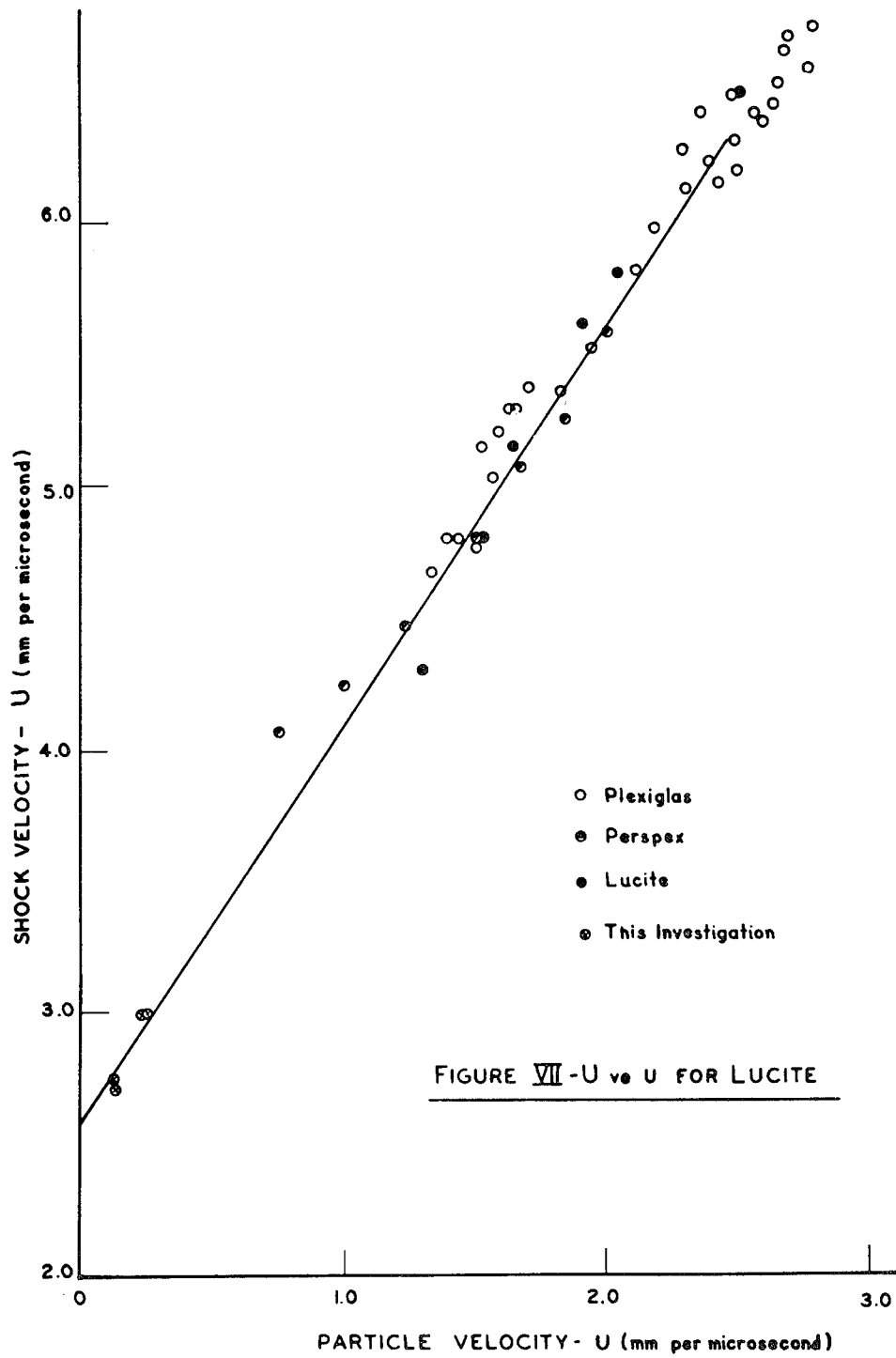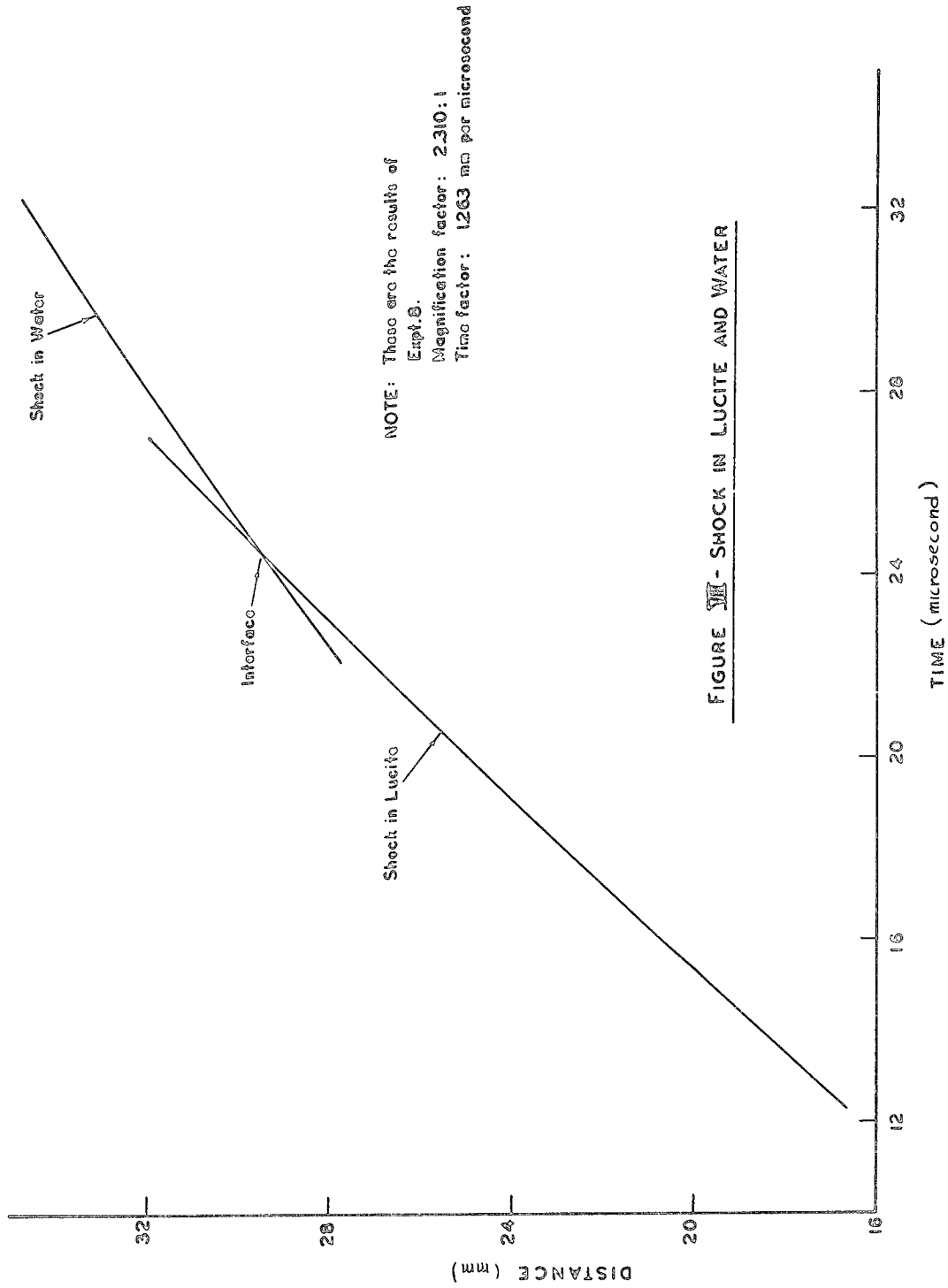
FIGURE VIII - SHOCK IN LUCITE AND WATER

Shock in Water

Interface

Shock in Lucite

NOTE: These are the results of
Expt.8.
Magnification factor: 2310:1
Time factor: 1.263 mm per microsecond

TIME (microsecond)

DISTANCE (mm)

extrapolated value is approximately equal to the hydro-
dynamic sound velocity calculated as 2.44 mm per micro-
second.

All the data required to develop a pressure-
distance curve (P vs X) are available. From experiments
5 thru 8 a U - X curve (shock velocity vs distance, Fig. VI)
was obtained for the specified geometry. In addition these
experiments provided the data (Table III) required to
calculate and complete the U - u curve (shock velocity vs
particle velocity, Fig. VII). Using these two curves and
Eqn. (1) (P = $\rho_0 Uu$) it is possible to calculate P - X
(pressure vs distance, Table IV) and obtain the curve in
Figure IX in which the pressure appears to vary expo-
nentially with the distance. Figure X is a plot of log P
vs X and may be approximated by the equation

$$P = 105e^{-0.0358X} \tag{3}$$

These curves will allow direct interpretation of gap
length in terms of shock pressure obtained at the end of
the Lucite gap. While this pressure is somewhat higher
than the pressure entering the acceptor because of the

TABLE III

SHOCK VELOCITY IN LUCITE AND H_2O, OPTICAL DATA

Expt.No.	Conversion Factor**	U_L mm/μsec	U_{H_2O} mm/μsec	μ_{H_2O} mm/μsec	U_L(calc) mm/μsec
5	4.043	2.701	1.840	0.162	0.128
6	4.274	2.744	1.817	0.160	0.125
7	2.938	2.990	2.130	0.312	0.250
8	2.911	2.952	2.069	0.281	0.224

** The conversion factor contains both the magnification
factor and time factor.

FIGURE IX. P VS. X FOR LUCITE

FIGURE 10- Ln Pressure vs. Distance
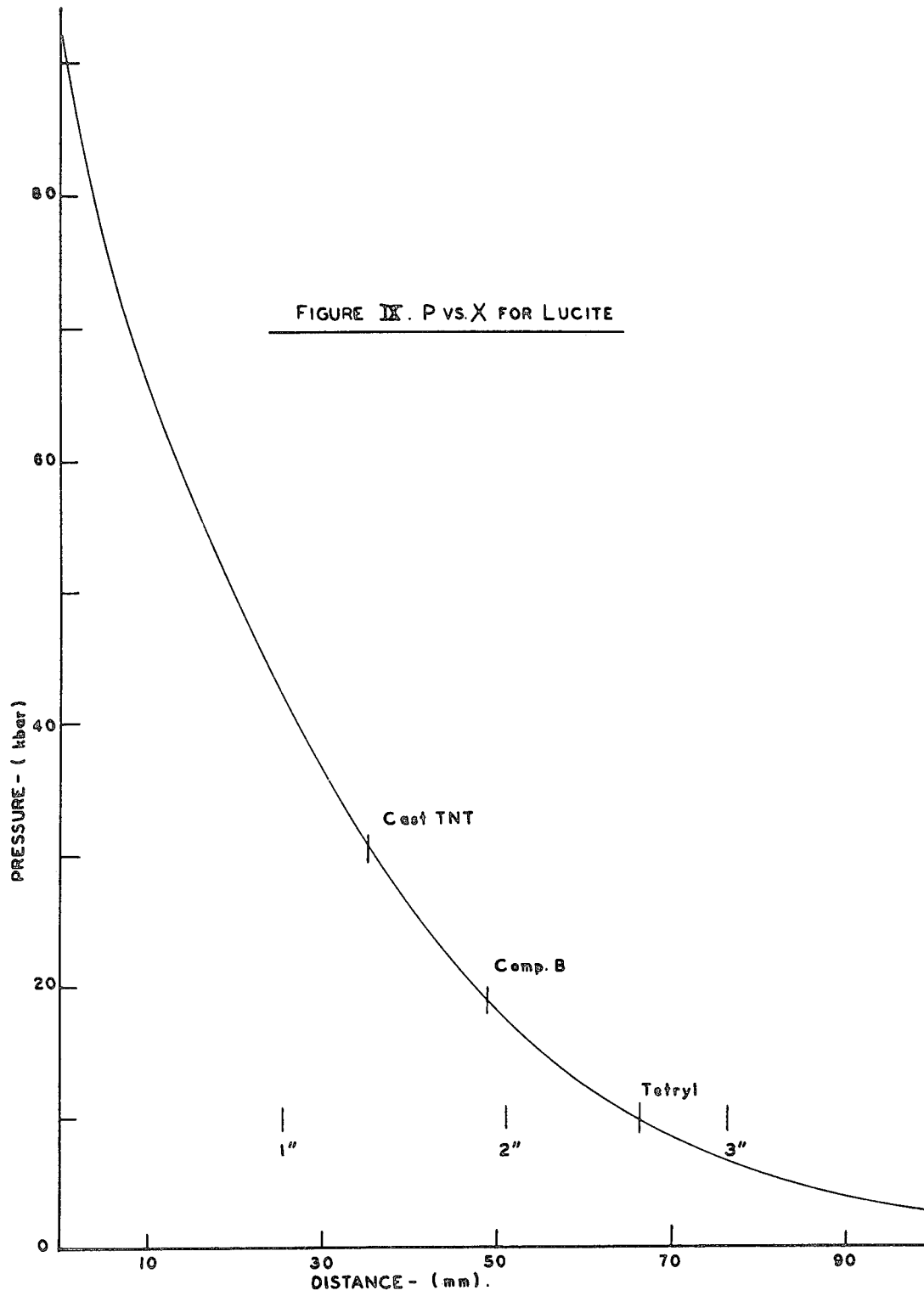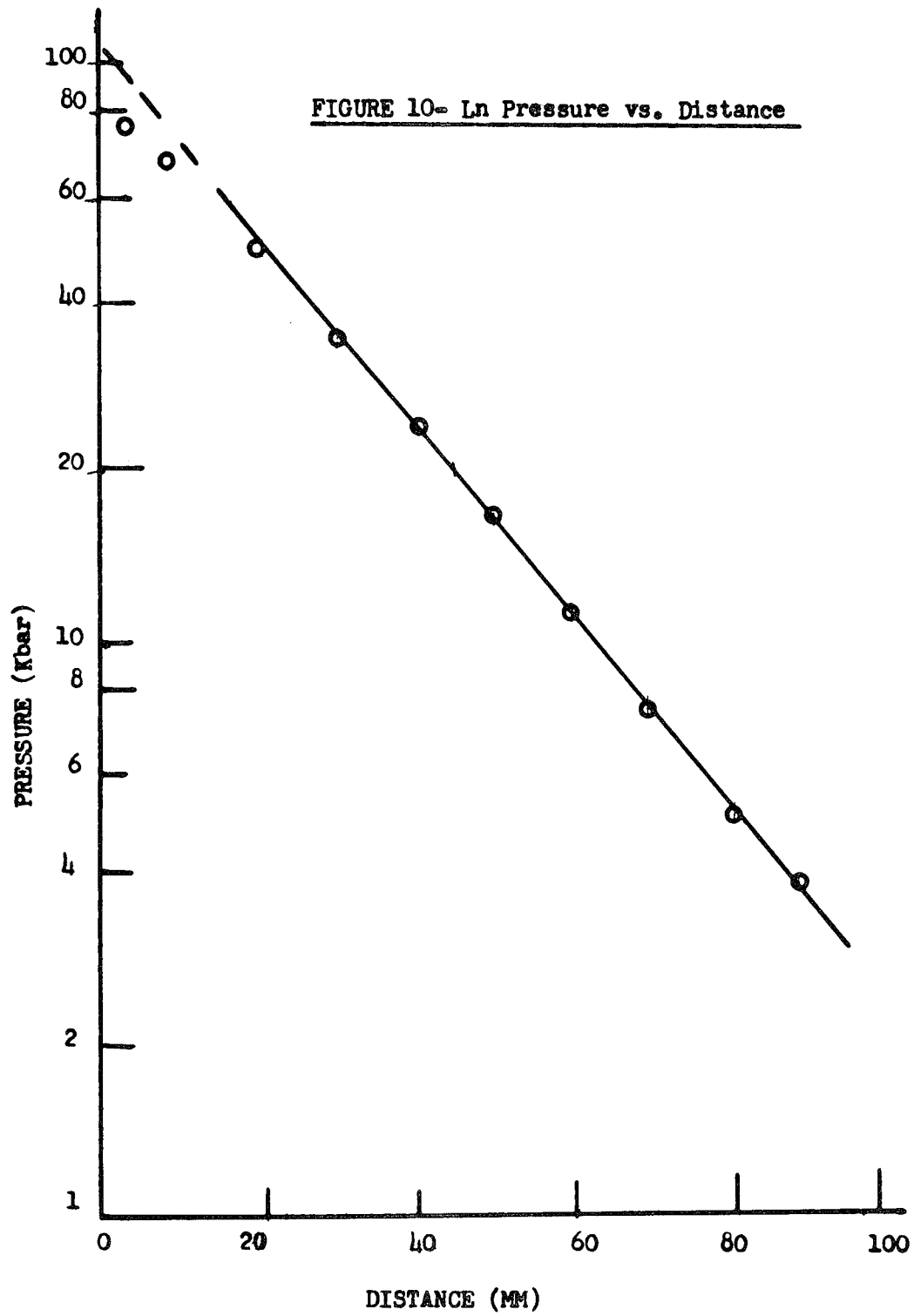
impedance mismatch between the donor and acceptor, it is hoped that this scale of P vs X will offer additional guidance in the sensitivity work. This is especially so since the impedance of Lucite is so near the range found for most explosives. The pressures required to initiate the explosives TNT (34.5 kbar), Composition B (19 kbar) and tetryl (10 kbar) have been indicated in Figure IX.

TABLE IV

CALCULATED PRESSURE AND DISTANCE DATA FOR LUCITE

Distance mm	Pressure Kbar
5	75.47
10	66.08
20	50.95
30	36.83
40	26.31
50	18.29
60	12.44
70	8.51
80	6.06
90	4.35
100	2.89

REFERENCES

1. A. B. Amster, R. L. Beauregard, G. J. Bryan, and E. K. Lawrence, NavOrd Report 5788, Detonability of Solid Propellants, 1. Test Methods and Instrumentation, 3 February 1958.

2. A. B. Amster, R. L. Beauregard, and G. J. Bryan, NavOrd Report 6222, Detonability of Solid Propellants, II. Sensitivity of Some Double Base and Composite Propellants, 15 December 1958, Confidential.

3. A. B. Amster, R. L. Beauregard, G. J. Bryan, and E. K. Lawrence, NavOrd Report 6091, Current Status of the Propellant Sensitivity Program at NOL, 20 May 1958, Confidential.

4. A. B. Amster and R. L. Beauregard, Rev. Sci. Inst. 30, 942 (1959).

5. Los Alamos Scientific Laboratory, private communication.

6. N. Coleburn, Naval Ordnance Laboratory, private communication.

7. J. S. Buchanan, H. J. James, and G. W. Teague, Armament Research and Development Establishment ARDE Memorandum (MX)20/59, April 1959.

8. H. D. Mallory, NavOrd Report 1883, The Measurement of Detonation Pressures in Explosives, 5 March 1953, Confidential.

9. W. C. Holton, NavOrd Report 3968, The Detonation Pressures in Explosives as Measured by Transmitted shocks in Water, 1 December 1954, Confidential.

10. M. H. Rice and J. M. Walsh, J. Chem. Phys. 26, No. 4, 824 (1957).

11. C. B. Officer, Introduction to the Theory of Sound Transmission, McGraw-Hill Book Co., Inc., N.Y., 1958.

12. American Institute of Physics Handbook, McGraw-Hill Book Co., Inc., New York, 1957.

A COMPUTATIONAL TREATMENT OF THE TRANSITION
FROM DEFLAGRATION TO DETONATION IN SOLIDS

C. T. Zovko and A. Macek
U. S. Naval Ordnance Laboratory
Silver Spring, Maryland

ABSTRACT: Experimental results of the study of
spontaneous transition from deflagration to detonation at
the Naval Ordnance Laboratory indicate that the approach
to the problem can be in two stages; the first is the
formation of a shock from pressure waves engendered by a
confined deflagration, and the second the shock-initiation
of detonation. Since a preliminary analytical treatment
of the first stage, reported previously, led to promising
results, a more extensive IBM-704 program has now been
undertaken. Two numerical codes have been tested, a pre-
viously developed one based on the so-called "q-method"
and a special one written for this program which avoids
amplitude fluctuations inherent in the "q-method" and thus
gives a more realistic representation of a shock wave.
Representations of spontaneous shock formation obtained by
the two numerical codes and by the analytical treatment
are discussed and compared. The numerical methods yield
the temperature as a function of time and location during
growth of the shock and thus allow a study of simple
chemical kinetic models. Introduction of chemical ki-
netics into the program gives a basis for elucidation of
the second stage of the transition problem, namely shock-
initiation of detonation.

While the phenomena of deflagration (slow, pressure-
dependent burning) and detonation are reasonably well
understood, spontaneous transition from one regime to the
other is still in early exploratory stages, and it is one
of the major unsolved problems in explosives technology.
Gross experimental features of the phenomenon have emerged
only recently (1,2,3,4,5). It appears that the onset of
detonation in condensed explosives is preceded by a rela-
tively long (up to 80 μsec) interval of rapid burning
which propagates at a fraction (1/10 to 1/5) of the steady

state detonation velocity. There is also evidence that the actual transition from rapid burning (sometimes termed "low order detonation") to steady state detonation takes place rapidly (within several microseconds) at a plane some distance ahead of the burning front.

The evidence thus far is consistent with the hypothesis that the onset of detonation is due to a shock wave which arises spontaneously as a result of deflagration, and which initiates detonation in unburnt explosive. The hypothesis was subjected to quantitative scrutiny at this Laboratory; in addition to experiments mentioned above, a preliminary theoretical treatment was carried out (6) by means of the following model:*

A thermally initiated (slow) laminar flame progresses into a homogeneous solid explosive charge. Pressure of the hot products, because of rigid confinement, increases steeply and, in consequence, sends compression waves into unburnt explosive.

On this basis it was shown that compression waves thus formed coalesce into a shock wave within 10-15 cm from the region of thermal initiation. Since, experimentally, the typical pre-detonation distance is in the same range (6-14 cm), it appears reasonable to suppose that the theoretically computed shock is the direct cause of detonation.

While the analytical methods thus give promising results, it is very desirable to extend the treatment in two ways: first, by repeating the computation using different equation of state parameters and different shock-generating pressure pulses; and second, by calculating the energy (or temperature) as a function of time and distance. The latter computation can then, in principle, be used to study the chemical kinetics of the explosive reaction during build-up and thus elucidate the transition phenomenon. Such an extension clearly calls for machine computation. This report gives an introduction to the computational program which is now in progress.

The report consists of four parts. The first part describes the scope of the program treated so far and the equation of state used. The second and third parts describe two different numerical codes for the IBM-704 computer and compare the results from these codes with the previously obtained analytic results. The fourth part describes the shock formation, chemical kinetics and shock initiation.

---

* Reference 6 gives the conceptual and analytical basis of the computational work described below, and it will be frequently referred to in the subsequent pages.

SCOPE OF THE PROBLEM

A. Hydrodynamics

As has been stated above, the approach to the problem of transition to detonation at the Naval Ordnance Laboratory has been via two stages. The first one is formation of a shock from pressure waves engendered by a confined deflagration. The second one is shock-initiation of detonation.

The shock formation problem is programmed in the following way: The difference equations for conservation of mass, momentum and energy are written down as applied to a one-dimensional flow problem. The explosive charge, which obeys an equation of state described below, is divided into N zones ($0 < N < 500$). At time $t = 0$ the pressure throughout the charge is fixed at a low but finite value ($P(t=0) = 0.08$ kbar). At subsequent times, the near boundary is subjected to prescribed pressures increasing with time. The result is that compression waves of increasing amplitudes travel forward from the near boundary.

For a realistic description of the transition process the pressure at the near boundary must simulate the backing pressure rise in a confined deflagration. In such a case the theoretical relationship between P and t, derived in Ref. 6, is given by

$$t = K \int_{P_0}^{P} \frac{dP}{P(A-P)^2} \qquad , \qquad (1)$$

where K and A are constants; at low pressures this is sufficiently well approximated by the exponential $P = P_0 e^{kt}$ where P_0 (i.e. pressure at t=0) and k are experimental parameters. The exponential form, which was used previously in the analytical treatment, is used also in the machine computations. However, an indefinitely long exponential pressure increase would be unrealistic, because it would lead to unreasonably high pressures as well as to extremely high values of dP/dt. In reality, such a situation does not occur; rather, the pressure will increase until the confinement is broken and then decrease. As a crude simulation of such behavior the pressure in the computation is allowed to increase exponentially until about 10 microseconds after the estimated bursting pressure of the steel casing has been attained; thereafter, the pressure is assumed constant. The last stipulation may be at least partly justified if one assumes that the actual pressure decrease is relatively slow; it appears rather more

realistic than the other extreme, namely a discontinuous pressure drop to zero, which would cause too rapid a rear-rarefaction to set in. Thus the assumed near boundary condition is

$$P = P_o e^{kt} \qquad t \leq t(P_{max})$$

$$P = P_{max} \qquad t \geq t(P_{max})$$

Hydrodynamically, the problem of coalescence of compression waves into a shock can be divided in two parts. In the first part the compression is isentropic and the flow is simple. The compression energy is E_s and the temperature attained, T_s, is given by $T_s - T_o = \frac{E_s}{C_v}$, where C_v is heat capacity of the explosive and T_o the ambient temperature. This part was treated analytically in Ref. 6 by the method of characteristics. The method, in fact, is valid only for such simple flow (i.e. no shocks); it does not give a basis for further calculation; in particular, it cannot show where and when the shock becomes strong enough to initiate detonation.

The second part of the problem starts with the overlap of simple waves. The flow then ceases to be simple and there is an increase of entropy across the compression wave. As P and dP/dt at the near boundary increase, shock compression conditions, described by the Rankine-Hugoniot relations, may ultimately be reached at the front of the disturbance. Since the most important part of the problem is expected to be the region of shock formation, i.e. region intermediate between simple flow and shock conditions, a parameter ζ , which measures the extent of shock nature is hereby defined such that

$$0 < \zeta = \frac{E - E_I}{E_H - E_I} < 1 \qquad (2)$$

Here E, E_I and E_H are actual (computed), isentropic and shock (Hugoniot) compression energies respectively, corresponding to a given pressure. (Since simple flow is isentropic ($\Delta S = 0$), an alternative parameter, $0 < \zeta' = \frac{\Delta S}{S_H} < 1$, could be defined to measure the extent of shock nature). The two parts of the hydrodynamic problem are thus characterized by $\zeta = 0$ and $\zeta > 0$ respectively; the upper limit of the parameter, $\zeta = 1$, corresponds to a full grown shock.

While in a condensed medium the difference, for a given pressure, in energy (and consequently in temperature) between the two modes of compression characterized by the extreme values of ζ will not be large, the difference in chemical reaction rates should be quite considerable and may mean a difference between failure and initiation of detonation. Hence it is convenient that, in addition to pressure, another parameter specifying the energy be known. ζ has been chosen because it gives a direct indication of deviation from simple flow conditions.

B. Equation of State

A generalized Tait equation of state has been chosen to represent the solid explosive

$$(P + B) V - (P_0 + B) V_0 = (\gamma - 1) (E - E_0) \quad (3)$$

With appropriate values of the constants B, and γ, the equation gives a remarkably realistic representation of the compression of solid explosives over a wide range of pressures*. Combined with the isentropic condition,

$$dE = -PdV, \quad (4)$$

the equation reduces to the form used in Ref. 6 (which does not include the energy):

$$P = \frac{B}{\gamma} \left((\frac{V_0}{V})^\gamma - 1 \right) \quad (5)$$

Explicit equations relating the various properties for isentropic compression and for shock compression on the basis of Eqn. 3 are collected in Table I.

The arbitrary parameters chosen in Ref. 6 were B = 105 kbar, γ = 3. The choice deserves a comment.

If Eqn. (3) is to be fitted to a set of data in a certain range of pressures, the constants B and γ can, in general, be assigned any convenient values. If, however, the lower limit of the range is P = o, by virtue of the relation

$$C = V \sqrt{-\left(\frac{\partial P}{\partial V}\right)_s} = \sqrt{V(\gamma P + B)}, \quad (6)$$

---

* The authors are indebted to Dr. S. J. Jacobs for having pointed out the promising possibilities of this extremely simple equation.

TABLE I

SUMMARY OF ISENTROPIC AND HUGONIOT FORMS OF THE EQUATION OF STATE USED IN THIS REPORT

The equation of state in its ordinary form is

$$(P + B) V - (P_0 + B) V_0 = (\gamma - 1)(E - E_0).$$

Isentropic

$$V = V_0 \left(\frac{\gamma P_0 + B}{\gamma P + B} \right)^{\frac{1}{\gamma}}$$

$$E - E_0 = \frac{V_0}{\gamma - 1} \left((P+B) \; \frac{\gamma P_0 + B}{\gamma P + B}^{\frac{1}{\gamma}} - (P_0 + B) \right)$$

Hugoniot

$$V = V_0 - \frac{2 V_0 (P - P_0)}{(\gamma+1)P + 2B + (\gamma - 1) P_0}$$

$$E - E_0 = \frac{V_0 (P^2 - P_0^2)}{(\gamma+1)P + (\gamma-1)P_0 + 2B}$$

the value of B is fixed by

$$B = \frac{C_o{}^2}{V_o} \qquad (6')$$

This is certainly the case in the shock formation problem, where in the early stages of shock growth, the pressure is quite low. The value $B = 105$ kbar used in Ref. 6 corresponds to an initial sonic velocity $C_o = 2.56$ mm/μsec, which is an average of the range of $2.25 - 2.85$ mm/μsec found by Majowicz (7) for a series of explosives. Thus the value of this parameter is realistic.

There is no doubt that the value of $\gamma = 3$, used in Ref 6 (and by some earlier workers), is too low, because it gives an unrealistically high compressibility. The reason why the value has been used at all is twofold. First, it is a carry-over from calculations of high pressure gases, such as detonation products, in which the Eqn. 3 with $B = 0$ and $\gamma \approx 3$ gives reasonable results. Second, and perhaps more important, the choice of $\gamma = 3$ lends convenient tractability to hydrodynamic equations. In particular, it allows the boundary path in the shock formation problem to be evaluated in closed form (see Ref. 8); this would be impossible for any value $\gamma > 3$ (and probably for most non-integral values).

Figure 1 shows a comparison of the computed $P - V$ relation for two different sets of parameters B and γ as well as experimental data of Majowicz and Jacobs (9). The high compressibility of a hypothetic material for which $\gamma = 3$ is evident. The value of $\gamma = 4.5$, on the other hand (combined with $B = 100$ kbar) is very realistic, and it is the current choice for the machine computations. However, since the analytical treatment exists (Ref. 6) in which the first set of values was used ($\gamma = 3$, $B = 105$), the preliminary computations discussed below, were run with this set of parameters for the sake of comparison.

The sonic velocity, corresponding to $B = 100$ kbar, is 2.5 mm/μsec, a most reasonable value.

NUMERICAL SOLUTION OF HYDRODYNAMIC PROBLEMS (GENERAL)

The general hydrodynamic problem is a solution of the equations of motion, state and energy release subject to appropriate boundary conditions. The equations of motion for a one dimensional case are

$$\rho_o \frac{\partial u}{\partial t} = -\frac{\partial P}{\partial x} \qquad \text{(conservation of momentum)} \qquad (7)$$
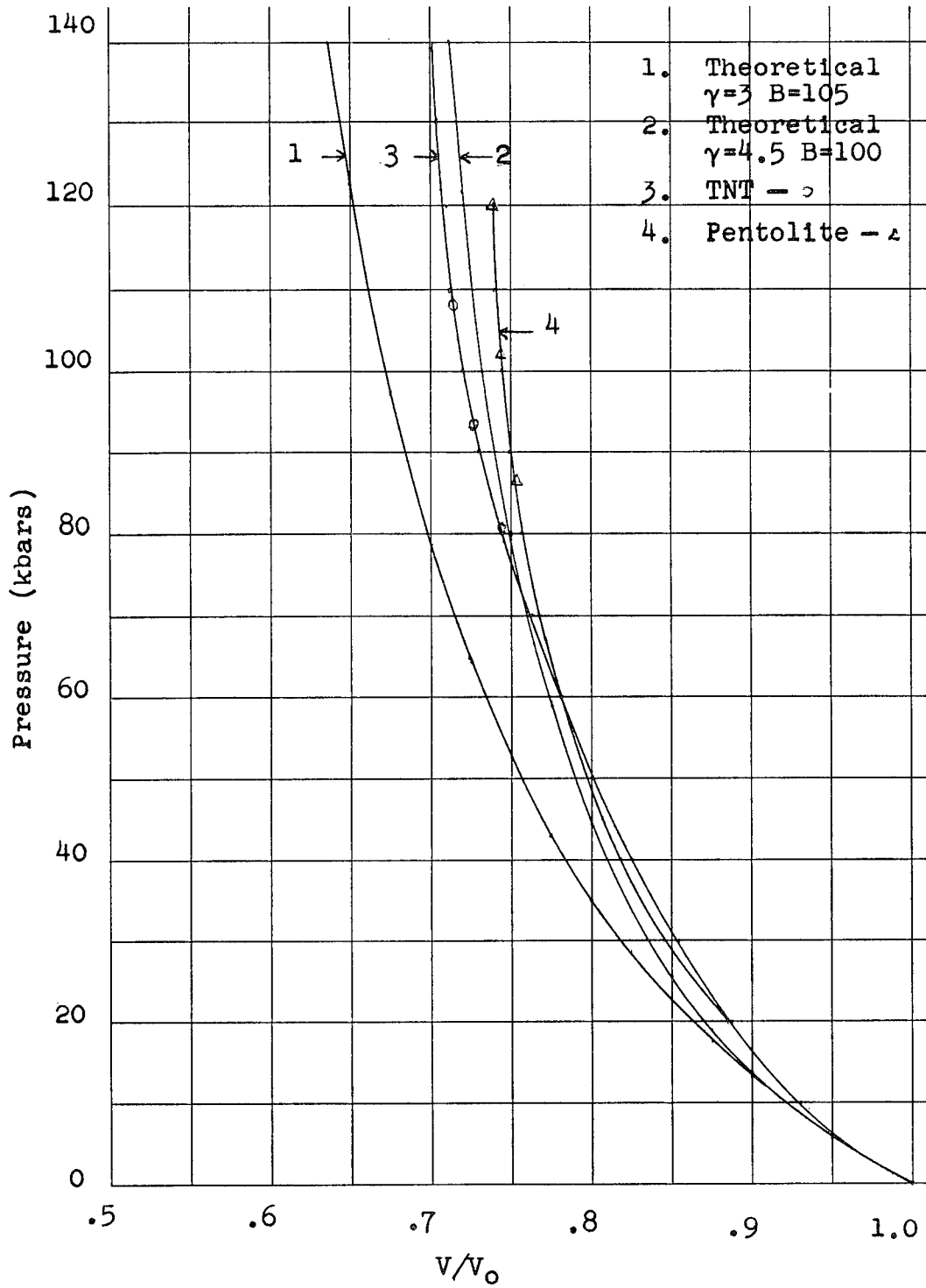
FIGURE 1 - Experimental and Theoretical Hugoniot
Curves for Unreactive Explosives

$$\frac{\partial E}{\partial t} - \frac{\partial Q}{\partial t} + P \frac{\partial V}{\partial t} = 0 \quad \text{(conservation of energy}$$

$$(8)$$

$$\text{and} \quad \rho_0 \frac{\partial V}{\partial t} = \frac{\partial u}{\partial x} \quad \text{(conservation of mass)}, \quad (9)$$

where   t   =   time

ρ_0 =   initial density

u   =   particle velocity

P   =   pressure

E   =   specific internal energy

Q   =   heat added per unit mass (from chemical reaction)

V   =   specific volume

X   =   distance

x   =   Lagrange coordinate defined by the relation

$$\frac{\partial X(x,t)}{\partial x} = \rho_0 V(x,t) .$$

The equation of state is

$$P = \Phi(E,V) . \quad (10)$$

The equation of chemical energy release is

$$\frac{\partial Q}{\partial t} = R(Q,E,V) . \quad (11)$$

One way to obtain a solution is by numerical techniques. This consists of dividing the Lagrange space coordinate (x) into a number of equal zones and approximating the differentials in equations 7, 8, 9 and 11 by finite difference ratios. In the difference equations, the dependent variables are usually specified at the interfaces between the zones or at the centers of the zones.

The boundary conditions must specify the values of the dependent variables for all values of the Lagrangian space coordinate (x) at time zero and for the end points (x = 0 and x = x_{max}) at all times. Once the boundary conditions are specified the difference equations can then be solved to obtain the values of the variables at the interior points.

Most differencing schemes have the limitation that they cannot handle discontinuities. The equations of motion (Eqns. 7, 8 and 9) admit discontinuous solutions; in fact, the discontinuities are the most interesting parts of the solutions. Two methods of overcoming this difficulty will be discussed in the next section.

The time increment (Δt) used cannot be chosen arbitrarily. A stability analysis (Ref. 10) of the problem will yield a maximum value of Δt with which reasonable results can be obtained. Stability analysis is an analysis of the history of an arbitrarily introduced error. Usually a critical value of Δt will be determined such that if Δt were to be made larger than this critical value, the error will increase, if Δt were to be made smaller than this critical value, the error will decrease and if Δt is made equal to this critical value the error will remain constant.

TWO SPECIFIC METHODS OF OBTAINING NUMERICAL SOLUTIONS TO HYDRODYNAMIC PROBLEMS

Two methods of handling discontinuities will be discussed in this section. They are the Richtmyer-von Neumann "q" method (Ref. 11) and the Lax method (Ref. 12). In both methods discontinuities are approximated by steep but finite slopes.

The "q" method eliminates discontinuities by the inclusion of an artificial dissipative term. Physically it can be considered as a one-dimensional viscosity. This dissipative term "q" is defined by the equation

$$q = -\frac{(K \Delta x)^2}{V} \cdot \frac{\partial u}{\partial x} \cdot \left| \frac{\partial u}{\partial x} \right| , \qquad (12)$$

where $K\Delta x$ = arbitrary constant.* $K\Delta x$ is approximately 1/3 the distance over which the shock is spread.

The term "q" is added to the pressure (P) and Eqns. (7) and (8) became respectively,

$$\rho_0 \frac{\partial u}{\partial t} = - \frac{\partial}{\partial x} (P + q) \quad \text{and} \qquad (13)$$

$$\frac{\partial E}{\partial t} - \frac{\partial Q}{\partial t} + (P + q) \frac{\partial V}{\partial t} = 0 . \qquad (14)$$

Equation (9), which does not contain pressure, is unchanged.

The resultant set of equations (Eqns. (9), (10), (11), (13) and (14) do not have discontinuous solutions. The solutions of the modified equations and the original equations are very nearly the same except in regions where the solution of the original equations would have a discontinuity. Equations (9), (10), (11), (13) and (14) approximate the discontinuity by a smooth but steep curve.

The Hugoniot relation across a shock,

$$E_f - E_i = \frac{1}{2} (P_i + P_f) (V_i - V_f) , \qquad (15)$$

is not affected by the inclusion of q.

Thus the "q" method is successful in that it eliminates discontinuities and gives a good approximation to the true solution in every aspect except details of the shock.

A computer (IBM 704) program which utilizes the "q" method and a second order differencing scheme was constructed at the Naval Ordnance Laboratory by W. Walker. Some results from this code will be discussed in the next section.

Another method for handling the problem of discontinuities was devised by Lax (Ref. 12). While the "q" method involves a quasi-physical concept and a modification of the equations of motion, the Lax method does neither. Rather, it handles discontinuities by the nature of its unusual differencing scheme. The Lax scheme

* Considering the arbitrary constant as the product of K and Δx is superfluous at this stage of the discussion. However, when the differential equations are replaced by finite difference equations the Δx mentioned above and the Δx used as the increment of the independent variable are identical. K is a dimensionless constant usually near unity.

requires that all of the differential equations be in perfect differential form, i.e,

$$A \ \frac{\partial Y}{\partial t} = \frac{\partial Z}{\partial x} \quad , \tag{16}$$

where A is a constant. This differential equation is then differenced in the following way

$$\frac{A}{\Delta t} \ \left(Y_x^{t+\Delta t} - \frac{1}{2} \ (Y_{x+\Delta x}^t + Y_{x-\Delta x}^t) \right)$$

$$= \frac{1}{2\Delta x} \ (Z_{x+\Delta x}^t - Z_{x-\Delta x}^t) \tag{17}$$

In so-called normal regions where $\frac{\partial^2 Y}{\partial x^2}$ is small,

$$\frac{1}{2} \ (Y_{x+\Delta x}^t + Y_{x-\Delta x}^t) \approx Y_x^t \quad . \tag{18}$$

In this case the Lax difference scheme approaches an ordinary forward difference scheme. Therefore, in normal regions, the solution obtained by the Lax scheme approaches the analytic solution.

In regions where $\frac{\partial^2 Y}{\partial x^2}$ is high (at shocks) Eqn. (18)

is not valid and the Lax scheme comes into effect. It causes any discontinuities (or other extreme changes) to be replaced by a steep but smooth change.

As mentioned earlier, the equations of motion must be in perfect differential form if the Lax scheme is to be used. The equations of conservation of mass (Eqn. (9)) and momentum (Eqn. (7) and the equation of chemical energy release (Eqn. (11)) are already in perfect differential form. A fourth, independent, perfect differential equation must be constructed. This can be done by multiplying Eqn. (7) by u, Eqn. (8) by ρ_0 and Eqn. (9) by -P and adding the results

$$\rho_0 \ \left(u \ \frac{\partial u}{\partial t} + \frac{\partial E}{\partial t} - \frac{\partial Q}{\partial t} + P \ \frac{\partial V}{\partial t} - P \ \frac{\partial V}{\partial t} \right)$$

$$= - u \ \frac{\partial P}{\partial x} - P \ \frac{\partial u}{\partial x} \tag{19}$$

Simplifying;

$$\rho_0 \; \frac{\partial}{\partial t} \; (\frac{1}{2} u^2 + E - Q) = - \frac{\partial}{\partial x} \; (Pu) \qquad (20)$$

One of the results of this task is a computer (IBM 704) program to solve hydrodynamic problems by the Lax method. Appendix I gives a description of this program.

Comparison of Analytic, "q" and Lax Methods

The general hydrodynamic problem solved numerically by the "q" and Lax methods as described above, will now be compared to the previously obtained analytic solution (6). The same equation of state and boundary conditions were used in all three calculations. Equation (3) was used as the equation of state. It was assumed that no reaction took place so $Q(x,t)$ was set equal to zero.

The following boundary conditions were used in all three calculations

$$P(0,t) = P(0,0) e^{kt} \qquad \text{for } t \leqq 60 \; \mu sec;$$

$$k = .1 \; \mu sec^{-1}$$

$$P(0,t) = P(0,60) \qquad \text{for } t \geqq 60 \; \mu sec;$$

$$P(x_{max},t) = P(0,0)$$

$$P(x,0) = P(0,0)$$

$$u(x,0) = 0$$

$$P(0,0) = .08 \; kbars$$

$V(x,0) = .6245$ cc/gm and $E(x,0) = 2 \times 10^4$ ergs/gm were the values calculated for an adiabatic compression from .001 to .08 kbars. These boundary conditions approximate the boundary conditions realized in the experimental work.

Figure 2 compares the P - X plots at 66 μsec obtained from the analytic, "q" and Lax methods. Except for fluctuations in the plateau, the "q" method agrees more closely with the analytic method than does the Lax method.

Figure 3 compares P - X plots at 100 μsec obtained from the "q" and Lax methods. At this time a real solution would have a discontinuity extending slightly below the plateau. The "q" method gives a somewhat closer approximation to this discontinuity than does the Lax method. However, the "q" method gives severe fluctuations in the plateau, while the Lax method gives none.
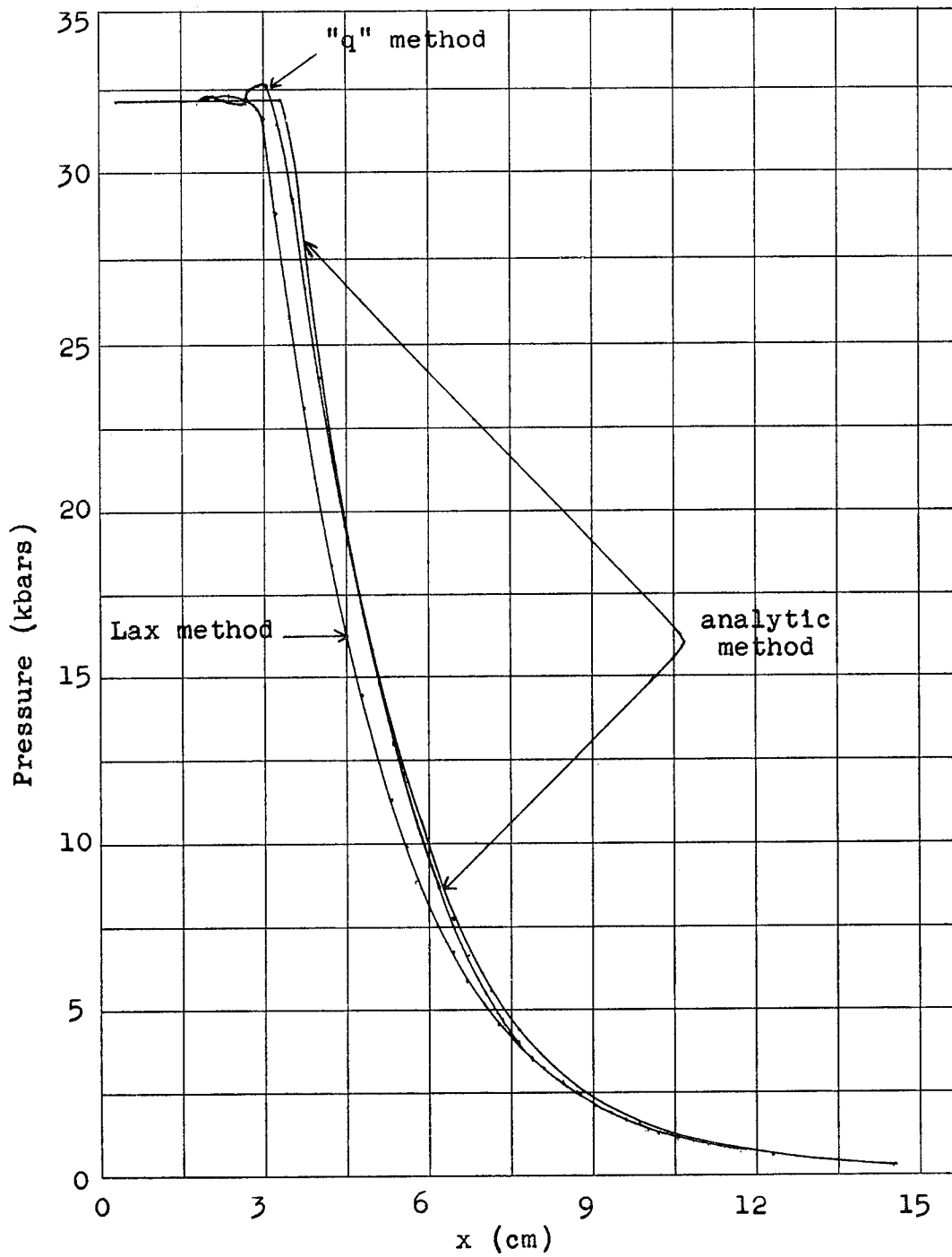
FIGURE 2

Pressure-Distance Profiles as Computed by the
Lax, "q" and Analytic Methods

The time of the computation is 66.1 μsec after
the first application of pressure.
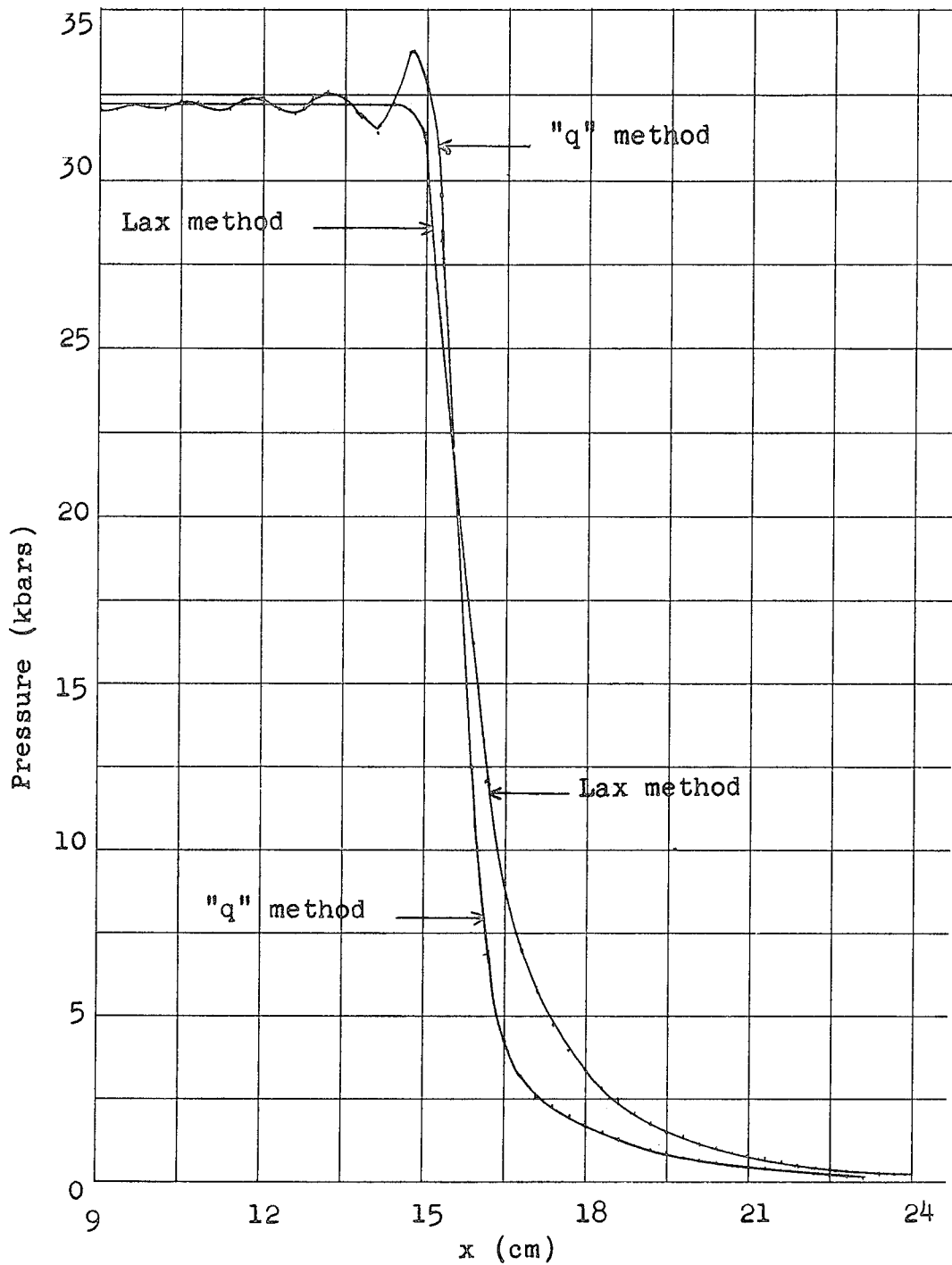
FIGURE 3

Pressure-Distance Profiles as Computed by the
Lax and "q" Methods

The time of the computation is 100 μsec after
the first application of pressure.

Because of the exponential dependence of reaction rates on temperature (i.e. energy), the spurious fluctuations inherent in the "q" method render the "q" method almost useless for reaction rate studies. Therefore all further numerical work discussed in this report is based on the Lax scheme.

SHOCK FORMATION AND INITIATION

A. Shock Formation

The analytic solution (Ref. 6) to this problem showed that a shock had started to form at about 12 cm from the boundary at 90 μsec. The analytic method cannot give the rate of shock growth.

The rate of growth of the shock is illustrated in Fig. 4 which gives energy-distance (or temperature-distance) profiles at several different times as computed numerically by the Lax method using the previously defined boundary conditions and equation of state. The generating pressure pulse was allowed to increase exponentially for 60 μsec so that the maximum pressure reached was P_{max} = 32.27 kbars; thereafter the boundary pressure remained at 32.27 kbars. In Fig. 4, the upper horizontal line gives the energy that would result from a shock compression to 32.27 kbars; the lower line gives the energy that would result from an isentropic compression to 32.27 kbars. The actually computed energy has increased perceptibly above the limiting isentropic value at 72.1 μsec, at which time the compression front is about 5.3 cm from the boundary. However, the transition from the isentropic compression to the shock compression is continuous; there is no sharp point of shock formation.

The growth of the shock is also shown in Fig. 5, in which the parameter ζ (evaluated at the compression front) is plotted against time. The figure also gives the location of the compression front as a function of time, so that the extent of the shock nature (ζ) in the front can be read both as a function of time and distance.

B. Shock Initiation

Figures 4 and 5 show that, assuming a chemically inert medium, the shock wave is half developed (ζ = .5) when the compression wave has travelled about 16 cm into the charge. The next step was to see whether the temperatures generated were sufficient to start a detonation in an actual (i.e. chemically reactive) explosive, and
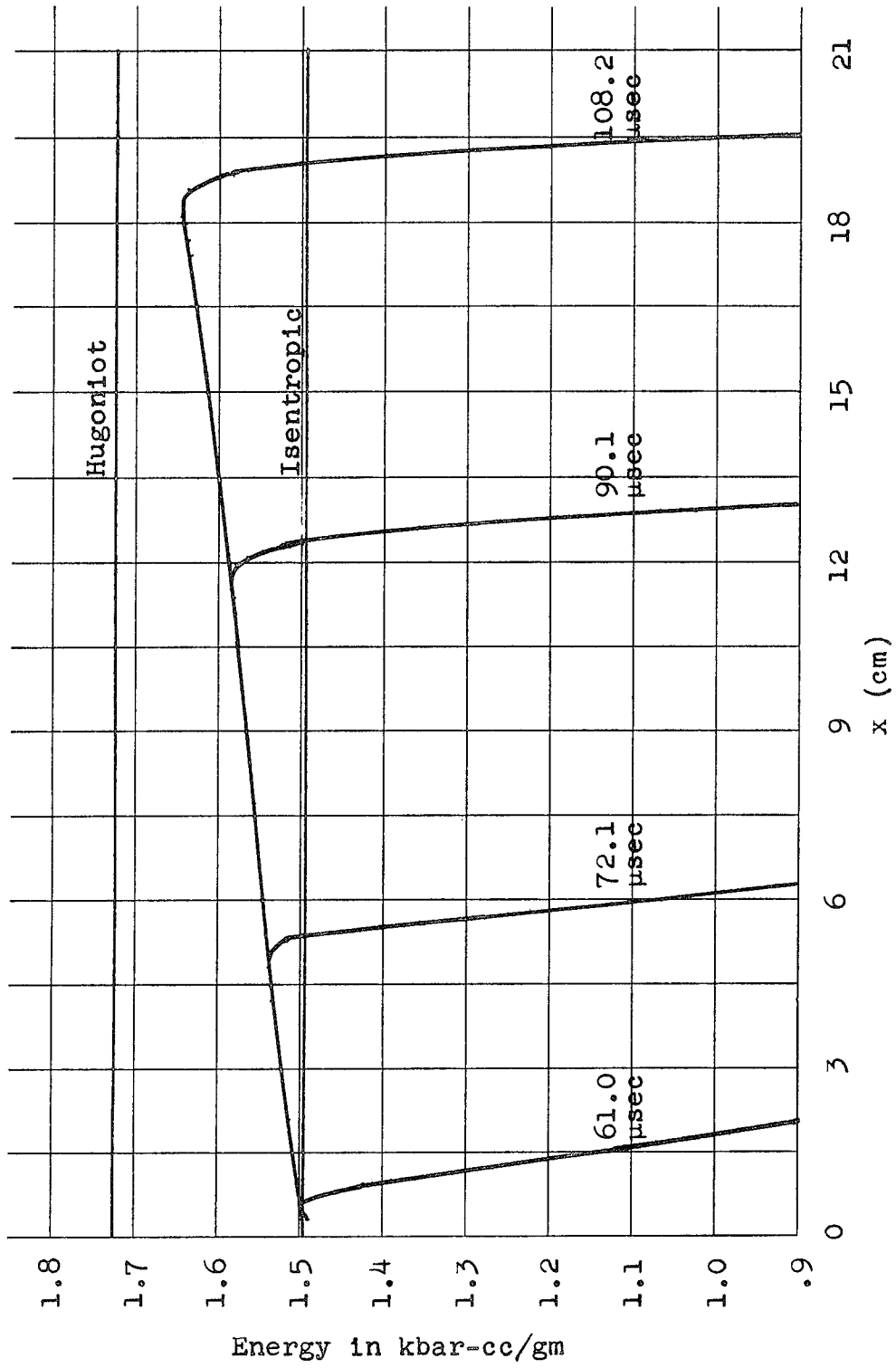
FIGURE 4 - Energy vs Distance at Several Different Times in a Non-Reactive Material
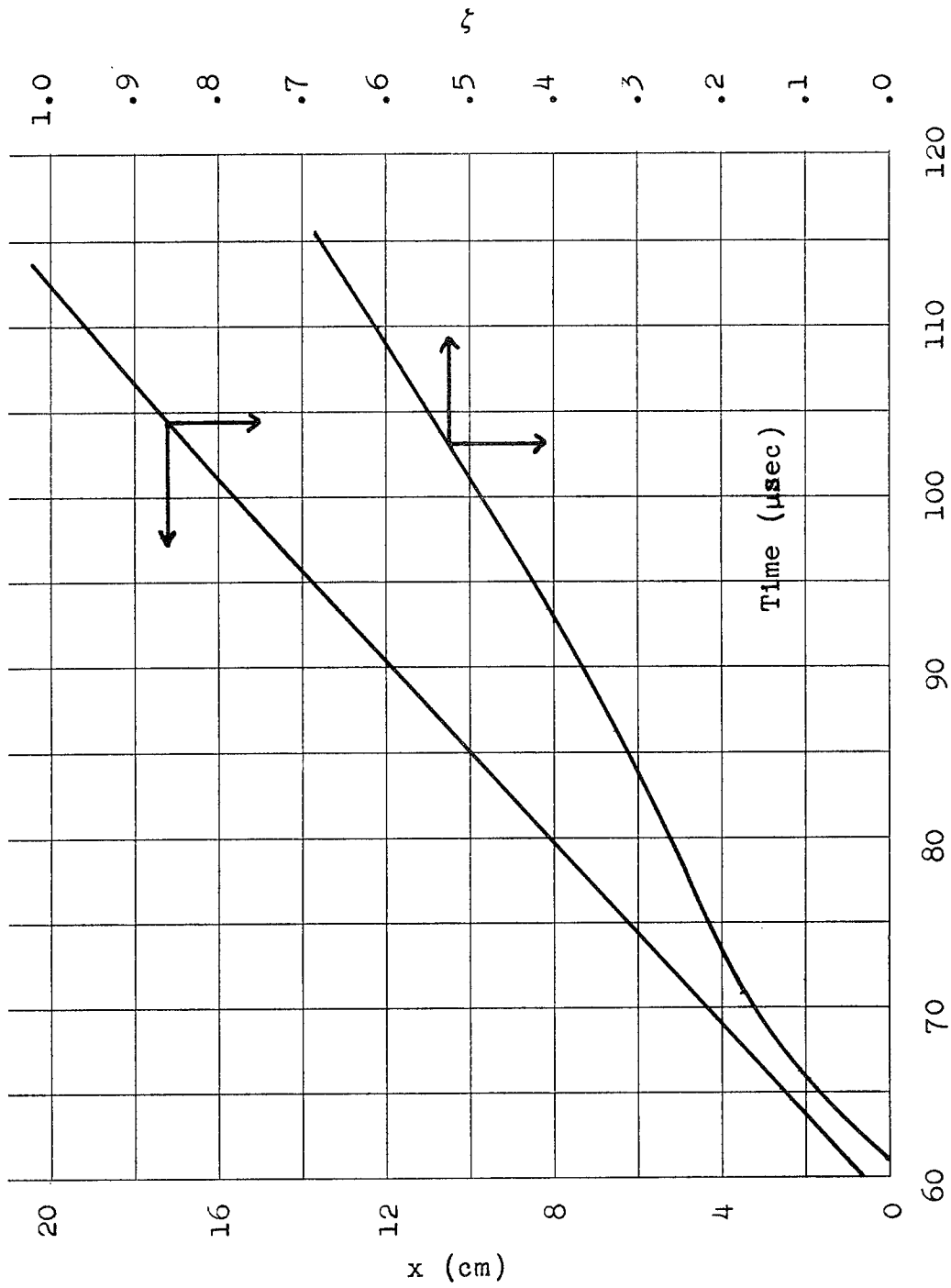
FIGURE 5 - x and ζ vs Time

where the detonation would start. The latter point is of particular interest because, experimentally in the NOL-DDT test (Ref. 6), the detonation starts about 15 cm. into the charge.

The computed point of initiation, in general, could be located anywhere between the boundary and the wave front. As seen in Fig. 4, the layer of explosive near the compression front is at a temperature higher than that of the boundary, but its residence time at that temperature is shorter. The point at which the chemical reaction rate becomes sufficiently high to generate a detonation wave will evidently depend on the specific parameters used in the computation.

In order to see if the theoretical model agrees with the experiments, a simple first order kinetic model was used, i.e.

$$\frac{\partial F(x,t)}{\partial t} = \left(1 - F(x,t)\right) Ae^{-\frac{E_a}{RT(x,t)}} \tag{21}$$

where,

$F(x,t)$ = mass fraction of burnt explosive,

A = preexponential factor,

E_a = activation energy,

R = gas constant,

and $T(x,t)$ = temperature.

$T(x,t)$ is defined by the equation

$$T(x,t) = T_0 + \frac{E(x,t)}{C_v} \tag{22}$$

Since $Q(x,t)$ is the energy liberated by the chemical reaction at a point (x,t) and ΔH is the heat of explosion of the explosive, then

$$F(x,t) = \frac{Q(x,t)}{\Delta H} \tag{23}$$

Therefore, equation (21) can be rewritten as

$$\frac{\partial Q(x,t)}{\partial t} = \Delta H \left(1 - \frac{Q(x,t)}{\Delta H}\right) Ae^{-\frac{E_a}{RT(x,t)}} \tag{24}$$

624

This is the explicit form of equation (11) that was used in the following calculations. The constants in equations (22) and (24) are

$$C_v = 1.254 \times 10^7 \; \text{ergs}/\text{gm}°\text{C}$$

$$\Delta H = 5.016 \times 10^{10} \; \text{ergs}/\text{gm}$$

$$A = 10^{14} \; \text{sec}^{-1}$$

$$E_a = 35,000 \; \text{cal}/\text{mole}.$$

A computer run was made using the previously discussed boundary conditions and equation (24) to compute the reaction rate. The maximum pressure was 32.27 kbars. The computed temperatures were too low to cause any appreciable reaction. The run gave results almost identical to the run represented in Fig. 4.

Figure 6 illustrates the most important result of this run. It is a plot of $F(x,t)$ vs x at several different times. It shows that after the shock is partly developed, the greater reaction rate in the interior (due to the greater temperature increase from the partly developed shock) causes the reaction to proceed farther than it does at the boundary.

A subsequent run was made with one important change. The near boundary pressure was,

$$P(0,t) = .08 \; e^{kt} \; \text{kbars for } t \leqq 67.5 \; \mu\text{sec}$$

$$k = .1 \; \mu\text{sec}^{-1}$$

$$P(0,t) = .08 \; e^{6.75} \; \text{kbars} = 68.32 \; \text{kbars for}$$

$$t \geqq 67.5 \; \mu\text{sec}$$

The higher pressure caused the temperature (i.e. energy) to reach higher values than in the previous run. The reaction rates from these higher temperatures were great enough to cause the reaction to go to completion.* The reaction first went to completion* 17.7 cm in from the

---

* The first order reaction assumed here would never actually go to completion, but in a numerical computation the reaction goes to completion. The error is completely neglibible.
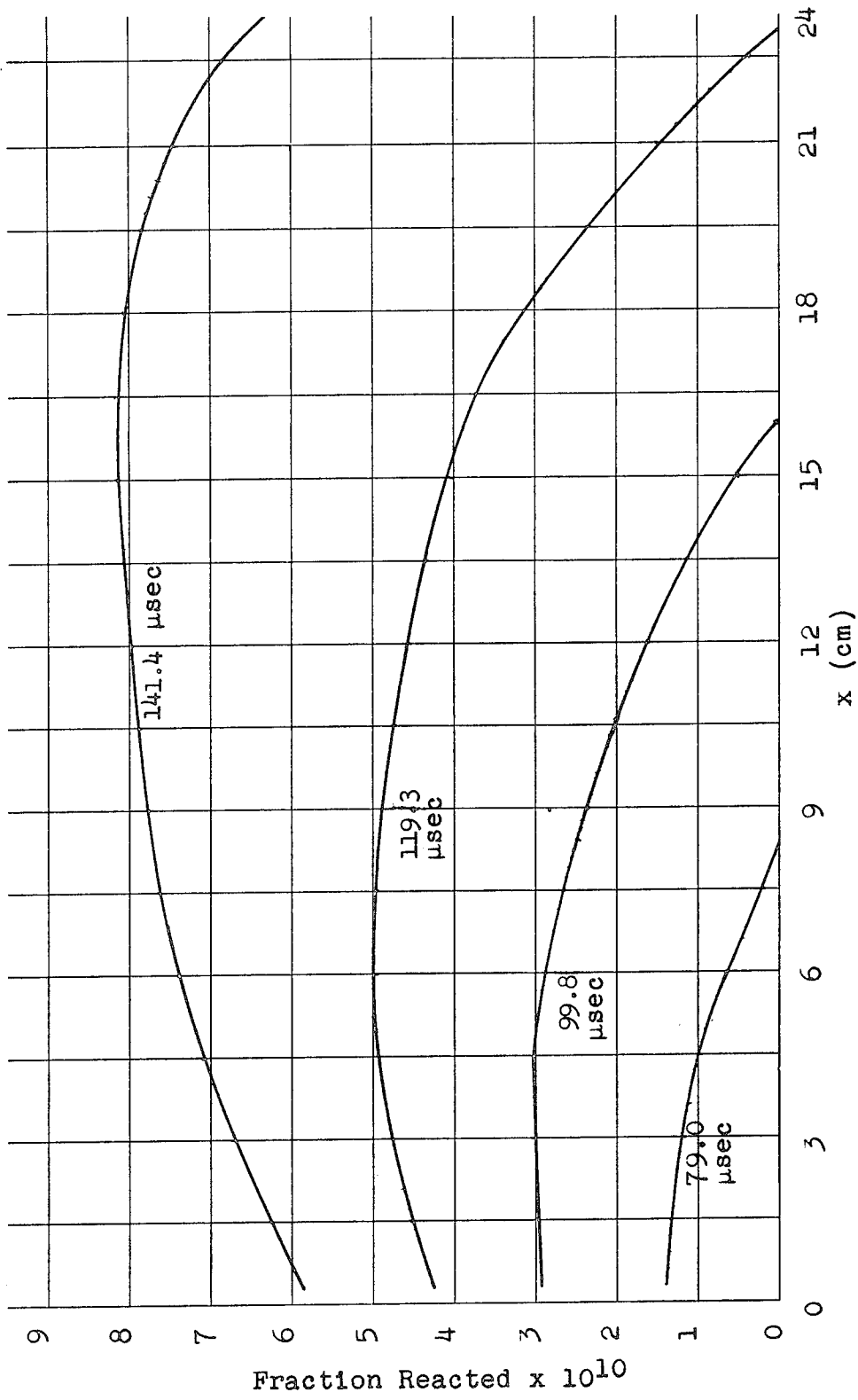
FIGURE 6 – Fraction Reacted vs Distance at Several Different Times

x (cm)

Fraction Reacted x 10^{10}

141.4 µsec

119.3 µsec

99.8 µsec

79.0 µsec

boundary. Figure 7 illustrates the course of the reaction. It is a plot of $F(x,t)$ vs x at several different times.

Figure 8 is a plot of $T(x,t)$ vs x at two different times from two different computer runs. In one run the material was assumed to be non reactive; in the other run the material was assumed to be reactive. The times chosen were slightly before and slightly after the reaction went to completion in the reactive run. The interior temperature is higher than the boundary temperature; this coupled with the exponential dependence of reaction rate on temperature caused the reaction to go to completion in the interior before it went to completion at the boundary.

Figure 9 is a plot of pressure vs x at several different times for the 68.32 kbar maximum pressure, reactive explosive calculation. It shows the development of the detonation wave.

DISCUSSION

Measurements and rough calculations (Ref. 6) indicate that the maximum boundary pressure attained in the NOL-DDT test is about 32 kbars. Calculations based on this maximum pressure and homogeneous first order kinetics show no appreciable reaction. This is not surprising since it is almost certain that initiation by weak stimuli (e.g. weak shocks) requires some mechanism of stress concentration (e.g. occluded grit or gas bubbles). The important result from the 32 kbar calculation was the observation that the reaction inside the charge surpassed the reaction at the boundary.

A later calculation was made based on a maximum boundary pressure of 68 kbars. This was done to compensate for the absence of stress concentrating mechanisms in the model used. This pressure was adequate to cause initiation of the explosive. The initiation started in the interior at a location comparable to the experimental results.

It was concluded from these calculations that the shock formation-shock initiation model for the transition from deflagration to detonation is essentially correct.
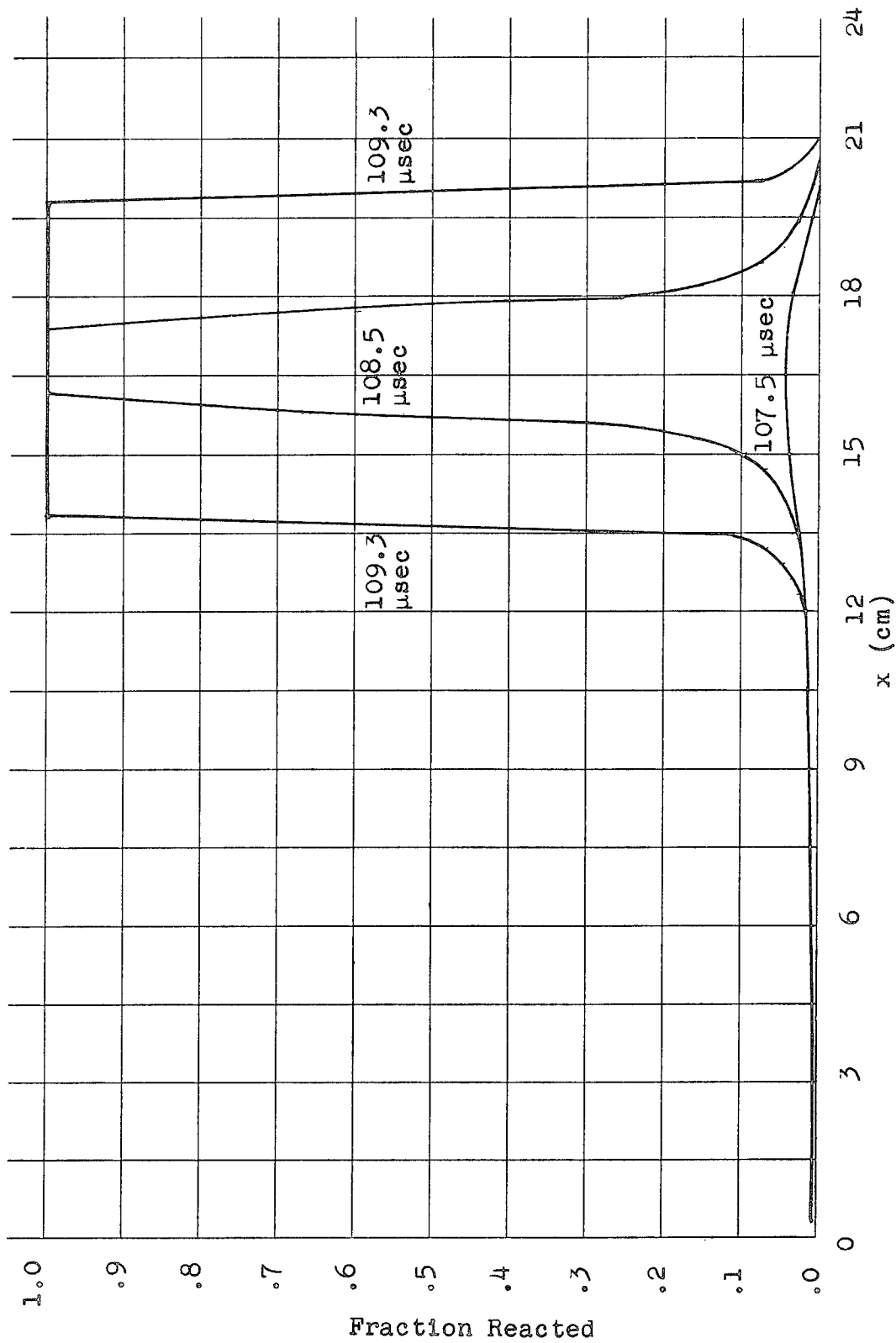
FIGURE 7 — Fraction Reacted vs Distance at Several Different Times
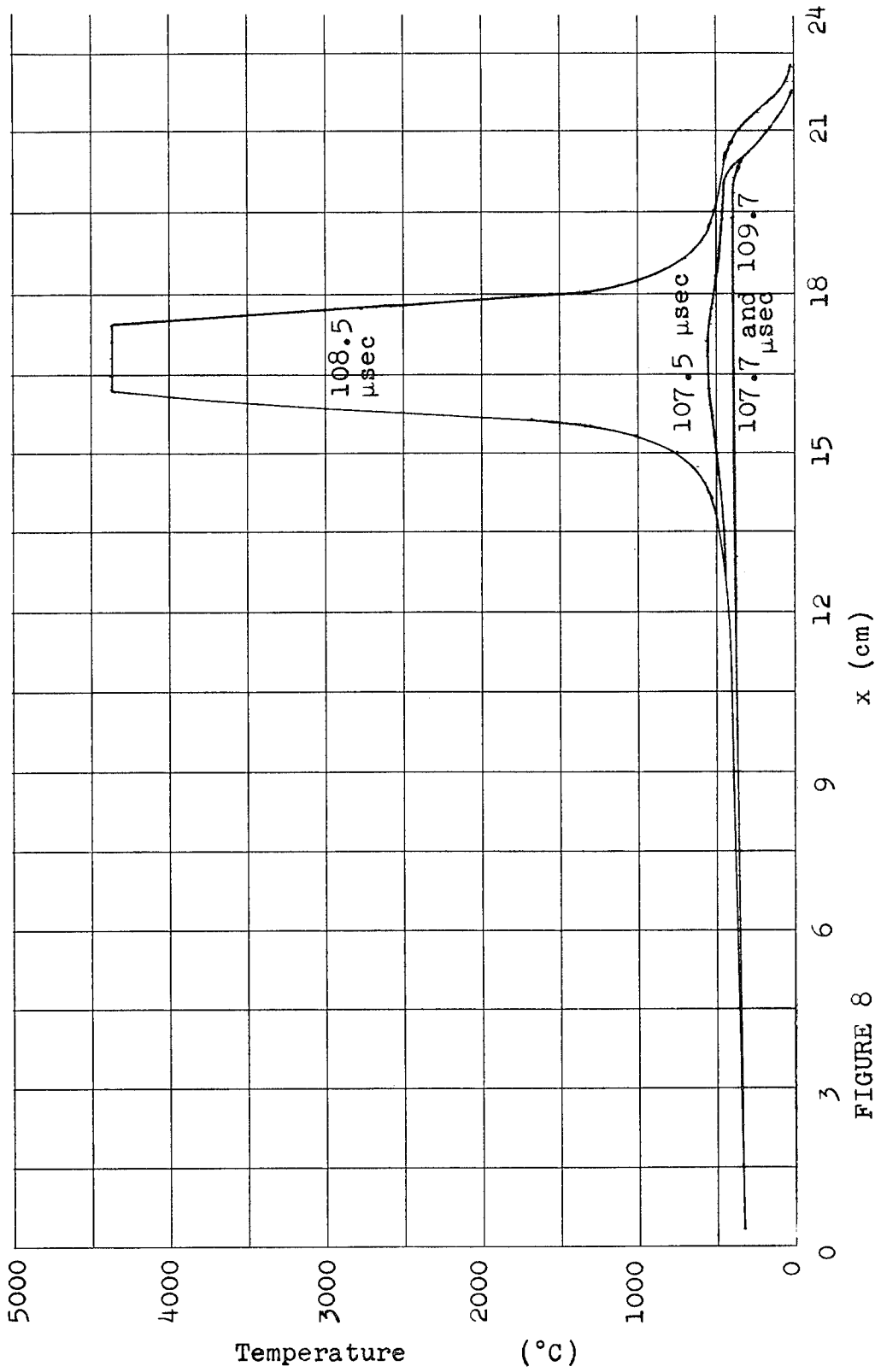
FIGURE 8

Temperature vs Distance at Several Different Times with Reactive and Non-Reactive
Materials
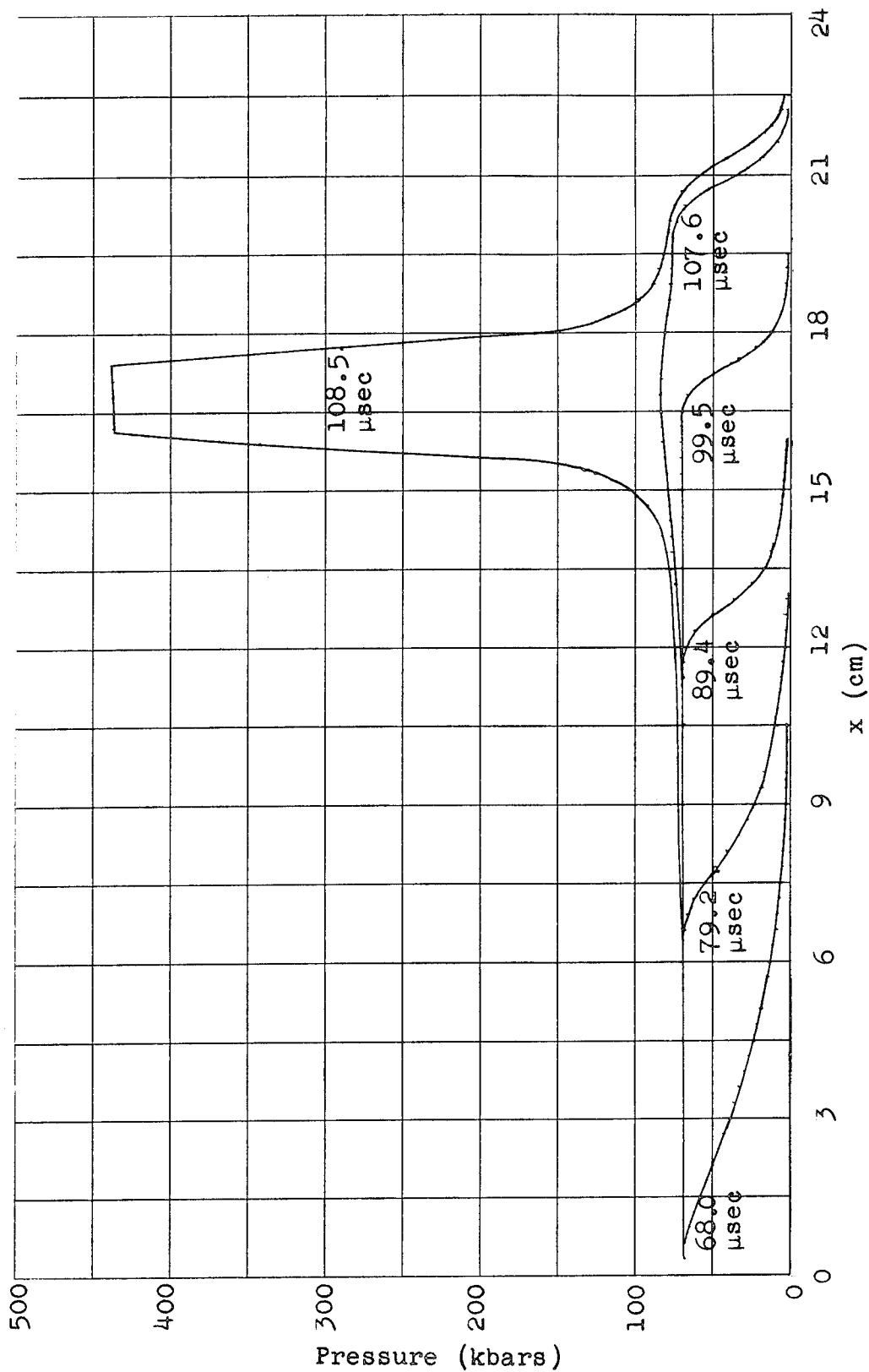
FIGURE 9 – Pressure vs Distance at Several Different Times with a Reactive Material

Start

| Read in initial conditions and constants |

Store initial values of P, V, Q, u and X

Calc. and store initial values of E — Equation of State Subroutine

Calc. sound speed at all interfaces — Sound Speed Subroutine

Calc. time increment from stability cond. Note 1

Integrate for new internal values of V and u Note 2

Calc. reaction rates — Reaction Rate Subroutine

Integrate for new internal values of Q, E and X Note 3

Calc. new internal values of P — Equation of State Subroutine

Evaluate variables at boundaries — Boundary Value Subroutine Note 4

Stop? — Yes → Stop

No

Print? — Yes → Print results — Output Subroutine

No

FIGURE 10. Flow Chart of Computer Program

REFERENCES

1. F. P. Bowden and O. A. Gurton, Proc. Roy Soc., 198A, 337 (1949); 198A, 350 (1949).

2. A. Macek and R. W. Gipson, NavOrd 5758, 1 November 1957; NavOrd 6104, 12 May 1958.

3. N. Griffiths and J. M. Groocock, ARDE Rep. (MX) 6/59. March 1959.

4. M. A. Cook, R. T. Keyes, W. S. Partridge and W. O. Ursenbach, JACS, 79, 32 (1957).

5. C. H. Winning, Proc. Roy. Soc., 246A, 288 (1958).

   (References 4 and 5 deal with initiation by relatively weak shocks, not by deflagration).

6. A. Macek, J. Chem. Phys., 31, 162 (1959).

7. J. M. Majowicz, unpublished.

8. A. Macek, NavOrd 6105, 12 May 1958.

9. J. M. Majowicz and S. J. Jacobs, NavOrd 5710, November 1957.

10. R. D. Richtmyer, "Difference Methods for Initial Value Problems", Interscience Publishers, Inc., N.Y., 1957.

11. J. von Neumann and R. D. Richtmyer, J. Appl. Phys., 21, 232 (1950).

12. P. D. Lax, Communications on Pure and Applied Math., 7, 199 (1954).

APPENDIX I

As a part of this task a computer (IBM 704) program was constructed to solve hydrodynamic problems on the basis of the Lax scheme. The program consists of a main routine in which the equations of motion are integrated and certain other unchanging operations are performed. Calculations involving the equation of state, reaction rates, boundary conditions and stability are carried out in subroutines. Thus if any of these things must be changed, only the appropriate subroutine need be re-programed.

The program runs according to the flow diagram in Figure 10. The following are notes to Figure 10:

(1) The stability analysis of this system shows that

$$\Delta t \; < \; \rho_o \; \Delta x \; \frac{V}{C} \qquad .$$

Δt is computed at every interface and the smallest value is used.

(2) At this step the equations of conservation of mass and momentum are integrated. The equation of conservation of mass (Eqn. 9), when differenced according to the Lax scheme, becomes

$$\frac{\rho_o}{\Delta t} \left(V_x^{t+\Delta t} - \frac{1}{2} (V_{x+\Delta x}^t + V_{x-\Delta x}^t) \right) \; = \; \frac{1}{2\Delta x} (U_{x+\Delta x}^t - U_{x-\Delta x}^t).$$

Since the values of all of the variables are known at t, this equation can be used to evaluate $V_x^{t+\Delta t}$. Likewise, the equation of conservation of momentum (Eqn. 7) when differenced according to the Lax scheme becomes,

$$\frac{\rho_o}{\Delta t} \left(U_x^{t+\Delta t} - \frac{1}{2} (U_{x+\Delta x}^t + U_{x-\Delta x}^t) \right) \; = \; \frac{1}{2\Delta x} (P_{x+\Delta x}^t - P_{x-\Delta x}^t).$$

Since the values of all of the variables are known at t, this equation can be used to evaluate $U_x^{t+\Delta t}$.

Since $0 < x < x_{max}$, the above two equations cannot be used to evaluate the variables at $t+\Delta t$ where $x = 0$ or x_{max} because this would demand values of the variables at x outside the range $0 < x < x_{max}$.

(3) At this step the equations of chemical energy release and conservation of energy are integrated. The equation of chemical energy release, when differenced according to the Lax scheme, becomes

$$\frac{1}{\Delta t} \left(Q_x^{t+\Delta t} - \frac{1}{2} (Q_{x+\Delta x}^t + Q_{x-\Delta x}^t) \right) = R_x^t \quad .$$

Since the right hand side of this equation can be evaluated directly, it will not be differenced or averaged. R_x^t are evaluated in the reaction rate subroutine. Therefore, this equation can be used to evaluate $Q_x^{t+\Delta t}$.

(4) The values of the variables at the boundaries (i.e. at $x = 0$ and $x = x_{max}$) are computed in the boundary value subroutine. The values of the pressure P are specified by the equations,

$$P(0,t) = .08 \, e^{0.1t} \text{ kbar for } t \leq t_{co}$$

$$P(0,t) = .08 \, e^{0.1t_{co}} \text{ kbar for } t \geq t_{co}$$

$$P(x_{max},t) = .08 \qquad \text{kbar for all values of } t$$

The values of the other variables at the boundaries are computed from $P(0,t)$, $P(x_{max},t)$ and equations 7, 9, 11 and 19. The Lax differencing scheme cannot be used at the boundaries because it would require values of the variables outside the range of $0 < x < x_{max}$. Therefore a different differencing scheme is used. For a partial differential equation of the following general type,

$$A \, \left(\frac{\partial Y}{\partial t}\right) = \left(\frac{\partial Z}{\partial x}\right),$$

the following differencing scheme is used;

$$\frac{A}{2\Delta t} \left(Y_x^{t+\Delta t} - Y_x^t + Y_{x+\Delta x}^{t+\Delta t} - Y_{x+\Delta x}^t \right)$$

$$= \frac{1}{2\Delta x} \left(Z_{x+\Delta x}^t - Z_x^t + Z_{x+\Delta x}^{t+\Delta t} - Z_x^{t+\Delta t} \right) \quad .$$

A METHOD FOR DETERMINATION OF DETONABILITY OF PROPELLANTS AND EXPLOSIVES

S. Wachtell & C. E. McKnight
Picatinny Arsenal
Dover, New Jersey

ABSTRACT

A new quantitative approach to establishing the detonability of propellants and explosives through a study of the deflagration to detonation transition (DDT) has shown promising results. Results indicate that each explosive material has a critical pressure above which the transition from deflagration to detonation will occur.

The measurement depends on the determination of burning rate as a function of pressure. By comparing the burning rates obtained in a strand burner with those obtained for large solid cylinders in a closed bomb at high pressure, a pressure is found for each explosive above which the closed bomb burning rate vs pressure curve turns sharply upward from the normal burning rate vs pressure curve obtained with the strand burner.

This deviation is believed to be the result of a crazing or surface cracking of the explosive causing a large increase in burning area. This rapid increase in burning area is considered to be the basic intermediate step in transition from deflagration to detonation.

The pressure at which this increase in burning surface begins and the rate at which it occurs can be used as the basis for a quantitative classification of the detonability of explosives.

This method has been applied to a number of explosives and propellants and the results are reported.

INTRODUCTION

The development of new high energy solid propellants which go into the manufacture of modern missles has reemphasized the gap in our understanding of the mechanism of transition from deflagration,

to detonation (DDT). While the number of cases in which actual transition has occurred in propellants is extremely small, the advent of larger and larger solid propellant motors with higher and higher energy propellants makes the prediction of the possibility of such an occurrence more and more urgent.

Existing test methods for evaluation of sensitivity fall into two basic categories, those involving initiation by shock and those involving thermal initiation. None of the methods give information about a property of the propellant or explosive which defines its susceptibility to undergo transition from deflagration to detonation. In this paper I will present a method by which we can quantitatively measure this property.

Kistiakowsky [1] described the following mechanism for the development of detonation in a large mass of granular or crystalline explosive ignited thermally at a localized region within the bulk:- As the explosive burns, the gases formed cannot readily escape between the explosive crystals and a pressure gradient develops. This increase in gas pressure in turn causes an increase in burning rate which in turn causes increase in pressure with constantly increasing velocity. This condition results in the formation of shock waves which are reinforced by the energy released by the burning explosive and they eventually reach an intensity where the entire energy of the reaction is used for propagation of the shock wave, and a stable detonation wave is produced. A critical size exists for each material above which this deflagration can pass over into detonation under proper conditions. Below this size the burning will first increase, and then decrease as the material is consumed.

The transition to detonation is considered to be essentially a physical process in which the linear burning rate of the bed of material increases to the rate of several thousand meters per second although the individual particles are consumed at the rate of only several hundred inches per second.

The validity of this mechanism for propellants in granular form has been demonstrated by a number of workers (2), (3). While this mechanism is applied to granular material why should it not apply as well to composite or homogeneous propellants, if the growth of a shock front can be shown (4) which is accompanied by an increasing break-up of the surface of the propellant?

The apparent non-detonability (through transition) of nitro-cellulose propellants is due to the dense surface preventing deflagration from taking place in the interstices of the materials. For composite propellant the continuous and highly elastic nature of the binder probably prevents this type of reaction. However, it has been shown (5), (6) that many highly elastic materials will undergo brittle failure when stress at very high strain rates is applied.

636

GENERAL APPROACH

In the light of experience with some cannon propellants in closed bomb tests in which unexpectedly high rates of change of pressure were observed, it was considered possible that this technique might be used to demonstrate this property for rocket propellants. It had been found that when the tested lot of cannon propellant deviated from normal, the occurrence of high rates of change of pressure started at a specific pressure, which was reproducible. Since the burning rate law has been shown to hold for these propellants, a reasonable explanation is that surface cracking or crazing occurred under the pressure and thermal stress of the reaction. This increase in burning surface is believed to be the initial step in the transition from deflagration to detonation and the critical pressure and the rate at which the increase in surface area occurs can be calculated from measurements made in the closed bomb.

The calculation of linear burning rate from closed bomb measurements has been standard procedure for many years, (7), (8). From a consideration of the original geometry of a grain of material and a knowledge of the rate of change of pressure in the bomb when the grain is burned, the linear burning rate at any particular pressure can be calculated. This calculation assumes that the grain is ignited uniformly over its entire surface and always burns normal to that surface. However, if surface cracking or crazing should occur, the calculated linear burning rates will be far in excess of the value expected, and the increase in surface area can be calculated from this apparent increase in linear burning rate. A detailed discussion of these calculations is given in Appendix A.

EXPERIMENTAL APPROACH

TNT

To determine whether this method would throw any light on the burning of high explosives, cylinders of TNT were prepared with diameters of 1" to $1\frac{1}{4}$" and lengths of from 1" to 3". These cylinders were machined from solid blocks of TNT which had been carefully cast to make certain that they contained no voids or porosity. All the cylinders were machined from the same block and were considered to have approximately the same crystalline structure. These cylinders were placed in a standard 200cc closed bomb with a reinforced cylinder wall and fired with a small amount of Grade A5 black powder and an M1A1 Squibb. Tracings of typical oscillograms resulting from the firings are shown in Figure 1. These represent a series of firings made with cylinders of TNT at various loading densities. In the first of these is inserted a line representing the trace which should have been obtained if the cylinder of TNT had burned normally. However, in each case note that a marked deviation from normal occurred at 6000-8000 psi. In examining these tracings it must be born in mind that the standard closed bomb instrumentation produces
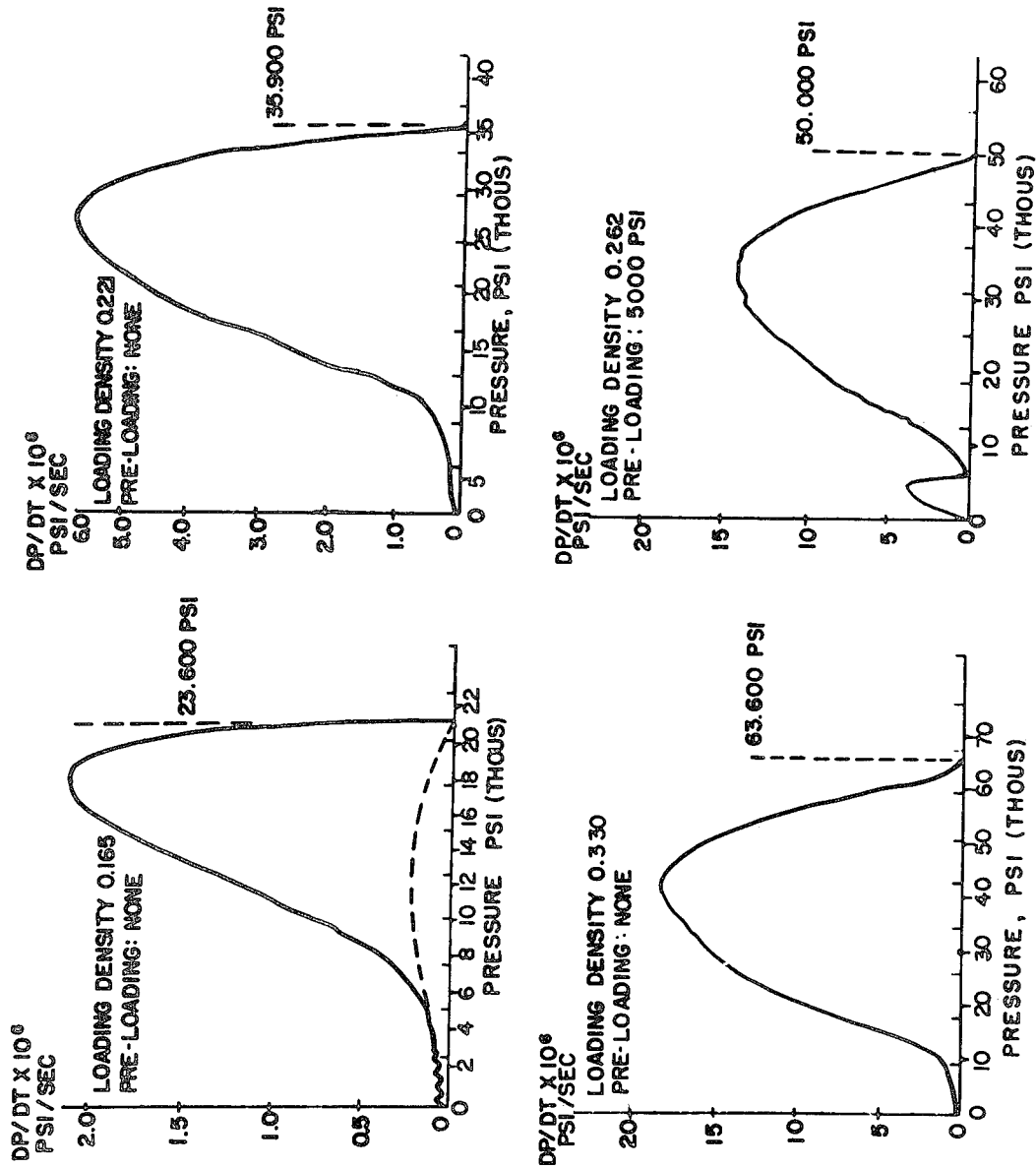
Fig. 1 – Closed bomb test TNT

an oscillogram of dp/dt vs P and that the horizontal axis represents P and the vertical axis represents rate of change of P. The scale is varied to have the trace fill the oscillogram. The calculated scales of P and dp/dt are added to the tracings.

When linear burning rates were calculated from these traces, the results shown in Figure 2 were obtained. An average line is drawn for burning rates calculated from the closed bomb test.

In order to establish the true burning rate for TNT, strands 1/8" x 1/8" x 7" long were prepared by cutting them from a block of TNT similar to the one used previously. These were burned in a strand burner using the standard technique at pressures of from 1,000 psi to 20,000 psi. The results of these tests are included in Figure 2.

These results show that the calculated closed bomb burning rates approximately coincides with the strand burner result up to about 6,000 psi and then curves sharply upward. This "apparent" increase in burning rate is consistent with the assumption of an increase in burning surface which occurs on the cylinder due to surface crazing or cracking. Figure 3 shows a graph of the expected surface area vs pressure due to consumption of the TNT in the bomb (assuming normal burning of the grain) and the actual surface area of the crazed TNT calculated from the dp/dt of the bomb test and the actual linear burning rate of the TNT. This shows for TNT an increase in surface area of close to 20 times.

It was desired to determine whether this change in slope was strictly a pressure and thermal effect and independent of the amount of TNT burned. Therefore a technique was devised whereby a quantity of thin sheets of a very fast burning propellant was loaded into the bomb with the TNT. On ignition, this material burned quickly, giving an initial high pressure and temperature to the bomb before any appreciable burning of the TNT took place. This technique permits a larger mass of TNT to be present at higher pressure. Measurement made in this way showed no change in the pressures at which the change in slope took place in the lower part of the curve or in the slope of the middle part of the curve. However, an increase in the slope of the upper part of the burning rate curve did result. This indicates that there is possibly some minimum mass of explosive necessary to maintain the formation of increasing burning surface. Further work will be done to investigate this.

Composition B

Cylinders of Composition B which had been prepared in a manner similar to the TNT were then burned in the bomb at varying loading densities. In order to obtain adequate ignition of the Composition B it was necessary to use a small amount of sheet propellant as igniter. This masked that part of the curve below about 5,000 psi. However,
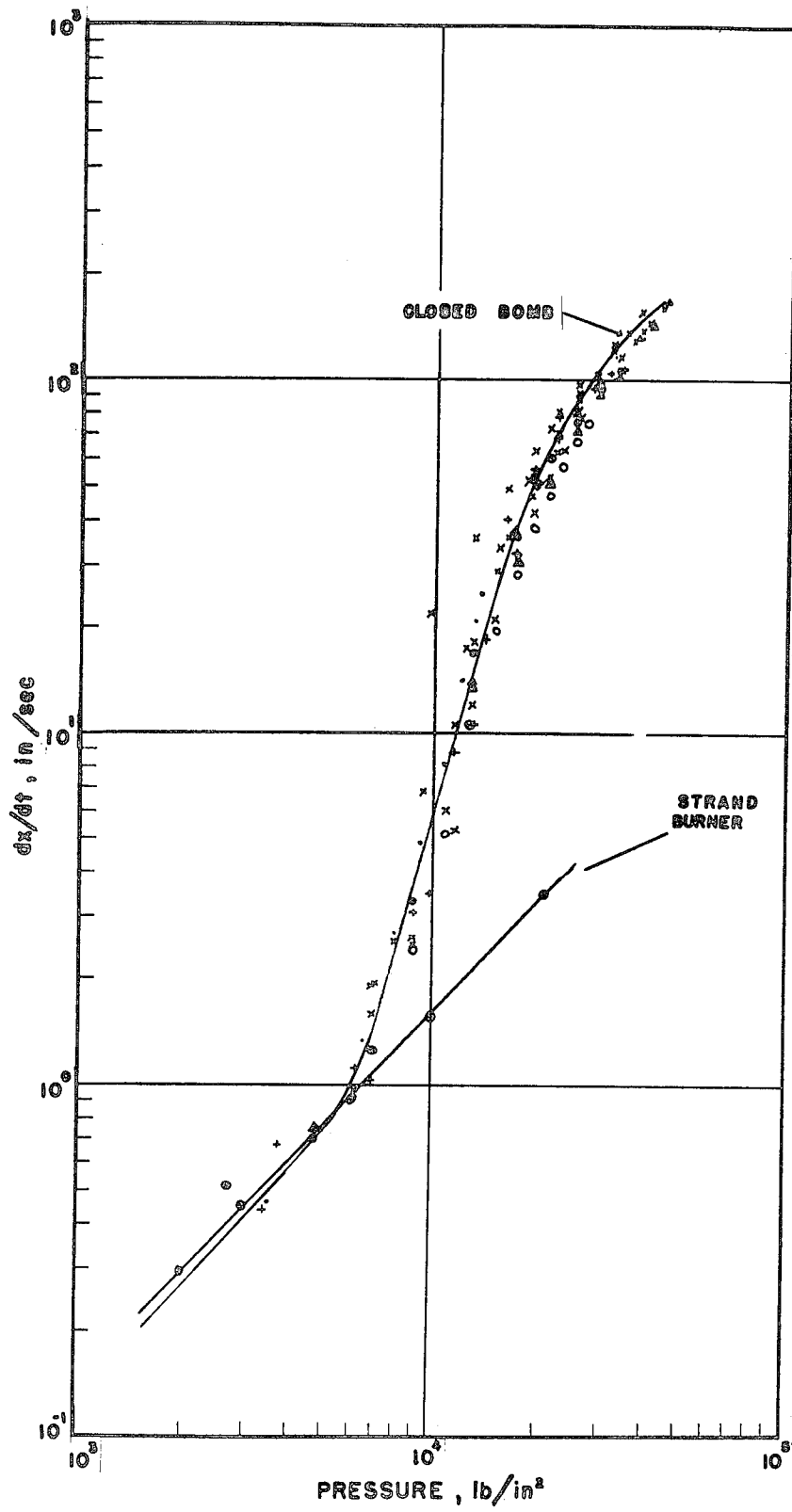
Fig. 2 - Linear burning rates of TNT obtained
with closed bomb and strand burner
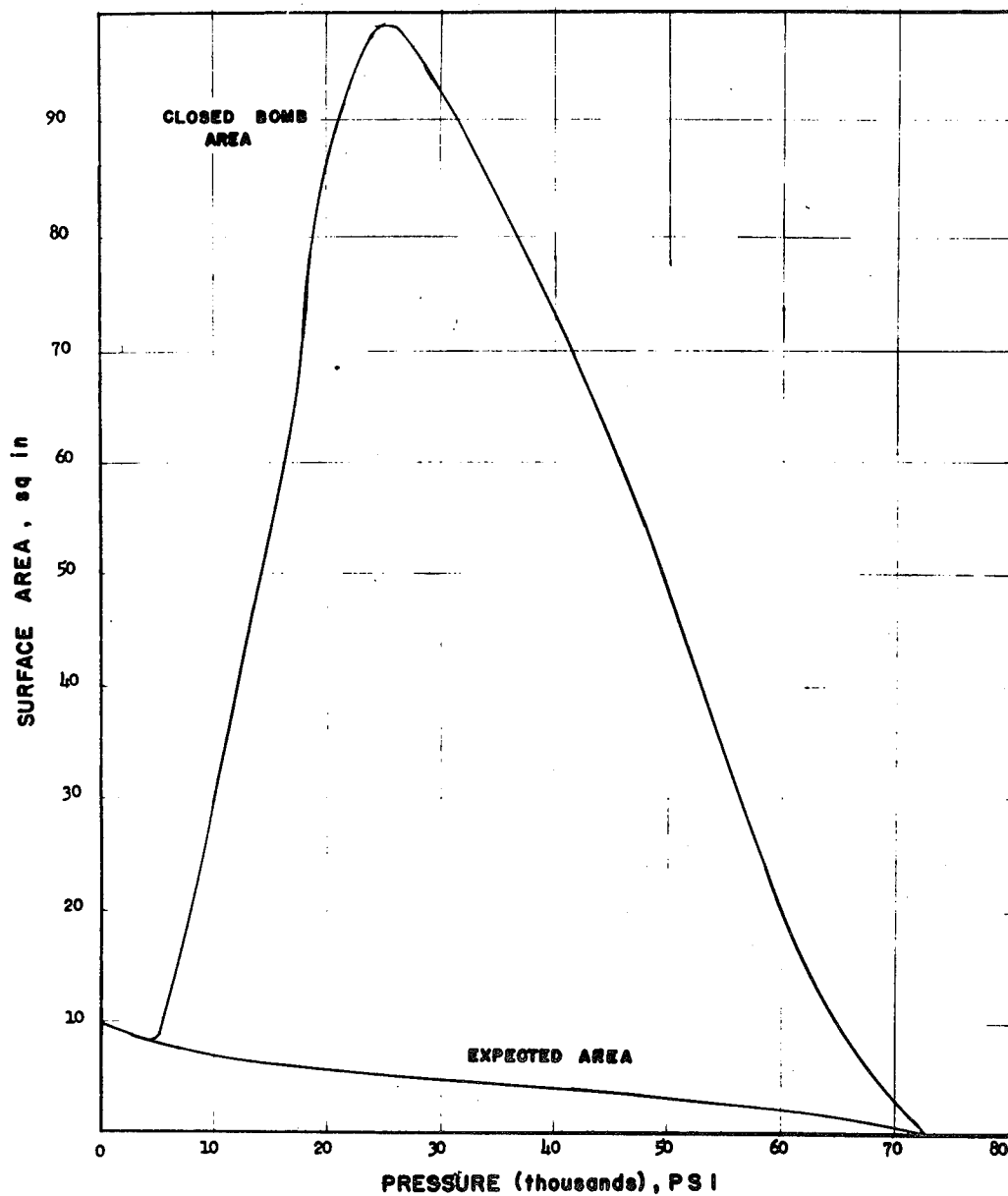
Fig. 3 - Expected surface area vs actual area obtained
for TNT cylinder burned in closed bomb

strands cut from the same block of Composition B as the cylinders were burned in the strand burner to obtain the normal burning rate vs pressure curve (Figures 4 & 5). This shows that the break in the Composition B curve occurs about 4,000 - 5,000 psi. The slope of the Closed Bomb curve past the transition may be even greater than that obtained for TNT. The surface area vs pressure curves for calculated normal burning vs actual closed bomb burning of a sample of Composition B are given in (Figure 6).

ARP Propellant

In order to establish the applicability of this technique to high energy propellants, a sample of ARP propellant was subjected to this closed bomb test. Figure 7 shows a series of tests resulting from increasing loading densities up to about .40. When this was increased to .43 by preloading with sheet propellant, a change in slope occurred at about 35,000 - 40,000 psi similar to those which were obtained for TNT and Composition B. This was accompanied by a disintegration of one of the seals in the bomb. Unfortunately, each time conditions were used in which the transition was expected to show, the rate of pressure rise was so great that some part of the bomb seal was destroyed and the trace was lost. A bomb is being designed in which we hope to hold the pressures produced and measure transition pressures similar to those obtained for TNT and Composition B.

Figure 8 shows a plot of linear burning rate vs pressure calculated from the available data for the ARP propellant burned with and without preloading. The linear burning rates obtained with the strand burner are almost coincident with those calculated from the closed bomb at pressures of 10,000 psi and above.

Experimental Propellant

A sample of highly sensitive experimental propellant was then subjected to this detonability test. This material had been found to be detonable with a No. 6 blasting cap. Cylinders of different diameters were tested and pressures up to 85 thousand psi were obtained. A very sharp transition was obtained at about 15 thousand psi. Also the fall off from the maximum dp/dt begins at a much lower percentage of the maximum pressure than for the high explosive samples. Figure 9 shows a plot of the linear burning rates calculated from the closed bomb traces. The strand burner curve was extrapolated from low pressure data since strands of this material were not available for high pressure testing. Figure 10 shows the surface area relationship between expected area and actual area obtained.

A preliminary study of the data obtained for the ratio of cylinder area to actual area obtained indicates the existance of a diameter below which the continued cracking or increase in surface area stops and the explosive returns to normal burning since there is not
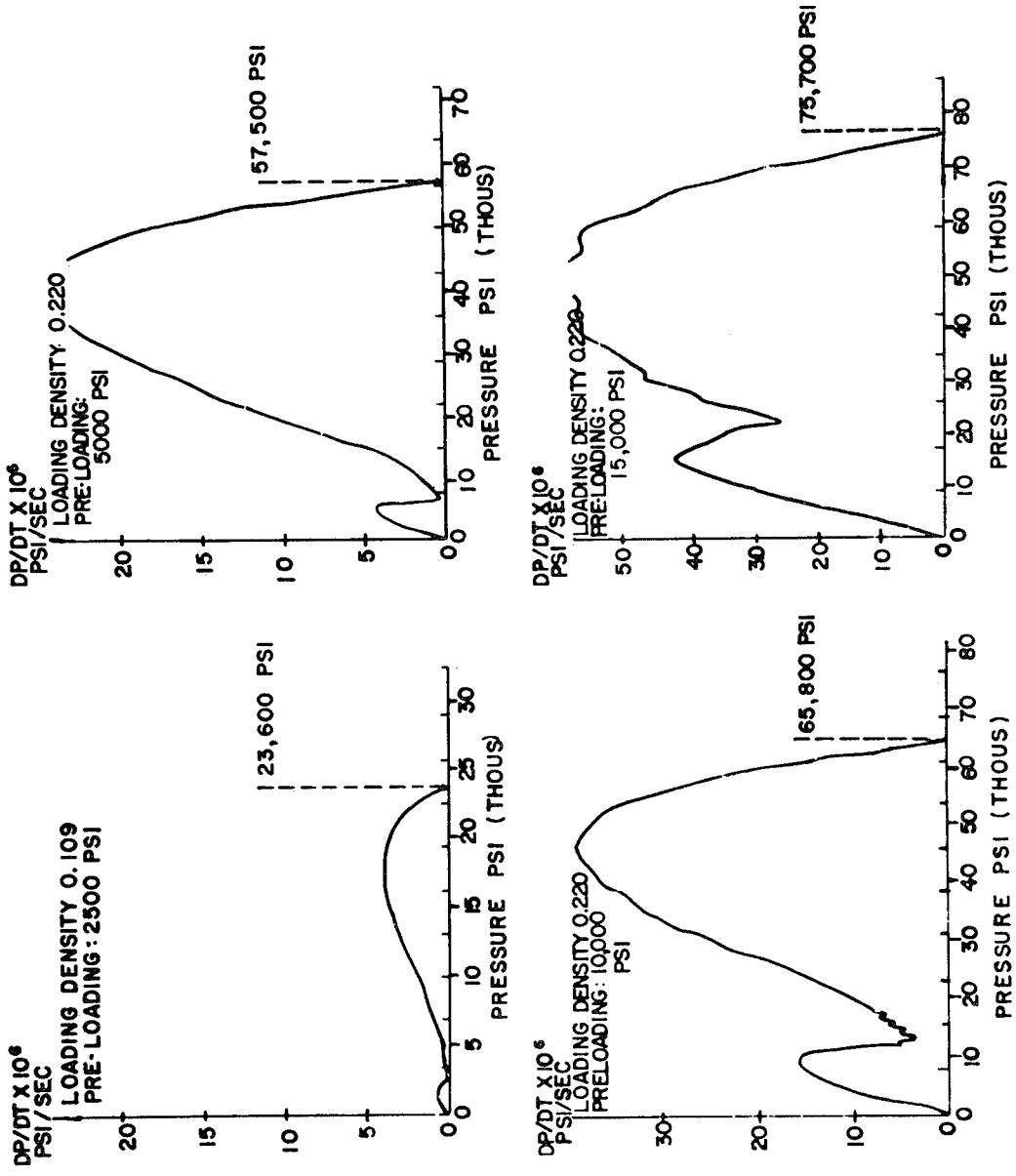
Fig. 4 - Closed bomb test composition B
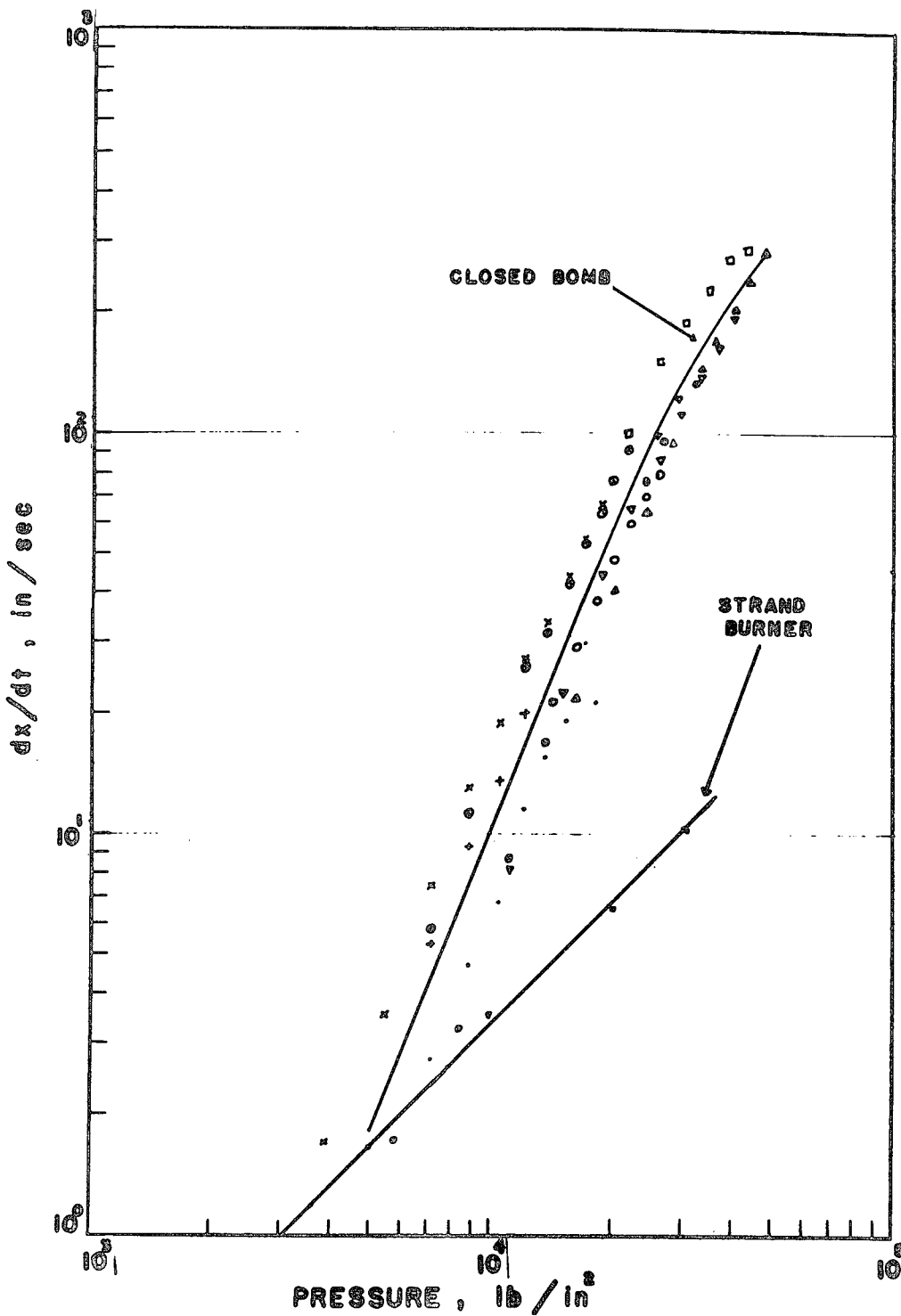
Fig. 5 - Linear burning rates of composition B obtained
with closed bomb and strand burner
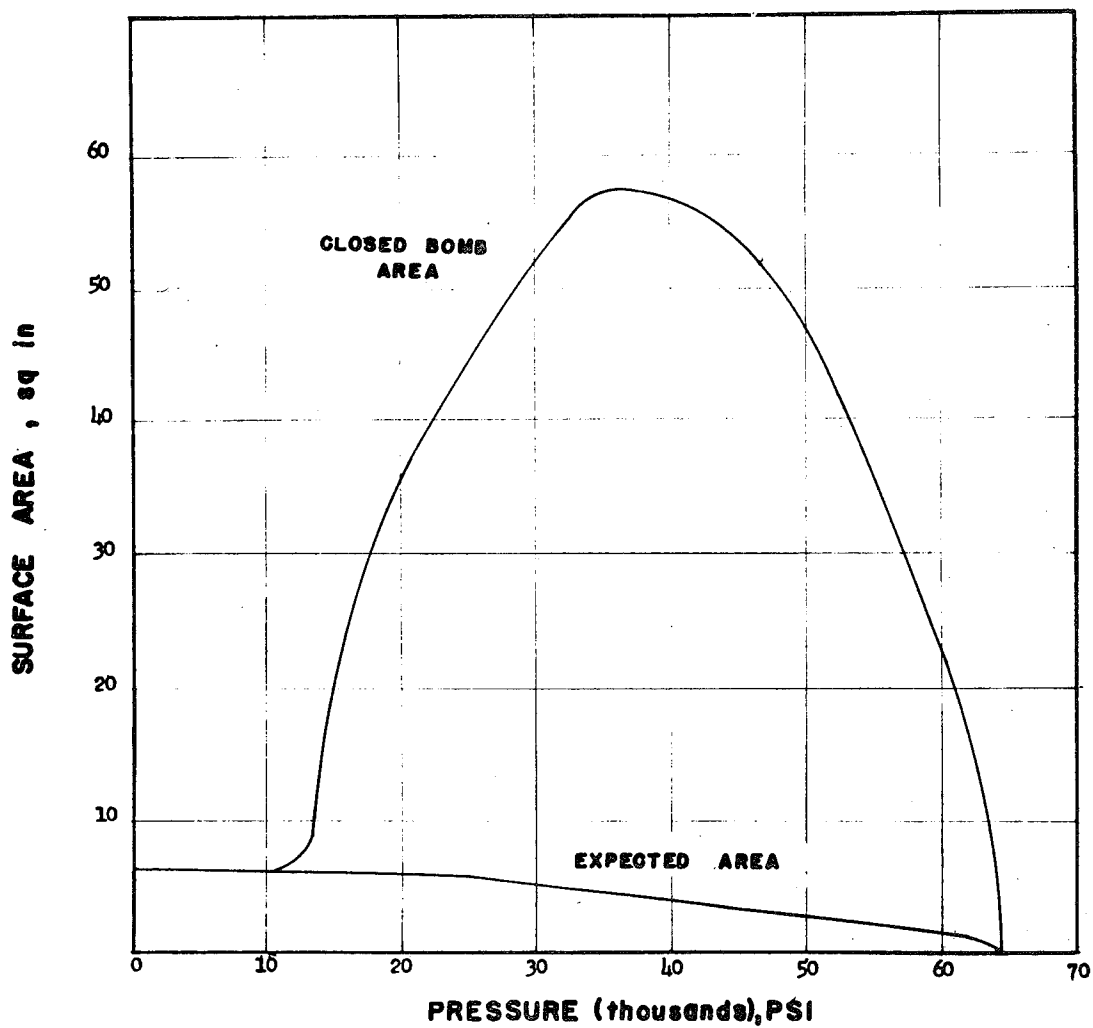
Fig. 6 - Expected surface area vs actual area obtained for composition B cylinder burned in closed bomb
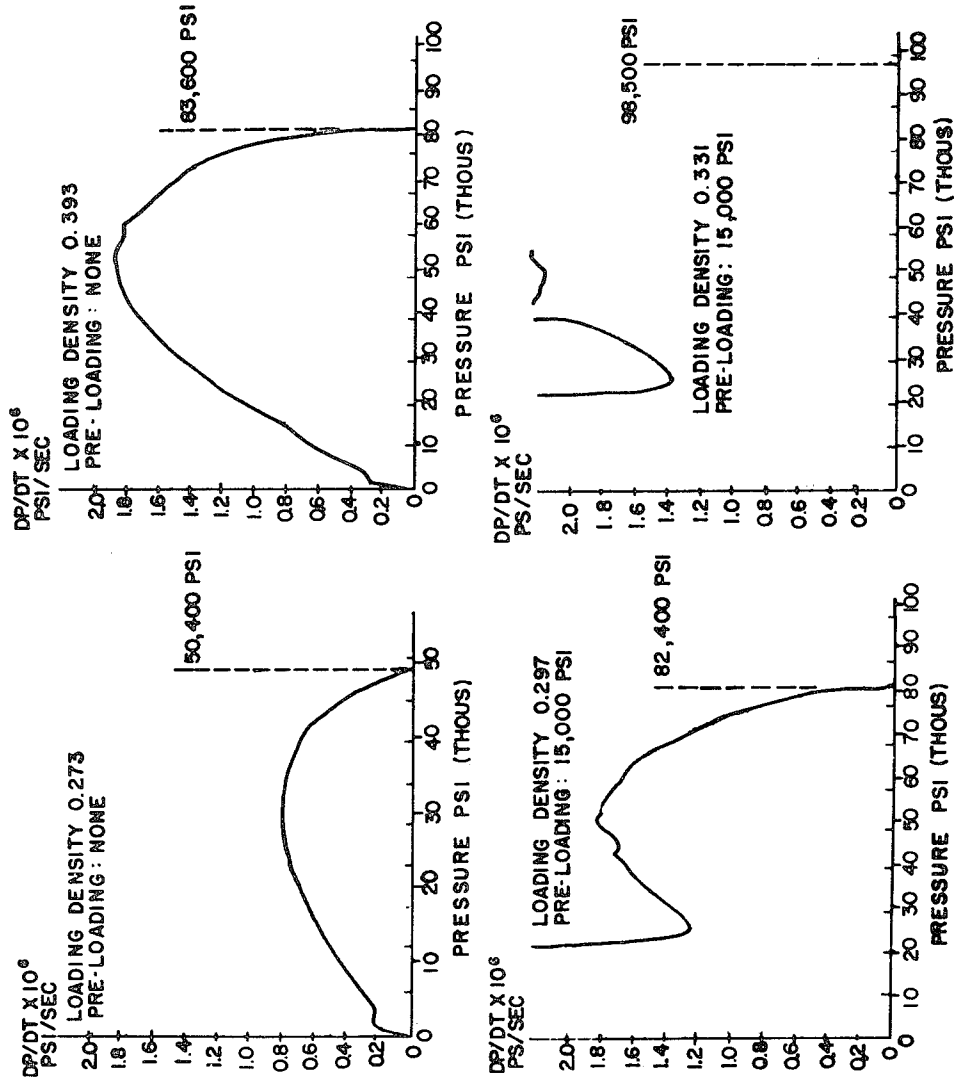
Fig. 7 – Closed bomb test ARP propellent
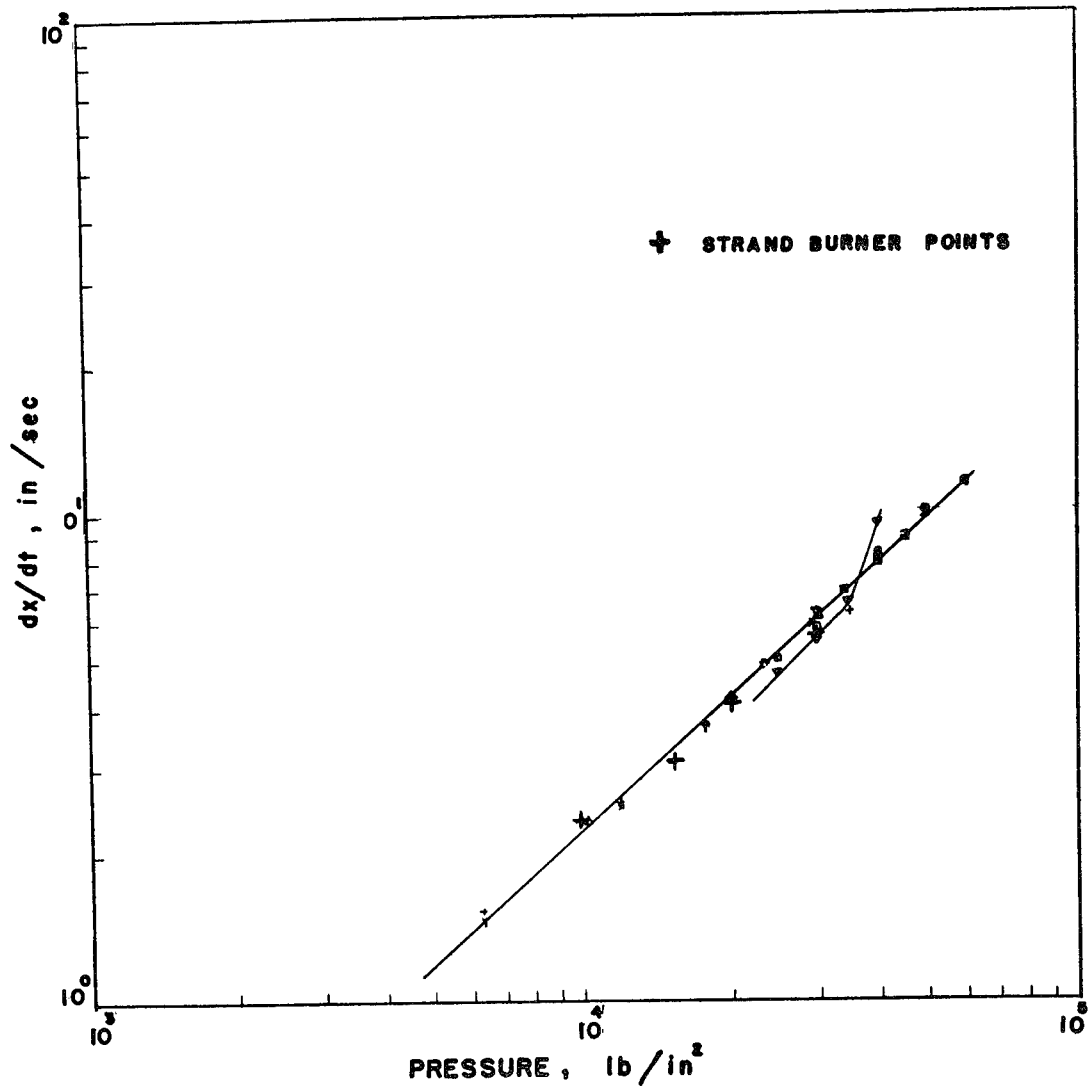
Fig. 8 - Linear burning rates of ARP propellant obtained
with closed bomb and strand burner
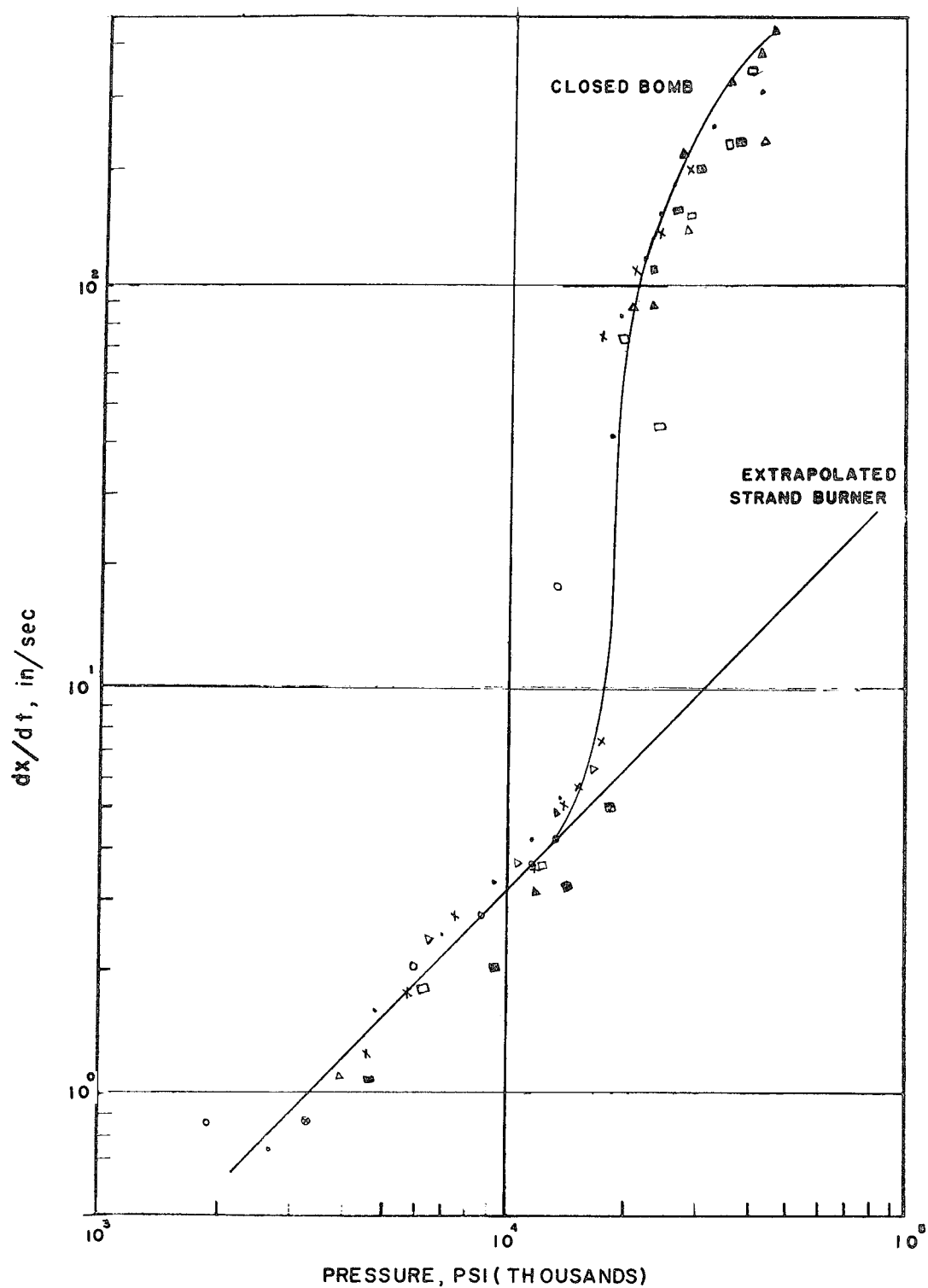
Fig. 9 - Linear burning rate of experimental propellant
obtained with closed bomb
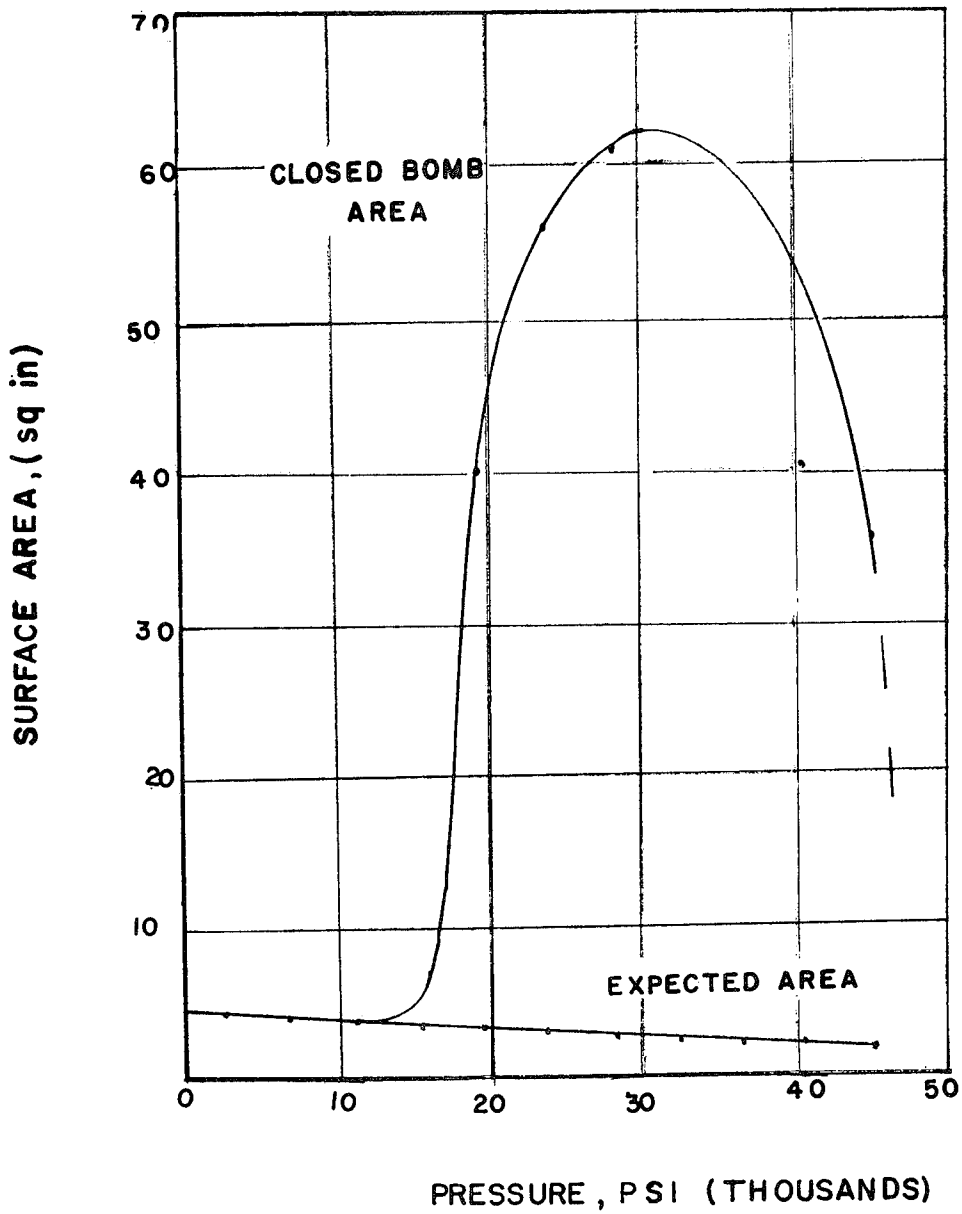
Fig. 10 - Expected surface area vs actual area obtained
for experimental propellant burned in closed bomb

sufficient material available to develop a shock wave of sufficient intensity to go to stable detonation.

Figure 11 shows the ratio of surface area from closed bomb over expected surface area for the same cylinder of TNT presented in Figure 3. This shows that the ratio increased until about 35% of the grain was consumed then remained constant till about 30% of the grain was left.

An equivalent study for a Composition B cylinder in Figure 12 shows that here, the increase in surface area did not start to level off until about 70% of the grain was consumed.

The experimental propellant was tested in cylinders of different diameters and the changes in burning rate as a function of geometry were calculated. It was found that for cylinders of two different diameters, increases in surface areas were obtained down to a specific diameter which was the same for both sizes tested. This indicates the possibility that there is a minimum diameter which is characteristic of each material. This may explain the fact that in earlier work on burning of explosives in a closed bomb done by Buck, Epstein and Jacobs (Ref. 7) under the NDRC the high burning rates reported here, were not observed, since the explosives were burned in small grains.

CONCLUSION AND APPLICATIONS

It would appear from results of these tests that for each of the materials studied, there is a critical pressure above which the transition from deflagration to detonation can occur. This is believed to be the result of a surface cracking or crazing which increases the burning surface to a point where a shock front can form. The existance of this condition is considered necessary for DDT to occur. If sufficient explosive material were available, the shock front could reach sufficient intensity to establish a stable detonation front in the explosive.

The application of this test to explosives and propellants should give us a basis for a quantitative evaluation of these materials in terms of critical transition pressure, slope of the transition curve and minimum charge diameter. This will make it possible to classify these materials as to the severity of the conditions to which they can be subjected before the danger of DDT will exist. It will also make possible a study of the effects of temperature, porosity, particle size, crystal size and other physical variables on the detonability of existing propellants and for new materials as they are developed. It will be a valuable tool in the development of new formulations to study the effects of composition and processing modifications on the detonability of high energy materials.
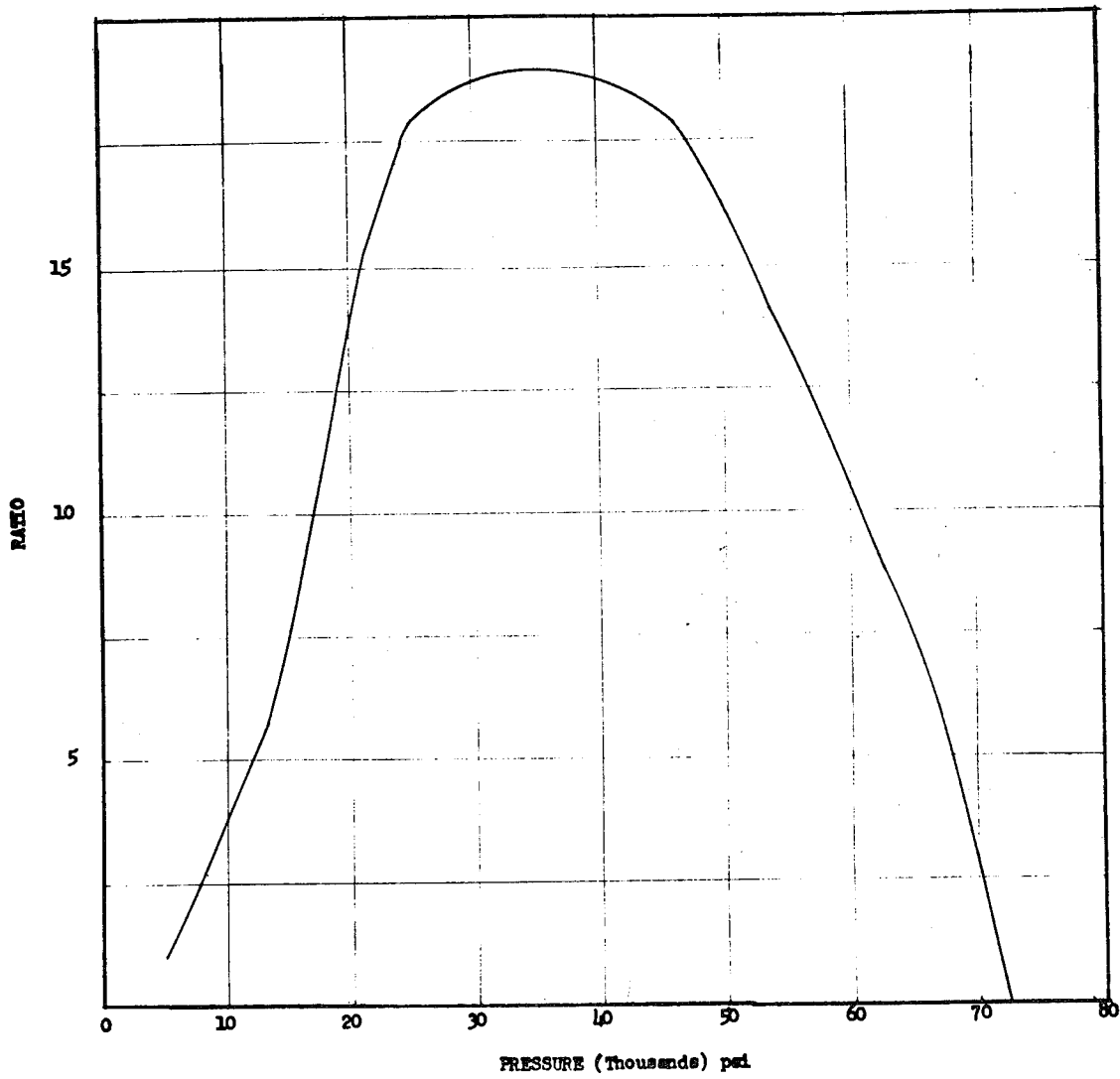
Fig. 11 - Ratio of expected area to actual area
found for TNT cylinder

651
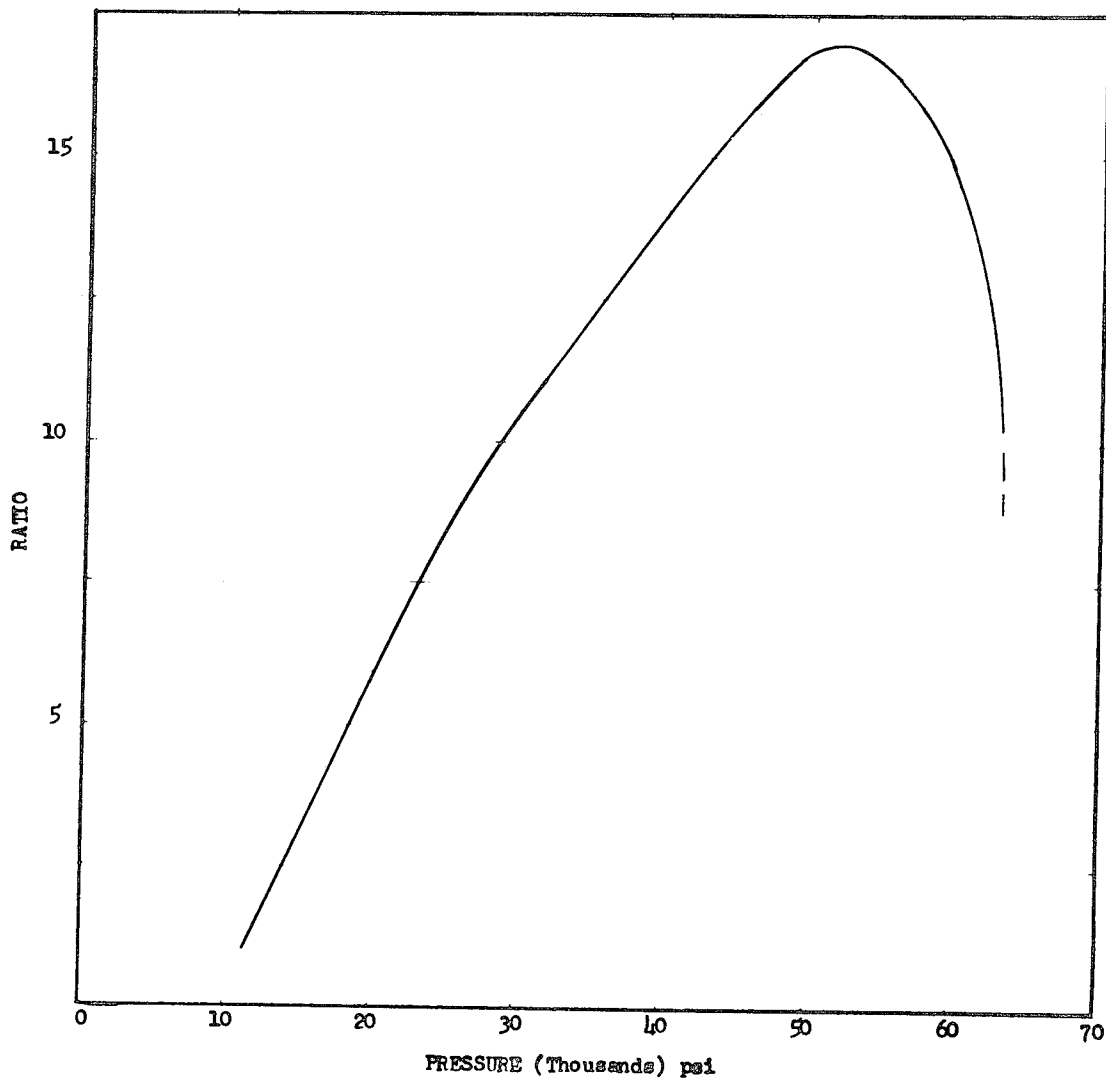
Fig. 12 - Ratio expected area to actual area found
for composition B cylinder
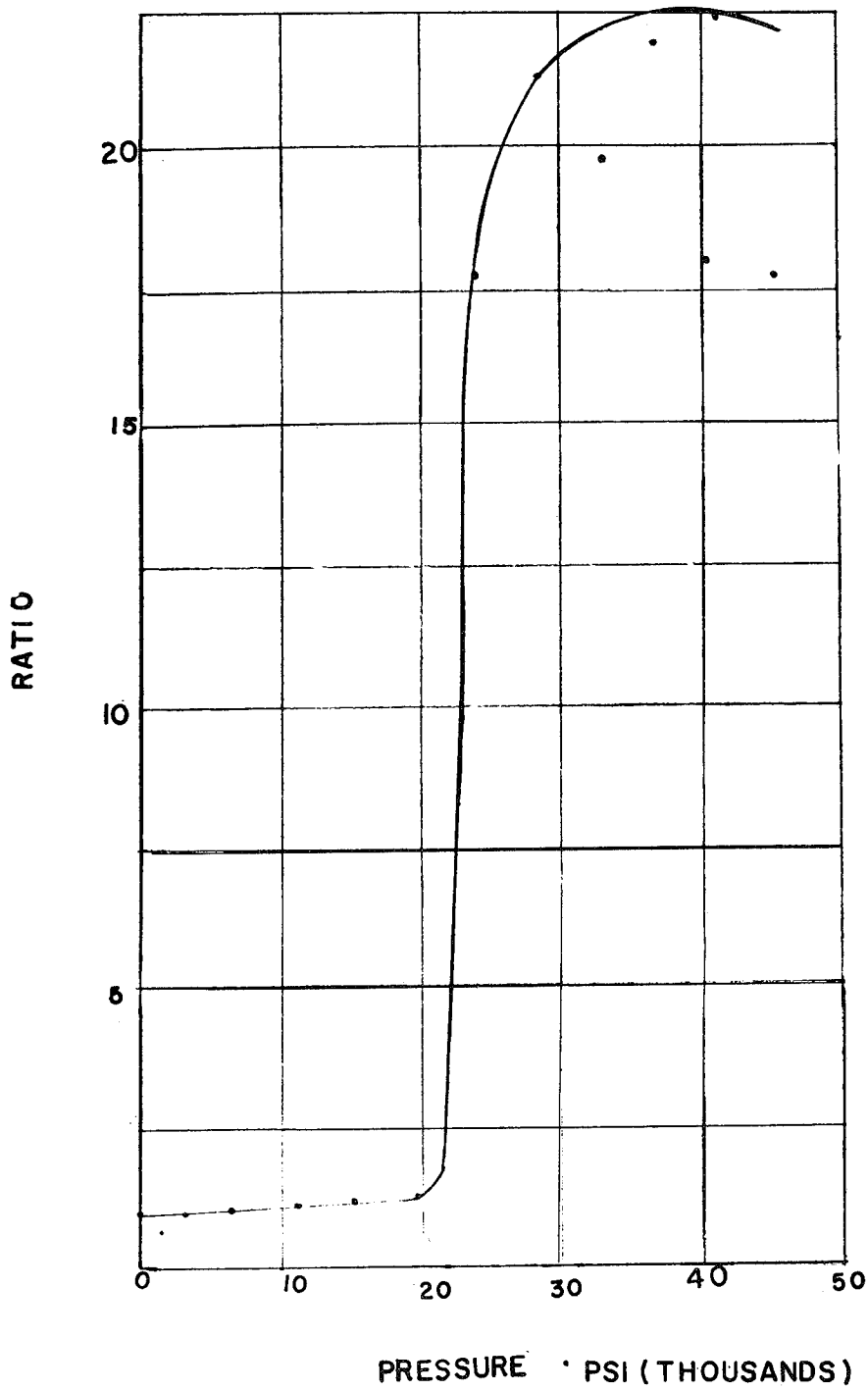
Fig. 13 - Ratio of expected area to actual area for
experimental propellant

REFERENCES

1. Kistiakowsky, G.B., Initiation of Detonation in Explosives
   Third Symposium on Combustion Flame and Explosion Phenomena
   Williams and Wilkins (1949).

2. Hyndman, J.R. et al, Rohm and Haas Co. Ballistics Section
   Progress Report #67 October 1957.

3. Mason, C.N. et al, (U.S. Dept. of Interior, Bureau of Mines)
   Final Summary Report #3734. Investigation of Susceptibility
   to Detonation of Propellants.

4. Macek, A. (Naval Ordnance Laboratory) NAVORD 6105, Sensitivity
   of Explosives VII. Transition from Slow Burning to Detonation:
   A Model for Shock Formation in a Deflagrating Solid. 3 Feb.1958.

5. Jones, J.W., Sagers, D.L., and Nolan, E.J., Fracture Mechanics
   of Solid Propellants. Progress Report No. ELab-A-19, Feb. 16,
   1959 to Feb. 15, 1960, Eastern Laboratory, E. I. du Pont
   de Nemours & Company (confidential).

6. Jones, J.W., Prediction of Catastrophie Rocket Motor Explosion
   Conditions from Broad Spectrum Mechanical Property Analysis.
   Preprints of Sixteenth Meeting, JANAF Solid Prepellant Group,
   Vol 5.

7. Pallingston, A.O., Weinstein, M., Method of Calculation of
   Interior Ballistic Properties of Propellants from Closed Bomb
   Data, Picatinny Arsenal Technical Report #2005 June 1954.

8. Wallace, W.F., New Formulas for Rapid Calculation of Linear
   Burning Rates of Solid Propellants. Picatinny Arsenal
   Technical Report #2488, April 1958.

APPENDIX A

1. Linear Burning Rate

A. Theory

The linear burning rate is the rate at which the burning surface of a propellant recedes in a direction normal to the flame front.

If dx be the distance burning proceeds during anytime interval dt, then dx/dt is the linear burning rate.

By assuming that all surfaces of the burning propellant burn at the same rate and by using a known geometry the linear burning rate can be deduced from the mass rate of burning. By the assumption of a suitable equation of state the mass rate of burning can be deduced from the rate of change in pressure surrounding the burning propellant in a closed vessel.

For particles of known shape, such as perforated or solid cylinders the closed bomb fitted with a rapid response pressure gage is suitable experimental apparatus for determining the linear rate of burning of propellants or explosives at any pressure.

The apparatus produces an oscillographic trace of piezo-originated voltages as measures of the rate of change of pressure, dp/dt and pressure, P. Sample traces are shown in Figure 7. The rate of change of pressure is calculated from the ordinate voltage V_x, and the pressure from the abscissa, V_y, after appropriate calibration and determination of gage constants.

$$P = K_g \, C_x \, V_x + K_1 \qquad (1)$$

$$dp/dt = \frac{K_g \, V_y}{R} \qquad (2)$$

The maximum pressure (at the end of burning) can be used to measure the combined temperature and gas molecular weight function, thus completing an expression for the equation of state in terms of Z, the weight fraction burned, and p_i the pressure due to prepressurizing and igniter, if any, where K_g, C_x and K_1 are equipment constants:

$$P_{max} = K_g \, C_x \, V_{xmax} + K_1 \qquad (3)$$

$$P = p_i + \frac{Z \, (1 - (\frac{m_i \, a_i + a}{m_0}) \, Do)}{1 - (b + \frac{m_i}{m_0} \, a_i + (a-b) \, Z) \, Do} \, (P_{max} - p_i) \qquad (4)$$

655

To simplify calculations the term (m_i/m_o) a_i is considered negligible because of the relatively small quantity involved in m_i, the mass of igniter and prepressurizing materials.

The geometry for solid cylinders of propellant or explosives burning on all surfaces is stated in terms of fraction burned, Z, and dimension remaining, $(d-2x)$ and $(h-2x)$, at anytime:

$$Z = 1 - \frac{(d - 2x)^2 (h - 2x)}{d^2 h} \qquad (5)$$

The derivative, dp/dZ, may be found from equation (4) and the derivative dZ/dx from equation (5):

$$dp/dZ = f_1 (Z) \qquad (6)$$

$$dZ/dx = f_2 (x) \qquad (7)$$

The linear burning rate can be calculated from equations (2), (6) and (7):

$$dx/dt = \frac{dp/dt}{(dp/dZ)(dZ/dx)} \qquad (8)$$

B. Calculation Method

The equations (4) through (8) have, in principle, been rearranged by Wallace [8] to a form suitable for direct solution. The solution was made in terms of the surface area (S_x) at any value of x. With slight modifications, the equations of Wallace were used to convert the closed bomb data to linear burning rates.

The equations used for this solution for a solid cylinder are listed below. These equations were programmed for solution in an IBM 650 computer.

$$K6 = (d-h)^2 / 1.5\ hd^2 \qquad (9)$$

$$K5 = 27\ hd^2 / 2\ (d-h)^3 \qquad (10)$$

$$B = (P_{max}-P_i)\ (1-aD) / (a-b)D \qquad (11)$$

$$C = (1-bD) / (a-b)D \qquad (12)$$

$$Z = \frac{(P-p_i)\ (1-bD)}{(P_{max}-p_i)\ (1-aD) + (P-p_i)\ (a-b)D} \qquad (13)$$

$$E = 1 + K5\ (1-Z) \qquad (14)$$

If $E < 1$

$$\phi = \cos^{-1} E \qquad (15)$$

$$S_x/V_o = \left[1 - 2\cos\left(60° + 2/3\ \phi\right)\right] K6 \qquad (16)$$

If $E \geq 1$ $\qquad (17)$

$$S_x/V_o = \left\{\left[\left[E + (E^2 - 1)^{1/2}\right]^{1/3} + \left[E - (E^2 - 1)^{1/2}\right]^{1/3}\right]^2 - 1\right\} K6$$

$$dx/dt = \frac{dp/dt}{\dfrac{B}{C}\left(1 + \dfrac{P}{B}\right)^2 \dfrac{S_x}{V_o}} \qquad (18)$$

In these equations certain special cases had to be recognized to allow for discontinuities introduced by algebraic and trigonometric solutions. When diameter exactly equals length, a discontinuity arises in Eq (9) for K6. An increment of 0.01 inch is therefore added to one dimension for this special case. If the quantity E is less than unity a cosine procedure is used (Eq 15); if equal to or greater than unity a cube-root procedure is used (Eq 17). Either procedure leads to S_x/V_o which is then used in the final equation (Eq 18) with the experimentally observed dp/dt to calculate the linear burning rate dx/dt.

II. Equivalent Surface Areas.

A. Theory

When linear burning rates are found from closed bomb data from single cylinders of propellant or explosive using the solid cylinder geometry as described above the results compare well with strand burner results below a certain characteristic pressure. At other pressures the burning rate so calculated must be regarded as an "apparent" burning rate because it deviates a great deal from strand burner results.

This suggests that the general configuration may be cylindrical, but the surface may be full of cracks or breaking into small pieces, with the strand burning rate governing the reaction for each burning particle. Combining experimentally determined rate of pressure rise, dp/dt, and pressure, P, with strand burning rates, dx/dt, permits solving for a surface area, S_x, will reflect the abnormally high mass rate of burning.

Thus P, dp/dt, and P_{max} are found as before (Eq 1,2,3). The equation of state showing total pressure as function of fraction burned is also applicable (Eq 4). Likewise the fraction burned is related to the burning cylinder dimensions by (Eq 5) for a smooth cylinder. In (Eq 8, and 18), however, the predicted linear burning

657

rate $dx/dt = aP^n$ would be used. Then from (Eq 18) the equivalent area S_x is found representing surface area of cracks and convolutions on the surface of a rough cylinder. The equivalent areas are found to proceed through a maximum before reaching zero during burning.

SENSITIVENESS TESTING AND ITS RELATION TO THE PROPERTIES OF EXPLOSIVES

E.G. Whitbread
Explosives Research and Development Establishment,
Waltham Abbey, Essex, England.

Scope

It is proposed to review the subjects of section one as seen from E.R.D.E.   This is necessarily a biased view with a considerable emphasis on this establishments work, but it is thought that this description of our problems will be useful to the meeting as a whole.

1.   The Selection and Standardisation of Tests

1.i   Safety Certificate Testing.   The need for sensitivity testing in research has long been recognized.   A great deal of effort is currently expended, in those establishments concerned, on the development of empirical tests and rather less on basic research leading to an understanding of sensitivity phenomena.

There are two major objectives in sensitivity testing, (1) to obtain a measure of the hazard associated with the manufacture, use and storage of explosive materials, and (2) to determine the reliability in operation of explosive devices.   To some extent these require a different philosophical approach although the tests used may be similar or even identical.   In one case the desired state is a very low probability of initiation, whereas in the other the optimum is a very high probability of detonation which must itself be as efficient as possible.

For either objective the work falls into two natural classes: the development of efficient tests, and a study of the mechanism of the physical and chemical processes by which the material is brought to explosion.

The choice of tests by a given establishment is often arbitrary and dictated by availability of facilities or similar

factors.   The commonest, in order of popularity, are:-

1   Impact machine.
2   Some form of thermal (temperature of explosion) test.
3   Some form of friction test.
4   Gap test.
5   Projectile attack test.

It is a chastening thought that of all the tests and test facilities the impact test is the only one which is universally used.

There is a considerable advantage in the collective use of the results of several tests to describe an explosive.   In the United Kingdom this principle is used in a document known as the "Safety Certificate", and this has been the basis of a certain amount of standardisation.

The "Safety Certificate" is issued by the authority of the Director of Safety Services and is available to the technical staff of any establishment (e.g. a filling factory) having to handle the explosive certified.   It contains a great deal of information on the hazards (not necessarily explosive) associated with the use and storage of the explosive to which it refers.   Six tests of sensitivity are included, viz. impact, friction, temperature of ignition, ease of inflammation, behaviour on inflammation and sensitivity to electrostatic discharge.   Of these tests only the friction and impact are commonly carried out in more than one laboratory and as a result the effort on standardisation has been confined to these two tests.

The friction test specified for safety certificate purposes is crude but surprisingly effective.   To test for friction sensitivity between two materials the explosive is spread on an anvil made of one material and struck a glancing blow with a mallet made from the other, the operation being entirely manual and its efficiency and reproducibility entirely dependent on the skill of the operator.   The results are reported as the number of ignitions in 10 trials.

Several unsuccessful attempts have been made to mechanize this test or to substitute some other less subjective test but to the present time the improvement and standardization has been limited to the tools (i.e. anvils and mallets) which are drawn by all laboratories from a common source.

The original impact machine technique was worked out by Dr. Godfrey Rotter in about the year 1908.   In the construction of his machine he employed, as indeed many laboratories must do to-day, materials readily to hand, in his case those stores to be found in the Royal Arsenal at Woolwich.   For example the base of the machine consists of two 15 inch proof shots, and the explosive is loaded

into small brass caps which were the primer caps for the 12 pounder gun of that day. As picric acid was then the major high explosive he decided to employ it as a standard against which all other materials would be measured. He was greatly concerned with the probability that some materials would only partially explode and devised a somewhat complicated procedure for the computation of the result which depended on the integration of the various volumes of gas evolved from caps of explosive struck at different heights. Because the numerical result produced by the machine is larger for less sensitive materials, the result, expressed as a percentage of the result for picric acid, was termed the "figure of insensitiveness" (or F.I.).

This procedure lasted almost unchanged until about 1950 - 52. At about this time at E.R.D.E., Waltham Abbey we satisfied ourselves on two points: 1. For high explosives the volume of gas evolved yields no more information than that the shot has "fired" or "failed". 2. Picric acid is a very bad material to use as a standard.

It is not however in our tradition to make changes lightly, and in the minds of those who have to handle explosives there is a firm pattern of "figures of insensitiveness" built up over the last half century. We therefore retained the use of picric acid as a primary standard but have substituted RDX for daily use; we have adopted the "Bruceton staircase" determination of median heights but express the result as the ratio of the median height of the substance under test to the median height of the reference standar•, RDX, and multiply this ratio by one hundred times the ratio of the median height of this RDX to the median height for picric acid, thus obtaining a result numerically similar to (but more precise than) the F.I.

It is interesting to note that A.W.R.E., working quite independantly of E.R.D.E., arrived at the same final method, and with its adoption by A.R.D.E. and the Chemical Inspectorate there is now a broad measure of agreement among the Government Establishments on the actual method of measurement.

There are eight machines in use at various establishments in the U.K. and a number of trials have been made to compare the data obtained by each. Table 1 shows the kind of scatter obtained.

It has become clear that before any useful standardisation was possible the following requirements must be met:-

1. The machines must be identical in construction.

2. The expendable machine parts (i.e. the "tools"; in the Rotter machine the anvils and caps) must be drawn from a uniform stock common to all machines.

3. The operating procedure must be identical in all cases. For example, all are agreed that a modified Bruceton procedure is a good basis for the determination of the median height, but agreement has not yet been reached on the spacing of the intervals.

4. The method of reporting the results must be identical.

5. A reference standard explosive must be used, and this must be drawn from a stock common to all users.

Table 1

Explosive	Median height calculated relative to agreed standard					
	A.W.R.E.	E.R.D.E.		A.R.D.E.		D.C.I.
		Machine 1	Machine 2	Machine 1	Machine 2	
Picric Acid	129	137	132	110	91	106
RDX/TNT Holston	105	117	104	103	88	119
RDX/TNT Bridgwater	103	118	106	103	93	116
PETN	69 & 49	51	51	44	-	59
TNT	158	202	211	159	122	146

The value of this standardisation is a fit subject for discussion in its own right. In this case (i.e. in the U.K.) it is necessary that certain explosives are tested batch by batch and that the data are accepted by several authorities; to have value the test must be as discriminating as possible. If the need is assumed, careful standardisation is essential; but it is quite expensive for a test as simple as the impact test and could be prohibitively so if applied to all testing.

In the more general case it is necessary only that the sensitivity of a new explosive is assigned to a certain class and as pointed out by G.F. Strollo (1) there is much virtue in testing any new explosive by a variety of tests even if these are nominally of the same type.

1.ii Other Standard Test Methods. In the U.K. we have not had the widespread and diverse interest in liquid monopropellants that has occurred in the U.S.A. and there is no equivalent to the

American "Committee for Standardisation of Monopropellant Test Methods". Extensive work on liquid monopropellant sensitiveness has been confined almost entirely to Waltham Abbey and the question of standardisation has not arisen.

Three points of contact with American work may be noted:

(a) At E.R.D.E. a locally modified version of the Olin Matherson impact tester for liquids is used. This appears entirely satisfactory provided that it is recognised that only the risk of initiation from adiabatic compression of occluded air is measured.

(b) The "gap" test used at E.R.D.E. for liquid propellants is related to the one which is (or was) the American standard; but has a fundamental difference in that in the American pattern only high order detonations are recognised as "fires" whereas in the British test a much lower order explosion is counted as a positive result.

(c) Interest in liquid oxygen in contact with other materials is centred mainly at Rolls Royce Ltd. who intend to use an exact copy of the Douglas Aircraft Company impact machine. (2) (3)

1.iii **Future Extension of Standardisation.** Unless some central authority has the power to specify exactly a method and to enforce its adoption, standardisation on the lines followed by the work on the Rotter machine is extremely expensive because of the lengthy discussions and experimental work made necessary by small differences in technique in the different laboratories.

There is however one feature of the Rotter procedure that is to be commended to all laboratories, and that is the use of a reference material. Frequently data are reported solely (for example, considering the impact machine) as drop heights and unless the reader has an intimate knowledge of the machine used he is unable to form any real estimate of the sensitivity of the material. This principle can be extended, within reason, to other tests and would form a satisfactory substitute for full standardisation. Basically the idea is that with any sensitivity test the data are reported either relative to some well known standard explosive; or alternatively, a figure for this material is reported with the new data.

For laboratories that needed a closer degree of standardisation, samples of materials could be exchanged, although the physical barrier of the Atlantic will impose an obvious limitation.

This scheme is not new, data for several monopropellants have been suggested as standards for the N.O.L. gap test and Technoproducts (4) give n-propylnitrate as a standard for their liquid impact tester.

2. **Effects of Scale and Ad Hoc Trials.** It is a fundamental
limitation of all laboratory tests of sensitiveness that they will
grade explosives only in an order defined by the test, they will not
give any measure of the absolute probability of an explosion in a
particular set of circumstances other than those obtaining in the
actual test.

It frequently happens that a question is posed in the
following form: "It is intended to process a large bulk of
propellant material (say 5000 lbs) in one batch. As the design of
the buildings to house the plant and the layout of the explosives
area is affected by the possible consequences of an explosion, will
the effects following an ignition resemble those of a detonation or
those of a fire?" This is one of the most important types of ad
hoc experiment and its design poses a number of difficult questions.

If replicas are constructed of the piece of plant in
question, for the conclusions to be drawn with reasonable confidence,
either a large number of shots must be fired or the stringency of
the conditions increased over those found in the original.

As full scale replica firing is extremely expensive, use is
made of reduced scale charges. This also calls for an increased
stringency to compensate for the smaller scale. In both full and
reduced scale experiments we need to know the effect of stringency,
in whatever way this is applied, (e.g. confinement) on the
probability of an explosion. Finally, as the result is usually an
explosion intermediate between a detonation and a fire, some method
must be devised to measure the destructive potential.

As yet no comprehensive solution is available. The method
adopted by E.R.D.E. in a recent series of trials (16) on a new
propellant was to lay on a few trials in full scale replica con-
tainers, supported by a larger number in 1/10 scale, much stronger
containers. In all shots the blast output was measured by canti-
lever blastmeters. When the trial was fired, the blast from the
1/10 scale containers, because of their greater strength, exceeded
that from the full scale replicas, but in all cases the blast output
was acceptably low. In these circumstances the smaller shots were
held to provide evidence supporting the larger.

It is thought that this solution is unsatisfactory in that
a definite result cannot be predicted, e.g. the small containers
might be made too strong and give an unacceptable amount of blast
even when the full scale ones did not; and it is suggested that
systematic work on the effect of scale is necessary before a satis-
factory solution can be found.

3. **Relation of Experimental Results and Explosive Properties.**
The field of work in sensitivity is very wide and any one laboratory
can hope to investigate only some of the questions.

In the last ten years at E.R.D.E. we have studied some aspects of the influence on sensitiveness of kinetics, crystal habit, crystal imperfections and the acoustic properties of explosives.

3.i Kinetics. The early work was concerned with liquid propellants, a large part of this was reported at the second detonation conference (5) (6) (7) (8). Liquids were chosen because of their importance at the time (1950 - 55) and because they offered freedom from the effects of grain, structure and density variations. The most important reason for working with these materials however was that they permitted a new approach to the application of chemical kinetics to sensitiveness, viz. by the use of the rate of burning at standard pressures instead of the rate of decomposition.

The overall conclusion from this work was that, in a liquid monopropellant the probability of an explosion was a function of the rate of growth of the explosive reaction after initiation, and that this could be estimated from the rate of burning and energy of explosion of the explosive concerned. It is probable that this correlation owes its existance to the elimination of all other factors: the acoustic properties of the liquids were similar, crystal form and structure and voids were absent.

No attempt has been made at E.R.D.E. to find correlations between oxygen balance or the kinetics of decomposition and sensitivity. The most significant recent work is that of Kamlet (9) (10) and Wenograd (11). Both workers used the ERL machine with the use of added grit in the form of sandpaper. Under these conditions an adequate supply of initiation centres are always available and the effects of crystal structure or hardness are submerged; the correlation of sensitivity measured under these conditions with the kinetics of decomposition is reasonable. It would be interesting to study the effects of decomposition kinetics or oxygen balance with a "pure" impact machine, (i.e. one which initiates by impact alone), certainly neither the Rotter nor the E.R.L. fill this requirement but an exciting new device devised by Cachia and reported at this conference may well provide the necessary data.

3.ii Crystal Structure. An obviously fruitful line of attack into the problem of the mechanism of initiation is to study those materials which show anomalous behaviour rather than those which fit neatly into patterns. One example in the impact test is the differing sensitivity of the various polymorphs of HMX. This was investigated by Jeffers at E.R.D.E. (12). He found that the greatest sensitivity arose from what might be termed "mixed polymorphs", that is, where crystals were in process of transformation; and that to some forms of the impact test e.g. the so called adiabatic compression test, all forms had a similar sensitiveness.

It is possible that in this case the "mixed polymorph" is harder than the normal crystal, the apparently greater sensitivity

could then be explained by the greater efficiency of the impact machine considered as a whole, i.e. including the explosive. In effect this means that with the harder crystal more energy has been extracted by the explosive from the falling weight than with the normal kind.

It might be thought that impact and gap tests would show a correlation. Some data have been determined at E.R.D.E. with the Olin Matheson machine on liquid propellants which tend to support this. The data are too scanty for firm conclusions but the gap test used is known to correlate with combustion processes (5) and in the Olin Matheson machine the propellant is burned rather than detonated.

With the gap tests used on liquid propellants the criterion of a "fire" was carefully chosen to be below a full detonation as the object of the test was the estimation of hazard. With high explosives the gap test is usually employed to measure the efficiency of an explosive train and a detonation is taken as a criterion of a "fire". With high explosives in the impact machine the criterion is not so well defined, it is often violent and called a detonation but in fact may be only a rapid burning. This difference must be borne in mind when comparing data arising from impact and gap tests.

We have made an interesting study of the effect of crystal perfection on sensitivity as measured by gap and impact tests. The material chosen was RDX. It had been found that the sensitivity of an RDX/TNT mixture, to the gap test, was controlled by the RDX. Two RDX/TNT mixtures of similar nominal composition but with widely differing sensitivity to the gap test were taken, the TNT and wax extracted with benzene from each sample and reincorporated with the RDX from the other sample.

Table 2

Material	Gap test	Impact
Holston composition B	0.083	115
Bridgwater RDX/TNT grade A	0.027	116
TNT and wax from Holston Comp. B, RDX from Bridgwater RDX/TNT grade A	0.027	119
TNT and wax from Bridgwater grade A RDX from Holston Comp. B	0.086	117

Table 2 shows that there is no correlation between the impact and the gap test data for these samples, and that the gap test result is influenced sharply by the RDX.

Next an attempt was made to sensitise the Bridgwater material to the Holston level. Impact results are easily influenced by the addition of grit which provides initiation centres, but the addition of either grit or cork dust to the RDX/TNT failed to affect the gap test sensitivity. The most interesting addition was that of sensitive HMX. The sensitivity of HMX to the impact test varies considerably as has been discussed. If β HMX is heated to 190°C for two hours a mixture of α β and δ is formed and this material has an impact sensitivity comparable to lead azide. This material was made into a 60/40 octol with TNT and then the TNT was extracted with solvent and the HMX was found to have retained nearly all its high impact sensitivity, yet the addition of 1% of this material to Bridgwater RDX/TNT raised the critical gap to only 0.031" and 3.75% raised it to no more than 0.038" (compare data in Table 2). It might be expected that material of this character would, in the gap test, act as nuclei and greatly increase the sensitivity of the charge as a whole, in fact this is not so.

A careful microscopic examination of the various samples of RDX available showed that the more sensitive the RDX/TNT made therefrom, the greater the number of microscopic inclusions in the RDX crystal. The particular sample of Holston RDX/TNT was particularly rich in these inclusions, presumably introduced during formation of the crystal from the reaction mixture and preserved by recrystallisation by partial solution. A simple method was then devised for the addition of small inclusions to RDX. (13) The procedure is simply to heat the RDX until a limited amount of decomposition occurred. The products were then trapped in the crystal at numerous points throughout the crystal lattice.

Table 3

Temperature and Time of Heating Hours °C	Impact sensitivity of RDX (picric acid = 100)	Density of RDX g/ml	Gap test 60/40 RDX/TNT
0 130	74	1.804	0.027
24 130	74	1.797	0.042
72 130	72	1.793	0.045
167 130	75	1.789	0.047
42 160	77	1.790	0.093

The increase in the number of these inclusions may be varied easily in a controlled manner. Reference to Table 3 shows that the effect on the gap test of RDX/TNT made from the RDX is not paralleled by any effect on the impact sensitivity of the RDX itself.

This behaviour raises a number of interesting possibilities but for the purposes of this paper it will suffice to note that it is possible to vary the sensitivity of RDX/TNT to the gap test by modifications to the RDX crystal which do not affect its impact sensitivity.

It then seemed pertinent to examine the behaviour of RDX alone, and in particular the behaviour of single crystals of RDX. Dr. James Holden of N.O.L. worked on this interesting study whilst at E.R.D.E. (14). The crystals ranged from 20 - 45 g in weight and were relatively free from internal flaws. The results may be summarized as follows

(1) The sensitivity to shock of these single crystals is about equal to 60/40 RDX/TNT (i.e. is less than might be thought for pure RDX).

(2) In the majority of cases the crystals did not detonate until the shock had passed through the crystal completely and they then detonated "backwards".

(3) The sensitivity was affected by the nature of the material in contact with the crystal, i.e. different results were obtained if the crystal was in contact with a block of steel, aluminium or TNT, and the data could not be explained by the different acoustic impedences.

3.iii Physical Properties. The experimental problem in initiation by shock waves is to do so with a shock of accurately known intensity and duration. The method used at E.R.D.E. is to employ a discarding sabot gun to fire cylindrical projectiles at the explosives. The projectile velocity corresponding to a 50% probability of detonation is measured.

The pressure of the shock wave is determined by the velocity of the projectile and the shock properties of the explosive and projectile. The duration is determined by the projectile length. By using projectiles of different shock properties and of different lengths it is possible to compute the duration and pressure in the pulse which will just produce detonation.

Some interesting results arise from this study. (15). It was found that for the longest pulses the critical shock pressure was independant of duration. However for each explosive there was a minimum duration below which the critical pressure was strongly dependant on duration. For RDX/PWX 83/17 a critical duration of

0.6μ seconds was found, and for pulses longer than this, a critical pressure of 0.05 megabars.

The interesting aspect is this: if we apply to this explosive a pressure of 0.05 megabars for a duration of exactly 0.6μ seconds there will be a 50% probability of detonation, but at the time when the pressure at the entry face falls, because the end of the pulse has now reached the entry face, the shock front will have penetrated for no more than 2 to 3 mm into the explosive. It is a commonly observed phenomenon that with shock waves of border-line intensity the transition to detonation does not occur at the entry face but at some distance into the explosive. It is reasonable to assume that this happens in this case. We therefore have the circumstance that at the end of 0.6μ sec. (in this particular case) the shock has started a sequence which will lead inevitably to a detonation but has not yet in fact done so.

4. <u>Conclusion.</u> It would be inappropriate to draw purely technical conclusions in a review made in a biased fashion and without reference to the papers to be presented with it. It appears, however, at the present time that the interest in sensitivity is much healthier than at the time of the last detonation conference with many more laboratories taking a keen interest in these important problems and we can look forward to the future with confidence.

5. <u>Acknowledgement.</u> This review would not have been possible without the work of the author's colleagues both in E.R.D.E. and in other Establishments and grateful acknowledgement is hereby made.

6. <u>Bibliography</u>

(1) "Report of the Conference on Explosive Sensitivity held at the U.S. Naval Ordnance Laboratory" Navord 4197 p.20.

(2) "Impact Sensitivity of Materials with Liquid Oxygen" L.A. Nelson, Report MP 11,076 Douglas Aircraft Co.

(3) "Impact Sensitivity of Materials with Liquid Oxygen" L.A. Nelson, Report MP 10792 Douglas Aircraft Co.

(4) "Drop Weight Test for Liquids", p.14, Oct. 23 1958, Technoproducts Inc.

(5) "The Correlation of the Sensitiveness of Explosives with Combustion Data", E.G. Whitbread and L.A. Wiseman Second ONR Symposium on Detonation 1955.

(6) "Problems of Initiation in Tests of Sensitiveness", E.G. Whitbread, Second ONR Symposium on Detonation 1955.

(7)   "An Investigation into the Mechanism of Rifle Bullet and
      Fragment Attack Tests", P.C. Hobbins and E.G. Whitbread,
      E.R.D.E. Report 5/R/55.

(8)   "An Investigation into the Pressure History of an Explosive
      under Projectile Impact", P.C. Hobbins, E.L. Kendrew and
      E.G. Whitbread, E.R.D.E. Report 26/R/55.

(9)   "A Correlation of Impact Sensitivities of Explosives with
      Oxidant Balances", M.J. Kamlet, Navord 6126.

(10) "Variation of Heat of Detonation with Oxidant Balance for
      Structurally Related Compounds", M.J. Kamlet, Navord 6117.

(11) "The Correlation of the Impact Sensitivity of Organic High
      Explosives with their Decomposition Rates", J. Wenograd,
      Eigth Tripartite AXP Conference 1957.

(12) "The Impact Sensitiveness of HMX Polymorphs", W. Jeffers,
      E.R.D.E. Report 1/R/58.

(13) U.K. Patent Application No. 29255/59 (confidential
      application).

(14) "The Explosive Initiation of a Single Crystal of Cyclo-
      trimethylene Trinitramine", G.K. Adams, J. Holden,
      E.G. Whitbread, 31st International Congress Ind. Chem.
      Liege Sept. 1958.

(15) "Sensitivity of High Explosives: Projectile and Gap Tests",
      S.M. Brown, D.A. Steel, E.G. Whitbread, E.R.D.E. Report
      6/R/59.

(16) "An Investigation of the Explosive Hazards of Ammonium
      Perchlorate - Polyurethane Rubber Propellants in the
      Uncured and Cured Conditions", J. Clark, P.D. Verschoyle,
      E.R.D.E. Tech. Memo. 6/M/60.

SENSITIVITY RELATIONSHIPS

M. J. Kamlet
U. S. Naval Ordnance Laboratory
White Oak, Silver Spring, Maryland

ABSTRACT: Since individual impact results are not closely reproducible and since such effects are often small, it has hitherto been impossible to determine the effect on sensitivity of incorporating a specific chemical linkage within the structure of a molecule. It has now been found for large classes of structurally related compounds that impact errors tend to cancel out and that a plot of logarithmic impact sensitivity as a function of OB/100 shows points distributing about a straight line, called the "true trend" for the class of compounds in question. OB/100 is defined as the number of equivalents of oxidant per 100 g of explosive above the amount necessary to burn all C to CO and all H to H_2O.

For compounds containing a nitro group bound to nitrogen (nitramines, nitramides) the "true trend" is described by

$$\log h_{50\%} \pm 0.02 = 1.38 - (0.18)(OB/100).$$

For other polynitroaliphatic compounds the pertinent equation is

$$\log h_{50\%} \pm 0.02 = 1.76 - (0.22)(OB/100).$$

Separate trends are also shown for polynitroaromatic compounds whose sensitivity varies to a great degree depending on whether there are hydrogen atoms on a carbon alpha to the ring and for the surprising impact behavior of polynitrostilbenes.

These relationships enable us for the first time to
compare specific effects of specific structural features
on sensitivity. Mixtures of explosive plus wax are shown
to be about as sensitive as would be predicted from the
relevent "true trend" for pure explosives at equivalent
values of OB/100. Thus conventional "desensitization" is
merely a process of dilution.

I. INTRODUCTION

The impact sensitivity of an explosive varies to an
extent depending on the operator, the preparation and
condition of the impact sample and multifold other, as yet
undetermined, causes. Thus it is at present possible to
distinguish only gross differences in sensitivity between
structurally similar organic compounds. The present study
was undertaken with the purpose of establishing a rela-
tionship whereby we might judge how the impact sensitivities
of a recently prepared series of compounds containing the
terminal fluorodinitromethyl group (4b) compared with
other polynitroaliphatic compounds at similar levels of
"explosive power." In developing the relationship herein
described it soon became apparent that there might be
ramifications extending far beyond this original limited
objective.

In view of the unreliability of individual impact
results it appeared that any correlation would necessarily
be based on large numbers of impact sensitivities deter-
mined for related compounds. Our hope was that errors
would average out and that a plot of these data as a
function of whatever parameter was chosen for comparison
would show distribution around a "true trend." The trend
would then serve as a tool for predicting variation of
impact behavior with the chosen parameter.

The parameters compared were logarithm of 50% impact
height as determined on the ERL machine and Oxidant
Balance per 100 grams of explosive. Impact heights were
determined for 30/50 sieve cuts using Type 12 tools on
sandpaper. The other quantity, abbreviated as OB/100, is
defined as the number of equivalents of oxidant per 100 g
of compound above the amount necessary to burn all hydro-
gen to water and all carbon to carbon monoxide.

In calculating OB/100 an atom of oxygen represents two
equivalents of oxidant per mole, an atom of fluorine one
equivalent. Hydrogen represents one equivalent of reduc-
tant, carbon two equivalents. Since carboxyl groups are
considered as "dead-weight", two equivalents of oxidant
per mole are subtracted for each such group in the

molecule. For compounds containing only carbon, hydrogen, nitrogen and oxygen, the applicable equation is

$$OB/100 = \frac{100 \left(2\, n_O - n_H - 2\, n_C - 2\, n(\text{-COO-})\right)}{Mol.\ Wt.}$$

where n_O, n_H and n_C represent the number of atoms of oxygen, hydrogen and carbon in the molecule and $n(\text{-COO-})$ the number of carboxyl groups. For compounds balanced to the carbon monoxide level, $OB/100 = 0$. Above the CO level, $OB/100$ has a positive sign, below the CO level a negative sign.

II. POLYNITROALIPHATIC COMPOUNDS (1)

An attempt was made to eliminate the possibility that preformed prejudices might influence the choice of examples. The first one hundred compounds encountered in a search of the periodic NavOrd Reports listing sensitivities of explosive samples received by the Explosives Properties Division (2) during the period 1 January 1950 to 1 November 1956 were taken. The following criteria were then set for inclusion: The compound was solid at room temperature, contained no heteroaromatic ring, contained no acetylenic or azido groups and was not a salt. Of the original hundred, seventy-eight met all criteria.

These compounds, divided into categories according to structure, are listed in Table I. Listed also for each is the molecular formula, molecular weight, oxidant balance per mole, OB/100 and impact sensitivity. A plot of OB/100 vx. impact sensitivity for these compounds is given in Figure 1.

A first glance at this figure in which no distinction is made between types of compounds shows the expected general increase in impact height with increasing OB/100. The band within which all compounds fall is quite broad with impacts ranging from 5 to 16 cm at $OB/100 = + 3.0$, from 11 to 72 cm at $OB/100 = + 0.30$ and from 34 to 220 cm at $OB/100 = - 1.25$. Closer inspection of the plot, however, shows several areas of regularity.

Categories 1 - 5, Nitramines and Nitramides ●

These compounds, which share the common property that each has at least one nitro group attached directly to nitrogen, almost uniformly show lower impact values than the other polynitroaliphatics at equivalent values of OB/100. It appears, indeed, that points for the compounds

TABLE I
IMPACT SENSITIVITY AND OB/100
OF SELECTED NITROALIPHATIC EXPLOSIVES

No.	Compound Name	Mol. Formula	M.W.	O.B.	OB/100	I.S.
	1. Nitramines					
1	MEDINA	$CH_4N_4O_4$	136	+2	+1.47	13
2	EDNA	$C_2H_6N_4O_4$	150	+2	-1.33	34
3	RDX	$C_3H_6N_6O_6$	222	0	0	24
4	N-methyl EDNA	$C_3H_8N_4O_4$	164	-6	-3.65	114
5	HMX	$C_4H_8N_8O_8$	296	0	0	26
6	3-nitraza-1,5-pentanedinitramine	$C_4H_{10}N_6O_6$	238	-6	-2.52	39
7	3,6-dinitraza-1,8-octanedinitramine	$C_6H_{14}N_8O_8$	326	-10	-3.07	53
8	Tetryl	$C_7H_5N_5O_8$	287	-3	-1.04	32
	2. Nitramine plus gem-Dinitro					
9	3,3-dinitropentanedinitramine	$C_5H_{10}N_6O_8$	282	-4	-1.42	35
10	N,3,3,5,5-pentanitropiperidine	$C_5H_6N_6O_{10}$	310	+4	-1.29	14
11	bis-dinitropropylnitramine	$C_6H_{10}N_6O_{10}$	326	-2	-0.61	29
12	bis-dinitrobutylnitramine	$C_8H_{14}N_6O_{10}$	354	-10	-2.82	80
13	2,2,4,7,9,9-hexanitro-4,7-diazadecane	$C_8H_{14}N_8O_{12}$	414	-10	-1.45	72
14	2,2,4,7,7,10,12,12-octanitro-4,7-diazatridecane	$C_{11}H_{18}N_{10}O_{16}$	546	-8	-1.47	44
15	2,2,5,7,9,12,12-octanitro-4,7-diazatridecane	$C_{11}H_{18}N_{10}O_{16}$	546	-8	-1.47	57
	3. Nitramine plus Trinitromethyl					
16	methyl trinitroethylnitramine	$C_3H_5N_5O_8$	239	+5	+2.09	9
17	BTNEN	$C_4H_4N_8O_{14}$	388	+16	+4.12	5
18	trinitroethyl trinitropropylnitramine	$C_5H_6N_8O_{14}$	402	+12	+2.98	6
19	N,N'-bis-trinitroethyl MEDINA	$C_5H_6N_{10}O_{14}$	462	+16	+3.46	5
20	N-methyl-N'-trinitroethyl EDNA	$C_5H_9N_7O_{10}$	327	+1	+0.30	11
21	trinitroethyl N-trinitroethylnitraminoacetate	$C_6H_6N_8O_{16}$	446	+12	+2.69	9
23	trinitroethyl 4-nitrazavalerate	$C_6H_9N_5O_{10}$	311	-3	-0.97	35
24	trinitroethyl 3,3-dinitrobutylnitramine	$C_6H_9N_7O_{12}$	371	+3	+0.81	20
25	bis-trinitroethyl 3-nitrazaglutarate	$C_8H_8N_8O_{18}$	504	+8	+1.58	14
26	1,1,1,3,6,9,11,11,11-nonanitro-3,6,9-triazaundecane	$C_8H_{12}N_{12}O_{18}$	564	+8	+1.42	12
27	1,1,1,3,6,9,11,11,11-decanitro-3,9-diazaundecane	$C_9H_{12}N_{12}O_{20}$	608	+10	+1.64	10
28	1,1,1,4,6,8,11,11,11-decanitro-4,8-diazaundecane	$C_9H_{12}N_{12}O_{20}$	608	+10	+1.64	11
29	bis-trinitroethyl 4-nitrazaheptandioate	$C_{10}H_{12}N_8O_{18}$	532	0	0	29
30	1,1,1,3,6,9,12,14,14,14-decanitro-3,6,9,12-tetrazatetradecane	$C_{10}H_{16}N_{14}O_{20}$	652	+4	+0.61	19
31	bis-trinitroethyl 3,6-dinitraza-1,8-octandioate	$C_{10}H_{12}N_{10}O_{20}$	592	+4	+0.67	29
32	1,1,13,6,8,10,13,15,15,15-tridecanitro-3,8,13-triazapentadecane	$C_{12}H_{16}N_{16}O_{26}$	800	+12	+1.50	23

TABLE I (Cont'd.)

No.	Compound Name	Mol. Formula	M.W.	O.B.	OB/100	I.S.
	4. Nitramine plus Nitrate Ester					
33	trinitroethylnitraminoethyl nitrate	$C_4H_6N_6O_{11}$	314	+10	+3.19	7
34	trinitroethylnitraminopropyl nitrate	$C_5H_8N_6O_{11}$	328	+ 6	+1.83	12
35	3,5,5-trinitro-3-azahexyl nitrate	$C_5H_9N_5O_9$	283	- 1	-0.35	21
	5. Nitramides					
36	N-nitro-N-trinitropropyl trinitroethyl carbamate	$C_6H_6N_8O_{16}$	446	+12	+2.70	9
37	trinitroethyl 2,5-dinitrazahexanoate	$C_6H_9N_7O_{12}$	371	+ 1	+0.27	15
38	trinitroethyl 2,5,5-trinitro-2-azahexanoate	$C_7H_9N_7O_{14}$	415	+ 3	+0.72	22
39	trinitroethyl 2,4,6,6-tetranitro-2,4-diazaheptanoate	$C_7H_9N_9O_{16}$	475	+ 7	+1.47	18
40	N,N'-dinitro-N,N'-bis-(trinitropropyl)-oxamide	$C_8H_8N_{10}O_{18}$	532	+12	+2.26	9
41	2,2,6,9,9-pentanitro-4-oxa-5-keto-6-azadecane	$C_8H_{12}N_6O_{12}$	384	- 6	-1.56	47
42	1,1,1,5,7,10,14,14,14-nonanitro-3,12-dioxa-4,11-diketo-5,7,10-triazatetradecane	$C_9H_{10}N_{12}O_{22}$	638	+12	+1.88	11
43	N,N'-dinitro-N,N'-bis-(3,3-dinitrobutyl)-oxamide	$C_{10}H_{14}N_8O_{14}$	470	- 6	-1.28	37
44	1,1,1,5,8,11,14,18,18,18-decanitro-3,16-dioxa-4,15-diketo-5,8,11,14-tetrazaoctadecane	$C_{12}H_{16}N_{14}O_{24}$	740	+ 4	+0.54	19
45	N, N'-dinitro-N,N'-bis-(3-nitrazabutyl)-oxamide	$C_8H_{14}N_8O_{10}$	382	-10	-2.61	90
	6. Trinitromethyl Compounds					
46	trinitroethylcarbamate	$C_3H_4N_4O_8$	224	+ 4	+1.79	18
47	methyl trinitroethyl carbonate	$C_4H_5N_3O_9$	239	+ 3	+1.25	28
48	1,1,1,3-tetranitropropane	$C_4H_4N_4O_8$	236	+ 4	+1.70	33
49	methylene-bis-trinitroacetamide	$C_5H_4N_8O_{14}$	400	+14	+3.50	9
50	heptanitropentane	$C_5H_5N_7O_{14}$	387	+13	+3.36	12
51	BTNEC	$C_5H_4N_6O_{15}$	388	+14	+3.60	16
52	BTNEU	$C_5H_6N_8O_{13}$	386	+10	+2.60	17
53	5,5,5-trinitropentanone-2	$C_5H_7N_3O_7$	221	- 3	-1.36	125
54	TNETB	$C_6H_6N_6O_{14}$	386	+ 8	+2.07	18
55	ethyl trinitroethyl carbonate	$C_5H_7N_3O_9$	253	- 1	-0.39	81
56	trinitroethyl orthoformate	$C_7H_7N_9O_{21}$	553	+21	+3.80	7
57	1,1,1,7,7,7-hexanitroheptanone-4	$C_7H_8N_6O_{13}$	384	+ 4	+1.04	34
58	nitroisobutyl trinitrobutyrate	$C_8H_{12}N_4O_{10}$	324	-10	-3.09	279
59	trinitrobutyric anhydride	$C_8H_8N_6O_{15}$	428	+ 4	+0.93	30
60	N,N'-bis-trinitropropyloxamide	$C_8H_8N_8O_{14}$	442	+ 2	+0.45	45
61	bis-trinitroethylsuccinate	$C_8H_8N_6O_{16}$	444	+ 4	+0.90	30
62	TNEOC	$C_9H_{12}N_{12}O_{28}$	732	+28	+3.83	7
63	methylene-bis-trinitrobutyramide	$C_9H_{12}N_8O_{14}$	456	- 2	-0.44	113
64	ethylene-bis-trinitrobutyrate	$C_{10}H_{10}N_6O_{14}$	470	- 2	-0.43	120

TABLE I (Cont'd.)

No.	Compound Name	Mol. Formula	M.W.	O.B.	OB/100	I.S.
	7. Trinitromethyl plus gem-Dinitro					
65	N-trinitroethyl-3,3,5,5-tetranitropiperidine	$C_7H_8N_8O_{14}$	428	+6	+1.40	18
66	trinitroethyl dinitrovalerate	$C_7H_9N_5O_{12}$	355	-1	-0.28	70
67	dinitropropyl trinitrobutyramide	$C_7H_{10}N_6O_{11}$	354	-2	-0.57	72
68	dinitrobutyl trinitrobutyrate	$C_8H_{11}N_5O_{12}$	369	-5	-1.33	101
69	trinitroethyl dinitrohexanoate	$C_8H_{11}N_5O_{12}$	369	-5	-1.33	138
70	N,N'-bis-dinitropropyl trinitrobutyramide	$C_{10}H_{14}N_8O_{15}$	486	-4	-0.82	72
71	dinitropropandiol bis-trinitrobutyrate	$C_{11}H_{12}N_8O_{20}$	576	+2	+0.35	50
72	bis-trinitroethyl 4,4-dinitrohepandioate	$C_{11}H_{12}N_8O_{20}$	576	+2	+0.35	68
73	bis-trinitroethyl 4,4,6,6,8,8-hexanitroundecanedioate	$C_{15}H_{16}N_{12}O_{28}$	812	+6	+0.74	32
	8. gem-Dinitro Compounds					
74	3,3,4,4-tetranitrohexane	$C_6H_{10}N_4O_8$	266	-6	-2.25	80
75	2,2,4,6,6-pentanitroheptane	$C_7H_{11}N_5O_{10}$	325	-5	-1.54	56
76	2,2,4,4,6,6-hexanitroheptane	$C_7H_{10}N_6O_{12}$	370	0	0	29
77	bis-dinitropropyl oxalate	$C_8H_{10}N_4O_{12}$	354	-6	-1.70	227
78	dinitropropyl dinitrovalerate	$C_8H_{12}N_4O_{10}$	324	-10	-3.09	320
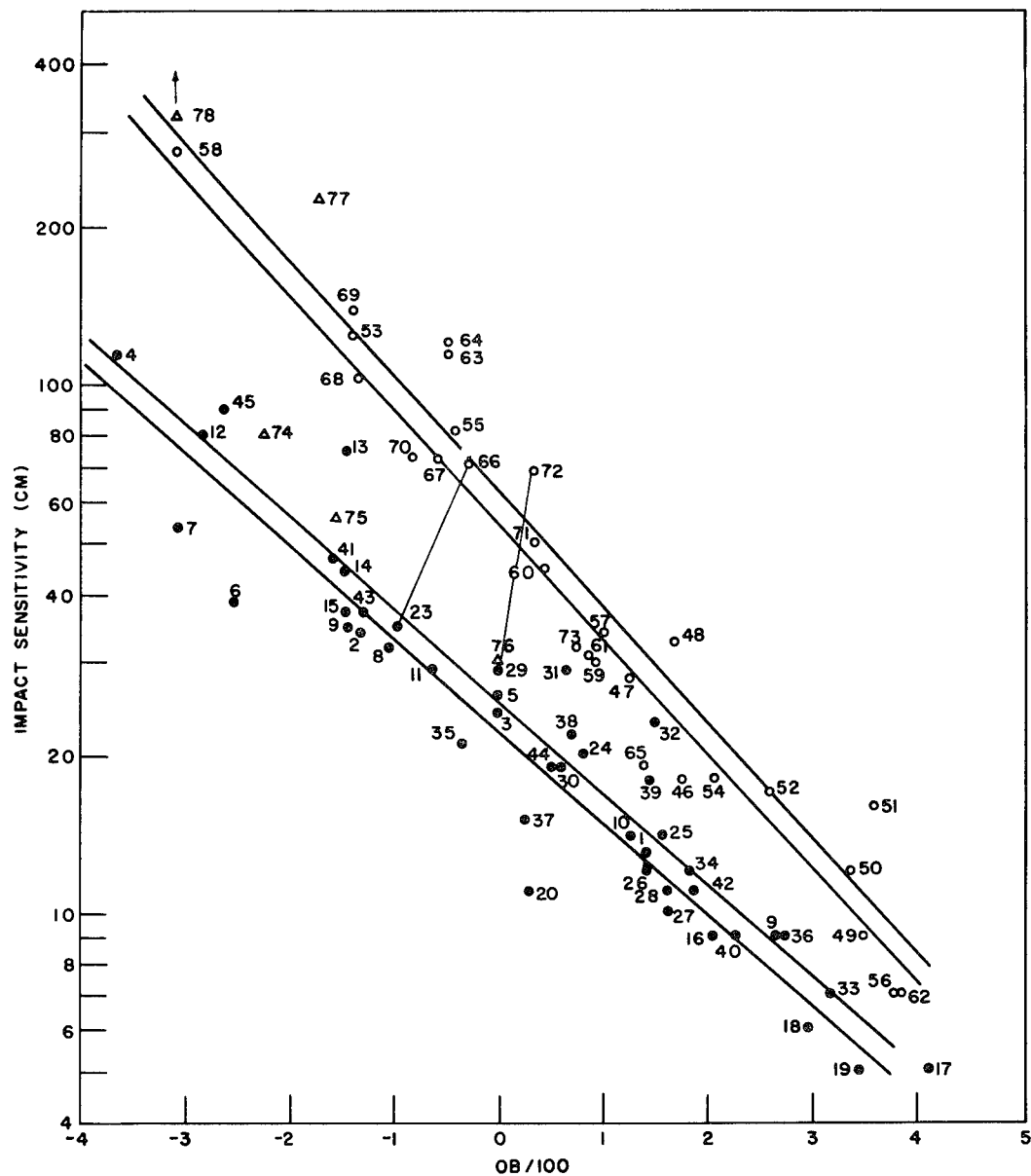
FIG. I IMPACT SENSITIVITY AS A FUNCTION OF OB/IOO, ALIPHATIC
COMPOUNDS

in these five categories, represented by filled-in circles on the plot, show the hoped-for statistical distribution about a straight line relating OB/100 with the logarithm of the impact height.

Since it would be overly precise to attempt a least-squares treatment based on measurements as inexact as these, we have by inspection delineated an area within which it is expected a least-squares line would fall and whose width at any impact height is equal to 10% of that height. This area, hereafter called the "true trend for N-nitro compounds, may be described by the approximation

$$\log I. S. \pm 0.02 = 1.38 - (0.18)(OB/100)$$

where I. S. represents the 50% impact height.

Of the forty-five nitramino and nitramido compounds, fifteen fall in the area of the "true trend", an additional seventeen within 10% of the area and an additional seven within between 10 and 30% of the area. Of the other six, none is more than 80% off the value predicted by the "true trend." Since TNT, a standard for impact determinations, has shown impact values ranging from below 100 to 250 cm, and considering that for a period of over three months impact sensitivities of TNT consistently ran between 20 and 40% high, the distribution is as good as could be hoped for if the relationship claimed is truly a fact of nature.

An attempt was made to determine whether within the overall classification "N-nitro compounds" there was any preferred concentration of points above or below the "true trend" according to structure. The five individual categories comprising the group each show more-or-less random distribution as do categories based on the number of nitramino groups in the molecule or molecular weight. There is a slight tendency for compounds containing "dead weight" carboxyl groups to fall above the "true trend" and for primary nitramines to fall below.

Categories 6 and 7, Trinitromethyl Compounds ◎

Points for these two classes, represented by empty circles in Figure 1, also distribute about a straight line relating the logarithm of impact sensitivity with OB/100. A "true trend" for polynitroaliphatic compounds based on these points is shown in the plot and may be described by

$$\log I. S. \pm 0.02 = 1.76 - (0.22)(OB/100).$$

Of the twenty-eight compounds, eight fall in the area of the "true trend", an additional thirteen within 10%, four within between 10 and 30% and three within between 30 and 60%.

At OB/100 = + 2.0 this "true trend" predicts an impact height twice that of the N-nitro "true trend"; at OB/100 = - 2.0, impact heights are three times as great. The question of why polynitroaliphatics and N-nitro compounds follow separate trends is discussed separately (1) as is the suggestion that lower heats of formation and higher heats of detonation of N-nitro compounds cause lower impact heights at equivalent values of OB/100. It is meanwhile instructive to consider two pairs of compounds, structurally identical with the exception that in each case a nitramino group replaces a gem-dinitro. Tie-lines between the compounds considered are drawn in Figure 1.

No.	Compound (X = NO_2)	OB/100	Heat of Det. Cal/g	Impact Sensitivity
66	$CH_3CX_2CH_2CH_2COOCH_2CX_3$	-0.28	1035	70
23	$CH_3NXCH_2CH_2COOCH_2CX_3$	-0.97	970	35
72	$CX_3CH_2OOCCH_2CH_2CX_2CH_2CH_2COOCH_2CX_3$	+0.35	1115	68
29	$CX_3CH_2OOCCH_2CH_2NXCH_2CH_2COOCH_2CX_3$	0.0	1065	29

In each instance the nitramino compound has a lower value of OB/100 and a lower calculated heat of detonation but is still much more sensitive.

Category 8, gem-Dinitro Compounds △

Compounds 77 and 78 lie well above the "true trend" for polynitroaliphatic compounds while with compounds, 74, 75 and 76 the points fall much lower. The last three share in common the fact that each has a gem-dinitro group in a position alpha or beta to another secondary nitro linkage and it may be that this is a sterically unfavorable situation as far as impact sensitivity is concerned. This seems borne out by the fact that compounds 65 and 73 of Category 7 which contain this structural feature also exhibit the same behavior.

III. POLYNITROAROMATIC COMPOUNDS

With the nitroaliphatic compounds discussed above, the division into two major classes, depending on whether the compound had a nitro group attached directly to nitrogen, was made by first plotting all available data, then ascertaining from an examination of the plot the particular structural feature which appeared to impart greater sensitivity. With polynitroaromatic compounds (including mixed nitroaliphatics-nitroaromatics), an a priori reason existed for a division into two main categories and an examination of the plot showed the existence of an interesting third category.

Dacons, Kamlet and Sickman (5) had used chromatographic techniques to isolate some of the initial thermal decomposition products of TNT and had identified among these the oxidized derivatives trinitrobenzyl alcohol, trinitrobenzaldehyde and dinitroanthranil together with reduced derivatives which appeared to be the isomeric tetranitroazoxytoluenes and azotoluenes. These results implied that the initial steps in this thermal decomposition involved oxidative attack on the methyl group by nitro groups in the same or neighboring molecules. Coupled with Dacons' observation (6) that trinitrobenzene, hexanitrobiphenyl and nonanitroterphenyl show very much greater thermal stability both as solids or in solution than TNT and hexanitrobibenzyl, these findings indicated that polynitroaromatic compounds decompose by different mechanisms depending on whether or not there is an aliphatic residue containing a hydrogen atom on the carbon attached directly to the ring. This furnished an excellent preliminary basis for categorizing the polynitroaromatics.

Data for these compounds are listed in Table II and plotted in Figures 2 and 3.

Category 9, Nitroaromatics with no Hydrogen on alpha Carbon ○

The twenty three members of this class, which includes polynitroarylamines, polynitrophenols, alkyl polynitroaryl ethers, polynitroalkyl polynitrobenzoates and other polynitrobenzoic acid derivatives are represented by open circles in Figure 2. Although the scatter is somewhat greater than is the case with the aliphatics, these compounds similarly appear to follow a trend which may be described approximately by

$$\log \text{ I. S. } \pm 0.02 = 1.74 - (0.28)(\text{OB}/100).$$

TABLE II

IMPACT SENSITIVITY AND OB/100 OF SELECTED NITROAROMATIC EXPLOSIVES

No.	Compound Name	Mol. Formula	M.W.	O.B.	OB/100	I.S.
	9. No Alpha Hydrogen on Carbon					
79	Pentanitroaniline	$C_6H_2N_6O_{10}$	318	+6	+1.88	15
80	Trinitroethyl trinitrobenzoate	$C_9H_4N_6O_{14}$	420	+4	+0.95	24
81	Trinitroresorcinol	$C_6H_3N_3O_8$	245	+1	+0.41	43
82	2,3,4,6-Tetranitroaniline	$C_6H_3N_5O_8$	273	+1	+0.37	41
83	Trinitroethyl 3,5-dinitrosalicylate	$C_9H_5N_5O_{13}$	391	+1	+0.26	45
84	Trinitroethyl 3,5-dinitrobenzoate	$C_9H_5N_5O_{12}$	375	-1	-0.28	73
85	Picric acid	$C_6H_3N_3O_7$	229	-1	-0.44	87
86	2,4,6-Trinitro-3-aminophenol	$C_6H_4N_4O_7$	244	-2	-0.81	138
87	Nonanitroterphenyl	$C_{18}H_5N_9O_{18}$	635	-5	-0.79	39
88	Hexanitrobiphenyl	$C_{12}H_4N_6O_{12}$	424	-4	-0.94	85
89	Trinitrobenzoic acid	$C_7H_3N_3O_8$	257	-3	-1.17	109
90	Fluorodinitroethyl 3,5-dinitrobenzoate	$C_9H_5N_4O_{10}F$	348	-4	-1.15	140
91	Dinitropropyl trinitrobenzoate	$C_{10}H_7N_5O_{12}$	389	-5	-1.28	214
92	Trinitrobenzene	$C_6H_3N_3O_6$	213	-3	-1.46	100
93	Trinitrobenzonitrile	$C_7H_2N_4O_6$	238	-4	-1.68	149
94	Picramide	$C_6H_4N_4O_6$	228	-4	-1.75	177
95	4,6-Dinitroresorcinol	$C_6H_4N_2O_6$	200	-4	-2.00	>320
96	2,4-Dinitroresorcinol	$C_6H_4N_2O_6$	200	-4	-2.00	296
97	Trinitroanisole	$C_7H_5N_3O_7$	243	-5	-2.06	192
98	Dimethoxytrinitrobenzene	$C_8H_7N_3O_8$	273	-7	-2.56	251
99	3-Methoxy-2,4,6-trinitroaniline	$C_7H_6N_4O_7$	258	-6	-2.32	>320
100	Diaminotrinitrobenzene	$C_6H_5N_5O_6$	243	-5	-2.06	>320
101	Hexanitrodiphenylamine	$C_{12}H_5N_7O_{12}$	439	-5	-1.14	48
	10. Alpha Hydrogen on Carbon					
102	Trinitroethyltrinitrobenzene	$C_8H_4N_6O_{12}$	376	+4	+1.07	13
103	Trinitropropyltrinitrobenzene	$C_9H_6N_6O_{12}$	390	0	0.00	21
104	Trinitroethyl-2,4-dinitrobenzene	$C_8H_5N_5O_{10}$	331	-1	-0.30	31
105	Trinitrobenzaldehyde	$C_7H_3N_3O_7$	241	-3	-0.80	36
106	Hexanitrobibenzyl	$C_{14}H_8N_6O_{12}$	452	-12	-2.64	114
107	TNT	$C_7H_5N_3O_6$	227	-7	-3.08	160
108	Trinitrobenzyl alcohol	$C_7H_5N_3O_7$	243	-5	-2.06	52
109	Trinitrobenzaldoxime	$C_7H_4N_4O_7$	256	-4	-1.56	42
110	Trinitro-m-cresol	$C_7H_5N_3O_7$	243	-5	-2.06	191
	11. Stilbene Derivatives					
111	2,2',4,4',6,6'-Hexanitrostilbene	$C_{14}H_6N_6O_{12}$	450	-10	-2.22	39
112	2,2',4,4',6-Pentanitrostilbene	$C_{14}H_7N_5O_{10}$	405	-15	-3.71	107
113	2,4,4',6-Tetranitrostilbene	$C_{14}H_8N_4O_8$	360	-20	-5.56	140
114	2,2',4,4'-Tetranitrostilbene	$C_{14}H_8N_4O_8$	360	-20	-5.56	109
115	2,3',4,6-Tetranitrostilbene	$C_{14}H_8N_4O_8$	360	-20	-5.56	314
116	2,4,6-Trinitrostilbene	$C_{14}H_9N_3O_6$	315	-25	-7.92	218
117	2,4,6-Trinitrostyrene	$C_8H_5N_3O_6$	239	-9	-3.76	41
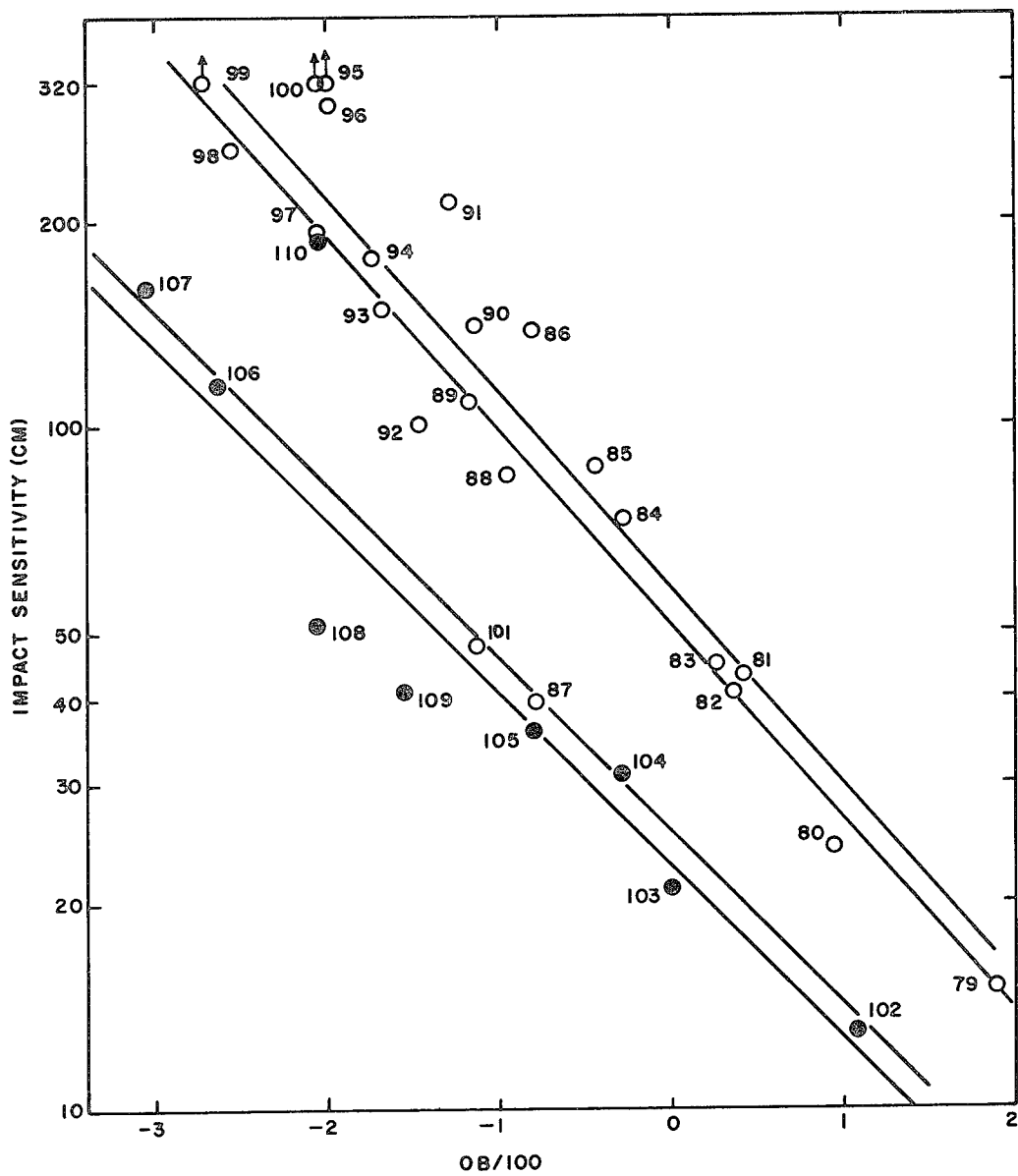
FIG. 2 IMPACT SENSITIVITY AS A FUNCTION OF OB/I00,
AROMATIC COMPOUND
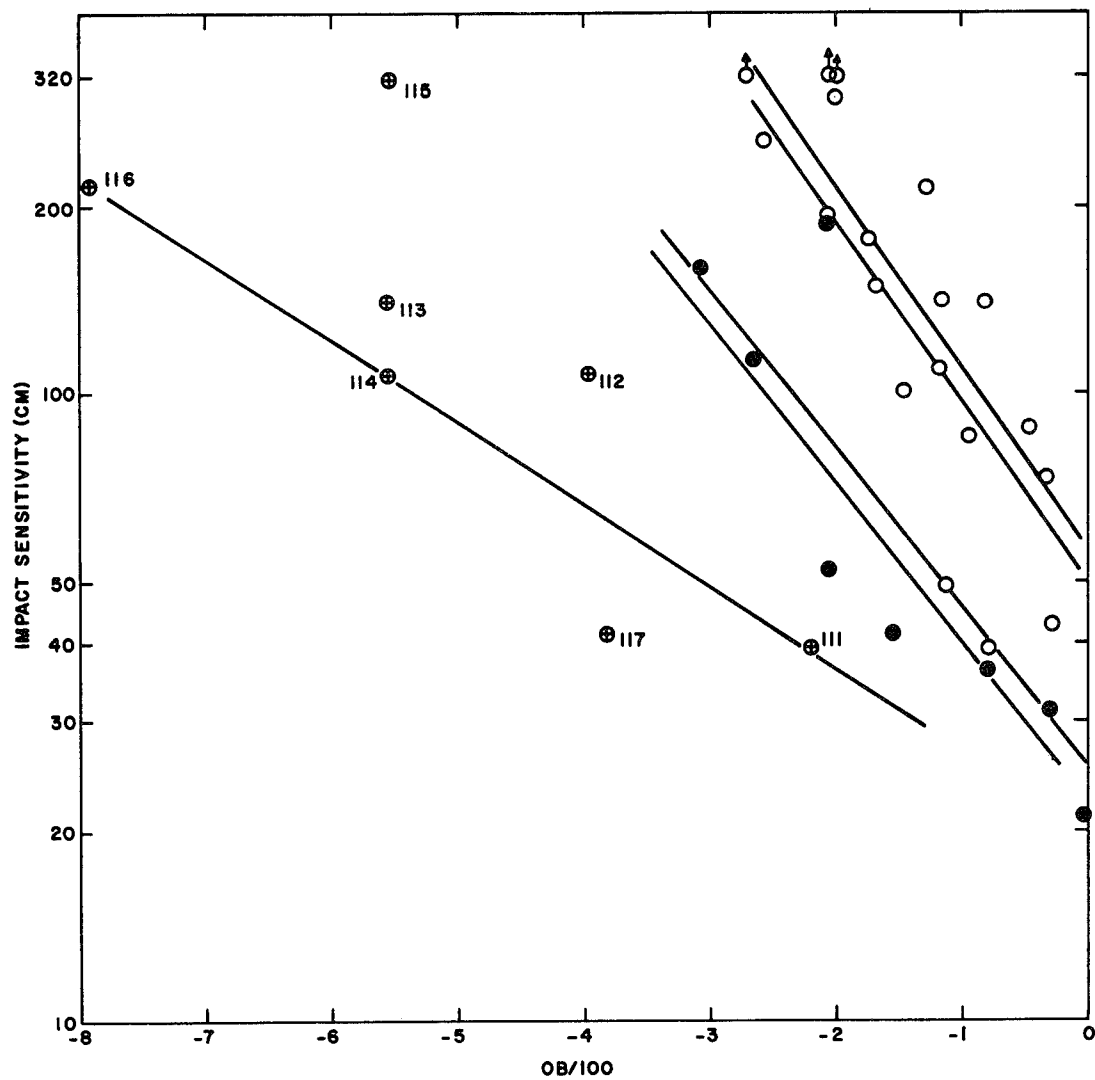
FIG. 3 IMPACT SENSITIVITY AS FUNCTION OF OB/100, STILBENES

Of the compounds in this broad category, seven fall within the area of the "true trend", eight within 10% and two between 10 and 40%, while six fall rather badly out of line. Since it is unlikely that these compounds all decompose by similar mechanisms, the "spread" is not surprising. It is perhaps noteworthy that of the six compounds which fall badly out of line, the increased sensitivity of two (numbers 87 and 101) may be explained on the basis of intramolecular crowding similar to that which imparts greater sensitivity in the nitroaliphatic series where gem-dinitro groups are alpha or beta to other secondary nitro linkages. The decreased sensitivities of 95 and 96 are also not surprising since with each compound two of the six oxygens are phenolic rather than nitro.

Category 10. Nitroaromatics with Hydrogen on alpha Carbon

The greater sensitivity of this category (filled circles in Figure 2) relative to category 9 is readily evident from an inspection of the plot. Of nine compounds in this class, six follow closely the trend

$$\log I. S. \pm 0.02 = 1.38 - (0.25)(OB/100),$$

while two are 50-60% low and one (trinitro-m-cresol, No. 110) is 150% high. No explanation can yet be offered for the anomolous behavior of compound 110 which has been repeated in a sufficient number of impact determinations to convince us that it is real.

Category 11. Polynitrostilbenes ⊕

Data for six polynitrostilbenes (Nos. 111-116) and 2,4,6-trinitrostyrene (No. 117) are plotted in Figure 3. Although these compounds conform with the definition offered for category 10, it is apparent that as a class they are uniformly more sensitive. 2,4,6-Trinitrostilbene (No. 116), with three nitro groups for fourteen carbon atoms, is perhaps the poorest explosive yet to register on the NOL impact machine. The remarkable sensitivity of this class may be due to the close proximity of the nitro group to the readily oxidizable C=C linkage.

IV. TWO-COMPONENT MIXTURES

In considering the sensitivity of pure compounds one has to contend only with the vagaries of the impact machine. With more than one component there is the additional complication that the method of mixing is also suspect. One never knows whether the 35 mg sample taken for the individual shot fairly represents the overall composition of the aggregate. Unfortunately, such phenomena as segregation and clustering appear to be the rule rather than the exception.

Since systemic errors in multi-components systems are more to be expected than with single compounds, we have been more selective in the choice of examples for consideration. We have confined ourselves to pairs for which large numbers of measurements are available and for which results taken over a span of years by a number of workers show a measure of agreement. The data have, as before, been taken from the periodic NavOrd Reports of the Explosives Properties Division covering the interval 1 January 1950 to 1 November 1956 (2).

Explosive Plus Explosive

Plots of logarithmic 50% impact heights as functions of OB/100 are shown in Figure 4 for mixtures of RDX with TNT and with bis-dinitropropyl fumarate (DNPF). In both cases the points distribute about straight lines connecting the logarithmic impact heights of the individual components. Probably the most reliable of the points on the plot is that for Composition B at OB/100 = - 1.50. Although not strictly a two-component system since it contains 1% wax, it seems significant that the accepted impact sensitivity of 60-65 cm agrees well with the 62 cm predicted if the linear relationship should apply.

Other explosive pairs, for which it appears that mixtures show logarithmic impact heights between those of the individual components and for which a similar linear relationship with OB/100 may hold, involve RDX-TNETB, RDX-BTNEU and HMX-BTNEN. With these pairs the amount of data available is sufficient only for the qualitative observation.

Without further experimental results any conclusions must be tentative and it can only be expressed as an opinion that where mixing is ideal, the logarithmic impact sensitivity of a mixture of explosive plus explosive is a linear function of the composition of that mixture.
It should be noted that the frequently made qualitative
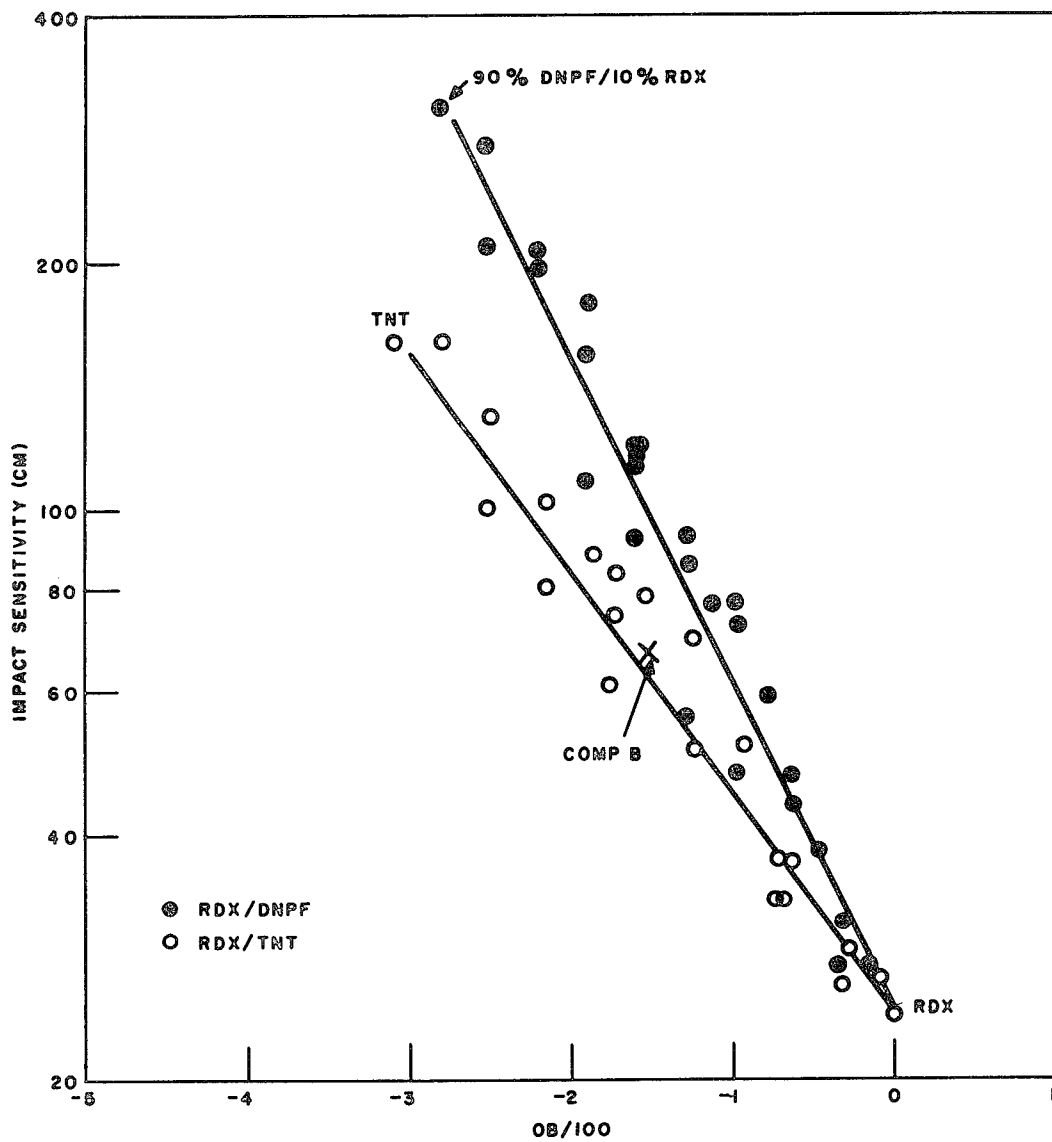
FIG. 4 IMPACT SENSITIVITIES OF RDX-TNT AND RDX-DNPF
MIXTURES AS FUNCTIONS OF OB/100

observation that the sensitivity of a mixture approaches
more closely that of the more sensitive component is not in
conflict with the above opinion. A linear relationship
with logarithmic heights would on a non-logarithmic basis
have this as a necessary consequence*.

Explosive Plus Wax

Because of their differing physical properties,
segregation and clustering are even more to be expected
with mixtures of explosive plus wax. It is disconcerting
but not surprising to find presumably the same RDX-wax
composition shooting at heights ranging from 25 cm to
250 cm. Of the multitude of data collected for explosive-
wax mixtures only a single value may be considered as
reliable and this only over a range.

Based on an average of tens of thousands of shots, Com-
position A (91% RDX-9% wax) has an impact sensitivity of
70-75 cm. OB/100 for this mixture is -2.58**. At an
equivalent value of OB/100 a pure explosive, if it fol-
lowed the "true trend" for N-nitro compounds, would be
predicted to have an impact sensitivity of 67-73 cm.

Additional data for this and other proportions of
RDX and Stanolind wax are plotted in Figure 5. It can be
seen that for compositions ranging from 2 to 15% wax
there is an approximately equal distribution of points
above and below the "true trend" (solid lines).

Also plotted in Figure 3 are data for TNETB -
Stanolind wax mixtures at compositions from 1 to 15% wax
together with the "true trend" for polynitroaliphatic com-
pounds. Here it appears that if a least-squares line
should be drawn through these points the line would closely
parallel the "true trend" for this class of compounds.

---

* Note added in proof: It has recently come to our atten-
tion that a similar linear relationship between composition
and logarithmic impact heights of RDX-PETN mixtures as
measured on the ERL machine, "Design No. 3", was des-
cribed fifteen years ago (3).
** In the calculations waxes are considered to be
mainly polymethylene, OB/100 = - 28.6
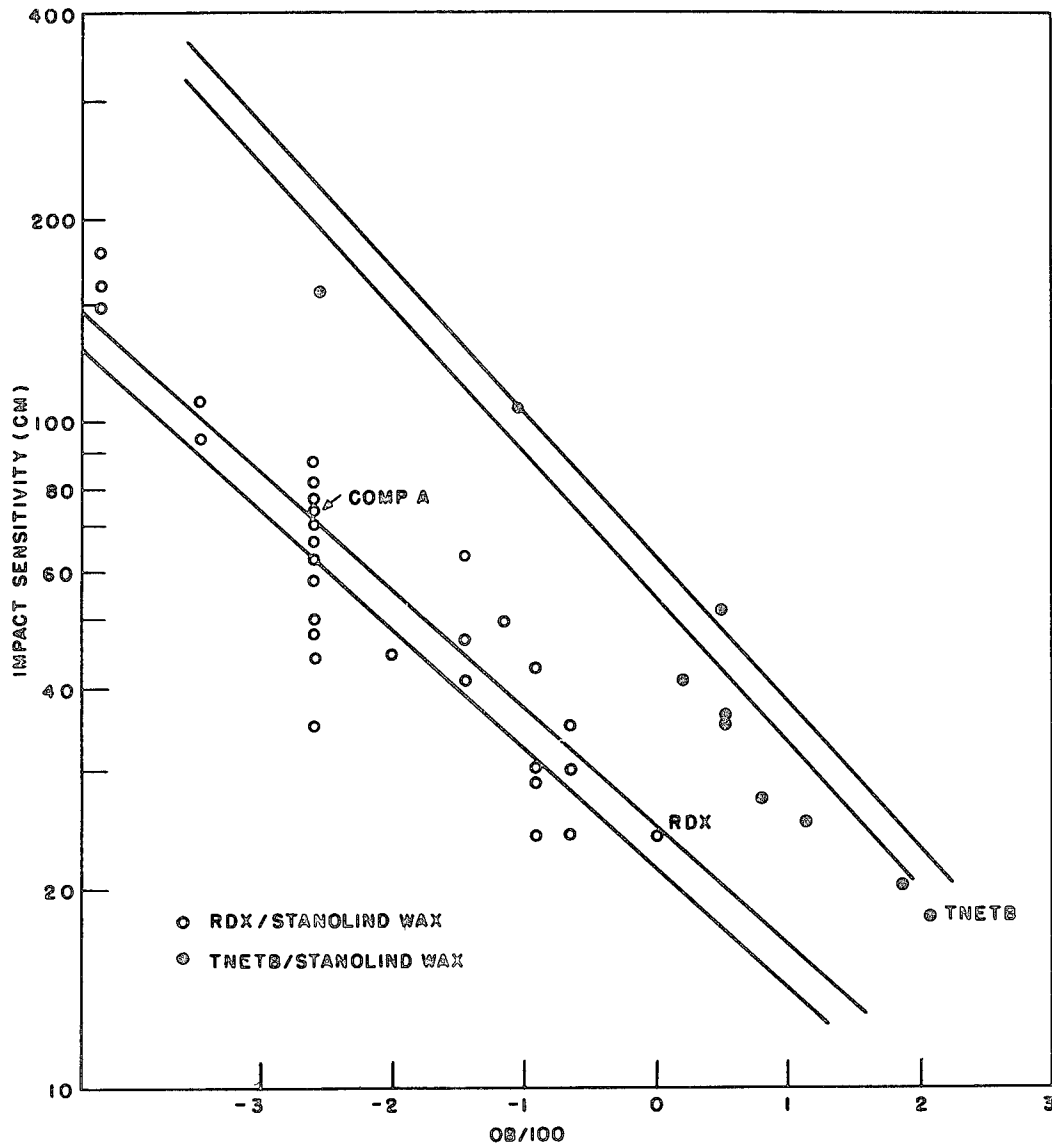
FIG. 5 "DESENSITIZATION" OF RDX AND TNETB WITH STANOLIND WAX
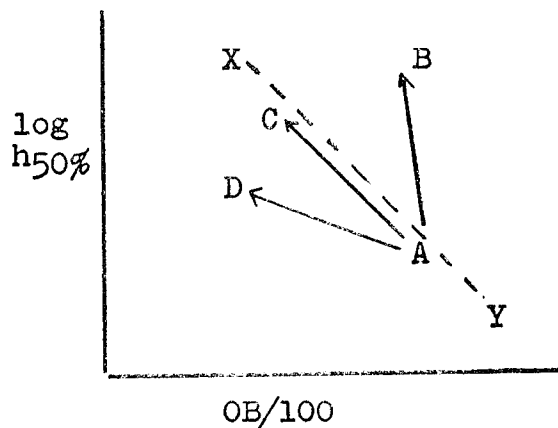
If the point A represents an explosive compound and the broken line X-Y the "true trend" of the class into which that compound falls, the arrow A-C describes the behavior of both RDX and TNETB on addition of wax. This effect is one of dilution, not desensitization. The same result was obtained on adding methylene groups in the form of a wax coating on the explosive crystal as would be predicted had the same quantity of methylene groups been incorporated within the structure of the molecule.

True desensitization would imply the behavior described by the arrow A-B. The decrease in sensitivity on coating crystal surfaces with wax would be greater than that anticipated simply by dilution. Many cases of A-B behavior have been reported, but none has ever been reproduced and it appears that in conventional "desensitization" it has never truly occurred. If it had, the composition would probably now be in service use.

Behavior described by the arrow A-D has also often been reported. It is a necessary consequence of segregation that if A-C represents ideal behavior and if one portion of a mixture follows A-B behavior, another portion will follow A-D.

It is our belief that the impact sensitivity of an explosive on "desensitization" approaches that anticipated on dilution as mixing and sampling approach ideality. While the validity of all other evidence is suspect, the value for Composition A seems unassailable and strongly supports this belief.

CONCLUSIONS

A number of conclusions may be drawn from this study. If correct, they support recommendations on future research and development in the field of explosive chemistry.

(1) Nitramines are more sensitive than other poly-nitroaliphatic compounds at equivalent values of OB/100 and at equivalent heats of detonation. The N-nitro linkage appears to be a built-in sensitizing group. It is perhaps unfortunate that of the three compounds most commonly used in explosive chemistry, RDX, tetryl and TNT, two are of this class. In the further synthesis of new high explosives and propellants, the N-nitro linkage should be avoided. Conversely, at every value of OB/100, poly-nitroaliphatic compounds not containing the N-nitro linkage are less sensitive than pure explosives and explosive compositions now in use.

(2) For separate classes of explosive compounds there are linear relationships between logarithmic impact heights and OB/100. These relationships have a number of potential uses.

(2-a) One can predict the sensitivity of a compound prior to making it. This furnishes a preliminary indication of how the compound should be handled.

(2-b) One can determine whether within a class additional structural features tend to sensitize or desensitize. Fluorodinitromethyl compounds, for example, appear quite promising as a group because their impact sensitivities generally fall above the "true trend" for polynitro-aliphatics (4). Conversely, compounds with the gem-dinitro linkage alpha or beta to a secondary nitro group appear not to be promising because impacts fall well below the "true trend."

(3) With ideal mixing the impact sensitivity of explosive plus wax is that predicted at an equivalent value of OB/100 by the "true trend" of the class into which that explosive falls. Conventional "desensitization" appears merely to be a process of dilution. If this be the case, why "desensitize"? The same result may be achieved by incorporating the same quantity of methylene groups within the structure of the explosive molecule, i.e., "tailor-making" a molecule with the same value of OB/100 as explosive plus wax. A number of advantages result.

Problems of segregation, stratification, preferential exudation, sampling, etc. are eliminated. Batch to batch

reproducibility is much easier. In "desensitizing" RDX we must build around the physical characteristics of this compound; in tailor-making we can choose between many possible sets of physical properties since a wide variety of compounds is potentially available at any value of OB/100 desired.

NOTE WELL: In recommending against "desensitization" we confine ourselves to the conventional method of coating explosive crystals with wax. Work currently being done on desensitization by solution is promising and may offset many of the arguments made here.

ACKNOWLEDGMENT

BIBLIOGRAPHY

(1) The material in this section is discussed in greater
detail in the following references: (a) M. J. Kamlet,
NavOrd Report (NOL) 6126, "A Correlation of Impact
Sensitivities of Explosives with Oxidant Balances,"
26 September 1958; (b) Idem., NavOrd Report (NOL)
6117, "Variation of Heat of Detonation with Oxidant
Balance for Structurally Related Compounds,"
26 September 1958.

(2) N. D. Mason, G. Svadeba, L. E. Starr, S. F. Duck,
G. W. Reynolds and L. D. Hampton, NavOrd Reports
(NOL) 2184, 1 August 1951; 2433, 5 May 1952;
2940, 1 July 1953; 3955, 27 November 1954; 4058,
1 May 1955; 4202, 13 March 1956; 4352, 30 July 1956;
4394, 20 December 1956; 4458, 17 January 1958,
"Sensitivity of Explosives to Impact."

(3) H. D. Mallory, NavOrd Report (NOL) 4236, "The Develop-
ment of Impact Sensitivity Tests at the Explosives
Research Laboratory, Bruceton, Pennsylvania, During
the Years 1941-1945," 16 March 1956.

(4) Discussed in greater detail in the following
references: (a) M. J. Kamlet, NavOrd Report (NOL)
6206, "Compounds Containing the Terminal Fluorodini-
tromethyl Group, I. Theoretical Background,"
23 January 1959; (b) Idem., NavOrd Report (NOL) 6207,
"Compounds Containing the Terminal Fluorodinitromethyl
Group, II. A New Class of High Explosives,"
2 February 1959.

(5) J. C. Dacons, M. J. Kamlet and D. V. Sickman,
NavOrd Report (NOL) 6831, "Thermal Decomposition of
TNT," 1 May 1960.

(6) J. C. Dacons, NavOrd Report (NOL) 6904, "Heat
Resistant Explosives, VIII. 2,2',4,4',6,6'-
Hexanitrobiphenyl (HNB) and 2,2',2",4,4',4",6,6',6"-
Nonanitroterphenyl," 15 June 1960.

A STATISTICAL CORRELATION OF IMPACT SENSITIVITY
WITH OXYGEN BALANCE FOR SECONDARY EXPLOSIVES

By

Jack Alster

Picatinny Arsenal
Dover, New Jersey

Introduction

In a compilation of the impact sensitivities of a variety of primary and secondary explosives, Arthur D. Little, Inc. (1) noted an apparent correlation of the Figure of Insensitiveness (which is a measure of impact sensitivity) with oxygen balance. The "correlation" was not subjected to a statistical test nor was its theoretical justification explored. More recently, with Bowden's and Yoffe's (2) hot spot theory of impact initiation as a basis, Wenograd (3) demonstrated the existence of a correlation between the impact sensitivities of secondary CHNO explosives and their extrapolated rates of thermal decomposition at 500°C. Having attributed the thermal decomposition rate to ease of breaking of the weakest bond in a molecule, Kamlet (4) reasoned that for groups of structurally related explosives containing the weak C-nitro or N-nitro bonds one should find a relationship between the rate of decomposition and oxygen balance. (The latter is obviously a function of the number of C-nitro and N-nitro bonds in the molecule.) Consequently, impact sensitivity, too, should correlate with oxygen balance.

Kamlet's investigation of some eighty-four explosive compounds has, in fact, substantiated this notion; in particular, the logarithmic impact heights corresponding to 50% probability of explosion were found to vary in an inverse linear manner with increasing oxidant balance, where the latter is defined as the number of equivalents of oxidant per 100 gms of compound above the amount necessary to burn all hydrogen to water and all carbon to carbon monoxide.

Since some of the ramifications (4) of these and related findings are reportedly of great consequence to the military, it was deemed desirable 1) to search for a similar correlation among an independent set of impact sensitivity data and 2) to test the extent of the correlation, if any.

Comparison of Impact Tests

The data which will be analyzed in this report consist of the British Figures of Insensitiveness (FI) which are compiled in the aforementioned Reference 1 and are also available in the convenient form of IBM punched cards (5)[*]. The FI Index is defined as the relative area under the per cent gas evolved versus impact height curve based on picric acid as the standard. It is determined by means of the Rotter impact machine (7) in which a brass cap containing a known volume of explosive is acted upon by a falling weight and the extent of the ensuing evolution of gas is taken as a measure of explosion probability. Four repeat runs at each of five or six drop heights generally constitute the raw data for each explosive whence the FI value is obtained.

The data which served as a basis for the analyses of Wenograd and Kamlet, however, were obtained by means of the ERL impact machine (8) employing Type 12 tools on sandpaper. Here the sample is, relatively speaking, unconfined and the occurrence of an explosion is registered on a noise meter (9). Generally, 50 trials are carried out near the 50% explosion height in accordance with the AMP "up and down" method (10).

Owing to the relatively low statistical uncertainty surrounding the 50% explosion height and the greater number of trials employed, the AMP test procedure is, no doubt, capable of yielding more reliable relative impact sensitivities than the British procedure (11). Accordingly, British investigators (12) have in recent years largely abandoned their traditional test procedure in favor of the "up and down" method, while still retaining the basic features of the Rotter machine. The newer results are, however, quite limited in quantity. Thus, in order to provide the ensuing correlation study with the broadest possible base, it was decided to exploit the older, more complete set of FI data.

Oxygen Balances

Two types of oxygen balances are considered as correlation parameters in the present study.

One is the familiar weight per cent oxygen balance to CO_2 and H_2O which is a measure of the relative weight of oxygen in deficiency or excess of what is required to burn all carbon to carbon dioxide and all hydrogen to water. For CHNO compounds the applicable equation is

$$OB = \frac{100 \left(N_O - \frac{N_H}{2} - 2N_C \right)}{\frac{MW}{16}} = \frac{100 \ MOB}{\frac{MW}{16}} \quad (1)$$

[*]Footnote: A catalog (6) which has been prepared from the card file also contains all the data reported here but in less convenient form.

where N_O, N_H and N_C are the number of atoms of oxygen, hydrogen and carbon, respectively, in the molecule, $\frac{MW}{16}$ is the ratio of the molecular weight to the atomic weight of oxygen and MOB is the molar oxygen balance to CO_2 and H_2O. It should be noted that the main difference between Equation 1 and Kamlet's expression for oxidant balance resides in the difference between the CO and CO_2 reference levels of combustion. In essence, however, they measure the same quantity which is the relative amount of oxygen in the explosive.

Another expression for oxygen balance has recently been introduced by Martin and Yallop (13) for the purpose of differentiating among oxygen atoms which, on the one hand, are either completely or only partially available for combustion of the fuel elements to CO_2 and H_2O and, on the other hand, are altogether unavailable. Thus oxygen atoms attached to a nitrogen which is loosely linked with either a carbon or another nitrogen as in the plosophoric* nitro and nitramine groups, respectively, are completely available for combustion; oxygens which link the nitrate group to a carbon atom are only partially available for further combustion; finally, oxygens which occur in the auxoplosive* keto, carboxyl, hydroxyl or ether groups are essentially unavailable. For CHNO explosives this modified oxygen balance takes the form

$$OB^1 = \frac{100\ (MOB - w)}{n} \qquad (2)$$

where n is the number of atoms in the molecule and w** is a factor which corrects for the extent of "non-availability" of certain oxygen atoms. In particular, the values*** of w employed in the calculation

---

*Footnote: For a definition of the terms primary plosophoric and secondary plosophoric and auxoplosive see Reference 1.

**Footnote: In Martin's and Yallop's paper w is preceded by $\pm$ which signifies that when MOB is positive w is positive and when MOB is negative w is negative. Presumably, the authors anticipated that the "trend" of increasing detonation velocity with increasing oxygen balance would reverse itself at a negative oxygen balance near zero owing perhaps to an increasing degree of disassociation of CO_2 and H_2O followed by dilution of the detonation energy by the presence of excess oxygen.

In the present study, however, one would expect impact sensitivity to increase monotonically with increasing oxygen balance so long as the oxygen is carried by plosophoric as contrasted with auxoplosive groups. The effect of auxoplosive oxygen should, as a result, always be subtracted in Equation 2.

***Footnote:
These values are taken directly from Reference 13.

of OB^1 in this paper are the following:

Nature of Oxygen Linkage		w
O	(N = O)	O
O	(C-O-N)	1
O	(C = O)	1.8
O	(C-O-H)	2.2

Besides the appearance of w in the expression for OB^1, a second feature which differentiates between OB and OB^1 is that the former is a weight ratio whereas the latter is an atom ratio. It will be later shown, however, that this does not materially affect the correlation with FI.

From Kamlet's investigation, one infers that impact sensitivity increases with oxygen balance provided the oxygen is associated with weak linkages as, for example, the C-nitro and C-nitramine bonds. The more firmly bound auxoplosive groups bearing oxygen, however, cannot be expected to contribute to the impact sensitivity of the parent compound. Thus, OB^1 should be superior to OB as a correlation parameter. As a result, an attempt is made to ascertain whether this is borne out by the data.

Criteria for Selection of Compounds

Compounds were selected in accordance with the following criteria:

a. They must be -

(1) CHNO secondary explosives containing the primary plosophoric groups, nitro and nitramine, (compounds containing, for example, the primary plosophoric nitrate group or the secondary plosophoric groups - azide, diazo, peroxide, acetylenic, etc. were excluded from this study).

(2) Solids at room temperature

b. They must not be -

(1) Organic or inorganic salts.

(2) Polymeric substances.

Results

Forty-eight compounds were found to satisfy the above requirements. In Figures 1 and 2 FI is plotted versus OB and OB^1, respectively. Each symbol represents a compound in one of five conveniently chosen structure classifications; viz, aromatic nitro $\triangle$, aliphatic nitro O, open chain nitramine $\square$, nitramine containing

FIGURE OF INSENSITIVENESS
VS
CONVENTIONAL OXYGEN BALANCE
(OB)

FIG. 1
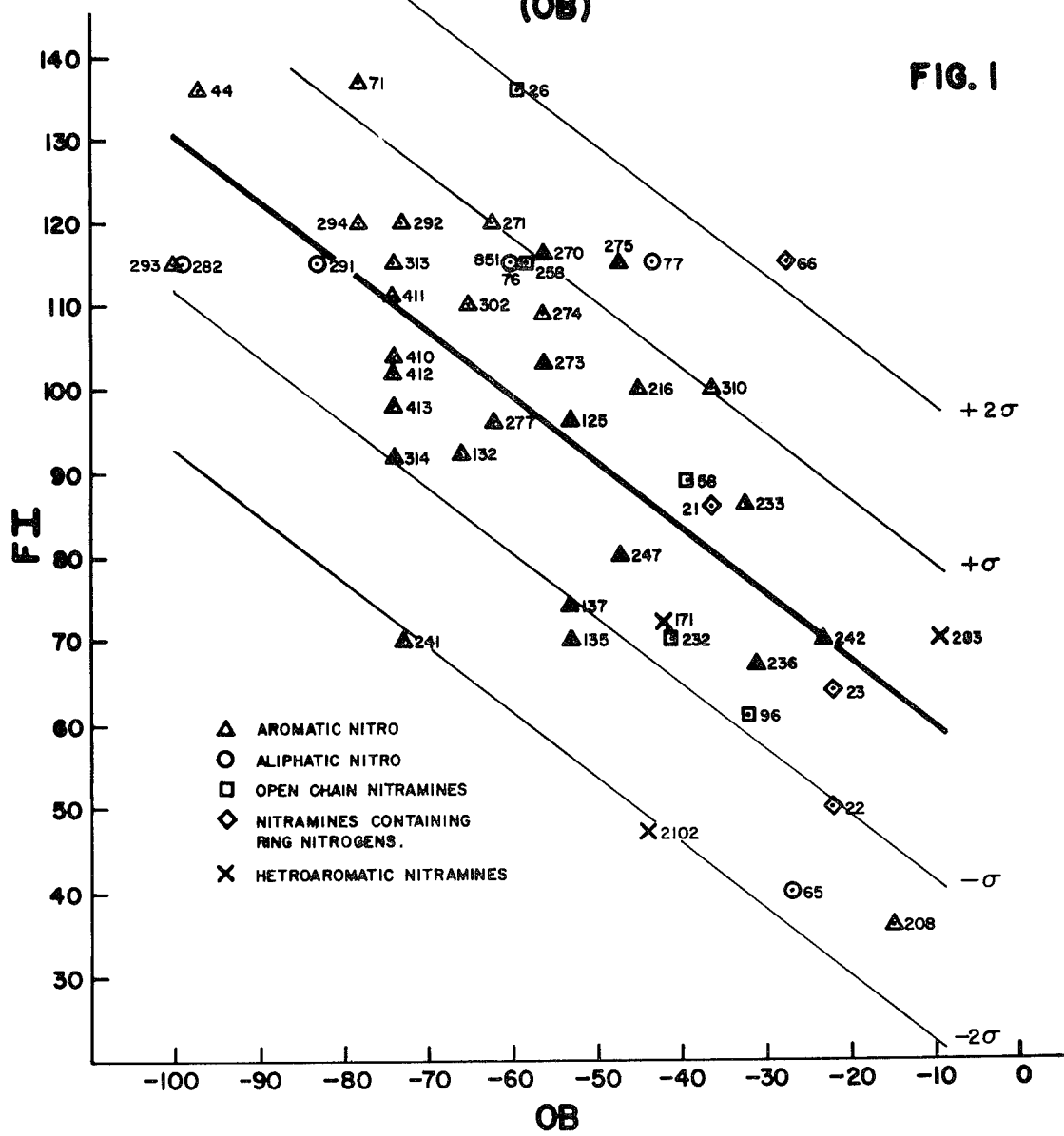
FIGURE OF INSENSITIVENESS
VS
MODIFIED OXYGEN BALANCE
(OB')

FIG. 2
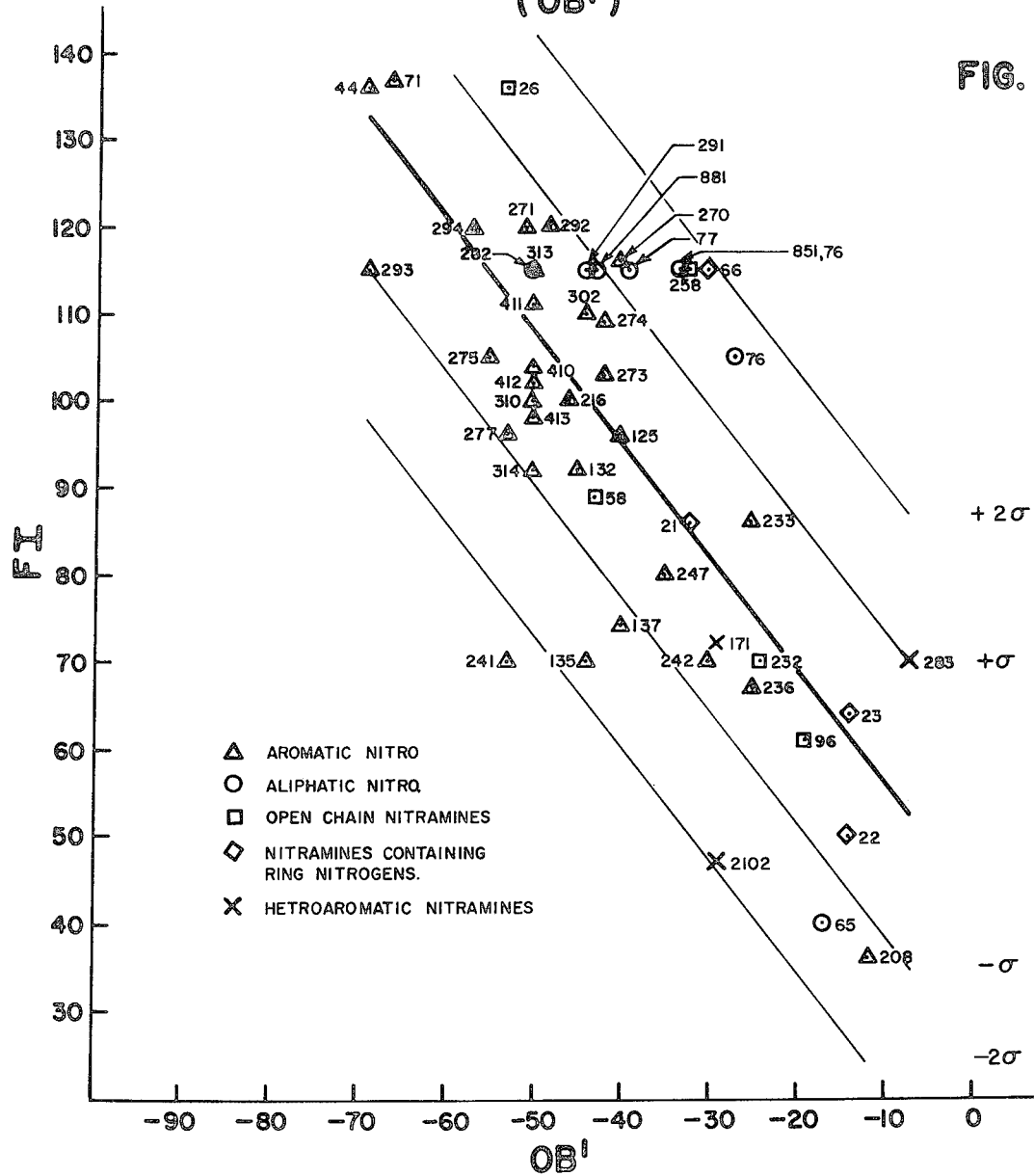
TABLE I

FIGURES OF INSENSITIVENESS AND FUNDAMENTAL DATA OF SELECTED EXPLOSIVES

Code Serial Nr	Compound Name	Elem. Comp.				OB	OB¹	FI
		C	H	N	O			
	1. Open Chain Nitramines □							
* 26	1,7 Diacetoxy tetramethylene - 2, 4, 6 Trinitramine	8	14	6	10	-59	-53	136
* 58	N,N¹ - Dinitrodimethyloxamide	4	6	4	6	-39	-43	89
96	Ethylenedinitramine	2	6	4	4	-32	-19	61
232	Tetra (nitraminomethyl)methane	5	12	8	8	-41	-24	70
258	Trimethylene - 1,2 - Dinitramine	3	8	4	4	-58	-32	115
	2. Nitramines Containing Ring Nitrogens ◇							
* 21	Cyclonite Oxide	3	6	4	5	-36	-32	86
22	Cyclotetramethylene Tetranitramine	4	8	8	8	-22	-14	50
23	Cyclotrimethylene Trinitramine	3	6	6	6	-22	-14	64
* 66	N,N¹ - Dinitroethylene Urea	3	4	4	5	-27	-30	115
	3. Heteroaromatic Nitramines X							
171	5 - Nitramine 1,2,4 - Triazole	2	3	5	2	-42	-29	72
283	Trinitromelamine	3	3	9	6	- 9	-7	70
2102	Diaminonitro 1,2,4 H Triazole	2	4	6	2	-44	-29	47

TABLE I (cont)

Code Serial Nr	Compound Name	Elem. Comp.				OB	OB[1]	FI
		C	H	N	O			
	4. Aliphatic Nitro Compounds ○							
65	1,1 Dinitroethane	2	4	2	4	− 27	−17	40
76	1,1 Dinitropropane	3	6	2	4	− 60	− 33	115
*77	2,2 Dinitro − 1 − propanol	3	6	2	5	− 43	− 39	115
282	2,2,3 Trinitro − 3 − ethylpentane	7	13	3	6	− 99	− 50	115
291	2,2,3 Trinitro − 3 − methylpentane	6	11	3	6	− 83	− 44	115
851	Dinitropropane	3	6	2	4	− 60	− 33	115
	5. Aromatic Nitro Compounds △							
*44	2,4 Dinitroanisole	7	6	2	5	− 97	− 69	136
*71	2,4 Dinitrophenol	6	4	2	5	− 78	− 66	137
125	2,2,4,4,6,6 Hexanitrodiphenylamine	12	5	7	12	− 53	− 40	96
132	N Methyl 2,2,4,4,6,6 Hexanitrodiphenylamine	13	7	7	12	− 66	− 45	92
*135	Hexanitrodiphenyl urea	13	6	8	13	− 53	− 44	70
137	2,2,4,4,6,6 Hexanitrohydrazobenzene	12	6	8	12	− 53	− 40	74
208	Pentanitroaniline	6	2	6	10	− 15	− 12	36
*216	Picric Acid (PA)	6	3	3	7	− 45	− 46	100
233	2,3,4,6 Tetranitroaniline	6	3	5	8	− 32	− 25	86
236	1,2,3,5 Tetranitrobenzene	6	2	4	8	− 31	− 25	67
241	1,3,6,8 Tetranitronaphthalene	10	4	4	8	− 73	−53	70

TABLE I (cont)

Code Serial Nr	Compound Name	Elem. Comp.				OB	OB[1]	FI
		C	H	N	O			
* 242	2,3,4,6 Tetranitrophenol	6	2	4	9	− 23	− 30	70
247	2,3,4,6 Tetranitrotoluene	7	4	4	8	− 47	− 35	80
270	2,4,6 Trinitroaniline	6	4	4	6	− 56	− 40	116
* 271	2,4,6 Trinitroanisole	7	5	3	7	− 63	− 51	120
273	1,2,4 Trinitrobenzene	6	3	3	6	− 56	− 42	103
* 274	1,3,5 Trinitrobenzene	6	3	3	6	− 56	− 42	109
* 275	2,4,6 Trinitrobenzoic Acid	7	3	3	8	− 47	− 55	115
277	2,4,6 Trinitro-m-cresol	7	5	3	7	− 62	− 53	96
292	2,4,6 Trinitromonomethylaniline	7	6	4	6	− 73	− 48	120
293	1,3,8 Trinitronaphthalene	10	5	3	6	−100	− 69	115
* 294	2,4,6 Trinitrophenetole	8	7	3	7	− 78	− 57	120
302	2,4,6 Trinitrophenylguanidine	7	6	6	6	− 65	− 44	110
* 310	2,4,6 Trinitroresorcinol	6	3	3	8	− 36	− 50	100
313	2,4,6 Trinitrotoluene	7	5	3	6	− 74	− 50	115
314	2,3,4 Trinitrotoluene	7	5	3	6	− 74	− 50	92
410	2,3,5 Trinitrotoluene	7	5	3	6	− 74	− 50	104
411	2,3,6 Trinitrotoluene	7	5	3	6	− 74	− 50	111
412	2,4,5 Trinitrotoluene	7	5	3	6	− 74	− 50	102
413	3,4,5 Trinitrotoluene	7	5	3	6	− 74	− 50	98

ring nitrogens ◇ and heteroaromatic nitramine X . The number
adjacent to each symbol is a code designation of the compound which
is identical with that found in References 1, 5 and 6, whence the
data were extracted. Table 1 enables one to identify the compound
names corresponding to their code serial numbers, the latter being
listed in Table 1 in numerical sequence under the appropriate struc-
ture classification.

In view of the considerable spread of the points in both
Figures 1 and 2, a simple linear correlation was assumed to a first
approximation between both FI and OB and FI and OB^1. A least-squares
treatment was then applied to the points. This yielded the following
analytical expressions for the lines representing the points in
Figures 1 and 2, respectively:

$$F.I. (\angle 38) = 52 - 0.79 \ OB \qquad (3)$$

and
$$for \quad -100 \leq OB \leq -9$$

$$F.I. (\angle 35) = 43 - 1.3 \ OB^1 \qquad (4)$$

$$for \quad -69 \leq OB^1 \leq -7$$

The parenthetic number in each of the above equations repre-
sents a value which is twice the (adjusted) standard deviation of the
differences between the actual FI corresponding to a given OB or OB^1
and the estimated FI. This value which is known to statisticians as
2x the standard error of estimate (i.e. 2 σ) implies that at least
95% of all the points should fall within two lines drawn above and be-
low the lines represented by Equations 3 and 4 of vertical distances
38 and 35 units from it, respectively (see Figures 1 and 2). Further-
more, these equations must not be extrapolated beyond the indicated
ranges of validity of the independent variable.

Of particular importance is the (adjusted) correlation co-
efficient which has been determined for each of the above graphs.
This coefficient (12) measures the proportion of the variation in FI
which is associated with the independent variable. It may vary between
0 and 1, 0 representing no correlation and 1 perfect correlation. The
particular (adjusted) correlation coefficients for the data in Figures
1 and 2 are 0.67 and 0.74, respectively. Application of Fisher's
statistical techniques (15, 16) to these values indicates that corre-
sponding to 95% confidence, 1) a correlation exists between FI and OB
to the extent that at least 27% of the variance in FI can be associ-
ated with OB, 2) a correlation exists between FI and OB^1 to the extent
that at least 37% of the variance in FI can be associated with OB^1,
and 3) while OB^1 gives a somewhat better correlation than OB there is
insufficient evidence to indicate that this improvement is significant.

It should be noted that of the forty-eight explosives in-
cluded in this study only fifteen contained oxygen-bearing auxoplosive
groups such as ether, hydroxyl, carboxyl, keto, etc. These are label-
led in Table 1 by means of an asterisk. The remaining thirty-three

compounds carry oxygen only in the form of the plosophoric nitro or nitramine groups. The correction factor w for these explosives is therefore zero. Thus, OB^1 differs from OB only in the change of the denominator in Equations 1 and 2 from $\frac{MW}{16}$ to n. In view of the insignificantly small increase in correlation coefficient associated with the conversion $OB \rightarrow OB^1$ it was thought that perhaps some of the efficiency of OB^1 was lost due to the change in denominator from $\frac{MW}{16}$ to n. Accordingly, the data of the thirty-three pure plosophores were analyzed, as before, using both OB and OB^1 as independent variables. A decrease in correlation coefficient from .76 corresponding to OB to .71 corresponding to OB^1 was indeed observed; however, no significance can be attached to this small difference. This, therefore, confirms the previous conclusion that, insofar as the present study is concerned, both OB and OB^1 are equally well suited as correlation parameters.

Discussion of Results

The principal outcome of the present investigation is that the figures of insensitiveness of solid, secondary CHNO explosives in the nitro and nitramine category can be correlated with oxygen balance. That this correlation is unambiguously established (by statistical means) is, in a sense, surprising when one considers that many factors other than oxygen balance could conceivably affect relative impact sensitivity. To name but a few, consider such factors as the variation in over-all physical and surface condition among samples of the same or different explosives, uncontrollable variations in environmental conditions and, above all, the variation in chemical structure among explosives of identical or nearly identical oxygen balance. It is highly improbable that we are dealing with a fortuitous phenomenon, particularly since Kamlet has already demonstrated the existence of a correlation between impact sensitivity and oxygen balance on the basis of an entirely different set of data. Moreover, as was discussed earlier, the basic hypothesis is not without some theoretical justification. The results, therefore, strongly suggest that oxygen balance is certainly an important factor, among undoubtedly others, affecting the relative impact sensitivity of an explosive.

Figures 1 and 2 reveal at a glance that, contrary to Kamlet's findings, the nitro and nitramine compounds do not distribute about separate regression lines. Presumably, the resolving power of the figure of insensitiveness is impaired by the error surrounding its determination which is undoubtedly greater than that of the 50% explosion height. By the same token, the failure of OB^1 to perform significantly better as a correlation parameter than OB might be similarly explained. The situation naturally demands that as the new British impact data become available in sufficient quantity they be subjected to the same analysis as carried out here on the older British data.

Acknowledgments

The author wishes to acknowledge the assisstance of Mr. J. N. Nielsen of Picatinny Arsenal in programming the stastical computations on the IBM 650 computer. The author is likewise indebted to Dr. W. Hess of Picatinny for his reading of the manuscript.

References

1. A. D. Little, Inc, "Report on Study of Pure Explosive Compounds" to OCO - Contract Nr W-19-020-ORD-6435, Pt I. p. 166, 2 January 1947 (Confidential).

2. F. P. Bowden and A. D. Yoffe, "Initiation and Growth of Explosion in Liquids and Solids" - University Press, Cambridge, 1952.

3. J. Wenograd, "The Correlation of the Impact Sensitivity of Organic Explosives with Their Thermal Decomposition Rates" - NAVORD 5730, 30 September 1957 (Confidential).

4. M. J. Kamlet, "A Correlation of Impact Sensitivities of Explosives with Oxidant Balances" - NAVORD 6126, 26 September 1958 (Confidential).

5. A. D. Little, Inc., "Explosives IBM Punched Card File" - housed at Picatinny Arsenal, Dover, N. J. and A. D. Little, Inc., Cambridge, Mass., April 1958 (Confidential).

6. A. D. Little, Inc., "Explosives IBM Punched Card Catalog" - includes latest supplement dated April 1958. (Confidential).

7. "Summary of Experimental Methods for the Determination of Explosive Constants", Advisory Council (of Gr. Britain) - Report Nr 294, 6 August 1940 (Secret).

8. D.P. MacDougall, E. H. Eyster, and R. F. Davis, "Progress Report on Physical Testing of Explosives. Pt II - Sensitivity Studies with the Drop-Weight Impact Machine" - OSRD 5744, 27 December 1945.

9. E. H. Eyster and L. C. Smith, "Studies of the ERL Type 12 Drop-Weight Impact Machine at NOL" - NOLM 10,003, 25 January 1949.

10. "Statistical Analysis for a New Procedure in Sensitivity Experiments" - AMP Report Nr 101, IR.

11. P.W.J. Moore and R. Pape, "The Significance of the Figure of Insensitiveness Obtained from Impact Tests on the Rotter Machine" - British Ministry of Supply - E.R.D.E. 14/M/54, June 1954.

12. J. Wilby, "Impact Sensitiveness of Explosives. Pt I Measurements Made During 1957" - ARDE Memorandum (MX) 41/58, August 1958 (Confidential).

13. A. R. Martin and H.J. Yallop, "Some Aspects of Detonation" Pt 1 "Detonation velocity Velocity and Chemical Constitution" - Trans. Far. Soc. 54, February 1958.

14. M. Ezekiel, "Methods of Correlation Analysis" - John Wiley & Sons, Incorporated, New York, N. Y., Second Edition, July 1953.

15. Ibid, Figure B Appendix 3.

16. R. A. Fisher, "Statistical Methods for Research Workers" - Eleventh Edition, Oliver & Boyd, London, 1950.

THE ELECTRIC-SPARK INITIATION OF MIXTURES OF
HIGH EXPLOSIVES AND POWDERED ELECTRICAL CONDUCTORS

T. P. Liddiard, Jr. and B. E. Drimmer
U. S. Naval Ordnance Laboratory
Silver Spring, Maryland

The initiation by an electric spark and the subsequent build-up to detonation in a pure, powdered high explosive, such as PETN or RDX, requires considerable energy, typically amounting to several joules. Little experimental data have been reported on the events occurring within the first 0.1 microsec or so after the establishment of a spark within the explosive powder. Initiation may occur, but this does not necessarily mean that build-up to full detonation will result. The steps leading to such full detonation can be listed in the following order: 1) the initiation of chemical reaction within a localized region; 2) the simultaneous increase in the dimensions of this region, and an increase in the burning rate due primarily to an increase in the local pressure; 3) transition from rapid burning into a low-velocity detonation due to an accumulation of small shocks; and 4) rapid acceleration to high-velocity steady-state detonation.

The minimum spark energy required to produce detonation in high explosives depends on such things as the inherent sensitivity of the explosive to sparks, the circuit parameters, the explosive particle-size distribution, the form, habit and uniformity of the explosive crystals, and finally, the density of loading. As has been found elsewhere with primers made conductive with graphite, we have found that the minimum electric energy needed to produce detonation in high explosives is greatly reduced by adding a few per cent of aluminum powder.

The effects of adding aluminum are, in general, manifested in several ways: a) the spark is established at a lower voltage; b) the spark break-down time for a

706

given voltage is greatly reduced and is more reproducible; c) the threshold voltage for initiation is lowered considerably; and d) the rate of build-up to detonation is increased. Of many additives tested at the Naval Ordnance Laboratory, only a fine-flake aluminum would substantially produce all of the above effects. For a fine RDX powder (20 microns average particle size: all less than 44 microns), 3 per cent aluminum by weight is about optimum for producing these effects. The size and shape of the aluminum particles are important. The aluminum used in these experiments (Alcoa No. 422) was composed of flakes that passed through a 325-mesh screen, about 0.3 micron thick with an average diameter of about 10 microns. Spherical particles of roughly the same mass distribution were significantly less efficient than this flake variety.

We have taken detailed smear-camera photographs of the phenomena occurring during the build-up to detonation in several high-explosive powders, both with and without the addition of aluminum. A typical example is shown in Figure 1. The explosive, RDX/Al(97/3), was completely confined by Plexiglas to the shape of a thin circular wafer, 4 mm thick and 25 mm in diameter. The loading density was 0.8 g/cm^3. (This was the usual loading density, except where the effect of density change was studied. In general, for a given explosive mixture in this experimental arrangement initiation became increasingly difficult as the density increased beyond about half of the theoretical maximum density. As a matter of fact, charges with densities above 1.0 g/cm^3 were not reliably detonated with the circuit conditions described below.) Aluminum-foil electrodes, 0.05 mm thick by 2.5 mm wide with 30 degree taper, typically forming a 0.3 to 0.8-mm gap, were pressed between the explosive and the Plexiglas cover. The slit of the smear camera was aligned through the middle of the spark gap, perpendicular to the line joining the electrode tips, as in Figure 1. For much of the study, the energy to the spark was supplied by a 1.0 mfd capacitor, charged to 5 kv and discharged through a 7.6-meter long 30-ohm coaxial cable (Figure 2). The initial rate of rise of the current (E/L, the capacitor voltage divided by the circuit inductance) was determined to be 2200 amp/microsec. The peak current was 2300 amp, reached in 2.0 microsec.

The instantaneous power and accumulated energy in the spark within the explosive mixture have been determined for the condition used in the example (Figure 3). The resistance of the spark, after the first 0.1 microsec or so, was considered to be fairly constant. (Our measurements were consistent with spark resistance values ranging from 0.15 to 0.20 ohm, or about one-fifth of the
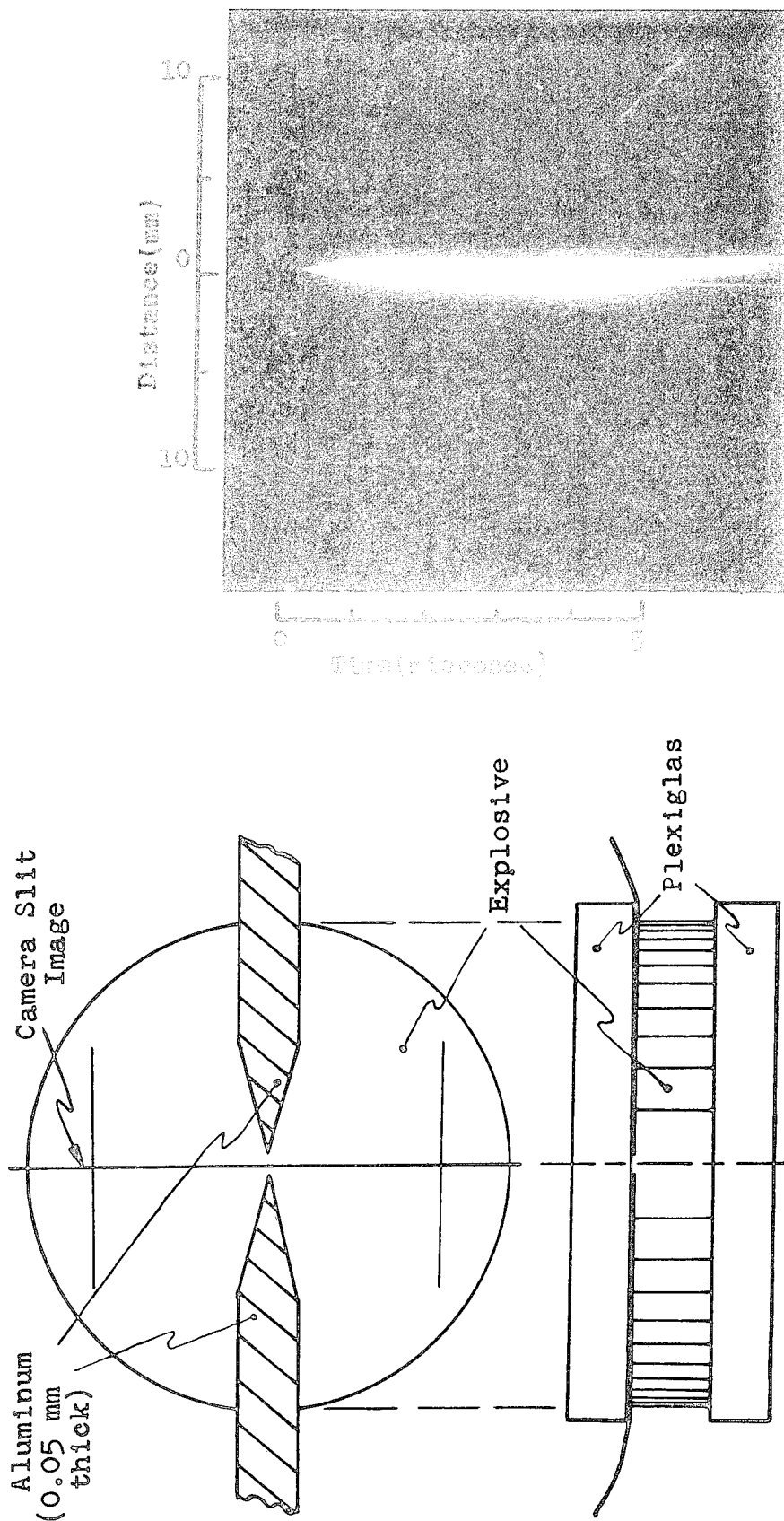
Figure 1. Smear-camera record of build-up to detonation of RDX/Al(97/3) powder having a density of 0.8 g/cm3. The explosive cavity, represented by the circle, was 25 mm in diameter and 4 mm thick. Spark energy supplied by discharge of 1.0 mfd capacitor charged to 5 kv.

708
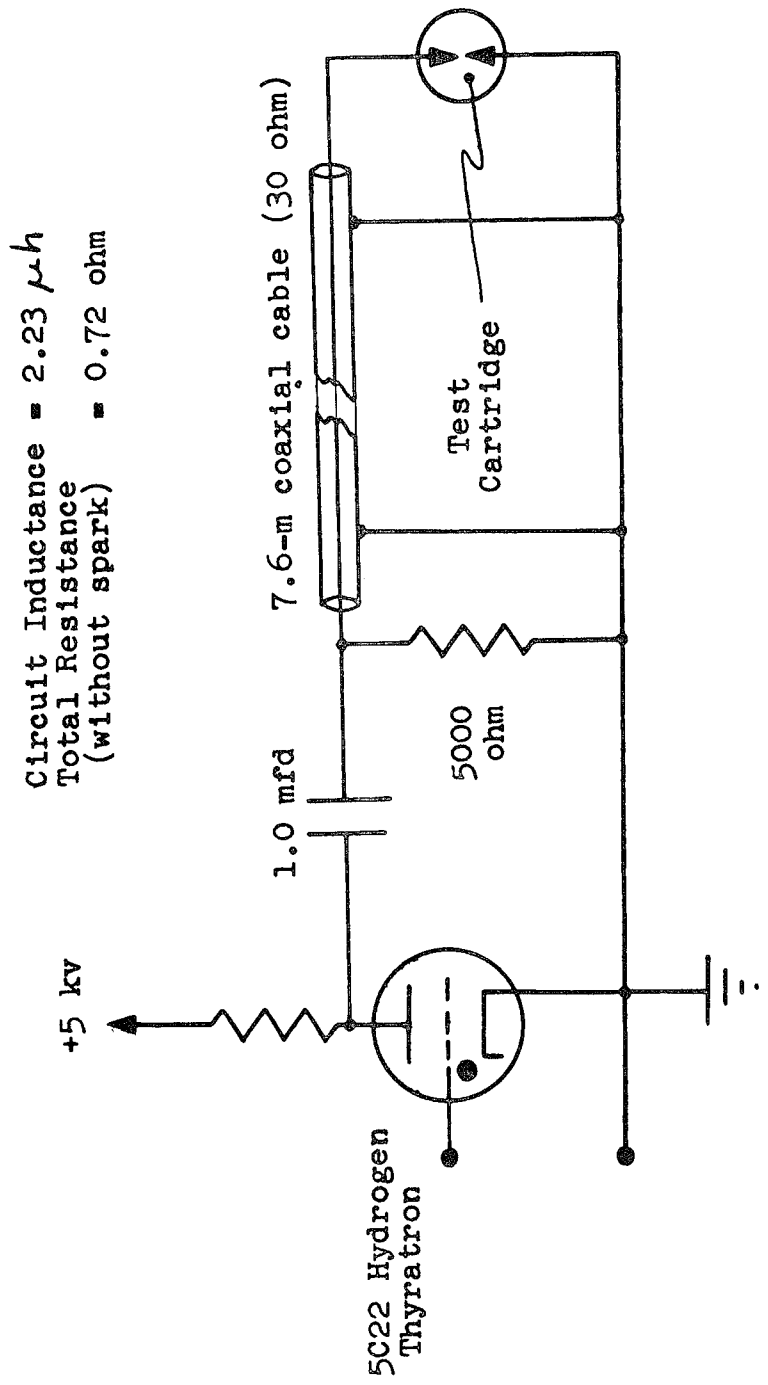
Figure 2. Electrical circuit used in studies of electric-spark initiation of explosive-conductor mixtures.
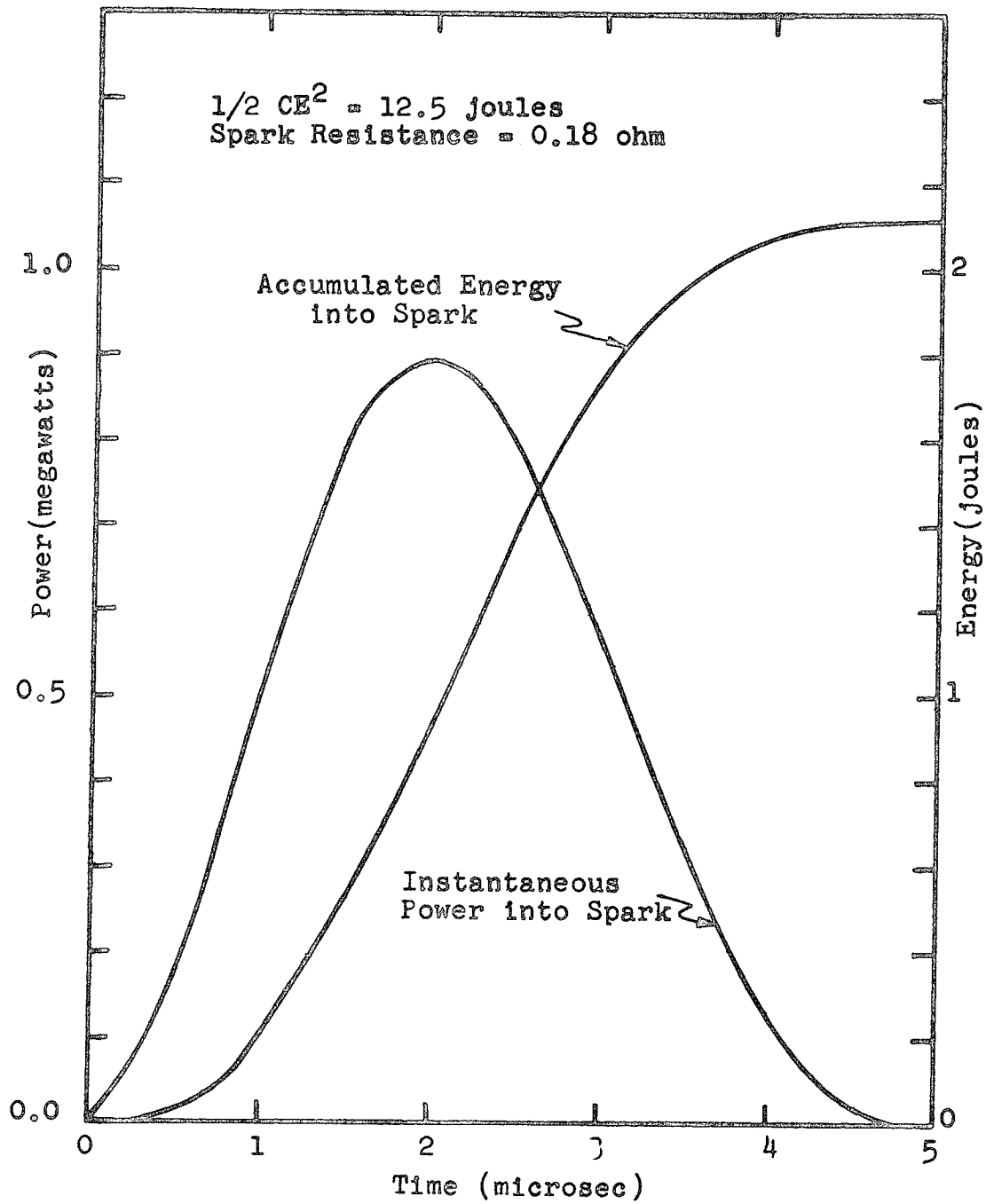
Figure 3. Power and energy of a spark within a typical conductive mix as a function of time.

total circuit resistance.) As a consequence the power
input into the spark (I^2R) follows the general shape of
the current curve. On the other hand, the energy is
absorbed by the spark rather slowly: in one microsecond,
less than 2 per cent of the capacitor energy has been
absorbed, and only some 7 per cent after 2 microseconds.
As will be seen shortly, by the end of 2 microseconds the
chemical energy from the reacting explosive appears to
have taken over as the driving force.

The build-up to detonation (distance-time curve)
for RDX/Al(97/3) is shown in Figure 4. A corresponding
plot for PETN/Al(97/3) is also included. (The explosive
particle size in both cases was less than 44 microns.)
Velocity-distance curves, obtained from slopes of the
curves in Figure 4, are given in Figure 5. Note that the
initial velocity is about 800 m/sec for both mixes; the
build-up of velocity in the RDX/Al powder increases slowly
for a radial distance of about 3.5 mm, and then acceler-
ates rapidly. The PETN/Al(97/3) shows no such region of
gradual acceleration. Instead it begins immediately to
accelerate rapidly. However, similar tests of mixes con-
taining coarser PETN do show such a region of slow accel-
eration. (Possibly the dominant reason for PETN exhibiting
a faster build-up than RDX, for comparable particle size,
is that the PETN crystals have a greater surface area
than the RDX crystals. Not only are PETN crystals rather
elongated, but they also seem to contain large axial
cavities. In contrast, the RDX crystals are nearly spher-
ical and free of observable voids.)

The first wave appearing within the explosive, af-
ter spark break-down, appears to be a weak, essentially
non-luminous shock. This was clearly observed, (Fig-
ure 6) when we placed a strip of aluminized Mylar film
on the outer surface of the Plexiglas, over the region
of the spark. This film served two purposes: 1) it
allowed enough light from the brilliant spark to pass
through, making observable the expansion of the spark
column; 2) it reflected light back to the Plexiglas-
explosive interface, where, on reflection again, it made
observable the presence of a weak shock within the explo-
sive powder. (This shock caused modifications in the
reflectivity of the Plexiglas surface, at the interface,
recorded by the camera: Figure 6.) The weak shock,
originating with the establishment of the spark, appears
to be maintained by that spark, plus, perhaps, by a series
of weak reaction waves. This, in turn, is overtaken by a
much stronger reaction wave. The spark column itself
appears to behave as an expanding cylinder of intensely-
heated "plasma". When detonation fails to develop, the
spark column continues to expand, as shown in Figure 7,
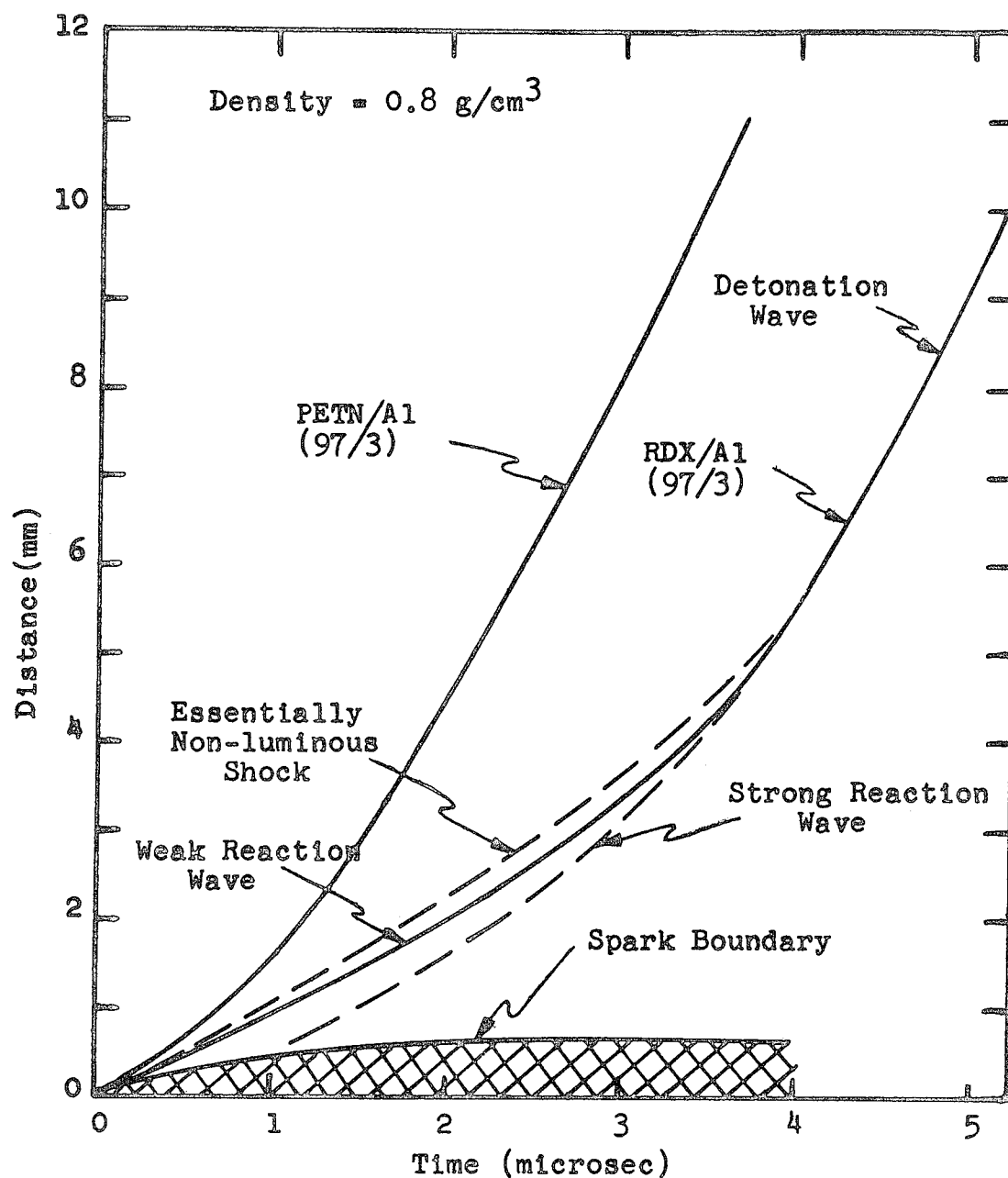
Figure 4. Re-plot of data taken directly from smear-camera photographs, showing the build-up to detonation of RDX/Al(97/3) and PETN/Al(97/3).
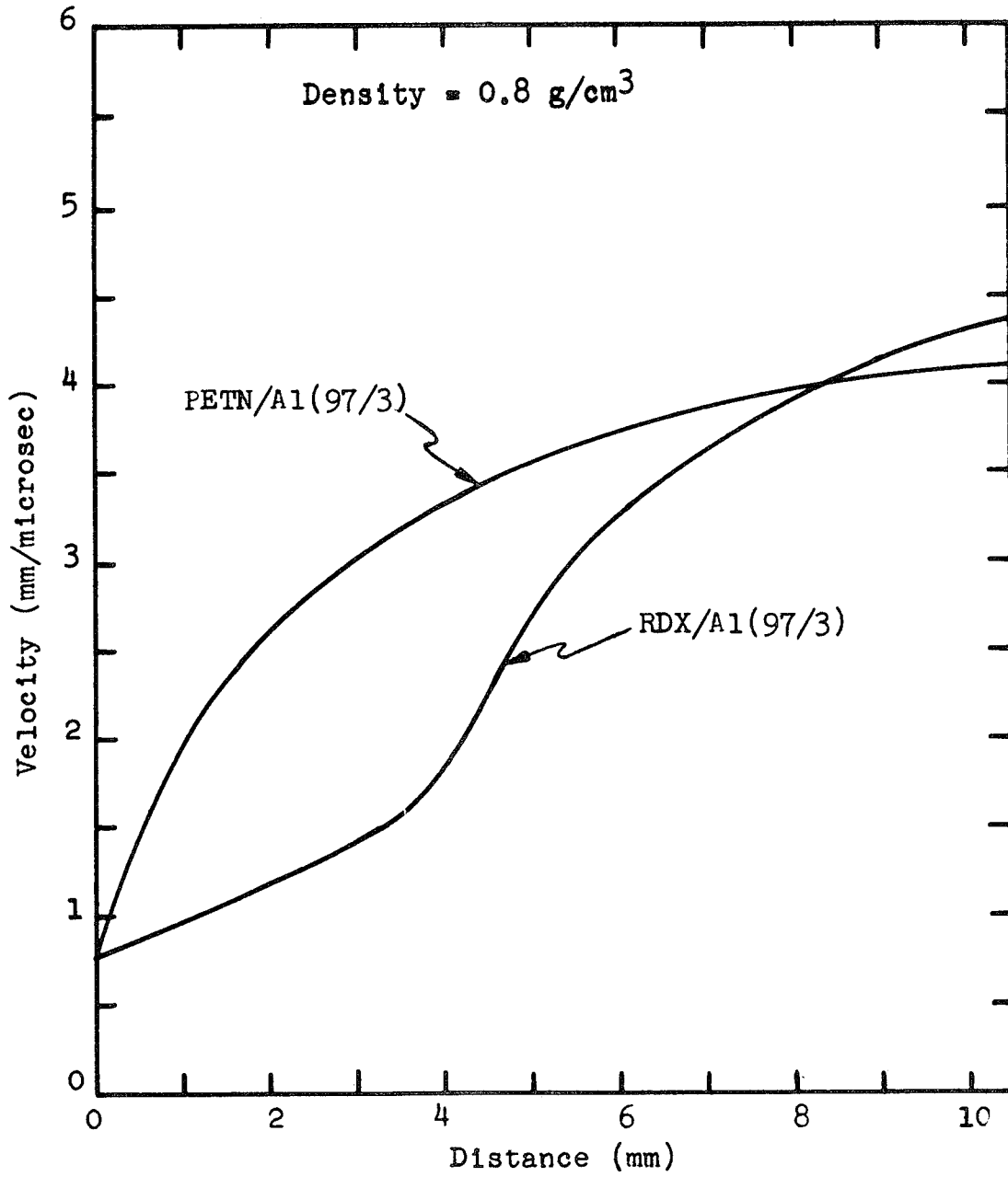
Figure 5. Build-up toward steady-state detonation
velocity.
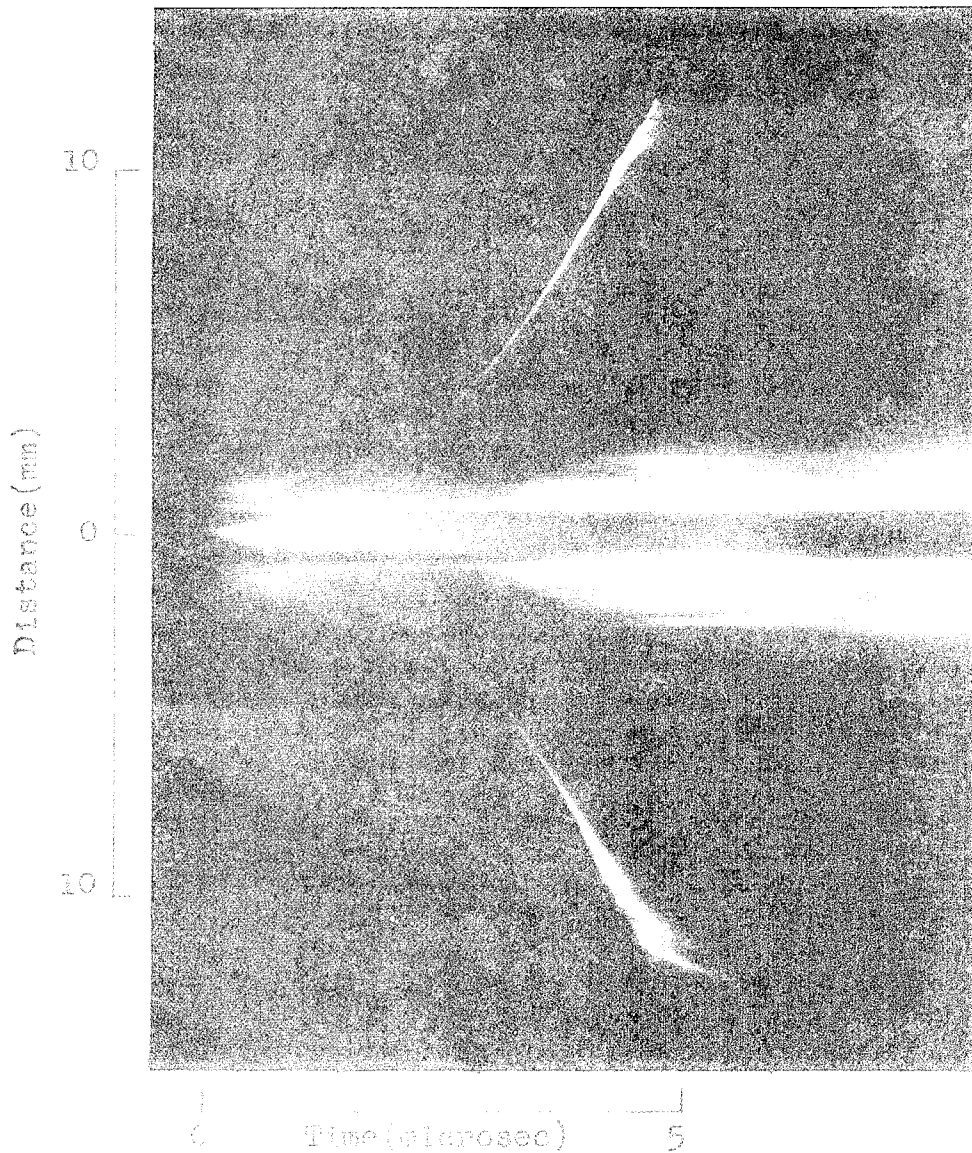
Figure 6. Smear-camera record obtained as in
Figure 1, except that a narrow strip of alumi-
nized Mylar film was placed on exterior of
Plexiglas. (See Figure 4, curve for RDX/Al,
for explanatory diagram.)
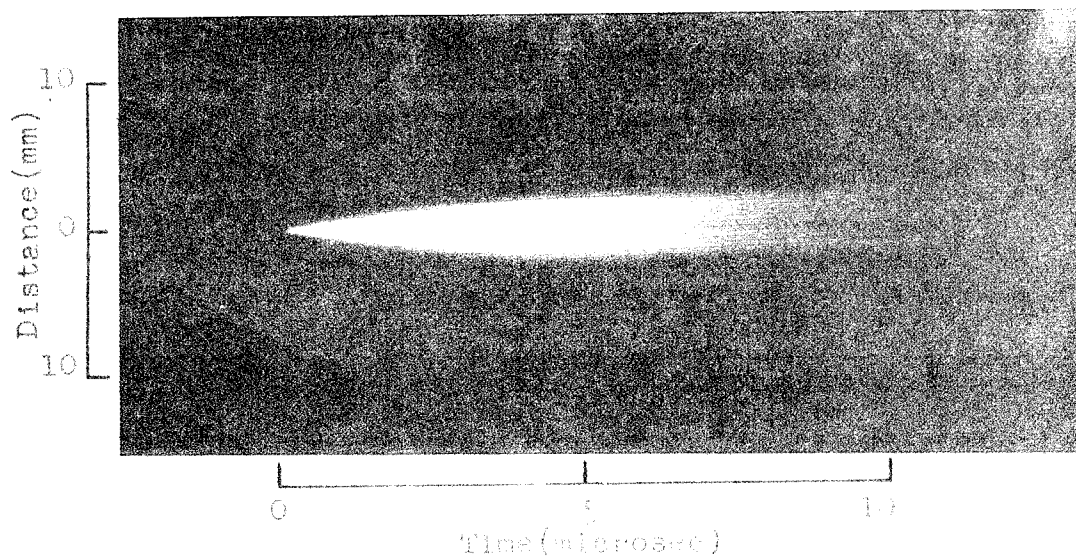
Figure 7. Continued expansion of spark in PETN when no chemical reaction is observed.

in pure PETN. When build-up occurs, as in Figure 8 for PETN/Al(97/3), expansion of the spark is greatly restricted by the pressure generated by the reaction products.

In one series of tests a higher-voltage pulsing-circuit was used to study the effect on the build-up to detonation, of higher rates of energy input to the spark. The energy from this generator (labelled "B", to distinguish it from generator A, described above) was obtained from a 0.1-mfd capacitor, charged to 10 kv. This gave a maximum current of 4900 amp, measured without spark load, reached in 0.29 microsec. The initial rate of rise was 28,600 amp/microsec. (Contrary to the behavior of pulse generator A, which used a uni-directional switch, this one oscillated with resonant frequency, because a spark switch was used.) This circuit (generator B) produced high-order detonation in both pure PETN and in pure RDX, whereas the other circuit (generator A) did not. (This underscores our earlier statement that the minimum energy required to cause detonation is dependent on the circuit parameters: note that the energy stored in the capacitors of generator A (12.5 joules) is greater than that in generator B (10.0 joules)). A comparison is made in Figure 9 of the detonation build-up curves for PETN/Al and for RDX/Al mixtures, using generators A and B. It is seen that a substantial increase in the rate of build-up to detonation is produced by using generator B. Note that PETN still preserves a considerable superiority over RDX in its rate of build-up.

Using generator B, a study was made of the effect of adding fine-flake aluminum to finely-divided RDX and PETN powders (density = 0.8 g/cm^3). The detonation build-up curves are shown in Figure 10. The increase in the rate of build-up over that of the pure explosive is most pronounced in the RDX/Al(97/3) mixture; only a slight increase was obtained in the corresponding PETN/Al mixture.

In summary, the initiation and build-up to detonation of high-explosive powders, such as PETN and RDX, by electric sparks is, in general, enhanced by the addition of a few per cent of fine-flake aluminum. Many factors affect the degree of enhancement. In addition to the factors described above there were a number of variations studied which can only be mentioned in passing: changes in explosive-aluminum ratio; density variations in the range from 0.5 to 1.3 g/cm^3; explosive particle size and shape; aluminum particle size and shape; explosive composition (e.g. tetryl, HMX, DATB); and the electrode configuration. Details of these studies may be found in NAVWEPS Report 6915, now in preparation.
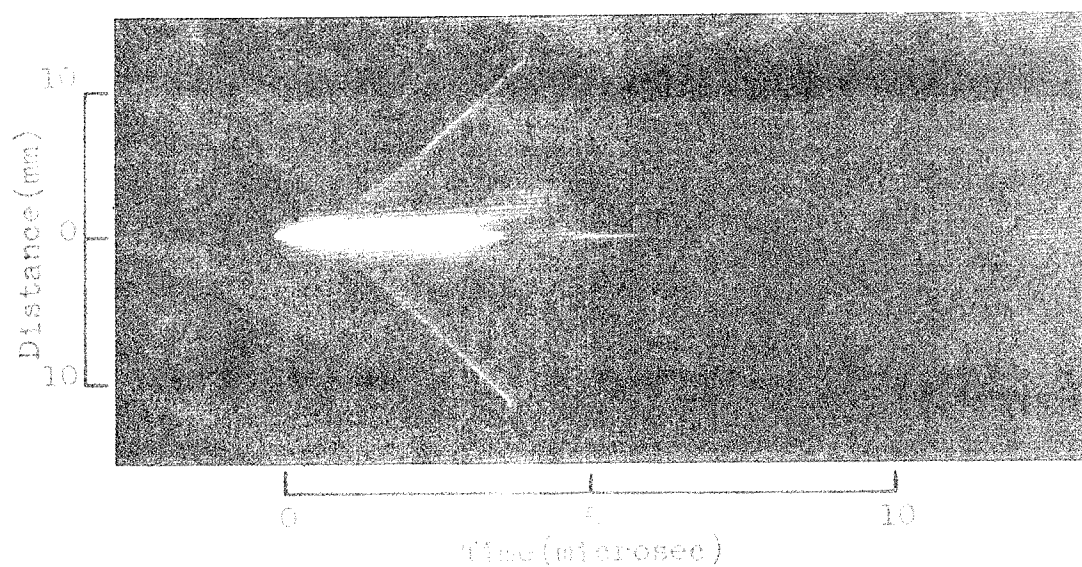
Figure 8. Restricted expansion of spark in PETN/Al
(97/3) when chemical reaction occurs. (For Figures
7 and 8, explosive density was 0.8 g/cm^3; spark
generation with 5 kv, 1 mfd.)
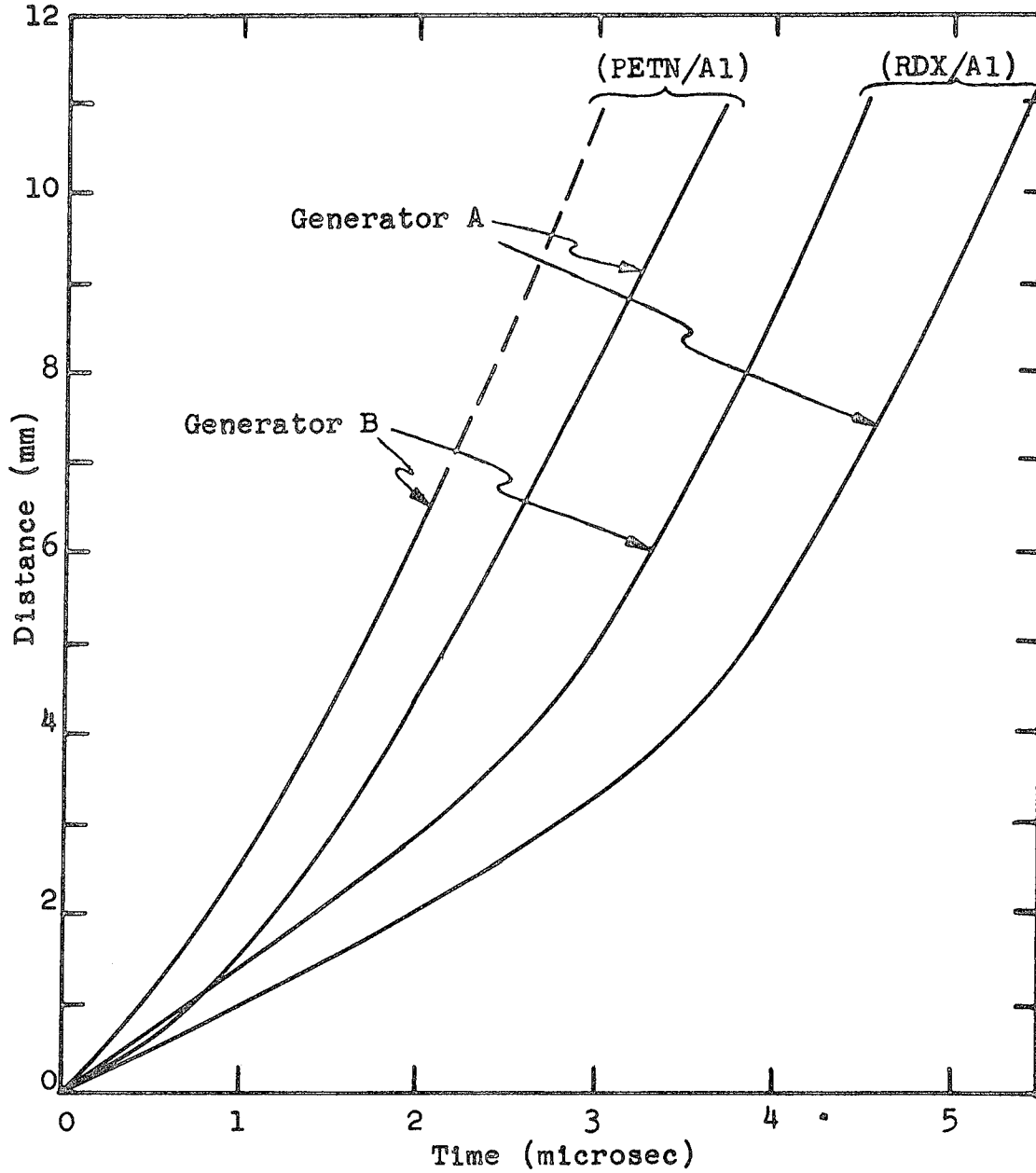
Figure 9. Influence of circuit parameters on detonation build-up. Pulse generator A:5.0 kv, 1.0 mfd, E/L=2200 amp/microsec. Pulse generator B:10.0 kv, 0.1 mfd, E/L=28,600 amp/microsec.
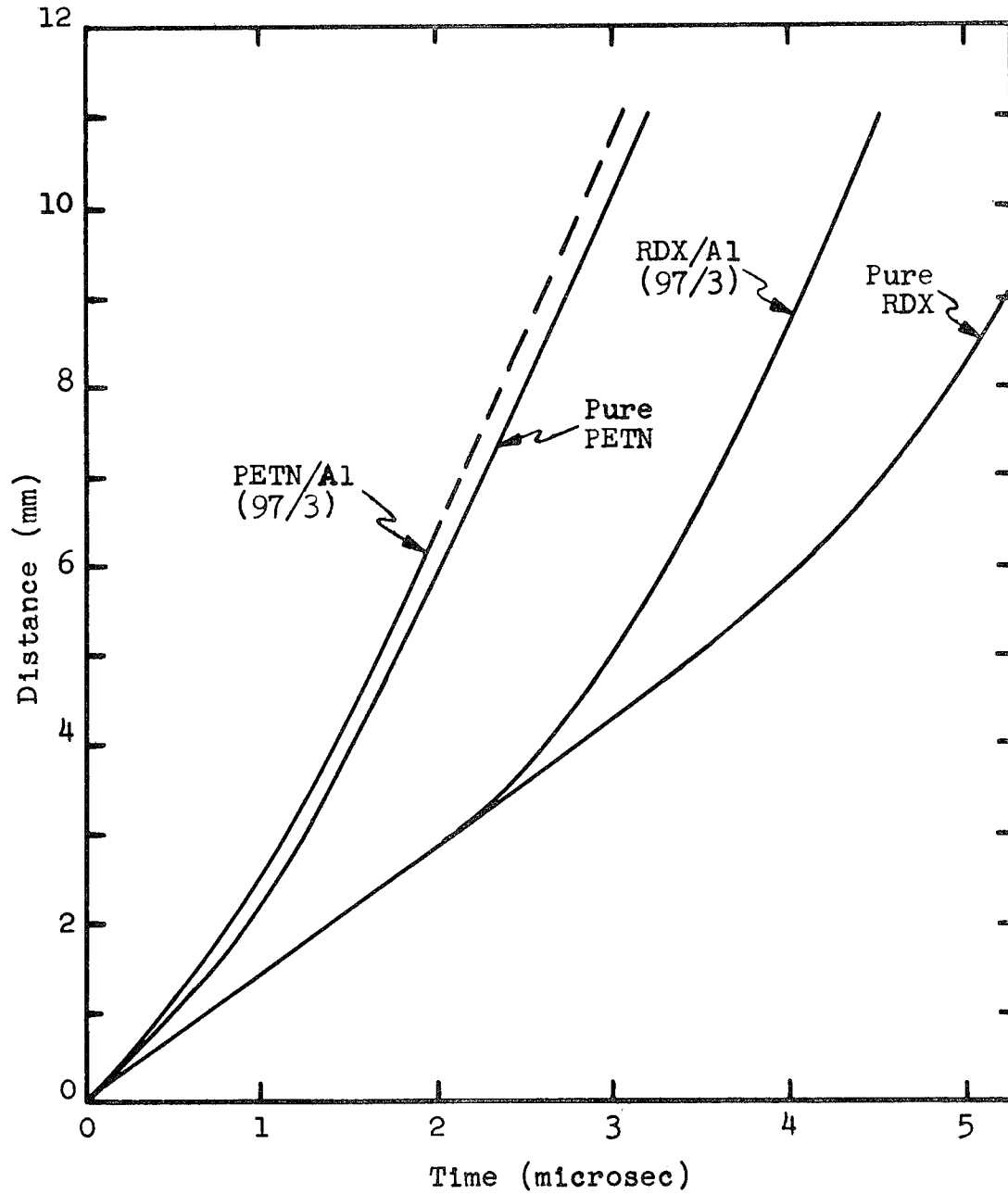
Figure 10. Influence of addition of aluminum on detonation build-up of RDX and PETN, initiated by sparks (generator B).

It is possible that in some of the tests made during this investigation, failure to detonate was due to an absence of the ability to propagate through the porous explosive mass, and not due to a failure to initiate. This report covers some penetration into this region of difficult observation, however, much still remains to be done to explain fully the mechanism of electric spark-initiation and build-up to detonation, especially within the first 0.1 microsec or so after spark formation.

The authors wish to thank James Schneider for his excellent, painstaking execution of most of the experiments cited above. The assistance of James Counihan in preparing many electronic components is gratefully acknowledged. Many stimulating discussions with S. J. Jacobs, M. Solow, A. D. Solem, I. Kabik, H. Leopold, and V. Menichelli of this Laboratory contributed a great deal to the success of this work.

Bibliography

1. NAVORD Report 5746, "Proceedings of the Gilbert B. L. Smith Memorial Conference on Explosive Sensitivity", held at NOL September 16, 17, 1957.

2. Robert DiPersio, "Exploding Wire and Spark Gap Control Initiator for High Explosives", BRL Memorandum Report No. 851, 1954.

3. F. P. Bowden and A. D. Yoffe, "The Initiation and Growth of Explosion in Liquids and Solids", Cambridge University Press, 1952.

4. F. P. Bowden and A. D. Yoffe, "Fast Reactions in Solids", Butterworths Scientific Publications, 1958.

5. Proceedings of the Royal Society, "A Discussion on the Initiation and Growth of Explosion in Solids", (Lead by F. P. Bowden), No. 1245, Vol. 246, July 29, 1958.

6. Beckman Instruments, Inc., Summary Report on Contract NOrd 15894, March 31, 1957 (Confidential).

7. H. Leopold, "Investigation of High Explosive Conductive Powder Mixes for Use in Insensitive Electric Initiators." NAVWEPS Report 6902. (In preparation).

DETONATION AND SHOCKS REVIEW

M. Wilkins
Lawrence Radiation Laboratory
Livermore, California

This paper is intended to review the equations of state and calculation techniques used by the Atomic Energy Commission installations for calculating high explosive detonations. I should like to point out that we are first of all interested in calculating explosively driven plate systems and only include the physics descriptions into the HE that help us correctly describe what is happening inside the plates being driven by the HE. This paper is divided into two parts:

I. HE Equation of State
II. Calculation of Detonations

Most of the forms of the equation of state and the reference to articles that will be discussed are neatly summarized in Dr. Sigmund Jacob's articles in the American Rocket Society Journal of February 1960, so I will not review in detail here.

PART I

A.   For the past few years the Lawrence Radiation Laboratory has used the results of R. Cowan and W. Fickett work on the Kistiakowsky-Wilson equation of state for Comp B and cyclotol. These results have worked quite well in calculating HE driven systems. The least square fit that we made to the Cowan-Fickett data gave an effective gamma around the C-J point of 2.78 for Comp B and 2.85 for cyclotol. The gammas changed to 2.4 and 2.5 respectively at expansions of about 5 from the C-J point. Since the results were very much like the gamma law equation of state, in the 2-dimensional calculations of detonations we used a constant gamma law equation as it took less machine time to calculate. Later, the work of W. E. Deal showed that this was a very good description.

B.   Los Alamos Scientific Laboratory uses in their detonation calculations the constant beta equation derived by W. Fickett and W. W. Wood which uses the experimental results of Deal. The form

looks like this:

$$P = \frac{k_1}{V} + \frac{k_2}{V} \cdot E$$

The adiabats for this equation are the same as those for a gamma law equation.

C. The British use a form somewhat like the Jones form:

$$E = \frac{PV}{\alpha} - A\ P^a \qquad\qquad a = \frac{\gamma - 1}{\gamma}$$

and was developed by H. H. Pike and E. R. Woodcock. This equation also has gamma law adiabats.

D. The French Atomic Energy Commission group working on explosives uses the Paterson equation of state with a correction term for long range molecular forces. The lack of a description for molecular interaction was one of the objections to this form raised by Cowan and Fickett in their paper on the Kistiakowsky-Wilson equation of state.

E. The LASL and British forms give the same adiabats as a gamma law equation however, for the over driven case or when the HE is shocked beyond the C-J point, the adiabats will start from different points and will deliver less energy than a simple gamma law equation. I do not know of any experimental data for over-driven HE that could check the calculated parameters.

In 1-dimensional geometry like the following:

```
                    30 cm   0.5 cm    V_al = 0.515 cm/μsec
detonate →  | cyclotol | Al |              after 15 cm free run
```
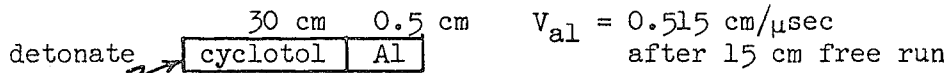
the calculated and experimental value of the velocity agreed to less than 1%. However, the HE volume at the end of the free run has only expanded to about three times its reference volume, so it turns out that as far as calculated 1-dimensional HE plate assemblies are concerned gamma law equations are very good since the accelerations are over before the HE reaches an expansion where the gamma has changed very much from its value at the C-J point. So this is not a good way to examine the equation of state for large expansions.

However, in calculating 2-dimensional detonations where there are strong rarefactions as for example a slab of HE detonating along a piece of metal, the geometry of a lens,

```
detonate →  | HE |
            | Al |
```

one is faced with the problem of calculating the metal acceleration from expanded gases. For some time we have found that for expansion of the order of 3 we must allow the gamma to drop sharply to a low value, like 1.5 in order to correctly calculate the system. (See Figure on page 3) This was also found to be required to correctly calculate a 1-dimensional plate that was accelerated by HE that had expanded into a void before driving the plate.
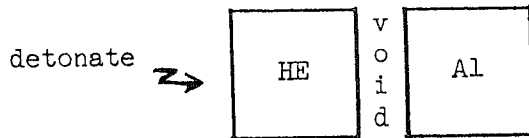
If the HE were in contact with the plate we could correctly calculate its position time history with the equation of state mentioned before. However, the void allows the HE to expand to volumes three to four times the reference volume and the calculations do not agree using a constant gamma equation of state. When an equation of state, with a variable γ was used we were able to get, once again, very close agreement with the experiment.

$$V = \frac{\rho_o}{\rho}$$
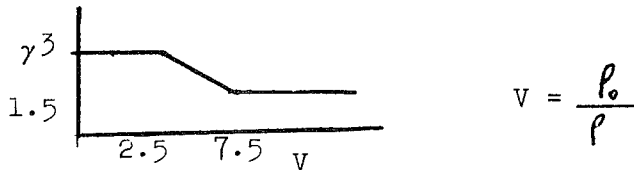
The French are doing some HE work with RDX where the effective γ changes sharply from 3 to about 1.7 at expansions of 3 (Memorial des Poudre 1959, Tome XL1), the reference applies to TNT, however the authors informed me they got similar results with RDX. A reasonable assumption is that more energy is being released in the cooler gases behind the C-J point. This could account for why the experiment and calculation agree when the γ is allowed to change.

PART II

A. The Lawrence Radiation Laboratory uses the "q" method of Von Neumann and Richtmeyer to calculate hydrodynamic problems on the high speed computer. The method is used in 1-dimensional and 2-dimensional hydro problems in both Lagrange and Eulerian coordinates.

To calculate a detonation we introduce a parameter f which multiplies the pressure.

$$\frac{df}{dt} = -\beta \frac{dV}{dt} \qquad\qquad V = \frac{\rho_o}{\rho}$$

in difference form this becomes:

$$f^n = \beta(1-V^n)$$
$$\beta = \frac{1}{1-V_{C-J}}$$

as V goes from $1 \longrightarrow V_{C-J}$

f goes from $0 \longrightarrow 1$ and is set equal to one from then on.

This allows us to get from the unburned state, with the relative volume equal to one and the energy in the material equal to the available chemical energy, to the C-J point.

723
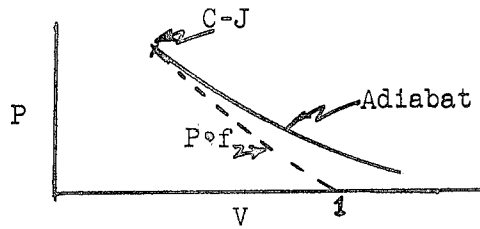
The HE will burn over the same number of zones that the "q" is acting on (about 3-4 zones).

The method also works in the over-driven case.

Several years ago we used the method of characteristics to burn HE, but the burn fraction method is much simpler and can give just as good results.

The burn fraction method also works in Eulerian coordinates. Where:

$$\frac{d(\quad)}{dt} = \frac{\partial(\quad)}{\partial t} + \frac{U\ \partial(\quad)}{\partial x}$$

B.   LASL uses a sharp shock method to burn HE in 1-D. This gives a sharper burn front than the burn fraction method can give.

C.   The British have been using the method of characteristics to solve hydrodynamic problems and burning HE doesn't complicate the problem any more than it already is. They also use the Von Neumann "q" method together with the burn fraction routine.

D.   The French also use the method of characteristics to solve their hydro problems. They are just starting to use the "q" method.

E.   Even though the "q" method has been in the literature for a number of years, people haven't appreciated how well it works for shock hydrodynamics and have tended to adopt the method of characteristics instead. The method of characteristics is inherently more accurate, but it is also very complicated when there are several shocks in a problem.

As yet I do not know of a 2-D characteristic routine that can readily solve time dependent shock hydrodynamic problems. The problem is being worked on in Germany, Switzerland and England.

DETONATION PERFORMANCE CALCULATIONS USING
THE KISTIAKOWSKY-WILSON EQUATION OF STATE*

C. L. Mader
Los Alamos Scientific Laboratory
Los Alamos, New Mexico

ABSTRACT

During the last three years the Kistiakowsky-Wilson
equation of state as modified by Cowan and Fickett has been used to
estimate the detonation performance of explosives composed of various
combinations of the elements carbon, hydrogen, nitrogen, boron, alumi-
num, oxygen, and fluorine. A comparison of the computed performance
with the available detonation velocity, Chapman-Jouget pressure, and
brightness temperature data has been made. Over a wide range of
density and composition the computed and experimental performance have
agreed to within 20%. The KW equation of state suggests an interest-
ing though not thoroughly verified model of the inter-relationships
between temperature, pressure, and the particle density of the CJ
products for explosive systems.

BKW CALCULATIONS

The theoretical estimation of the detonation parameters is
based on the Kistiakowsky-Wilson equation of state as modified by
Cowan and Fickett (9). To make the calculations as unbiased as possi-
ble in predicting the effect of various combinations of elements, the
Cowan and Fickett treatment was taken unchanged as the starting point,
and the new product species were incorporated in it without adding
any adjustable parameters. This was done by using geometrical
covolumes for the new species and the same covolume scaling factor
as was used by Cowan and Fickett for all the products except the
carbon-fluorine products. The 704 code was written, with Fickett's
assistance, so that it would handle mixtures containing up to five
elements and fifteen components, one of which may be solid carbon or
solid (uncompressed) aluminum oxide. This generalized version of
Cowan and Fickett's technique is called the BKW calculation.

The BKW calculation computes the equilibrium composition of the explosion products at temperatures and pressures of interest, the detonation Hugoniot, and the values of the hydrodynamic and thermodynamic variables at the C-J point. The isentrope of the reaction products also can be obtained in either the pressure-volume or the pressure-particle velocity plane. As input data the calculation requires, for the explosive, its elemental composition, heat of formation, density, and molecular weight; and for the explosion products, their elemental compositions, heats of formation, covolumes, and cubic fits of their ideal gas free energies, enthalpies, and entropy values as a function of temperature. The thermodynamic data used was taken from references 13 and 30. The covolumes used are given in Table I. The constants used in the K-W equation of state are $\theta = 400$, alpha = 0.5, beta = 0.09, and K = 11.85.

The C-J state was computed by an iteration procedure which was terminated when the convergence error in temperature was less than $\pm 10°C$. The corresponding convergence errors in P and D are not the same for all systems, but are of the order of ± 5 kilobars and ± 25 meters/second, respectively.

EXPERIMENTAL PERFORMANCE MEASUREMENTS

The methods used at Los Alamos to measure the C-J pressure and detonation velocity of an explosive have been described previously in the open literature and are adequately referenced in Table II. The brightness measurements of W. C. Davis of this Laboratory will be published some time in the future. The temperatures reported are those of a black body of equivalent photographic brightness, probably with relative accuracy of $50°K$, since each shot has a nitromethane internal standard, and absolute accuracy of about $200°K$. The relationship between these numbers and the actual detonation temperature is not known. Since the agreement between Davis's temperatures and those of other investigators for void-free systems is rather good, we shall assume, as previous investigators have, that the temperatures we are measuring are the C-J temperatures.

The estimated errors given in Table II for some of the pressure and velocity measurements are considerably larger than normally associated with the techniques used. The accuracy of the results suffered primarily as a result of the necessity to design the shot setup in such a way as to use a minimum amount of material and the necessity of preparing and loading the hazardous mixtures by remote control.

CHNO Systems
Cowan and Fickett's version of the Kistiakowsky-Wilson equation of state was calibrated for RDX, Cyclotol, Composition B, and TNT. They obtained their poorest agreement for TNT.

726

Table I

Covolumes Used in BKW Calculations

Specie	Covolume	Specie	Covolume
B_2O_3	730	C	180
HBO_2	1270	B_2O_2	1740
BO	610	NO	386
B_2	674	N	148
B	215	BN	619
BH	533	NH_3	476
BF_3	800	CH_4	528
BF	685	Al_2O_3	1350
F	108	Al_2O_2	1800
F_2	387	Al_2O	1300
HF	389	AlO	1160
CO_2	670	AlH	948
CO	390	Al	350
H_2O	360	CF_4	1330
OH	413	CF_3	1330
H_2	180	CF_2	1330
O_2	350	CHF_3	1920
O	120	CH_2F_2	1330
H	760	CH_3F	1920
N_2	380	CF_2O	1330

CoVolume $= 10.46\, V_i$ where V_i has the dimensions A^{o3}.

Table II

Experimental and BKW Calculated Performance of Explosives

System No.	Empirical Formula of System	Composition	Solid (S) or Liquid (L)	ΔH_f° (kcal/mole HE)	Reference to ΔH_f°	Density (grams/cc)
CHNO SYSTEMS						
1	$C_3H_6N_6O_6$	RDX	(S)	14.71	(9)	1.80
2	$C_{5.045}H_{7.461}N_{6.876}O_{7.753}$	Cyclotol (17)	(S) mixture	9.5	(10)	1.755
3	$C_{6.851}H_{8.750}N_{7.650}O_{9.300}$	Comp. B (18)	(S) mixture	4.9	(10)	1.715
4	$C_7H_5N_3O_6$	TNT	(S)	-17.81	(9)	1.640
5	$C_7H_5N_3O_6$	TNT	(L)	-12.95	(11)	1.447
6	CH_3NO_2	Nitromethane	(L)	-21.28	(13)	1.128
7	$C_{1.071}H_3N_{1.284}O_{2.568}$	NM/TNM (20)	(L) solution	-20.66	(10)	1.197
8	$C_{1.25}H_3N_2O_4$	NM/TNM (21)	(L) solution	-19.08	(10)	1.310
9	$C_{1.5}H_3N_3O_5$	NM/TNM (22)	(L) solution	-16.88	(10)	1.397
10	$C_{7.29}H_6N_{5.16}O_{10.32}$	C_6H_6/TNM (23)	(L) solution	+22.98	(10)	1.362
11	$C_3H_5N_3O_9$	Nitroglycerine	(L)	-84.6	(14)	1.590
12	$C_4H_8N_4O_8$	Dina	(L)	-70.0	(15)	1.430

Table II
Continued

BKW Calculated

System No.	CJ Gas Volume (cc/mole gas)	Moles Gas/ Mole HE	CJ Solid Carbon Volume (cc/mole)	Moles Solid Carbon/ Mole HE	Gamma	Mole Fraction of Gaseous Products for Species Present More Than 1×10^{-3}						
						H_2O	H_2	O_2	CO_2	CO	NH_3	N_2
CHNO SYSTEMS												
1	11.47	7.55	3.77	1.42	2.92	.391	--	--	.195	.014	.005	.395
2	11.95	9.26	3.87	2.91	2.87	.395	--	--	.211	.019	.005	.369
3	12.43	10.78	3.97	4.20	2.92	.396	--	--	.220	.025	.006	.352
4	13.98	5.87	4.21	5.10	2.97	.417	--	--	.281	.043	.005	.253
5	15.54	6.04	4.46	4.91	2.81	.399	.002	--	.248	.098	.008	.244
6	15.33	2.35	4.56	0.60	2.53	.596	.009	--	.086	.084	.023	.202
7	15.28	2.85	4.50	0.32	2.54	.494	.007	--	.144	.120	.017	.217
8	15.78	3.78	--	0	2.46	.395	--	.009	.312	.018	.003	.264
9	15.38	4.76	--	0	2.52	.315	--	.054	.311	.004	--	.315
10	15.86	10.39	4.46	2.39	2.60	.270	.005	--	.251	.221	.009	.244
11	14.22	7.26	--	0	2.61	.344	--	.035	.412	.002	--	.207
12	13.96	8.24	4.26	1.68	2.68	.470	.001	--	.219	.063	.009	.238

Table II
Continued

System No.	BKW Calculated			Experimental Data		
	CJ Pressure (mbs.)	CJ Temp. (°K)	Det. Vel. (cm/μsec)	CJ Pressure (mbs.)	Detonation Velocity (cm/μsec)	Brightness Temperature (°K)
CHNO SYSTEMS						
1	.338	2677	.8584	.341 ±.005 (1)	.859 ±.005 (1)	
2	.311	2730	.8281	.313 ±.005 (1)	.829 ±.002 (1)	
3	.284	2760	.8068	.292 ±.005 (1)	.802 ±.002 (1)	
4	.225	2757	.7361	.190 ±.005 (1)	.695 ±.002 (1)	
5	.173	2960	.6747	.170 ±.002 (31)	.658 ±.001 (31)	3030 (5)
6	.151	2960	.6871	.133 ±.015 (4)	.629 ±.001 (4)	3380 (5)
7	.168	3200	.7045	.138 ±.010 (2)	.657 ±.010 (2)	3480 (5)
8	.195	3850	.7177	.156 ±.010 (2)	.688 ±.010 (2)	3750 (5)
9	.200	3570	.7099		.678 ±.015 (6)	3580 (5)
10	.182	3700	.6948		.685 ±.015 (6)	3520 (5)
11	.256	3270	.7630		.758 ±.010 (7)	3470 (5)
12	.217	2960	.7469			3480 (5)
13	.191	4520	.6930		.671 ±.015 (6)	4000 (5)

Table II
Continued

System No.	Empirical Formula of System	Composition	Solid (S) or Liquid (L)	ΔH_f^o (kcal/mole HE)	Reference to ΔH_f^o	Density (grams/cc)
13	$C_{4.25}H_3N_6O_{10}$	AN/TNM (24)	(L) solution	+55.0	(10)	1.380
CHNOF SYSTEMS						
14	$C_5H_7N_4O_6F_3$	TFNA (25)	(S)	-180	(12)	1.692
15	$C_2H_3N_2O_2F_3$	TFENA (26)	(L)	-162	(12)	1.523
16	$C_{3.7}H_{6.35}N_{5.3}O_6F_{1.05}$	RDX/TFNA (27)	(S) mixture	-53.4	(10)	1.754
CHNOAl SYSTEMS						
17	$C_{1.873}H_{2.469}N_{1.613}O_{2.039}Al_{0.7338}$	Alex 20 (28)	(S) mixture	-1.0	(10)	1.801
18	$C_{1.647}H_{2.093}N_{1.365}O_{1.744}Al_{1.142}$	Alex 32 (29)	(S) mixture	-1.1	(10)	1.880
BCHNOF SYSTEMS						
19	$B_{10}H_{18}C_{5.75}N_{15}O_{30}$	(19)	(L) solution	+40	(16)	1.40
20	$B_{10}H_{18}C_{6.45}N_{17.8}O_{35.6}$	(32)	(L) solution	+46	(16)	1.427
21	$B_{10}H_{18}C_{17}F_{30}O_{30}N_{15}$	(33)	(L) solution	-1290	(16)	1.467
22	$B_{2.159}C_{11.0226}H_{4.6477}N_8O_8$	(34)	(S) mixture	-10.9	(10)	1.665

Table II
Continued

BKW Calculated

Mole Fraction of Gaseous Products for Species Present More Than 1×10^{-3}

System No.	CJ Gas Volume (cc/mole gas)	Moles Gas/Mole HE	CJ Solid Carbon Volume (cc/mole)	Moles Solid Carbon/Mole HE	Gamma	Species and mole fractions
13	17.05	9.01	--	--	2.46	H_2O .165, H_2 --, O_2 .018, CO_2 .415, CO .056, NH_3 --, N_2 .323, NO .020
CHNOF SYSTEMS						
14	14.13	7.61	4.08	2.93	2.74	HF .026, CO_2 .173, CO .007, H_2O .436, NH_3 .007, N_2 .259, CF_4 .092
15	17.58	3.62	4.43	0.97	2.55	HF .068, CO_2 .092, CO .003, H_2O .365, NH_3 .010, N_2 .271, CF_4 .190
16	12.42	7.60	3.91	1.95	2.88	HF .016, CO_2 .188, CO .012, H_2O .402, NH_3 .005, N_2 .346, CF_4 .030
CHNOAl SYSTEMS						
17	13.20	1.97	4.24	1.66	3.40	Solid Al_2O_3 .3669, H_2O .354, H_2 .051, CO_2 .012, CO .098, NH_3 .148, N_2 .336
18	14.58	1.30	4.52	1.64	3.33	Solid Al_2O_3 .5708, H_2O .015, H_2 .271, CO_2 --, CO .009, NH_3 .343, N_2 .353

Solid B_2O_3 not present in equilibrium composition

System No.	CJ Gas Volume (cc/mole gas)	Moles Gas/Mole HE	CJ Solid Carbon Volume (cc/mole)	Moles Solid Carbon/Mole HE	Gamma	Species and mole fractions
BCHNOF SYSTEMS						
19	16.51	27.07	--	--	2.42	B_2O_3 .184, HBO_2 .0007, H_2O .292, NH_3 .007, CO_2 .047, CO .166, H_2 .028, N_2 .273, O_2 --
20	16.94	29.94	--	--	2.42	B_2O_3 .166, HBO_2 .0010, H_2O .293, NH_3 .0004, CO_2 .138, CO .077, H_2 .005, N_2 .297, O_2 .018
21	17.2	44.9	--	--	2.47	B_2O_3 *.012, HBO_2 --, H_2O .119, NH_3 --, CO_2 .120, CO .259, H_2 .004, N_2 .167, O_2 .003
22	12.56	10.11	4.04	4.36	2.70	B_2O_3 .107, HBO_2 --, H_2O .429, NH_3 .075, CO_2 .014, CO .014, H_2 .003, N_2 .358, O_2 --

*Also 0.198 BF_3 and 0.071 HF

Table II
Continued

System No.	BKW Calculated			Experimental Data		
	CJ Pressure (mbs.)	CJ Temp. (°K)	Det. Vel. (cm/μsec)	CJ Pressure (mbs.)	Detonation Velocity (cm/μsec)	Brightness Temperature (°K)
CHNOF SYSTEMS						
14	.247	2300	.7387	.249 +.010 (3)	.740 +.005 (3)	
15	.164	1950	.6176	.174 +.010 (3)	.665 +.005 (3)	
16	.298	2530	.8120	.324 +.010 (3)	.822 +.005 (3)	
CHNOAl SYSTEMS						
17	.251	4860	.7671	.230 +.005 (8)	.753 +.002 (8)	
18	.211	6340	.6971	.215 +.005 (8)	.730 +.002 (8)	
BCHNOF SYSTEMS						
19	.192	5180	.6849	.172 +.015 (16)	.674 +.01 (16)	4460 (5)
20	.194	5240	.6825	.167 +.015 (16)	.682 +.01 (16)	
21	.185	4500	.6620	.206 +.015 (16)	.691 +.01 (16)	
22	.273	3150	.7782	.275 +.010 (3)	.80 +.02 (3)	

Systems 6, 7, 8, and 9 show the effect of changes in oxygen balance. The C-J pressures and velocities of the CO_2 balanced system compared to the CO balanced system is disappointing if one considers the heats of explosion and simple gamma law predictions. If one assumes that the detonation velocity increases with density at about 3,000 meters/second/gram/cc. then the velocity difference between the CO and the CO_2 balanced systems may be attributed entirely to the difference in density. The temperature increases as the amount of CO_2 increases until an excess of oxygen is present and then the temperature decreases. The observed C-J performance may be explained by the lower particle density at the C-J state for systems producing CO_2 instead of CO. The extra energy present in such a system is primarily thermal energy rather than intermolecular potential energy. Thus the temperature would be expected to increase as the amount of CO_2 formed was increased and the pressure and velocity remain relatively unchanged.

BCHNOF Systems

Systems 19, 20, and 21 are homogeneous systems which produce B_2O_3 and BF_3 as detonation products. Although the heats of explosion are almost twice that of conventional CHNO explosives, the observed C-J pressures and velocities are not as high as those of the better CHNO explosives at the same densities. A possible explanation for the poor C-J pressures and velocities of the boron explosives relative to the CHNO explosives can be proposed on the basis of these calculations. Because the product molecules B_2O_3 and BF_3 are complex, the particle density at the C-J point is lower than for systems containing the product molecules CO, CO_2, H_2O, and N_2. Thus the energy is partitioned unfavorably with the intermolecular potential energy low and the thermal energy high. At C-J densities the intermolecular potential energy is the primary pressure-determining part of the energy; thus the C-J pressures of the boron explosives are low and the C-J temperatures are high. We have no reason to doubt that the heats of explosion of these mixtures are high, and the possibility remains that they would perform well in applications which rely importantly on the equilibrium expansion of the detonation products.

CHNOAl Systems

Systems 17 and 18 are nonhomogeneous systems, but the C-J pressures and velocities may be explained by assuming that the HE/Al behaves as if it is a homogeneous explosive and the product molecule Al_2O_3 is formed as an equilibrium C-J product. Again the computed and experimental C-J pressures and velocities are lower than one might expect from heat of explosion considerations because of the low particle density of the detonation products. One expects that the C-J temperature would be high and that HE/Al systems would perform well in applications which rely on the equilibrium expansion of the detonation products.

CHNOF Systems

Systems 14, 15, and 16 show the computed and experimental C-J pressures and velocities of systems containing fluorine.

of the Rohm and Haas Company, the Callery Chemical Company, the Olin-
Mathieson Chemical Company, and the Lawrence Radiation Laboratory for
making available some of the materials used in the experimental
program.

NOTES AND REFERENCES

1. Deal, W. E., J. Chem. Phys., 27, 796 (1957)
   (Values adjusted for density differences)

2. Garn, W., LASL unpublished data. (Values adjusted for density
   differences) Used technique described in Reference 1.

3. Urizar, M. J. and Craig, B. J., LASL unpublished data. Used
   technique described in Reference 1.

4. Davis, W. C., LASL unpublished data. Used technique described
   in Reference 1.

5. Davis, W. C., LASL unpublished data. Used brightness measure-
   ment technique.

6. Davis, W. C., LASL unpublished data. Used smear camera technique.

7. Mautz, C. W., LASL unpublished data. Used smear camera technique.

8. Deal, W. E., LASL unpublished data. Used technique described in
   Reference 1.

9. Cowan, R. D., and Fickett, W., J. Chem. Phys., 24, 932 (1956).

10. Computed from heats of formation of individual components.

11. Heat of Fusion = 4.86 kcal/mole. Ency. Chem. Tech., Vol. 6,
    p. 44 (1951).

12. Loughran, E. D., LASL private communication.

13. National Bureau of Standards, Circular 500.

14. Taylor, Detonation in Condensed Explosives (1952).

15. Blatt, A. H., OSRD 2014.

16. Mader, C. L., Smith, L. C., "The Performance of Boron
    Explosives", LA-2341 (1959). Report classified Confidential D.I.

17. 77/23 wt % RDX/TNT

18. 64/36 wt % RDX/TNT

19. One mole $B_{10}H_{13}C_2H_5$ to 3.75 mole tetranitromethane.

20. One mole of nitromethane to 0.071 mole of tetranitromethane.

21. One mole of nitromethane to 0.25 mole of tetranitromethane.

22. One mole of nitromethane to 0.50 mole of tetranitromethane.

23. One mole of benzene to 1.29 mole of tetranitromethane.

24. One mole of acrylonitrile to 1.25 mole of tetranitromethane.

25. 1,1,1-trifluoro-3,5,5-trinitro-3-azahexane.

26. Trifluoroethyl nitramine.

27. 65/35 wt % RDX/TFNA.

28. 44/32.2/19.8/4.0 wt % RDX/TNT/Al/Wax.

29. 37.4/27.8/39.8/4.0 wt % RDX/TNT/Al/Wax.

30. Mader, C., "Ideal Gas Thermodynamic Properties of Detonation Products", Los Alamos Scientific Laboratory Report GMX-2-R-59-3 and GMX-2-R-60-1 (1960).

31. Garn, W., J. Chem. Phys., 32, 653 (1960).

32. One mole $B_{10}H_{13}C_2H_5$ to 4.45 moles tetranitromethane.

33. One mole $B_{10}H_{13}C_2H_5$ to 7.5 moles tetranitromethane.

34. 10.35/89.65 wt % methyl carborane/HMX.

ENERGY RELEASE FROM CHEMICAL SYSTEMS

John W. Kury, Gus D. Dorough, Robert E. Sharples
Lawrence Radiation Laboratory
Livermore, California

I. INTRODUCTION

The "energy release" of a detonating high explosive has
been defined in a number of ways. Many of the definitions, however,
are not useful for the general understanding and prediction of
explosive performance. Energy release as defined by such traditional
tests as the Trauzl block test or the sand test falls in this
category. Even the widely used fundamental definition[1] which
expresses energy release in terms of the internal energy change
(ΔE) of the reaction,

$$\text{High explosive} \longrightarrow \text{products in equilibrium at the Chapman-Jouguet point,}$$

is not completely applicable. This is because the definition can
take no cognizance of compositional changes (and thus energy changes)
which can occur in the post Chapman-Jouguet (C-J) states.

The definition of energy release which we find most useful*
for performance predictions is in terms of an adiabat relating
pressure (P) to the volume (V) of the detonation products. The
energy release is then explicitly defined as the $\int P dV$ or the area
under the applicable portion of the PV curve. It is not necessary
that a single adiabat represent the post C-J behavior of a given
explosive. This will depend on the kinetics of the chemical
reactions occurring after the C-J state. If there are no composi-
tional changes, or if the changes occur in times shorter than a few

---

*This definition is not general for every application, for it
excludes energy transfer by mechanisms other than PV work (heat
conduction, etc.)

738

tenths of a μsec, then for all practical purposes there is but one adiabat. If, however, compositional changes take place more slowly, a family of adiabats results with time as a parameter. In this case the energy release will not be single-valued, but will exhibit a range of values dependent upon the time of expansion of the detonation products.

Where experimental information is insufficient to define the adiabat, or family of adiabats, representative of the energy release of a system, it may still be possible to define minimum and maximum limits of the energy release. The true energy release is then known to be bracketed, at least, between these two extremes.

An approximation of the minimum energy release can be obtained in the following way. First a value for γ is calculated* from the Chapman-Jouguet pressure (P_{CJ}), the detonation velocity (D), the loading density (ρ_o), and the assumption that PV^γ = a constant is descriptive of the behavior of the detonation products. This γ** which we shall term the Chapman-Jouguet gamma (CJG), then defines an adiabat which can be integrated for energy release over the appropriate pressure-volume change. The integration cannot realistically be taken to pressures below about a kilobar because the value of CJG is invariably too high in the low pressure range (thus predicting too low an energy). The main justification that the CJG adiabat represents a minimum in energy release is that experimentally measured adiabats (which have been obtained from impedence matching experiments[2] with a time scale of a few tenths of a microsecond) have given values of γ equal to or slightly less than CJG. Such experiments allow minimum time for energy release due to post C-J compositional changes.

The maximum energy release can be obtained from a simple thermo-chemical calculation (see Section II). To express this maximum energy in the form of an adiabat, we calculate* an <u>average</u> γ from the energy, P_{CJ}, ρ_o, and PV^γ = constant. We call this γ a maximum energy gamma (MEG). The MEG, like the CJG, is also invariably too high in the lower pressure ranges. Being an average, however, it must be low in the high pressure ranges and will therefore tend to predict too high an energy release.

In the remainder of this paper we will discuss the calculated maximum and minimum limits of energy release for a variety of systems (Section II), and describe some methods useful for measuring energy release (Section III).

---

*See Appendix I for appropriate equations.

**We use γ in this paper to mean the slope of an adiabat for the detonation products in the ln P-ln V plane.

II. CALCULATED MINIMUM AND MAXIMUM ADIABATS
FOR SOME NEW SYSTEMS

One of the objectives of explosives research is to find new materials which are better sources of chemical energy than those currently available. Since most explosive systems can be considered simply in terms of internal oxidation-reduction reactions, the search for new materials is reduced in part to a search for new oxidizing and reducing elemental combinations. That the search cannot be confined to just such groupings, however, is illustrated by system E described below. This system, containing only the elements boron, nitrogen and hydrogen, is devoid of any oxidizing groups.

In Table I we have listed examples* of the most promising chemical explosive systems currently known, together with their thermochemical properties and probable maximum densities. RDX, one of the better organic explosives, is also included in the table as a convenient reference material. System A is representative of what might be nearly the ultimate in organic explosives. The density and composition chosen are based on known materials (a CO_2-balanced mixture of bis-trinitroethylnitramine (BTNEN) and diacetylene). System B is representative of what one might expect from organic explosives containing the NF_2 grouping in place of the traditional nitro group. Systems C and D are boron analogs of the carbon systems A and B. The compositions chosen for C and D are not pure nitro and difluoroamino boranes, however, because some carbon would likely be a necessary component of such materials. System E is the unusual formulation without oxidizing groups. It relies upon the formation of boron nitride for energy release, and hydrogen gas as the medium for PV work. Because of the large hydrogen content of System E, the maximum estimated density is low. The final system tabulated, F, is an extreme example of what might be possible in aluminized systems. The composition and density are based on a BTNEN-Al mixture.

We should restate that synthetic chemistry cannot provide these compositions at the present time; the systems cited are merely best estimates of what could probably be achieved in the synthetic line. In terms of maximum possible specific energy, all the systems in the table are superior to RDX. Whether such systems, if synthesized, would indeed deliver these energies is of course not known a priori. However, by the calculation of CJG and MEG adiabats, we can bracket the energy release. This has been done; the data is collected in Table II.

As discussed before, the calculation of MEG requires a knowledge of the Chapman-Jouguet pressure; for CJG the detonation velocity must also be known (see Appendix I). Since none of these values have been measured, we have relied on BKW (3) calculational

---

*These examples may also be taken as representative of promising lithium, beryllium, and magnesium containing systems.

TABLE I. NEW EXPLOSIVES SYSTEMS

System	Explosive System		Maximum Estimated Density (g/cc)	ΔH_f (kcal/mole)	Most Stable Possible Products	Maximum Specific Energy (kcal/g)
	Type	Composition				
Reference	Nitro-organic	$C_3H_6N_6O_6$	1.80	+21	$1.5CO_2(g)$, $1.5C(s)$, $3H_2O(g)$, $3N_2(g)$	1.53
System A	Nitro-organic	$C_{5.78}H_{4.88}N_8O_{14}$	1.90	+52	$5.78CO_2(g)$, $2.45H_2O(g)$, $4N_2(g)$	1.81
System B	difluoro-amino organic	$C_2H_4N_2F_4$	1.90	~0	$2C(s)$, $4HF(g)$, N_2	1.97
System C	nitro borane	$CB_{1.5}H_2N_2O_{4.25}$	1.70	~0	$CO(g)$, $0.75B_2O_3(s)$, $H_2O(g)$, $N_2(g)$	2.47
System D	difluoro-amino borane	$C_2B_2H_2N_4F_8$	1.70	~0	$2C(s)$, $2BF_3(g)$, $2HF(g)$, $2N_2(g)$	2.59
System E	amino-borane	$B_5N_5H_{19}$	1.20	+38	$5BN(s)$, $9.5H_2(g)$	2.40
System F	Aluminized Nitro-organic	$Al_3C_4H_8N_8O_{14}$	2.02	+4	$3.5CO_2(g)$, $1.5Al_2O_3(s)$, $2H_2O(g)$, $4N_2(g)$, $0.5CO(g)$	2.28

TABLE II. CALCULATED DETONATION PROPERTIES

System	Explosive Composition	Density (g/cc)	BKW Calculations		CJG	MEG
			P_{CJ} (kbars)	D (mm/μsec)		
Reference	$C_3H_6N_6O_6$	1.80	346	8.61	2.85	2.52
A	$C_{5.78}H_{4.88}N_8O_{14}$	1.90	414	9.01	2.73	2.44
B	$C_2H_4N_2F_4$	1.90	330	7.76	2.47	2.05
C	$CB_{1.5}H_2N_2O_{4.25}$	1.70	252	7.22	2.52	1.92
D	$C_2B_2H_2N_4F_8$	1.70	266	7.37	2.47	1.72
E	$B_5N_5H_{19}$	1.20	436	12.87	3.55	2.82
F	$Al_3C_4H_4N_8O_{14}$	2.02	341	8.33	3.11	1.88

results* for these two quantities. That this is appropriate is based on the fact that for a variety of explosives (including boron ones, see Section III) where measurements are available, the BKW calculations have agreed well with experiment[3].

By combining the data in Table II with hydrodynamic calculations, we can assay the possible performance of these explosive systems in various short-time applications. As an example, we have done this for the case of metal plate acceleration, using the calculational code KO** (based on the methods of von Neumann and Richtmeyer (4)) and a simple geometry of the type discussed in Section III. We find the results shown in Table III. We see that

Table III

System	Metal Velocity Calculated Using CJG (Relative to RDX)***	Metal Velocity Calculated Using MEG (Relative to RDX)***
A	1.17	1.25
B	1.10	1.23
C	0.94	1.10
D	0.98	1.20
E	0.95	1.10
F	0.98	1.32

if the CJG defines the behavior of the detonation products, none of the boron or aluminum systems are superior to RDX. If, however, the MEG defines the behavior of the detonation products, all of the systems are superior to RDX. These calculations thus provide a good indication of the possible performance range of the systems of Table I in metal acceleration applications (fragmentation, shaped charge effects, nuclear weapons, etc.).

For long-time applications (air blast and underwater effects, etc.) the total energy release is the determining factor. The numbers given in Table I represent the maximum values of this energy. These values do not differ appreciably from those of numerous aluminized organic explosives that have been in military use for some time. We therefore cannot expect the systems of Table I to offer much improvement in "long-time" applications.

---

*These results were kindly supplied by Mr. Charles Mader of the Los Alamos Scientific Laboratory.

**Reference 4 is the basis of an IBM 704 code (KO) used in all the calculations reported in this paper.

***Values in table equal velocity calculated for the system divided by velocity calculated for RDX.

III. EXPERIMENTAL EVALUATION OF ENERGY RELEASE

One new high energy system that has been investigated experimentally is a homogeneous solution of ethyldecaborane in tetranitromethane (ET). This is an example of System C although its density (1.40 g/cc) is lower than the probable maximum density of such a system. The elementary composition of this solution is $B_{10}C_{5.75}H_{18}H_{15}O_{30}$ (at a mole ratio of ethyldecaborane to tetranitromethane of 1:3.75). ET is an extremely sensitive mixture.

What follows in this section is a discussion of the experimental work planned and completed for ET and similar explosives. This discussion serves to describe the experiments necessary to define the energy release of new systems in general.

The detonation velocity and the Chapman-Jouguet pressure have been measured for ET at the Los Alamos Scientific Laboratory[3]. Isentrope measurements have also been performed at Los Alamos for a "Hi-cal" - tetranitromethane system almost identical in composition to ET[3,5]. This isentrope was measured using an impedance matching technique[2] in which the C-J products are very rapidly expanded. The results of the impedance experiments agree with the CJG equation of state. Table IV summarizes the Los Alamos experimental data on ET

Table IV

Explosive	Density (gm/cc)	Detonation Velocity (mm/μsec)	P_{CJ} (kbars)	Calc. CJG
ET (ethyldecaborane-tetranitromethane)	1.40	6.74	172	2.70
Comp B (64% RDX, 36% TNT)	1.71	7.99	290	2.77
PBX 9404 (94% HMX, 6% plastic binder)	1.84	8.72	347	3.03

along with similar values for PBX 9404[5] and Composition B[6]. The results of impedance matching experiments agree with the CJG equation of state for these materials also.

Another type of experiment which has been performed on ET is the "small scale plate test"[7]. This test employs a configuration shown schematically in Fig. 1. It consists simply of a heavily confined column of HE, with a detonator and booster at one end, and a metal plate at the other. The length of the column is such that the results are independent of the detonator system. The test is run in a carefully standardized way with a constant volume of test explosive; the measurement consists of determining the final plate
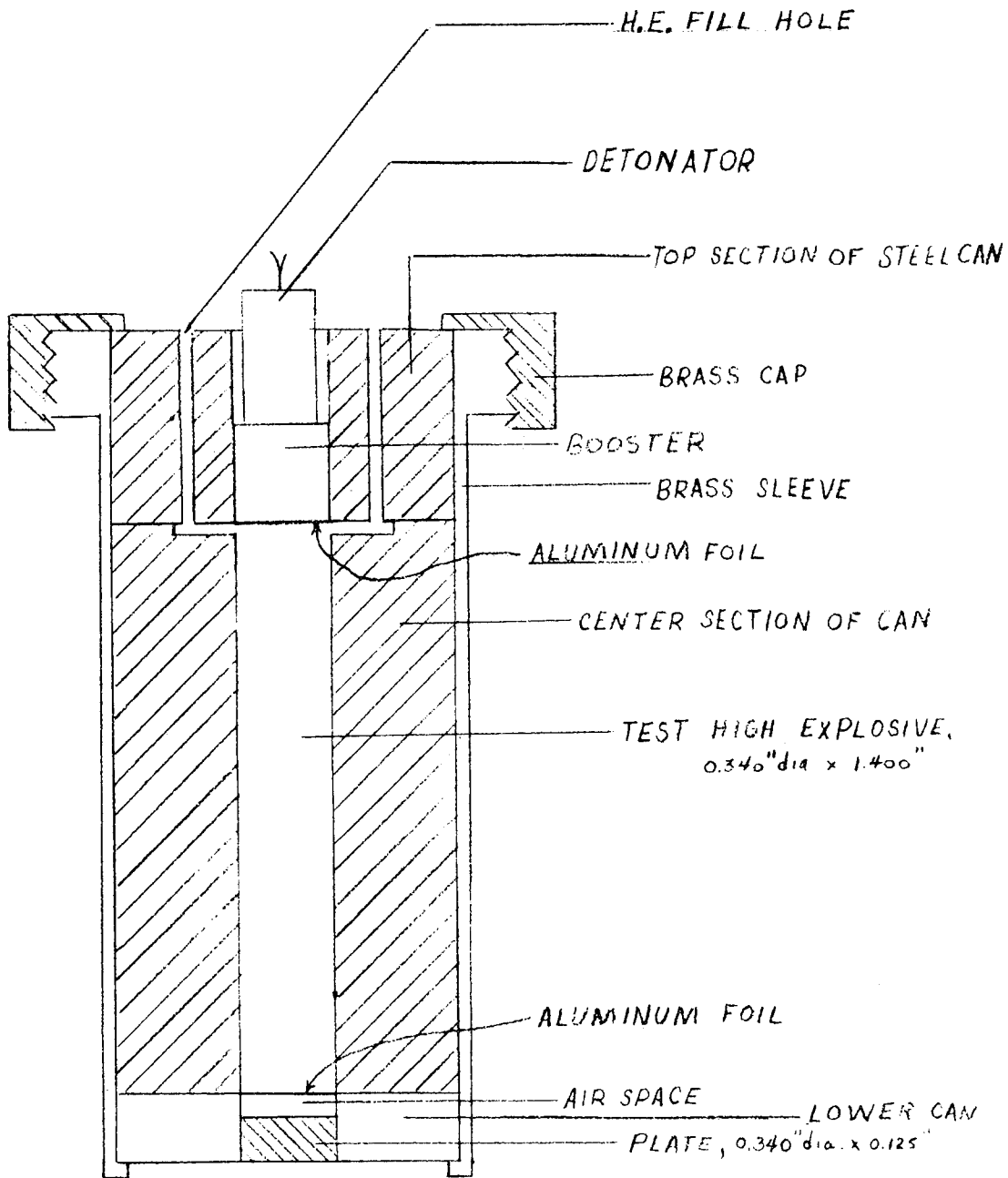
SMALL SCALE PLATE TEST
LIQUID CONFIGURATION

FIG. 1

velocity by optical techniques. The plate is under acceleration for a time period of 2 to 4 μsec. Some final plate velocities obtained in the small scale plate test are presented in Table V.

Table V

Explosive	Density (gm/cc)	Experimental Plate Velocity (mm/μsec)	Calculated Plate Velocity Using 9404 for Normalization and CJG Equation of State (mm/μsec)
ET	1.40	1.12	0.89
Comp B	1.70	1.09	1.10
LASL 9404	1.82	1.17	1.17

We have conducted one-dimensional hydrodynamic calculations (employing KO) on the small scale plate test configuration using the CJG equations of state. The calculated final plate velocities are also presented in Table V (normalized to PBX 9404)*. The agreement between the experimental and calculated normalized velocity for Comp B is very good. The discrepancy between the calculated and experimental values for the boron explosive, however, suggests that in the small scale plate test a higher energy release is obtained than the CJG equation of state would predict.

A way of reconciling this discrepancy is to assume that the energy release of the boron explosive, unlike that of Comp B and PBX 9404, is markedly time dependent. Experiments more readily interpretable than the small scale plate test, however, are required to verify this assumption. We have started such experiments, but they are not complete at the time of writing of this article. We report here only what these experiments are, and what information we hope to gain from them.

The largest of the experiments is known as the "flat-plate test". The configuration employed is shown in Fig. 2. Pin techniques[8] are used to measure final plate velocity. For large scale testing of highly sensitive, expensive systems, the flat plate test has advantages over end-on tests in that lens and edge effects may be eliminated without using large amounts of explosive. The flat plate test also tends to accentuate the importance of the lower pressure regions of the adiabat. The plate is under acceleration for a longer period (the range is some 2-20 μsec) in this test compared to the small scale plate test. To illustrate how sensitive

---

*The normalized velocity $= \dfrac{V_{calc}}{V_{9404}\ calc} \times V_{9404}\ exp$

9x 12"x 1/4" ALUMINUM PLATE ⟶

HIGH EXPLOSIVE SLAB, 6"x 6"x t" ⟶

CONFIG. 1 , t = 1/2"
CONFIG. 2 , t = 1"
CONFIG. 3 , t = 2"

DIRECTION
of
DETONATION

⟵ 50 PINS OVER
2"x 2" SQUARE
AT CENTER

PLANE-WAVE GENERATOR ⟶

FLAT PLATE TEST

FIG. 2
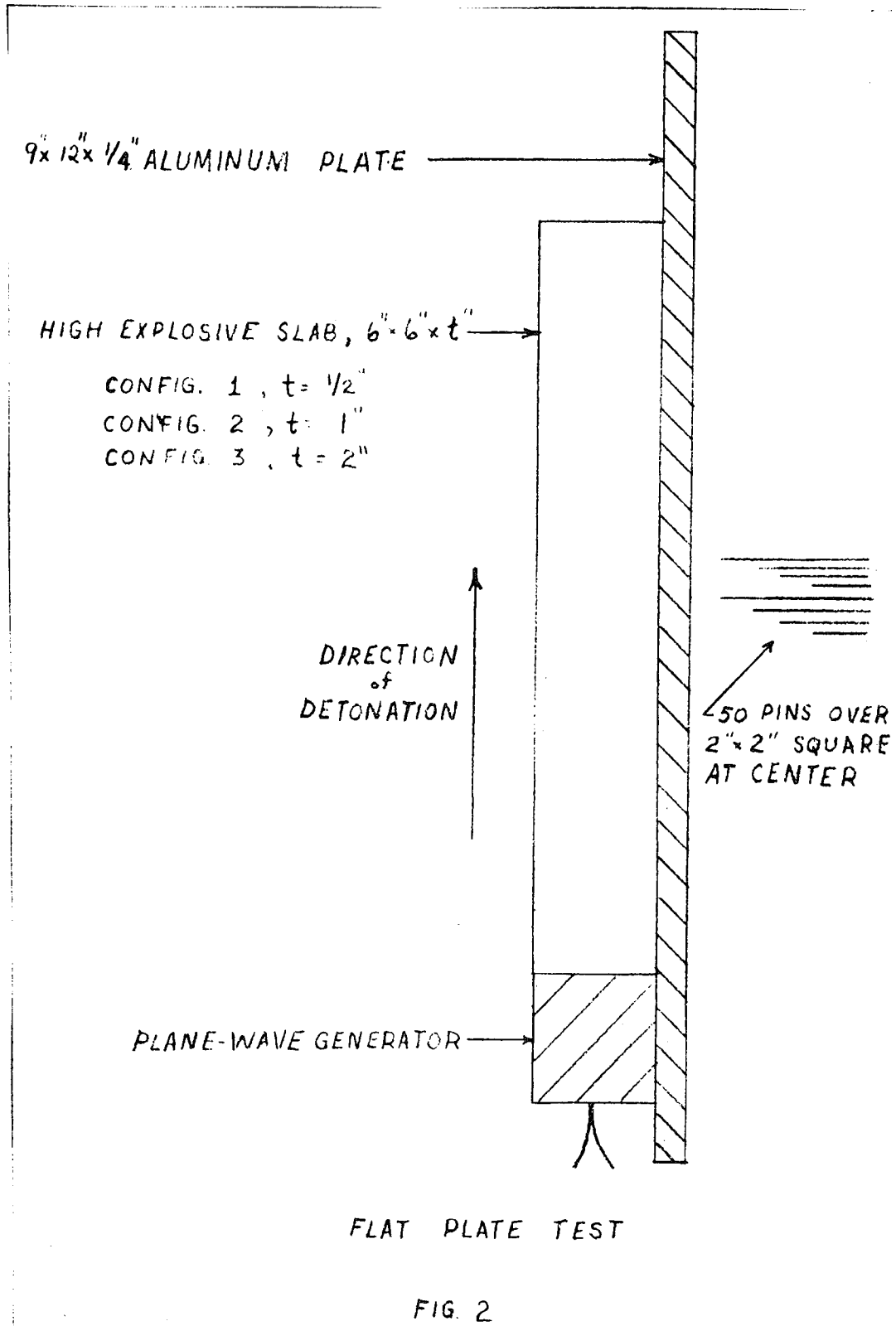
final plate velocity should be to changes in the equation of state of
the detonation products, hydrodynamic calculations have been made
using the three different types of flat plate configurations and the
CJG and MEG* equations of state for the ET system. The results are
presented in Table VI.

Table VI

Flat Plate Test Configuration	Final Plate Velocity Calculated for ET Using CJG Equation of State (mm/μsec)	Final Plate Velocity Calculated for ET Using MEG Equation of State (mm/μsec)
1	1.6	2.2
2	2.4	3.0
3	3.0	3.9

Another test which shows considerable promise for exploring
time-dependent adiabats with small amounts of explosive is the
"cylinder test" depicted in Fig. 3. The KO-calculated final wall
velocities for ET in two configurations of the cylinder test are
presented in Table VII. These values were again calculated using

Table VII

Cylinder Configuration	Final Wall Velocity Calculated for ET Using CJG Equation of State (mm/μsec)	Final Wall Velocity Calculated for ET Using MEG Equation of State (mm/μsec)
1	3.2	4.8
2	2.5	3.4

both the CJG and MEG equations of state.

An entirely different type of energy measurement is offered
by the calorimeter. This test measures directly the total energy
change involved in the overall reaction:

high explosive ⟶ C-J products ⟶ products found in bomb
(at 298°K and 1 atm)   (at 298°K and several atm)
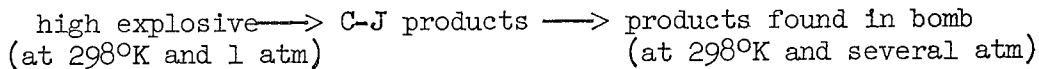
One does not necessarily obtain a unique energy release by this
method since charge diameter and extent of confinement influence
the composition of the final products. The maximum possible energy

---

*The value of γ calculated from the maximum thermochemical ΔE
is 1.58.

H.E. CYLINDER, DIA.= d

·ALUMINUM CYLINDRICAL SHELL, WALL THICKNESS: t"

WALL VELOCITY MEASURED BY FRAMING CAMERA

DIRECTION of DETONATION

PLANE-WAVE GENERATOR

CONFIG. 1, d=½, t=.024"
CONFIG. 2, d=2", t=0.22"

CYLINDER TEST
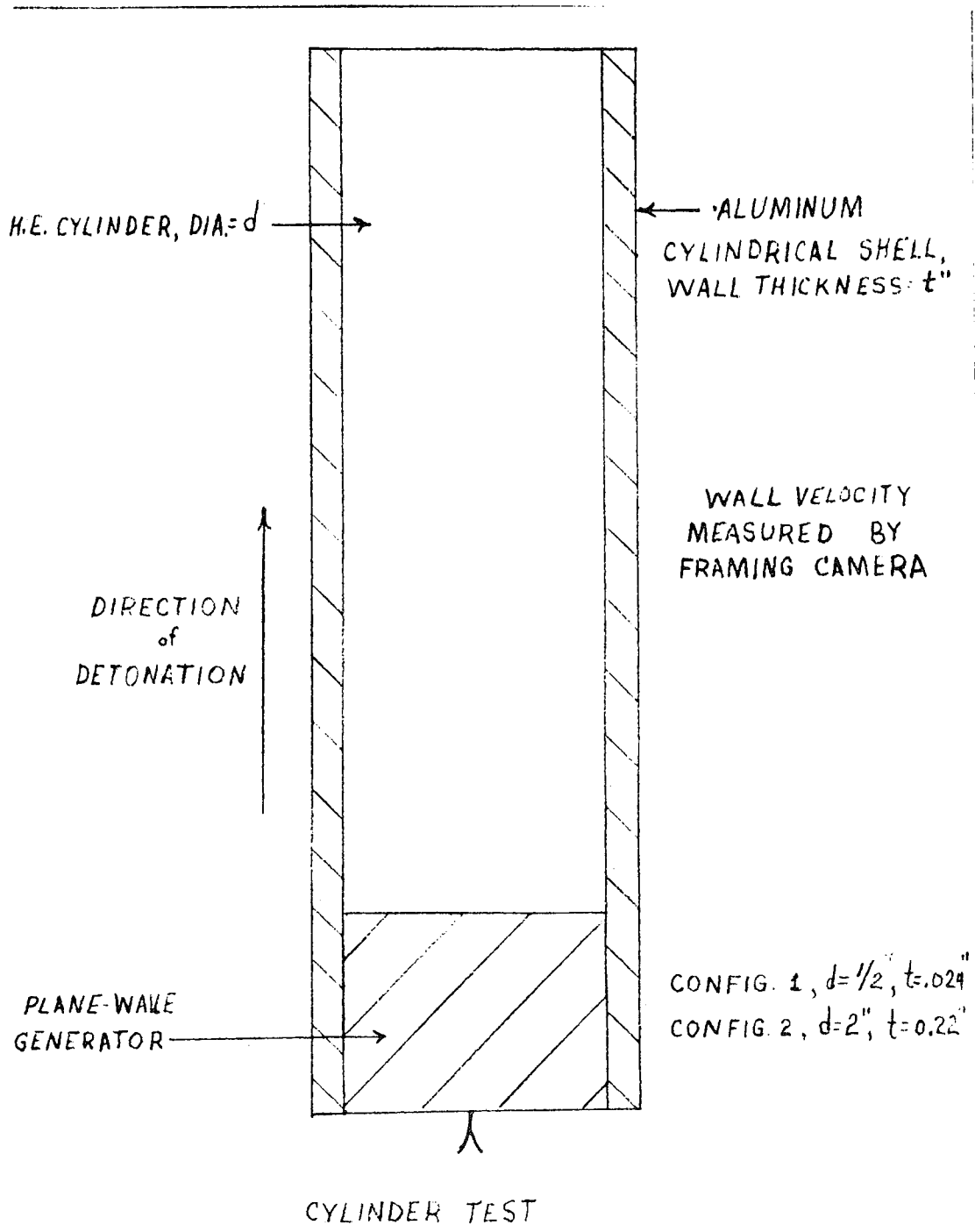
FIG. 3

release, therefore, has to be determined by measuring the heat of detonation as a function of charge diameter and extrapolating to infinite diameter.

A small-scale detonation calorimeter has been constructed at LRL, and a larger one is in the planning stage. The heats of detonation, Q, obtained for several reference explosives (both confined and unconfined) using the small calorimeter are presented in Table VIII. (The Q's given are for water liquid.)

Table VIII

Explosive	Confined		Unconfined	
	Weight of Charge (g)	Heat of Detonation (kcal/g)	Weight of Charge (g)	Heat of Detonation (kcal/g)
PETN	4.551	1.473	0.982	1.467
Density = 1.73 g/cc	4.598	1.497	2.893	1.508
			4.638	1.507
	Avg.	1.49	Avg.	1.49
PBX 9404			1.800	1.295
Density = 1.80 g/cc	3.601	1.388	3.597	1.280
	Avg.	1.39	Avg.	1.29
Composition B	4.032	1.213	1.764	0.976
Density = 1.69 g/cc	4.046	1.225	4.038	0.968
	Avg.	1.22	Avg.	0.97
			0.870	0.903
			0.871	0.928
Tetryl	4.372	1.139	2.603	0.916
Density = 1.69 g/cc	4.376	1.141	2.608	0.917
	Avg.	1.14	4.340	0.908
			4.356	0.919
			4.357	0.951
			4.363	0.911
			4.374	0.924
			Avg.	0.92

The fact that the heat of detonation of PETN is the same confined and unconfined, even in the small diameter used, suggests that 1.49 kcal/gm is its maximum possible energy release. The values

for the other explosives, however, show a marked dependence of energy release on confinement.

The various experiments described above run the gamut of time dependence for energy release. To illustrate this, we have plotted in Fig. 4 the average internal energy of the detonation products of ET versus time. The values for the flat plate and cylinder tests are calculated from KO using the CJG equation of state; the values for the impedance matching and calorimetry experiments are estimated. We plan to use this entire set of tests to explore the system*, $B_XC_{20-x}H_{18}N_{20}O_{40}$. This system is a homogeneous mixture of tetranitromethane, tetralin, and a derivative of decaborane. The boron content can be varied from $x = 0$ to $x = 10$ without changing the density or heat of formation of the mixture. The calculated maximum energy release, however, changes from 1.6 to 2.4 kcal/gm as x goes from 0 to 10. We fully expect that these new results will establish clearly whether the discrepancy noted for ET in the small-scale plate test is an artifact of the test, or a real indication that a family of time dependent adiabats must be used to represent the performance of boron containing explosives.

---

*Developed for the Lawrence Radiation Laboratory by Reaction Motors, Inc. LRL Purchase Order No. 3187106.
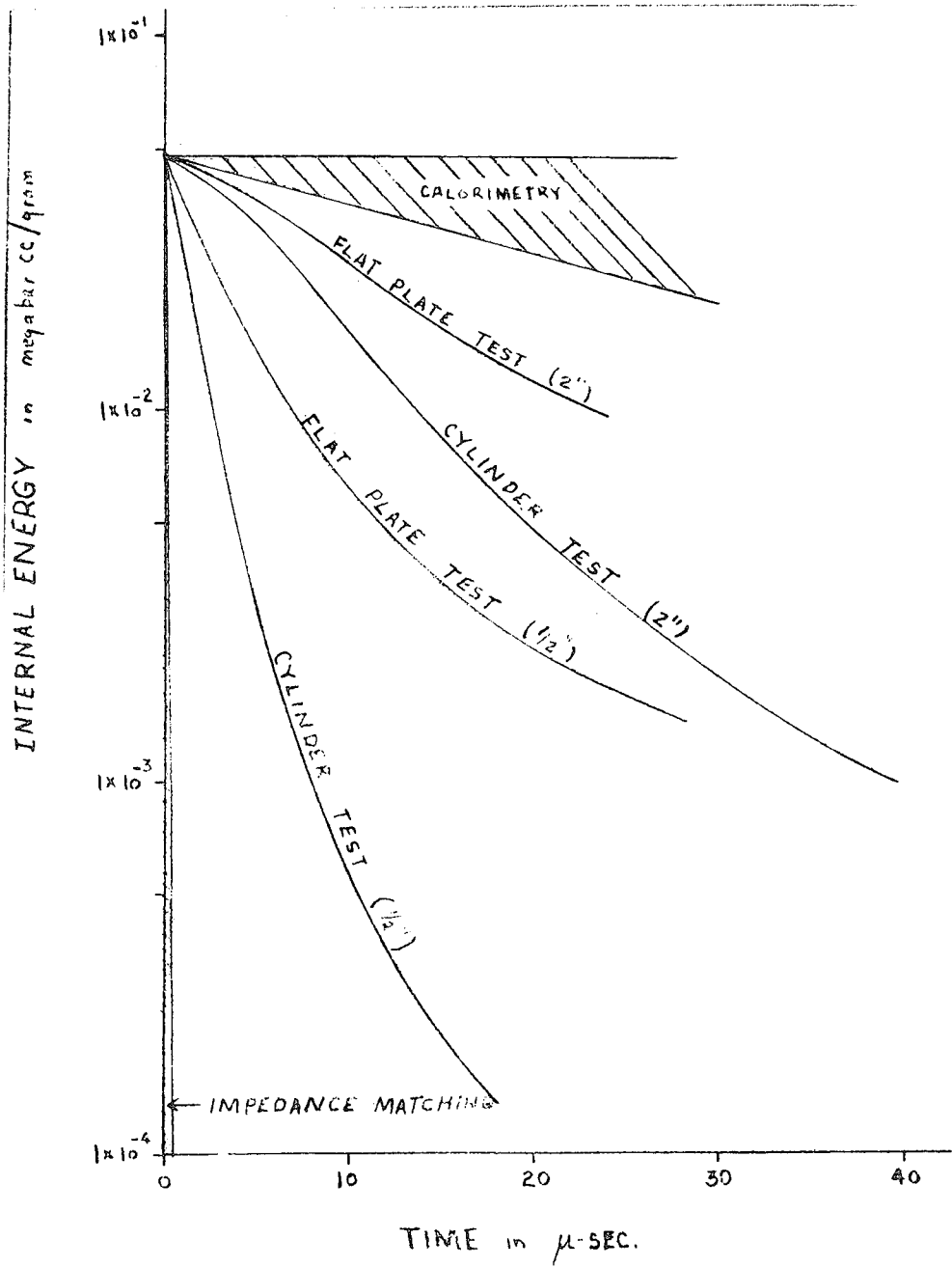
VARIATION OF THE INTERNAL ENERGY OF THE
(ET) DETONATION PRODUCTS AS A FUCTION OF TIME

FIG. 4

ACKNOWLEDGEMENTS

Kury et al.

APPENDIX I

Relations among the Detonation Parameters of a γ-law High Explosive.

We first list the well known conservation equations associated with the passage of an inert, one-dimensional shock through a fluid confined in a rigid-walled cylinder. The subscripts o and 1 denote, respectively, the states before and after the passage of the shock. The polytropic equation of state, the C-J hypothesis, and the definition of the sound speed are also given for reference.

Mass conservation: $\rho_o D = \rho_1 (D - u_1)$

Momentum conservation: $P_1 = \rho_o D u_1$

Energy conservation: $e_1 - e_o = 1/2\, P_1 (1/\rho_o - 1/\rho_1)$

Chapman-Jouguet Hypothesis: $c_1 = D - u_1$

Definition of sound speed: $c^2 = (dP/d\rho)_s$

Polytropic equation of state: $P/(\gamma-1)\rho = e$

It should be noted that the conservation equations given here assume the unshocked medium to be at rest, i.e., $u_o = 0$, and to have $P_o = Q$. If now state o describes a region of undisturbed high explosive, and state 1 is associated with the C-J state, i.e., we assume a negligible reaction zone thickness, then the following relations can be derived[9] for the quantity γ:

$$\gamma = \rho_o D^2 / P_{CJ} - 1$$
$$\gamma = P_{CJ} / 2e_o + 1$$

REFERENCES

(1) Taylor, J., "Detonation in Condensed Explosives", Oxford
University Press, London, England, p. 40.

(2) Deal, W. E., Phys. of Fluids, $\underline{1}$, 523 (1958).

(3) Mader, C. L. and Smith, L. C., "The Performance of Boron
Explosives", LA-2341, Nov. 6, 1959.

(4) von Neumann, J. and Richtmeyer, R. D., J. Applied Physics, $\underline{21}$,
232 (1950).

(5) Private communication from Los Alamos Scientific Laboratory,
Los Alamos, New Mexico.

(6) Deal, W. E., J. Chem. Phys. $\underline{27}$, 796 (1957).

(7) Ornellas, D., Dorough, G., Kury, J., and Finger, M., UCRL
Report in preparation.

(8) Duff, R. E., and Houston, E., J. Chem. Physics $\underline{23}$, 1268, (1955).

(9) Jacobs, S. J., "The Energy of Detonation", NAVORD 4366,
Sept. 17, 1956.

ADDENDUM

ADDITIONAL EXPERIMENTAL RESULTS AVAILABLE
AT THE TIME PAPER WAS PRESENTED

Preliminary results for the systems $B_{10}C_{10}H_{18}N_{20}O_{40}$ and
$C_{20}H_{18}N_{20}O_{40}$ (Table 1) have been obtained from the following
experiments:

1) Measurement of detonation velocity and
Chapman-Jouguet pressure. (Table 2)

2) Measurement of a point on the isentrope
of the detonation products. (Table 3)

3) Small scale plate test. (Table 4)

4) Cylinder and flat plate hydrodynamic
performance tests. (Tables 5 and 6)

5) Heat of detonation. (Table 7)

Table 1.

Explosive	Composition	Formula	Density (gms/cc)	ΔH_f^{298} (kcal/gm)	Calculated Maximum E_0° (kcal/gm)
TT 51.5 (Organic)	5 moles Tetra-Nitromethane - 1.5 moles Tetralin	$C_{20}H_{18}N_{20}O_{40}$	1.47	0.00	1.77
TI 51 (Boron)	5 moles Tetra-Nitromethane - 1 mole IPrθ	$B_{10}C_{10}H_{18}N_{20}O_{40}$	1.47	-0.06	2.42

Table 2.

Explosive	Density (gms/cc)	P_{CJ} (kbars)	D (mm/μsec)
PBX 9404*	1.83	360	8.80
Comp B*	1.71	290 (287)	7.99 (8.10)
Organic	1.47	215 (220)	7.39 (7.31)
Boron	1.47	*215* (203)	7.00 (6.85)

*LASL experimental values.
()LASL calculated values using BKW codes.

Table 3.

Isentrope P-U Points

Explosive	U_p (cm/μsec)	P (bars)
Organic	0.75	1000
Boron	0.75	670

Table 4.

Small Scale Plate Test Results

Explosive	Density (gms/cc)	Final Plate Velocity (mm/μsec)
Organic	1.47	1.16
Boron	1.47	1.16
Comp B	1.72	1.08
PBX 9404	1.83	1.18

Table 5.

Flat Plate Test Results

Explosive	Density (gms/cc)	Experimental Velocity (mm/μsec)
Organic	1.47	1.58
Boron	1.47	1.62
Comp B	1.72	1.76
PBX 9404	1.83	1.96

Kury et al.

Table 6.

Cylinder   Test Results

Explosive	Density (gms/cc)	Experimental Velocity (mm/µsec)
Organic	1.47	1.43
Boron	1.47	1.46
Comp B	1.72	1.55
PBX 9404	1.83	1.70

Table 7.

Experimental Heat of Detonation

Explosive	Density (gms/cc)	E_0 (H_2O-liquid) (kcal/gm)	(kcal/cc)
Organic	1.47	1.56	2.29
Boron	1.47	2.31	3.40
Comp B	1.72	1.22	2.10
PBX 9404	1.83	1.39	2.54

The above experimental data combined with hydrodynamic calculations lead to the following conclusions:

1) Boron-oxygen explosives perform about as predicted by the CJG equation of state, not the MEG equation of state.

2) There is no evidence for time dependent adiabats in the boron explosive.

3) The small scale plate test does not order explosives in the same manner as larger more significant hydrodynamic tests.

THE DETONATION PROPERTIES OF DATB
(1, 3-DIAMINO, 2, 4, 6-TRINITROBENZENE)

N. L. Coleburn, B. E. Drimmer, T. P. Liddiard, Jr.
U. S. Naval Ordnance Laboratory
Silver Spring, Maryland

ABSTRACT: The detonation parameters of the relatively new heat-resistant, shock-insensitive explosive DATB have been measured. At the normal, pressed-loaded density (1.80 g/cm^3), the detonation velocity is 7600 m/sec, and the Chapman-Jouguet pressure is 257 kb. The detonation velocity (m/sec) varies with density (g/cm^3) according to D = 2480 + 2852ρ. The energy of detonation is 847 cal/g. The failure diameter was found to be 0.53 cm. When mechanical shocks are slowly applied, as in the impact-hammer machine, DATB is less sensitive than TNT, but when the shock is more rapidly applied, as in the NOL wedge test, the explosive behaves more like Composition B. Addition of 5% plastic binder desensitizes DATB to rapidly-applied shocks, causing it to fail to build up to detonation in the wedge test even though the pressure within the explosive may be as high as 82 kb.

Introduction

The speeds of modern aircraft, and especially those of unmanned missiles, have produced many difficult problems in ordnance design. The ability of the explosive component to tolerate severe thermal cycles experienced during the mission of such ordnance is an important parameter in these designs. A promising, new, shock-insensitive explosive, 1, 3-diamino, 2, 4, 6-trinitrobenzene (DATB)[1, 2], has superior thermal stability under these conditions. DATB is a yellow solid having a crystal density of 1.837 g/cm^3; it melts at 286°C, and decomposes at a negligible rate at 204°C, while at 260°C its decomposition rate is only about 1% (by weight) per hour. It does not initiate at the maximum height of the NOL impact machine (320 cm), in sensitivity testing,

761

showing that it is much less sensitive to such slowly-
applied mechanical shocks than even TNT (200 cm). The
detonation parameters of DATB and its sensitivity to
rapidly-applied shocks are reported herein.

Detonation Velocity of DATB and DATB-Plastic-
Bonded Compositions

Detonation velocities as a function of charge
density were measured for pure DATB and DATB/EPON 1001*
(95/5) with a rotating-mirror smear camera. The veloc-
ities obtained from the photographic measurements (when
the charge density was a maximum) checked to within
10 m/sec when camera and electronic pin probes were
employed simultaneously. Simple pelleting techniques
produced 5.0-cm diameter pellets for these tests, with
densities ranging from 1.4 to 1.8 g/cm^3. To obtain charges
with densities below 1.4 g/cm^3, the powder (average
particle size 4 to 5 microns) was loaded in 15-gram
increments into 5.1-cm internal diameter, 0.15-cm thick
aluminum or glass tubes and pressed (in the aluminum
tubes only) at pressures up to 8,000-10,000 psi. When
confined by the aluminum the detonation wave was observed
through a series of small, evenly spaced holes drilled
through the metal casing. Each test charge was initiated
by an explosive train consisting of a U. S. Engineer's
Special Detonator, a 5.1-cm diameter plane-wave generator
(Baratol-Composition B), and a 5.1-cm diameter, 5.1-cm
long tetryl pellet.

The detonation velocities are listed in Table I and
plotted in Figure 1. At densities normally obtainable,
1.80 g/cm^3 (98.0% of crystal density), the detonation
velocity of pure DATB is 7600 m/sec. The detonation
velocity varies linearly with the charge density according
to the equation

$$D = 2480 + 2852\rho \ (\pm 25) \ \text{m/sec.} \tag{1}$$

The diameter effect was studied by detonating a
pyramidal charge of three cylindrical pellets, 2.54-,
1.22- and 0.64-cm diameter, stacked in order of de-
creasing diameter. On top of the 0.64-cm diameter pellet
was placed a 1.25-cm long truncated conical section
tapering from 0.64-cm diameter at its base to 0.32-cm
diameter at the top. Detonation of the pyramidal charge
resulted in a normal velocity with detonation failure

---

* Epoxy Resin; Shell Epon 1001; (Shell Chemical Company,
Emeryville, California.)

TABLE I

DETONATION VELOCITY OF DATB

Charge no.	Diameter (cm)	Length (cm)	Confinement	Density (g/cm^3)	Detonation velocity (m/sec)
1*	Conical**	1.250	None	1.816	***
	0.64	2.540	"	1.816	7620
	1.27	2.644	"	1.815	7620
	2.54	7.861	"	1.809	7620
2	5.47	13.40	Glass	0.901	5050
3	5.47	15.31	Lucite	1.427	6600
4	4.48	15.53	"	1.375	6470
5	4.44	15.26	Aluminum	1.381	6470
6	4.44	15.27	"	1.285	6130
7	4.44	15.27	"	1.205	5880
8	5.08	15.80	None	1.788	7570
9	5.08	20.47	"	1.793	7580

* Charge 1 was the pyramid charge in four sections.
** Diameter uniformly decreased from 0.64 to 0.32 over 1.25 cm-length.
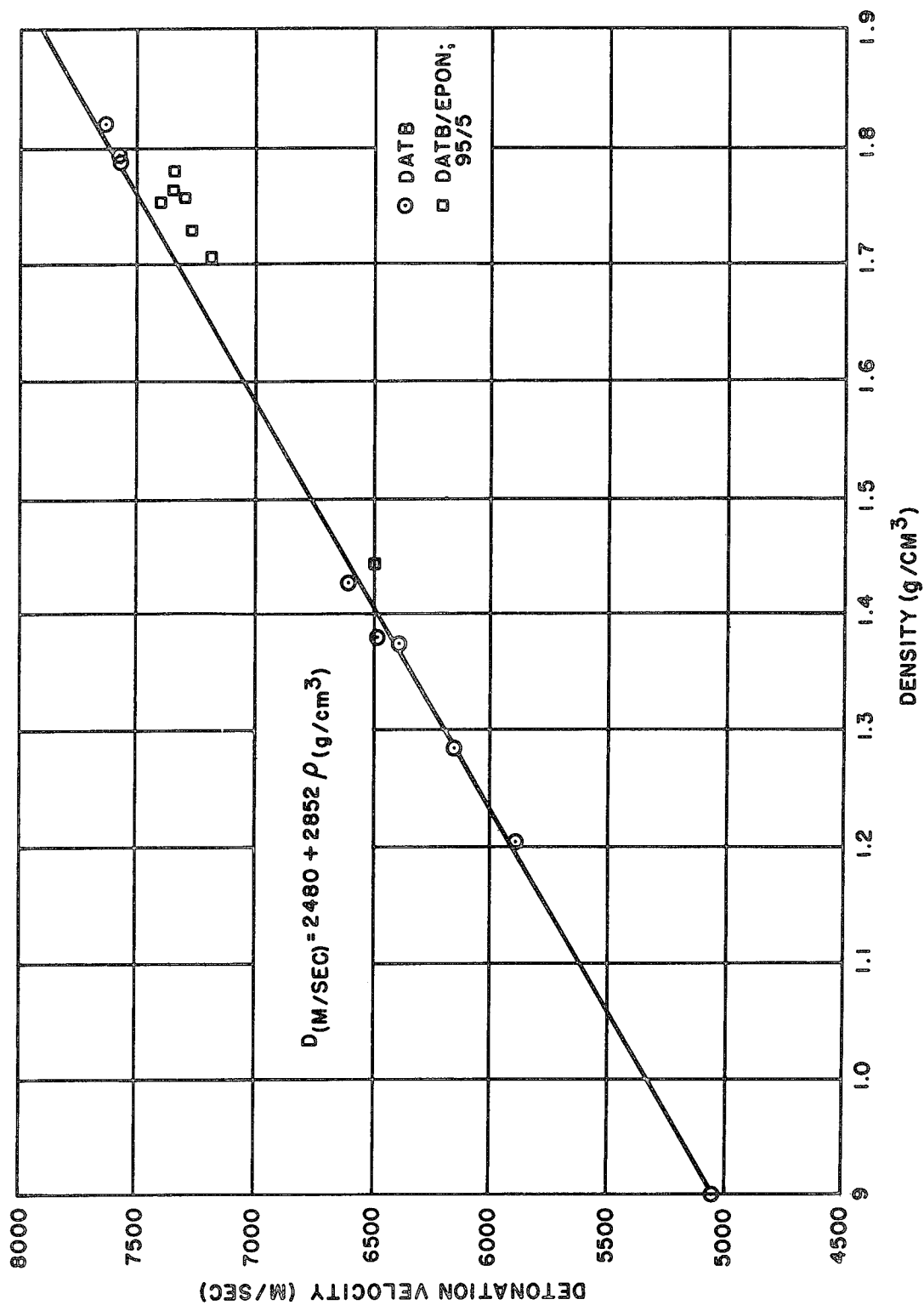*** Failure diameter = 0.53 cm.

Fig. 1 - Detonation velocity of DATB as a function of charge density

occurring at a charge diameter of 0.53 cm, i.e. within the tapered region.

Results obtained with DATB/EPON 1001 (95/5), Table II and Figure 1, show that at a given charge density this plastic-bonded explosive detonates about 150 m/sec slower than does pure DATB. A tapered section was not used in the DATB/EPON 1001 (95/5) pyramidal charge. Therefore the failure diameter of this composition was not ascertained. However, its ability to propagate stable detonation up to the end of a 2.54-cm long cylindrical pellet 0.64 cm in diameter demonstrated that its failure diameter is near to that of pure DATB.

The Chapman-Jouguet Pressure of DATB

Using a method reported by W. C. Holton[3], we have measured the Chapman-Jouguet pressure of DATB. This method involves the measurement of the velocity of the shock wave transmitted into water from the end of a plane-wave-initiated charge; then, employing an equation of state of water to obtain the pressure at the water-explosive interface, the Chapman-Jouguet pressure is inferred. In the experimental arrangement, a charge 15.2-cm long by 5.1-cm diameter, initiated by a Baratol-Composition B plane-wave generator, was immersed in distilled water to a depth of 6.4 cm. The bottom end of the charge was positioned parallel to, and 1.3 cm above, the optical axis of the smear camera. The shock wave within the water, "back-lighted" by collimated light from an exploding wire, produced a time-resolved shadowgraph. From measurements of this photographic trace the detonation pressure of the explosive is calculated using the water-shock wave data of Rice and Walsh[4]. Their data are represented by the following equation:

$$U - 1,483 = 25,306 \log_{10} (1 + u/5,190) \qquad (2)$$

where U is the shock velocity and u is the particle velocity of the water in m/sec. Thus a measurement of U at the explosive-water interface produces a corresponding value of u. The pressure, P, in the water at this interface is then obtained from the familiar hydrodynamic equation

$$P = Uu/V_0 \qquad (3)$$

where V_0 is the specific volume of material in the unshocked state. The Chapman-Jouguet pressure of the explosive, P_{CJ}, is related to the pressure, P_{H_2O}, of

765

TABLE II

DETONATION VELOCITY OF DATB/EPON 1001 (95/5)

Charge no.	Diameter (cm)	Length (cm)	Density (g/cm3)	Detonation velocity (m/sec)
1*	0.638	2.545	1.776	7350
	0.953	2.545	1.765	7350
	1.267	2.436	1.756	--
	1.267	2.629	1.761	7280
	2.537	2.573	1.752	7400
	2.537	2.614	1.708	7180
2	5.053	15.00	1.733	7260
3	2.527	15.67	1.448	6480

* Charge 1 was a pyramid charge in six sections.

the water at the explosive-water interface by a simple equation[5]:

$$P_{CJ} = \frac{P_{H_2O}(\rho_o U)_{H_2O} + (\rho_o D)_E}{2(\rho_o U)_{H_2O}} \qquad (4)$$

where $(\rho_o D)_E$ is the product of the initial density and detonation velocity of the explosive.

Three DATB charges were fired, each at an initial density of 1.790 ± 0.001 g/cm^3, yielding the following mean values:

$$D = 7585 \text{ m/sec},$$
$$U = 5980 \ (\pm 28) \text{ m/sec},$$
$$u = 2624 \text{ m/sec},$$
$$P_{H_2O} = 157 \text{ kb}.$$

Therefore, the Chapman-Jouguet pressure of DATB is 257 kb. This is some 36% greater than that of TNT (189 kb)[6] and only 12% less than that of Composition B (290 kb)[7].

The Energy of Detonation and the Isentropic Exponent

The energy of detonation can be estimated from the assumption that on detonation the oxygen in the explosive forms $H_2O_{(g)}$, $CO_{(g)}$, and $CO_{2(g)}$ in that order. For DATB this reaction is

$$C_6H_5N_5O_6 \longrightarrow$$

$$2.5 \ H_2O_{(g)} + 3.5 \ CO_{(g)} + 2.5 \ N_{2(g)} + 2.5 \ C_{(c)} \qquad (5)$$
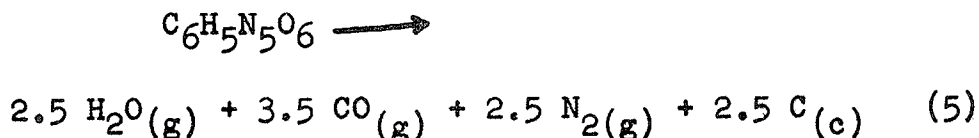
The measured heat of formation of DATB is 29.23 k cal/mole[8]. Using available heat-of-formation data for the decomposition products, the heat of detonation is calculated to be 875 cal/g.

The heat of detonation also can be calculated from the hydrodynamic properties determined above. The relation

$$P_{CJ} = \frac{1}{V_o} \frac{D^2}{(k+1)} \qquad (6)$$

is readily derived from the Chapman-Jouguet condition,

$$\left(\frac{\partial P}{\partial V}\right)_S = -\frac{P_{CJ}}{V_o - V_{CJ}} \tag{7}$$

(the term P_o has been neglected here since $P_{CJ} \gg P_o$), the hydrodynamic relation,

$$D^2 = V_o P_{CJ}/ (V_o - V_{CJ}) \tag{8}$$

and the definition of k, the isentropic exponent,

$$k = -\left(\frac{\partial \ln P}{\partial \ln V}\right)_S \tag{9}$$

Thus equation (6) yields a value of k from the experimentally determined values of D and P_{CJ}. The energy of detonation, Q, is then calculated by the equation

$$Q = \frac{D^2}{2(k^2 - 1)} \tag{10}$$

as shown by Jacobs[9] and Price[10]. From these relations k for DATB is 3.02, and Q is 847 cal/g, checking to within some 3%, the energy calculated from thermal data. For convenience these results are assembled in Table III, where they are compared to corresponding values for TNT.

Sensitivity to Rapidly-Applied Shocks

Evaluation studies were performed on pure DATB, DATB/EPON 1001 (95/5), and DATB/BRL 2741* (95/5) using the NOL wedge test[11]. In this test, Figure 2, the explosive, formed into a 25-degree wedge with a maximum thickness of 1.27 cm, is subjected to a plane shock wave delivered by an explosively-driven brass plate. Plates of 1.27-, 2.34-, and 3.81-cm thicknesses are used in order to vary the shock pressure transmitted into the explosive. The shock wave within the metal is formed by the detonation of a 1.27-cm thick Composition B slab, 12.7 cm square, initiated by a 10.8-cm diameter plane-wave generator. The shock velocity within the unreacted explosive, as a function of explosive thickness, and the build-up to the steady detonation rate, are inferred from an analysis of the smear-camera photograph of the shock arrival at the free surface of the wedge (Figure 3, central region)

---

*Phenolic resin (Bakelite Corporation, New York City, New York.)

TABLE III

PROPERTIES OF DATB COMPARED TO TNT

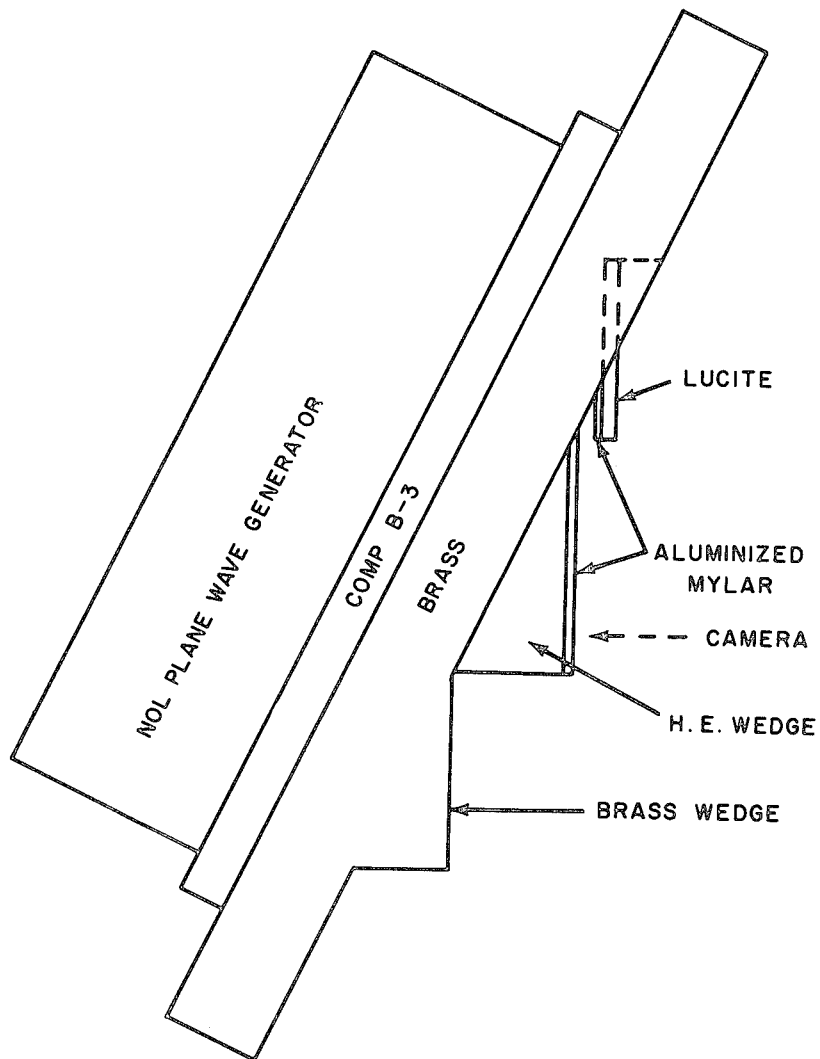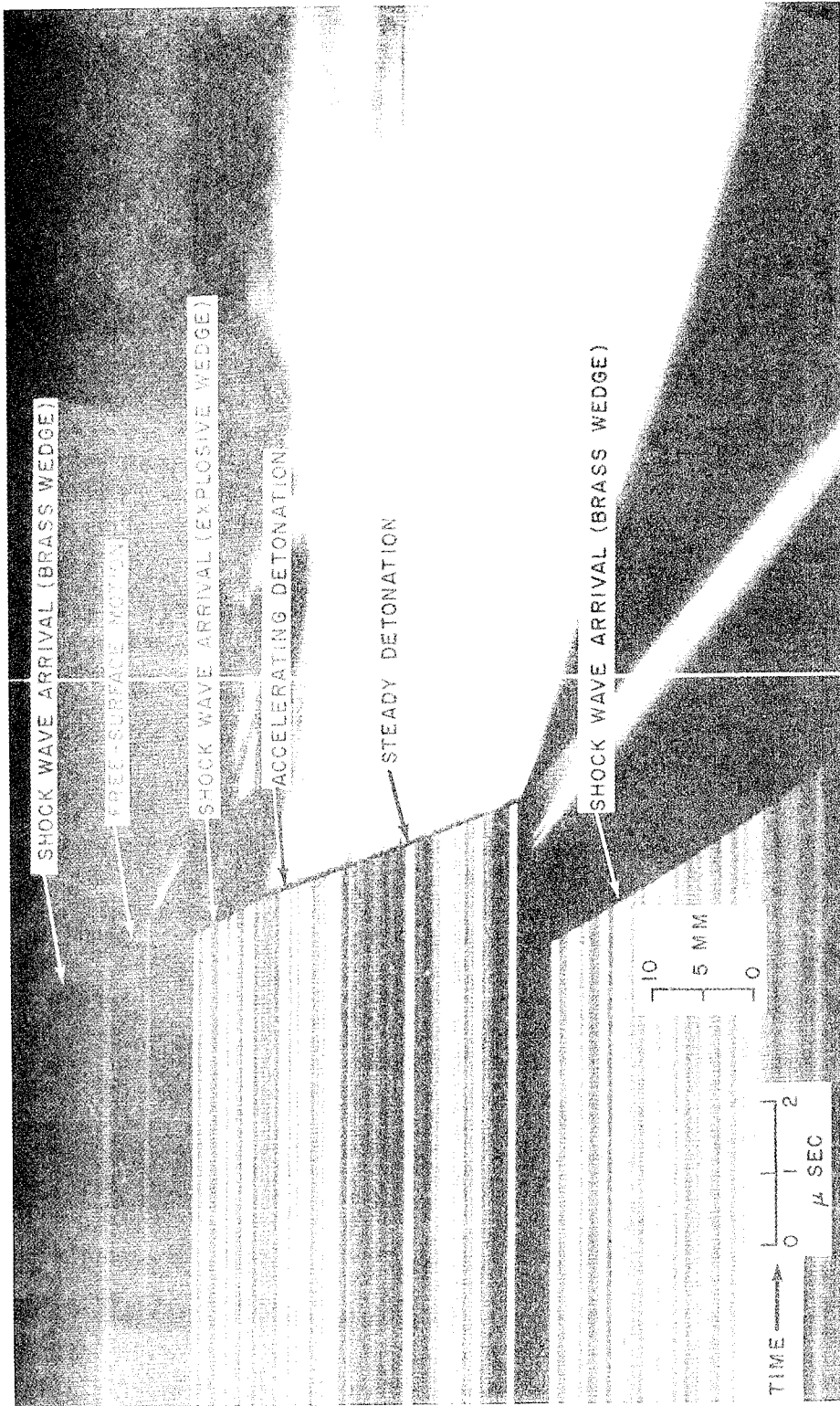| Property	DATB	TNT
Experimental Density (g/cm3)	1.800	1.637
Detonation Velocity (m/sec)	7600	6940
$\dfrac{d\,D}{d\rho}\,\dfrac{(m/sec)}{(g/cm3)}$	2852	3225
Failure Diameter (cm)	.53	1.3[14]
Detonation Pressure (kb)	257	189[6]
Detonation Energy (cal/g)	847	636
50% Impact Initiation Height (cm)	320	200
Isentropic Exponent, k	3.02	3.17
Plate-Push Value, (ft/sec)	3130	2930

Fig. 2 - Side view of NOL
wedge-test arrangement

Fig. 3 – Smear camera record of the detonation of DATB in the NOL wedge test using 1.27 cm-thick brass

Reflected-light technique is used to record the shock arrival and to measure the shock-wave parameters of the brass plate.

The results obtained for the build-up-to-detonation tests on DATB using the three brass thicknesses are shown in Figures 4-6, where they are compared to those obtained for Composition B. The outstanding feature of these curves is the fact that the instantaneous shock velocity within the explosive rises 10-20% above the normal detonation velocity before settling down to that value. An example of this velocity "overshoot" can be seen in the smear-camera photograph for Shot 1 (Figure 3). In this respect DATB behaves like other pressed explosives. No cast explosive has exhibited such an "overshoot", while pressed explosives characteristically do[12]. Another feature shown in Figures 4-6 is that the build-up-to-detonation of DATB under this rapid shock-loading is not significantly different (other than the "overshoot") from that of cast Composition B[11]. Thus the sensitivity of DATB to mechanical shocks is strongly dependent on the rate of shock-loading; when applied slowly, as in the impact-hammer machine, DATB is very insensitive (the 50% initiation point exceeds 320 cm, while for TNT it is 200 cm and for Composition B it is 60 cm)[13]. When the shock is applied rapidly, as in the wedge test, the sensitivity of DATB is comparable to that of cast Composition B (TNT fails completely to build-up to normal detonation velocity in the wedge test[11].)

The NOL wedge test was designed to permit for each shot a determination of one point on the Hugoniot curve for the unreacted explosive. Analysis of the upper region of Figure 3 yields the free-surface velocity and the shock velocity of the brass at its free surface, and thus, by equation (3), the pressure in the brass at the brass, explosive-wedge interface (assuming that the particle velocity of the brass is one half its free-surface velocity). An equation analogous to equation (4) then produces the pressure within the unreacted explosive at the same interface. If its compression, V/V_o (where V_o and V are respectively, the specific volume of the explosive before and after being shocked), is determined for the same state, then the point on the Hugoniot curve will have been determined. The compression is calculated from the continuity equation for the explosive

$$\frac{V}{V_o} = \frac{U - u}{U} \qquad (11)$$

using equation (3) to obtain the particle velocity, u, of the unreacted explosive. In this manner three points
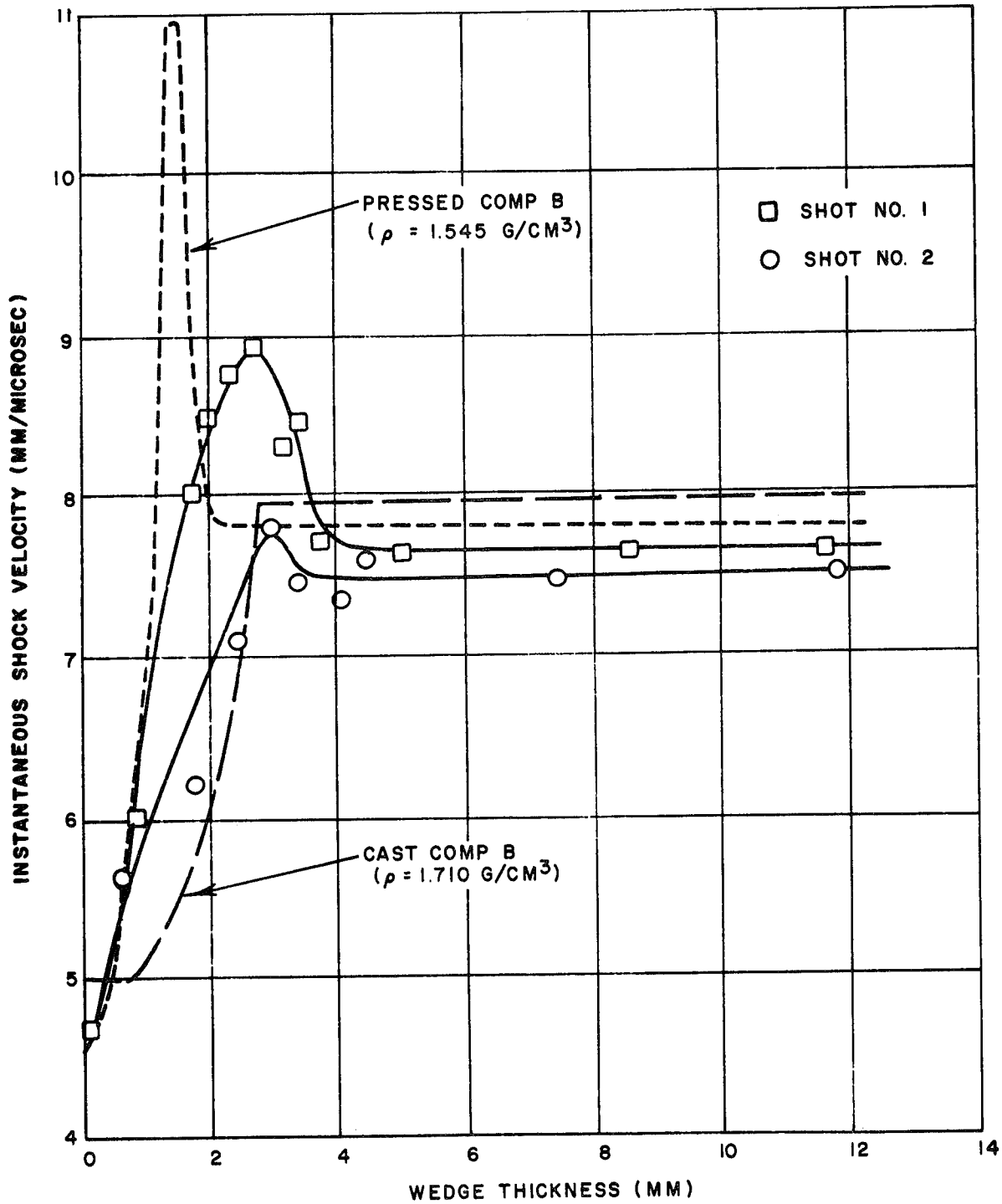
Fig. 4 - Instantaneous shock velocities in DATB for 1.27-cm
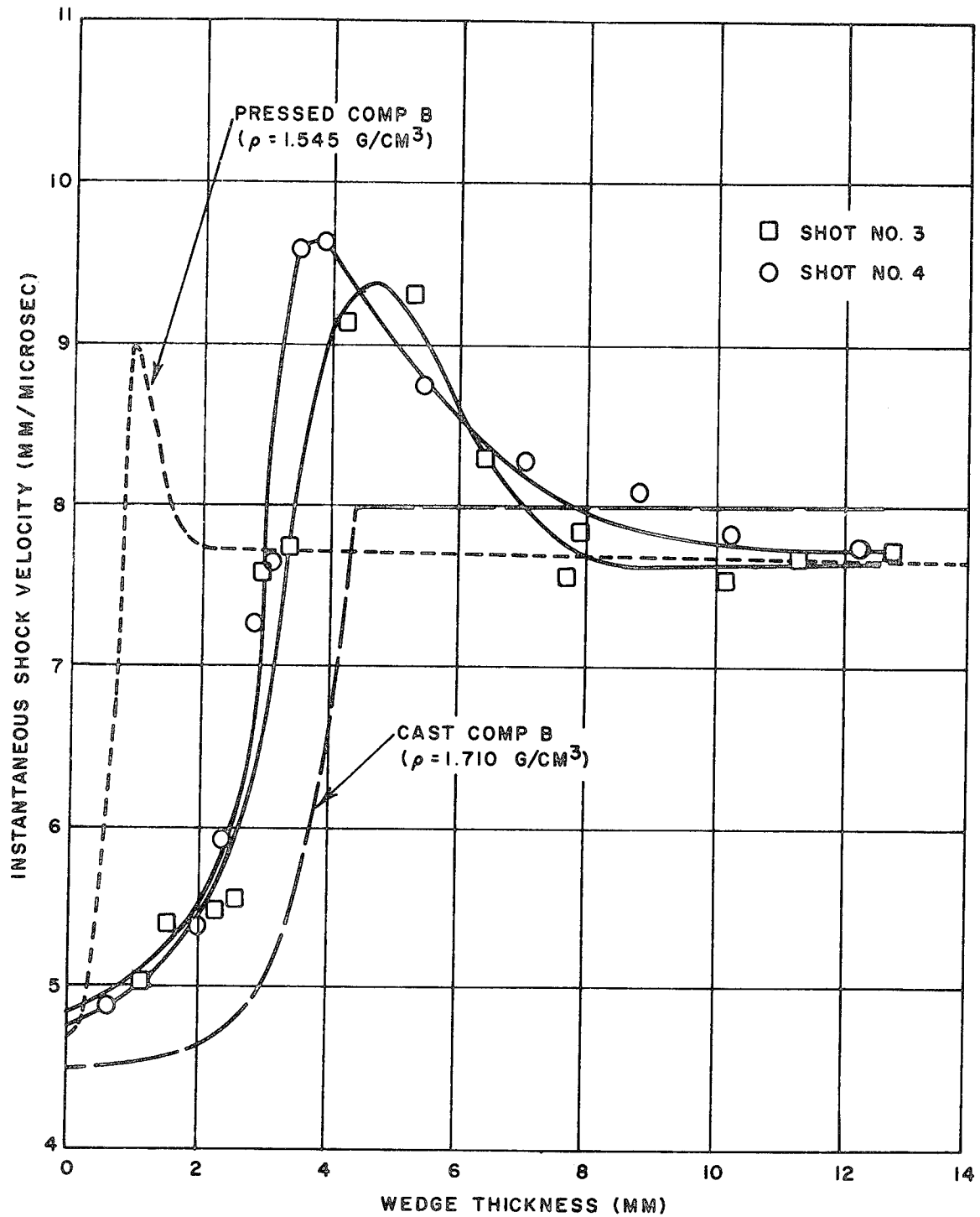thick brass compared with comp B

Fig. 5 - Instantaneous shock velocities in DATB for 2.54-cm
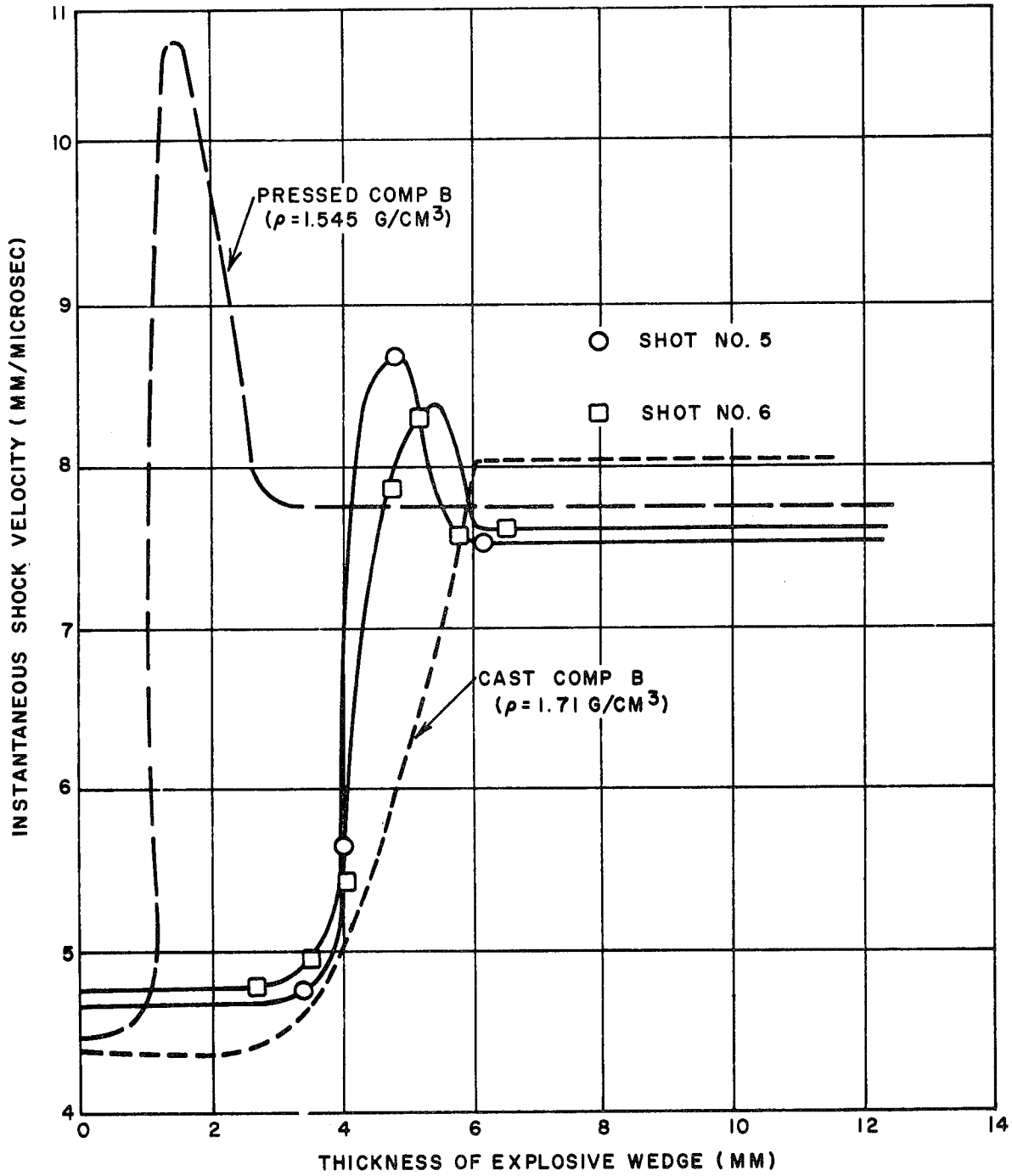thick brass compared with comp B

Fig. 6 - Instantaneous shock velocities in DATB for 3.81-cm
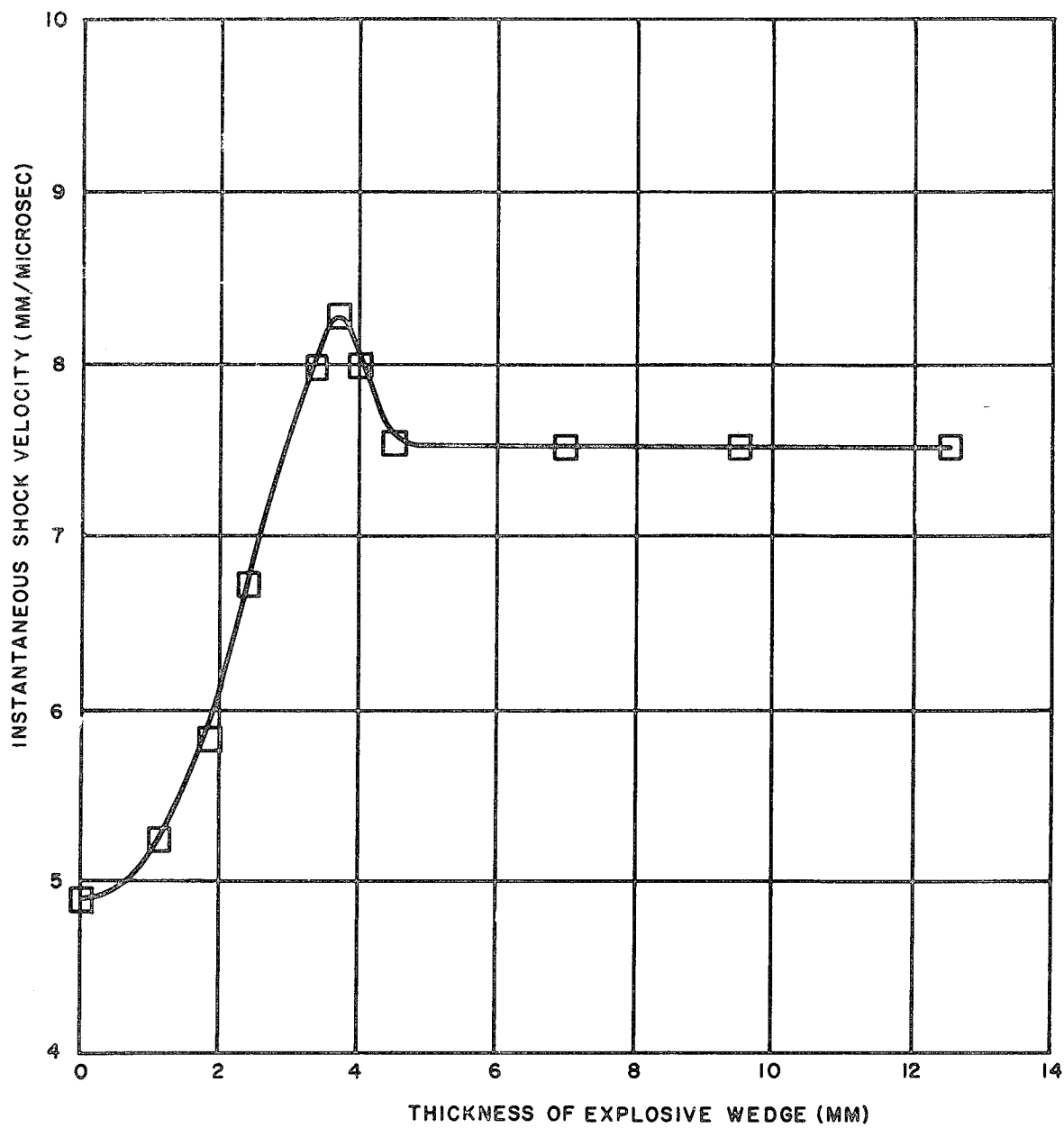thick brass compared to comp B

Fig. 7 - Instantaneous shock velocities in DATB/BRL
2741 (95/5), for 1.27-cm thick brass

on the Hugoniot curve for the unreacted explosive have been determined for pressures of approximately 75, 85, and 100 kb. The exact values, as well as the other parameters derived from the wedge test are tabulated in Table IV.

A few explanatory remarks on the data in Table IV are appropriate. The final, or steady value of the instantaneous velocity, D, should be identical with the normal detonation velocity. The observed deviations from this value are merely the result of the difficulties of making a precision velocity measurement by this method. The smallest tilt, or non-planarity of the wave as it emerges from the explosive wedge would alter the value of D. Thus the measurement of D, while not good enough for a determination of a precision detonation velocity, serves as a useful measure of the normal, plane-wave propagation assumption of the wedge test.

The fact that the shock within the explosive wedge does not move always at its normal detonation velocity means that the shock (or detonation) wave is "delayed" in reaching a given depth in the explosive. The "delay time" is defined as the difference in time of arrival of the wave within the explosive between its actual time of arrival and the time it would have arrived had it moved always at its steady detonation velocity:

$$\text{Delay time} = (\text{time-of-arrival})_{\text{"observed"}} - (\text{time-of-arrival})_{\text{"steady shock"}} \quad (12)$$

(Of course, these times of arrival are calculated for some point beyond that where the steady velocity has been attained). The fact that velocity "overshoots" occur, produces the possibility that negative "delays" could be obtained, i.e., the shock could arrive even before it would have, had it travelled at its steady velocity at all times. Thus Shot 1 (with a 1.27-cm thick brass plate) exhibit a delay time of only 0.07 microsec as contrasted with 0.20-0.30 microsec for the other five shots.

Wedge tests also were run for plastic bonded DATB/BRL 2741 (95/5) and DATB/EPON 1001 (95/5). With DATB/BRL 2741 (95/5) the standard 25-degree wedge failed to build-up to detonation when a 2.54-cm thick brass plate was used, even though the pressure developed within the explosive was 82 kb. Build-up to detonation was obtained with DATB/EPON 1001 (95/5) in the 2.54-cm thick brass plate wedge test.

TABLE IV

WEDGE-TEST PARAMETERS FOR PURE DATB

Shot no.	Brass thick (cm)	Shock velocity brass (m/sec)	Particle velocity brass (m/sec)	Shock velocity H.E. (m/sec)	Particle velocity H.E. (m/sec)	Shock pressure H.E. (kb)	Relative volume H.E. (V/V_o)	H.E. (g/cm^3)	D (m/sec)	Delay time (micro-sec)
1	1.27	4630	710	4670	1167	99.2	.750	1.820	7640	.07
2	1.27	4630	710	4660	1167	99.3	.750	1.825	7460	.16
3	2.54	4460	600	4870	972	85.4	.800	1.803	7620	.24
4	2.54	4460	600	4700	979	82.8	.792	1.799	7700	.20
5	3.81	4380	550	4736	892	76.6	.810	1.813	7590	.29
6	3.81	4380	550	4767	892	76.5	.815	1.810	7500	.26

TABLE V

WEDGE-TEST PARAMETERS FOR PLASTIC-BONDED COMPOSITIONS OF DATB

Shot no.	Brass thick (cm)	Shock velocity brass (m/sec)	Particle velocity brass (m/sec)	Shock velocity H.E. (m/sec)	Particle velocity H.E. (m/sec)	Shock pressure H.E. (kb)	Relative volume H.E. (V/V_o)	H.E. (g/cm^3)	D (m/sec)	Delay time (micro-sec)
DATB/ BRL 2741 (95/5)										
1	1.27	4630	710	4820	1164	99.4	.759	1.77	7350	.17
2	2.54	4460	600	4720	982	82.0	.792	1.77	Failed to Detonate	
DATB/ EPON (95/5)										
1	2.54	4460	600	5120	971	86.0	.810	1.73	7350	.17

Plate-Push Tests

The NOL plate-push test measures the ability of a 5.4-cm diameter by 6.3-cm long cylinder of explosive to project a 5.4-cm diameter steel disc (200 g) from a small, expendable 1.25-cm thick steel mortar. The velocity imparted to the disc, in ft/sec, is the "plate-push" value of the explosive. Pure DATB gives a value of 3130 ft/sec and is thus intermediate to TNT (2930) and Composition B (3320).

Conclusions

1. At normal densities (1.78-1.80 g/cm^3) the detonation velocity of DATB is about 7600 m/sec, or more exactly, its velocity is represented by

$$D = 2480 + 2852\rho \text{ (m/sec).}$$

At a density equal to the crystal density of TNT (1.654 g/cm^3), charges of DATB have a detonation velocity of 7200 m/sec, or 200 m/sec greater than that of TNT of the same density.

2. The sensitivity of DATB to rapidly-applied, large-amplitude shocks (as in the wedge test) is comparable to that of cast Composition B. This contrasts strongly to its behavior under slowly-applied, low-amplitude shocks (as in the drop-hammer impact test), where it is much less sensitive than even TNT.

3. The shock sensitivity of DATB is markedly reduced even for rapidly-applied, large-amplitude shocks by the addition of only 5% of certain plastic binders.

4. In the wedge test (and presumably for mechanical impacts of a similar nature) the velocity of the shock wave passing through DATB starts at 4500-5000 m/sec and accelerates to a value exceeding the normal detonation velocity before finally settling back to normal detonation velocity. In this regard, DATB behaves similarly to other pressed explosives, which also exhibit this velocity "overshoot".

5. The small failure diameter of DATB, 0.53 cm, appears surprising at first glance. Its very large impact-hammer 50% height would lead one to expect a much larger failure diameter, say something comparable to the 1.3-cm diameter found for TNT[14]. However, our wedge tests

indicate that for high pressure, rapidly-applied shocks (such as it might also receive from its own detonation) the sensitivity of DATB is comparable to that of Composition B. The small failure diameter lends further support to conclusion 2 above, since the failure diameter of Composition B is approximately 0.4 cm[15].

6. Using water as a calibrated manometer, the measured Chapman-Jouguet pressure of DATB was found to be 257 kb, thus exceeding that of TNT by about 40% (considering each explosive at its normally-obtainable charge density).

7. Using this pressure value, the isentropic exponent of product gases from DATB at the detonation front is calculated to be 3.02.

8. With this value of k, the energy of detonation of DATB is calculated from equation (10) to be 847 cal/g, or some 3% less than the value of 875 cal/g obtained from its measured heat of formation.

9. The plate-push value for DATB is 3130 ft/sec, about 6% higher than that of TNT.

References

1. Shipp, K. G. and Hill, M. E., "Heat Resistant Explosives II; 1, 3-Diamino - 2, 4, 6,- Trinitrobenzene, DATB", NAVORD Report 6016 (31 March 1958) (Confidential).

2. Holden, J. R., Rosen, A. H.; Rosen, J. M., "Heat Resistant Explosives VI; Properties of 1, 3-Diamino-2, 4, 6-Trinitrobenzene, DATB", NAVORD Report 6299 (17 March 1959).

3. Holton, W. C., "The Detonation Pressures in Explosives as measured by Transmitted Shocks in Water", NAVORD Report 3968 (1 December 1954) (Confidential).

4. Rice, M. H. and Walsh, J. M., "Equation of State of Water to 250 Kilobars", J. Chem. Phys. 26, 824 (1957).

5. Mallory, H. D., "The Measurement of Detonation Pressures in Explosives", NAVORD Report 1883 (5 March 1953) (Confidential).

6. Deal, W. E., "The Measurement of C-J Pressure for Explosives", J. Chem. Phys. 27, 796 (1957).

7. Deal, W. E., "Measurement of the Reflected Shock Hugoniot and Isentrope for Explosion Reaction Products", Phys. Fluids, 1, 523-527 (1958).

8. McEwan, William S., NOTS, Informal communication.

9. Jacobs, S. J., "The Energy of Detonation", NAVORD Report 4366 (17 September 1956).

10. Price, O., "Inter-Relationship of Explosive Characteristics III", NAVORD Report 4510 (26 April 1957).

11. Majowicz, J. M. and Jacobs, S. J., "Initiation to Detonation of High Explosives by Shocks", NAVORD Report 5710 (1 March 1958) (Confidential).

12. Jacobs, S. J., "Recent Advances in Condensed Media Detonations", ARS Journal 30b, 151 (1960).

13. Heller, H., NOL; Informal communication.

14. Cybulski, W. B., Payman, W., and Woodhead, D. W., "Explosive Waves and Shock Waves. VII. The Velocity of Detonation in Cast TNT", Proc. Roy. Soc., A 197, 51 (1949)

15. Malin, M. E., Campbell, A. W. and Mautz, C. W., "Particle Size Effects on Explosives at Finite and Infinite Diameters", J. Appl. Phys. <u>28</u>, 63 (1957).

NON-STEADY DETONATION - A REVIEW OF PAST WORK

Sigmund J. Jacobs
U. S. Naval Ordnance Laboratory
White Oak, Silver Spring, Maryland

Introduction

When this paper was invited for presentation at the Third Detonation Symposium (ONR, NOL) the above title was given as the subject. It was pointed out that the ground to be covered should include effect of chemical reaction rates on detonation, i.e., transition from deflagration to detonation, growth of detonation from an initiating shock, factors affecting the failure of detonation, and failure diameters. This fairly well covers the scope of the present review. One might argue that the effect of scaling on the rate of detonation in charges of constant cross-section should also be included since here, too, there is an effect of reaction rate on the hydrodynamics of the flow. Detonations under these circumstances can be considered as steady despite the fact that the reactions are perturbed by the lateral rarefaction. The so-called "diameter effect" will therefore be briefly considered. It is apparent to most of us that the area of non-steady detonations is of utmost importance. From a practical point of view it is here that the problems of safety on the one extreme and reliability on the other must be attacked. From the scientific point of view it is an area of challenging problems. At one time not too long ago the "Theory of Detonation" was the theory of steady flows. Today we recognize that this is only a special case of a much broader problem, namely, to develop: "The Theory of Non-steady Flows with Exothermal Reactions". Before this theory can be spelled out unambiguously we must define the important variables and determine their properties. Some of the variables are apparent, some are still to be found. Much of the early work largely concerned with shock initiation suffered from lack of understanding of the amplitude, position and time

variations in the initiating shock. There was further
lack of even qualitative understanding of the role played
by rarefaction waves. Though the situation is somewhat
better today there is still a tendency in some of the
work going on to ignore the importance of these factors.
The search for other variables of importance is meanwhile
going on. We seem to have a need to go beyond the simple
concepts of grain burning theory versus homogeneous
reaction theory. The mechanism for the chemical reaction
under shock seems now to require greater sophistication.
A promising area of study seems to be emerging from the
disciplines of solid state physics and chemistry. Mean-
while new effects are being discovered, and these must
be fitted into the picture. The papers of Winning(1) and
Gibson, et al(2) should prove to furnish interesting food
for thought. Recently it was discovered at UCLRL that a
solid explosives could be made insensitive to detonation
by preshocking the explosive. A detonation was found to
fail if it entered a region in which a weak shock had
already passed. The observation is very reminiscent of
what has been called "dead pressing". (This experiment
will be illustrated later.) The results of this new work
may be of great value in filling out the picture on the
shock initiation in finite cylinders. Electrical effects
(conduction and charge formation) have been found in
dielectrics including explosives subjected to shock. The
consequences of these effects need to be placed in proper
perspective. The author has taken advantage of this
opportunity to collect a bibliography of the papers which
he has found useful in the field of non-steady detonations.

Early Work

It has long been known that detonation could be
initiated by the effect of a detonation from a donor
charge separated from the test charge by an air gap or an
inert gap. Most detonators, for example, are cased in
metal sheathes, yet they can cause detonation in many
explosives. As far back as 1931 a bulletin of the Bureau
of Mines(3) described a gap test (air) for the determi-
nation of the sensitivity of an explosive to detonation by
"influence". This test is undoubtedly much older than the
bulletin date. Other early gap tests have been cited by
Eyring, et al(4), without source reference. Prior to 1944
the interest in non-steady effects was largely tied to
practical problems. There was work on minimum booster
requirements and work on failure diameter. A few smear
camera observations were made on fading of detonation.
I have some old slides by Messerly and MacDougall who
worked at the Bureau of Mines (Bruceton) on an OSRD

contract showing fading, low rate detonation*and the effect of inert gaps on the propagation of detonation.

It was about the end of 1944 before any serious attempt was made to study initiation of solids and liquids by shocks. A project of the National Research Council (Canada) to study initiation by shocks was undertaken at this time by Herzberg of the University of Saskatchewan. Using both still photography (time average observation) and smear photography Herzberg and Walker(5, 6) brought to light a number of interesting observations. Using "point" initiation, the point being a detonator or a cylinder of comparable diameter ($\sim$1/4 inch). They unambiguously showed the existence of the hook in smear camera records when a large cylindrical charge was initiated at one end on its axis. When the detonator was moved to the edge of the charge a "dark zone" was apparent. They found that cardboard sheets placed between the detonator and the test charge caused the point of detonation emergence in a receptor charge to move away from the point of initiation. They found the critical gap at which no detonation would propagate was quite sharp, like ±1 card in 20 (see Eyring(4), p. 139). The observation of the hook led Herzberg to the hypothesis that a displaced center of initiation existed, that the shock from the detonator caused a "low order" detonation to propagate into the acceptor and that this low order suddenly jumped to high order. In the last of his papers(6) it was said that this was a new kind of low-order detonation. One sees here a groping for words to describe a phenomena and a choice of words which really had never been defined, that is, "low order detonation". When Herzberg first presented a discussion of his early work at a meeting at McGill University (Toronto) late in 1944 it excited considerable interest and stimulated Elizabeth Boggs(7) of the Explosives Research Laboratory, ERL (Bruceton) into considering a number of new experiments to establish the facts of the "hook effect". She first set down a number of working hypotheses. These centered on two basic conflicting arguments: a) the displaced center argument of Herzberg, and b) a propagation theory of her own. The latter may be paraphrased as follows: "a) The wave may propagate from the 'point' of initiation with a non-spherical front arising from variation in velocity with direction, and b) The wave velocity, in addition, may be a function of distance from the initiating point". The experiments

---

* As far back as 1928 records of this type had been obtained. E. Jones(24) reported such records and, incidentally, the curved front in normal detonation at that date.

showed clear evidence that the wave in TNT was not propagating as a true spherical front and that the wave also varied in velocity with distance and direction. The discussion of Boggs anticipated many later explanations. It is striking that neither worker ever mentioned rarefaction wave or shock wave in connection with their experiments. It seems that at that date waves with reaction were just called detonations. If the ideas of "shocks with reaction" and "rarefactions with reaction" are introduced and applied to the interpretation of the experiments discussed by them the results become quite clearly explained. The works of Herzberg and of Boggs are worthy references. They contain much of value despite their age. Ground covered by Herzberg has included: a) "Hook" observations, b) Dark zone, c) Preferential detonation in an axial direction ("channel" detonation), d) Gap test, e) Non-uniform spreading of detonation in liquids, f) Re-initiation after fading in thin layers of explosive detonated at a center. Boggs has described: a) Acceleration from shock to detonation, b) Effect of off-axis propagation, c) Detonation around a corner or around an arc.

During the war Jones[8] added some approximations to the ideas of Prandtl-Meyer flow (see ref. 9) behind a detonation wave to estimate the perturbation of lateral rarefaction on the detonation velocity in cylinders (the diameter effect). Eyring[10, 11, 4] used theoretical arguments to show that the detonation in cylinders would have a curved front due to lateral expansion and then developed an alternate perturbation theory on diameter effect. In addition the group under Eyring at Princeton undertook to explain many of the non-steady effects in detonation by use of approximate theory. Many of these approximations can now be improved upon but they still are useful in giving a mathematical "feel" for the problems. The papers remain an interesting and useful source of ideas. Another source of theoretical concepts is the work of Finklestein and Gamow[12]. A number of additional references pertinent to the early work on non-steady detonation is to be found in a recent survey paper by the author[13].

Post World War II Research

The period 1945-1950 saw limited activity in non-steady detonations. Eyster, Smith and Walton[14] developed a gap test in which wax was used as the inert barrier. They reported 50% gaps for a number of explosives. They explored the effect of gap material and

donor charge height as well. The result of the work gave us relative values for minimum shock strength needed to initiate explosives of various composition, density and state.

Bowden stimulated considerable thought on explosive initiation by his papers of this period. The work is summed up in Bowden and Yoffe(15). Of particular interest is the experimental work concerning deflagration to detonation transition. Deflagration was initiated by mild impact or by spark discharge. Along similar lines Roth(16) described a number of experiments on deflagration to detonation at the First ONR Symposium on Detonation. The non-steady aspects of detonation were touched on in several other papers of that symposium. The following should be mentioned: a) Initiation of detonation in PETN by an exploding wire (Dewey); b) Small scale gap test, Anomalies in the Detonation of Hydrazine Mononitrate (Price); c) Comments on Chemical Aspects of Detonation (Lewis); d) Non-stationary Detonation Waves in Gases (Kistiakowsky); e) Some comments on the reaction zone in detonation of finite charges (Jacobs); f) An introduction to the Goranson experiment on detonation pressure and shock Hugoniots for solids (Ablard); g) Boundary Effects on Detonation Velocity (Parlin and Eyring).

An important result concerning the shock to detonation transition was found by Mooradian and Gordon(17) in a study on gases. They observed that both the shock front velocity and peak pressure increased in the reactive gas after entry of a shock leading in most cases to an "overshoot"; i.e., a value in excess of that for a steady detonation. They remarked:

"There can be little doubt that the pressure rise
behind the shock front is due to combustion of
the gases in this region. Flames situated some
distance behind a shock front have often been
observed photographically. The gas, compressed
and heated in the shock front, begins to react
slowly, and the reaction accelerates from self-
heating. Accompanying the rise in pressure due
to the combustion, there will be a flow of gas
out of the burning region. This gas flow will
serve to reinforce the shock wave, which, thus
intensified, will initiate a still more rapid
combustion in the fresh gas. Thus the effect can
be rapidly accumulative, until at some point,
presumably when the shock wave is sufficiently
strong, the phenomenon takes on the characteristics
of a detonation. In this "build-up" period, just

prior to detonation, pressures considerably
higher than the stable detonation pressure
sometimes appear,---".

This observation and interpretation for gaseous initiation
appears applicable to the shock initiation of solids and
liquids as well. (See comments by the writer(18). Many
other workers have independently arrived at the same con-
clusion.)

In the course of studies on the shock initiation of
nitromethane at Los Alamos an interesting experiment was
devised by T. P. Cotter(19) to observe the time of initial
shock entry into a bath of the explosive, the luminosity
developed by reaction as a function of time and the shock
pressure responsible for the initiation. The transparent
liquid was shocked by an oblique shock through a barrier
containing a mirrored surface. The experiment was arranged
so that light from a region already reacting reflected off
the mirror into a smear camera. The time of shock entry
was clearly obtained in this way by light cut-off. Later
the camera sees light due to reaction. Varying the barrier
thickness permitted observations on "induction time" vs.
shock amplitude. The use of velocity synchronization of
the phase velocity across the boundary to the smear camera
velocity sharpened up the details considerably. Shock
strengths were determined in separate experiments by using
reflected light intensity at the shock front to determine
the index of refraction of the shocked explosive. Index
changes were related by the Lorenz law to the density in
the shocked liquid. Control experiments with Lucite
showed the index of refraction measurements to give den-
sities in agreement with those found by more conventional
methods. In nitromethane mixtures the records showed a
dark zone, an abrupt change to a zone of moderate light
intensity followed by a second abrupt change to a high
luminosity which gradually decayed to a steady value. In
interpreting the records Cotter made no distinction as to
where the luminosity was arising in relation to distance
from the boundary. He interpreted the brightest flash as
indicating quite nearly the time to complete reaction.
The earlier intensity increase was hypothesized to be due
to partial reaction. Times from shock entry to either
light change are proportional to each other so that
selecting either as an induction time would cause no great
error in interpreting the records in terms of an Arrhenius
equation for chemical reaction. Chaiken(20) has raised
a question as to the interpretation of the observed time
of peak luminosity. He has suggested (and there is good
argument to follow his suggestion) that the peak luminos-
ity arises from a detonation in pre-shocked explosive

overtaking the shock front. The decay to normal luminosity
is then easily explained as the decay of an overdriver
detonation. The first luminosity to appear has been sug-
gested by Chaiken to be light from a detonation originating
at the interface with the shock degrading mirror. (A paper
by Chaiken(21) at the 3rd Detonation Symposium indicates
that he will discuss this point in greater detail.)
A question raised by this interpretation is "why should
the luminosity of a shock in a precompressed region be less
than that in an uncompressed region?" One answer suggested
is that the temperature of this detonation is, in fact,
lower than that of a normal detonation. This could be the
case if the internal energy in a highly compressed medium
is very large. Many workers on equation of state believe
this is so. The paper by Cotter makes interesting reading.
It contains many novel ideas and techniques for the study
of detonation phenomena.

Smear camera records of the initiation of an explo-
sive (Pentolite) by an air shock from a donor charge were
discussed by Sultanoff and Bailley(32) in a BRL Report.
It was shown that the steady detonation trace in the
acceptor (seen on the charge surface) when extrapolated
back to the air-acceptor boundary always indicated a time
later than the time of arrival of the air shock at the
boundary. Through this observation the expression
"delay-time" seems to have been coined. Delay times were
reported for several air gap distances. A later paper from
BRL by McVey and Boyle(33) extends the work on "sympathetic
detonation" to Composition B. The Sultanoff paper contains
a few flash radiographs of the initiation of the acceptor.
It is unfortunate that the reproductions are rather poor
because the technique should be of great value in answering
some key questions concerning the flows occurring behind
the initial shock.

At the 27th International Congress of Industrial
Chemistry (Brussels, 1954) two papers of interest were
presented. Shamgar(22) describes a gap test similar to
that of Eyster. To show the precision of the cut-off gap,
data was presented on the percentages of detonations vs.
gap height using 20 trials at each of seven gap heights.
The data shows a normal distribution in the frequency of
detonations for both TNT and Pentolite. The standard
deviation of the 50% point is about 1% of the critical
gap. Winning and Sterling(23) presented some interesting
Argon flash-bomb photographs on the initiation of Pentolite
cylinders by spherical shocks in water from the detonation
of a Pentolite sphere initiated at its center. Features
of the shocks and product of detonation are clearly seen
for various stages of the initiation process.

It was about the time of the Second ONR Symposium on Detonation (February 1955) that we began to see an upsurge of interest in the study of non-steady detonations. By this time a "feel" had been acquired for hydrodynamical problems associated with detonation through the work of Gorenson, Walsh, Schall, and Pack to mention a few of many contributors. (See reference 13 for bibliography). The idea of reaction in shocks and rarefaction waves was beginning to replace the ambiguous concept of low order detonation. At the Second ONR Symposium on Detonation a paper given by Kirkwood and Wood(25) described the structure of steady state plane detonation waves with finite reaction rates in formal mathematical terms. A second paper on diameter effect(26) was discussed by these authors with equal formalism. A particularly inter- esting report on non-steady effects in the detonation of liquids and single crystals was presented by Campbell, Malin and Holland(27). They described failure waves in nitromethane, showed the effect of thin foils in sustaining detonation, illustrated a failure in detonation in nitro- methane on emerging into a large container after propa- gating in a tube and described the first wedge experiment to observe the transient wave propagation when a single crystal of PETN was shocked by a plane shock wave. This latter experiment showed initially a shock in the crystal (it was called low-order detonation) followed by an over- shoot in velocity which subsequently dropped back to normal detonation velocity. The result is strikingly similar to that described by Mooradian and Gordon for gases. An amplification of the single crystal experiment appears in reference 28. Some very precise measurements on the effect of particle size and diameter on detonation velocity were presented by Malin, Campbell and Mautz(29). New experimental evidence on the low velocity detonations in liquids and loose solids was presented by Gurton(30). Dewey(31) reported on the results of projectile impact in initiating detonation. The most significant conclusion in this paper was that when blunt nosed cylinders were fired at the explosive the velocity of impact to cause detonation was independent of the projectile length but dependent on its diameter. The shortest projectile used was 1/2" long. Diameters were 0.3 and 0.5". Work by Whitbread and his associates to be described later confirmed this result and added significantly to its interpretation.

A classified meeting concerned with detonation wave shaping held at the Jet Propulsion Laboratory in June 1956 brought out several unclassified papers on shock initiation and a lively discussion on the subject. Majowicz(34) described an experiment in which pellets of explosive were initiated by an oblique shock. The

"delay-time" was correlated with the surface velocity
induced in an aluminum gap when the explosive pellet was
not present. Sultanoff(35) showed both smear and framing
camera records of the initiation of an acceptor through
air and steel for both end shocks from a donor and oblique
shocks in a sandwich arrangement. The latter showed the
arrival of the shock in the acceptor quite clearly by a
surface effect and showed break-out of detonation to occur
at a point removed from the interface as is customarily
observed for axially symmetric donor-gap-acceptor arrange-
ments. Cosner and Sewell(36) presented smear camera
results on the initiation of cylindrical Composition B
charges by cylindrical donors through blocks of steel of
varying thickness. The charges were 2-1/8 inch diameter,
3 inches long and the barrier plates were 7" diameter. It
was found that break-out of detonation in the acceptor
occurred as far as 68 mm (over 2-1/2 inches) from the
acceptor-barrier interface. An unusual result was that
within experimental error the break-out distance for
varying barrier plate thickness was linear with time
reckoned from the time of entry into the acceptor in the
range of 15 to 68 mm from the interface. The apparent
velocity of the primary wave deduced from the slope of
the break-out distance-time curve was given as 2.54
mm/μ sec, a value very nearly that of an acoustic wave,
i.e., a wave of low pressure amplitude which could be
either an elastic or a plastic wave. The results of
Cosner and Sewell have been verified by other workers
(41, 42, 45). An impromptu discussion of the shock to
detonation transition was presented by the writer at this
meeting(18). The problem was primarily discussed in one-
dimensional hydrodynamic terms because under these con-
ditions the description of the flow and compression effects
is considerably simplified. In essence it was postulated
that the temperature rise accompanying compression due to
the shock entering an explosive initiated a reaction first
at the boundary to the barrier and later behind the shock
as it progressed. When significant reaction is complete
at the boundary it will result in additional temperature
rise and a pressure increase. The temperature rise
accelerates the reaction; the pressure increase propagates
as a wave to accelerate the shock in a manner as previously
quoted from Mooradian and Gordon. Eventually the reaction
is so fast that at some point in the medium a true deto-
nation is formed. It may develop as a continuous acceler-
ation of the shock front or it may develop behind the
primary shock and overtake the latter. In the event that
a high pressure wave develops behind the primary shock it
is probable that the wave front will temporarily exper-
ience an "overshoot" in velocity, i.e., an overdriven
detonation is formed. This overdriven wave will then

decay to a normal detonation for lack of support. It was pointed out that in the initiation of cylinders one must add the effect of rarefaction waves due to lateral expansion. Transition to detonation appears to be a competition between acceleration effects on the shock wave due to reaction and decelerating effects due to rarefaction. The same thesis had been voiced, though in less detail, in the Cosner-Sewell paper. It has apparently been accepted, in principle, by most workers in the field. In extending this theory to apply to finite charges only rarefaction effects have seemed to be required as a dominant variable. A few workers, notably the explosives group at Utah University, have held to the theory that long range heat transfer is a dominant factor in the growth of detonation from a shock. The papers of this group first considered heat transfer through the barrier plate as a necessary condition for detonation. As a consequence their papers have repeatedly referred to the barrier as a "shock pass heat filter". Later the idea of a heat pulse from the donor seems to have been dropped in favor of a heat pulse from the early reaction at the boundary. To account for a strong thermal pulse observations which indicate that strong shocks cause the explosive medium to become an electrical conductor (formation of a metallic state) are used. In applying these arguments the "heat pulse" seems to have been given properties not described by the usual heat conduction equations. Recent theoretical work being reported by Enig based on the Navier-Stokes equation (equations of motion with heat transfer and viscosity included) lead us to believe that even abnormally large heat transfer coefficients cannot cause the thermal term in the equations to take precedence over the momentum terms in determining the transient flow or the reaction. Heat transfer is a contributing factor whenever a surface burning reaction is present. It has been found to have some small effect in rounding off the shock fronts but this appears to be extremely short range in the mathematical analysis.

The reactions taking place behind a shock wave can be considered as deflagrations if one chooses. Courant and Friedrichs (reference 9, p. 208) have discussed deflagrations in this sense. They go even further to show a Chapman-Jouguet detonation as a combination of a shock and a Chapman-Jouguet deflagration. We could therefore call a shock initiation event as a transition from non-CJ to CJ deflagration behind a shock. When the workers studying potential runaway of the burning in solid propellants coined the amusing letters DDT they

implied a definition which referred to transition from
flame initiated burning to detonation. Since DDT has
now been given more than one meaning it seems necessary
that the specific meaning be more precisely spelled out.

In May of 1957 the Royal Society (London) sponsored
a "Discussion on the Initiation and Growth of Explosion in
Solids" under the leadership of Dr. F. P. Bowden(37).
Seven papers were presented on the growth of explosion.
Yoffe(38) confined his remarks largely to growth of explo-
sion from small centers in primary materials. He pointed
out the importance of break-up of crystals in reaction of
solids. This may be a worthy clue to follow in regard to
some of the yet unexplained details in the initiation of
cylindrical acceptors by relatively weak shocks. Andreev
(39) also pursued the thesis of break-up in the initiation
of solids, suggesting that fast reaction rates develop due
to a suspension of solid explosive in the gaseous products.
His arguments concerning charges of low bulk density
require no mechanism for break-up since the porosity is
already present. In this case the discussion resembles
that of Kistokowsky(58). He suggests that liquids can
form droplets near a shock front due to instability and
turbulent effects. The remarks made seem well worth
considering in regard to both shock to detonation transition
and in regard to the runaway deflagration of explosives
and propellants.

Various aspects of the donor-gap-acceptor experi-
ment were discussed in the 5 remaining papers. Cachia
and Whitbread(40) discussed details of a small scale gap
test. They indicate how the shock pressure decays with
distance in a brass cylinder shocked by a donor charge
and show examples of shock velocity acceleration and decay
in acceptor charges. Their theory of the mechanism of
shock initiation parallels the picture previously dis-
cussed. Eichelberger and Sultanoff(41) describe gap tests
with smear and framing cameras and point out that initi-
ation by impact from a high speed projectile produces the
same transition history as does the shock from an inert
barrier. The discussion supports the theory on initiation
already mentioned. Air shock pressures from donor charges
were given. They show an apparent order of magnitude
difference between amplitude of shocks through air and
shocks through solids in the initiation of an acceptor.
This apparent difference is likely to vanish when reflected
pressures and subsequent pressure build-up due to gas flow
from the donor is taken into consideration. Further
evidence confirming the findings of Cosner and Sewell are
to be found in the paper by Cook, Pack and Gey(42).
A later paper by this group and L. N. Cosner(45) amplifies

on the experimental work and discusses the "heat pulse" hypothesis.

Marlow and Skidmore(43) used a pin probe method to determine the shock front velocity in both gap material and acceptor charge of a typical gap experiment. From their measurements shock pressure in the gap material (steel or aluminum) was determined as a function of "initiation delay". Application of impedance conditions between barrier and acceptor indicated that a 20 kilobar peak pressure in the explosive (Composition B) was about the lower limit for causing detonation in 2 inch diameter charges. They inferred that both peak pressure and the shape of the pressure decay behind the shock wave are important in determining the transition to detonation. The conditions for build-up to detonation are interpreted in terms of the model in which competition of rarefaction waves and reaction effects determine whether the shock will accelerate to a detonation. Winning(44) described some new experimental work following the underwater shock methods previously used by him(23). The experimental arrangement using a spherical donor charge in a large water bath is particularly attractive because the shock wave in the water has spherical symmetry. Consequently the peak pressure and the pressure-time relation behind the shock can be defined with precision. Winning has used the results published in Cole's "Underwater Explosions" (Princeton Press, 1948) to define pressure in the water with distance. Somewhat better results could be obtained today by using the shock velocity in the water and the better Hugoniot equation of state for water which is now available. The data indicate that shock pressure of the order of 10 kilobars in the water will initiate detonation in the 50/50 Pentolite charges investigated. A number of experiments with modified boundaries near the acceptor are described.

The gap experiments used by most investigators yield useful results on relative shock sensitivity and permit one to see qualitative features of the processes taking place. They are difficult to interpret quantitatively in terms of pressure vs. time since the waves and flows in both barrier and acceptor are influenced by both lateral rarefactions and rarefactions in the direction of the donor charge (the so-called Taylor wave). Though more difficult to perform, experiments with large donor charges which are plane wave initiated should be easier to interpret since one-dimensional hydrodynamic equations should be very nearly applicable to their analysis. The wedge experiment of references 27 and 28 and the large

scale experiment of reference 19 suggested to Majowicz and Jacobs(46) a method for observing the shock to detonation transition in essentially a one-dimensional system. In order to be able to work with weak shocks in the acceptor and to apply the method to relatively opaque solids a wedge experiment was devised in which the arrival of a shock on a 25° wedge of acceptor was signalled by the interruption of light reflected from an exploding wire by a metallized plastic film attached to the surface. The shallow wedge angle of 25° makes it almost certain that the surface blow-off after shock arrival on the thin side of the wedge will not perturb subsequent shock and reaction effects associated with the remainder of the shocked explosive. Smear camera records were made of both the boundary effect in the acceptor wedge and the motion of the barrier plate through which the explosive was shocked. This gives sufficient data to determine points on the non-reaction Hugoniot for the explosive as well as to determine the progress of the shock wave in its transition to detonation. Much as predicted the transition in several cast explosives appears as a continuous build-up to detonation velocity without overshoot. In some solids more recently studied, e.g. TNT and Composition B at about 90% of theoretical density the transition involved an overshoot to a velocity in excess of normal followed by a decay to normal detonation velocity. This result is very much like that described in reference 28 for a single crystal of PETN. The Hugoniot data published in reference 46 was later found to be in error due to a drop-off in free surface velocity of the barrier plate in the region where the measurement was made. A second error was introduced by using shock impedance relations to determine the initial particle velocity and pressure in the acceptor explosive. After correcting the data, using the measurements of Drimmer for the free surface velocity of the brass barrier and Walsh's data for the Hugoniot of brass it is found that the shock pressures for the HE previously quoted should be reduced by approximately 20%. The compressed density will also decrease. Details will be reported in the unclassified write-up to be issued in the not too distant future.

A classified conference on explosive sensitivity held at NOL in 1957 resulted in several papers on shock initiation. These may be found in Reference 47. One report (Rice and Levine) will be singled out because it describes a new approach to the study of the effect of shocks on chemical decomposition. A perchlorate polyurethan propellant, 1" square cross-section, was subjected to a modest shock from a 1-5/8" diameter plane wave booster (baritol-pentolite) through 1 inch of steel.

The shocked charge was recovered, sectioned, and analyzed. It was found that the amount of perchlorate in the samples had decreased; the greatest decrease occurring at points in the charge where the shock amplitude would have been greatest. The shocks were much too weak to have resulted in appreciable temperature rise on the average. One must conclude that local regions had been subjected to sufficiently high energy to cause decomposition. Hot spots were postulated as being formed. One should not rest with this conclusion. Local inhomogeneities can cause shears or fractures and these could be the means of hot spots for motion.

The mechanism for build up to detonation from shock has been one of the problems undertaken by Aernutronics under a Bureau of Ordnance Contract on the "Study of Detonation Behavior of Solid Propellants". Their first and second Quarterly Reports(48) describe the computation of shock to detonation transition in a one dimensional model based on the equations of motion without heat transfer and viscosity terms and based on an Arrhenius equation for chemical reaction. Although the number of points used in a von Neumann Richtmyer approach to the numerical solution is small, the results show clearly the onset of reaction at the point where the shock begins and a reactive wave overtaking the primary relatively unreactive shock. Two examples are shown in which the initial pressure pulse is cut off after a time, . They show a distinction between failure to detonate and build-up to detonation. The time difference is very small in the examples chosen being τ = 0.70 μ sec as sufficient to establish a detonation and τ = 0.69 for failure to detonate. The work was subsequently published by Hubbard and Johnson(49). Later work under this contract(50) has included a) the varying of the parameters; b) introduction of a model for decomposition combining homogeneous and surface burning reaction in competition with each other; c) addition of dissipation to simulate lateral expansion; and recently d) an attempt to introduce heat transfer and viscosity terms in the equation of motion. At this stage of the work it is quite evident that the build-up to detonation can be demonstrated mathematically without recourse to the inclusion of heat transfer or viscosity effects.

Brown, Steel and Whitbread(51) reporting on the impact of metal cylinders to initiate explosives showed that the velocity for 50% probability of detonation was independent of length until the length was in the vicinity of 1/4 to 1/10 of the diameter. For 3 metals at a given diameter it was shown a) that the time for sustaining the shock to effect detonation in the explosives was independent

of the metal used, and b) the amplitude of the shock in
the explosive was also independent of the metal used.
This result may be taken as experimental evidence of the
amplitude-time dependence for go-no go predicted by
numerical calculations as cited above. The critical
thickness in cylinder impact at a given velocity is indic-
ative of the condition that for long cylinders lateral
rarefaction in either the HE, or the metal, or both deter-
mine the effective duration of the pressure pulse. For
thin disks the thickness determines the pulse duration.
The critical cylinder height may be assumed as that at
which rarefactions from the rear are strongly adding to
the lateral rarefaction to quench reaction build-up. One
would expect for higher impact velocities in a given
diameter that the back rarefaction would become completely
controlling.

In the studies of detonation propagation and also
in shock initiation some unusual effects have been
reported. In discussion of the card gap test using nitro-
methane as the acceptor, Van Dolah and his coworkers(52)
showed the 50% gap was increased when aluminum was sub-
stituted for steel as the confining tube. Both tubes were
of equal wall thickness. One might attribute this
reversal of expectation to a catalytic effect of the
aluminum. In another report by this group(53) on an
amine-nitric acid mixture, however, one finds that the gap
height is also increased when the wall thickness of alu-
minum, steel and glass is decreased. This result suggests
that either a flow effect at the boundary between the
acceptor and the container or a rarefaction may be respon-
sible for the apparent increase in sensitivity. Adams,
Holden and Whitbread(54) reporting on the shock initiation
of single crystals of RDX have shown a related anomaly.
They found instances in which the crystal was initiated at
the free boundary of the crystal. They suggest fracture
and spalling into air as a possible explanation of their
result. Winning(55, 1) has found a case in which nitro-
glycerine was not initiated by the shock from a detonator
or through a gap but in which subsequent initiation
occurred in a region where rarefactions from the lightly
confined boundaries was undoubtedly present. Similar
results were found by the Bureau of Mines group(2).

An opposite effect has been found by a number of
workers. Johansson, et al(56) found that detonation in a
dynamite charge in a polyethylene tube of greater inner
diameter than the charge diameter could be quenched after
initiation. The effect was explained by noting that air
shocks could travel ahead of the detonation and precompress
the charge. This explanation, which appears to be correct,
indicates that for mild compressions the effect of change

in density due to compression can more than offset the
adiabatic heating in determining whether a detonation will
propagate in a given diameter. More recently a similar
but even more unexpected result was found by workers at
UCLRL (Weingart and Eby). A follow-up on the latter work
by Liddiard and Drimmer(57) has confirmed that detonation
in thin layers of duPont's EL-506 could be quenched when
the detonation encountered a region in which a shock of
about 10-20 kilobars peak amplitude was traveling. The
Livermore group has actually recovered part of the explo-
sive in these experiments. These results lend further
evidence to the interpretation that mild shock compression
in solids can reduce the sensitivity to subsequent shock
of high amplitude. Work on a liquid explosive has not
produced as clean-cut a result.

Detonations from Deflagating Explosives or Propellants

The use of large rocket motors containing solid
propellant charges has pointed up questions regarding
development of detonation when the motor is ignited in its
normal mode of operation. Deflagration to detonation
transition (DDT) was coined by workers interested in this
problem as a covering description of the research effort.
The build-up to detonation from a shock has been envisioned
as the final step of a series of events in which deflagration
might accelerate to form shocks followed by the transition
to detonation. In view of this concept, gap tests were
first undertaken to establish the intrinsic detonability
of the materials of interest. It was found that many
propellants could not be detonated even in very large scale
gap tests as long as they were tested in manufactured form.
This result seems to indicate that the explosion hazard
of large propellant grains falling in this category must be
investigated in experiments to determine conditions for
deflagration run-away far short of the actual detonations.

The literature on burning to detonation from fires
is not very extensive at the present time. Kistiakowsky(58)
discussed the mechanism whereby a mildly initiated defla-
gration could accelerate to a detonation in porous beds of
explosive or propellant. Griffiths and Grecock(59) have
discussed experimental measurements and the theory of
burning to detonation. A study of deflagration acceleration
in cast solids has been in progress at the NOL. Maček and
his coworkers(60-63) have found that in heavily confined
steel tubes, cast Pentolite and DINA, relatively shock
sensitive explosives would not accelerate to a detonation
for a relatively long distance after ignition by a hot
wire. Their experiments and theory tend to confirm the

belief that the problem can be separated into deflagration
and shock transition events. It may be pointed out that
gap tests, to be successful, must be conducted in diameters
greater than the critical failure diameter for the material
being tested. Failure diameters for many propellants
appear to be so large that they have not been detonated
without introduction of gross porosity. The Maček experi-
ments showed 1/2" diameter DINA charges (failure diameter
$\sim$ 1/4" unconfined) under heavy confinement to require
several inches of wave travel from the initiator before
detonation would develop. This result leads the writer
to believe that the propellant problem is largely in an
area unexplored by the explosives workers, an area linked
to the effect of compressions on physical properties of
the propellant. Explosives workers can undoubtedly con-
tribute to this area of study as much as they have in
more familiar territory.

An Interpretive Summary

The influence of reaction rate on the initiation of detonation and on the rate of detonation seems to have been recognized long before 1940. There was, however, a vagueness in describing known experimental results. The materials used in a detonator, for example, were classed as primary explosives because they could be detonated when stimulated by a mild thermal energy source such as a hot wire or a spark. The classing of primary explosives as more sensitive might also be accepted as recognition that their reaction rates were higher. Initiation of detonation by influence was experimentally known but the nature of the influence does not appear to have been understood. The effect of diameter and confinement on detonation rates was also experimentally known. The existence of detonations which propagated at low velocity had been established and transition from low rate to high rate under certain conditions was an experimental fact. During World War II two theories of diameter effect were born (H. Jones, H. Eyring). Both recognized that a finite reaction zone or reaction time must exist in the wave and that it was the interplay between lateral expansion and this reaction time which contributed to a slowing down of the detonation. In the early 40's a number of people struggled with the problem of how the reaction was initiated in a detonation and how it proceeded. There was a strong feeling that reactions in homogeneous materials like liquids could not be completed in times of the right order of magnitude if the reaction was initiated by adiabatic compression to detonation pressures. This stumbling block was removed to a great extent when von Neumann suggested that a steady detonation first displays a shock compression at the front and the shock pressure could exceed that of the reacted medium. Meanwhile an explanation for reaction in porous solids leaned in the direction of surface burning reactions initiated at "hot spots". The latter idea was put into a mathematical description by Eyring and his coworkers. The case for cast solids remained as a problem area. Closely linked to the diameter effect were the observations that tapered charges exhibited abrupt failure to detonate when the propagating wave passed from the large diameter end toward the small. The effect has been treated by Eyring as a perturbation of the diameter effect. The abrupt failure was not too satisfactorily explained until much later.

The period 1944-45 saw the beginnings of fruitful studies on the shock initiation of detonation. Herzberg in Canada and Boggs in the United States investigated the transition from shock to detonation and transition effects

in propagating from small diameter columns to large diameter charges of the same composition and density. Both types of experiment gave very similar results in smear camera observations even though it is now apparent that there were some fundamental differences in the boundary conditions. In the experiments where cards were placed between a detonator or a donor charge and the acceptor one may expect that the initial shock in the acceptor will be weaker than that when the initiating column is of the same composition as the acceptor. In both types of experiment we now see that rarefaction waves will influence shock velocity and reaction rates in some regions of the acceptor. The theories of Herzberg (displaced detonation center) and Boggs (non-isotropic propagation) regarding the observations are brought into line when their experiments are examined in the light of hydrodynamic flows with reaction in which shocks, rarefactions and reaction rates are considered to mutually influence each other at the same time. In cylindrically symmetric experiments it is apparent that the shock amplitude in the acceptor is a function of the radius and of the time, being highest in amplitude on the charge axis. When detonators, detonators separated by cards, columns separated by cards or low density donor charges are used the boundary conditions invariably result in shocks weaker than detonations in the acceptor. Under these conditions the reaction must be initiated and then must catch up to the shock front in order to have a detonation in the acceptor. Meanwhile rarefactions follow the shock compression due to the outward motion at several boundaries. The result seen at the charge surface is invariably a hook or a dark zone in the smear camera trace. When the donor column is the same composition and density as the acceptor one might expect the detonation to continue steadily into the acceptor in a cylindrical zone of diameter equal to that of the donor column. This detonation will cause a "bow wave" in the external zone and detonation may be expected to spread radially but show a delay relative to uniform spherical detonation as it propagates due to transition effects behind this weaker shock wave. Herzberg has records which show just this. Even though the detonation never had to develop from a weaker shock in the acceptor core the result is a hook in the wave arrival as seen at the charge surface. It is clear from just the experimental examples of Herzberg and of Boggs that one cannot treat all cases of transition to detonation as manifestations of the same thing unless that same thing includes the interplay between reactions, shock, and rarefactions. Likewise one cannot treat all reactions in shocks as being alike. Some appear to follow homogeneous reaction laws, others seem to require surface burning, and undoubtedly many require consideration of the

competition or cooperation of more than one mechanism in the reaction model.

Except for a lull during the few years following the war one finds the subject of shock initiation of detonation as one of the dominant areas being investigated in regard to non-steady propagation influenced by reaction effects. The investigations are shedding light on the problem. This preoccupation is quite logical. In steady detonations the perturbations on the reaction are relatively small. The steady-state conditions tend to make people lose sight of the chemical reaction as something associated with a particular region in the charge. We think of moving with the wave not the particle in examining the results of our diameter effect experiments. In shock initiation we are more inclined to begin to look at each region in a charge and ask ourselves "What is happening to the material here and how does this compare with what is happening elsewhere?" The recognition of rarefactions as influences on reactions lead us naturally to attempt to eliminate them or minimize their effect. The ideal shock initiation experiment would be that in which an explosive is subjected to a step-shock and then studied to determine its response hydrodynamically and chemically to this shock. We approach this ideal by going to plane wave systems. The work in this direction has demonstrated that it is possible to learn much about explosives in this way. Equally important is the fact that reducing experiments to one-dimensional geometry, even though the shocks may be followed by rarefactions, leads to results that can be analyzed or independently substantiated by numerical computations. In programming a numerical calculation it is now possible to throw in almost any variable for examination. All conservation laws are rigorously adhered to and many models may be examined for the reactions. If one wishes to establish the effect of heat transfer and viscosity; this, too, can be done. In the few instances where these terms have been introduced into computation their influence has been found to be small even when coefficients of viscosity and heat transfer have been made unrealistically large. The computation methods have directed our attention to the need for more precise data in certain areas. For example, we now find need for the equation of state of unreacted explosive, and this equation must define the temperature to a reasonable degree of precision. Even without the best available input data we find computer runs confirming in a general way both the experimental observations and our more recent theoretical guesses based on hydrodynamic considerations concerning the events taking place when an explosive is shocked. By varying the reaction parameters one can find

either a smooth increase in velocity to detonation velocity or a detonation forming behind the shock leading to an abrupt jump in shock front velocity followed by a decay to the normal Chapman-Jouguet detonation velocity.

Experiments which have approximated one-dimensional flows have given us information on the shock Hugoniots for explosives which have not yet reacted. This information has been correlated to the subsequent transition event. It is found that liquids free from bubbles appear to have reaction rates due to adiabatic compression in agreement with thermal decomposition rates for homogeneous fluids. The same appears to be approached fairly well by single crystals. Cast, pressed and loose solids seem to require surface burning concepts to explain the relatively small dependence of transition times on shock amplitude. These materials also show dependence of transition time on particle size (the RDX/TNT system is a good example). To be sure some of the results have been anticipated from old data. Reduction of grain size in TNT castings by cream casting, for example, has long been a requirement for assuring reliable propagation in charges of usual ordnance application. The one-dimensional experiments may be expected to guide us in the better understanding of all initiation problems in which the boundary conditions are more complex. They can supply input data for 2-dimensional non-steady state calculations. We already are able to interpret much of the gap test results in terms of a hydrodynamic model. A fuzzy area develops in gap experiments when it is found that a wave can propagate almost two diameters into a charge at nearly acoustic velocity before a truly high pressure reaction takes place. This can be explained by a slight advantage in the unbalance between reaction effects and rarefaction in favor of the reaction. This would imply that the wave slowly accelerates in rate until at some point reaction is rapid enough to cause rapid speed up of the wave. Although this idea seems to be a satisfactory explanation it would seem to need further confirmation.

The rarefactions behind a shock in a cylinder of explosive are worthy of further examination. Calculations on a one-dimensional cylindrical rarefaction were used by the writer to approximate the condition behind a shock. The results show pressure dropping to zero in the axis region while positive pressures exist farther out. One might expect cavitation behind a shock under these conditions and such cavitation has, in fact, been observed by Vodar in plastic rods. The experiments of Gibson also seem to show cavitation in a column of liquid explosive in which a shock is moving down the axis. It seems

reasonable that cavitation in solids and even liquids can be considered as a fracture phenomenon. This approach could give some accounting for initiation of reaction in a region of rarefaction thus giving a clue to the results of Winning and of Gibson. The argument, if substantiated, could possibly have bearing on the weak shock case for gap experiments in solids.

The effect of acceptor confinement in the 50% gap test for liquids has appeared to be anomalous to the shock-reaction hypothesis in at least two liquids. In searching for new variables to examine for explaining the results we find several to consider. First there is the meeting of rarefactions at the axis. Second, we note that shocks moving along boundaries between two media will generally result in a flow discontinuity at the boundary. The result can be a shear, or a build-up of a viscous or turbulent boundary layer; any of which effects could be the source of enough local energy concentration to start a reaction. In the case of thin walls there is a further possibility of fracture of the moving wall leading to a localized flow of liquid to create frictional heating. In the case of some metals, as for example aluminum, the metal could enter into reaction with the explosive when new surfaces are exposed as a consequence of plastic flow. The experimental result found by UCLRL that weak shocks can make an explosive solid less sensitive to detonation appears to have some bearing on the gap experiment. One can see the possibility that immediately behind the shock in those cases where thick barriers are used the explosive will not be capable of initiation by a second shock even if it is relatively strong. The experiments of Cook, et al, involving colliding shock might find a hydrodynamic explanation in this experimental observation.

The disk impact experiments of Brown and Whitbread have given us useful information on the required pulse duration to cause transition to detonation. In this regard they give more pertinent information than the "delay time" in establishing the induction time. The experiments suggest that for thick disks it is the radial rarefaction in the explosive which is responsible for quenching a reaction initiated by adiabatic compression. If we estimate the sound speed in solid HE from the slope of the Hugoniot p-ρ curve at about 50 kilobars we find a value of about 5 to 6 mm/μsec. This is about the velocity one might expect in aluminum (the metal of highest wave velocity used) at this pressure. The experiment suggests that promising results could be obtained by the use of flying sheets of metal of larger diameter in an experiment employing wedges of explosive and smear camera observations.

The study of detonation effects influenced by chemical reaction rates is seen to be largely concentrated, at the moment, in studies of the initiation of detonation by shocks. This approach appears to be paying off, leading to the acquisition of knowledge which can be applied to the interpretation of results of other experimental conditions in which reaction rates play a significant role. We find experimental evidence which is forcing us to include variables other than adiabatic compression and rarefaction for explanation. The writer believes the variables to be examined are boundary flow discontinuities and localized discontinuities which may be broadly stated as being due to the imperfections in the medium.

* * * * *

NOTE: This review paper has been classified CONFIDENTIAL because of a few references to classified reports. An unclassified version will be written later in order to make the material more accessible.

REFERENCES

1.   C. H. Winning, "Initiation Characteristics of Mildly Confined, Bubble-Free Nitroglycerine", Third Detonation Symposium, (Sept. 1960)

2.   F. C. Gibson, C. R. Summers, C. M. Mason, R. W. Van Dolah, "Initiation and Growth of Detonation in Liquid Explosives", Third Detonation Symposium, (Sept. 1960)

3.   "Physical Testing of Explosives", U. S. Dept. of Commerce, Bureau of Mines, Bull. No. 346 (1931)

4.   H. Eyring, R. E. Powell, H. Duffey and R. H. Parlin, "The Stability of Detonation", Chem. Revs., 45, 1, 70-181 (1949)

5.   G. Herzberg and G. R. Walker, "Optical Investigations of Initiation and Detonation", I, II, III. Project XR-84, Dept. of Physics, Univ. of Saskatchewan, (Mar. 1945-Aug. 1946)

6.   G. Herzberg and G. R. Walker, "Initiation of High Explosives", Nature (London) 161, 647-8, (Apr. 24, 1948)

7.   E. M. Boggs, G. H. Messerly, and H. A. Strecker, "Initiation Studies on Solid Explosives", OSRD 5617 (Dec. 14, 1945)

8.   H. Jones, "A Theory of the Dependence of the Rate of Detonation of Solid Explosives on the Diameter of the Charge", Proc. Roy. Soc. London, A-189, 415 (1947)

9.   R. Courant and K. O. Friedrichs, "Supersonic Flow and Shock Waves", Interscience Publ., Inc., N. Y. (1948)

10.   H. Eyring, R. E. Powell, G. H. Duffey, and R. B. Parlin, "The Chemical Reaction in a Detonation Wave", OSRD 3796, (June 17, 1944)

11.   H. Eyring, R. E. Powell, H. Duffey and R. H. Parlin, "The Stability of Detonation", NavOrd Report 70-46, (15 June 1946) Conf.

12. Finklestein and G. Gamow, "Theory of the Detonation Process", NavOrd Report 90-46, (20 Apr. 1947), Conf.

13. S. J. Jacobs, "Recent Advances in Condensed Media Detonations", ARS Journal, 30, 2, 151-158 (Feb. 1960)

14. E. H. Eyster, L. C. Smith, S. R. Walton, "The Sensitivity of High Explosives to Pure Shocks", NOLM 10,336 (14 July 1949), Conf.

15. F. P. Bowden and A. D. Yoffe, "Initiation and Growth of Explosion in Liquids and Solids", Cambridge Univ. Press, (1952)

16. J. Roth, "Experiments on the Transition from Deflagration to Detonation", p. 51, The Chemistry and Physics of Detonation, Office of Naval Research, (11-12 Jan. 1951), Conf.

17. A. J. Mooradian and W. E. Gordon, "Gaseous Detonation. I. Initiation of Detonation", J. Chem. Phys, 19, 9, 1166-1172 (1951)

18. S. J. Jacobs, "A Theory Concerning the Initiation of Detonation by Shocks", Proceedings of Detonation Wave Shaping Conference, JPL, Pasadena, California (5-7 June 1956)

19. T. P. Cotter, Jr., "The Structure of Detonation in Some Liquid Explosives", A thesis for the Ph. D Cornell Univ. (Sept. 1953)

20. R. F. Chaiken, "Kinetic Theory of Detonation of High Explosives", Mastov's thesis, Polytechnic Inst. of Brooklyn, (June 1958)

21. R. F. Chaiken, "Comments on Hypervelocity Wave Phenomena in Condensed Explosives", Third Symposium on Detonation, Princeton, (ONR, NOL), (Sept. 1960)

22. A. Shamgar and I. Bordman, "Determination de la
     Sensibilite des Explosifs a L'Initiation", Comm. 27th
     Congress International de Chimie Industrielle, Brussels
     (11-20 Sept. 1954)

23. C H. Winning and E. Sterling, "Etude Photographique
     de L' Amorcage de la Pentolite a Travers L'Eau", Ibid

24. E. Jones, "Photographic Study of Detonation in Solid
     Explosives. I. The Development of a Photographic Method
     for Measuring Rate of Detonation", Proc. Roy. Soc. A 120,
     603-620 (1928)

25. J. G. Kirkwood and W. W. Wood, "The Structure of Steady-
     State Plane Detonation Waves with Finite Reaction Rate",
     Second ONR Symposium on Detonation, Washington, D C.,
     (Feb. 9-11, 1955), J. Chem. Phys. 22, 1915-19 (1954)

26. W. W. Wood, J. G. Kirkwood, "Diameter Effect in
     Condensed Explosives. The Relation Between Velocity and
     Radius of Curvature of the Detonation Wave", 2nd ONR
     Symposium Det. (1155); J. Chem. Phys., 22, 1920-24
     (1954)

27. A. W. Campbell, M. E. Malin, and T. E. Holland, "Detonation
     in Homogeneous Explosives", 2nd ONR Symposium Det.
     (1955)

28. T. E. Holland, A. W. Campbell, and M. E. Malin, "
     Phenomena Associated with Detonation in Large Single
     Crystals", J. Appl. Phys. 95, 1217 (1957)

29. M. E. Malin, A. W. Campbell and C. W. Mautz, "Particle
     Size Effect in One- and Two- Component Explosives",
     2nd ONR Symposium Det. (1955); "Particle Size Effects in
     Explosives at Finite and Infinite Diameters", J. Appl.
     Phys., 28, 63-69 (1957)

30. O. A. J. Gurton, "The Role of Gas Pockets in the
     Propagation of Low Velocity Detonation", 2nd ONR Sym.
     Det. (1955)

31.   J. M. Dewey, "Initiation of Military Explosives by
        Projectile Impact", 2nd ONR Sym. Det. (1955)

32.   M. Sultanoff and R. A. Bailley, "Induction Time to
        Sympathetic High Order Detonation in an Explosive Receptor
        Induced by Explosive Air Shock", BRL Rept. No. 865, (May'53)

33.   G. R. McVey and V. M. Boyle, "Sympathetic Detonation in
        Composition B Induced by Air Shock from Pentolite and
        from Composition B", BRL Rept. No. 1048, (Nov. 1956)

34.   J. M Majowicz, "The Effect of Shock Strength on the
        Initiation of High Explosives", Proceeding of Detonation
        Wave Shaping Conference, JPL, Pasadena, Calif.,
        (June 5-7, 1956), Conf.

35.   M. Sultanoff, "Explosive Wave Shaping", (see ref. 34)

36.   L. N. Cosner and R. G. Sewell, "Initiation of Explosives
        Through Metal Barriers", (see ref. 34)

37.   F. P. Bowden, Leader, "A Discussion on the Initiation and
        Growth of Explosion in Solids", Proc. Roy. Soc., A 246,
        145-297 (1958)

38.   A. D. Yoffe, "The Growth of Explosions in Solids", Ibid
        (p. 254)

39.   K. K. Andreev, "Some Considerations on the Mechanism
        of Initiation of Detonation in Explosives", Ibid (p. 257)

40.   G. P. Cachia and E. G. Whitbread, "The Initiation of
        Explosive by Shock", Ibid (p. 265)

41.   R. J. Eichelberger and M. Sultanoff, "Sympathetic
        Detonation and Initiation by Impact", Ibid (p. 274)

42.   M. A. Cook, D. H. Pack, and W. A. Gey, "Deflagration to
        Detonation Transition in Solid and Liquid Explosives",
        Ibid (p. 281)

43. W. R. Marlow and I. C. Skidmore, "The Initiation of Condensed Explosives by Shock Waves from Metals", Ibid (p. 284)

44. C. H. Winning, "The Underwater Shock Wave Initiation of Cast Pentolite", Ibid (p. 288)

45. M. A. Cook, D. H. Pack, L. N. Cosner, and W. A. Gey, "Instrumented Card-Gap on SPHF-Plate Test", J. Appl. Phys. 30, 10, 1579-84 (1959)

46. J. M. Majowicz and S. J. Jacobs, "Initiation to Detonation of High Explosives by Shocks",
a) 8th Tripartite AXP Conference, London (1957), Conf.; b) NavOrd Report 5710, (March 1958), Conf.;
c) Bull. APS. Series II, Vol. 3, No. 4, p. 293 (1958)

47. "Proceedings of the Gilbert B. L. Smith Memorial Conference on Explosive Sensitivity", NavOrd Report 5746, (June 1958), Conf.

48. "Study of Detonation Behavior of Solid Propellants". BuOrd Contract No. NOrd 17945, Aernutronics Systems, Inc., a) 1st Quarterly Rept. Publ. No. U-121(Nov. 1957), b) 2nd Quarterly Rept. Publ. No. U-154(Feb. 1958)

49. H. W. Hubbard and M. H. Johnson, "Initiation of Detonation", J. Appl. Phys., 30, 5, 765-769 (1959)

50. (See Ref. 48) 3rd-10th Quarterly reports (May 1958 to Apr. 1960)

51. S. McM. Brown, D. A. Steel, E. G. Whitbread,
a) 9th Tripartite AXP, Ottawa, Canada (1959);
b) "Sensitivity of High Explosives: Projectile and Gap Tests", British E.R.D.E. Rept. 6/R/59, Conf.

52. R. W. Van Dolah, J. A. Herickes, J. Ribovich, and G. H. Damon, "Shock Sensitivity Studies of Nitromethane Systems", Section on Powders and Explosives, 31st Int. Congr. of Ind. Chem., Liege (Sept. 1958) (Reprinted by Centre de Rechorches Sci at Tech pour l'Ind des Prod Expl, p. 121)

53. R. W. Van Dolah, et al, "Characteristics of Monopropellants", Interim Report, U.S. Bureau of Mines (3/3/58), Conf.

54. G. K. Adams, J. Holden, and E. G. Whitbread, "The Explosive Initiation of a Single Crystal of Cyclotrimethylenetrinitramine", (See ref. 52, p. 1 (1958))

55. Private communication from C. H. Winning, March 1959

56. C. H. Johansson, H. L. Solberg, A. Persson, T. Sjoelin, "Channel Effect in Detonation in Tubes with an Open Space Between the Charge and the Tube Wall", (see ref. 52, p. 57 (1958))

57. NOL Interim Reports. To be summarized in a NAVWEPS Report

58. G. B. Kistiakowsky, "Initiation of Detonation of Explosives", 3rd Sym. Comb., Flame, and Explosion, Williams and Watkins Co., Baltimore, p. 560 (1949)

59. N. Griffiths, J. M. Groocock, "The Burning to Detonation of Solid Explosives", 9th AXP Tripartite, Paper B.3 (4) (1958), Conf.

60. A. Maček, R. W. Gipson, "Sensitivity of Explosives to Transition from Slow Burning to Detonation in Cast Pentolite", NavOrd Report 5758 (1957)

61. A. Maček, R. W. Gipson, P. F. Donovan, "Sensitivity of Explosives, VI Transition from Slow Burning to Detonation; Pressure and Velocity Measurements", NavOrd Report 6104, (1958); b) Ibid, VII, "A Model for Shock Formation in a Deflagrating Solid", NavOrd Report 6105 (1958)

62. A. Maček, "Transition from Deflagration to Detonation in Cast Explosives", J. Chem. Phys., 31, 1, 162-167, (1959)

63. R. W. Gipson and A. Macek, "Transition from Slow Burning to Detonation; Flame Fronts and Compression Waves During Growth of Detonation", NavOrd Report 6759 (1960)

THE SHOCK INITIATION OF DETONATION IN
LIQUID EXPLOSIVES

William A. Gey and Karl Kinaga
U. S. Naval Ordnance Test Station
China Lake, California

Shock Initiation. This study was undertaken in order to
obtain more experimental data on the transition from deflagration to
detonation in explosives which have been subjected to shock compression
from a detonating explosive through an inert barrier. Transparent
liquid explosives were used in order to follow the reaction inside the
explosive, and a streak camera used to obtain high time-space resolu-
tion. The effectiveness of the method is illustrated by Fig. 1, which
is a streak camera picture of the initiation of detonation.

The initiation of detonation of liquid TNT, nitroglycerine
(NG), nitromethane (NM), ethyl nitrate (EN), and trimethylolethane
trinitrate (TMETN), was studied by this technique. The main feature
which appeared is that all these liquids are relatively insensitive to
compressional shocks, compared to solid explosives. This statement
must be qulaified, in that observations were made of detonation of
nitroglycerine through barriers of several centimeters of glass, but
the mechanism is fundamentally different from the initial shock
compression initiation, since detonation does not occur until the
explosive has expanded. This second phenomenon may be more pertinent
to the transition to detonation in solid explosives when subjected to
weak shocks, and deserves more study.

Experimental Procedures. The initiations were photographed
with a .010" slit Beckman-Whitley streak camera operated at 300 to
450 rps, corresponding to a writing speed of 1.9678 to 2.9516 mm/μ
second. The mirror speed was checked on each firing with an electronic
chronograph counter. Eastman Kodak Royal X Pan film was used to obtain
the highest light collection possible. The donor charges were all
3.5 cm. (d) Composition B, 10 to 12.5 cm. in length; the interruptors
6.5 - 8.0 cm. square glass plates; and the receptor explosive was
contained in 4 to 7.5 cm. diameter glass cylinders, with, in some
cases, mirrors mounted on top to view the charge axially on the same
film. Figure 1 shows a typical setup with nitroglycerine as the
receptor with a mirror on top. In most experiments a backlight

FIG. 1. Streak Camera Record of Initiation of Detonation in Nitroglycerine in 5.2 cm. Diameter Cylinder.

consisting of a 3.7 cm. diameter Tetryl pellet in the end of a cardboard 15" tube was used to illuminate the shock transmission in the glass and the events in the explosives.

The explosives used were TNT, Picatinny Arsenal Grade 1; Nitromethane, Eastman Kodak Yellow Label; Ethyl Nitrate, Eastman Kodak White Label; and Nitroglycerine, extracted from special dynamite with acetone and precipitated and washed with water at the firing site. Several analyses of the nitroglycerine showed 99+% purity in each case.

Temperatures of the liquid TNT were measured with a thermocouple. Film data was measured with a travelling microscope to determine , the time between entrance of the shock into the receptor and the transition.

Results of Liquid TNT. The results of a series of shock tests on liquid TNT at various temperatures are shown in Fig. 2 and Table 1. The critical glass thickness for initiation of detonation appears to increase only from 7 mm at 100°C to 9 mm at 170°C. The delay time to transition, measured as the time from entrance to the shock in the receptor to speedup of the shock front viewed in the mirror, cannot simply be plotted vs. glass interruptor thickness because of the influence of ambient temperature. A temperature effect of the shock was calculated from the time delay by the equation

$$\log \mathcal{T} = \frac{A}{RT_o} + B \qquad (1)$$

where
$$A = \frac{\Delta H^{\ddagger}}{2.303}, \text{ and}$$

$$B = \frac{Ch\,RT_o}{Qk\,\Delta H^{\ddagger}}\, e^{-\Delta S/R} \qquad (2)$$

with
$$\Delta H^{\ddagger} = 34.4 \text{ kcal/mole (3)}, \quad Q = 2.23 \text{ kcal/mole,}$$

$$C = 90 \text{ cal/mole/deg}, \quad \Delta S^{\ddagger} = 3.2 \text{ eu. (2)}$$

h is the Planck constant, k the Boltzmann constant, and plotted in Fig. 3.

The data are reasonably self-consistent with temperature rise in the range of 400-500° for detonation.

Figure 4 shows a plot of measured initial shock velocity in liquid TNT vs. glass interruptor thickness, the data including shocks which resulted in detonations as well as failures as indicated. The coincidence of the initial velocities of the shocks in the experiments which resulted in detonations and non-detonations appear to support the postulate that the initial compression wave is relatively
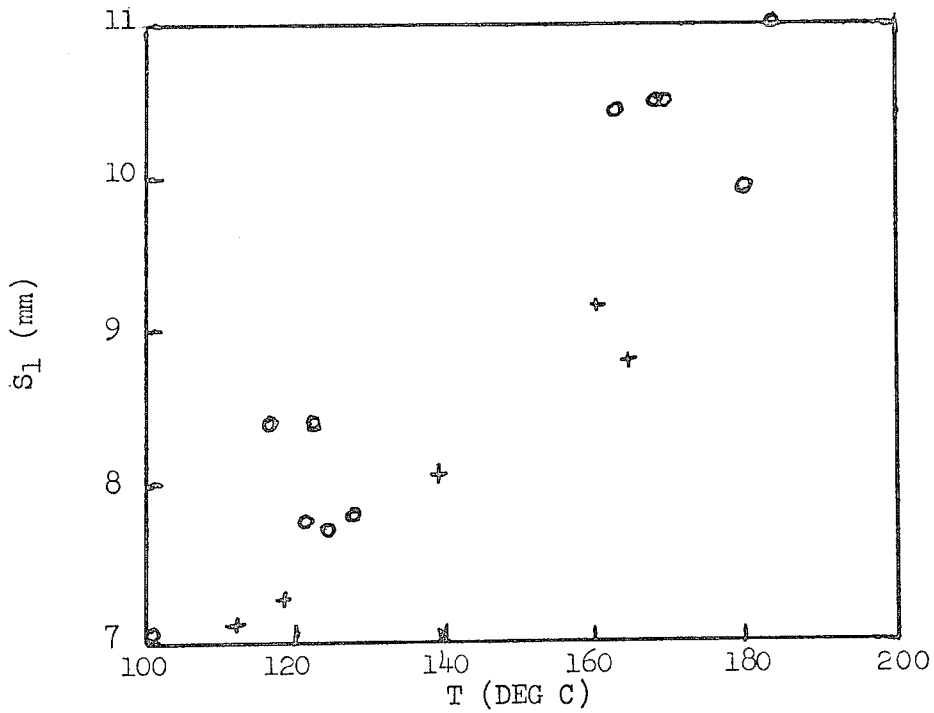
Fig. 2. Glass Interruptor Thickness S_1 vs. Test Temperature Results For Hot TNT. 0, + Incidate No-Go And Go.
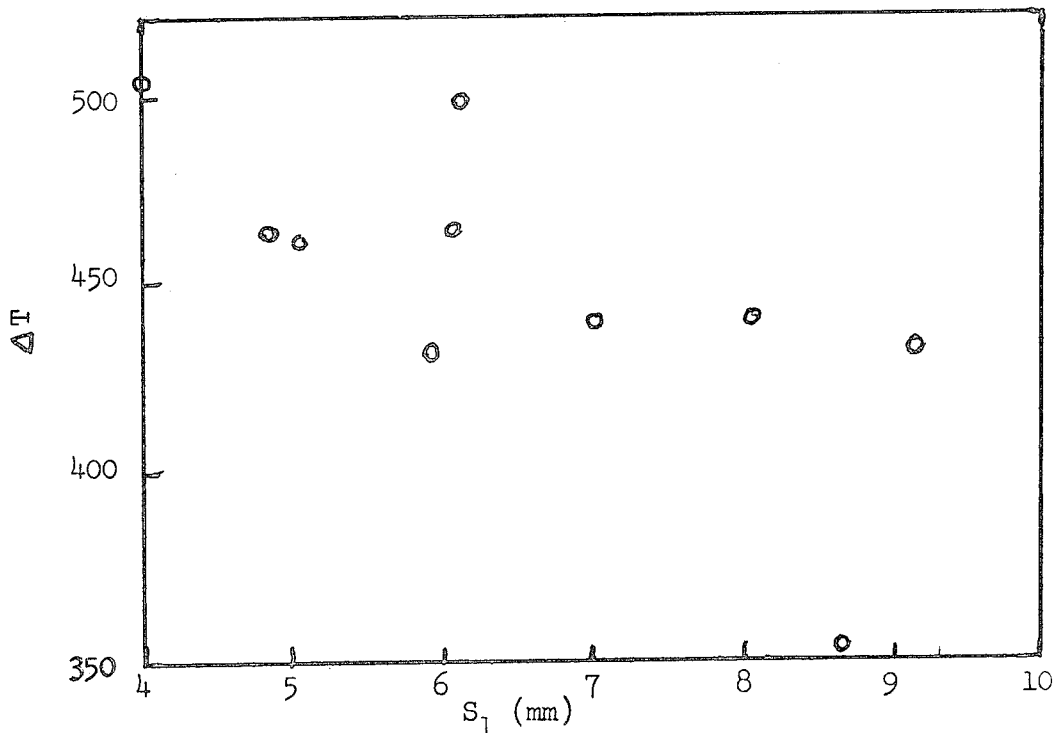

Fig. 3. Calculated Temperature Rise In Liquid TNT vs. Glass Interruptor Thickness.

unsupported by any energy supplied by reaction of explosive (4). There is in the case of initiation of detonation therefore an induction period before the reaction becomes rapid enough to contribute energy to the wave, as outlined by Jacobs. The higher density in the compressed explosive contributes to higher velocity but cannot explain wave velocities above 15,000 m/sec., the appearance of which in detonation wave pictures are probably phase phenomena (5 and 6).

Other Liquid Explosives. The effect of shock on the other liquid explosives all exhibit similar phenomena. Table 2 summarizes the data and Fig. 5 presents the initial velocity vs S_1 results of all these explosives. Again it appears that the initial compression wave is not supported by reaction. Figure 6 shows another initiation of nitroglycerine in a 7.0 cm (d) cylinder, illustrating almost planar initiating wave surface in the image observed by the mirror on top.

TABLE 1. Shock Velocity and Delay to Detonation in
Liquid TNT

Temperature, °C	S_1,[a] mm	Initial wave velocity, mm/μsec	Delay to detonation,[b] μsec	Result
100	4.01	....	0.5	go
100	4.01	....	0.5	go
108	10.46	4050	...	no
110	5.05	....	1.1	go
110	5.1	....	0.5	go
112	7.11	....	...	go
118	7.26	....	...	go
119	6.07	4700	0.8	go
120	4.83	4700	0.8	go
122	8.40	4650	...	no
122	8.4	4250	...	no
124.5	7.7	4350	...	no
127.6	5.92	....	1.4	go
128	7.80	4310	...	no
129	4.83	....	0.5	go
139	8.05	4340	0.9	go
159	12.44	3600	...	no
160	9.14	5300	0.8	go
160	12.20	3890	...	no
162	10.44	3950	...	no
164	8.69	4530	3.8	go
166.5	7.01	....	0.5	go
168	10.50	4150	...	no
180	9.93	4350	...	no
184	10.97	4290	...	no

[a] Glass interruptor thickness.
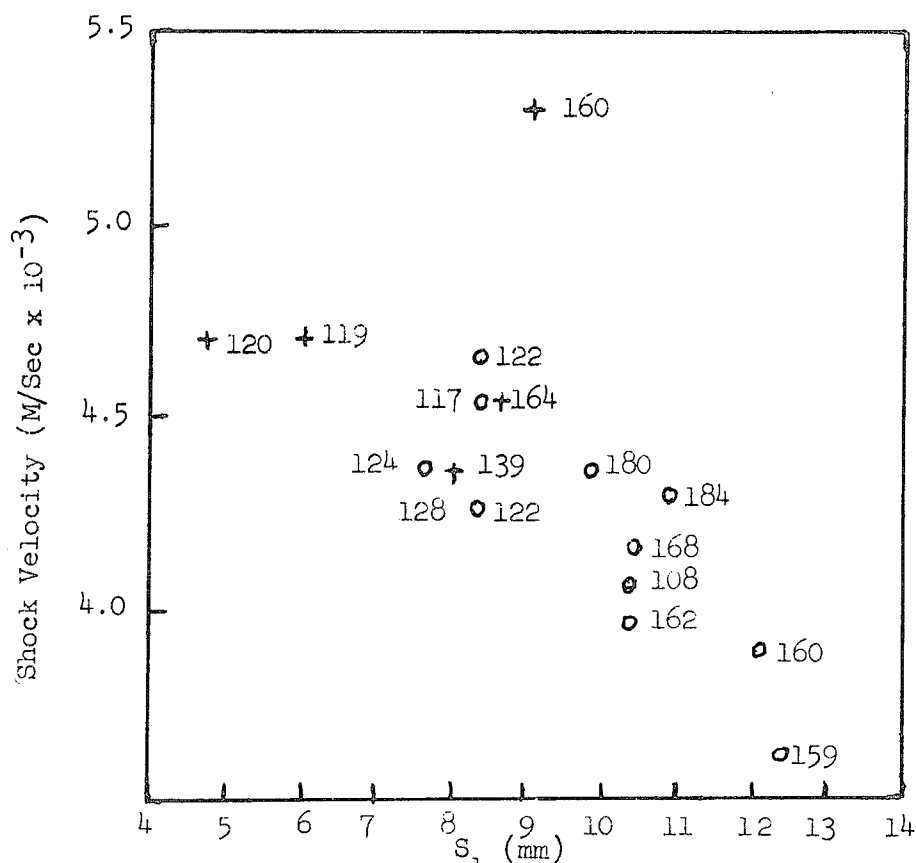[b] Measured as time from shock entering receptor to wave speedup.

Fig. 4. Initial Shock Velocity In Liquid TNT vs. Interruptor Thickness. O, + Indicates No-Go and Go. (Figures Show Liquid Temp.)
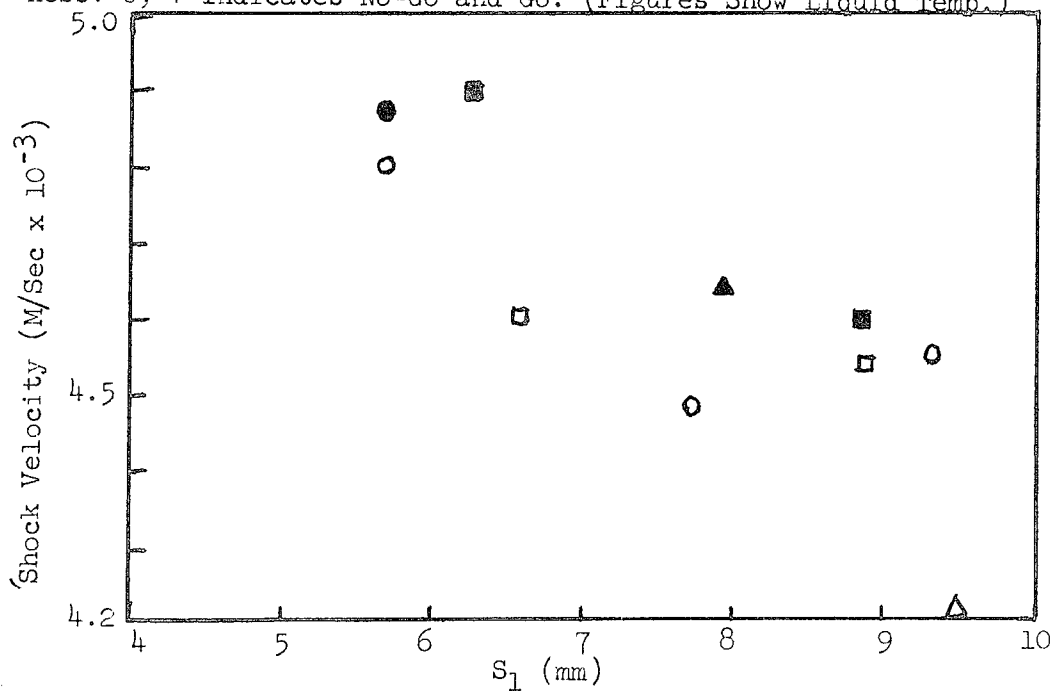

Fig. 5. Initial Shock Velocity in Liquid Explosive vs. Interruptor Thickness. O TMETN, ⌑ Nitroglycerine, △ Ethyl Nitrate ● ▦ ▲ Indicates Detonation Occured.

FIG. 6. Streak Camera Record of Initiation of Detonation of Nitroglycerine in 7.0 cm cylinder.

Summary. A study was made of the initiation of detonation
by shock in transparent liquid explosives in the region of critical
shock intensity. In most cases the velocity of the transmitted shock
in the liquid receptor, for cases which did or did not result in
detonation, was not appreciably different. Delay time to detonation
was used in the case of TNT, with thermal decomposition data, to
calculate the temperature rise in the compression wave as 420 to 500°.

TABLE 2. Shock Velocity and Delay to Detonation
in Other Liquid Explosives

Explosive	S_1, mm	Initial wave, velocity, mm/μsec	Delay to detonation, mm/μsec	Result
NM	6.18	....	0.6	go
NG	4.83	....	0.5	go
	4.95	5800	0.9	go
	6.25	4900	1.8	go
	6.60	4600	...	no
	8.86	4600	2.0	go
	8.89	4540	...	no
	14.38	3140	...	no
	19.3	3988	...	no
TMETN	3.19	....	0.6	go
	4.22	4470	...	no
	5.69	4800	...	no
	5.69	4870	0.7	go
	7.72	4480	...	no
	9.32	4550	...	no
EN	6.02	....	0.45	go
	6.10	....	0.6	go
	6.12	....	0.4	go
	9.5	4220.	1.8	go
÷0.5% quinone	7.92	4640	3.0	go

REFERENCES

1. Ubbelohde, A. R., Phil. Trans A241 (1948) 281.

2. T. K. Collins and M. A. Cook, Tech. Report XLVIII, 15 Dec 1955 Inst. for Study of Rate Processes, U. Utah.

3. A. J. B. Robertson, Trans Far. Soc. $\underline{44}$,977 (1948).

4. S. J. Jacobs, ARS Journal, Feb 1960.

5. C. W. Mautz, N. Y. meeting of APS. Jan 1959.

6. Cook, Pack, Cosner, and Gey. J. Appl. Phys. 30, 1579 (1959).

SENSITIVITY OF PROPELLANTS

W. W. Brandon and K. F. Ockert
Rohm & Haas Company
Redstone Arsenal Research Division
Huntsville, Alabama

ABSTRACT - High explosives are capable of propagating
stable detonation at very small diameters (less than 1/4 inch). Solid
propellants containing reactive binders, such as nitro compounds or
nitrate esters, require larger diameters (from 1/2 to 2 inches), de-
pending upon a number of factors, and are generally less sensitive
to shock initiation than conventional explosives, as measured by the
card gap sensitivity test.

Alumi nized ammonium perchlorate-containing plastisol ni-
trocellulose composite propellant exhibits regular differences in both
minimum diameter and card gap value between steel and cardboard
confinement. Initiation is easier in the heavier confinement. These
differences vanish at charge diameters appreciably above minimum.
As has been shown with ammonium perchlorate alone, perchlorate
particle size in propellant affects minimum diameter in light confine-
ment but not gap sensitivity. Thus larger (65-micron) oxidizer par-
ticle size raises the minimum diameter without correspondingly re-
ducing detonation hazard. The omission of the oxidizer or substitu-
tion of potassium chloride has no effect on propellant critical diameter
or card value in heavy confinement; in light confinement, the highest
gap value and smallest minimum diameter are shown by the base
alone, without dispersed crystalline phase.

A liquid monopropellant, hydrazine saturated with dekazene,
has been found to have a minimum diameter and card gap value simi-
lar to those of petrin acrylate composite solid propellant.

Brandon, Ockert

Introduction - Solid rocket propellants and many of their constituents are explosives. As such they constitute hazards in synthesis, manufacture, transportation and handling, and ultimate utilization. In the course of an investigation by this Division into the nature and definition of detonation sensitivity as applied to solid propellants, it became useful to have a simple means of ranking the materials under study. Such a means was the card gap test[1]. This test has been successfully applied to the examination of the effect of oxidizer particle size, of charge confinement, and of temperature on shock sensitivity of composite propellant; the effect of solids loading on apparent sensitivity; and comparative minimum diameters and gap sensivities of a number of propellant types.

Effect of Acceptor Confinement - Degree of confinement has a significant effect on the detonability of propellants. Charges of composite formulation 116bw (17% double-base powder, 32% triethylene glycol dinitrate, 1% resorcinol, 20% aluminum (Alcoa 140), 30% ammonium perchlorate (35-micron weight median diameter, 95% between 4. 4 and 93 microns)) were cast in steel water pipe and in cardboard cylinders, and minimum diameter and card gap values were determined.

Plots of card value against charge size gave two straight lines, intercepting the abscissa at the respective minimum diameters (Figure 2)[2]. The limiting diameter indicated in the Figure is the largest subcritical diameter experimentally tested, i. e., stable detonation does not propagate at that diameter. The limiting diameter is higher in cardboard than in steel but the slope of the line in the former case is greater, so that at 2 inches, the two lines intersect. Above

---

[1] Owing to considerations of minimum or critical diameter, a certain measure of flexibility in this test as regards charge size is necessary. The distinctive features of the test referred to here are 1) the use of a heavy booster of Composition C-4 explosive, 2) maintenance of fixed scaling between donor and acceptor, regardless of charge size (Figure 1), and 3) determination of gap sensitivity above the experimentally established minimum diameter. (Cf. Ref. (1))

[2] The reader unfamiliar with this form of presentation should bear in mind that booster size is increased with acceptor size. Consequently an increase in card value is to be expected. In these tests donor, gap, and acceptor always have diameters equal to each other. Donor length-to-diameter ratio is maintained at 3 and that of the acceptor is 4 or greater.
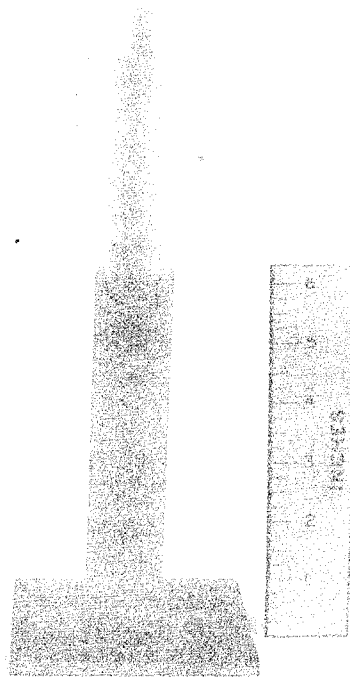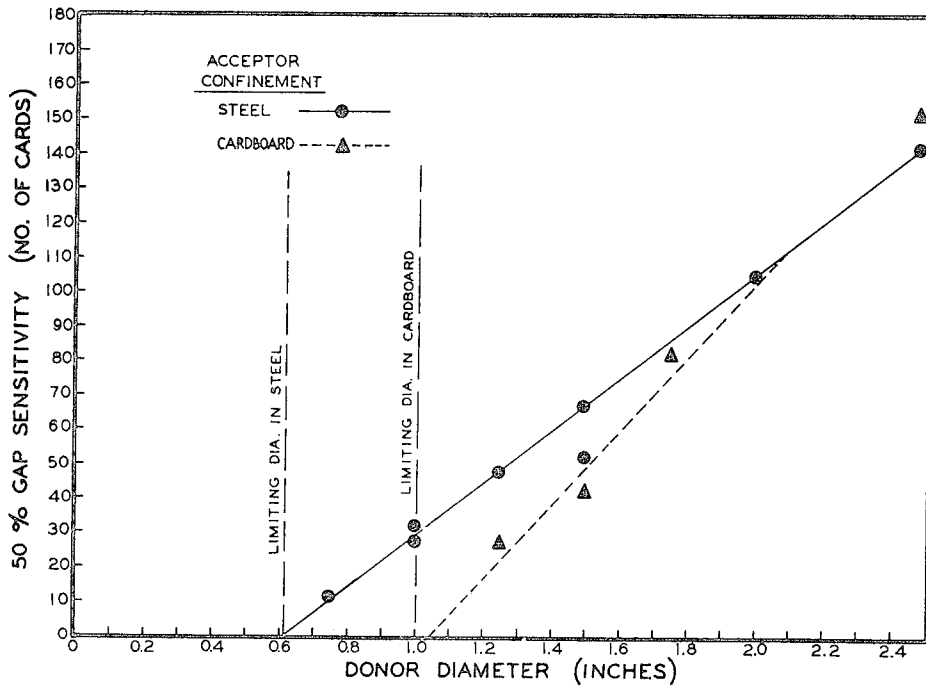
Fig. 1 CARD GAP SENSITIVITY TEST ARRANGEMENT

Fig. 2 CARD GAP SENSITIVITY OF PLASTISOL
FORMULATION 116 bw (35μ NH$_4$ClO$_4$)

this diameter the charges are effectively self-confined and no further differences in card value are observed. (Data obtained at 3 inches, since the Figure was drawn, indicate continued linear congruence. Gap values were 202 and 192 in steel and cardboaru, respectively.)

Effect of Oxidizer Particle Size - Of the different substances examined in the earlier study (1), all but one exhibited the type of relationship shown in Figure 2, viz., a linear function of positive slope intercepting the abscissa at critical diameter. The exception was ammonium perchlorate containing a small amount of fuel (0.5% magnesium stearate). Although the card values plotted in the usual straight-line fashion, regardless of perchlorate particle size, the minimum diameters varied widely with particle size in light confinement and were significantly larger than the extrapolated intercept. An abrupt change was observed such that the card values were not low near minimum diameter.

The effect of oxidizer particle size has been confirmed in propellant (Figure 3). Propellant formulation 116bn has the identical chemical composition as that represented in Figure 2; the sole difference between the two is the substitution of 65-micron perchlorate (95% between 6 and 130 microns). Card values of cardboard-confined charges decrease linearly as diameter is reduced to 1.6 inches; diminishing the diameter by another quarter of an inch places it below critical. (The graph implies that the change is discontinuous, owing to the fact that quarter-inch increments are customary. Smaller increments would show a rapid but continuous drop to the base line.)

Comparison of the data for the two propellants (Figure 4) shows that changing the oxidizer particle size has little effect on gap sensitivity in either light or heavy confinement, but makes its influence felt on critical diameter alone.

Sensitivity of Propellant Ingredients - The constituents of plastisol-type propellants, with the exception of aluminum, have positive heats of explosion, i.e., evolve heat. This includes the double-base powder, the plasticizer (triethylene glycol dinitrate), and ammonium perchlorate. Each can be expected to contribute to the support of stable detonation once initiated. In order to compare the ease of initiation of each constituent minimum diameters and card gap values were determined (Table I).

In steel confinement, the presence or absence of a dispersed crystalline phase has no effect on either minimum diameter or card value. Under conditions of light confinement, on the other hand, the
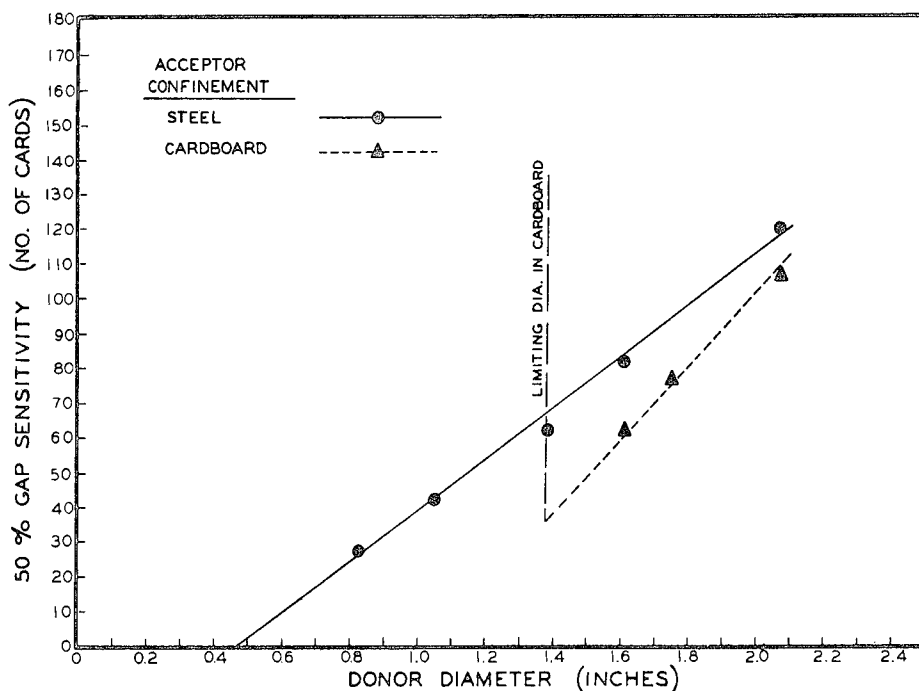
Fig. 3 CARD GAP SENSITIVITY OF PLASTISOL FORMULATION
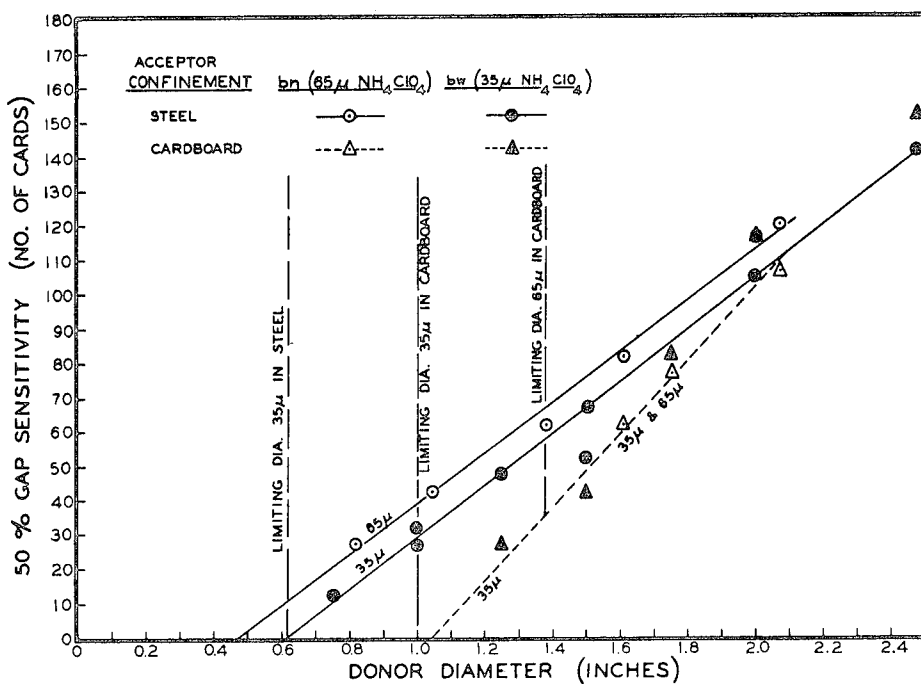116 bn (65μ NH$_4$ClO$_4$)

Fig. 4 CARD GAP SENSITIVITY OF PLASTISOL FORMULATION 116
AS A FUNCTION OF OXIDIZER PARTICLE SIZE

Table I

Minimum Diameters and Card Gap Values of Plastisol
Propellant Formulation 116bn and Its Components

Component	Cardboard-confined		Steel-confined	
	Minimum Diameter D_c, in.	50% Gap Value @ 2.07"	Minimum Diameter D_c, in.	50% Gap Value @ 1.05"
Base (no oxidizer)	$1.05 < D_c < 1.38$	127	$0.36 < D_c < 0.62$	47
Base + oxidizer (116bn)	$1.38 < D_c < 1.61$	107	$D_c < 0.62$	42
Base + dummy oxidizer	$1.75 < D_c < 2.07$	82	$0.36 < D_c < 0.62$	37
Plasticizer	--	--	$1.05 < D_c < 1.38$	57 (2.07")

homogeneous base has the smallest critical diameter and the highest gap sensitivity at 2 inches. The inert-loaded propellant has a high minimum diameter and relatively low card value, while the perchlorate-containing formulation occupies intermediate positions. The insensitivity of the plasticizer is emphasized by the fact that the gap value in steel is less than that of the other constituents in cardboard.

The relationship among the three formulations is more readily seen in Figure 5. It is interesting to note that the limiting diameter of the base alone in light confinement appears exactly at the extrapolated point for normal propellant and, in fact, coincides with that of 116bw, which contains the smaller-size oxidizer.

These results strongly suggest that initiation is effected through the plasticized nitrocellulose continuous phase. Introduction of a crystalline dispersed phase reduces the energy release per unit cross-sectional area, either by simple dilution and/or by absorption of energy in the dispersed phase. The intermediate values with the live oxidizer indicate that energy absorption by the dispersed phase is in some measure offset by energy released by decomposition of the perchlorate. The invariance of the results determined in steel contrasted with the differences in cardboard serve to demonstrate the delicacy of the balance between internal and external energy losses.

(The base formulation still contains aluminum, which comprises 20% of the finished propellant. Recently determined minimum diameters of base from which this aluminum is absent have been significantly greater than those shown in Table I: between 0.82 and 1.05 inches in steel and greater than 2.07 inches in cardboard. These are a half-inch more in heavy confinement and at least 3/4 inch more in light confinement than corresponding values for aluminum-containing base. If minimum diameter be taken as an index of detonation sensitivity, then aluminum would appear to increase the sensitivity of the plasticized double-base powder matrix. The physical consolidation of the charges was so poor and nonhomogeneous that further experiments must be made.)

<u>Effect of Charge Temperature on Apparent Sensitivity</u> - The card gap values of plastisol-type propellant change very slowly with conditioning temperature. Over the range from -40° to +130°F, the numbers increase linearly at 28 cards per 100 Fahrenheit degrees (Figure 6). Since normal variation is $\pm$ 5 cards, these results indicate that card gap values are unaffected by temperature under normal ambient conditions.
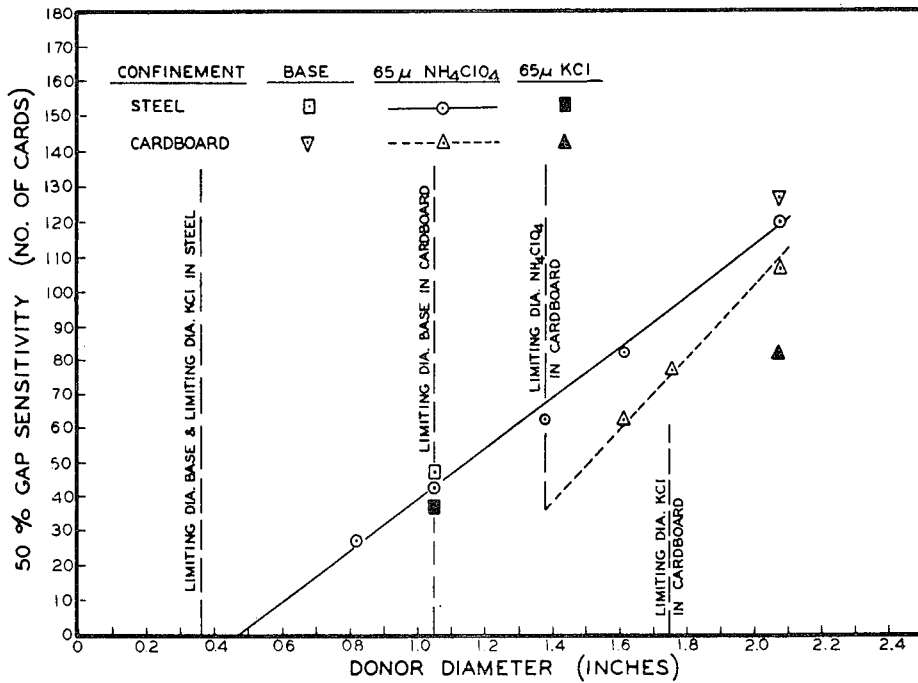
Fig. 5 CARD GAP SENSITIVITY OF PLASTISOL FORMULATIONS:
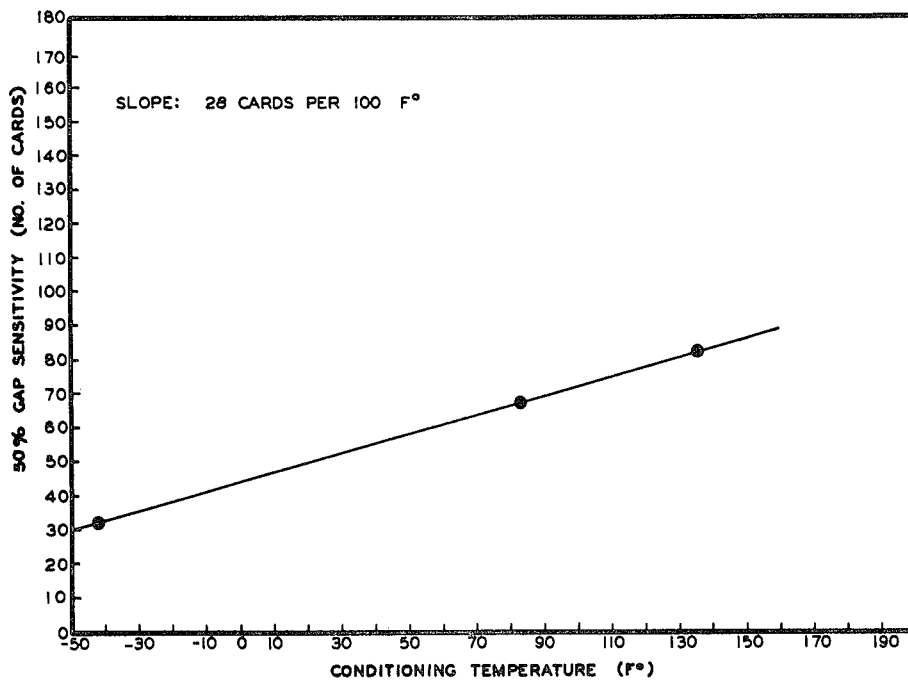116 bn (65μ NH₄ClO₄), 116 BASE, 116 bn WITH 65μ KCl REPLACING NH₄ClO₄

Fig. 6 TEMPERATURE SENSITIVITY OF CARD GAP VALUE OF
PLASTISOL FORMULATION 116 bw AT 1.61 INCHES
DIAMETER IN CARDBOARD CONFINEMENT

829

Comparative Gap Sensitivities - Although screening of materials is not the primary object of this program, sufficient data have accumulated to compare a number of substances as regards minimum diameter and card gap value under various conditions of confinement and size.

Despite the exceptions noted above, the data (Table II) confirm the general relationship between critical diameter and card gap value, namely, the smaller the minimum diameter, the greater the sensitivity. Thus Composition C-4 explosive (1.33 gm/cc)(91% RDX) has a very small critical diameter and high card value. RDX-containing composite propellant (petrin acrylate base) shows nearly the same properties, although the RDX concentration is down to 28%. The extruded double-base (N-5), plastisol nitrocellulose composite (116bn), and mixed-binder (plasticized nitrocellulose and polyurethane) composite (BRL-1) propellants have similar card gap values. Saturated (35%) solution of dekazene (1:1 adduct of hydrazine and decaborane) in hydrazine, a liquid monopropellant, ammonium perchlorate/petrin acrylate composite propellant (without RDX), and TEGDN consistently show decreasing gap sensitivity with increasing minimum diameter.

The characteristics of petrin acrylate propellant with and without RDX are in marked contrast. Comparison of the two liquid substances gives a striking example of the importance of a little latitude in conducting card gap sensitivity tests. The dekazene/hydrazine solution has a minimum diameter 3/4 inch in steel; that of TEGDN lies above 1 inch. Yet at 2 inches the two have nearly the same card value. Had this test been run at 1 inch according to the procedure recommended by the Joint Army-Navy-Air Force Panel on Liquid Propellant Test Methods (2), a negative result would have been obtained with TEGDN, implying it to be an insensitive material.

In general, we have found explosives and propellants to fall into three loosely-defined categories. High explosives are characterized by very low minimum diameters. They appear indifferent to degree of confinement, probably because the diameters at which card gap values have been determined are still significantly larger than critical diameter. Solid propellants containing reactive binders, such as nitro compounds and nitrate esters, have minimum diameters which vary with confinement and range from 1/2 to 2 inches. The liquid substances tested also fall in this range. Solid propellants having inert binders of polyurethane, polysulfide, polybutadiene-acrylic acid copolymer, etc., have minimum diameters above 8 inches and they cannot be ranked owing to limitations of test facilities. It should be noted in conclusion that these generalities apply to normally consoli-

Table II

Minimum Diameters and Card Gap Values
of Propellants and Explosives

Material or Propellant Type	Light Confinement				Heavy Confinement			
	Minimum Diameter D_c, in.	50% Gap Value Charge Diameter			Minimum Diameter D_c, in.	50% Gap Value Charge Diameter		
		1"	1.5"	2"		1.05"	1.61"	2.07"
Compn. C-4 explosive	$0.15 < D_c < 0.16$	82	142	187	$D_c < 0.62$	92	147	--
RDX-contg. comp.	$0.19 < D_c < 0.25$	67	--	--	--	--	--	--
Extruded double-base	--	--	77	--	--	--	--	--
Plastisol NC comp.	$1.38 < D_c < 1.6$	--	62	107	$D_c < 0.62$	42	82	120
Mixed binder comp.	--	--	--	--	--	--	--	110^a
Satd. dekazene/hydrazine	--	--	--	--	$0.62 < D_c < 0.82$	--	--	62
Petrin acrylate comp.	$2.0 < D_c < 2.5$	--	--	--	$0.82 < D_c < 1.05$	12	37	--
TEGDN	--	--	--	--	$1.05 < D_c < 1.38$	--	--	57

[a] 100-125

dated propellant. Where mechanical defects or interconnected porosity exist, transition from deflagration to detonation takes place with all types of solid propellants.

REFERENCES

(1) Brandon, W. W., "The Importance of Flexibility in Gap Sensitivity Testing, " Bull. 16th Mtg. JANAF Solid Prop. Group $\underline{V}$, 109 (1960)

(2) "Liquid Propellant Test Methods, " Test No. 1, Card Gap Test, Liquid Propellant Information Agency, March 1960

SOME STUDIES ON THE SHOCK INITIATION OF EXPLOSIVES
by

E. N. Clark and F. R. Schwartz

Explosives Research Section
Picatinny Arsenal
Dover, New Jersey

Introduction

This work was supported by Ordnance Corps Project TB3-0134. Figure 1 illustrates the experimental technique used in this study. The donor explosive has a length to diameter ratio of approximately 3 to 1 and is coated with an aluminum silicofluoride paste to facilitate the observation of its detonation rate. The inert barrier used was mild steel "boiler plate" with both faces ground smooth and parallel. The barrier was large enough that the detonation products were delayed sufficiently long so that they did not interfere with the observation of the phenomena occurring in the receptor explosive.

So as to observe the "low order" phenomena occurring, a reflective technique was used similar to that at NOL[1]. A 0.0003" thick strip of silver foil was cemented to the side and top of the donor explosive. Light from an argon bomb is reflected from the foil into the slit of the 194 Beckman and Whitley streak camera. Thus, any disturbance of the foil will interrupt the beam of light and the disturbance will be noted by the extinction of the light on the film. The exit of the wave from the end of the acceptor is also observed using the foil by means of a mirror placed at 45° to the horizontal.

Figure 2 is a good film record showing the propagation of the low order wave, its transition to high order, the retonation wave, which is obviously slower than the detonation wave, and the wave shape coming out the rear of the receptor. Each shot was observed with the Model 189 B&W framing camera normal to the direction of observation of the streak camera.

The explosive studied was Composition B machined from billets having a density of 1.70 grams/cc detonation rate of 7.88 mm/micro second and a standard deviation of 0.23 mm/microsecond as determined
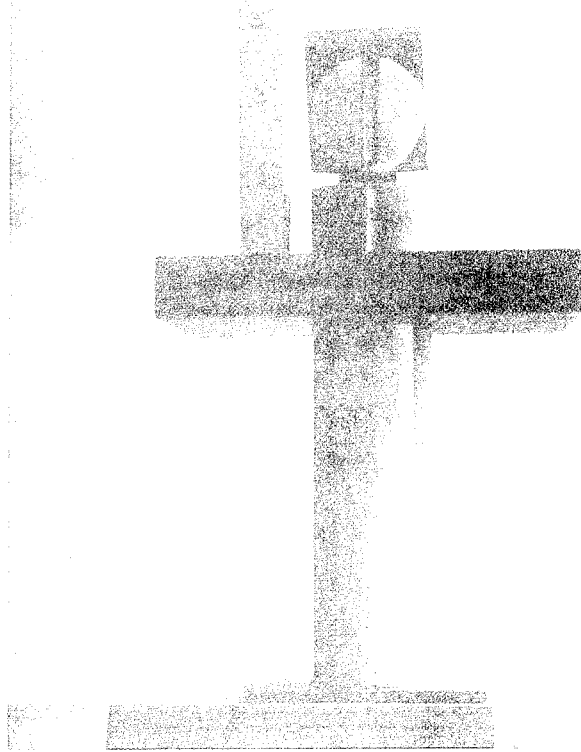
833

Figure I - Charge Set Up

from streak camera records during these experiments. Since the foil
technique described permits observation only on the surface of the
charge, and in order to deduce what was going on inside the explosive
charge, it was necessary to vary the length of the acceptor and note
the time of arrival and the shape of the wave out the end of the ac-
ceptor as a function of length.

Experimental Results

Figure 3 shows a plot of the peripheral shock velocity in
Composition B as a function of thickness of steel for a donor geome-
try of 1 1/16" diameter x 3" long. Those points which have a standard
deviation as shown are an average of 8 or more shots. It will be
noted that there is a decided change in the slope of the curve for the
two points indicated by triangles. The magnitude of the pressure
pulse which corresponds to a given thickness of steel has not as yet
been measured. It is anticipated, however, that this increase in
velocity is greater than would be expected from the increase in
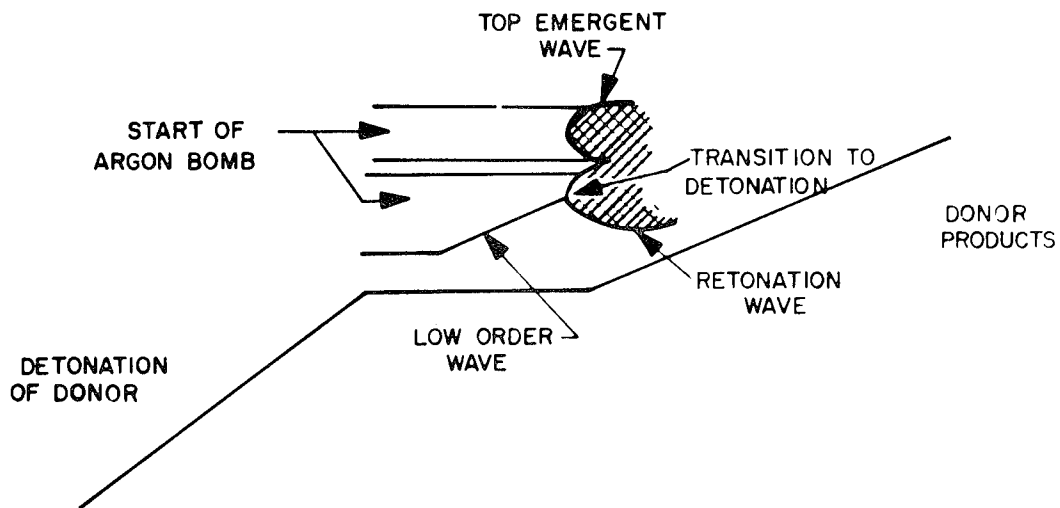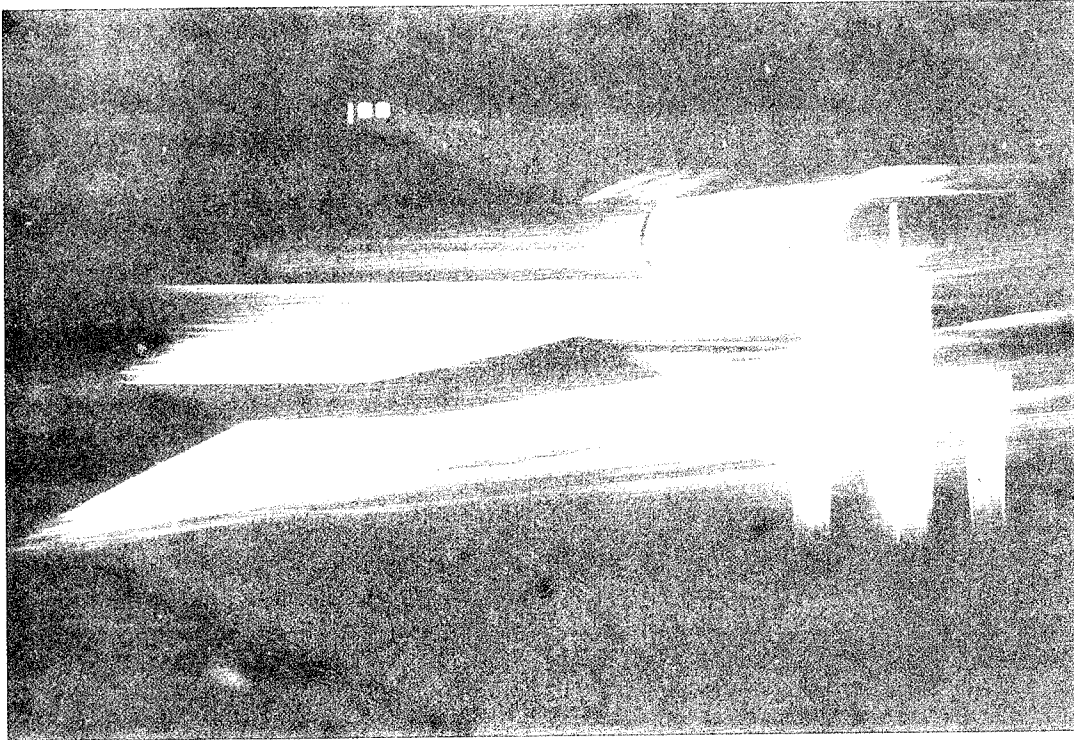pressure represented by a decrease in thickness by 1/8" of steel.

TOP EMERGENT
WAVE

START OF
ARGON BOMB

TRANSITION TO
DETONATION

DONOR
PRODUCTS

RETONATION
WAVE

LOW ORDER
WAVE

DETONATION
OF DONOR

FIG. 2

FIG. 3

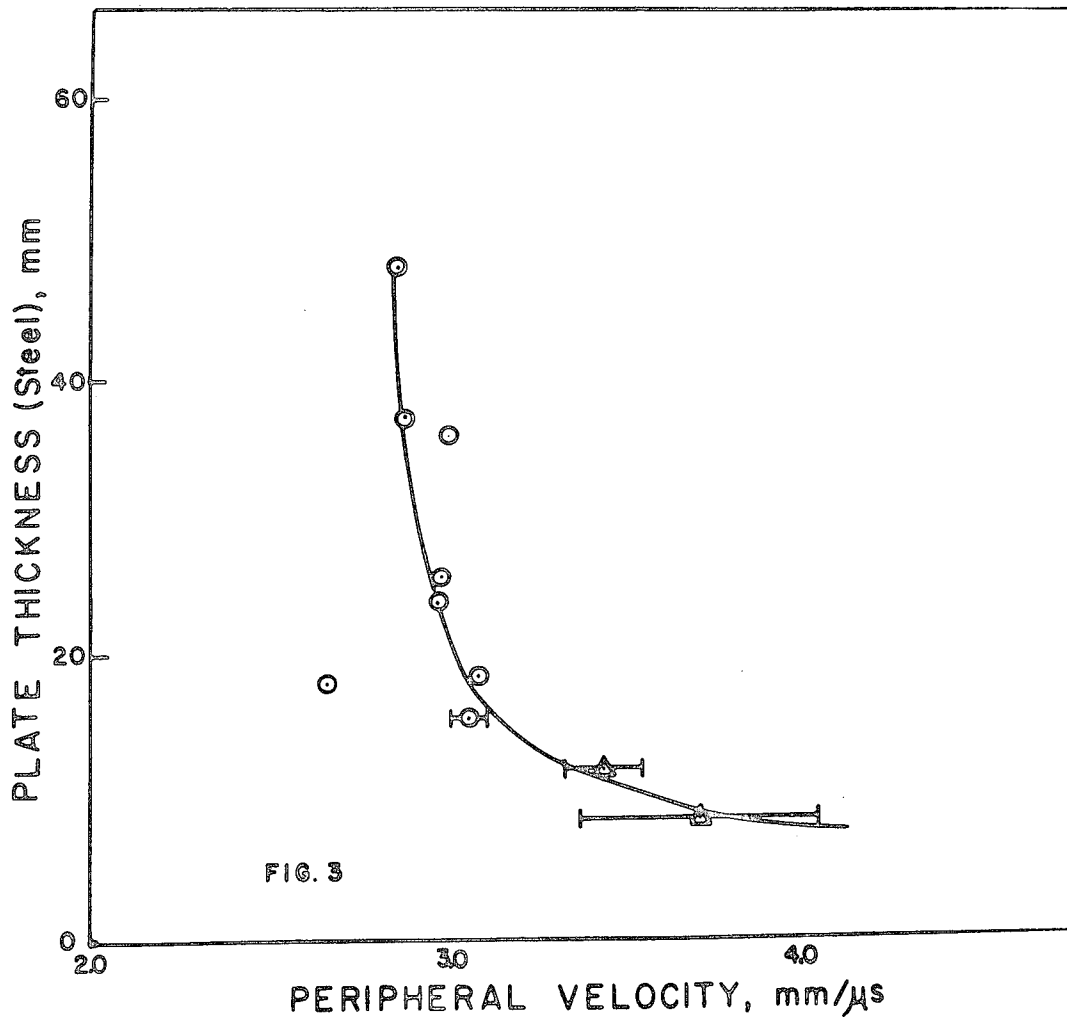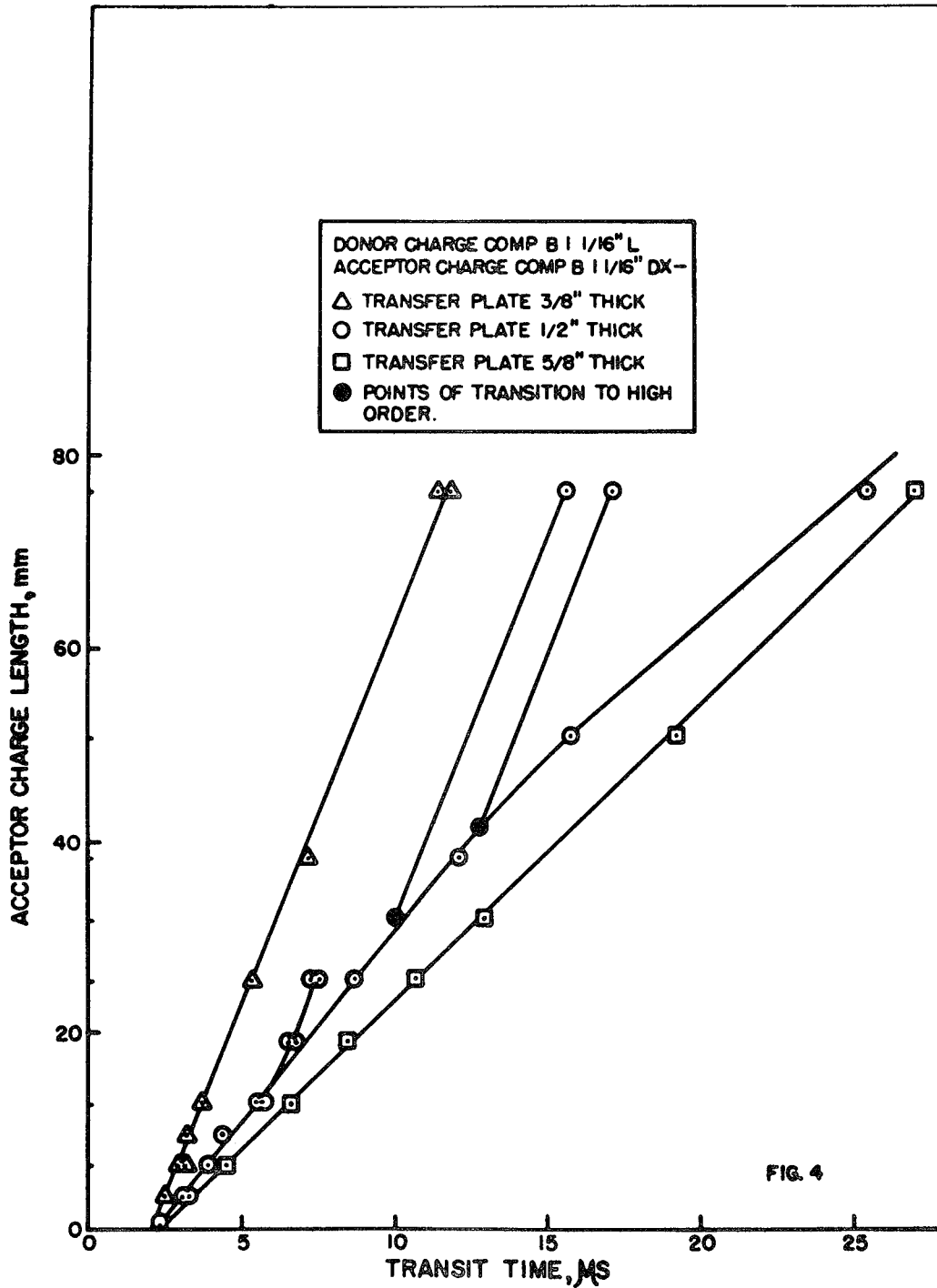PLATE THICKNESS (Steel), mm — PERIPHERAL VELOCITY, mm/μs

Figure 4 shows a plot of the arrival time of the wave out of the acceptor as a function of acceptor length for various thicknesses of steel plate using the aforementioned donor geometry. The acceptor charges were 1 1/16" in diameter. It will be noted that for the case of the 5/8" steel all the arrival times plotted against acceptor length fall on a straight line the slope of which is the velocity of the shock wave along the axis of the acceptor. A least squares fit of the data shows the velocity to be 3.078 mm/microsecond. The average of the velocities observed along the edge of the explosive is 3.061 mm/microsecond, with a standard deviation of 0.05 mm/microsecond. Thus, there is no significant variation between velocities taken along the axis of the charge and along its periphery. The pertinent fact here is that the thickness of the steel is such that the shock wave is somewhat slower than any with which detonation has been observed to date.

DONOR CHARGE COMP B 1 1/16" L
ACCEPTOR CHARGE COMP B 1 1/16" DX—
△ TRANSFER PLATE 3/8" THICK
○ TRANSFER PLATE 1/2" THICK
□ TRANSFER PLATE 5/8" THICK
● POINTS OF TRANSITION TO HIGH
ORDER.

FIG. 4

In Figure 4 for the case of the 1/2" thick steel the plot is somewhat more complicated. This is so because this particular configuration sometimes transfers to high order detonation and sometimes does not. Detonation was not observed in acceptors less than 0.6" and the few points below this value lie on a straight line. A continuation of this straight line can be seen to go through those points up to about 1 1/4" where no high order detonation was observed and beyond which, the velocity of the axial shock appears to fall off. The velocity of the axial shock for acceptors 1 1/4" and less was determined by the method of least squares to be 4.054 mm/microsecond. The average peripheral velocity observed for these samples is 3.44 mm/microsecond with a standard deviation of 0.11 mm/microsecond. Thus, in the instance of a stronger shock, there is a significant difference between the axial velocity and the peripheral velocity.

Times of arrival less than 1 1/4" which did not detonate were also measured at a distance of 1/4 R, 1/2 R, 3/4 R and 1 R from the axis of the charge for all acceptors. Velocities were determined for each of these distances from the axis, Figure 5 shows the variation of this velocity with the radius of the charge. Although the curve does show a continual and significant change in velocity from the axis to the edge of the charge, the actual shape of the curve may not vary significantly from a straight line relationship.

As can be seen from Figure 2, the shock wave in the donor travels at a constant velocity until such time as a transition takes place to high order detonation. However, the transition to detonation apparently takes place at some point within the explosive since the detonation wave shows a distinct curvature at the side of the explosive. This curvature makes the measurement of the detonation rate in the acceptor somewhat difficult and, therefore, is not being reported. However, this rate can be deduced from time of arrival data.

Consider in Figure 4 those longer acceptors which transferred over to detonation. Let us assume that the distance along the side of the stick, at which the transition to high order is seen, represents the distance on the axis of the charge where the transition did occur. Since we know the velocity of the shock at the center this point determines the actual time at which detonation started. Thus, with this distance and time, and the exit time from the end of the stick, we may calculate a detonation velocity. This has been done for all the charges that detonated in the 1/2" steel series. All the detonation rates observed were higher than the rate for the donor. However, there is considerable scatter for most of the data, as they represent the measurement of detonation rates over only a few tenths of an inch. For the two instances where there is over an inch in which to measure the detonation rate, the value obtained was 8.1 mm/microsecond; which is not significantly different from the detonation rate of the donor.

FIG. 5
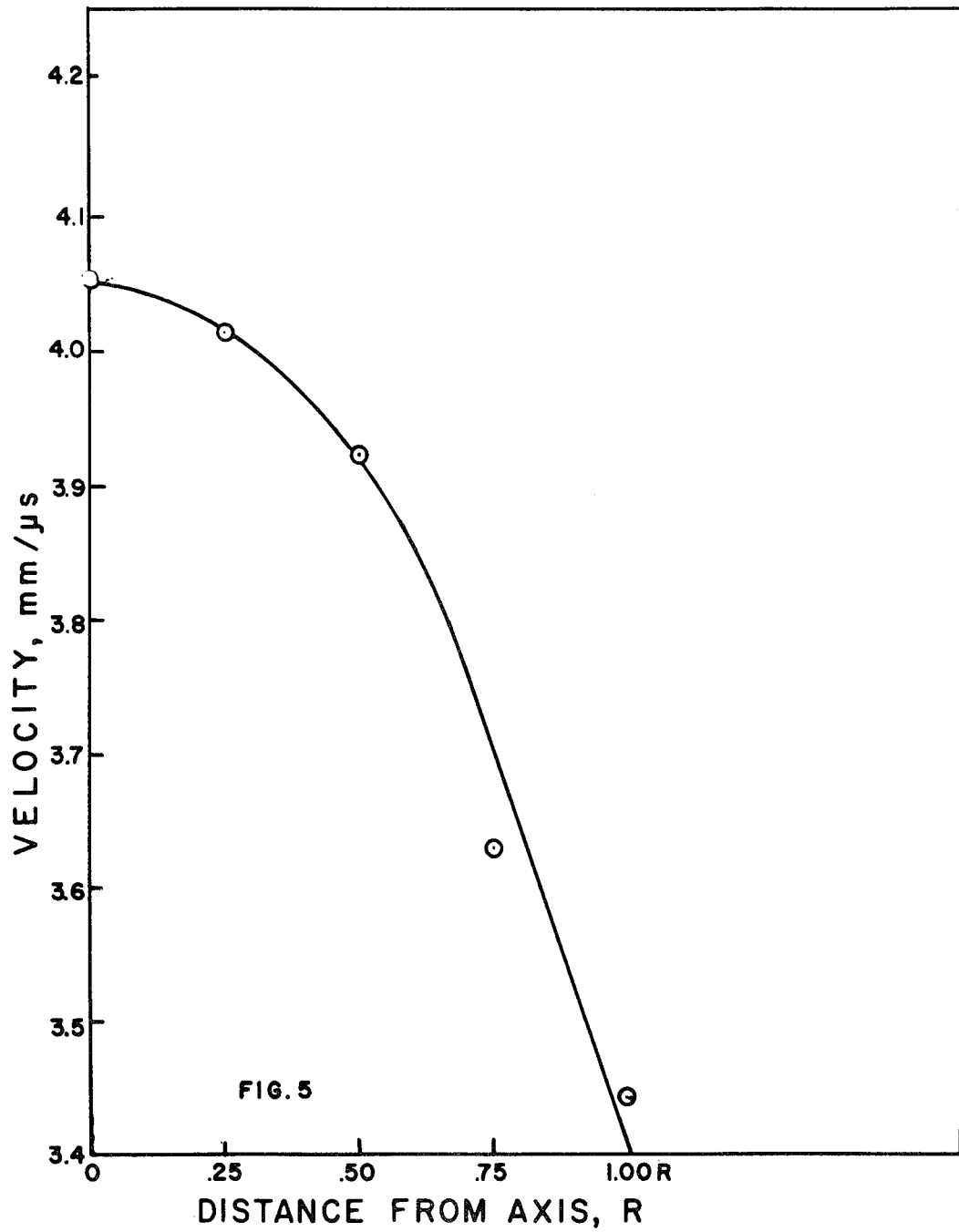
For the series with the 3/8" steel plate, the point where the transition to detonation took place was less than 0.5" and the detonation always took place so that the axial velocity of the shock wave could not be determined. However, the low order wave was observed on the side of the acceptor. Its velocity spread was somewhat greater than in other instances, possibly because of the shorter distance over which it could be measured. A least squares fit of the points with acceptors longer than 0.5" was made, and a value of 8.032 mm/microsecond was obtained. This value again does not differ significantly from the detonation rate of the donor. Therefore, these few measurements are insufficient to show any differences in the detonation rates of the donor and the acceptor.

Discussion

Possibly the easiest manner in which the sudden increase in shock velocity in Figure 3 can be explained is that this discontinuity represents a sudden onset of chemical reaction or at least an increase in chemical reactions which then supports the shock wave. This hypothesis is further supported by the fact that there is a considerable difference between the velocities on the axis and the periphery.

Thus, it appears that a necessary condition for a shock wave to initiate detonation is that the shock pressure should be sufficiently high so as to initiate chemical reaction and to support a shock on the axis of the charge markedly faster than at its periphery. It is not clear that this is a sufficient condition since some charges of this type did not detonate. However, the transition point was quite variable, and it might be argued that these charges were not long enough for the transition to take place. Also, there is some indication that the shock might be starting to slow down but, since this represents the results of only two shots, it is not conclusive and more firings are necessary to settle this point.

At this time, it is not clear as to what other conditions must be satisfied for this reactive shock to transfer to high order. The fact that the distance to the transition is quite variable, suggests that the condition at least in part is statistical, possibly having to do with the location of voids or other imperfections in the explosive. In order to determine if this is indeed the case, we are presently studying the same phenomena in very good quality plastic bonded explosives.

It seems obvious, however, from the fact that with thinner steel plates the distance to transition decreases and the spread in this distance also decreases, that the condition is not completely statistical. The fact that the velocity of the wave is greater in the center of the stick than in the periphery leads to an instability, which might explain what we have observed so far. The velocity gradient results in a continually decreasing radius of curvature for

this low order detonation, similar to what might be observed with a convergent detonation wave. At some time, the decrease in the radius of curvature would be expected to result in higher pressures in this region, with a consequent increase in velocity resulting in a further decrease in radius of curvature. Consequently the transition from this low order process should be expected to take place in a catastrophic manner.

Further, this process has in it the elements of being affected by statistical variations in the charge, as various small voids in the explosive might be expected by a jetting process to form the small radius of curvature somewhat earlier than in the normal process and, thus, cause the transition to take place at an earlier stage.

Thus, the picture develops of a shock pressure sufficiently high to induce chemical reaction to support the shock wave. The radial pressure gradient induces a velocity gradient which, in turn, reduces the radius of curvature which, when sufficiently small, transfers suddenly to high order detonation. For larger charges where the pressure gradient and consequently the velocity gradient across the stick is small, or in instances where the shock wave would have a uniform impulse across the acceptor, the transition to detonation should take place further along. In similar work with charges 1 1/2" in diameter and suitable transfer plates, we find that the transition takes place at 1.0" rather than 0.6". As yet we have not performed the uniform impulse experiment although this is planned for the near future. At present, the experimental evidence is insufficient to prove this mechanism; however, it does seem to contain within it the elements to explain some of the experimental results that have been observed to date.

References

(1) Initiation to Detonation of High Explosives by Shocks - NAVORD Rpt #5710, Naval Ordnance Laboratory.

Acknowledgements

THE INFLUENCE OF ENERGY OF DECOMPOSITION OF THE TRANSITION FROM INITIATION TO DETONATION

Z. V. Harvalik
U. S. Army Engineer Research and Development Laboratories
Fort Belvoir, Virginia

During the past two decades a considerable amount of research has been undertaken to determine the nature of initiation of explosives and of the transition of initiation to detonation. The first satisfactory theory of initiation was proposed by Bowden and co-workers (1), who assumed that the presence of thermal hot spots is responsible for the breaking of the bond. Many phenomena of initiation could be explained by the hot spot theory. To cite a few examples: initiation by heat, by hot wires, by stab, percussion, and by shock. However, as new experiments were invented and data gathered, the hot spot theory was not considered satisfactory for explaining certain phenomena associated with gap-type initiation and with spontaneous detonations during crystal growth of metastable materials (2), (3), (4). In addition to these phenomena, multiple energy exposures including phase transformation indicate that a purely thermal model of initiation is not too satisfactory (5), (6), (7), (8), (9), (10), (11). This author (12) proposed a theory of initiation which attempts to explain initiation processes in terms of rapidly changing field gradients within the intra-atomic and intramolecular spaces of a metastable compound. The rapid changes of the field gradients which ultimately would lead to the severance of the chemical bonds can be achieved by influx of various energy forms either singularly or multiply applied. They have to be absorbed in the compound in order to produce an intra-atomic or intramolecular disturbance. Absorption coefficients of various metastable compounds for various radiant and vibrational energies have been only sparsely determined as well as the interaction cross sections for ionizing radiations and particles.

When multiple exposure is used in the study of initiation of metastable materials usually one of the energy forms applied is heat. The particular specimen material is heated to certain temperatures and another energy form such as stab or light, for instance, is applied to the material. The measurements reveal that as the temperature of the specimen is increased the additional heterogeneous

energy can be reduced to affect initiation. This is also true for radiant energy (UV) when used instead of heat as a pre-exposed energy form (6), (7). Since the pre-exposed radiant energy magnitudes are very small and do cause significant reduction of the amount of heterogeneous energy to affect decomposition, it is considered that the hot spot theory fails to explain this phenomenon (5).

Photolysis and thermolysis experiments of metal azides carried out by numerous investigators including those at the Basic Research Group were able to point out that in the early stages of initiation, color centers and excitons were formed and perhaps also short lifetime free radicals of N_3 (13), (14). Thus, even in exceedingly pure compounds the stoichiometric equilibrium is disturbed due to the appearance of nitrogen, colloidal metal, and compounds of lower nitrogen content which in turn accelerate catalytically the decomposition of the compound (15), (16). These "catalysts" seem to be the sites of electronic disturbances thus modifying field gradient distribution in the vicinity of undecomposed molecules and with further influx of external energy more and more undecomposed material will be affected.

In the process of breaking of the chemical bond, a significant amount of energy is generated. Because of its spectral distribution, specific for a given compound, a large portion of this energy will be absorbed in the undecomposed compound thus increasing the field disturbances in front of the reaction zone. When large enough in magnitude, the bond will break thus ensuing an additional production of energy, accelerating the decomposition to detonation (17).

It is well known that detonating materials produce, besides heat and shock, also radiant energies in the form of light as well as microwaves and soft X-Rays (18),(19). It is also known that electric charges are amply produced not only in the form of electrons but also in the form of positively and negatively charged ions of various velocities (20), (21). These energy forms are always observed simultaneously when a metastable compound detonates. The energy distribution and spectrum of individual energy forms vary from substance to substance (17). Preliminary investigations performed by members of the Basic Research Group and by its contractors indicate that not all of the energy of decomposition is heat (22), (23). Perhaps up to 30 percent and more could be assigned to radiant energy alone. The remainder could be classified as heat and shock.

To attempt to understand the phenomena which lead from initiation to detonation one would have to acquire a thorough knowledge of the phenomena associated with initiation. If initiation is essentially an electric phenomenon, namely, interaction of external electromagnetic energies with the intra-atomic and intramolecular fields, the generation of electric energy forms will result. However, as the interaction progresses from the color center and exciton formation into the free radical production and molecular fragmentation of rather

unexpected combinations (24), heterogeneous energy forms are generated by these processes. A transition from a prevalent electromagnetic energy stage to a vibratory (thermal) stage will now be observed. When the detonation stage is reached the production of thermal energies and shock waves prevails. However, it should be pointed out that a still considerable amount of other energy forms (electromagnetic) will be present. These energy forms will penetrate into the not yet decomposed portion of the detonating specimen thus conditioning it for subsequent decomposition (17). The presence of electromagnetic energy forms in the transition from initiation to detonation is proved by the influence of strong magnetic and electric fields on detonating metastable materials. An apparent decrease of sensitivity and a reduction of detonation velocities was observed when detonating compounds were exposed to these fields (21). This seemed to indicate that certain electric component energies have to be available in the transition period for appropriate acceleration.

The disregard of the role of electric energy forms explains the difficulty of establishing valid prediction of decomposition temperatures of metastable materials. Many attempts have been made but none of the predictions approached the observed temperature ranges closely enough (21), (22), (23). It is realized that the problem of establishing a satisfactory model of the transition from initiation to detonation is a very complex one and, therefore, difficult to establish. The inclusion of electric and magnetic phenomena into this model will probably simplify the understanding of the phenomena and ultimately enable one to predict the circumstances leading to detonation of metastable substances.

1. F. P. Bowden, O. A. J. Gurton: Proc. Roy. Soc. (London), Vol. A198, page 350, (1949).

2. J. G. Dodd, Jr.: Quarterly Progress Report, 11 Dec 1955-10 Mar 1956, Contract DA-44-009-ENG-2439, Univ. of Arkansas, page 2.

3. M. D. Kemp, Proc. of the 1959 Army Research Conference, West Point, N. Y., Vol. 2, page 1, (1959).

4. J. G. Dodd, Jr.: Final Report, Contract DA-44-009-ENG-3132, 9 Oct 1957, Univ. of Arkansas, page 33.

5. Z. V. Harvalik: Quarterly Progress Report, 11 June 1955-10 Sep 1955, Contract DA-44-009-ENG-2439, Univ. of Arkansas, page 10.

6. B. Meerkaemper: Ztsch. f. Electrochemie, Vol. 58, page 387, (1953).

7. J. Eggert: Proc. Roy. Soc. (London), Vol. A246, page 240, (1958).

8. Yao Chiang: Quarterly Progress Report, 1 May-31 Jul 1954, Contract NOrd 10417, Univ. of Arkansas, page 25.

9. L. G. Bolkhovitinov: Dokl. Akad. Nauk, USSR, Vol. 125, page 570, (1959).

10. L. G. Bolkhovitinov: Dokl. Akad. Nauk, USSR, Vol. 126, page 322, (1959).

11. G. J. King: Private Communication, BRG, USAERDL, (1960), (to be published).

12. Z. V. Harvalik: Proc. of the 1957 Army Research Conference, West Point, N. Y., Vol. 3 page 189 (1957).

13. J. G. Dodd, Jr.: Technical Report, Contract DA-44-009-ENG-2439 15 Aug 1956, Univ. of Arkansas.

14. H. M. Dumas, Jr.: Technical Report, Contract DA-44-009-ENG-2439, 31 Aug 1956, Univ. of Arkansas.

15. G. J. King, B. S. Miller, F. F. Carlson, R. C. McMillan: Journal Chem. Phys., Vol. 32, page 940, (1960).

16. B. S. Miller: Journ. Chem. Phys., (1960), (in press).

17. Z. V. Harvalik: Proc. Contractors Conference, Project 8-07-11-440, page 1, (1959).

18. H. Kolsky: Nature, Vol. 173, page 77, (1954).

19. T. Takakura: Publ. Astron. Soc., Japan, Vol. 7, page 210, (1955).

20. W. A. Bone, R. P. Frazer, W. H. Wheller: Transact. Phil. Soc., (London), Vol. A235, page 29, (1935).

21. M. A. Cook: The Science of High Explosives, Reinhold Publ. Co., New York, (1958), page 143 ff.

22. S. Ling: 1st Quarterly Rpt, 9 Oct 1959-5 Feb 1960, Contract DA-44-009-ENG-4158, PEC, Boulder, Colorado, page 1.

23. M. Misushima: 2nd Quarterly Report, 5 Feb-6 May 1960, Contract DA-44-009-ENG-4158, PEC, Boulder, Colorado, page 1.

24. D. P. Easter: Private Communication, BRG, USAERDL, (1960), (to be published).

AUTHOR INDEX

Smith, L.C.	327		Van Dolah, R.W.	436
Sternberg, H.M.	205,226		Verhoek, F.H.	50
Stresau, R.H.	309,396,420			
Sultanoff, M.	520		Wachtell, S.	635
Summers, C.R.	436		Wenograd, J.	10,60
			Whitbread, E.G.	202,574,659
Taylor, B.C.	267		Wilkins, M.	721
Taylor, J.W.	77		Winning, C.H.	455
Travis, J.R.	469,499			
			Zovko, C.T.	606
Udy, L.L.	150			
Urizar, M.J.	327			
Ursenbach, W.O.	357			